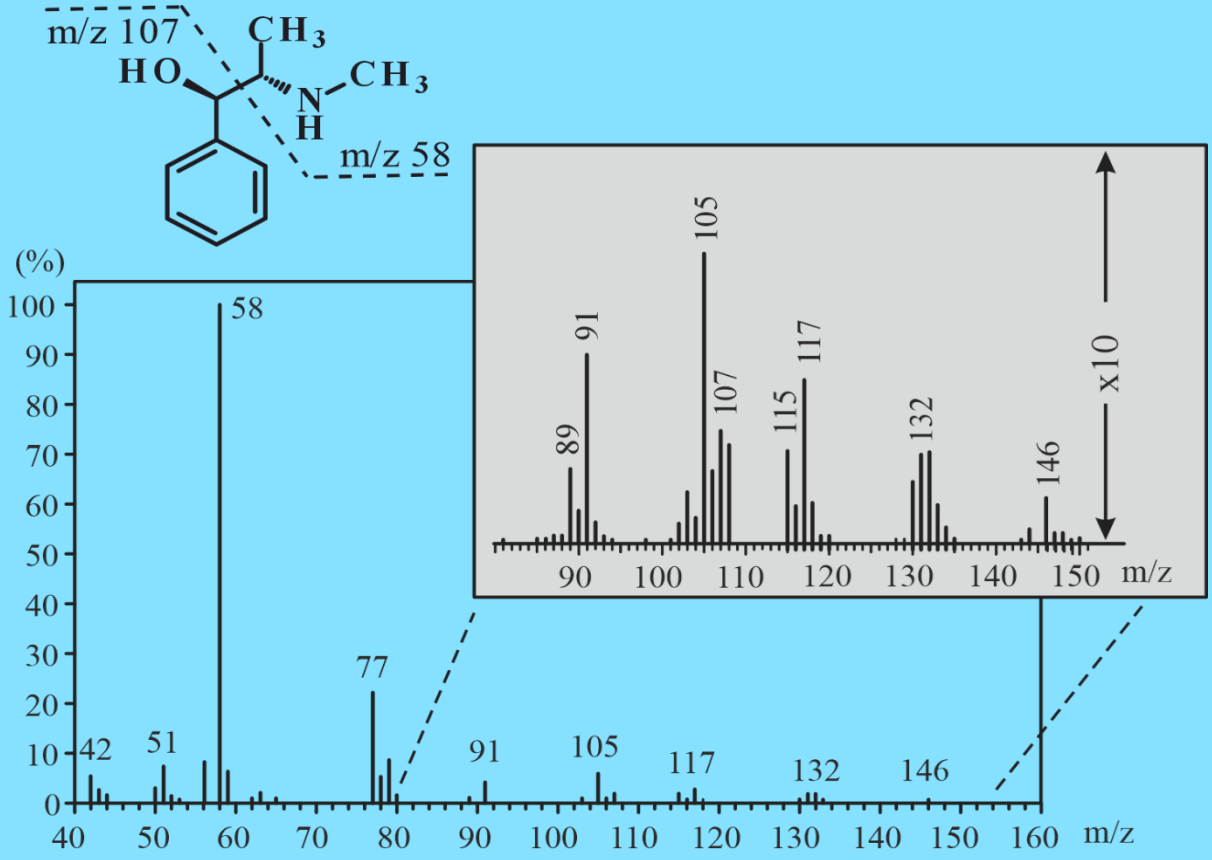
UNIVERSITATEA
DE MEDICINĂ ȘI FARMACIE
„VICTOR BABEȘ“ DIN TIMIȘOARA

*Szabadai Zoltán*

# Mass Spectrometry in Drug Analysis and Development




ACADEMICA

Editura “Victor Babeş”
Timişoara, 2026

*Szabadai Zoltán*

# Mass Spectrometry in Drug Analysis and Development

Editura “Victor Babeş”
Timişoara, 2026

**Editura „Victor Babeș”**
Piața Eftimie Murgu nr. 2, cam. 316, 300041 Timișoara
Tel./ Fax 0256 495 210
e-mail: evb@umft.ro
**https://www.umft.ro/ro/organizare-evb/**

**Director: Prof. univ. dr. Sorin Ursoniu**

**Colecția: ACADEMICA**

**Coordonatori colecție:** **Prof. univ. dr. Andrei Anghel**
**Prof. univ. dr. Victor Dumitraşcu**

**Referenţi științifici:** **Prof. univ. Dr. Ludovic Kurunczi**
**Prof. univ. Dr. Vincențiu Vlaia**

**Indicativ CNCSIS: 324**

© 2026
Toate drepturile asupra acestei ediții sunt rezervate.
Reproducerea parțială sau integrală a textului, pe orice suport, fără acordul scris al autorilor este interzisă și se va sancționa conform legilor în vigoare.

**ISBN 978-606-786-544-8**

## Preface

This volume is dedicated to describing methods of physical and chemical analysis of drugs based on mass spectrometry, as practiced in laboratories focused on control, research development and toxicological studies. In addition to presenting the physical and chemical bases of mass spectrometry, it provides examples of significant analytical applications in quality control, authenticity testing, and development of new drugs and pharmaceutical preparations. Examples, cited with references to relevant literature, are taken from data that has been published or are contained in established databases.

The material in this book is based on the Drug Analysis course taught in the final year of the University and Pharmacy of Timișoara in Romania. The goal is to thoroughly explain the physical and chemical principles behind high-performance methods for analyzing substances of pharmaceutical interest, as well as their respective advantages and limitations.

Mass spectrometry has undergone unprecedented diversification in terms of ionization and ion separation techniques in recent decades, making it a particularly powerful analytical tool.

The content and presentation style focus on understanding the essence of mass spectrometry techniques and providing a rigorous theoretical understanding of the underlying phenomena of analytical methods. Mathematical formalism is used only when strictly necessary; instead, a qualitative and intuitive presentation is preferred.

To illustrate the usefulness of mass spectrometric techniques, the book provides several examples of concrete applications taken, adapted and appropriately commented from specialized literature. This book is addressed to academics and specialists in laboratories involved in developing new drugs and solving toxicological problems.

Szabadai Zoltán

**Contents**

1. Basic concepts and some specific physical details of mass spectrometry (1)
2. Construction and operating modules of mass spectrometers (10)
    2.1. Sample introduction and ionization (10)
        2.1.1. Electron Ionization – EI (12)
        2.1.2. Electrospray Ionization – ESI (16)
        2.1.3. Chemical Ionization – CI (17)
        2.1.4. Fast Atom Bombardment Ionization – FAB (18)
        2.1.5. Plasma Desorption – PD (19)
        2.1.6. Matrix Assisted Laser Desorption Ionization – MALDI (20)
    2.2. Mass spectrometer analysis unit (23)
        2.2.1. General concepts and performance characteristics of mass analyzers (23)
        2.2.2. Magnetic analyzer and magnetic-electrostatic assembly (25)
        2.2.3. Quadrupole analyzer (30)
        2.2.4. Analyzer with a series of quadrupoles ("triple quad analyzer") (38)
        2.2.5. Time of Flight – TOF analyzer (41)
        2.2.6. Ion trap analyzers (45)
            2.2.6.1. Quadrupole linear ion trap (45)
            2.2.6.2. Ion trap with three electrodes (47)
            2.2.6.3. Electrostatic trap (“Orbitrap”) (49)
    2.3. Detection of the ions (52)
    2.4. Ion Mobility Mass Spectrometry – IMS (53)
        2.4.1. Drift-Time Ion Mobility Spectrometry – DTIMS (54)
        2.4.2. High-Field-Asymmetric Waveform Ion Mobility Spectrometry FAIMS (57)
        2.4.3. Travelling Wave Ion Mobility Spectrometry – TWIMS (60)
    2.5. Direct Analysis in Real Time – DART (61)
3. Tandem chromatography - mass spectrometry analysis (65)
    3.1. Total Ion Chromatogram – TIC (66)
    3.2. Selected Ion Monitoring – SIM (68)
    3.3. Selected Reaction Monitoring – SRM (70)
    3.4. Neutral Loss Monitoring – NLM (72)
4. Analytical interpretation and valuation of mass spectra (74)
    4.1. Detection of molecular ion signal and calculation of molecular weight (76)
    4.2. The nitrogen rule (81)
    4.3. "M+1" signals (81)
    4.4. 4.4. Isotopic discrimination of isotopologues (82)
    4.5 Finding the number of atoms of a chemical element in an ionic species (106)
    4.6. Quantitative analysis (109)
            4.9.2.11. Amines (181)
            4.9.2.12. Amides (184)
            4.9.2.13. Nitriles (186)
            4.9.2.14. Nitroderivatives (187)
            4.9.2.15. Halogenated compounds (188)

4.9.2.16. Fragmentation of peptide chains. The *Roepstorff - Fohlman* convention (190)
4.9.2.17. Fragmentation of saccharides. The *Domon-Costello* convention (194)
5. Application examples for the analysis of pharmaceutically relevant substances (case studies) (195)
5.1 Differential identification of paclitaxel and related compounds by mass spectrometry (195)
5.2 MS analysis of the major constituents of *Zingiber officinale* (200)
5.3 Control of photodegradation of metronidazole (208)
5.4 Detection and quantification of illicit stimulants in sport (213)
5.5 MS spectrum and fragmentation of morphine and other narcotics by electron beam ionization (EI) (225)
5.6 Analytical mass spectrometric characterization of non-steroidal anti-inflammatory drugs (NSAIDs) (231)
5.7 Monitoring illicit drugs in wastewater and surface water (236)
5.8 Identification of ramipril by comparative positive and negative $MS^2$ fragmentation (242)
5.9 Special features of the $MS^2$ fragmentation of Aspirin (acetylsalicylic acid) (246)
5.10 Identification and quantification of N,N-dimethyl barbiturates by gas chromatography coupled to mass spectrometry (264)
5.11 Particularities of some phosphodiesterase ($PDE_5$) inhibitors in mass spectrometric analysis (272)
5.12 Determination of β-Methasone 17-valerate by HPLC and mass spectrometry (282)
5.13 Study of buspirone metabolites (384)
5.14 Detection and determination of tetrahydrogestrinone in doping control (288)
5.15 Detection and analytical determination of diuretics abused in sports (292)
Appendix - $MS^1$-EI spectra of some pharmaceutically and toxicologically relevant substances (verified against established databases: NIST, SDBS, MoNa, MassBankRecord) (300)

## 1. Basic concepts and some specific physical details of mass spectrometry

Mass spectrometry (MS) occupies an important place among physical and chemical analytical methods, particularly in biochemistry, protein chemistry, toxicology, drug discovery, and drug metabolism monitoring, because of its unique characteristics: high sensitivity, detection limits unmatched by most other analytical methods, speed of analysis, and advanced technical and application versatility. Mass spectrometry is essential for monitoring environmental and food contamination, as well as pharmaceuticals. There are several mass spectrometric techniques, each tailored to specific analytical problems. Between 1995 and 2000, mass spectrometry made significant advances due to the development of various ionization methods and the emergence of hybrid assemblies such as gas chromatograph (GC) coupled to mass spectrometer, liquid chromatograph (HPLC) coupled to mass spectrometer, and capillary electrophoresis coupled to mass spectrometer. Various methods have been developed to separate and detect ionized species, including quadrupole analyzer, ion trap, orbitrap analyzer, multiple mass spectrometric analysis (MS/MS) with induced and controlled fragmentation of ionic species, and *Fourier* transform mass spectrometry. Currently, mass spectrometry is highly diverse in terms of both production methods and separation strategies for ionic species. Due to the abundance of technical and procedural details, this description is limited to pharmaceutically and toxicologically relevant methods, and to case studies and several examples. Figure 1 shows the building blocks of a mass spectrometer, and the processes involved in the primary stages of analysis.

The modules in Figure 1 have the following roles.

(1) For sample introduction, the spectrometer is equipped with a specialized part with the role of bringing the sample from different initial states of aggregation into a vapor state. Sometimes the sample introduction unit is connected to the outlet of a chromatography column, so the inlet unit is the interface between the chromatograph and the mass spectrometer and has the additional function of separating and sending to the mass spectrometer only a small fraction of the effluent leaving the chromatography column.

(2) The ionization unit operates according to different physical principles, but its common function is to convert the neutral sample molecules into positive or negative ions. In most cases, the ionization of molecules is accompanied - to some extent, depending on the type of ionization - by their fragmentation, so that even a single type of molecule results in different ionized fragments with different degrees of ionization. This phenomenon is usually a disadvantage, but sometimes it is a source of additional information about the molecular structure of the sample.

(3) The confined ions are accelerated and focused by an electric field. In some configurations the ions are brought to the same velocity by the concerted action of an

electric and magnetic field with appropriate mutual orientation (*Wien* velocity filter).

(4) The ions enter the analyzer where the combination of electric and/or magnetic fields causes them to follow different trajectories depending on the ratio of their mass to electrical charge. In some designs, the analyzer acts as a filter, allowing only ions with a specific mass/charge ratio (**m/z**) to pass. By progressively changing the operating parameters, the analyzer selects ions with different **m/z** ratios.

(5) The selected ions with the known **m/z** ratio are captured in the detection unit where their presence is converted into an electrical signal. The intensity of the electrical signal generated is proportional to the number of ions reaching the detector per unit of time, i.e. the abundance of ions with a specific **m/z** ratio.

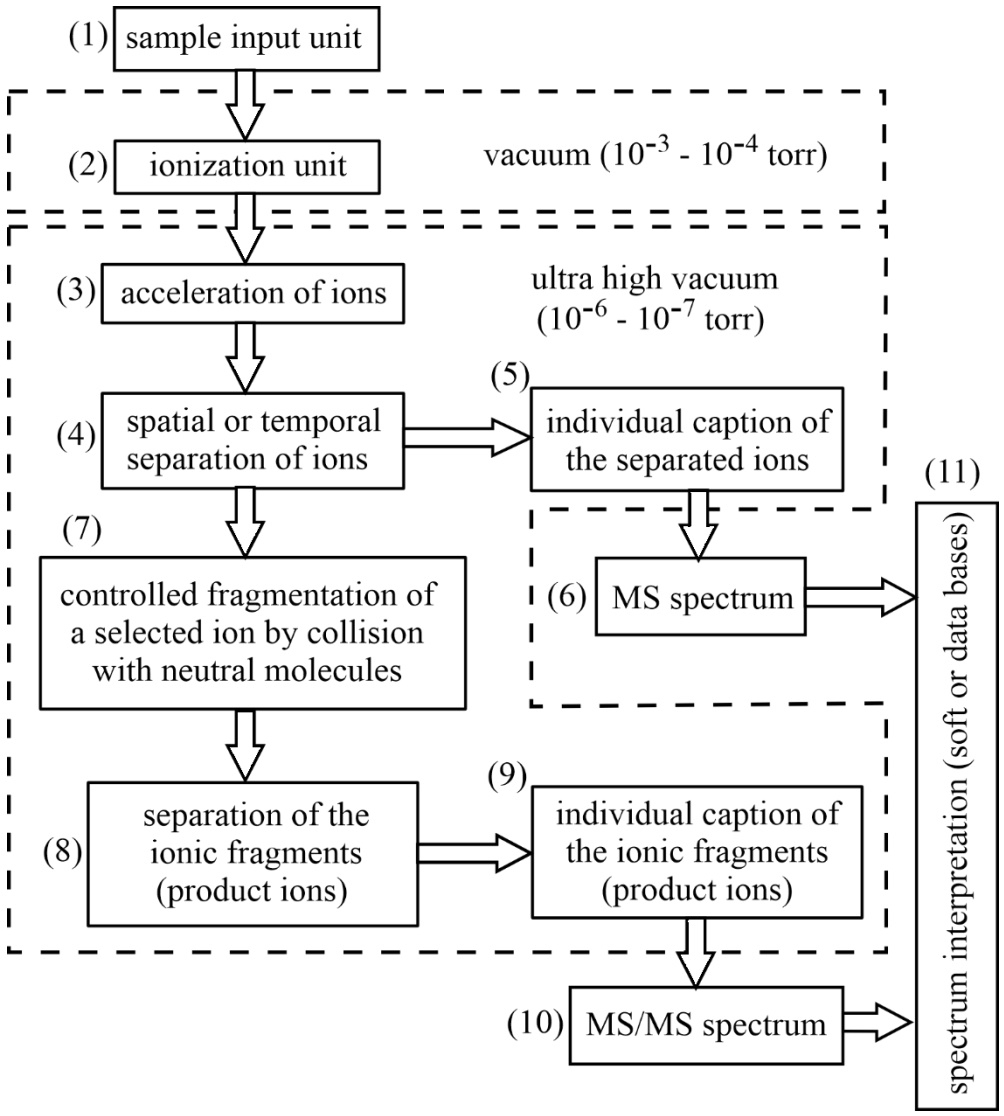



**Fig. 1. Building blocks and key events in a mass spectrometer**

6) The first order mass spectrum ($MS^1$) is the graphical representation of the ion abundance as a function of the **m/z** ratio.

(7) For further analysis of the sample, one ionized species (precursor ion) with a specific value of the **m/z** ratio (precursor ion) is sometimes selected, which undergoes further fragmentations by collision with neutral molecules (like argon, helium, ammonia, etc.), resulting in several ions of lower molecular mass (product ions), producing the second order mass spectrum (MS/MS or $MS^2$). As a result, the information about the molecular structure of the sample becomes richer and the molecule of the original sample can be identified with much greater certainty.

(9) The fragments are trapped in the detector unit and their presence is converted into an electrical signal proportional to the flux of incoming ions, as shown in point (5).

(10) The spectrum obtained (MS/MS) is derived from the fragmentation of the precursor ion. In principle, a complete $MS^2$ spectrum can be obtained for each precursor ion (selected from the $MS^1$ spectrum). The procedure can be repeated by selecting a new precursor ion from the $MS^2$ spectrum and obtaining the $MS^3$ spectrum after subsequent fragmentation (and so on).

(11) The analysis data is processed with specialized programs or compared with data contained in appropriate databases, such as:

- NIST (National Institute of Standards and Technology),
- CHEMDATA.NIST.GOV.(Mass Spectrometry Data Center),
- Wiley Library,
- MPW Drug Library,
- FFNSC (Flavor and Fragrance Natural and Synthetic Compound Library),
- Smart Forensic Database,
- Smart Environmental Database,
- Smart Metabolites Database,
- Forensic Toxicological Database,
- Method Package Residual Pesticides in Foods.

The sample is converted into positive or negative ions (in "positive working mode" or "negative working mode" respectively) and then separated according to their **m/z** (mass to ionic charge) ratio. The mass of the ions (**m**) is conventionally expressed in atomic mass units (the $12^{th}$ part of the mass of the $^{12}C$ isotope of the carbon atom). The electrical charge (**z**) of ions is expressed as the number of electrons deficient (in the case of positive ions) or excess (in the case of negative ions) compared to the corresponding neutral species. In other words, the electrical charge is expressed by the oxidation number of the ionic species. The separation of the ionic species in all variants of mass spectrometry is carried out according to the **m/z** ratio.

The mass spectrum is the graphical representation of the abundance of ions (expressed in relative percent) as a function of the **m/v** ratio. Figure 2 shows the typical form of the mass spectra of salicylamide and of a pentacyclic triterpenoid derivative

(betulin). In practice, both forms of presentation are used: either in "portrait" format (Figure 2 **(A)** and **(C)**), or in "centroid" format (Figure 2 **(B)** and **(D)**).

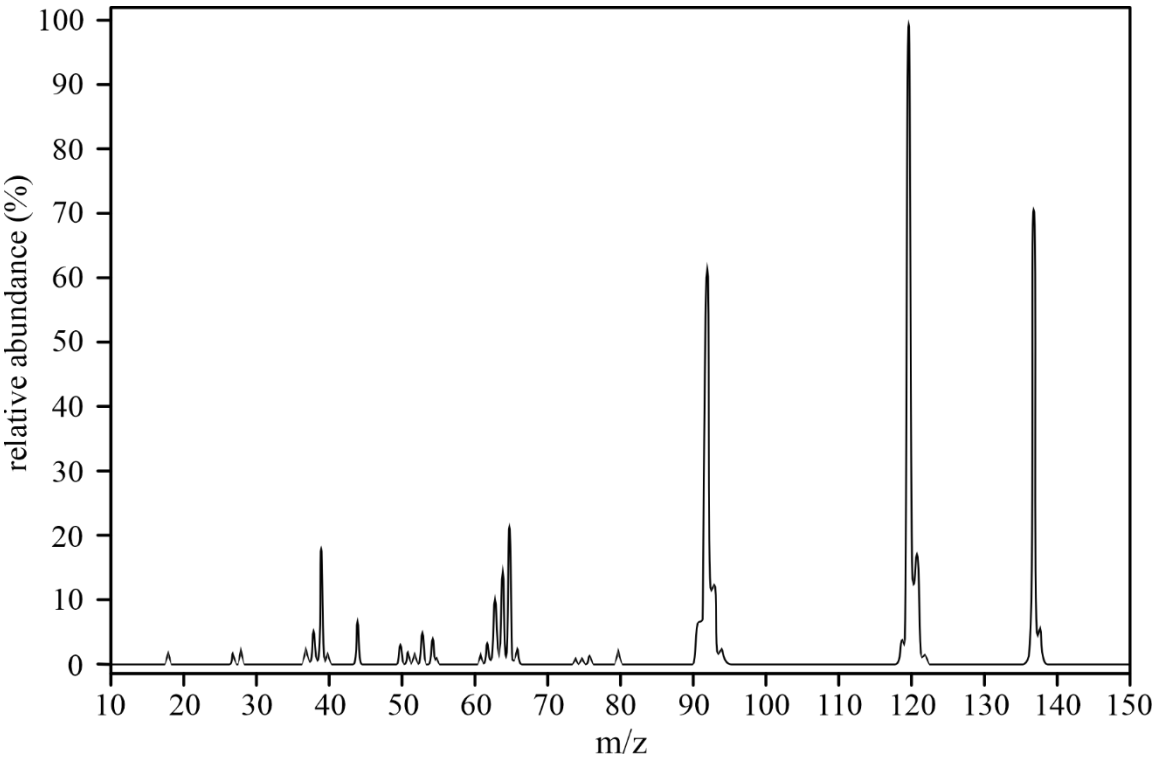



**Fig. 2 (A) Common "portrait" view of a mass spectrum (salicylamide)**

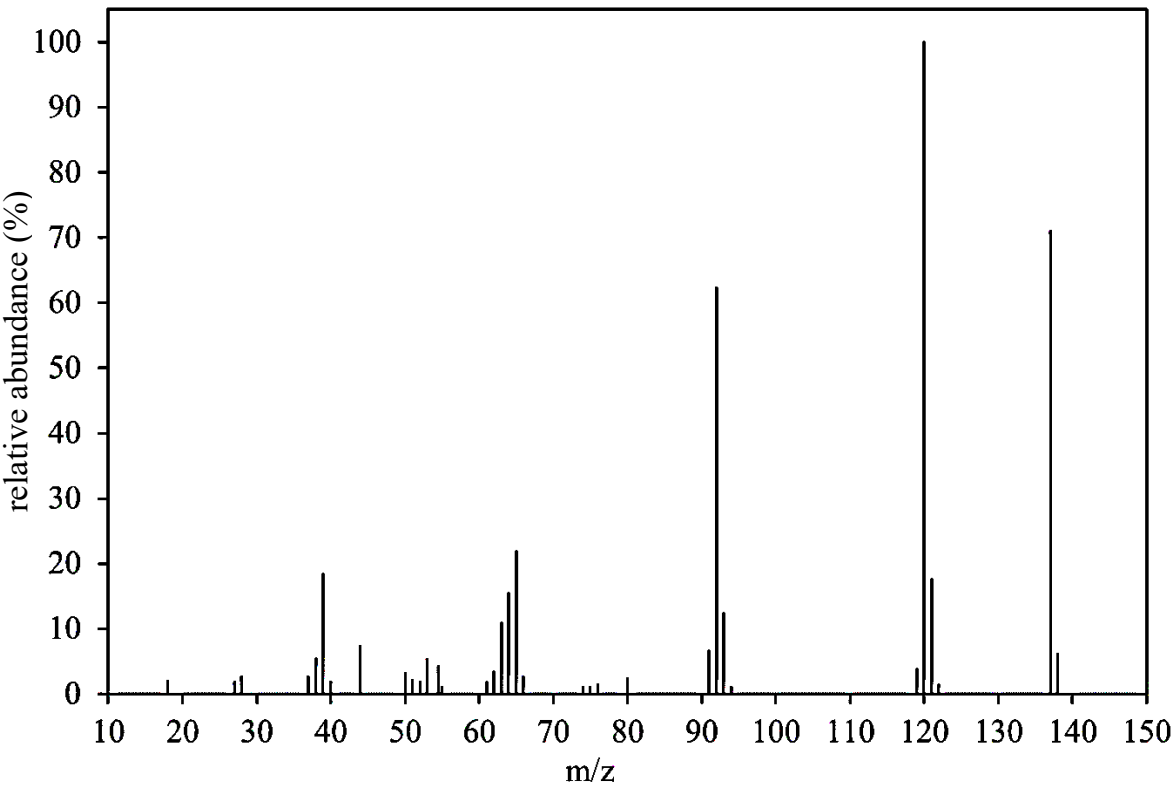



**Fig. 2 (B) Common presentation of a mass spectrum (salicylamide) in" centroid" format.**

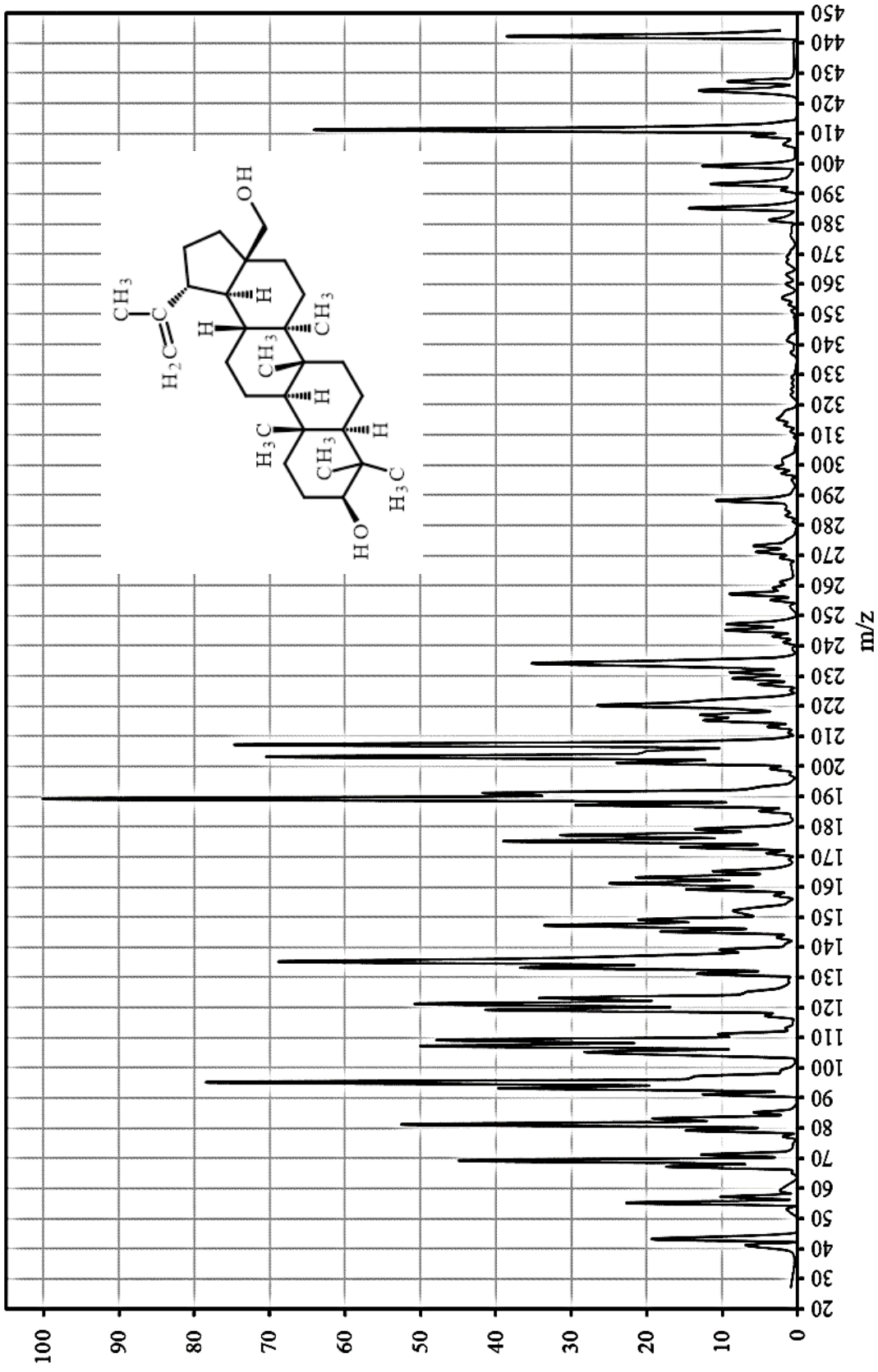



**Fig 2 (C) MS spectrum of betulin in "portrait" format**

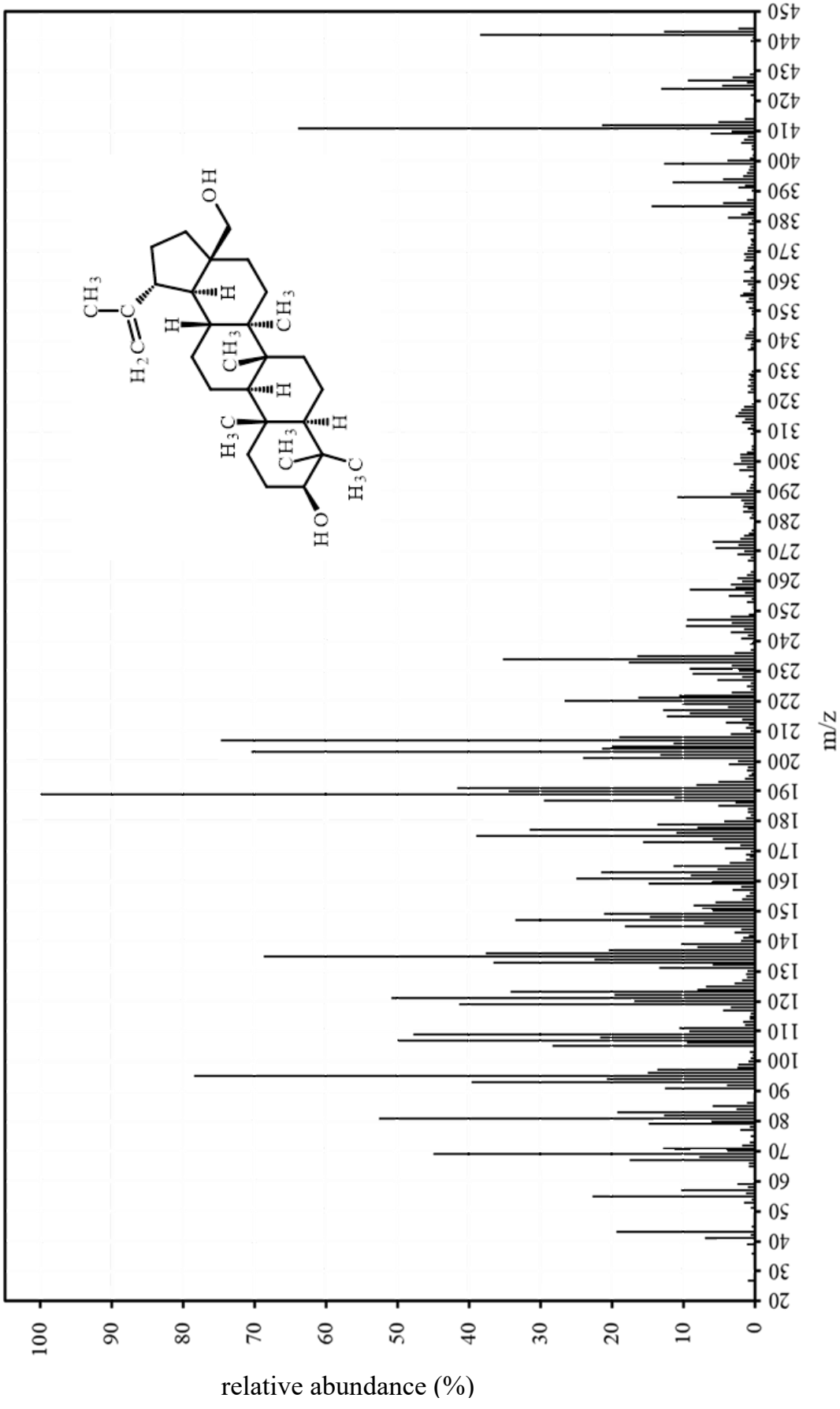



**Fig 2 (D) MS spectrum of betulin in centroid format**

Each signal is identified by its position, intensity and width. The position is determined by the value of the **m/z** ratio, while the intensity is expressed on a scale relative to the most intense signal. The signal width is only visible in the portrait view. In the portrait view, the signals correspond to either a *Lorenz* or a *Gauss* curve. The centroid display uses vertical segments located at the **m/z** values corresponding to the local maximum of the portrait signal. The portrait shape of the signals has a non-zero width due to the presence of multiple isotopes with different abundances in the chemical elements that make up the molecules. The mass spectra can be used to determine the relative molecular mass of the sample, although this process is not always straightforward.

The non-zero width of the portrait signals is also due to the limited physical resolution of mass spectrometers. The width of the signals in the portrait display decreases as the resolution of the instrument increases. In a lower resolution spectrometer, signals with nearby **m/z** values merge into a single, wider signal. A high-resolution mass spectrometer, however, can distinguish between these signals. The resolution "res" at mass "**m**" is defined as the ratio of the mass value "**m**" to the minimum detectable mass difference "**Δm**".

$$\text{res} = \frac{\text{m}}{\Delta\text{m}} \qquad (1)$$

Obviously, the higher the resolution, the more efficient the spectrometer. Since most chemical elements contain several isotopes of different masses (in other words, they are not "monoisotopic"), the spectral signal associated with a given molecule can, with sufficient resolution (monoisotopic resolution), distinguish ionic species with the same elemental composition but different isotopic compositions. At lower resolution, the signals associated with the different isotope distributions merge into a single signal from which the "average relative molecular mass" of the sample can be determined. Isotopic differentiation is illustrated in Figure 3 using the simple example of the chlorine atom (Cl) and the chlorine molecule ($Cl_2$). The spectra in Figure 3 distinguish the $^{35}Cl$ and $^{37}Cl$ isotopes of the chlorine atom and the three species ($^{35}Cl$-$^{35}Cl$, $^{35}Cl$-$^{37}Cl$ and $^{37}Cl$-$^{37}Cl$) of the diatomic chlorine molecule. The relative intensities of the signals are consistent with the natural abundance of the $^{35}Cl$ and $^{37}Cl$ isotopes.

After ionization, the next main event is the differentiation of the ionized fragments and their separation (spatial or temporal, depending on the design characteristics of the mass spectrometer). The differentiation and separation unit operates under the influence of a magnetic field, an electrostatic field or various combinations of these fields in the analysis unit.

Figure 4 illustrates the deflection (change in path) of a positive (point-like) charge

entering a homogeneous magnetic field with induction $\vec{B}$, due to the *Lorentz* force $\vec{F}_L$. The *Lorentz* force is perpendicular to the current direction of motion of the particle and is also perpendicular to the magnetic field lines. The direction of the *Lorentz* force is determined by the "right hand" rule (Figure 5).

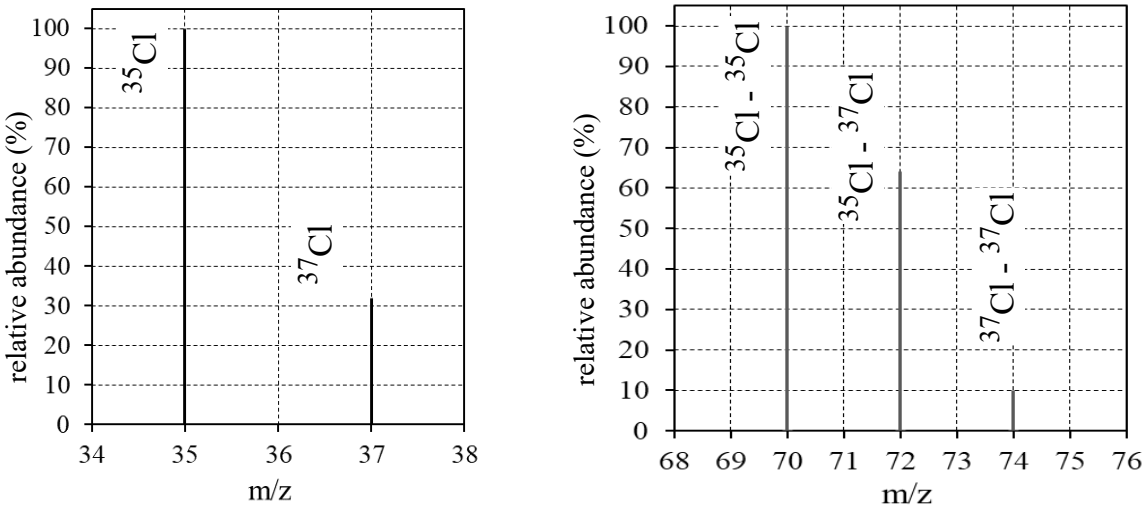



**Fig. 3 Mass spectrum of the isotopes of the chlorine atom and the isotopologues of the chlorine molecule at high resolution (monoisotopic resolution)**

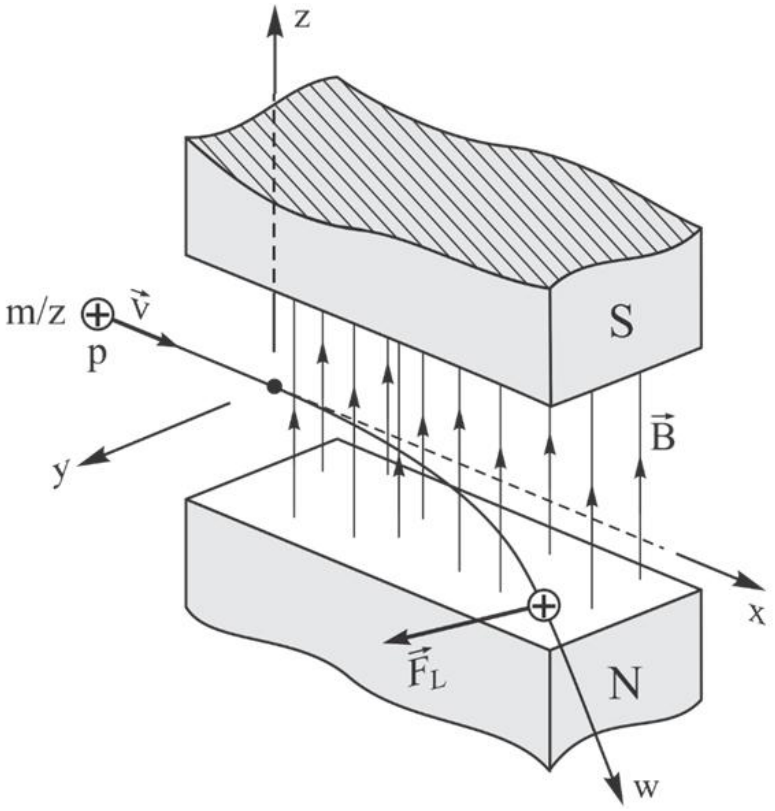



**Fig. 4 The origin of the *Lorenz* force $\vec{F}_L$ and the motion of a positive particle in a homogeneous magnetic field**

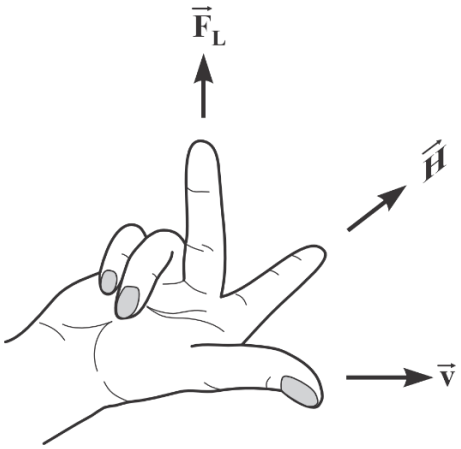



**Fig. 5**
**Mutual orientation of the velocity vector ($\vec{v}$), the magnetic field lines ($\vec{H}$) and the *Lorentz* force ($\vec{F}_L$) for a positively charged particle ("right hand rule")**

The *Lorentz* force acts on a charged particle only when it is moving in a magnetic field. With a suitable geometry of the magnetic field, deflections can be made to the desired extent, e.g. $90^o$ to the original direction (Figure 6).

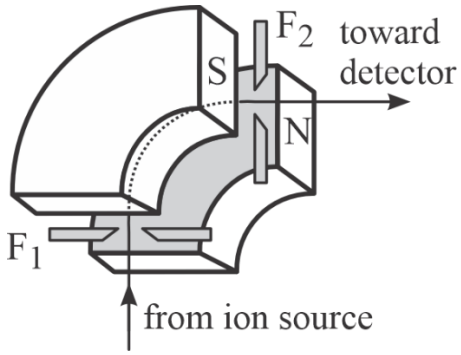



**Fig. 6 Deflection with $90^o$ of a positively charged particle in a uniform magnetic field**

Equation (2) expresses the relationship between the displacement velocity vector **($\vec{v}$ )** of the particle carrying the electric charge "**q**", the magnetic field intensity vector **($\vec{H}$)** and the *Lorentz* force vector **($\vec{F}_L$)**.

$$\vec{F}_L = \vec{v} \times \vec{H} \;;\; F_L = v \cdot H \cdot \sin(\vec{v},\vec{H})$$
$$\vec{F}_L \perp \vec{v} \;;\; \vec{F}_L \perp \vec{H} \qquad (2)$$

The module of the *Lorentz* force vector is proportional to the module of the velocity vector $\vec{v}$ , the magnetic field intensity vector $\vec{H}$, and to the sinus of the angle between these vectors.

Another way to control the deflection of a beam of electrically charged particles is to drive them between the armatures of a capacitor subjected to a continuous voltage. Figure 7 shows the deflection of a positive particle by $180^o$ from the direction of incidence.

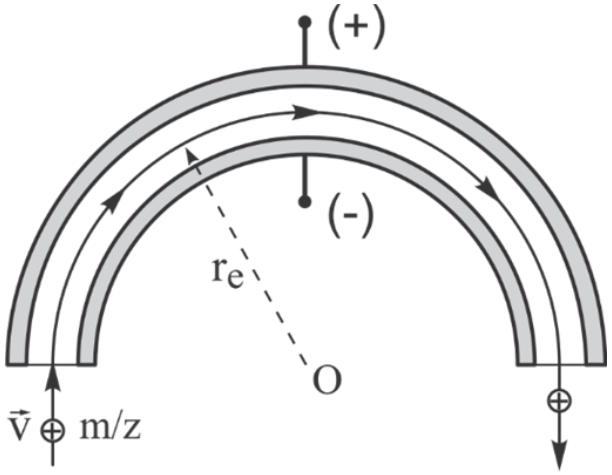



**Fig. 7 The trajectory of a particle with positive electric charge in a cylindrical electrostatic field**

If the electrostatic force between the armatures is balanced by the centrifugal force, the particle can pass through the gap between the armatures. Otherwise, it will collide with one of them and be stopped. If a particle has mass "**m**", charge "**q**" and moves with velocity "**v**", the condition for passing through the space between cylindrical armatures with average radius "$r_e$" is expressed by relation (3).

$$\frac{m \cdot v^2}{r_e} = \frac{U \cdot q}{d} \qquad (3)$$

In relation (3), "**U**" represents the continuous electric voltage applied between the armatures, and "**d**" is the distance between them.

The final event is the capture of the ions in a detector, which produces an electric current or voltage proportional to the electric charge arriving in the time unit. The detector captures the ions as such or detects the light signal produced when the incoming ions collide with a light emitting surface.

## 2. Construction and operating modules of mass spectrometers

### 2.1. Sample introduction and ionization

The sample is introduced into the spectrometer either directly (via a dedicated interface) or from the outlet end of a chromatography column. The sample introduction unit can operate at atmospheric pressure or moderate vacuum. The amount of sample introduced, either in vapor or liquid form, is generally of the order of micrograms. In some cases, molecules, free radicals and ions are removed from the solid sample by irradiation with laser light (**L**aser **D**esorption **I**onization, **LDI**) or by bombardment with atoms or ions of high kinetic energy. Table 1 lists the ionization methods with their common names and abbreviations.

**Table 1 Ionization methods, names, common acronyms, physical phenomena involved and typical applications**

| Method, consecrated name and acronym | Physical phenomenon involved | Resulting ionic species | Typical applications and characteristics |
|---|---|---|---|
| Gas Discharge | Electric discharge | Ionized atoms | The first ionization method in MS |
| Thermal Ionization (TI) | ionization by heating | Ionized atoms | Determination of the isotopic ratio |
| Spark Source (SS) | Electric discharge | Ionized atoms | Trace analysis<br>Solid samples |
| Glow discharge (GD) | Electric discharge | Ionized atoms | Trace analysis |
| Inductively Coupled Plasma (ICP) | Transformation of the sample into plasma state | Ionized atoms | Determination of the isotopic ratio<br>Trace analysis |
| Electron Ionization (EI) | Electron impact | Volatile molecular ions | Small molecules<br>Coupling with gas chromatograph<br>Creation of databases |
| Chemical Ionization (CI) | Reagent-induced ionization | Volatile molecular ions | Connection to a gas chromatograph via an interface |
| Atmospheric Pressure Chemical Ionization (APCI) | Reagent-induced ionization | Non-volatile molecular ions | Small molecules<br>Connection to a gas chromatograph via an interface |
| Photo-ionization (PI) | Photolytic ionization | Volatile molecular ions | Small molecules<br>Connection to a gas chromatograph via an interface |
| Multiphoton Ionization (MPI) | Photolytic ionization | Atomic and molecular ions | The MPI resonance separation method has advanced selectivity.<br>Trace analysis |
| Atmospheric Pressure Photoionization (APPI) | Photolytic ionization | Non-volatile molecular ions | Connection to liquid chromatograph (HPLC) via an interface;<br>Analysis of non-polar substances |
| Field Ionization (FI) | Ionization with an intense electric field | Volatile molecular ions | Molecular compounds |
| Field Desorption (FD) | Desorption/ionization in an intense electric field | Non-volatile molecular ions | The first gentle method of ionization<br>Analysis of large molecules |

**Table 1 Ionization methods, names, common acronyms, physical phenomena involved and typical applications (continued)**

| Method, consecrated name and acronym | Physical phenomenon involved | Resulting ionic species | Typical applications and characteristics |
|---|---|---|---|
| Thermospray Ionization (TSI) | Misty dispersion | Non-volatile molecular ions | Connection to a liquid chromatograph (HPLC) via an interface; |
| Electrospray Ionization (ESI) | Misty dispersion | Non-volatile molecular ions | Connection to a liquid chromatograph (HPLC) via an interface; Analysis of large molecules |
| Desorption Electrospray Ionization (DESI) | Misty dispersion | Non-volatile molecular ions | Direct analysis without prior sample preparation |
| Direct Analysis in Real Time (DART) | Electrical discharge | Non-volatile molecular ions | Direct analysis without prior sample preparation |
| Secundary Ion Mass Spectrometry (SIMS) | Particle-induced desorption/ionization | Non-volatile molecular ions | Semiconductor analysis. Surface analysis. |
| Fast Atom Bombardment (FAB) | Particle-induced desorption/ionization | Non-volatile molecular ions | Gentle method of ionization. Analysis of large molecules |
| Laser Desorption Ionization (LDI) | Photon-induced desorption/ionization | Non-volatile atomic and molecular ions | Isotope ratio determination. Trace analysis |
| Matrix-Assisted Laser Desorption Ionization (MALDI) | Desorption and ionization | Non-volatile molecular ions | Gentle method of ionization. Analysis of large molecules |

In all variants the sample molecules are converted into positive ions ("positive working mode") or negative ions ("negative working mode"). Depending on the ionization conditions, some fragmentation occurs in addition to ionization, resulting in ions of lower mass. The following discussion is limited to the ionization methods commonly used in the analysis of substances of pharmaceutical and/or toxicological interest.

### 2.1.1. Electron Ionization – EI

One way to convert the neutral molecules of the sample into molecular ions or ionized fragments is to expose the sample to a beam of electrons of appropriate energy (typically tens of electron volts). Figure 8 illustrates the design elements and operation

of an electron impact ionization system. A heated ruthenium filament (**F**) emits electrons that are accelerated toward the positively charged anode (**A**). Along the way, the electrons collide with neutral molecules in the sample (**M**), resulting in the formation of molecular ions ($\mathbf{M}^+$), molecular radical ions ($\mathbf{M}^{+\bullet}$), or ionized fragments. The ionic species are accelerated by the negative electrode assembly ($\mathbf{V_{AC}}$) and move toward the entrance hole of the spectrometer analyzer due to the repulsive action of the electrode (**R**). To increase the efficiency of electron-molecule collisions, a magnetic field of modest intensity is applied to the space (with the poles of the magnet labeled **N** and **S**), resulting in a longer path for the electrons (Figure 8).

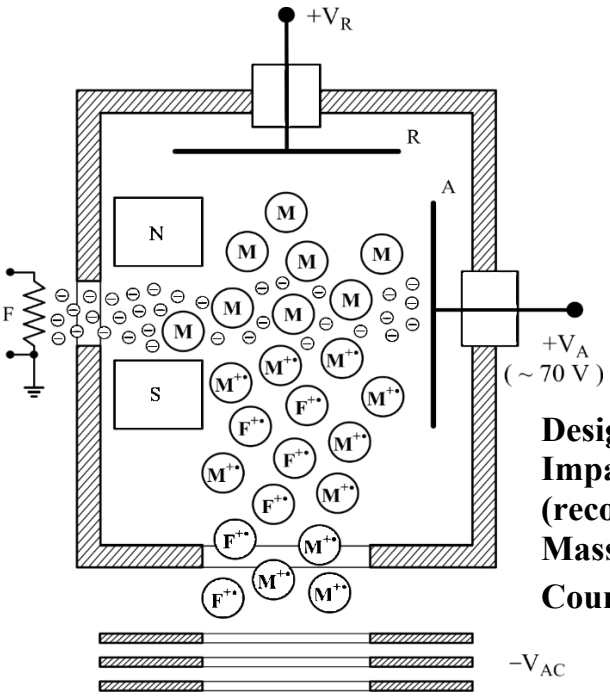



**Fig. 8**
**Design principles of the Electron Impact Ionization (EI) Unit (reconstructed after *K. Downard*: Mass Spectrometry. A Foundation Course RS·C 2004)**

The voltage commonly used for electron acceleration is about 70 V. An electron energy of 70 eV corresponds to $6.8 \bullet 10^3$ kJ/mol, which is sufficient to ionize most organic molecules (which typically require 8-15 eV) and to fragment them to some extent. The pressure inside the electron impact ionization module is around $10^{-6}$ Torr ($1.3\ 10^{-4}$ Pa). Figure 9 shows the potential fragmentation modes of the hypothetical radical ion $ABYZ^{+\bullet}$. The breaking of covalent bonds may result in the release of radical species, while fragmentation with rearrangement (indicated by the symbol  ) involves the elimination of a smaller neutral molecule. Figure 10 shows the events that take place and the resulting ionic and/or radical species that are formed when a hypothetical ABC molecule collides with electrons.

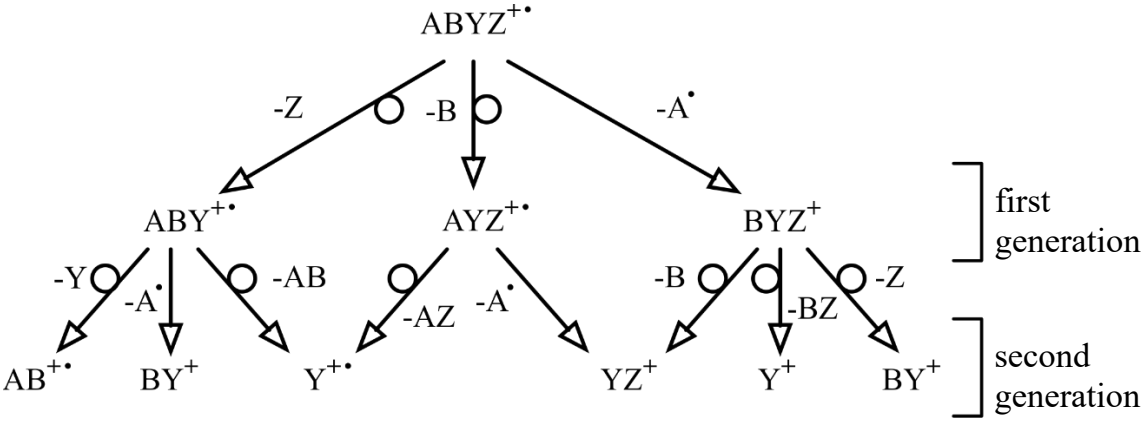



**Fig. 9 Characteristic events during electron beam ionization of a hypothetical radical ion $ABYZ^{+\bullet}$. ( ⟶○ denotes a process with preservation of electron number parity; ⟶ indicates a process with a change in electron number parity.)**

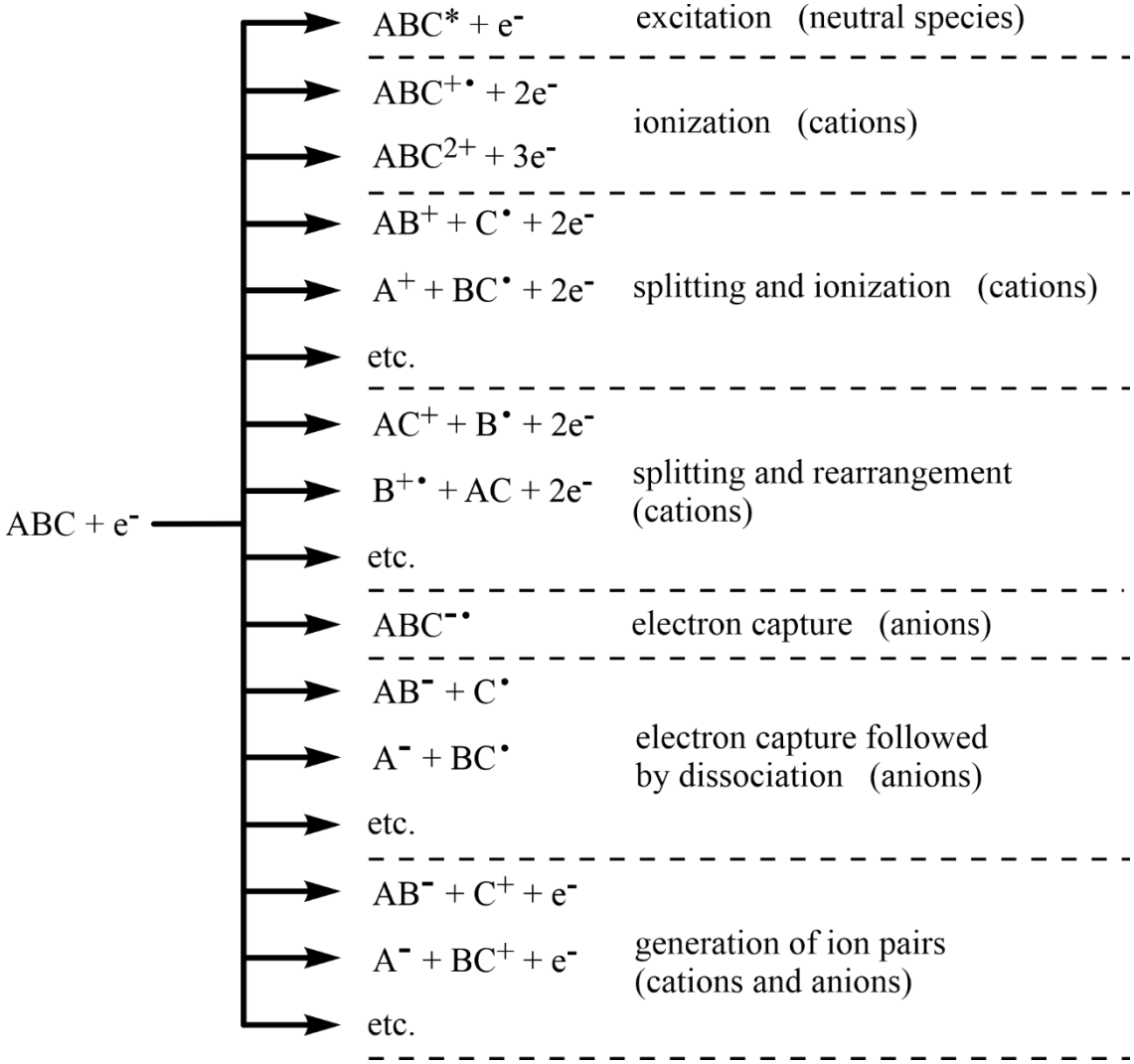



**Fig. 10 Characteristic events during electron beam ionization of a hypothetical molecule ABC**

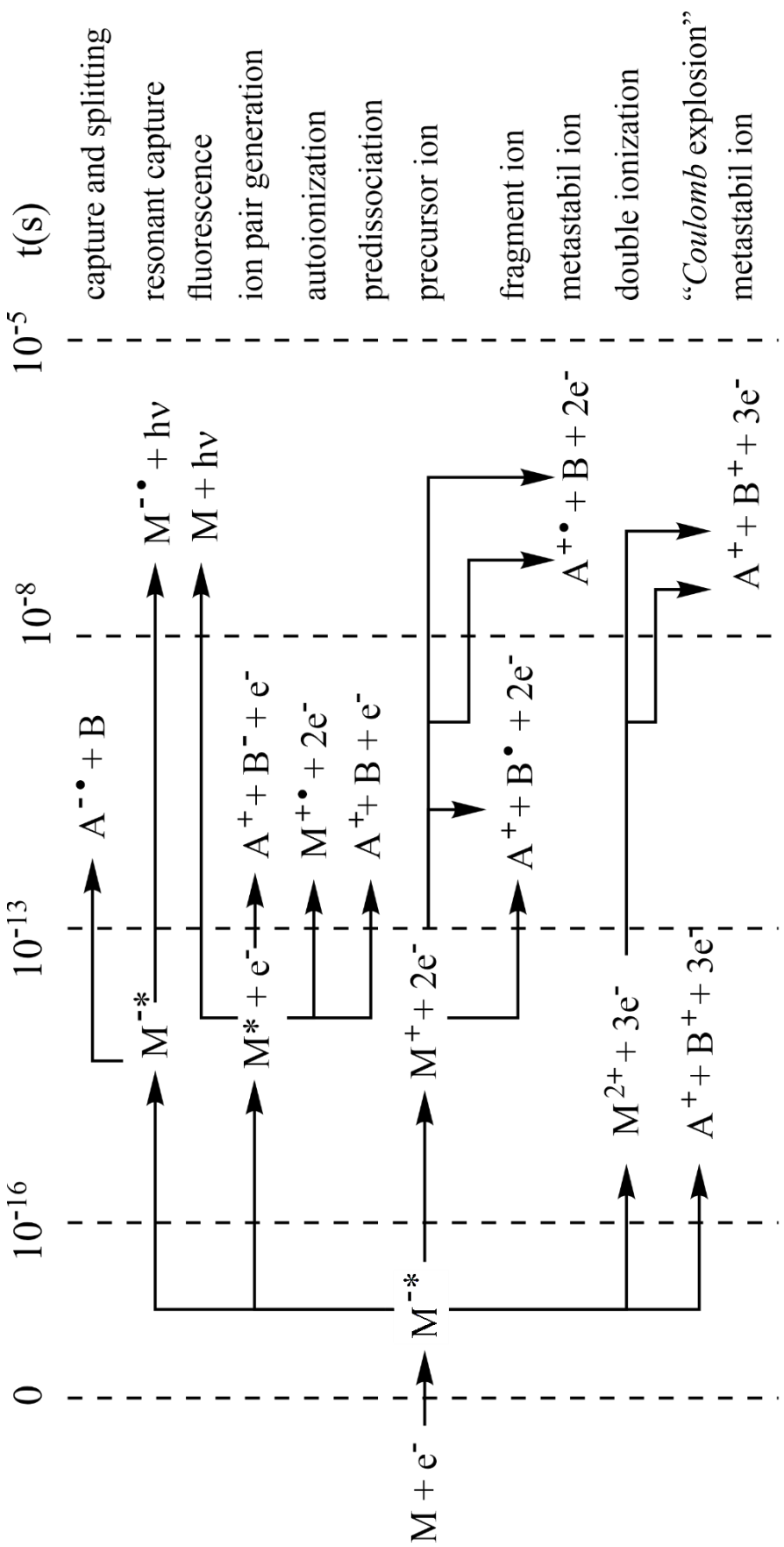



**Fig. 11 Time course of events during ionization of sample (M) with an electron beam using electron ionization (EI). (adapted and rebuilt after *J.H. Gross*: Mass Spectrometry – A Textbook, Springer Int. Publ., 2017)**

Figure 11 illustrates the time course of events during electron beam ionization. Electrons can produce positive and negative molecular ions as well as free radicals. The type of analyzer determines whether positive or negative ions are used.

### 2.1.2. Electrospray Ionization – ESI

A common method for ionizing organic compounds is to spray the sample solution in the form of a mist. The sample solution passes through a capillary tube whose end is charged with a voltage of several kilovolts. The droplets become electrically charged as they form and the solvent evaporates, causing them to fragment into smaller droplets with increasing charge density. This results in the formation of mostly molecular ions and a smaller proportion of ionic fragments. Electrospray ionization has a significant advantage over electron impact ionization because of the reduced fragmentation. Consequently, it provides a simpler interpretation of the mass spectra. Figure 12 shows the design and operation of the electrospray ionization unit.

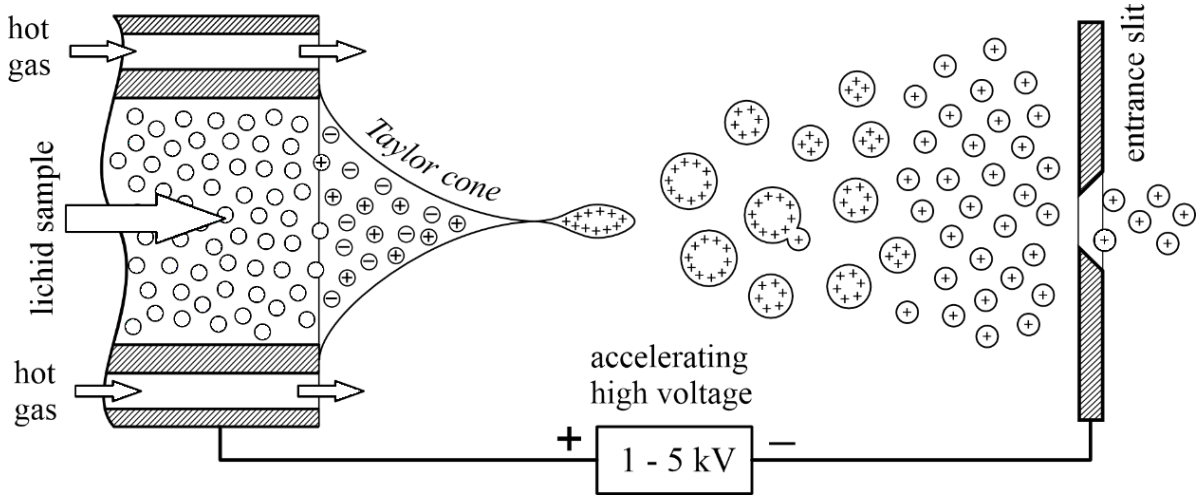



**Fig. 12 The principle of electrospray ionization (ESI) (redrawn after *Westman-Brinkmalm, G. Brinkmalm*: "A Mass Spectrometer's Building Bloks" in "Mass Spectrometry – Instrumentation, Interpretation and Applications", *R. Ekman, J. Silberring, A. Westman-Brinkmalm* editors, John Wiley & Sons Inc., Hoboken, New Jersey, 2009 Cap. 2. pg. 15-87)**

The sample solution is injected through a capillary tube into a space exposed to an electrical voltage of several kilovolts applied between the end of the tube and the nozzle. At the end of the capillary, the solution forms a liquid cone (known as a *Taylor* cone) that releases charged droplets. A jet of hot gas is introduced coaxially with the capillary tube to assist in evaporating the solvent from the droplets. The density of electric charge increases as the volume of the droplet gradually decreases. Due to the repulsive electrostatic force, the droplets disintegrate when they reach a critical size and electrical charge density, known as the "*Rayleigh* limit". This process results in

the formation of electrically charged molecules, which is the predominant process, and ionic fragments, which are produced at a more limited rate. The negative ions are repelled by the negative potential of the nozzle, while the positive ions enter the analyzer. Electrospray ionization is commonly used as a chromatographic detector for enhanced specificity and sensitivity when the mass spectrometer is coupled to a gas- or liquid chromatograph.

### 2.1.3. Chemical Ionization – CI

Chemical ionization is like electron impact ionization except that in the first step, the electron beam ionizes a gaseous reactant other than the actual sample molecules. Next, a chemical process transfers the electrical charge from the reactant gas to the sample molecules (Figure 13). The collision of the atoms or molecules with the surface of the solid sample (**S**) releases ions from its structure which, after being accelerated and focused, enter the spectrometer analyzer. This type of ionization is used to analyze solid samples, such as pharmaceutical preparations in tablet form.

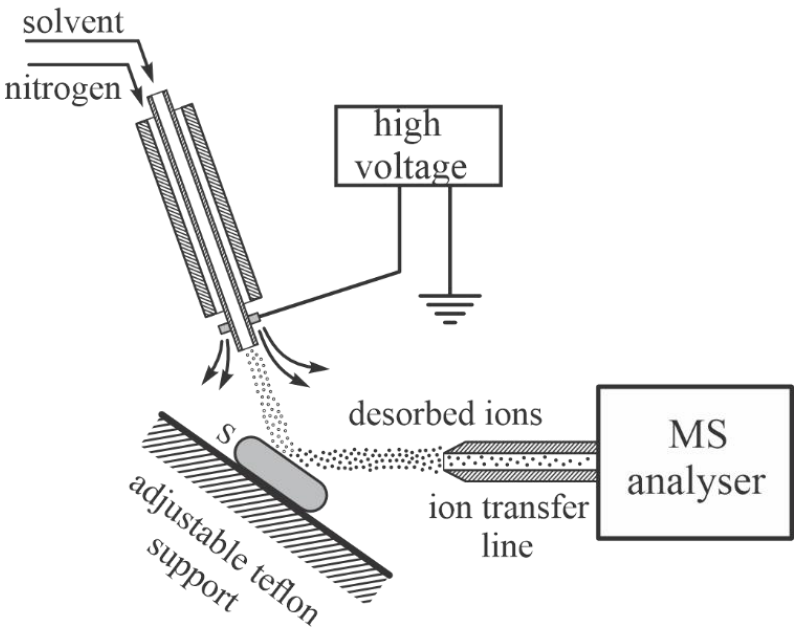



**Fig. 13 Basic configuration of the chemical ionization unit (after *G. Hopfgartner*: "Overview of the Various Types of Mass Spectrometers that Are Used in Drug Discovery and Drug Development", in "Mass Spectrometry and Drug development", *W.A. Korfmacher* editor, chapter. 1. p. 8., John Wiley & Sons Inc., Publ. 2013)**

Methane is often used as a reactant gas. Initially, the radical ion $CH_4^{+\bullet}$ is formed which, upon collision with another methane molecule, produces the reactive species $CH_5^+$:

$$CH_4 \xrightarrow[-2e^-]{+e^-} CH_4^{+\bullet} \xrightarrow{+CH_4} CH_5^+ + CH_3^\bullet \quad (4)$$

The $CH_5^+$ ion, an efficient proton donor, reacts with the sample molecule (**M**) to form the protonated and ionized species **[M+H]**$^+$ by proton transfer:

$$CH_5^+ + M \rightarrow [M+H]^+ + CH_4 \quad (5)$$

To prevent direct ionization of the sample molecules by electron impact, methane is introduced into the ionization chamber at a concentration much higher than the sample concentration. The chemical ionization source therefore operates at a much higher pressure, $10^{-3}$ – $10^{-4}$ Torr or 0.1 - 1.0 Pa, than the electronic impact ionization source.

Other chemical processes that occur during chemical ionization besides proton transfer are also known for example, charge transfer to another molecule (**N**),

$$M^{+\bullet} + N \rightarrow M + N^{+\bullet} \quad (6)$$

adduct formation with another molecule (**N**),

$$M^+ + N \rightarrow [M+N]^+ \quad (7)$$

or nucleophilic substitution of a nucleophilic species (**Nu**$^-$) on the molecule (**AB**):

$$Nu^- + AB \rightarrow NuAB + B^- \quad (8)$$

### 2.1.4. Fast Atom Bombardment Ionization – FAB

In FAB ionization, the sample is bombarded with a beam of atoms or ions (primary beam) of high energy (typically 10-30 eV), such as argon atoms or **Xe**$^+$ or **Cs**$^+$ ions (Figure 14). The sample is suspended or dissolved in a viscous, non-volatile liquid (liquid matrix) whose role is to dissipate the energy of the primary beam to minimize damage to the sample. Another reason for using a liquid matrix is that otherwise the incident primary beam would progressively modify the surface of the sample, changing the efficiency of the collision with the sample molecules. If the target of the primary fascicle is a liquid surface (state provided by the liquid viscous matrix), it can remodel its shape and ensure a better stability of the interaction with the primary fascicle.

A typical practical solution is to bombard the sample with high energy argon atoms from an "atom gun" where the argon is at high temperature and relatively high pressure ($10^{-3}$ - $10^{-4}$ Torr or 0.1-1 Pa). In the first stage, argon radical ions are formed:

$$Ar + e^- \rightarrow Ar^{+\bullet} + 2e^- \quad (9)$$

$$Ar^{+\bullet}(fast) + Ar(slow) \rightarrow Ar(fast) + Ar^{+\bullet}(slow) \quad (10)$$

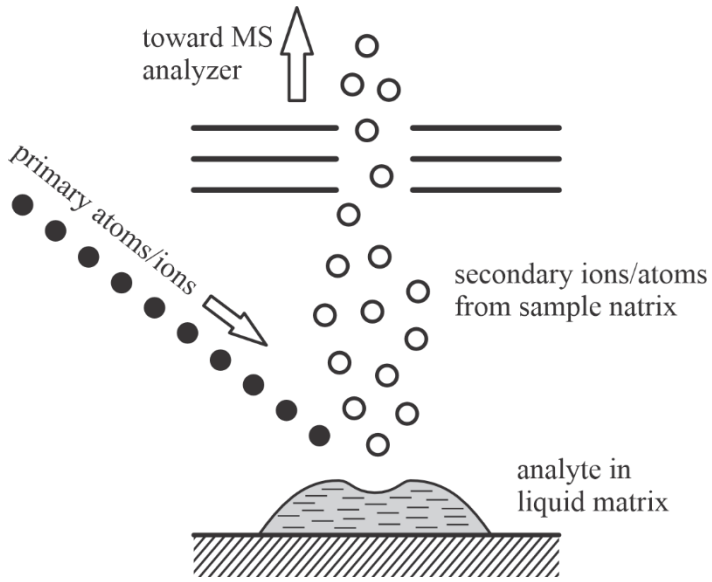



**Fig. 14**
**The principle of fast atom/ion ionization (Fast Atom Bombardment Ionization – FAB) (after to *K. Downard*: Mass Spectrometry. A Foundation Course RS•C 2004)**

When the primary atoms or ions collide with the liquid surface, the electrical charge is transferred to the molecules of the non-volatile liquid matrix (**M**) and then to the molecules of the sample (**A**).

$$\begin{aligned} Ar^{+\bullet} + M &\rightarrow M^{+\bullet} + Ar \\ M^{+\bullet} + MH &\rightarrow MH^{+} + M^{\bullet} \\ MH^{+} + A &\rightarrow AH^{+} + M \end{aligned} \qquad (11)$$

Among the ionic species there can be protonated forms that appear in the spectrum with **m/z** values one unit higher than the **m/z** values corresponding to the non-protonated species.

The secondary ions ($\mathbf{M^{+\bullet}}$ and $\mathbf{MH^{+}}$) sent to the spectrometer analyzer come from the matrix and from the sample ($\mathbf{AH^{+}}$). Because the abundance of $\mathbf{M^{+\bullet}}$ and $\mathbf{MH^{+}}$ ions is much higher than that of $\mathbf{AH^{+}}$ ions, mass spectra obtained with FAB ionization show an intense, characteristic background, especially at low **m/z** values (below 500). This phenomenon can make it difficult to detect ions with **m/z** values below 500, especially when the amount of sample is small.

### 2.1.5. Plasma Desorption – PD

PD ionization was the first method suitable for the analysis of non-volatile, high molecular weight samples (higher hydrocarbons, proteins). The sample is placed on a thin nickel or aluminum foil and irradiated with a flux of neutrons produced by the radioactive isotope $^{252}$Cf (half-life 2.6 years), an efficient neutron source (1 μg $^{252}$Cf produces $1.7 \cdot 10^{8}$ neutrons/minute). Neutrons colliding with sample molecules pro-

duce primarily **[M+H]**$^+$ and **[M+Na]**$^+$ ions. Due to the special requirements associated with handling radioactive isotopes, the PD method is increasingly being replaced by the Fast Atom Bombardment (**FAB**) ionization method.

### 2.1.6. Matrix Assisted Laser Desorption Ionization – MALDI

Until 1966, MALDI ionization was used for the analysis of organic and inorganic compounds with relatively low molecular mass. Since 1980, this ionization method has proven useful for the analysis of samples containing large molecules (such as proteins).

Two methods of sample preparation have been tested and proposed. In the method developed by *Tanaka*, the sample is mixed with glycerol and irradiated with light from a laser emitting at 337 nm. Another method, developed by *Karas* and *Hillenkamp*, involves mixing the sample solution with a solution of a compound capable of absorbing UV radiation ("matrix"), followed by application of 266 nm radiation from a Nd:YAG laser. Both ionization methods produce predominantly mono-ionized species. The matrix compound is used in large excess compared to the analyte. Table 2 shows some of the matrices used in the MALDI technique. Several microliters of solution are applied to a solid support where the analyte crystallizes. The crystallized sample is placed in the vacuum chamber of the ionization module and irradiated with short pulses of laser radiation to detach and ionize the sample molecules. The role of the matrix is to efficiently absorb the UV radiation and transfer the absorbed energy to the molecules of the matrix and the analyte.

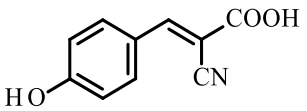
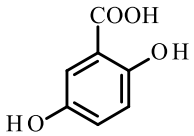
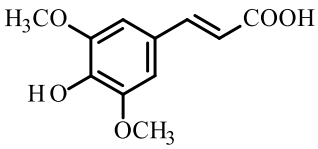
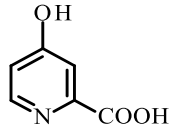
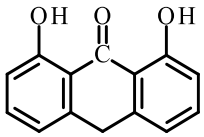
The typical operating frequency of the laser pulses used is between 20 - 200 Hz (more recently up to 1000 Hz). MALDI ionization has largely replaced other ionization methods (e.g. fast atom bombardment ionization - FAB), especially in the analysis of macromolecules (proteins, peptides, nucleic acids, lipids). In most cases, intact mono-ionized species are obtained. Figure 15 shows the principle of MALDI ionization. The sample and analyte solution are applied to a support (Figure 15 **(A)**) and the solvent is evaporated. The matrix and analyte crystals are irradiated with ultraviolet light from a laser (Figure 15 **(B)**). The energy of the photons affects the molecules of the matrix and the analyte, ionizing and protonating them. An electric field accelerates the positive ions and directs them toward the inlet of the analyzer.

[*K. Tanaka, H. Waki, Y. Ido, S. Akita, S. Yoshida, Y. Yoshida, T. Matsuo*: Protein and Polymer Analysis up to m/z 100,000 by Laser Ionization Time-of-Fly Mass Spectrometry. **Rapid Commun. Mass Spectrom., 1988:2**(8), 151-153]

[*M. Karas, U. Bahr, F. Hillenkamp*: UV Laser Matrix Desorption Ionization Mass Spectrometry of Proteins in the 100,000 Dalton Range. **Int. J. Mass Spectrom. Ion Process 1989:92**(15 Sept.) 231-242]

[*M. M. Karas, F. Hillenkamp*: Laser Desorption Ionization of Proteins with Molecular Masses Exceeding 10,000 Daltons. **Anal. Chem., 1988:69**(20), 2299-2301]

**Table 2 Compounds used as matrix for MALDI ionization**

| Matrix | Chemical name (acronym) | Practical use |
|---|---|---|
|  | α-cyano-4-hydroxy-cinnamic acid (4-HCCA) | analysis of peptides and low molecular weight compounds |
|  | 2,5-dihydroxy-benzoic acid (DHB) | protein analysis |
|  | sinapic acid (SA) | protein analysis |
|  | 4-hydroxy-picolinic acid (HPA) | analysis of oligonucleotides |
|  | 9(10H)-anthrachinon-1,8-diol (dithranol) | polar and non-polar polymers |

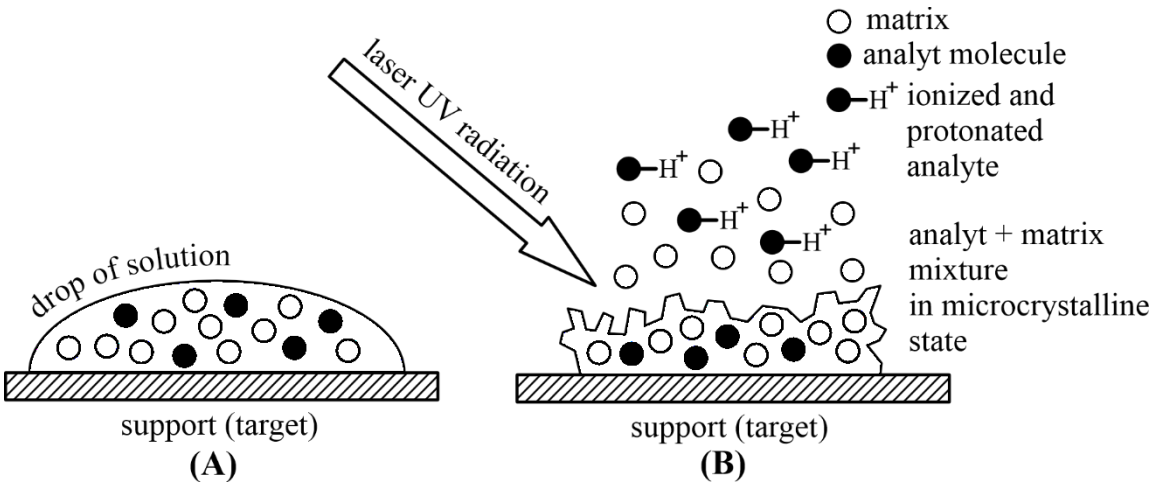



**Fig. 15 Principle of MALDI ionization**

Mass spectra contain, in addition to the signals of the ions of the analyte, the signals of the ions and ionic fragments of the matrix (spectral background attributed to the matrix), especially in the range of low **m/z** values. This inconvenience does not occur

when analyzing macromolecular samples whose signals appear at high **m/z** values. The spectral background generated by matrix ions can be eliminated by the more recent matrix-independent desorption ionization technique. In this method, the analyte is deposited on a photoactive support that effectively absorbs ultraviolet radiation but does not desorb.

*D.S. Peterson*: matrix-Free Methods for Laser Desorption/Ionization Mass Spectrometry. **Mass Spectrom. Rev., 2007:26**(1), 19-43]

[*J. Wei, J.M. Buriak, G. Siuzdak*: Desorption-Ionization Mass Spectrometry on Porous Silicon. **Nature 1999:399**(20 May), 243-246]

[*E.P. Go, J.E. Prenni, J. Wei, A. Jones, S.C. Hall, H.E. Witkowska, Z. Shen, G. Siuzdak*: Desorption/Ionization on Silicon Time-of-Flight/Time-of-Flight Mass Spectrometry. **Anal. Chem., 2003:75**(10), 2504-2506]

[*W.G. Lewis, Z. Shen, M.G. Finn, G. Siuzdak*: Desorption/Ionization on Silicon (DIOS) Mass Spectrometry: Background and Applications. **Int. J. Mass Spectrom., 2003:226**(1), 107-116]

MALDI ionization offers the possibility of storing and archiving the samples deposited on the support so that the analysis can be repeated if necessary. Another advantage of MALDI ionization over EI or ESI ionization is the coupling of the mass spectrometer to the HPLC separation of complex mixtures, in the sense that the separated chromatographic fractions can be deposited on the support and the mass spectrometric analysis can be performed later, independently of the chromatographic separation. An important difference between ESI and MALDI ionization is that ESI ionization produces multicharged ions that can be analyzed on almost any type of mass analyzer, whereas MALDI ionization requires a time-of-flight (TOF) mass analyzer, mainly in a linear configuration, to cover the range of high molecular masses typical of proteins.

Although the typical and most used configuration has the sample on the support in a vacuum environment, atmospheric pressure MALDI (AP-MALDI) methods have also been developed.

[*V.V. Laiko, M.A. Baldwin, A.L. Burlingame*: Atmospheric Pressure Matrix Assisted Laser Desorption/Ionization Mass Spectrometry. **Anal. Chem., 2000:72**(4), 652-657]

Comparative studies of vacuum MALDI and AP-MALDI ionizations have shown that similar results are obtained for peptide samples, but the optimization of working conditions in AP-MALDI is more difficult due to the partial thermal degradation of peptides.

[*B.B. Schneider, C. Lock, T.R. Covey*: AP and Vacuum MALDI on a QqLIT Instrument. **J. Am. Soc. Mass Spectrom., 2005:16**(2), 176-182]

In AP-MALDI ionization, the sample is positioned near the inlet of the mass analyzer at an appropriate angular orientation (sometimes even parallel to the axis of the spectrometer). After desorption and ionization, the resulting species enter the vacuum section of the analyzer.

## 2.2. Mass spectrometer analysis unit

### 2.2.1. General concepts and performance characteristics of mass analyzers

The mass analyzer is the most representative unit of the mass spectrometer, since the overall performance of the instrument depends critically on the design and operation of this module. The mass analyzer has two basic functions.

(1) The analyzer sends the ions from the previous (ionization) phase on different spatial trajectories according to their mass-to-electrical charge ratio (**m/z**).

The mass (**m**) of an ion is expressed as the ratio of the absolute mass to 1/12 of the absolute mass of the $^{12}C$ carbon isotope (equal to $1.660540 \bullet 10^{-27}$ kg; this ratio is also known as the *Dalton* unit, "Da"), and the charge (**z**) is the ratio of the absolute electric charge of the ion (expressed in coulombs) to the absolute charge of the electron ($1.602176 \bullet 10^{-19}$ coulombs). For example, the **m/z** ratio for the mono-ionized $^{12}C$ isotope of carbon is, by definition, equal to 12.

(2) The analyzer focuses ions with the same **m/z** ratio to a single point (exit slit) regardless of the diversity of their initial velocities.

Figures 4 and 6 show the trajectory of a positive ion in a magnetic field. Figure 5 shows the correlation between the orientations of the magnetic field vector ($\vec{\mathbf{H}}$), the *Lorentz* force vector ($\vec{\mathbf{F}}_{\mathbf{L}}$) and the velocity vector ($\vec{\mathbf{v}}$) for a positive ion and Figure 7 shows the trajectory of a positive ion in the electrostatic field between the armatures of a cylindrical capacitor.

In practice, the differentiation of ions is achieved because of the action of a magnetic field, the action of an electric field, the combined action of these fields or because of the time taken for the ions to travel a fixed distance (time-of-flight (TOF) analyzers). Analyzers can therefore be divided into four classes according to their mode of operation:

- analyzers that selectively deflect ions in a magnetic field alone or in combination with an electrostatic field,
- analyzers with selective ion transmission by means of a time-varying electric field (quadrupolar, octupolar analyzers),
- analyzers with selective sequential reception of the ions at the exit of the analyzer (Time of Flight Analyser, **TOF**),

- analyzers based on captive maintenance (ion traps) and selective release of individual ions according to **m/z** ratio (quadrupolar trap, orbitrap, *Fourier* transform analyzer).

The performance of mass analyzers is qualified according to the following characteristics.

(a) Mass range covered - defined as the maximum value of the **m/z** ratio detected by the analyzer.

(b) Resolving power, "**res**" - is the ability to distinguish two ions with close **m/z** ratios that produce distinct signals in the spectrum. Two close signals, with the distance "**Δ(m/z)**" between their maximum, are separate if the minimum between them does not exceed 10 % of their maximum height (Figure 16). From a quantitative point of view, the resolution ("**res**") is expressed by the equation (12), where **$(m/z)_1$** and **$(m/z)_2$** are the values corresponding to the maxima of signals "**1**" and "**2**", respectively, and $(\Delta m/z)_{12}$ is the difference between the individual maxima.

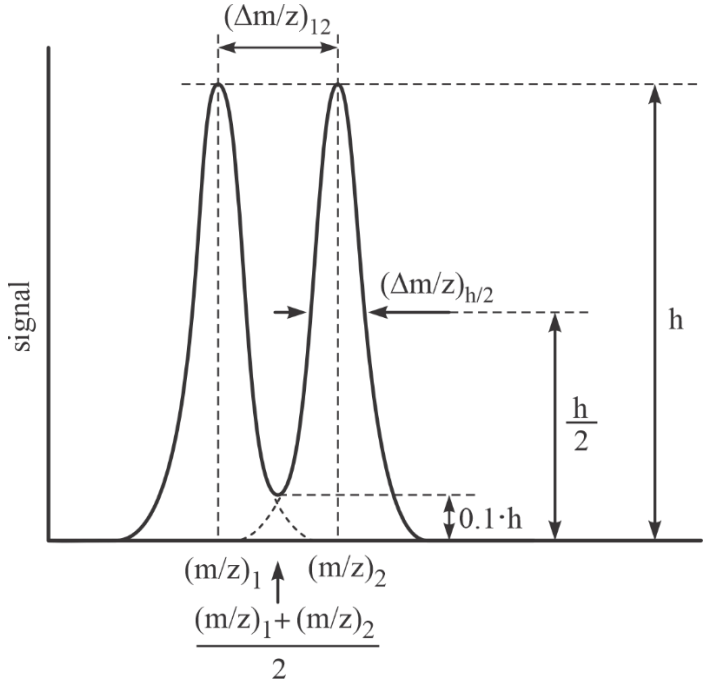



**Fig. 16 Definition of mass analyzer resolution (res)**

$$res = \frac{(m/z)_1 + (m/z)_2}{2 \cdot (\Delta m/z)_{12}} \qquad (12)$$

Another definition of resolving power uses the signal width **$(\Delta m/z)_{h/2}$** at half the maximum height, **h/2**. Of course, these definitions of resolving power assume that the mass spectrum is displayed in format "portrait" (Figure 2 **(A)**).

The high resolution of the mass analyzer is necessary (i) for the determination of the molecular mass with very high accuracy (which in turn allows the determination of the molecular formula of the analyzed compound), (ii) for the differentiation of chemical species labeled with stable isotopes, in which case it is necessary to deter-

mine the percentage presence of a specific isotope (other than the dominant one) in the analyte, and (iii) for the exact quantification of the precursor ion in "tandem" $MS^2$ analyses. The **m/z** ratios of ions may be expressed with 6-7 decimal accuracy on some mass analyzers with appropriate resolution.

Regarding their performance, the analyzers are characterized through several additional parameters.

(c) Efficiency – defined as the fraction of ions detected at the output of the analyzer in a single ionization cycle.

(d) Accuracy - refers to the error in reporting the **m/z** ratio of an ion divided by the exact **m/z** ratio of that ion.

(e) Dynamic range of linearity - refers to the maximum amount of analyte that produces a signal at the detector level proportional to the amount of analyte introduced.

(f) Analysis speed - represented by the number of spectra recorded (the number of scans) per unit of time. A high scan rate is important when tracking and analyzing events that occur at high speed.

(g) Ability to record MS/MS-type spectra (second order, "tandem"). These analyzers are composed of at least three subunits: the first subunit selects a representative (precursor ion) from the primary ion mixture; this enters the second subunit where it undergoes fragmentation according to different mechanisms depending on the local physical conditions; the last subunit of the analyzer separates the ionized fragments, producing the second order, MS/MS spectrum. For each precursor ion generated in the first subunit, a complete MS/MS spectrum results. This technique increases the certainty of chemical identification (confirmation or denial of chemical identity) of an analyte.

### 2.2.2. Magnetic analyzer and magnetic-electrostatic assembly

The first mass analyzer was designed based on the deflection of the ion path in a magnetic field due to the *Lorentz* force. The initial path of the ions is perpendicular to the lines of magnetic field, and the *Lorentz* force is perpendicular to the instantaneous direction of motion and to the magnetic field lines. (Figures 4, 5, 6).

An ion with absolute mass "$\mathbf{m_i}$" and electric charge "$\mathbf{q_i}$" is accelerated by a potential difference "**V**" as it leaves the ionizing unit. As a result, the ion reaches the velocity "$\mathbf{v_i}$". These quantities satisfy the relation (13), which expresses the fact that the kinetic energy of the ion is equal to the mechanical work done by the accelerating electric field.

$$q_i \cdot V = \frac{m_i \cdot v_i^2}{2} \qquad (13)$$

The condition for an ion of absolute mass "$\mathbf{m_i}$" and absolute electric charge "$\mathbf{q_i}$" to follow a circular path of radius "$\mathbf{r_m}$" in the presence of a magnetic field of induction "**B**" is that the modulus of the *Lorentz* force is equal to the modulus of the centrifugal force acting on the ion (14):

$$B \cdot q_i \cdot v_i = \frac{m_i \cdot v_i^2}{r_m} \qquad (14)$$

The radius "$\mathbf{r_m}$" of the circular trajectories, imposed on the ion by the design details of the analyzer, is expressed by equation (15).

$$r_m = \frac{m_i}{q_i} \cdot \frac{v_i}{B} \qquad (15)$$

Ions with different "$\mathbf{m_i/q_i}$" ratios follow different circular trajectories with radii "$\mathbf{r_m}$" (Figure 17). Equation (15) shows that the radius "$\mathbf{r_m}$" of the circular trajectory depends not only on the ratio "$\mathbf{m_i/q_i}$" of the ion, but also on its velocity "$\mathbf{v_i}$".

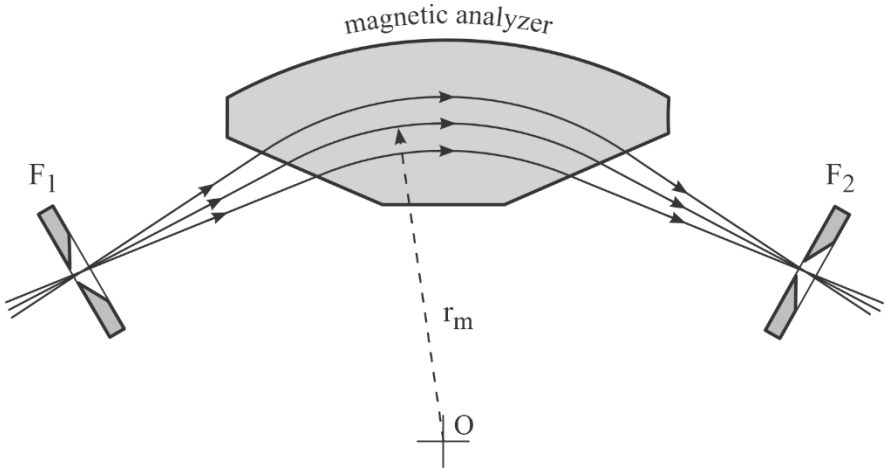



**Fig. 17 Deflection and focusing of an ion beam using a homogeneous magnetic field**

The discrimination power of the magnetic analyzer strictly according to the "$\mathbf{m_i/q_i}$" ratio criterion (implicitly the resolution power) depends on the condition that all the ions entering the analyzer have the same velocity (in other words, "$\mathbf{v_i}$" does not depend on "$\mathbf{i}$"). However, this condition is difficult to satisfy, first because the ions may have different initial thermal velocities (even before they are accelerated), and second because it is difficult to define the point at which the acceleration of the ions begins. The uncertainty in the "$\mathbf{v_i}$" velocities works against the resolution of a purely magnetic analyzer. This problem can be solved by combining the magnetic analyzer with an electrostatic analyzer (acting as a velocity filter). The electrostatic analyzer consists of

two cylindrical electrodes (the armatures of a cylindrical capacitor) between which an electrostatic field "**E**" is applied. (Figure 18).

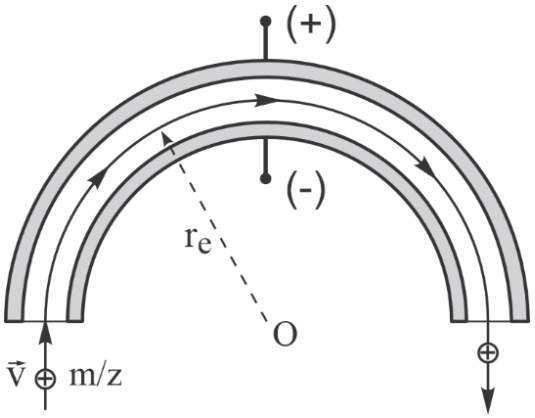



**Fig. 18**
**Electrostatic velocity filter**
**(shown for positive ion)**

The condition for the ion "**i**" of absolute mass "$\mathbf{m_i}$" and absolute electric charge "$\mathbf{q_i}$" to move along the circular orbit of radius "$\mathbf{r_e}$" (the condition that ensure passage through the space between the cylindrical armatures) is the equality between the modules of the electrostatic and centrifugal forces at each point of the circular orbit.

$$q_i \cdot E = \frac{m_i \cdot v_i^2}{r_e} \qquad (16)$$

Removing the product "$\mathbf{m_i \bullet v_i^2}$" from (13) and (16) gives:

$$r_e = \frac{2 \cdot V}{E} \qquad (17)$$

According to relation (17), the condition that all ions "**i**" with different values of the "$\mathbf{m_i/q_i}$" ratio follow a circular trajectory with a given radius "$\mathbf{r_e}$" depends only on the ratio between the acceleration potential "**V**" and the intensity of the electric field "**E**" between the armatures. The device thus acts as a velocity filter: it allows ions with a given velocity to pass, whatever the "$\mathbf{m_i/q_i}$" ratio.

Analyzers consisting of an electrostatic unit and a magnetic analyzer (dual electromagnetic analyzer) provide better resolution because the velocity filter removes the uncertainty associated with the initial velocities of the ions.

The influence of the variety of the initial velocities can be eliminated (or at least reduced) by associating an electrostatic analyzer with a magnetic analyzer (resulting in a double electro-magnetic analyzer). In this case, the passage of an ion through the system requires the satisfaction of both relations (13) and (14). By squaring relation (14) and then dividing by relation (16), the variable "$\mathbf{v_i}$" is eliminated:

$$\frac{m_i}{q_i} = \frac{B^2 \cdot r_m^2}{E \cdot r_e} \qquad (18)$$

According to relation (18), the condition to obtain the "transparency" of the analyzer (with the radii of curvature "$\mathbf{r_e}$" and "$\mathbf{r_m}$" constructively imposed) for different values of the "**m/q**" ratio (in other words, to *scan* the values of "**m/q**") is that the magnetic induction "**B**" and the intensity of the electric field "**E**" vary simultaneously, keeping the ratio "$\mathbf{B^2/E}$" constant. Hybrid analyzers, consisting of an electrostatic and a magnetic unit, offer a higher resolution than pure magnetic analyzers.

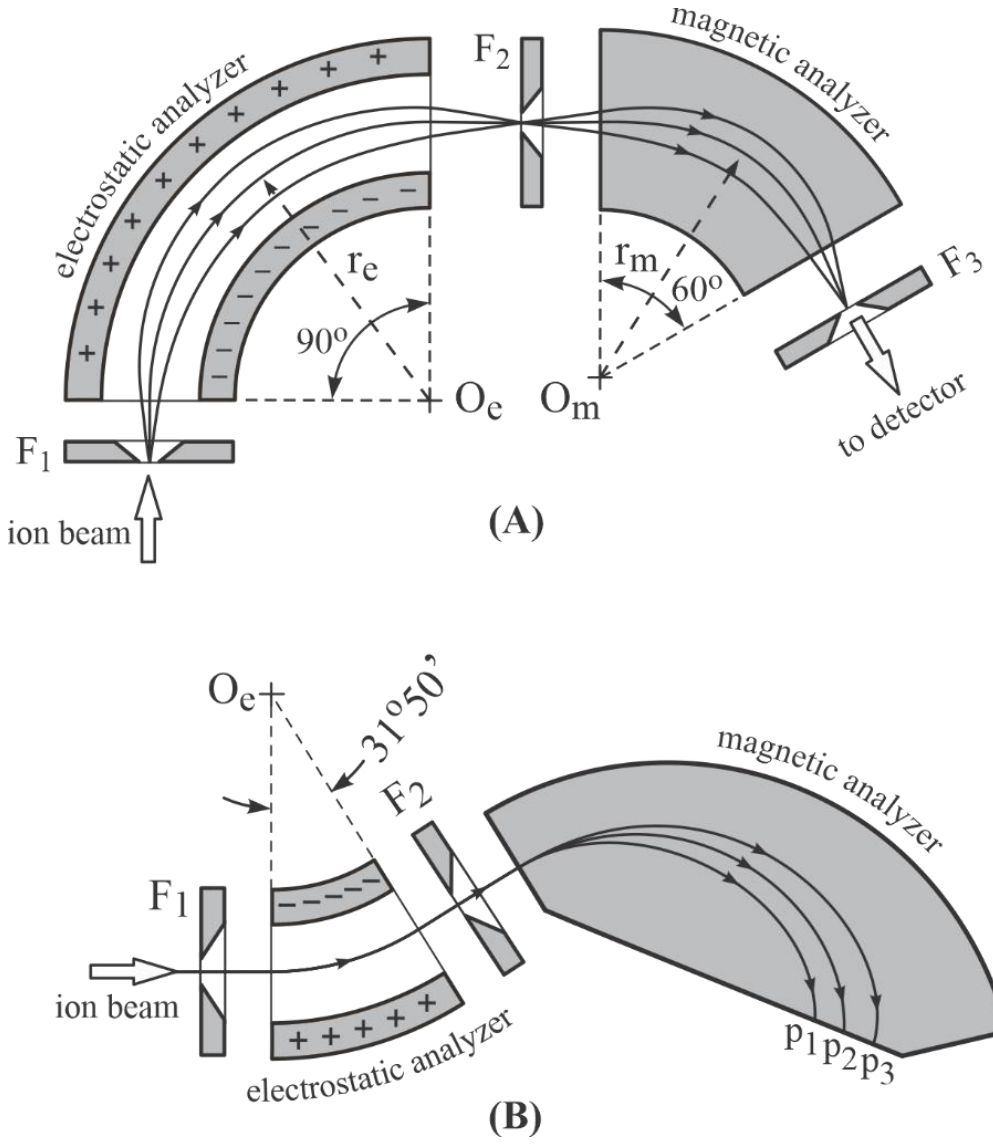



**Fig. 19 Design scheme of the mass analyzer with *Nier-Johnson* geometry (A) and *Mattauch-Herzog* geometry (B) (paths shown for a positive ion)**

Figure 19 **(A)** shows the design elements and operating principles of an analyzer with dual electric and magnetic focus (*Nier-Johnson* geometry), a configuration common for many mass spectrometers. The electrostatic analyzer is placed in front of the

magnetic analyzer. The angle covered by the electrostatic analyzer is $90^o$ and the angle covered by the magnetic sector is $60^o$.

In the *Mattauch-Herzog* geometry analyzer (Figure 19 **(B)**), the magnetic and electric fields deflect the ions in opposite directions (on a global sigmoidal trajectory) and the ions are focused on a common plane. The *Mattauch-Herzog* configuration is advantageous when using a multichannel detector. Due to the simultaneous detection of ions with different values of the "**m/q**" ratio, this configuration provides increased sensitivity compared to the *Nier-Johnson* configuration.

To overcome the problem of different initial ion velocities, some spectrometers use a linear velocity filter (*Wien* filter) before the magnetic analyzer (Figure 20). The ions coming from the ionization unit, with different "$\mathbf{m_i/q_i}$" values and with different initial velocities "$\mathbf{v_i}$", pass through a region with a magnetic field and a crossed electrostatic field. Figure 20 illustrates the effect of the magnetic force $\mathbf{F_m}$ and the electrostatic force $\mathbf{F_e}$ in the case of a positive ion. The forces $\mathbf{F_m}$ and $\mathbf{F_e}$ have opposite directions. The condition for the non-deviated passage of an ion through the selector is that it has the right velocity $\mathbf{v_o}$ for which the two forces are equal in module.

$$F_e = F_m \quad ; \quad q \cdot E = B \cdot q \cdot v_o \quad ; \quad v_o = \frac{E}{B} \tag{19}$$

The condition of non-deviated passage of ions through the velocity filter depends only on the "**B**" and "**E**" values, characteristics of the velocity filter, and not on the "**m/q**" ratio of the ions. In other words, the filter allows ions with different "**m/q**" values to pass, but only ions with the velocity "$\mathbf{v_o}$" given by equation (19).

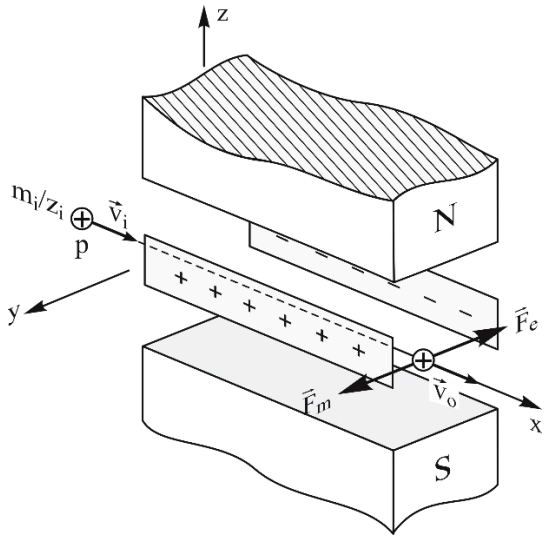



**Fig. 20**
**Working principle of a linear velocity (*Wien*) filter. The figure corresponds to a positive ion.**

Dual focus mass spectrometers (electrostatic and magnetic) are high performance instruments. With a magnetic induction of 2 T and an acceleration potential of 10 kV,

a resolution of 100,000 can be achieved, covering the mass range up to 15,000 Da. The accuracy of molecular mass determination can exceed 1 ppm (parts per million). The sensitivity increases with the acceleration potential.

Another important advantage of the double focus analyzer is the possibility of fragmentation any ion selected by the first module in the space between the electrostatic and magnetic modules (field-free space) by controlled collision with neutral atoms (for example helium or argon). On the other hand, their excessive cost limits their use in laboratories with modest financial resources. Another drawback is the difficulty of coupling them to a chromatographic system (gas or liquid) in which the mass spectrometer acts as a detector.

### 2.2.3. Quadrupole analyzer

The quadrupole analyzer is often used when high resolution is not essential. The analyzer consists of four electrodes in the form of parallel bars with a hyperbolic cross-section (ideal profile, Figure 21 **(A)** and **(C)**) or with a circular cross-section in less demanding systems.

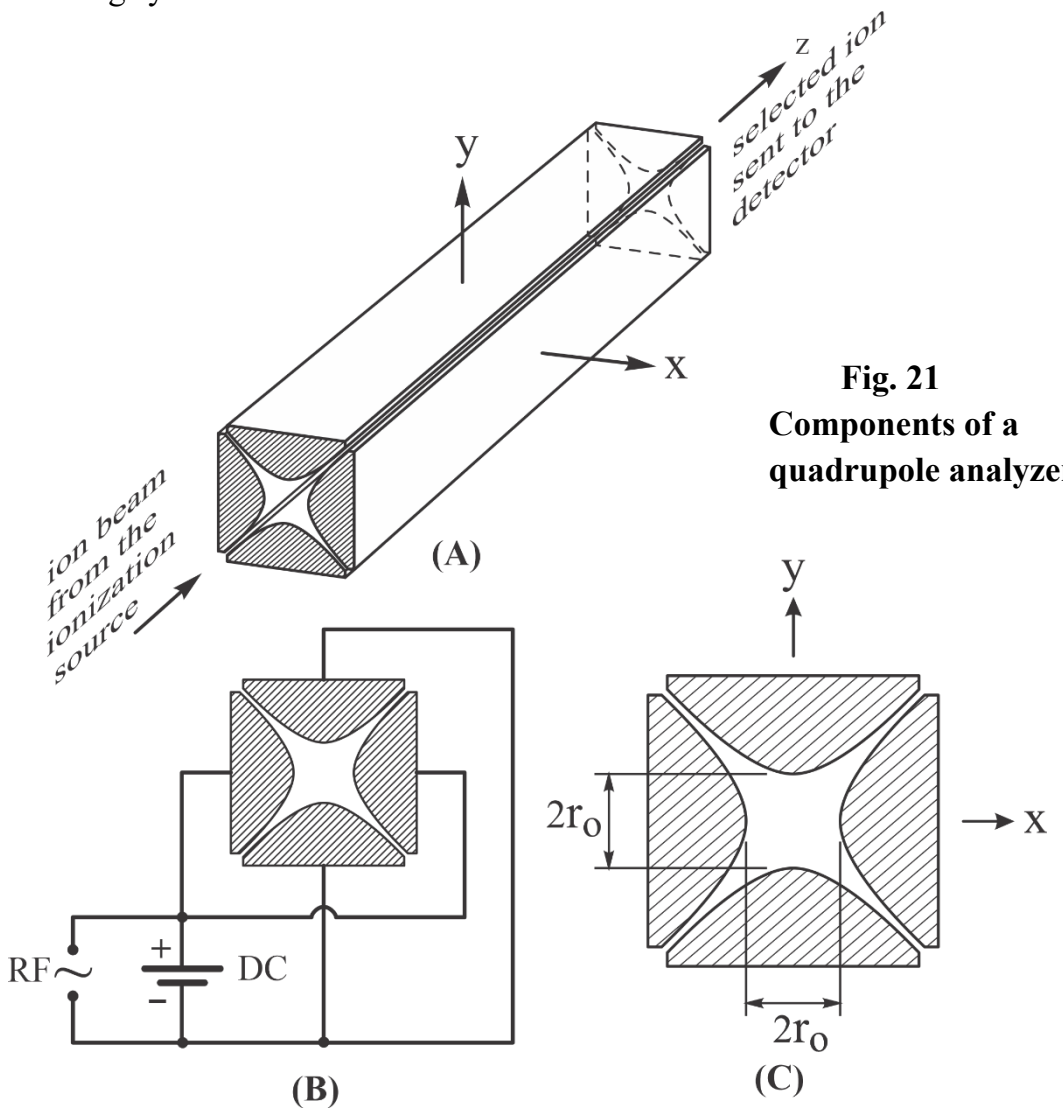



**Fig. 21**
**Components of a quadrupole analyzer**

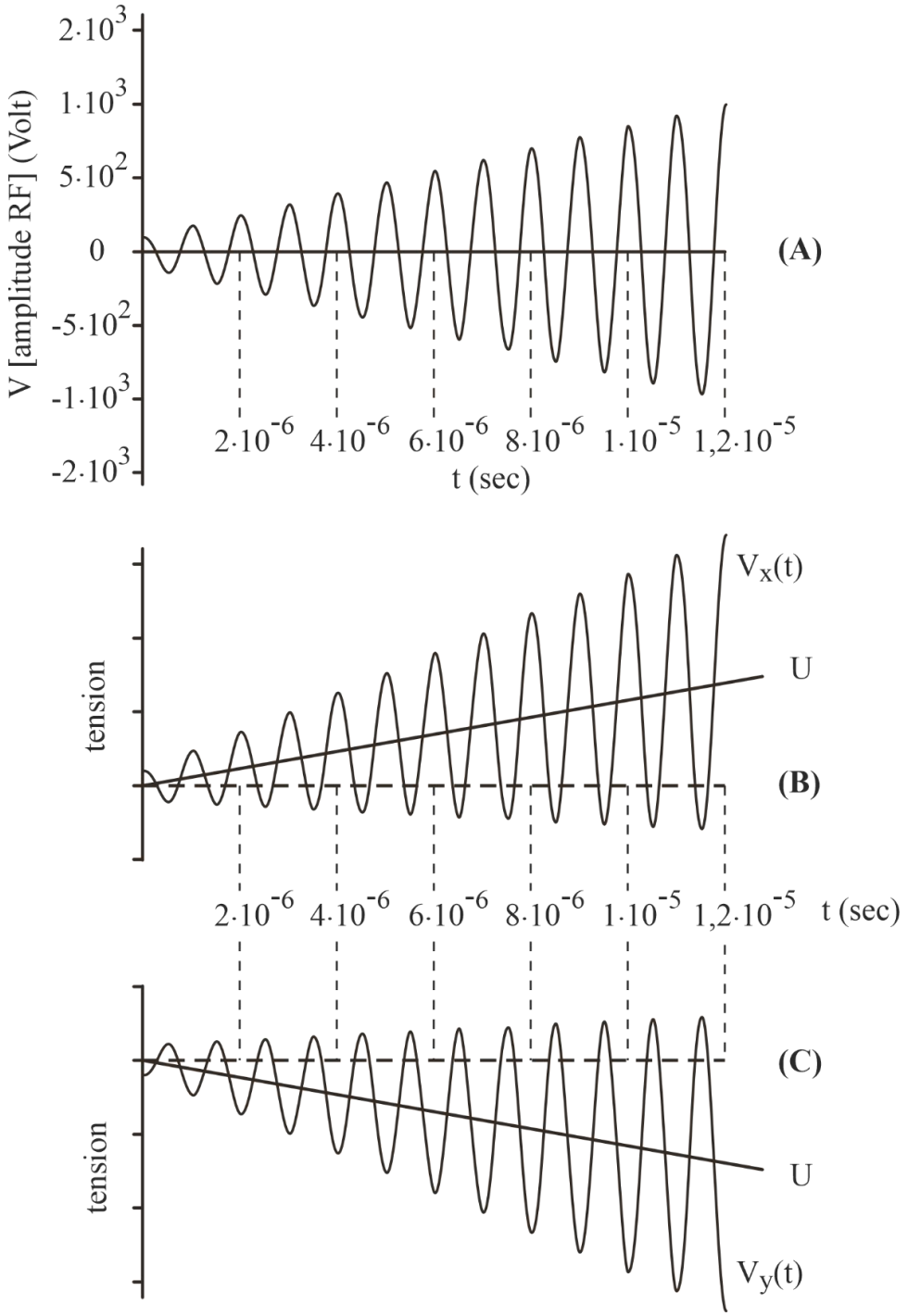



**Fig. 22 The evolution over time of the direct voltage and the alternating potential applied to the electrodes. The ratio between the direct voltage and the amplitude of the alternating potentials is maintained at a constant value (adaptation and reconstruction from *R.E. March and J.F.J. Todd*: Quadrupole Ion Trap Mass Spectrometry. John Wiley & Sons, Inc., Hoboken, New Jersey, 2005 [ISBN: 978-0-471-48888-0])**

The ions arriving from the ionization unit penetrate in the axial direction (**z**-axis direction in Figure 21 **(A)**) and, if the time-varying electrical potential of the electrodes is suitable, the ions cross the electrode assembly and leave the analyzer along the **z**-axis direction. The separation of the ions (spectrum scanning) according to the **m/q** ratio criterion is performed by applying a combination of direct voltage (**DC**) and alternating voltage (**RF** Radio Frequency) to the electrodes (Figure 21 **(B)**). Selecting the characteristics of the **DC** and **AC** voltages, it is ensured that only an ion with the suitable "**m/q**" ratio passes through the analyzer, while the other ions collide and discharge on the surfaces of the electrodes. By progressively varying the value of the **DC** voltage and the amplitude of the **AC** voltage, while keeping their ratio constant, the analyzer becomes "transparent" to ions with different "**m/q**" values. During the scan, the **DC** voltage, **U**, and the amplitude of the **RF** voltage, $\mathbf{V_o}$,are progressively varied while keeping their ratio constant and the frequency of the **AC** voltage is kept constant as well.

Figure 22 shows the evolution over time of the **DC** voltage **U** and the **AC** potential values $\mathbf{V_x(t)}$ and $\mathbf{V_y(t)}$ applied to the electrodes. The analyzer acts as a tunable filter for varied "**m/q**" values without the need for a magnetic field. The condition of passage for an ion imposes stability (limited oscillation) both along the **x**-axis and along the **y**-axis. The electric potential "**V(x,y,t)**" in an interior point of coordinates "**x**" and "**y**" at time "**t**" is expressed by relation (20).

$$V(x,y,t) = \left[U(t) - V_o(t) \cdot \cos(2 \cdot \pi \cdot f \cdot t)\right] \cdot \frac{x^2 - y^2}{r_o^2} \qquad (20)$$

In equation (20), "**U(t)**" is the value of the **DC** voltage, "$\mathbf{V_o(t)}$" is the amplitude of the high-frequency voltage, both in time "**t**", "**f**" is the frequency of the **AC** voltage, and "$\mathbf{r_o}$" is half the distance between the opposite electrodes (Fig. 21 **(C)**).

Figure 23 shows the equipotential lines due to the **DC** component at a given instant in the space defined by the electrodes.

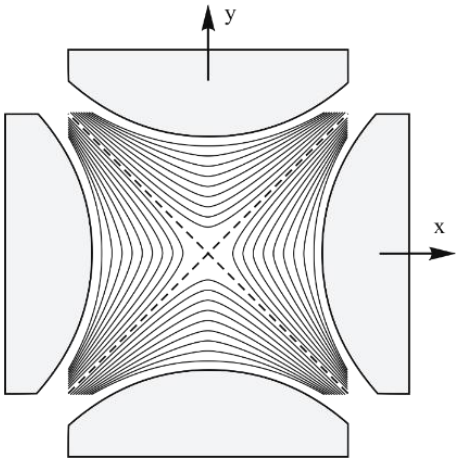



**Fig. 23**
**Equipotential lines in the space between the hyperbolic profile electrodes of the quadrupole analyzer**

The oscillatory motion of an ion in the "**x**" and "**y**" directions is described by the differential equation (21) (*Matheu* equation).

$$\frac{d^2u}{d\xi^2} + \left[a_u - 2 \cdot q_u \cdot \cos(2 \cdot \xi)\right] \cdot u = 0 \qquad (21)$$

where "**u**" is the transverse displacement of the ion (in "**x**" and "**y**" directions) from the center of the electrode assembly and the variable "**ξ**" is the product "**π·f·t** " where "**f**|" is the frequency of **AC** voltage. The solution of the *Mathieu* equation includes two dimensionless parameters "$\mathbf{a_u}$" and "$\mathbf{q_u}$" defined by relations (22).

$$a_u = a_x = -a_y = \frac{8 \cdot z \cdot e \cdot U}{m \cdot 4 \cdot \pi^2 \cdot f^2 \cdot r_o^2}$$
$$q_u = q_x = -q_y = \frac{4 \cdot z \cdot e \cdot V_o}{m \cdot 4 \cdot \pi^2 \cdot f^2 \cdot r_o^2} \qquad (22)$$

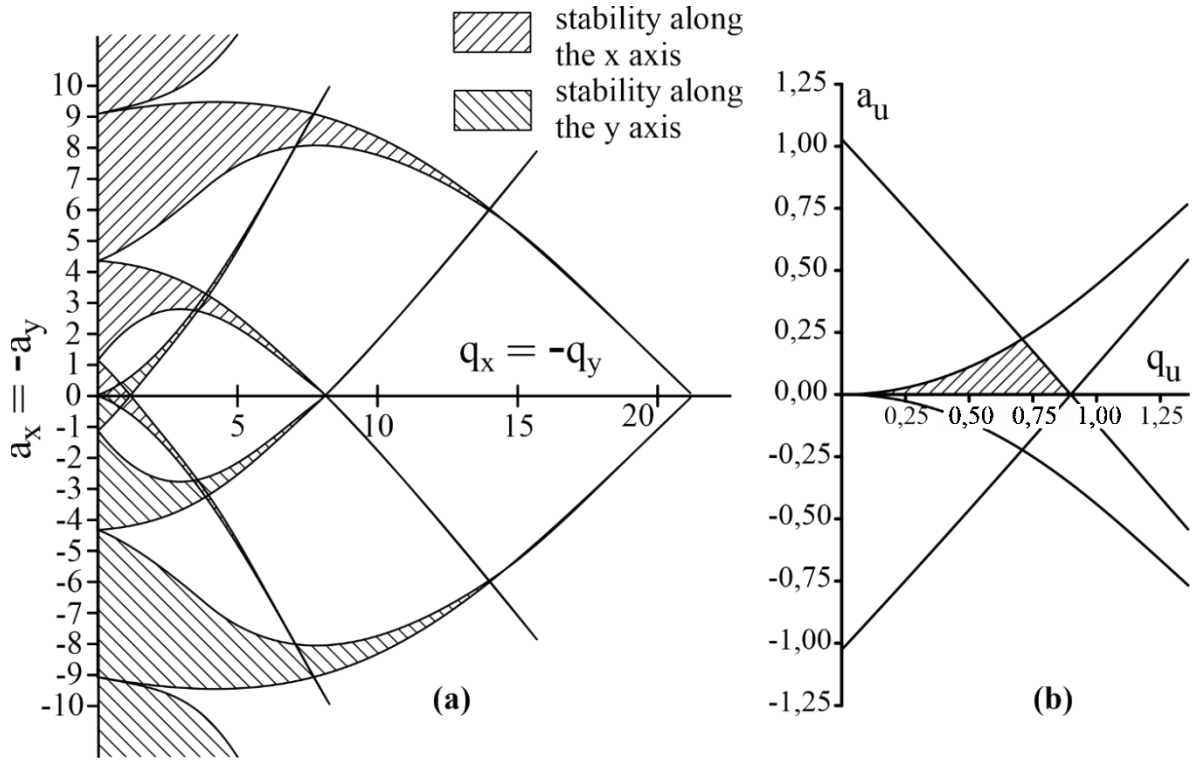



**Fig. 24 Stability zones of ion movement in the quadrupole analyzer resulting from the *Mathieu* equation (a) and the first stability zone involved in real operations (b). (taken from *R.E. March şi J.F.J. Todd*: Quadrupole Ion Trap Mass Spectrometry. John Wiley & Sons, Inc., Hoboken, New Jersey, 2005 [ISBN: 978-0-471-48888-0])**

The graphical representation of the values of the "$a_u$" parameter as a function of the values of the "$q_u$" parameter delimits some regions of stable oscillation in the directions of the "**x**" and "**y**" axes (Figure 24). From the stability domains of Figure 24**(a)**, the domain near the origin of the graphs is used (Figures 24**(b)**, 25 and 26).

Scanning consists in simultaneously increasing the voltage **U** and the amplitude $V_o$, an operation which corresponds to simultaneously increasing the variables "$a_u$" and "$q_u$" in relation (22), while keeping their ratio constant. In the graph in Figure 25, scanning means moving the figurative point on a straight line whose points correspond to different values of the **m/z** ratio. Only the ion with an **m/z** value whose point is within the stability region (in Figure 25 the ion with $m_2/z_2$) can pass through the analyzer.

The ions with figurative points outside the stability zone cannot pass through the quadrupole analyzer. The mass resolution is inversely proportional to the width of the stability domain intersected by the scan line. Therefore, the slope of the scan line is chosen to intersect the stability domain as close as possible to its peak.

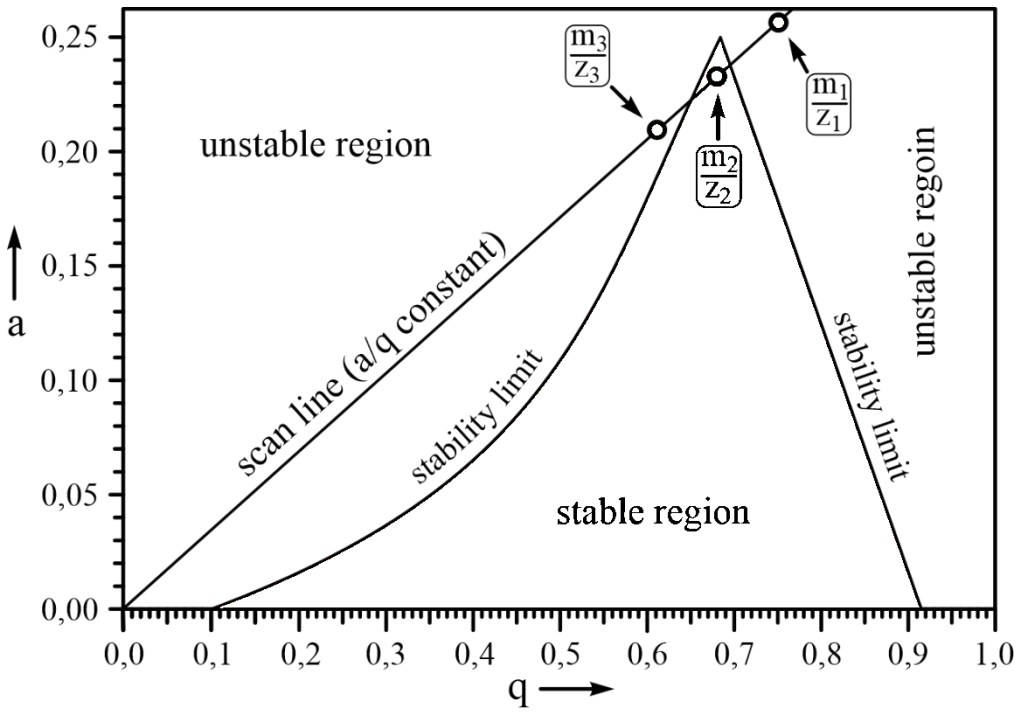



**Fig. 25 The stability zone used in practice for scanning the mass spectrum**

Stability regions are sometimes presented in **U** and $V_o$ coordinates (Figure 26). In this case, for a pair of "$a_u$" and "$q_u$" values, **U** and **Vo** values may correspond to the **m/z** ratio of the ion in question. In other words, different stability regions correspond to different **m/z** ratios in the **U** vs. $V_o$ plot. Only ions for which the figurative point on

the scan line is in its own stability region can pass through the quadrupole analyzer (Figure 26).

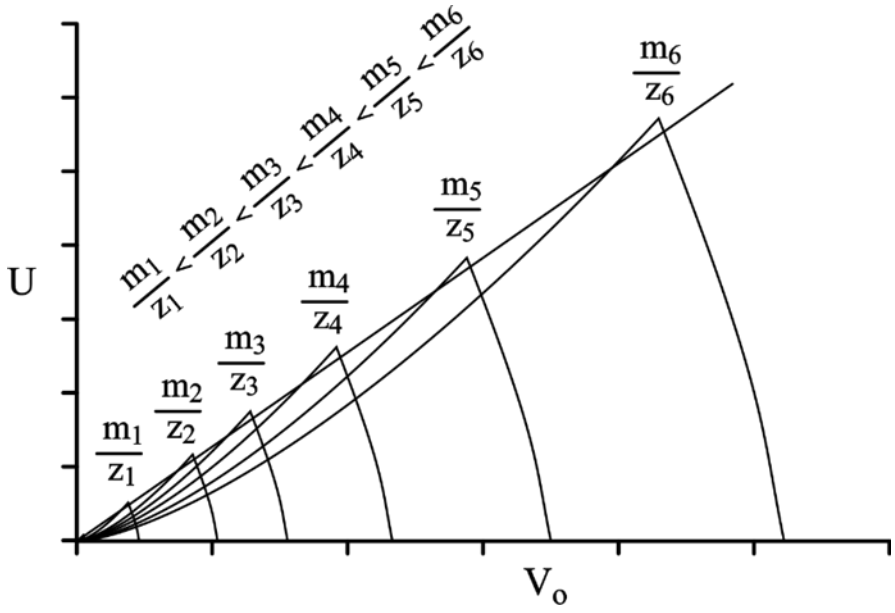



**Fig. 26 Display of stability domains in "U" and "$V_o$" coordinates, where each m/z ratio corresponds to a distinct stability domain (contrasted to the display in "$a_u$" and "$q_u$" coordinates as in Figure 25). (redrawn according to *K.Blaum, C. Geppert, P. Müller, W. Nörtershäuser, E.W. Otten, A. Schmitt, N. Trautmann, K. Wendt, B.A. Bushaw*: Properties and Performance of a Quadrupole Mass Filter Used for Resonance Ionization Mass Spectrometry. Int. J. Mass Spectrom., 1998:181(1-3), 67-87)**

The motion of an ion passing through the quadrupole analyzer is composed of two transverse oscillations along the **x** and **y** axes (Figure 27). If the stability condition is satisfied, the amplitude of the transverse oscillation will remain between limited values, smaller than the distance between the electrodes.

Mass spectrometers equipped with a quadrupole analyzer are compact, but their resolution does not match that of instruments with a combined electrostatic/magnetic analyzer. The typical upper limit of accessible mass, around 4000 Da, can be extended somewhat by increasing the amplitude of the radiofrequency voltage (**$V_o$**), reducing its frequency ("**f**"), and reducing the diameter of the rods that make up the electrodes. For example, by reducing the frequency to 262 kHz, the upper mass limit can be extended to 45,000 Da, but at the categorical disadvantage of resolution.

Quadrupole analyzers are particularly well suited for the analysis of low-molecular-weight compounds. With the advent of ESI ionization, a method that produces

significant amounts of ions with multiple electrical charges, it became possible to use the quadrupole for much higher molecular mass compounds.

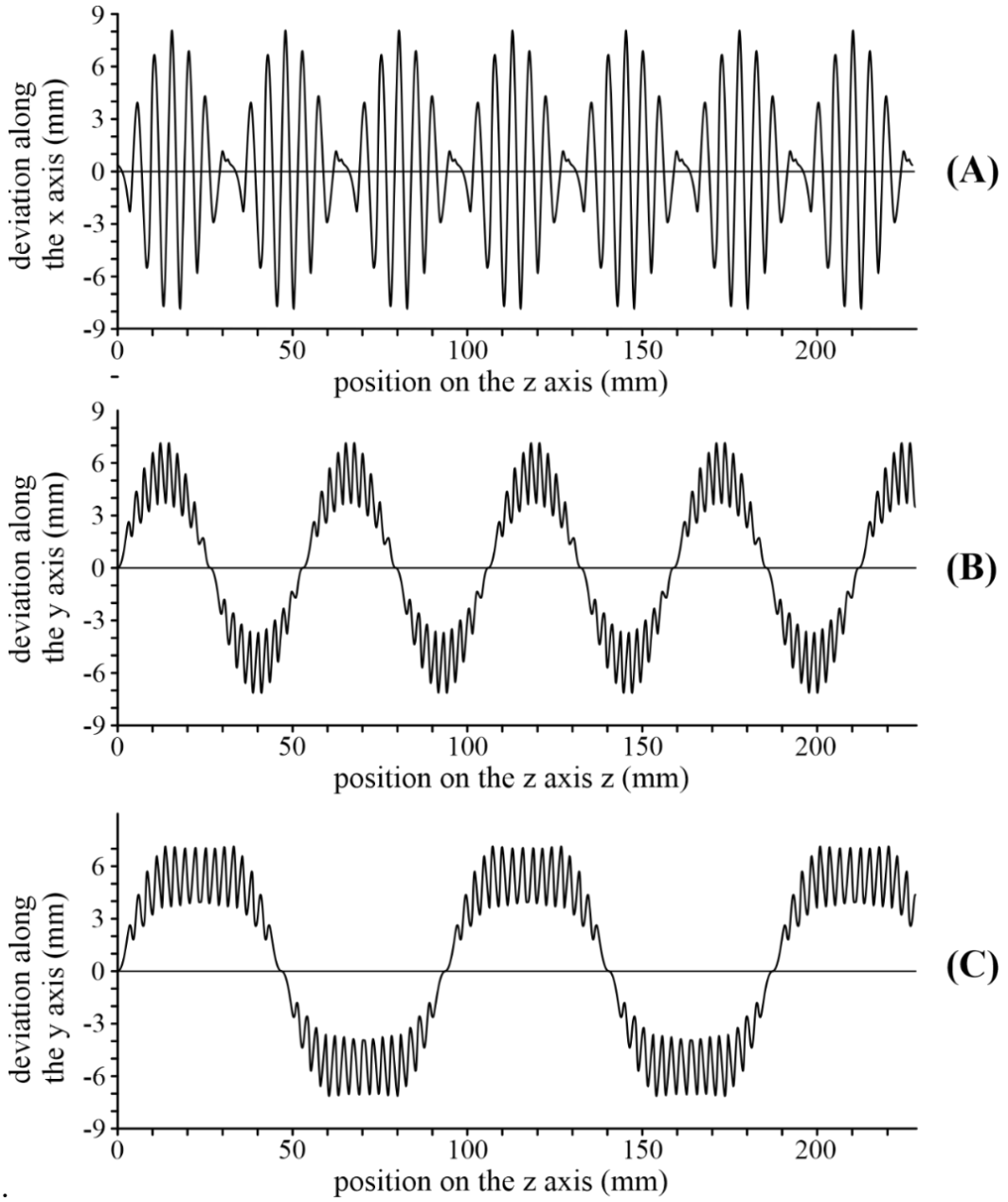



**Fig. 27 The stable oscillations of an ion along the "x" (A) and "y" (B) axes as it passes through the quadrupole analyzer. Oscillation along the "y" axis of an ion passing through the quadrupole analyzer for a hyperbolic (B) and circular (C) profile of the electrodes. (redrawn after *K.Blaum, C. Geppert, P. Müller, W. Nörtershäuser, E.W. Otten, A. Schmitt, N. Trautmann, K. Wendt, B.A. Bushaw*: Properties and Performance of a Quadrupole Mass Filter Used for Resonance Ionization Mass Spectrometry. Int. J. Mass Spectrom., 1998:181(1-3), 67-87)**

The resolution, "**res**", around the ion with the "**m/q**" ratio is given by the equation (23).

$$res = \frac{m \cdot f^2 \cdot L^2}{q \cdot V_{acc}} \qquad (23)$$

where "**L**" is the length of the electrode bars, "$\mathbf{V_{acc}}$" is the acceleration voltage (which determines the kinetic energy "**q•Vacc**" of the ions entering the analyzer), "**m**" and "**q**" are the mass and the electric charge of the ion respectively, and ("**f**") is the frequency of the **RF** voltage.

According to relation (23), the resolution can be improved by increasing the frequency ("**f**"), decreasing the acceleration voltage "$\mathbf{V_{acc}}$" and increasing the length of the electrode "**L**". Due to the inherent design imperfections of the electrodes, the practical limit for mass discrimination of quadrupolar analyzers is 1 Da. Much better resolution (sometimes up to 15,000) can be obtained using electrodes with a strictly hyperbolic profile (the ideal case).

To simplify the design, some quadrupolar analyzers use a circular profile of the electrodes rather than a hyperbolic one. Figures 27 **(B)** and **(C)** compare the transverse oscillation of an ion (in the direction of the **y**-axis) in the case of the hyperbolic (ideal) and circular profiles. The macro-oscillation frequency is lower in the case of electrodes with a circular profile than in the case of electrodes with a hyperbolic profile, which means a slightly lower resolution in the first case according to relation (23).

Because the quadrupole analyzer does not require a sophisticated vacuum or magnetic component, it is ideal for coupling to a gas chromatograph (GC/MS tandem), liquid chromatograph (HPLC/MS tandem), or capillary electrophoresis instrument (CE/MS tandem).

In some special applications, the analyzer is supplied only with **AC** voltage without the **DC** component ("**U**" = 0, "**RF** only" mode). In this case, for all operating conditions, the "$\mathbf{a_u}$" parameter in the *Mathieu* equation is zero (relation (22)), the scan line coincides with the "$\mathbf{q_u}$" axis (Figure 25), and the quadrupole behaves as a broadband mass filter. All ions for which "$\mathbf{q_u}$" < 0.908 pass through the analyzer. If the quadrupole is bounded at the ends by additional electrodes, the ions can be held inside the quadrupole analyzer without colliding with the electrodes (ion trap). The **AC**-only quadrupole is used to provide an intermediate region in which multiple ions can undergo chemical reactions (e.g., fragmentation by collision with neutral atoms of a gas), or as a guide only to deflect the ions in more powerful instruments.

### 2.2.4. Analyzer with a series of quadrupoles ("triple quad analyzer")

Quadrupole analyzers connected in series are used to record the fragmentation products of primary ions. Figure 28 shows an assembly of three quadrupole analyzers, **Q1**, **q2** and **Q3**, connected in this manner.

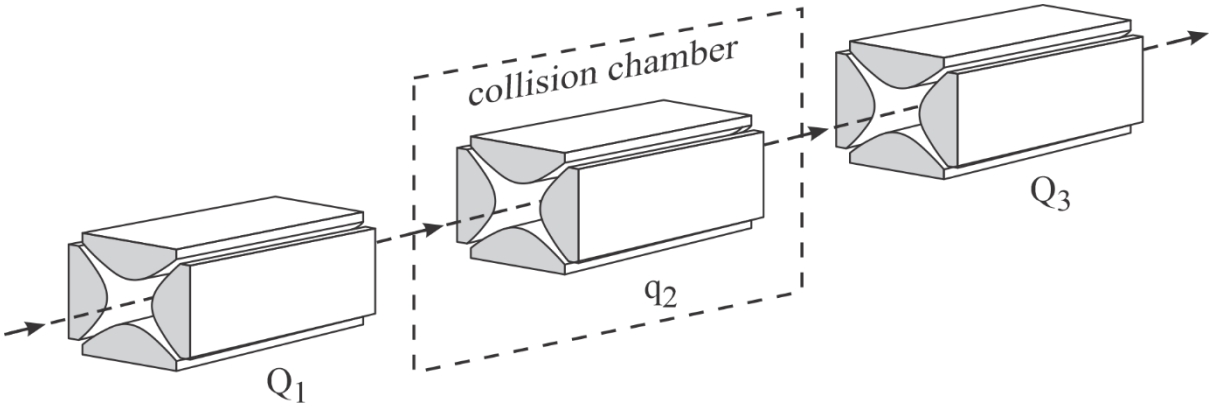



**Fig. 28 Quadrupole analyzers connected in series ("triple quad" assembly)**

Ions from the ionization unit enter the quadrupole analyzer **Q1**, which can scan all ions or transmit only a specific ion (the primary ion) with a selected **m/z** ratio. The selected ion enters the quadrupole **q2**, which is powered only by the radio frequency voltage "**V**", without the **DC** voltage "**U**", and is therefore open to ions with a wide range of "**m/z**" values. This quadrupole is in a separate chamber where a gas can be introduced whose molecules collide with the primary ion, causing them to split into smaller ions (fragmentation). The **Q3** quadrupole separates the ions produced by fragmentation. For each primary ion selected by quadrupole **Q1**, the action of quadrupole **Q3** produces a complete fragment spectrum. Quadrupole **q2** has a different role from the other two (it is the chamber for the fragmentation reaction, or it has only the role of ion guide). For this reason, the notation **q2** is used instead of **Q2** to emphasize this functional difference.

By choosing the collision energy in the **q2** quadrupole, it is possible to control the type and degree of fragmentation and, implicitly, the final mass spectrum. This procedure is called MS/MS (sometimes referred to as $MS^2$). The "triple quad" assembly is often used as a detector for chromatographs or capillary electrophoresis instruments with particularly high specificity, allowing very reliable identification of efficiently separated chemical species. Table 3 and Figure 29 show the standard operating modes of the triple quad analyzer.

**Table 3 Operating modes of quadrupoles in the "triple quad" analyzer**

| Procedure | Desired goal | Quadrupoles regime |
|---|---|---|
| Product Ion Scanning | Information on the chemical structure of the ions formed in the ionization phase | In **Q1** a precursor ion is selected<br>In **Q3** the full MS spectrum of the ion fragments is generated. |
| Precursor Ion Scanning | Detection of compounds that produce common ion fragments | In **Q1**, all ions are scanned.<br>**Q3** selects a particular ion fragment |
| Neutral Loss Scanning | Detection of compounds that lose a neutral molecular species by cleavage | Both quadrupoles (**Q1** and **Q3**) are in scanning mode but are permanently set to a specific difference in m/z values. |
| Single Ion Reaction | Monitoring of a selected reaction | **Q1** is set for an established precursor ion.<br>**Q3** is set for an established ionized fragment |

**(A)** ***Scanning of produced ions (fragments)***

The **Q1** quadrupole is in selection mode. From the ion stream coming from the ionization unit, the **Q1** quadrupole selects the ion of interest (precursor ion, $\mathbf{(m/z)_p}$). The selected ion is fragmented by Chemical Impact Dissociation (CID) in the **q2** quadrupole and the **Q3** quadrupole (in scanning mode) separates the ionized fragments and generates their spectrum.

**(B)** ***Precursor ion scanning***

The **Q1** quadrupole, set in scanning mode, separates the ions from the ionization and sends them in sequence to the **q2** quadrupole. Here, upon impact with a reactive gas (nitrogen, helium, etc.), the ions dissociate into ionic fragments that are sent to the **Q3** quadrupole. The **Q3** quadrupole selects a particular ionic fragment, specific to each sequentially released ion, from the **Q1** quadrupole and sends it to the detector.

**(C)** ***Neutral Loss Scanning***

Quadrupoles **Q1** and **Q3** are in scanning mode so that during scanning there is a fixed difference between the **m/z** ratios to which the quadrupoles are transparent.

**(D)** ***Single Ion Reaction***

Both quadrupoles, **Q1** and **Q3**, are in select mode. This mode of operation provides greater confidence in the identification of a compound and minimizes the possibility of misinterpretation of results.

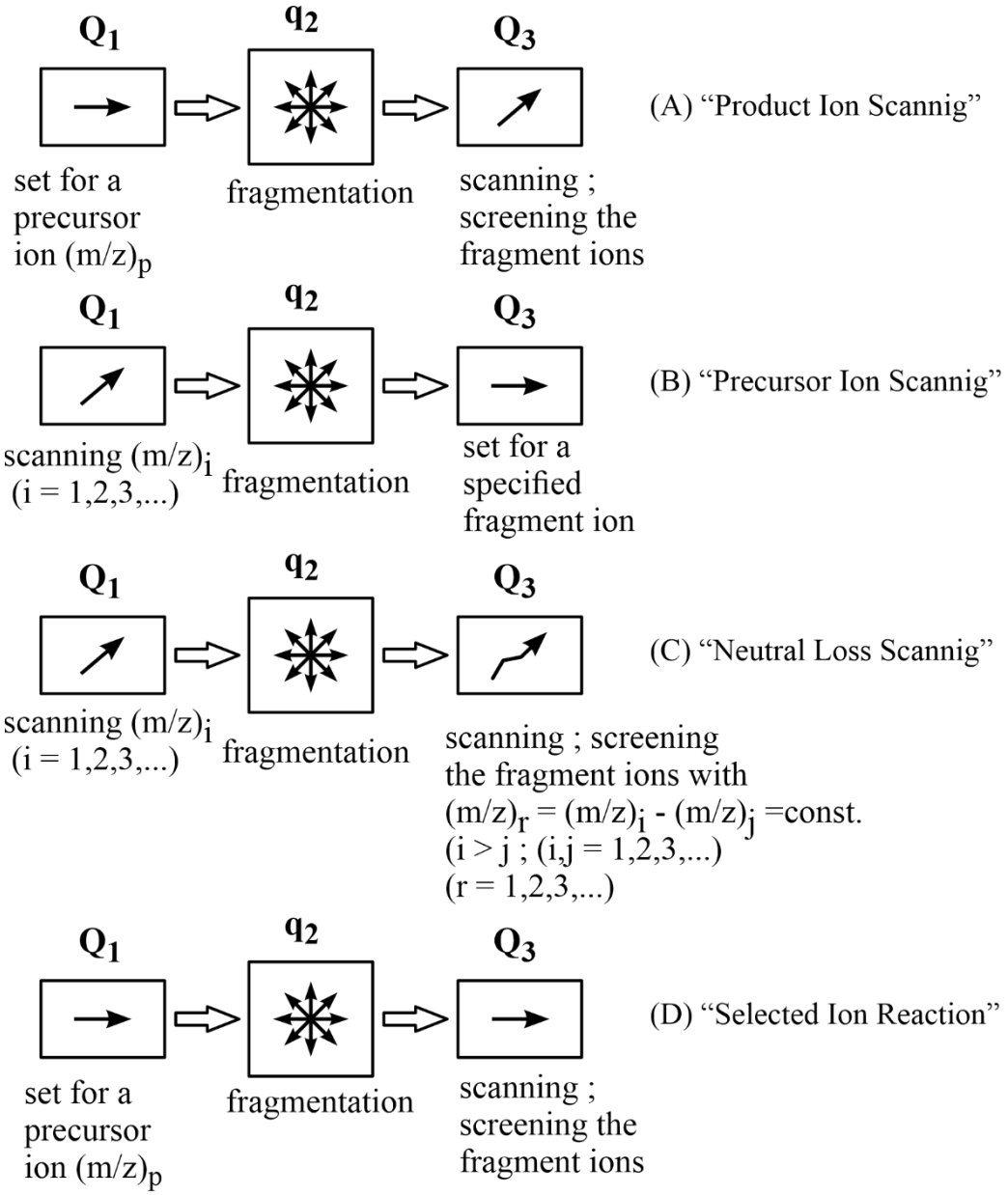



**Fig. 29 Illustration of the standard operating modes of the "triple quad" analyzer**

The **q2** quadrupole, where fragmentation takes place, works only with the **RF** voltage applied to the electrodes, so it acts only as a guide for the ions. This quadrupole is not necessarily linear; in some mass spectrometer designs, this quadrupole is bent at $90^{o}$ or even $180^{o}$ from the ion entrance direction (Figure 30).

In addition to reducing size, the curved shape of the **q2** quadrupole offers the advantage of longer ion paths in the fragmentation space and the exclusion of neutral molecular fragments and photons from the ion flux, thus reducing background noise.

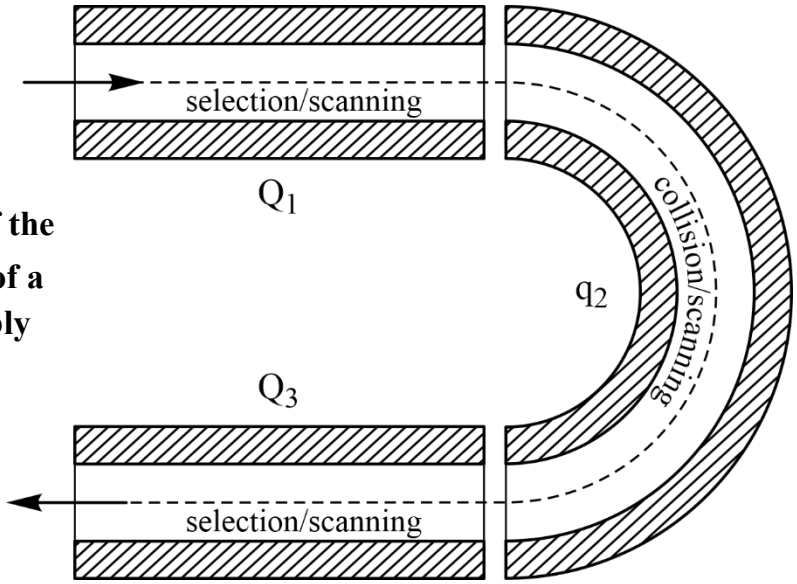



**Fig. 30**
**Bent configuration of the q2 quadrupole, part of a "triple quad" assembly**

### 2.2.5. Time of Flight – TOF analyzer

The Time of Flight (TOF) analyzer separates ions according to the time ("time of flight") between their departure from the ionization unit and their arrival at the detector. The principle of operation is shown in Figure 31.

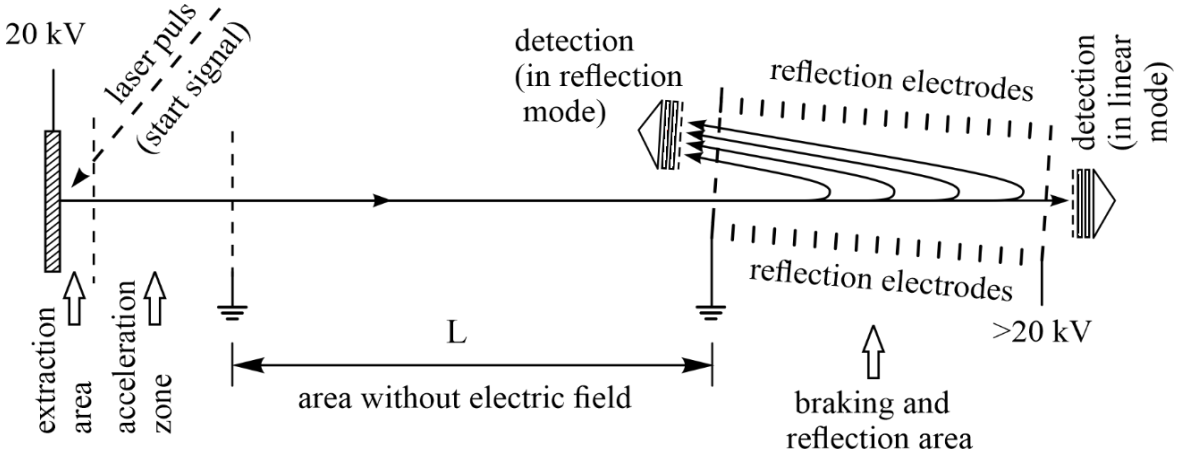



**Fig. 31 Design principle of the Time of Flight (TOF) analyzer (redrawn with changes after *R. Ekman, J. Silberring, A.M. Westman-Brinkmalm, A. Kraj*: Mass Spectrometry – Instrumentation, Interpretation and Applications. Joh Wiley & Sons, Inc., 2009 [ISBN: 978-0-741-71395-1])**

The operating condition of the TOF analyzer is a well-defined ion start signal against which the time is measured for ions of different masses and charges to arrive sequentially at the detector after a fixed distance. The TOF analyzer is suitable for pulsed ion sources, such as MALDI, where the laser pulse is the start signal.

The sample holder is at a positive or negative potential (depending on the preferred mode of operation with positive or negative ions) between 5 - 30 kV. The ions released by the laser pulse are accelerated towards the grounded electrode (at zero potential). After leaving the acceleration zone, all intact ions with the same electrical charge have the same kinetic energy but different mass-dependent velocities. The ions then enter a region with no electric field and finally reach the detector. The time from the start signal (ionization-initiating laser pulse) to the arrival of the ions at the detector is the time of flight "$\mathbf{t_{TOF}}$", expressed by equation (24).

$$\left(t_{TOF}\right)_i = \frac{L}{v_i} = L \cdot \sqrt{\left(\frac{m}{z}\right)_i \cdot \frac{1}{2 \cdot e \cdot U_{acc}}} \qquad (24)$$

where "**L**" is the length of the zone without electric field (Figure 31), "$\mathbf{v_i}$" is the velocity of the ion "**i**" due to the accelerating voltage "$\mathbf{U_{acc}}$", "$\mathbf{(m/z)_i}$" refers to the mass/ionization state ratio of the ion "**i**", and "**e**" is the elementary electric charge.

The faster or lighter an ion is, the shorter the time interval during which the ion travels through space without an electric field. The correlation between the time of flight and the "**m/z**" ratio of an ion is achieved by calibration with ions of known mass.

The resolution of the TOF analyzer is limited by the diversity of the initial ion velocities. This diversity is minimized by special procedures such as the use of electrostatic reflectors or delayed extraction of the ions ("time-lag" procedure).

The TOF analyzer can operate in two ways: either by capturing the ions at the detector without deflecting them from their original path (linear detection mode), or by modifying the path because of applying a deflection potential and sending the ions to a different detector (reflection detection mode). In the case of detection by electrostatic reflection, the path of the ions is not straight to the detector (linear detection mode), but they are reflected by applying an electric potential higher than the acceleration potential, after which they reach another detector (Figure 31). The axis of the reflection electrodes is tilted about $1^o$ from the main axis and the resulting path deviates about $178^o$ from the original direction.

The effect of ion deflection by reflection is to increase the distance traveled, but the more important effect is to compensate for the difference in initial ion velocities. The ions with a higher initial velocity penetrate deeper into the space of the reflecting electrodes and travel a longer effective path compared to the ions with a lower initial

velocity which, by penetrating less deeply into the reflector, travel a shorter effective path (Figure 31). By optimizing the ratio between the accelerating voltage and the voltage of the reflecting electrodes, ions with the same "**m/z**" ratio but different initial velocities arrive at the detector almost simultaneously. This ratio, once optimized, is suitable for the entire mass range covered by the analyzer.

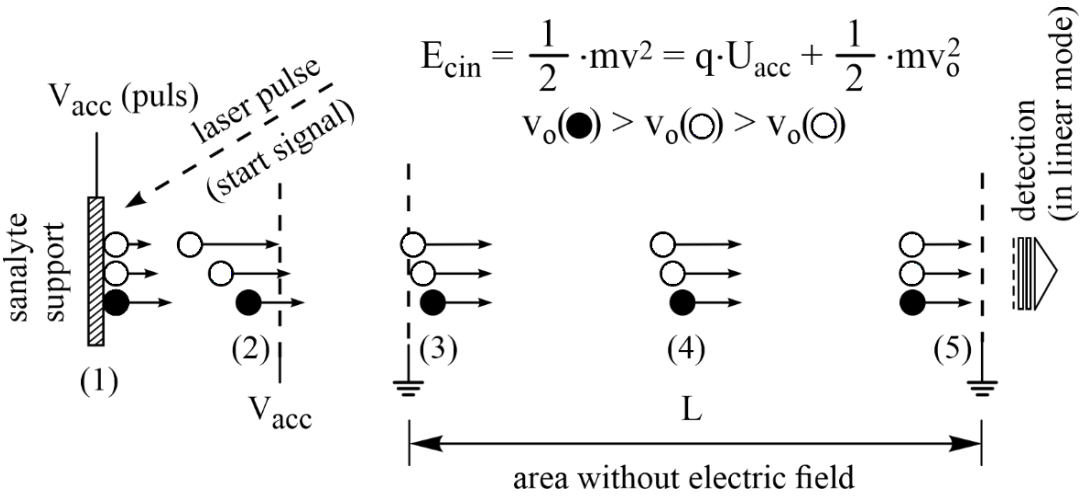



**Fig. 32 The principle of "time-lag" extraction (redrawn with modifications after *R. Ekman, J. Silberring, A.M. Westman-Brinkmalm, A. Kraj*: Mass Spectrometry – Instrumentation, Interpretation and Applications. Joh Wiley & Sons, Inc., 2009 [ISBN: 978-0-741-71395-1])**

The time-lag (delayed extraction) method is based on the linear path of the ions (like the linear detection mode in the reflection configuration) (Figure 32). The laser pulse directed at the sample **(1)** induces desorption of the ions. Initially, the desorbed ions (even those with the same "**m/z**" ratio) have different initial velocities. In the moment of laser irradiation, the sample support is at the same electrical potential ($\mathbf{V_{acc}}$) as the first grating **(2)** and the ions are not subjected to an effective acceleration voltage in this region, furthermore the ions cross the space **(1)** - **(2)** at their initial velocities "$\mathbf{v_o}$".

A few hundred nanoseconds (delay time, "**τ**") after the impact of the laser pulse, the potential of the sample support **(1)** is suddenly increased, accompanied by the instantaneous generation of an accelerating force in space **(1)** - **(2)** acting towards the grid **(2)**. The initially slower ions (labeled "○" in Figure 33) are surprised closer to the electrode **(1)** and are accelerated over a greater distance than the initially faster ions (labeled "●" in Figure 33), so that the former increase their velocity more than the latter. As a result, the speeds of the ions approach a common value. When the ions enter the space without electric field (between grids **(3)** and **(4)**), their velocities gradually approach a common value (mark **(4)**). If the acceleration voltage "$\mathbf{U_{acc}}$" and the delay time "**τ**" are set to optimal values, ions with different "**m/z**" ratios and initial

velocities "$\mathbf{v_0}$" arrive (almost) simultaneously at the grid **(5)** and implicitly at the detector. Thus, an "**m/z**" value corresponds to a well-defined time of flight "$\mathbf{t_{TOF}}$" without being affected by the diversity of initial velocities.

Regarding the initial velocity problem and the extent to which it affects resolution, TOF with reflection detection is superior to TOF with linear detection or even to time-lag extraction. Figure 33 compares (in portrait format) the resolutions of three TOF modes for the 18-39 fragment of the peptide hormone ACTH.

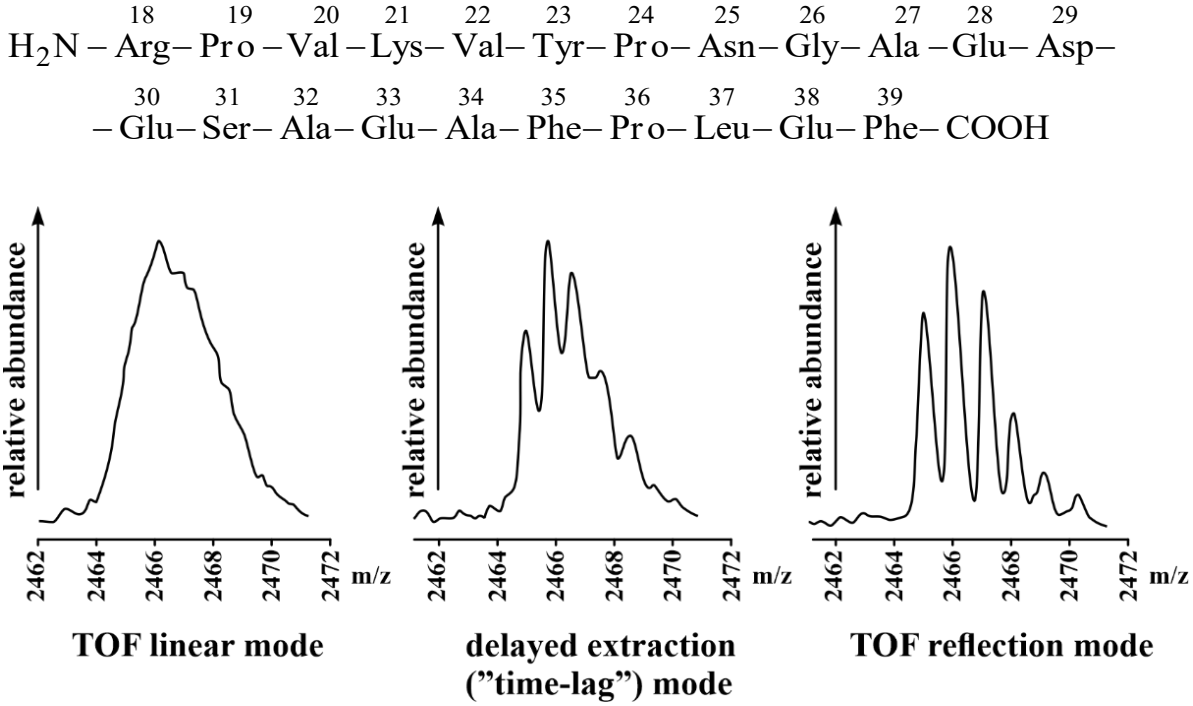



**Fig. 33 Comparative resolution performance of three TOF operating modes (after *K. Downard*: Mass Spectrometry – A Foundation Cours (RS•C, 2004 [ISBN: 0-85404-609-7])**

In some design configurations, time-of-flight analysis is performed in the direction perpendicular to the initial ion incidence (Figure 34). Ions selected by quadrupole $\mathbf{Q_1}$ and subjected to chemical reaction/fragmentation in quadrupole $\mathbf{q_2}$, are deflected and accelerated by a combination of electrodes in the direction perpendicular to incidence. After reflection, by a process like that shown in Figure 31, ions with a defined **m/z** ratio reach the detector simultaneously, even though they left the quadrupole $\mathbf{q_2}$ with different initial velocities. Thus, the travel time of the space defined by the orthogonal accelerator and the reflection electrode ("**reflectron**") is characteristic for a given ion.

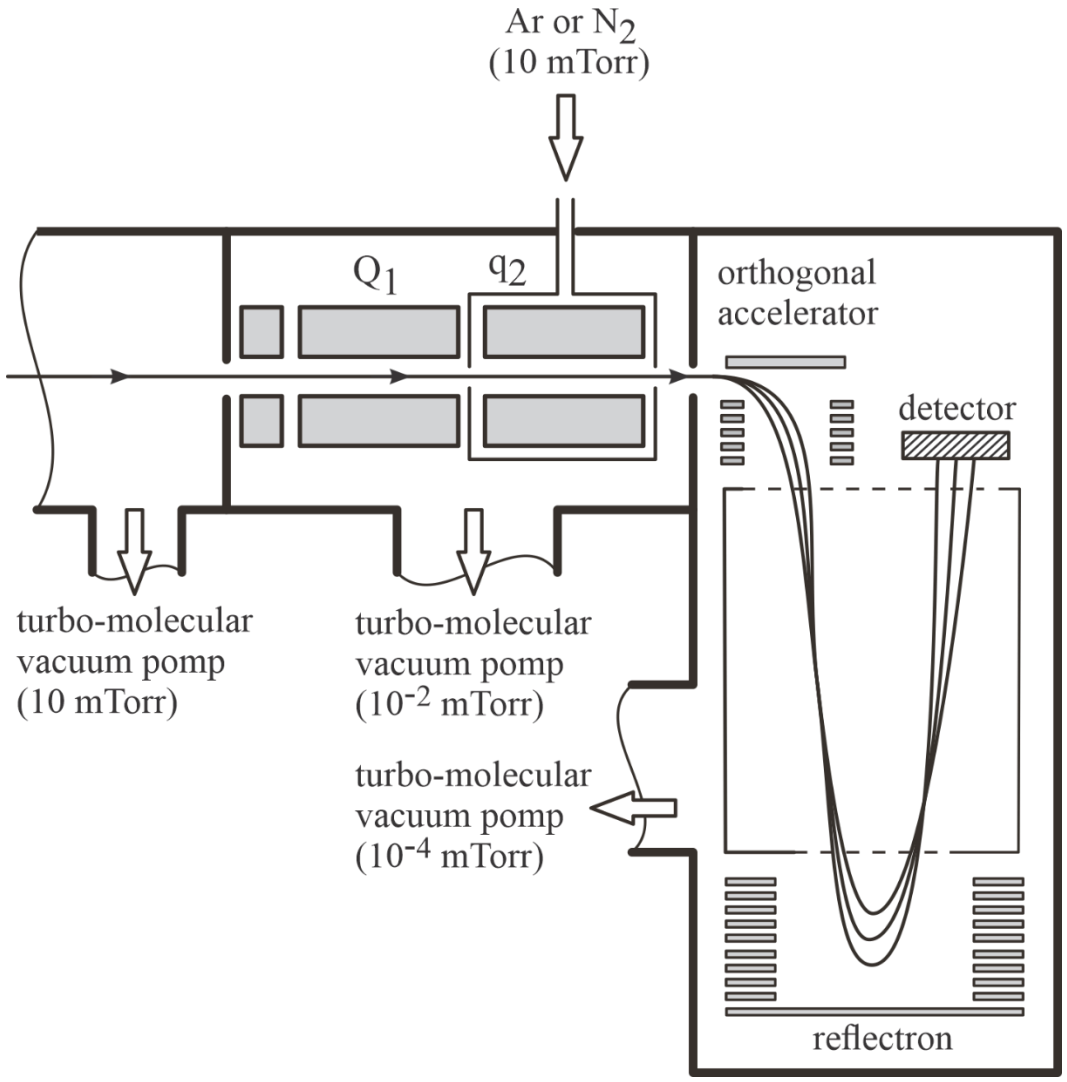



**Fig. 34 Details on the design and operation of the orthogonal TOF analyzer (redrawn with modifications after *E. de Hoffmann* şi *V. Strobant*: Mass Spectrometry – Principles and Applications. John Wiley & Sons Ltd., 2007 [ISBN: 978-0-470-03310-4])**

### 2.2.6. Ion trap analyzers

Unlike the analyzers described in previous chapters, which act on the sample ions either by producing deviations in the trajectories depending on the "**m/z**" ratio or by recording the time taken to travel a fixed distance, ion traps capture the ions arriving from the ionization unit and release the individual ions one at a time.

#### 2.2.6.1. Quadrupole linear ion trap

The quadrupole can be used as a linear ion trap if an appropriate combination of continuous voltage and radio frequency is applied to the electrodes to satisfy the condition of transverse oscillation stability for ions with "**m/z**" values between predefined limits. To prevent ions from escaping in the axial direction, additional electrodes (front

and end section) are located at the ends of the quadrupole (Figure 35), which are loaded with an appropriate electrical potential and can return the ions towards the center. This ensemble is known in literature as a linear ion trap ("LIT").

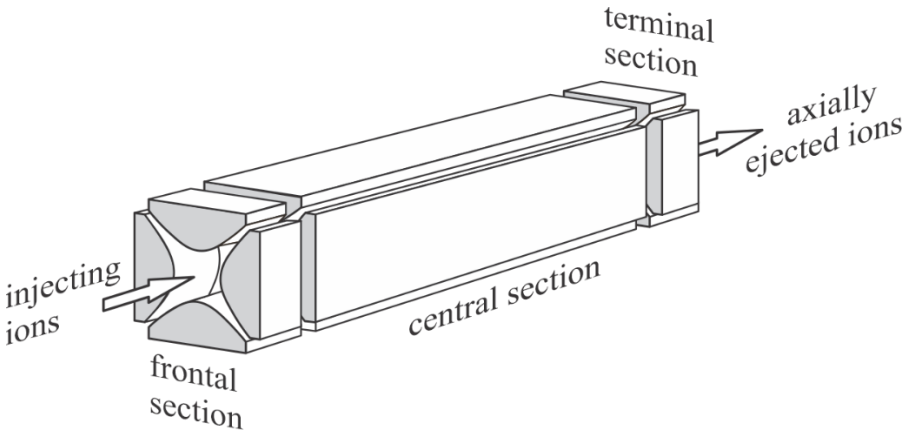



**Fig. 35 Construction details of axial ejection quadrupole ion trap**

Figure 36 shows the operating mode of the linear quadruple ion trap for the case of positive ions. In the ion uptake phase, the front section is at a potential that allows the ions to enter the space between the electrodes (Figure 36 **(a)**). The transverse oscillation is stable for the incoming ions so that they don't hit the surface of the electrodes. The higher positive potential of the terminal electrode prevents the ions from escaping in the axial direction. Once trapped, the potential of the front section is increased (Figure 36 **(b)**). By modifying the potential of the terminal section (at -10 V in Figure 36 **(c)**), the possibility of sequential ejection of ions in the axial direction is achieved.

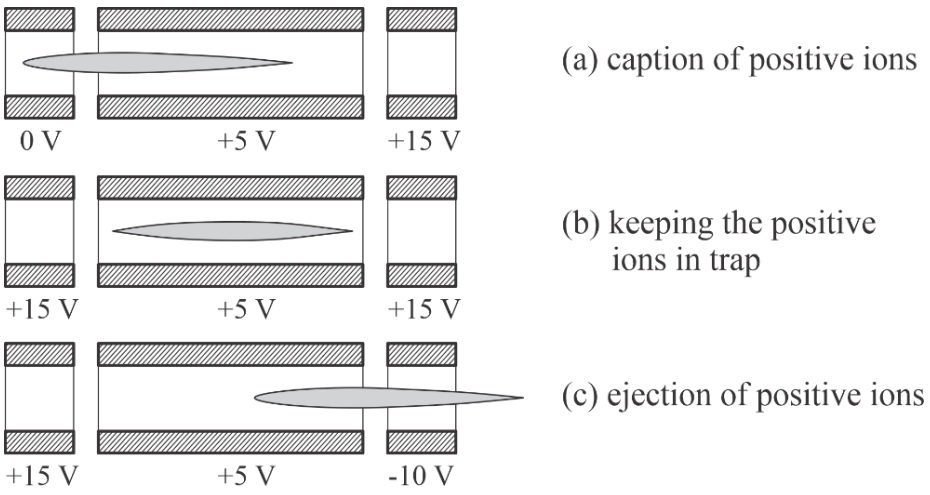



**Fig 36 Operation of a quadruple ion trap with axial ejection (for positive ions)**

In other configurations, the quadrupolar ion trap releases the ions perpendicular to the incident direction through a slit in one of the electrodes (Figure 37).

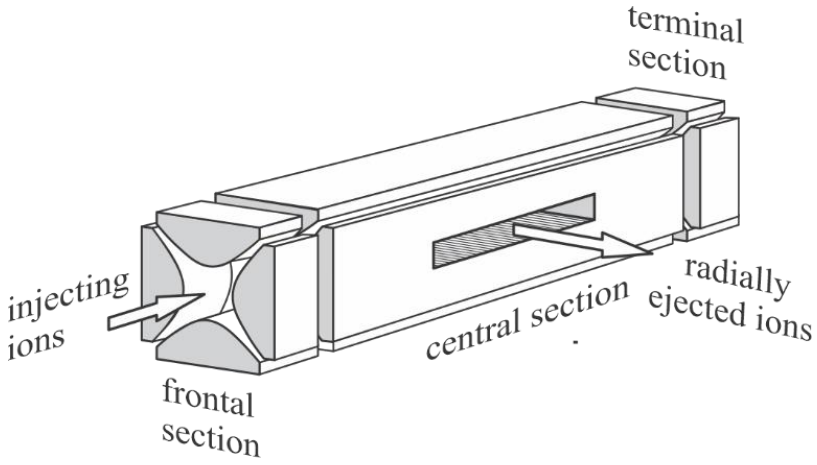



**Fig. 37 Design details of a radial ejection quadruple trap**

### 2.2.6.2. Ion trap with three electrodes

Another type of ion trap consists of three electrodes, each with a hyperboloid profile (Figure 38). At the ring electrode **a**, an alternative voltage of radio frequency **V(t)** with amplitude $\mathbf{V_o}$ and frequency "**f**" (pulse **ω**) is superimposed on a continuous voltage **U**. Electrodes **b** and **c** are grounded (zero potential).

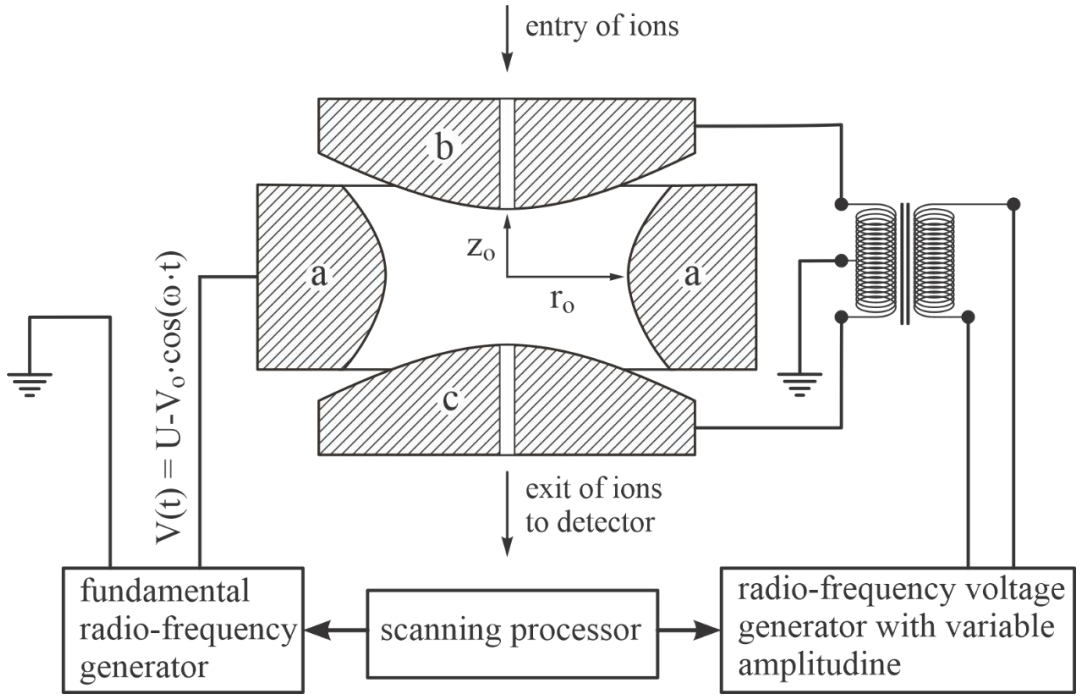



**Fig 38 Sectional view of a three-electrode ion trap (adapted and redesigned after *Chhabil Dass*: Fundamentals of Contemporary Mass Spectrometry. John Wiley & Sons, Inc., Hoboken, New Jersey, 2007 [ISBN: 978-0-471-68229-5] and after *E. de Hoffmann* & *V. Stroobant*: Mass Spectrometry. Principles and Applications. John Wiley & Sons, Ltd., 2007 Wesr Sussex [ISBN: 978-0-470-03310-4])**

The ions enter the space between the electrodes through a channel in the center of electrode **b**. Inside the electrode assembly, the ions perform complicated oscillating motions in three directions (the path is a three-dimensional *Lissajous* curve, Figure 39) without colliding with the electrode wall.

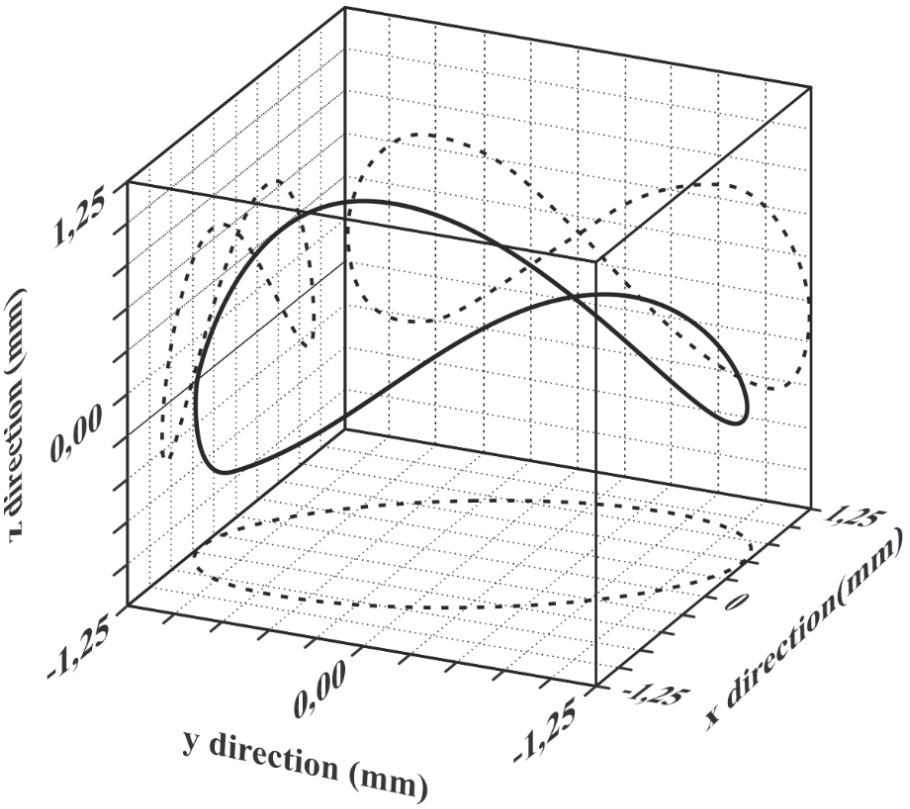



**Fig. 39 Typical ion trajectory inside the ion trap (adapted and redesigned after *Chhabil Dass*: Fundamentals of Contemporary Mass Spectrometry. John Wiley & Sons, Inc., Hoboken, New Jersey, 2007 [ISBN: 978-0-471-68229-5] and after *R.E. March şi J.F.J. Todd*: Quadrupole Ion Trap Mass Spectrometry. John Wiley & Sons, Inc., Hoboken, New Jersey, 2005 [ISBN: 978-0-471-48888-0])**

By changing the voltage of the input and output electrodes (electrodes **b** and **c** in Figure 38), ions enter the trap, are retained for a period (in the order of picoseconds), or are selectively released towards the detector, depending on the "**m/z**" ratio. The residence time of an ion in the trap depends on the "**m/z**" ratio, the inner radius of the ring electrode ($\mathbf{r_o}$), the distance between the electrodes **b** and **c** ($2 \cdot \mathbf{z_o}$), the frequency of the **AC** voltage "**f**" applied between the electrodes **b** and **c**, the **DC** voltage **U** and the amplitude $\mathbf{V_o}$ of the radiofrequency voltage. From the differential equation of motion of an ion of mass "**m**" and electric charge "**z•e**", two quantities, "$\mathbf{a_z}$" and "$\mathbf{q_z}$", can

be defined which delimit the stability zones analogous to the quantities, "$\mathbf{a_u}$" and "$\mathbf{q_u}$", mentioned in equation (22) of the quadrupole analyzer:

$$a_z = -2 \cdot a_r = -\frac{16 \cdot z \cdot e \cdot U}{m \cdot (r_o^2 + z_o^2) \cdot 4 \cdot \pi^2 \cdot f^2}$$
$$q_z = -2 \cdot q_r = \frac{8 \cdot z \cdot e \cdot V_o}{m \cdot (r_o^2 + z_o^2) \cdot 4 \cdot \pi^2 \cdot f^2} \qquad (25)$$

Using the "$\mathbf{a_z}$" and "$\mathbf{q_z}$" values as coordinates, the stability diagram is built and the areas corresponding to the retention of ions inside the trap can be determined (like in diagrams of Figures 24 and 25). The movement of ions for which the figurative points of the "$\mathbf{a_z}$" and "$\mathbf{q_z}$" values are within the stability zones is restricted to the inside of the trap. In modern spectrometers, an inert gas is introduced inside the trap, often helium at a pressure of $10^{-3}$ Torr, to reduce the kinetic energy of the ions by collision. The important feature of the ion trap is its ability to store the ions until a suitable concentration is reached and only then to release them towards the detector.

In other conventional analyzers (quadrupolar or electric/magnetic), a continuous flow of ions is obtained whose concentration depends on the efficiency of the ionization unit. Instead, in the case of the ion trap, the ability to store ions provides a greatly increased detection sensitivity.

The three-electrode ion trap was invented by *W. Paul* and *H.S. Steinwedel* in 1960 and perfected for mass spectrometry by *G.C. Stafford* in 1984, hence the name "*Paul*'s trap".

### 2.2.6.3. Electrostatic trap (“Orbitrap”)

The name "Orbitrap" refers to an electrostatic ion trap that generates the actual mass spectrum by a *Fourier* transform of the captured electrical signal. The basic concept was developed and published by *Makarov* in 1999 [U.S. Pat. 5886346], in 2000 **[Anal. Chem., 2000:72(6), 1156-1162]** and in 2004 **[U.S. Pat. 2004108540]**.

Figure 40 shows the longitudinal section of the "Orbitrap" analyzer and the location of its electrodes. Figure 41 **(A)** shows a transversal section of the electrode assembly that makes up the parts of the "Orbitrap" trap. The outer part consists of two identical parts separated by a narrow electrically insulating space (longitudinal section, Figure 41 **(B)**). The spindle-shaped central electrode has a maximum diameter of 8 mm. The ions are injected into the space between the electrodes tangentially to the central electrode (Figure 41 **(A)**). The central electrode is at a positive or negative potential (depending on the mode of operation) of several kilovolts, while the outer electrodes are at zero potential (connected to ground).

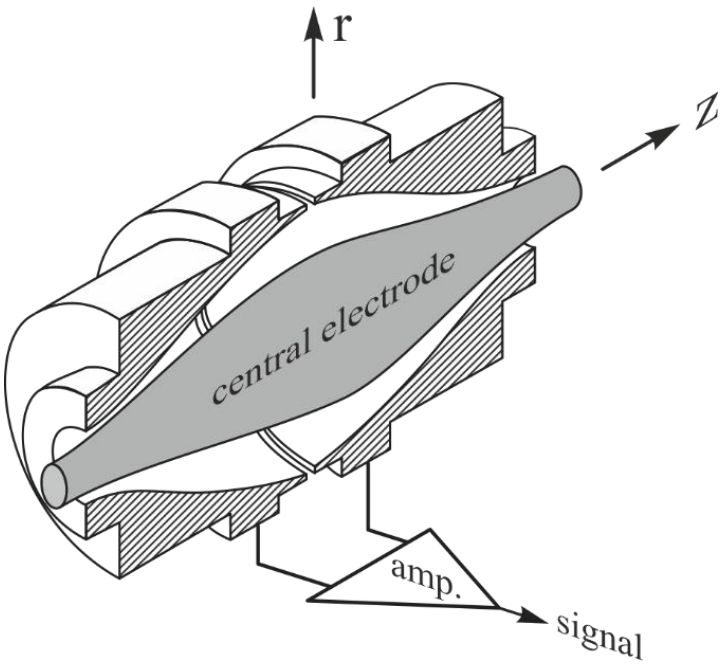



**Fig. 40 Longitudinal section through "Orbitrap" analyzer (redesigned after: *M. Scigelova, M. Hornshaw, A. Giannakopulos, A. Makarov*: Fourier Transform Mass Spectrometry. Mol. Cell. Proteomics 2011:10(7), M111.009431)**

The ions are injected into the orbitrap with a kinetic energy of a few kiloelectronvolts and are forced to follow circular trajectories around the central electrode. At the same time, they are made to oscillate along the longitudinal axis (**z**-axis in Figure 41 **(B)**) by the action of the electric field between the electrodes. The oscillation frequency "**f**" of an ion of mass "**m**" and electric charge "**z•e**" in the direction of the **z**-axis is given by equation (26):

$$f = \frac{1}{2 \cdot \pi} \cdot \sqrt{\frac{z \cdot e}{m} \cdot \frac{\partial U(r,z)}{\partial z}} \qquad (26)$$

where the factor $\frac{\partial U(r,z)}{\partial z}$ is the voltage gradient **U(r,z)** (depending on the coordinates **r** and **z**) along the **z**-direction. It can be seen from relation (26) that the oscillation frequency of the ion depends on the "**m/z**" ratio but not on the kinetic energy of the ion entering the trap, a fact that gives the "Orbitrap" a much higher resolution than other analyzers.

Figure 42 shows graphically the dependence of the axial oscillation frequency associated with a potential of -2500 V of the inner electrode as a function of the "**m/z**" ratio of the captive ion in the "Orbitrap". The alternating voltage generated by the oscillation of the ions in the direction of the **z**-axis, as perceived by the two halves of the outer electrode (Figure 41 **(B)**), is subjected to a *Fourier* transform, resulting in the mass spectrum of the ions inside the "Orbitrap".

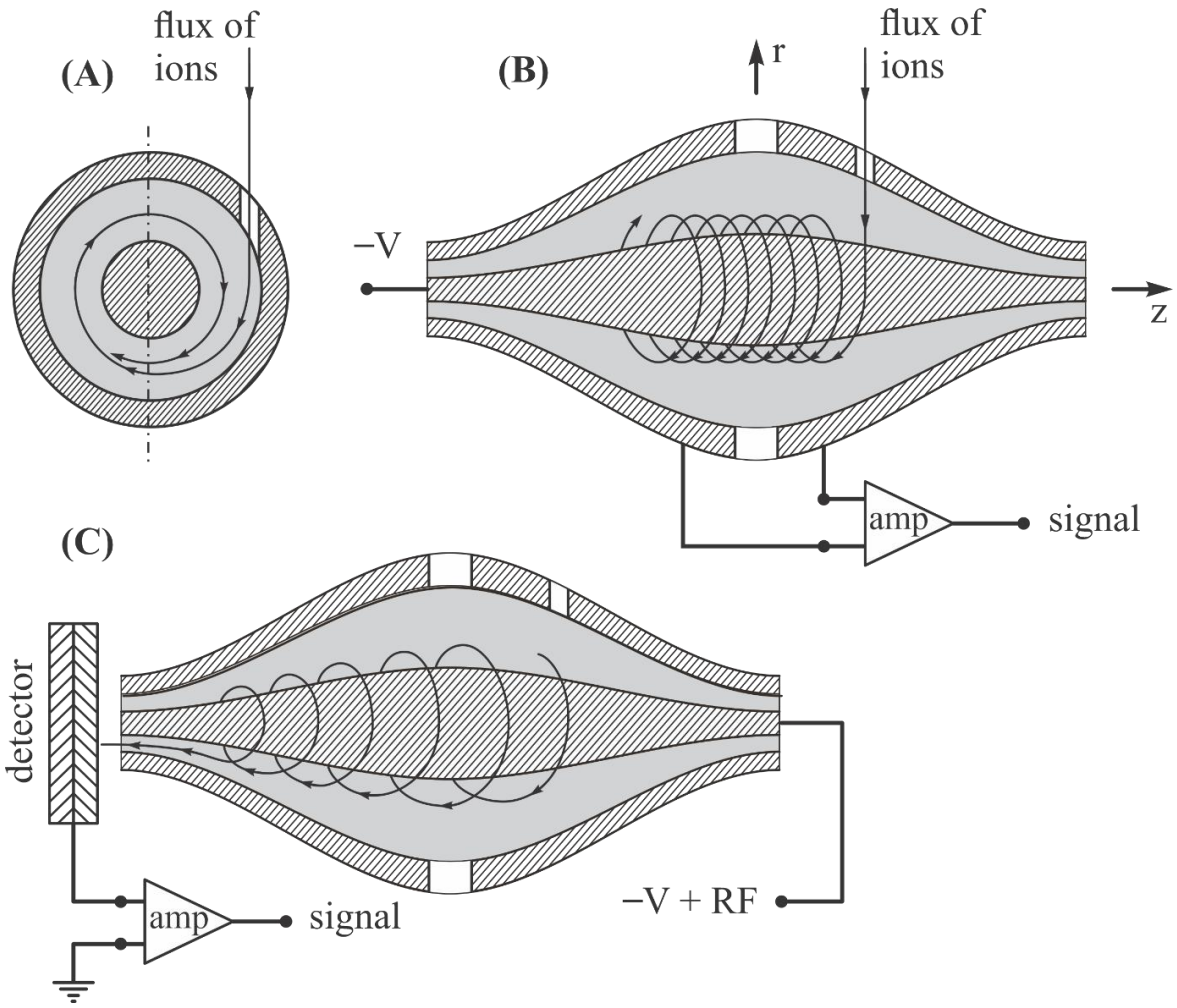



**Fig. 41 Construction details and operation of the "Orbitrap" analyzer**
**(A) transversal section and ion injection**
**(B) longitudinal section and image current detection**
**(C) mass-selective detection**

Another mode of operation is the sequential ejection of ions from the interior of the "Orbitrap" by superimposing a radio frequency (**RF**, Figure 41 **(C)**) voltage on the continuous potential (**-V**) of the central electrode. The sequentially ejected ions are directed towards the detector, which generates the final electrical signal.

Figure 42 shows the variation of the axial oscillation frequency of a positive ion as a function of the "**m/z**" ratio at -2500 V potential of the central electrode. This analyzer is of particular interest to MS analysis of biological samples because of its high resolution and high mass limit. The mass range covered by the "Orbitrap" is 50 kDa to 100 kDa. Samples of biological origin with 100 kDa, and a charge of "**z = 1**" is detectable on the "Orbitrap" analyzer. This is due to the high sensitivity of "Orbitrap" having one of the highest resolutions compared to other mass analyzers.

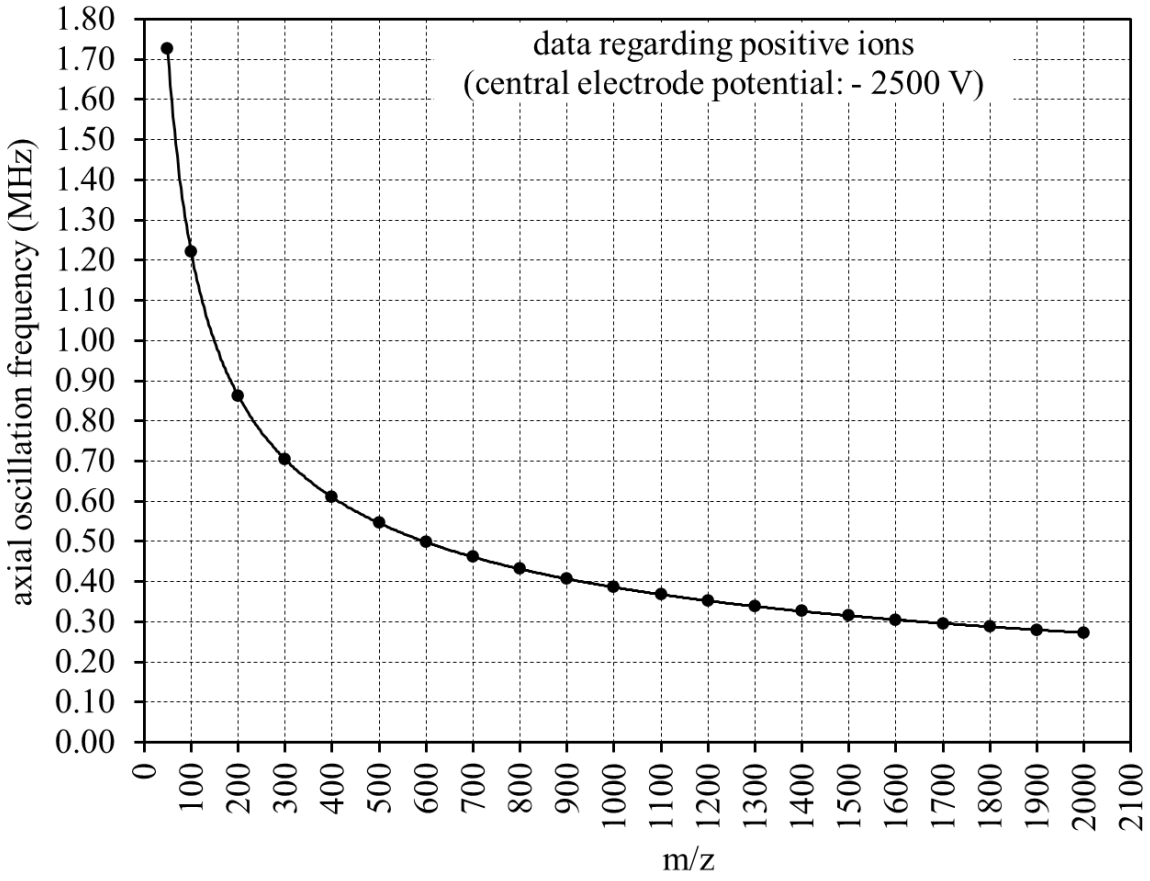



**Fig. 42 Axial oscillation frequency of a positive ion in the "Orbitrap" analyzer vs. "m/z" ratio at −2500 V potential of the central electrode**

### 2.3. Detection of the ions

The final capture of the ions arriving from the analyzer and the quantitative characterization of the ion flux is accomplished by the detector, the unit designed to convert the flow of incoming ions into an electrical signal. The simplest detector is a *Faraday* cage in which the trapped ions give up their electrical charge. The electrical current generated is passed through a high-impedance resistor, creating a potential difference across the resistor's terminals. The *Faraday* cage is still used in some designs. Early models of mass spectrometers, such as the *Mattauch-Herzog* electrostatic-magnetic analyzers (Figure 19 **(B)**), used a photographic plate as the detector. Ultimately, the function of modern detectors is to generate an electrical signal proportional to the flux of ions received.

With the development of scanning spectrometers, electron multiplier detectors were introduced (Figure 43). Their operation is based on the emission of electrons due to the collision of ions with the detector cathode ("converter" in Figure 43). The emitted electrons are accelerated toward additional electrodes, where their collisions progressively produce an increasing number of electrons (and an increasing electric

current). Inside the photomultiplier, there are additional electrodes ("dinodes" **d1**, **d2**, **d3**, etc.) that are charged to increasingly positive potentials by a series of resistors ("**R**"). The incoming ions collide with the converter electrode, emitting a flux of electrons which, after progressive acceleration, collide with the "dinodes", producing a progressively increasing current. The final current creates a potential drop between terminals **A** and **B**, which is the final signal.

In *Fourier* transform based analyzers (such as the "Orbitrap" analyzer), the useful signal is the alternating current generated by the axial oscillation of the trapped ions.

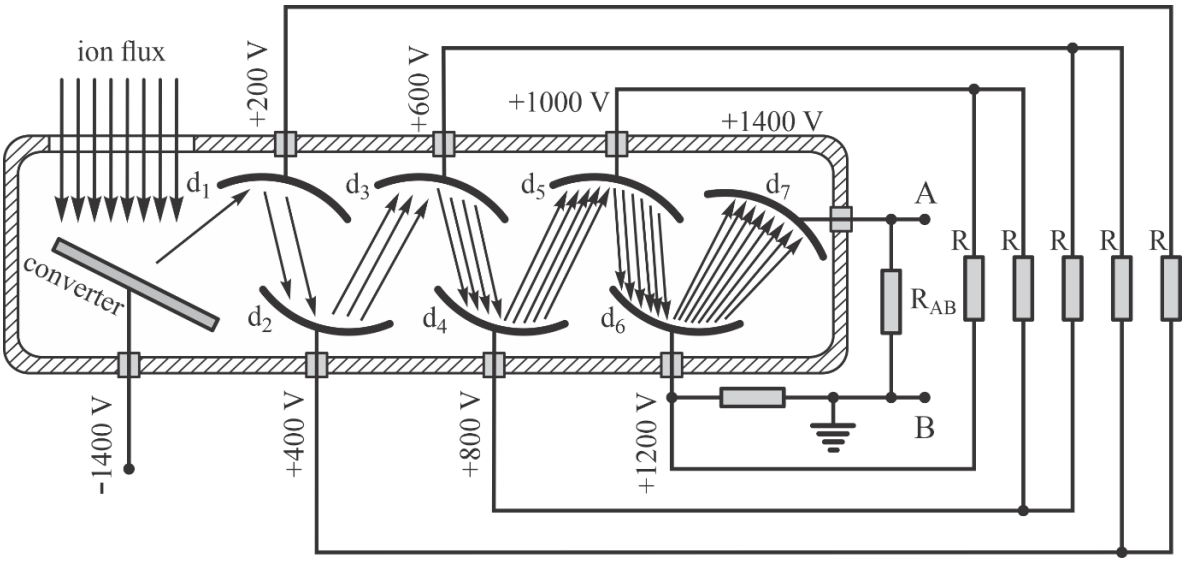



**Fig. 43 Design and operation of the electron multiplier**

## 2.4. Ion Mobility Mass Spectrometry - IMS

Ion Mobility Spectrometry separates the ion species resulting from the primary sample according to their overall mobility under the combined action of an accelerating electric field and the braking action of an inert gas countercurrent.

The global mobility of ionic species depends not only on their mass-to-charge ratio and their size and shape, but also on their effective collision cross section with the atoms of the inert gas. Thus, IMS provides information about the structure of ionic species, even distinguishing between isomeric forms. Combined with a conventional mass spectrometer, the assembly is a powerful hybrid analytical tool with applications in biochemistry, pharmaceutical chemistry or environmental pollution problems involving small polyatomic molecules, polymers, peptides, proteins or even viruses. There are three common design and operating variants of ion mobility spectrometers:

- Drift-Time Ion Mobility Spectrometry – **DTIMS**),
- High-Field-Asymmetric Waveform Ion Mobility Spectrometry – **FAIMS,**
- Travelling Wave Ion Mobility Spectrometry – **TWIMS**

### 2.4.1. Drift-Time Ion Mobility Spectrometry – DTIMS

DTIMS is the most widely used version because it is the only one that allows direct measurement of the collision cross section with the braking inert gas atoms.

Figure 44 shows the principle of DTIMS ion mobility spectrometry. Ionic species from the ion source move along a channel formed by a series of annular electrodes (Figure 44 **(A)**). An inert gas (nitrogen, argon, etc.) traverses the electrode channel in the opposite direction to the ion motion and acts to discriminatively slow the ion motion.

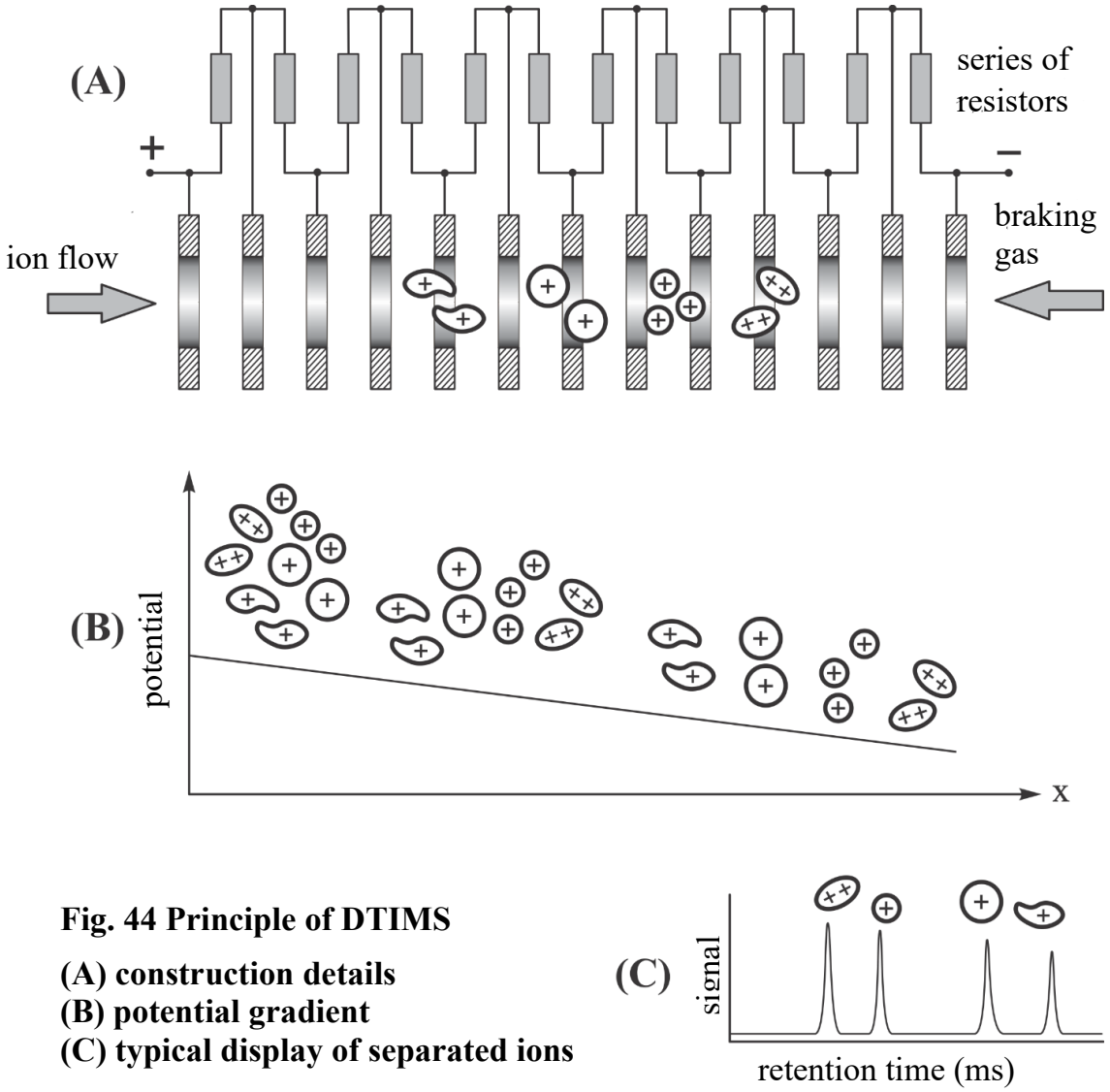



**Fig. 44 Principle of DTIMS**

**(A) construction details**
**(B) potential gradient**
**(C) typical display of separated ions**

A linear gradient of electrical potential is applied along the channel using a series of resistors. The time taken to travel through the channel depends on the mass and electrical characteristics of the individual ions, but also on the efficiency of their collision with the brake gas. The final information from the analysis is therefore the time taken to travel the length of the annular electrodes channel (Figure 44 **(B)** and **(C)**). The required time interval '**t**' is expressed by the equation (27).

$$t = \frac{L}{K_o} \cdot \frac{T_o}{T} \cdot \frac{p}{p_o} \cdot \frac{1}{V} + t_o \qquad (27)$$

where "**L**" is the length of the annular electrodes channel, "**p**" and "**T**" are the actual pressure and the actual absolute temperature of the brake gas respectively, $\mathbf{p_o}$ is the atmospheric pressure, 1 atm (101.325 kPa), $\mathbf{T_o}$ = 0 $^{o}$C (273.15 K), "**V**" is the continuous electric voltage applied to the ends of the resistive battery that ensures the formation of the potential gradient, "$\mathbf{t_o}$" is the time interval that the ion spends outside the annular electrodes channel and "$\mathbf{K_o}$" is the quantity that characterizes the effective collision section between the ion and the atoms of the brake gas. The spectrum is obtained by scanning the voltage value "**V**". The ion mixture is injected into the DTIMS analyzer in discrete pulses.

Figure 45 **(A)** illustrates the ability of DTIMS to discriminate between two isomeric pentapeptides (containing the same set of amino acids but with opposite amino acid sequence) with different secondary structures and thus different shapes (and implicitly different effective collision cross sections). Figure 45 **(B)** shows the DTIMS separation of two hexapeptides whose primary structures differ by only two amino acids: serine or glycine at the N-terminus and serine or threonine at position 5 of the peptide chain.

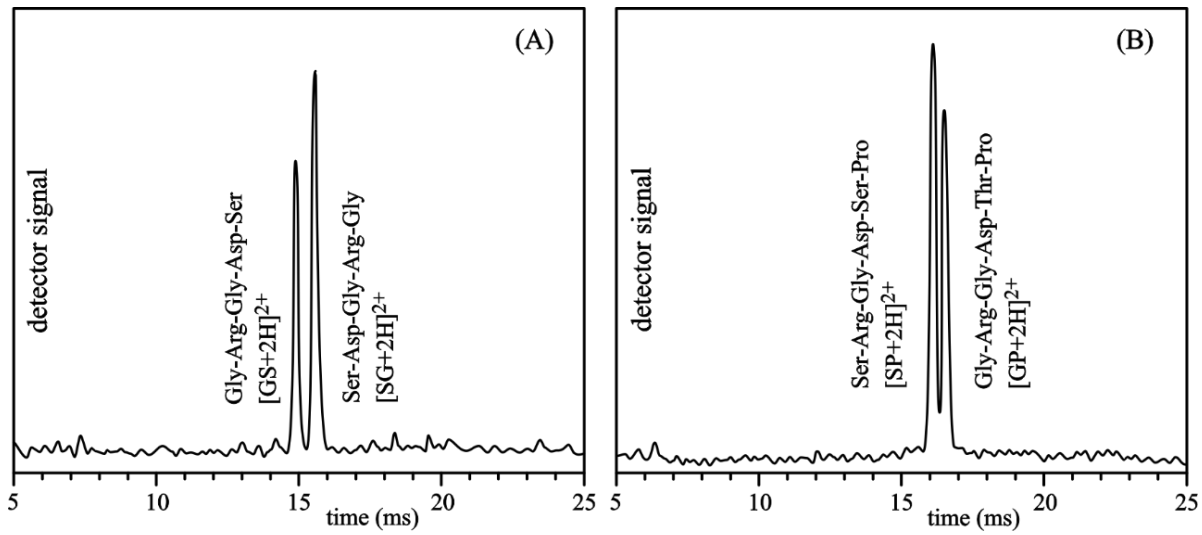



**Fig. 45 DTIMS spectra of peptide mixtures (brake gas: $N_2$ at 250$^{o}$C)**
**(after *G.A. Eiceman* and *Z. Karpas*: Ion Mobility Spectrometry Taylor & Francis Group, 2005 [ISBN: 0-203-50475-5]], Ch. 7., p.283)**
**(A) pentapeptide Gly-Arg-Gly-Asp-Ser and Ser-Asp-Gly-Arg-Gly (monitored for m/z 246)**
**(B) hexapeptide Ser-Arg-Gly-Asp-Ser-Pro and Gly-Arg-Gly-Asp-Thr-Pro (monitored for m/z 302)**

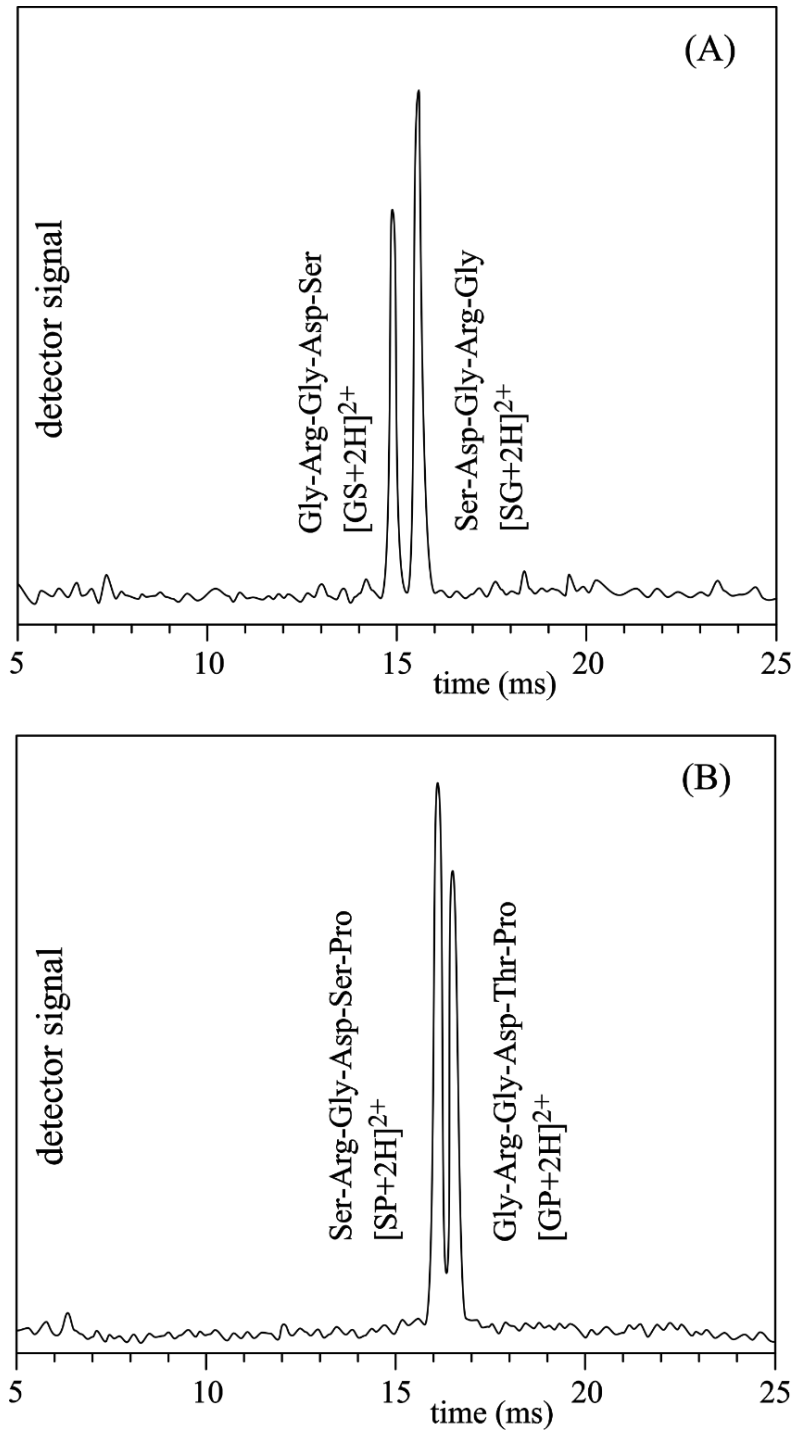



**Fig. 45 DTIMS spectra of peptide mixtures (brake gas: $N_2$ at 250$^{o}$C) (after *G.A. Eiceman* and *Z. Karpas*: Ion Mobility Spectrometry Taylor & Francis Group, 2005 [ISBN: 0-203-50475-5]], Ch. 7., p.283)**

**(A) pentapeptide Gly-Arg-Gly-Asp-Ser and Ser-Asp-Gly-Arg-Gly (monitored for m/z 246)**

**(B) hexapeptide Ser-Arg-Gly-Asp-Ser-Pro and Gly-Arg-Gly-Asp-Thr-Pro (monitored for m/z 302)**

The principle of operation is like the separation of components of a mixture by isotachophoresis or capillary electrophoresis with mobile phase countercurrent, where the driving force for the movement of ions in solution is the electrical voltage applied between the ends of the system, and the role of the brake gas in DTIMS is analogous to that of the solvent countercurrent in capillary electrophoresis. DTIMS can also be compared to the chromatographic separation of components of a mixture, where the electrical potential gradient in DTIMS is analogous to the mobile phase in the chromatographic system and the brake gas in DTIMS has the role of the stationary phase in the chromatographic column.

### 2.4.2. High-Field-Asymmetric Waveform Ion Mobility Spectrometry - FAIMS

FAIMS (High-Field Asymmetric Waveform Ion Mobility Spectrometry) separates ions based on their mobility at atmospheric pressure. This technique was developed in 1993. **[*I.A. Buryakov, E.V. Krylov, E.G. Nazarov, U. Kh. Rasulev*: A New Method of Separation of Multi-Atomic Ions by Mobility at Atmospheric Pressure Using a High-Frequency Amplitude-Asymmetric Strong Electric Field. Int. J. Mass Spectrom., Ion Process, 1993:128(3), 143-148]**

In FAIMS, ions are separated according to their mobility difference in the strong and weak electric fields (Figure 46 **(A)**). Figure 46 **(B)** shows the typical path of a positive ion, which has increased mobility when the strong electric field is applied (with increased deflection in one direction) and decreased mobility when the weak electric field is applied (with limited deflection in the opposite direction), perpendicular to the path of the carrier gas. When the sequence of weak and strong fields is cyclically repeated, the displacements of the ion toward one of the electrodes are added up. To allow a particular ion to pass through the analyzer, a compensation potential, **CP**, specific to that ion, is applied to one of the electrodes, counteracting the summation of its displacements (Figure 46 **(C)**). Changing the compensation potential opens the analyzer to different ions. The spectrum is the graphical representation of the detector signal as a function of the current value of the compensation potential (Figure 46 **(D)**). Unlike DTIMS, FAIMS allows the ion mixture to be continuously injected into the analyzer. The operation of this analyzer is like a quadrupole analyzer that is transparent to only one selected ion at a time. Because ion mobility also depends on the geometric shape of the ion, FAIMS can separate the isomeric structures of an ion.

Figure 47 shows the separation of the positional isomers of phthalic acid. The separation was performed in negative working mode using a mixture of 5 % carbon dioxide and 95 % nitrogen as the carrier gas.

FAIMS can even distinguish ionized diastereoisomers. Figure 48 shows the FAIMS spectra of $\mathbf{[M+H]^+}$ positive ions, and Table 4 shows the compensation potentials (**CP** expressed in volts) for six ephedrine derivatives.

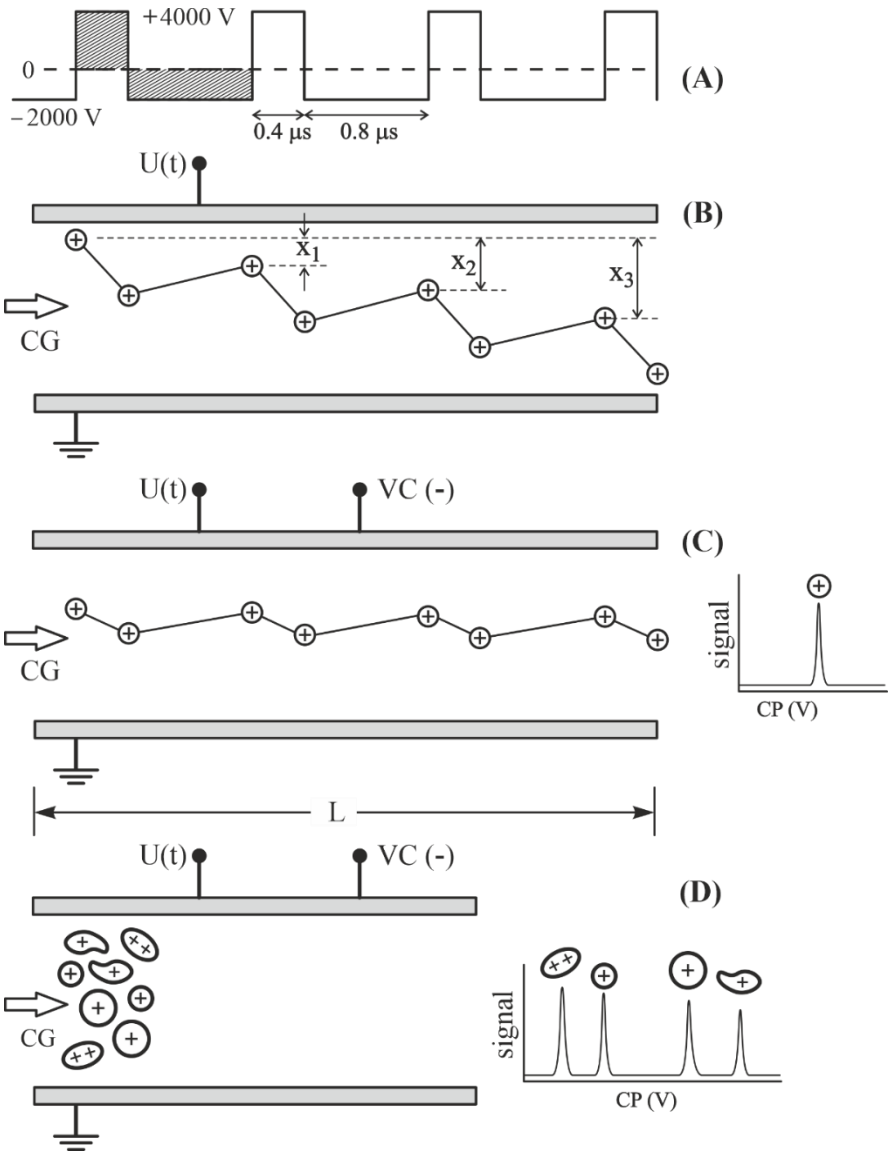



**Fig. 46 Principle of FAIMS**

**Table 4 FAIMS compensation potentials for the detection of *Ephedra* alkaloids (after *M.A. Cooeye, L. Ding, G.J. Gardner, C.A. Fraser, J. Lam, R.E. Sturgeon, Z. Mester*, Anal. Chem., 2003:75(11), 2538-2542)**

| *Ephedra* alkaloid | **m/z** $[M+H]^+$ | Compensation potential (**CP**) (**V**) |
|---|---|---|
| (-)-ephedrine | 166 | -4,47 |
| (+)-pseudoephedrine | 166 | -5,76 |
| (-)-norephedrine | 152 | -4,84 |
| (+)-norpseudoephedrine | 152 | -6,25 |
| (-)-methylephedrine | 180 | -2,46 |
| (+)-methylpseudoephedrine | 180 | -2,89 |

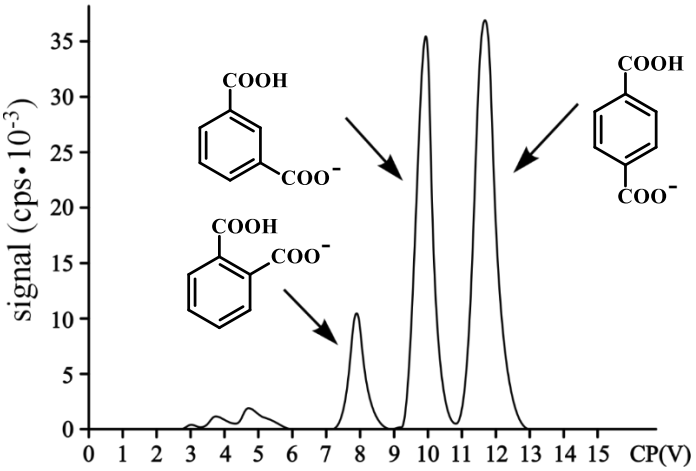



**Fig.47 FAIMS separation of phthalic acid isomers**
**(after *D.A. Barnett, R.W. Purves, B. Elis, R. Guevrement*: Separation of *o*-, *m*- and *p*-phthalic acids by High-Field Asymmetric Waveform Ion Mobility Spectrometry (FAIMS) Using Mixed Carrier Gases. J. Mass. Spectrom., 2000:35(8), 976-980)**

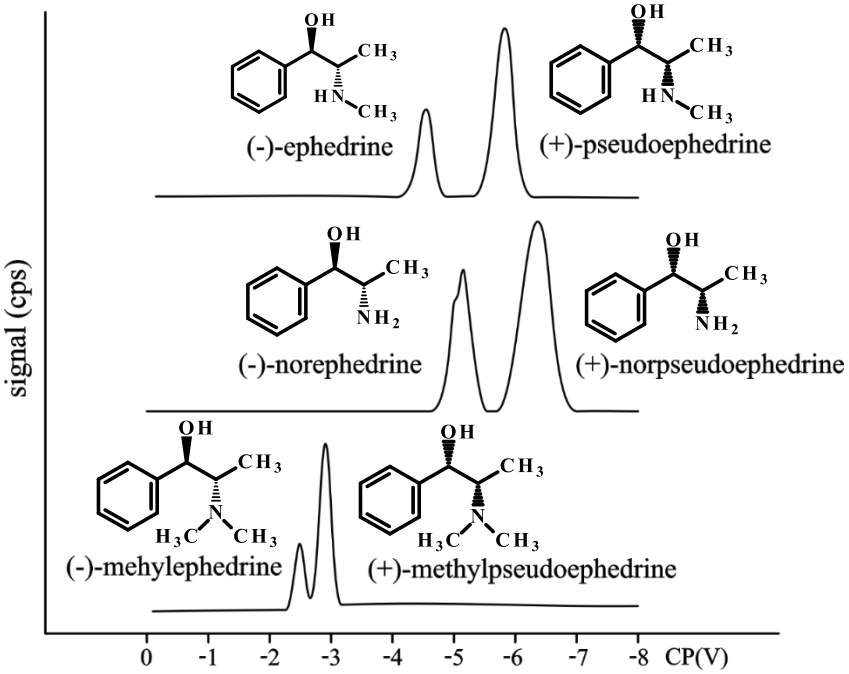



**Fig. 48 FAIMS discrimination of *Ephedra* alkaloids**
**(*M.A. Cooeye, L. Ding, G.J. Gardner, C.A. Fraser, J. Lam, R.E. Sturgeon, Z. Mester*: Separation and Quantification of the Stereoisomers of *Ephedra* Alkaloids in Natural Health Products Using Flow Injection-Electrospray Ionization-High Field Asymmetric Waveform Ion Mobility Spectrometry-Mass Spectrometry. Anal. Chem., 2003:75(11), 2538-2542, and *R. Gouevremont*: High Field Waveform Ion Mobility Spectrometry: A New Tool for Mass Spectrometry. J. Chromatogr. A. 2004:1058(1-2), 3-19)**

### 2.4.3. Travelling Wave Ion Mobility Spectrometry - TWIMS

The TWIMS analyzer consists of a series of ring electrodes connected to a high frequency voltage source (**RF** in Figure 49 **(A)**) superimposed on a continuous potential drop generated by a resistive battery (**R**). The result is the formation of a waveform train that carries the analyzed ions along the axial direction of the electrode assembly.

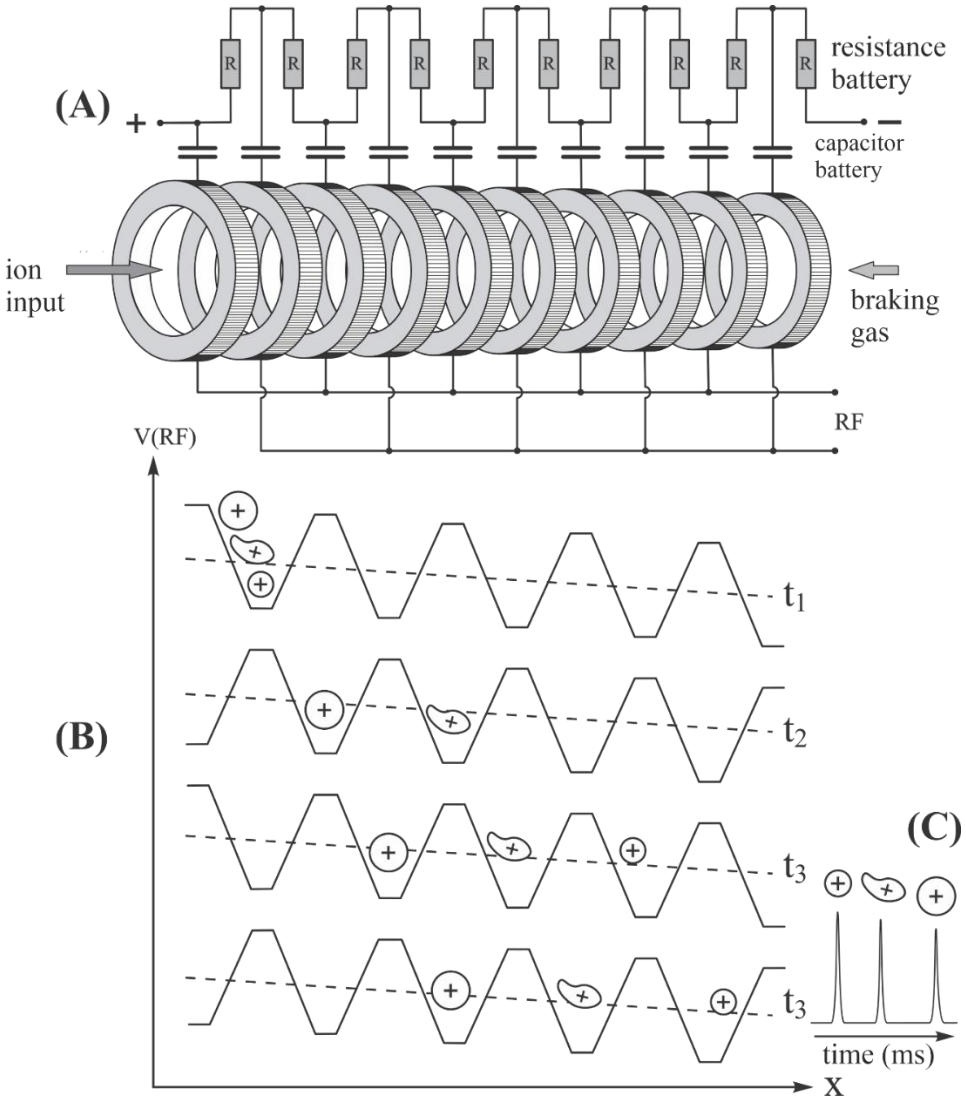



**Fig. 49 Principle of TWIMS**

The ion train is selectively braked, depending on the effective collision cross section, by a braking gas current (atomic or molecular) introduced in the opposite direction to the ion motion. The displacement of the ions is caused by the concerted action of a continuous potential drop and a radio frequency (**RF**) voltage waveform applied to the electrodes, creating a half-periodic phase difference between two adjacent electrodes ($\pi$ radians, Figure 49 **(B)**). The principle is like the chromatographic separation of components in a mixture: the electrical accelerator field is analogous to the mobile phase, and the brake gas is analogous to the stationary phase of a chromatographic

system. Similarly to DTIMS, the ion mixture is introduced into the analyzer in the form of individual pulses. The result is obtained graphically by plotting the signal generated by the ions reaching the detector as a function of the time the ions spend in the ring electrode assembly (Figure 49 **(C)**).

### 2.5. Direct Analysis in Real Time - DART

DART (Direct Analysis in Real Time) uses a special primary ionization of the sample at ambient pressure, outside the vacuum space of the mass analyzer, by collision with neutral atoms in an excited electronic state (metastable state) of a suitable gas (often helium or nitrogen) heated to 200-500 $^{o}$C (process known as "*Penning* ionization"). The special feature of DART ionization is that the sample is placed outside the vacuum chamber of the analyzer, allowing the sample to be analyzed in its native state without the need for any pre-treatment (extraction, derivatization, etc.) required by other ionization methods. The specific spectrum of the sample is obtained virtually instantaneously.

DART analysis is generally not coupled with separation methods (HPLC, gas chromatography, capillary electrophoresis); the high specificity of component identification is ensured by the high resolution imposed by the analyzer used (TOF, magnetic sector, orbitrap), since all sample components are ionized simultaneously.

The ions released from the sample are accelerated towards the capillary inlet of the analyzer module by an extraction and acceleration voltage of the order of tens of volts. Figure 50 shows a simplified longitudinal section of the DART ion source.

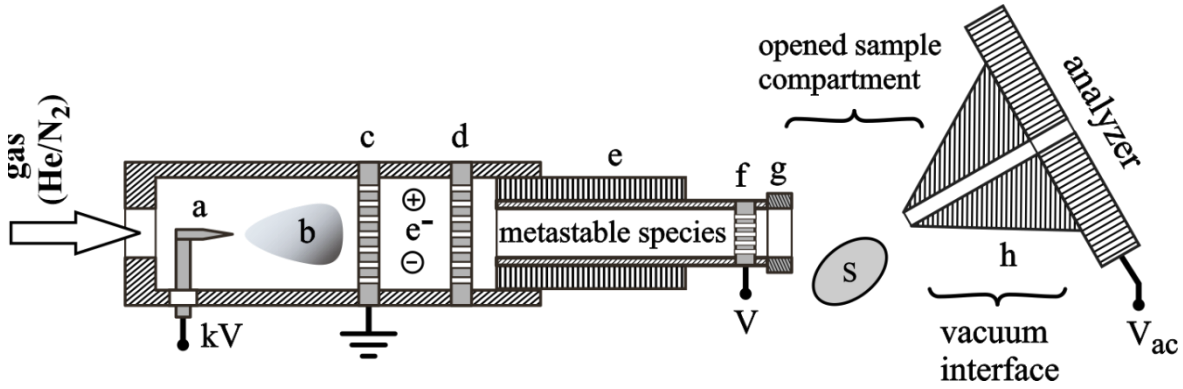



**Fig 50 Longitudinal section of the DART ion source**

The neutral gas (He or $N_2$) passes close to an electrode with a sharp tip (**a**) under a voltage of the order of kilovolts, forming a cloud of atoms in an excited electronic (metastable) state (**b**). Collisions with other atoms can produce not only neutral metastable species but also ionized atoms of the gas together with free electrons. The electrically charged species are trapped by the perforated electrode (**c**) connected to ground (zero electrical potential) and only the neutral metastable species continue their way to the zone (**e**) heated to 200-500 $^{o}$C. After passing through a second perforated elec-

trode (**f**), the metastable neutral species reach the surface of the sample (**s**) after passing through the electrically isolated hole (**g**).

Positive and negative ions specific to the sample are released from the surface of the sample placed in the open space. Depending on the polarity (positive or negative) of the capillary hole (**h**), the accelerating voltage $\mathbf{V_{ac}}$ introduces the positive or negative ions into the spectrometer analyzer.

In the positive ion mode, the energy of the excited neutral He atoms or $N_2$ molecules forms the protonated molecular ion $\mathbf{[M+H]^+}$. The helium atoms are used in the following processes after the transition from the fundamental electronic singlet state ($1^1S$) to the excited triplet state ($2^3S$) in the presence of atmospheric water.

$$He(1^1S) \xrightarrow{\text{energy form (a)}} He(2^3S) \quad \text{process in the DART ionization unit}$$

$$He(2^3S) + H_2O \longrightarrow H_2O^{\bullet +} + He(1^1S) + e^-$$

$$H_2O^{\bullet +} + H_2O \longrightarrow H_3O^+ + HO^{\bullet}$$

$$H_3O^+ + nH_2O \longrightarrow [(H_2O)_{n+1}H]^+$$

$$[(H_2O)_{n+1}H]^+ + M \longrightarrow [M + H]^+ + (n+1)H_2O$$

} processes in open space

The energy of the $2^3S$ excited state of helium (19.6 eV) is sufficient to react effectively with water; therefore, DART ionization performance is not significantly affected by changes in humidity.

The ionization mechanism differs in the negative ion mode. Fast (rapid) electrons ($\mathbf{e_r}$) emitted from the electrode (**a**) are slowed down by collisions with neutral gas atoms (e.g., helium), converting them to slow electrons ($\mathbf{e_s}$).

$$e_r^- + He(1^1S) \longrightarrow e_s^- + He(2^3S)$$

The slow electrons ("$\mathbf{e_s}$") are captured by oxygen molecules in the vacuum-free space, forming oxygen anions ($O_2^-$): $e_s^- + O_2 \longrightarrow O_2^-$

The $O_2^-$ anion forms the molecular anion, $\mathbf{[M-H]^-}$, by removing a proton from the analyte molecule (M): $M + O_2^- \longrightarrow [M-H]^- + HO_2$

In negative mode, the mass spectrum of analyte M is essentially the same for $N_2$, Ne, or He. However, the detection efficiency depends on the choice of inert gas because the *Penning* ionization efficiency varies in the following order: $N_2 < Ne < He$.

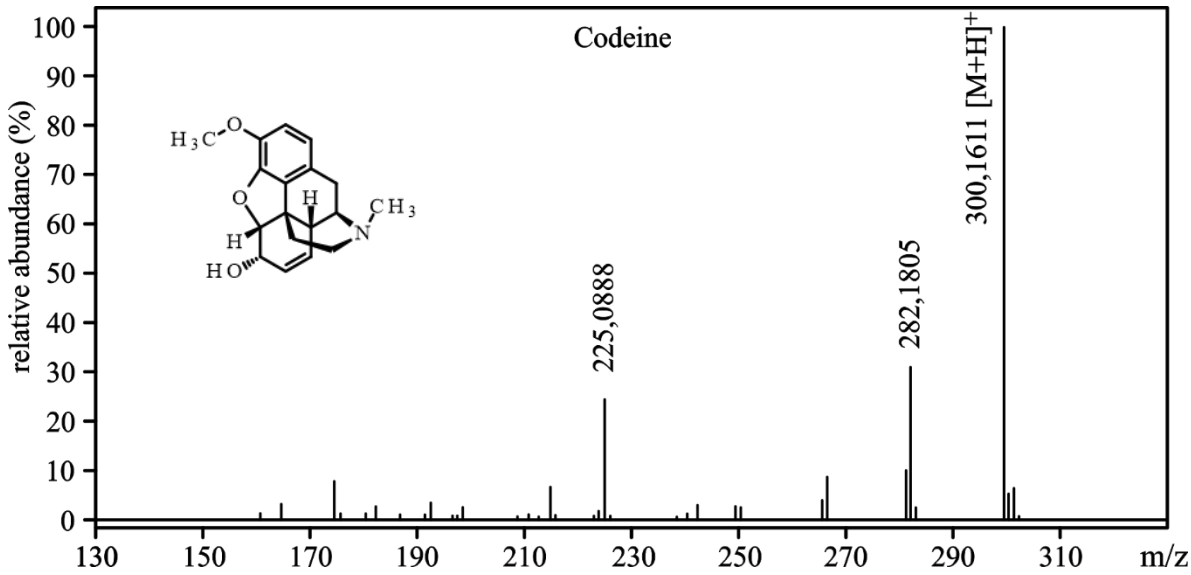
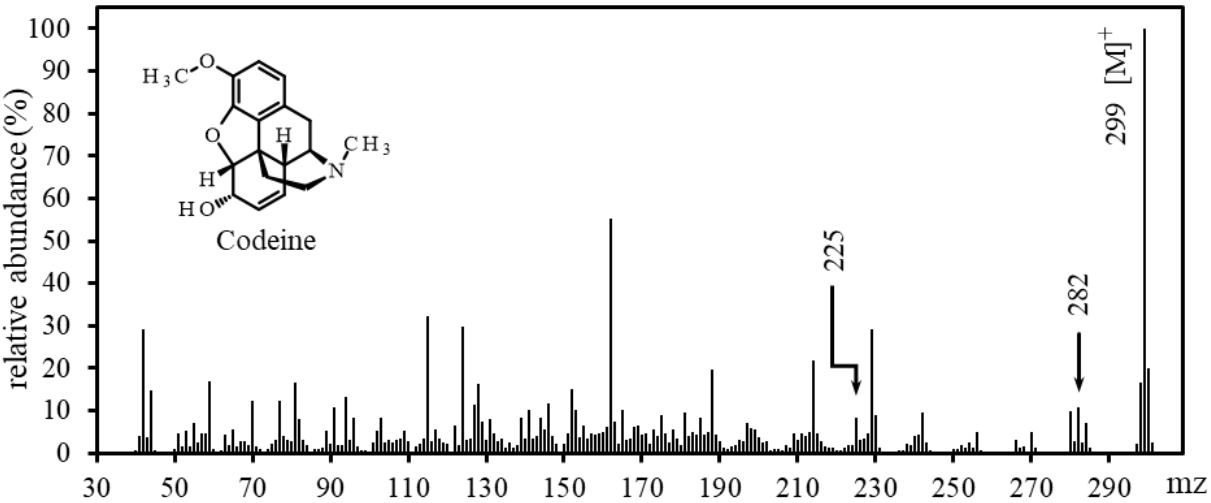



**Fig. 51 DART spectrum of codeine (after *A.D. Lesiak, J.R.E. Shepartd*: Recent Advances in Forensic Drug Analysis by DART-MS. Bioanalysis 2014:6(6), 819-842)**




**Fig, 52 Mass spectrum of codeine with 70 eV EI ionization (rebuilt from digitized NIST data, nr. 335560)**

In addition to analyzing high-molecular-weight compounds such as proteins and polypeptides, DART is also useful for identifying and quantifying low-molecular-weight compounds such as pharmaceuticals, illicit drugs, athletic performance-enhancing drugs, forensic substances, explosives, and drug metabolites.

Because of the limited fragmentation, DART spectra are easier to interpret than those obtained by more vigorous ionization techniques such as Electronic Impact Ionization (EI). Mass spectra of codeine obtained by DART and EI ionization techniques are compared in Figures 51 and 52. It is evident that the analyte undergoes more significant fragmentation during EI ionization.

Table 5 provides a list of the ionized forms of non-polar and medium-polar molecules ("**M**") after DART ionization in both the positive and negative modes of operation.

**Table 5 Ions formed often during DART ionization.**

| | Common ionic species in positive working regime | Common ionic species in negative working regime |
|---|---|---|
| non-polar molecule (**M**) | $M^{\bullet+}$ ; $[M+H]^+$ ; $[M+O+H]^+$ | $M^{\bullet-}$ ; $[M-H]^-$ ; $[M+O_2-H]^-$ ; $[M+O_2]^{\bullet-}$ ; $[M+Cl]^-$ |
| molecule (**M**) with medium polarity | $[M+H]^+$ ; $[M+O+H]^+$ ; $[M+NH_4]^+$ | $[M-H]^-$; $[M+OH]^-$ ; $[M+CN]^-$ ; $[M+Cl]^-$ |

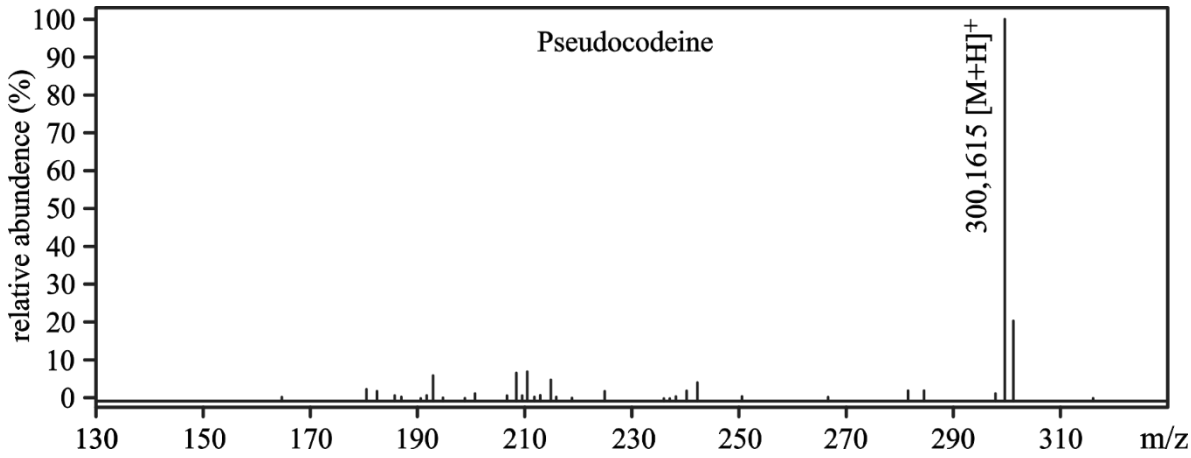



**Fig. 53 DART spectrum of pseudocodeine (after *A.D. Lesiak, J.R.E. Shepartd*, Bioanalysis 2014:6(6), 819-842)**

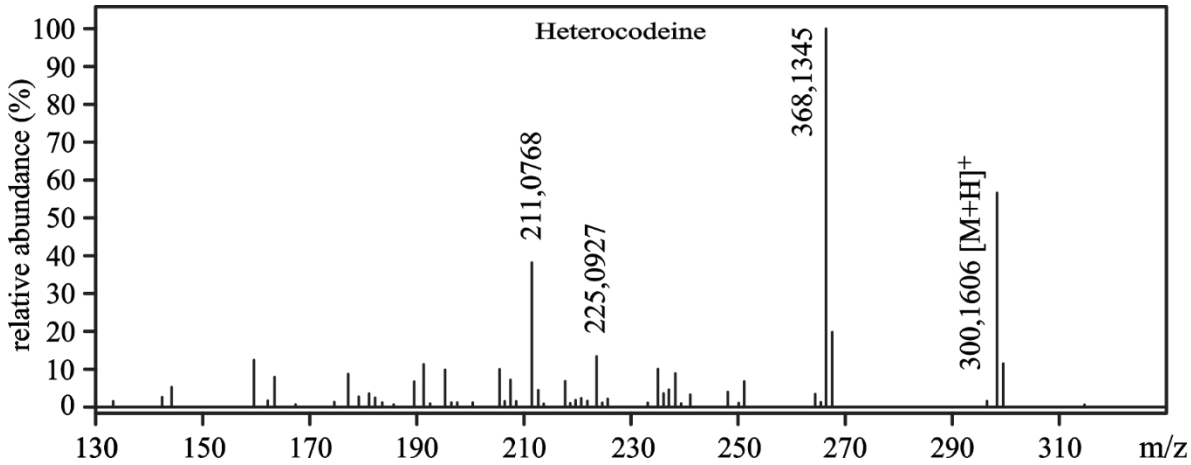



**Fig. 54 DART spectrum of heterocodeine (after *A.D. Lesiak, J.R.E. Shepartd*, Bioanalysis 2014:6(6), 819-842)**

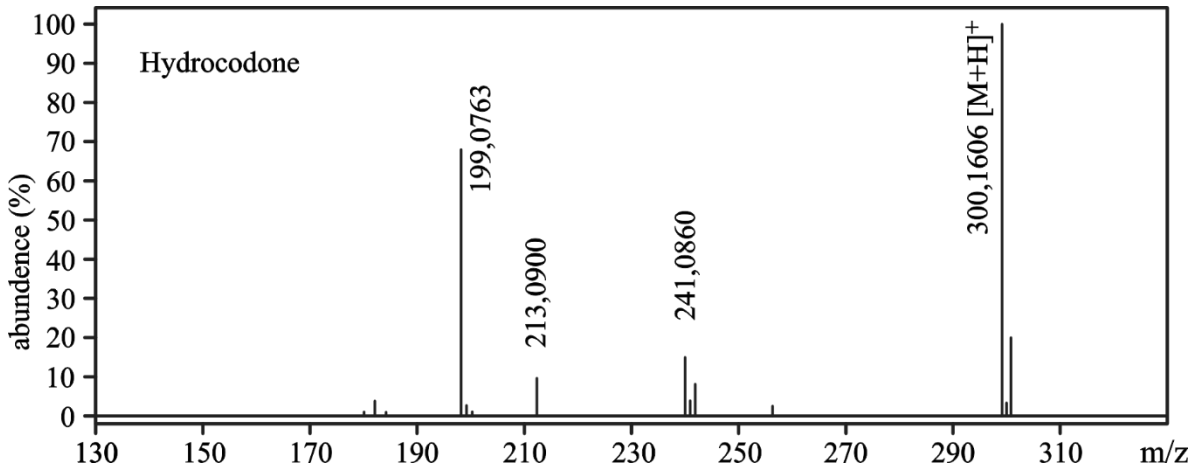



**Fig. 55 DART spectrum of hydrocodone**
**(after *A.D. Lesiak, J.R.E. Shepartd*: Recent Advances in Forensic Drug Analysis by DART-MS. Bioanalysis 2014:6(6), 819-842**

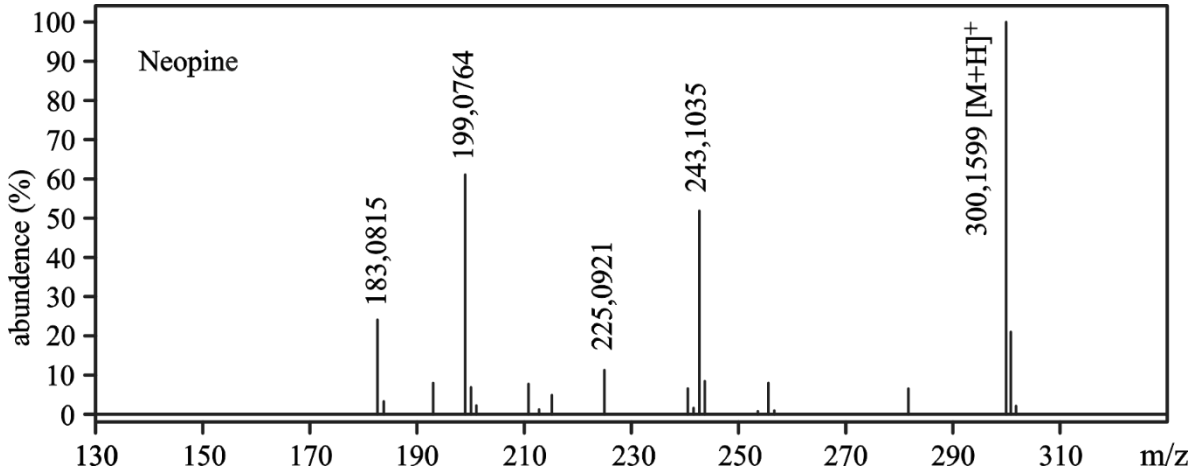



**Fig. 56 DART spectrum of Neopine**
**(after *A.D. Lesiak, J.R.E. Shepartd*, Bioanalysis 2014:6(6), 819-842)**

Figures 53 to 56 show the DART spectra of pseudocodeine, heterocodeine, hydrocodone, and neopine, demonstrating only limited fragmentation of them.

### 3. Tandem chromatography - mass spectrometry analysis

The analytical potential of mass spectrometry is greatly enhanced by coupling it to an appropriate separation method. Gas-liquid chromatography, liquid-liquid chromatography, and some electrokinetic separation methods such as capillary electrophoresis and isotachophoresis are the most used methods in combination with mass spectrometry.

Figure 57 shows the functional cooperation between the chromatographic separation and mass spectrometry. In this configuration, the mass spectrometer is a dedicated detector that not only detects a component at the output of the chromatography co-

lumn, forming a chromatographic peak (**p1**, **p2**, **p3**, etc. for components **C1**, **C2**, **C3**, etc.), but also provides a unique fingerprint of each component in the form of the corresponding mass spectrum (**MS(C1)**, **MS(C2)**, **MS(C3)**, etc.). In addition to separation, chemical component identification is also achieved with a high degree of confidence.

Depending on the analyzer setting of the mass spectrometer, the chromatogram can show all ions formed during the ionization of the components coming from the chromatographic column (Total Ion Chromatography, "**TIC**") or only some selected ions (Selected Ion Monitoring, **SIM**, - Selected Reaction Monitoring, **SRM** - Multiple Reaction Monitoring **MRM**, - Neutral Loss Monitoring, **NLM**).

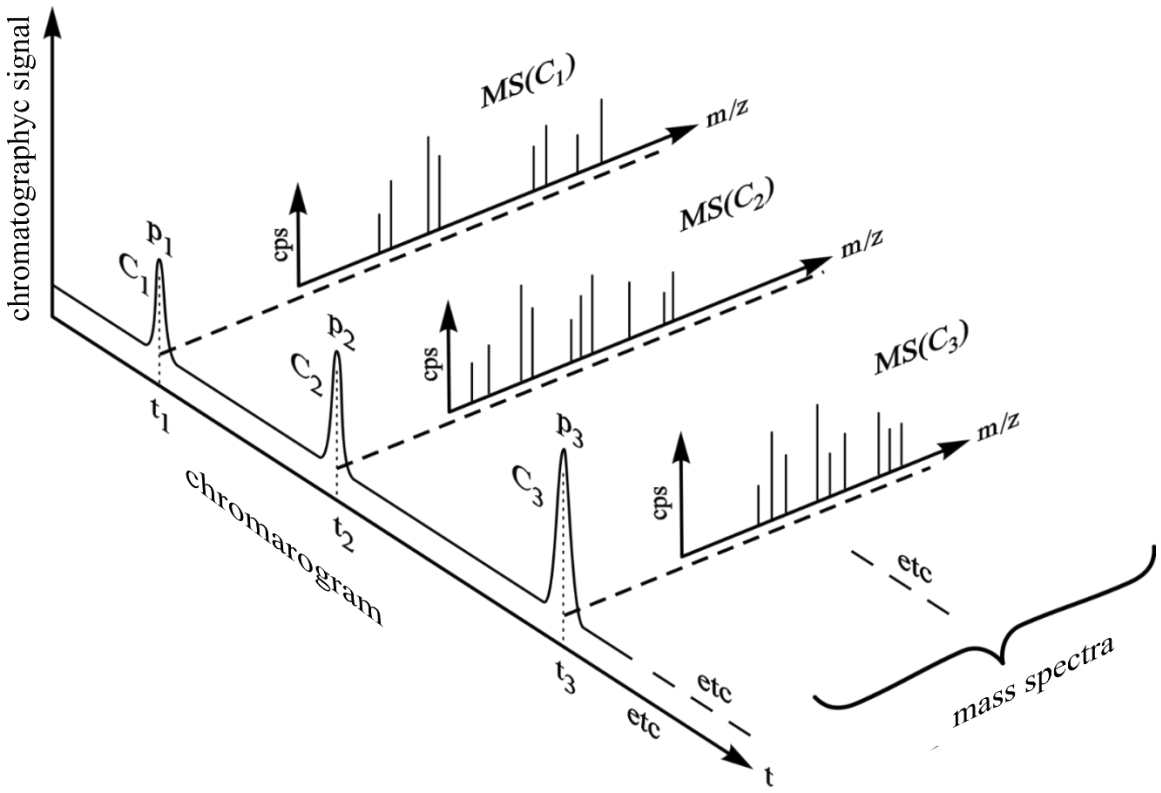



**Fig. 57 The logistical link between chromatography and mass spectrometry.**

### 3.1. Total Ion Chromatogram – TIC

The simplest mode of operation of the chromatograph-mass spectrometer assembly is to ionize the effluent from the chromatographic column and detect all the resulting ions. The mass spectrometer analyzer is transparent to all **m/z** values within a predetermined limit and works as a universal detector, able to respond non-specifically to all components, etc. of the analyzed mixture (Figure 58). The advantage of the TIC regime lies in the small volume of software resources involved in data storage.

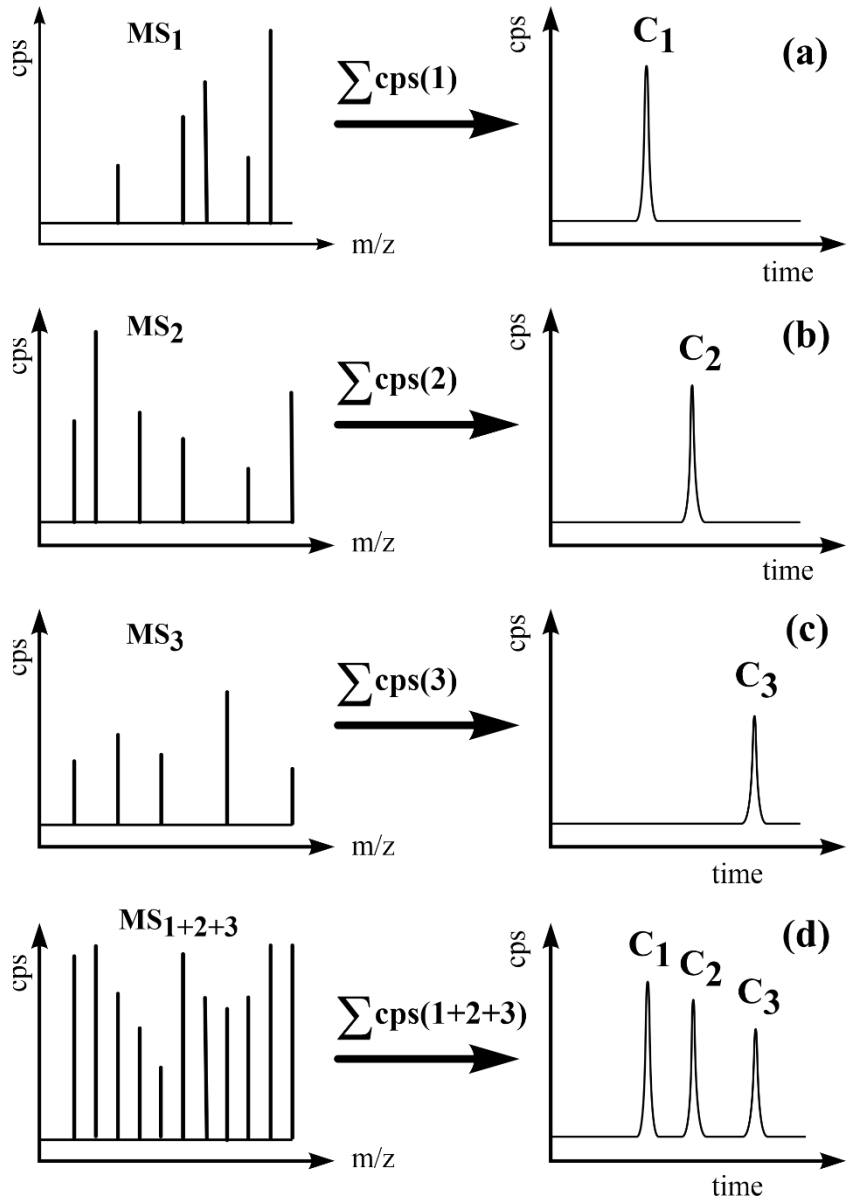



**Fig. 58 TIC analysis scheme**

If the analyzed sample contained only component **C1**, it would give the individual mass spectrum $MS_1$, and by summing the signals (**∑cps(1)**, Fig. 58 **(a)**) would result in a single **C1** peak in chromatogram **(a)**. If only the **C2** component were to leave the chromatographic column, it would produce the individual mass spectrum **MS2**, and by summing its signals ((**∑cps(2)**, Figure 58 **(b)**), the single peak (**C2**) would appear in the chromatogram **(b)**. The single component **C3** would be characterized by the individual mass spectrum **MS3** and by summing the signals (**∑cps(3)**, (Figure 58 **(c)**) will lead to the unique **C3** "peak" in the chromatogram. **(c)**. In the TIC mode, the data pro-

cessing software sums the signals (cps - "count per second", (**∑cps(1+2+3)**,) from all the individual mass spectra in every moment of the chromatographic process, generating the reunited (amounted) mass spectrum (**$MS_{1+2+3}$** and the TIC chromatogram contains all of the "peaks", (**$C_1$**, **$C_2$**, **$C_3$**, Figure 58 **(d)**).

### 3.2. Selected Ion Monitoring – SIM

The specificity of combined chromatography/MS (GC/MS or HPLC/MS) analysis can be enhanced by limiting the transparency of the MS analyzer to the selected ion(s) with the preferred **m/z** ratio. Thus, only those components appear as peaks in the resulting chromatogram that, after ionization, contain in their individual mass spectrum the ion(s) of the selected **m/z** ratio(s).

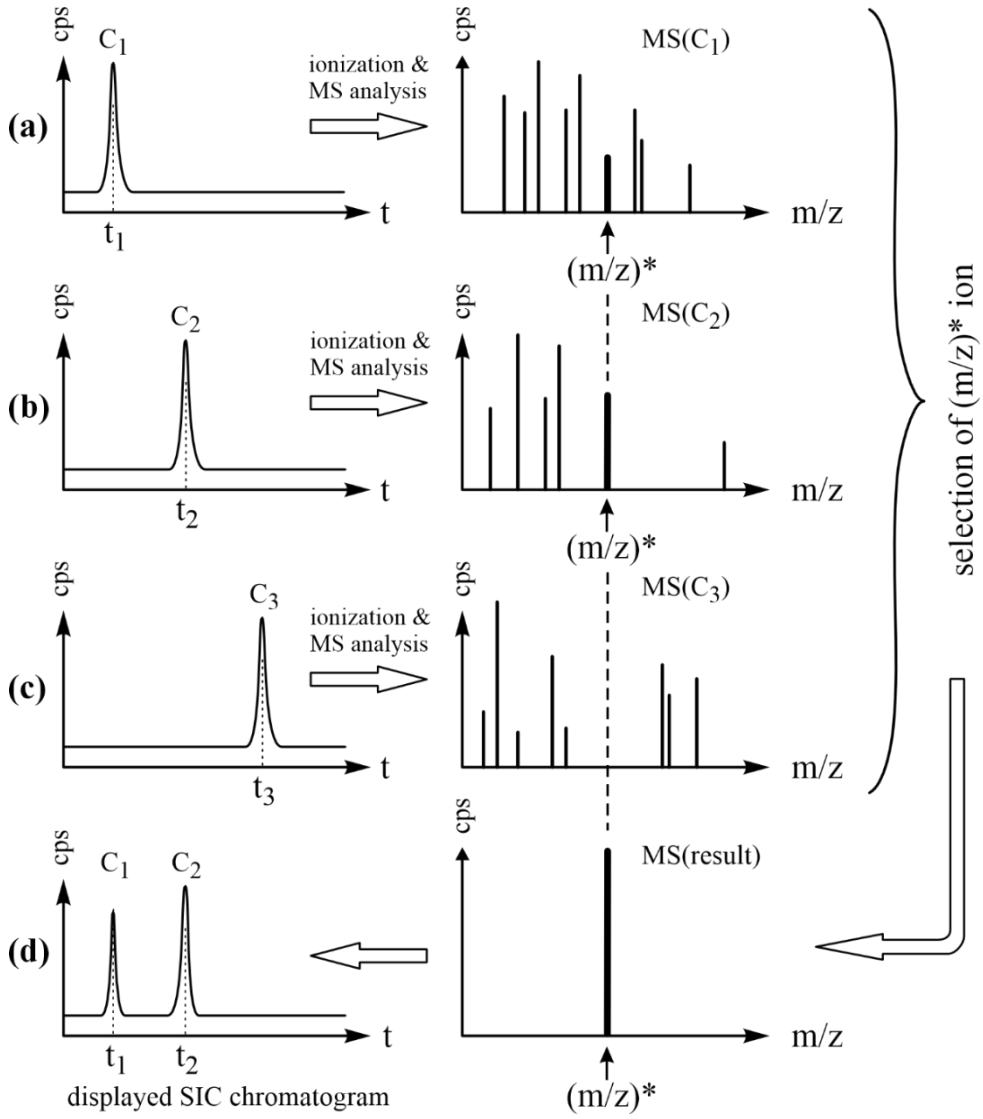



**Fig. 59 SIC analysis scheme – selecting the ion with (m/z)* ratio**

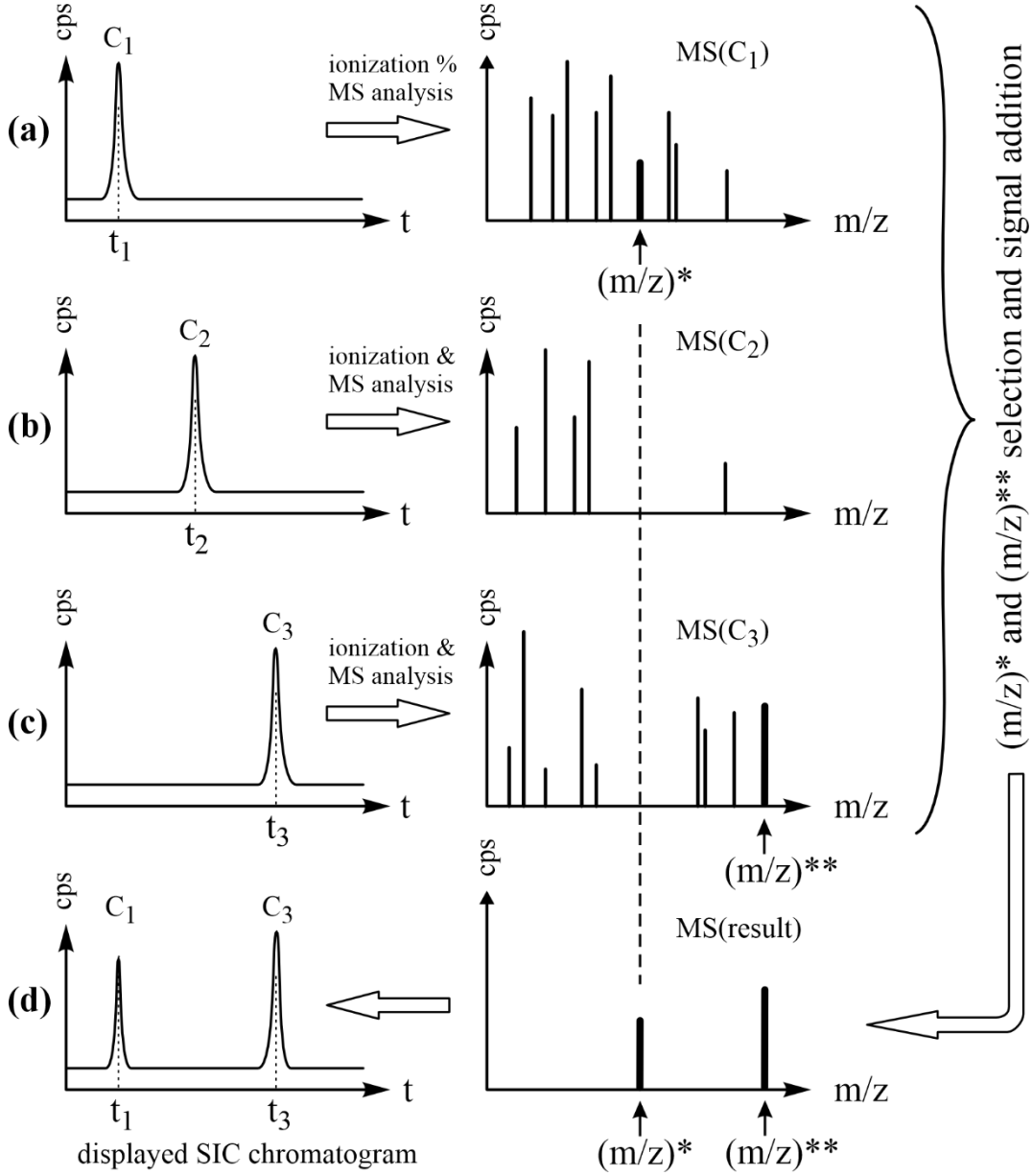



**Fig. 60 SIC analysis scheme – selecting the ions with (m/z)* and (m/z)** rations**

If the retention times of two different components are identical (i.e. components that cannot be differentially detected by a universal detector) but produce different mass spectra then, by selecting the appropriate **m/z** ratio, only the component that produced the selected ion(s) after ionization will contribute to the peak in the resulting chromatogram. This method is particularly effective when the goal is not only to detect the components in the original sample, but also to determine their quantity.

Figure 59 shows the peculiarity of SIC (Selected Ion Chromatography) analysis. If the analyzed sample contained only component **C1**, the individual mass spectrum

would be **MS($C_1$)** (Figure 59 **(a)**). If only component **$C_2$** would leave the chromatographic column, it would generate the individual mass spectrum MS**($C_2$)** (Figure 59 **(b)**), and the individual component **$C_3$** would be characterized by the individual mass spectrum **MS($C_3$)** (Figure 59 **(c)**), and so on.

In SIC mode the analyzer selects from all the individual mass spectra only the signal with the selected **(m/z)*** ratio and in the chromatogram only the peaks of the components which, after ionization, produce the ion with the selected **(m/z)*** ratio (Figure 59 **(d)**) is displayed. In the example in Figure 59 the displayed chromatogram does not show the component **$C_3$** because it did not produce the ion with the selected **(m/z)*** ratio.

To further increase the selectivity of the detection, the data processing software algorithm allows multiple ion selection. Figure 60 shows the essence of the analysis when selecting an ion pair (**(m/z)*** and **(m/z)****). Component **$C_1$** produces (among others) the selected ion with the **(m/z)*** ratio and component **$C_3$** produces the selected ion with the **(m/z)**** ratio. Ionization of component **$C_2$** does not produce any of the selected ions. Consequently, only the peaks of components **$C_1$** and **$C_3$** appear in the chromatogram without the peak of component **$C_2$**. If, at retention time **$t_1$** or **$t_3$**, a component other than **$C_1$** or **$C_3$** of no analytical interest should occur by chance, the application of SIM analysis will ensure that this component no longer contributes to the signal intensity in the final chromatogram, thus ensuring the selective quantitative determination (unperturbed by this component) of the components of interest **$C_1$** or **$C_3$**.

The data processing programs of the high-performance instruments allow the selection of a larger number of ions both for the entire chromatographic separation time and for specific time intervals of the chromatographic separation process.

### 3.3. Selected Reaction Monitoring - SRM

To further increase the selectivity of component detection and the possibility of their chemical identification, different variants of $MS^2$ analysis are practiced. After sequential ionization of the components leaving the chromatographic column, a primary **$MS^1$** mass spectrum is obtained (Figure 62). To obtain a selective response for only one of the components (e.g. for **$C_1$**, Figure 62**(a)**), a suitable precursor ion (the **$pre_1$** ion) is selected and subjected to fragmentation by collision with atoms of a gas

(helium, argon, nitrogen). **Collision Induced Dissociation** (CID) fragmentation results in a second mass spectrum associated with the **$C_1$** component, **$(MS^2)_1$**.

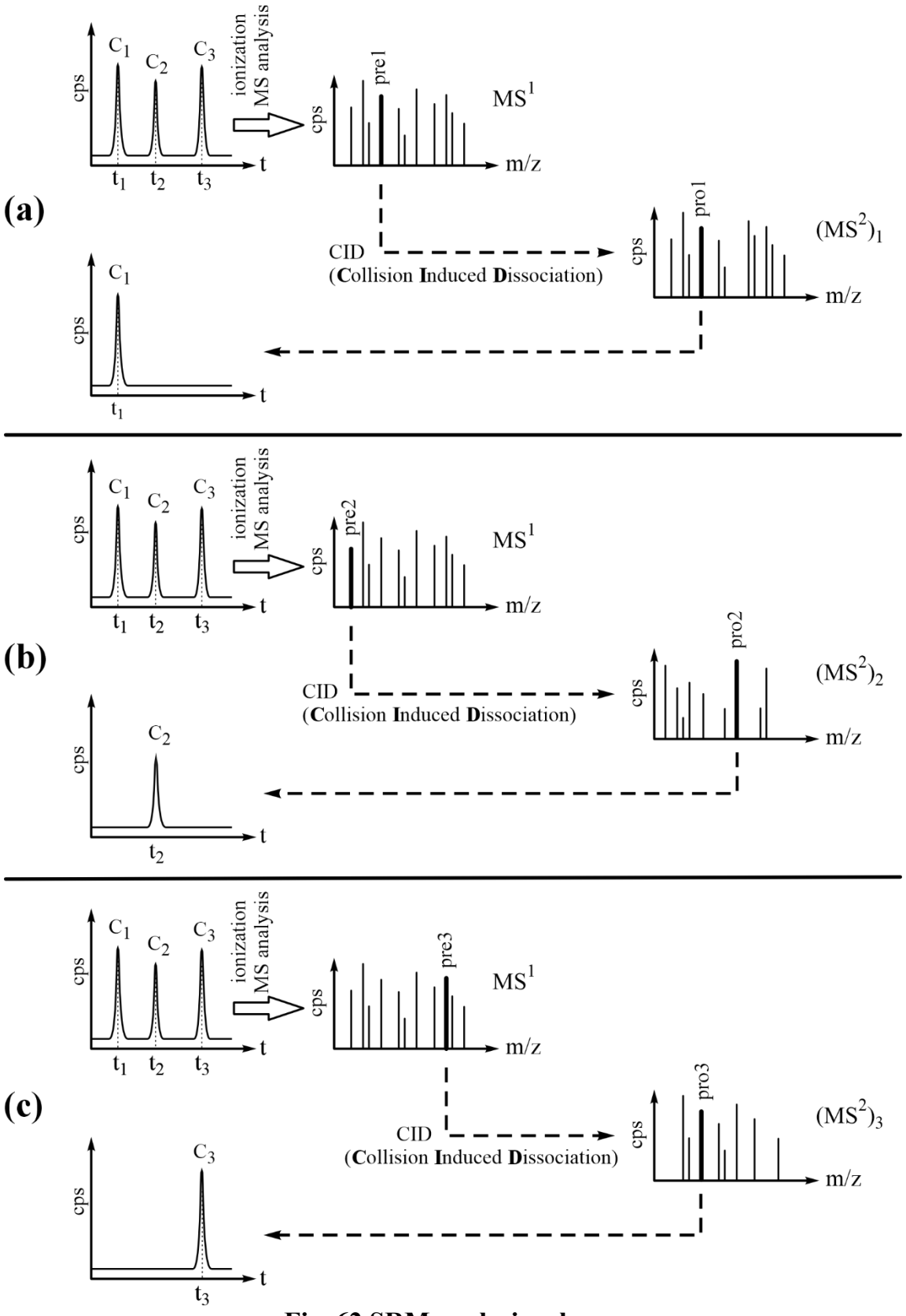



**Fig. 62 SRM analysis scheme**

From the second spectrum, a product ion (the **pro$_1$** ion) appropriate for the monitored component **C$_1$** is selected, and its ionic current is the final signal. The chromatogram shows only the peak associated with component **C$_1$**, even if other components than **C$_1$** are emerging at the end of the chromatographic column. This method guarantees twice the specificity of detection compared to methods based on a single MS analysis (TIC and SIC). With the appropriate choice of precursor (**pre$_1$** or **pre$_2$**) and product (**pro$_1$ or pro$_2$**) ion, the final response can be selective for component **C$_2$** only (Figure 62**(b)**) or for component **C$_3$** only (Figure 62**(c)**).

One variant of SRM analysis is to select several suitable precursor ions from the **MS$^1$** spectrum and/or several suitable product ions from the **MS$^2$** spectrum. This is known as Multiple Reaction Monitoring (MRM). Obviously, MRM provides even more selective discrimination of the components of interest and offers the possibility of more reliable chemical identification of sample components.

### 3.4. Neutral Loss Monitoring - NLM

Another way to increase the specificity of component identification in a chromatograph-mass spectrometer assembly is to detect the removal of electrically neutral chemical species. The mixture of chemical species leaving the chromatographic column is ionized by one of the common methods (EI, ESI, etc.), resulting in the **MS$^1$** mass spectrum characteristic either of the entire chromatographic elution process or of defined elution time intervals. The second order mass spectrum (**MS$^2$**) is generated from the **MS$^1$** mass spectrum for each selection of precursor ions. The essence of the NLM method is to select and detect ions in the **MS$^2$** spectrum whose **m/z** ratio is shifted by a constant value, lower relative to the **m/z** ratio of the selected ions in the **MS$^1$** spectrum. The shift is due to the removal of a neutral chemical species, and the chromatographic signal is the sum of the signals thus selected from the **MS$^2$** spectrum.

Figures 63**(a)** and 63**(b)** illustrate the peculiarity of the NLM detection method for selective signal display in the chromatogram. Ions from the chromatographic eluate produce the first-order spectrum, **MS$^1$**. In the example in Figure 63 **(a)**, the precursor ions **(pre)$_{a1}$**, **(pre)$_{a2}$** and **(pre)$_{a3}$**, after chemical fragmentation (CID), produce the **MS$^2$** spectrum in which the product ions **(pro)$_{a1}$**, **(pro)$_{a2}$** and **(pro)$_{a3}$** are at the same distance **$\Delta$(m/z)$_a$** from the signal of the precursor ions from which they originate due to the removal of the same neutral fragment, a process specific to the **C$_a$** component.

The chromatographic signal ('peak'), the pooled ionic current of these produced ions, is characteristic of the $\mathbf{C_a}$ component. Figure 63 **(b)** illustrates the selection of $\mathbf{(pre)_{b1}}$ and $\mathbf{(pre)_{b2}}$ precursor ions to obtain the specific chromatographic signal for the $\mathbf{C_b}$ component. Precursor ions are selected that, upon chemical fragmentation, produce $\mathbf{(pro)_{b1}}$ and $\mathbf{(pro)_{b2}}$ ions that are at the same distance $\mathbf{\Delta(m/z)_b}$ from the precursor ions from which they originate. The chromatographic "peak" signal is the combined ionic current of the $\mathbf{(pro)_{1b}}$ and $\mathbf{(pro)_{2b}}$ ions produced and is characteristic of the $\mathbf{C_b}$ component. In practice, the commonly removed neutral species are small molecules: $NH_3$, $CO_2$, CO, $H_2O$, HCOOH, $CH_3COOH$, $CH_3CN$ etc.

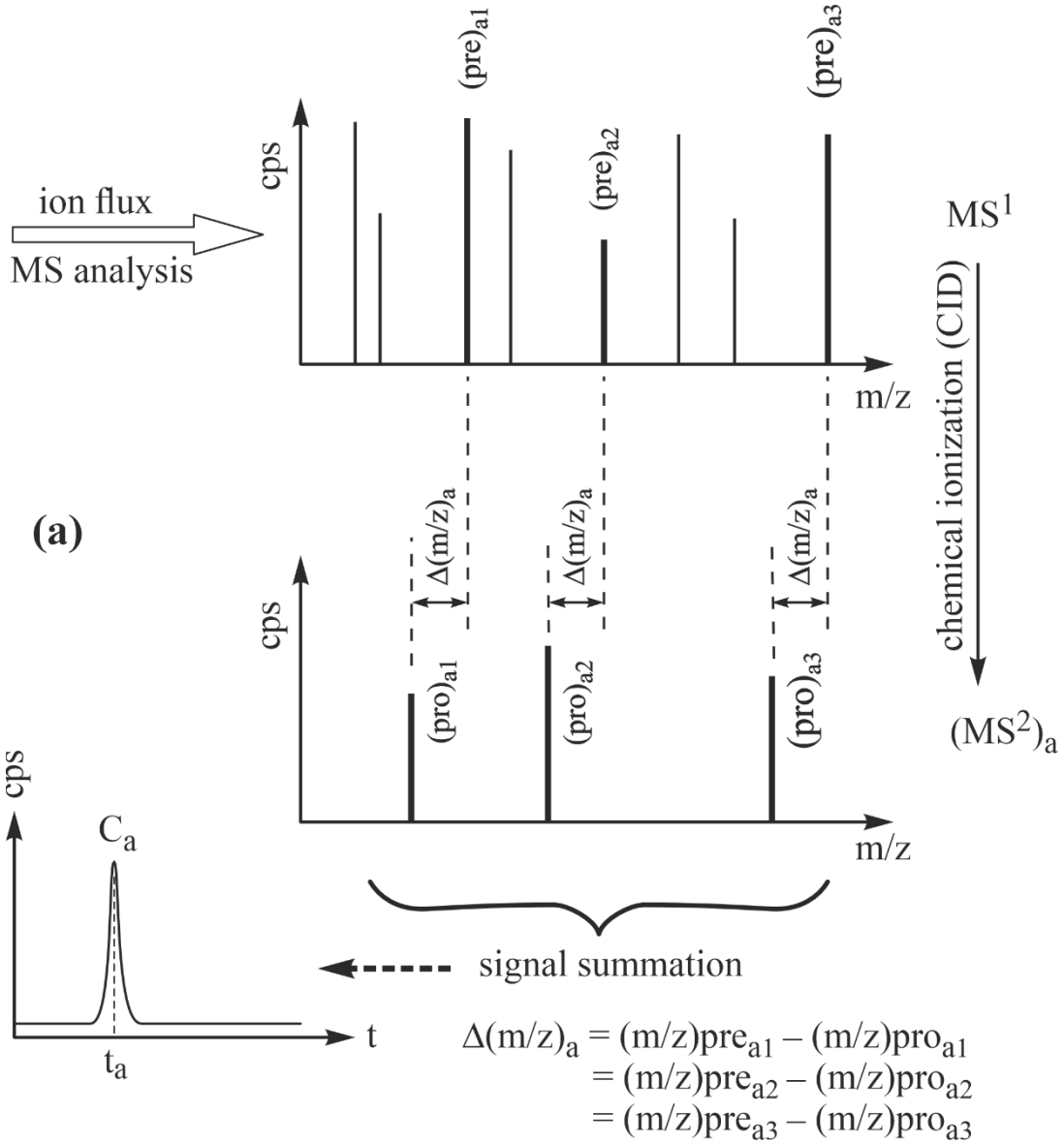



**Fig. 63 (a) The principle of "Neutral Loss Monitoring" analysis**

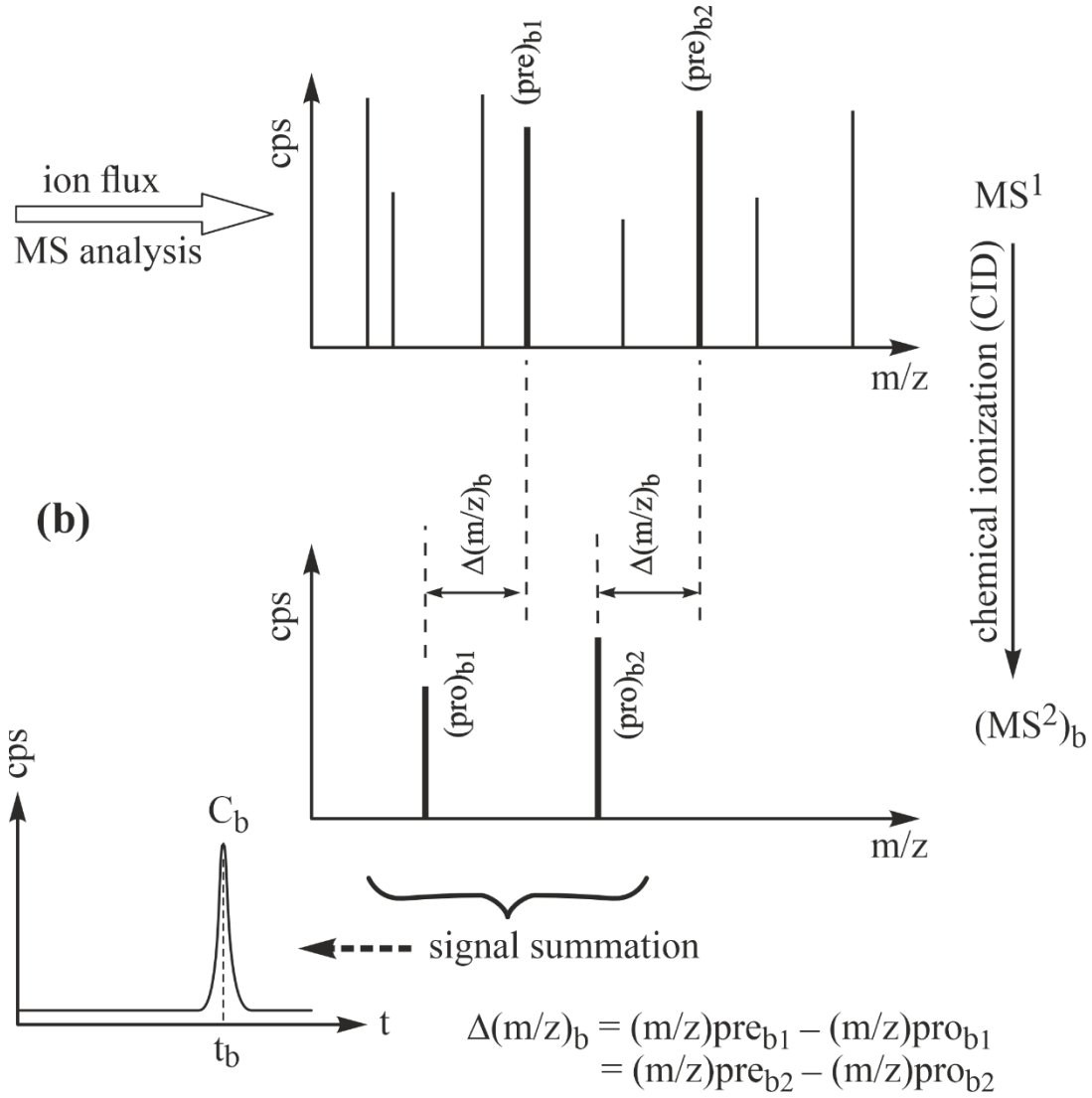



**Fig. 63 (b) The principle of "Neutral Loss Monitoring" analysis**

**4. Analytical interpretation and valuation of mass spectrum**

The mass spectrum is recorded for one of the following reasons:

a) verification/confirmation of the identity of a chemical compound by comparison with the true standard substance or by comparison with a spectrum accessible from established databases,

b) quantitative analysis of mixtures where the chemical identity of the components is known,

c) determination of the exact molecular mass and establishment of molecular formula of an unknown compound,

d) obtaining data on the molecular structure of an unknown compound from the fragmentation image of the primary ion.

Purposes a) and b) do not require knowledge or hypotheses about how and under what conditions fragmentation occurs. Quantitative determination involves calibration of the method with known amounts of the component of interest.

Mass spectrometers equipped with high performance analyzers allow the calculation of **m/z** ratios with advanced resolution (**m/z** value determination to the seventh decimal place). The precise determination of the mass of the molecular ion allows, in principle, the determination of the elemental formula of the chemical compound analyzed.

The fragmentation of the primary ion under different ionization conditions and energies provides valuable information about the molecular structure of the primary ion and thus about the molecule being analyzed. When most organic compounds are ionized by electronic impact (EI), the energy of the electron flow usually falls between 50-75 eV. It generally leads to ion fragmentation, resulting in the presence of several ions with lower **m/z** ratios in addition to the molecular ion in the spectrum. As fragmentation increases, the relative intensity of the molecular signal decreases. Figure 63 shows the intensity of the molecular ion signal in the mass spectrum of pyridine obtained by EI ionization as a function of the energy of the ionizing electrons.

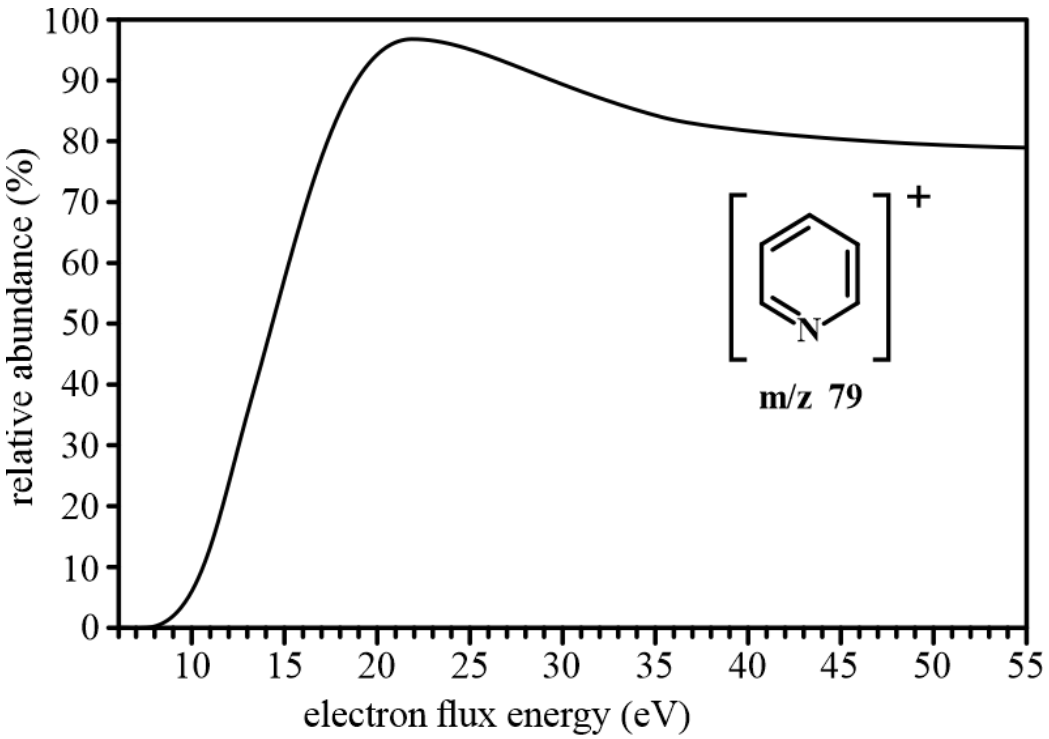



**Fig. 63 The signal intensity of the molecular ion in the pyridine spectrum as a function of ionization energy. (after *I. Oprean*: Spectrometria de masă a compuşilor organici. Editura Dacia, Cluj 1974)**

When it comes to the comprehensive interpretation of mass spectra, there are several peculiarities, and it is recommended to follow some useful procedures and rules.

### 4.1. Detection of molecular ion signal and calculation of molecular weight

After electron impact, the neutral molecule ("**M**") loses an electron and becomes a positively charged radical ion.

$$M + e^- \rightarrow M^{\bullet +} + 2e^-$$

Efficient ionization occurs when the energy of the electron flow is equal to or greater than the ionization energy threshold of the primary molecule. For most organic molecules their ionization energies are in the range of 7-15 eV.

In addition to the energy of the electron current, the ionization efficiency depends on the collision probability, also called the effective collision cross section, between the electrons and the primary molecules. Therefore, when the energy of the electrons is identical to the ionization energy of the primary molecule, the signal intensity of the molecular ion is small. When the energy of the electron beam exceeds the minimum threshold, both the collision probability and the ionization efficiency increase.

Figure 63 shows the intensity of the molecular ion in the mass spectrum of pyridine obtained by EI ionization as a function of the energy of the ionizing electrons. Up to 10 eV of ionizing electron energy, the molecular ion signal is relatively weak. As the energy of the electrons increases beyond this point, the ionization efficiency gradually increases, reaching a maximum value at about 20 eV of electron energy. Beyond this point, further increases result in a decrease in the molecular ion signal that gradually reaches a constant limit at about 80 eV of ionizing electron energy as fragmentation processes begin to replace the molecular ion formation.

Despite efficient ionization of the analyte molecule, an unstable molecular ion undergoes significant fragmentation as it travels from the ionization unit to the detector. As a result, the signal intensity of the molecular ion is often significantly reduced or becomes undetectable.

Identifying the molecular ion is the first step in interpreting a mass spectrum. In about 70 % of the cases the molecular ion is present in the spectrum and the signal corresponding to the maximum of the **m/z** ratio can be attributed to the mono-ionized molecular ion. Otherwise, detailed interpretation of the mass spectrum is more difficult and some additional rules from practice are used.

When analyzing high molecular weight samples such as peptides and proteins, particularly in electrospray ionization (ESI), both the molecular ion and molecular fragments may have multiple elemental charges due to the incorporation of varying numbers of protons. In the analysis of peptides and proteins, this can be advantageous because ions of a given mass but with multiple elemental charges produce a signal at

lower **m/z** values than those with a single elemental charge. Therefore, it is possible to detect high molecular mass samples even with spectrometers that have a limited mass range. For example, an ion with a nominal molecular mass of 80,000 Da bound to 40 protons will produce a signal at **m/z** of 2,000.

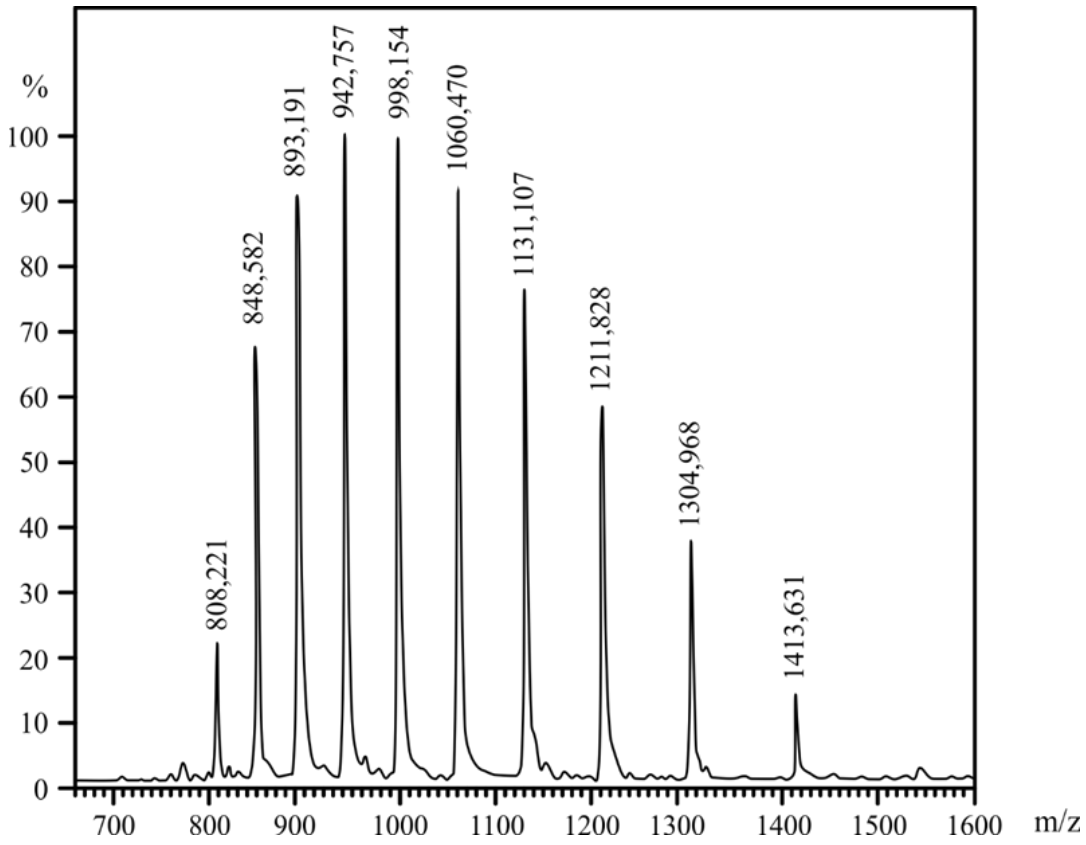



**Fig. 64 ESI mass spectrum of horse myoglobin (rebuild after the data of C.G. *Herbert* & *R.A.W. Johnstone*: Mass Spectrometry Basics CRC Press LLC, 2003 [ISBN: 0-8493-1354-6])**

The ions with multiple elementary electric charges (resulting from "**n**", "**n+1**", "**n+2**", "**n+3**", etc. bound protons) are usually observed as a continuous series of signals at "**m/z**" values occurring at one-unit intervals. When the molecular ion (mass "**M**") is the proton carrier, both the molecular ion mass and the number of bound protons can be determined. If we can conclude that two closely related intense signals with values "$(m/z)_1$" and "$(m/z)_2$" result from the uptake of "**n**" and "**n+1**" protons (and therefore have "**n**" and "**n+1**" elementary electric charges), then we can describe the situation with the following system of two equations:

$$\begin{aligned}(m/z)_1 &= \frac{M + n \cdot M_H}{n} \\ (m/z)_2 &= \frac{M + (n+1) \cdot M_H}{n+1}\end{aligned} \qquad (28)$$

where "**M**" is the molecular mass of the suspected species without attached protons and "$\mathbf{M_H}$" is the atomic mass of one proton (1.0078250 Da).

Solving the equation system (28) with respect to "**M**" and "**n**" yields:

$$M = \frac{[(m/z)_1 - M_H] \cdot [(m/z)_2 - M_H]}{(m/z)_1 - (m/z)_2}$$

$$n = \frac{M}{(m/z)_1 - (m/z)_2} = \frac{(m/z)_2 - M_H}{(m/z)_1 - (m/z)_2} \qquad (29)$$

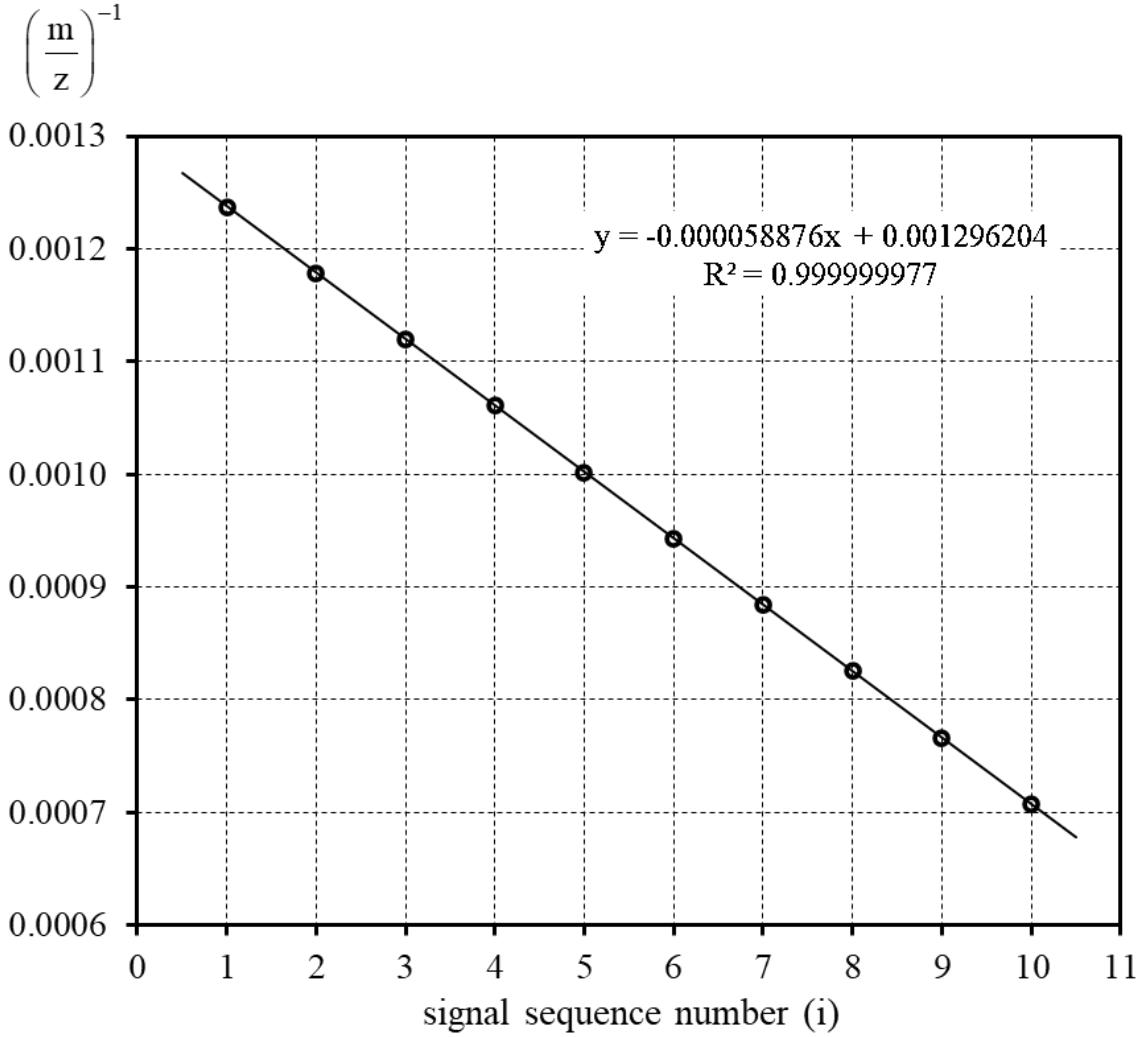



**Fig. 65 Reciprocal values of the m/z ratios of the mass spectrum shown in Figure 64 as a function of signal sequence number**

The process of determining the molecular ion mass and the number of attached protons is illustrated by the mass spectrum of horse myoglobin (Figure 64) obtained by electron spray ionization. Within the **m/z** range of 700-1500, 10 signals form a regular sequence, indicating the presence of species of progressively higher protonation. A signal in the mass spectrum corresponds to an ionic species with one additional

proton compared to the previous signal. This can be shown graphically by plotting the reciprocal values of the "**m/z**" ratios or the "**z/m**" ratios against the signal sequence number (see Figure 65).

**Table 2.6 Interpretation of the data shown in Figure 64**

| nr | m/z | m/z - $M_H$ | Calculation details |
|---|---|---|---|
| 1 | 808,221 | 807,213 | |
| 2 | 848,582 | 847,574 | $M = \frac{847,574 \cdot 807,213}{847,574 - 807,213} = \mathbf{16951,3330}$ ; $n_2 = \frac{16951,333}{847,574} = 19,9998 \approx \mathbf{20}$ |
| | (i = 1 ; i + 1 = 2) | | |
| 3 | 893,191 | 892,183 | $M = \frac{892,183 \cdot 847,574}{892,183 - 847,574} = \mathbf{16951,5370}$ ; $n_3 = \frac{16951,5370}{892,183} = 19,0000 = \mathbf{19}$ |
| | (i = 2 ; i + 1 = 3) | | |
| 4 | 942,857 | 941,749 | $M = \frac{941,749 \cdot 892,183}{941,749 - 892,183} = \mathbf{16951,3870}$ ; $n_4 = \frac{16951,3870}{941,749} = 17,9999 \approx \mathbf{18}$ |
| | (i = 3 ; i + 1 = 4) | | |
| 5 | 998,154 | 997,146 | $M = \frac{997,146 \cdot 941,749}{997,146 - 941,749} = \mathbf{16951,4820}$ ; $n_5 = \frac{16951,4820}{997,146} = 17,0000 = \mathbf{17}$ |
| | (i = 4 ; i + 1 = 5) | | |
| 6 | 1060,470 | 1059,462 | $M = \frac{1059,462 \cdot 997,45}{1059,462 - 997,45} = \mathbf{16952,9221}$ ; $n_6 = \frac{16952,9221}{1059,462} = 16,0014 \approx \mathbf{16}$ |
| | (i = 5 ; i + 1 = 6) | | |
| 7 | 1131,107 | 1130,099 | $M = \frac{1130,099 \cdot 1059,462}{1130,099 - 1059,462} = \mathbf{16949,9971}$ ; $n_7 = \frac{16749,9971}{1130,099} = 14,9987 \approx \mathbf{15}$ |
| | (i = 6 ; i + 1 = 7) | | |
| 8 | 1211,828 | 1210,820 | $M = \frac{1210,820 \cdot 1130,099}{1210,820 - 1130,099} = \mathbf{16951,5550}$ ; $n_8 = \frac{16951,5550}{1210,820} = 14,0000 = \mathbf{14}$ |
| | (i = 7 ; i + 1 = 8) | | |
| 9 | 1304,968 | 1303,960 | $M = \frac{1303,960 \cdot 1210,820}{1303,960 - 1210,820} = \mathbf{16951,4800}$ ; $n_9 = \frac{16951,4800}{1303,960} = 13,0000 = \mathbf{13}$ |
| | (i = 8 ; i + 1 = 9) | | |
| 10 | 1413,631 | 1412,623 | $M = \frac{1412,623 \cdot 1303,960}{1412,623 - 1303,960} = \mathbf{16951,5280}$ ; $n_{10} = \frac{16951,5280}{1412,623} = 12,0000 = \mathbf{12}$ |
| | (i = 8 ; i + 1 = 9) | | |

The perfect alignment of the figurative points on a straight line indicates that the signals considered have the same mass value and that their electric charge (implicitly the number of protons attached) varies by constant increments (assumed to be one unit) between the adjacent signals. Therefore, it is justified to treat the group of signals according to the algorithm outlined above to calculate the molecular weight "**M**" of the molecular ion and the number of protons ("**n**") attached to each ion species.

Table 6 shows the "**m/z**" ratios for the ten signals, labeled **i** = 1 to 10. The table also shows the difference between the "**m/z**" ratio and the mass of a proton ($M_H$ = 1.0078250 Da) for each signal, along with the method used to calculate the molecular ion mass "**M**" and the number of protons "**n**" present in each species of the spectrum. The updated calculation formulas (30) for the molecular mass ("**M**") and the number of protons (**$n_i$+1**), considering the successive pairs of signals "**i**" and "**i+1**", include the "**m/z - $M_H$**" data.

$$M = \frac{\left[\left(\frac{m}{z}\right)_{i+1} - M_H\right] \cdot \left[\left(\frac{m}{z}\right)_{i} - M_H\right]}{\left[\left(\frac{m}{z}\right)_{i+1} - M_H\right] - \left[\left(\frac{m}{z}\right)_{i} - M_H\right]} \; ; \; n_{i+1} = \frac{M}{\left(\frac{m}{z}\right)_{i+1} - M_H} \qquad (30)$$

The molecular weight calculated for horse myoglobin is in good agreement with the published value (16951.48) determined using various ionization techniques and mass spectrometry analysis. **[*J. Zaia, R.S. Annan, K. Biemann*: The Correct Molecular Weight of Myoglobin, a Common Calibrant for Mass Spectrometry, Rapid Communication in Mass Spectrometry 1992:6(1), 32-36].**

A typical technique used to verify the determined molecular mass is to compare it with the mass of the ion that is one atomic unit lighter in the spectrum. If the assumed molecular mass is correct, there are certain limits to the values of this difference, since it should correspond to a legitimate group of atoms or to a hydrogen atom. In organic compounds, no atom or group of atoms corresponds to masses in the ranges of 3-4 and 21-25 atomic mass units. The difference between the assumed molecular mass and the mass immediately below it in the spectrum, which belongs to these limits, is an argument either for the presence of an impurity in the sample or against the assumed molecular mass. For example, if there is a difference of 3 mass units between two signals, it is more reasonable to assume that the ions originated from an unstable shared ion that eliminated two fragments with a mass difference of 3 than to assume that the lower mass ion originated from a heavier ion by removing a hydrogen atom and then a hydrogen molecule.

### 4.2. The nitrogen rule

A useful rule for interpreting mass spectra of organic compounds concerns molecules containing nitrogen atoms. If the molecular ion contains an odd number of nitrogen atoms, then (and only then) its signal (if observable) appears at an odd **m/z** ratio. If the molecule does not contain nitrogen and yet the last signal (with the maximum **m/z** ratio) in the spectrum occurs at an odd **m/z** ratio, then that signal does not belong to the molecular ion.

The rule given in this form applies only to the unfragmented molecular ion but can be extended to ionic fragments as follows: except for ions with an odd number of nitrogen atoms, ions with an even number of electrons, whereas those with an odd number of electrons, have a mass expressed by an even number. For example, the odd-mass ion $\mathbf{CHO}^{+}$ (relative mass 29) contains an even number of electrons, so it is in the singlet or triplet electronic state, but not in the doublet state - in other words, it is not a radical ion ($\mathbf{CNO}^{+\bullet}$).

### 4.3. "M+1" signals

If the molecular ion of a chemical compound is unstable, its signal will not appear in the mass spectrum. In these cases, an artifact is used to determine the molecular weight.

Normally, the pressure inside the ionization source is reduced (below atmospheric pressure), so the probability of the ions formed colliding with the neutral molecules is negligible. By increasing the pressure in the ionization source, the probability of collisions between particles increases. When a molecular ion collides with a neutral molecule, the neutral molecule can give up a hydrogen atom to the molecular ion; the $\mathbf{[M]}^{+}$ ion (with molecular mass "**M**") becomes the $\mathbf{[M+H]}^{+}$ ion (with molecular mass "**M+1**"). If the ion formed is stable enough, it will appear in the spectrum as a detectable signal. Subtracting one unit of mass from the **m/z** value of this ion gives the molecular mass of the compound.

The gradual and controlled increase of the pressure in the ion source is achieved by the introduction (at the same time as the sample) of an auxiliary substance capable of easily yielding a hydrogen atom (water, methanol, etc.). The $\mathbf{[M+H]}^{+}$ ion generation method can be used for substances that form very stable $\mathbf{[M+H]}^{+}$ ions, such as heteroatomic compounds with electron pairs not involved in covalent bonding (alcohols, amines, ethers, nitriles, amino alcohols, amino acids, but also many natural compounds: peptides or alkaloids).The $\mathbf{[M+H]}^{+}$ ion is produced by bimolecular collision; therefore its signal strength depends on both the concentration of molecular ions and neutral molecules, i.e. on the square of the total vapor pressure in the ion source,

whereas the ion signal from monomolecular fragmentation is directly proportional to the vapor pressure of the sample in the ion source. Consequently, when recording mass spectra of a compound at different pressures in the ion source, the **M+1** signal is easily distinguished because its intensity increases more than the signal intensity of the other ions with increasing pressure in the ion source.

The molecular ion of substances that thermally fragment prior to ionization cannot be detected. This category includes polyhydroxy compounds (e.g. carbohydrates). In this situation the sample components are first converted ("derivatized") into non-polar and more volatile products, for example by conversion to organosilicon derivatives.

### 4.4. Isotopic discrimination of isotopologues

In the previous chapters, only stable isotopes with the dominant natural abundance of chemical elements relevant to the analysis of organic compounds (the category to which most active drug compounds belong) were considered. But almost every chemical element occurs as a mixture of isotopes with different masses, producing additional (low intensity) signals in addition to those of species containing only the dominant isotopes. Table 7 lists the stable isotopes of chemical elements found in most organic molecules. It gives their exact relative mass (in atomic mass units, au), natural abundance, and natural variation limits of their abundance (in molar fractions).

Different isotopes of a chemical element in an ion give rise to multiple signals (isotopologues) of different intensities for that ion. By knowing the relative intensities of the component signals associated with an ion, the elemental composition of that ion can be determined. To determine the isotopic weight of an ion, the natural abundance of the isotopes, expressed in mole fractions, is considered.

The relative weights "$\mathbf{P_e}$" ($\mathbf{e} = 1, 2, ..., $) of the ionic species, with exact masses $\mathbf{M_1}$, $\mathbf{M_2}$, ... , $\mathbf{M_m}$, which have "**m**" isotopes of the chemical element "**e**" with a natural abundance "$\mathbf{x_e}$", satisfy the relation (30).

$$P_e = \frac{n!}{k_1! \cdot k_2! \cdots k_m!} \cdot \left({}^1x_e\right)^{k_1} \cdot \left({}^2x_e\right)^{k_2} \cdots \left({}^m x_e\right)^{k_m} \qquad (30)$$

The symbol "$\mathbf{k_m!}$" in relation (30) represents the "$\mathbf{k_m}$" factorial. Each value "**e**" corresponds to a set of natural numbers $\mathbf{k_1}$ , $\mathbf{k_2}$ , ... $\mathbf{k_m}$ ($k_i \in \mathbb{N}$) with the restriction that their sum is equal to the number of atoms "**n**" of the chemical element "**e**" in the molecule under consideration (31). Note that, for mathematical reasons, a zero factorial is 1 (0! = 1). Also, any non-zero number raised to the power of zero is 1 ($a^0 = 1$).

$$\sum_{i=1}^{m} k_i = n \qquad (31)$$

**Table 7 Stable isotopes of chemical elements relevant to drug analysis**

| Isotope | Exact mass (au) | Natural abundance (molar fraction) | Variation of natural abundance (molar fraction) |
|---|---|---|---|
| $^{1}H$ | 1.0078250 | 0.999885 | 0.999816 – 0.999974 |
| $^{2}H$ | 2.0141018 | 0.000115 | 0.000026 – 0.000184 |
| $^{10}B$ | 10.012937 | 0.199 | 0.18929 – 0.20386 |
| $^{11}B$ | 11.009305 | 0.801 | 0.79614 – 0.81071 |
| $^{12}C$ | 12.000000 | 0.9893 | 0.98853 – 0.99037 |
| $^{13}C$ | 13.003355 | 0.0107 | 0.00963 – 0.001147 |
| $^{14}N$ | 14.003074 | 0.99636 | 0.99579 – 0.99654 |
| $^{15}N$ | 15.000109 | 0.00304 | 0.00346 – 0.00421 |
| $^{16}O$ | 15.994915 | 0.99757 | 0.99738 – 0.99776 |
| $^{17}O$ | 16.999132 | 0.00038 | 0.00037 – 0.00040 |
| $^{18}O$ | 17.999161 | 0.00205 | 0.00188 – 0.00222 |
| $^{19}F$ | 18.998403 | 1.00000 | |
| $^{23}Na$ | 22.989769 | 1.00000 | |
| $^{28}Si$ | 27.976926 | 0.92223 | 0.92205 – 0.92241 |
| $^{29}Si$ | 28.976495 | 0.04685 | 0.04678 – 0.04692 |
| $^{30}Si$ | 29.973770 | 0.03092 | 0.03082 – 0.03102 |
| $^{31}P$ | 30.973761 | 1.00000 | |
| $^{32}S$ | 31.972071 | 0.9493 | 0.94454 – 0.95281 |
| $^{33}S$ | 32.971459 | 0.0076 | 0.00730 – 0.00793 |
| $^{34}S$ | 33.967867 | 0.0429 | 0.03976 – 0.04734 |
| $^{36}S$ | 35.967080 | 0.0002 | 0.00013 – 0.00027 |
| $^{35}Cl$ | 34.968853 | 0.7576 | 0.75644 – 0.75923 |
| $^{37}Cl$ | 36.965902 | 0.2424 | 0.24077 – 0.24356 |
| $^{79}Br$ | 78.918337 | 0.5069 | |
| $^{81}Br$ | 80.916291 | 0.4931 | |
| $^{127}I$ | 126.904473 | 1.00000 | |

The variables $^{1}\mathbf{x}$ , $^{2}\mathbf{x}$ , . , $^{\mathbf{m}}\mathbf{x}$ in equation (30) represent the mole fractions of the "**m**" isotopes of the chemical element in question. The relative intensity of an ionic species (associated with a given combination of the quantities $\mathbf{k_1}$ , $\mathbf{k_2}$ , ... $\mathbf{k_m}$) contaiinning the isotopes of the chemical element "**e**" is proportional to the weight "$\mathbf{P_e}$" expressed by equation (30).

Flowchart 66 shows the variables involved in the calculation of the relative signal strength of ions containing isotopes of the chemical elements present in the respective ions.

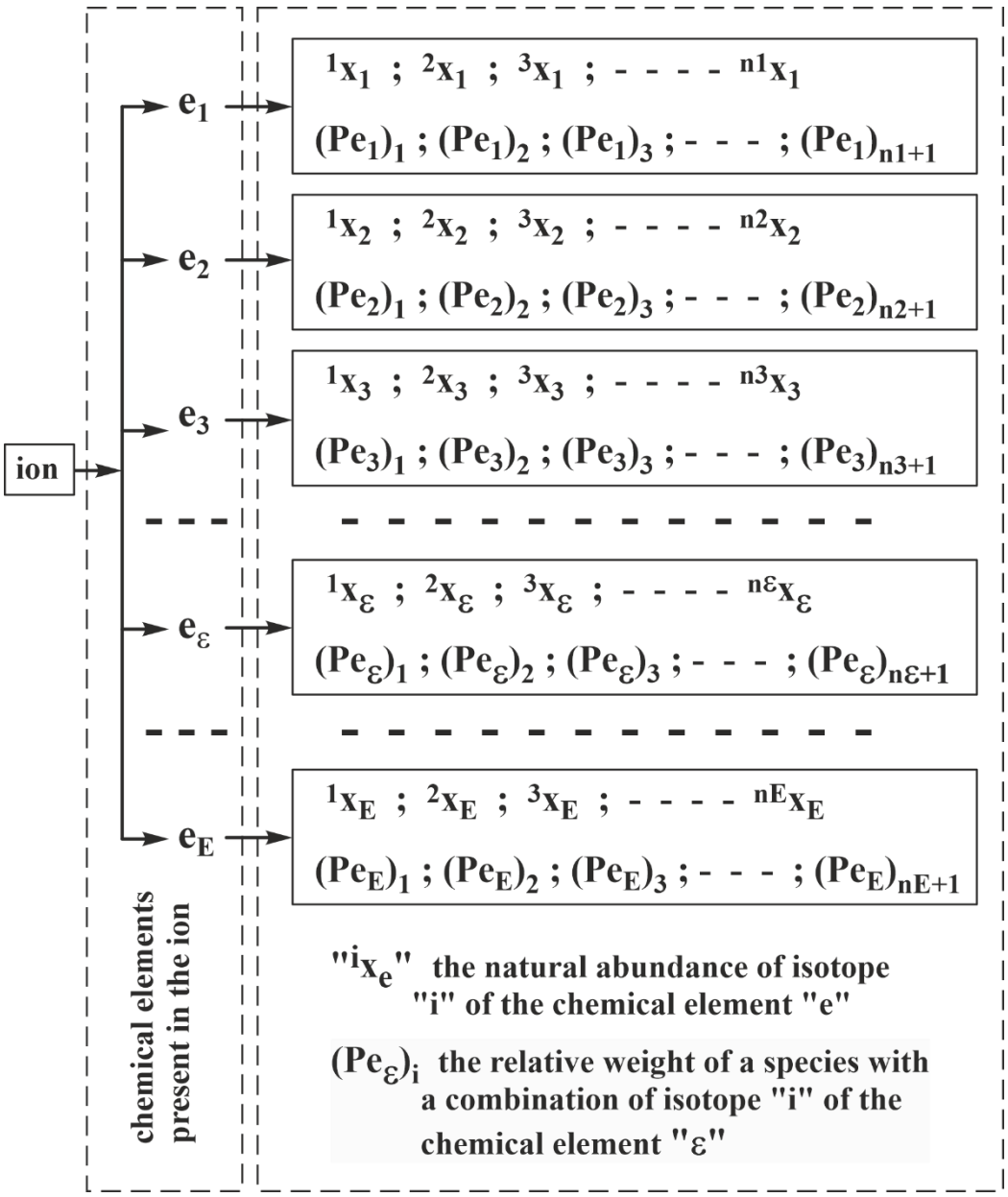


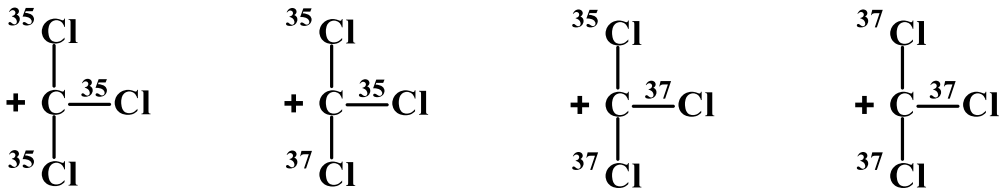

**Fig. 66 Flowchart of variables involved in calculating relative signal intensity for ionic species with different isotopic configurations**

If the ion contains isotopes of more than one chemical element (chemical elements "**e1**" , "**e2**" , . . . , "**eε**" , . . . , "e**E**"), then the weight of the isotopic form of this ion is the product of the specific weights of the individual chemical elements.

$$P = \prod_{i=1}^{E} P_i \qquad (32)$$

The following examples illustrate the concrete application of the general relations (30) and (32).

a) The $\mathbf{[CCl_3]^+}$ ion contains one carbon and three chlorine atoms. If the ionic species contained only the dominant carbon ($^{12}C$) and chlorine ($^{35}Cl$) isotopes, then in the mass spectrum the $\mathbf{[CCl_3]^+}$ ionic species would give a single signal at **m/z** 12.000000 + 3•34.968853 = 116.906559 a.u. (atomic units). The carbon atom has two isotopes ($^{12}C$ and $^{13}C$), but the $^{13}C$ isotope is present in a very small proportion (about 1%) next to the dominant $^{12}C$ isotope, so to first approximation the isotopic diversity of the carbon atom can be neglected by considering only the dominant $^{12}C$ isotope. Chlorine atoms are a different case. The two chlorine isotopes ($^{35}Cl$ with an exact mass of 34.968853 and $^{37}Cl$ with an exact mass of 36.965902) have comparable weights. It means that the $\mathbf{[CCl_3]^+}$ ion exists in four isotopic forms (isotopologues):




| **m/z 116.906559** | **m/z 118.903608** | **m/z 120.900657** | **m/z 122.897706** |
|---|---|---|---|
| **$P_1$** | **$P_2$** | **$P_3$** | **$P_4$** |

with the indicated **m/z** ratios (in atomic units, a.u.) and individual relative weights '$\mathbf{P_1}$', '$\mathbf{P_2}$' , '$\mathbf{P_3}$' and '$\mathbf{P_4}$'. In this case **n** = 3 and **m** = 2. The set of "$\mathbf{k_1}$" and "$\mathbf{k_2}$" values associated with the $^{35}Cl$ and $^{37}Cl$ isotopes respectively, the calculated weights ($\mathbf{P_{Cl}}$) and the normalized weights (%) are given in Table 8. Figure 67 shows the percentage signal intensities associated with the four isotopic forms.

**Table 8 Possible values of exponents '$k_1$' and '$k_2$', calculated weights and normalized weights (%) for $[CCl_3]^+$ ion**

| $k_1$ | $k_2$ | **Relative weight:** $\left(P_{Cl}\right)=\frac{n!}{k_1!\cdot k_2!}\cdot\left({}^{35}x_{Cl}\right)^{k_1}\cdot\left({}^{37}x_{Cl}\right)^{k_2}$ | **Normalized weight (%)** |
|---|---|---|---|
| 3 | 0 | $\left(P_{Cl}\right)_{30}=\frac{3!}{3!\cdot 0!}\cdot\left({}^{35}x_{Cl}\right)^{3}\cdot\left({}^{37}x_{Cl}\right)^{0}=$ $=1\cdot\left(0.7576\right)^{3}\cdot\left(0.2424\right)^{0}=0.43483$ **m/z** $[C\text{-}{}^{35}Cl{}^{35}Cl{}^{35}Cl]^+$ = 116.906559 au. | 100.00 |

**Table 8 (continued)**

| k1 | k2 | **Relative weight:** $(P_{Cl}) = \frac{n!}{k_1! \cdot k_2!} \cdot \left({}^{35}x_{Cl}\right)^{k_1} \cdot \left({}^{37}x_{Cl}\right)^{k_2}$ | **Normalized weight (%)** |
|---|---|---|---|
| 2 | 1 | $(P_{Cl})_{21} = \frac{3!}{2! \cdot 1!} \cdot \left({}^{35}x_{Cl}\right)^2 \cdot \left({}^{37}x_{Cl}\right)^1 = 3 \cdot (0.7576)^2 \cdot (0.2424)^1 = 0.41738$ **m/z** $[C\text{-}^{35}Cl^{35}Cl^{37}Cl]^+ = 118.903608$ au. | 95.97 |
| 1 | 2 | $(P_{Cl})_{12} = \frac{3!}{1! \cdot 3!} \cdot \left({}^{35}x_{Cl}\right)^1 \cdot \left({}^{37}x_{Cl}\right)^2 = 3 \cdot (0.7576)^1 \cdot (0.2424)^2 = 0.13354$ **m/z** $[C\text{-}^{35}Cl^{37}Cl^{37}Cl]^+ = 120.900657$ au. | 30.71 |
| 0 | 3 | $(P_{Cl})_{03} = \frac{3!}{0! \cdot 3!} \cdot \left({}^{35}x_{Cl}\right)^0 \cdot \left({}^{37}x_{Cl}\right)^3 = 1 \cdot (0.7576)^0 \cdot (0.2424)^3 = 0.01424$ **m/z** $[C\text{-}^{37}Cl^{37}Cl^{37}Cl]^+ = 122.897706$ au. | 3.27 |

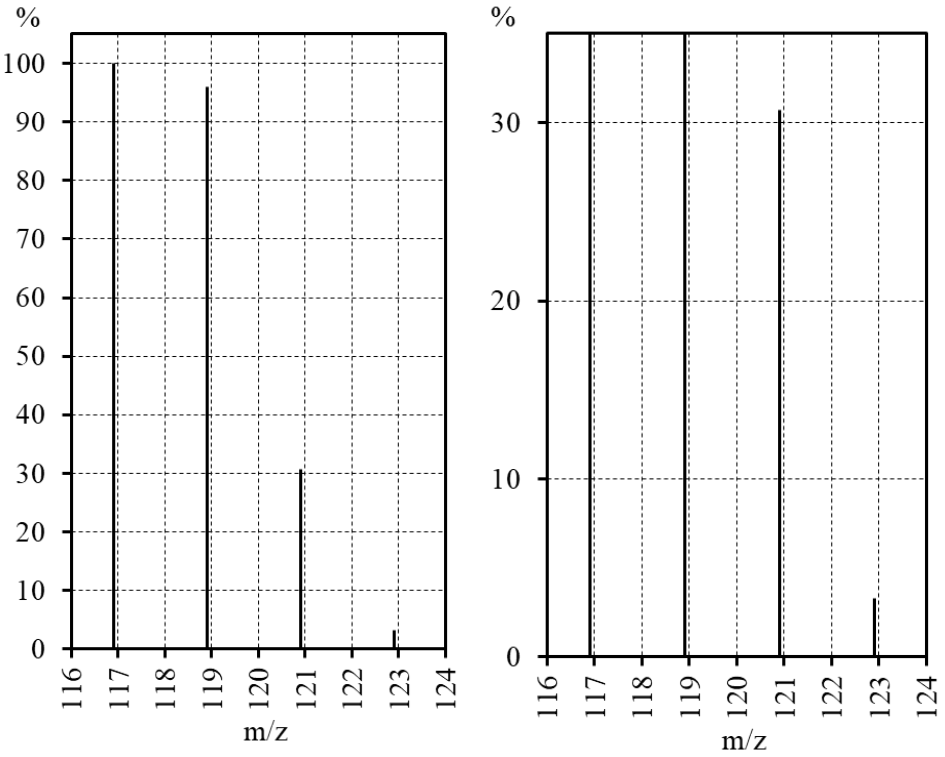
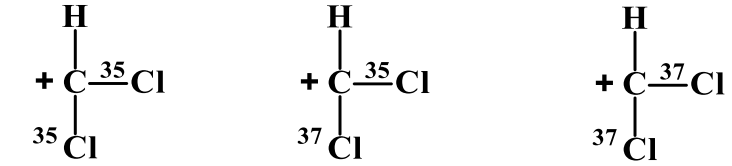



**Fig. 67 Relative abundance (normalized weights) of the isotopic forms of the $[CCl_3]^+$ ion**

b) The ion $[HCCl_2]^+$ contains one carbon, one hydrogen, and two chlorine atoms. If the ionic species contained only the dominant isotopes of carbon ($^{12}C$) and chlorine ($^{35}Cl$), then the ionic species $[HCCl_2]^+$ would give a single signal at **m/z** 13.007825 + 2•34.968853 = 82.945631 a.u. in the mass spectrum. The carbon atom has two isotopes ($^{12}C$ and $^{13}C$), but the $^{13}C$ isotope is present in a small fraction (about 1%) of the dominant $^{12}C$ isotope hence, as a first approximation, the isotopic diversity of the carbon atom can be neglected by considering only the dominant $^{12}C$ isotope. Similarly, the presence of minor hydrogen isotope $^{2}H$ can be neglected (see Table 7). On the other hand, the chlorine isotopes ($^{35}Cl$ with an exact mass of 34.968853 and $^{37}Cl$ with an exact mass of 36.965902) have comparable weights, and the $[HCCl_2]^+$ ion appears in three isotopic forms:



**m/z 82.945531** **m/z 84.942580** **m/z 86.939629**

**$P_1$** **$P_2$** **$P_3$**

with the indicated **m/z** ratios and with the individual relative weights " **$P_1$** ", " **$P_2$** " and " **$P_3$** ". In this case **n** = 2 and **m** = 2. The set of values " **$k_1$**" and " **$k_2$**" associated with the isotopes $^{35}Cl$ and $^{37}Cl$ respectively, the calculated weights ( **$P_{Cl}$** ) and the normalized weights (%) are shown in Table 9.

Example b) refers to the case where the "**P**" weights are calculated for a chemical element that has two stable isotopes, and the ion contains "**n** = 2" atoms of this chemical element. In this case the value of the coefficient $\frac{n!}{k_1! \cdot k_2!}$ in the calculation relation can be obtained by a simple algorithm that gives the coefficients of the binomial development of $(a+b)^n$ (*Pascal* triangle Figure 68).

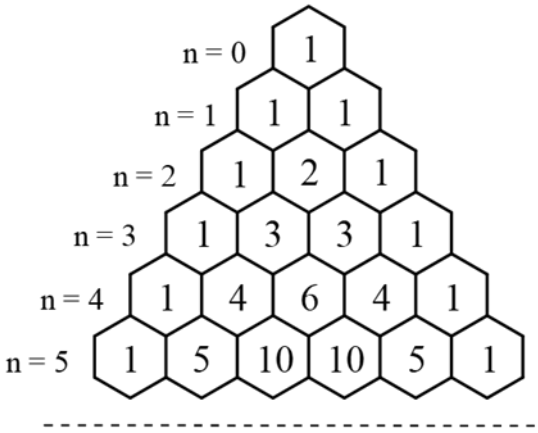



**Fig. 68**
***Pascal* triangle for the binomial coefficients (the value each given position is the sum of the values in the two positions just above it)**

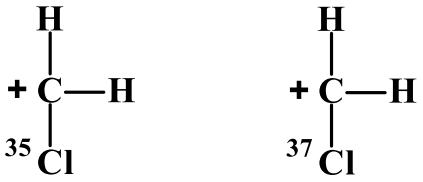
**Table 9 Possible values of exponents '$k_1$' and '$k_2$', calculated weights and normalized weights (%) for $[HCCl_2]^+$ ion**

| $k_1$ | $k_2$ | **Relative weight:** $(P_{Cl}) = \frac{n!}{k_1! \cdot k_2!} \cdot \left({}^{35}x_{Cl}\right)^{k_1} \cdot \left({}^{37}x_{Cl}\right)^{k_2}$ | **Normalized weight (%)** |
|---|---|---|---|
| 2 | 0 | $(P_{Cl})_{20} = \frac{2!}{2! \cdot 0!} \cdot \left({}^{35}x_{Cl}\right)^2 \cdot \left({}^{37}x_{Cl}\right)^0 =$ $= 1 \cdot (0.7576)^2 \cdot (0.2424)^0 = 0.57396$ **m/z** $[HC\text{-}{}^{35}Cl{}^{35}Cl]^+ = 82.945531$ au. | 100.00 |
| 1 | 1 | $(P_{Cl})_{11} = \frac{2!}{1! \cdot 1!} \cdot \left({}^{35}x_{Cl}\right)^1 \cdot \left({}^{37}x_{Cl}\right)^1 =$ $= 2 \cdot (0.7576)^1 \cdot (0.2424)^1 = 0.36728$ **m/z** $[HC\text{-}{}^{35}Cl{}^{37}Cl]^+ = 84.942580$ au. | 63.99 |
| 0 | 2 | $(P_{Cl})_{02} = \frac{2!}{0! \cdot 2!} \cdot \left({}^{35}x_{Cl}\right)^0 \cdot \left({}^{37}x_{Cl}\right)^2 =$ $= 1 \cdot (0.7576)^0 \cdot (0.2424)^2 = 0.05876$ **m/z** $[HC\text{-}{}^{37}Cl{}^{37}Cl]^+ = 86.939629$ au. | 10.24 |

The continuation rule of the series in Figure 68 is easy to deduce. The algorithm comes from the mathematical theory of combinations and is based on the recurrence formula (33) known from mathematical combinatorics:

$$\binom{n}{k} = \binom{n-1}{k-1} + \binom{n-1}{k} \qquad (33)$$

c) The ion $[H_2CCl]^+$ contains one carbon atom, two hydrogen atoms and one chlorine atom.



**m/z 47.976678** **m/z 50.981552**

**$P_1$** **$P_2$**

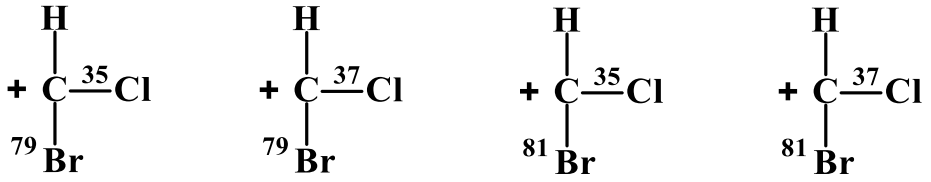
If only the dominant isotopes with respect to the hydrogen and carbon atoms are considered then, due to the isotopes $^{35}Cl$ and $^{37}Cl$ (with comparable abundances), two specific signals appear in the mass spectrum of this ion: one for the **$[H_2C\text{-}^{35}Cl]^+$** ion and another for the **$[H_2C\text{-}^{37}Cl]^+$** ion.

Their relative intensities (normalized to 100 %) are calculated similarly to the previous algorithm. In this case n = 1 and m = 2 and the ion appears in two isotopic forms: with the indicated **m/z** ratios and the individual relative weights "**$P_1$**" and "**$P_2$**". The values "**$k_1$**" and "**$k_2$**", associated with the $^{35}Cl$ and $^{37}Cl$ isotopes respectively, the calculated weights (**$P_{Cl}$**) and the normalized weights (%) are given in Table 10. In this case, the ratio of the signal intensities for the **$[H_2C\text{-}^{35}Cl]^+$** and **$[H_2C\text{-}^{37}Cl]^+$** ions correspond exactly to the ratio between the natural abundances of the $^{35}Cl$ and $^{37}Cl$ isotopes.

**Table 10 Possible values for the exponents '$k_1$' and '$k_2$', calculated weights and normalized weights for the $[H_2CCl]^+$ ion**

| **$k_1$** | **$k_2$** | **Relative weight:** $(P_{Cl}) = \frac{n!}{k_1! \cdot k_2!} \cdot \left(^{35}x_{Cl}\right)^{k_1} \cdot \left(^{37}x_{Cl}\right)^{k_2}$ | **Normalized weight (%)** |
|---|---|---|---|
| 1 | 0 | $(P_{Cl})_{10} = \frac{1!}{1! \cdot 0!} \cdot (35x_{Cl})^1 \cdot \left(^{37}x_{Cl}\right)^0 =$ $= 1 \cdot (0.7576)^1 \cdot (0.2424)^0 = 0.7576$ **m/z** $[H_2C\text{-}^{35}Cl]^+ = 48.984503$ au. | 100.00 |
| 0 | 1 | $(P_{Cl})_{01} = \frac{1!}{0! \cdot 1!} \cdot \left(^{35}x_{Cl}\right)^0 \cdot \left(^{37}x_{Cl}\right)^1 =$ $= 1 \cdot (0.7576)^0 \cdot (0.2424)^1 = 0.2424$ **m/z** $[H_2C\text{-}^{37}Cl]^+ = 50{,}981552$ au. | 31.99 |

d) The ion **$[HCClBr]^+$** contains one hydrogen, one carbon, one chlorine and one bromine atom. Considering only the dominant isotopes for the hydrogen and carbon atoms, due to the $^{35}Cl$ and $^{37}Cl$ isotopes with comparable abundances on the one hand, and the $^{79}Br$ and $^{81}Br$ isotopes with comparable abundances on the other hand, there are (theoretically) four signals corresponding to the following ions in the mass spectrum: **$[HC\text{-}^{35}Cl^{79}Br]^+$**, **$[HC\text{-}^{37}Cl^{79}Br]^+$**, **$[HC\text{-}^{35}Cl^{81}Br]^+$** and **$[HC\text{-}^{37}Cl^{81}Br]^+$**. Their relative intensities and normalized intensities are calculated similarly to the previous algorithm. The ion exists in four isotopic forms:



| m/z 126.859015 | m/z 128.892064 | m/z 128.892969 | m/z 130.890018 |
|---|---|---|---|
| **P1** | **P2** | **P3** | **P4** |

with the indicated **m/z** ratios and the individual relative weights '**P1**', '**P2**', '**P3**' and '**P4**'. For the two chlorine isotopes $n_{Cl} = 1$ and $m_{Cl} = 2$ and for the two bromine isotopes $\mathbf{n_{Br}} = 1$ and $\mathbf{m_{Br}} = 2$. The sets of values "**$k_1$**" and "**$k_2$**", associated with these isotopes $^{35}Cl$, $^{37}Cl$, $^{79}Br$, $^{81}Br$, the calculated weights (**$P_{Cl}$**), (**$P_{Br}$**) and the normalized weights (%) are given in Tables 11 and 12.

**Table 11 Possible values for the exponents '$k_1$' and '$k_2$' and calculated weights for the chlorine isotopes in the $[HC\text{-}Cl\text{-}Br]^+$ ion**

| k1 | k2 | **Relative weight:** $(P_{Cl}) = \frac{n!}{k_1!\cdot k_2!}\cdot\left(^{35}x_{Cl}\right)^{k_1}\cdot\left(^{37}x_{Cl}\right)^{k_2}$ |
|---|---|---|
| 1 | 0 | $(P_{Cl})_{10} = \frac{1!}{1!\cdot 0!}\cdot\left(^{35}x_{Cl}\right)^{1}\cdot\left(^{37}x_{Cl}\right)^{0} = 1\cdot(0.7576)^{1}\cdot(0.2424)^{0} = 0.7576$ **m/z** $[HC\text{-}^{35}Cl^{79}Br]^+ = 126.895015$ au. |
| 0 | 1 | $(P_{Cl})_{01} = \frac{1!}{0!\cdot 1!}\cdot\left(^{35}x_{Cl}\right)^{0}\cdot\left(^{37}x_{Cl}\right)^{1} = 1\cdot(0.7576)^{0}\cdot(0.2424)^{1} = 0.2424$ **m/z** $[H_2C\text{-}^{37}Cl^{79}Br]^+ = 128.892064$ au. |

**Table 12 Possible values for the exponents 'k1' and 'k2' and calculated weights for the bromine isotopes in the $[HC\text{-}Cl\text{-}Br]^+$ ion**

| k1 | k2 | **Relative weight:** $(P_{Br}) = \frac{n!}{k_1!\cdot k_2!}\cdot\left(^{79}x_{Br}\right)^{k_1}\cdot\left(^{81}x_{Br}\right)^{k_2}$ |
|---|---|---|
| 1 | 0 | $(P_{Br})_{10} = \frac{1!}{1!\cdot 0!}\cdot\left(^{79}x_{Br}\right)^{1}\cdot\left(^{81}x_{Br}\right)^{0} = 1\cdot(0.5069)^{1}\cdot(0.4931)^{0} = 0.5069$ **m/z** $[HC\text{-}^{35}Cl^{81}Br]^+ = 126.892969$ au. |
| 0 | 1 | $(P_{Br})_{01} = \frac{1!}{0!\cdot 1!}\cdot\left(^{79}x_{Br}\right)^{0}\cdot\left(^{81}x_{Br}\right)^{1} = 1\cdot(0.5069)^{0}\cdot(0.4931)^{1} = 0.4931$ **m/z** $[H_2C\text{-}^{37}Cl^{81}Br]^+ = 130.890018$ au. |

The relative weights ("**P1**","**P2**","**P3**","**P4**") of the isotopic forms of the **[HCClBr]**$^+$ ion can be obtained by multiplying the specific relative weights of the chlorine and bromine atoms (Tables 11 and 12). The masses of the "**P2**" and "**P3**" forms are almost identical (to the third decimal place), so the "**P2**" and "**P3**" weights are added together, since these two signals practically overlap at **m/z** 128.892 (Table 13). Figure 69 shows the percentage intensities of the signals associated with the isotopic forms.

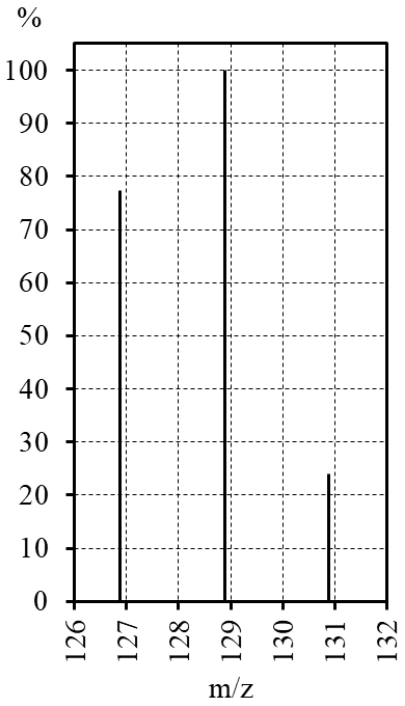



**Fig. 69**
**Relative abundance (normalized weights) of isotopic forms of [H-C-Cl-Br]$^+$ ion**

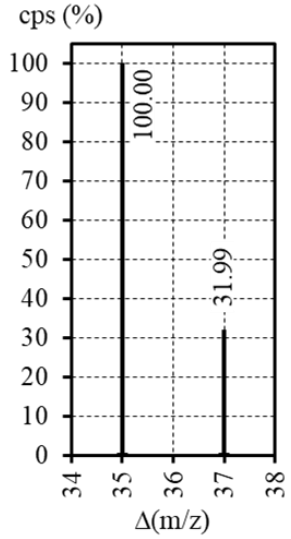
**Table 13 Isotopic signal weights of the [HCClBr]$^+$ ion**

| m/z | Individual relative weights of the isotopic forms of [HCClBr]$^+$ ion | m/z to three decimals | Cumulative weight (P2 + P3) | Normalized weight (%) |
|---|---|---|---|---|
| 126.895015 | $P_1 = (P_{Cl})_{10} \cdot (P_{Br})_{10} = 0.7576 \cdot 0.5069 = 0.3840$ | 126.895 | | 77.34 |
| 128.892064 | $P_2 = (P_{Cl})_{10} \cdot (P_{Br})_{01} = 0.7576 \cdot 0.4931 = 0.3736$ | 128.892 | 0.4965 | 100.00 |
| 128.892969 | $P_3 = (P_{Cl})_{01} \cdot (P_{Br})_{10} = 0.2424 \cdot 0.5069 = 0.1229$ | 128.892 | | |
| 130.890018 | $P_4 = (P_{Cl})_{01} \cdot (P_{Br})_{01} = 0.2424 \cdot 0.4931 = 0.1195$ | 130.890 | | 24.07 |

e) The isotopic compositions of some ions with different general structures are shown below (Figures 70-92).

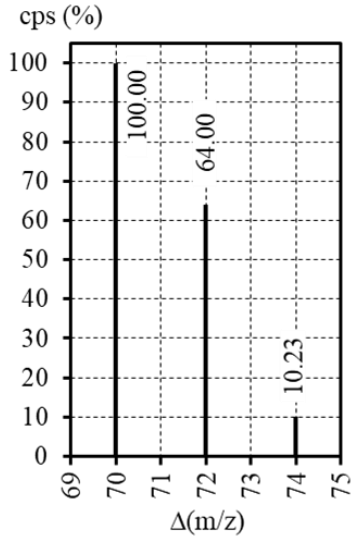
**$[R+Cl]^+$ ; $[R+Cl_2]^+$ ; $[R+Cl_3]^+$ ; $[R+Cl_4]^+$ ; $[R+Cl_5]^+$ ; $[R+Cl_6]^+$ ; $[R+Br]^+$ ; $[R+Br_2]^+$ ; $[R+Br_3]^+$ ; $[R+Br_4]^+$ ; $[R+Br_5]^+$ ; $[R+Br_6]^+$ ; $[R+Cl-Br]^+$ ; $[R+Cl-Br_2]^+$ ; $[R+Cl-Br_3]^+$ ; $[R+Cl_2-Br]^+$ ; $[R+Cl_2-Br_2]^+$ ; $[R+Cl_3-Br]^+$ ; $[R+Cl-Br_4]^+$ ; $[R+Cl_2-Br_3]^+$ ; $[R+Cl_4-Br]^+$ ; $[R+Cl_3-Br_2]^+$ ; $[R+Cl_4-Br_2]^+$.**

The symbol "**R**" represents the structural residue of the ion. The "**Δm/z**" values in the tables associated with the figures do not include the mass of the residue "**R**". The "**Δm/z**" contributions of the chlorine and bromine isotopes to the "**m/z**" ratio of the complete ion and the signal intensities generated by the isotopic species are determined by an algorithm like that shown in the previous examples. The masses of the isotopic species (isotopologues) are given to 6 decimal places (High Resolution - HR) and rounded to integers. The "**P**"-weights, which are different for isotopologues at high resolution, but belong to species of the same mass at low resolution, are added. The percentage abundance of the species (and thus the percentage signal value) is related to the maximum abundance (abundance and intensity of the base signal), which corresponds to 100 %.



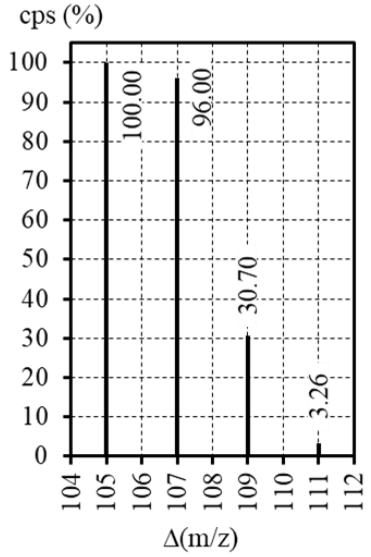

| Isotopologues $\Delta(m/z)_{HR}$ | Δ(m/z) | $(P)_{HR}$ | % |
|---|---|---|---|
| $[R+(^{35}Cl)]^+$ 34.968853 | 35 | 0.7576 | 100.00 |
| $[R+(^{37}Cl)]^+$ 36.965902 | 37 | 0.2424 | 31.99 |

**Fig. 70 Relative signal intensities of $[R+Cl]^+$ type ions**



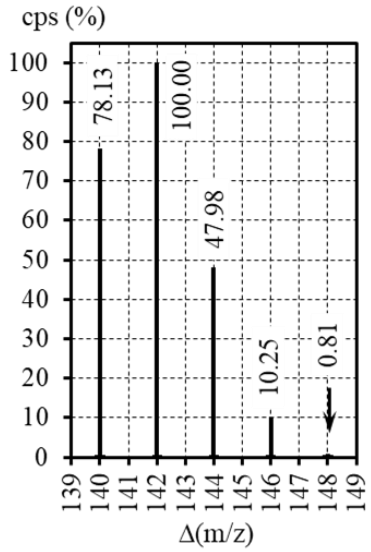

| Isotopologues $\Delta(m/z)_{HR}$ | Δ(m/z) | $(P)_{HR}$ | % |
|---|---|---|---|
| $[R+(^{35}Cl)_2]^+$ 69.937706 | 70 | 0.5739 | 100.00 |
| $[R+(^{35}Cl)(^{37}Cl)]^+$ 71.934755 | 72 | 0.3673 | 64.00 |
| $[R+(^{37}Cl)_2]^+$ 73.931804 | 74 | 0.0587 | 10.23 |

**Fig. 71 Relative signal intensities of $[R+Cl_2]^+$ type ions**




| Isotopologues $\Delta(m/z)_{HR}$ | Δ(m/z) | $(P)_{HR}$ | % |
|---|---|---|---|
| $[R+(^{35}Cl)_3]^+$ 104.906559 | 105 | 0.4348 | 100.00 |
| $[R+(^{35}Cl)_2(^{37}Cl)]^+$ 106.903608 | 107 | 0.4174 | 96.00 |
| $[R+(^{35}Cl)(^{37}Cl)_2]^+$ 108.900657 | 109 | 0.1335 | 30.70 |
| $[R+(^{37}Cl)_3]^+$ 110.897706 | 111 | 0.0142 | 3.26 |

**Fig. 72 Intensities of $[R+Cl_3]^+$ type ions**




| Isotopologues $\Delta(m/z)_{HR}$ | Δ(m/z) | $(P)_{HR}$ | % |
|---|---|---|---|
| $[R+(^{35}Cl)_4]^+$ 139.875412 | 140 | 0.3294 | 78.13 |
| $[R+(^{35}Cl)_3(^{37}Cl)]^+$ 141.872461 | 142 | 0.4216 | 100.00 |
| $[R+(^{35}Cl)_2(^{35}Cl)_2]^+$ 143.869510 | 144 | 0.2023 | 47.98 |
| $[R+(^{35}Cl)(^{37}Cl)_3]^+$ 145.865706 | 146 | 0.0432 | 10.25 |
| $[R+(^{37}Cl)_4]^+$ 147.863608 | 148 | 0.0034 | 0.81 |

**Fig. 73 Intensities of $R+Cl_4]^+$ type ions**

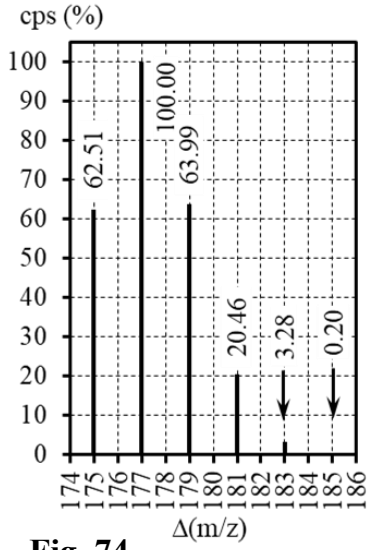



**Fig. 74 Intensities of $[R+Cl_5]^+$ type ions**

| Isotopologues $\Delta(m/z)_{HR}$ | Δ(m/z) | $(P)_{HR}$ | % |
|---|---|---|---|
| $[R+(^{35}Cl)_5$ 174.844265 | 175 | 0.2496 | 62.51 |
| $[R+(^{35}Cl)_4(^{37}Cl)]^+$ 176.841314 | 177 | 0.3993 | 100.00 |
| $[R+(^{35}Cl)_3(^{37}Cl)_2]^+$ 178.838363 | 179 | 0.2555 | 63.99 |
| $[R+(^{35}Cl)_2(^{37}Cl)_3]^+$ 180.835412 | 181 | 0.0817 | 20.46 |
| $[R+(^{35}Cl)(^{37}Cl)_4]^+$ 182.832461 | 183 | 0.0131 | 3.28 |
| $[R+(^{37}Cl)_5]^+$ 184.829510 | 185 | 0.0008 | 0.20 |

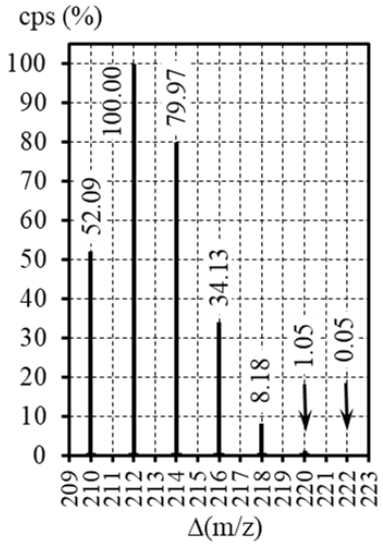
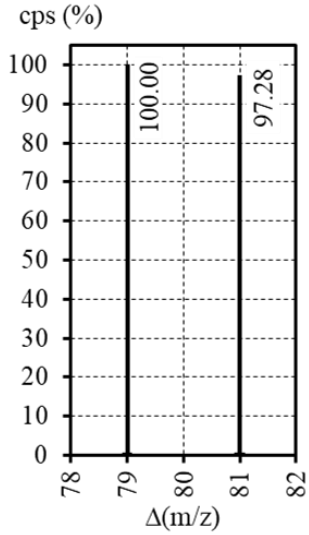


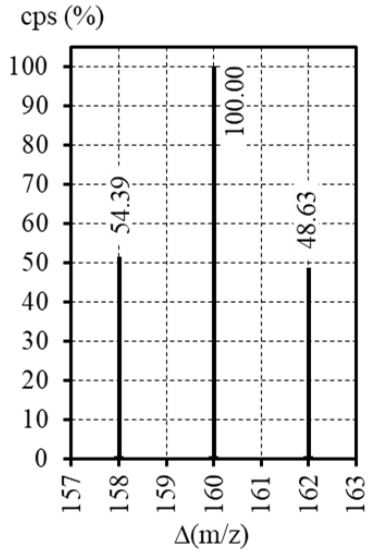

**Fig. 75 Intensities of $[R+Cl_6]^+$ type ions**

| **Isotopologues** **Δ(m/z)HR** | **Δ(m/z)** | **(P)HR** | **%** |
|---|---|---|---|
| $[R+(^{35}Cl)_6]^+$ 209.813118 | 210 | 0.1891 | 52.09 |
| $[R+(^{35}Cl)_5\ (^{37}Cl)]^+$ 211.810167 | 212 | 0.3630 | 100.00 |
| $[R+(^{35}Cl)_4\ (^{37}Cl)_2]^+$ 213.807216 | 214 | 0.2903 | 79.97 |
| $[R+(^{35}Cl)_3\ (^{37}Cl)_3]^+$ 215.804265 | 216 | 0.1239 | 34.13 |
| $[R+(^{35}Cl)_2\ (^{37}Cl)_4]^+$ 217.801314 | 218 | 0.0297 | 8.18 |
| $[R+(^{35}Cl)\ (^{37}Cl)_5]^+$ 219.798363 | 220 | 0.0038 | 1.05 |
| $[R+(^{37}Cl)_6]^+$ 221.795412 | 222 | 0.0002 | 0.05 |



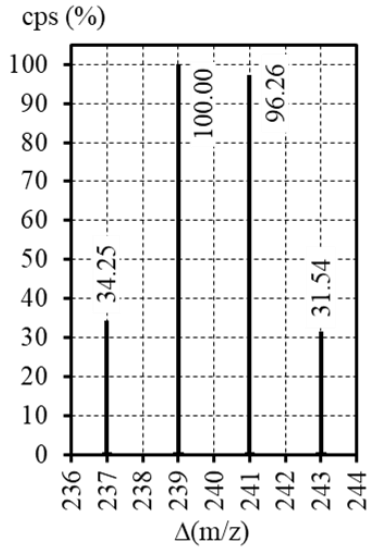

| **Isotopologues** **Δ(m/z)HR** | **Δ(m/z)** | **(P)HR** | **%** |
|---|---|---|---|
| $[R+(^{79}Br)]^+$ 78.918327 | 79 | 0.5069 | 100.00 |
| $[R+(^{81}Br)]^+$ 80.916291 | 81 | 0.4931 | 97.28 |

**Fig. 76 Intensities of $[R+Br]^+$ type ions**



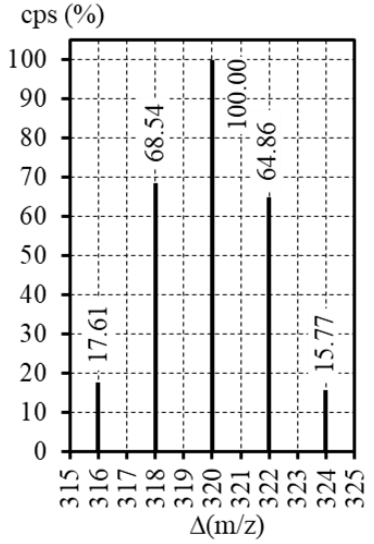

| **isotopologues** **Δ(m/z)HR** | **Δ(m/z)** | **(P)HR** | **%** |
|---|---|---|---|
| $[R+(^{79}Br_2)]^+$ 157.836674 | 158 | 0.2569 | 51.39 |
| $[R+(^{79}Br)\ (^{81}Br)]^+$ 159.834628 | 160 | 0.4999 | 100.00 |
| $[R+(^{81}Br_2)]^+$ 161.832582 | 162 | 0.2431 | 48.63 |

**Fig. 77 Intensities of $[R+Br_2]^+$ type ions**




| Isotopologues $\Delta(m/z)_{HR}$ | Δ(m/z) | $(P)_{HR}$ | % |
|---|---|---|---|
| $[R+(^{79}Br_3)]^+$ 236.755011 | 237 | 0.1302 | 34.25 |
| $[R+(^{79}Br_2)\ (^{81}Br)]^+$ 238.752965 | 239 | 0.3801 | 100.00 |
| $[R+(^{79}Br)\ (^{81}Br_2)]^+$ 240.750919 | 241 | 0.3697 | 97.26 |
| $[R+(^{81}Br)_3]^+$ 242.748873 | 243 | 0.1199 | 31.54 |

**Fig. 78 Intensities of $+Br_3]^+$ type ions**




| isotopologues $\Delta(m/z)_{HR}$ | Δ(m/z) | $(P)_{HR}$ | % |
|---|---|---|---|
| $[R+(^{79}Br_4)]^+$ 315.673348 | 316 | 0.0660 | 17.61 |
| $[R+(^{79}Br_3)\ (^{81}Br)]^+$ 317.671302 | 318 | 0.2569 | 68.54 |
| $[R+(^{79}Br_2)\ (^{81}Br_2)]^+$ 319.669256 | 320 | 0.3748 | 100.00 |
| $[R+(^{79}Br)\ (^{81}Br_3)]^+$ 321.667210 | 322 | 0.2431 | 64.86 |
| $[R+(^{81}Br_4)]^+$ 323.665164 | 324 | 0.0591 | 15.77 |

**Fig. 79 Intensities of $[R+Br_4]^+$ type ions**

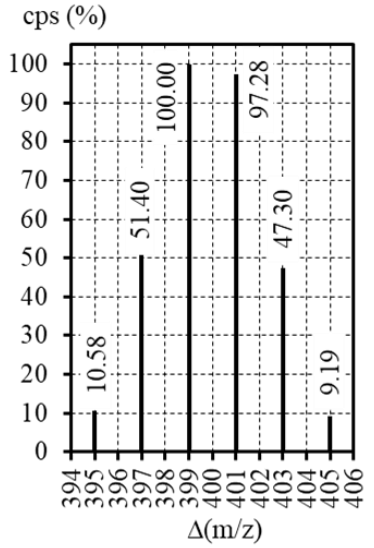



**Fig. 80 Intensities of $[R+Br_5]^+$ type ions**

| Isotopologues $\Delta(m/z)_{HR}$ | Δ(m/z) | $(P)_{HR}$ | % |
|---|---|---|---|
| $[R+(^{79}Br_5)]^+$ 394.591685 | 395 | 0.0335 | 10.58 |
| $[R+(^{79}Br_4)\ (^{81}Br)]^+$ 396.589639 | 397 | 0.1628 | 51.40 |
| $[R+(^{79}Br_3)\ (^{81}Br_2)]^+$ 398.587593 | 399 | 0.3167 | 100.00 |
| $[R+(^{79}Br)_2\ (^{81}Br_3)]^+$ 400.585547 | 401 | 0.3081 | 97.28 |
| $[R+(^{79}Br)\ (^{81}Br_4)]^+$ 402.583501 | 403 | 0.1448 | 47.30 |
| $[R+(^{81}Br_5)]^+$ 404.581455 | 405 | 0.0291 | 9.19 |

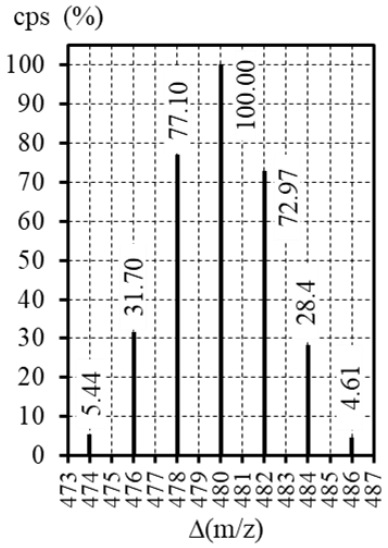
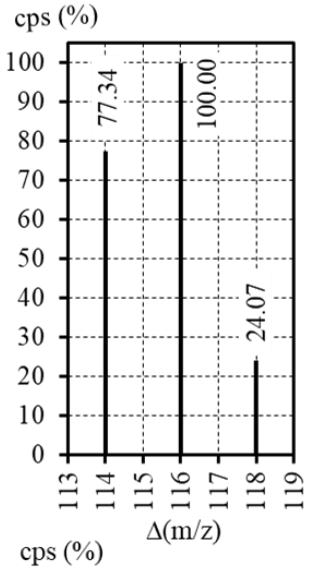



**Fig. 81 Intensities of $[R+Br_6]^+$ type ions**

| Isotopologues $\Delta(m/z)_{HR}$ | Δ(m/z) | $(P)_{HR}$ | % |
|---|---|---|---|
| $[R+(^{79}Br_6)]^+$ 473.510022 | 474 | 0.0170 | 5.44 |
| $[R+(^{79}Br_5)\ (^{81}Br)]^+$ 475.507976 | 476 | 0.0990 | 31.70 |
| $[R+(^{79}Br_4).\ (^{81}Br_2)]^+$ 477.505930 | 478 | 0.2408 | 77.10 |
| $[R+(^{79}Br_3)\ (^{81}Br_3)]^+$ 479.503884 | 480 | 0.3123 | 100.00 |
| $[R+(^{79}Br_2)\ (^{81}Br)_4]^+$ 481.501838 | 482 | 0.2279 | 72.97 |
| $[R+(^{79}Br)\ (^{81}Br_5)]^+$ 483.499792 | 484 | 0.0887 | 28.40 |
| $[R+(^{81}Br)_6]^+$ 485.497746 | 486 | 0.0144 | 4.61 |




| Isotopologues $\Delta(m/z)_{HR}$ | Δ(m/z) | $(P)_{HR}$ | % |
|---|---|---|---|
| $[R+(^{35}Cl)(^{79}Br)]^+$ 113.887190 | 114 | 0.3840 | 77.34 |
| $[R+(^{35}Cl)(^{81}Br)]^+$ 115.885144 | 116 | 0.3736 | 100.00 |
| $[R+(^{37}Cl)(^{79}Br)]^+$ 115.884239 | | 0.1229 | |
| $[R+(^{37}Cl)(^{81}Br)]^+$ 117.882193 | 118 | 0.1195 | 24.07 |

**Fig. 82 Intensities of $[R+Cl-Br]^+$ type ions**

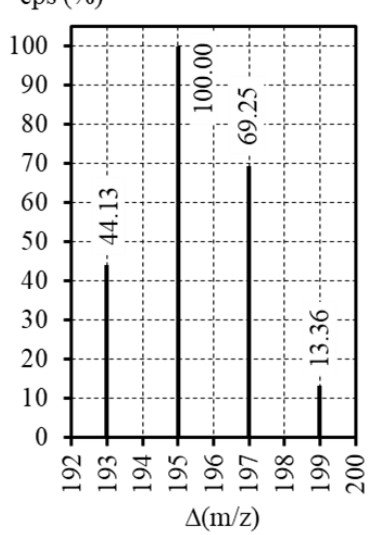
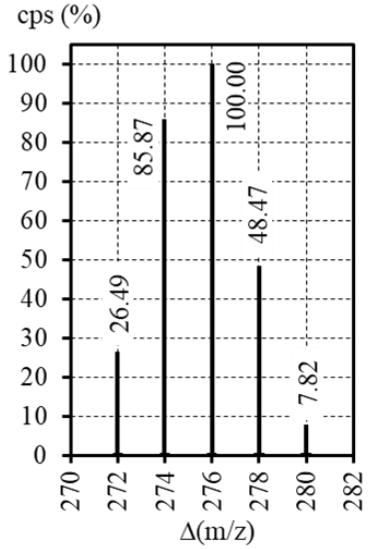
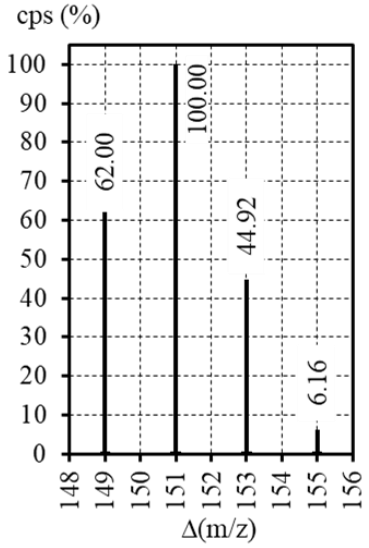



**Fig. 83 Intensities of $[R+Cl-Br2]^+$ type ions**

| Isotopologues $\Delta(m/z)_{HR}$ | Δ(m/z) | $(P)_{HR}$ | % |
|---|---|---|---|
| $[R+(^{35}Cl)(^{79}Br)_2]^+$ 192.805527 | 193 | 0.1946 | 44.13 |
| $[R+(^{35}Cl)(^{79}Br)(^{81}Br)]^+$ 194.803481 | 195 | 0.3787 | 100.00 |
| $[R+(^{37}Cl)(^{79}Br)_2]^+$ 194.80257 | | 0.0623 | |
| $[R+(^{35}Cl)(^{81}Br)_2]^+$ 196.801435 | 197 | 0.1842 | 69.25 |
| $[R+(^{37}Cl)(^{79}Br)(^{81}Br)]^+$ 196.800530 | | 0.1212 | |
| $[R+(^{37}Cl)(^{81}Br)_2]^+$ 198.798484 | 199 | 0.0589 | 13.36 |




| Isotopologues $\Delta(m/z)_{HR}$ | Δ(m/z) | $(P)_{HR}$ | % |
|---|---|---|---|
| $[R+(^{35}Cl)(^{79}Br)_3]^+$ 271.723864 | 272 | 0.0986 | 26.49 |
| $[R+(^{35}Cl)(^{79}Br)_2(^{81}Br)]^+$ 273.721818 | 274 | 0.2880 | 85.87 |
| $[R+(^{37}Cl)(^{79}Br)_3$ 273.720913 | | 0.0316 | |
| $[R+(^{35}Cl)(^{79}Br)(^{81}Br)_2]^+$ 275.719772 | 276 | 0.2801 | 100.00 |
| $[R+(^{37}Cl)\ (^{79}Br)_2\ (^{81}Br)]^+$ 275.718867 | | 0.0921 | |
| $[R+(^{35}Cl)(^{81}Br)_3]^+$ 277.717726 | 278 | 0.0908 | 48.47 |
| $[R+(^{37}Cl)\ (^{79}Br)\ (^{81}Br)_2]^+$ 277.716821 | | 0.0896 | |
| $[R+(^{37}Cl)(^{81}Br)_3]^+$ 279.714775 | 280 | 0.0291 | 7.82 |




| Isotopologues $\Delta(m/z)_{HR}$ | Δ(m/z) | $(P)_{HR}$ | % |
|---|---|---|---|
| $[R+(^{35}Cl)_2(^{79}Br)]^+$ 148,866043 | 149 | 0.2909 | 62.00 |
| $[R+(^{35}Cl)_2(^{81}Br)]^+$ 150,853997 | 151 | 0.2830 | 100.00 |
| $[R+(^{35}Cl)(^{37}Cl)(^{79}Br)]^+$ 150,853092 | | 0.1862 | |
| $[R+(^{35}Cl)(^{37}Cl)(^{81}Br)]^+$ 152,851046 | 153 | 0.1811 | 44.92 |
| $[R+(^{37}Cl)_2(^{79}Br)_3$ 152,850141 | | 0.0297 | |
| $[R+(^{37}Cl)_2(^{81}Br)]^+$ 154,848095 | 155 | 0.0289 | 6.16 |

**Fig. 85 Intensities of $[R+Cl_2-Br]^+$ type ions**

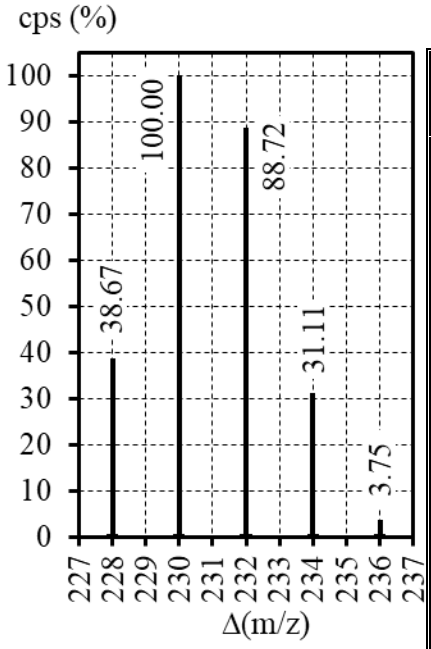



**Fig. 86 Intensities of $[R+Cl_2-Br_2]^+$ type ions**

| Isotopologues $\Delta(m/z)_{HR}$ | Δ(m/z) | $(P)_{HR}$ | % |
|---|---|---|---|
| $[R+(^{35}Cl)_2(^{79}Br)_2]^+$ 227,774380 | 228 | 0.1474 | 38.67 |
| $[R+(^{35}Cl)_2(^{79}Br)(^{81}Br)]^+$ 229,772334 | 230 | 0.2869 | 100.00 |
| $[R+(^{35}Cl)(^{37}Cl)(^{79}Br)_2]^+$ 229,771429 | | 0.0943 | |
| $[R+(^{35}Cl)_2(^{81}Br)_2]^+$ 231,770288 | 232 | 0.1395 | 88.72 |
| $[R+(^{35}Cl)(^{37}Cl)(^{79}Br)(^{81}Br)]^+$ 231,769383 | | 0.1836 | |
| $[R+(^{37}Cl)_2(^{79}Br)_2]^+$ 231,768478 | | 0.0151 | |
| $[R+(^{35}Cl)(^{37}Cl)(^{81}Br)_2]^+$ 233,767337 | 234 | 0.0893 | 31,11 |
| $[R+(^{37}Cl)_2(^{79}Br)(^{81}Br)]^+$ 233,766432 | | 0.0293 | |
| $[R+(^{37}Cl)_2(^{81}Br)_2]^+$ 235,764386 | 236 | 0.0143 | 3.75 |

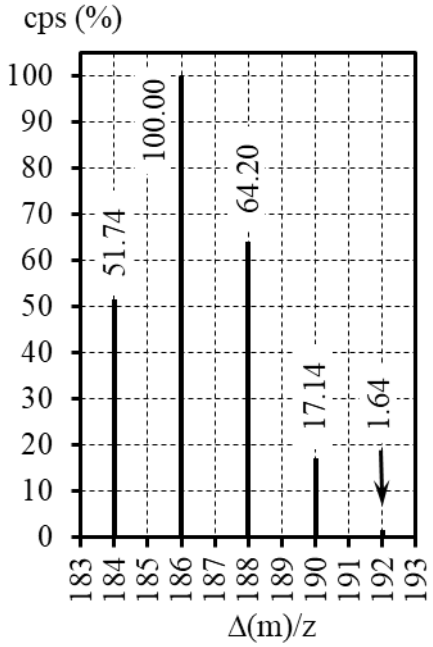



**Fig.87 Intensities of $[R+Cl_3-Br]^+$ type ions**

| Isotopologues $\Delta(m/z)_{HR}$ | Δ(m/z) | $(P)_{HR}$ | % |
|---|---|---|---|
| $[R+(^{35}Cl)_3(^{79}Br)]^+$ 183.824896 | 184 | 0.2204 | 51.74 |
| $[R+(^{35}Cl)_3(^{81}Br)]^+$ 185.822850 | 186 | 0.2144 | 100.00 |
| $[R+(^{35}Cl)_2(^{37}Cl)(^{79}Br)_2]^+$ 185.821945 | | 0.2116 | |
| $[R+(^{35}Cl)_2(^{37}Cl)(^{81}Br)_2]^+$ 187.819899 | 188 | 0.2058 | 64.20 |
| $[R+(^{35}Cl)(^{37}Cl)_2(^{79}Br)]^+$ 187.818994 | | 0.0677 | |
| $[R+(^{35}Cl)(^{37}Cl)_2(^{81}Br)]^+$ 189.816948 | 190 | 0.0658 | 17.14 |
| $[R+(^{37}Cl)_3(^{79}Br)]^+$ 189.816043 | | 0.0072 | |
| $[R+(^{37}Cl)_3(^{81}Br)]^+$ 191.813997 | 192 | 0.0070 | 1.64 |

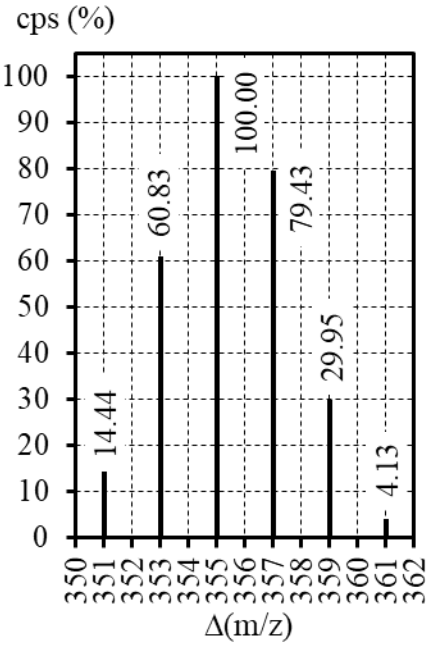



**Fig. 88 Intensities of $[R+Cl\text{-}Br_4]^+$ type ions**

| **Isotopologues** $\Delta(m/z)_{HR}$ | **Δ(m/z)** | **(P)HR** | **%** |
|---|---|---|---|
| $[R+(^{35}Cl)(^{79}Br)_4]^+$ 350,642201 | 351 | 0.0500 | 14.44 |
| $[R+(^{35}Cl)(^{79}Br)_3(^{81}Br)]^+$ 352,640155 | 353 | 0.1946 | 60.83 |
| $[R+(^{37}Cl)(^{79}Br)_4]^+$ 352,639250 | | 0.0160 | |
| $[R+(^{35}Cl)(^{79}Br)_2(^{81}Br)_2]^+$ 354,638109 | 355 | 0.2839 | 100.00 |
| $[R+(^{37}Cl)(^{79}Br)_3(^{81}Br)]^+$ 354,637204 | | 0.0623 | |
| $[R+(^{35}Cl)(^{79}Br)(^{81}Br)_3]^+$ 356,636063 | 357 | 0.1842 | 79.43 |
| $[R+(^{37}Cl)(^{79}Br)_2(^{81}Br)_2]^+$ 356,635158 | | 0.0908 | |
| $[R+(^{35}Cl)(^{81}Br)_4]^+$ 358,634017 | 359 | 0.0448 | 29.95 |
| $[R+(^{37}Cl)(^{79}Br)(^{81}Br)_3]^+$ 358,633112 | | 0.0589 | |
| $[R+(^{37}Cl)(^{81}Br)_4]^+$ 360,631066 | 361 | 0.0143 | 4.13 |

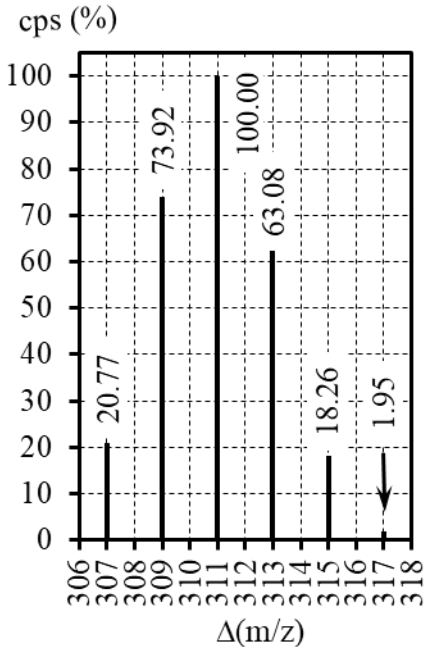



**Fig. 89 Intensities of $[R+Cl_2-Br_3]^+$ type ions**

| **Isotopologues** **Δ(m/z)HR** | **Δ(m/z)** | **(P)HR** | **%** |
|---|---|---|---|
| $[R+(^{35}Cl)_2(^{79}Br)3]^+$ 306.728717 | 307 | 0.0747 | 20.77 |
| $[R+(^{35}Cl)_2(^{79}Br)_2(^{81}Br)]^+$ 308.726671 | 309 | 0.2181 | 73.92 |
| $[R+(^{35}Cl)(^{37}Cl)(^{79}Br)_3]^+$ 308.707766 | | 0.0478 | |
| $[R+(^{35}Cl)_2(^{79}Br)_2(^{81}Br)_2]^+$ 310.724625 | 311 | 0.2122 | 100.00 |
| $[R+(^{35}Cl)(^{37}Cl)(^{79}Br)_2(^{81}Br)]^+$ 310.705720 | | 0.1396 | |
| $[R+(^{37}Cl)_2(^{79}Br)_3]^+$ 310.686815 | | 0.0076 | |
| $[R+(^{35}Cl)_2(^{81}Br)_3]^+$ 312.722579 | 313 | 0.0688 | 63.08 |
| $[R+(^{35}Cl)(^{37}Cl)(^{79}Br)(^{81}Br)_2]^+$ 312.703674 | | 0.1358 | |
| $[R+(^{37}Cl)(^{79}Br)_2(^{81}Br)]^+$ 312.684769 | | 0.0223 | |
| $[R+(^{35}Cl)(^{37}Cl)(^{81}Br)_3]^+$ 314.701628 | 315 | 0.0440 | 18.26 |
| $[R+(^{37}Cl)(^{79}Br)(^{81}Br)_2]^+$ 314.682723 | | 0.0217 | |
| $[R+(^{37}Cl)(^{81}Br)_3]^+$ 316.680677 | 317 | 0.0070 | 1.95 |

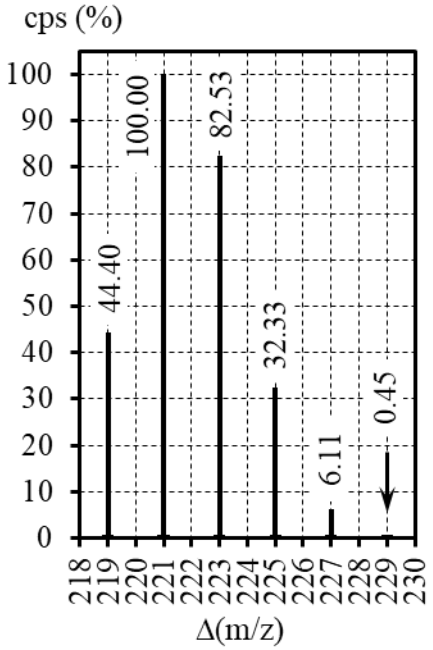



**Fig. 90 Intensities of $[R+Cl_4-Br]^+$ type ions**

| **Isotopologues $\Delta(m/z)_{HR}$** | **Δ(m/z)** | **(P)HR** | **%** |
|---|---|---|---|
| $[R+(^{35}Cl)_4(^{79}Br)]^+$ 218.865749 | 219 | 0.1670 | 44.40 |
| $[R+(^{35}Cl)_4(^{81}Br)]^+$ 220.863703 | 221 | 0.1624 | 100.00 |
| $[R+(^{35}Cl)_3(^{37}Cl)\ (^{79}Br)]^+$ 220.844798 | | 0.2137 | |
| $[R+(^{35}Cl)_3(^{37}Cl)(^{81}Br)]^+$ 222.842752 | 223 | 0.2079 | 82.53 |
| $[R+(^{35}Cl)_2(^{37}Cl)_2(^{79}Br)]^+$ 222.823847 | | 0.1025 | |
| $[R+(^{35}Cl)_2(^{37}Cl)_2(^{81}Br)]^+$ 224.821801 | 225 | 0.0997 | 32.33 |
| $[R+(^{35}Cl)(^{37}Cl)_3(^{79}Br)]^+$ 224.802896 | | 0.0219 | |
| $[R+(^{35}Cl)(^{37}Cl)_3(^{81}Br)]^+$ 226.800850 | 227 | 0.0213 | 6.11 |
| $[R+(^{37}Cl)_4(^{79}Br)]^+$ 226.781945 | | 0.0017 | |
| $[R+(^{37}Cl)_4(^{81}Br)]^+$ 228.779899 | 229 | 0.0017 | 0.45 |

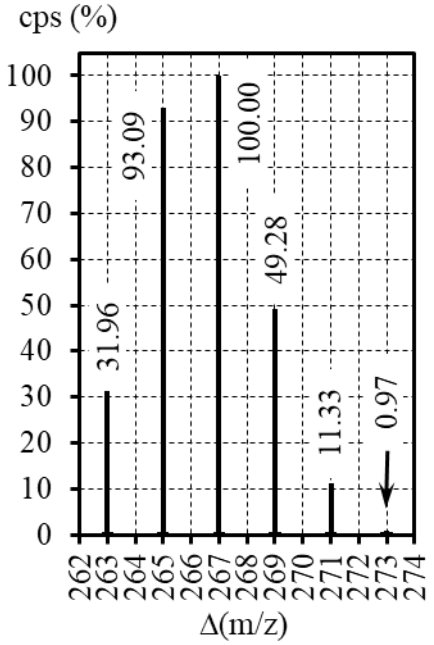



**Fig. 91 Intensities of $[R+Cl_3\text{-}Br_2]^+$ type ions**

| **Isotopologues** $\Delta(m/z)_{HR}$ | **Δ(m/z)** | **(P)HR** | **%** |
|---|---|---|---|
| $[R+(^{35}Cl)_3(^{79}Br)_2]^+$ 262.797233 | 263 | 0.1114 | 31.96 |
| $[R+(^{35}Cl)_3(^{79}Br)_1(^{81}Br)]^+$ 264.795187 | 265 | 0.2173 | 93.09 |
| $[R+(^{35}Cl)_2(^{37}Cl)(^{79}Br)_2]^+$ 264.776282 | | 0.1072 | |
| $[R+(^{35}Cl)_3(^{81}Br)_2]^+$ 266.793141 | 267 | 0.1057 | 100.00 |
| $[R+(^{35}Cl)_2(^{37}Cl)(^{79}Br)(^{81}Br)]^+$ 266.774236 | | 0.2086 | |
| $[R+(^{35}Cl)(^{37}Cl)_2(^{79}Br)_2]^+$ 266.755331 | | 0.0343 | |
| $[R+(^{35}Cl)_2(^{37}Cl)(^{81}Br)_2]^+$ 268.772190 | 269 | 0.1015 | 49.28 |
| $[R+(^{35}Cl)(^{37}Cl)_2(^{79}Br)(^{81}Br)]^+$ 268.753285 | | 0.0667 | |
| $[R+(^{37}Cl)_3(^{79}Br)_2]^+$ 268.734380 | | 0.0036 | |
| $[R+(^{35}Cl)(^{37}Cl)_2(^{81}Br)_2]^+$ 270.751239 | 271 | 0.0324 | 11.33 |
| $[R+(^{37}Cl)_3(^{79}Br)(^{81}Br)]^+$ 270.732334 | | 0.0071 | |
| $[R+(^{37}Cl)_3(^{81}Br)_2]^+$ 272.730288 | 273 | 0.0034 | 0.97 |

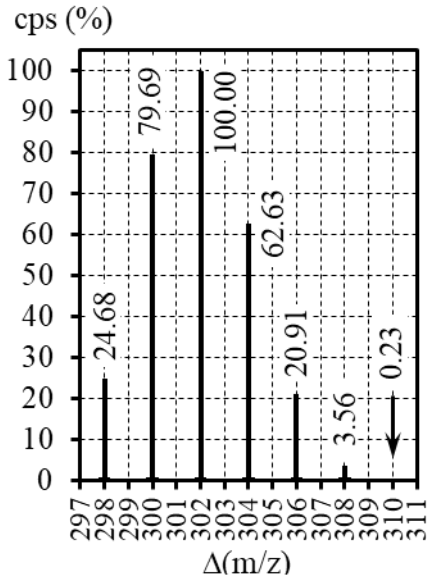



**Fig.92 Intensities of $[R+Cl_4-Br_2]^+$ type ions**

| **Isotopologues** $\Delta(m/z)_{HR}$ | **Δ(m/z)** | **(P)HR** | **%** |
|---|---|---|---|
| $[R+(^{35}Cl)_4(^{79}Br)_2]^+$ 297.784086 | 298 | 0.0846 | 24.68 |
| $[R+(^{35}Cl)_4(^{79}Br)(^{81}Br)]^+$ 299.782040 | 300 | 0.1647 | 79.69 |
| $[R+(^{35}Cl)_3(^{37}Cl)(^{79}Br)_2]^+$ 299.763135 | | 0.1083 | |
| $[R+(^{35}Cl)_4(^{81}Br)_2]^+$ 301.779994 | 302 | 0.0801 | 100.00 |
| $[R+(^{35}Cl)_3(^{37}Cl)(^{79}Br)(^{81}Br)]^+$ 301.761089 | | 0.2107 | |
| $[R+(^{35}Cl)_2(^{37}Cl)_2(^{79}Br)_2]^+$ 301.742184 | | 0.0520 | |
| $[R+(^{35}Cl)_3(^{37}Cl)(^{81}Br)_2]^+$ 303.759043 | 304 | 0.1025 | 62.63 |
| $[R+(^{35}Cl)_2(^{37}Cl)_2(^{79}Br)(^{81}Br)]^+$ 303.740138 | | 0.1011 | |
| $[R+(^{35}Cl)(^{37}Cl)_3(^{79}Br)_2]^+$ 303.721233 | | 0.0111 | |
| $[R+(^{35}Cl)_2(^{37}Cl)_2(^{81}Br)_2]^+$ 305.738092 | 306 | 0.0492 | 20.91 |
| $[R+(^{35}Cl)(^{37}Cl)_3(^{79}Br)(^{81}Br)]^+$ 305.719187 | | 0.0216 | |
| $[R+(^{37}Cl)_4(^{79}Br)_2]^+$ 305.700282 | | 0.0009 | |
| $[R+(^{35}Cl)(^{37}Cl)_3(^{81}Br)_2]^+$ 307.717141 | 308 | 0.0105 | 3.56 |
| $[R+(^{37}Cl)_4(^{79}Br)(^{81}Br)]^+$ 307.698236 | | 0.0017 | |
| $[R+(^{37}Cl)_4(^{81}Br)_2]^+$ 309.696190 | 310 | 0.0008 | 0.23 |

The relative signal intensities of ionic species with different configurations of chlorine and bromine isotopes can be more easily determined using an algorithm based on matrix calculation. The matrix method, which lends itself to the realization of suitable computer programs, is illustrated in several cases with the advantage of solving the problem for ionic species with a given number of chlorine and/or bromine atoms from the distribution of relative intensities of simpler ionic species, exploiting the additivity and recurrence properties of the procedure.

a) To determine the relative signal intensity distribution for $\mathbf{[R\text{-}Cl_2]^+}$ ions (target ion species), the ionic species is considered a composite of two (in this case identical) $\mathbf{[R\text{-}Cl]^+}$ species. Ion species of type $\mathbf{[R\text{-}Cl]^+}$ have two signals (one more than the number of chlorine atoms in the species) with relative percentage intensities 100 : 31.99 ) (Figure 70). With these values of relative percentage intensities, two matrices are constructed (identical this time, but with different roles in the following), $\mathbf{(I[R\text{-}Cl]^+)_a}$ and $\mathbf{(I[R\text{-}Cl]^+)_b}$:

$$\mathbf{(I[R\text{-}Cl]^+)_a} = \begin{bmatrix} 100 & 31.99 \end{bmatrix} \; ; \; \mathbf{(I[R\text{-}Cl]^+)_b} = \begin{bmatrix} 100 & 31.99 \end{bmatrix} \tag{34}$$

To determine the convolution of these matrices, the $\mathbf{(I[R\text{-}Cl]^+)_b^*}$ matrix (similar to a *Töplitz* matrix) is constructed from the $\mathbf{(I[R\text{-}Cl]^+)_b}$ matrix with two rows (the same number of rows as the number of elements in the $\mathbf{(I[R\text{-}Cl]^+)_a}$ matrix) and three columns (one more than the number of halogen atoms in the target ionic species):

$$\mathbf{(I[R\text{-}Cl]^+)_b^*} = \begin{bmatrix} 100.00 & 31.99 & 0 \\ 0 & 100.00 & 31.99 \end{bmatrix} \tag{35}$$

By multiplying the matrices $\mathbf{(I[R\text{-}Cl]^+)_a}$ and $\mathbf{(I[R\text{-}Cl]^+)_b^*}$ the matrix of the target ion $\mathbf{(I[R\text{-}Cl_2]^+)}$is obtained with elements representing the relative intensities (but not yet normalized to 100%):

$$\begin{aligned} \mathbf{(I[R\text{-}Cl_2]^+)} &= \begin{bmatrix} 100 & 31.99 \end{bmatrix} \cdot \begin{bmatrix} 100.00 & 31.99 & 0 \\ 0 & 100.00 & 31.99 \end{bmatrix} \\ &= \begin{bmatrix} 10000 & 6398 & 1023.3601 \end{bmatrix} \end{aligned} \tag{36}$$

The elements of the final matrix, $\mathbf{(I[R\text{-}Cl_2]^+)_n}$, are obtained by normalizing the elements of the matrix $\mathbf{(I[R\text{-}Cl_2]^+)}$ to 100% (the largest value is taken as 100 % and the others with proportionally smaller values).

$$\begin{aligned} \mathbf{(I[R\text{-}Cl_2]^+)_n} &= \frac{100}{10000} \cdot \begin{bmatrix} 10000 & 6398 & 1023.3601 \end{bmatrix} \\ &= \begin{bmatrix} 100.00 & 63.98 & 10.23 \end{bmatrix} \end{aligned} \tag{37}$$

The relative intensity values are almost identical to those shown in Figure 71, with small differences due to rounding of intermediate values to two decimal places.

b) Whit an analogous algorithm, the relative signal intensities of the $[\mathbf{R\text{-}Cl_2Br}]^+$ ions can be obtained by combining the data on the isotopic configurations of the $[\mathbf{R\text{-}Cl_2}]^+$ and $[\mathbf{R\text{-}Br}]^+$ ions. The matrix representations of the relative signal intensity distribution of these latter matrices, $(\mathbf{I[R\text{-}Cl_2]^+})$ and $(\mathbf{I[R\text{-}Br]^+})$ respectively, are (see Figures 69 and 92 for comparison):

$$(\mathbf{I[R-Cl_2]^+}) = [100 \quad 64 \quad 10.23] \; ; \; (\mathbf{I[R-Br]^+}) = [100 \quad 97.28] \tag{38}$$

The *Töplitz*-form matrix $(\mathbf{I[R\text{-}Br]^+})^*$ for the ionic species $[\mathbf{R\text{-}Br}]^+$ consists of three rows and four columns:

$$(\mathbf{I[R-Br]^+})^* = \begin{bmatrix} 100.00 & 97.28 & 0 & 0 \\ 0 & 100.00 & 97.28 & 0 \\ 0 & 0 & 100.00 & 97.28 \end{bmatrix} \tag{39}$$

The target matrix, $(\mathbf{I[R\text{-}Cl_2Br]^+})$, is the product of $(\mathbf{I[R\text{-}Cl_2]^+})$ and $(\mathbf{I[R\text{-}Br]^+})^*$ matrices:

$$(\mathbf{I[R-Cl_2Br]^+}) = [100.00 \quad 64.00 \quad 10.23] \cdot \begin{bmatrix} 100.00 & 97.28 & 0 & 0 \\ 0 & 100.00 & 97.28 & 0 \\ 0 & 0 & 100.00 & 97.28 \end{bmatrix} = \tag{40}$$

$$= [10000 \quad 16128 \quad 7248.92 \quad 995.1744]$$

The elements of the matrix $(\mathbf{I[R\text{-}Cl_2Br]^+})\mathbf{n}$ are the values normalized to 100 %.

$$(\mathbf{I[R-Cl_2Br]^+})_\mathbf{n} = \frac{100}{16128} \cdot [10000 \quad 16128 \quad 7248.92 \quad 995.1744] = \tag{41}$$

$$= [62.00 \quad 100.00 \quad 44.95 \quad 6.17]$$

The result is the same as in Figure 85 (small differences are due to rounding in the calculations).

(c) The ion $[\mathbf{R\text{-}Cl_4Br_2}]^+$ can be considered as the composition of the following ions $[\mathbf{R\text{-}Cl_4}]^+$ and $[\mathbf{R\text{-}Br_2}]^+$. The matrices associated with the constituent ions are (see Figures 71 and 75):

$$\begin{aligned} (\mathbf{I[R-Cl_4]^+}) &= [78.13 \quad 100.00 \quad 47.98 \quad 10.25 \quad 0.81] \\ (\mathbf{I[R-Br_2]^+}) &= [51.39 \quad 100.00 \quad 48.63] \end{aligned} \tag{42}$$

The *Töplitz*-form matrix corresponding to the ion $[\mathbf{R\text{-}Br_2}]^+$ is:

$$(\mathbf{I[R-Br_2]^+})^* = \begin{bmatrix} 51.39 & 100.00 & 48.63 & 0 & 0 & 0 & 0 \\ 0 & 51.39 & 100.00 & 48.63 & 0 & 0 & 0 \\ 0 & 0 & 51.39 & 100.00 & 48.63 & 0 & 0 \\ 0 & 0 & 0 & 51.39 & 100.00 & 48.63 & 0 \\ 0 & 0 & 0 & 0 & 59.39 & 100.00 & 48.63 \end{bmatrix} \tag{43}$$

The result (without normalization), $\mathbf{I[R\text{-}Cl_4Br_2]^+}$, is the matrix product between the matrices $\mathbf{I[R\text{-}Cl_4]^+}$ and $\mathbf{(I\ [R\text{-}Br_2]^+)^*}$,

$$\mathbf{I[R-Cl_4Br_2]^+ = I[R-Cl_4]^+ \cdot (I[R-Br_2]^+)^* =}$$
$$= [4015.10 \quad 12952.00 \quad 16265.15 \quad 10269.75 \quad 3406.37 \quad 579.46 \quad 39.39] \tag{44}$$

and the normalized result

$$\mathbf{(I[R-Cl_4Br_2]^+)_n} = [24.68 \quad 79.63 \quad 100.00 \quad 63.14 \quad 20.94 \quad 3.56 \quad 0.24] \tag{45}$$

is almost identical (within rounding errors) to that shown in Figure 92.

### 4.5 Finding the number of atoms of a chemical element in an ionic species

If a group of signals belonging to an ion can be identified in the spectrum, the relative intensities of the isotopic configurations of a chemical element can be used to determine the number of atoms of that chemical element in the ion. The procedure is illustrated in Figure 93, which shows the signals of a group of isotopic configurations of a chemical element where the mass difference between successive signals is two units (due to chlorine or bromine isotopes). The signals are numbered from the lowest value of the '**m/z**' ratio. The normalized relative intensities, $\mathbf{I_i(\%)}$ , (i = 1, 2 ,…, n, n+1)) (100 % for the base signal) are also given.

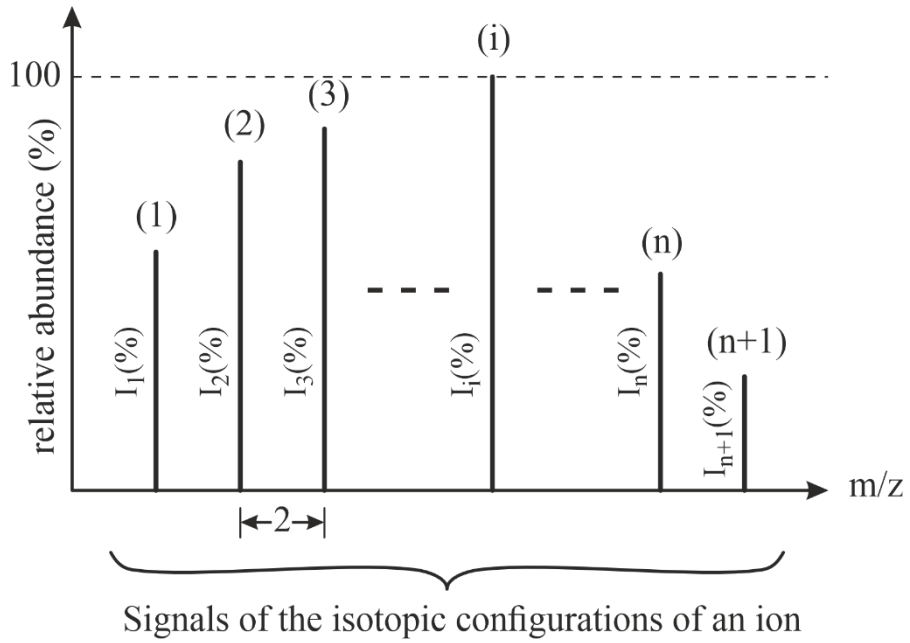



**Fig. 93 Finding the number of atoms of a chemical element in an ion containing two isotopes of that chemical element**

The determination of the number of atoms of a chemical element in the ion associated with a group of signals is based on a special form of the relation (30). In the case of a chemical element ('**E**') having two stable isotopes (denoted by superscripts

'**1**' and '**2**') with relative abundances '$^{1}\mathbf{x_E}$' and '$^{2}\mathbf{x_E}$' (normalized to the value '**1**', see Table 7, where the superscript '**1**' refers to the lighter isotope), the number of atoms '$\mathbf{n_E}$' of the chemical element ('**E**') in this ion is given by:

$$n_E = \frac{\log\left[I_1(\%)\right] - \log\left[\sum_i I_i(\%)\right]}{\log\left[{}^{1}x_E\right]} \qquad (46)$$

In relation (46) "$\mathbf{I_i(\%)}$" is the intensity of the signal with order number "(**i**)" (expressed as a percentage of the strongest signal in the group) and the sum is made over all the signals in the group. The symbol "**log**" represents the logarithmic function in base 10.

To give a concrete example of the use of relation (46), consider the group of signals shown in Figure 94, assigned to an ion containing "$\mathbf{n_{Cl}}$" chlorine atoms.

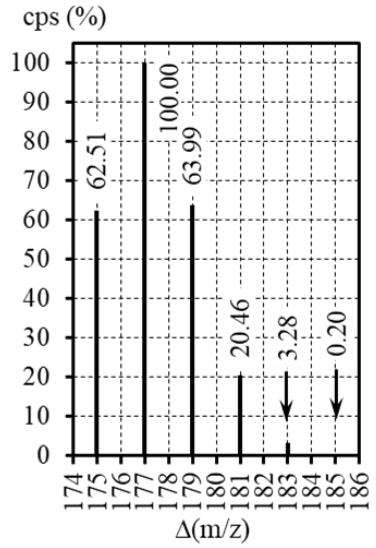



**Fig. 94**

**Intensity distribution of species with the isotopic configuration of an ion with "$\mathbf{n_{Cl}}$" chlorine atoms**

The sum of signal intensities (expressed as a percentage of the maximum intensity in the group) is as follows:

$$\sum_i I_1(\%) = 62.51 + 100.00 + 63.99 + 20.46 + 3.28 + 0.20 = 250.44 \qquad (47)$$

The percentage intensity of the signal with the minimum **m/z** ratio (the signal labeled (**1**)) is:

$$I_1(\%) = 62{,}51 \qquad (48)$$

The natural abundances of stable chlorine isotopes (Table 7) are:

$$\begin{aligned} {}^{1}x_{Cl} &= 0.7576 \text{ (for the isotope } {}^{35}Cl) \\ {}^{2}x_{Cl} &= 0.2424 \text{ (for the isotope } {}^{37}Cl) \end{aligned} \qquad (49)$$

Substitution the above values into equation (46) yields:

$$n_{Cl} = \frac{\log 62.51 - \log 250.44}{\log 0.7576} = 4.99962 \approx 5 \qquad (50)$$

Therefore, the ion in question contains 5 chlorine atoms.

A limitation of the approach described (and illustrated) above, based only on the signal with the minimum "**m/z**" ratio, is that in order to calculate the sum of the intensities involved in the relation used, it is necessary to observe all the signals in the group, including the signal with the maximum "**m/z**" ratio, which is often too small to be visible (as in the example shown in Figure 94). This drawback can be overcome by considering two consecutive signals of the group $\mathbf{I_i(\%)}$ and $\mathbf{I_{i+1}(\%)}$ with order numbers "**i**" and "**i+1**" respectively, which have sufficient intensities to be detected. Applying the equation (30) to these two signals gives the equation (51) for the chemical element '**E**' with isotopic weights '$\mathbf{^1x_E}$' (lighter isotope) and '$\mathbf{^2x_E}$' (heavier isotope).

$$\frac{I_i(\%)}{I_{i+1}(\%)} = \frac{i}{n_E - i + 1} \cdot \frac{^1x_E}{^2x_E} \qquad (51)$$

The number "$\mathbf{n_E}$" is expressed from the equation (52):

$$n_E = i \cdot \left[ 1 + \frac{I_{i+1}(\%)}{I_i(\%)} \cdot \frac{^1x_E}{^2x_E} \right] - 1 \qquad (52)$$

The procedure can be illustrated in the case of the chlorine atom, for which the group of signals in Figure 94 is analyzed. If we consider the first two signals with **i**=1 and **i+1** = 2 and the percentage intensities are $\mathbf{I_1(\%)}$ = 62.51 and $\mathbf{I_2(\%)}$ = 100.00, the number of chlorine atoms "$\mathbf{n_{Cl}}$" is calculated from equation (52) adapted to these data.

$$n_{Cl} = 1 \cdot \left[ 1 + \frac{100,00}{62,51} \cdot \frac{0,7576}{0,2424} \right] - 1 = 4,99986 \approx 5 \qquad (53)$$

The result is practically identical to (50) obtained with the method based on considering all the signals in the ion spectrum.

Applying the intensity ratio method to the intensity distribution in Figure 94 for the third (**i** = 3) and fourth (**i + 1** = 4) signals gives (52):

$$n_{Cl} = 3 \cdot \left[ 1 + \frac{20,46}{63,99} \cdot \frac{0,7576}{0,2424} \right] - 1 = 4,99793 \approx 5 \qquad (54)$$

If the group of signals represents the satellites of the molecular ion (unfragmented), the presented algorithm allows us to calculate the number of atoms of the chemical element even in the sample molecule itself.

### 4.6. Quantitative analysis

Mass spectrometry is a particularly reliable means of confirming the chemical identity of a compound, but it also offers the possibility of quantitatively determining the component of interest even when it is mixed with other substances. Quantitative determination methods are based on the (often linear) relationship between the intensity of the signal associated with the compound of interest and its amount in the sample. Like all methods of physicochemical analysis, quantitative mass spectrometry (in practice) relies on the use of standards containing a known amount of the substance of interest and consists of comparing the signal intensities produced by the standards and the sample under analysis.

#### 4.6.1. Quantitative analysis with external standard

One method of comparing the signals of a series of standards (with known content of the substance of interest) with the signal of the sample under analysis is to record the spectra of the series of standards and the spectrum of the sample in separate steps. The first step is to establish the relationship (linear or non-linear) between the signals in the mass spectrum and the amounts of the substance of interest in the series of standards and to construct a calibration line (assuming that the reported relationship is linear) (Figure 95). For this purpose, a signal (preferably strong) with a characteristic **m/z** ratio for the substance of interest is selected in the spectrum and a series of standards is prepared containing the known masses "$\mathbf{m_{e1}}$", "$\mathbf{m_{e2}}$", "$\mathbf{m_{e3}}$", ..., "$\mathbf{m_{en}}$" producing signals of respective intensities "$\mathbf{I_{e1}}$", "$\mathbf{I_{e2}}$", "$\mathbf{I_{e3}}$", ..., "$\mathbf{I_{en}}$". Plot the respective values "$\mathbf{I_{e1}}$", "$\mathbf{I_{e2}}$", "$\mathbf{I_{e3}}$", ... "$\mathbf{I_{en}}$" as a function of the "$\mathbf{m_{e1}}$", "$\mathbf{m_{e2}}$", "$\mathbf{m_{e3}}$", ..., "$\mathbf{m_{en}}$" values (Figure 95).

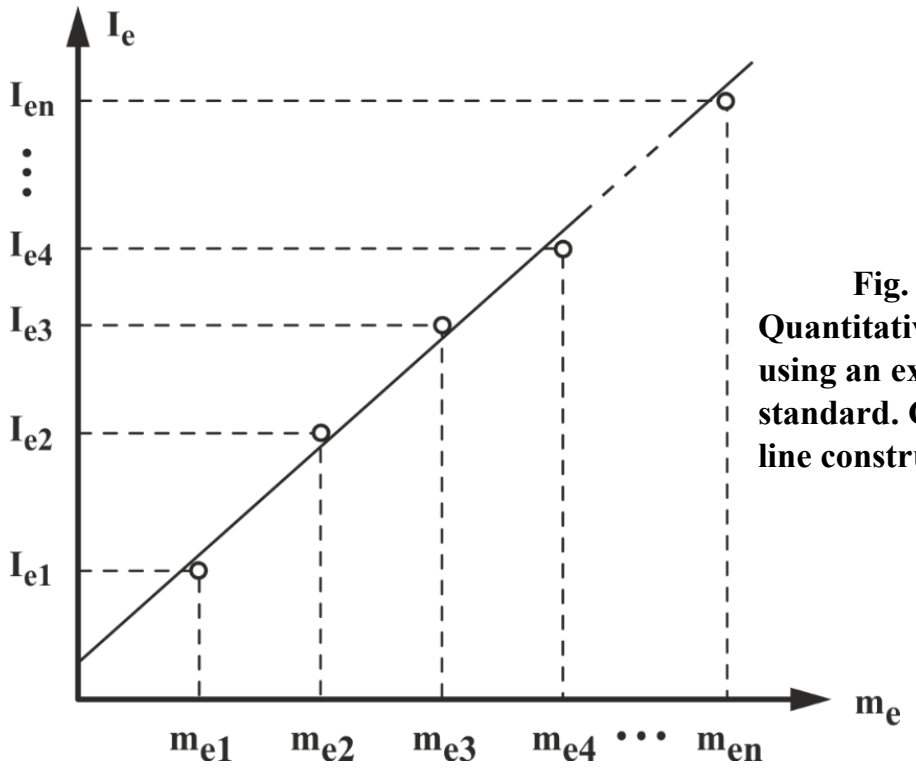



**Fig. 95 Quantitative analysis using an external standard. Calibration line construction**

Although the relationship is linear in principle, in real cases the points on the graph show deviations (due to inherent measurement errors) from the strictly linear relation. The most reliable calibration line, for which it is plausible that deviations from strict linearity are compensated, is determined by a well-known mathematical formalism (linear regression). The equation for the calibration line has the form (55).

$$I_{ei} = q + r \cdot m_{ei} \;\; ; \;\; (i = 1,2,3,...,n) \tag{55}$$

In equation (55) "**q**" is the intercept at the origin and "**r**" is the slope of the line (with respect to the reference system "$\mathbf{I_e}$" vs. "$\mathbf{m_e}$") in Figure (96). The problem is to express the variables "**q**" and "**r**" (for the equation of the calibration line) in terms of the pairs of values "$\mathbf{m_{ei}}$" and "$\mathbf{I_{ei}}$" (**i** = 1 , 2 , 3 , . . . , n). The essence of the mathematical formalism is that the sum of the squares of the deviations of the individual values from the optimum line must be minimum (for this reason it is also called the "least squares method"), i.e. the value of the quality function "**Φ(q,r)**", which depends on the variables "**q**" and "**r**" and is defined by the relation (56), must be minimum with respect to "**q**" and "**r**".

$$\Phi(q,r) = \sum_{i=1}^{n} \left( I_{ei} - q - r \cdot m_{ei} \right)^2 = \min \tag{56}$$

The necessary (but not always sufficient) condition to minimize the relation (56) is to cancel the partial derivatives of the function "**Φ(q,r)**" with respect to variables "**q**" and "**r**":

$$\begin{aligned} \frac{\partial \Phi(q,r)}{\partial q} &= \sum_{i=1}^{n} 2 \cdot \left( I_{ei} - q - r \cdot m_{ei} \right) \cdot (-1) = 0 \\ \frac{\partial \Phi(q,r)}{\partial r} &= \sum_{i=1}^{n} 2 \cdot \left( I_{ei} - q - r \cdot m_{ei} \right) \cdot (-m_{ei}) = 0 \end{aligned} \tag{57}$$

The development of relations (57) leads to following system of two linear equations concerning the unknowns **q** and **r**:

$$\begin{aligned} q \cdot n + r \cdot \sum_{i=1}^{n} m_{ei} &= \sum_{i=1}^{n} I_{ei} \\ q \cdot \sum_{i=1}^{n} m_{ei} + r \sum_{i=1}^{n} m_{ei}^2 &= \sum_{i=1}^{n} I_{ei} \cdot m_{ei} \end{aligned} \tag{58}$$

Solving the system (58) the intercept at origine (**q**) and the slope of the calibration line (**r**) are obtained, corresponding to the pairs of values '$\mathbf{m_{ei}}$' and '$\mathbf{I_{ei}}$' (**i** = 1, ..., n).

$$q = \frac{\sum_{i=1}^{n} I_{ei} \cdot \sum_{i=1}^{n} m_{ei}^2 - \sum_{i=1}^{n} I_{ei} \cdot m_{ei} \cdot \sum_{i=1}^{n} m_{ei}}{n \cdot \sum_{i=1}^{n} m_{ei}^2 - \left( \sum_{i=1}^{n} m_{ei} \right)^2}$$

$$r = \frac{n \cdot \sum_{i=1}^{n} I_{ei} \cdot m_{ei} - \sum_{i=1}^{n} I_{ei} \cdot \sum_{i=1}^{n} m_{ei}}{n \cdot \sum_{i=1}^{n} m_{ei}^2 - \left( \sum_{i=1}^{n} m_{ei} \right)^2} \qquad (59)$$

To determine the mass "**$m_p$**" of the compound of interest in the sample, the signal intensity "**$I_p$**" (located at the same "**m/z**" ratio for which the calibration line was constructed) is measured in the mass spectrum and the mass "**$m_p$**" is determined using the calibration line equation (55).

$$m_p = \frac{I_p - q}{r} \qquad (60)$$

### 4.6.2. Quantitative analysis by the addition method (enrichment method)

Quantitative analysis by stepwise addition of the standard to the sample is useful when it is suspected that the presence of accompanying substances (other than those of interest) may influence the sensitivity of the response to the substance of interest. In this case, all the the standards should contain the same set and the same amounts of interferents as the sample.

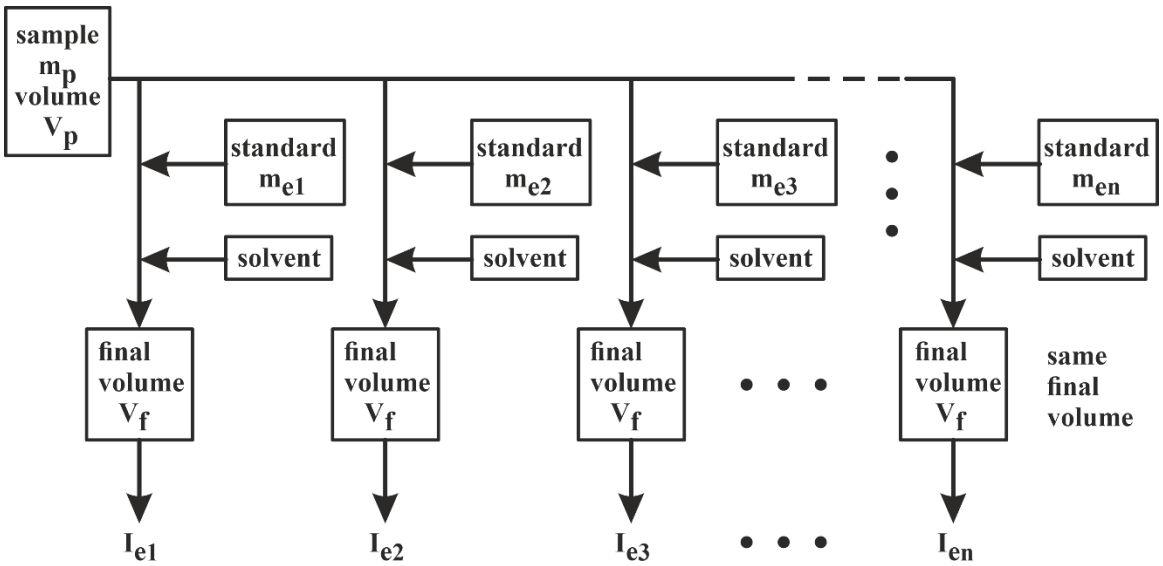



**Fig. 96 Preparation of the calibration set in the analysis by addition (enrichment)**

Figure 96 illustrates the steps in the preparation of the spiking series. To the same volume '$\mathbf{V_p}$' of sample containing the (unknown) mass '$\mathbf{m_p}$' of the substance of interest (analyte), increasing masses of standard ('$\mathbf{m_{e1}}$', '$\mathbf{m_{e2}}$', ..., '$\mathbf{m_{en}}$') are added and each mixture is made up to the same final volume '$\mathbf{V_f}$' with appropriate amounts of solvent. The solutions obtained contain, in addition to the unknown mass '$\mathbf{m_p}$', known amounts of the standard and the same amounts of accompanying substances as the sample. For each solution obtained, measure the signal intensity of the mass spectrum "$\mathbf{I_{e1}}$", "$\mathbf{I_{e2}}$", ..., "$\mathbf{I_{en}}$" at an appropriate value of the "$\mathbf{(m/z)_a}$" ratio and plot the values of "$\mathbf{I_{e1}}$", "$\mathbf{I_{e2}}$", ..., "$\mathbf{I_{en}}$" as a function of the added masses "$\mathbf{m_{e1}}$", "$\mathbf{m_{e2}}$", ..., "$\mathbf{m_{en}}$" (Figure 97).

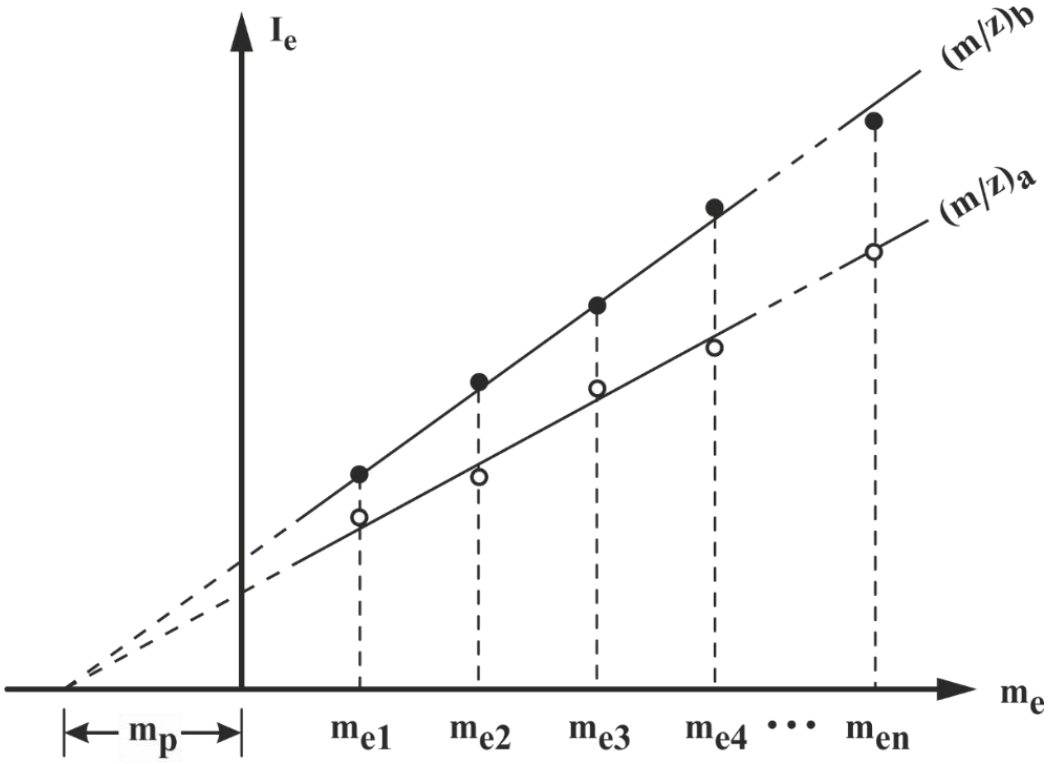



**Figure 97 Graphical display in the addition method**

The line determined by the pair of values, using the linear regression method, is extended in the negative direction of the "$\mathbf{m_e}$" axis to the intersection point with the negative part of this axis. The mass of the substance of interest ('$\mathbf{m_p}$') in the sample is expressed by the segment delimited by the point of intersection and the origin of the reference system.

For safety reasons the reading of the intensities "$\mathbf{I_{e1}}$", "$\mathbf{I_{e2}}$", ... "$I_{en}$" can be repeated for another ratio "$\mathbf{(m/z)_b}$". If the two signals "$\mathbf{(m/z)_a}$" and "$\mathbf{(m/z)_b}$" are specifically correlated with the compound of interest, the two lines will intersect the "$\mathbf{m_e}$" axis (practically) at the same point (Figure 97).

### 4.6.3. Quantitative analysis by isotope dilution mass spectrometry (IDMS)

For the analysis of very small amounts and concentrations, a suitable method has been developed, isotope dilution analysis, which is similar in principle to various forms of saturation analysis (radioimmunoassay - RIA, DELFIA, ELISA, etc.) used in biochemistry or medicinal chemistry. The essence of the variant adapted for mass spectrometry is shown in Figure 98.

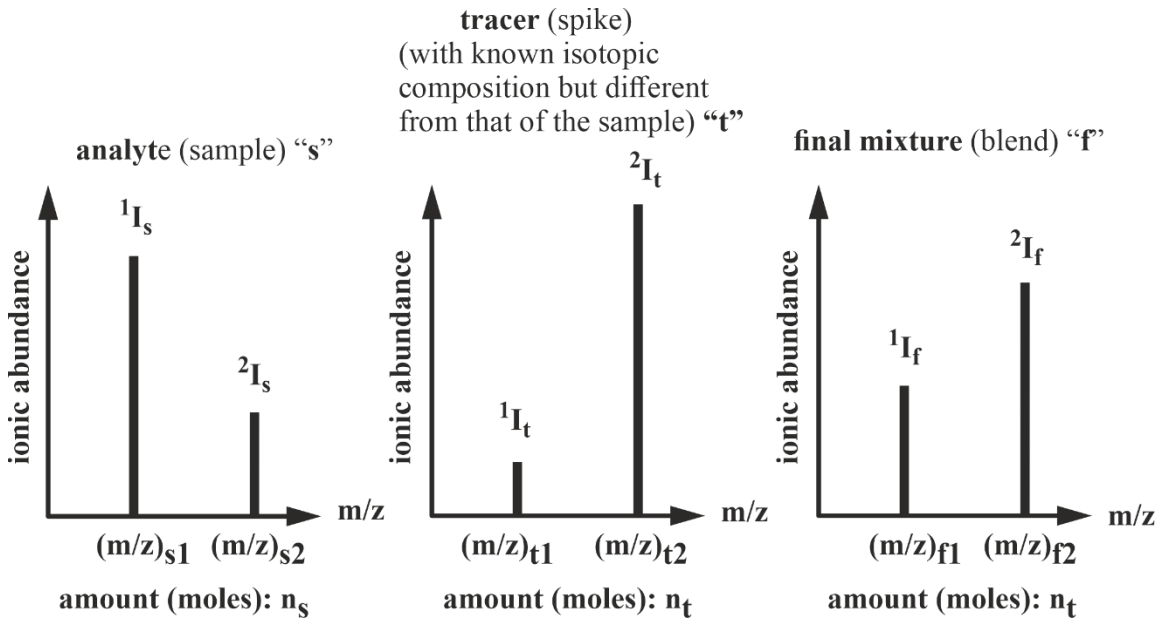



**Fig. 98 Illustration of the isotope dilution technique (IDMS)**

The method involves the identification of two signals of the chemical species of interest (analyte, sample, '**s**') associated with two forms (two isotopologues) with different isotopic configurations (isotopic configuration '**1**' with relative intensity $^1\mathbf{I_s}$ and isotopic configuration '**2**' with relative intensity $^2\mathbf{I_s}$) of the chemical compound of interest in the sample (the subscript '**s**' stands for 'sample'). The signals appear in the mass spectrum at the ratios **"$(m/z)_{s1}$"** and **"$(m/z)_{s2}$"** and their intensities depend on the relative abundance of the two isotopic forms of the sample (Figure 98). For example, the two signals may be associated with two species with different degrees of deuteration (i.e., different levels of heavy hydrogen isotope). The aim is to determine the number of moles ($\mathbf{n_s}$) of the substance of interest in the sample. To do this, a known amount ($\mathbf{n_t}$ moles) of the same chemical species (the subscript "**t**" indicates the "tracer" role), but with a different isotopic composition than that of the sample, is added to the sample. In the tracer spectrum, the isotopologue with isotopic composition "**1**" appears as a signal of intensity $^1\mathbf{I_t}$ and the isotopologue with isotopic composition "**2**" produces a signal of intensity $^2\mathbf{I_t}$. The final mixture (subscript "**f**") contains the two isotopic forms ("**1**" and "**2**") in a different ratio than in the sample and tracer and appears in the final mixture spectrum as intensity signals $^1\mathbf{I_f}$ and $^2\mathbf{I_f}$. The intensities $^1\mathbf{I_p}$ , $^2\mathbf{I_p}$ , $^1\mathbf{I_t}$ ,

$^2\mathbf{I_t}$ , $^1\mathbf{I_f}$ and $^2\mathbf{I_f}$ can be determined from the individual mass spectra of the sample, tracer and final mixture.

The material balance for the isotopically labeled form "**1**" is expressed by equations (61).

$$n_s \cdot \frac{^1I_s}{^1I_s + {}^2I_s} + n_t \cdot \frac{^1I_t}{^1I_t + {}^2I_t} = n_f \cdot \frac{^1I_f}{^1I_f + {}^2I_f} \qquad (61)$$

The intensity ratio ('**r**') expresses the ratio of isotopologue "**1**" in the sample, ('$\mathbf{r_s}$'), in the tracer ('$\mathbf{r_t}$') and in the final mixture ('$\mathbf{r_f}$'):

$$\frac{^1I_s}{^1I_s + {}^2I_s} = r_s \;\; ; \;\; \frac{^1I_t}{^1I_t + {}^2I_t} = r_t \;\; ; \;\; \frac{^1I_f}{^1I_f + {}^2I_f} = r_f \qquad (62)$$

With these notations, the relationship (61) is as follows:

$$n_s \cdot r_s + n_t \cdot r_t = (n_s + n_t) \cdot r_f \qquad (63)$$

Expressing the number of moles "$\mathbf{n_s}$" from relation (61), we get:

$$n_s = n_t \cdot \frac{r_f - r_t}{r_s - r_f} \qquad (64a)$$

The amount (number of moles) of tracer ("$\mathbf{n_t}$") added is known. If the ratios '$\mathbf{r_s}$', '$\mathbf{r_t}$' and $\mathbf{r_f'}$ can also be determined (from the individual mass spectra of the sample, tracer and final mixture), then the amount (number of moles) of sample ("$\mathbf{n_s}$") can be determined from equation (64-a). If, however, it is not possible to determine the isotopic ratio of the sample substance ('$\mathbf{r_s}$'), the analysis is repeated with the same quantity of primary sample ("$\mathbf{n_s}$") but with a different (also known) quantity of added tracer, $\mathbf{n_t'}$. As a result, the ratios '$\mathbf{r_s}$' and '$\mathbf{r_t'}$' do not change, but the isotopic ratio of the mixture changes to "$\mathbf{r_f}$" (measurable quantity in the spectrum). Equation (64-a) then becomes:

$$n_s = n_t' \cdot \frac{r_f' - r_t}{r_p - r_f'} \qquad (64b)$$

Removing the ratio " $\mathbf{r_s}$" from relations (64-a) and (64-b) yields:

$$n_s = \frac{n_t \cdot (r_f - r_t) - n_t' \cdot (r_f' - r_t)}{r_f' - r_f} \qquad (64c)$$

Once the result, expressed in number of moles ("$\mathbf{n_S}$") is available, the mass of the substance of interest in the sample ("$\mathbf{m_S}$") is calculated by multiplying the number of moles by the average molecular mass "$\overline{\mathbf{M}}_\mathbf{S}$" of the chemical substance of interest:

$$m_S = \overline{M}_S \cdot n_S \qquad (65)$$

For quantitative analysis by isotope dilution, many different and improved variants are known, but essentially like the one presented.

### 4.7. Impurity detection and mixture recognition

If the sample to be analyzed is impure in the sense that it contains unknown components in addition to the expected ones, then the mass spectrum will also contain their signals. If the impurity signals occur at mass values greater than the mass of the molecular ion of interest, they may be misattributed to the molecular ion. To avoid such errors, the spectrum is recorded at lower ionization energies. It is plausible that the spectra obtained at lower ionization energies may lack some or all the signals corresponding to sample fragmentation ions and impurities. Therefore, it can be assumed that signals at **m/z** values higher than that of the expected molecular ion are due to fragmentation ions of impurity molecules and tend to disappear at lower ionization energies. If the signal at the abnormally high **m/z** value is due to the molecular ion of an impurity, reducing the ionization energy is not a solution because the molecular ion of the impurity will remain in the spectrum in addition to the signal from the molecular ion of the component of interest. In this case, prior purification of the primary sample is required.

During MS analysis, several physical phenomena may influence and/or discriminate the components of the mixture.

a) Mixtures of isomers of a compound are very difficult to detect because they have identical molecular masses. The only way to distinguish the isomers is to compare how they are fragmented.

b) Two compounds in a mixture, neighbors in a homologous series, are recognized by the presence of a signal 14 mass units smaller (methylene fragment, $>CH_2$) than the signal of the molecular ion. It is unlikely that the signal 14 mass units away from the molecular ion is due to fragmentation of the molecular ion (forming the $\mathbf{[M-14]^+}$ ion, i.e. molecular mass minus 14 mass units), since removal of the methylene group from the molecular ion could only occur in the form of the energetically unfavorable carbene ($:CH_2$) species. For example, if in the recorded mass spectrum of a sample of myristic acid (relative molecular mass 228) there are two signals at m/z 214 and 200, this indicates the presence of two lower homologues in the sample: tridecanoic acid (at **m/z** 214) and lauric acid (at **m/z** 200).

c) A mixture of compounds belonging to different chemical classes can be identified by the presence of signals that cannot be attributed to the cleavage of a single molecular ion. For example, the presence of a signal at **m/z** 131 followed by another signal at **m/z** 121 indicates the presence of a mixture because no chemical species with a mass of 10 mass units are cleaved from a heavier ion. Such illogical signals have lower **m/z** ratios than the molecular ion signal with values between 3-14 mass units and between 21-25 mass units (signals with **m/z** values between M-3 and M-14 and between M-21 and M-25 are illogical).

d) If the sample is introduced directly into the ionization unit (by a route other than the chromatograph-mass spectrometer coupled assembly), fractional distillation of the components may occur, in the sense that the components of the mixture are gradually evaporated in the order of their volatility. For this reason, the mass spectrum recorded at the lower temperature of the ionization unit is richer in the signals of the more volatile components than those of the less volatile components. If the spectra recorded at different ionization unit, temperatures do not show a proportional relationship between the signals, it is suspected that the sample introduced is a mixture.

e) Another physical factor that can affect the relative intensity of the signals is the viscosity of the gaseous components. When the sample is introduced indirectly into the ionization unit, the sample vapor passes through an interface (capillary tube or porous disc) to control the pressure difference between the outside and inside the ionization unit. The laminar flow velocity of the vapor through small orifices is inversely proportional to the square root of the molecular mass. Lighter components of the mixture tend to move across the interface at higher velocities than heavier components. As a result, the gas mixture is initially richer in lighter components and, over time, the ratio of the components changes in favor of the heavier ones. When the spectrum of a pure substance is recorded at different injection velocities, the relative intensity of the signals remains approximately unchanged, which is not the case when a mixture is injected under similar conditions.

f) As an alternative method of highlighting a mixture, it is possible to progressively reduce the energy of the ionization electrons down to an energy of 8 eV. If the sample is pure (contains a single chemical species) then, from a certain ionization energy value downwards, only one signal appears in the spectrum corresponding to the molecular ion. If the sample is a mixture, the signals of all the molecular ions remain even at low ionization energy values.

Although each of the mixture detection methods has specific limitations, combined use of them provides reliable mixture detection in most cases.

### 4.8. Types of fragmentation of the organic compounds

Molecular ions formed during primary ionization can undergo fragmentation to produce ionic and/or radical species with masses smaller than the ions from which they originate. Fragmentation of an ion (splitting into lighter ions and neutral species) sometimes occurs spontaneously due to excess internal energy acquired in the ionization unit, or caused by collision with gas atoms (nitrogen, helium). Fragmentation is deliberately induced in $MS^2$ analysis when an ion (precursor) is selected from the primary spectrum and the spectrum of fragments resulting from the cleavage of the selected precursor ion is recorded in the second stage of the analysis.

a) Whether the molecular ion $\mathbf{[M]^+}$ can undergo multiple fragmentation pathways, producing fragments $F_1$ , $\mathbf{F_2}$ , $\mathbf{F_3}$ , ... associated with the energies required to produce them $\mathbf{\Delta E_1}$ , $\mathbf{\Delta E_2}$ , $\mathbf{\Delta E_3}$ ,.. such that $\mathbf{\Delta E_1 < \Delta E_2 < \Delta E_3}$ < ... then the abundance of the ionic fragments - and hence the intensity of the corresponding signals - varies in the order $\mathbf{I(F_1) > I(F_2) > I(F_3)}$ > ... (Figure 99).

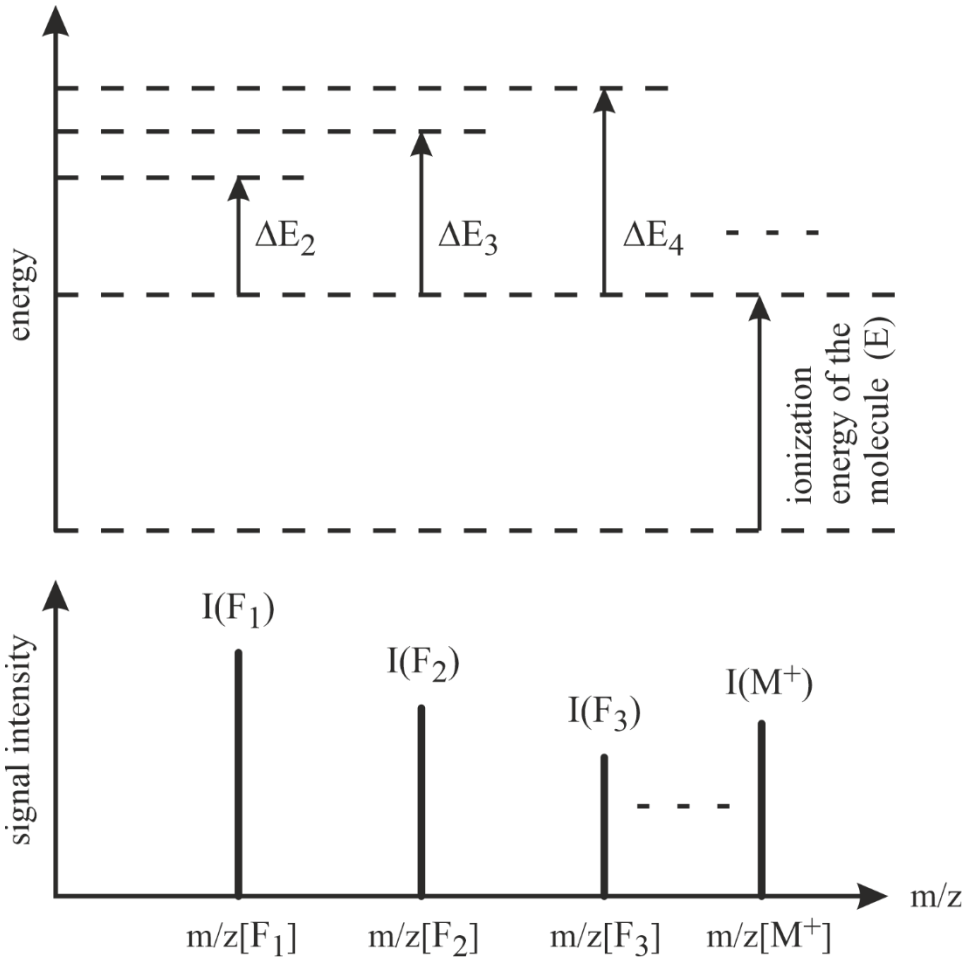
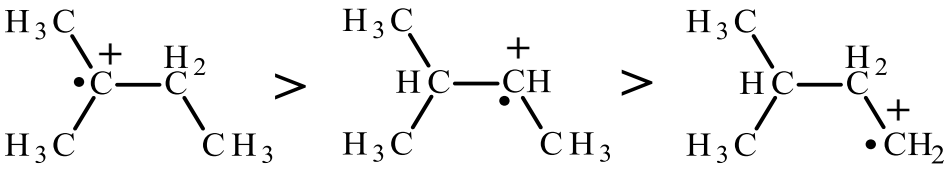



**Fig. 99 Relationship between the energies required for fragmentation and the relative abundance of fragments produced.**

b) Ionic fragments may undergo further transformation or fragmentation depending on their stability, in the sense that a more stable ionic fragment will show up more strongly in the spectrum than a less stable one. For example, the positively charged carbocation located on a tertiary carbon atom of an alkyl residue is more stable than the positively charged carbocation located on a secondary carbon atom, and the latter is more stable than the positively charged carbocation located on a primary carbon atom. Thus, among the radical carbocations resulting from the isopentane molecule, the order of stability is as follows:



c) The ions formed may be positive $[M]^+$ or negative $[M]^-$ ions with an even number of electrons (singlet state) or radical ions (e.g., $[M]^{+\bullet}$), that have both ionic and radical properties (odd number of electrons, doublet state), which may slightly affect their stability. Ions with an even number of electrons are more stable and therefore produce higher intensity signals than ions with an odd number of electrons.

For the interpretation of a mass spectrum, it is important to know the plausible fragmentation pathways. Fragmentation pathways are conventionally classified as follows.

(1) Simple fragmentation - is the removal of an electrically neutral fragment (neutral molecule or radical) from the primary ion by cleavage of a single chemical bond.

(2) Fragmentation with transposition of a hydrogen atom - involves the cleavage of multiple chemical bonds associated with the transfer of a hydrogen atom from one atom to another in the same ionic species.

(3) Complex fragmentations - are specific to ions with a cyclic or aromatic structure and result from the removal of fragments containing atoms from the cyclic structure.

(4) Fragmentation with double transposition of the hydrogen atom - consists in the simultaneous transposition of two hydrogen atoms from a neutral fragment to be removed to the ionic fragment to be formed.

(5) Fragmentation processes involving other types of transpositions - include those which are accompanied by - or preceded by - transpositions of groups or atoms other than hydrogen.

In the literature, the types of fragmentation listed are conventionally denoted by '**S**' (simple fragmentation), '**T**' (fragmentation with transposition of one hydrogen atom),

'**C**' (complex fragmentation), '**DT**' (fragmentation with transposition of two hydrogen atoms) and '**TS**' (transposition of different hydrogen groups or atoms). In most real cases, the fragmentation of molecular ions is the result of several processes occurring in parallel or in sequence, with weights depending on the nature of the substance analyzed.

### 4.8.1. Simple fragmentations - alkanes and cycloalkanes

Examples of **S**-type fragmentation are saturated hydrocarbons. Their molecules contain only σ bonds (C-C and C-H bonds). Since the strength of these bonds is approximately the same, the extraction of an electron and the cleavage of the σ bond after electron impact ionization can occur at different parts of the molecule. The radical ion can cleave in several ways, producing an alkyl ion (lower mass and positive charge) and an alkyl radical (electrically neutral) (Figure 100).

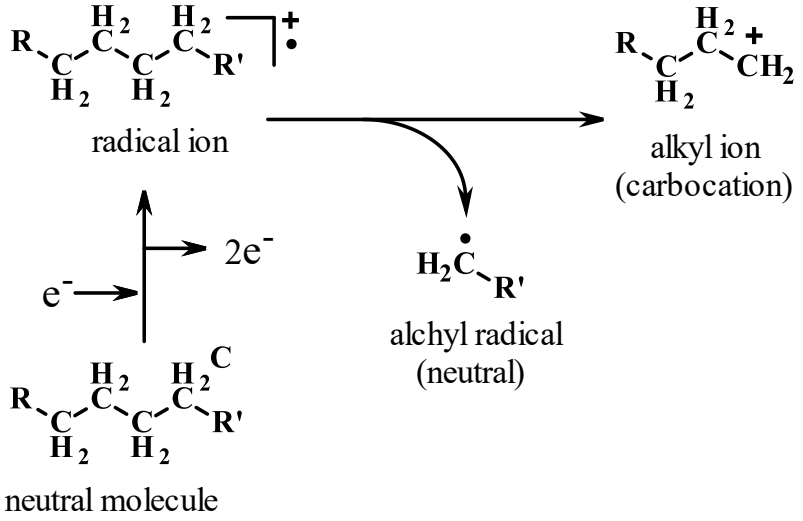



**Fig. 100 Simple fragmentation of the molecular ion of a saturated hydrocarbon**

Higher mass ionic fragments may undergo further fragmentation, while lower mass ions are relatively stable and produce a detectable signal in the spectrum. For saturated straight-chain hydrocarbons, the abundance of ionic fragments decreases progressively with increasing mass, and the signals have a typical shape. This phenomenon can be seen for example in Figure 101 in the mass spectrum of dodecane (EI ionization at energy 70 eV). The molecular ion appears at **m/z** 170. A series of signals at **m/z** 141, 127, 113, 99, 85, 71, 57, 43 and 29 Da are slightly highlighted. The mass difference between the positions of the consecutive signals is constant (14 Da), indicating that the corresponding fragments differ by one methylene group ( >CH2). The signals correspond to the following carbocations:

$[C_{10}H_{21}]^+$, $[C_9H_{19}]^+$, $[C_8H_{17}]^+$, $[C_7H_{15}]^+$, $[C_6H_{13}]^+$, $[C_5H_{11}]^+$, $[C_4H_9]^+$, $[C_3H_7]^+$ and $[C_2H_5]^+$.

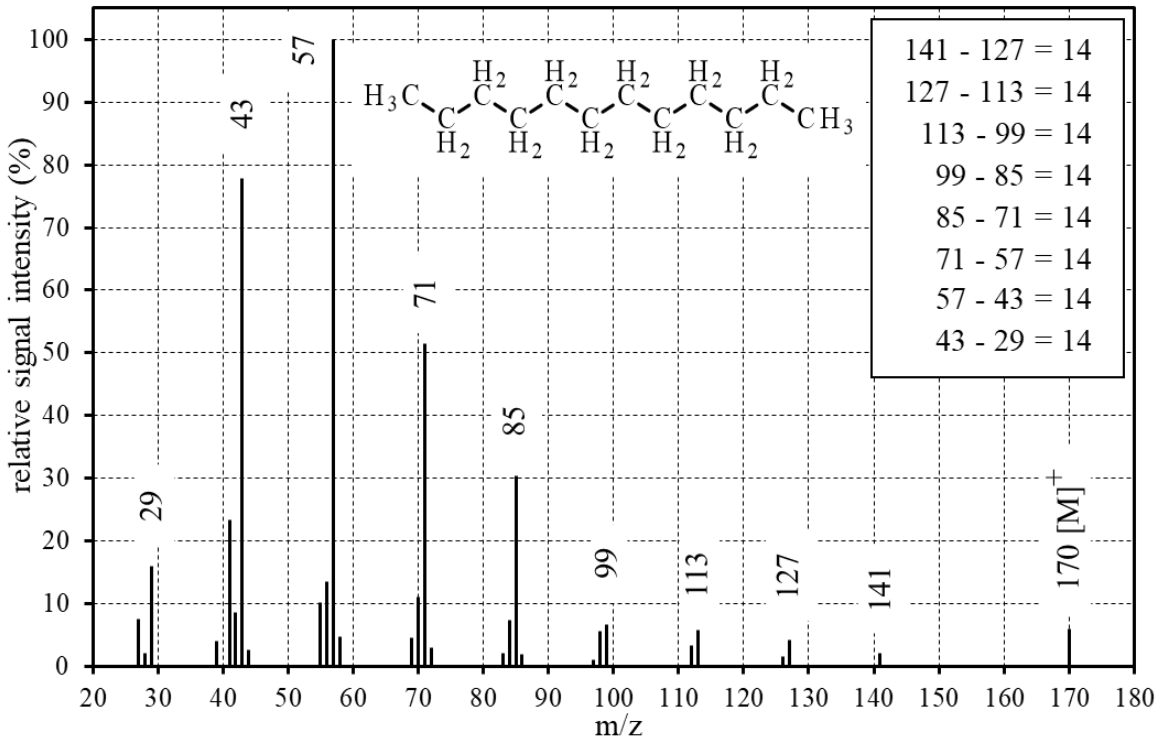



**Fig. 101 Mass spectrum of dodecane ($C_{12}H_{26}$) (EI ionization, energy: 70 eV) (reconstructed from data in T.A. Lee: A Beginner's Guide to Mass Spectral Interpretation, John Wiley & Sons, 1998 [ISBN: 0-741-97628-8] and from the SDBS spectral database https://sdbs.db.aist.go.jp)**

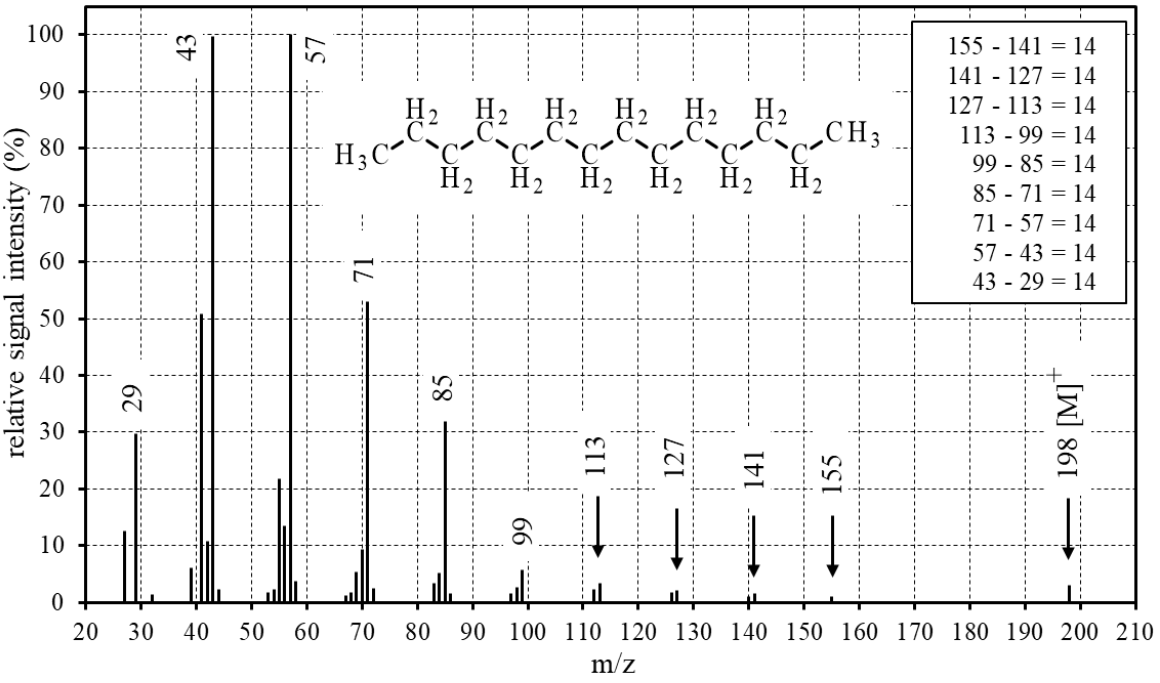



**Fig. 102 Mass spectrum of tetradecane ($C_{14}H_{30}$) (EI ionization, energy: 70 eV) (according to SDBS spectral database https://sdbs.db.aist.go.jp)**

Figure 102 shows the mass spectrum of tetradecane recorded using electron impact ionization (energy: 70 eV). The spectrum contains all the signals present in the dodecane spectrum and the mass difference between the consecutive signals (14 Da) also corresponds to a methylene group. Fragmentation of molecular ions of saturated and branched chain hydrocarbons preferentially occurs at the quaternary or tertiary carbon atom due to the higher stability of tertiary and secondary carbocations compared to primary carbocations.

### 4.8.2. Simple fragmentation - alkanes substituted with first order substituents

A category of fragmentation concerns hydrocarbon derivatives with substituents of order "I" (first order substituents): -F , -Cl , -Br , -I , -$NR_2$ , -OR , R = alkyl radical). A specific event is the cleavage of the chemical bond between the substituent and the alkyl radical. The cleavage of the bond can occur with the formation of a carbocation and the radical fragment of the substituent (process (**1**)) - on the one hand - or with the formation of an alkyl radical and the ionized substituent residue (process (**2**)) - on the other hand (Figure 103). The relative importance of the two processes depends on the electron affinity of the substituent **X** and the stability of the carbocation formed. If the substituent is iodine (**X** = I), then process (**2**) is favored over the case where the substituent **X** is another halogen (F, Cl, Br) because iodine has a lower electron affinity than the other halogens.

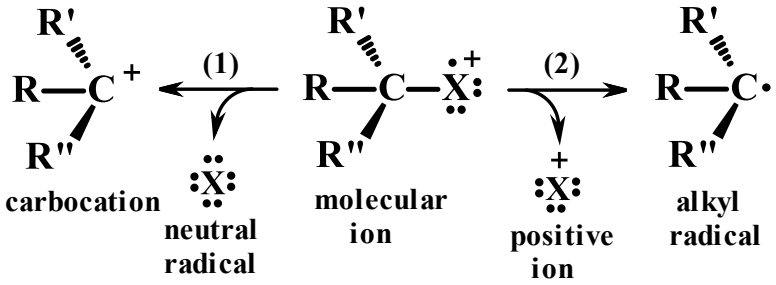



**Fig. 103 Fragmentation of a substituted alkane with a first order substituent**

The situation where the substituent **X** is the hydroxyl group (the case of alcohols) has been studied most thoroughly. In this case, processes **(1)** and **(2)** in Figure 103 form alkyl and alkoxy ions, but process **(1)** has an advantage because the alkyl ion is more stable than the positive hydroxy ion and because the alkyl radical is stabilized by the positive inductive effect of the alkyl radical.

This fragmentation category also includes ethers (where **X** = O-R). Figure 104 shows the mass spectrum of methyl 2-butyl ether in the positive mode. Ionization was realized by electron impact (EI) with electrons of 70 eV energy. The sample temperature was 270 $^{o}$C and the ion source temperature was 250 $^{o}$C. Signals marked with * are due to further rearrangements of the primary fragments.

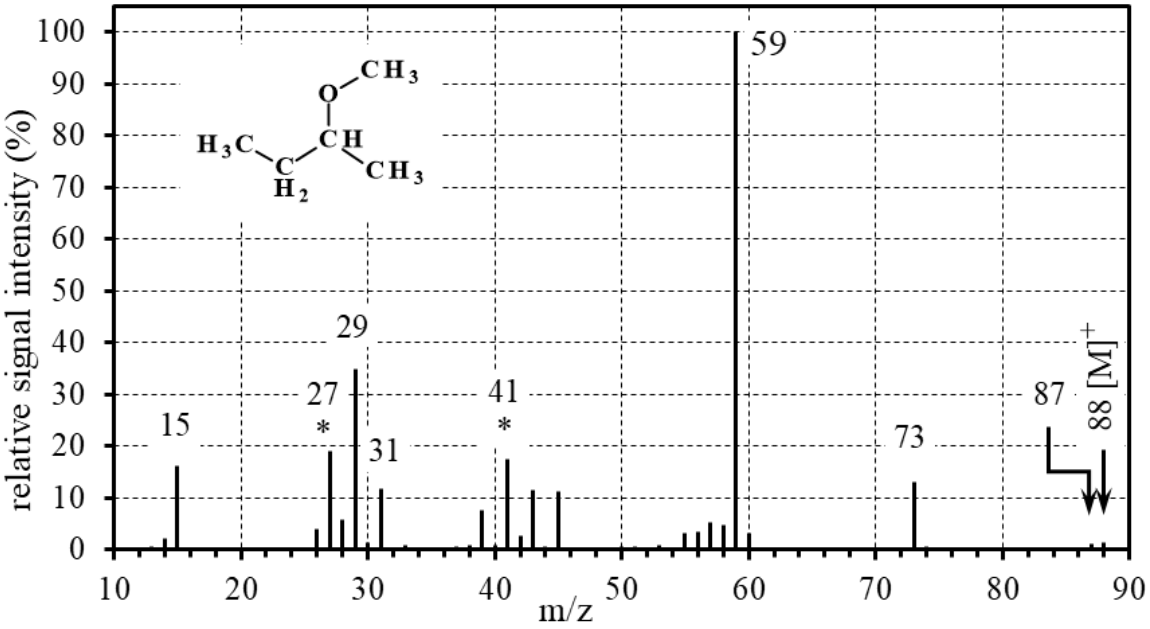



**Figure 104 MS[1] spectrum of methyl 2-butyl ether (ionization EI, 70 eV) (reconstructed from the data of SDBS spectral database https://sdbs.db.aist.go.jp)**

The primary signals can be attributed to the ionization fragments as follows (Figure 105).

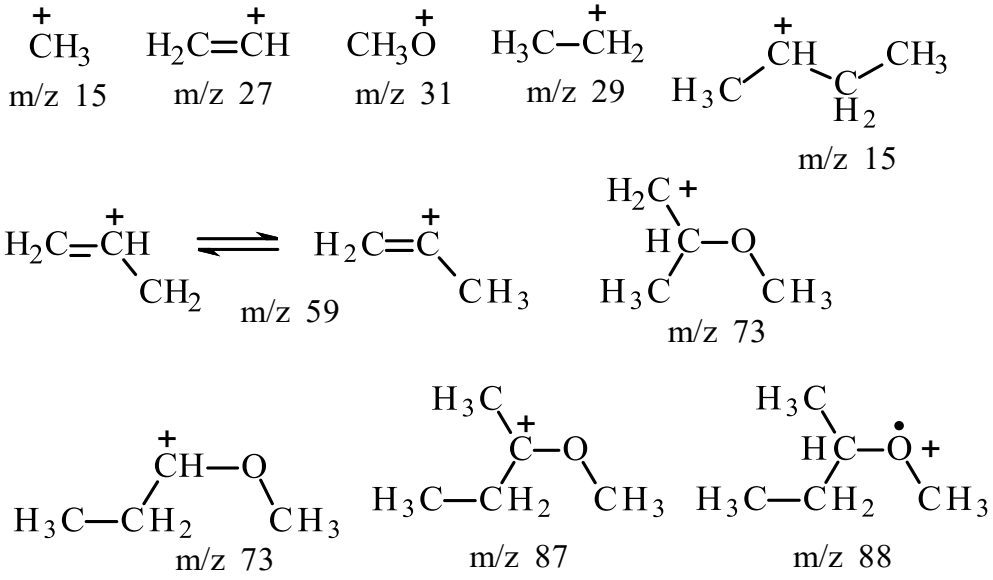



**Fig 105 Ions from the fragmentation of methyl 2-butyl ether**

Figure 106 suggests a possible fragmentation pathway for methyl 2-butyl ether.

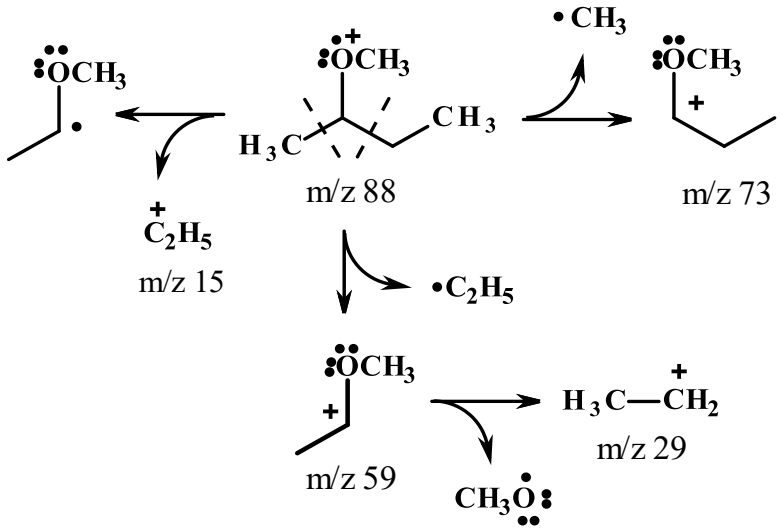



**Fig 106 Possible fragmentation scheme of methyl 2-butyl ether**

### 4.8.3. Simple fragmentation - unsaturated hydrocarbons

Fragmentation of molecular ions containing a double bond (bond "π") occurs preferentially at the "β" position over the double bond (allylic position, Figure 107). The resulting fragment is stabilized by delocalization of the electrons "π", a process conditioned by the possibility of successive displacement of the hydride ion ($H^-$) and/or the hydrogen atom (with radical character, $H^\bullet$).

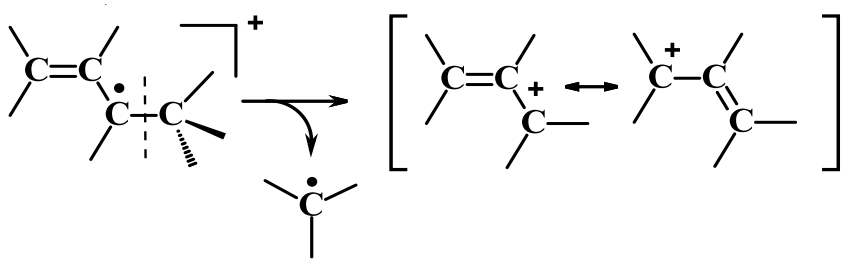


**Fig 107 Allylic fragmentation in alkenes with double bond migration**

Although one would expect the positional isomers to produce mass spectra with significantly different shapes, the mass spectra of the many alkenes that are unsubstituted at the alkenyl carbon atoms are very similar, sometimes identical; a phenomenon that suggests the possibility of double bond migration (Figure 107). For this reason, it is not possible to determine the position of the double bond from the mass spectra alone. Figure 108 compares the mass spectra of hexene isomers. The spectra were recorded using chemical impact ionization (with methane as impact gas) at 120 eV energy.

Figure 108 shows the similarity between the mass spectra of 1-hexene, trans-2-hexene, and trans-3-hexene. The problem of differentiating the positional isomers is solved by first converting the alkene to a suitable derivative (e.g. by an addition reaction) and then recording the mass spectrum of the derivative obtained.

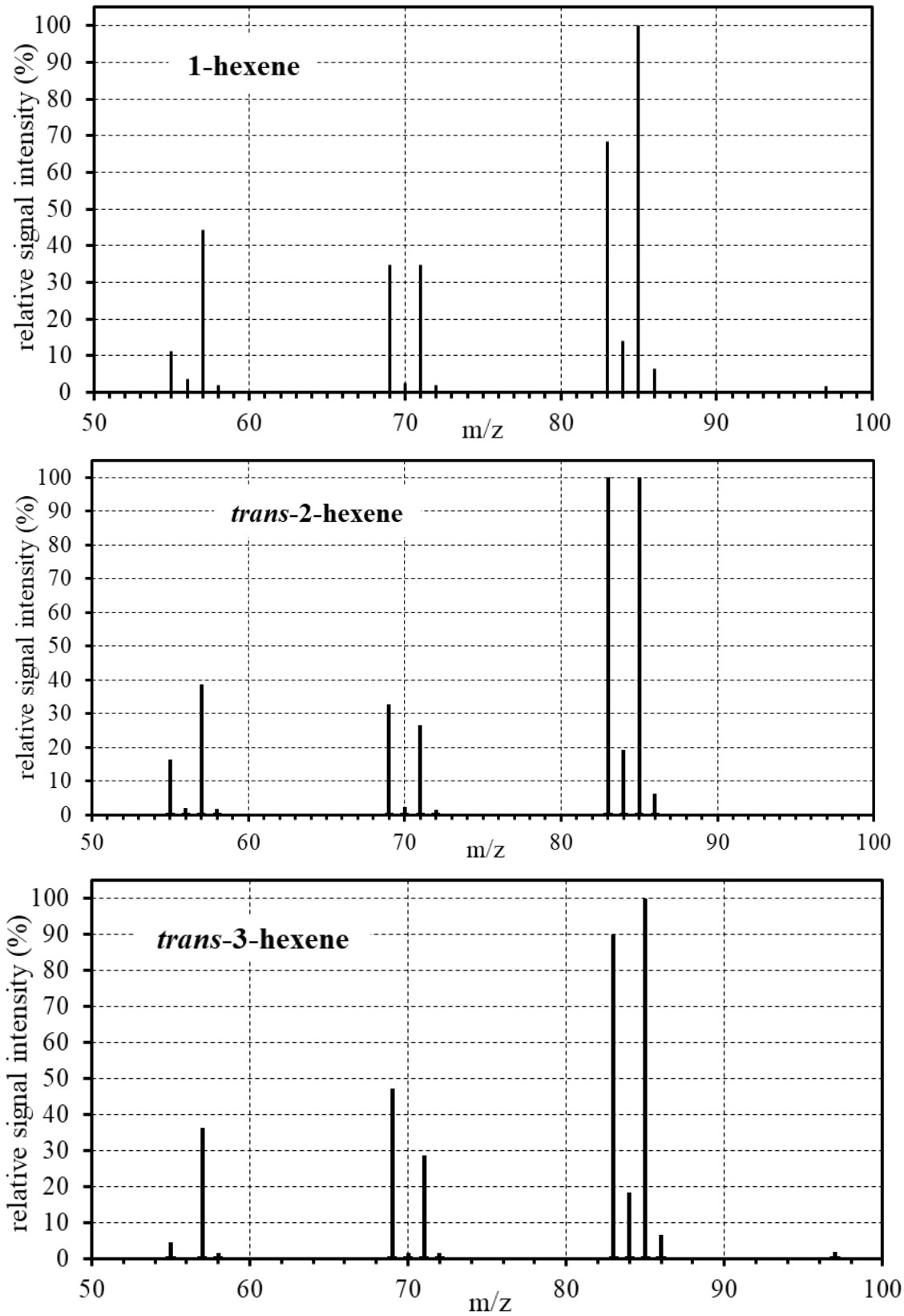



**Fig. 108 Mass spectra of positional isomers of hexene**

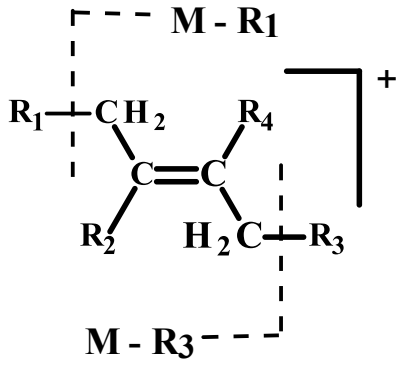



**Fig. 109**
**Characteristic fragmentation of fully substituted alkenes where migration of the double bond is hindered**

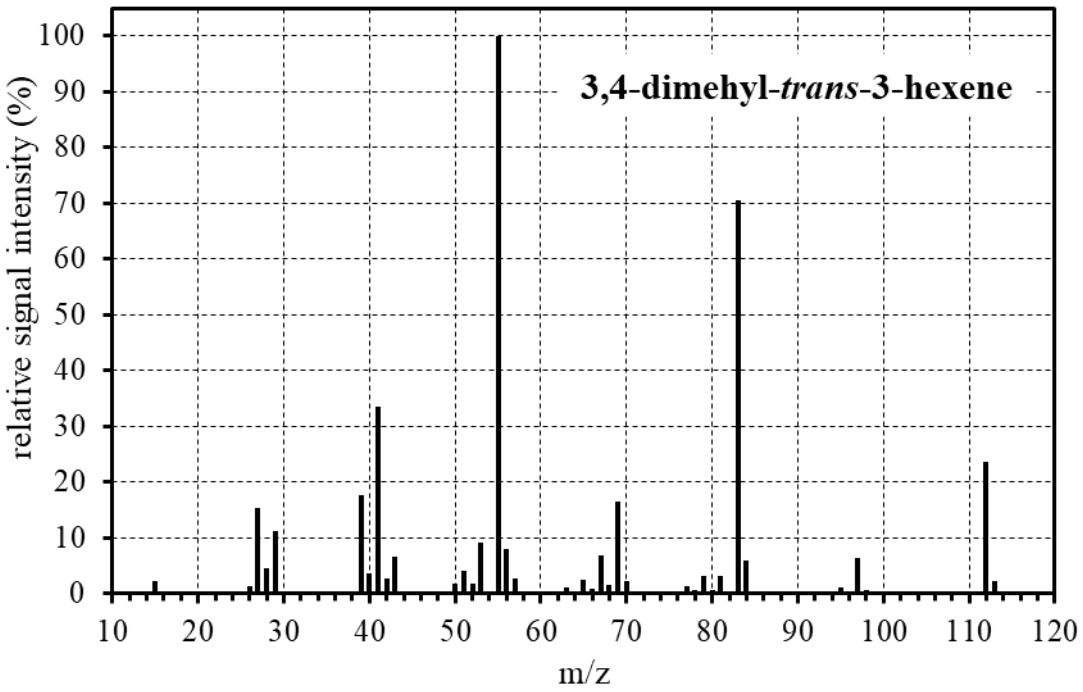



**Fig. 110 MS spectrum of 3,4-dimethyl-*trans*-hexene ionized by electron impact. (displayed according to NIST database values) https://webbook.nist.gov/cgi/inchi?ID=C19550879&Mask=200#Mass-Spec)**

If the carbon atoms involved in the double bond are fully substituted, migration of the double bond is prevented (Figure 109). In this case the mass spectrum will show characteristic signals associated with the **M - R1** and **M - R3** fragments (Figure 110).

### 4.8.4. Simple fragmentation - cleavage of the 'σ' carbon-carbon bond between the 'α' and 'β' positions of a substituent attached to an aromatic system. Tropical rearrangement

In alkyl-substituted aromatic compounds, primary cleavage occurs preferentially between the carbon atoms in the α and β positions to the aromatic nucleus (Figure 111).

In the mass spectra of alkyl derivatives of benzene (also of other substituted benzene derivatives), the signal with **m/z** ratio 91 always appears with high (sometimes even dominant) intensity, corresponding to the $C_7H_7^+$ ion resulting from the fragmentation of the σ bond between the atoms in positions α and β to the aromatic system. Labeling with $^{13}C$ isotope has shown that the carbon atoms in the $C_7H_7^+$ ion are equivalent, suggesting that cleavage **(1)** is followed by rearrangement **(2)** with formation of the tropylium ion (Figure 111).

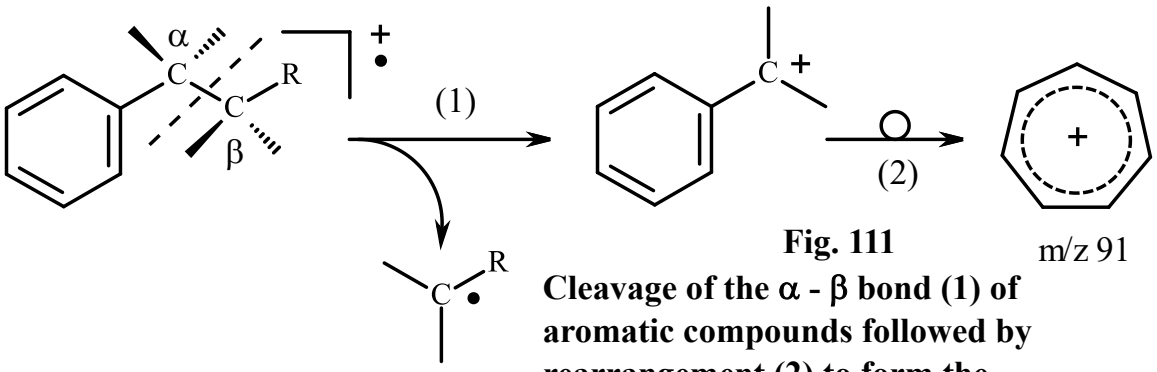



**Fig. 111**
**Cleavage of the α - β bond (1) of aromatic compounds followed by rearrangement (2) to form the tropylium ion (m/z 91).**

The signal strength of the tropylium ion, which is the dominant ion in most cases, depends on the substituent grafted to the aromatic system. The dominant appearance of the signal associated with the tropylium ion (**m/z** 91) is illustrated in the mass spectra obtained by electron impact ionization (EI) at an impact energy of 70 eV for ethyl-, propyl- and butyl-benzene (Figure 113) and for (2-bromethyl)-benzene, 3-phenyl-1-propanol and phenylacetic acid (Figure 114).

Similar cleavage occurs with alkylated derivatives of aromatic heterocyclic compounds. Alkyl-substituted pyridine also shows the characteristic signal at **m/z** 93 attributed to the azatropylium ion (Figures 112 and 118).

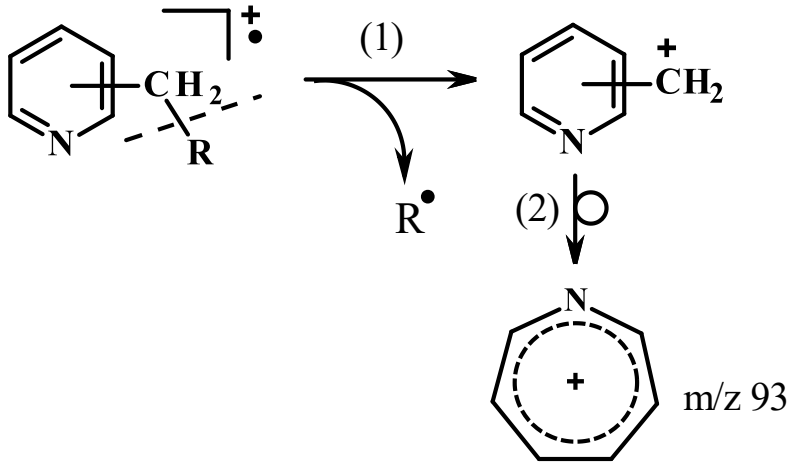



**Fig. 112 The α - β (1) cleavage of pyridine followed by rearrangement (2) to form the azatropylium ion. (m/z 93)**

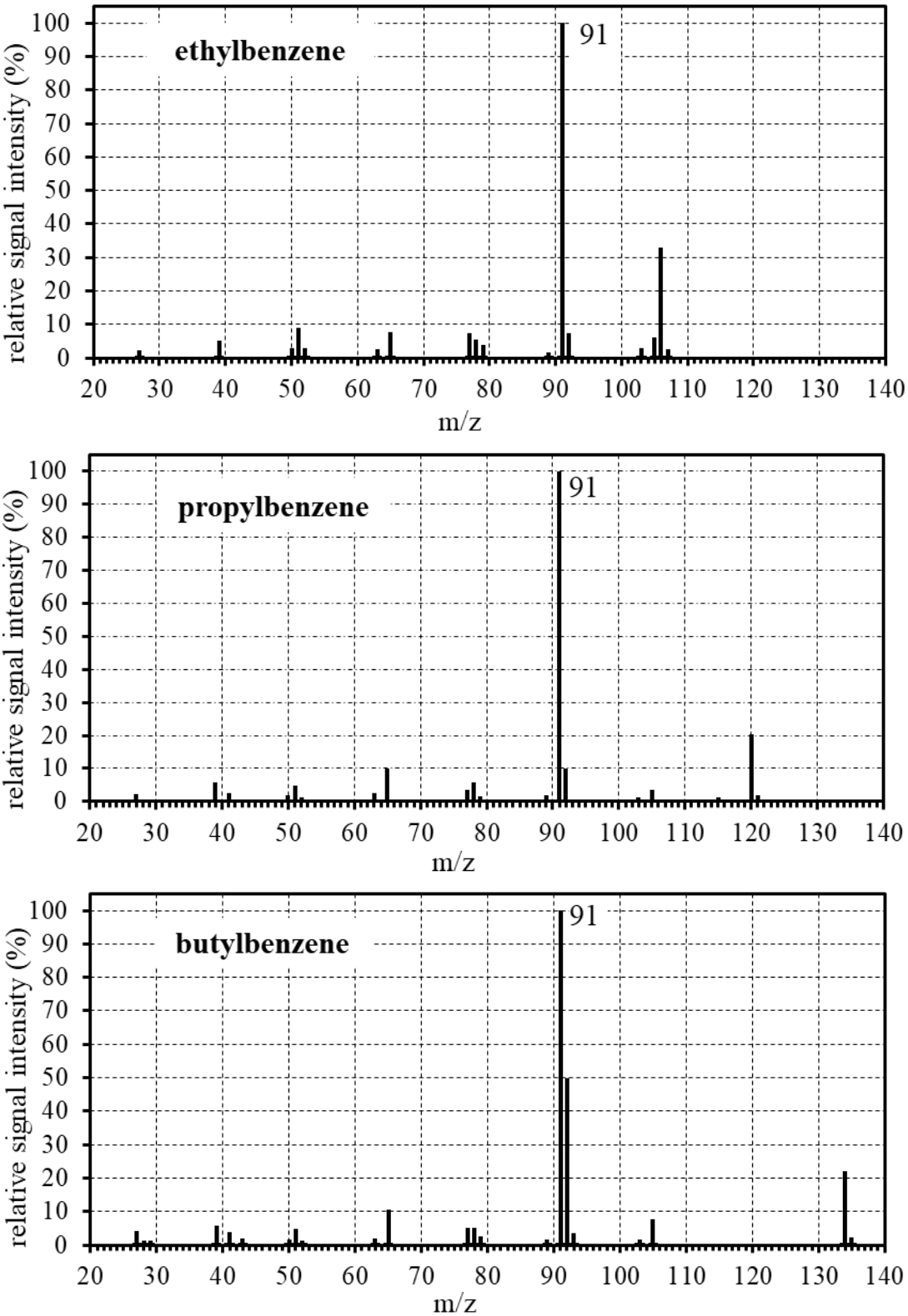



**Fig. 113 Comparison of the mass spectra of ethyl-, propyl- and butylbenzene (EI ionization, 70 eV)**

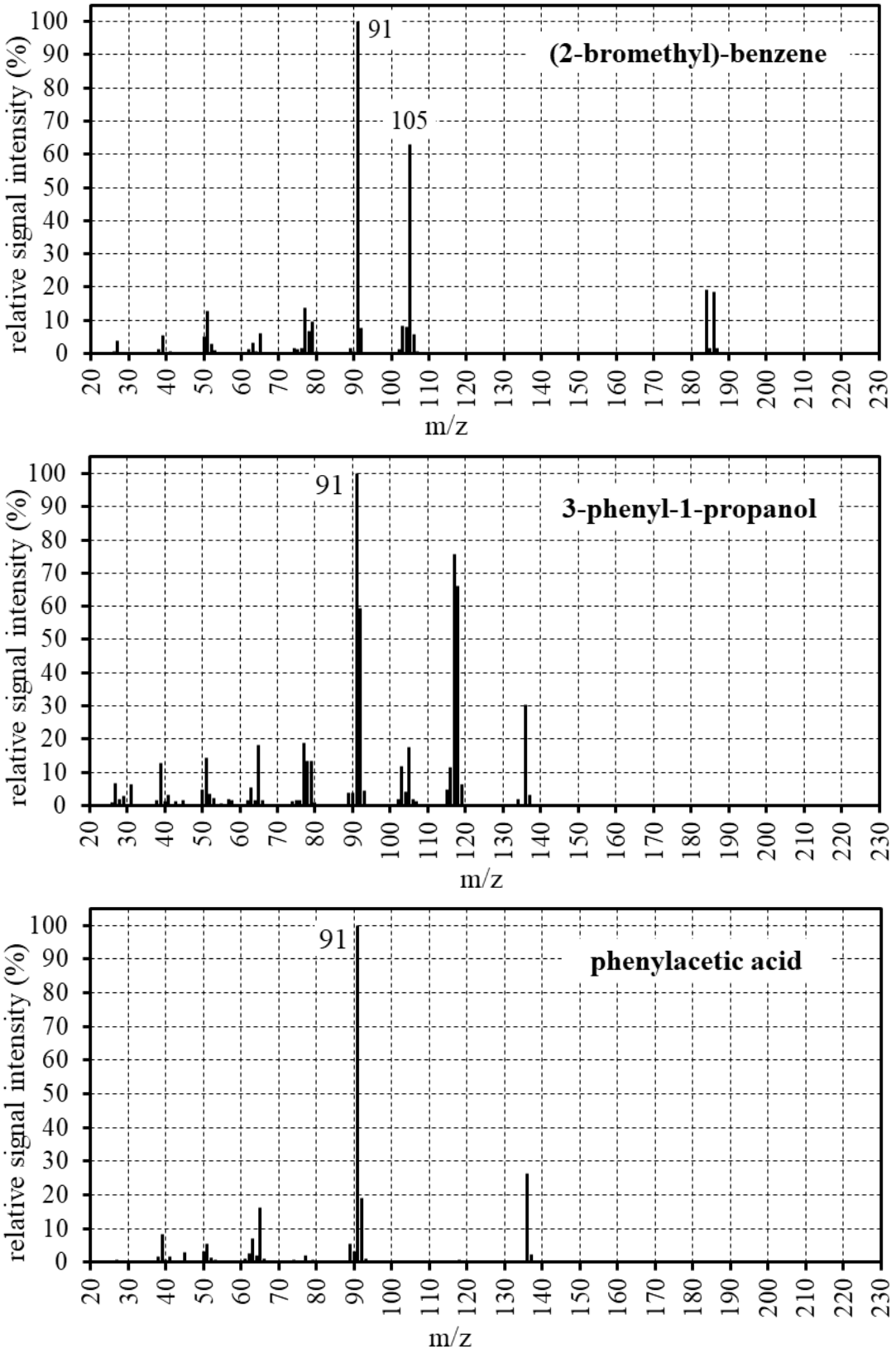



**Fig 114 Comparison of the mass spectra of (2-bromethyl)-benzene, 3-phenyl-1-propanol and phenylacetic acid. Signal m/z 91 is dominant in all three cases (EI ionization, 70 eV)**

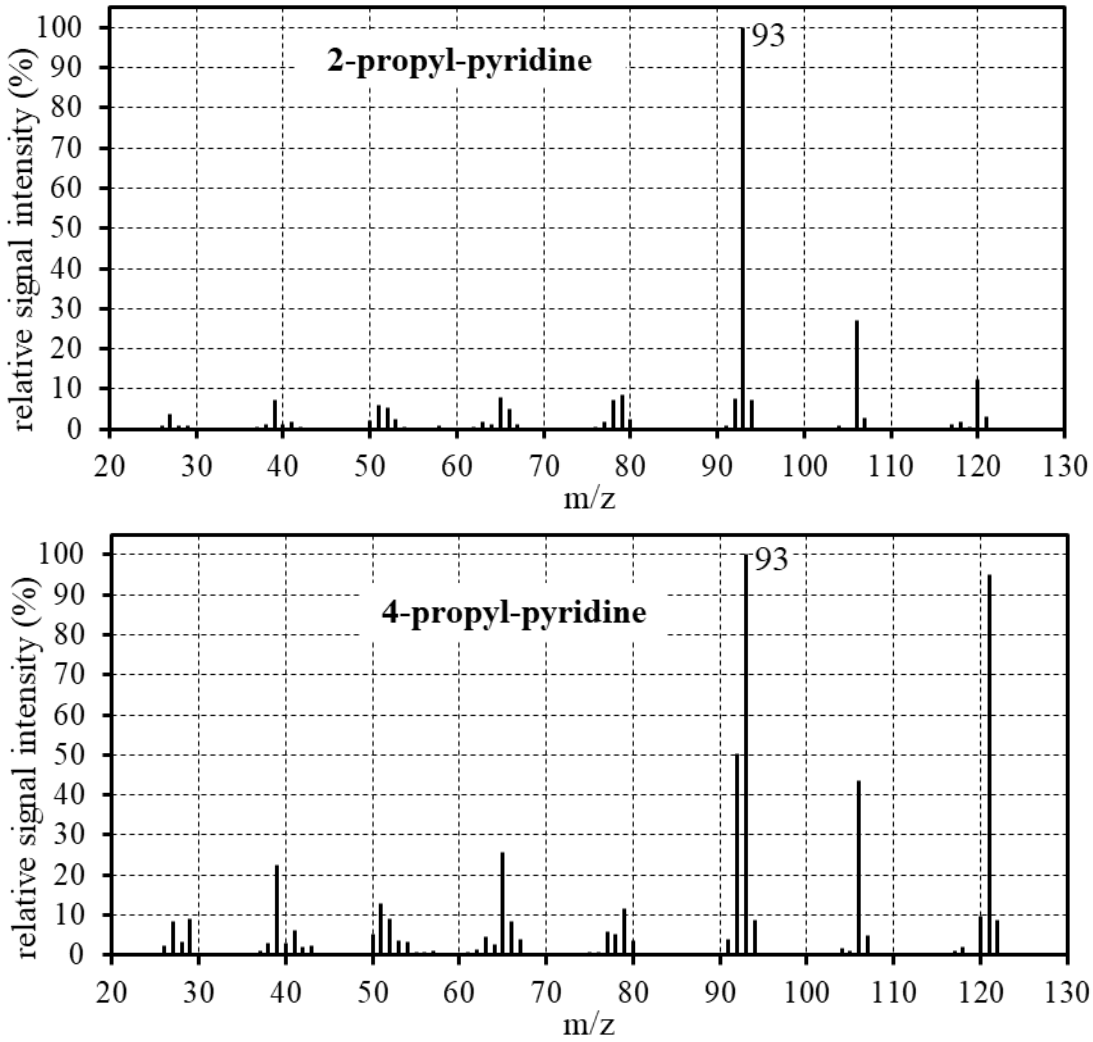



**Fig 115 Signal at m/z 93 (azatropylium ion) present in spectra of 2-propyl- and 4-propyl-pyridine. (EI ionisation, 70 eV)**

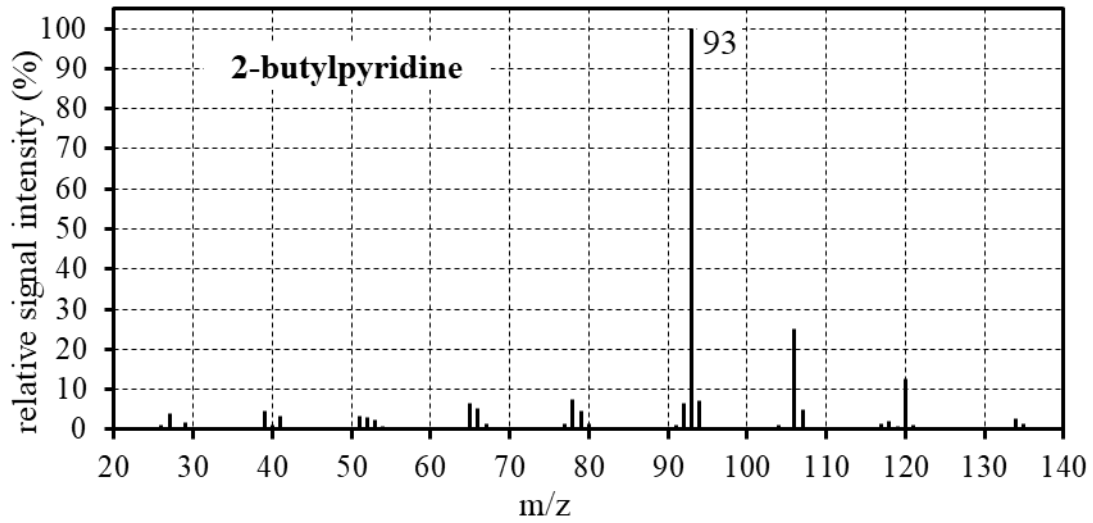



**Fig. 116 Azatropylium ion signal (m/z 93) in the 2-butylpyridine spectrum (EI, 20 eV)**

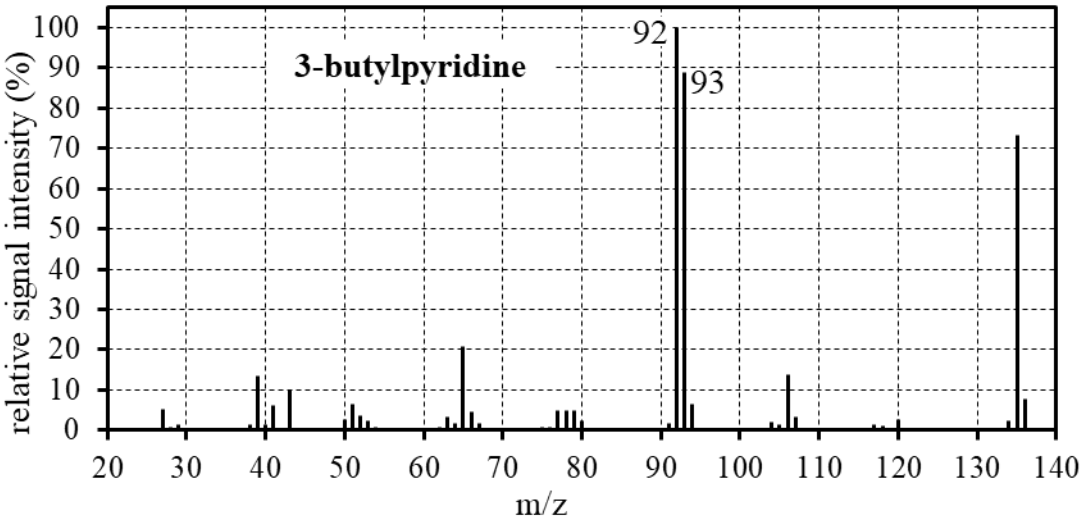



**Fig. 117 Azatropylium ion signal (m/z 93) in the 3-butylpyridine spectrum (EI, 20 eV)**

The formation of a seven-atom heterocyclic ion (azatropylium ion), like to the tropylium ion, is observed in the mass spectra of alkyl substituted pyridine derivatives (Figures 115 - 117). The azatropylium ion is dominant in almost all cases (except for 3-butylpyridine, but even here the intensity of the azatropylium ion is considerable).

Azatropylium ion formation is also observed for methyl pyridines (Figure 119). The spectra of the three positional isomers are almost identical, indicating a minor influence of the position of the methyl substituent on the pyridine nucleus.

In contrast to the first order substituents, the spectrum of pyridine derivatives with a second order substituent (e.g. nicotinic acid) does not show the signal of the azathropylium ion, but the fragmentation follows a different path due to the influence of the substituent on the aromatic system (Figure 118).

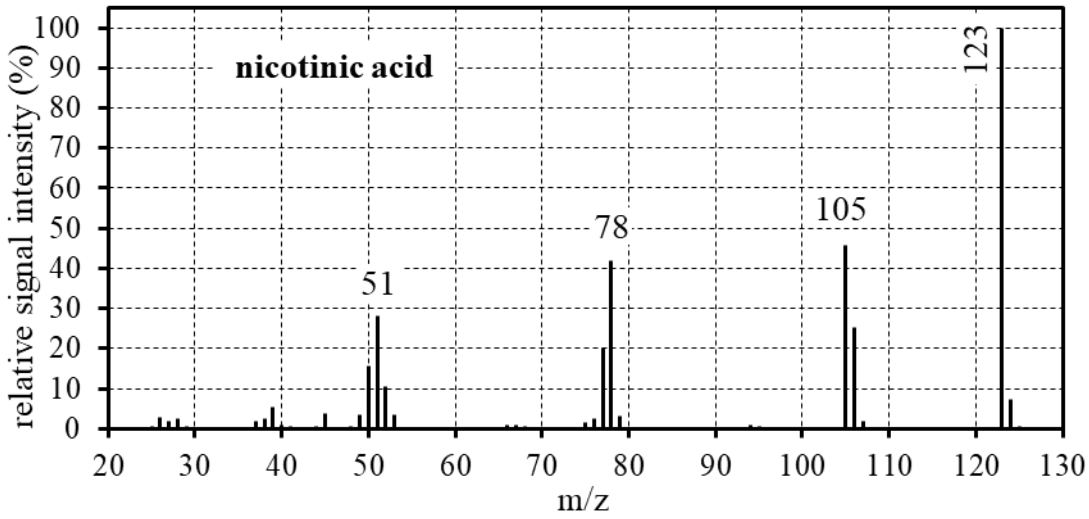



**Fig 118 Mass spectrum of nicotinic-3-carboxylic acid (Niacin) (EI ionization, 70 eV)**

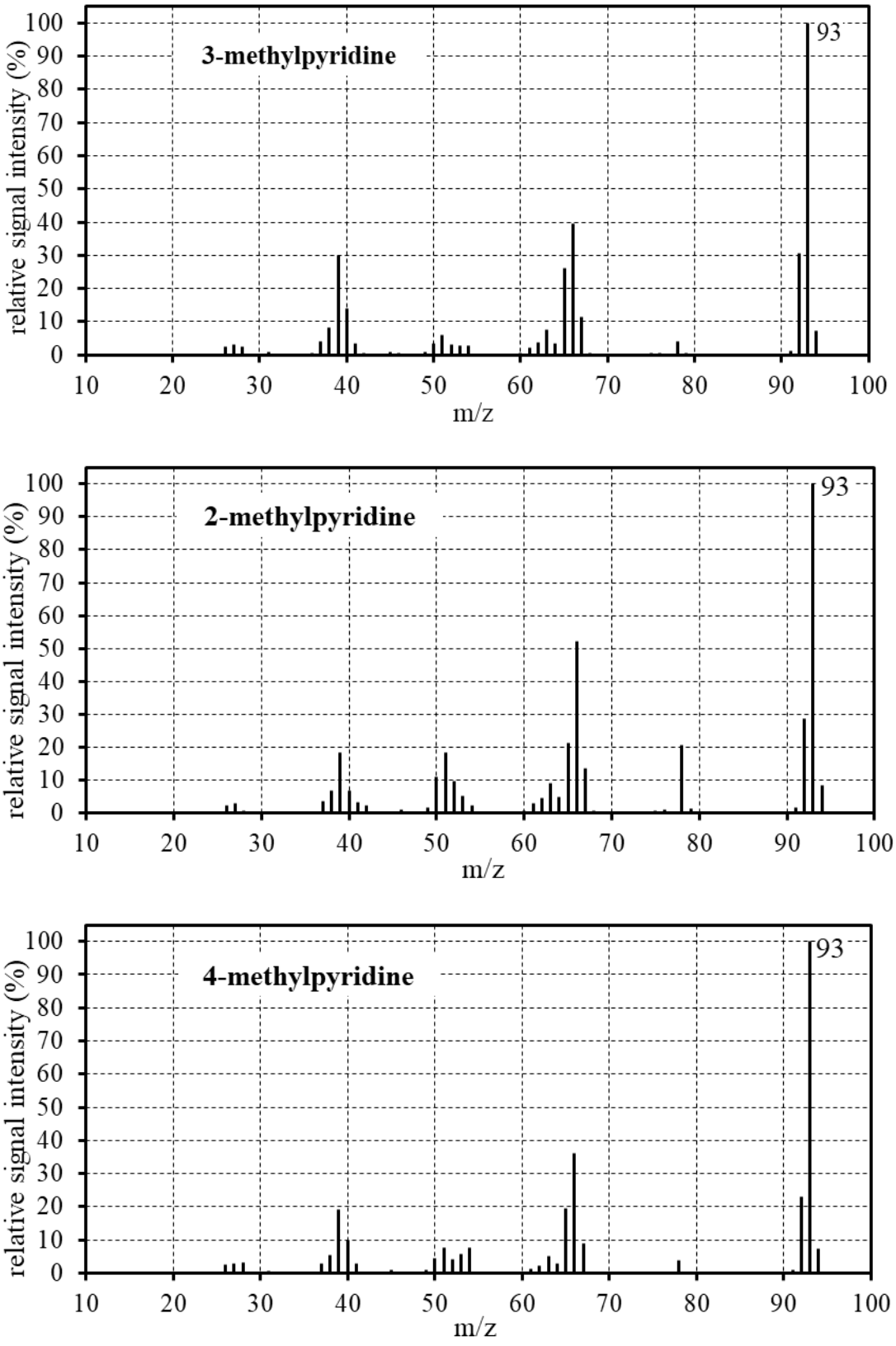



**Fig 119 Highlighting of the signal at m/z 93 (azatropylium ion) in 2-, 3- and 4-methylpyridine spectra (EI ionization, 70 eV)**

### 4.8.5. Simple fragmentation – "onium-type splitting" – at the link between the 'α' and 'β' positions to a heteroatom

Intramolecular transpositions, like those that produce the tropylium ion by ring enlargement, are also observed in 5-substituted heterocyclic compounds. The fragmentation of the primary ion is initiated by the removal of an electron from the heteroatom with the formation of an 'onium' type ion, regardless of the position of the substituent on the nucleus (Figure 120).

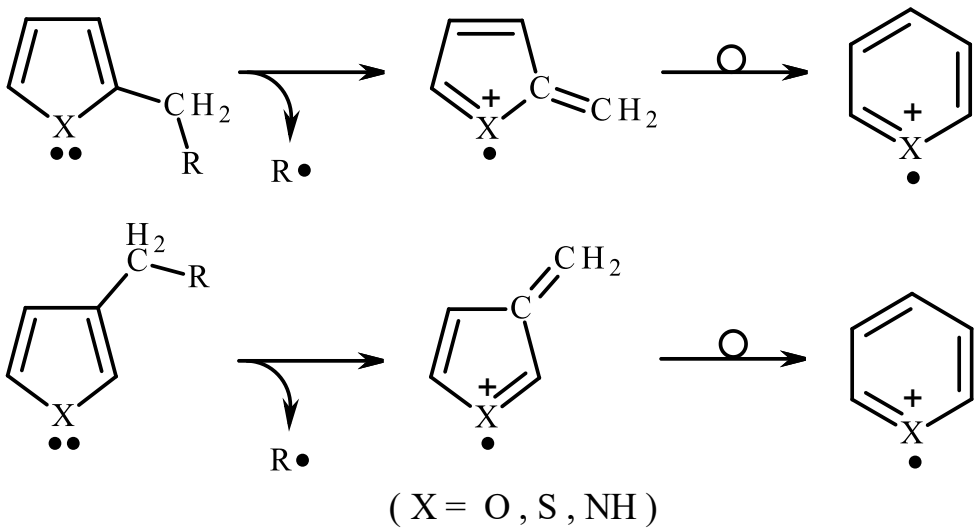



**Fig 120 Ionization followed by expansion of the heterocyclic nucleus to form an 'onium' ion.**

If a molecule contains a σ bond between a carbon atom and a heteroatom of a functional group, the bond between the carbon atoms at the α and β positions to the heteroatom is predominantly cleaved after primary ionization (Figure 121).

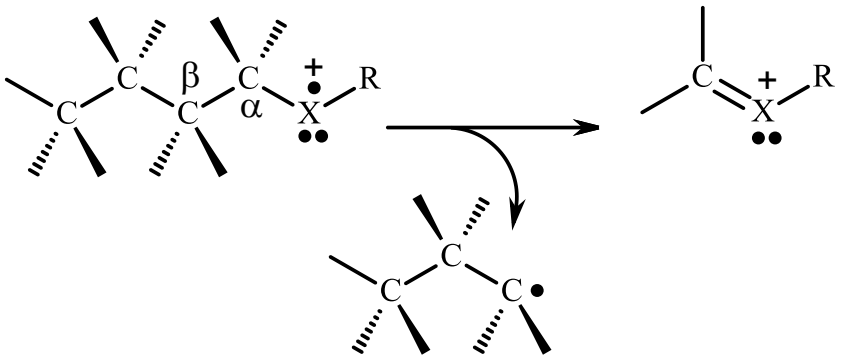



**Fig 121 Cleavage of the bond "σ" between the atoms in positions "α" and "β" to the heteroatom "X"**

The fragmentation results in a (relatively stable) "onium" ion and a neutral alkyl radical. This type of fragmentation occurs for heteroatoms **X** = NH, O, S present in the molecules of alcohols, ethers, thioethers, amines, amino acids, glucides (carbohydrates) and alkaloids.

This fragmentation pathway is illustrated by the specific example of 1-heptylamine (Figure 122) and confirmed by the appearance of the dominant signal at **m/z** 30 in the spectrum (Figure 123).

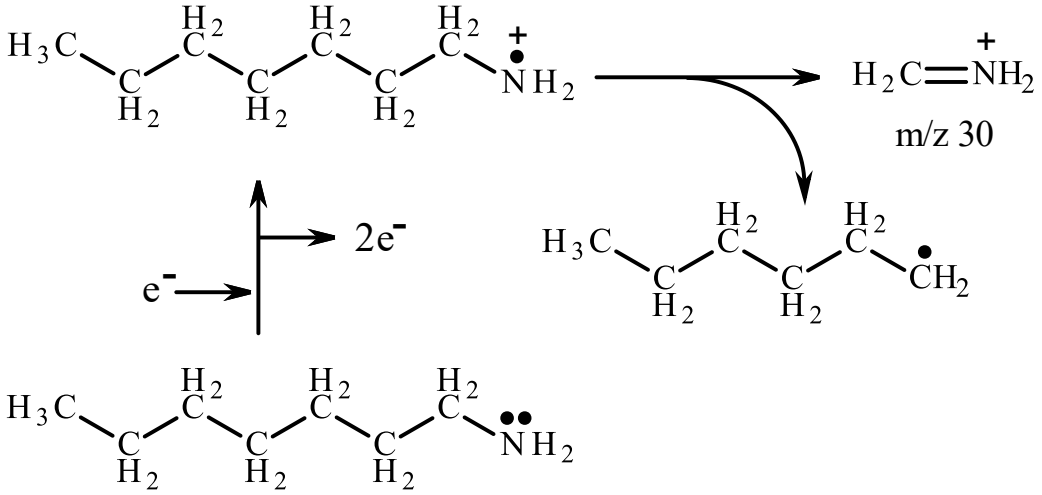



**Fig. 122 The "onium" cleavage of α–β bond to the heteroatom into 1-heptylamine (EI ionization energy: 70 eV)**

The splitting of the neutral radical is favored by its stability and thus implicitly by the size of the alkyl residue: the large size and advanced branching of the alkyl residue give it greater stability - and thus a higher probability of formation. This is illustrated in Figure 124 for the primary ion fragmentation of 3-octanol. In the experimental spectrum (Figure 125), the ion at **m/z** 59 gives a stronger signal than the ion at **m/z** 101, arguing for pathway **(1)**, i.e. the one that produces a longer chain neutral radical with greater stability.

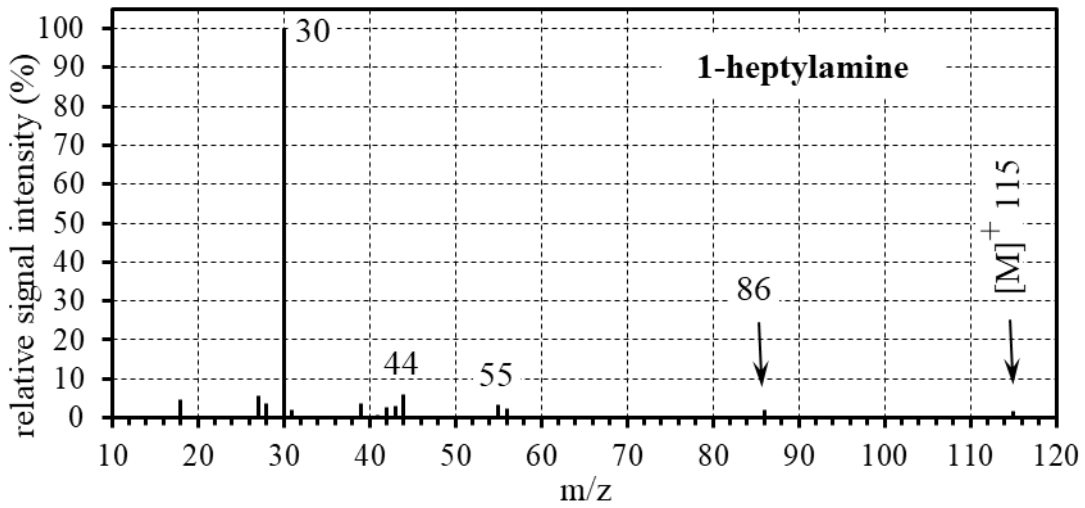



**Fig 123 Mass spectrum of 1-heptylamine (EI ionization energy 70 eV)**

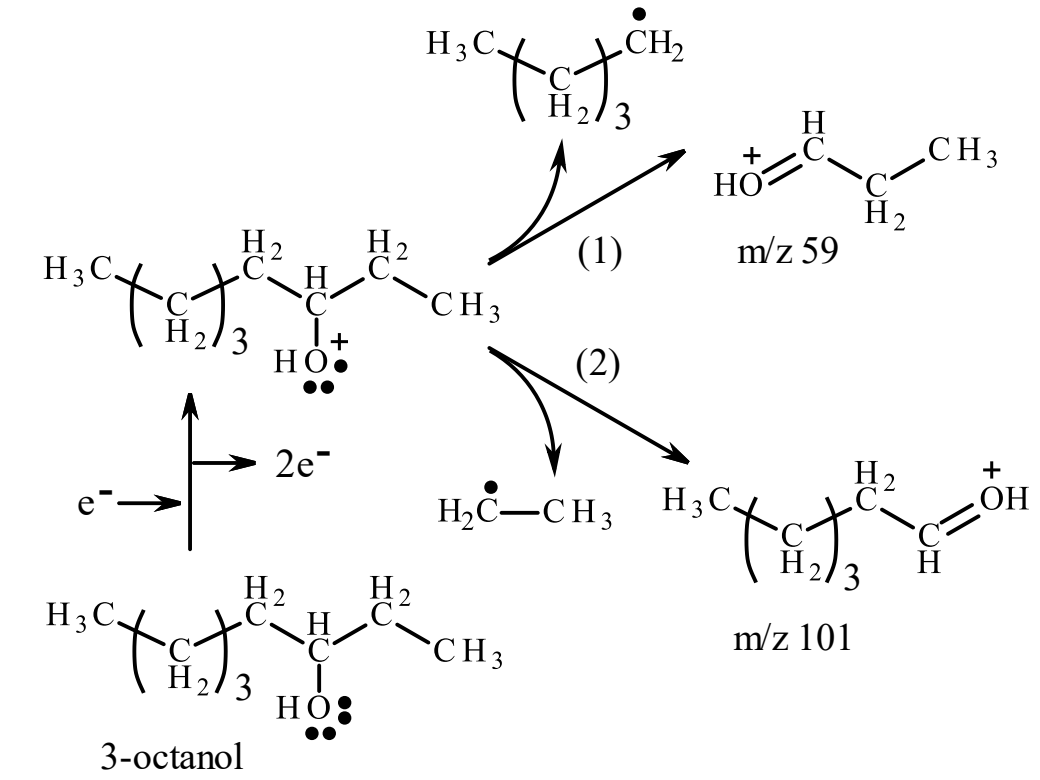



**Fig 124 The "Onium" fragmentation of 3-octanol**

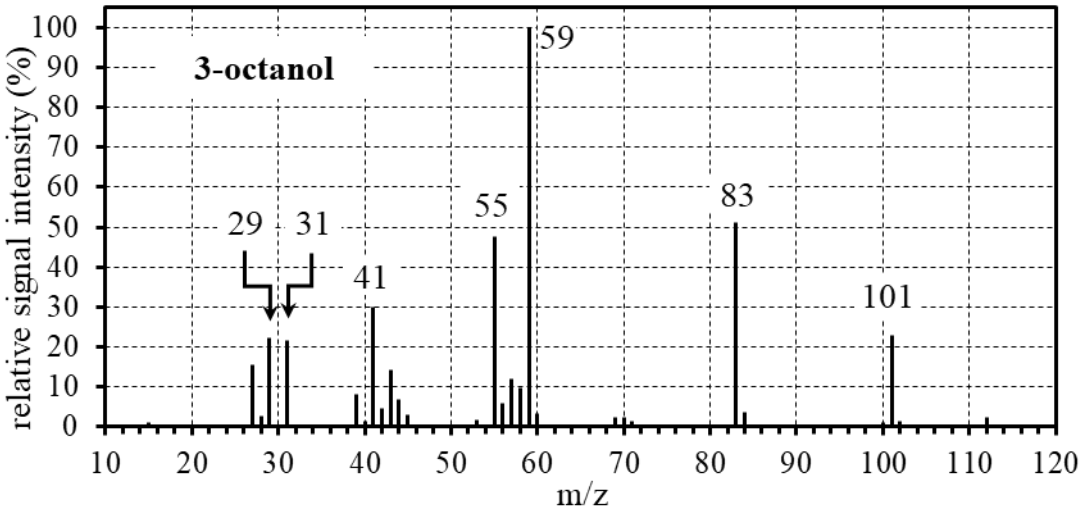



**Fig 125 Mass spectrum of 3-octanol (EI ionization energy: 70 eV)**

The other signals in the spectrum of 3-octanol can be attributed to the ionic fragments in Figure 126.

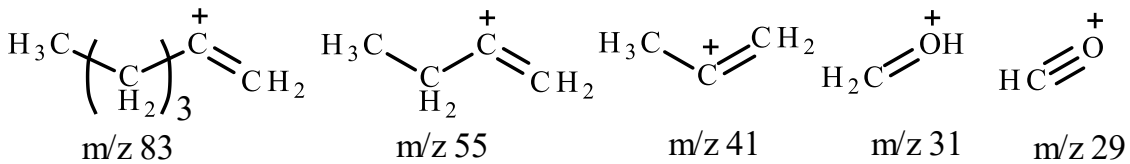



**Fig 126 Possible minor ionic fragments in the mass spectrum of 3-octanol**

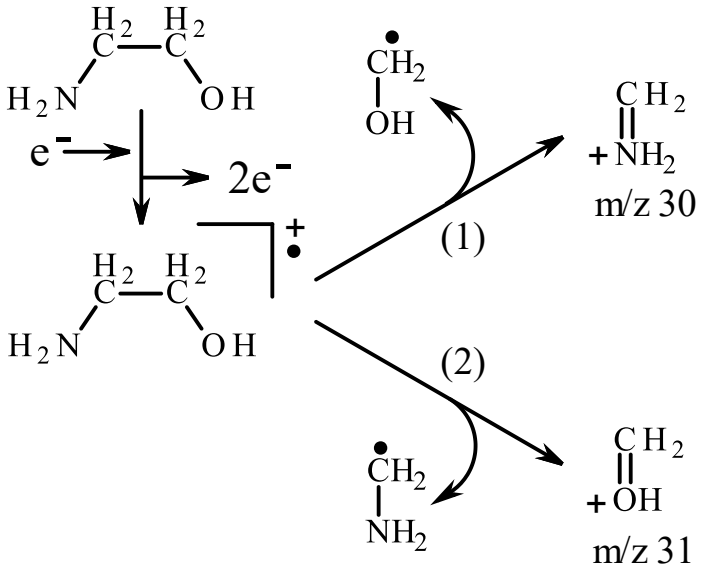



**Fig. 127 Fragmentation of the molecular ion of 2-aminoethanol**

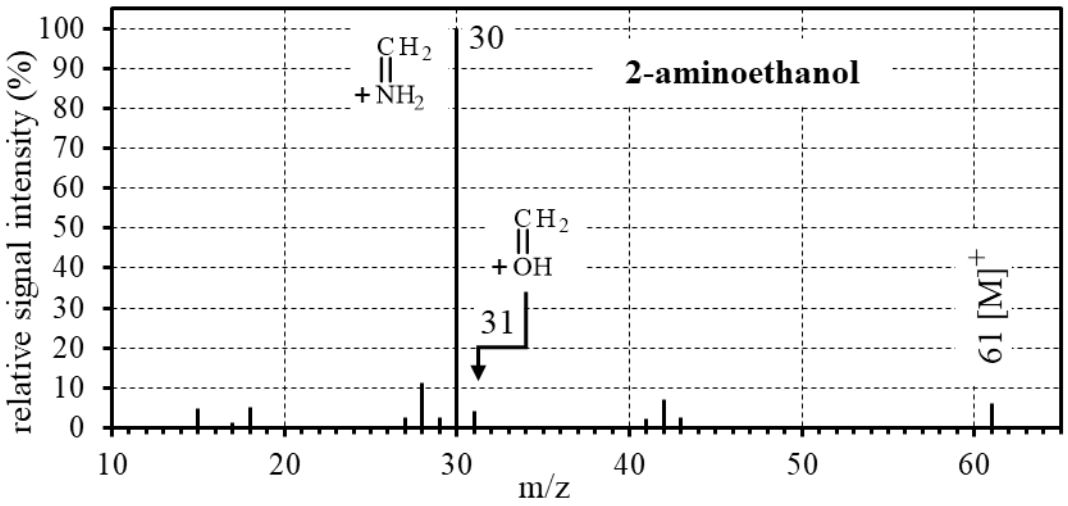



**Fig. 128 Mass spectrum of 2-aminoethanol (EI ionization, 75 eV) (reconstructed from data of SDBS database: http://sdbs.db.aist.go.jp/sdbs/cgi-bin/direct_frame_top.cgi)**

If the molecular ion binds via a heteroatom to different functional groups, the fragmentation pattern is the result of competition between the bonds at the "α–β" position to the heteroatom involved in the cleavage. The relative intensities of the signals corresponding to the different "onium" fragments formed are consistent with their stability. When the molecular ion of 2-aminoethanol (Figure 127) is fragmented, in terms of the signal intensities associated with the **(1)** and **(2)** pathways, the intensity ratio is clearly in favor of the **(1)** pathway (Figure 128) because the ion $\mathbf{[CH_2{=}NH_2]^+}$ is more stable than the $\mathbf{[CH_2{=}OH]^+}$ ion. The stability of this type of 'onium' ion decreases in the following order: $\mathbf{[CH_2{=}NH_2]^+ > [CH_2{=}SH]^+ > [CH_2{=}OH]^+}$ .

Because of their positive inductive effect on the heteroatom, the alkyl groups stabilize the positive fragment ion, the more so the longer they are. This is illustrated by the molecular ion of 1-dimethylamino-2-propanol, which can be cleaved in two ways **(1)** and **(2)** (Figure 129).

The effect of alkyl substituents in increasing the electron density on the nitrogen atom (through their positive inductive effect) is consistent with the effect of increasing the basicity of the target compound. In other words, the increased signal intensity of these ions is a measure of the increase in basicity with the degree of alkyl substitution of the nitrogen atom. Mass spectrometric study of the basicity of alkyl-substituted amines has the advantage that, unlike the method of measuring basicity in solution, it indicates the intrinsic basicity independent of the contribution of the solvent. It is known that secondary amines are more basic than tertiary amines in aqueous solution (apparently contradicting predictions of a positive inductive effect of alkyl groups), whereas in chloroform solution the natural order of basicity is observed:

tertiary amines > secondary amines > primary amines

which is identical to the order determined by mass spectrometry based on the signal intensities of the onium ions of alkyl-substituted amines.

Figure 129 predicts two possible direct molecular ion fragmentation routes in the case of 1-dimethylamino-2-propanol. In the mass spectrum (Figure 130), the **m/z** 58 signal is dominant, while the **m/z** 45 ion appears with much reduced intensity, details that confirm the preference of route **(1)** over route **(2)**.

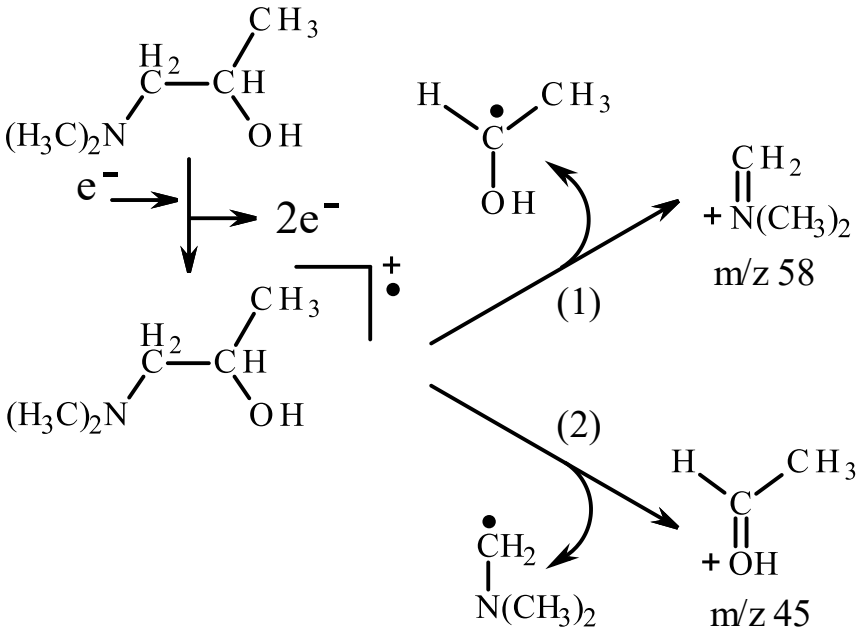



**Fig 129 Fragmentation of the molecular ion of 1-dimethylamino-2-propanol**

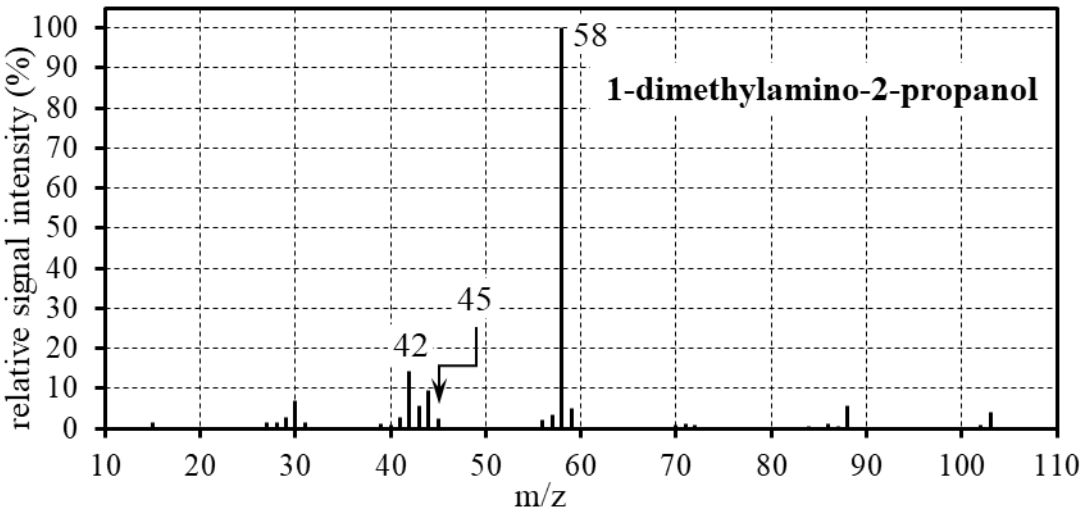



**Fig 130 Mass spectrum of 1-dimethylamino-2-propanol (EI ionization, 70 eV)**

Similar results to those shown above for relative signal intensities are obtained by considering the fragmentation of amines. The 'onium' ion resulting from a tertiary amine gives a stronger signal than the ion resulting from a secondary or primary amine.

If the substituent **R** of the heteroatom **X** in Figure 121 is an alkyl group (the case for ethers, thioethers, secondary or tertiary amines), the ions resulting from the primary cleavage will undergo further cleavage, removing an alkene. If the carbon atom attached to the heteroatom is part of a ring system, the cleavage will follow a path illustrated in the case of cyclohexanol (Figure 131).

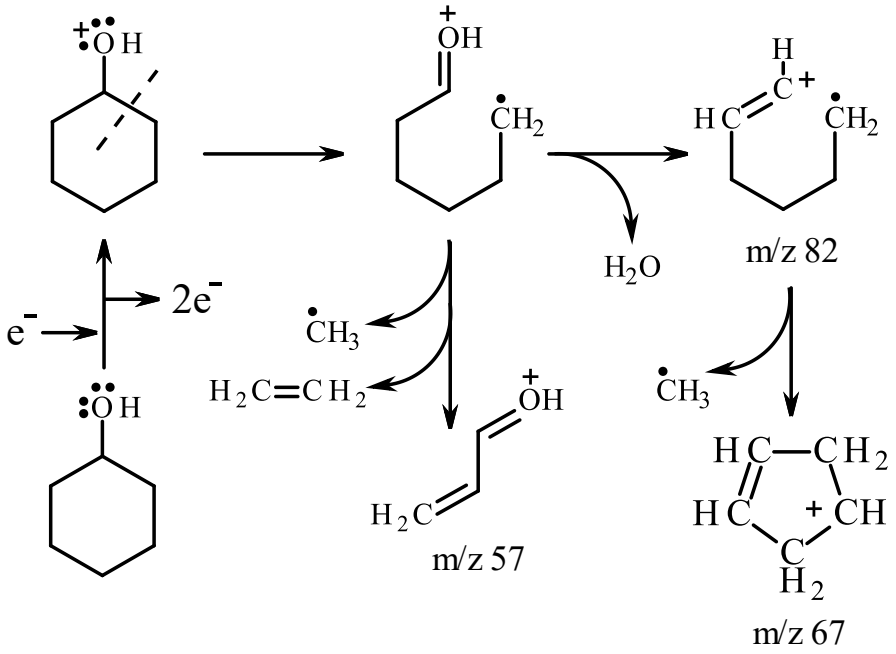



**Fig 131 Fragmentation of the molecular ion of cyclohexanol**

The mass spectrum of cyclohexanol (Figure 132) shows that the preferred pathway is the one ending with the formation of the ion at **m/z** 57. The relatively strong signal at **m/z** 82 is probably due to the removal of a water molecule from the molecular ion.

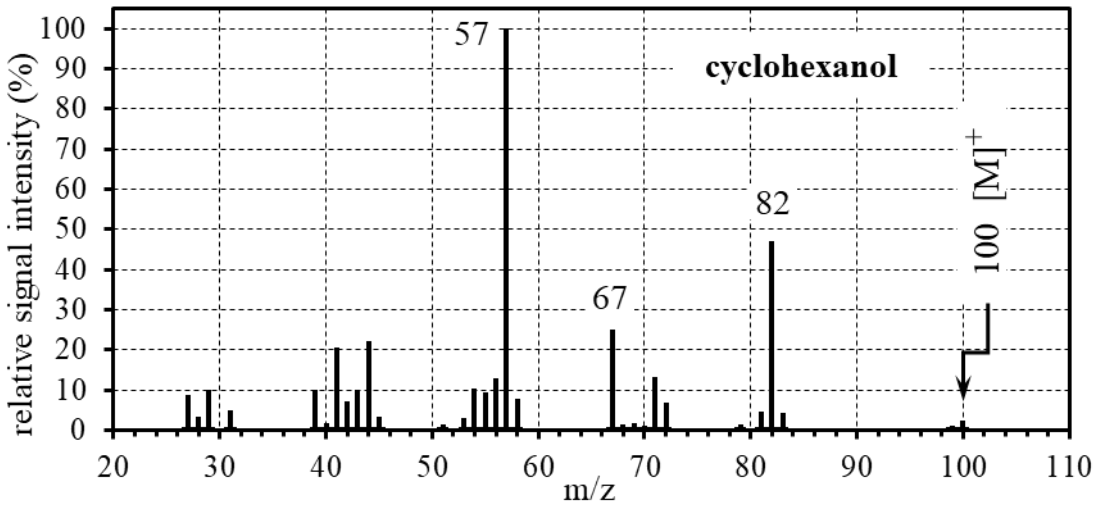



**Fig 132 Mass spectrum of cyclohexanol (EI ionization, 70 eV)**

### 4.8.6. Simple fragmentations - 'onion' fragmentation of the 'σ' bond between the carbon atoms at positions 'α' and 'β' from the heteroatom involved in a double bond.

Primary ions containing a double bond between a heteroatom and a carbon atom (>C=X) split predominantly at the bond between the carbon atoms in positions α and β to the heteroatom. The general course of the fragmentation process can in principle involve both σ bonds (bond **(1)** or **(2)** in Figure 133) of the adjacent carbon to the heteroatom **X**.

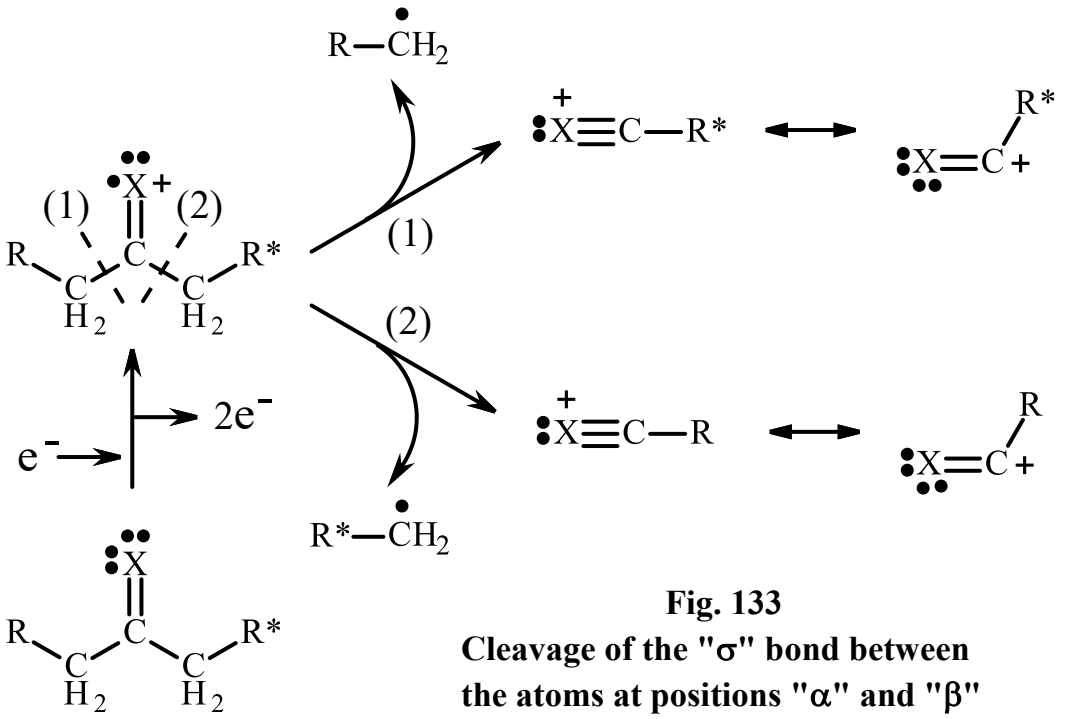



**Fig. 133**
**Cleavage of the "σ" bond between the atoms at positions "α" and "β" with respect to the heteroatom "X**

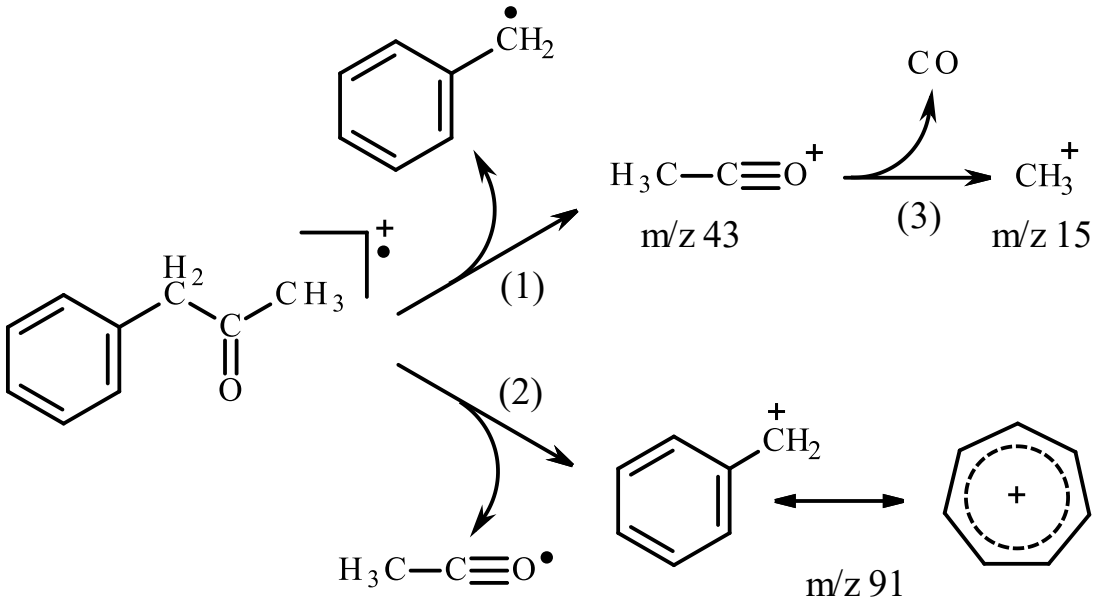



**Fig 134 Fragmentation of the molecular ion of phenylacetone**

The fragmentation shown in Figure 133 begins with the homolytic cleavage of a σ bond, after which either pathway **(1)** or pathway **(2)** may follow. The weight of the two pathways (and thus the appearance of the resulting "onium" ions in the spectrum) depends on the stability of the ions and radicals formed along the two pathways. This type of fragmentation is often found in substances containing the >C=N , >C=S , >C=O fragments. The stability of the corresponding "onium" ions decreases in the following order:

$$\mathbf{R{-}C{\equiv}NH^{+} > R{-}C{\equiv}S^{+} > R{-}C{\equiv}O^{+}}$$

The residue **R** can be hydrogen, alkyl, alkoxy, amino, covering several classes of compounds: aldehydes, ketones, quinones, esters, amides, peptides, steroids.

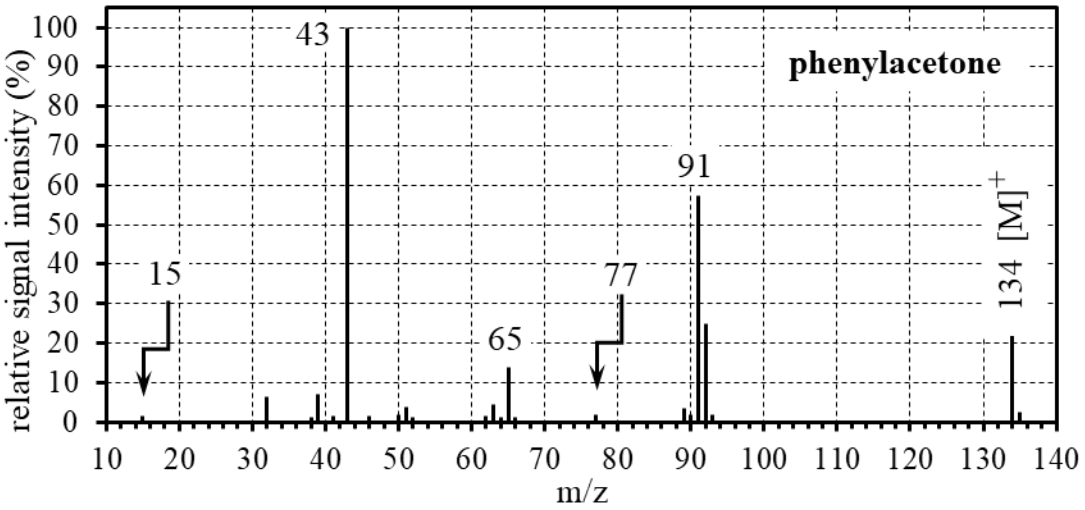



**Fig 135 Mass spectrum of phenylacetone (EI ionization, 70 eV)**

Phenylacetone is a relevant example of this type of fragmentation (Figure 134). In principle, there are two possible routes after cleavage of the σ bond from the benzyl residue, **(1)** and **(2)**. The higher stability of the benzyl radical compared to the acetyl radical results in a more pronounced appearance of the **m/z** 43 ion in the spectrum compared to the **m/z** 91 ion (Figure 135). The signal at **m/z** 15 (very weak) in the spectrum of phenylacetone (Figure 135) is due to the methyl carbocation ($\mathbf{CH_3^+}$) resulting from the removal of a carbon monoxide (**CO**) molecule (process (3) in Figure 134) from the acetyl cation ($\mathbf{CH_3\text{-}C{\equiv}O^+}$).

### 4.8.7. Simple fragmentation - removal of a neutral molecule from a fragmentation ion

Ionized fragments, formed from the molecular ion, can be further fragmented often by removing a neutral molecule (Figure 136).

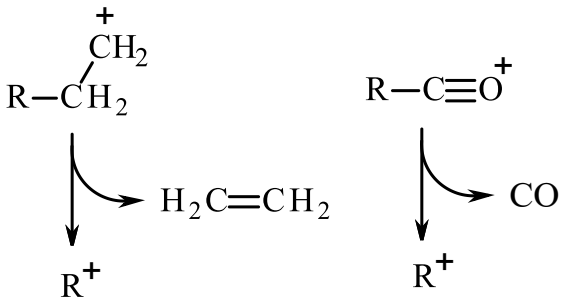



**Fig 136**
**Removal of a neutral molecule from a fragment ion**

### 4.8.8. Fragmentation with transposition of a hydrogen atom

Attempts to interpret mass spectra from simple fragmentation alone often fail. An example is the fragmentation of isobutane, where the mass spectrum shows a signal at **m/z** 29 (Figure 137) corresponding to ethyl ion, although the molecule contains no ethyl moiety. The appearance of this ion indicates that a process of intramolecular rearrangement is occurring simultaneously with the actual fragmentation. These are called ”transposition” ions. Their appearance is caused either by the migration of one or two hydrogen atoms (hydrogen transposition) or by the transposition of other atoms or groups of atoms from one position in the original ion to another (skeleton transposition).

Irrespective of the nature of the atoms transferred, the transposition of ions is conditioned by the following dynamic and steric aspects:

- transpositions occur via energetically and sterically favored cyclic intermediates,
- transposition is initiated by cleavage of a stable neutral fragment,
- the resulting transposed ion is stable,
- the spatial structure of the ion to be transposed requires that the centers involved in the transposition be close to each other.

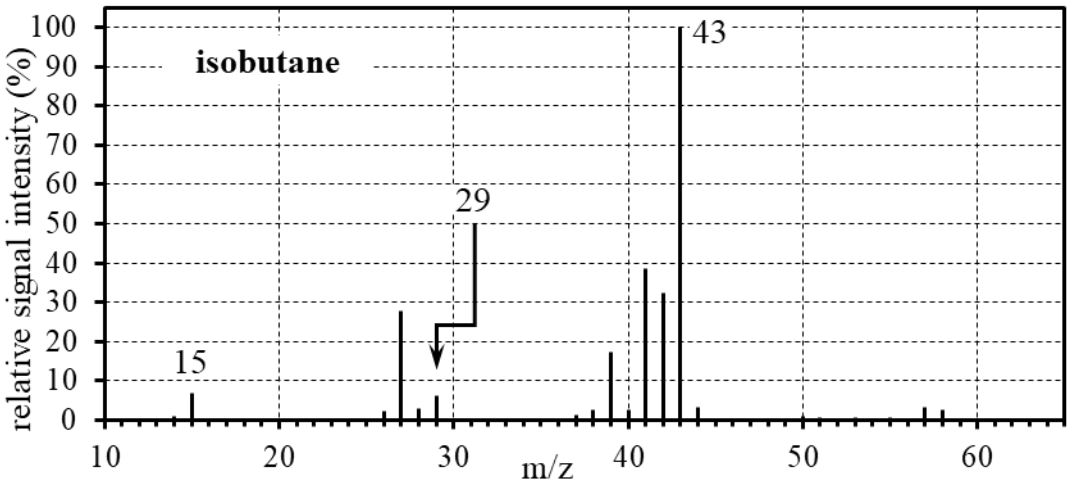



**Fig 137 Mass spectrum of isobutane showing a signal at m/z 29 (EI ionization, 70 eV)**

Due to transposition processes that occur under mild energetic conditions for some compounds (sometimes due to the temperature in the ionization unit), mass spectra often show a wealth of signals that are apparently uncharacteristic of the original molecular structure. On the other hand, transpositions often provide useful information for determining the molecular structure of the analyte.

A category of chemicals (alcohols, thiols, amines, esters, halogenated derivatives, nitriles), undergoes elimination of the functional group and a hydrogen atom from the rest of the molecule after electron flow ionization (Figure 138).

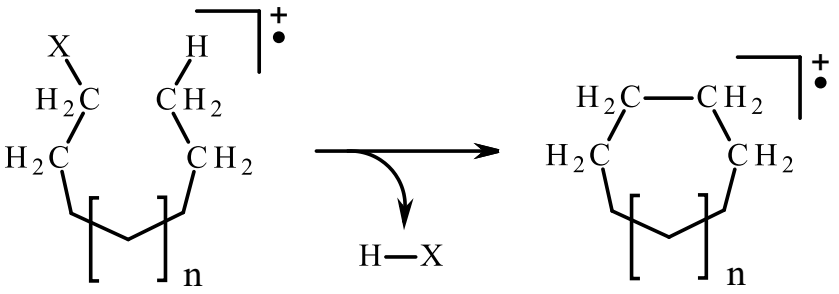



**Fig 138 Removal of the neutral H-X molecule and forming a cyclic intermediate**

Fragmentation accompanied by transposition of a hydrogen atom has been studied in detail for deuterated compounds by observing the position of the deuterium atom in the ionic fragment. For example, in the case of 1-butanol, both methyl-cyclopropane (by 1,3-elimination) and cyclobutane (by 1,4-elimination) are formed by the removal of a water molecule (Figure 139). The results confirm that the elimination of water from alcohol molecules does not occur only with the involvement of positions 1 and 2, so that the presence of a signal with **m/z** 18 Da, lower than the mass of the molecular ion, does not necessarily imply a hydrogen atom on the carbon atom in position "α" with respect to the hydroxyl group.

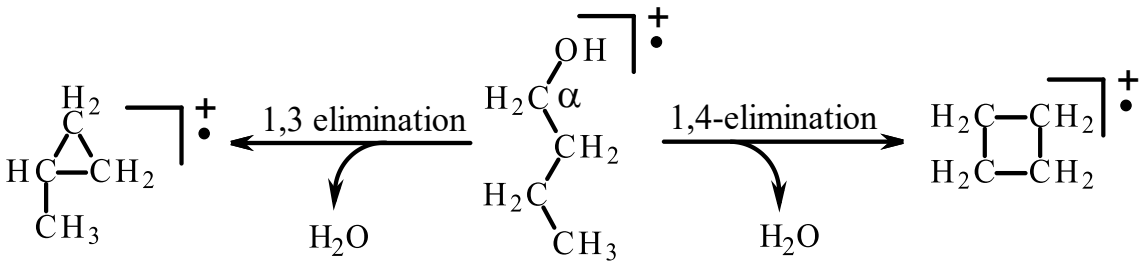



**Fig 139 Intramolecular transposition with removal of the neutral water molecule and subsequent formation of cyclic structures**

### 4.8.9. The *McLafferty* transposition

In studies of ketone fragmentation, *A.J.C. Nicolson* observed a rearrangement of ions with an intramolecular transposition of a hydrogen atom from the carbon atom at the position "γ" to the carbonyl group.

> [*A.J.C. Nicolson*: The Photochemical Decomposition of the Aliphatic Methyl Ketones **Trans. Faraday Soc., 1954:50**, 1067-1073].

The results were reviewed and generalized by *F.W. McLafferty*.:

> [*F.W. McLafferty*: Mass Spectrometric Analysis. Molecular Rearrangements. **Anal. Chem., 1959:31**(1), 82-87].

At present the transposition, generalized for a class of compounds with a double bond or an aromatic residue, is associated with the name of *McLafferty*. Figure 140 shows the *McLafferty* transposition of 2-octanone and Figure 141 shows the mass spectrum of 2-octanone.

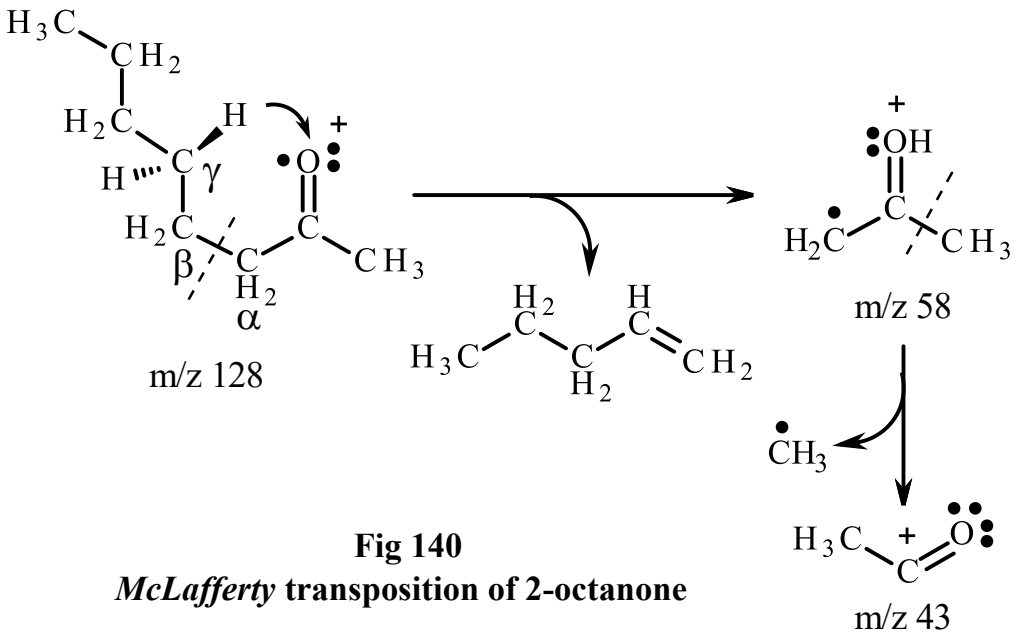



**Fig 140**
***McLafferty* transposition of 2-octanone**

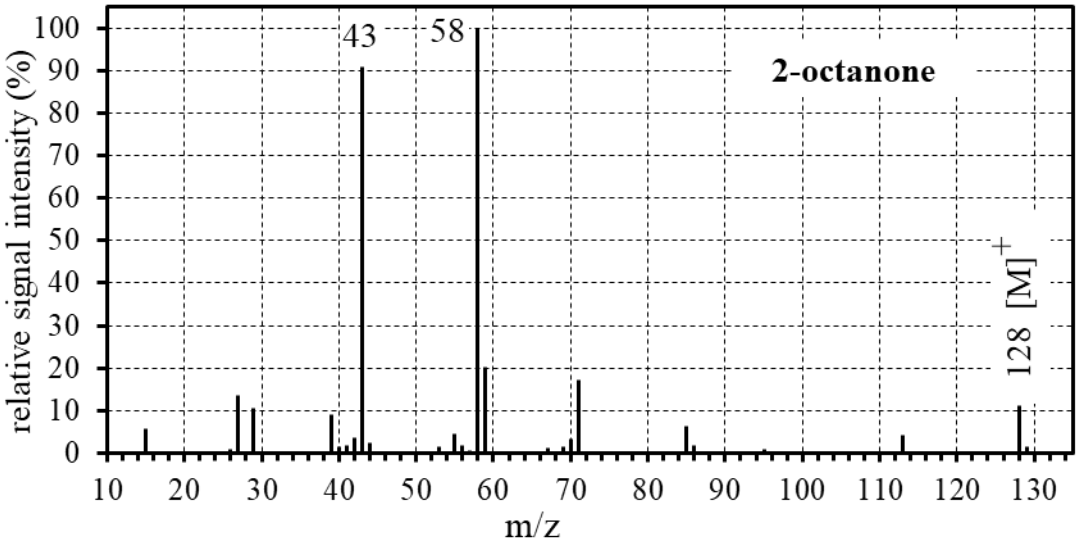



**Fig 141 Mass spectrum of 2-octanone (EI ionization, 70 eV)**

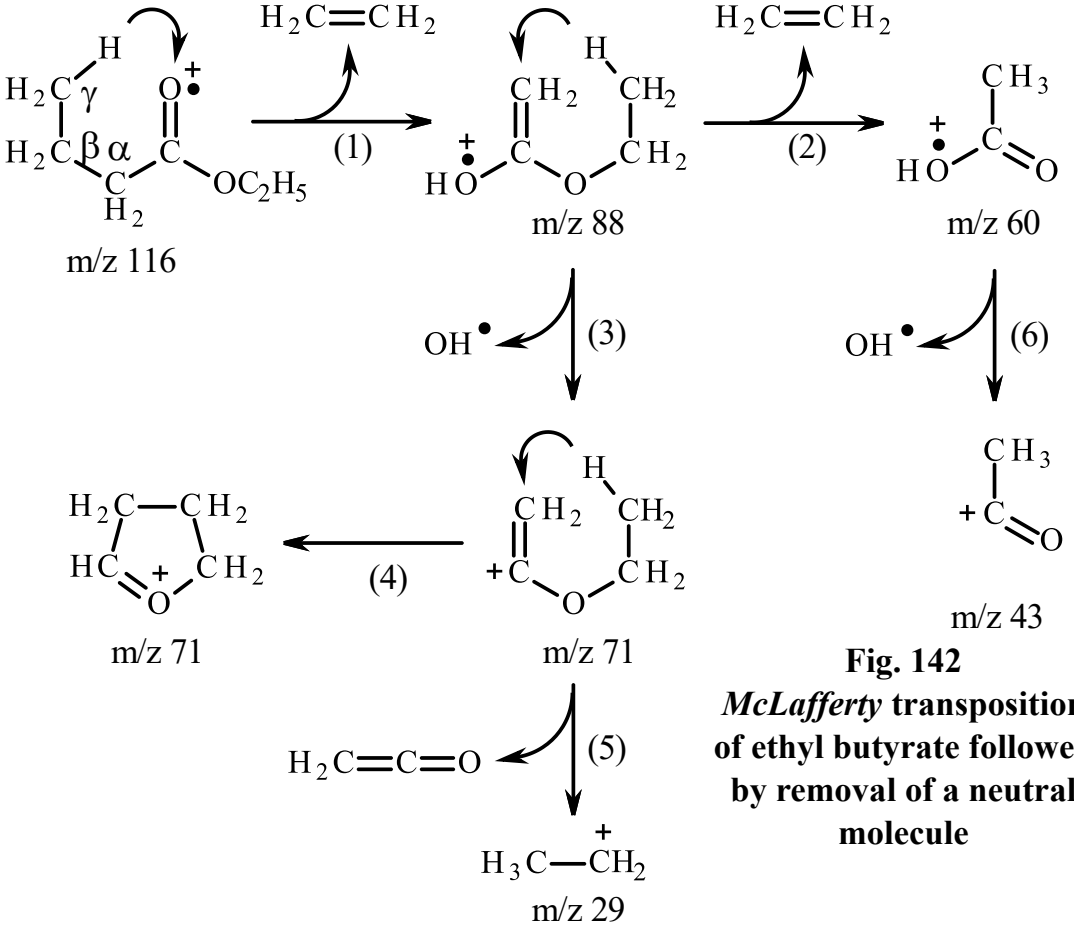



**Fig. 142 *McLafferty* transposition of ethyl butyrate followed by removal of a neutral molecule**

In molecules with a rigid steric structure (e.g. ketosteroids), the condition for *McLafferty* transposition is that the distance between the migrating hydrogen atom and the acceptor heteroatom is less than 18 Å. If all hydrogen atoms at the "γ" position are replaced by alkyl groups, then *McLafferty* transposition does not occur. If the hydro-

gen atom on the carbon atom at the "γ" position is involved in the double bond, then again, no transposition occurs.

If the structure of the ion formed in the *McLafferty* transposition is suitable for further transpositions, other signals characteristic of either radical ions (after removal of a neutral molecule) or ionic species will appear in the spectrum. A relevant example is the transposition of the radical ion of ethyl butyrate (Figure 142). The actual *McLafferty* transposition is the process **(1)**. In the radical ion resulting from the primary ionization, the hydrogen atom bonded to the carbon at the "γ" position of the carbonyl group is transferred to the oxygen atom, while a neutral molecule (in this case ethene) is eliminated **(2)**. Depending on the stability of the resulting ion, it may undergo a series of further fragmentations (processes **(2)-(6)**) in which radical ions are converted to ions with an even number of electrons, resulting in neutral molecules or small radicals (in Figure 142, ethene $CH_2{=}CH_2$, ketene $CH_2{=}C{=}O$, and hydroxy radical **HO•**). Figure 143 shows the mass spectrum of ethyl butyrate reconstructed from digitized spectra from an international collection:
**[https://mona.fiehnlab.ucdavis.edu/spectra/display/CCMSLIB00000075311]**.

The ions shown in Figure 142 are found in the spectrum (Figure 143) recorded with electron flow ionization (EI) at 70 eV.

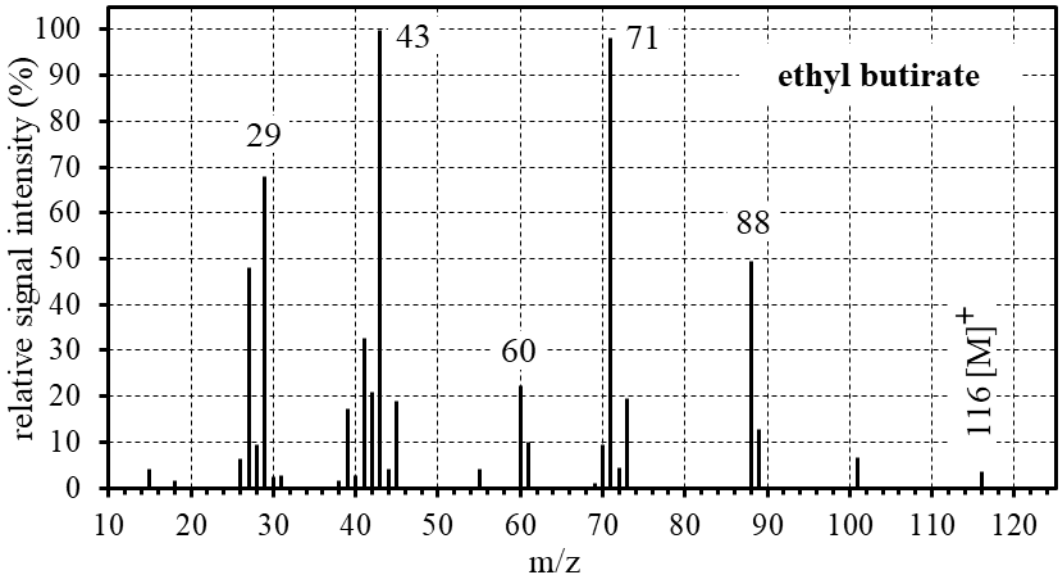



**Fig 143 The mass spectrum of ethyl butyrate (EI ionization, 70 eV). The ion at m/z 88 is the result of *McLafferty* transposition.**

### 4.8.10. Retro-addition 1,4

Fragmentation of a radical molecular ion containing two functional groups (**X** and **Y** in Figure 144) in adjacent positions (e.g., in the *ortho* configuration of an aromatic residue or in the *cis* configuration of an alkene) revealed the elimination of a neutral molecule containing a hydrogen atom from one of the functional groups (**X**) and an atom or groups of atoms (**Z-R** in Figure 144) from the other functional group.

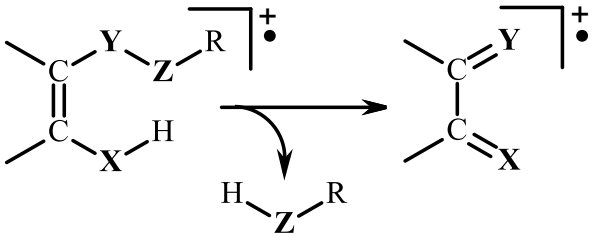


**Fig. 144**
**General representation of the "retro addition 1.4"**

Like *McLafferty* transposition, the process proceeds through a six-atom cycle transition state. The atoms **X**, **Y** and **Z** can be C, O, N, S and, depending on the identity of the **R** group, the neutral molecules removed can be water, an alcohol, a thiol, ammonia, an amine, or an acid.

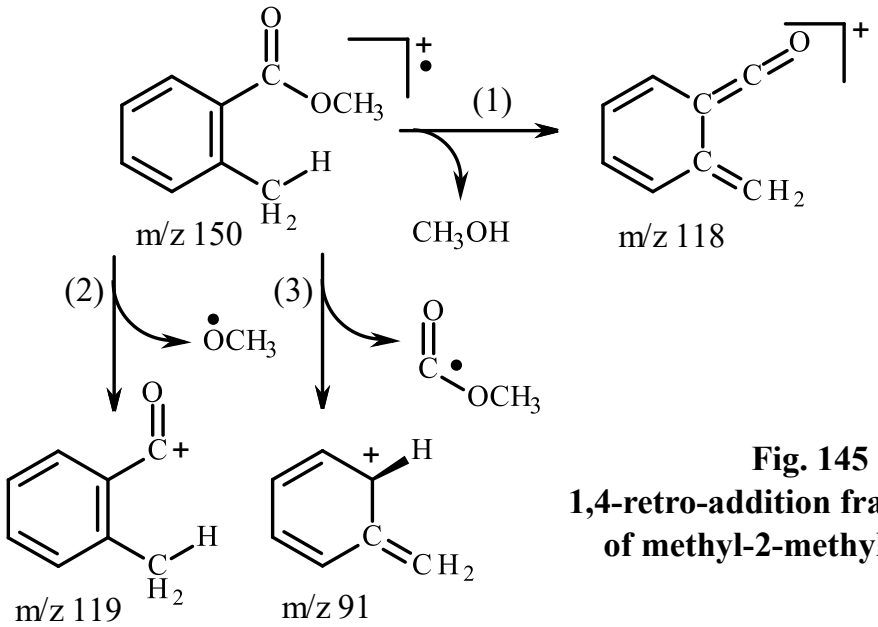



**Fig. 145**
**1,4-retro-addition fragmentation of methyl-2-methylbenzoate**

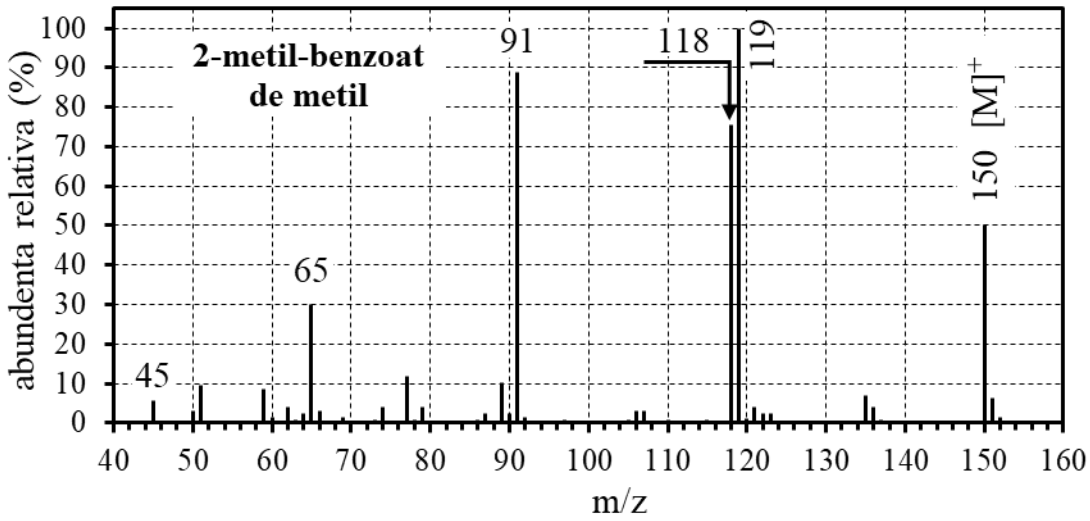



**Fig 146 Mass spectrum of methyl 2-methyl-benzoate (EI ionization, 70 eV)**

A relevant example is the fragmentation of the radical molecular ion of the methyl ester of 2-methylbenzoic acid (Figure 145). The 1,4-retro-addition fragmentation is

process **(1)** in which a neutral methanol molecule is removed and the ion of **m/z** 118 is formed. Processes **(2)** and **(3)** are additional fragmentation of a different type, producing ions of **m/z** 119 and 91, respectively. Figure 146 shows the mass spectrum of methyl 2-methyl-benzoate obtained after electron flow ionization (EI) with electron energy of 70 eV. The ions shown in Figure 145 are in the spectrum. The signal at **m/z** 150 corresponds to the radical molecular ion. The signal of the ion at **m/z** 118, which is the result of the 1,4-retro-addition process, appears with high intensity, indicating the high abundance of this ion. It is relevant to compare the mass spectrum of methyl-2-methyl-benzoate with that of methyl 4-methyl-benzoate recorded under identical conditions (Figure 147). In the latter spectrum the signal at **m/z** 118 is completely absent due to the unfavorable spatial arrangement of the groups involved.

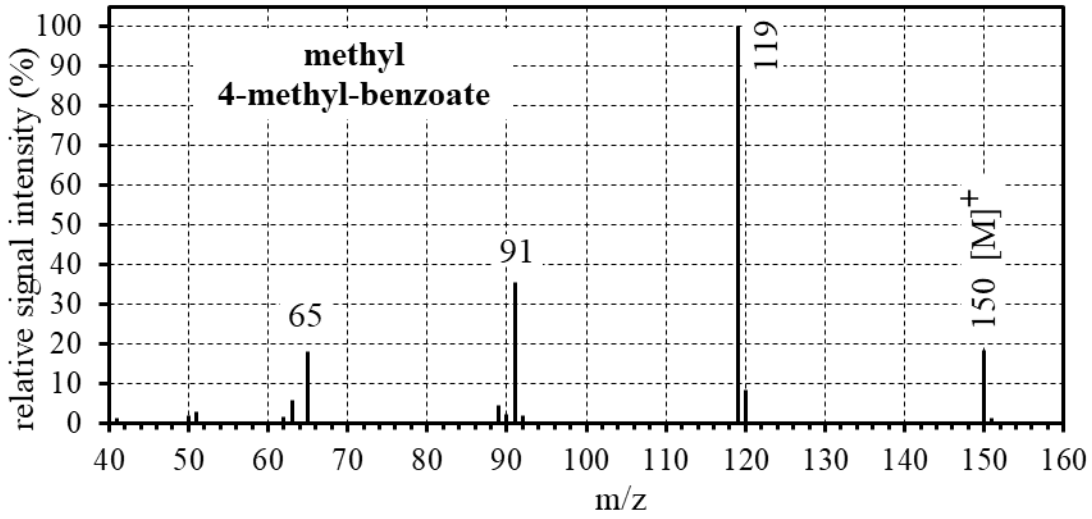



**Fig 147 Mass spectrum of methyl 4-methyl-benzoate (EI ionization, 70 eV)**

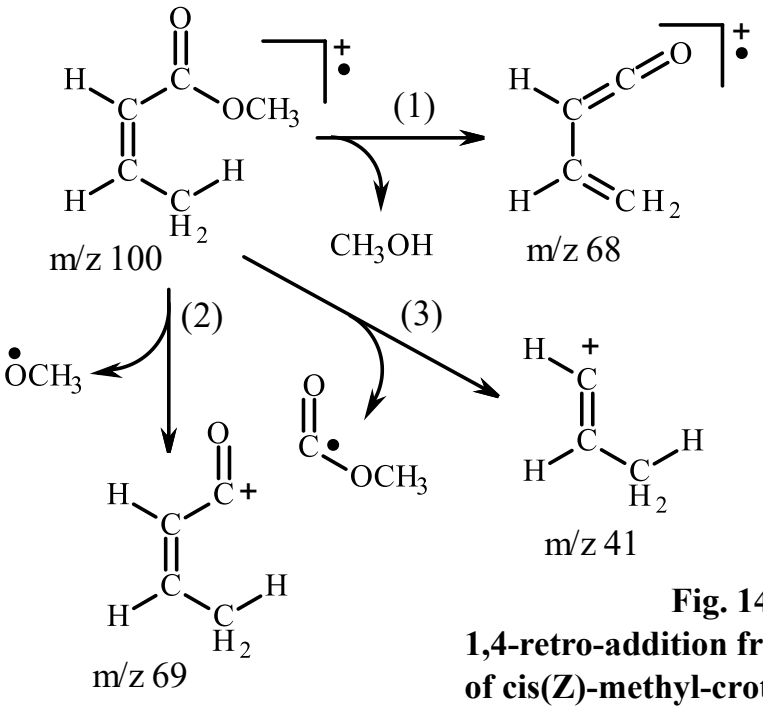



**Fig. 148**
**1,4-retro-addition fragmentation of cis(Z)-methyl-crotonate**

Another important example is methyl-crotonate (Figure 148). The role of group **X** in Figure 144 is played by the methylene group, **Y** is the carbonyl group, **Z** is the oxygen atom of the ester group, and **R** is a methyl residue. The result of the actual 1,4-retro-addition (process **(1)**) is the ion with **m/z** 68. In parallel with the 1,4-retro-addition, further fragmentation takes place to give the ions with **m/z** 69 (process **(2)**) and 41 (process **(3)**). Figure 149 shows the mass spectrum of the *cis*(*Z*) isomer of methyl-crotonate recorded using electron flow impact ionization (energy 70 eV). In addition to the signal from the 1,4-back addition (**m/z** 68, process **(1)**), ions resulting from other fragmentation appear.

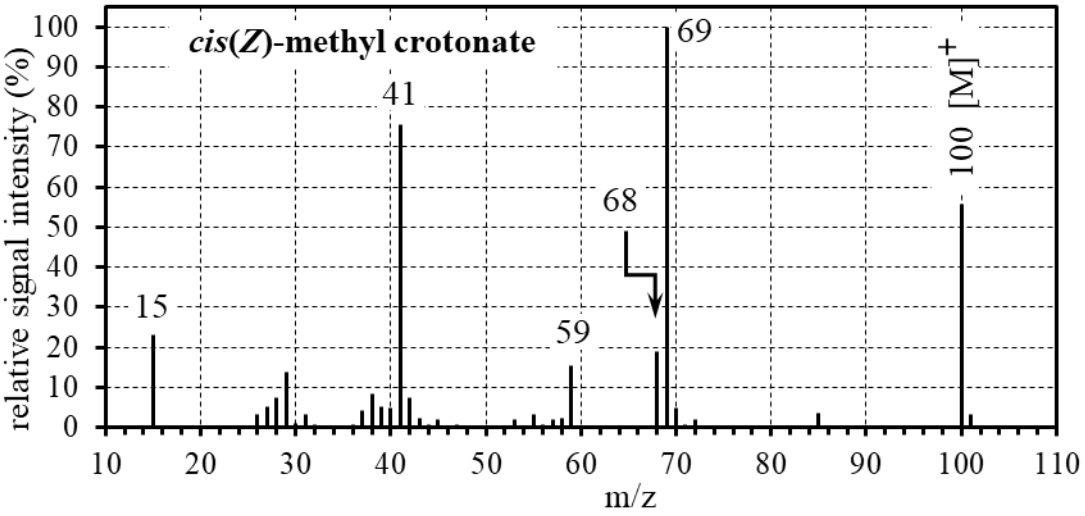



**Fig 149 Mass spectrum of methyl *cis*(*Z*)-crotonate (EI ionization, 70 eV)**

Note that the signal at **m/z** 68 is of medium intensity. In the case of the *trans*(*E*) isomer, where the hydrogen arrangement is not favorable for process **(1)**, the intensity of the signal at **m/z** 68 is much lower (Figure 150). In this case, to form the **m/z** 68 ion, the radical molecular ion must first change its configuration from *trans* to *cis*, and only after this change can process **(1)** start, hence the low intensity of the signal.

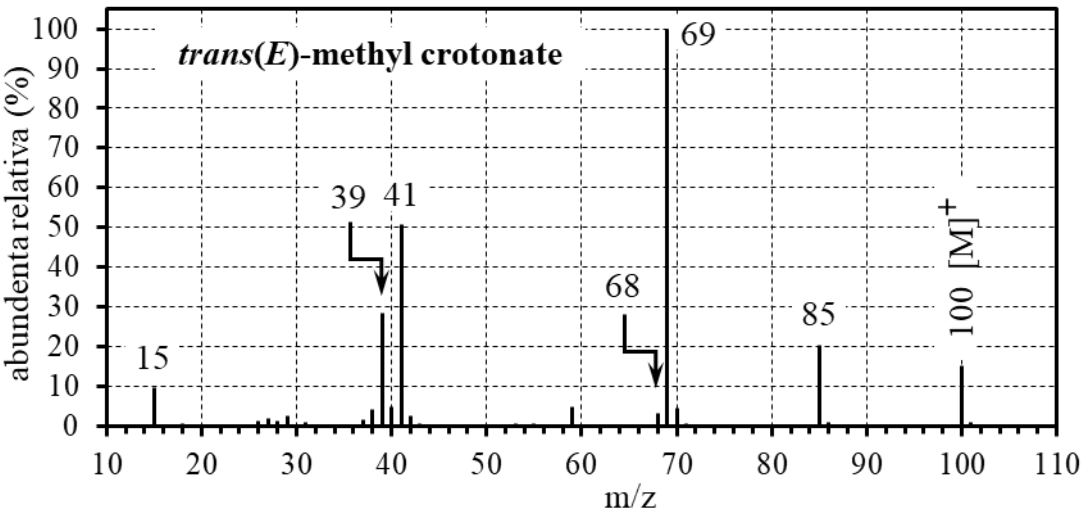
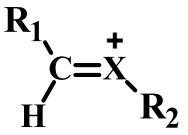



**Fig 150 Mass spectrum of methyl *trans*(*E*)-crotonate (EI ionization, 70 eV)**

### 4.8.11. Transposition of the hydrogen atom within an onium-type fragment ion

When the substituents **R1** and **R2** in an "onium" ion are alkyl radicals of at least 2 carbon atoms, then the onium ion undergoes an additional frag mentation with the removal of an alkene molecule and the migration of a hydrogen atom (Figure 151).



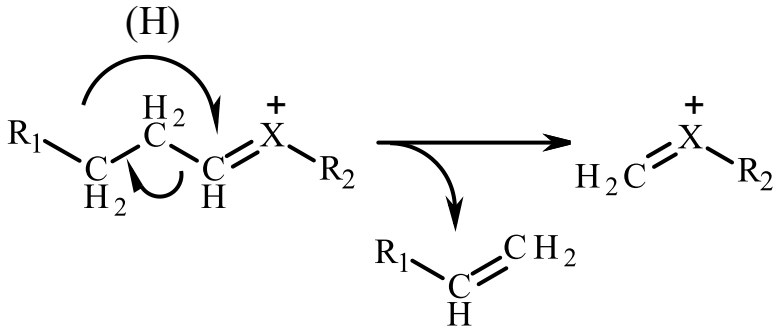


**Fig. 151 General scheme of the transposition of a hydrogen atom during the fragmentation of the "onium" ion**

If **R2** is a hydrogen atom (**R2** = H, as in the case of alcohols, thiols, primary amines where the amino group is attached to a secondary or tertiary carbon atom), the ion formed is stable and does not fragment further. However, if **R2** is an alkyl chain longer than or equal to the ethyl group (in the case of some ethers, secondary or tertiary amines), the fragmentation of the ion follows a slightly different mechanism (Figure 152), in that the process shown in Figure 151 involves the migration of a hydrogen atom to a carbon atom.

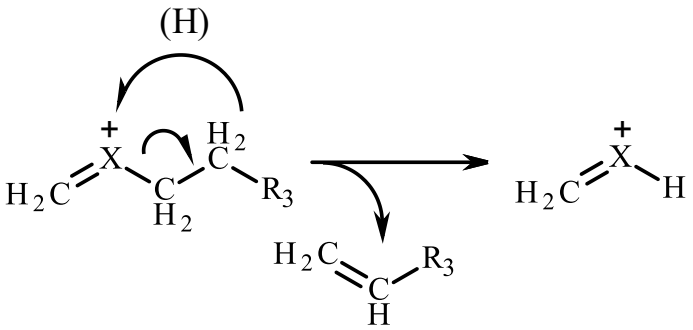


**Fig. 152 Scheme of further fragmentation of the "onium" ion formed in Figure 151**

In the process shown in Figure 152, a hydrogen atom is transferred to the heteroatom **X**. It follows that in the latter case, with a given heteroatom (with atomic mass '**MX**'), whether **R3** is an alkyl radical or a hydrogen atom, the final ion has molecular mass '$\mathbf{M_X+15}$'. If the heteroatom **X** is oxygen (secondary, tertiary and ether alcohols), the ion with **m/z** 31 is formed by both mechanisms.

Similar fragmentation with formation of the 'onium' ion is observed for 3-octanol (Figure 124). The **m/z** 31 signal is also present in the spectrum (Figures 125 and 126). This type of fragmentation, together with other secondary fragmentation, can be observed in the case of n-butyl-ethyl ether.

In Figure 153, processes **(1)** and **(2)** correspond to fragmentation mechanisms with transposition of the hydrogen atom with formation of the "onium" ion. Figure 154 shows the mass spectrum of n-butyl-ethyl ether obtained by electron flow ionization (EI) accelerated to the energy of 70 eV. It appears that the signals at **m/z** 31 and 59, corresponding to the "onium" ions produced by processes **(1)** and **(2)**, are dominant. The signals of other additional fragments, also shown in Figure 153, are also present in the mass spectrum.

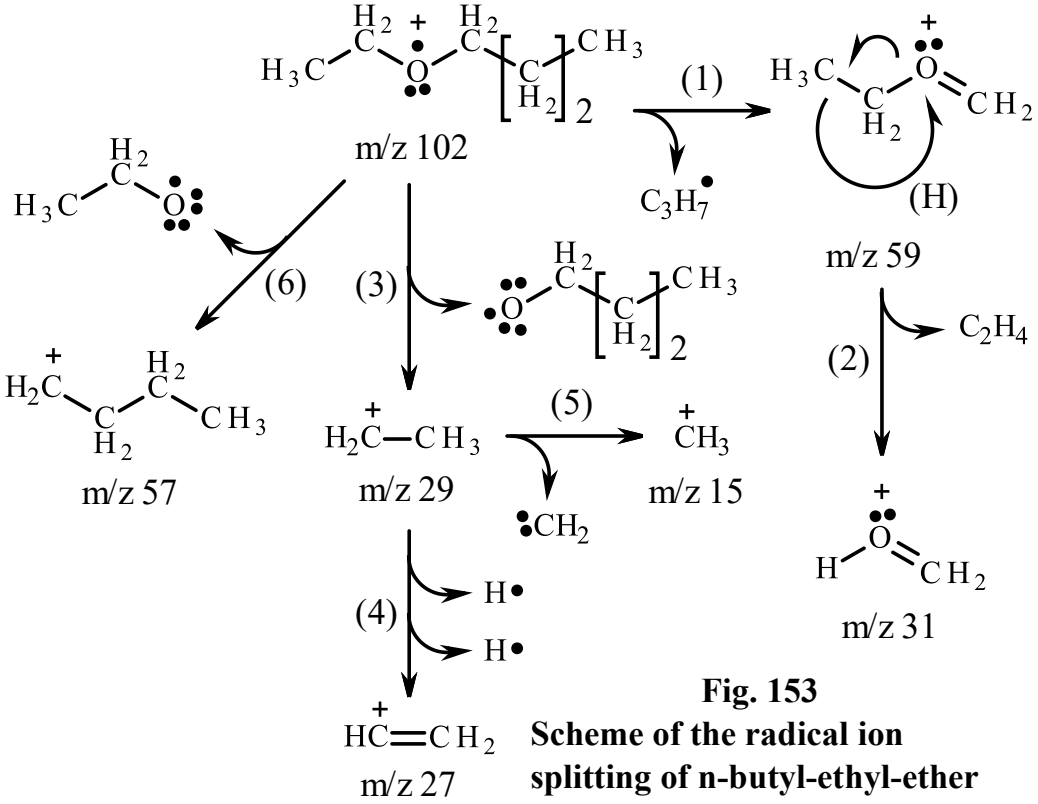



**Fig. 153**
**Scheme of the radical ion splitting of n-butyl-ethyl-ether**

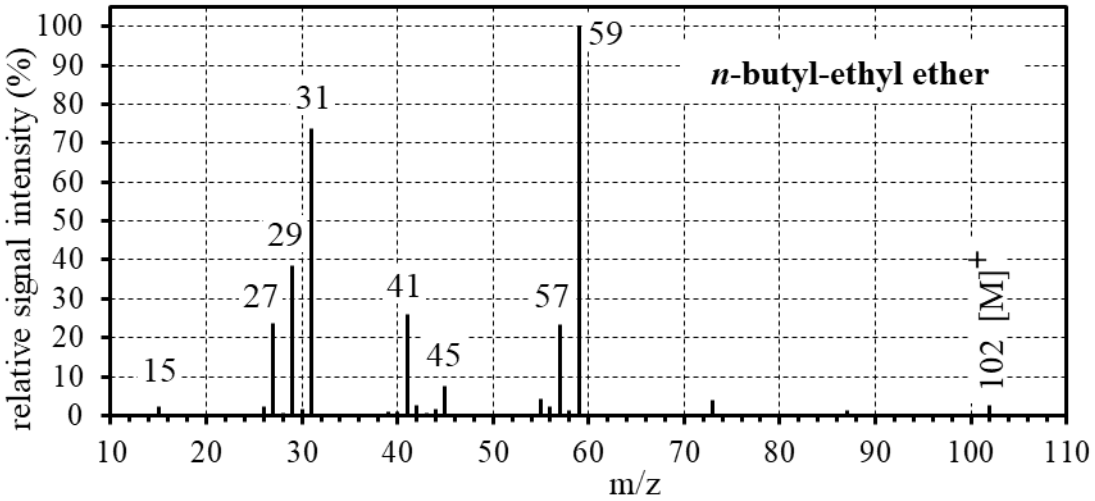



**Fig 154 Mass spectrum of *n*-butyl-ethyl ether (EI ionization, 70 eV) (reconstructed from digitized spectrum of collection MoNa, ID. JP007563)**

### 4.8.12. "Fragmentation "retro-*Diels-Alder*

In chapter 4.8.3 the fragmentation of unsaturated hydrocarbons (alkenes) was discussed and it was shown that during fragmentation the bond '**π**' can migrate to different positions in the chain. However, a bond '**π**' contained in a ring system cannot migrate but participates in a characteristic process known as 'retro-*Diels-Alder*' fragmentation (in the sense that it is the reverse of *Diels-Alder* synthesis known in hydrocarbon chemistry). Figure 155 shows, in general terms, the nature of the retro-*Diels-Alder* fragmentation.

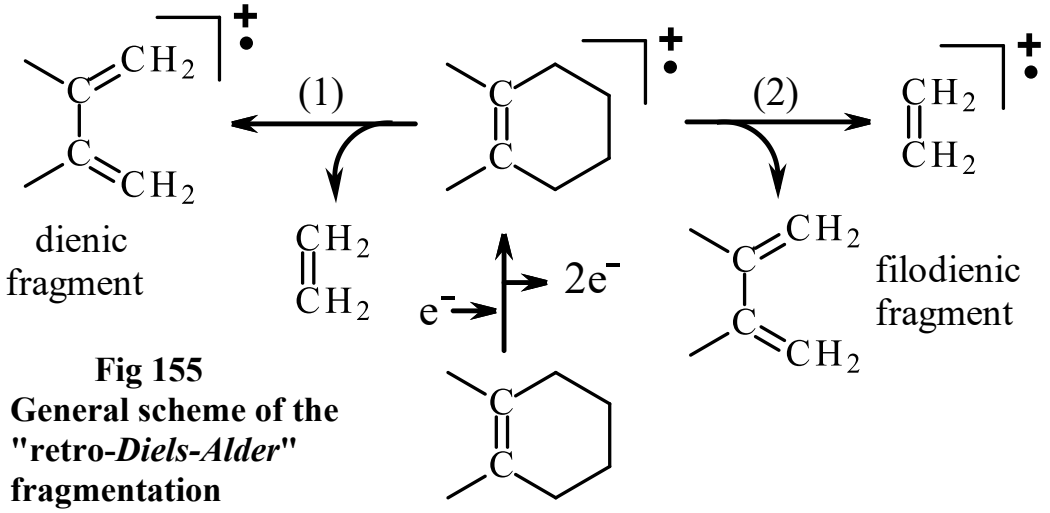



**Fig 155**
**General scheme of the "retro-*Diels-Alder*" fragmentation**

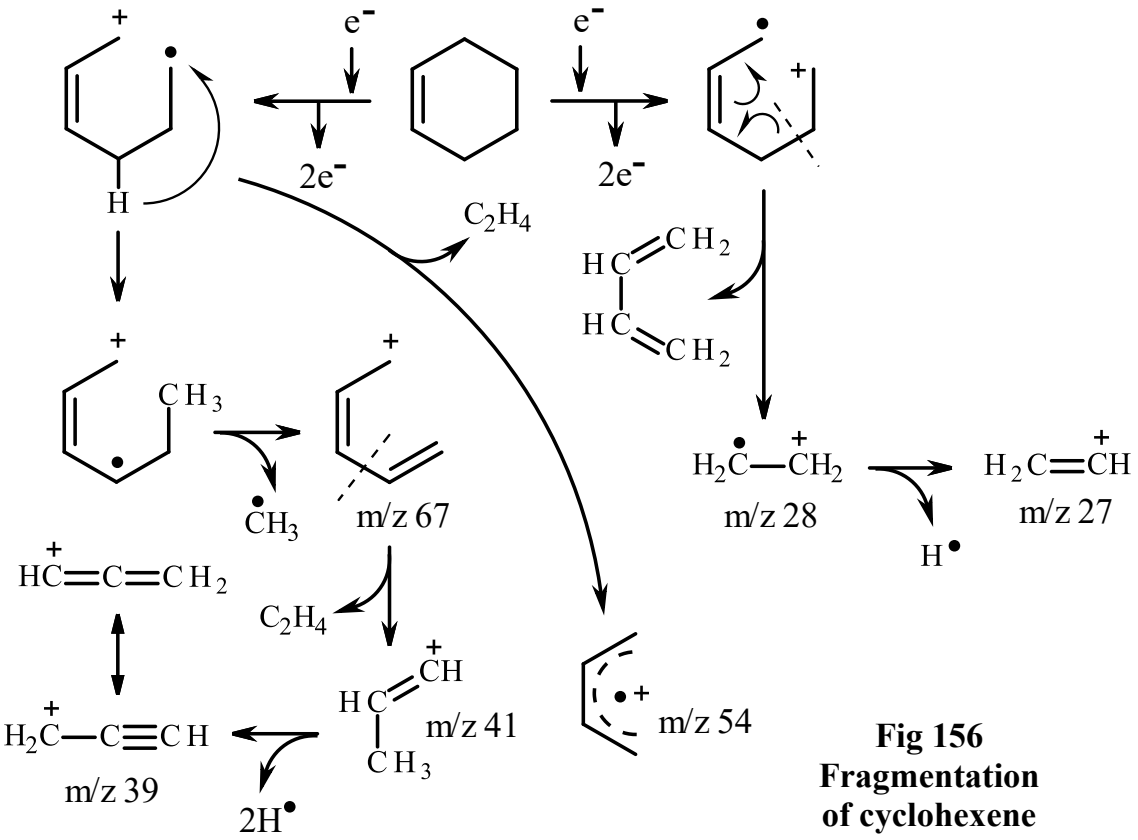



**Fig 156**
**Fragmentation of cyclohexene**

A relevant example is the fragmentation of cyclohexene. Figure 156 shows the fragmentation mechanism of cyclohexene after impact ionization by electrons with energy of 70 eV. Figure 157 shows the recorded mass spectrum. The ions predicted in the fragmentation scheme are found as prominent signals in the mass spectrum.

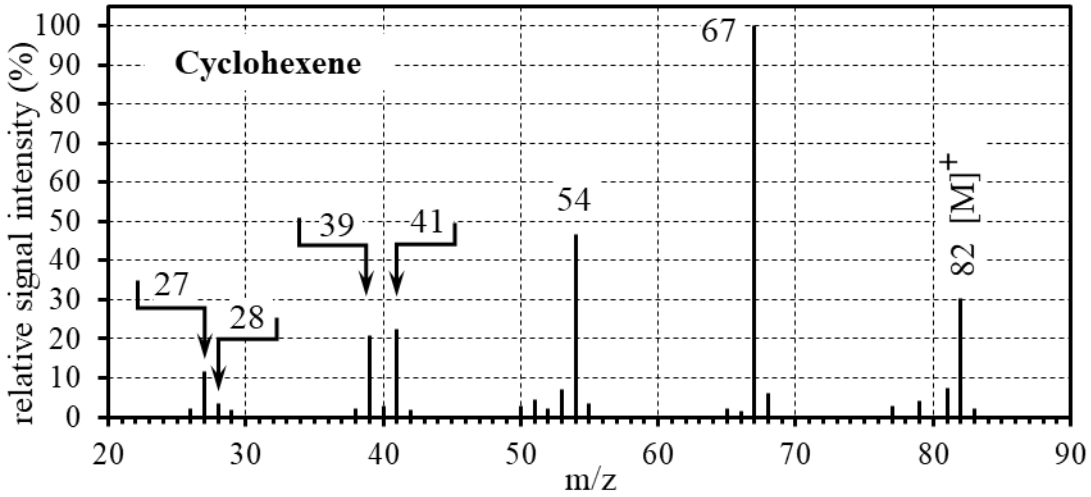



**Fig 157 Mass spectrum of cyclohexene (EI ionization, 70 eV) (after MoNa collection)**

The double bond, C═C, involved in retro-*Diels-Alder* fragmentation may be part of an aromatic system; an example is 1,2,3,4-tetrahydro-naphthalene (Figure 158).

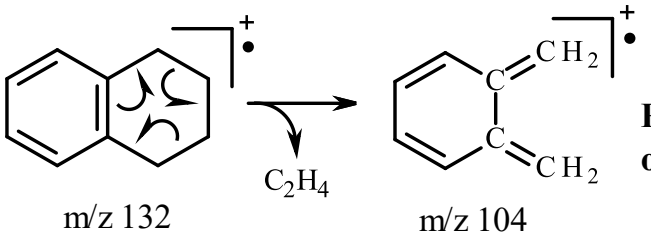



**Fig. 158**
**Retro-*Diels-Alder* fragmentation of 1,2,3,4-tetrahydronaphthalene**

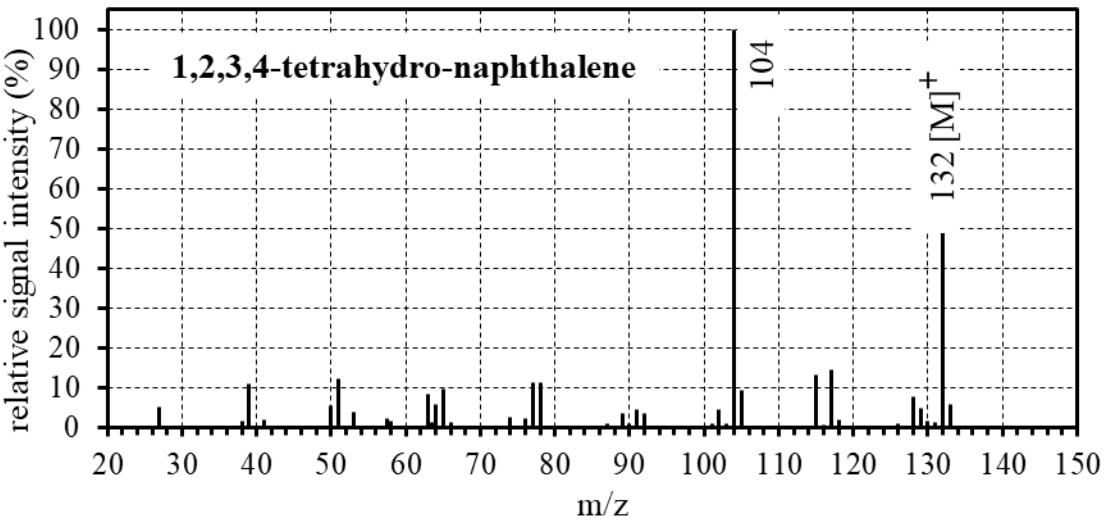



**Fig 159 Mass spectrum of 1,2,3,4-tetrahydro-naphthalene (EI ionization, 70 eV)**

Two ions with **m/z** ratios of 132 and 104 appear as dominant signals in the mass spectrum (Figure 159).

Retro-*Diels-Alder* fragmentation is an important tool for rational interpretation of mass spectra of unsaturated terpenes and some natural alkaloid compounds.

### 4.8.13. Fragmentation of mono-heteroatomic aromatic pentacyclic compounds

In addition to the bond cleavage between the atoms in the '$\alpha$' and '$\beta$' positions to the aromatic moiety (Figure 111), substances with a penta-atomic aromatic hetero cycle may undergo a bond cleavage between the heteroatom and one of its adjacent carbon atoms in the ring (Figure 160).

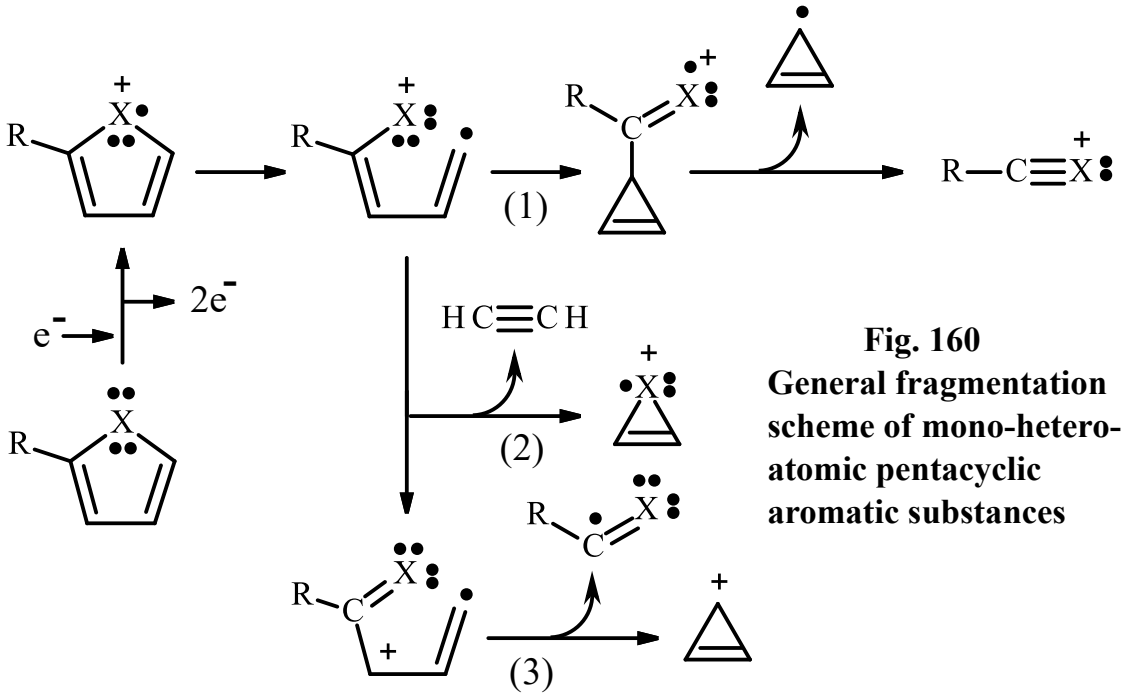



**Fig. 160**
**General fragmentation scheme of mono-hetero-atomic pentacyclic aromatic substances**

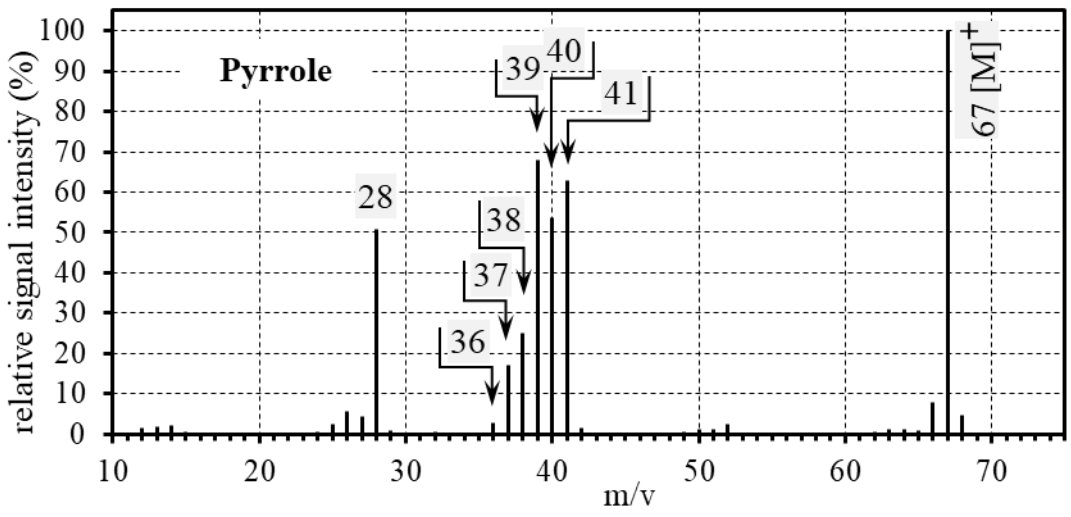



**Fig 161 Mass spectrum of pyrrole (EI ionization, energy: 75 eV)**

A simple example is the fragmentation of pyrrole. Figure 161 shows the mass spectrum of pyrrole obtained by impact ionization with electrons of 75 eV, and the process shown in Figure 162 is a possible interpretation of the signals.

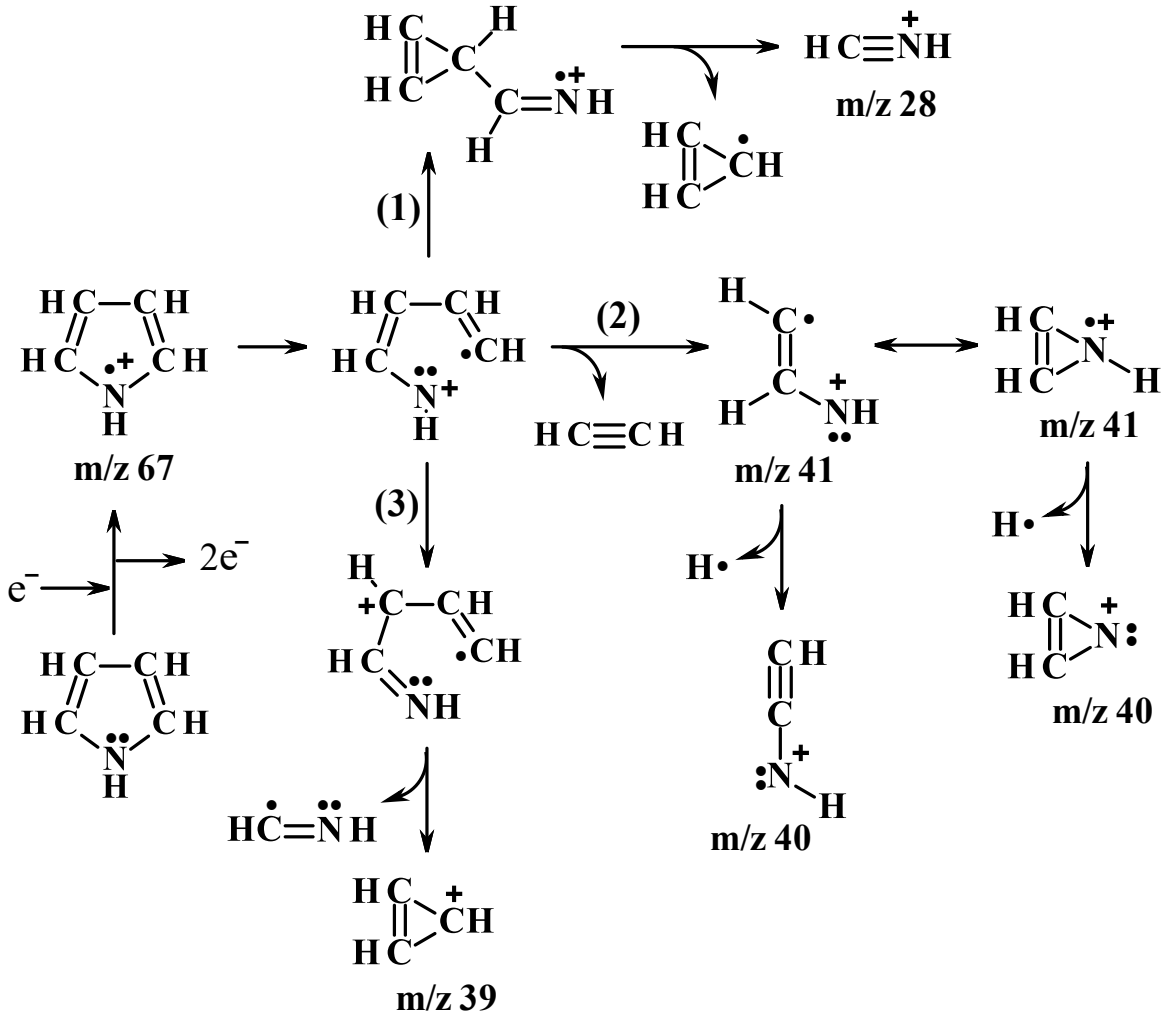



**Fig 162 Possible scenario for the fragmentation of pyrrole**

The relative preference of pathways **(1)**, **(2)**, and **(3)** depends on the energy factors and the stability of the ions formed. The driving force for pathway **(1)** is the stability of the "onium" ion at **m/z** 28. The removal of a neutral acetylene molecule energetically favors pathway **(2)** by increasing the probability of ion formation at **m/z** 41. The stability of the ion at **m/z** 39 formed in process **(3)** is due to the "**π**" electron pair. The cyclopropenium ion (**m/z** 39) is the simplest aromatic system (according to the *Hückel* rule, 2•n+2, for the system with "**n**" electrons "**π**" applied for the case **n** = 0), so its stability is comparable to that of the tropylium ion. Consequently, all three types of ions are present in the mass spectra of this class of heterocyclic chemical combinations.

### 4.8.14. Fragmentation of metastable ions

In most cases, the primary ions produced in the ionization unit are either stable enough to pass unchanged through the analyzer area and reach the detector, or unstable

enough to undergo fragmentation within the ionization unit before entering the analyzer. There is also a category of intermediately stable ions (lifetimes on the order of $10^{-5}$ seconds) that leave the ionization unit unchanged but undergo either total or partial fragmentation within the analyzer before reaching the detector. These ions are called "metastable" and the process is known as "metastable fragmentation".

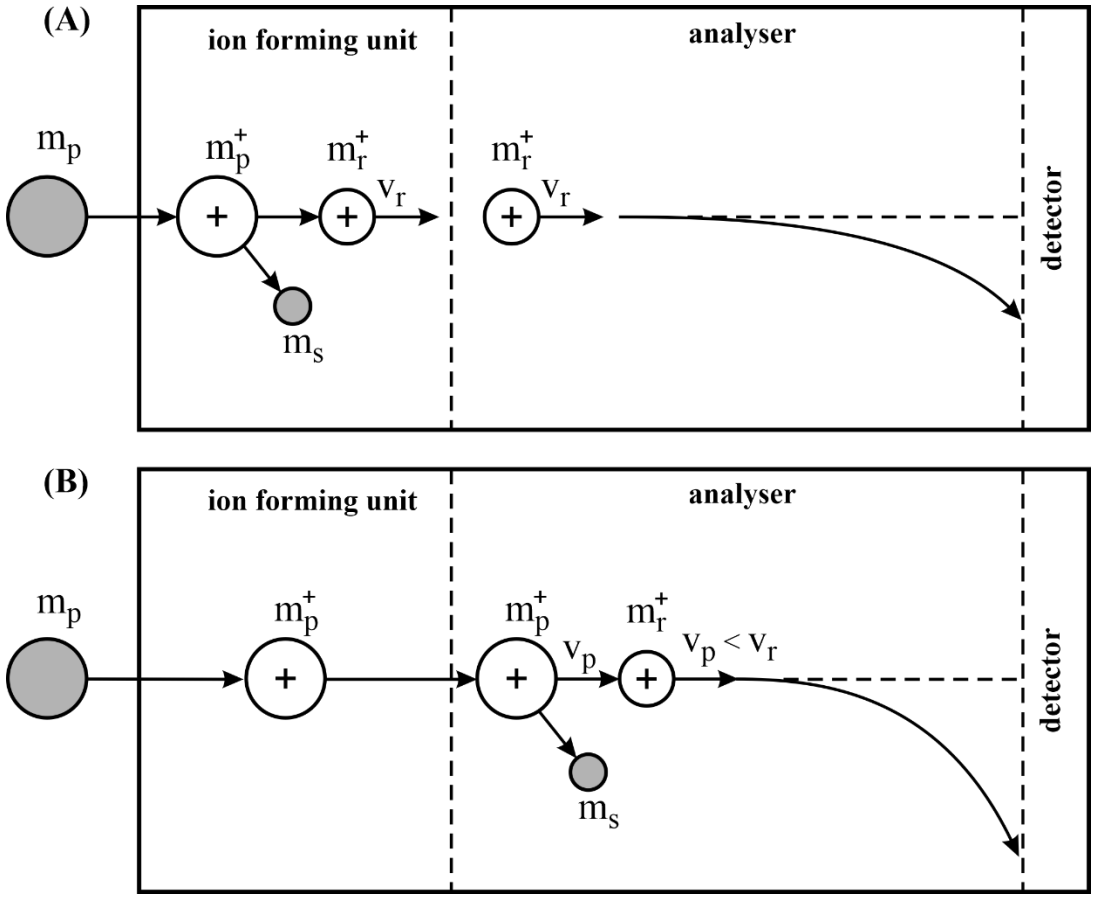



**Fig. 163 Formation of fragmentation ions (A) and metastable ions (B)**

Strictly speaking, the term "metastable fragmentation" refers to monomolecular splitting processes of primary ions due to internal energy and does not refer to post-ionization splitting of ions initiated by collision with atoms of an inert gas (as is the case in $MS^2$ spectrometry). Figure 163 compares the fragmentation of an ion of mass $\mathbf{m_p^+}$ into the ion of mass and $\mathbf{m_r^+}$ and a neutral species of mass $\mathbf{m_s}$ within the ionization unit **(A)** and the fragmentation of the ion of mass $\mathbf{m_p^+}$ within the analyzer region **(B)**, producing the same ion and neutral species pair. When the ions formed in the ionization unit are accelerated by the voltage "$\mathbf{V_{acc}}$", all the ions with electric charge "**e**" (i.e. monovalent ions "1", "2", ... , etc.) acquire kinetic energy "$\mathbf{e \cdot V_{acc}}$" related to their velocities ("$\mathbf{v_1}$", "$\mathbf{v_2}$", ... , etc.) by the relationship (66),

$$e \cdot V_{acc} = \frac{m_1 \cdot v_1^2}{2} = \frac{m_2 \cdot v_2^2}{2} = \cdots = \frac{m_i \cdot v_i^2}{2} = \cdots \frac{m_n \cdot v_n^2}{2} \qquad (66)$$

and the impulse ($\mathbf{P_i}$) of the ions is:

$$P_i = m_i \cdot v_i \;\; ; \;\; (i=1,2,...,n) \tag{67}$$

The relationship (66) also applies to the $\mathbf{m_p^+}$ and $\mathbf{m_r^+}$ ion pair (the latter resulting from the fragmentation of the former). If the fragmentation takes place in the ionization unit (Figure 163 **(A)**), then the velocity of the $\mathbf{m_r^+}$ ion is $\mathbf{v_r}$ and the relationship (66) becomes:

$$e \cdot V_{acc} = \frac{m_p^+ \cdot v_p^2}{2} = \frac{m_r^+ \cdot v_r^2}{2} \quad \Rightarrow \quad v_p^2 = v_r^2 \cdot \frac{m_r^+}{m_p^+} \tag{68}$$

Instead, if the fragmentation of the ion with mass $\mathbf{m_p^+}$ occurs inside the analyzer (the area where no further ion acceleration occurs, Figure 163 **(B)**), then the ion with mass $\mathbf{m_r^+}$ produced moves with the same velocity $\mathbf{v_p}$ as the ion with mass $\mathbf{m_p^+}$ acquired during the acceleration. From the point of view of the analyzer action, the ion with mass $\mathbf{m_r^+}$ (moving at velocity $\mathbf{v_p}$) behaves as an ion with velocity $\mathbf{v_r}$ (which it would have had if fragmentation had occurred in the ionization unit) but with apparent mass **m***. According to the principle of conservation of impulse, it follows that:

$$m_r^+ \cdot v_p = m_r^* \cdot v_r \tag{69}$$

Squaring both sides of the relationship (69) gives:

$$\left(m_r^+\right)^2 \cdot v_p^2 = \left(m_r^*\right)^2 \cdot v_r^2 \tag{70}$$

After removing the velocities $\mathbf{v_p}$ and $\mathbf{v_r}$ from equations (68) and (70), the apparent mass **m*** is expressed in terms of $\mathbf{m_r^+}$ and $\mathbf{m_p^+}$:

$$m_r^* = \frac{\left(m_r^+\right)^2}{m_p^+} \tag{71}$$

The signal produced by the fragmentation of a metastable primary ion can be recognized (in addition to its position in the spectrum at a non-integer **m/z** ratio) by its broadened shape, often corresponding to a *Gaussian* curve.

The relationship (71) can be transformed into the logarithmic form (72),

$$\log(m_r^+) = \frac{\log(m_p^+) + \log(m_r^*)}{2} \tag{72}$$

which can be plotted as a nomogram (Figure 164).

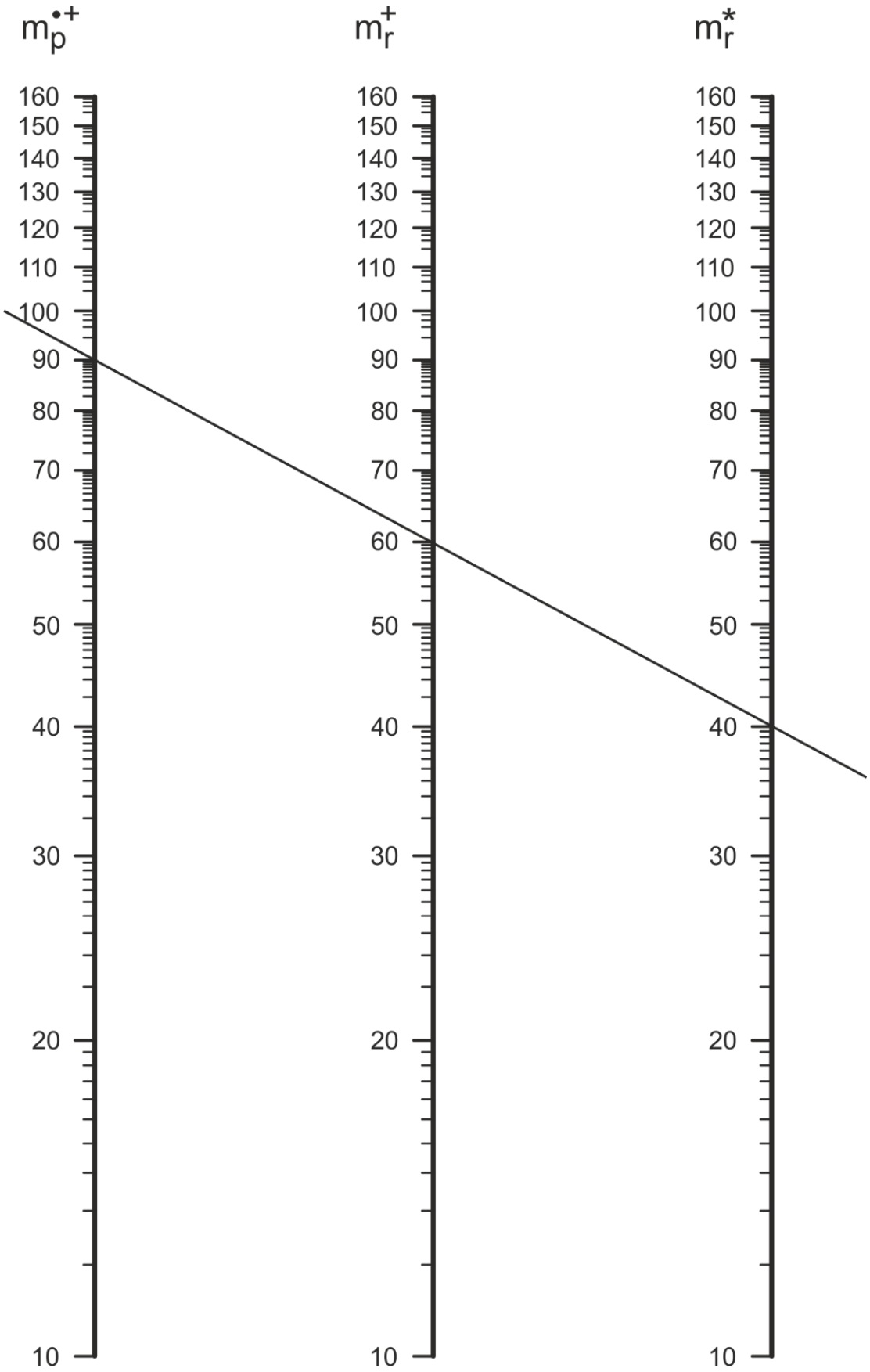



**Fig 164 Nomogram for calculating the mass of metastable ions**

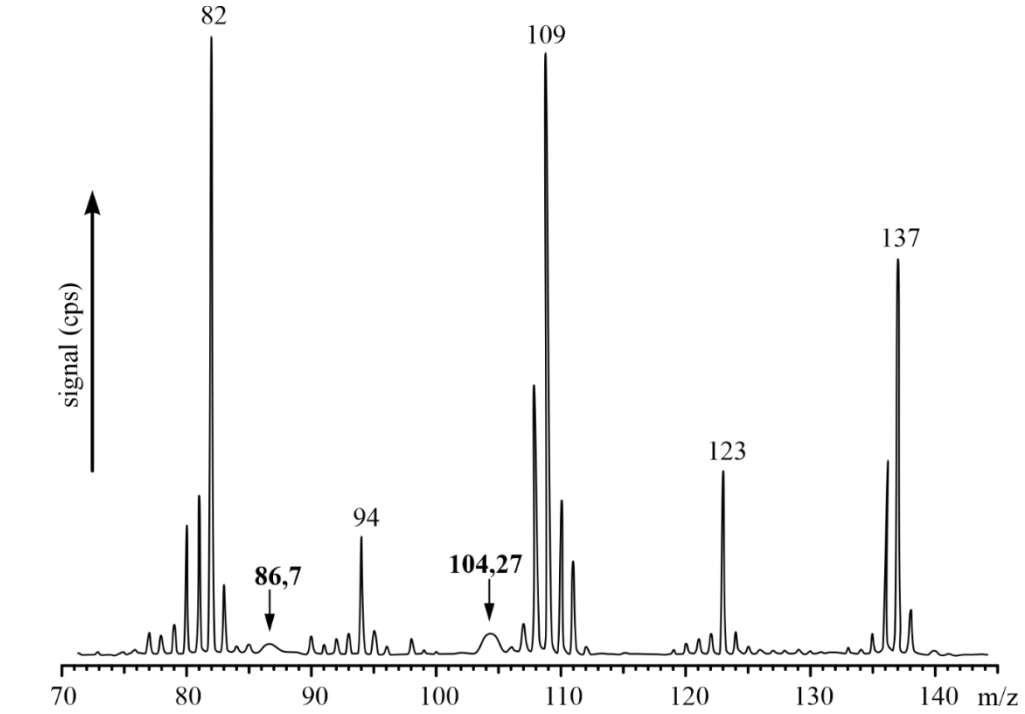



**Fig. 165 Mass spectrum of theobromine (after *L. Sleno, D.A. Volmer*: Ion Activation Methods for Tandem Mass Spectrometry. Journal of Mass Spectrometry 2004:39(10), 1091-1112**

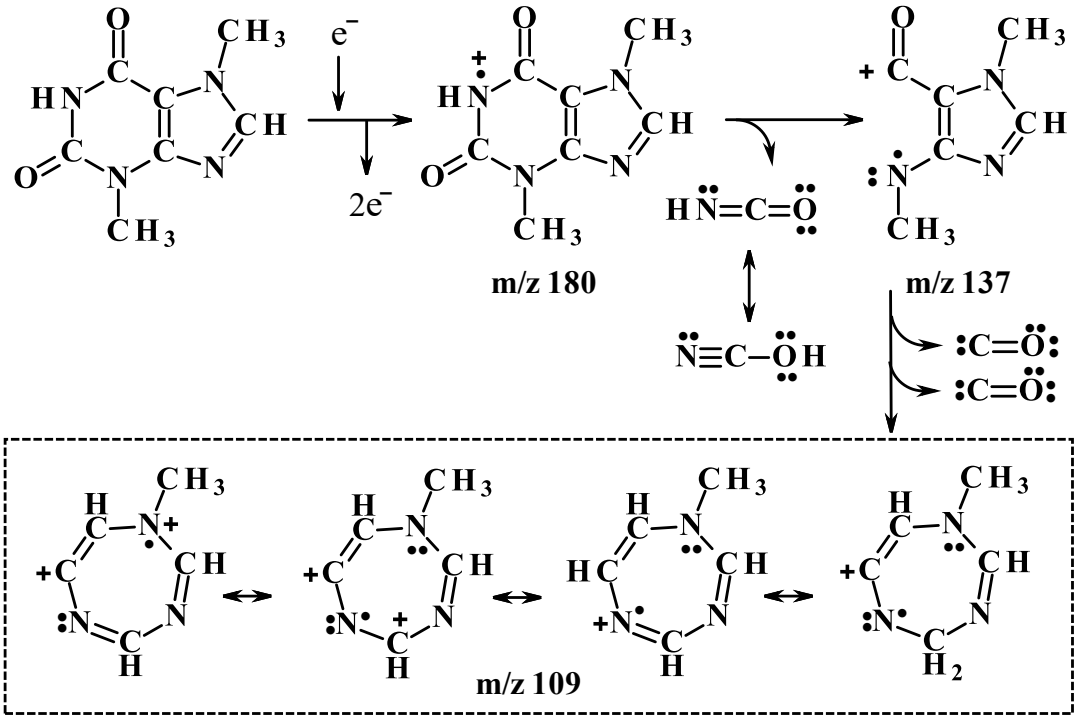



**Fig. 166 Fragmentation path of theobromine (after *L. Sleno, D.A. Volmer*: Ion Activation Methods for Tandem Mass Spectrometry. Journal of Mass Spectrometry 2004:39(10), 1091-1112 and *G. Spiteller, M. Spiteller-Friedmann*: Vergleichende massenspektrometrische Untersuchung einiger Purinderivate. Monatsh. Chem., 1962:93(3), 632-638)**

Consequently, in the mass spectrum obtained, the signal (corresponding to mass $\mathbf{mr^+}$) resulting from the fragmentation of a metastable ion (with mass $\mathbf{m_p^+}$) does not appear at the expected position but at the position corresponding to the apparent mass ("**m***"), often at a non-integer value.

The signal of an ion resulting from the fragmentation of a metastable ion is seen in the mass spectrum of pyrrole (Figure 161, signal at the non-integer value of **m/z** 33.5). Another appearance of signals resulting from fragmentation of metastable ions is seen in the mass spectrum of theobromine (**m/z** 86.7 and 104.27 in Figure 165). The interpretation of the other signals in the mass spectrum of theobromine is shown in Figure 166.

## 4.9. Elementary general rules and typical fragmentation processes of classes of organic substances

### 4.9.1 General rules for organic ion fragmentation

There are specialized databases for identifying or elucidating the molecular structure of an organic compound. Most databases provide information on electron flow ionization (EI) mass spectra. This mode of ionization is an energetic operation that results in significant fragmentation of the primary ion. The fragmentation mode provides useful information for elucidating the molecular structure of the analyte. Some explanations and rules are helpful. In the EI ionization unit, the first step produces a radical cation with an odd number of electrons, which usually is splitting into a smaller cation (even number of electrons) and a neutral radical (odd number of electrons). A covalent chemical bond (equivalent to a pair of electrons between the bonded atoms) can be broken "homolytically" (where the resulting fragments retain one electron of the original pair) or "heterolytically" (where both electrons of the bond are attached to one of the fragments) (Figure 167).

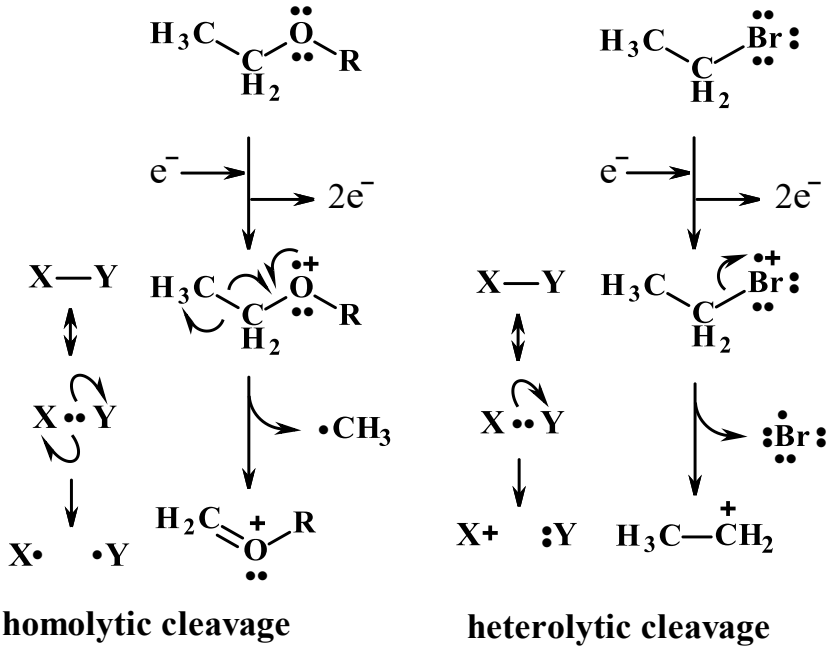



**Fig. 167 Homolytic and heterolytic cleavage of a covalent bond**

As shown in Figure 167, the displacement of an electron during the homolytic cleavage of a covalent bond is conventionally indicated by the half arrow., ). The displacement of an electron pair (an event in heterolytic cleavage) is represented by the usual full arrow, ) .

The ions formed in the ionization unit are usually radical ions with an odd number of electrons (doublet spectroscopic state). As a result of their fragmentation, either more radical ions are formed with the simultaneous elimination of electrically neutral molecules, or ions with an even number of electrons (singlet spectroscopic state) are formed together with neutral radical species.

The probability of a chemical bond cleavage (and hence the appearance of the resulting fragment signal in the spectrum) depends on the strength of the bond and the stability of the resulting ionic fragment. A cationic fragment may be fragmented into more stable cations. The fragmentation of a cyclic ion involves the cleavage of at least two covalent bonds.

Some rules are useful for interpreting mass spectra.

**Rule (1)** The spectral signal of the molecular ion, $\mathbf{[M]^+}$, is most prominent for linear species and its intensity decreases with increasing branching.

**Rule (2)** In a homogeneous series of linear molecules, the relative intensity of the molecular ion $\mathbf{[M]^+}$ decreases with increasing chain length.

**Rule (3)** Splitting is favored in alkyl-substituted carbon atoms, and its manifestation increases with increasing degree of substitution. This property is a consequence of the *Stevenson* rule concerning the relative stability of carbocations:

benzylic > allylic > tertiary > secondary >> primary

When an ionic radical is split, in most cases the larger fragment becomes a neutral radical and the smaller fragment retains the positive charge.

**Rule (4)** Double bonds ($\sigma$ and $\pi$ bond set), ring structures and especially aromatic rings stabilize the molecular $\mathbf{[M]^+}$ ion and increase the spectral intensity of the associated signal.

**Rule (5)** Double bonds ($\sigma$ and $\pi$ bond set) favor cleavage that produces a stabilized allylic carbocation; this phenomenon is particularly evident in cycloalkenes (Figure 168).

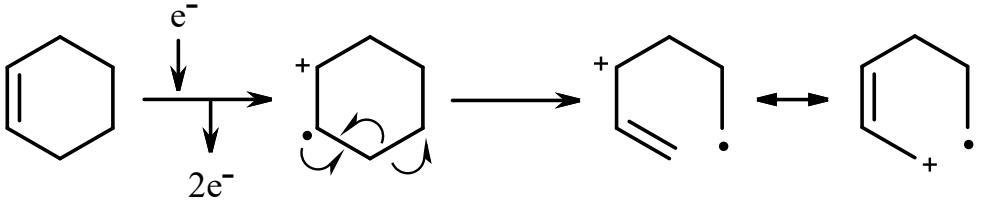



**Fig. 168 Fragmentation of cyclohexene with the positive charge in the allylic position**

**Rule (6)** In saturated cyclic compounds (e.g., substituted cyclohexane derivatives), the exocyclic bond tends to cleave first, leaving the positive charge on the cyclic moiety (Figure 169).

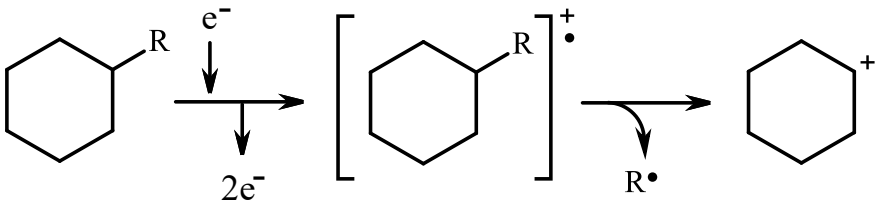



**Fig 169 Preferential cleavage of the exocyclic moiety in substituted cyclohexane**

**Rule (7)** The fragmentation reaction commonly observed for unsaturated cyclic ionic species is retro-*Diels-Alder* fragmentation with removal of a neutral molecule (Figure 170).

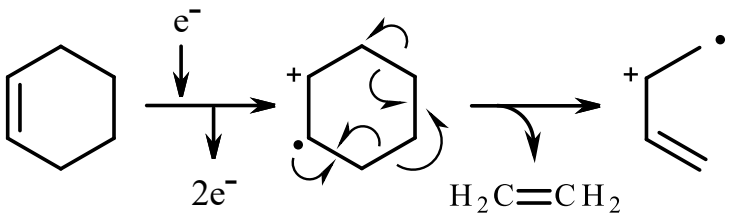



**Fig 170 Fragmentation retro-*Diels-Alder* of cyclohexene**

Again, the positive charge is preferentially located in the allylic position compared to the double bond.

**Rule (8)** Alkyl-substituted aromatic compounds tend to cleave to form a benzyl cation which, upon rearrangement, becomes a stable tropylium cation (Figure 171).

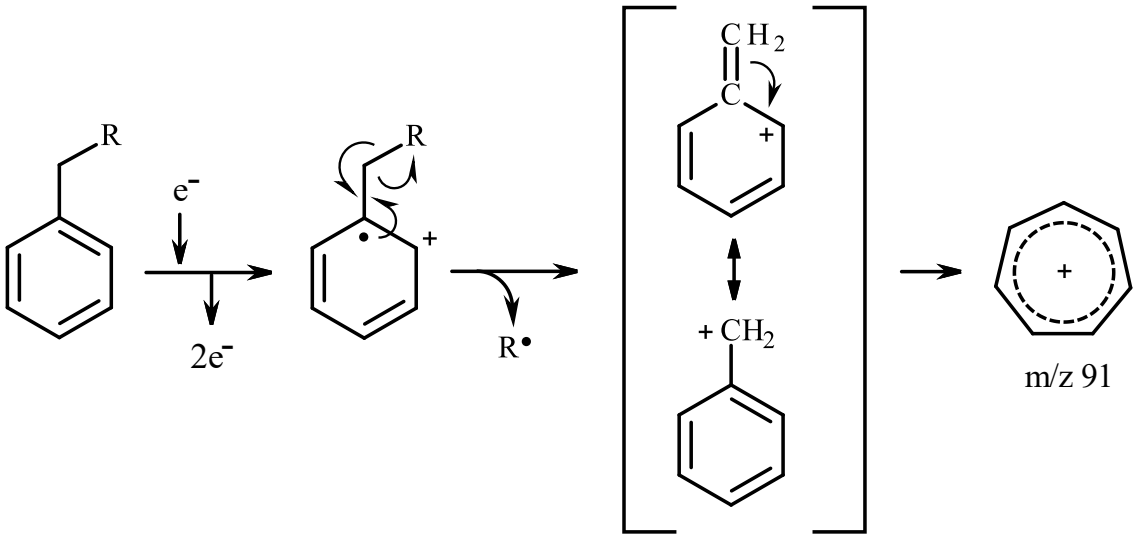



**Fig. 171 Conversion of alkyl substituted aromatic compounds with formation of a tropylium ion**

**Rule (9)** The σ(C-C) bond adjacent to a heteroatom often cleaves, leaving the positive charge on the carbon atom attached to the heteroatom (Figure 172).

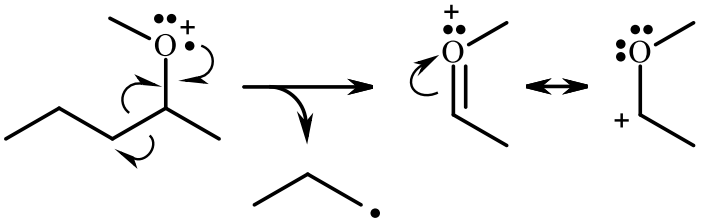


**Fig. 172 Cleavage of the σ(C-C) bond adjacent to a heteroatom**

**Rule (10)** Fragmentation associated with the removal of neutral, small, and stable molecules is usually likely to occur.

Fragmentation can be accompanied by intramolecular rearrangements, sometimes producing ions with unexpected structures. One such process is the *McLafferty* rearrangement observed in compounds containing a carbonyl group (Figure 142). Other forms of rearrangement are known, some of which are not mechanistically understood and are considered "random" (Figure 173).

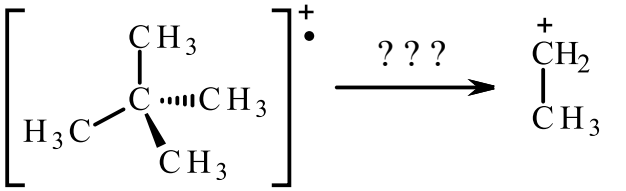



**Fig 173**
**Example of a "random" fragmentation**

### 4.9.2. Fragmentation peculiarities of some classes of compounds

#### 4.9.2.1. Saturated hydrocarbons (alkanes, isoalkanes, cycloalkanes)

The fragmentation rules **(1)-(3)** in the previous chapter are commonly applied to compounds in this class. Rearrangements are also possible but do not give strong signals. The signal of the molecular ion, $[M]^+$, of linear (unbranched) hydrocarbons is always detectable, but its relative intensity decreases with increasing chain length and/or branching (Figure 174).

The mass spectra of saturated hydrocarbons often have grouped signals separated by 14 mass units each corresponding to one methylene group, $-CH_2-$ (Figures 101 and 102). The most intense signals are those of fragments with three, four and five carbon atoms. The appearance of the mass spectra of saturated hydrocarbons with a branched chain is like that of unbranched alkanes, except for the increased intensity of some signals (for comparison, see the mass spectra of n-octane and 2-methyl-heptane in Figure 174). In both spectra there is a constant difference in the signals corresponding to a methylene group:

$$43 - 29 = 14\ ;\ 57 - 43 = 14\ ;\ 71 - 57 = 14\ ;\ 85 - 71 = 14\ .$$

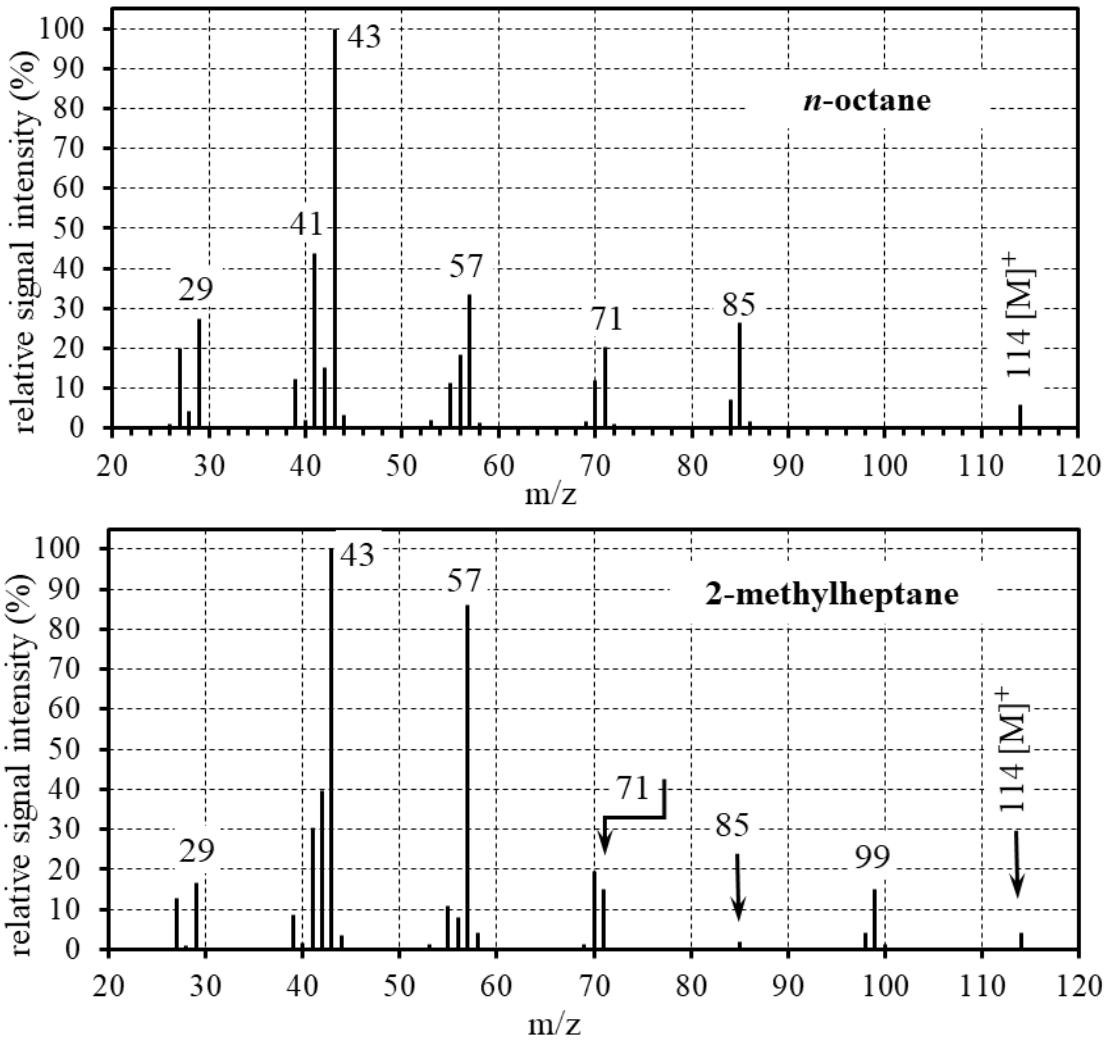



**Fig. 174 Comparison of mass spectra (EI ionization, 75 eV) of n-octane and 2-methylheptane (after database SDBS)**

In the spectrum of 2-methylheptane there is a signal at **m/z** 99 that is not present in the spectrum of n-octane. The difference 114 - 99 = 15 corresponds to the cleavage of a methyl group (-$CH_3$). The similarity of the positions of the signals is obvious; the differences are in their relative abundance.

In some exceptional cases, with electron impact ionization (EI), the molecular ion signal (**[M]**$^+$) may be very weak or even undetectable. In the chemical ionization of cyclic saturated hydrocarbons (cycloalkanes) the molecular ion signal is relatively strong (**Rule (4)**). The fragmentation of the cyclic molecular ion involves the cleavage of two covalent bonds, so the probability of the process is low.

### 4.9.2.2. Alkenes

In electron impact ionization (EI) of alkenes, the signal of molecular ion **[M]**$^+$ is usually easily identified. In acyclic alkenes the double bond may migrate to different positions in the fragment, making it difficult to determine the original position of the double bond. In cyclic alkenes the original position of the double bond is determined

more easily. Cleavage often occurs at the allylic position relative to the double bond (**Rule (5)**).

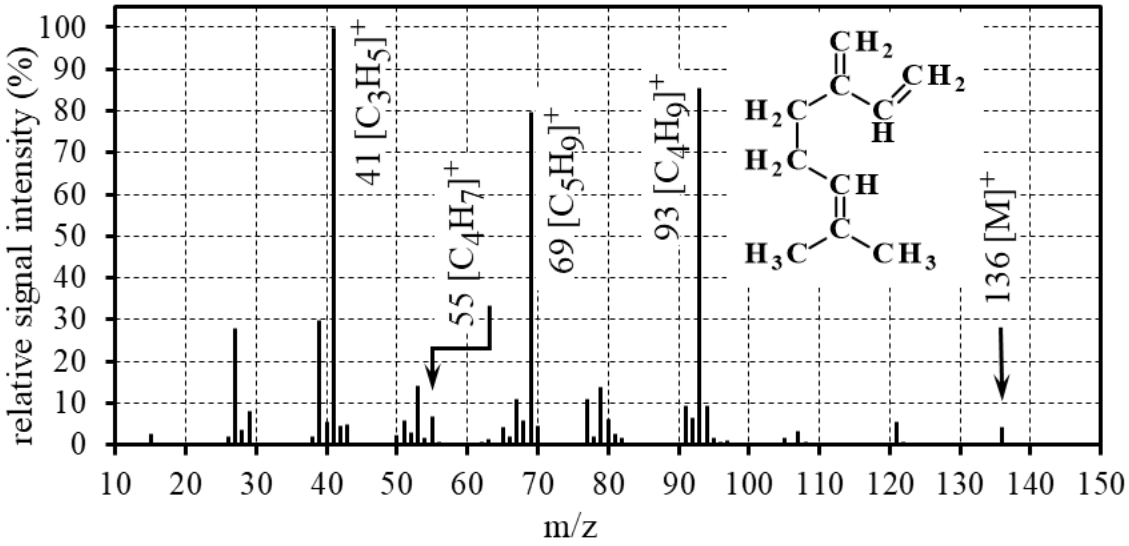



**Fig. 175 Mass spectrum of 7-methyl-3-methylene-1,6-octadiene (β-myrcene) (reconstructed from MoNa spectrum collection data, ID. JP007563)**

As an example, Figure 175 shows the mass spectrum of the compound β-myrcene, in which the signal of the molecular ion at **m/z** 136 is easily distinguishable.

### 4.9.2.3. Aromatic hydrocarbons

In the spectrum of aromatic hydrocarbons, the signal of the molecular ion **$[M]^+$** is more intense (**Rule (4)**) because aromatic structures, being stable, are less susceptible to fragmentation during EI ionization. Alkyl-substituted derivatives of benzene show a signal of significant intensity at **m/z** 91 due to the benzyl ion or the tropylium ion **$[C_7H_7]^+$** (**Rule (8)**).

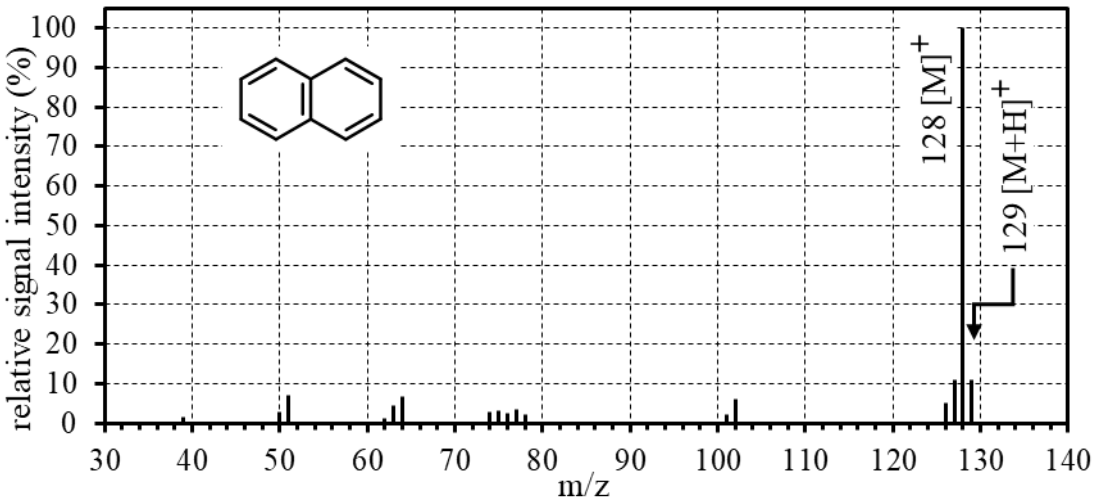



**Fig. 176 Mass spectrum of naphthalene (EI ionisation) (reconstructed from MoNa database)**

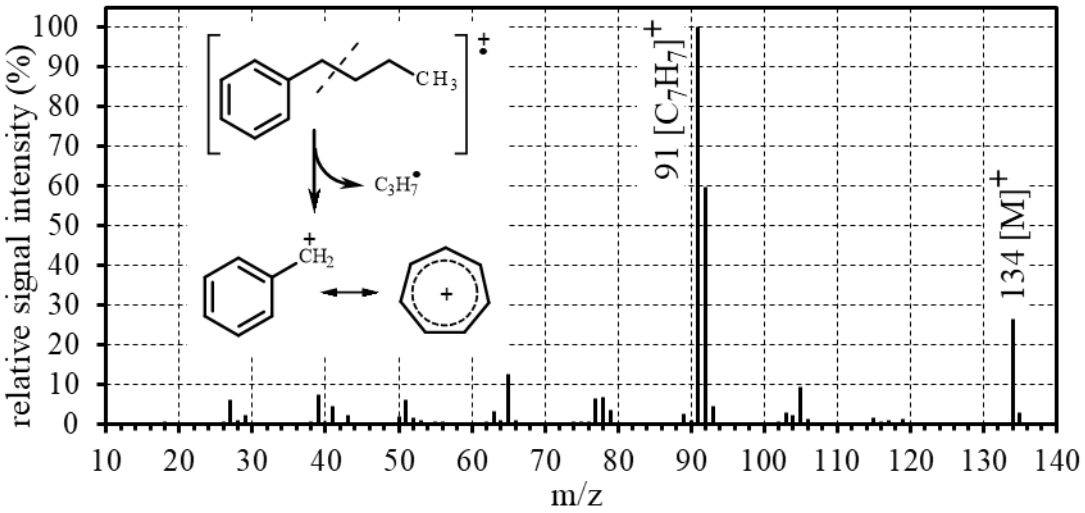



**Fig 177 Mass spectrum of n-butylbenzene (EI ionisation) (reconstructed from MoNa database)**

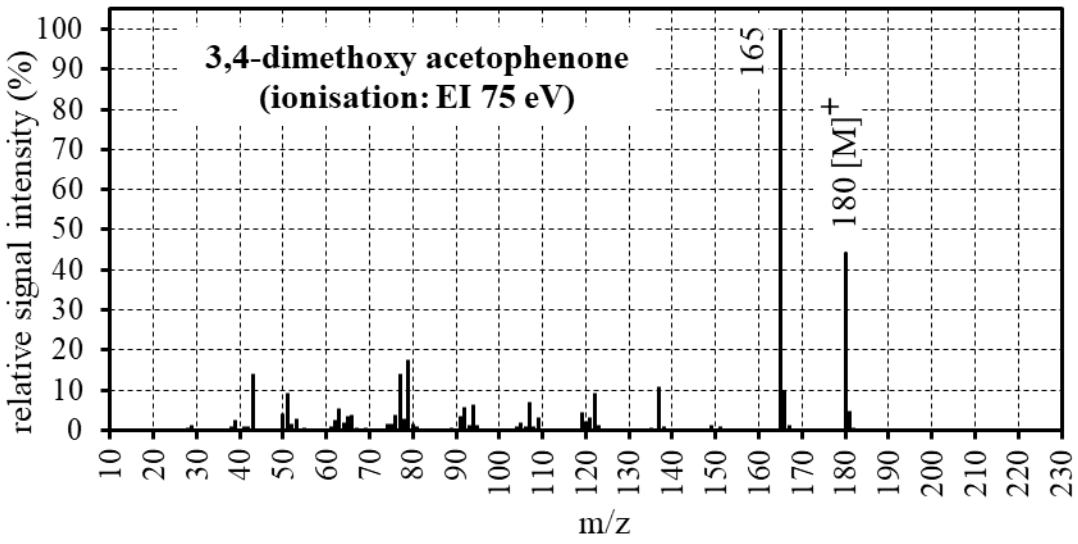



**Fig. 178 Mass spectrum of 3,4-dimethoxy-acetophenone obtained with EI ionization**

Figure 176 shows the mass spectrum of naphthalene obtained by electron impact ionization (electron flow energy: 75 eV, sample temperature 180 $^{o}$C, ionization source temperature: 260 $^{o}$C). Even under the drastic conditions of electron impact ionization, only the signal corresponding to the molecular ion is dominant and the smaller ion fragments appear only as signals of low intensity. In the case of n-butylbenzene, the $\mathbf{[C_7H_7]^+}$ ion signal (benzyl ion or tropylium ion) dominates the molecular ion signal (Figure 177). The extended fragmentation capability of electron flow ionization is illustrated by the mass spectrum of 3,4-dimethoxy-acetophenone. With electron flow ionization, the molecular ion (**m/z** 180, $\mathbf{[M]^+}$) is visible, but there are also signals that can be attributed to smaller fragments (Figure 178). In chemical ionization (CI) with reactive methane gas, only the molecular ion appears in the mass spectrum with dominant intensity. The $\mathbf{[M+C_2H_5]^+}$ and $\mathbf{[M+C_3H_5]^+}$ ions appear with much reduced intensity and the small fragment ions are virtually absent (Figure 179).

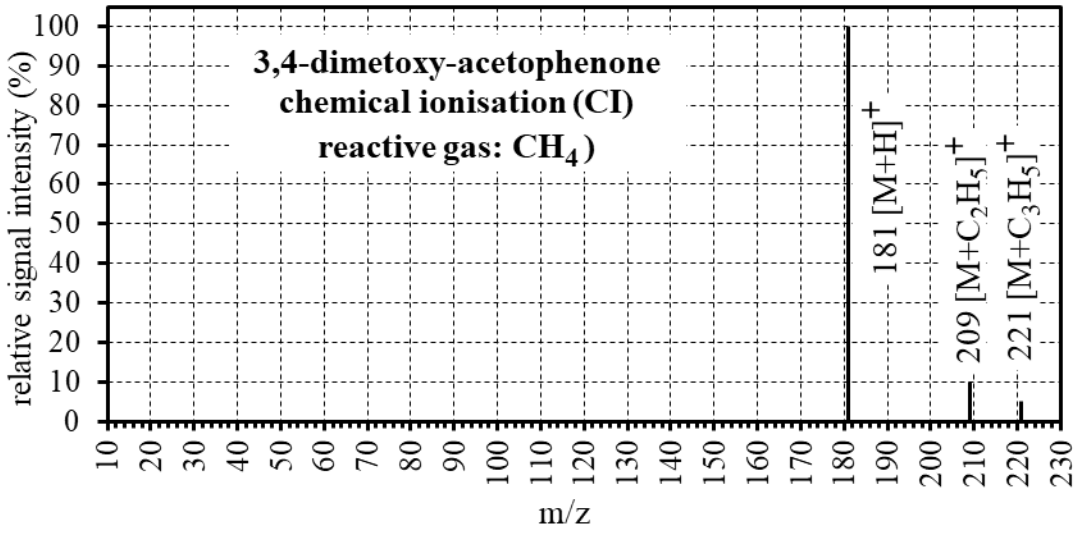



**Fig. 179 Mass spectrum of 3,4-dimethoxy-acetophenone obtained by chemical ionization**

### 4.9.2.4. Alcohols

Alcohols are sensitive to fragmentation. The molecular ion signal is weak for primary and secondary alcohols and often absent for tertiary alcohols. It is therefore preferable to derivatize the original sample (e.g. silanization) or use chemical impact ionization (CI) to determine the molecular mass of tertiary alcohols. The σ(C-C) bond near the hydroxyl group is the most easily cleaved. For this reason, a prominent signal at **m/z** 31 (the **$[CH_2\text{-}OH]^+$** ion, Figure 180) is often seen in the mass spectra of primary alcohols.

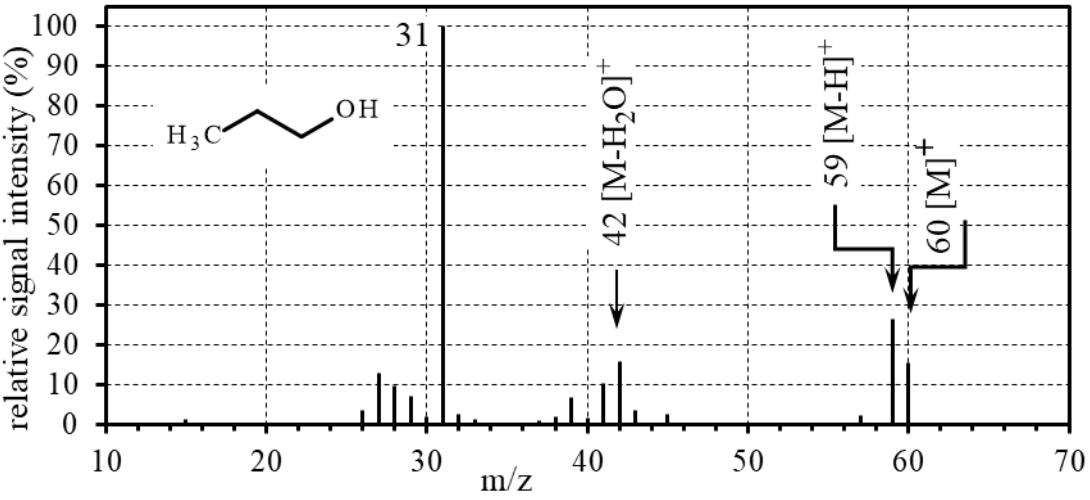



**Fig. 180 Mass spectrum of 1-propanol (EI, 70 eV, sample temperature: 250 $^oC$, ionization source temperature: 250 $^oC$) (reconstructed from SDBS database data, http://sdbs.db.aist.go.jp/sdbs/cgi-bin/direct_frame_top.cgi)**

The preferential cleavage of the σ(C-C) bond near the hydroxyl group is also observed for secondary alcohols. This is why the mass spectrum of 2-butanol shows

signals with **m/z** ratios of 45 (dominant signal) and 59 (relatively high intensity) (Figure 181). In agreement with the above, the signal of the molecular ion is also very weak in this case (practically invisible, with a relative intensity of 0.6 %). The signal of **m/z** 31, which is dominant in the spectrum of 1-propanol (primary alcohol), appears with much reduced relative intensity in the spectrum of 2-butanol (secondary alcohol). The decrease in intensity of the **m/z** 31 signal is also observed in the spectrum of 3-octanol (secondary alcohol) (Figure 125), while the molecular ion signal does not appear at all. In the fragmentation of the higher secondary alcohols the prominent **[CHR-OH]**$^+$ ion signal is generally observed.

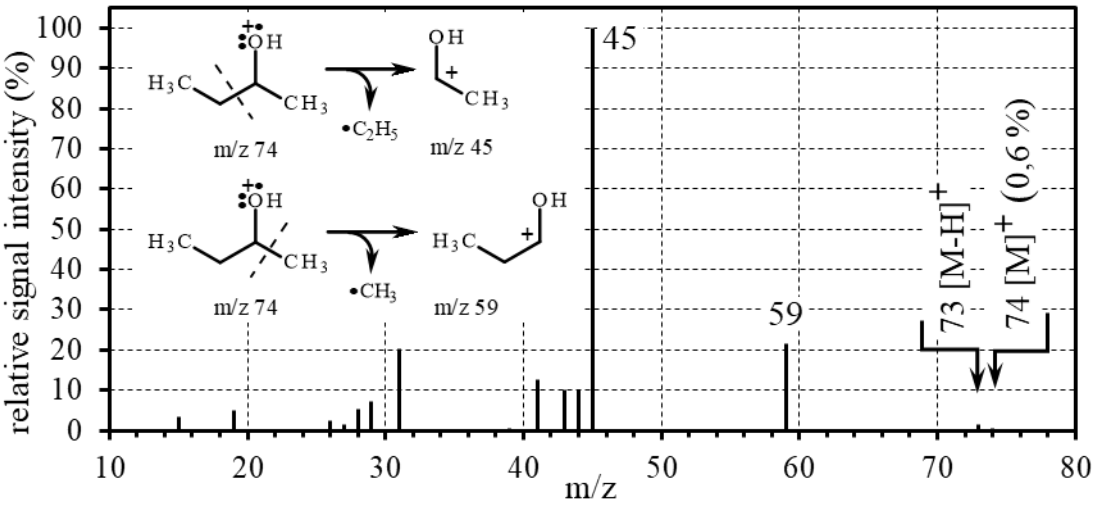



**Fig. 181 Molecular ion fragmentation of 2-butanol (spectrum reconstructed from MoNa database)**

In primary and secondary alcohol, the hydrogen atom bonded to the carbon atom attached to the hydroxyl group is sometimes even more easily cleaved than the alkyl group. The result is the signal of the **[M–H]**$^+$ ion (also seen in the spectra of Figures 180 and 181). Tertiary alcohols, like secondary alcohols, cleave to ionic fragments of the form **[CRR'-OH]**$^+$. Figure 182 is an example.

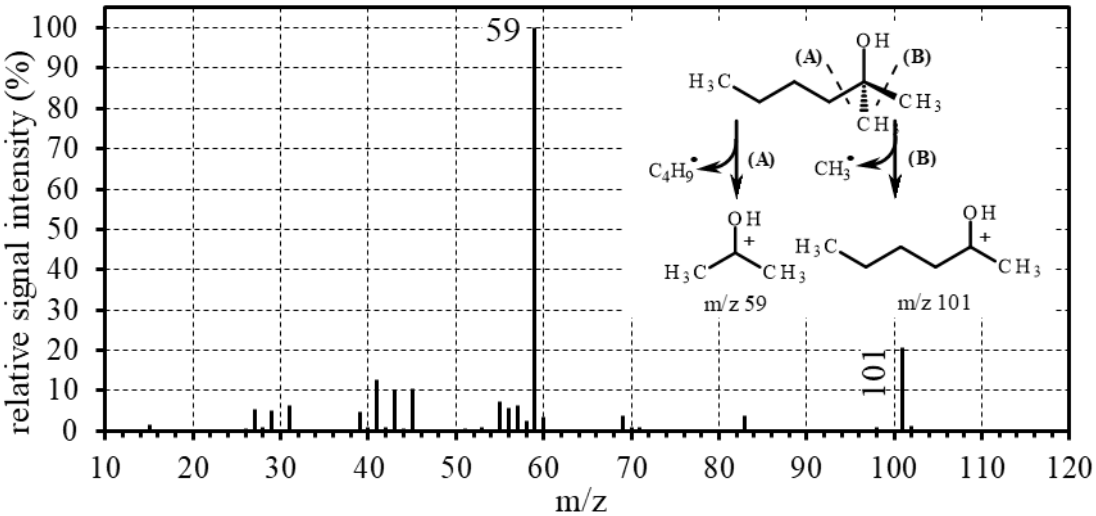



**Fig. 182 Mass spectrum of 2-methyl-2-hexanol (NIST Collection No. 231744)**

The ions with **m/z** ratios of 59 and 101 are the result of fragmentation at the bond between the carbon atoms at positions "α" and "β" to the hydroxyl group. Figure 182 shows the mass spectrum of 2-methyl-2-hexanol obtained by electron ionization (EI). As noted for secondary and especially tertiary alcohols, the molecular ion (**m/z** 116) is completely absent from the spectrum.

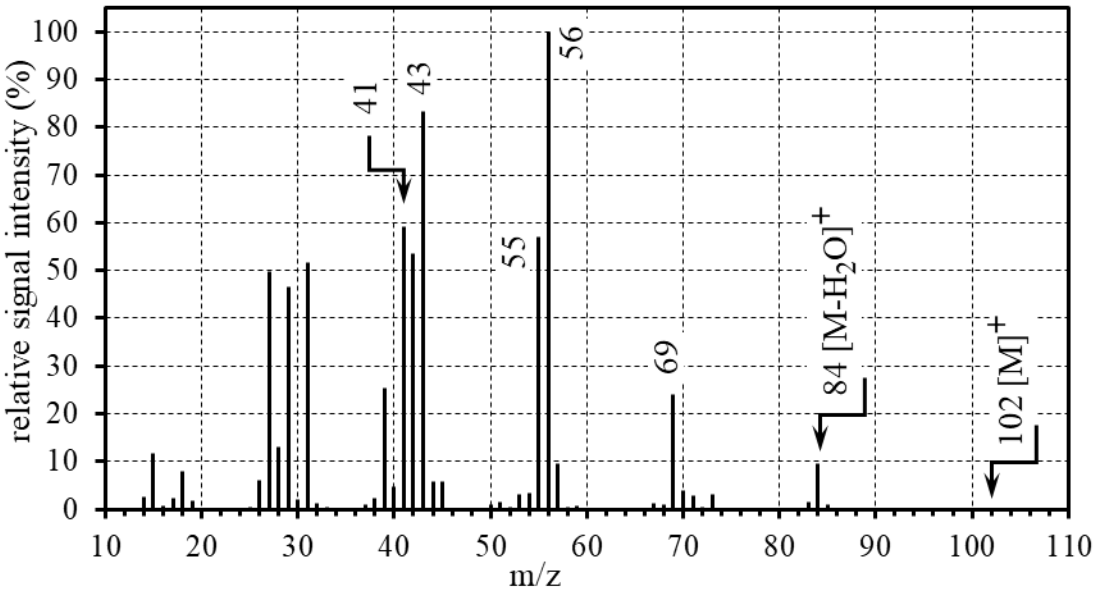



**Fig. 183 Mass spectrum (EI ionization) of 1-hexanol (reconstructed from NIST collection, spectral ref. 19937)**

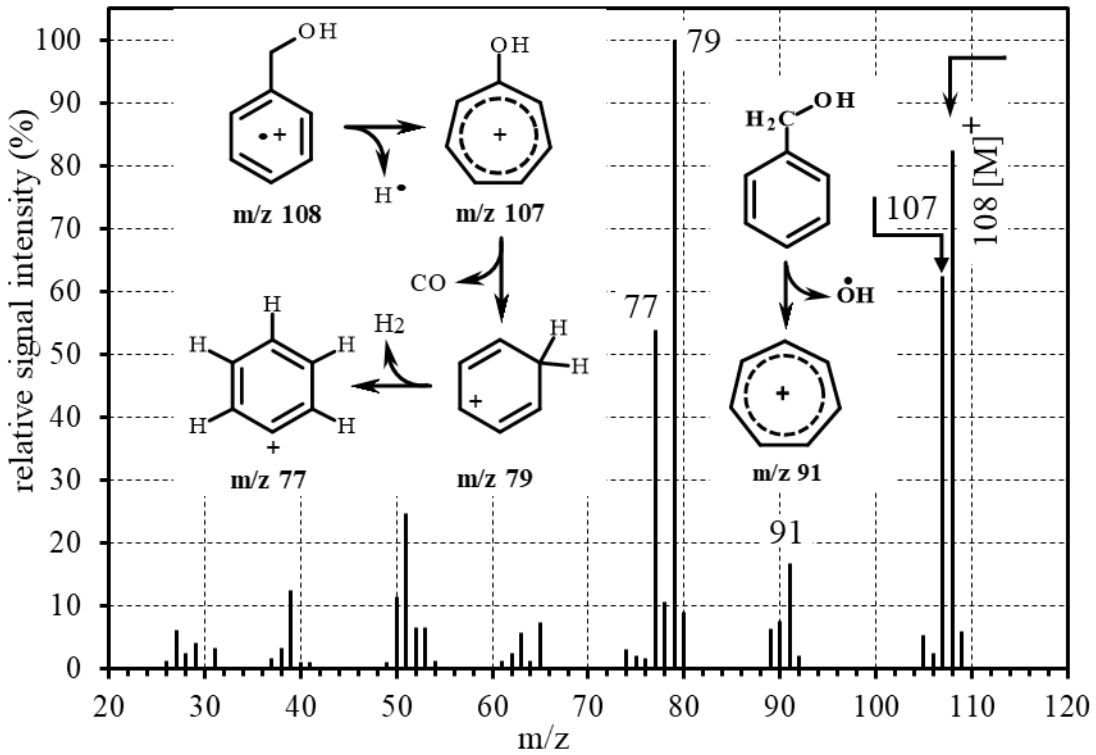



**Fig 184 Molecular radical ion fragmentation of benzyl alcohol (EI ionization, 75 eV (reconstructed from SDBS collection data)**

In some cases, particularly in primary alcohols, the radical molecular ion can lose a water molecule, and the result is manifested by the presence in the spectrum of the $[M-H_2O]^+$ signal at an **m/z** ratio 18 Da lower than the **m/z** ratio of the molecular ion. An example is the behavior of the radical molecular ion of 1-hexanol (Figure 183) and 1-propanol (Figure 180). In the first case the resulting signal is found at **m/z** 84 (102 – 18 = 84) and in the second case at **m/z** 42 (60 – 18 = 42).

Benzyl alcohol derivatives differ significantly from aliphatic alcohols in their fragmentation pathway. Fragmentation of benzyl alcohol proceeds according to **Rule (8)**, yielding ions with **m/z** ratios of 107, 79, and 77. In contrast to aliphatic alcohols, the signal of the molecular ion in the spectrum of benzyl alcohol derivatives is intense; in benzyl alcohol it is just after the dominant signal in terms of intensity (Figure 184).

The 2-methyl derivative of benzyl alcohol fragments in a different way from benzyl alcohol (Figure 185), but again the signal from the molecular ion is strong. Some derivatives of benzyl alcohol can remove a water molecule; the dominant signal in Figure 185 corresponds to the fragment resulting from such removal. (122 – 18 = 104).

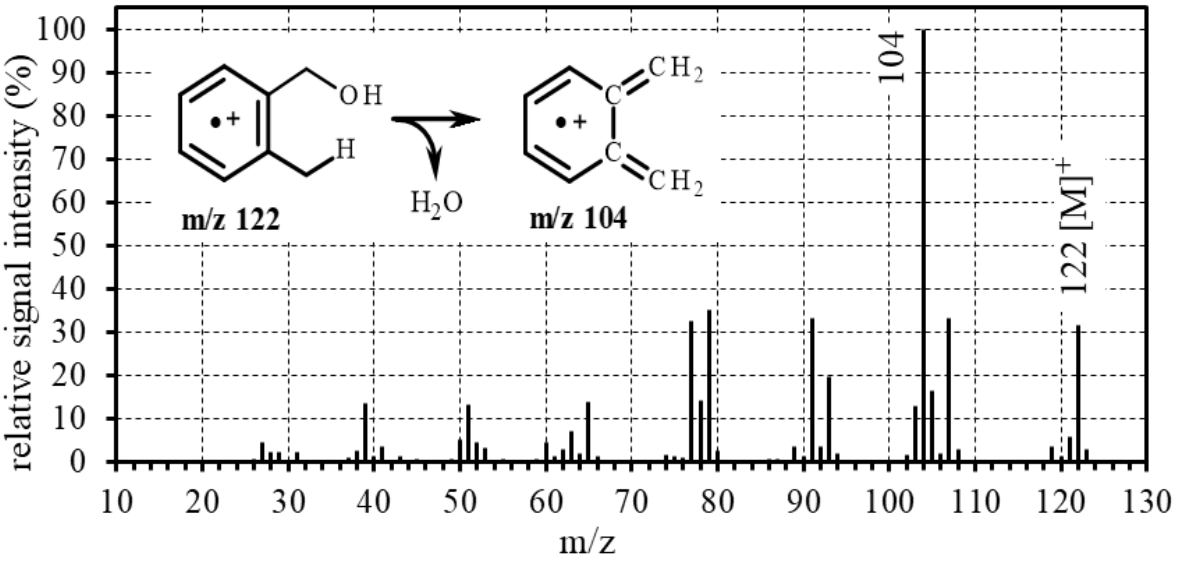



**Fig. 185 Molecular radical ion fragmentation of 2-methylbenzyl alcohol (EI ionization, 70 eV, reconstructed from data in NIST database)**

### 4.9.2.5. Phenols

The alkyl derivatives of phenol show, in addition to the molecular ion signal, two characteristic signals: at **m/z** 77 and 107 (Figure 186). The spectrum of phenol contains the molecular ion signal (it is even dominant), but the signals at **m/z** 77 and 107 are missing.

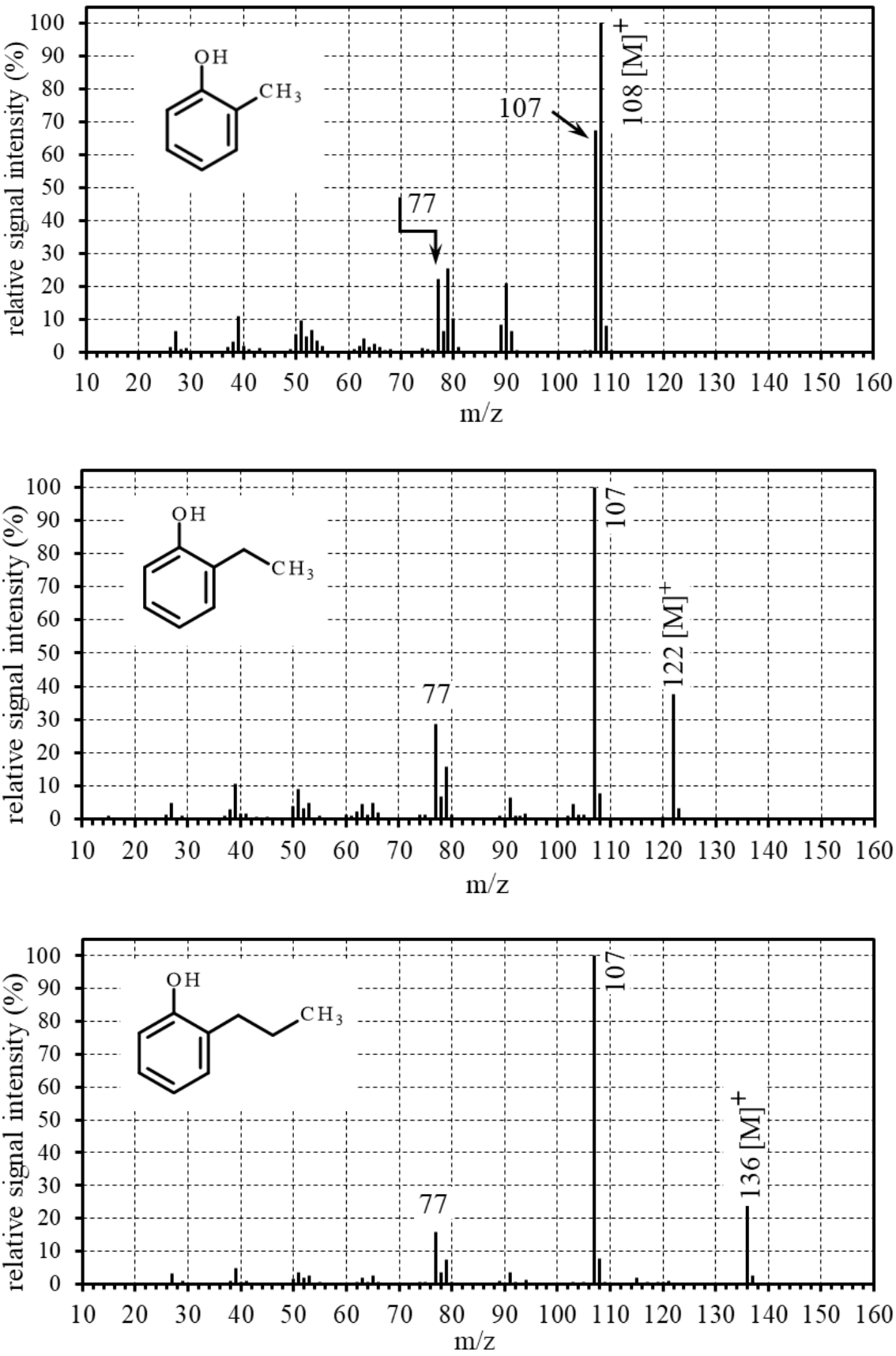



**Fig. 186 Mass spectra of 1-methyl-phenol, 1-ethyl-phenol and 1-propyl-phenol (EI ionization, NIST collection, spectra no. 228359 , 118669 , 229732)**

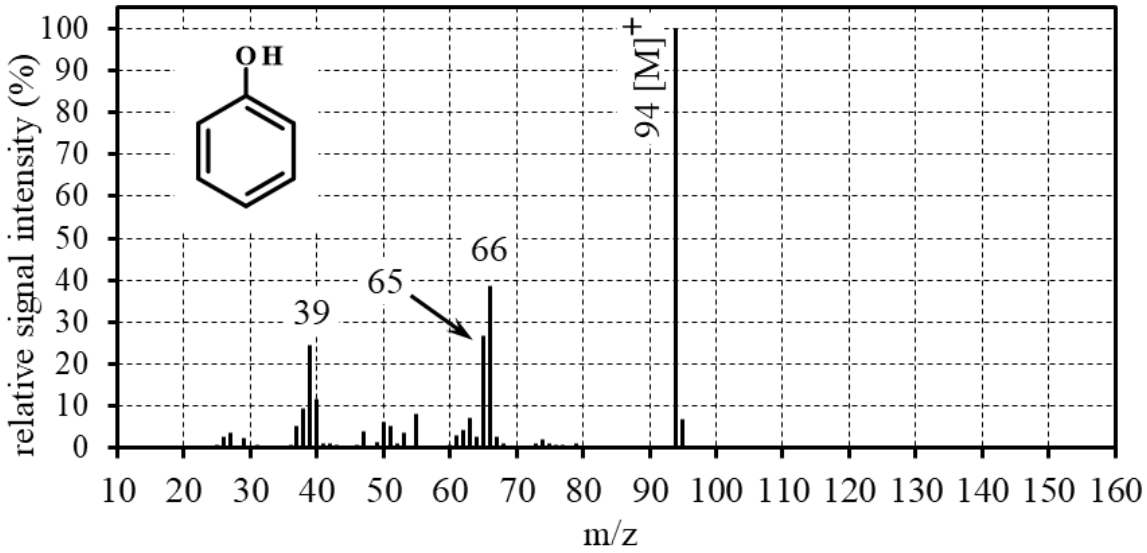



**Fig. 186 (continued) Mass spectrum of phenol (ionization EI – NIST)**

### 4.9.2.6. Ethers

Aliphatic ethers can follow two main fragmentation pathways:

a) cleavage of the σ(C-C) bond adjacent to the C-O bond (similar with alcohols) with positive charge on the oxygen atom fragment (Figure 187),

b) cleavage of the C-O bond with a positive charge on a carbon atom of the oxygen-free fragment (Figure 188).

The molecular ion signal is very weak or undetectable.

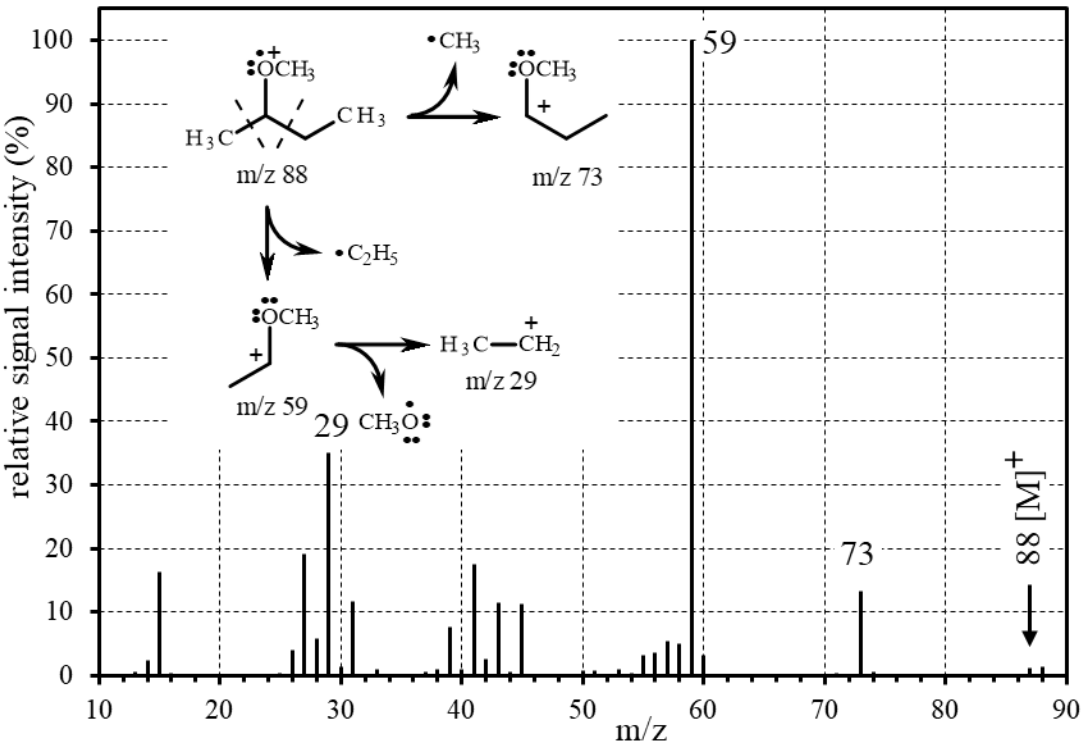



**Fig. 187 Fragmentation of 2-butyl methyl ether (EI ionization, 70 eV, NIST no. 664)**

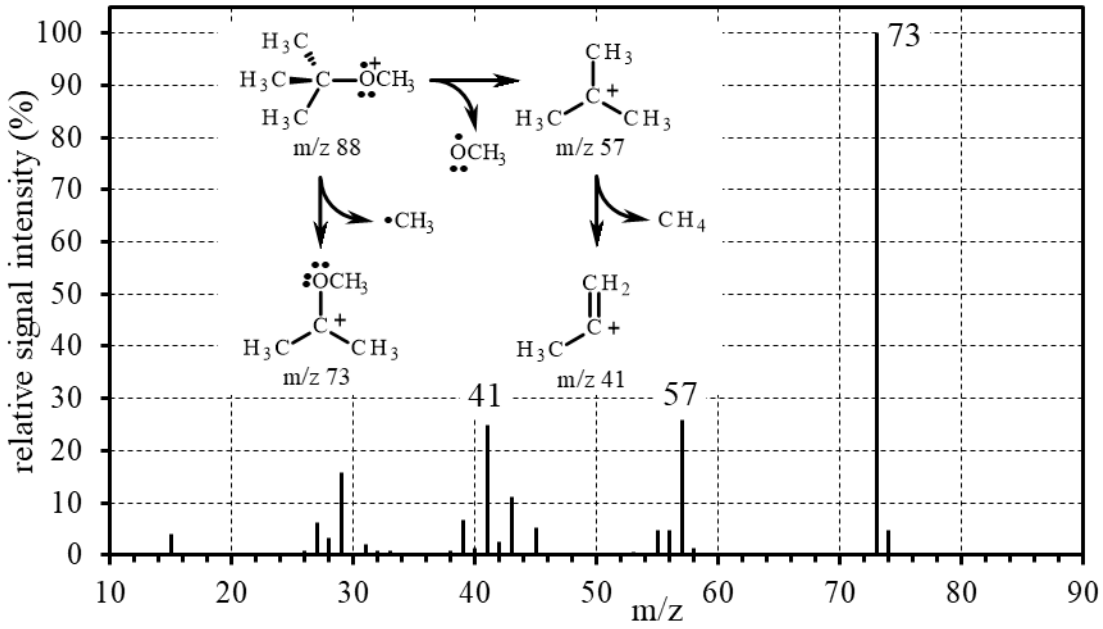



**Fig. 188 Fragmentation of t-butyl methyl ether (EI ionization, 70 eV, NIST no. 229277)**

In aromatic ethers the molecular ion signal is usually strong. The spectrum is like that of the corresponding phenol; in both cases the **m/z** 93 ion signal is characteristic. As an example, the cleavage path of phenyl methyl ether (anisole) is shown in Figure 189 and the mass spectrum obtained by electron flow impact ionization is shown in Figure 190.

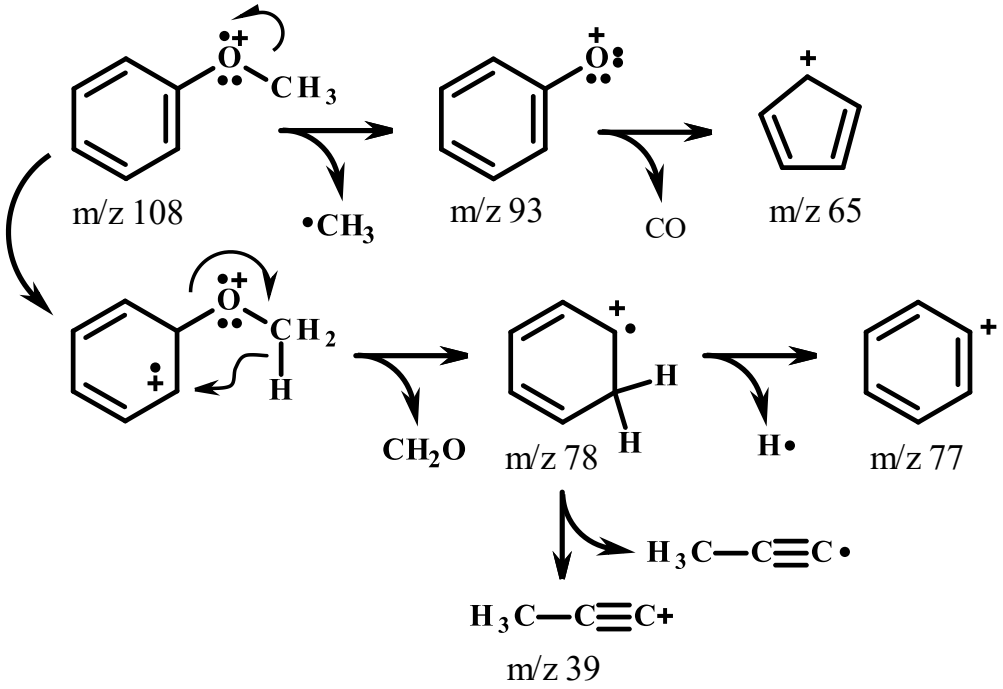



**Fig. 189 Molecular ion fragmentation of phenylmethyl ether by EI ionization**

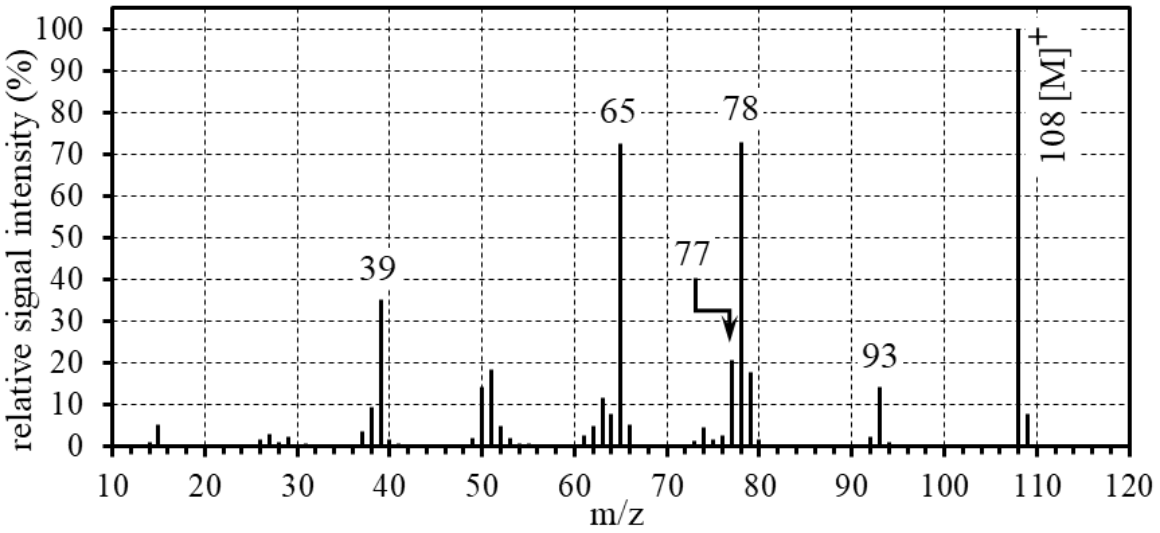



**Fig. 190 Mass spectrum of phenyl methyl ether (EI ionization, 70 eV, MoNa no. 118514)**

### 4.9.2.7. Ketones

In the mass spectra of ketones, the molecular ion signal is generally strong. The main fragmentation pathway involves cleavage of the σ(C–C) bond near the carbonyl group (C=O) to form an acylium ion (**R–C$^{+}$=O**). Another possible fragmentation pathway leads to an alkyl ion and an acylium radical (**R–C$^{\bullet}$=O**). The fragmentation of 3-hexanone (Figure 191) is an instructive example. In the mass spectrum of this compound (Figure 192), recorded by impact ionization with an electron flow energy of 70 eV, the signals of the species shown in Figure 191 are found. Consistent with this, the fragmentation of 2-octanone (Figure 140) also produces an acyl ion (**CH$_3$–C$^{+}$=O**) with the corresponding signal (**m/z** 43) in the mass spectrum (Figure 141).

For sufficiently long chain aliphatic ketones, *McLafferty* fragmentation may occur (shown for the example of 2-octanone in Figure 140).

Fragmentation of aromatic ketones results in a distinct molecular ion signal. The primary cleavage occurs at the σ bond adjacent to the carbonyl group, resulting in the formation of the aromatic ion **Ar–C$^{+}$=O**, which appears in the spectrum with significant intensity and is often the dominant signal. The resulting ion can easily eliminate a carbon oxide molecule and convert into the phenyl ion (**[C$_6$H$_5$]$^{+}$**) with an **m/z** ratio of 77.

An example of the fragmentation path of an aromatic ketone is the 4-chlorophenylbenzophenone. The mass spectrum obtained with EI ionization (electron flow energy 70 eV) is shown in Figure 193. The signals in the mass spectrum can be assigned to the ion fragments shown in Figure 194.

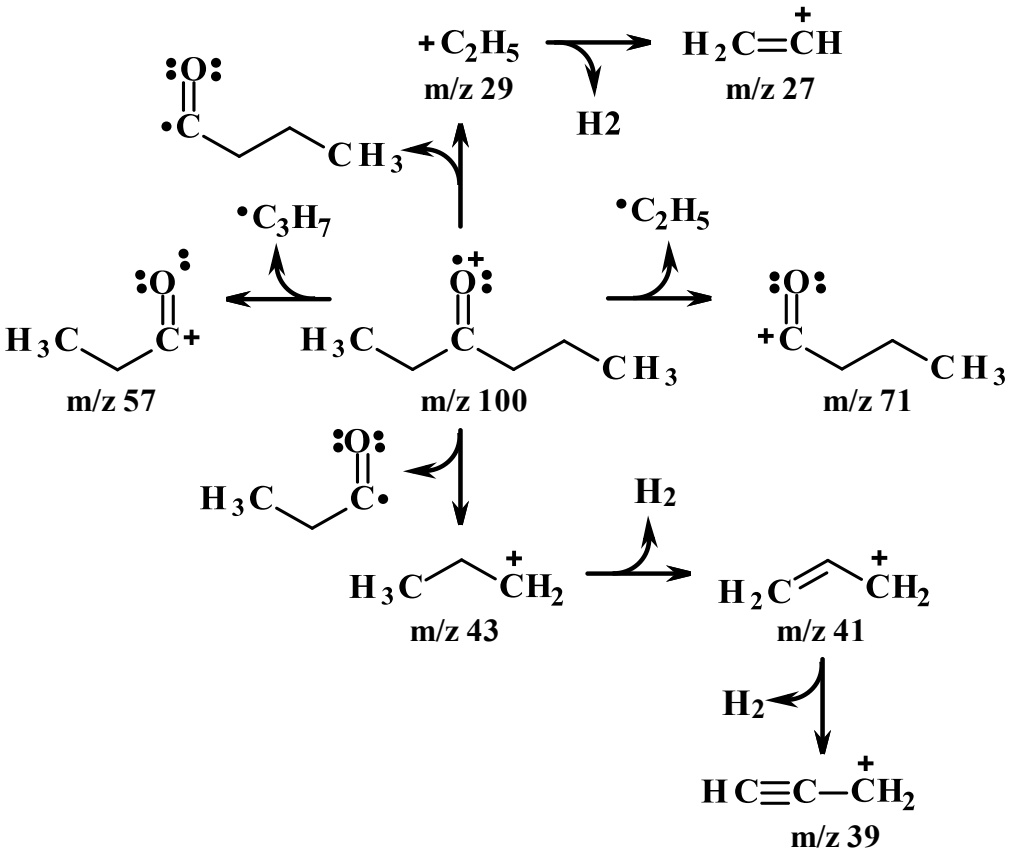



**Fig. 191 Fragmentation path of 3-hexanone (EI ionization, 70 eV)**

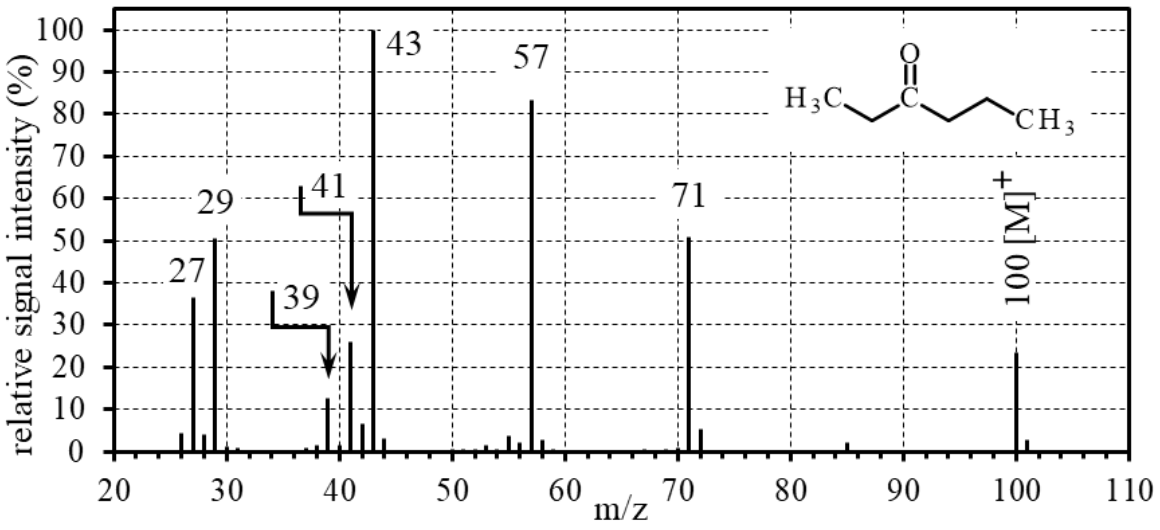



**Fig. 192 Mass spectrum of 3-hexanone using EI ionization, 70 eV (Reconstructed from NIST Data, spectrum no. 61741)**

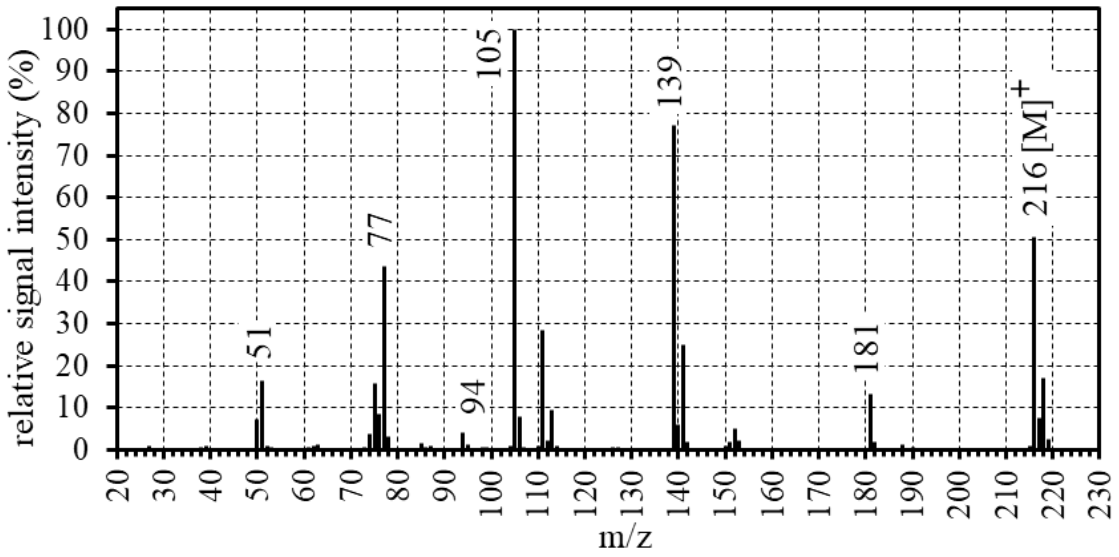



**Fig 193 Mass spectrum of 4-chlorophenyl-benzophenone, EI ionization, 70 eV (reconstructed from NIST data, spectrum no. 229197)**

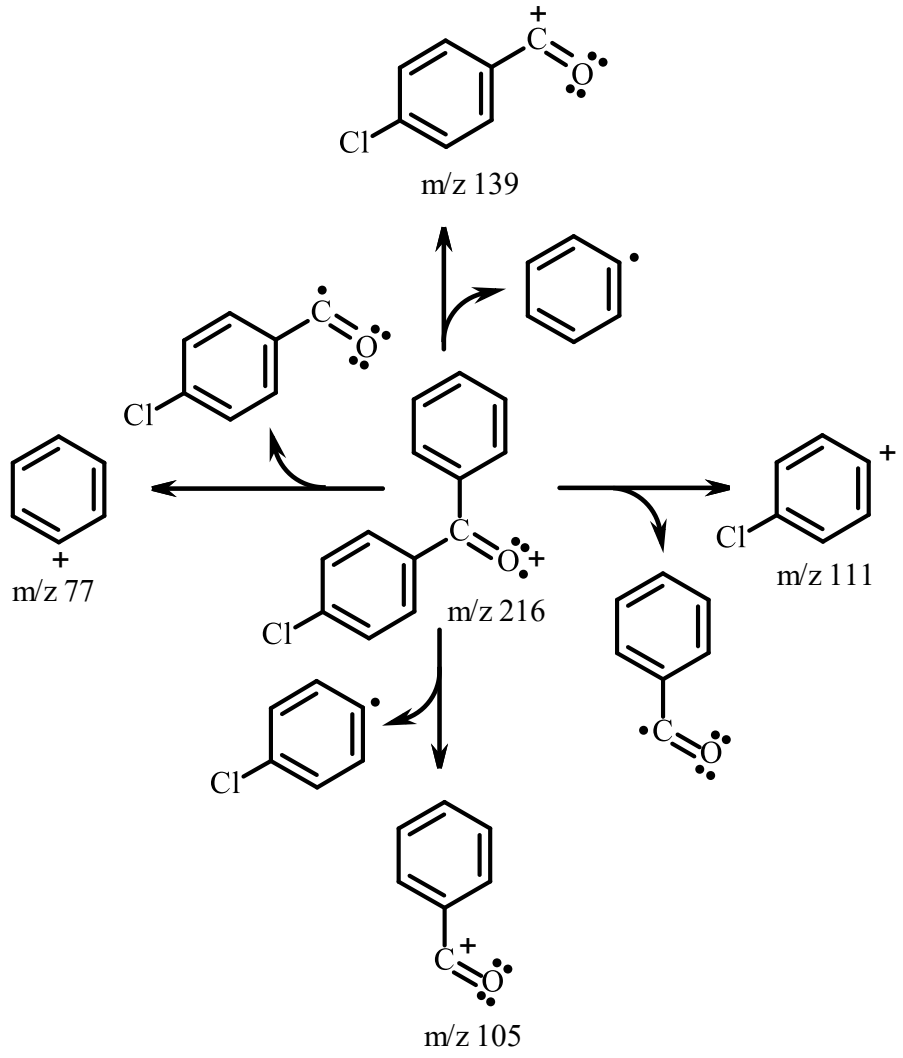



**Fig. 194 Fragmentation of 4-chlorophenyl-benzophenone**

### 4.9.2.8. Aldehydes

In the mass spectrum of aliphatic aldehydes, the signal from the molecular ion is weak but detectable. The main fragmentation pathway targets the σ (C-C) and (C-H) bonds in the vicinity of the carbonyl group - on the one hand - and follows *McLafferty* fragmentation - on the other. As a concrete example, Figure 195 shows the mass spectrum of pentanal (70 eV electron flow ionization) and Figure 196 details some of the fragmentation pathways of this compound.

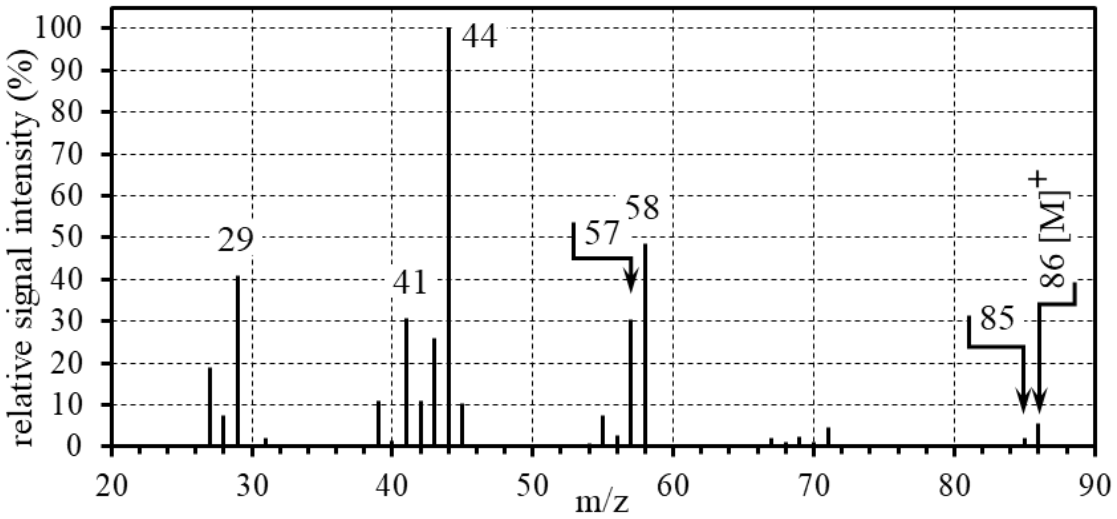



**Fig. 195 Mass spectrum of pentanal, EI ionization (according to NIST, spectrum no. 571)**

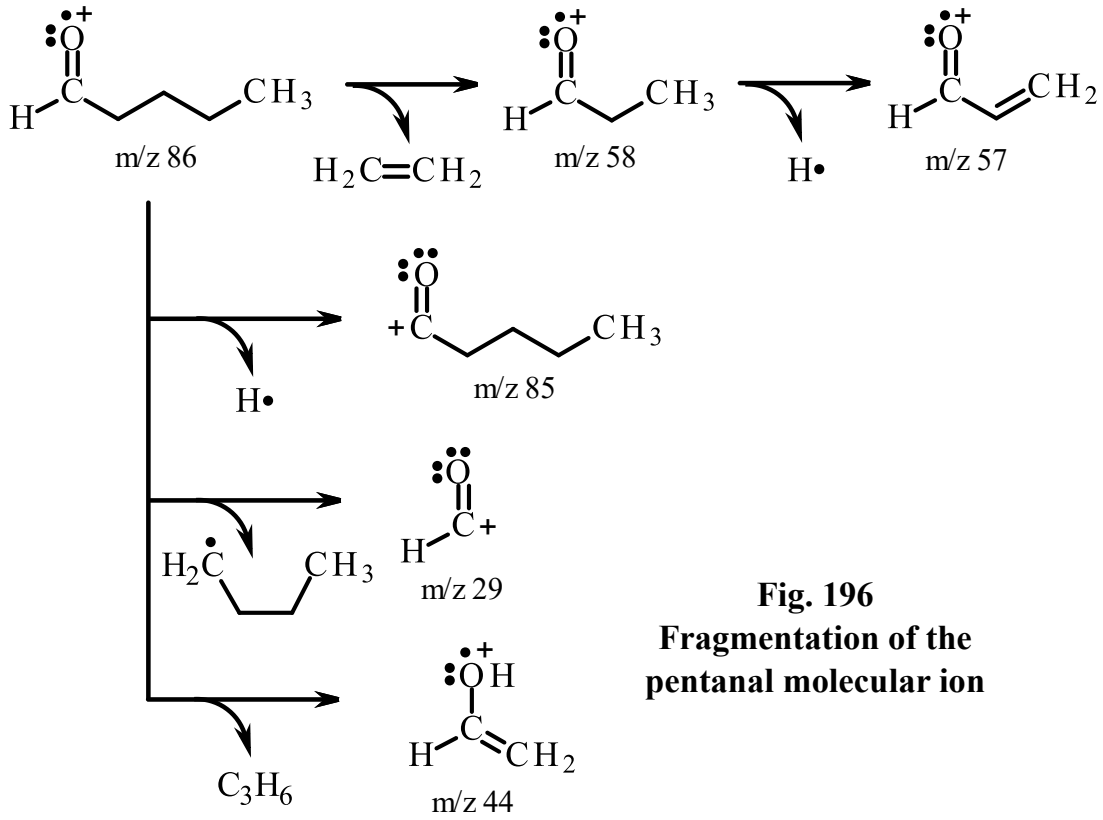



**Fig. 196 Fragmentation of the pentanal molecular ion**

Aromatic aldehydes behave similarly to aromatic ketones. The **[M]**$^+$ molecular ion signal is intense. The **[M-H]**$^+$ ion (acyl ion) also shows a strong signal. With the loss of a neutral carbon monoxide (CO) molecule, the acyl ion is converted to the **[Ar]**$^+$ ion (if the aromatic residue '**Ar**' is phenyl, this signal appears at m/z 77). Benzaldehyde is a simple example to illustrate the fragmentation of aromatic aldehydes. Figure 197 shows the mass spectrum of benzaldehyde with the ionic fragments of Figure 198 as the major signals.

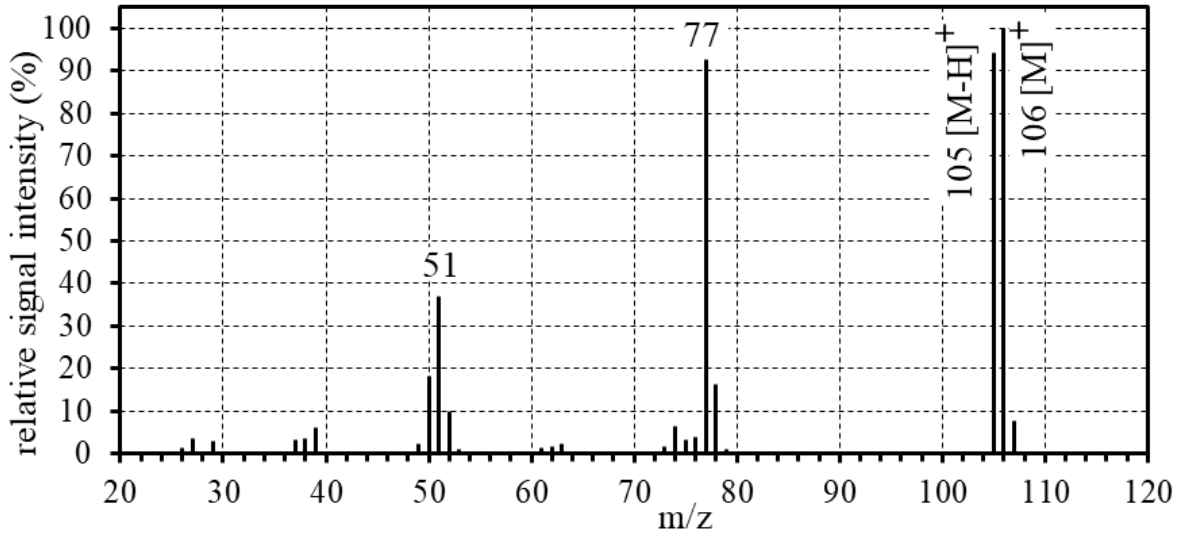



**Fig. 197 Mass spectrum of benzaldehyde, ionization EI 75 eV (reconstructed from SDBS database, spectrum no. 672)**

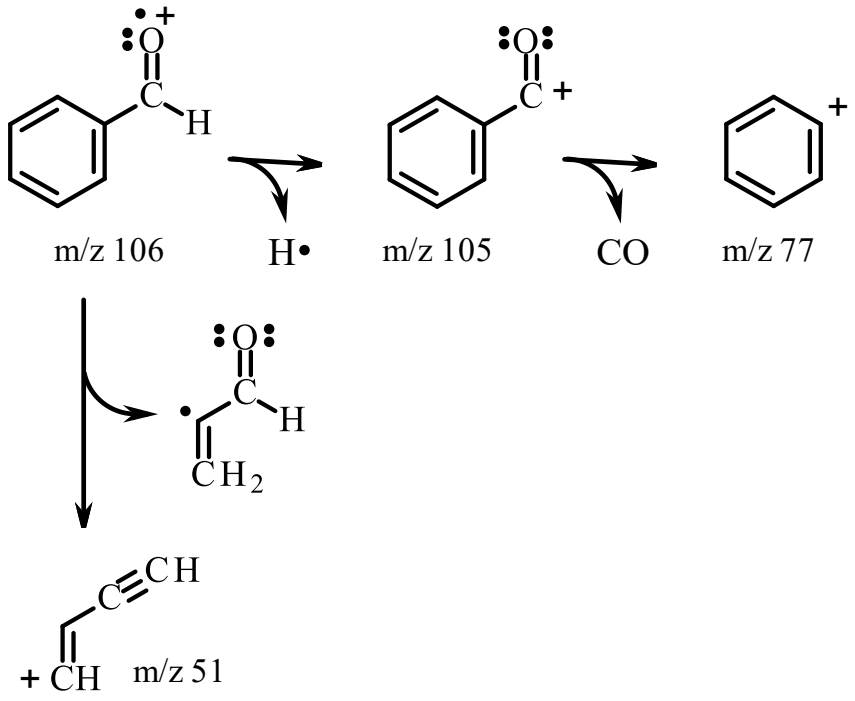



**Fig. 198 The benzaldehyde molecular ion fragmentation**

### 4.9.2.9. Carboxylic acids

The molecular ion signal of aliphatic carboxylic acids is weak, sometimes undetectable. Instead, a strong (often dominant) signal at **m/z** 60 is characteristic, due to the *McLafferty* rearrangement. The C-C bond between the atoms in the '**α–β**' position relative to the carboxyl group cleaves slightly to form **[M-OH]**$^+$ and **[M-COOH]**$^+$ ions.

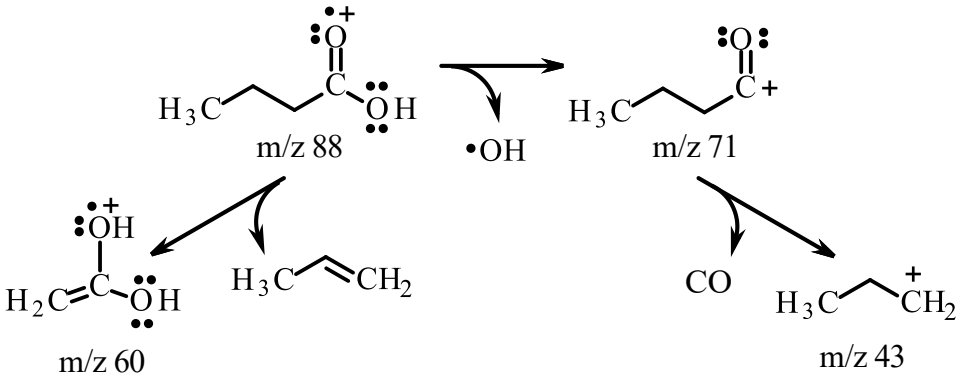



**Fig. 199 Fragmentation of butanoic acid**

As a specific example, Figure 199 shows the fragmentation of butanoic acid and Figure 200 shows the mass spectrum obtained by ionization with a 70 eV electron beam.

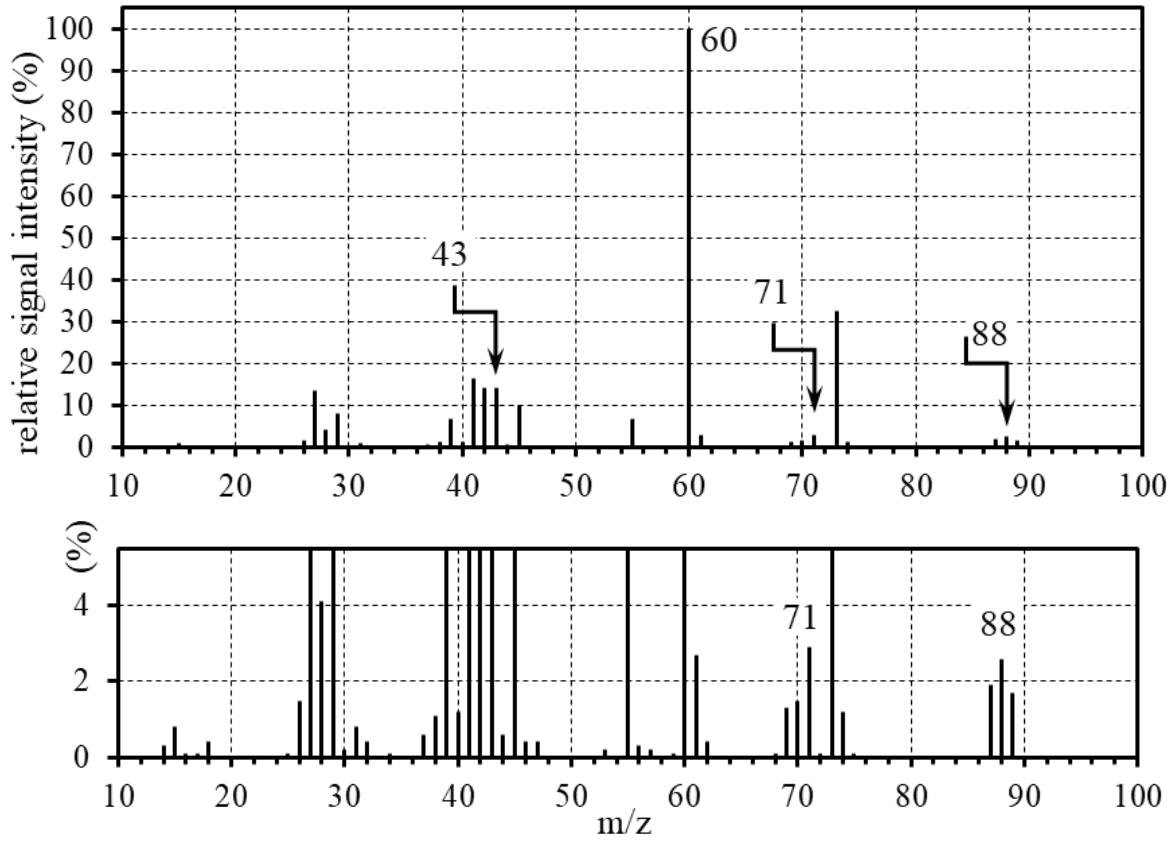



**Fig. 200 Mass spectrum of butanoic acid, EI 70 eV (reconstructed from NIST. no. 228230)**

In aromatic carboxylic acids the molecular ion **[M]**$^+$ appears as an intense signal in the spectrum. Other characteristic signals can be attributed to the ions **[M - OH]**$^+$ (**m/z** 119, because of hydroxyl radical elimination) and **[M - COOH]**$^+$ (**m/z** 91), because of carboxyl radical elimination); see the spectrum of 3-methylbenzoic acid, Figure 201. If the aromatic moiety contains a substituent in the *ortho* position that has a hydrogen atom, the **[M - H$_2$O]**$^+$ ion will appear in the spectrum due to the removal of a water molecule (e.g. 2-methylbenzoic acid, Figure 202).

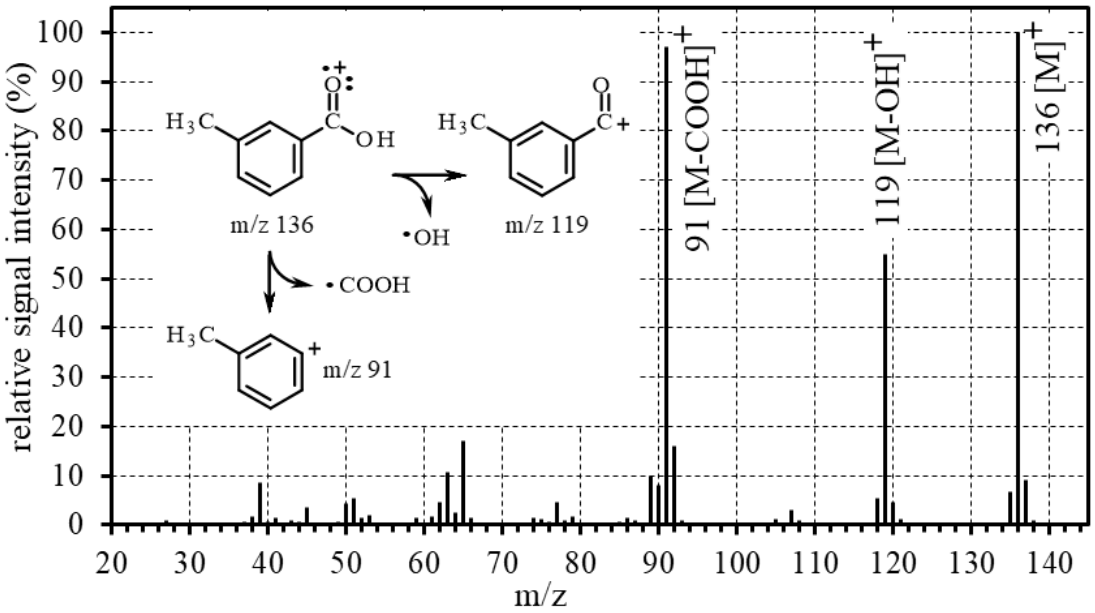



**Fig. 201 Mass spectrum of 3-methylbenzoic acid (reconstructed from the NIST database No. 291073, ionization EI 70 EV).**

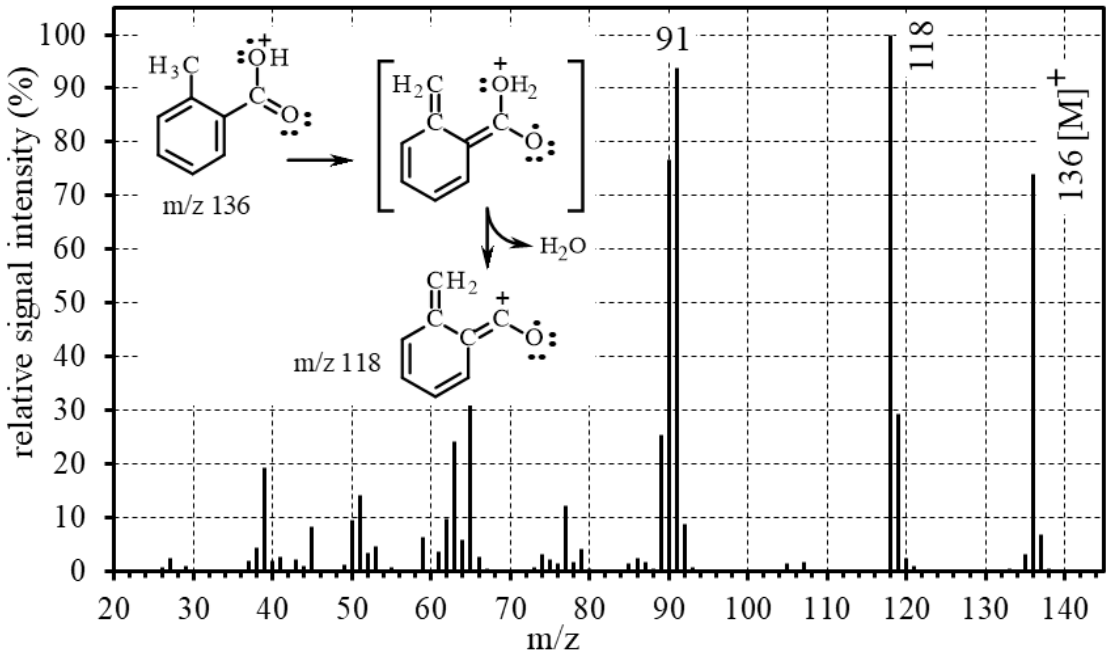



**Fig. 202 Mass spectrum of 2-methylbenzoic acid (reconstructed from the NIST database No. 290981, ionization EI 70 EV).**

### 4.9.2.10. Esters

For aliphatic esters, the molecular ion signal is weak but detectable. If the acid moiety has a relatively long chain, the characteristic intense (often dominant) signal can be attributed to *McLafferty* fragmentation. For example, Figure 203 shows the mass spectrum of ethyl hexanoate obtained by 70 eV electron-flow ionization, and Figure 204 shows some of the fragmentation steps corresponding to the mass spectrum. The dominant signal corresponds to the **m/z** 88 ion formed by the *McLafferty* process.

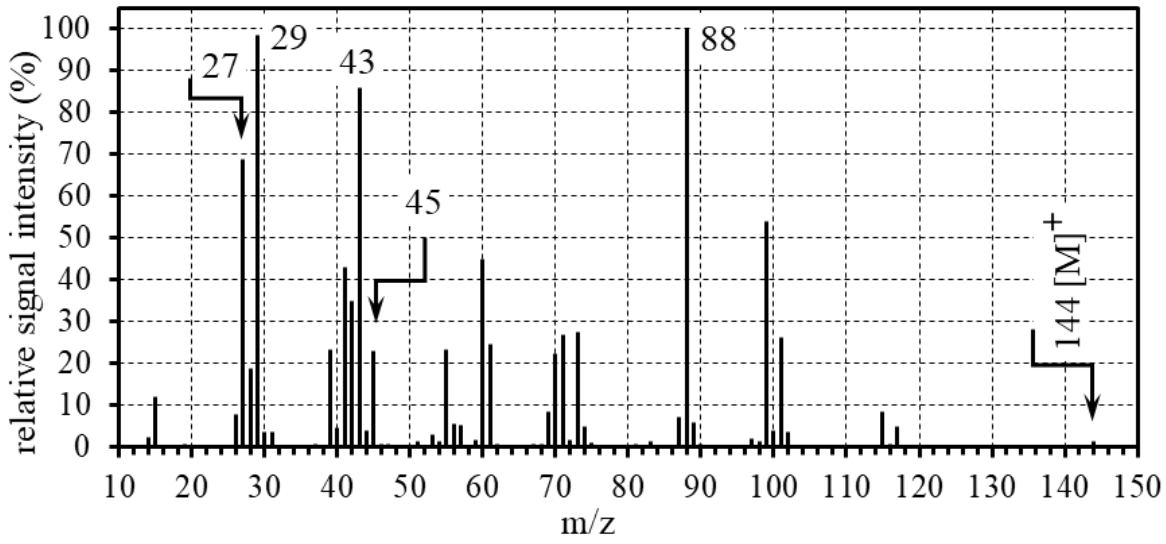



**Fig. 203 Mass spectrum of ethyl hexanoate (reconstructed from NIST, EI ionization, NIST no. 4085)**

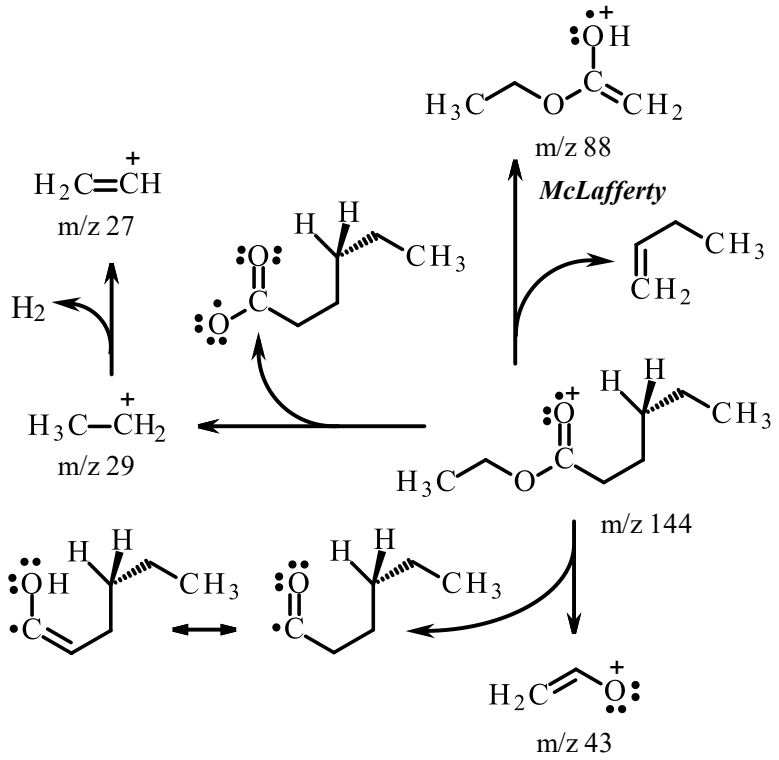



**Fig. 204 Fragmentation of ethyl hexanoate (*McLafferty* fragmentation and other fragmentations suggested by the mass spectrum)**

In the fragmentation of aromatic esters, the molecular ion signal is noticeable and slightly stronger than in the case of aliphatic esters. However, for long chains the molecular ion signal can be very weak, sometimes even absent. The main signal with dominant intensity corresponds to the ion formed by eliminating the alkoxy radical. The fragmentation of benzoyl propionate is an example: the dominant signal (at **m/z** 105) is due to the ion formed because of elimination of the propoxy radical (Figures 205 and 206).

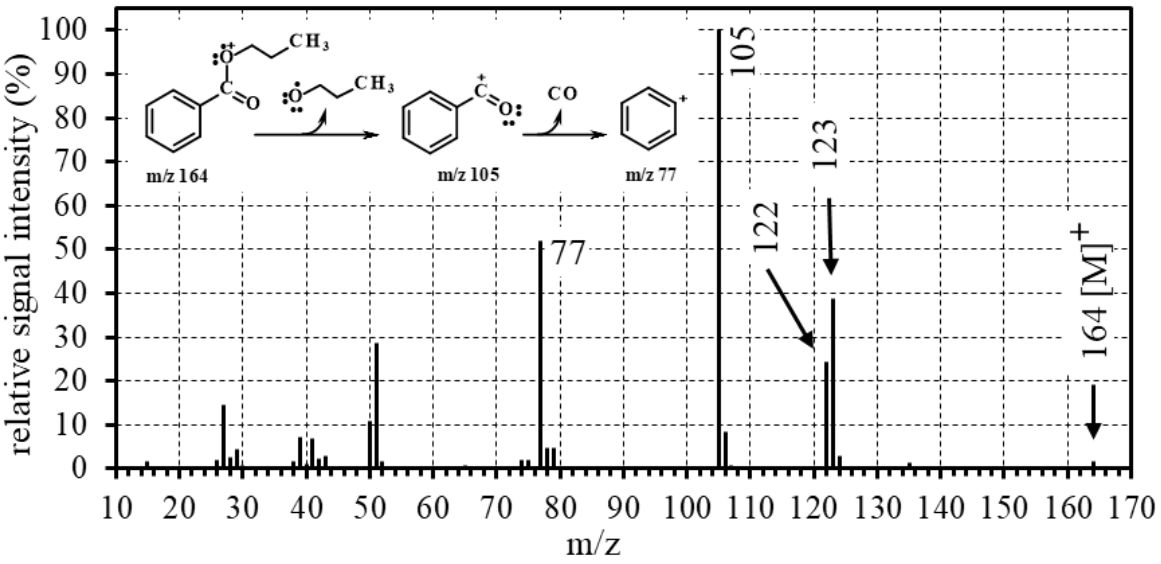



**Fig. 205 Mass spectrum of 1-propyl benzoate (reconstructed from NIST, no. 342339, EI 70 eV ionization)**

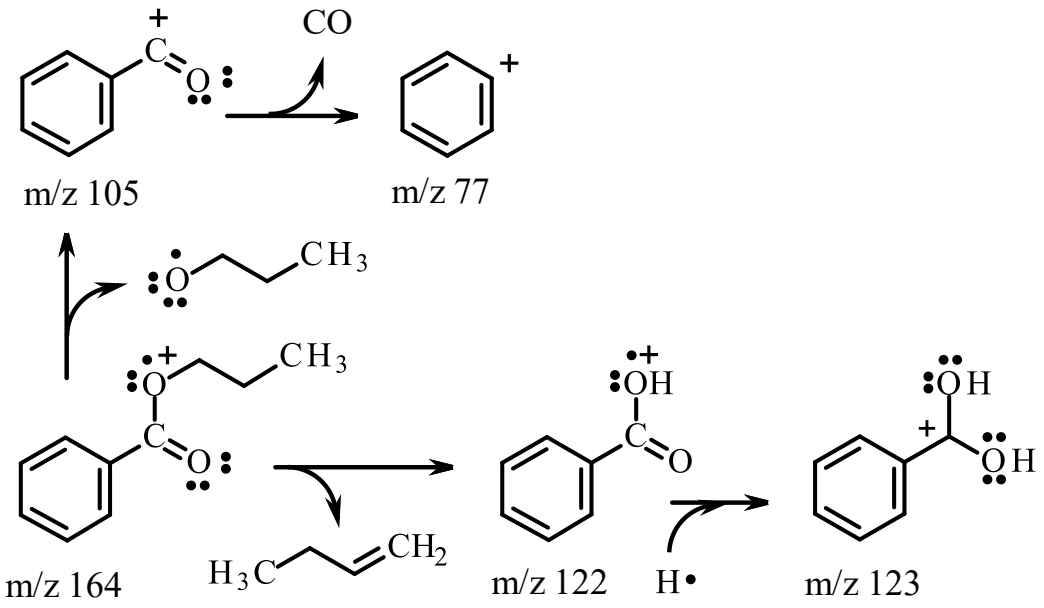



**Fig. 206 Fragmentation pathway of 1-propyl benzoate**

Under certain conditions the fragmentation picture is completed by the capture of a hydrogen atom with the formation of the $[M+H]^+$ ion (in the case of 1-propyl benzoate with the formation of the **m/z** 123 ion, Figures 205 and 206).

### 4.9.2.11. Amines

The molecular ion signal of aliphatic monoamines has a low intensity with an odd **m/z** ratio or is absent. The most important cleavage concerns the C-C bond adjacent to the C-N bond (e.g. fragmentation of 2-amino-butane and 1-amino-hexane, Figure 207 (A) and (B) and Figure 208). The dominant signal in almost all 1-aliphatic primary amines occurs at **m/z** ratio 30 (Figure 207 (B) and Figure 209).

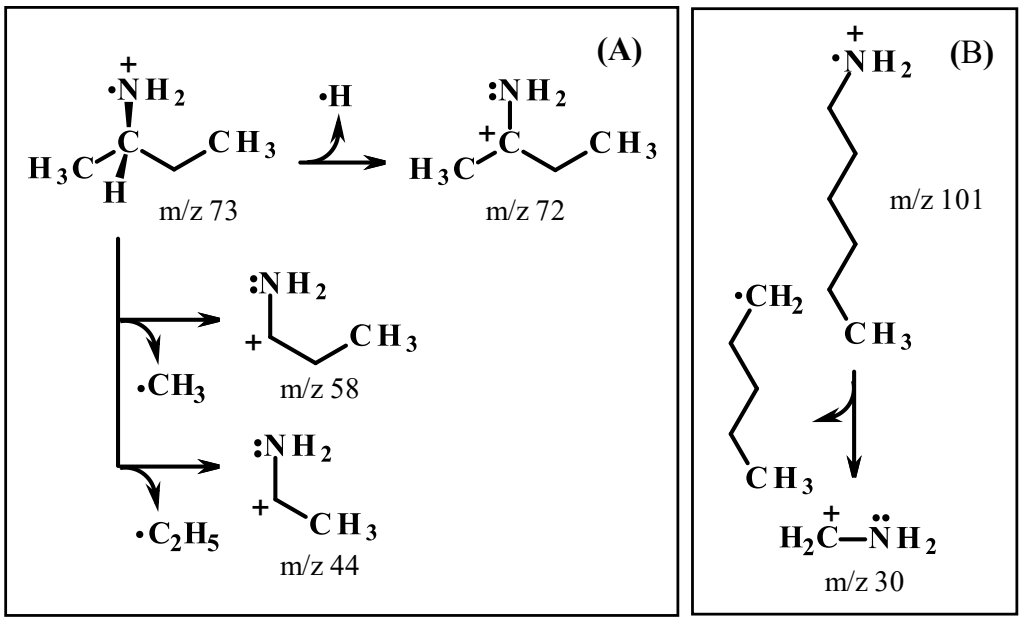



**Fig. 207 Fragmentation of 2-amino-butane (A) and 1-amino-hexane (B)**

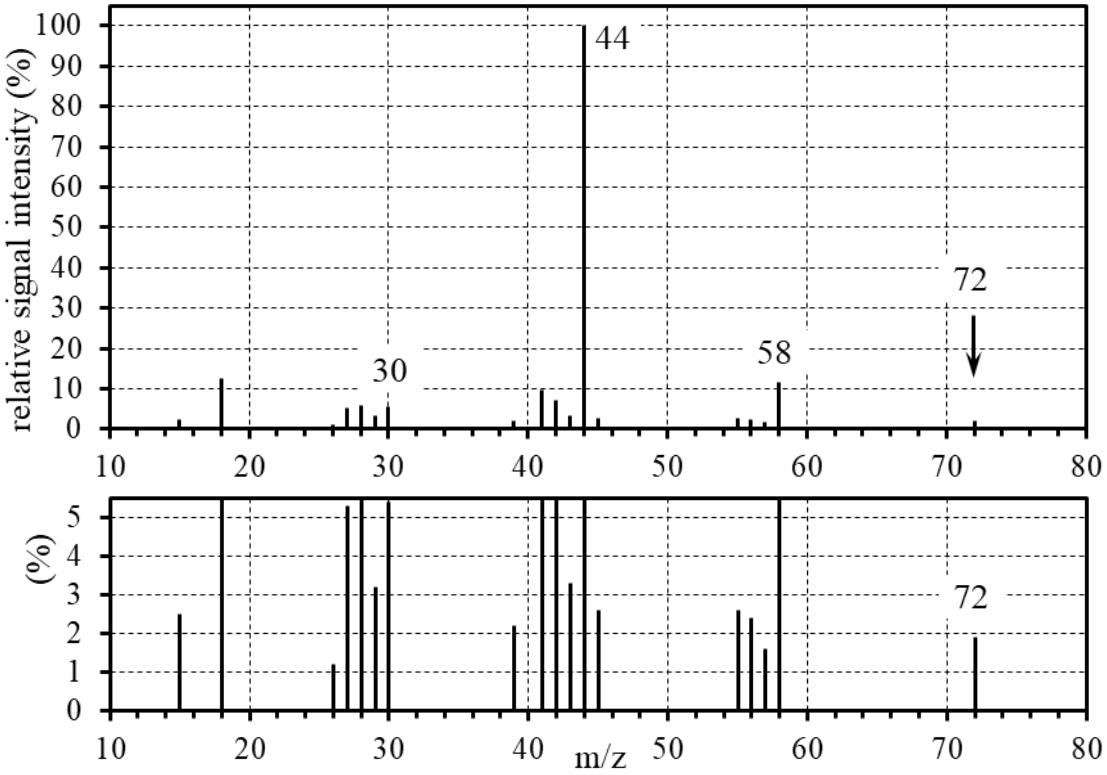



**Fig. 208 Mass spectrum of 2-amino-butane (reconstructed from SDBS, No. 1228, EI 70 eV ionization)**

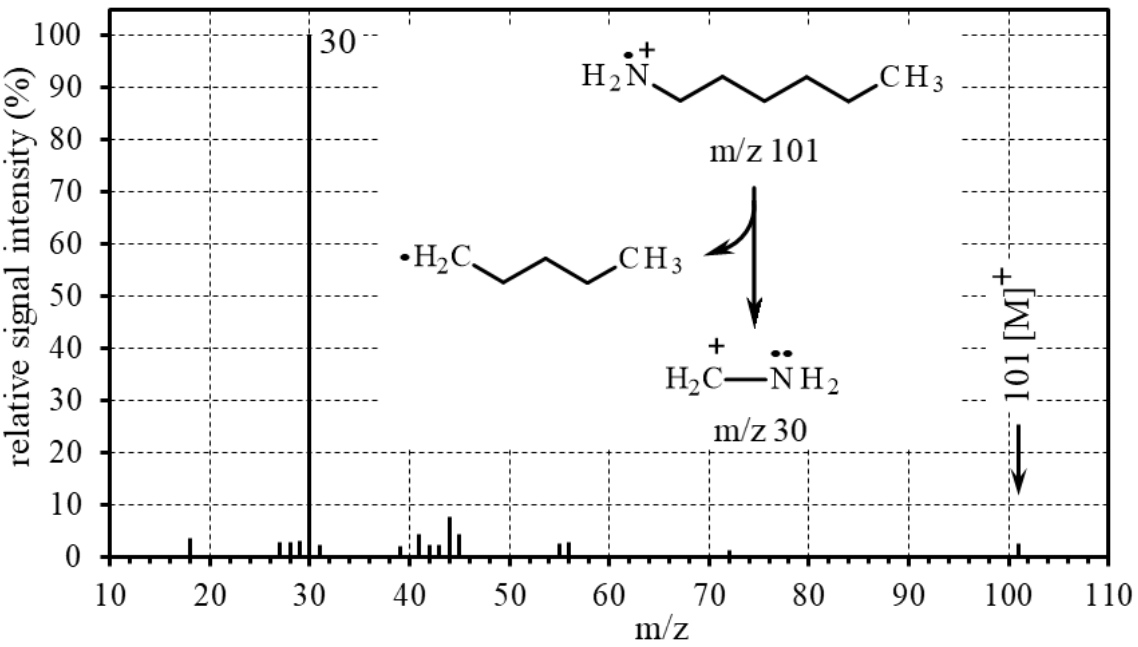



**Fig. 209 Mass spectrum of 1-amino-hexane (reconstructed from SDBS, No. 664, EI 70 eV ionization)**

In the mass spectra of aromatic amines, the molecular ion is represented as an intense, sometimes dominant, signal. In addition to the molecular ion, the **$[M - H]^+$** ion is produced by the homolytic cleavage of one of the N-H bonds, a process illustrated for aniline in Figure 210. Another type of fragmentation in aniline is the removal of the H-C≡N molecule or radicals **$CH_2N•$** or **$C_3H_2N•$**, producing ions with **m/z** ratios of 65 and 66 respectively. The molecular radical ion fragmentation path and mass spectrum of aniline are shown in Figures 210 and 211, respectively.

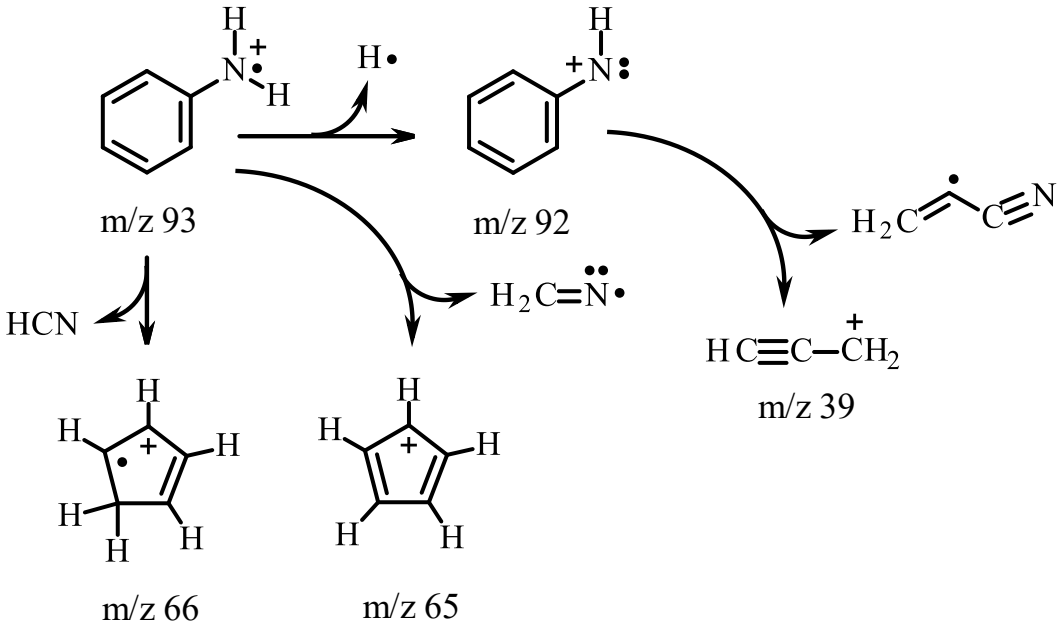



**Fig. 210 Fragmentation of the molecular ion of aniline**

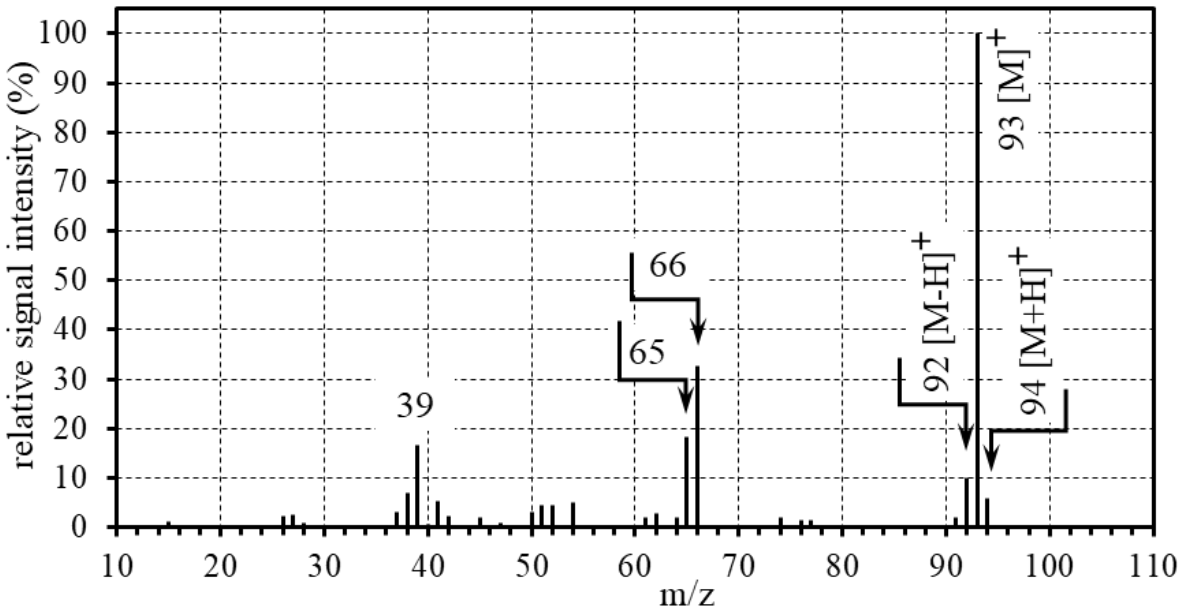



**Fig 211 Mass spectrum of aniline, EI 70 eV (MoNa database no. JP003982)**

A typical process for N-alkyl-substituted aromatic amines is a homolytic cleavage of the C-C bond adjacent to the C-N bond with the formation of an ion that appears as an intense signal. In the case of N-ethyl aniline, the ion formed (Figure 212) is at **m/z** 106 in the mass spectrum (Figure 213).

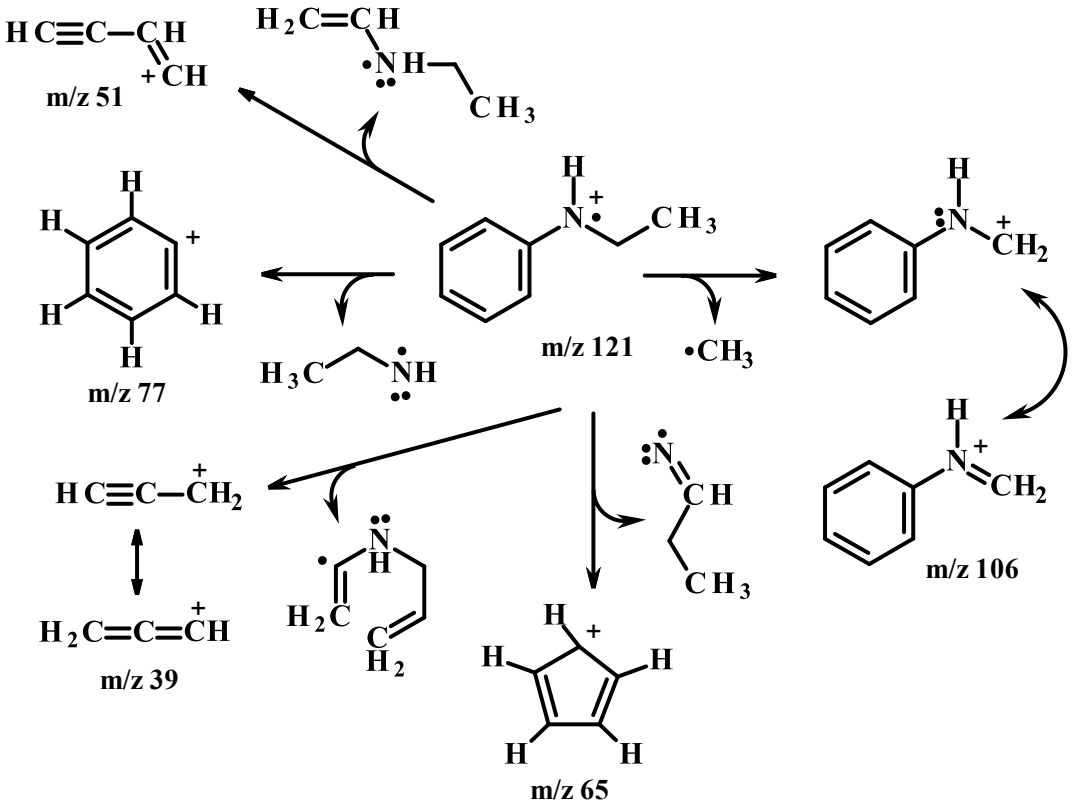



**Fig. 212 Fragmentation path of N-ethyl aniline molecular ion radical**

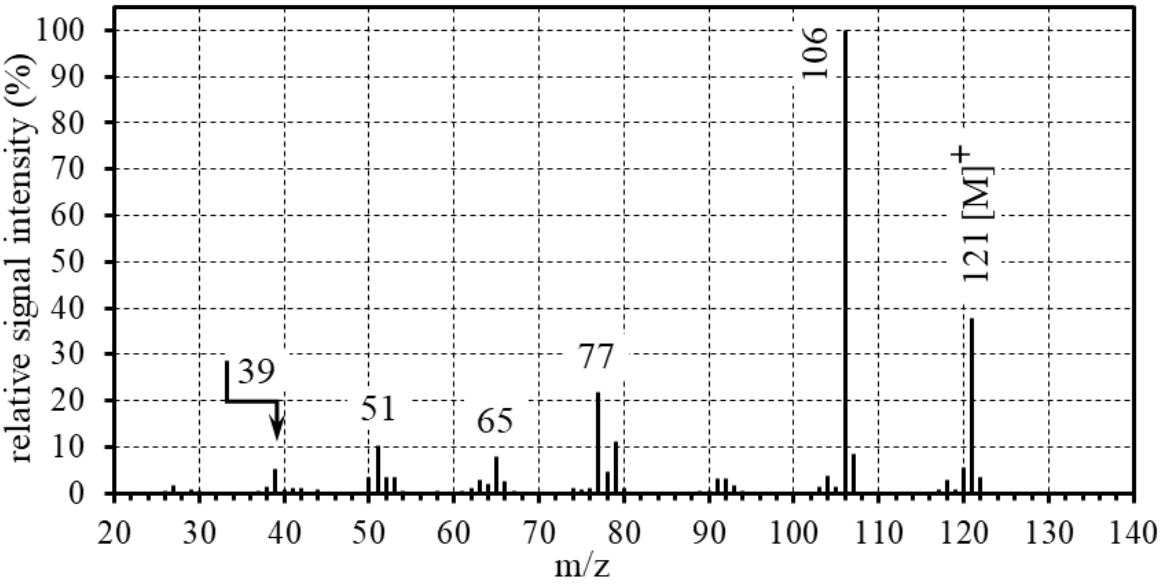



**Fig. 213 Mass spectrum of N-ethyl aniline (reconstructed from NIST, no. 291738, EI 70 eV ionization)**

### 4.9.2.12. Amides

In the fragmentation of primary amides, the formation of the **[O=C$^{+}$–NH$_2$]** ion associated with the intense signal at **m/z** 44 is characteristic, due to the cleavage of the bond between the carbon atom of the C=O group and the carbon atom in the "α" position to this group.

The signal from the molecular ion is very weak but in principle detectable. In aliphatic amides with chains longer than three carbon atoms, the dominant ion at **m/z** 59 is formed by *McLafferty* fragmentation.

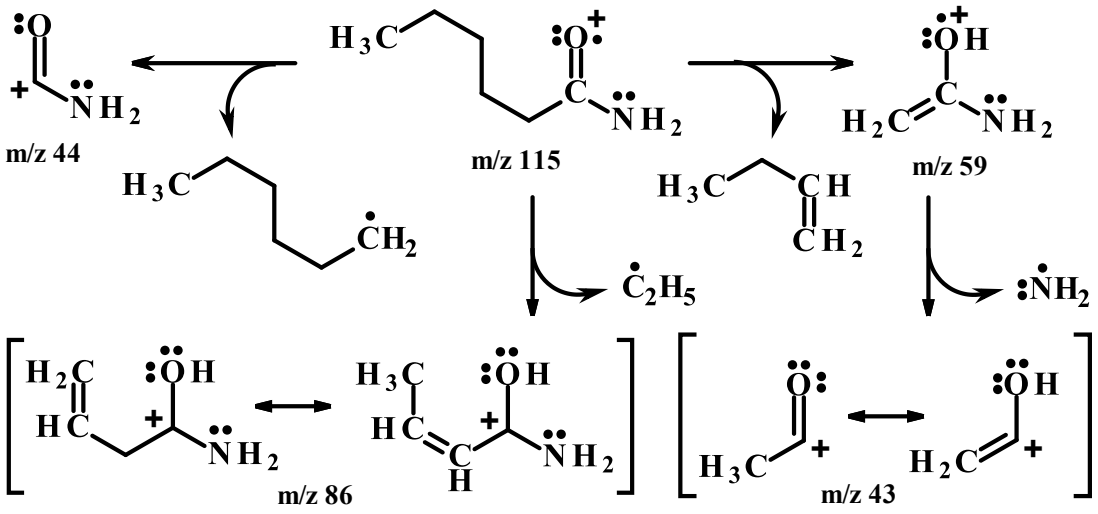



**Fig.214 Molecular ion fragmentation of hexanamide (molecular mass 115 g/mol)**

Figure 214 shows the formation of fragmentation ions in the hexanamide example and Figure 215 is the mass spectrum showing the signals of the ions formed.

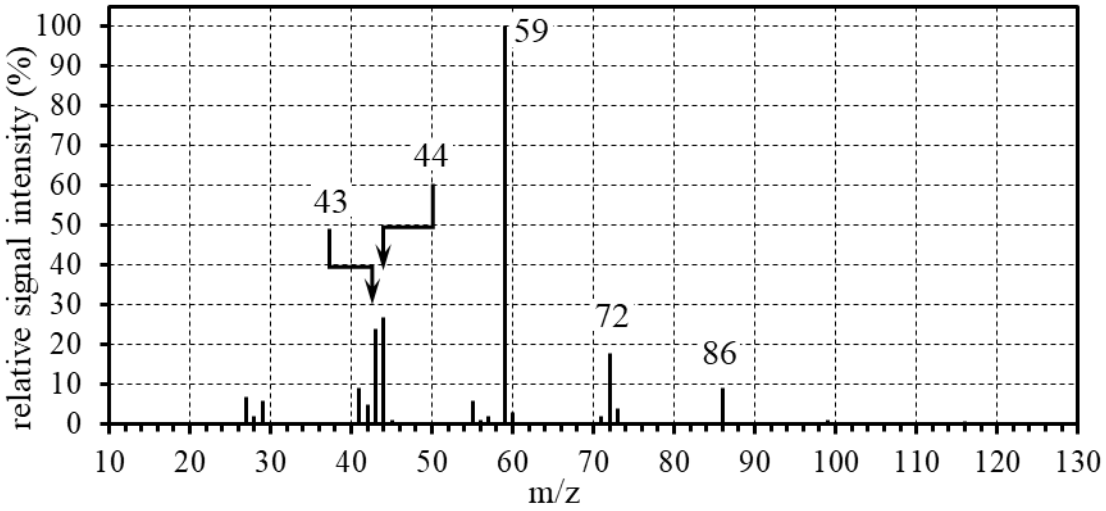



**Fig. 215 Mass spectrum of hexanamide (reconstructed from NIST, no. 20287, EI 70 eV ionization)**

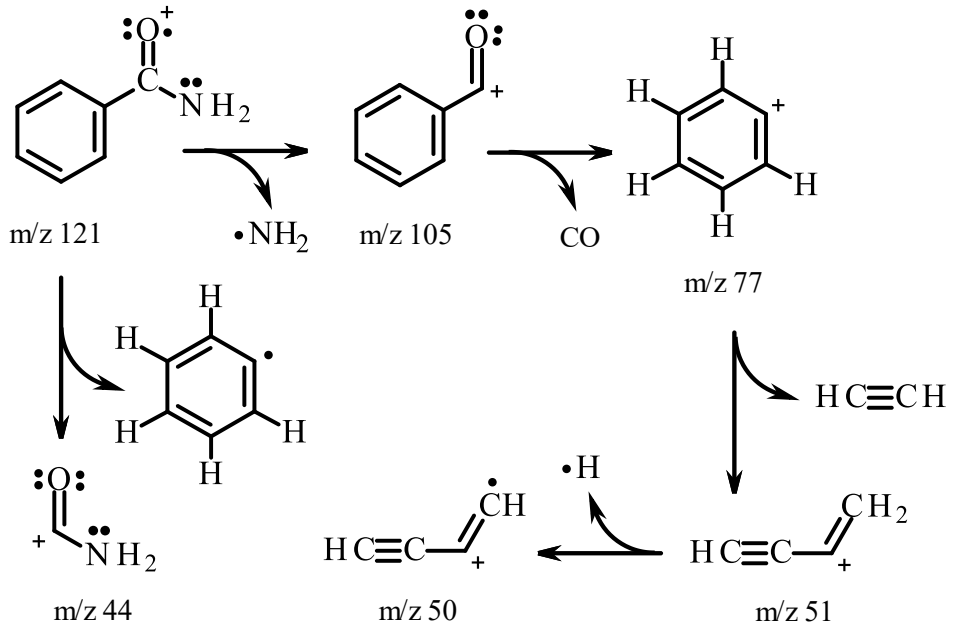



**Fig. 216 Molecular ion fragmentation of benzamide**

During fragmentation of aromatic amines, the molecular ion **[Ar–C(=O)–NH$_2$]** is found as an intense signal in the spectrum. After removing the **•HN$_2$** radical, the **[Ar–C=O]** ion is formed, which is then converted to the stable **[Ar$^+$]** losing a carbon monoxide [CO] molecule. Figure 216 shows the sequence of transformations and Figure 217 shows the mass spectrum of benzamide.

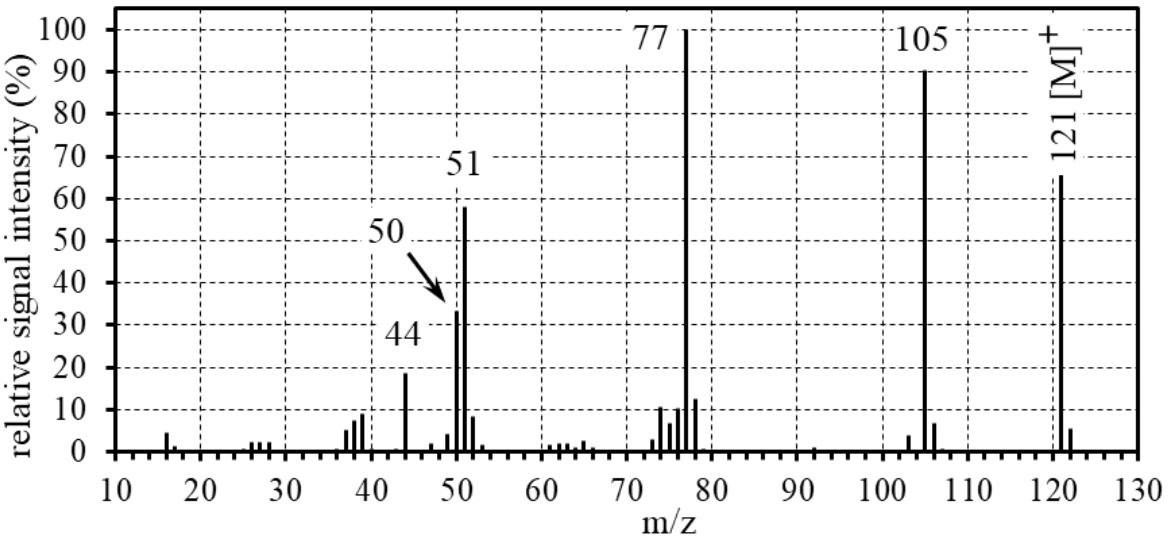



**Fig. 217 Mass spectrum of benzamide (reconstructed from NIST, no. 135755, EI 70 eV ionization)**

### 4.9.2.13. Nitriles

The molecular ion signal of nitriles is weak or absent. Removal of a hydrogen atom from the "α" position produces the **[M - H]**$^+$ ion, which also has a very weak signal. The dominant signal from *McLafferty* fragmentation at **m/z** 41 is of limited diagnostic value because the **[C$_3$H$_5$]**$^+$ ion has the same mass.

The fragmentation of nitriles is shown for butyronitrile in Figure 218 and the mass spectrum is shown in Figure 219.

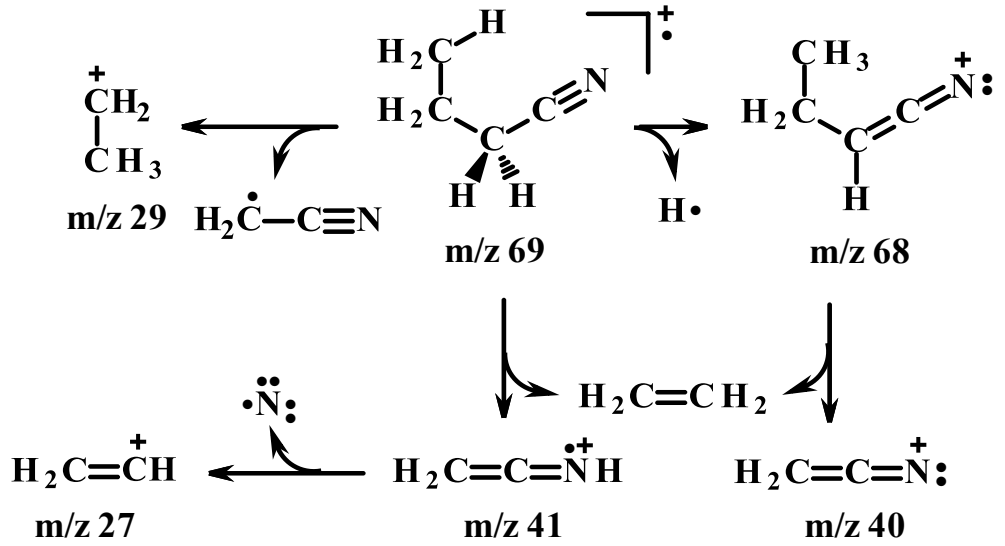



**Fig. 218 Fragmentation of the butyronitrile molecular ion**

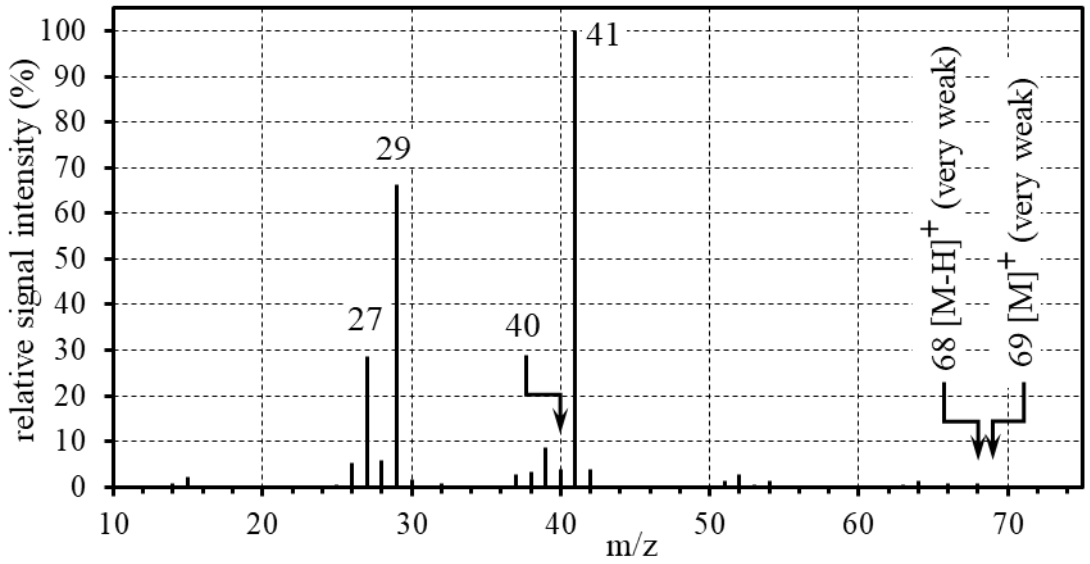



**Fig.219 Mass spectrum of butyronitrile (reconstructed from NIST, no. 228226, EI 70 eV ionisation)**

### 4.9.2.14. Nitroderivatives

The molecular ion of aliphatic nitro derivatives with an odd **m/z** ratio is represented by an extremely weak signal and in most cases is not present in the mass spectrum. The important signals are due to alkyl and alkenyl fragments resulting from chain cleavage. Figure 220 shows the mass spectrum of nitrohexane as an example.

The molecular ion signal of aromatic nitro derivatives is intense. Other prominent signals result from the removal of the anioni radical $\mathbf{[NO_2]^{\bullet}}$ (producing the ion $\mathbf{[M - 46]^+}$) and the removal of the NO fragment (producing the ion $\mathbf{[M - 30]^+}$). Figure 221 shows the spectrum of nitrobenzene as an example.

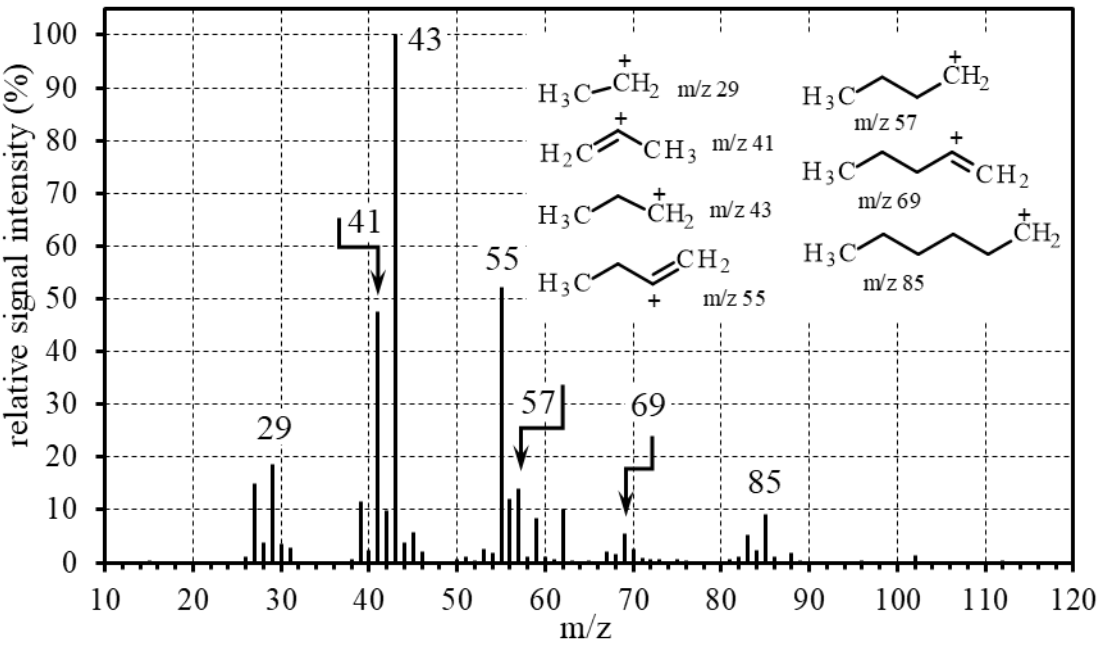



**Fig. 220 Fragmentation and mass spectrum of nitrohexane (reconstructed from NIST No. 238163, EI 70 eV ionization)**

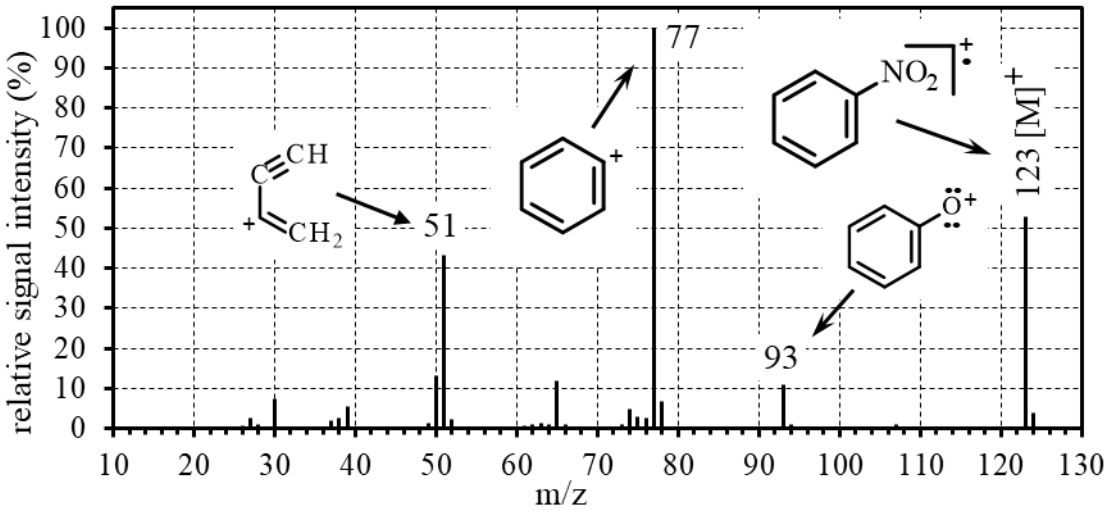



**Fig. 221 Mass spectrum of nitrobenzene**
**(reconstructed from NIST, No. 227769, EI 70 eV ionization)**

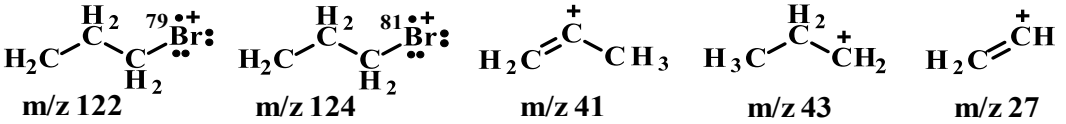
### 4.9.2.15. Halogenated compounds

With respect to the presence of signals in the mass spectrum, halogenated compounds can be divided into two categories:

***a) Compounds containing only chlorine and/or bromine atoms.*** These two chemical elements each have two stable isotopes of comparable natural abundance ($^{35}Cl$, $^{37}Cl$, $^{79}Br$ and $^{81}Br$). Therefore, chlorinated and/or brominated compounds have several isotopologues (chemical species with the same formula and molecular structure, with difference in the isotopic composition of one or more chemical elements). In the fragmentogram of these compounds, groups of isotopic signals are distinguished with a difference of 2 mass units between the signals, corresponding to the difference of 2 mass units between the isotopes of these halogens. The identity and number of halogen atoms in a fragment can be determined from the relative intensities of the grouped isotopologue signals (Figures 70-92 and 94). The number of grouped isotopologue signals is one unit greater than the total number of chlorine and/or bromine atoms in the molecule. Although the molecular ion signal is relatively strong in chlorinated and/or brominated derivatives, the fact that some grouped signals (especially those occurring at high **m/z** ratios) have low intensities can complicate data interpretation.

***(b) Compounds containing only fluorine and/or iodine atoms.*** The spectral behavior of fluorinated and/or iodinated derivatives differs from the previous category because the elements fluorine and iodine have only one stable isotope, so there is no problem of isotope discrimination. However, the interpretation of the fragmentation of fluorinated compounds presents real difficulties compared to iodinated representatives. The iodine atom splits more easily. This phenomenon is reflected by the loss of a neutral species and the appearance of a signal at an **m/z** ratio 127 mass units lower than that of the molecular ion. Interpretation of the fragmentation of fluorinated compounds is more difficult because the molecular ion (especially fluoroalkanes) is extremely weak in the spectrum. In general, the molecular ion is relatively easy to detect in the spectra of brominated and/or iodinated compounds.

For chlorinated alkanes, the intensity of the molecular ion signal depends on multiple factors: the number of chlorine atoms in the molecule, the length of the carbon chain, and the degree of branching of the molecular skeleton. The high degree of branching of the molecular backbone and the advanced alkyl chain length reduce significantly the signal intensity of the molecular ion. In the case of brominated or iodinated compounds, the above factors will affect the signal intensity of the molecular ion to a lesser extent. In most cases, the molecular ion signal does not appear in the spectra of fluorinated hydrocarbons. As an example, Figure 222 shows the spectrum of 1-brompropane. The signals in the spectrum can be assigned to the following ions:



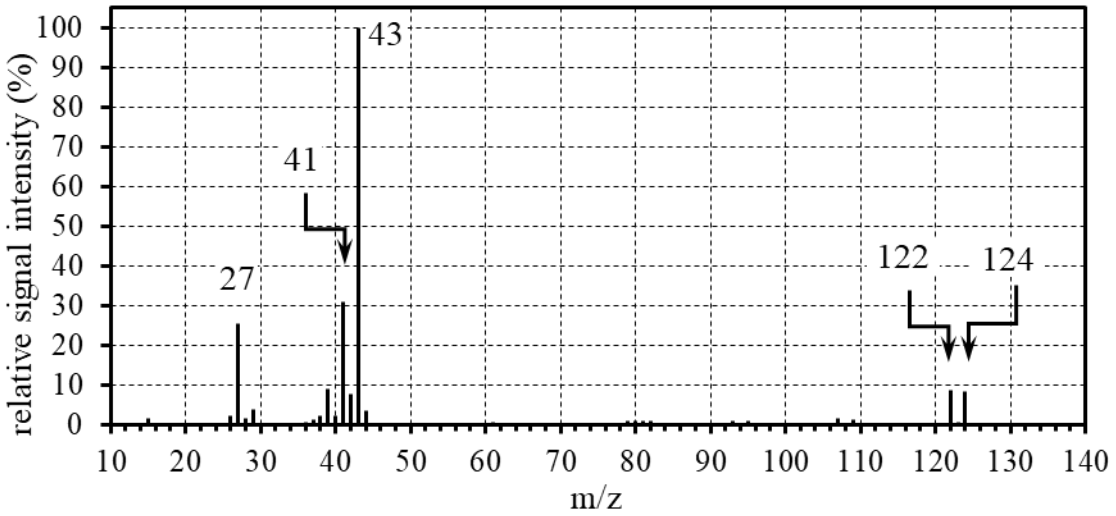




**Fig. 222 Mass spectrum of 1-brompropane (reconstructed from NIST, EI 70 eV)**

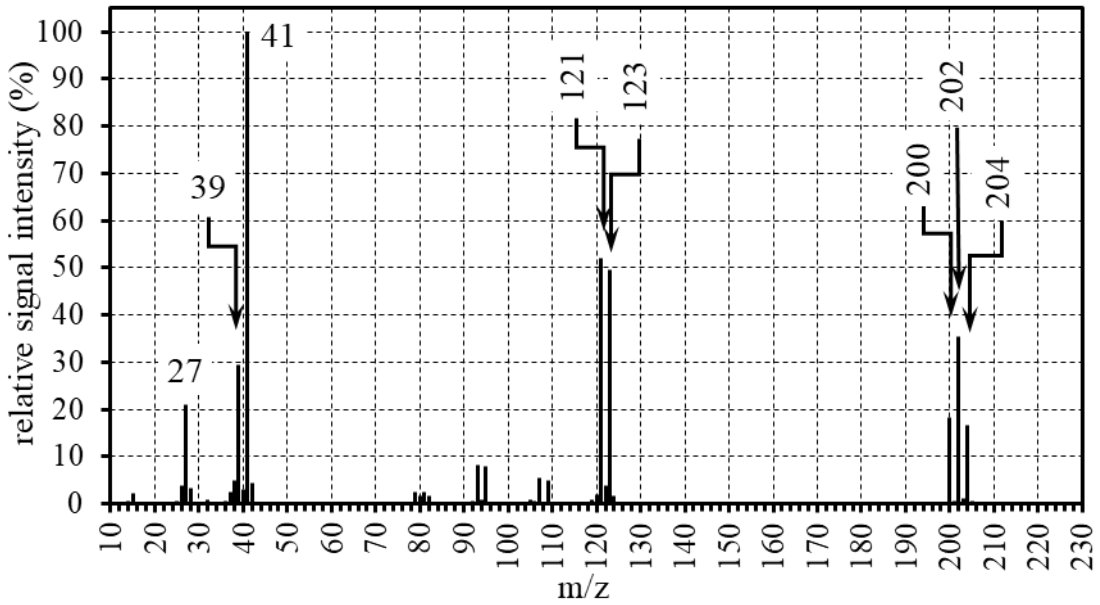
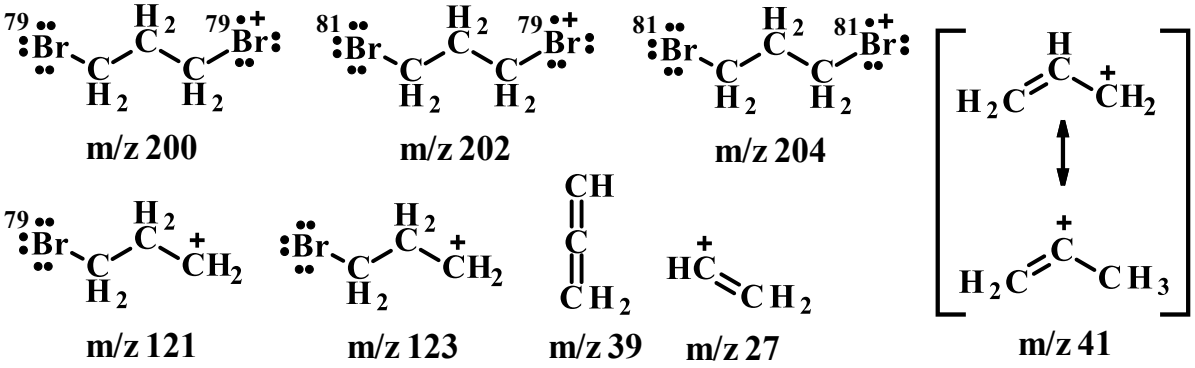



**Fig. 223 Mass spectrum of 1,3 dibrompropane (reconstructed from NIST, EI 70 eV)**

In the mass spectrum of 1,3-dibrompropane (Figure 223), the three-signal group of isotopologues of the molecular ion (the molecule contains two bromine atoms) can be easily identified. The signals in the spectrum can be assigned to the following ions:




### 4.9.2.16. Fragmentation of peptide chains. The *Roepstorff - Fohlman* convention

In the analysis of substances of the peptide and protein classes, composed of amino acids, fragmentation occurs mainly around the peptide bond, especially in electrospray ionization, producing ions formed from smaller groups of amino acids. Three main types of fragmentation affecting the bond between the carbonyl group and the adjacent atom are shown in Figure 224.

Figure 224 **(AX)** shows the cleavage of the bond between the carbonyl group "C=O" and the carbon atom at position α in comparison with this group (onto which the amino acid-specific **R** substituent is grafted). The ionic fragments resulting from the cleavage are designated by the symbol **A** (the ion at the N-terminal end of the original peptide chain) and by the symbol **X** (the ion at the C-terminal end of the peptide chain).

Figure 224 **(BY)** shows the cleavage of the bond between the carbonyl group "C=O" and the nitrogen atom of the bond "C(=O)-NH". The resulting ionic fragments after cleavage are denoted by **B** (the ion at the N-terminal end of the original peptide chain) and by **Y** (the ion at the C-terminal end of the peptide chain).

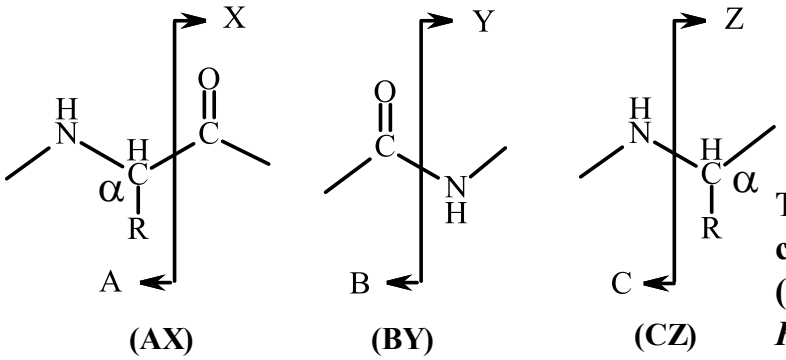



**Figure 224**
**Three types of peptides chain fragmentation (notation proposed by *Roepstorff and Fohlman*)**

Figure 224 **(CZ)** shows the cleavage of the "N-C" bond between the nitrogen atom and the carbon atom at position α (onto which the amino acid-specific **R** substituent is grafted). The resulting ionic fragments after cleavage are denoted by the symbol **C**

(the ion at the N-terminal end of the original peptide chain) and by the symbol **Z** (the ion at the C-terminal end of the peptide chain).

This notation, proposed by *P. Roepstorff* in 1984, is useful for the naming of ionic fragments in the analysis of peptides and proteins by mass spectrometry.
[*P. Roepstorff*, *J. Fohlman*: Proposal for a Common Nomenclature for Sequence Ions in Mass Spectrometry of Peptides. **Biomedical Mass Spectrometry 1984:11**(11), 601]

The symbols **A** , **B** , **C** , **X** , **Y** and **Z** are completed by a number indicating the number of amino acid units in the ion formed after cleavage (equal to the number of substituents R in the ion). Figure 225 illustrates the meaning of the symbols for a tetrapeptide. By selecting the mode and details of ionization and fragmentation, one type of cleavage can be favored over another, providing useful information about the primary structure (amino acid sequence) of the peptide or protein being analyzed. For the analysis of peptides and proteins, MALDI ionization in the positive mode is often preferred due to the relatively low fragmentation. Figure 226 shows the formation and structures of the positive ion fragments **A** , **X** , **B** , **Y** , **C** and **Z**.

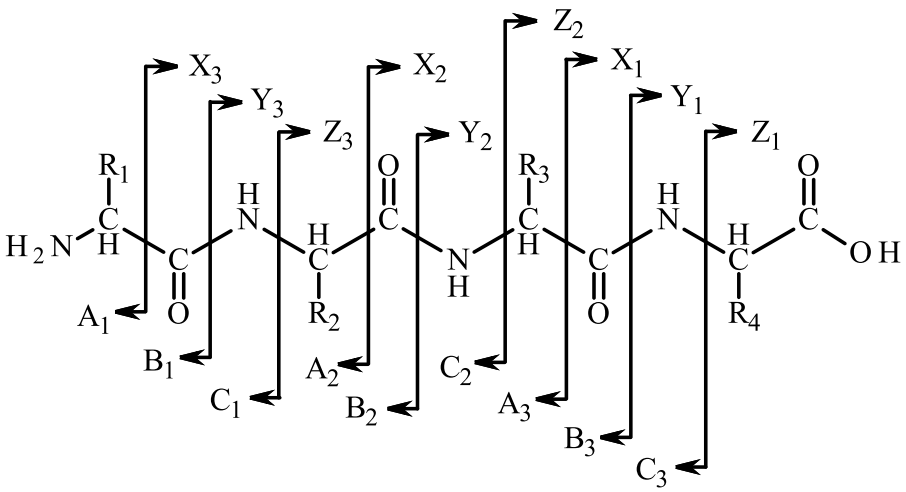



**Fig. 225 Conventional notation of peptide chain fragments according to *P. Roepstorff* and *J. Fohlman* [Letter to the Editors. Biomedical Mass Spectrometry 1984:11(11), 601]**

The formation of the ion types in Figure 226 is not equally plausible. The formation of **Y** ions is the most likely and therefore the most represented in the spectrum. **B**-type ions are also common, but the cyclic structure prevents the formation of the **B1**-type ions. The formation of the **A**-type ions is quite common, but less for long peptide chains. The occurrence of the **Z**-form ions is unlikely and uncertain in most cases.

Sometimes there are two other types of fragmentation: "internal" ion formation and "immonium" ion formation (Figure 227).

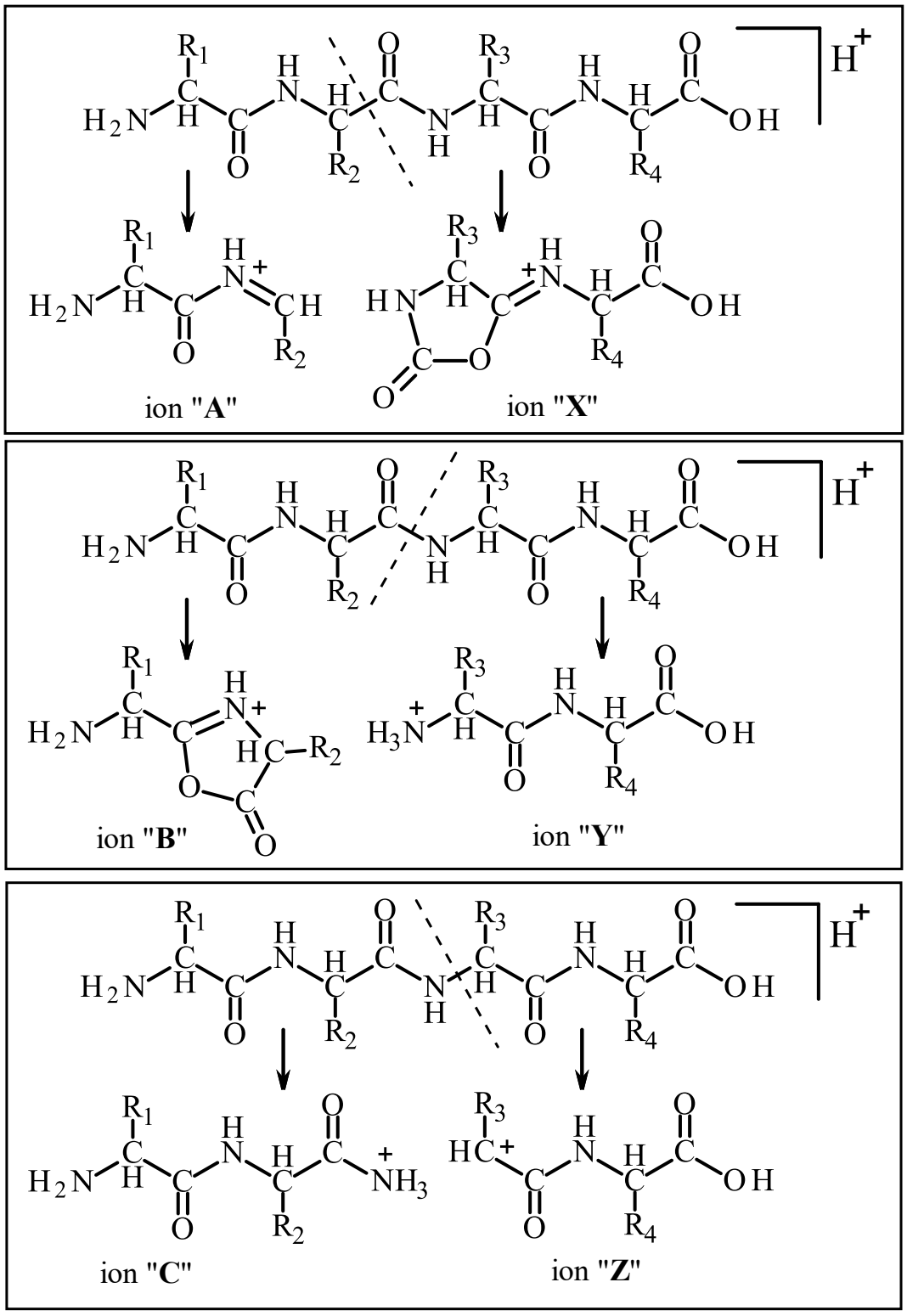



**Fig 226 Structure of ions resulting from $MS^2$ fragmentation of peptide chains 'A-X', 'B-Y' and 'C-Z' after MALDI ionization and argon atom bombardment.**

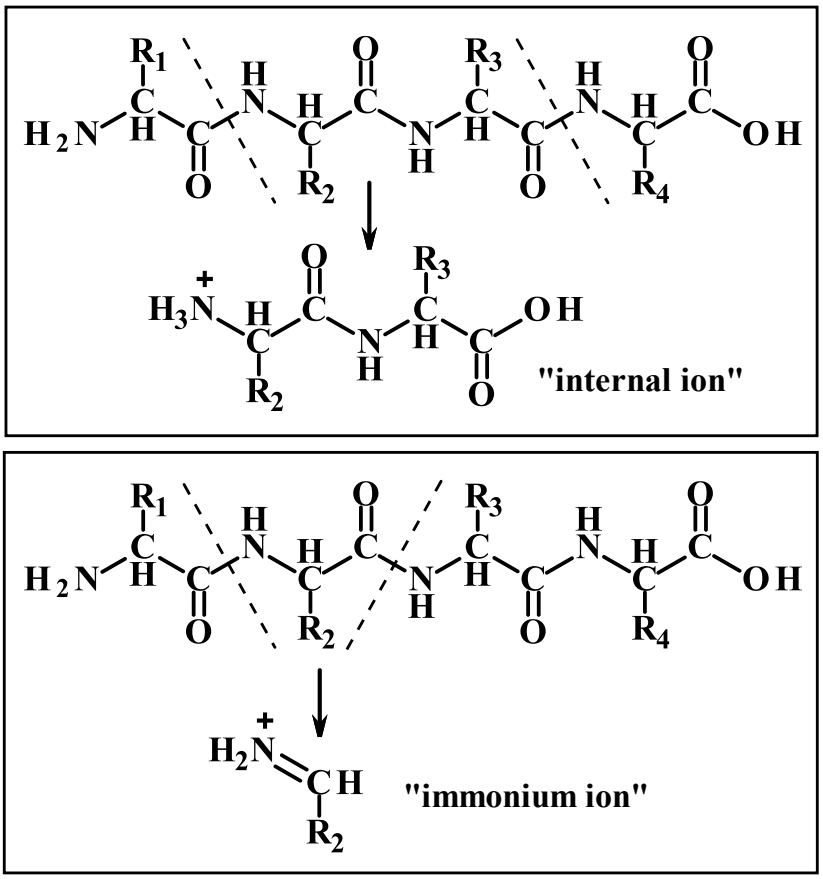



**Fig 227 Formation of an "internal" ion and an "immonium "ion during peptide fragmentation**

The usual procedure for identifying and characterizing peptides and proteins by $MS^2$ mass spectrometry (tandem spectrometry) is to select a narrow mass range from the primary MALDI spectrum, bombarding the ions within the selected range with argon atoms to induce their secondary fragmentation and separate the fragment ions. The selected mass range in the primary phase is 2-3 Da. The use of argon for fragmentation is justified by its chemical inertness to the analyte and its mass, which is high enough for efficient collision. The result is the generation and visualization of a variety of produced ions in the $MS^2$ spectrum. The $MS^2$ spectrum provides information about the ions produced and thus the structure of the precursor ions.

Sophisticated interpretation and processing of peptide mass spectral data allow determination of the type and number of amino acids in the molecule, as well as the amino acid sequence in the peptide chain (primary structure of the peptide, "*de novo*" amino acid sequence determination), sometimes even without recourse to other analytical techniques such as nuclear magnetic resonance (NMR) spectroscopy or prior enzyme fragmentation.

The study of peptides is often completed with negative ionization (negative mode) in addition to the positive ion mode. Electrospray ionization (ESI) or MALDI is chosen because of the low and largely predictable fragmentation, although these ioni-

zation methods can also produce ions with multiple elemental charges, a phenomenon that sometimes complicates the interpretation of results.

### 4.9.2.17. Fragmentation of saccharides. The *Domon-Costello* convention

Like the convention of *Roepstorff-Fohlman* for naming peptide fragments, *Domon* and *Costello* proposed a systematic nomenclature for fragments resulting from $MS^2$ mass spectrometry of saccharides and glycoconjugates using FAB (**F**ast **A**tom **B**ombardment) primary ionization followed by CID (**C**ollision **I**nduced **D**ecomposition) fragmentation of the precursor ion.
[*B. Domon*, *C.E. Costello*: A systematic nomenclature for carbohydrate fragmentation in FAB-MS/MS spectra of glycoconjugates. **Glycoconjugate J., 1988:5**(4), 397-409].

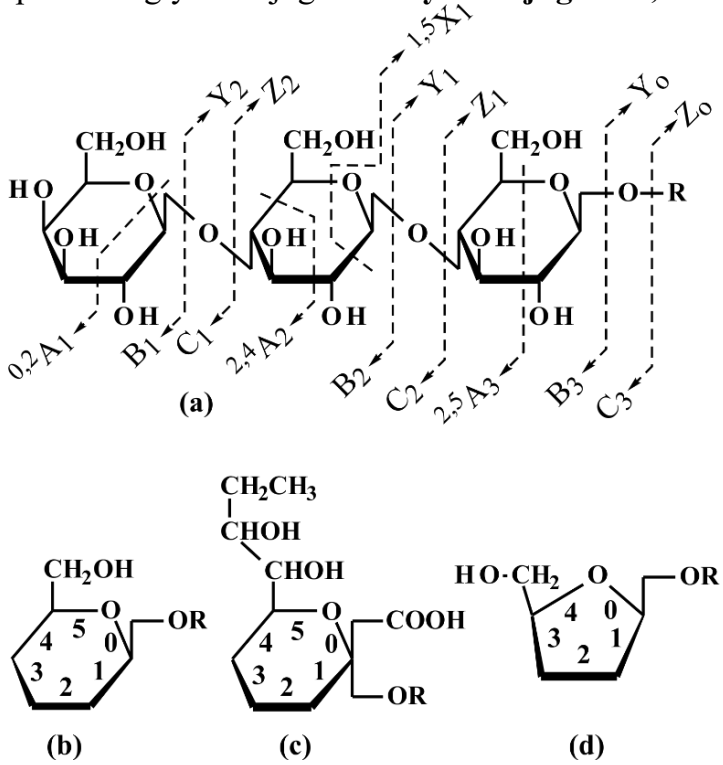



**Fig. 228 Illustration of the *Domon-Costello* convention**

The convention notation is illustrated in Figure 228 **(a)** for a group of three condensed hexoses. Ion fragments containing a terminal (non-reducing) carbohydrate moiety are denoted by $\mathbf{A_i}$ , $\mathbf{B_i}$ , $\mathbf{C_i}$ (i = 1, 2, 3, ...) and ions containing the aglycone (or reducing carbohydrate moiety) are denoted by $\mathbf{X_j}$ , $\mathbf{Y_j}$ and $\mathbf{Z_j}$ (j = 1, 2, 3, ...).

The subscript at the end of the notation indicates the sequence number of the carbohydrate unit (analogous to the convention used for peptides) and the superscript refers to the sequence number of the cleaved bond within the carbohydrate ring (Figure 228 **(b)**, **(c)** and **(d)**).

The proposed nomenclature is also relevant to other ionization techniques such as FD (**F**ield **D**esorption), DCI (**D**irect **C**hemical **I**onization), Laser Desorption and is useful for both positive and negative spectral recording.

## 5. Application examples for the analysis of pharmaceutically relevant substances (case studies)

### 5.1 Differential identification of paclitaxel and related compounds by mass spectrometry

Taxol (trade name: Paclitaxel) is an anticancer drug administered intravenously, often in albumin-bound form (nab-paclitaxel, Albraxane). Chemically, it is a diterpene alkaloid of the taxane class. It has several adverse effects and is the target of attempts to obtain chemically modified derivatives with reduced adverse effects.

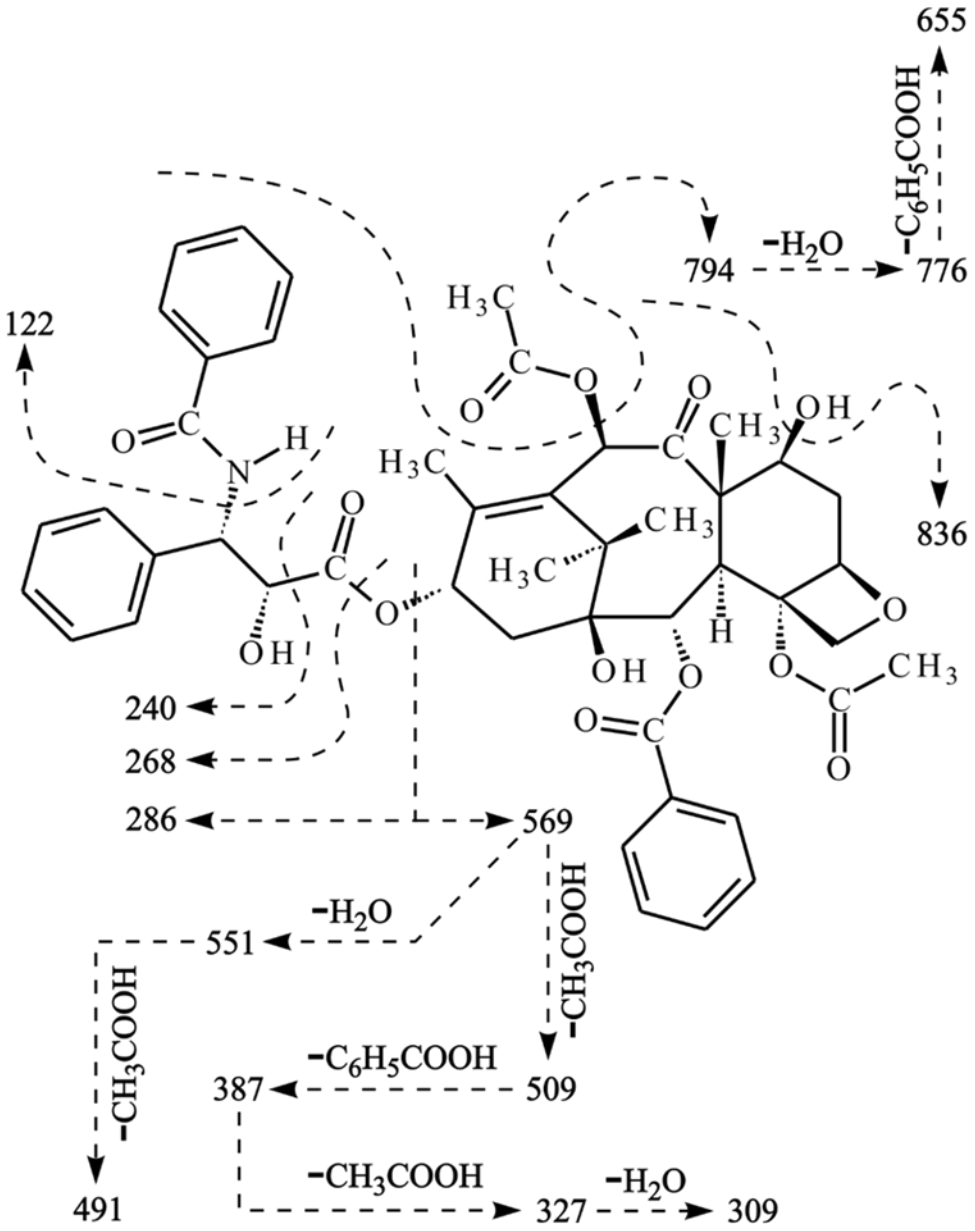



**Fig. 229 Fragmentation scheme of the paclitaxel molecule (reconstructed from [1])**

The compound was first isolated from the bark of the *Taxus brevifolia* tree [2] and its therapeutic use was approved in 1993. It is now produced by biotechnology. Due

to its highly complex molecular structure, analytical verification and reliable identifycation of the product obtained is essential. Several semi-synthetic methods have been developed since 1988, but none has yet proven to be industrially viable and cost effective.

A reliable method for identification and for molecular structure elucidation is mass spectrometry ($MS^1$) using electrospray ionization (ESI) with a nebulization voltage of +4500 V). The ions identified in the spectrum are consistent with the fragmentation mode shown in Figure 229 [2,3]. Figure 230 shows the MS mass spectrum of paclitaxel obtained by ESI ionization.

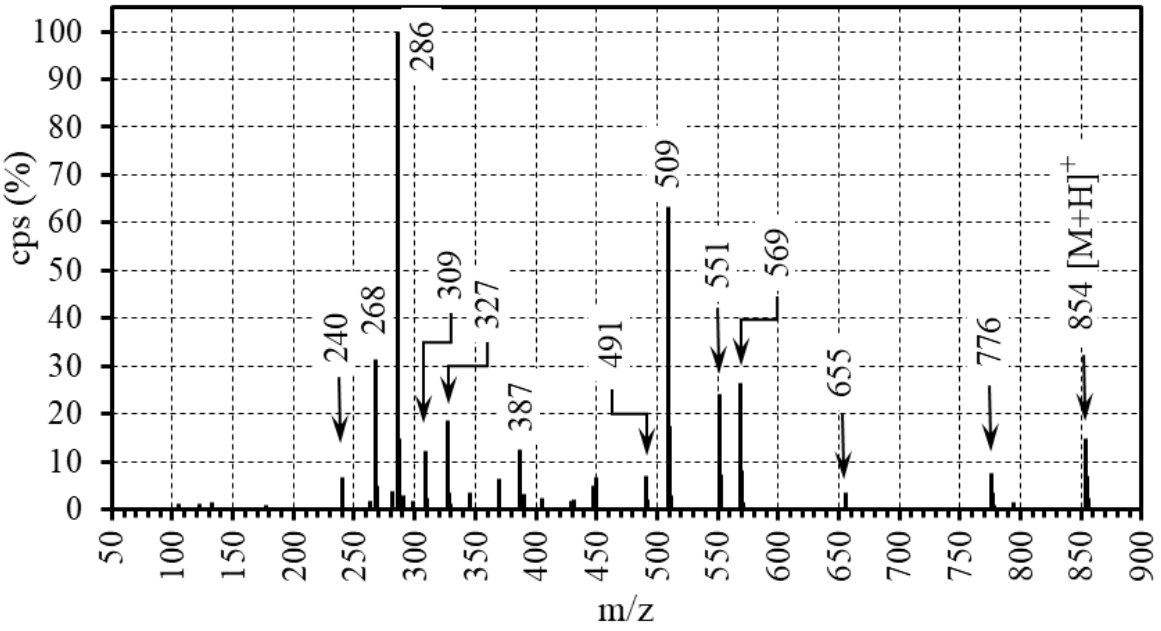



**Fig. 230 MS spectrum of paclitaxel (ESI ionization, reconstructed from the MassBank Record MSBNK Fiocruz – FIO 00536 [3])**

Other methods used for analytical purposes and to elucidate the fragmentation mechanism are based on matrix-assisted laser desorption ionization (MALDI) [4] and fast atom bombardment (FAB) [5]. The matrix for MALDI dissociation was 4-nitronaphthalene, dissociation was performed with laser radiation of 337 nm, at incidence angle of 50 degree to the normal of the sample surface, and the resulting ions were accelerated to a voltage of 10 kV. Sulfolane matrix was used for FAB ionization. Table 229 compares the **m/z** values of the ionic species resulting from MALDI [4] and FAB [5] ionization.

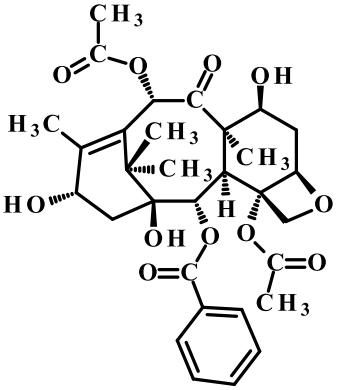
The signals at **m/z** 105.033461 (FAB ionization) and 196.027876 (MALDI ionization) are suitable for quantitative determinations, but it should be noted that the mode of fragmentation and therefore the shape of the MS spectrum depends on the specific technical conditions of the spectrum acquisition, such as the operating parameters of the ESI ionizer, the nature of the precursor ion, and the nature and energy of the collision gas.

**Table 14 Ion fragments resulting from MALDI ionization and FAB fragmentation**

| m/z | Ionic species | Relative abundance (%) | |
|---|---|---|---|
| | | FAB [5] | MALDI [4] |
| 892 | $[M+K]^+$ | missing | 19.2 |
| 876 | $[M+Na]^+$ | missing | 100.0 |
| 854 | $[M+H]^+$ | 13.4 | 16.7 |
| 794 | $[M-H-AcOH]^+$ | 1.9 | missing |
| 696 | $[M+H-BzOH-2H_2O]^+$ | missing | 3.6 |
| 569 | $[M-S]^+$ | 5.8 | 5.1 |
| 551 | $[M-S-H_2O]^+$ | 2.4 | 3.6 |
| 509 | $[M-S-AcOH]^+$ | 7.4 | 10.2 |
| 447 | $[M-S-BzOH]^+$ | 2.1 | missing |
| 286 | $[S+2H]^+$ | 61.8 | 13.0 |
| 268 | $[S-O]^+$ | 37.6 | 11.4 |
| 210 | $[S-O-CO-HCOH]^+$ | 49.4 | missing |
| 105 | $[BzO]^+$ | 100.0 | missing |

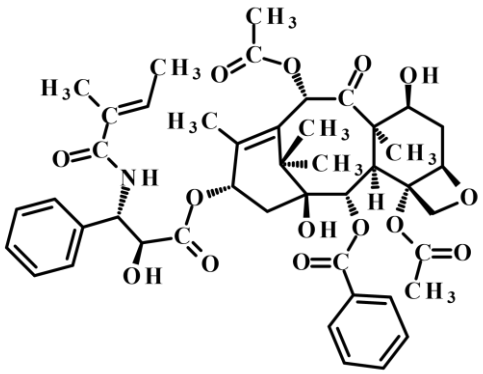
**AcOH = acetic acid; S = molecular "tail" m/z 284; BzOH = benzyl alcohol; BzO = benzyl alcohol minus one hydrogen atom.**

Other Taxol-related substances (Figure 231) that may appear as impurities, can be detected, and identified by MALDI-TOF ionization MS. Some characteristic signals of these compounds are listed in Table 15.



**Baccatin**

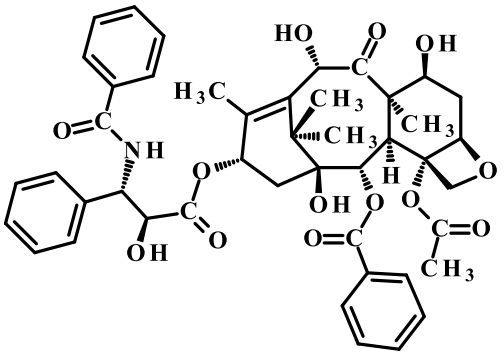
**($C_{31}H_{38}O_{11}$) M = 586.62677**



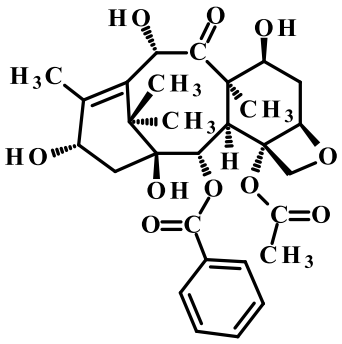
**Cephalomannine**

**($C_{45}H_{53}NO_{14}$) M = 831.9**

**Fig. 231 (A) Molecular structures of compounds in Table 15**

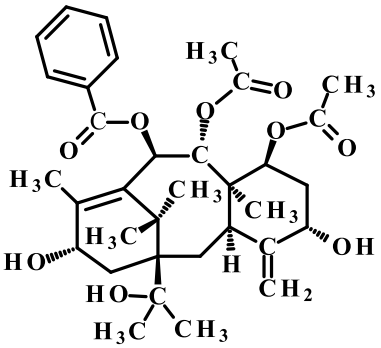


**10-deacetyl taxol**
**($C_{45}H_{49}NO_{13}$) M = 811.9**

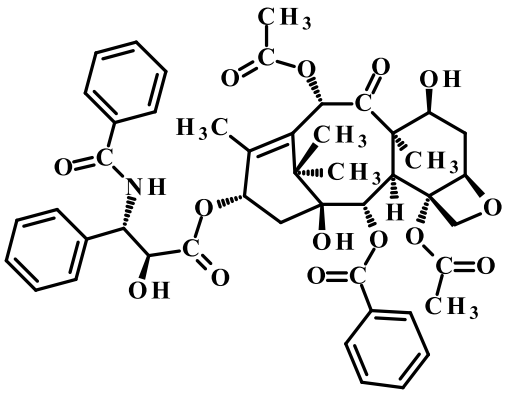


**10-deacetyl baccatin**
**($C_{29}H_{36}O_{10}$) M = 544.59**

**Fig. 231 (B) Molecular structures of compound in Table 15**



**Brevifoliol**
**($C_{31}H_{40}O_9$) M = 556.652**



**Taxol (Paclitaxel)**
**($C_{47}H_{51}NO_{14}$) M = 853.906**

**Fig. 231 (C) Molecular structures of compound in Table 15**

**Table 15 Main MALDI-TOF MS[1] signals of the compounds in Figure 231 (from [4])**

| Analyte | m/z | Ionic species | Analyte | m/z | Ionic species |
|---|---|---|---|---|---|
| baccatin | 625 | $[M+K]^+$ | 10-deacetil taxol | 850 | $[M+K]^+$ |
| | 609 | $[M+Na]^+$ | | 834 | $[M+Na]^+$ |
| | 587 | $[M+H]^+$ | | 812 | $[M+H]^+$ |
| | 527 | $[M+H-AcOH]^+$ | | 549 | $[M-S]^+$ |
| | 509 | $[M+H-AcOH-H_2O]^+$ | | 286 | $[S+2H]^+$ |
| cephalomannine | 870 | $[M+K]^+$ | 10-deacetil baccatin | 583 | $[M+K]^+$ |
| | 854 | $[M+Na]^+$ | | 567 | $[M+Na]^+$ |
| | 832 | $[M+H]^+$ | | 545 | $[M+H]^+$ |
| | 572 | $[M-S-H_2O]^+$ | | 527 | $[M+H-H_2O]^+$ |
| | 508 | $[M-S-AcOH]^+$ | | 405 | $[M+H- BzOH-H_2O]^+$ |
| | 265 | $[S+2H]^+$ | brevifoliol | 595 | $[M+K]^+$ |
| | | | | 579 | $[M+Na]^+$ |
| | | | | 417 | $[M+H-BzOH-H_2O]^+$ |

**S: ester fragment at position 13 of the diterpene skeleton**
**AcOH: acetic acid**
**BzOH: benzoic acid**

**Sources cited in application example 5.1**

**[1]** *E.H. Kernst, K.J. Volk, S.E. Hill*: Profiling Taxanes in *Taxus* Extracts Using LC/MS and LC/MS/MS Techniques.
**Journal of Natural Products 1994:57(10), 1391-1403**

**[2]** *M.C. Wani, H.L. Taylor, M.E. Wall, P. Coggon, A.T. McPhail*: Plant Antitumor Agents. VI. Isolation and Structure of Taxol, a Novel Antileukemic and Antitumor Agent from *Taxus brevifolia*.
**J. Am. Chem. Soc., 1971:93(9), 2325-2327**

**[3] MoNA - MassBank of North America, https://mona.fiehnlab.ucdavis.edu/**

**[4]** *E.H. Kernst, K.J. Volk, S.E. Hill*: Profiling New Taxanes Using LC/MS and LC/MS/MS Substructural Analysis Techniques.
**Rapid Communication in Mass Spectrometry 1995:9(15), 1539-1545**

**[5]** *M.E. Gimon, G.R. Kinsel, R.D. Edmondson, D.H. Russell*: Matrix Assisted Laser Desorption/Ionization Time-of-Flight Mass Spectrometry of Paclitaxel and Related Taxanes.
**Journal of Natural Products 1994:57(10), 1404-1410**

### 5.2 MS analysis of the major constituents of *Zingiber officinale*

Ginger (*Zingiber officinale*) has been used since ancient times for its impressive array of beneficial effects. More than 30 effects of ginger oil or products in other forms (extract, dried root powder) are listed in the literature [1].

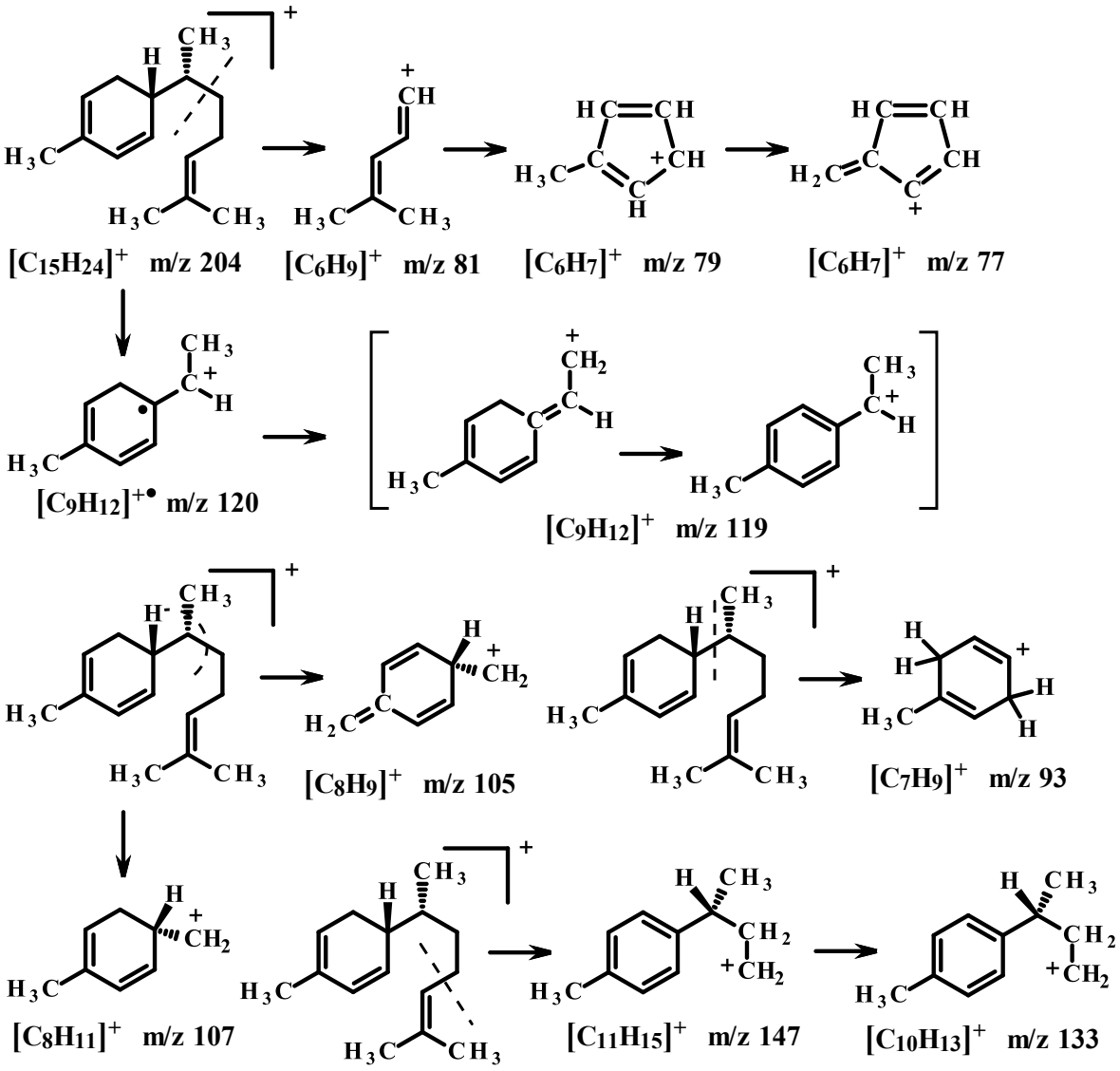



**Fig. 232 Ionic fragments formed from α zingiberene by mass spectrometric analyses (EI 70 eV, reconstructed and supplemented according to [2]).**

Positive effects include blood sugar regulation, stimulation of immune system, antioxidant behavior and efficacy in cases of respiratory infections. Generally, it does not cause adverse reactions or undesirable interactions with other drugs; however, prior medical consultation is recommended when taking concurrently with antihypertensive or cardioactive drugs.

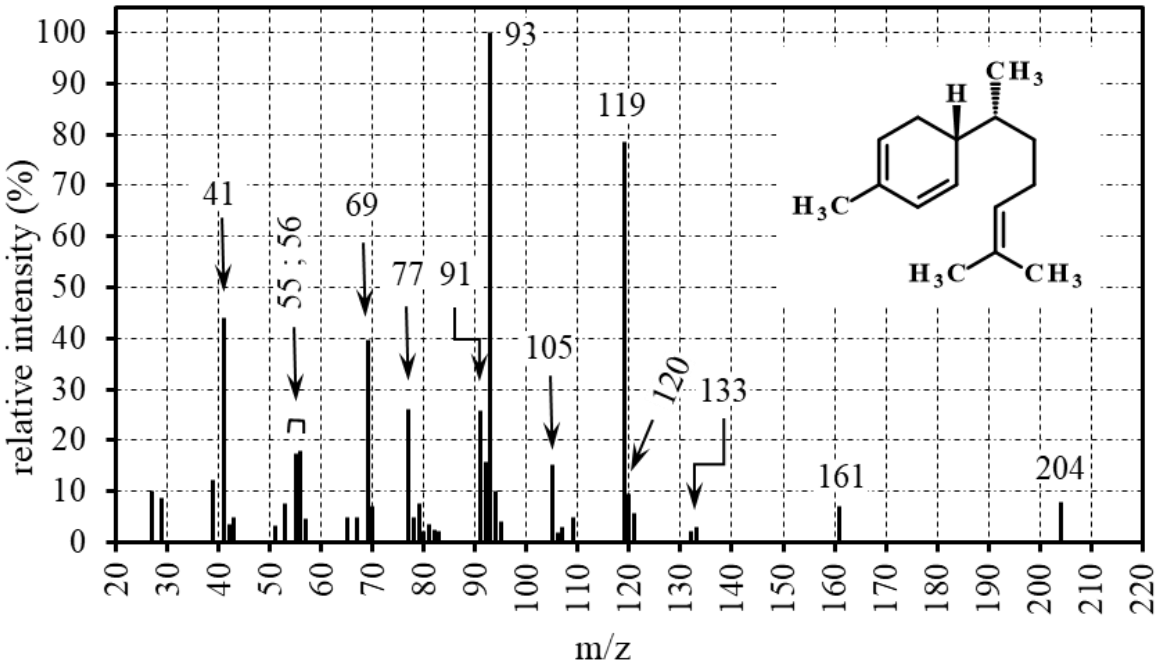



**Figure 233 Mass spectrum of the compound α–zingiberene (EI 70 eV ionization, reconstructed from data in NIST database no. 70231)**

Analytical procedures have been developed using a tandem gas chromatograph-mass spectrometer system to identify and quantify the composition of raw materials and determine the properties of their products [2]. These methods have identified over 50 constituents belonging to the mono- and sesquiterpene derivative categories. Gas chromatography uses electron impact (EI) ionization, with a preference for the positive mode and energy of 70 eV, to identify these compounds. Established databases contain a variety of reference spectra obtained under these conditions. Figure 232 shows the possible fragments resulting from the α-zingiberene molecule during EI ionization (70 eV), while Figure 233 shows the signals in the MS spectrum associated with the ionic fragments.

Gas chromatographic analysis of the essential oil of *Zingiber officinale* allowed the identification of a significant number of compounds. The mass spectra of some important representatives are shown in Figures 234 - 251, reproduced from digitized data taken from the literature [3] as well as from the NIST database [4], obtained after impact ionization with electrons (70 eV).

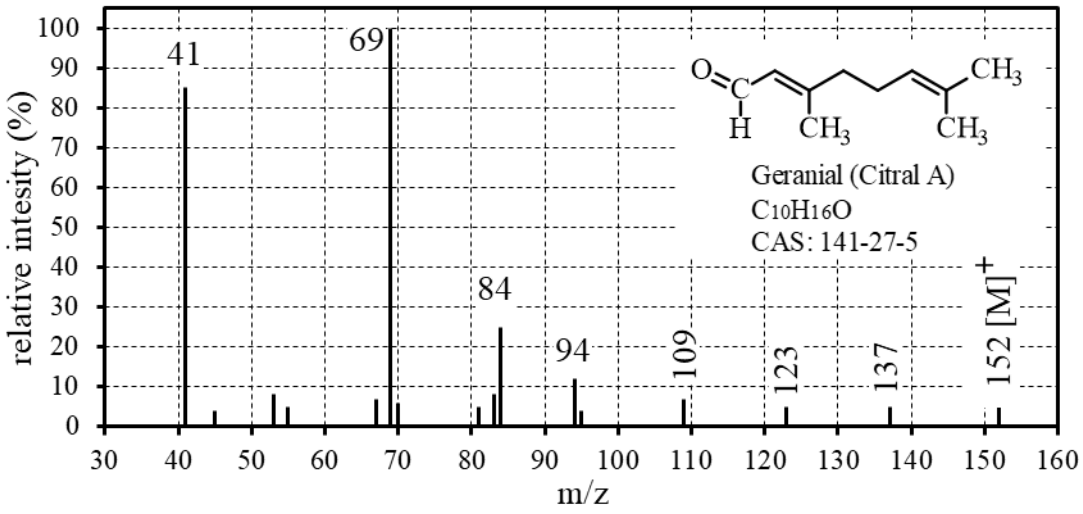



**Fig. 234 Geranial (Citral A) (MS EI, 70 eV) [3]**

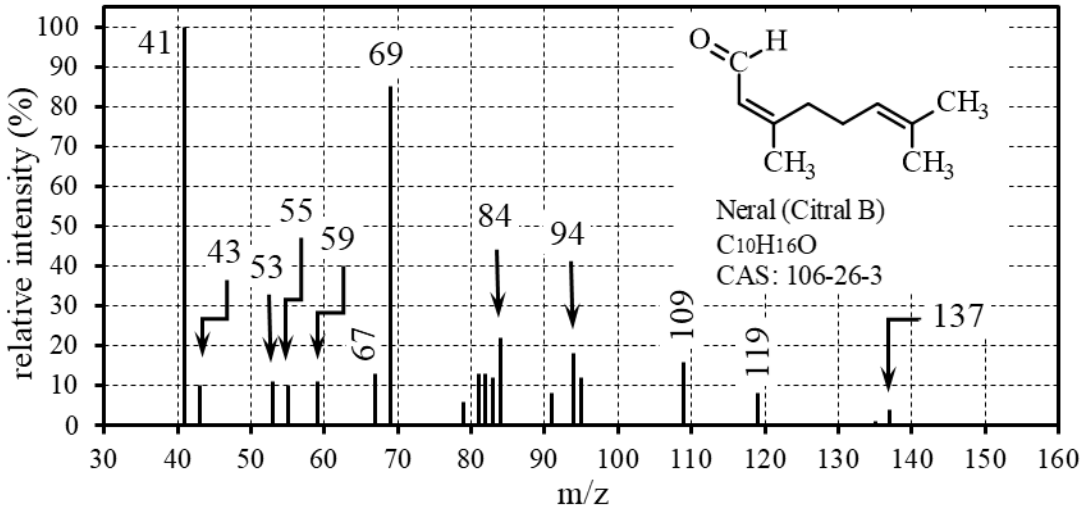



**Fig. 235 Neral (MS EI, 70 eV) [3]**

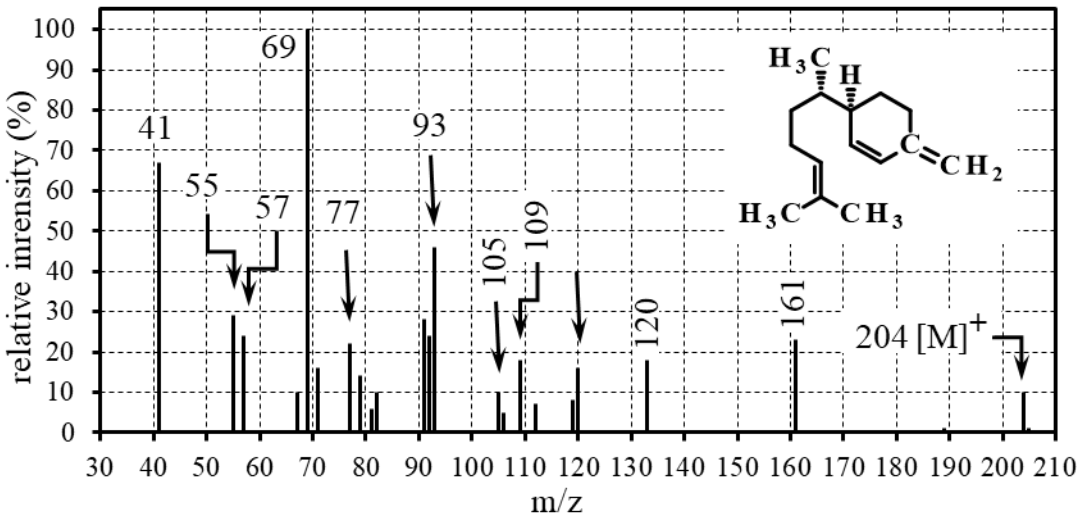



**Fig. 236 β – sesqui-phellandrene (MS EI, 70 eV) [3]**

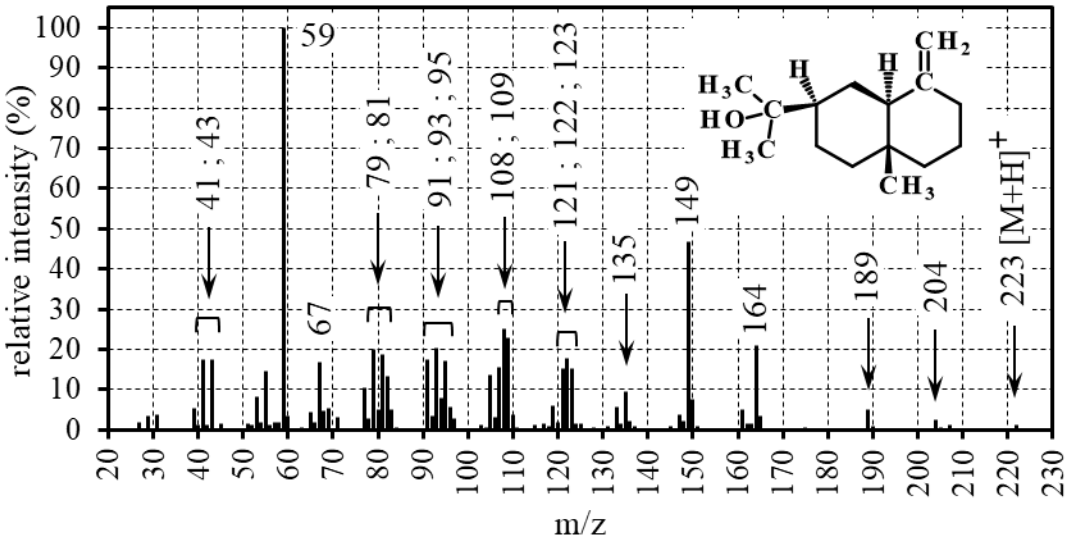



**Fig. 237 β-eudesmol (MS EI, 70 eV – NIST 334000)**

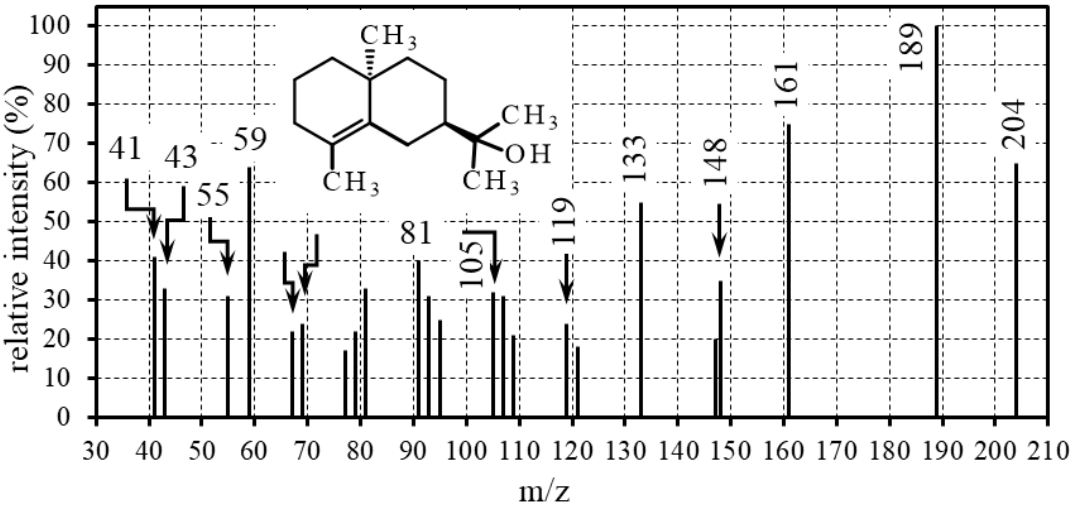



**Fig. 238 10-*epi*-γ-Eudesmol (MS EI 770 eV)**

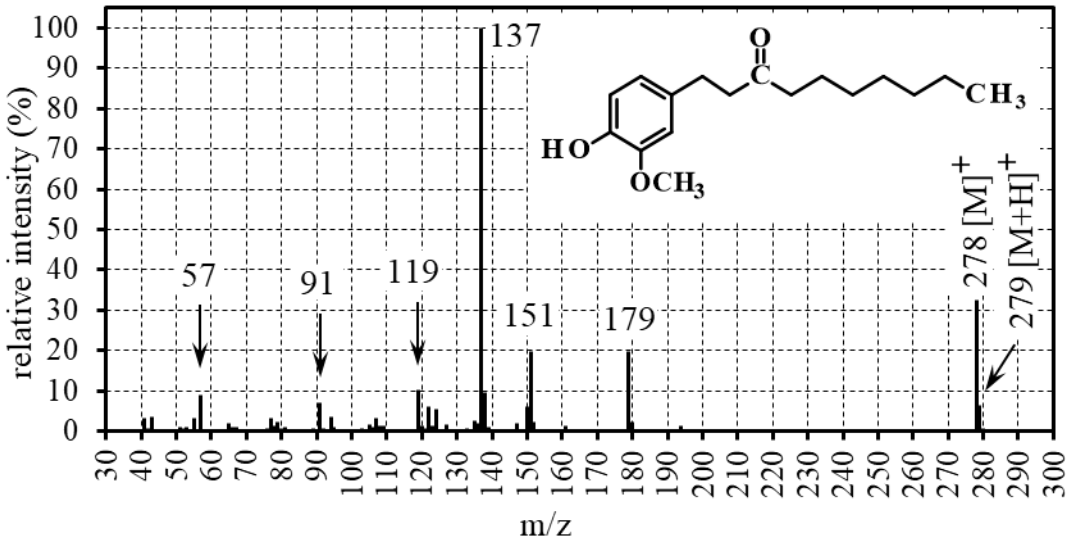



**Fig. 239 Paradol (MS EI, 70 eV – NIST 384092)**

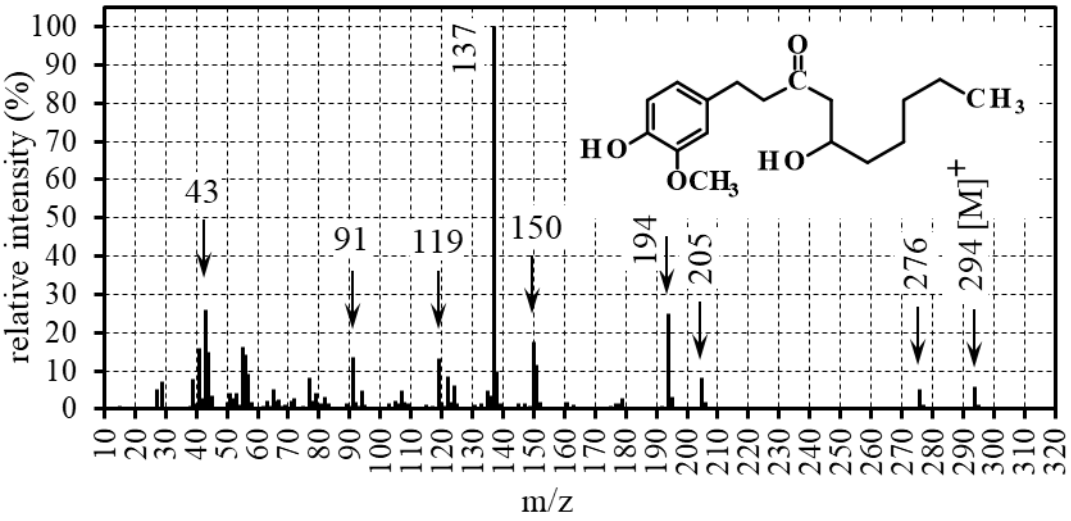



**Fig. 240 6-gingerol CAS 23513-14-6 (MS EI, 70 eV – NIST 291923)**

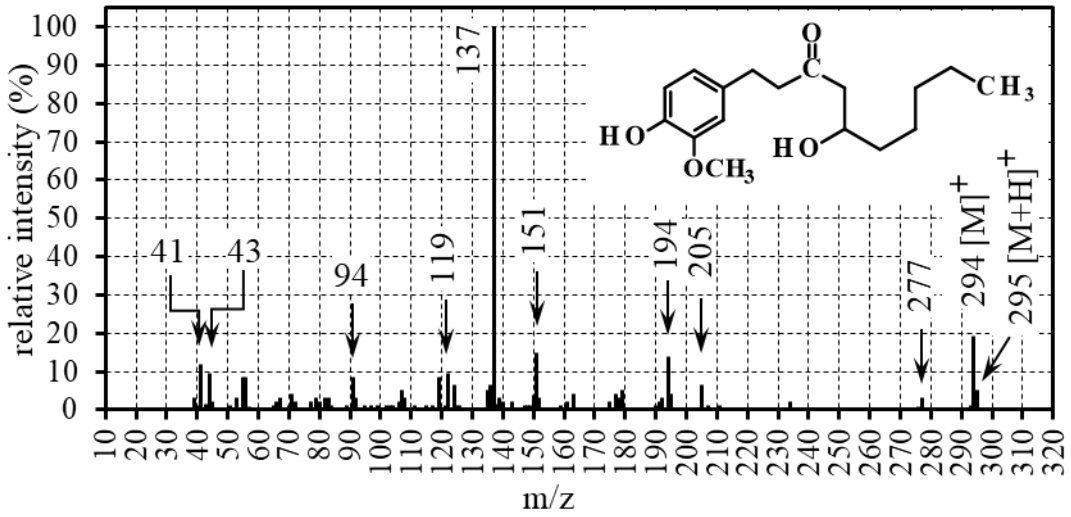



**Fig. 241 6-gingerol CAS 23513-14-6 (MS EI, 25 eV – MoNa)**

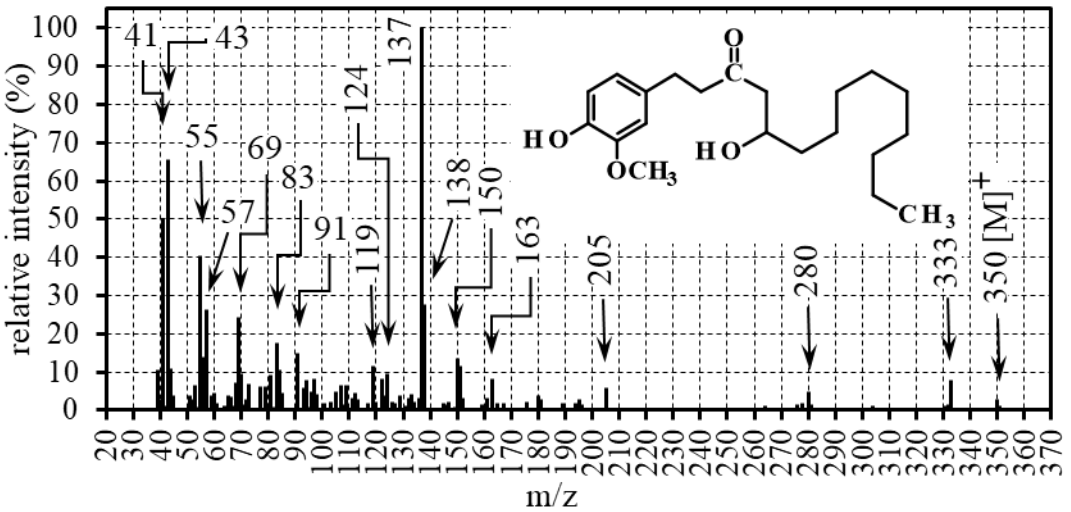



**Fig. 242 10-gingerol CAS 23513 (MS – EI, 25 eV MoNa)**

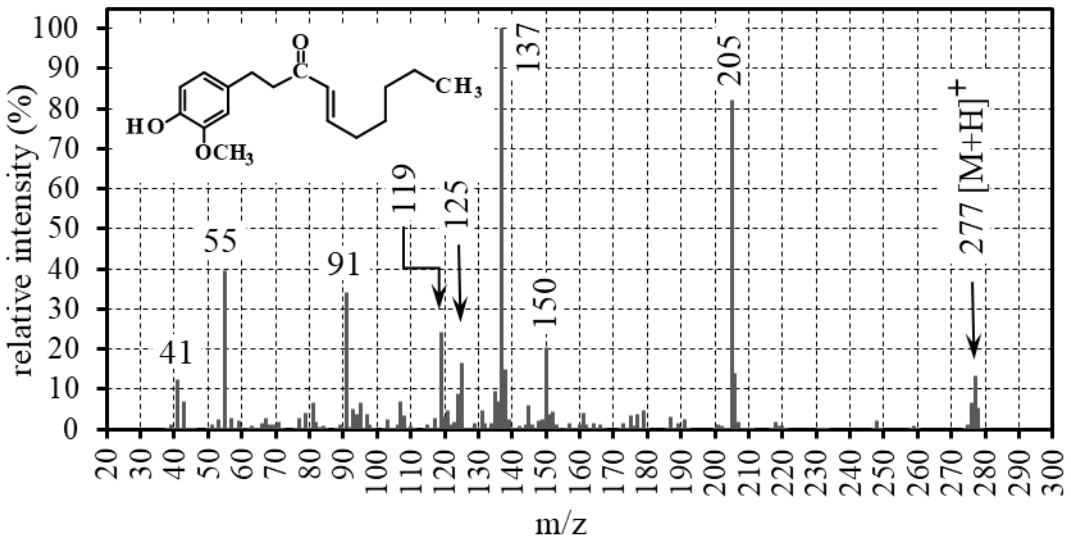



**Fig. 243 6-shogaol (MS positive, – EI, 26 eV – MoNa JP007241)**

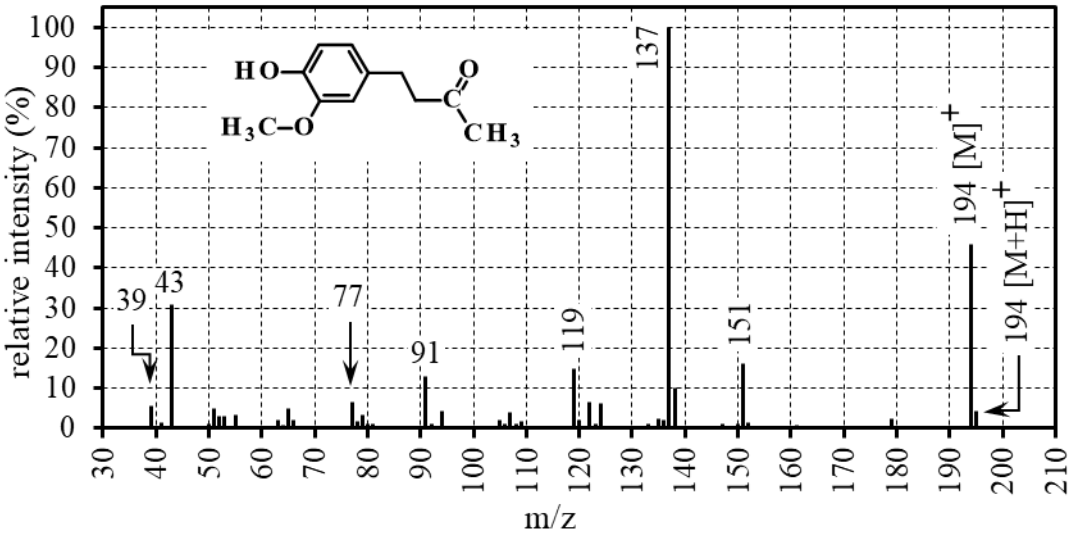



**Fig. 244 Zingerone (MS positive, EI, NIST 8502)**

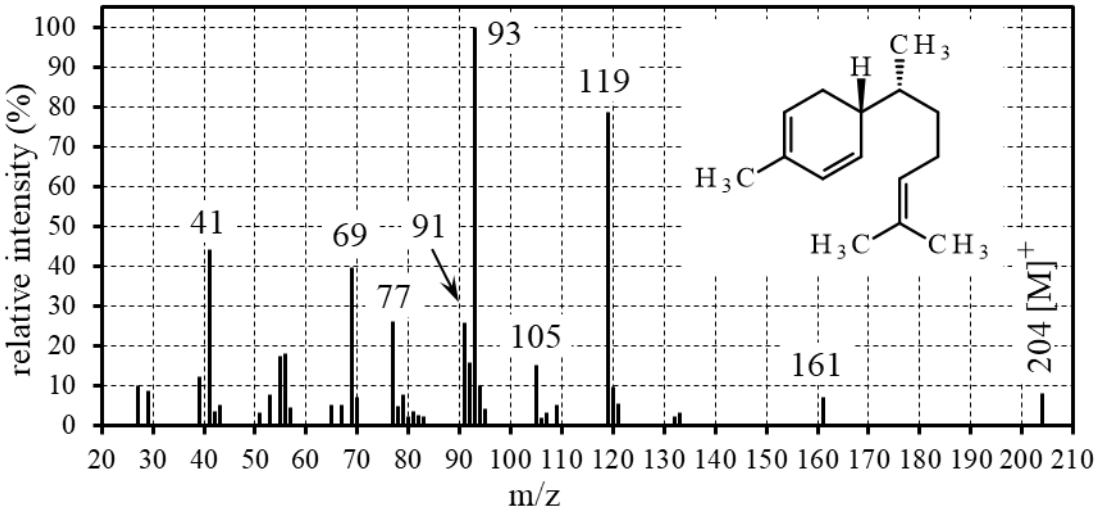



**Fig. 245 α-Zingiberene (MS positive, EI, NIST 70231)**

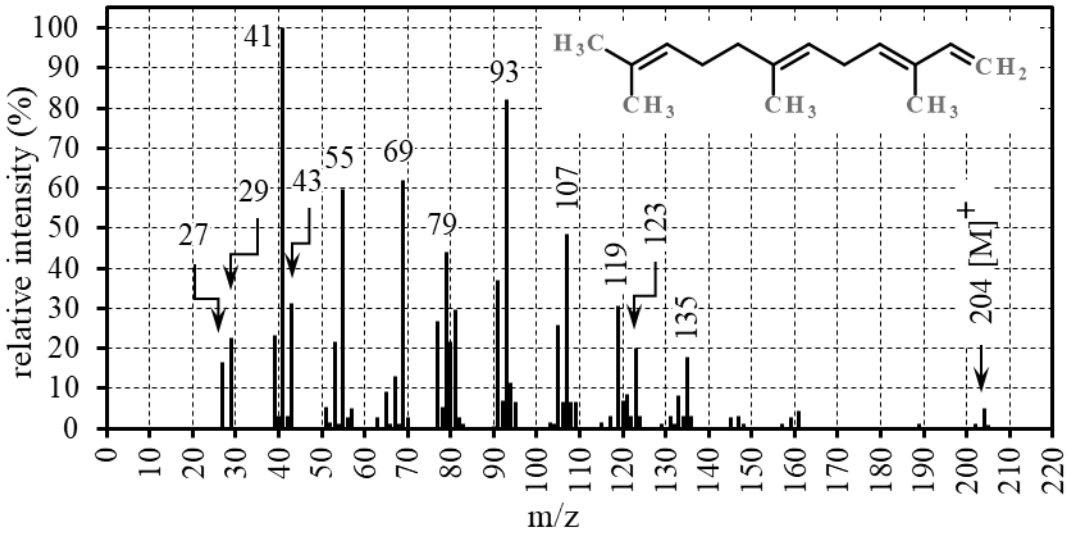



**Fig. 246 (E,E)-alpha-pharnesene (MS EI – NIST 9209)**

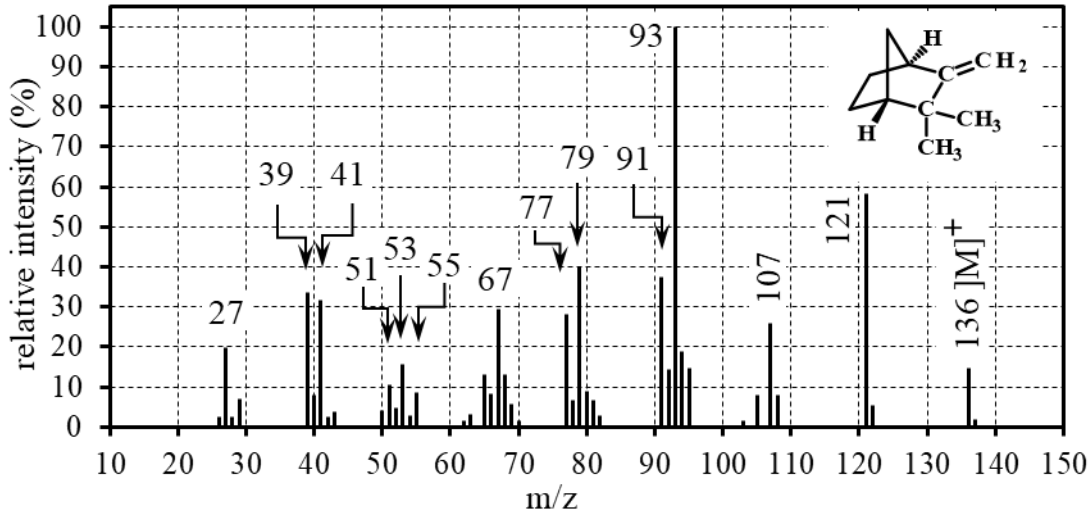



**Fig. 247 (E)-(+) camphene (MS EI – NIST 114297)**

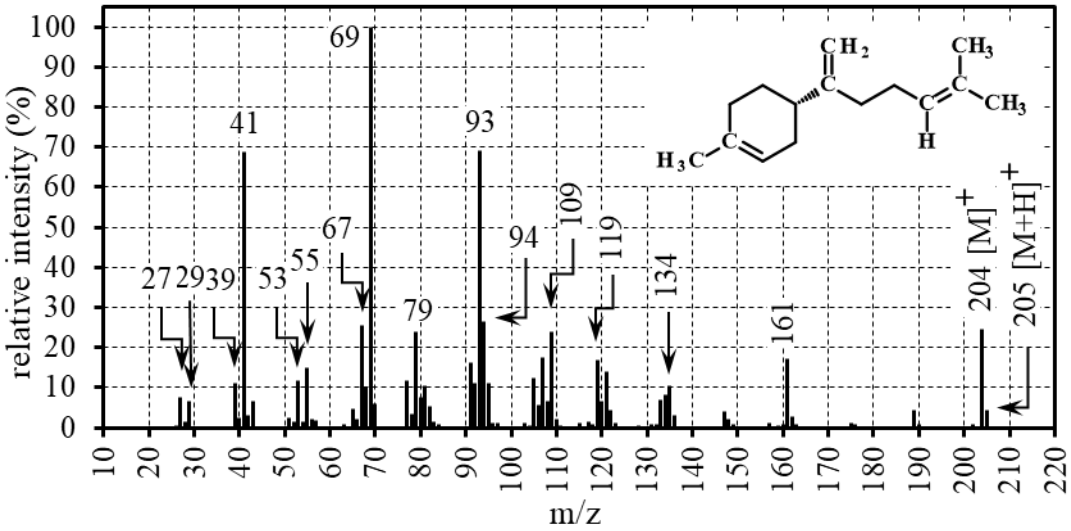



**Fig. 248 (E)-β-bisabolone (MS EI – NIST2919)**

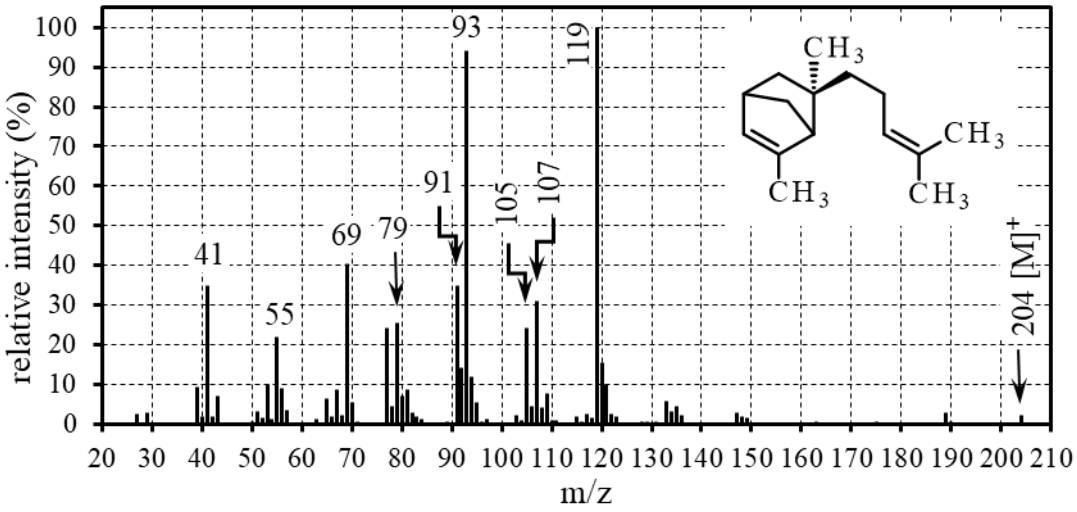



**Fig. 249 (E)-α-bergamotene (MS EI)**

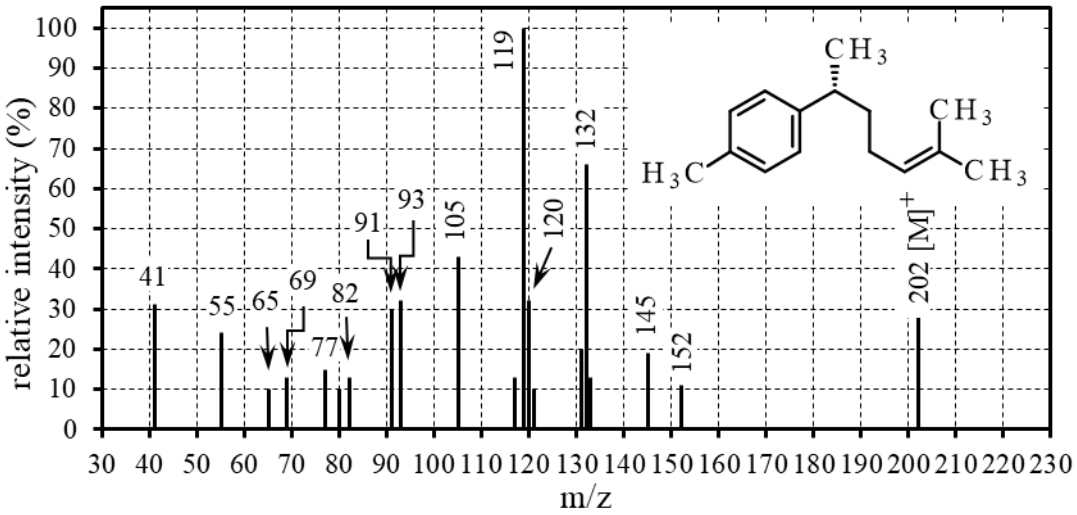



**Fig. 250 (R)-(-)-α-curcumene (MS EI)**

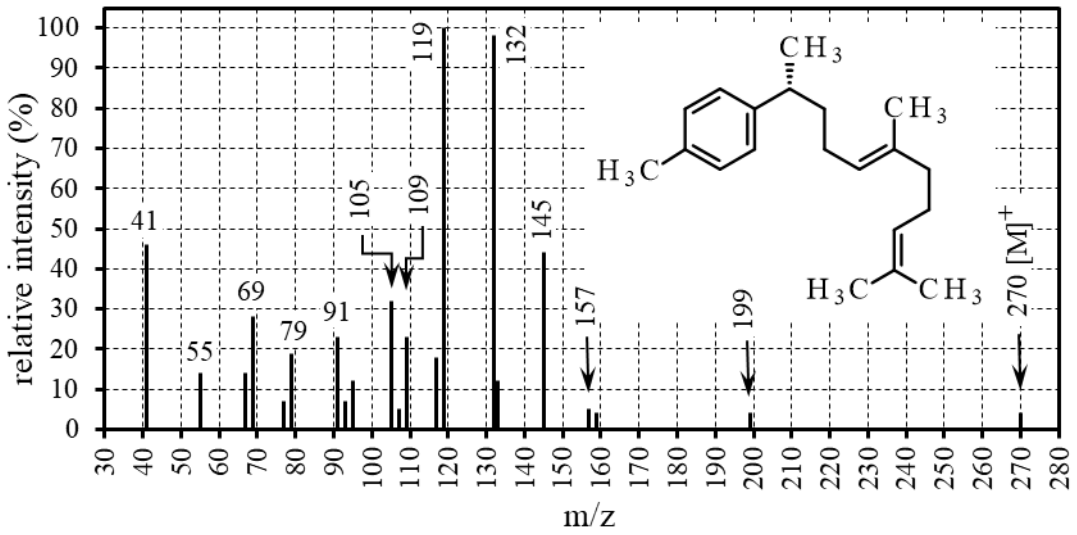



**Fig. 251 Pentenylcurcumene (MS EI)**

**Sources cited in application example 5.2**

[1] *P.Surain, N.K. Aggarwal*: *Zingiber officinale*: Clinical Aspects for Treatment of Candida infections.
**International Journal of Scientific and Research Publications 2019:9**(4), 561-573

[2] *M. Butu, M. Butnariu, S. Rodino, A. Butu*: Study of Zingiberene from *Lycopersicon esculentum* Fruit by Mass Spectrometry.
**Digest Journal of Nanomaterials and Biostructures 2014:9**(3), 935-941

[3] *G. Vernin*, *C. Parkanyi*: **Chemistry of Ginger** in **Ginger – The Genus *Zingiber***, *P.N. Ravindran* şi *K.N. Babu* editori, CRC Press, 2005, pag. 87-180
[ISBN: 0-415-32468-8]

[4] Spectral database **NIST**:
**https://webbook.nist.gov/cgi/inchi?ID=C19550879&Mask=200#Mass-Spec**

## 5.3 Control of photodegradation of metronidazole

Metronidazole is a 5-nitroimidazole chemotherapeutic agent used primarily against anaerobic bacteria. Because of its susceptibility to photodegradation, it has been the subject of publications to investigate natural sunlight-induced processes, to characterize the stability of the compound in common pharmaceutical formulations, and to monitor metronidazole-containing products that may become environmental pollutants [1,3]. The effect of gamma radiation on the transformations of this compound has also been studied [2].

Samples in different aqueous media exposed to ultraviolet radiation (xenon lamp with a power of 500 W/m$^2$) with a wavelength above 290 nm (spectrum corresponding to solar radiation) were analyzed by liquid chromatography (HPLC) and mass spectrometry [3].

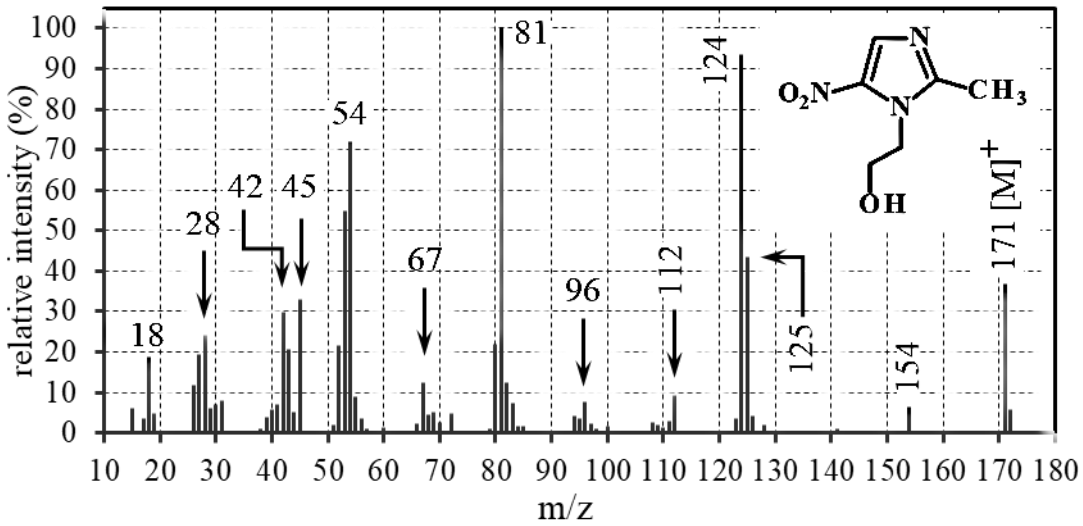



**Fig. 252 Mass spectrum of metronidazole (EI ionization) reconstructed from digitized spectrum from SDBS database:
mhttps://sdbs.db.aist.go.jp/sdbs/cgi-bin/direct_frame_top.cgi**

Figure 252 shows the mass spectrum of the metronidazole standard obtained by electron flow (EI) ionization at 70 eV. The advanced fragmentation is due to the energetic nature of the ionization process; therefore, electrospray ionization (ESI) was preferred, as ionization method that provides a finer fragmentation of the primary ion. Photodegradation studies [3] were based on liquid chromatography with hydrophobic stationary phase ($C_{18}$ column, 2.1x50 mm, particle size 1.7 μm, mobile phase: variable mixture of water and acetonitrile). To obtain the final chromatographic signal ($MS^2$), the selected molecular ion (precursor ion m/z 171) was bombarded with argon atoms providing a collision energy between 5 and 20 eV.

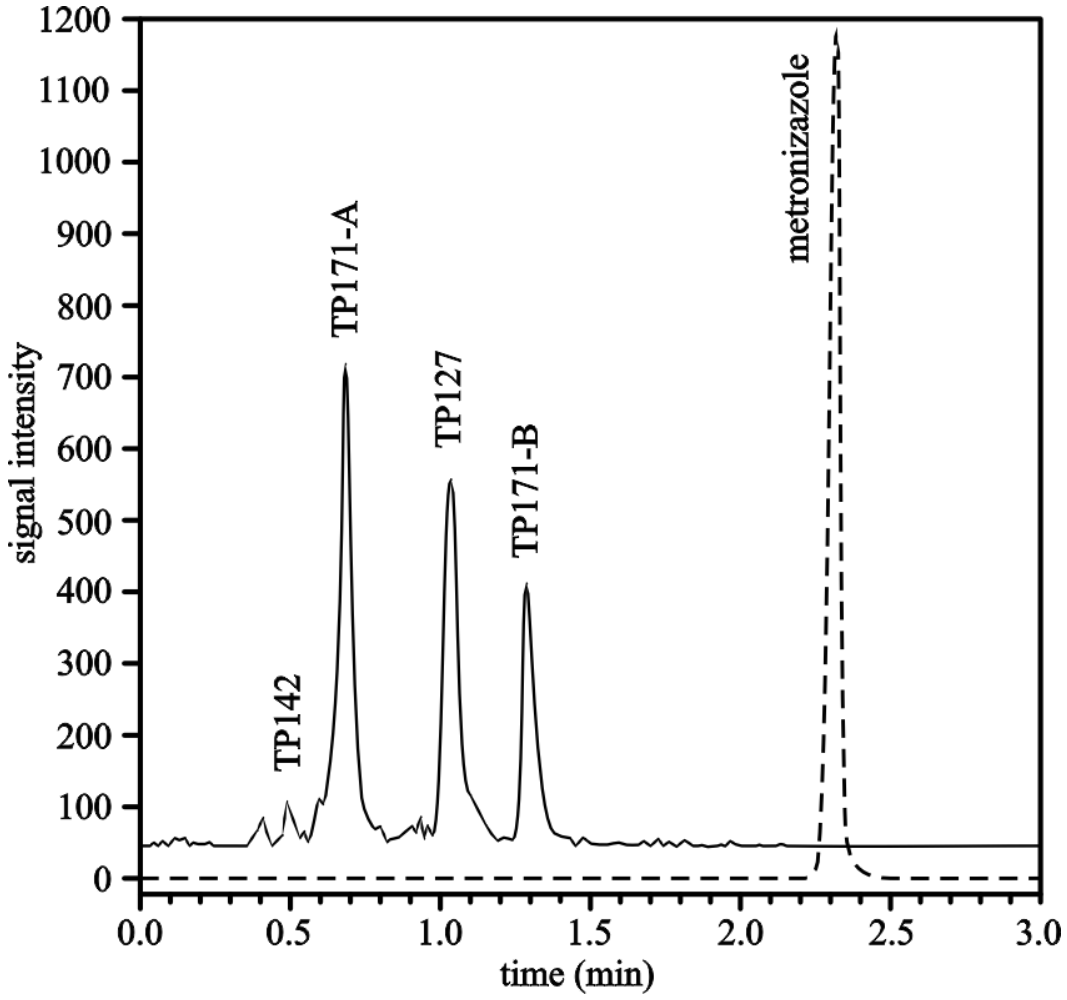



**Fig. 253 Chromatogram of metronidazole and its photochemical degradation products (reconstruction based on [3])**

Figure 253 shows the chromatographic signals of the photolysis products (designated as **TP142**, **TP171-A**, **TP127**, and **TP171-B**) and the metronidazole standard signal. The $MS^2$ mass spectra, recorded for both the metronidazole standard and photoproducts, are shown in Figures 254 **(a)-(d)** together with the assignment of the signals to the structures of the ionized fragments.

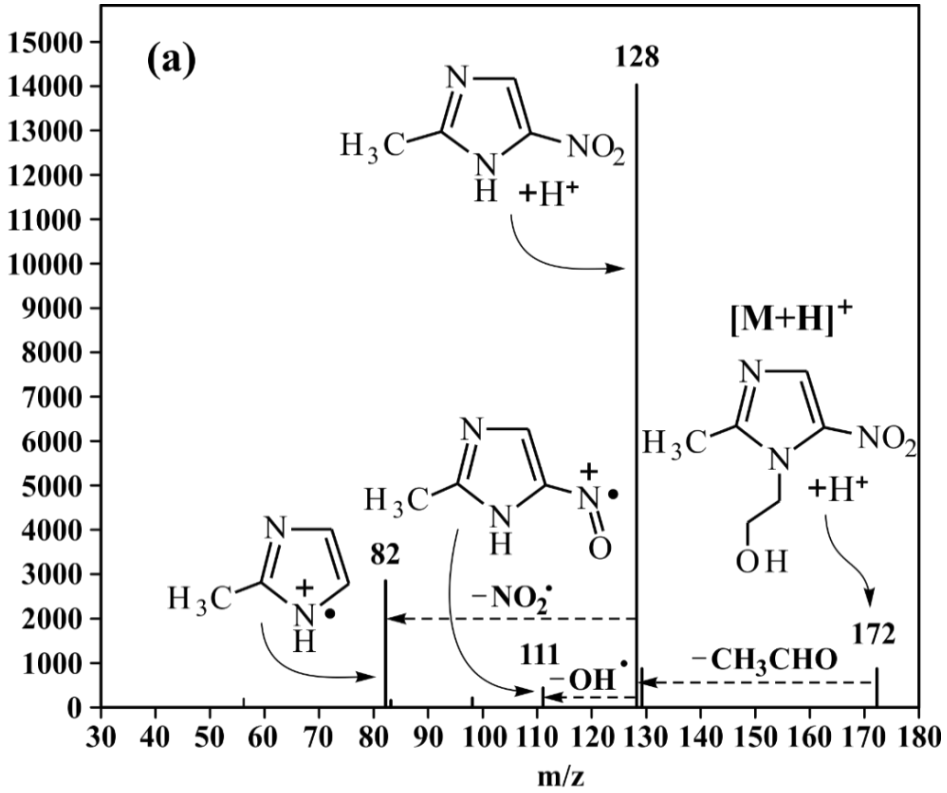



**Fig. 254 (a) ESI $MS^2$ spectrum of metronidazole**

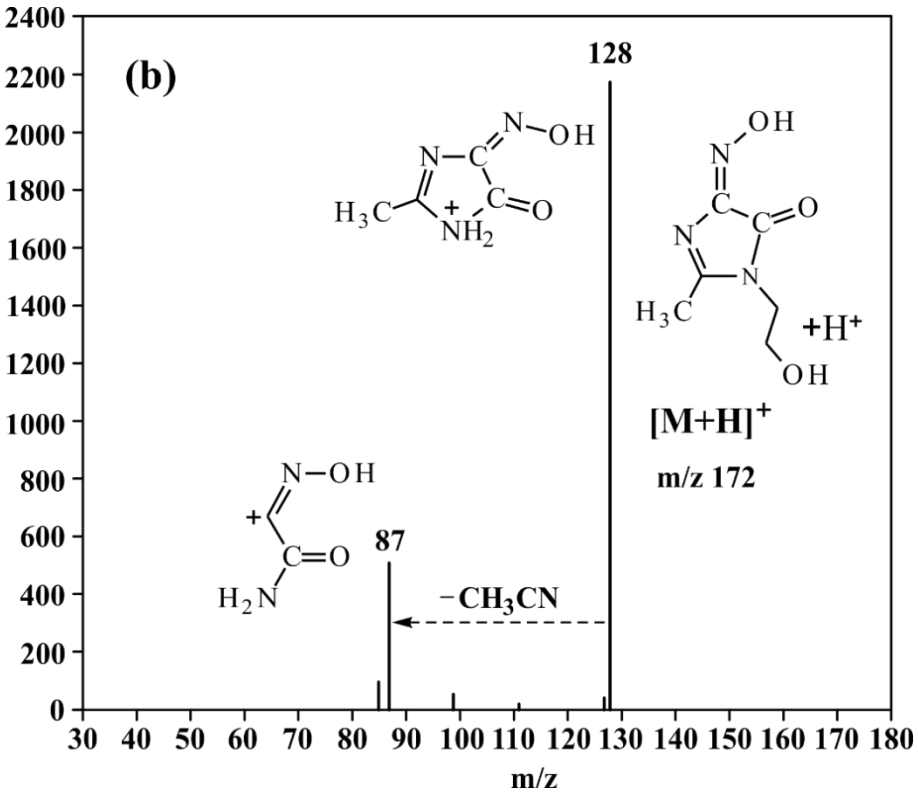



**Fig. 254 (b) ESI $MS^2$ spectrum of photolysis product TP171-A**

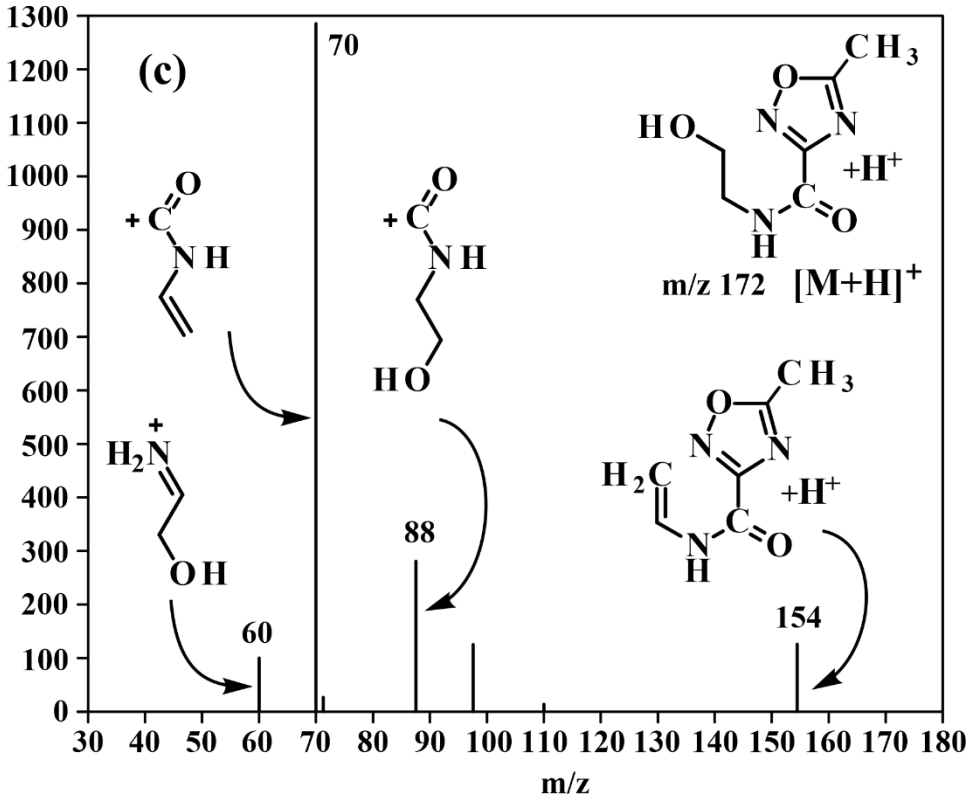



**Fig. 254 (c) ESI $MS^2$ spectrum of photolysis product TP171-B**

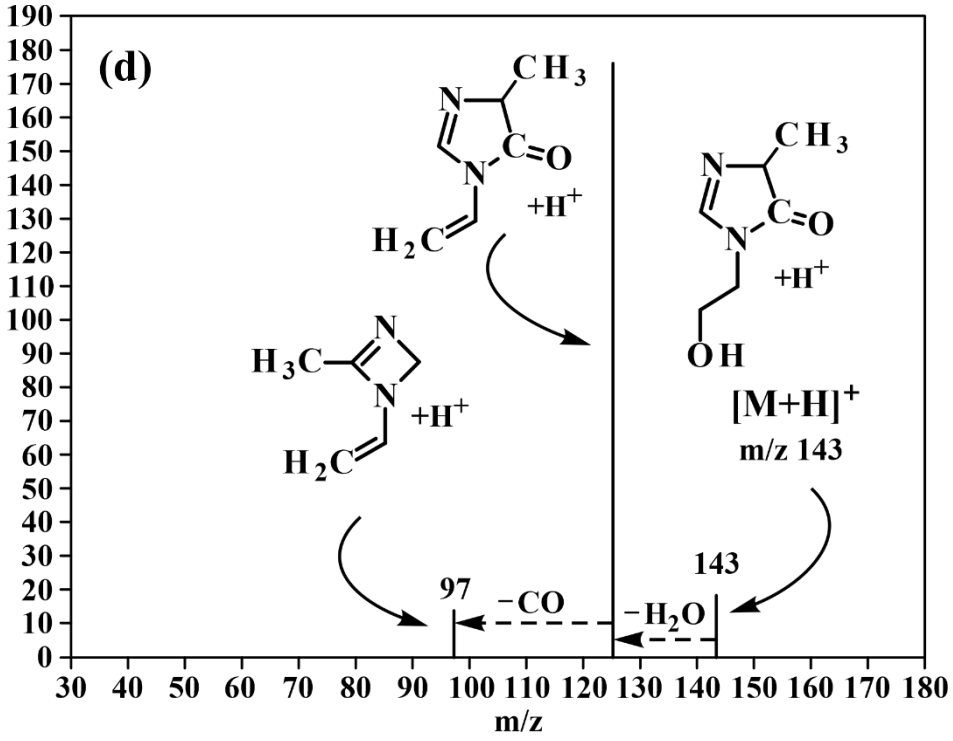



**Fig. 254 (d) ESI $MS^2$ spectrum of photolysis product TP142**

Based on the fragmentogram of the photolysis products, the authors deduced their chemical structures (except for the photoproduct designated **TP127**) (Figure 255).

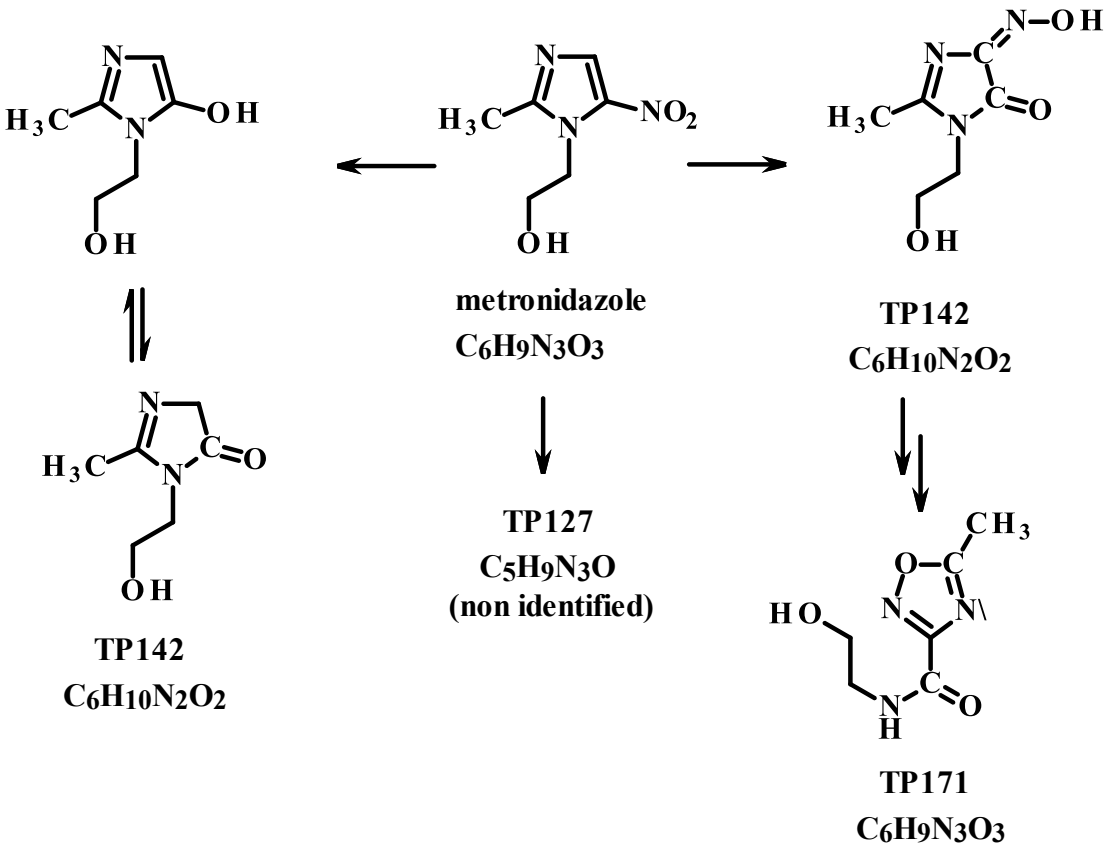



**Fig. 255 Structures of metronidazole photolysis products**

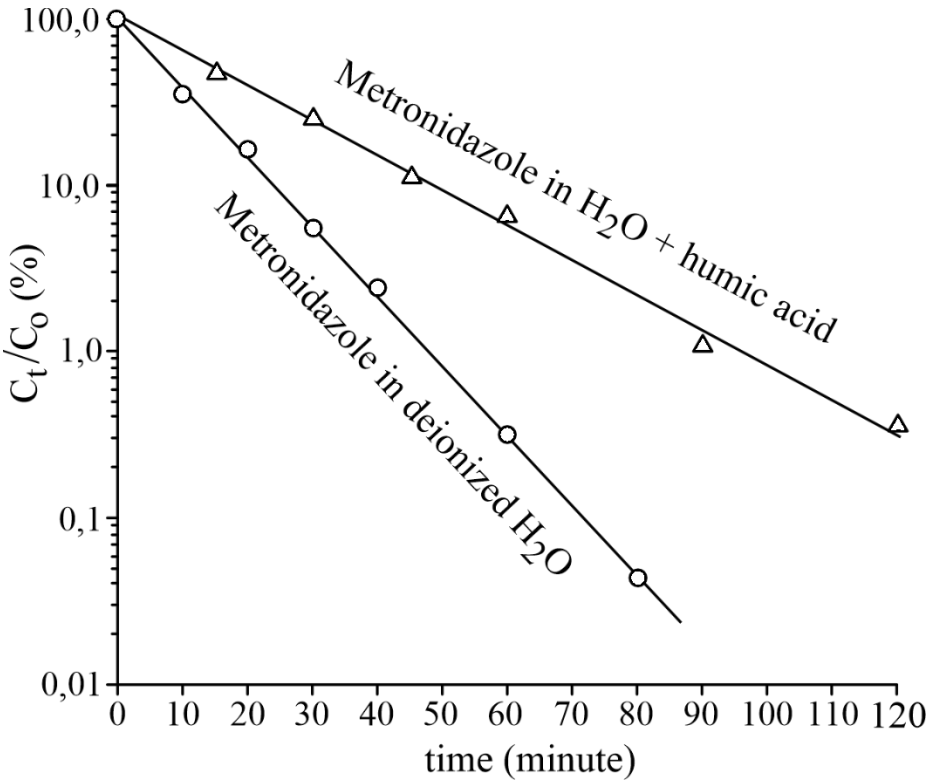



**Fig. 256 Kinetic curves of photolysis in deionized water with and without addition of humic acid ($C_0$ = 10 mg/L) (according to [3])**

In terms of the time course of the photochemical transformation, the reaction was found to be of pseudo-monomolecular order for both the deionized water medium and in the presence of humic acid (Figure 256). The presence of humic acid significantly decreases the rate-constant of the process ($9.2 \cdot 10^{-2}$ $min^{-1}$ in deionized water in comparation with $4.5 \cdot 10^{-2}$ $min^{-1}$ in water solution of humic acid).

**Sources cited in application example 5.3**

[1] *A.E.I. Karim, K.E. Ibrahim, M.E. Adam*: Studies on the Photochemical Decomposition of Metronidazole.
**Int. J. Pharm., 1991:76**(3), 261-264

[2] *D.E. Moore, B.J. Wilkins*: Common Products from Gamma-Radiolysis and Ultraviolet Photolysis of Metronidazole.
**Int. J. Radiat. Appl. Instrum. Part C. Radiat. Phys. Chem., 1990:36**(4), 547-550

[3] *L. Tong, S. Pérez, C. Gonçalves, F. Alpendurada, Y. Wang, D. Barceló*: Kinetic and Mechanistic Studies of the Photolysis of Metronidazole in Simulated Aqueous Environmental Matrices Using a Mass Spectrometric Approach.
**Anal. Bioanal. Chem., 2011:399**(1), 421-428

## 5.4 Detection and quantification of illicit stimulants in sport

Various performance-enhancing drugs are often used illicitly in sport competitions. Their detection, identification and quantification in biological samples are a real professional challenge. Most analytical control methods are based on chromatographic variants, but to increase the certainty of chemical identification and/or isomer differentiation, chromatographic separation with thermionic detection is coupled with mass spectrometric detection.

Without going into all the technical details, here is an example of a procedure studied in the literature and developed for the differential analysis of several stimulants [1]. Thermo-ionic and mass spectrometric detection methods were compared. One technical problem was the different pressure conditions inside the two detectors: the thermos-ionic detector operates at atmospheric pressure, while the mass spectrometer requires a high vacuum, so capillary chromatography columns of different lengths were used in the two modes, chosen that their hydraulic resistance to compensate for the pressure difference that is characteristic for these detectors.

Figure 257 **(A)** shows the gas chromatogram of the mixture containing heptaminol, amphetamine, methamphetamine, N,N-dimethylamphetamine, nicotine, ephedrine, phenmethazine, nikethamide, pentylentetrazole, phencamfetamine and caffeine, recording with a 19-meter capillary column and a thermo-ionic detector (NPD – Nitrogen Phosphor Detector) commonly used in the chromatographic analysis of nitrogen compounds. Figure 257 **(B)** shows the GC-MS detection of an identical mixture used with a capillary column with the same characteristics as the previous one, but 24 m long.

At these column lengths the difference between the optimum detector pressures is compensated for, so that the retention times are satisfactorily reproduced.

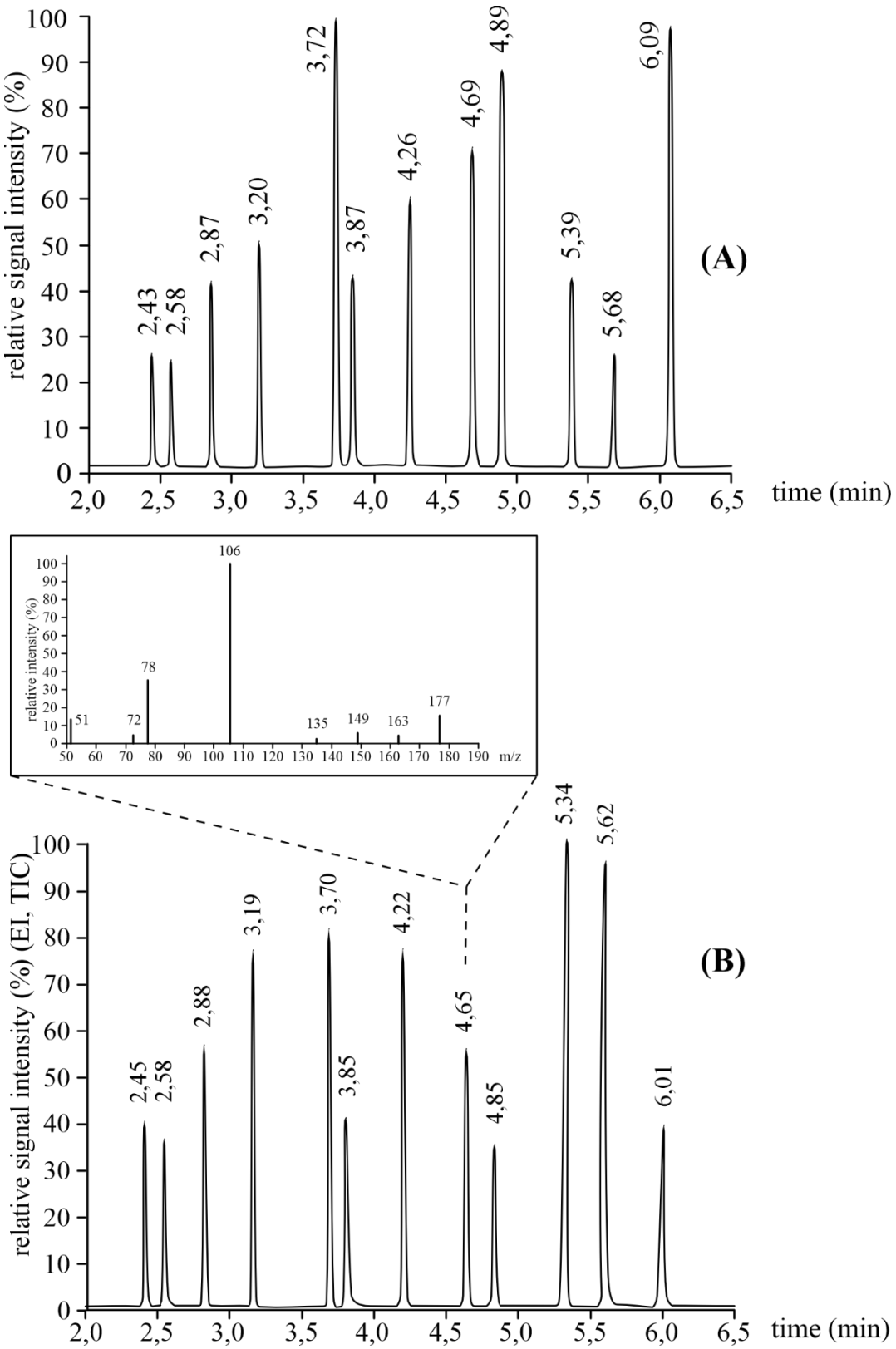



**Fig. 257 Gas chromatographic separation of stimulant substances (A) with NPD detection; (B) with MS detection (EI, TIC) (recreated from [1])**

The chromatogram in Figure 257 **(B)** was obtained in the total ionic detection (TIC) mode, which means that the chromatogram signal is the sum of the abundances of all ionic signals. For example, the chromatogram signal of nikethamide at the retention time of 4.65 minutes is the sum of the signals in the mass spectrum of this compound (Figure 258). The chromatographic peaks with retention times of 5.68 minutes (in case of PND detection) and 5.62 minutes (in case of MS-TIC detection with EI ionization) correspond to diisopropyl-amine used as internal standard.

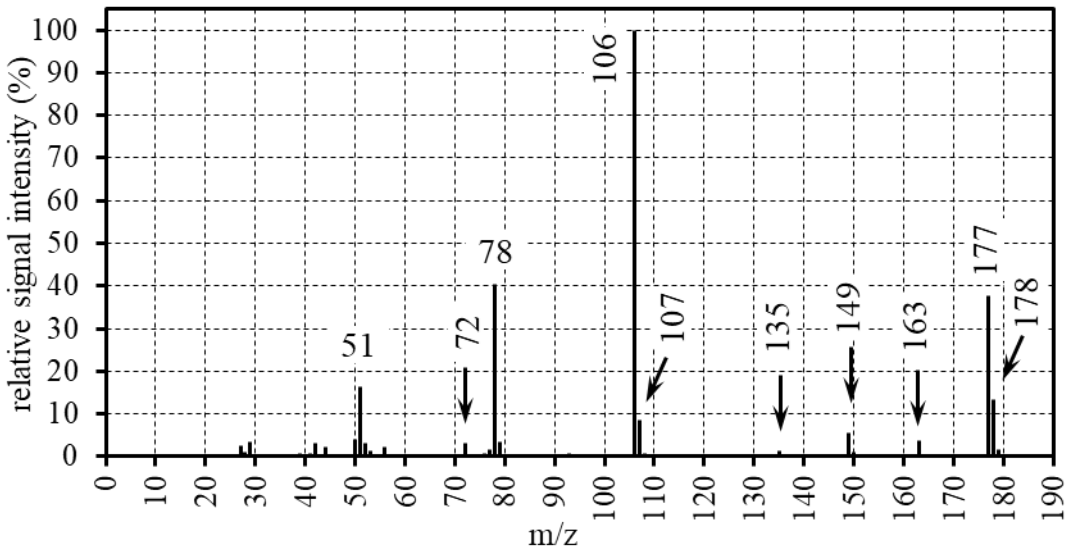



**Fig. 258 Mass spectrum of nikethamide (EI ionization, reconstructed from NIST data, spectrum no. 291418)**

**Table 16 -Electron impact ionization (EI) ion fragments suitable for the identification and quantitative analysis of various stimulants [1]**

| Active stimulant compound | Ionic fragments for analysis | | | Active stimulant compound | Ionic fragments for analysis | | |
|---|---|---|---|---|---|---|---|
| Amfepramone | 190 | 100 | 105 | Furfenorex | 138 | 91 | 81 |
| Amfetamine | 91 | 65 | 44 | p-hydroxyephedrine | 107 | 71 | 58 |
| Benzphetamine | 224 | 148 | 91 | Methylenedioxy-amphetamine | 138 | 77 | 44 |
| Cathine (*D*-norpseudo-ephedrine) | 107 | 105 | 44 | Methylenedioxy-metamphetamine | 193 | 135 | 58 |
| Cocaine | 198 | 182 | 105 | Methylamphetamine | 134 | 91 | 58 |
| Chlorphentermine | 125 | 107 | 58 | Methylephedrine | 105 | 77 | 72 |
| Dimethyl-amphetamine | 91 | 72 | 65 | Methylphenidate | 91 | 84 | 56 |
| Ephedrine | 105 | 77 | 58 | Nikethamide | 177 | 106 | 78 |
| Ethylamfetamine | 148 | 91 | 72 | Phendimetrazine | 176 | 85 | 57 |
| Etilefrine | 121 | 77 | 58 | Phenmetrazină | 177 | 77 | 71 |
| Fencamfamin | 186 | 115 | 98 | Phentermină | 134 | 91 | 58 |
| Fenfluramine | 216 | 159 | 72 | Strychnine | 334 | 319 | 306 |
| Fenproporex | 97 | 92 | 57 | Tuaminoheptane | 100 | 55 | 44 |

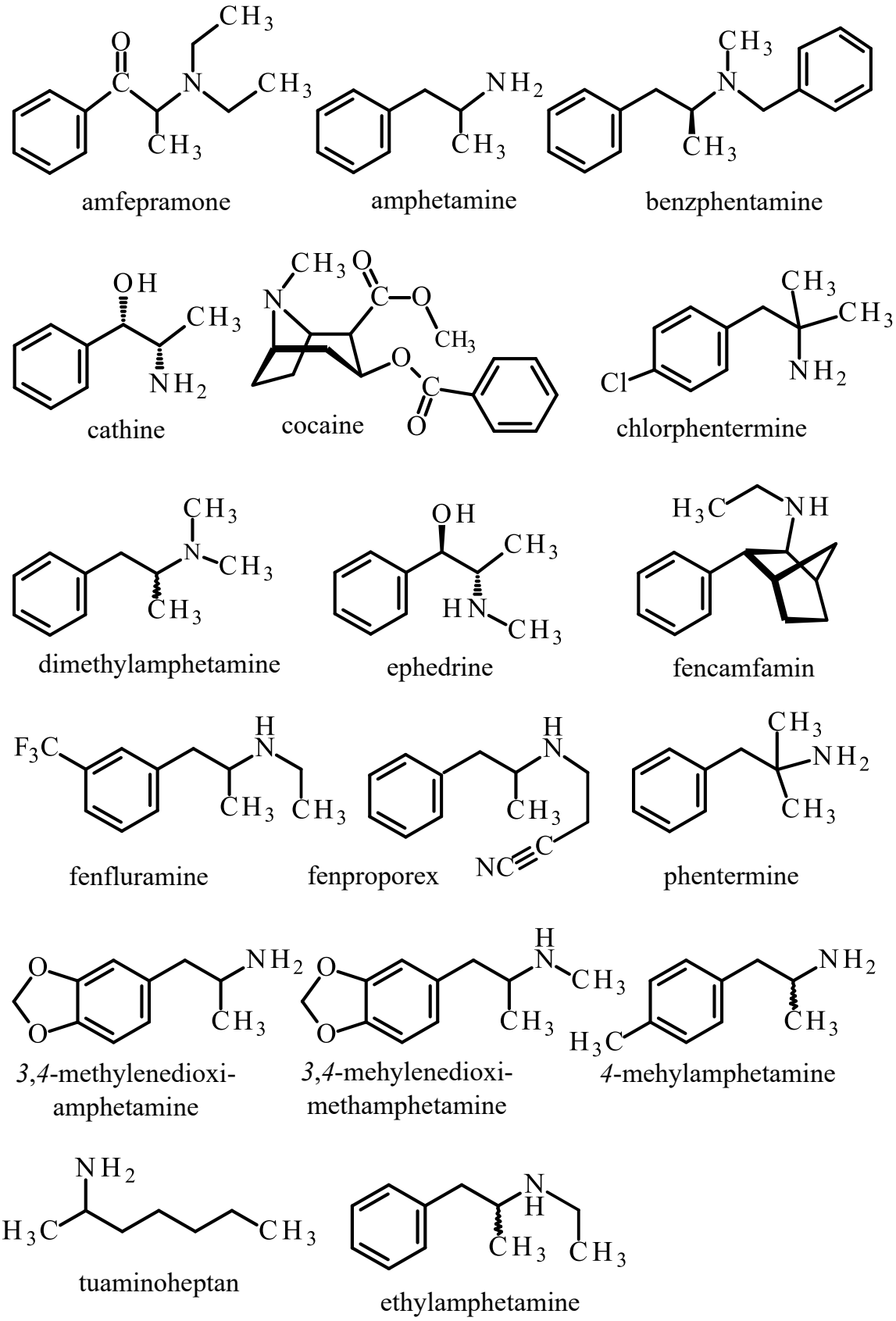



**Fig. 259 Chemical structures of the stimulants in Table 16**

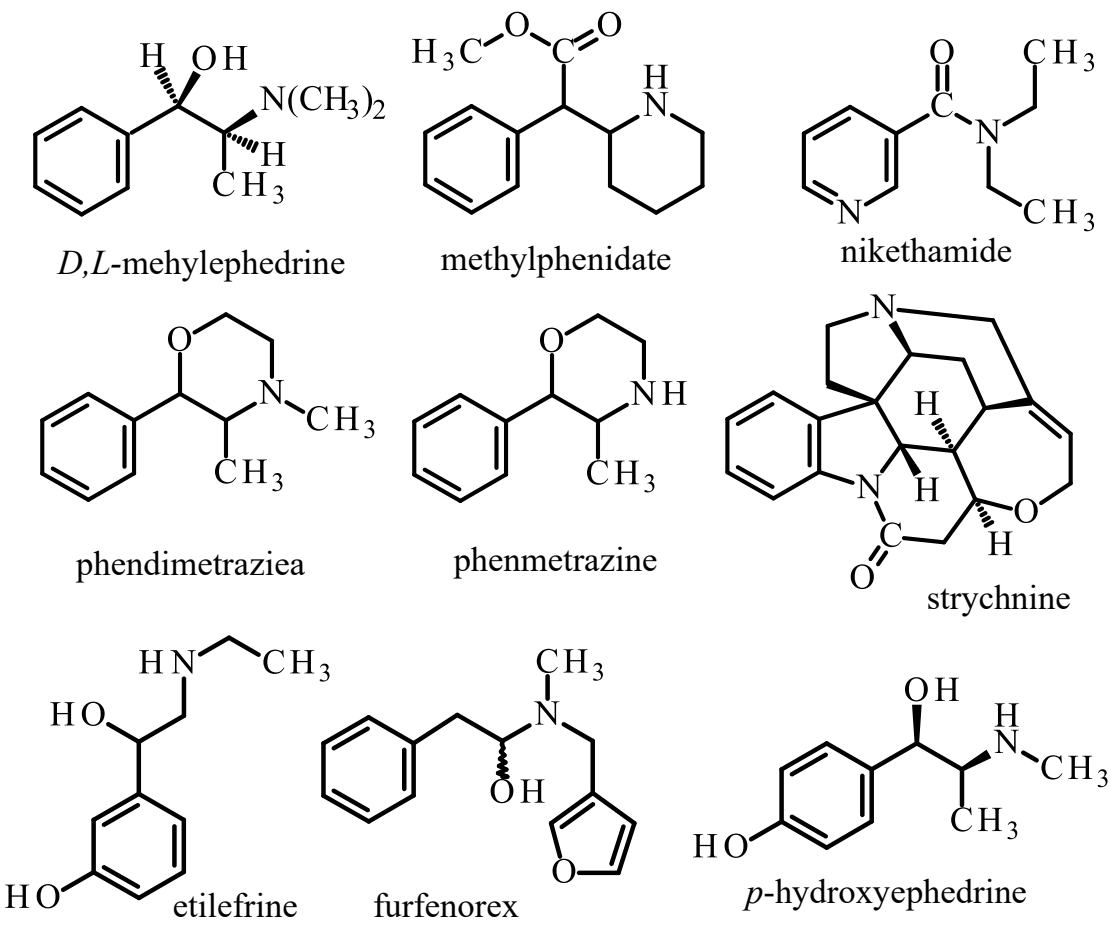



**Fig. 259 Chemical structures of the stimulants in Table 16 (continued)**

To increase the confidence of identifying stimulants in established dosage forms, three spectral signals were proposed for 26 representatives under EI ionization conditions (Table 16 and Figure 259).

The choice of electron impact ionization for stimulants is justified by the fact that established databases contain many spectra recorded with this ionization mode, facilitating reliable identification of compounds. On the other hand, electron impact ionization is a drastic process that often leads to advanced fragmentation of the primary molecules. Other ionization methods, some of which are more conservative, produce more limited fragmentation resulting in significantly different mass spectra that can provide an additional level of confidence in confirming analyte identity.

As an example, Figure 260 compares mass spectra of methamphetamine recorded with electron impact ionization (Figure 260 **(a)**) and chemical impact ionization with methane (Figure 260 **(b)**) and ammonia (Figure 260 **(c)**) as reactant gases. Upon chemical ionization, the signal of the molecular ion (protonated) is intense, while with electron impact ionization, the molecular ion, which is fragmented, does not appear at all.

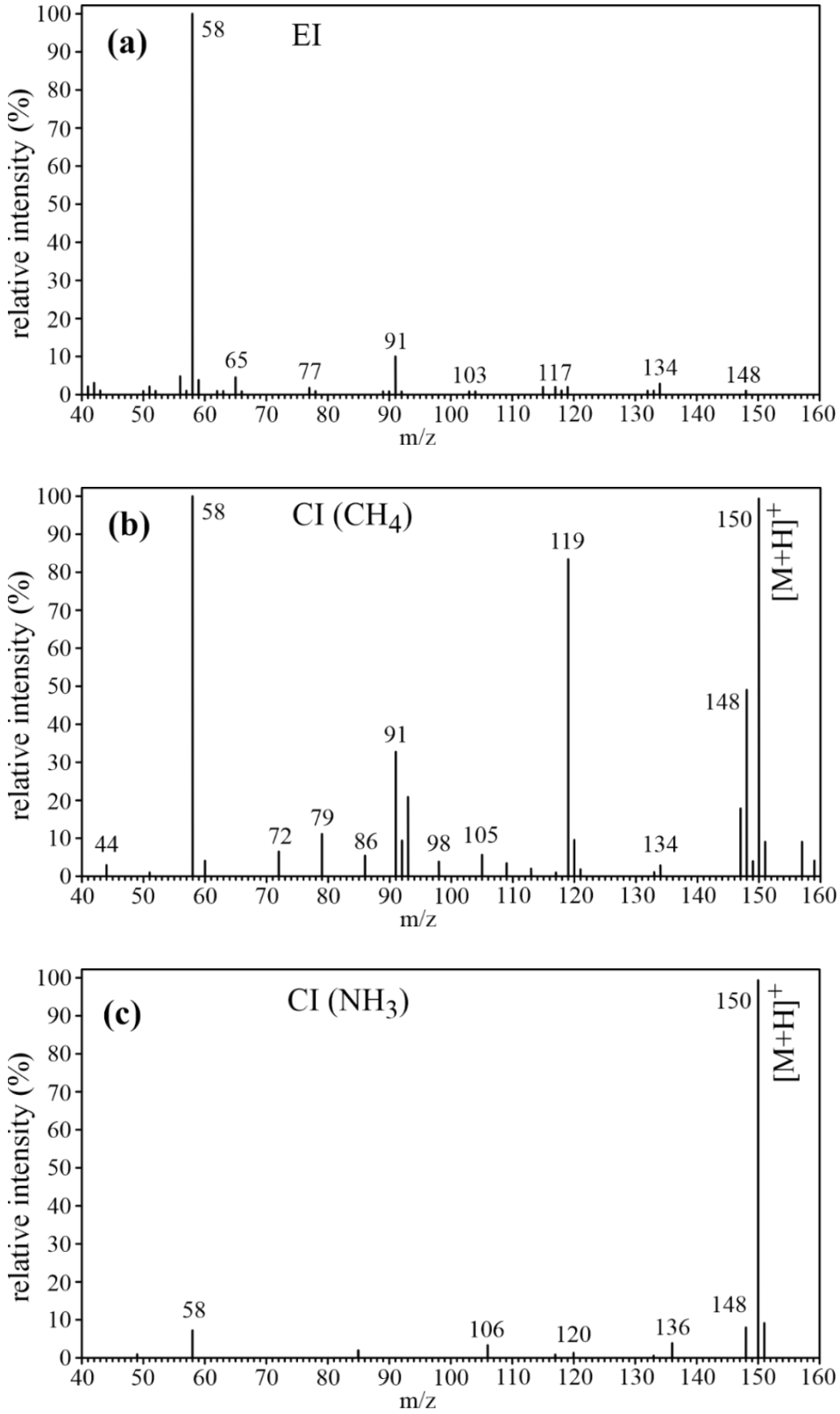



**Fig. 260 MS spectra of methamphetamine with electron impact ionization (a) and chemical impact with methane (b) and ammonia (c) (reconstructed from [1], p. 51).**

Figure 261 shows the mass spectrum of ephedrine obtained by electron flow ionization. Figure 262 shows the mass spectrum of cocaine for the same ionization mode. The fragmentation trajectories of ephedrine and cocaine under EI ionization conditions are shown in Figures 263 and 264.

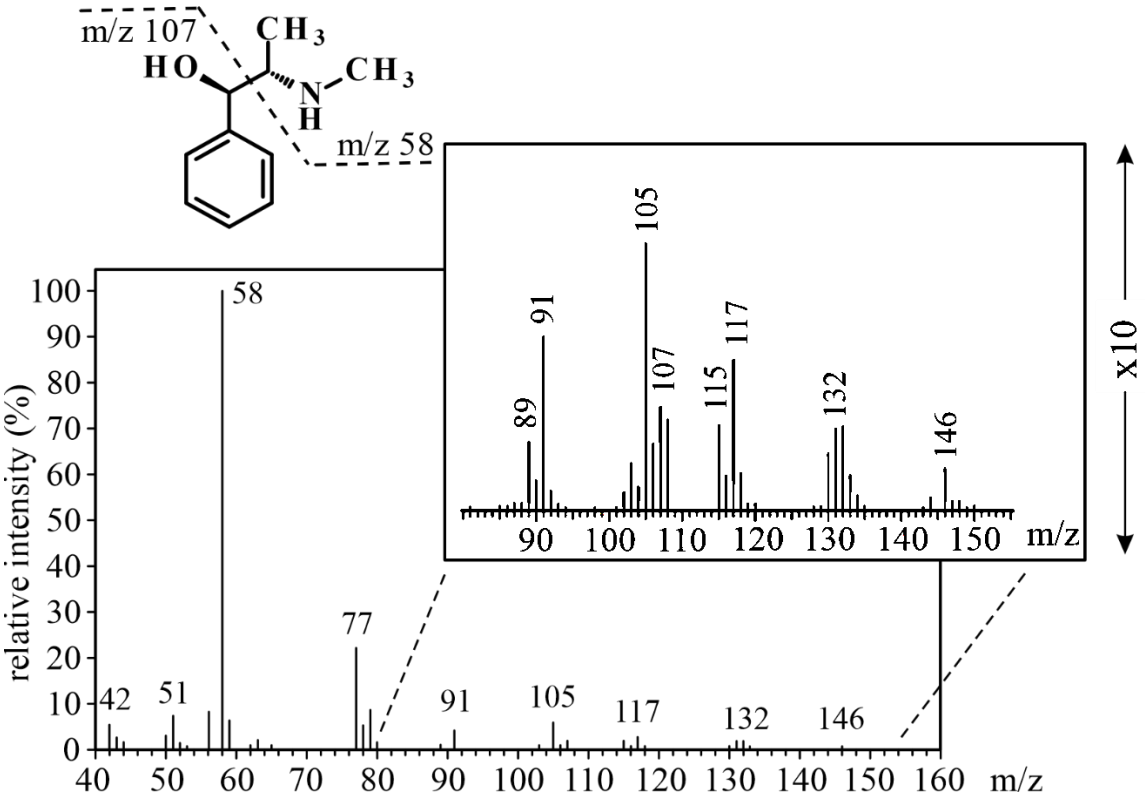



**Fig. 261 Mass spectrum (MS) of ephedrine (molecular mass 165 Da) (reconstructed from [1])**

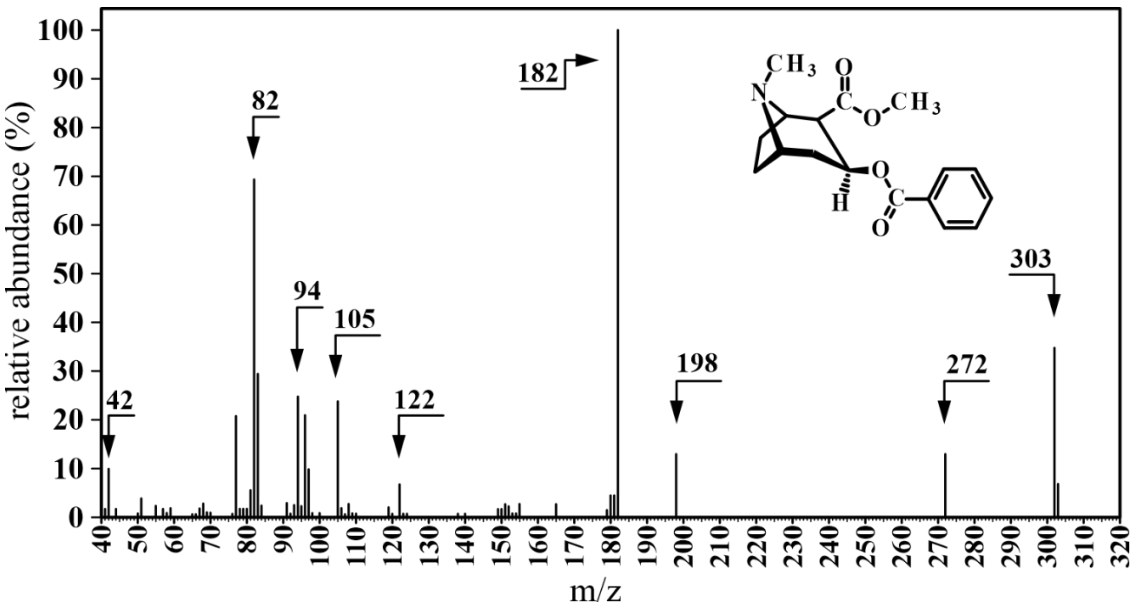



**Fig. 262 Mass spectrum of cocaine with electron impact ionization (EI) (reconstructed from [1,2])**

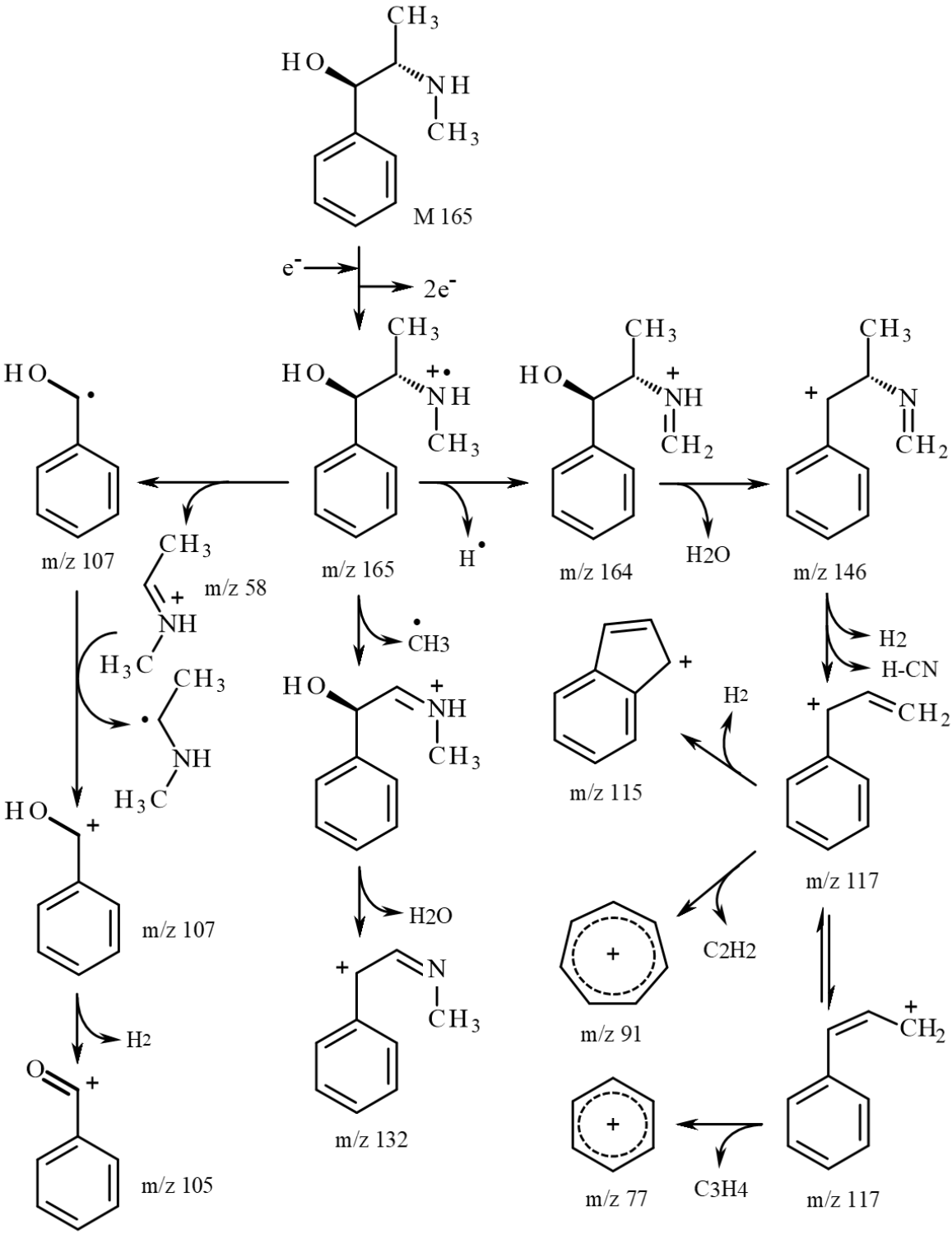



**Fig. 263 Mechanism of ephedrine fragmentation (electron flow impact ionization) (recreated according to [1] and [3])**

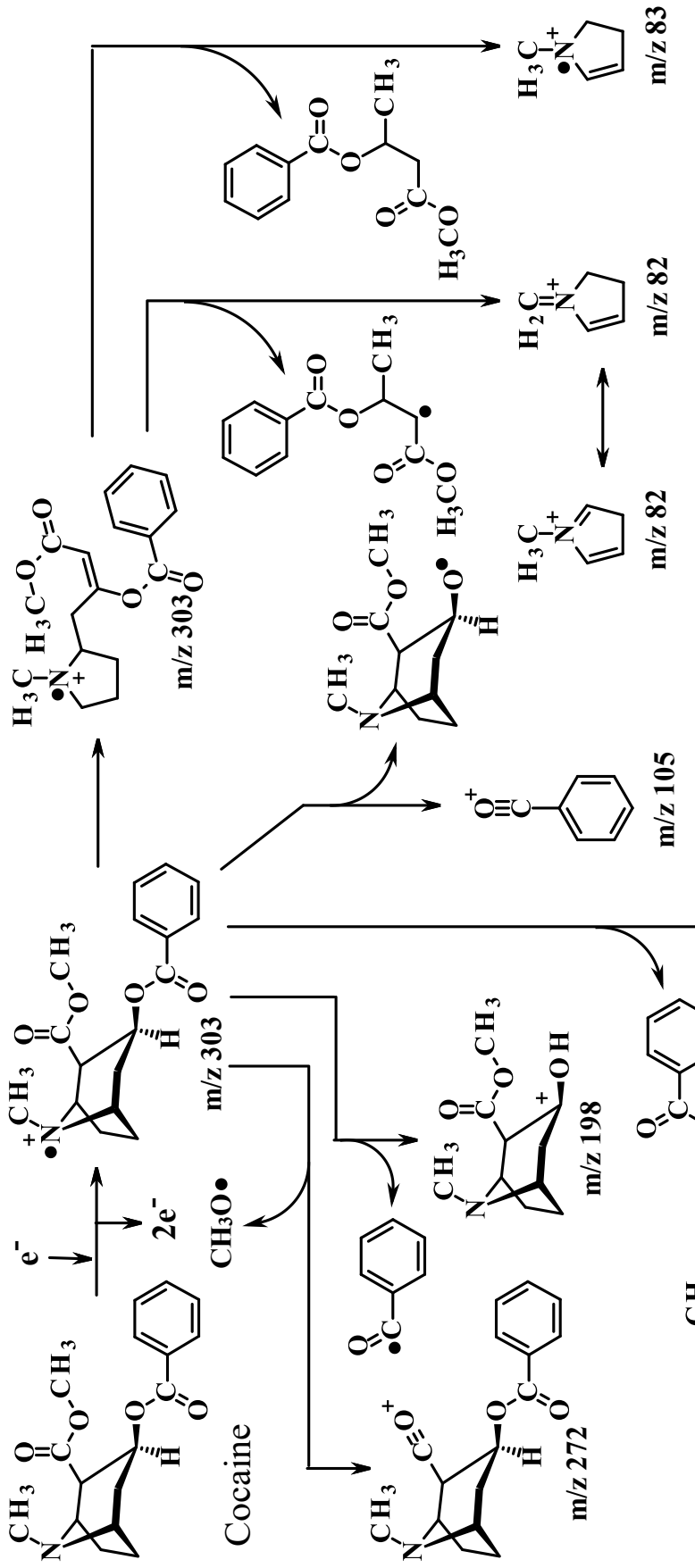



**Fig. 264**
**MS-EI fragmentation scheme of cocaine (reconstructed from [1] and [2])**

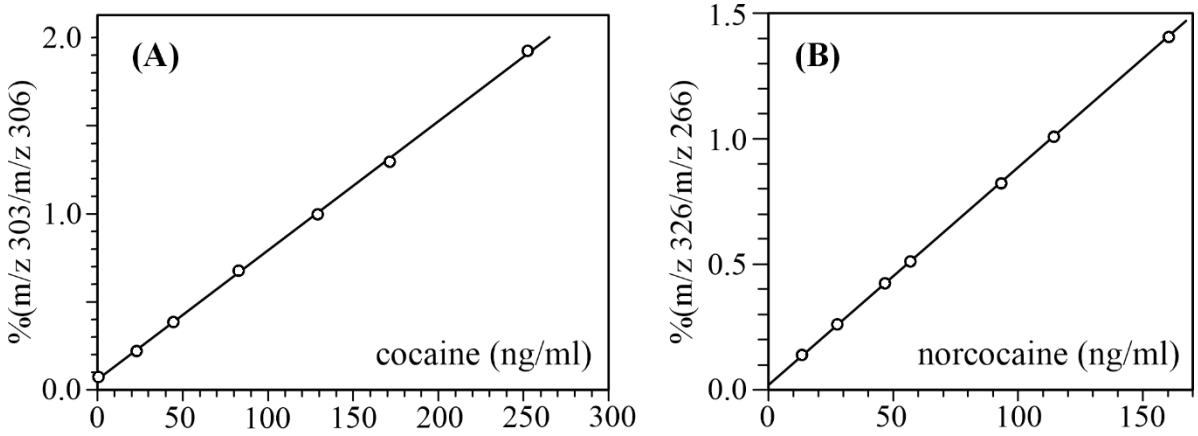



**Fig. 265 Determination of cocaine and norcocaine based on the ratio of MS signal intensities (figure adapted from [3]).**

The ratio of signal intensities associated with **m/z** 303 and 306 (for cocaine) and **m/z** 263 and 266 (for norcocaine) has been proposed and used for the quantitative determination of cocaine and norcocaine (the degradation and metabolic product of cocaine) [3]. For both substances, a linear response was confirmed for these drug concentrations between 0 - 255 ng/ml (for cocaine) and 0 - 160 ng/ml (for norcocaine) (Figure 265).

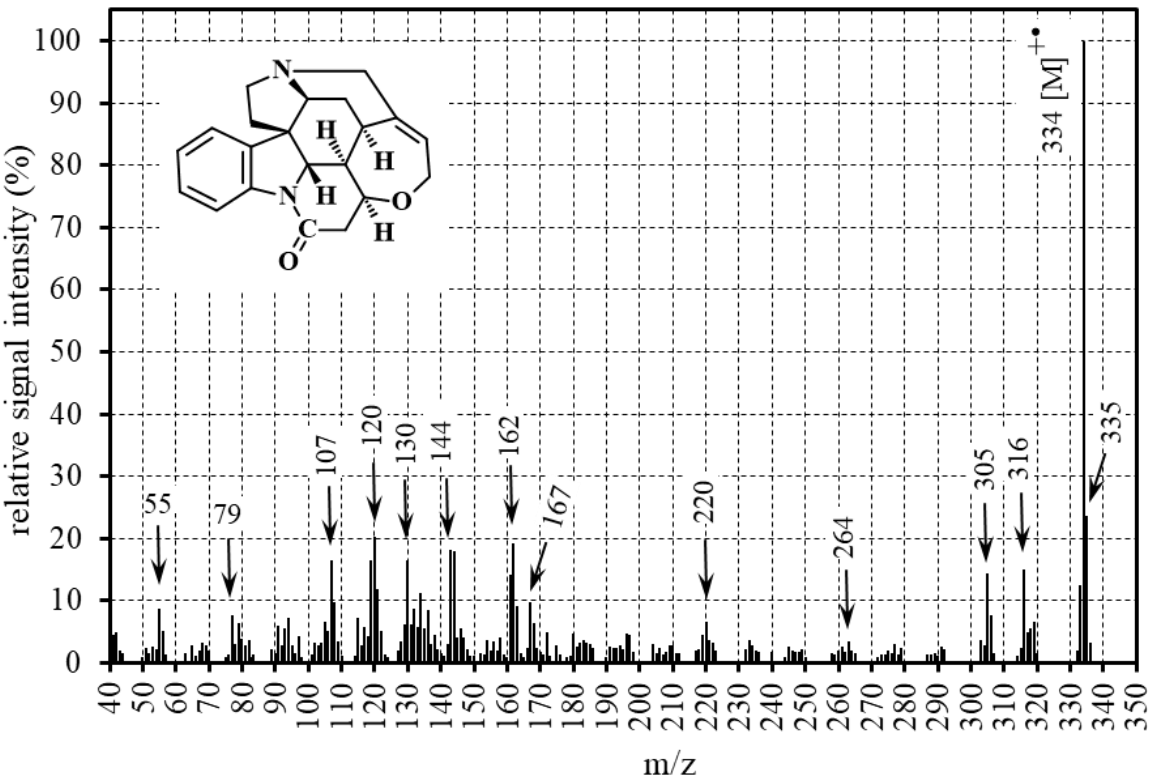



**Fig. 266 Mass spectrum (EI 75 eV ionization) and characteristic signals of strychnine base (reconstruction according to [5,6,7])**

A method for the identification and quantitative determination of strychnine recommends signals with **m/z** ratios of 334 and 130 in the spectrum (Figure 266) [8]. Indeed, in the mass spectrum of strychnine obtained by EI ionization (75 eV), the first two signals mentioned appear with remarkable intensities.

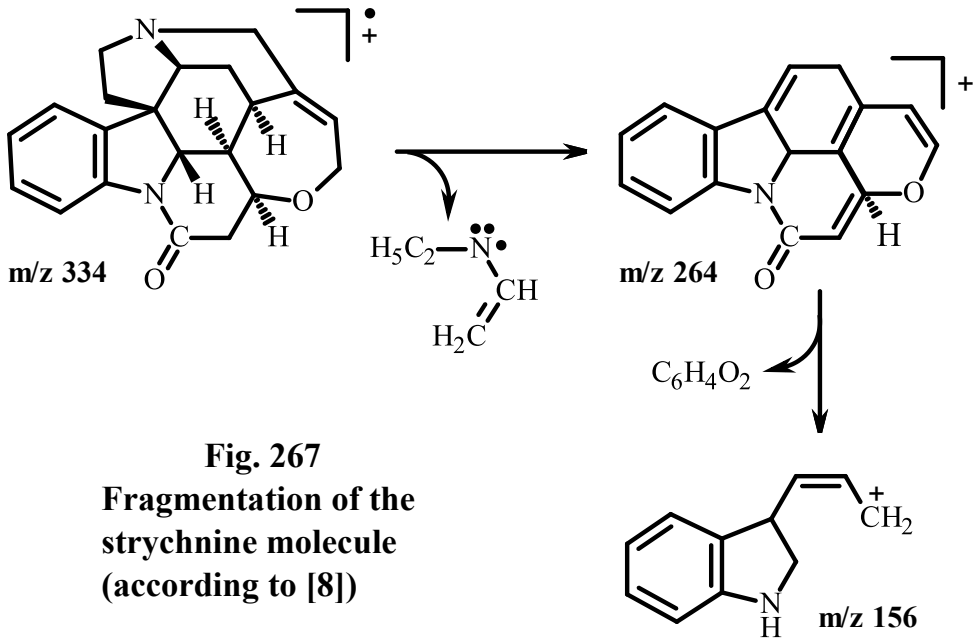



**Fig. 267**
**Fragmentation of the strychnine molecule (according to [8])**

In a publication, *J. Haneef* and coworkers [9] suggested a possible fragmentation pathway for strychnine (Figure 267) and proposed several ion signals in the $MS^2$ analysis of some stimuli (Table 17). The fragment-generating precursor ion was **$[M+H]^+$**.

**Table 17 Suggestion of $MS^2$ ion fragments for identification of various stimulants [9]**

| Stimulant | Molecular mass (Da) | Precursor ion $[M+H]^+$(m/z) | Secondary ions produced (m/z) |
|---|---|---|---|
| Amphetamine | 135,10480 | 136,2 | 119,2 ; 91,2 |
| MDA | 179,09463 | 108,2 | 163 ; 134,9 ;105 |
| MDMA | 193,11028 | 194,1 | 163,2 ; 105,1 |
| Strychnine | 334,16813 | 334 | 264 ; 184 ; 156 |
| Methylphenidate | 233,14158 | 234 | 174 ; 129 ; 84 ; 56 |

Another method uses tandem fragmentation ($MS^2$) of the analyte for the identification and quantification of some stimulants [4]. The preferred ionization is atmospheric pressure chemical ionization (**APCI**) with electrical discharge (corona effect). The collision energy for fragmentation, between 25 and 30 eV, is chosen to ensure complete fragmentation of the precursor ion. Table 18 lists some recommended technical details for the analysis of 18 ephedrine-related stimulants.

**Table 18 $MS^2$ signals recommended for the identification and quantification of ephedrine-related stimulants (from [4]) (relative abundance of ionic fragments in brackets)**

| Stimulant | Precursor ion $[M+H]^+$ (m/z) | Ionic fragments (m/z) |
|---|---|---|
| Amphetamine | 136 | 119(100) |
| Ephedrine | 166 | 148(100) |
| Ethyl amphetamine | 154 | 119(100) ; 91(12) |
| Fencamfamin (Euvitol) | 216 | 171(100) ; 159(10) ; 143(12) ; 129(32) |
| Phendimetrazine | 192 | 174(25) ; 159(6) ; 148(100) ; 147(90) ; 119(18) ; 100(14) ; 91(23) ; 86(6) ; 74(14) |
| Phenmetrazine | 178 | 160(100) ; 143(25) ; 134(70) ; 119(40) ; 117(20) ; 91(34) |
| Phentermine | 150 | 133(100) |
| Fenfluramine | 232 | 187(100) ; 159(28) |
| *3*,*4*-methylendioxy-amphetamine (MDA) | 180 | 163(100) |
| *3*,*4*-methylendioxy-N-ethyl-amphetamine (MDEA) | 208 | 163(100) |
| *3*,*4*-methylendioxy methamphetamine (MDMA) | 194 | 163(100) |
| Methamphetamine | 150 | 119(100) ; 91(8) |
| Methylephedrine | 134 | 117(100) |
| Nikethamide | 179 | 108(100) ; 75(18) |
| Norephedrine | 152<br>134 | 134(100)<br>117(100) |
| Norfenfluramine | 204 | 187(100) |
| Norpseudoephedrine | 152<br>134 | 134(100)<br>117(100) |
| Pseudoephedrine | 166 | 148(100) |

**Sources Cited in application example 5.4**

[1] *M. Thevis*: **Mass Spectrometry in Sports Drug Testing – Characterization of Prohibited Substances and Doping Control Analytical Assays**
John Wiley & Sons, Inc. Publication 2010 [ISBN: 978-0-470-41327-2]

[2] *M. Thevis, G. Optermann, W. Schänzer*: N-methyl-N-Trimethylsilyltrifluoroacetamide-Promoted Synthesis and Mass Spectrometric Characterization of Deuterated Ephedrines.
**European Journal of Mass Spectrometry 2004:10**(5), 673-681

[3] *S.P Jindal*, *T. Lutz, P. Vestergaard*: Mass Spectrometric Determination of Cocaine and Its Biologically Active Metabolite, Norcocaine, in Human Urine.
**Biomedical Mass Spectrometry 1978:5**(121), 658-663

[4] *K. Deventer*, *P. Van Eenoo*, *F.T. Delbeke*: Screening for Amphetamine and Amphetamine-type Drugs in Doping Analysis by Liquid Chromatography/Mass Spectrometry.
**Rapid Communications in Mass Spectrometry 2006:20**(5), 877-882

[5] MassBankData: (spectru nr. JP003086)
**(https://massbank.eu/MassBank/RecordDisplay.jsp?id=JP003086)**

[6] Baza de date NIST (spectru nr. 232994)
**(https://webbook.nist.gov/cgi/inchi?ID=C19550879&Mask=200#Mass-Spec)**

[7] Baza de date SDBS (spectru nr. 7596)
**https://sdbs.db.aist.go.jp/sdbs/cgi-bin/direct_frame_top.cgi**

[8] *V. Venugopal*, *S. Sudhaker*, *M. Afzal*, *S.N. Rasool*, *A.K. Srivastava*, *R.K. Sarin*: Simultaneous Detection of Strychnine and Brucine in Bl Matrix by Gas Chromatography-Mass Spectroscopy.
**Journal of the Indian Society of Toxicology (JIST) 2010:006**(001), 19-24

[9] *J. Haneef*, *M. Shaharyar*, *A. Husain*, *M. Rashid*, *R. Mishra*, *S. Parveen*, *N. Ahmed*, *M. Pal*, *D. Kumar*: Application of LC-MS/MS for Quantitative Analysis of Glucocorticoids and Stimulants in Biological Fluids.
**Journal of Pharmaceutical Analysis 2013:3**(5), 341-348

## 5.5 MS spectrum and fragmentation of morphine and other narcotics by electron beam ionization (EI)

Analytical interest in narcotics, particularly morphine and morphine-related compounds, has led to studies of fragmentation accompanying mass spectrometric analysis [1,2]. As an example, Figure 268 shows the ions formed because of morphine ionization by electron beam impact (EI ionization). The abundance of ionic fragments allows reliable identification of the compound, and the intensity of the signals correlates with the amount of analyte in the primary sample.

Figures 269 through 277 show mass spectra of various narcotics in the NIST collection for morphine (NIST 42472), dextromoramide (NIST 247090), fentanyl (NIST 250541), hydromorphone (NIST 352952), heroin (NIST 352937), oxycodone (NIST 125779), pentazocine (NIST 352200), pethidine (NIST 352938), and from the MoNa collection for methadone (MoNa JP002769). Based on the spectra obtained by EI ionization, characteristic signals have been proposed for these compounds (Table 19).

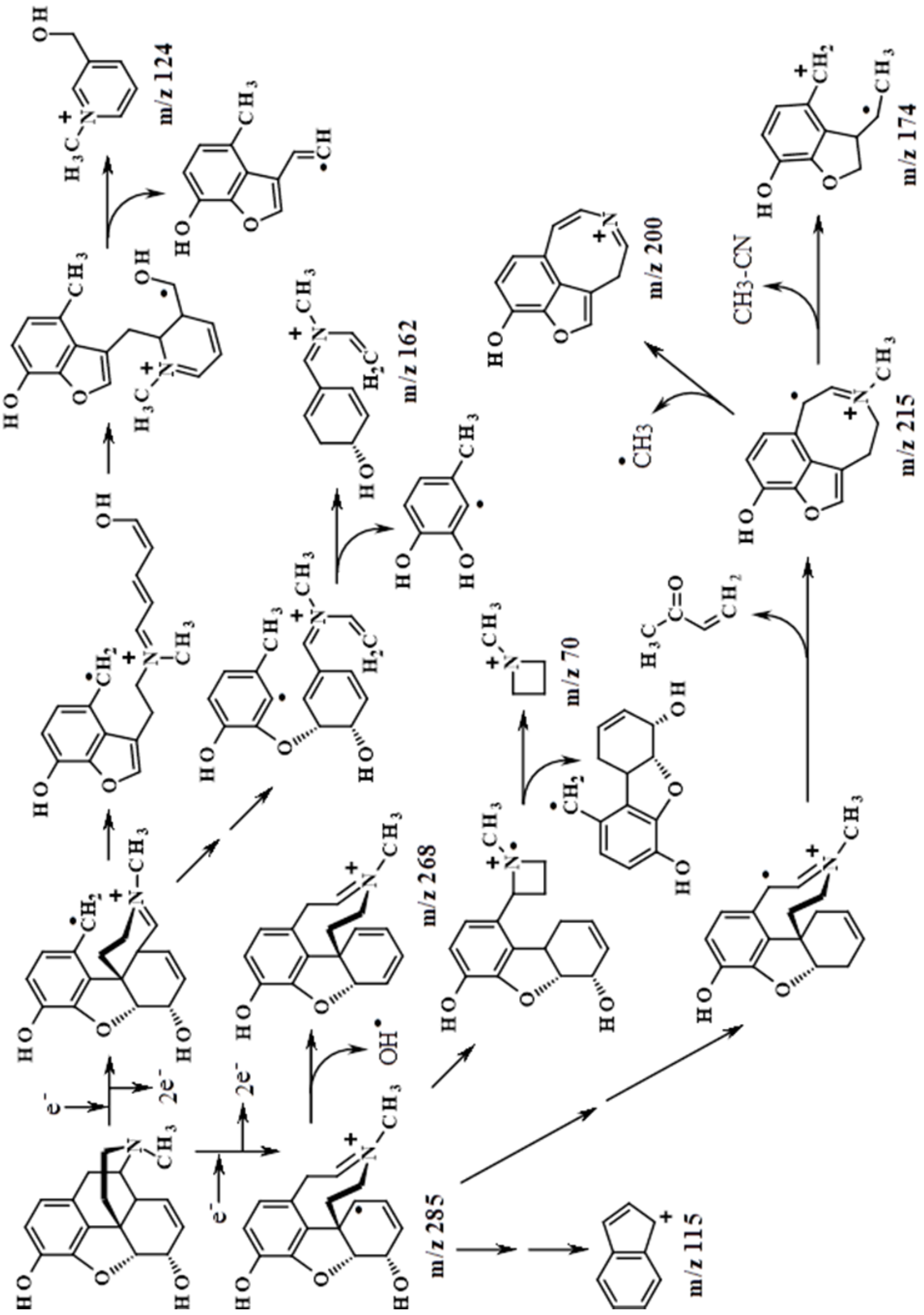



**Fig. 268 MS-EI fragmentation scheme of morphine (reconstructed from [1] and [2])**

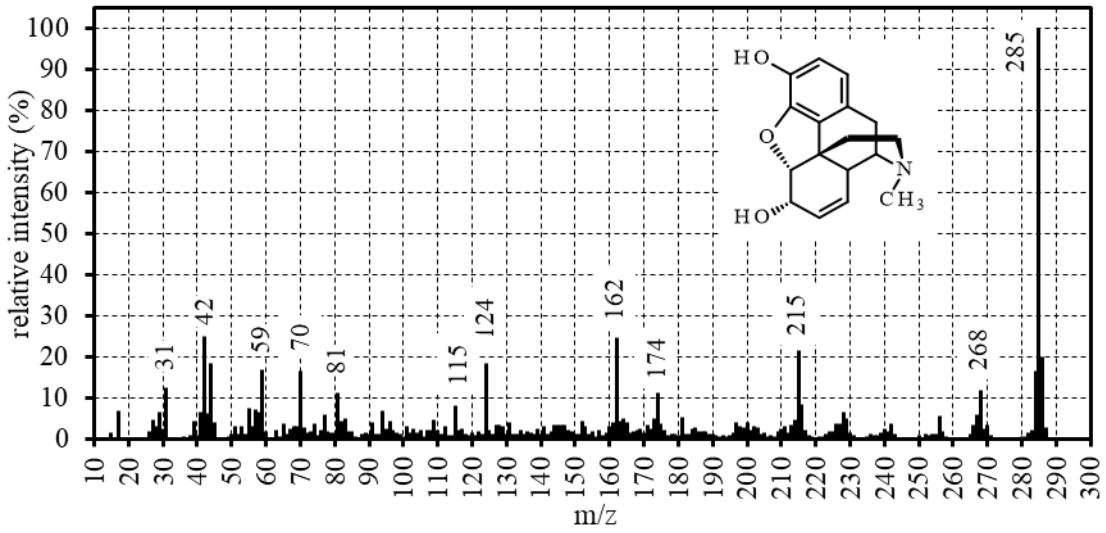



**Fig. 269 MS spectrum of morphine (EI ionization)**

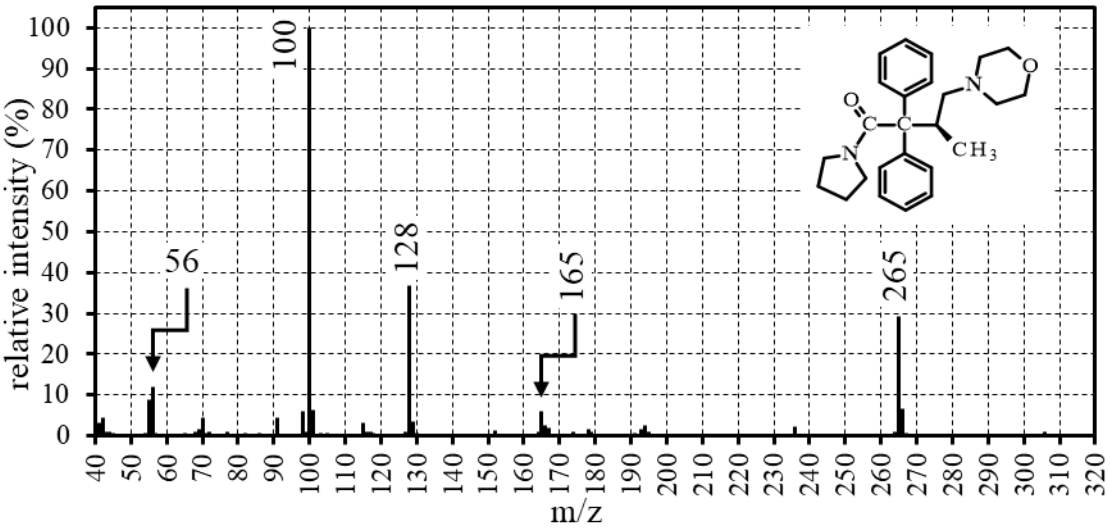



**Fig. 270 MS spectrum of dextromoramide (EI ionization)**

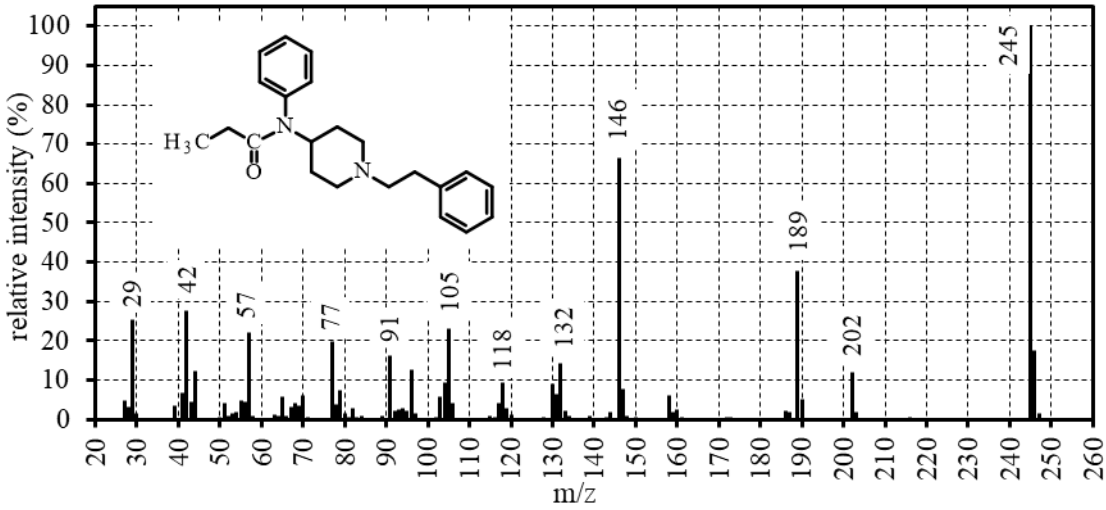



**Fig. 271 MS spectrum of phentanyl (EI ionization)**

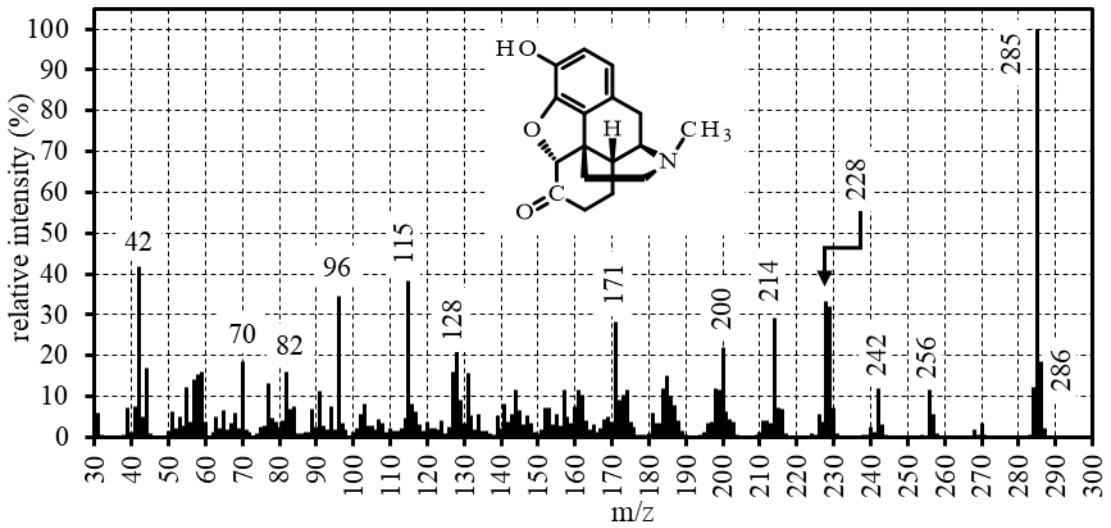



**Fig. 272 MS spectrum of hydromorphone (EI ionization)**

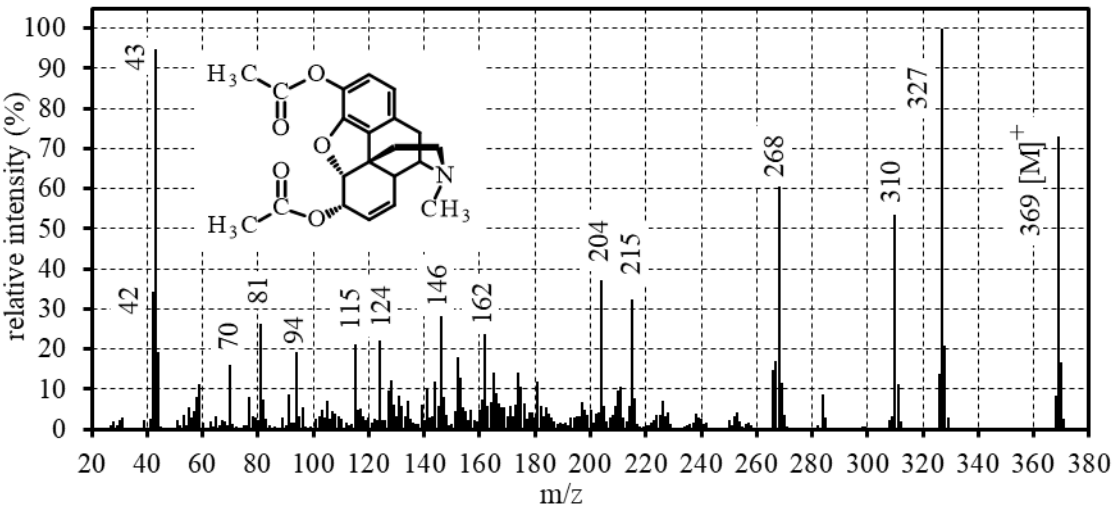



**Fig. 273 MS spectrum of heroin (diacetylmorphine) (EI ionization)**

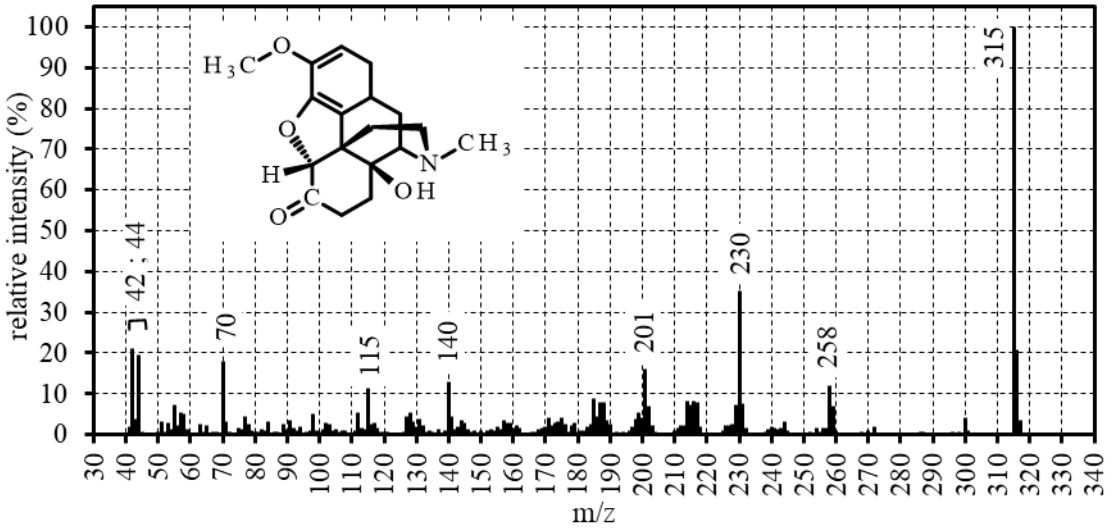



**Fig. 274 MS spectrum of oxycodone (EI ionization)**

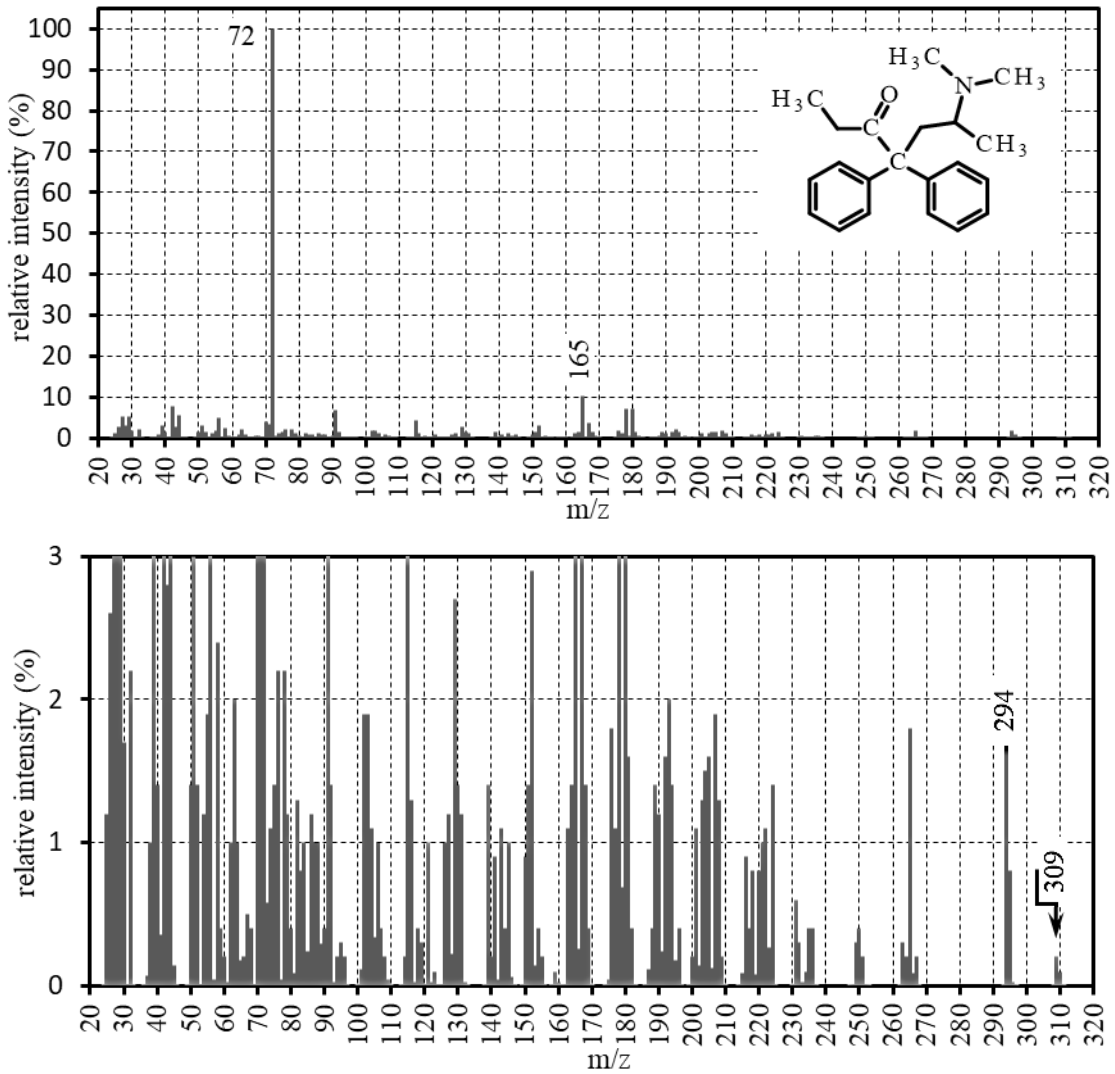



**Fig. 275 MS spectrum of methadone (EI ionization)**

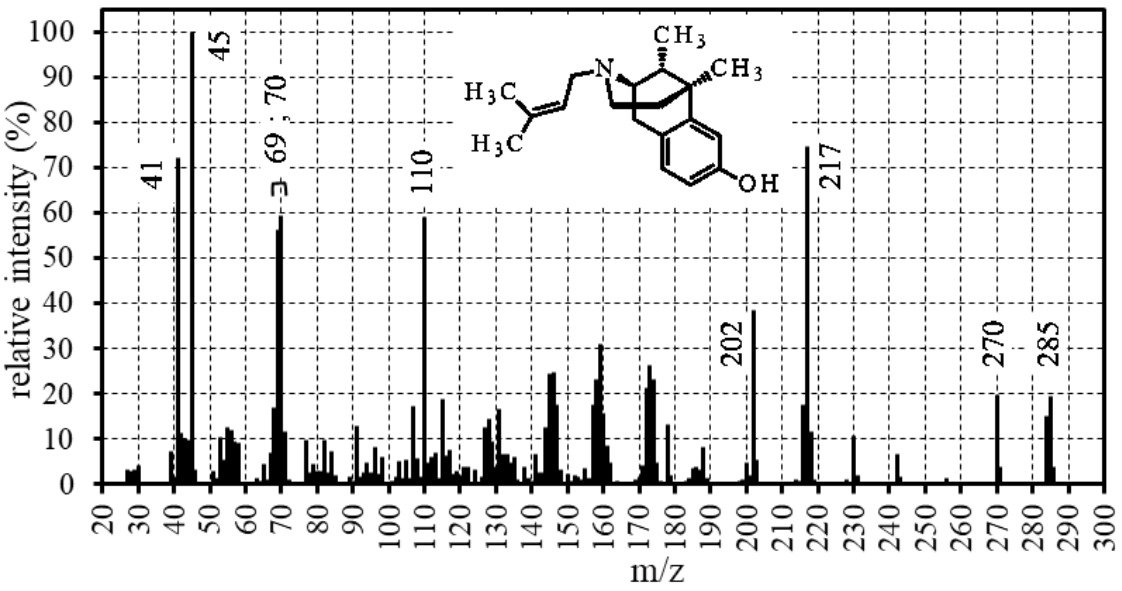



**Fig. 276 MS spectrum of pentazocine (EI ionization)**

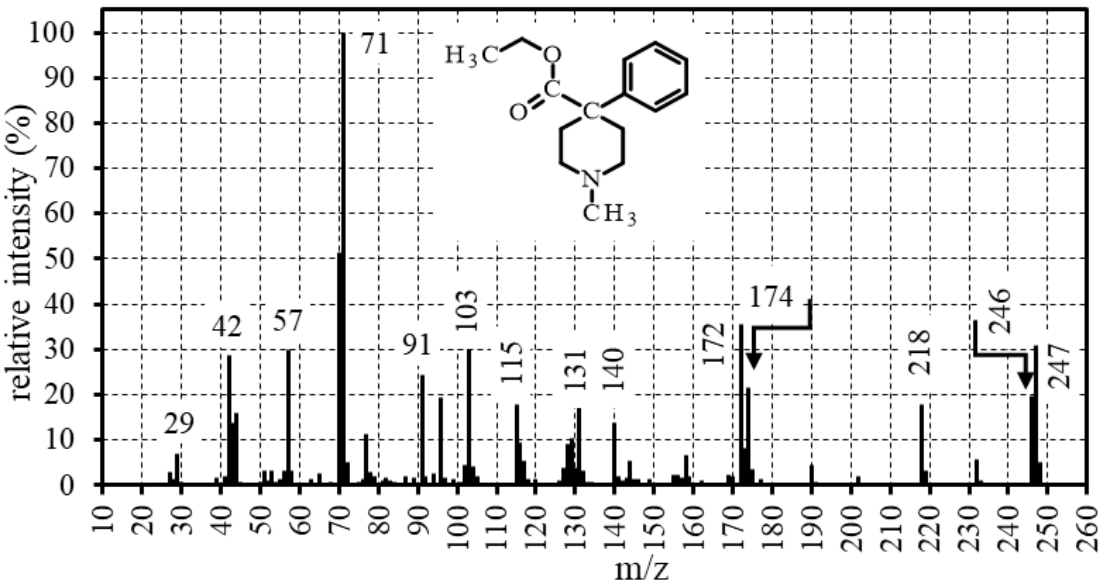



**Fig.277 MS spectrum of pethidine (meperidine) (EI ionization)**

**Table 19 Ionic fragments relevant for the identification and quantitative determination of narcotics by electron impact ionization (EI) mass spectrometry (according to [3])**

| Nr. | Active compound | Molecular mass (Da) | Ion fragments at EI ionization (m/z) | | | | | CAS number |
|---|---|---|---|---|---|---|---|---|
| 1 | Buprenorphine | 467 | 449 | 435 | 410 | 378 | 55 | 52485-79-7 |
| 2 | Dextromoramide | 392 | 265 | 165 | 128 | 100 | 56 | 357-56-2 |
| 3 | Phentanyl | 336 | 245 | 202 | 189 | 146 | 105 | 437-38-7 |
| 4 | Hydromorphone | 285 | 228 | 214 | 171 | 115 | 96 | 466-99-9 |
| 5 | Heroin | 369 | 327 | 310 | 268 | 204 | 162 | 561-27-3 |
| 6 | Methadone | 309 | 309 | 223 | 165 | 72 | | 76-99-3 |
| 7 | Morphine | 285 | 268 | 215 | 162 | 124 | 115 | 57-27-2 |
| 8 | Oxycodone | 315 | 258 | 230 | 201 | 140 | 70 | 76-42-6 |
| 9 | Pentazocine | 285 | 217 | 202 | 110 | 70 | | 359-83-1 |
| 10 | Pethidine | 247 | 246 | 218 | 174 | 172 | 71 | 57-42-1 |

**Sources Cited in application example 5.5**

[1] *H. Audier, M. Fetzion, D. Ginsburg, A. Mandelbaum, Th. Rüll*: Mass Spectrometry of the Morphine Alkaloids.
**Tetrahedron Letters 1965:6**(1), 13-22

[2] *D. Wheeler, T. Kinstle, K. Rinehart jr.*: Mass Spectral Studies of Alkaloids Related to Morphine.
**Journal of the American Chemical Society 1967:89**(17 ), 4494-4501

[3] *M. Thevis*: Characterization of Prohibited Substances and Doping Control Analytical Assays **John Wiley & Sons, 2010** [ISBN: 978-0-41327-2]

## 5.6 Analytical mass spectrometric characterization of non-steroidal anti-inflammatory drugs (NSAIDs)

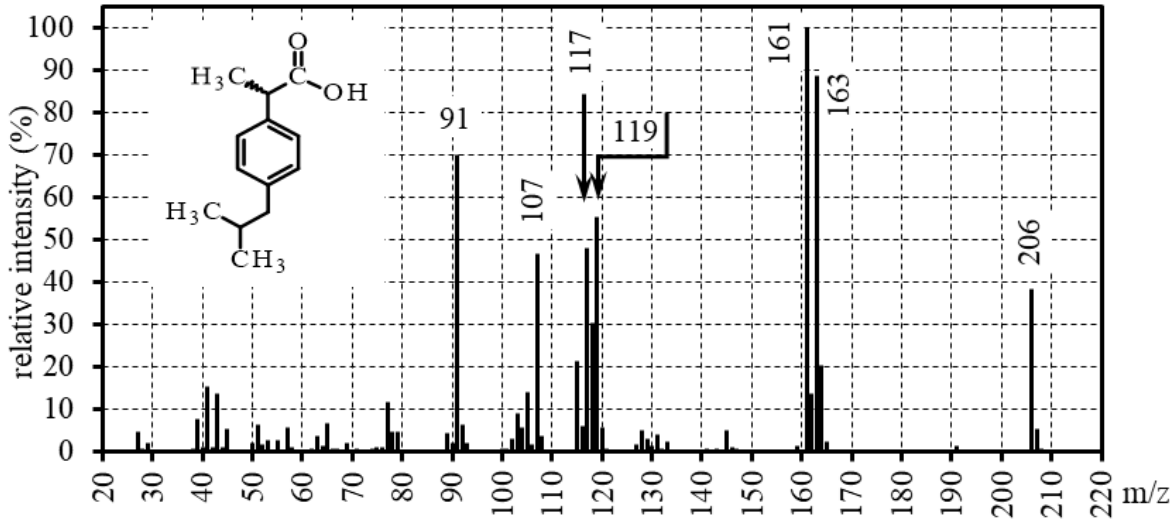



**Fig. 278 Mass spectrum of ibuprofen (EI ionization) (NIST nr. 352144)**

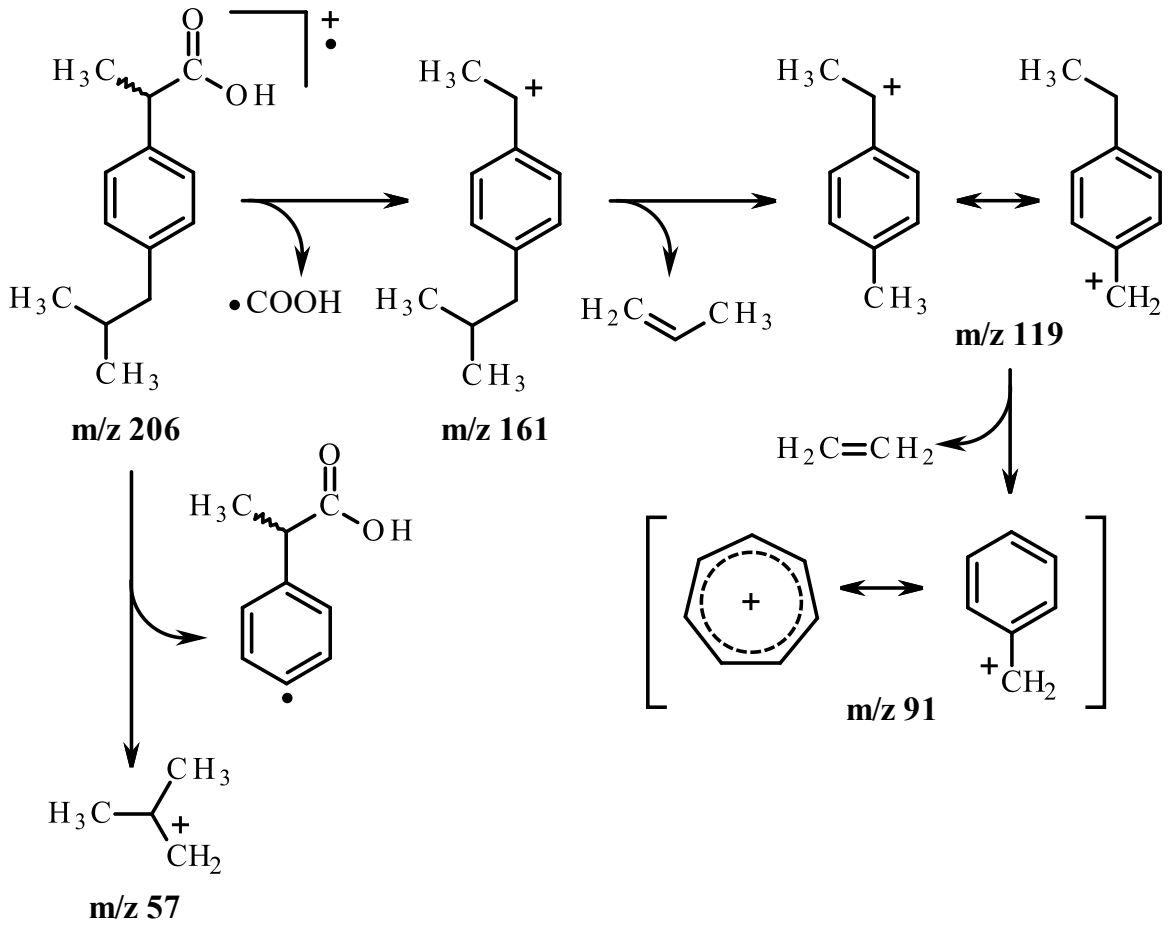



**Fig. 279 Fragmentation paths of ibuprofen in electron flow ionization (based on [1,2])**

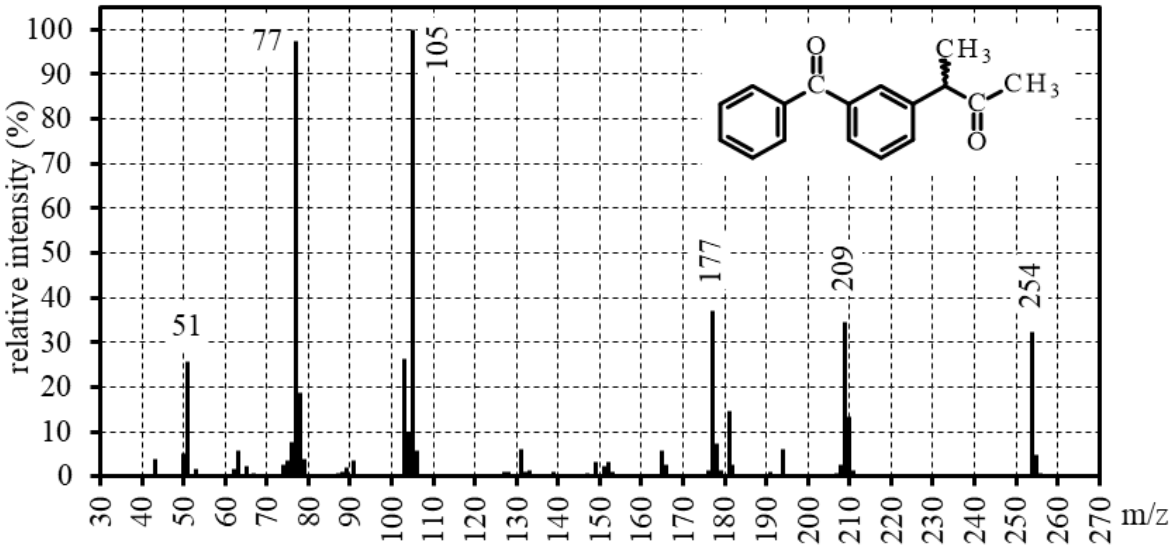



**Fig. 280 Mass spectrum of ketoprofen (EI ionization) (NIST no. 248419)**

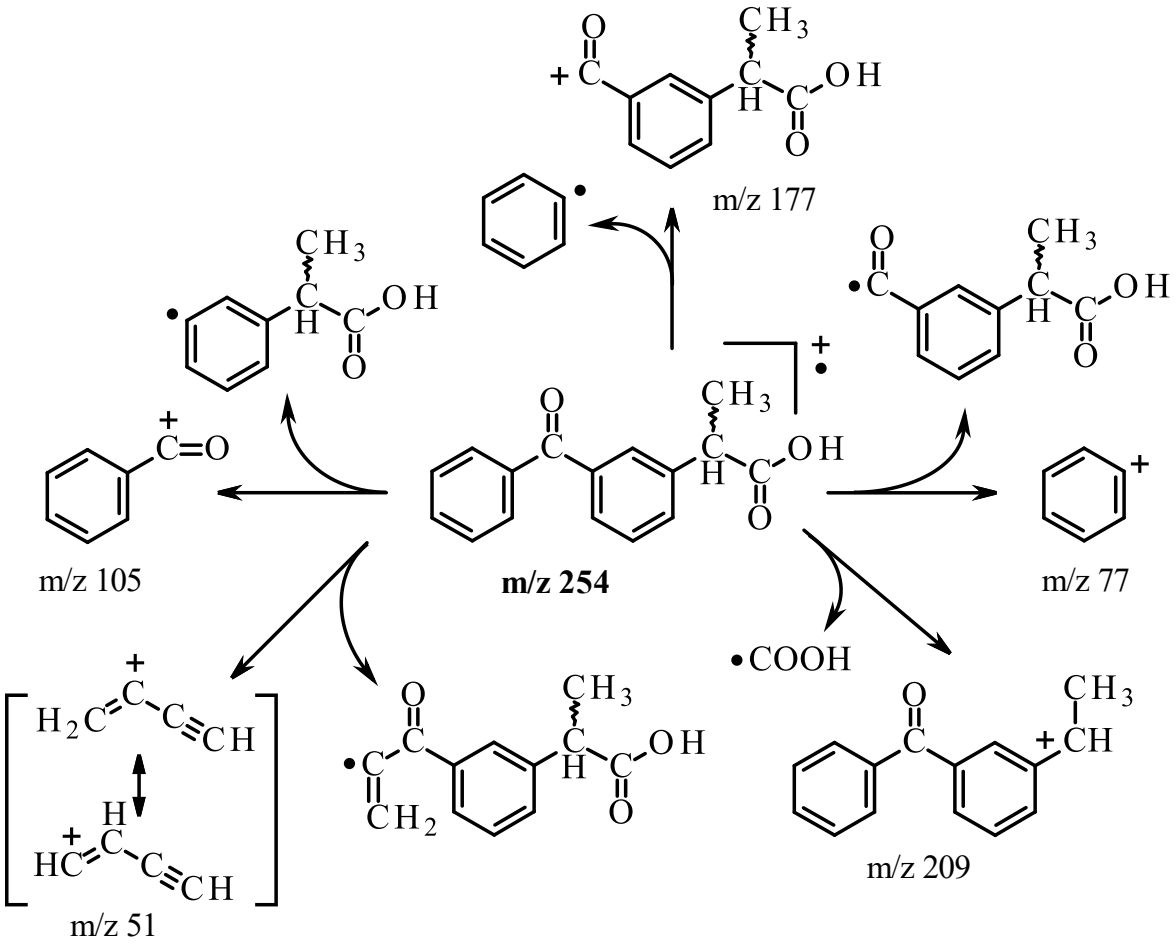



**Fig. 281 Fragmentation pathways of ketoprofen in electron flow ionization (based on [3])**

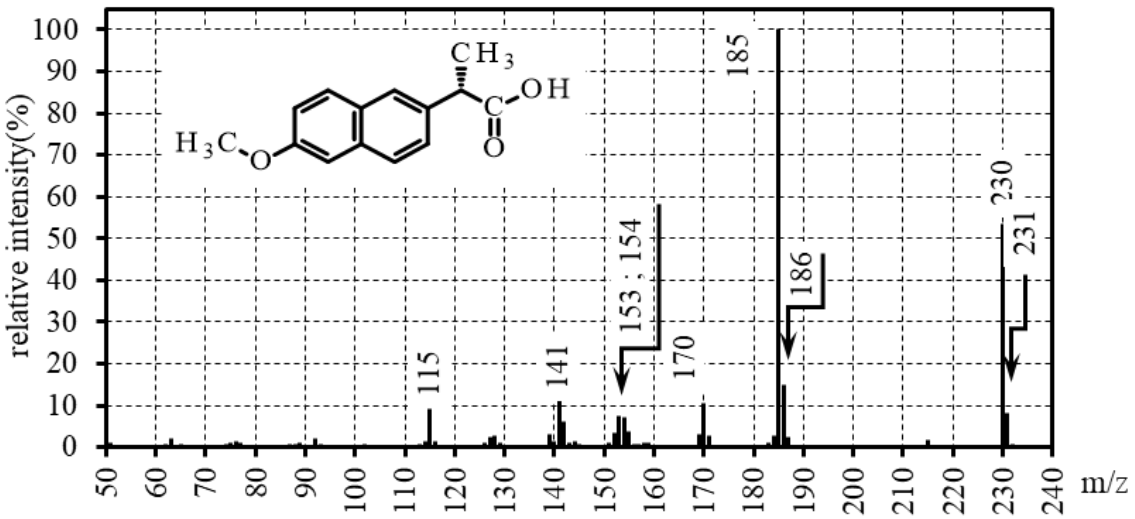



**Fig. 282 Mass Spectrum of Naproxen (EI Ionized) (NIST No. 237147)**

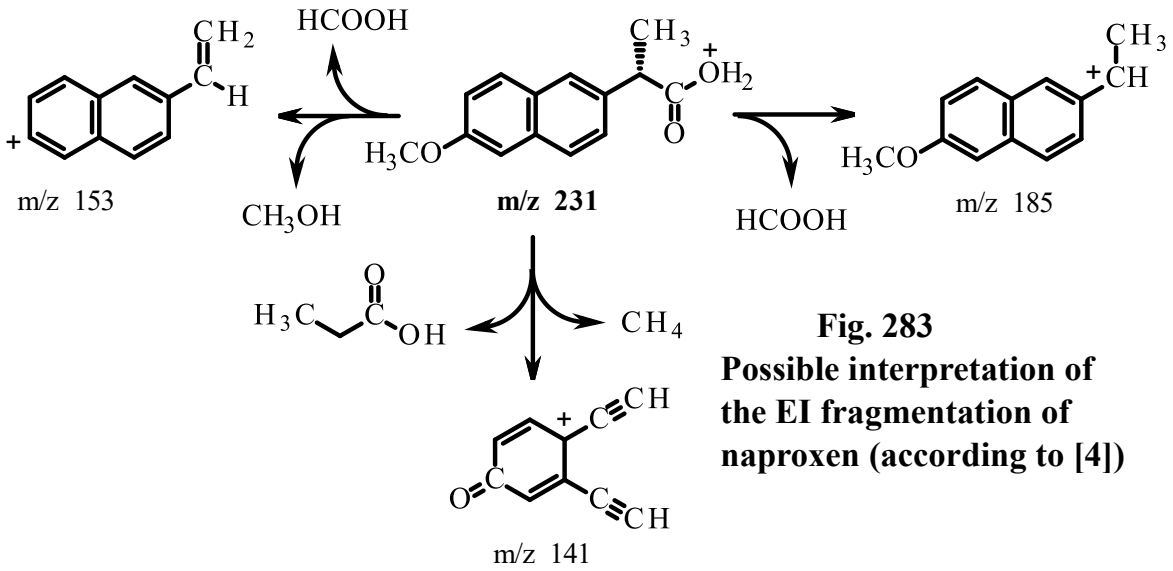



**Fig. 283**
**Possible interpretation of the EI fragmentation of naproxen (according to [4])**

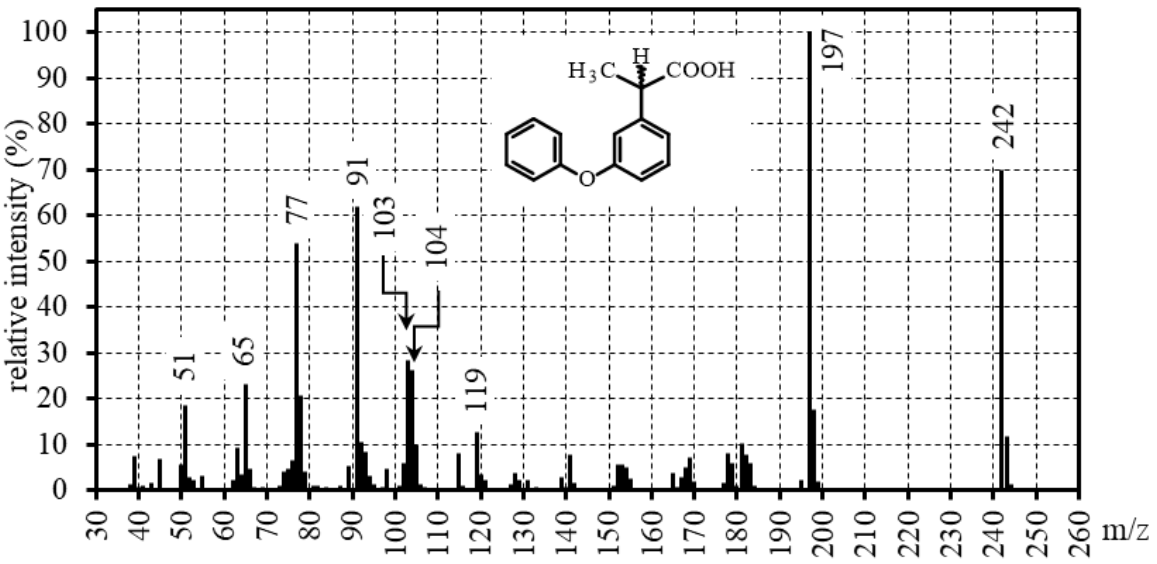



**Fig. 284 Mass spectrum of fenoprofen (EI ionization) (NIST no. 246389)**

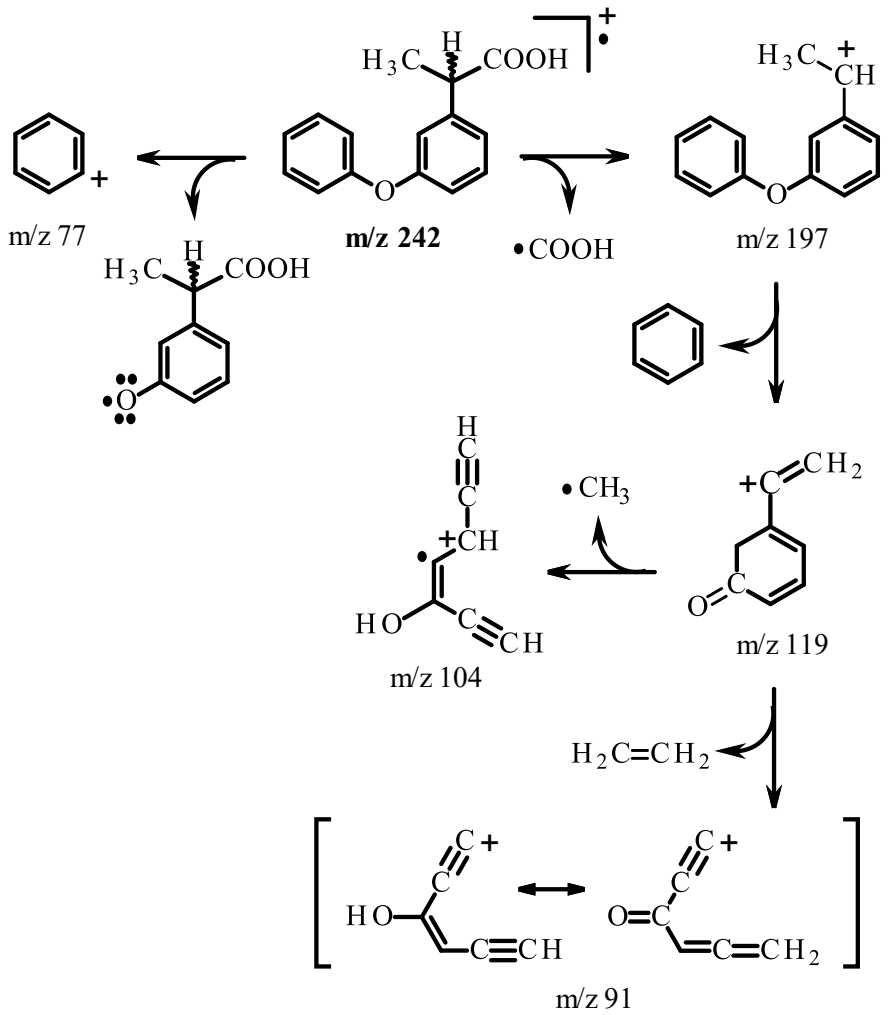



**Fig. 285 Possible interpretation of the EI fragmentation of fenoprofen [5].**

In order to characterize the stability and to elucidate the fragmentation mechanism of some NSAIDs, fragmentation studies under mass spectrometric and thermal degradation conditions have been initiated [1], especially in the case of the representatives ibuprofen, ketoprofen [2,3], naproxen and fenoprofen [4,5], where the experimental results are correlated with theoretical quantum chemical calculations carried out with the semi-empirical PM3 method, the **U**nrestricted ***Hartree-Fock*** (**URF**) level for neutral species and the **R**estricted ***Hartree-Fock*** (**RHF**) level for cationic species [1,4], targeting the relative strength of the chemical bonds in the molecules in question.

Figures 278, 280, 282 and 284 show the mass spectra of the compounds ibuprofen, ketoprofen, naproxen and fenoprofen obtained by electron flow ionization (EI). Figures 279, 281, 283 and 285 show the proposed pathways for the fragmentation of ibuprofen, ketoprofen, naproxen and fenoprofen. The **m/z** ratios of the indicated fragments correspond to the signals in the mass spectra of the corresponding compounds. The results of theoretical calculations of the relative cleavage energies of certain chemical bonds [1,4] were used in the development of possible fragmentation pathways.

Other studies have focused on the identification of photodegradation products and the kinetics of transformation under the action of light [2]. The photodegradation kinetic curve of ketoprofen, shown in Figure 286, illustrates the advanced photosensitivity of ketoprofen.

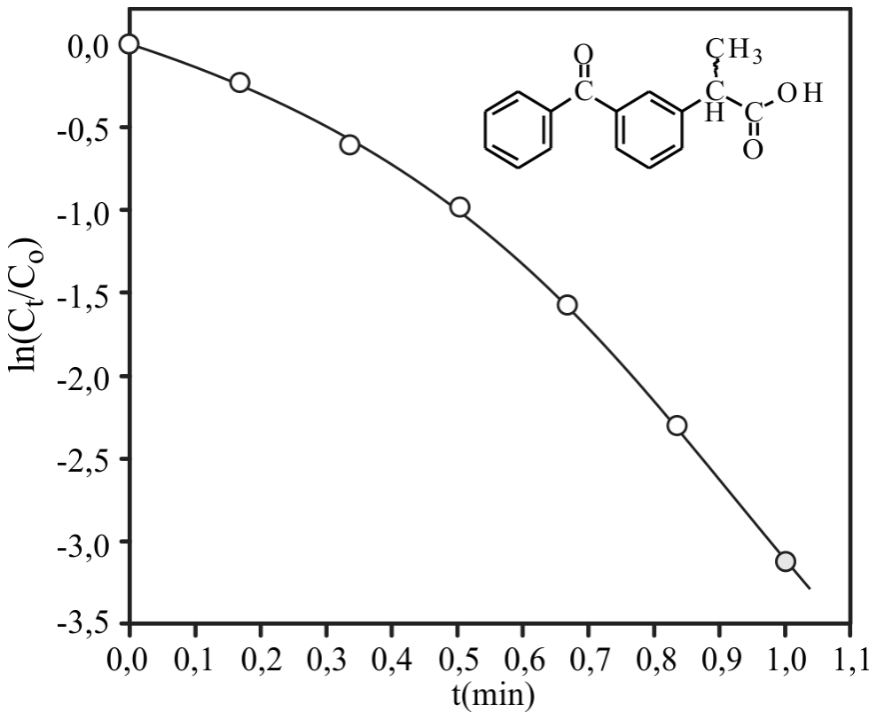



**Fig. 286 Photodegradation kinetic curve of ketoprofen (recreated after [2])**

**Sources cited in application example 5.6**

[1] *M.A. Zayed, M.F. Hawash, M.A. Fahmey, A.M.M. El-Gizouli*: Investigation of Ibuprofen Drug Using Mass Spectrometry, Thermal Analysis and Semi-empirical Molecular Orbital Calculation. **J. Therm. Anal. Calorim., 2012:108**(1), 315-322

[2] *A. Jakimska, M. Śliwka-Kaszińska, J. Reszczyńska, J. Namieśnik, A. Kot-Wasik*: Elucidation of Transformation Pathway of Ketoprofen, Ibuprofen and Furosemide in Surface Water and Their Occurence in the Aqueous Environment Using UHPLC-QTOT-Ms. **Anal. Bioanal. Chem., 2014:406**(15), 3667-3680

[3] *J. Assaf, A.S. Kollmeier, C. Müller, M.K. Parr*: Reconsidering Mass Spectrometric Fragmentation in EI-MS – New Insights from Recent Instrumentation and Isotopic Labelling Exemplified by Ketoprofen and Related Compounds. **DOI: 10.1002/rcm.8313**

[4] *M.A. Zayed, M.F. Hawash, M. El-Desawy, A.M.M. El-Gizouli*: Investigation of Naproxen Drug Using Mass Spectrometry, Thermal Analysis and Semi-empirical Molecular Orbital Calculation. **http://dx.doi.org/10.1016/j.arabjc.2013.09.025**

[5] *K.D. Ghaewad, P.A. Shah, P.S. Shrivastav, V.S. Sharma, P. Singhal*: Quantification of Fenoprofen in Human Plasma Using UHPLC-tandem Mass Spectrometry for Pharmacokinetic Study in Healthy Subjects. **DOI: 1002/bmc.4708**

## 5.7 Monitoring illicit drugs in wastewater and surface water

Supervising illicit drug residues and their metabolites in wastewater and surface water has become a necessity due to the hard-to-control drug use - on the one hand - and the impact on environmental integrity - on the other hand.

Among the numerous analytical methods, those based on chromatography (gas and/or liquid) coupled with mass spectrometry are characterized by their high identification specificity and the possibility of analyzing multiple samples. One method is based on SIM (**S**elected **I**on **M**onitoring) liquid chromatography coupled to $MS^2$ mass spectrometry with CID (**C**hemical **I**onization **D**issociation) fragmentation [1]. Primary ionization is performed by the ESI (**E**lectro-**S**pray **I**onization) method and for fragmentation different collision energies are recommended depending on the nature of the analyte of interest.

**Tabel 20 MS conditions for analytical determination of illicit drugs and their metabolites by LC-SIM ([1]) (in parentheses collision energy in eV)**

| Active compound and metabolite | Precursor ion m/z | Fragment ion (I) m/z | Fragment ion (II) m/z |
|---|---|---|---|
| amphetamine | 136 | 119 (14) | 91 (24) |
| methamphetamine | 150 | 119 (16) | 91 (26) |
| MDA | 180 | 133 (24) | 105 (20) |
| MDMA | 194 | 133 (30) | 105 (36) |
| MDEA | 208 | 133 (28) | 105 (36) |
| anhydroecgonine | 168 | 91 (32) | 122 (28) |
| anhydroecgonine methyl ester | 182 | 118 (32) | 122 (28) |
| ecgonine | 186 | 82 (38) | 100 (34) |
| ecgonine methyl ester | 200 | 82 (36) | 119 (32) |
| cocaine | 304 | 182 (28) | 105 (32) |
| norcocaine | 290 | 168 (24) | 136 (32) |
| cocaethylene | 318 | 196 (28) | 82 (44) |
| benzoylecgonine | 290 | 168 (24) | 105 (42) |
| norbenzoylecgonine | 276 | 154 (24) | 136 (30) |
| morphine | 286 | 201 (36) | 165 (54) |
| morfine-3β-D-glucuronid | 462 | 286 (40) | 201 (60) |
| 6-acetylmorphine | 328 | 211 (36) | 165 (50) |
| methadone | 310 | 265 (22) | 105 (36) |
| EDDP | 278 | 234 (42) | 186 (48) |
| 11-nor-9-carboxy-$\Delta^9$-tetrahydrocannabinol | 343 | 299 (30) | 245 (40) |

EDDP – 2-ethylene-1,5-dimethyl-3,3-difenylpyrrolidine (metabolit of methadone)
MDEA – 3,4-methylene-dioxyethyl-amphetamine
MDMA – 3,4-methylene-dioxyethyl-methamphetamine
MDA – 3,4-methylene-dioxy-amphetamine

Table 20 shows the precursor ion and two fragment ions, (I) and (II), produced by CID ionization of the precursor ion for several illicit drugs and their metabolites. Figures 287 through 292 show the mass spectra obtained by ESI ionization in positive and negative mode, followed by CID fragmentation for the $MS^2$ mass spectrum.

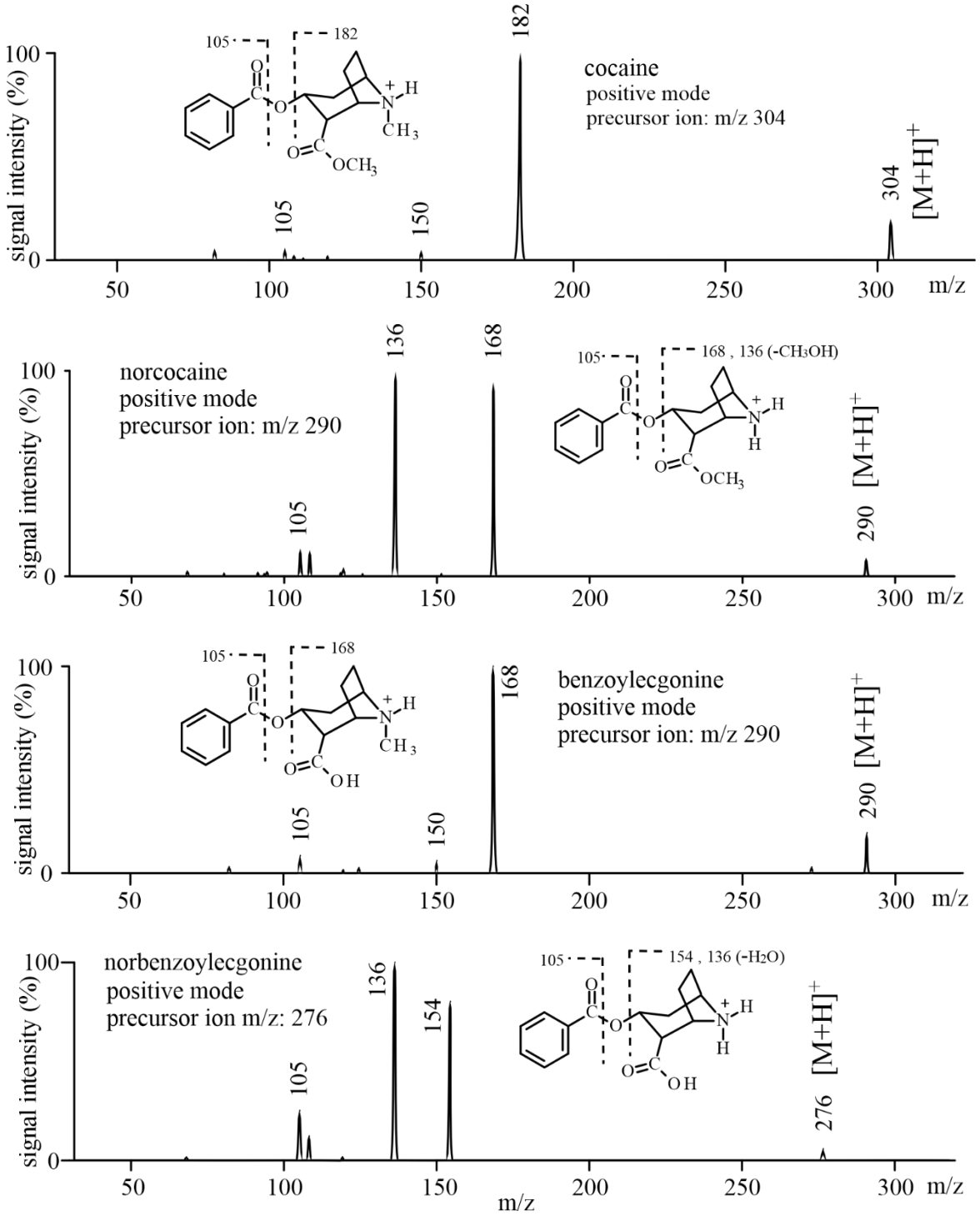



**Fig. 287 Positive $MS^2$ mass spectra of cocaine, norcocaine, benzoylecgonine and norbenzoylecgonine (recreated from [1])**

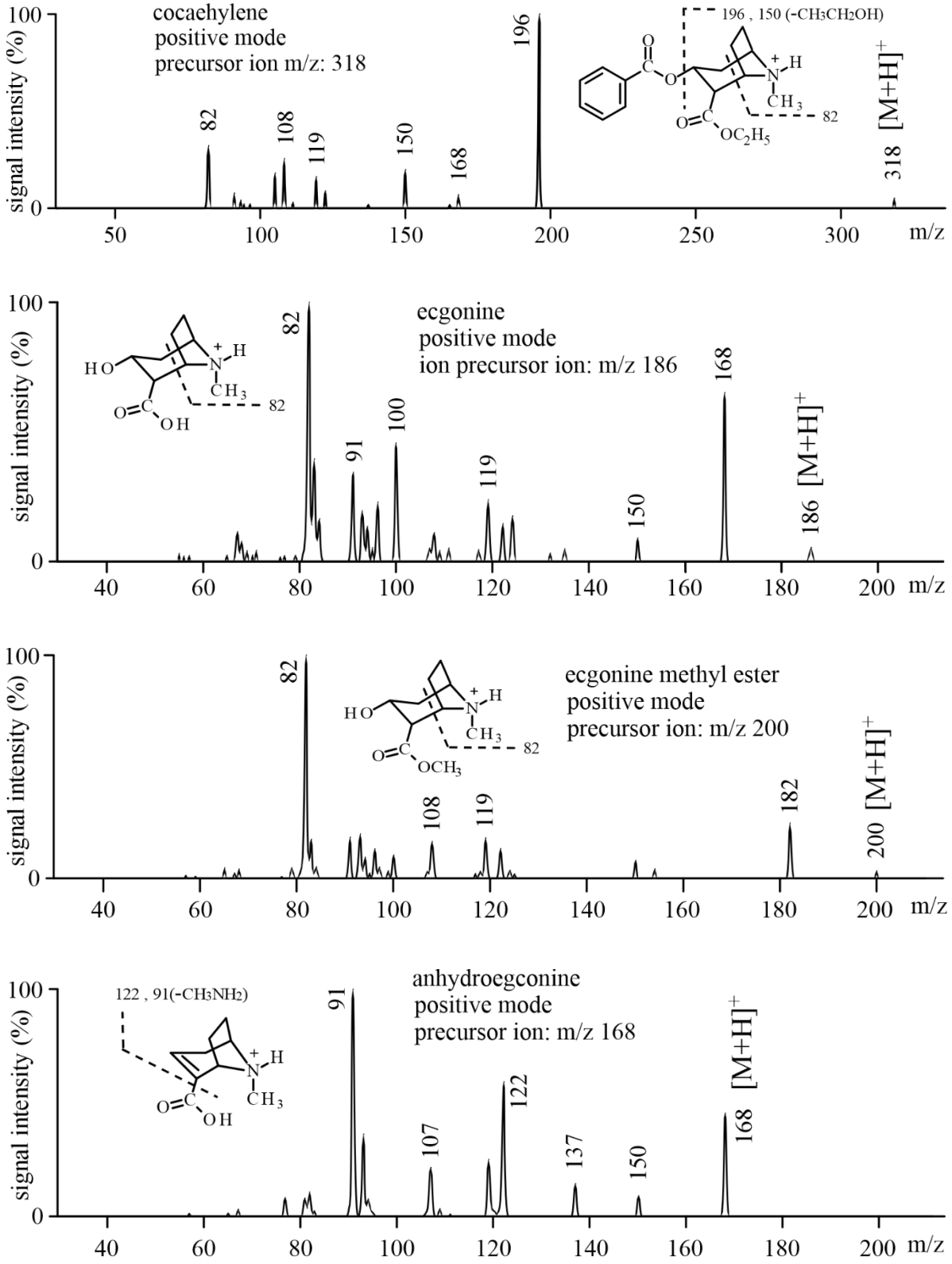



**Fig. 288 Positive $MS^2$ mass spectra of cocaethylene, ecgonine, ecgonine methyl ester and anhydroecgonine (recreated from [1])**

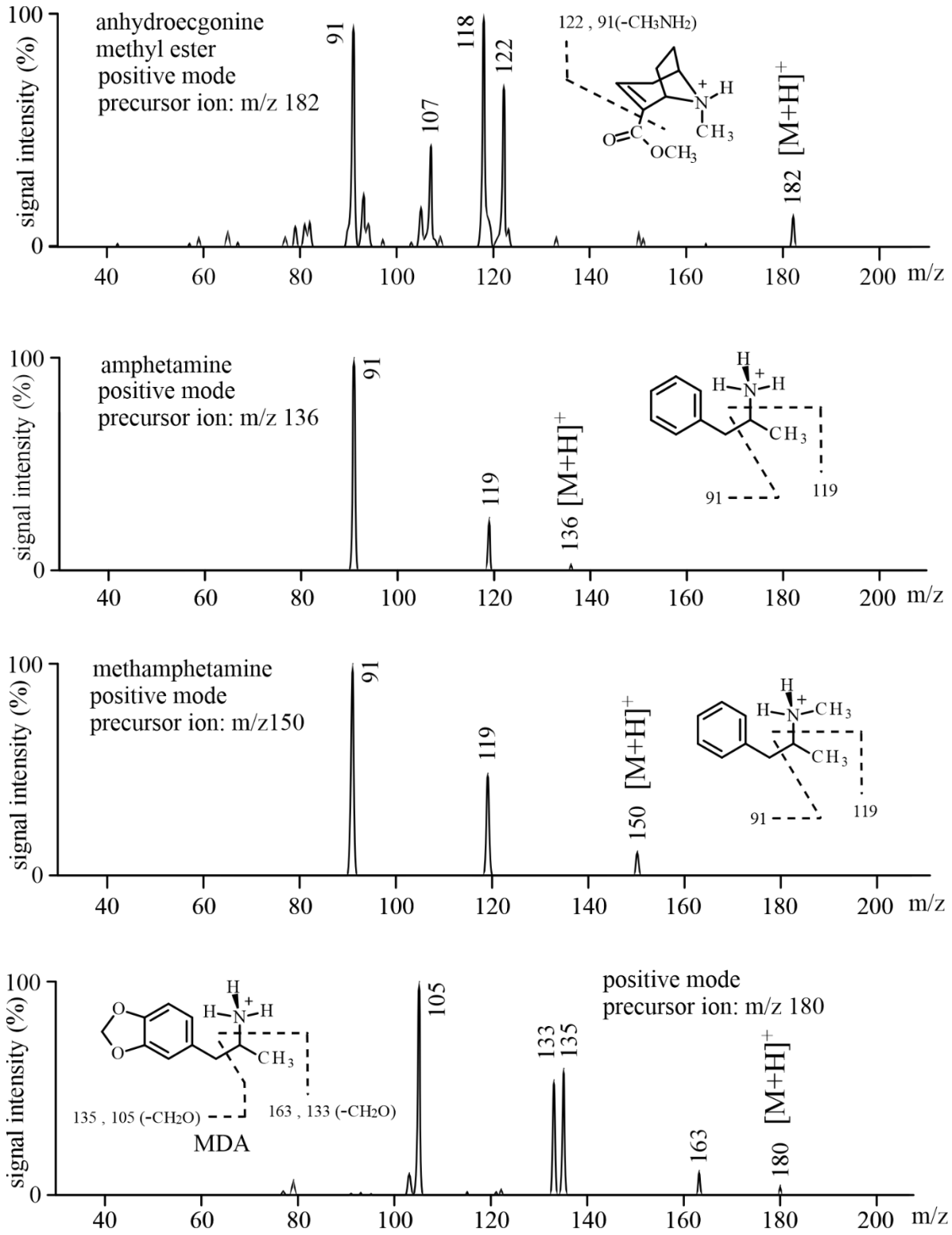



**Fig. 289 $MS^2$ mass spectra of the methyl ester of anhydroecgonine, amphetamine, methamphetamine and MDA in positive mode (recreated from [1,2])**

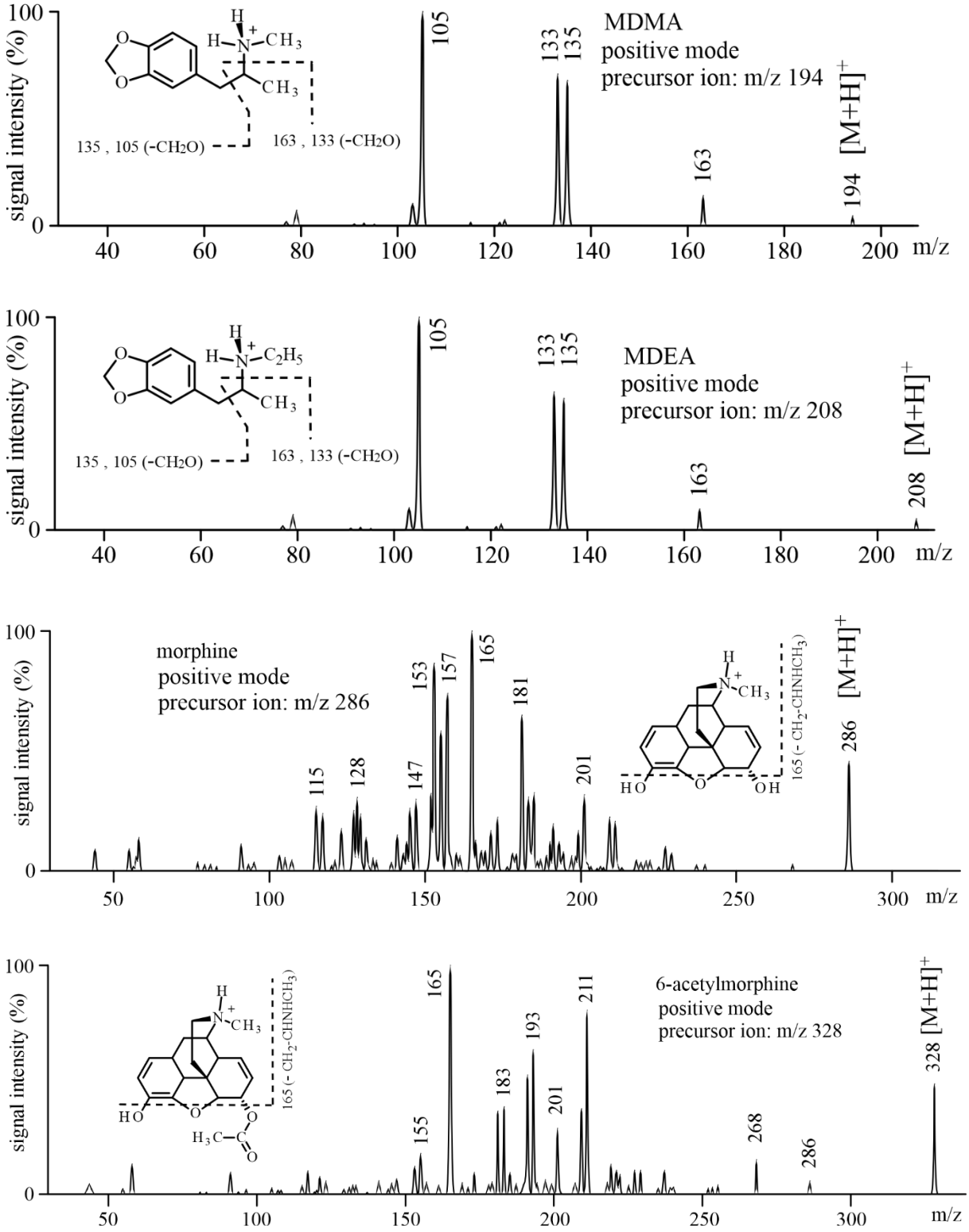



**Fig. 290 Positive $MS^2$ mass spectra of MDMA, MDEA, morphine and 6-acetylmorphine (recreated from [1,2])**

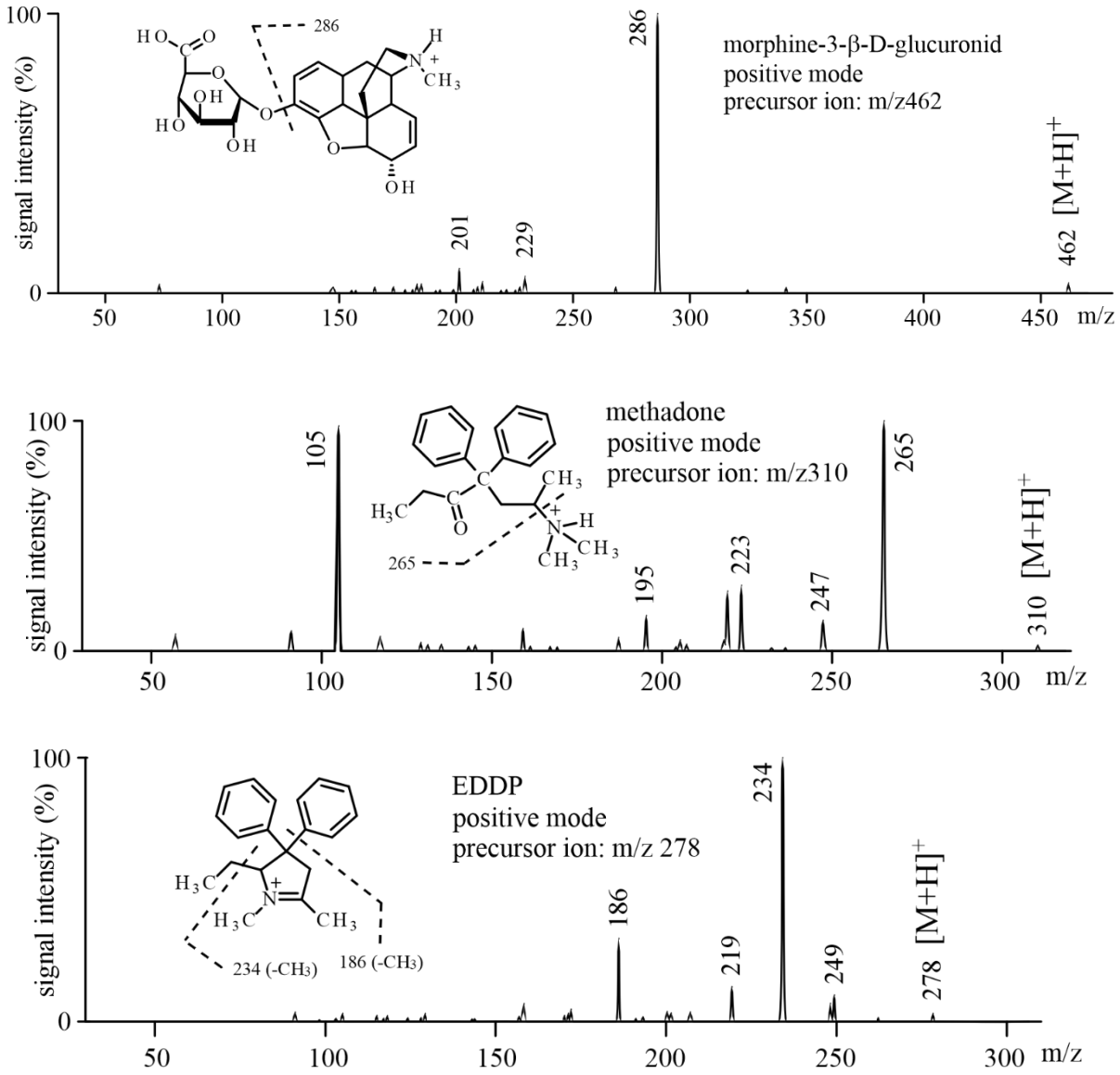



**Fig. 291 The $MS^2$ mass spectra of morphine-3-β-D-glucuronide, methadone and EDDP in positive mode [1].**

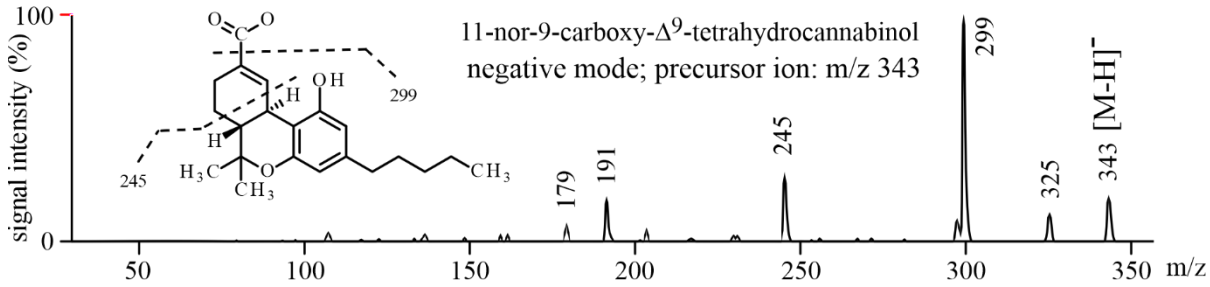



**Fig. 292 The $MS^2$ mass spectrum of 11-nor-carboxy-$\Delta^9$-tetrahydro-cannabinol in negative mode (recreated after [1,2])**

**Sources cited in application example 5.7**

[1] *S. Castiglioni, E. Zuccato, C. Chiabrando, R.Fanelli, R. Bagnati*: Mass Spectrometric Analysis of Illicit Drugs in Wastewater and Surface Water
**Mass Spectrometry Reviews 2008:27**(4), 378-394

[2] *L. Bijsma, J.V. Sancho, F. Hernández, W.M.A. Niessen*: Fragmentation Pathways of Drugs of Abuse and their Metabolites Based on QTOF MS/MS and $MS^E$ Accurate-mass Spectra.
**Journal of Mass Spectrometry 2011:46**(9), 865-875

## 5.8 Identification of ramipril by comparative positive and negative $MS^2$ fragmentation

Ramipril is an angiotensin-converting enzyme (**ACE**) inhibitor used to treat high blood pressure, heart failure and diabetic kidney disease [1]. It reduces the activity of the renin-angiotensin-aldosterone system. It was introduced into therapy in 1989 [2].

For the identification and analytical determination of ramipril, methods based mainly on different variants of chromatography were used. For more reliable analytical control, a mass spectrometric study was performed comparing fragmentation in positive [3] and negative [4] modes. Figure 293 shows the $MS^2$ mass spectrum of ramipril in positive mode. The signal with the highest **m/z** ratio (417) corresponds to the protonated molecular ion $\mathbf{[M+H]^+}$, which is the precursor ion. Due to the more advanced fragmentation process, the base signal (with maximum relative intensity) in the $MS^2$ spectrum corresponds to a lower **m/z** ratio.

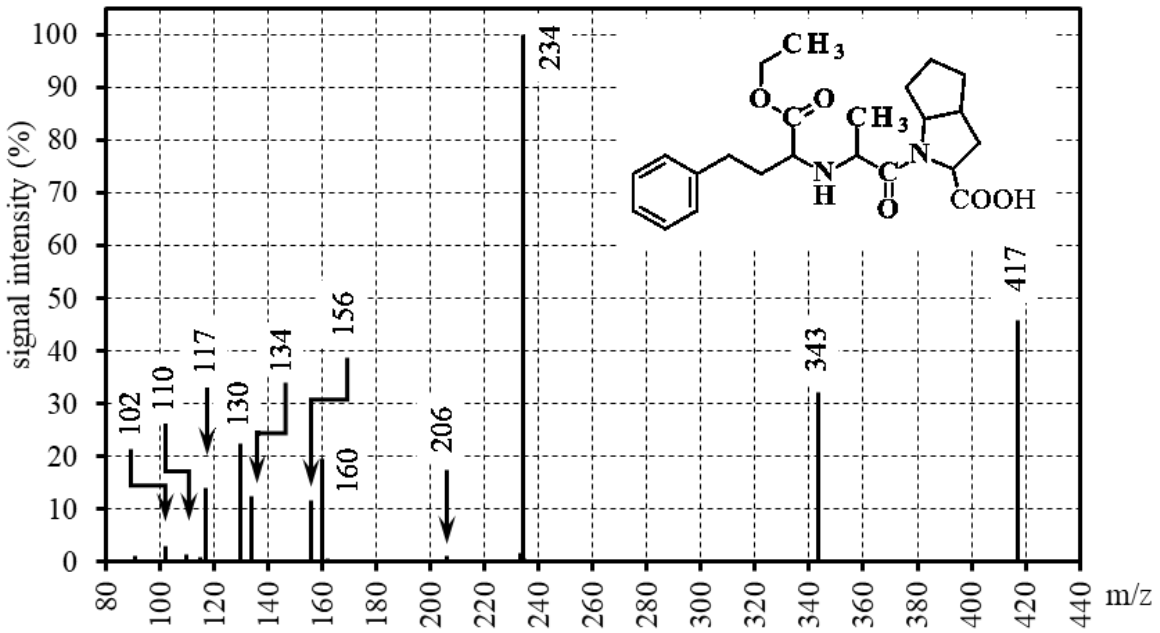



**Fig. 293 Mass spectrum of the compound ramipril - $MS^2$, positive mode, precursor ion $[M+H]^+$, ESI ionization (the signal at m/z 417 is assigned to the $[M+H]^+$ ion) (after MoNa spectra acquisition).**

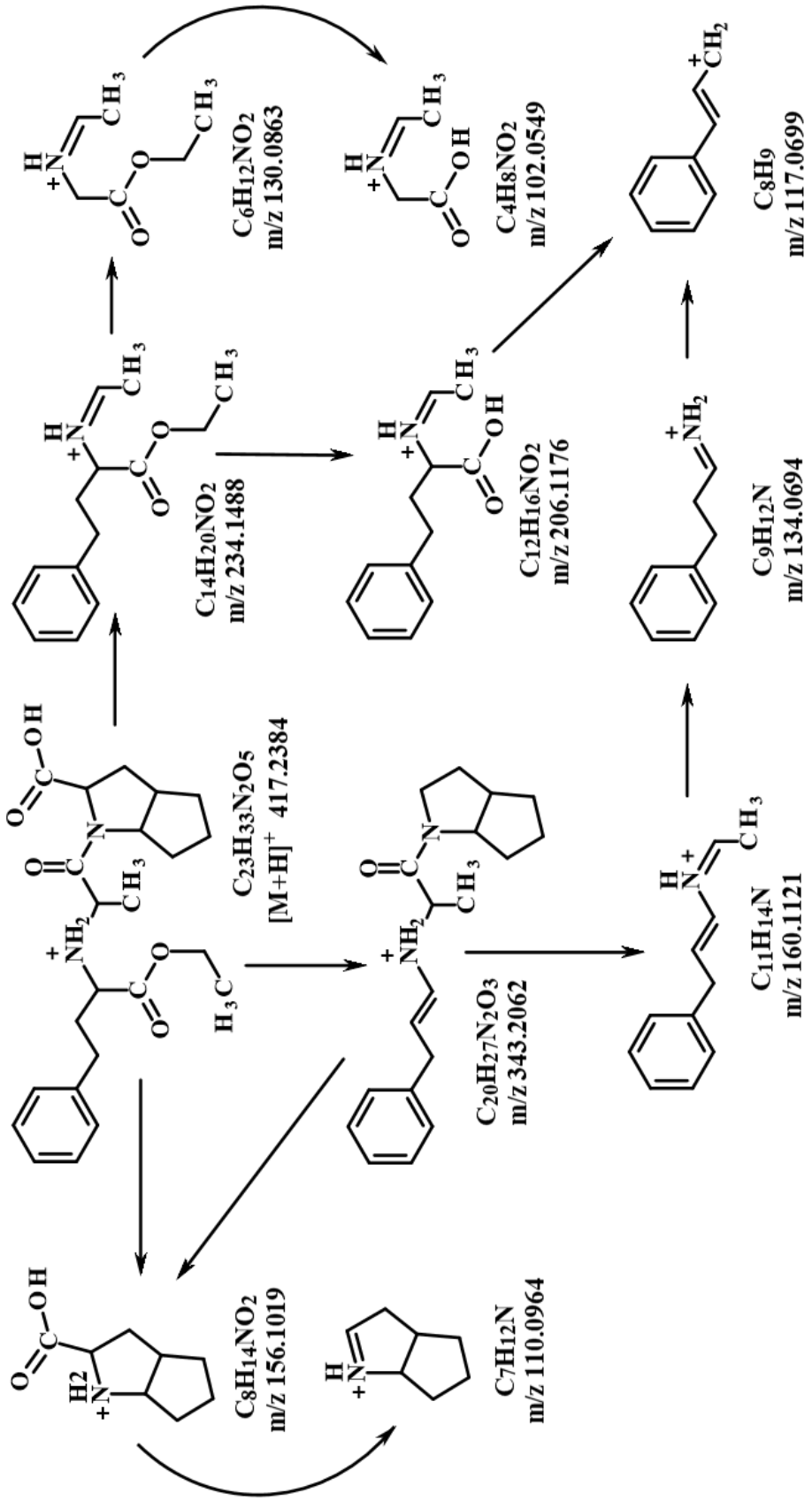



**Fig. 294**

**$MS^2$ fragmentation of ramipril in positive mode (according to [3])**

Figure 294 shows the interpretation of the fragmentation spectra indicating likely cleavage sites. The suggested fragments correspond to the major signals in the mass spectrum in Figure 293.

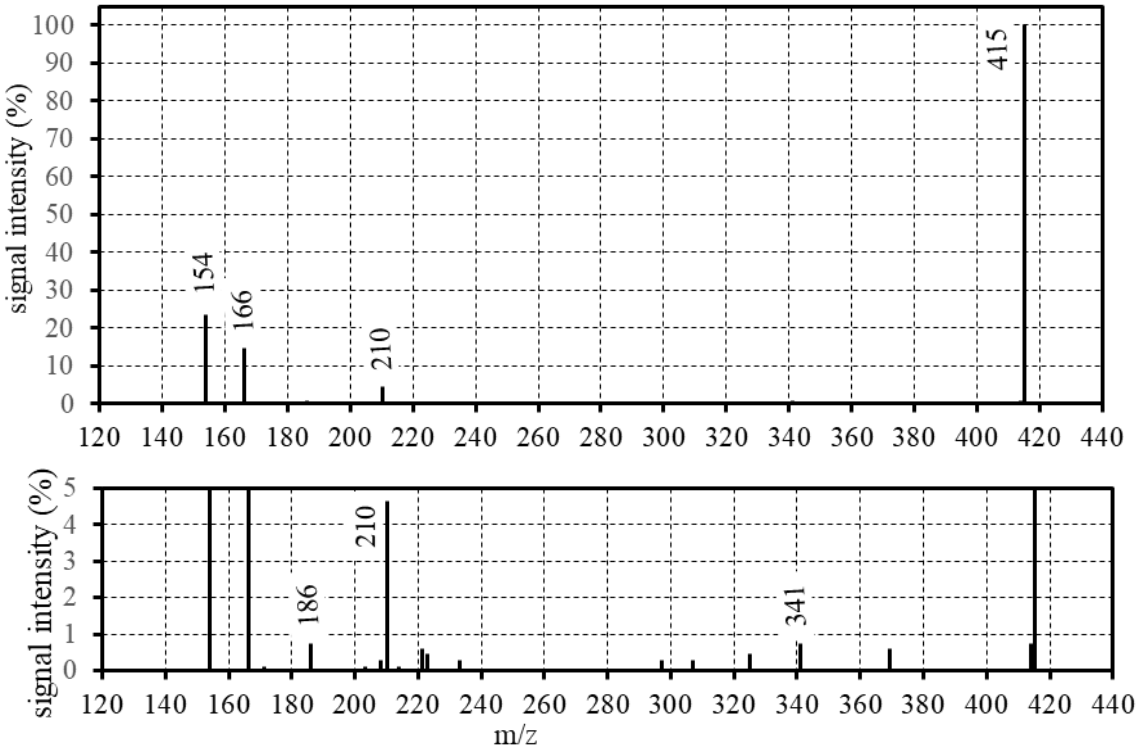



**Fig. 295 Mass spectrum of the compound ramipril - $MS^2$, negative mode, precursor ion $[M-H]^-$, ESI ionization (the signal at m/z 415 is assigned to the $[M-H]^-$ ion) (after MoNa spectra acquisition)**

Figure 295 shows the $MS^2$ mass spectrum of the compound ramipril in negative mode. The maximum signal at **m/z** 415 corresponds to the deprotonated molecular ion **$[M-H]^-$**, which is the precursor ion and the base signal (with maximum intensity), demonstrating that fragmentation is more tempered in the negative mode than in the positive mode.

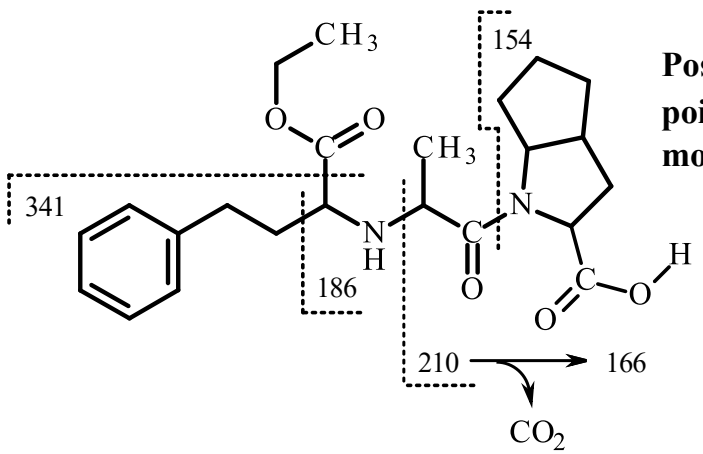



**Fig. 296 Possible $MS^2$ fragmentation points of ramipril in negative mode (according to [4])**

Figure 296 shows the interpretation of the fragmentation mode, which indicates likely cleavage sites. The suggested fragments correspond to the major signals in the mass spectrum in Figure 295. The signal at **m/z** 166 is due to the removal of a neutral carbon dioxide molecule from the fragment assigned to the **m/z** 210 signal.

Ramiprilat (species with the hydrolyzed ester group, Figure 297), the active metabolite of ramipril, was also the subject of a comparative analytical study [5]. The $MS^2$ mass spectrum with ESI ionization is shown in Figure 298.

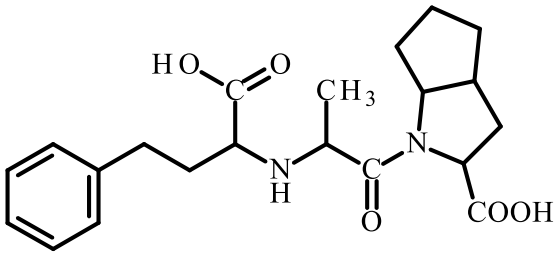



**Fig. 297**
**Structure of ramiprilat, the active metabolite of ramipril**

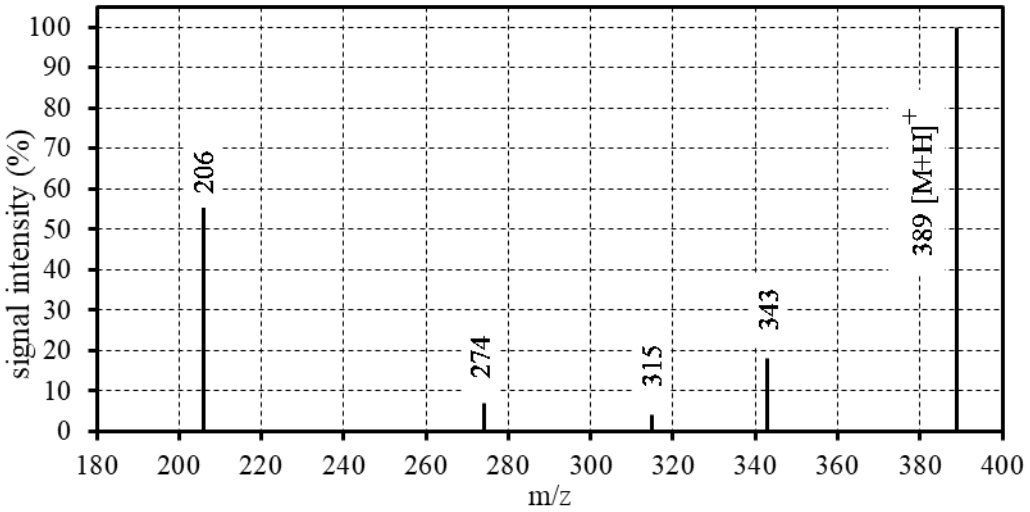



**Fig. 298 $MS^2$ mass spectrum of ramiprilat, positive mode, precursor ion $[M+H]^+$, ESI ionization (reconstructed from data in [5]).**

**Sources cited in application example 5.8**

[1] *J.E. Frampton, D.H. Peters*: Ramipril – An Updated Review of its Therapeutic Use in Essential Hypertension and Heart Failure.
**Drugs 1995:49**(3), 440-466

[2] *E.M. Alapi, J. Fischer*: **Tables of Selected Analogue Classes** în **Analogue-based Drug Discovery**, *J. Fischer & C.R. Ganellin* editors, pag. 469
Wiley-VCH Verlag GmbH & Co. KGaA, 2006
[ISBN: 3-527-31257-9]

[3] *W.M.A. Niessen*: Fragmentation of Toxicologically Relevant Drugs in Positive-ion Liquid Chromatography-Tandem Mass Spectrometry.
**Mass Spectrometry Reviews 2011:30**(4), 626-663

[4] *W.M.A. Niessen*: Fragmentation of Toxicologically Relevant Drugs in Negative-ion Liquid Chromatography-Tandem Mass Spectrometry.
**Mass Spectrometry Reviews 2012:31**(6), 626-665

[5] *Z. Zhu, A. Vachareau, L. Neirinck*: Liquid Chromatography-Mass Spectrometry Method for Determination of Ramipril and Its Active Metabolite Ramiprilat in Human Plasma.
**Journal of Chromatography B. 2002:779**(2), 297-306

## 5.9 Special features of the $MS^2$ fragmentation of Aspirin (acetylsalicylic acid)

Aspirin is a suitable compound to illustrate the change in $MS^2$ mass spectra as a function of the collision energy that produces the product ions. Figure 299 shows the $MS^1$ mass spectra of aspirin recorded in positive electrospray ionization (ESI) mode.

Figures 300 through 306 show the $MS^2$ spectra obtained by chemical impact ionization performed with progressively increasing impact energies (from 15 eV to 180 eV) and the **m/z** values together with the composition of the ion fragments assigned to the signals. The precursor ion is the protonated molecular ion **$[M+H]^+$** with **m/z** 181.0495. Fragmentation of the precursor ion is performed by chemical impact dissociation (**CID**).

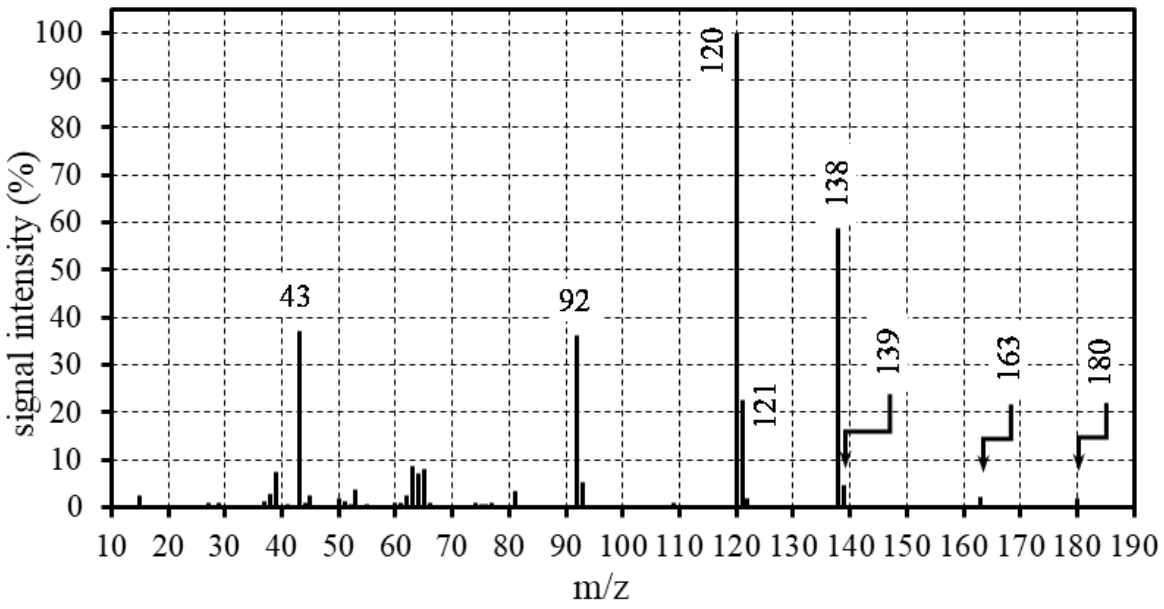
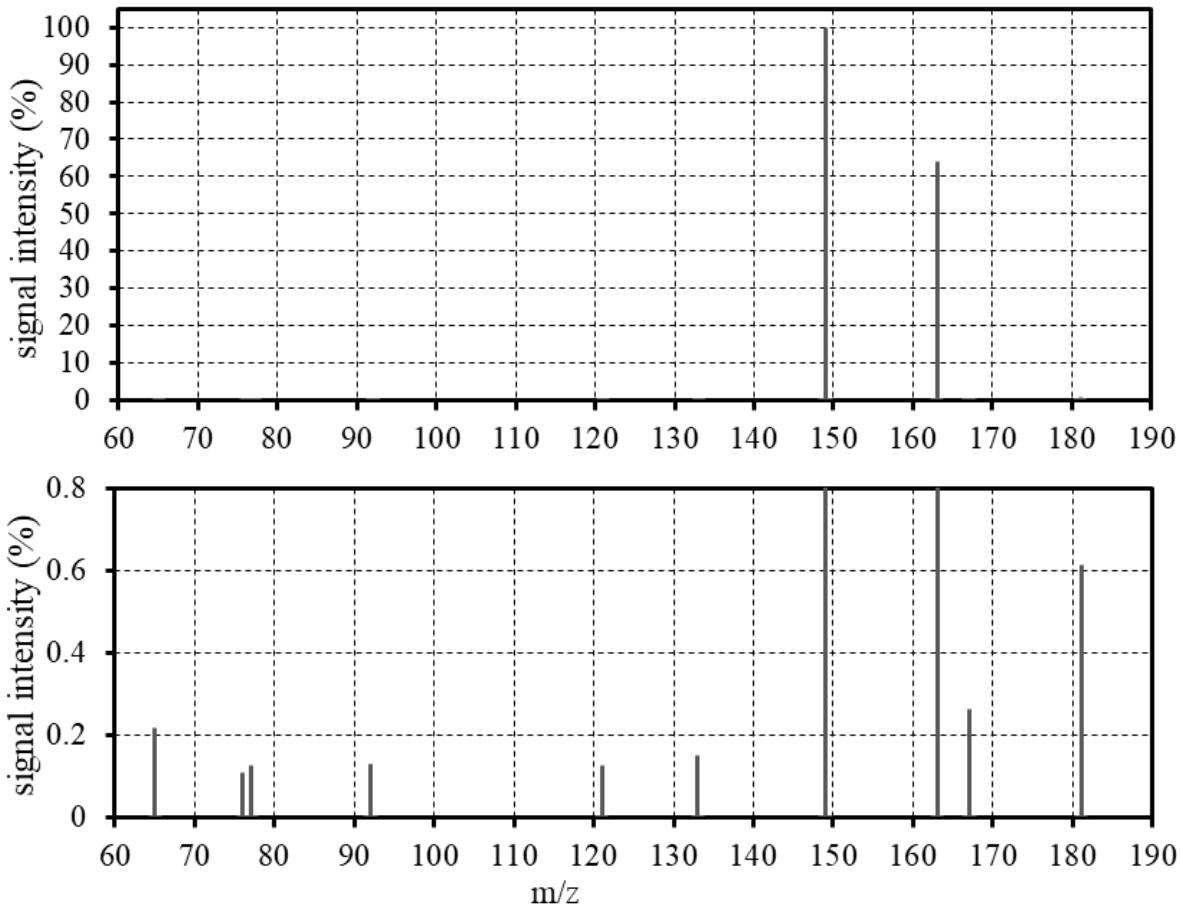
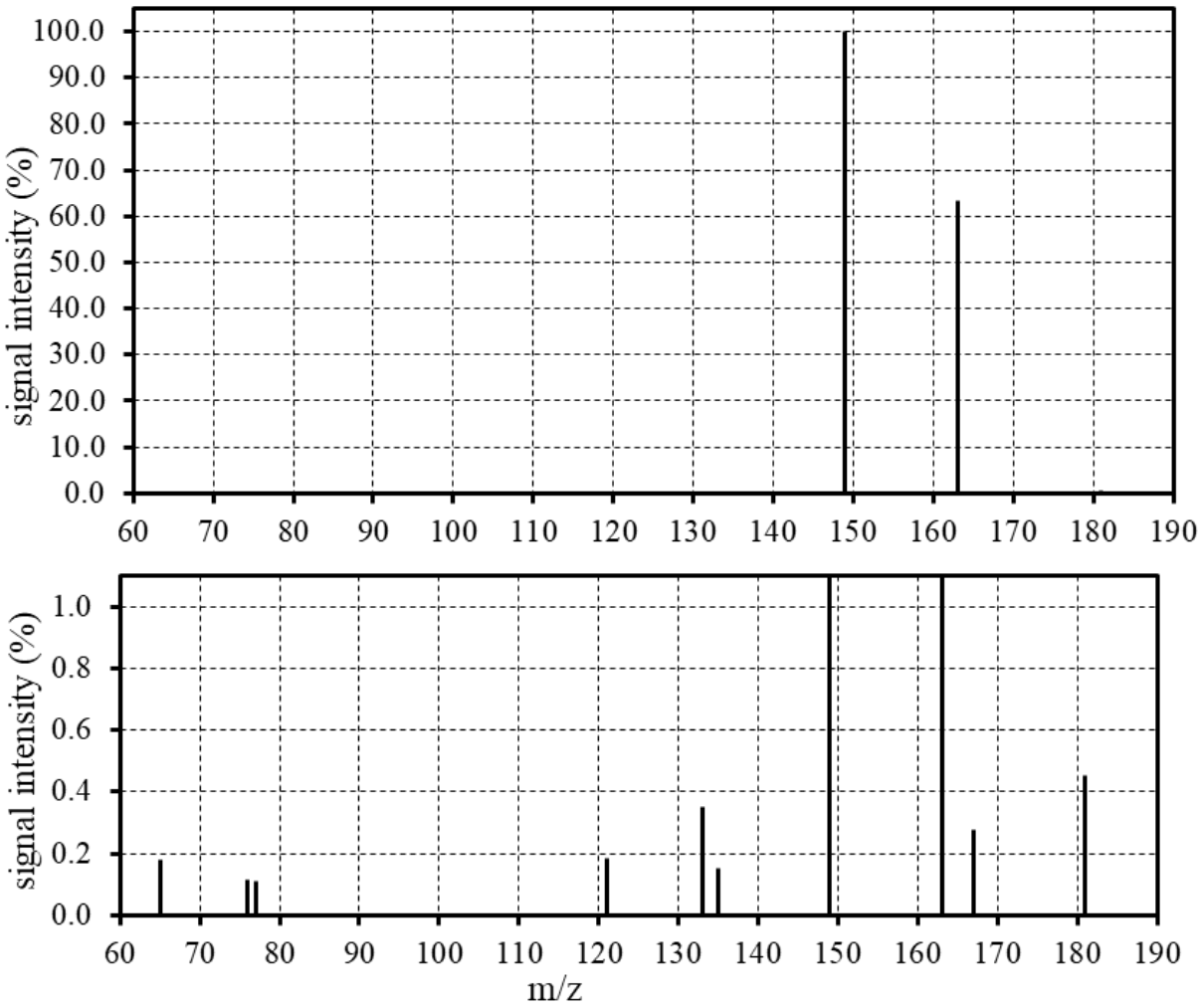



**Fig. 299 $MS^1$ mass spectrum of Aspirin (positive mode, ESI ionization, after MoNA collection, spectrum no. 250572)**



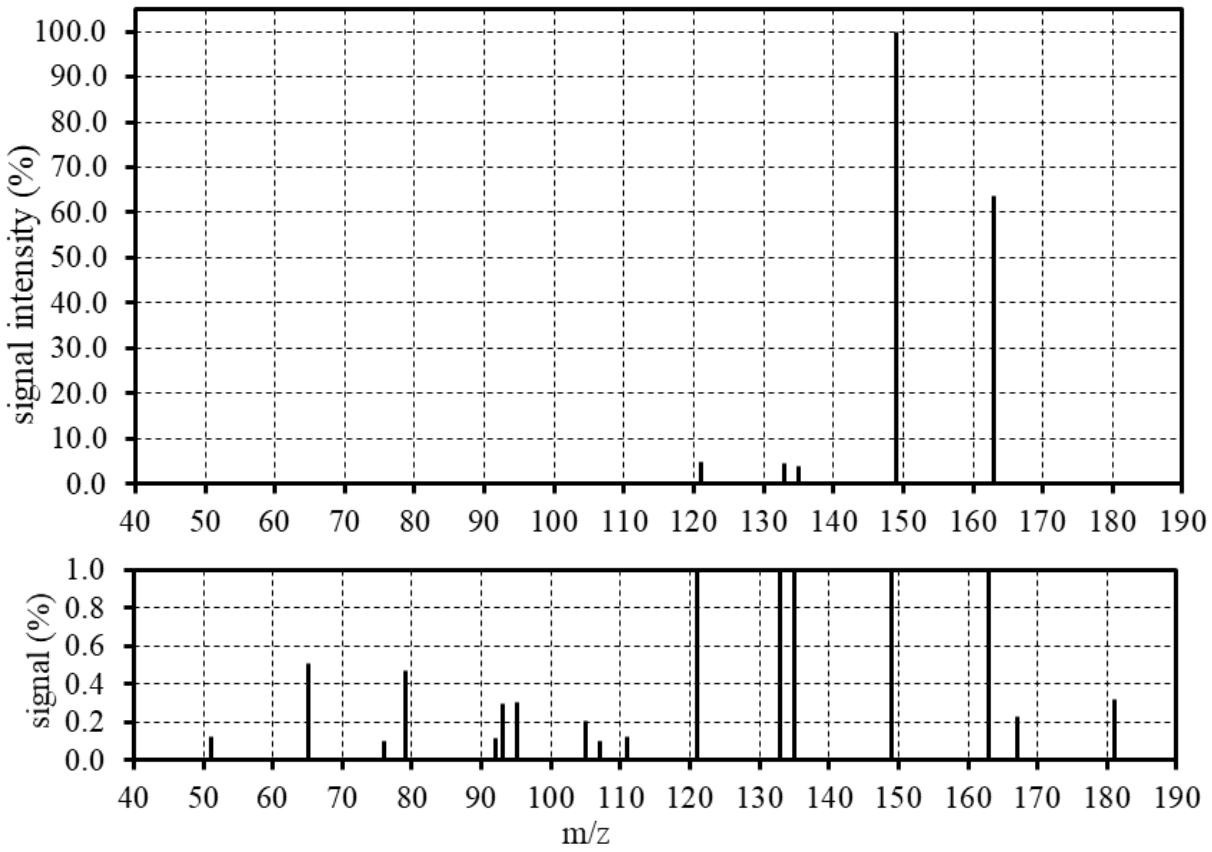

| Acetylsalicylic acid (Aspirin)<br>positive mode – $MS^2$ – 15 eV ; precursor ion: 181.0495 $[M+H]^+$ | | | | | |
|---|---|---|---|---|---|
| **m/z** | **Relative abundance (%)** | **Assigned ionic fragment** | **m/z** | **Relative abundance (%)** | **Assigned ionic fragment** |
| 65.0385 | 0.22 | $[C_5H_5]^+$ | 133.028 | 0.15 | $[C_8H_5O_2]^+$ |
| 76.0304 | 0.11 | $[C_6H_4]^+$ | 149.0231 | 100.00 | $[C_8H_5O_3]^+$ |
| 77.0383 | 0.12 | $[C_6H_5]^+$ | 163.0386 | 63.82 | $[C_9H_7O_3]^+$ |
| 92.0255 | 0.13 | $[C_6H_4O]^+$ | 167.0337 | 0.26 | $[C_8H_7O_4]^+$ |
| 121.0283 | 0.12 | $[C_7H_5O_2]^+$ | 181.0493 | 0.61 | $[C_9H_9O_4]^+$ |

**Fig. 300 $MS^2$ spectrum of Aspirin and the ion fragments assigned to the signals (reconstructed from digitized data of the Mass Bank of North America data)**



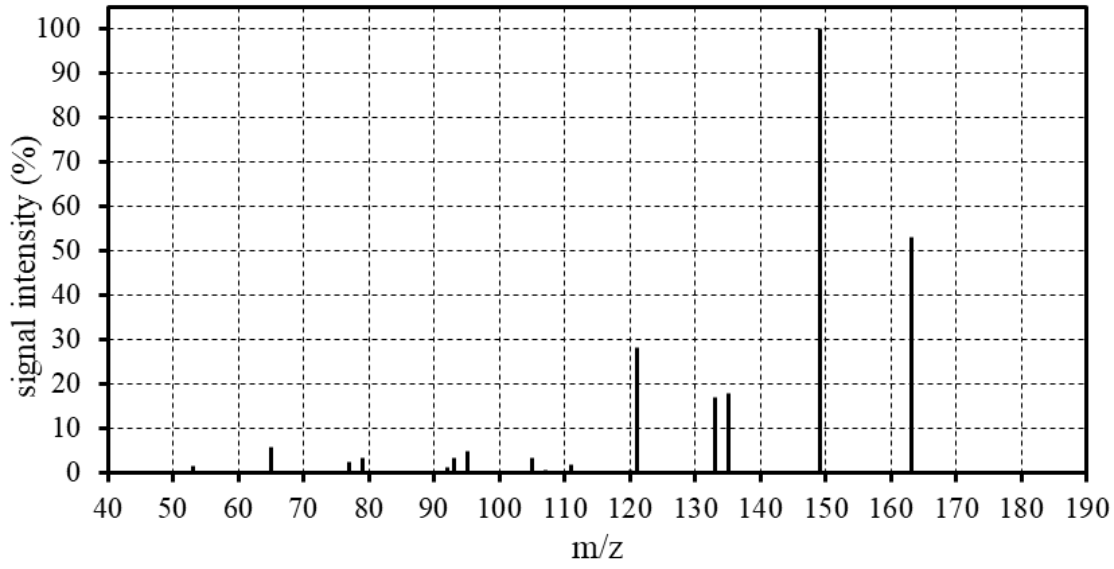

| Acetylsalicylic acid (Aspirin)<br>positive mode – $MS^2$ – 30 eV ; precursor ion: 181.0495 $[M+H]^+$ | | | | | |
|---|---|---|---|---|---|
| **m/z** | **Relative abundance (%)** | **Assigned ionic fragment** | **m/z** | **Relative abundance (%)** | **Assigned ionic fragment** |
| 65.0385 | 0.18 | $[C_5H_5]^+$ | 135.0436 | 0.15 | $[C_8H_7O_2]^+$ |
| 76.0305 | 0.12 | $[C_6H_4]^+$ | 149.0231 | 100.00 | $[C_8H_5O_3]^+$ |
| 77.0384 | 0.11 | $[C_6H_5]^+$ | 163.0386 | 63.31 | $[C_9H_7O_3]^+$ |
| 121.0281 | 0.18 | $[C_7H_5O_2]^+$ | 167.0336 | 0.27 | $[C_8H_7O_4]^+$ |
| 133.0282 | 0.35 | $[C_8H_5O_2]^+$ | 181.0493 | 0.45 | $[C_9H_9O_4]^+$ |

**Fig. 301 $MS^2$ spectrum of Aspirin and the ion fragments assigned to the signals (reconstructed from digitized data of the Mass Bank of North America data)**



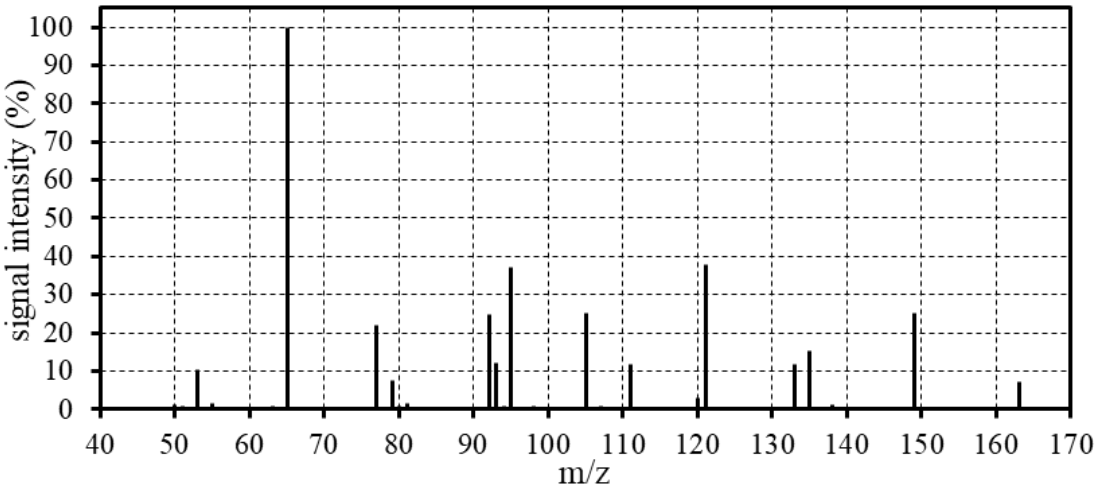

| Acetylsalicylic acid (Aspirin)<br>positive mode – $MS^2$ – 45 eV ; precursor ion: 181.0495 $[M+H]^+$ | | | | | |
|---|---|---|---|---|---|
| **m/z** | **Relative abundance (%)** | **Assigned ionic fragment** | **m/z** | **Relative abundance (%)** | **Assigned ionic fragment** |
| 51.0228 | 0.12 | $[C_4H_3]^+$ | 111.0438 | 0.12 | $[C_6H_7O_2]^+$ |
| 65.0383 | 0.51 | $[C_5H_5]^+$ | 121.0282 | 4.91 | $[C_7H_5O_2]^+$ |
| 76.0304 | 0.10 | $[C_6H_4]^+$ | 121.0394 | 0.66 | $[C_6H_5N_2O]^+$ |
| 79.054 | 0.47 | $[C_6H_7]^+$ | 133.0282 | 4.63 | $[C_8H_5O_2]^+$ |
| 92.0255 | 0.11 | $[C_6H_4O]^+$ | 135.0438 | 3.97 | $[C_8H_7O_2]^+$ |
| 93.0333 | 0.29 | $[C_6H_5O]^+$ | 149.0231 | 100.00 | $[C_8H_5O_3]^+$ |
| 95.049 | 0.30 | $[C_6H_7O]^+$ | 163.0386 | 63.51 | $[C_9H_7O_3]^+$ |
| 105.0334 | 0.18 | $[C_7H_5O]^+$ | 167.0337 | 0.23 | $[C_8H_7O_4]^+$ |
| 105.0447 | 0.20 | $[C_6H_5N_2]^+$ | 181.0492 | 0.32 | $[C_9H_9O_4]^+$ |
| 107.049 | 0.10 | $[C_7H_7O]^+$ | | | |

**Fig. 302 $MS^2$ spectrum of Aspirin and the ion fragments assigned to the signals (reconstructed from digitized data of the Mass Bank of North America data)**



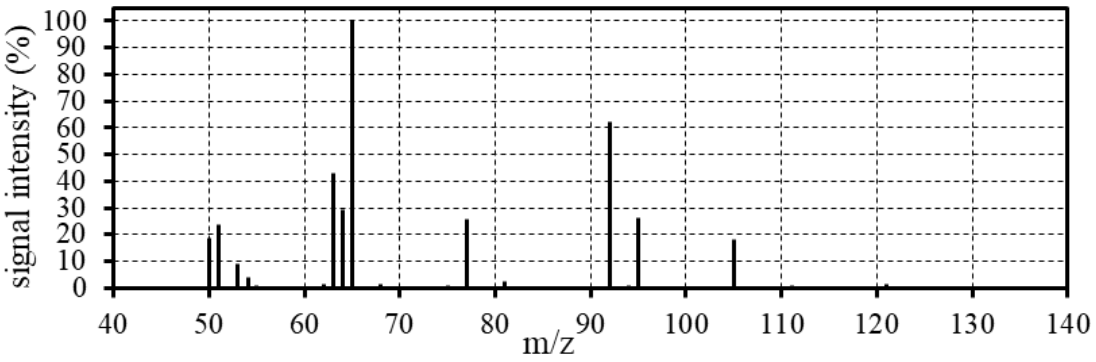

| Acetylsalicylic acid (Aspirin)<br>positive mode – $MS^2$ – 60 eV ; precursor ion: 181.0495 $[M+H]^+$ | | | | | | |
|---|---|---|---|---|---|---|
| **m/z** | **Relative abundance (%)** | **Assigned ionic fragment** | **m/z** | **Relative abundance (%)** | **Assigned ionic fragment** | |
| 50.0149 | 0.14 | $[C_4H_2]^+$ | 105.0333 | 2.06 | $[C_7H_5O]^+$ | |
| 51.0228 | 0.15 | $[C_4H_3]^+$ | 105.0445 | 3.26 | $[C_6H_5N_2]^+$ | |
| 53.0385 | 1.32 | $[C_4H_5]^+$ | 107.0489 | 0.60 | $[C_7H_7O]^+$ | |
| 55.0177 | 0.17 | $[C_3H_3O]^+$ | 111.0439 | 1.71 | $[C_6H_7O_2]^+$ | |
| 65.0384 | 5.83 | $[C_5H_5]^+$ | 120.0203 | 0.48 | $[C_7H_4O_2]^+$ | |
| 77.0383 | 2.41 | $[C_6H_5]^+$ | 121.0282 | 28.28 | $[C_7H_5O_2]^+$ | |
| 79.0540 | 3.36 | $[C_6H_7]^+$ | 121.0394 | 7.31 | $[C_6H_5N_2O]^+$ | |
| 80.0254 | 0.28 | $[C_5H_4O]^+$ | 133.0282 | 16.99 | $[C_8H_5O_2]^+$ | |
| 81.0334 | 0.17 | $[C_5H_5O]^+$ | 135.0438 | 17.86 | $[C_8H_7O_2]^+$ | |
| 91.0541 | 0.13 | $[C_7H_7]^+$ | 138.0308 | 0.23 | $[C_7H_6O_3]^+$ | |
| 92.0254 | 1.15 | $[C_6H_4O]^+$ | 149.0231 | 100.00 | $[C_8H_5O_3]^+$ | |
| 93.0333 | 3.29 | $[C_6H_5O]^+$ | 163.0386 | 53.06 | $[C_9H_7O_3]^+$ | |
| 94.0411 | 0.16 | $[C_6H_6O]^+$ | 167.0337 | 0.20 | $[C_8H_7O_4]^+$ | |
| 95.0490 | 4.82 | $[C_6H_7O]^+$ | 181.0491 | 0.35 | $[C_9H_9O_4]^+$ | |
| 98.0361 | 0.21 | $[C_5H_6O_2]^+$ | | | | |

**Fig. 303 $MS^2$ spectrum of Aspirin and the ion fragments assigned to the signals (reconstructed from digitized data of the Mass Bank of North America data)**



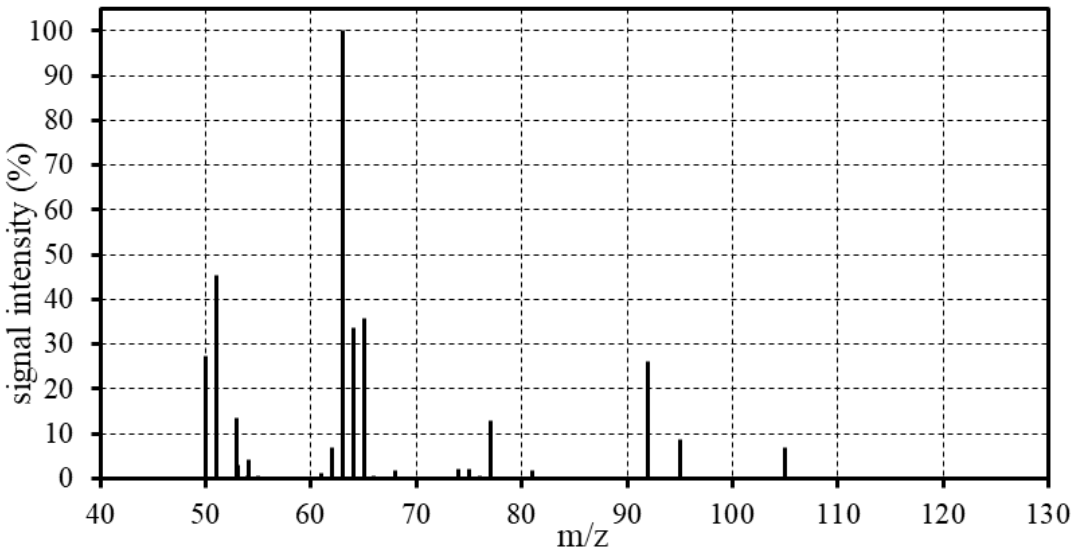

| Acetylsalicylic acid (Aspirin) positive mode – $MS^2$ – 90 eV ; precursor ion: 181.0495 $[M+H]^+$ | | | | | |
|---|---|---|---|---|---|
| **m/z** | **Relative abundance (%)** | **Assigned ionic fragment** | **m/z** | **Relative abundance (%)** | **Assigned ionic fragment** |
| 50.0150 | 1.24 | $[C_4H_2]^+$ | 98.0361 | 0.66 | $[C_5H_6O_2]^+$ |
| 51.0228 | 0.64 | $[C_4H_3]^+$ | 105.0333 | 11.09 | $[C_7H_5O]^+$ |
| 53.0021 | 0.78 | $[C_3HO]^+$ | 105.0446 | 25.189 | $[C_6H_5N_2]^+$ |
| 53.0385 | 10.36 | $[C_4H_5]^+$ | 106.0415 | 0.26 | $[C_7H_6O]^+$ |
| 55.0178 | 1.44 | $[C_3H_3O]^+$ | 107.049 | 0.81 | $[C_7H_7O]^+$ |
| 63.0228 | 0.68 | $[C_5H_3]^+$ | 108.0204 | 0.12 | $[C_6H_4O_2]^+$ |
| 64.0306 | 0.57 | $[C_5H_4]^+$ | 109.0646 | 0.18 | $[C_7H_9O]^+$ |
| 65.0384 | 100.00 | $[C_5H_5]^+$ | 110.036 | 0.20 | $[C_6H_6O_2]^+$ |
| 67.0541 | 0.26 | $[C_5H_7]^+$ | 111.0439 | 11.80 | $[C_6H_7O_2]^+$ |
| 68.9969 | 0.39 | $[C_3HO_2]^+$ | 120.0204 | 3.01 | $[C_7H_4O_2]^+$ |
| 77.0384 | 21.91 | $[C_6H_5]^+$ | 121.0282 | 37.72 | $[C_7H_5O_2]^+$ |
| 79.0541 | 7.55 | $[C_6H_7]^+$ | 121.0394 | 31.04 | $[C_6H_5N_2O]^+$ |
| 80.0255 | 0.93 | $[C_5H_4O]+$ | 122.0365 | 0.20 | $[C_7H_6O_2]^+$ |
| 81.0333 | 1.40 | $[C_5H_5O]^+$ | 133.0282 | 11.63 | $[C_8H_5O_2]^+$ |
| 91.0540 | 0.60 | $[C_7H_7]^+$ | 135.0438 | 15.24 | $[C_8H_7O_2]^+$ |
| 92.0255 | 24.63 | $[C_6H_4O]^+$ | 138.0309 | 1.31 | $[C_7H_6O_3]^+$ |
| 93.0334 | 12.25 | $[C_6H_5O]^+$ | 149.0231 | 25.13 | $[C_8H_5O_3]^+$ |
| 94.0412 | 0.80 | $[C_6H_6O]^+$ | 163.0387 | 7.27 | $[C_9H_7O_3]^+$ |
| 95.0490 | 37.23 | $[C_6H_7O]^+$ | | | |

**Fig. 304 $MS^2$ spectrum of Aspirin and the ion fragments assigned to the signals (reconstructed from digitized data of the Mass Bank of North America data)**




| Acetylsalicylic acid (Aspirin)<br>positive mode – $MS^2$ – 150 eV ; precursor ion: 181.0495 $[M+H]^+$ | | | | | |
|---|---|---|---|---|---|
| **m/z** | **Relative abundance (%)** | **Assigned ionic fragment** | **m/z** | **Relative abundance (%)** | **Assigned ionic fragment** |
| 50.0151 | 18.57 | $[C_4H_2]^+$ | 79.0178 | 0.11 | $[C_5H_3O]^+$ |
| 51.0229 | 23.82 | $[C_4H_3]^+$ | 79.0541 | 0.49 | $[C_6H_7]^+$ |
| 53.0021 | 8.76 | $[C_3HO]^+$ | 80.0255 | 0.39 | $[C_5H_4O]^+$ |
| 53.0385 | 8.16 | $[C_4H_5]^+$ | 81.0334 | 2.42 | $[C_5H_5O]^+$ |
| 54.0463 | 3.91 | $[C_4H_6]^+$ | 82.0412 | 0.13 | $[C_5H_6O]^+$ |
| 55.0177 | 0.65 | $[C_3H_3O]^+$ | 91.0541 | 0.15 | $[C_7H_7]^+$ |
| 61.0071 | 0.15 | $[C_5H]^+$ | 92.0255 | 62.05 | $[C_6H_4O]^+$ |
| 62.0150 | 1.62 | $[C_5H_2]^+$ | 92.0367 | 5.24 | $[C_5H_4N_2]^+$ |
| 63.0228 | 42.97 | $[C_5H_3]^+$ | 93.0334 | 0.43 | $[C_6H_5O]^+$ |
| 64.0307 | 29.06 | $[C_5H_4]^+$ | 94.0411 | 0.62 | $[C_6H_6O]^+$ |
| 65.0385 | 100.00 | $[C_5H_5]^+$ | 95.0490 | 26.31 | $[C_6H_7O]_+$ |
| 66.0099 | 0.17 | $[C_4H_2O]^+$ | 98.0361 | 0.11 | $[C_5H_6O_2]^+$ |
| 66.0463 | 0.32 | $[C_5H_6]^+$ | 105.0446 | 18.23 | $[C6H5N2]^+$ |
| 67.0541 | 0.18 | $[C_5H_7]^+$ | 106.0416 | 0.15 | $[C_7H_6O]^+$ |
| 67.9891 | 1.48 | $[C_3O_2]^+$ | 109.0645 | 0.16 | $[C_7H_9O]_+$ |
| 68.9969 | 0.17 | $[C_3HO_2]^+$ | 111.0439 | 0.62 | $[C_6H_7O_2]^+$ |
| 74.0149 | 0.34 | $[C_6H_2]^+$ | 119.0127 | 0.13 | $[C_7H_3O_2]^+$ |
| 75.0228 | 0.92 | $[C_6H_3]^+$ | 121.0282 | 0.37 | $[C_7H_5O_2]^+$ |
| 77.0384 | 25.67 | $[C_6H_5]^+$ | 121.0394 | 1.31 | $[C_6H_5N_2O]^+$ |

**Fig.305 $MS^2$ spectrum of Aspirin and the ion fragments assigned to the signals (reconstructed from digitized data of the Mass Bank of North America data)**




| Acetylsalicylic acid (Aspirin)<br>positive mode – $MS^2$ – 180 eV ; precursor ion: 181.0495 $[M+H]^+$ | | | | | |
|---|---|---|---|---|---|
| **m/z** | **Relative abundance (%)** | **Assigned ionic fragment** | **m/z** | **Relative abundance (%)** | **Assigned ionic fragment** |
| 50.0151 | 27.37 | $[C_4H_2]^+$ | 68.997 | 0.19 | $[C_3HO_2]^+$ |
| 51.0229 | 45.38 | $[C_4H_3]^+$ | 74.0150 | 2.15 | $[C_6H_2]^+$ |
| 53.0021 | 13.54 | $[C_3HO]^+$ | 75.0228 | 1.94 | $[C_6H_3]^+$ |
| 53.0385 | 2.92 | $[C_4H_5]^+$ | 76.0306 | 0.48 | $[C_6H_4]^+$ |
| 54.0100 | 0.44 | $[C_3H_2O]^+$ | 77.0384 | 12.77 | $[C_6H_5]^+$ |
| 54.0463 | 4.20 | $[C_4H_6]^+$ | 79.0176 | 0.11 | $[C_5H_3O]^+$ |
| 55.0177 | 0.48 | $[C_3H_3O]^+$ | 81.0333 | 1.78 | $[C_5H_5O]^+$ |
| 61.0072 | 1.27 | $[C_5H]^+$ | 82.0413 | 0.14 | $[C_5H_6O]^+$ |
| 62.0150 | 6.81 | $[C_5H_2]^+$ | 92.0255 | 26.22 | $[C_6H_4O]^+$ |
| 63.0228 | 100.00 | $[C_5H_3]^+$ | 92.0367 | 3.38 | $[C_5H_4N_2]^+$ |
| 64.0306 | 33.67 | $[C_5H_4]^+$ | 94.0412 | 0.21 | $[C_6H_6O]^+$ |
| 65.0385 | 35.83 | $[C_5H_5]^+$ | 95.0490 | 8.77 | $[C_6H_7O]^+$ |
| 66.0099 | 0.59 | $[C_4H_2O]^+$ | 98.0360 | 0.17 | $[C_5H_6O_2]^+$ |
| 66.0462 | 0.23 | $[C_5H_6]^+$ | 105.0446 | 6.76 | $[C_6H_5N_2]^+$ |
| 67.0542 | 0.11 | $[C_5H_7]^+$ | 119.0122 | 0.10 | $[C_7H_3O_2]^+$ |
| 67.9891 | 1.76 | $[C_3O_2]^+$ | | | |

**Fig. 306 $MS^2$ spectrum of Aspirin and the ion fragments assigned to the signals (reconstructed from digitized data of the Mass Bank of North America data)**

Figures 299 through 306 are the result of reconstructed spectra from digitized data in the MoNA spectral database (**M**ass Bank **o**f **N**orth **A**merica https://pubchem.ncbi.nlm.nih.gov/source/22043).

The positions and intensities of the signals in the $MS^2$ spectra depend on the CID ionization energies that produce the ions. Increasing the fragmentation energy produces a greater number of signals localized at lower **m/z** values at the expense of signals at higher **m/z** ratios. This dependence can be illustrated by a simple function, **F** (72):

$$F = \frac{E_{col}(eV) \cdot n}{\sum_{j=1}^{n} \left(\frac{m}{z}\right)_j \cdot I_j(\%)} \qquad (72)$$

in which:

"$\mathbf{E_{col}(eV)}$" is the collision energy (expressed in eV) that produces the fragmentation,

"$\mathbf{Ij(\%)}$" is relative abundance of $\mathbf{j}^{th}$ ion (expressed as percentage of the dominant signal);

"**n**" is the number of signals in the spectrum taken into account by the function "**F**".

Figure 307 shows the dependence of the function (72) on the energy of fragmentation. The shape corresponds to a power function.

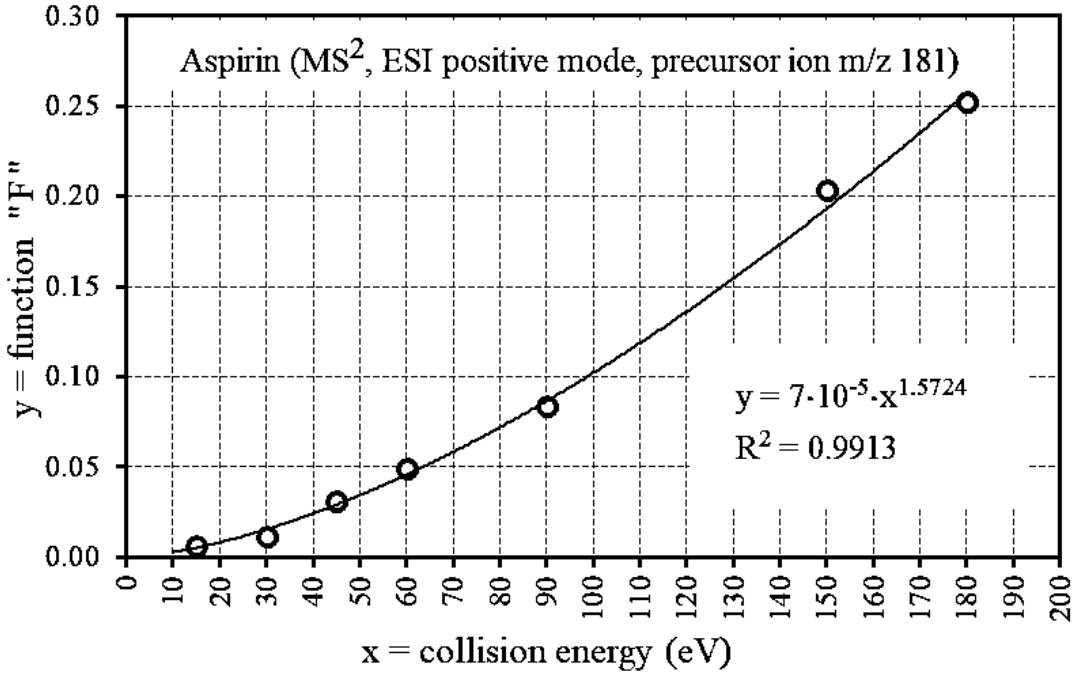
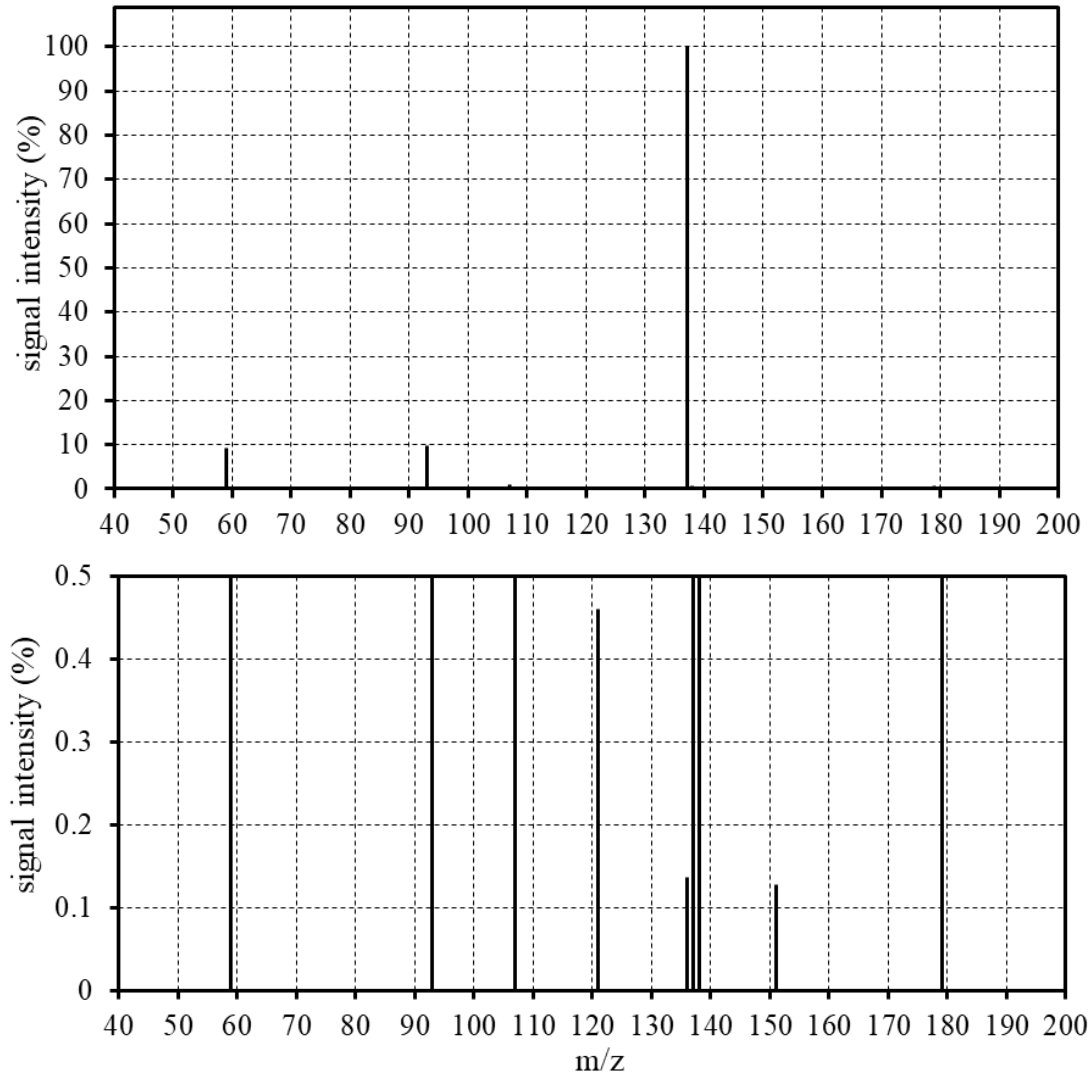
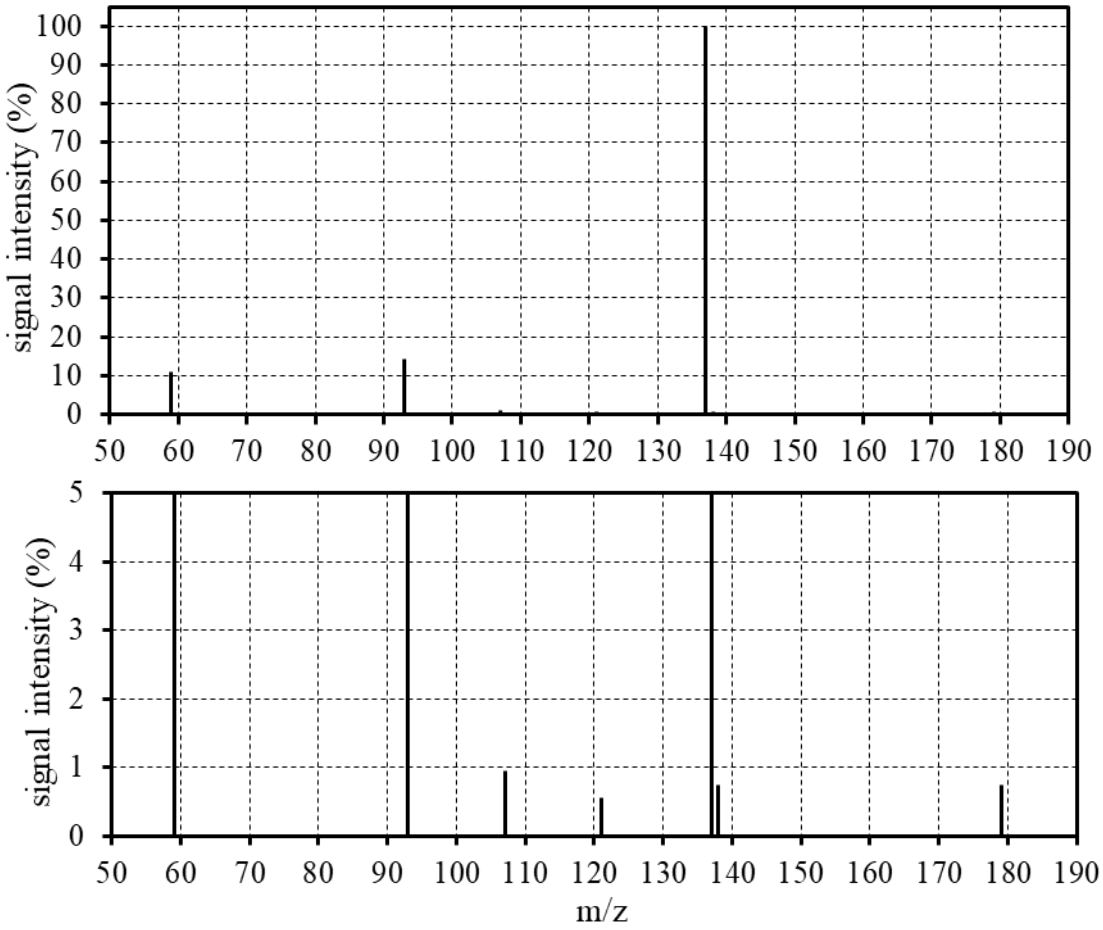



**Fig. 307 The dependence of the $MS^2$ fragmenting propensity of precursor ion (m/z 181) on the collision energy.**



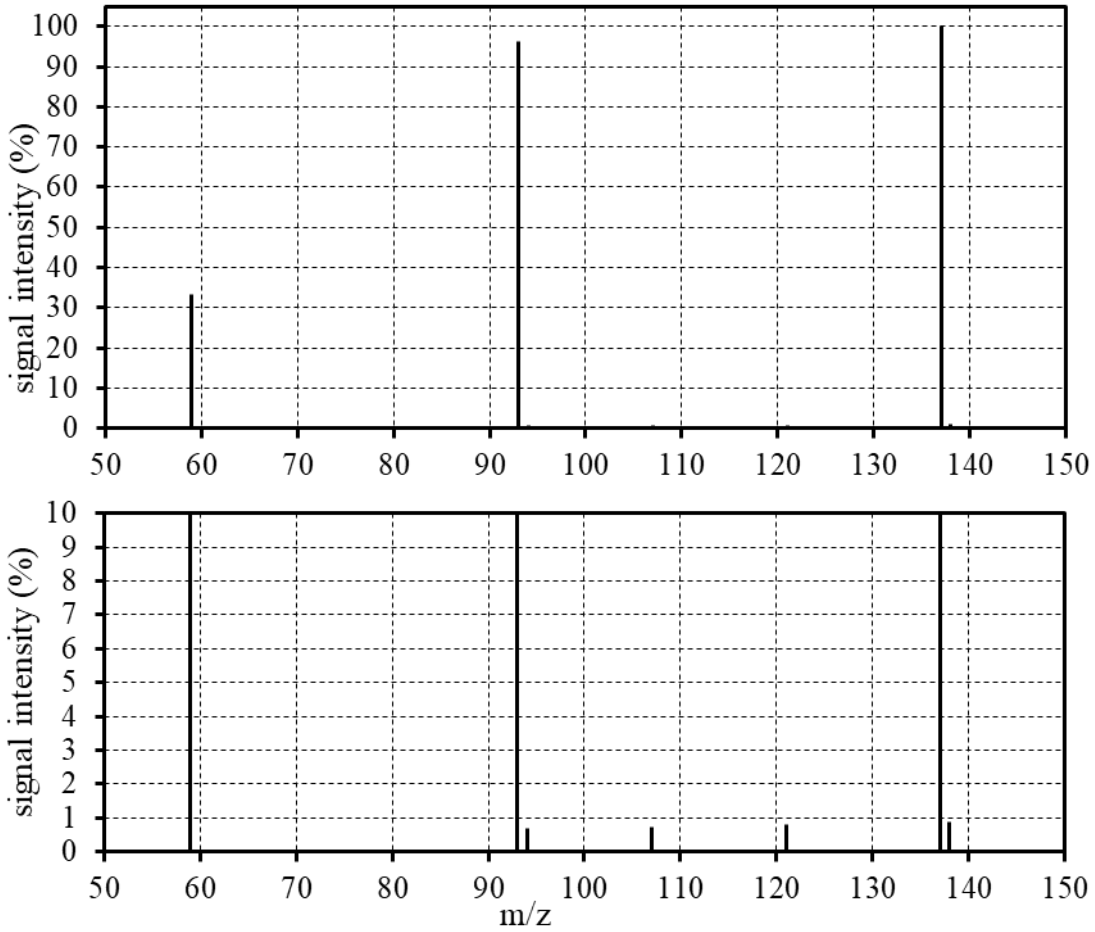

| Acetylsalicylic acid (Aspirin)<br>negative mode – $MS^2$ – 15 eV - precursor ion: 179.0350 $[M-H]^-$ | | | | | |
|---|---|---|---|---|---|
| **m/z** | **Relative abundance (%)** | **Assigned ionic fragment** | **m/z** | **Relative abundance (%)** | **Assigned ionic fragment** |
| 59.0138 | 9.20 | $[C_2H_3O_2]^-$ | 137.0243 | 100.00 | $[C_7H_5O_3]^-$ |
| 93.0345 | 9.83 | $[C_6H_5O]^-$ | 138.0277 | 0.79 | $[C_2H_6N_2O_5]^-$ |
| 107.0502 | 1.01 | $[C_7H_7O]^-$ | 151.0397 | 0.13 | $[C_8H_7O_3]^-$ |
| 121.0295 | 0.46 | $[C_7H_5O_2]^-$ | 179.0350 | 0.81 | $[C_9H_7O_4]^-$ |
| 135.9913 | 0.14 | $[C_5N_2O_3]^-$ | | | |

**Fig. 308 $MS^2$ mass spectrum of aspirin in negative mode at 15 eV collision energy (reconstructed from digitized data from the Mass Bank of North America).**



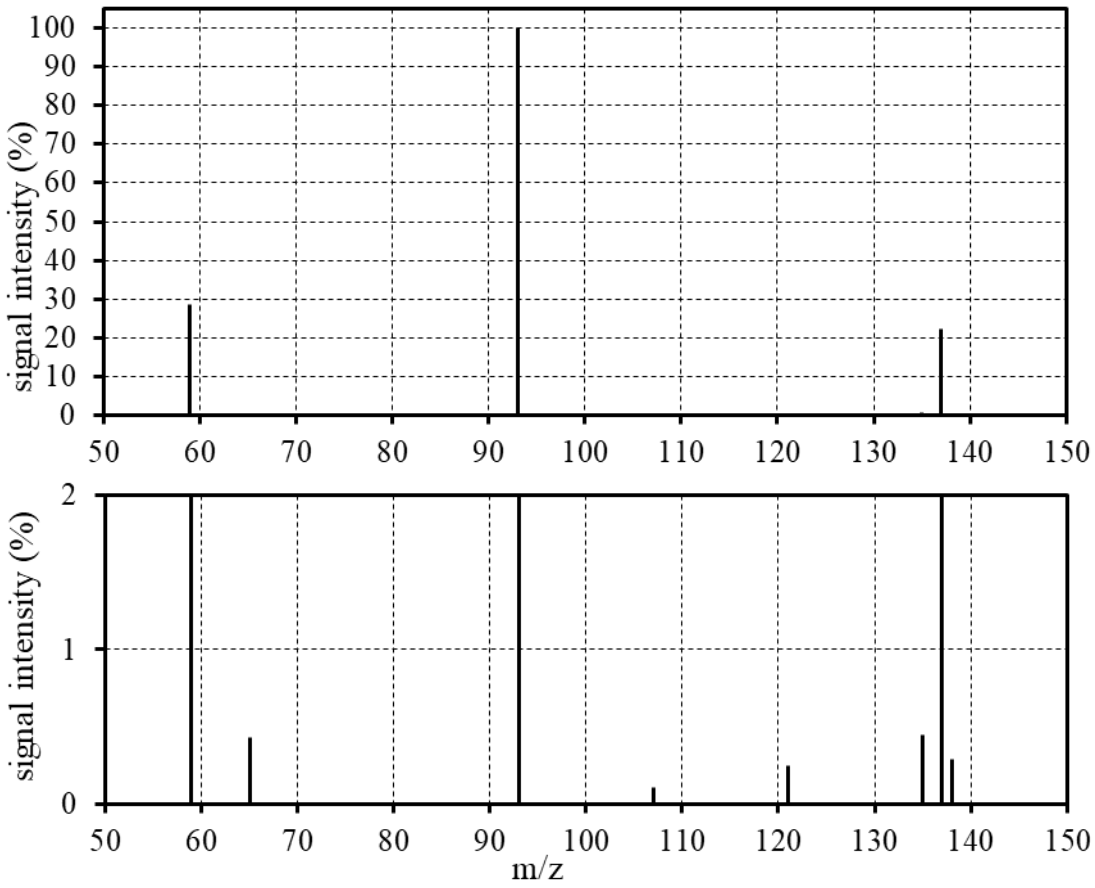

| Acetylsalicylic acid (Aspirin)<br>negative mode – $MS^2$ – 30 eV ; precursor ion: 179.0350 $[M-H]^-$ | | | | | |
|---|---|---|---|---|---|
| **m/z** | **Relative abundance (%)** | **Assigned ionic fragment** | **m/z** | **Relative abundance (%)** | **Assigned ionic fragment** |
| 59.0138 | 10.87 | $[C_2H_3O_2]^-$ | 137.0243 | 100.00 | $[C_7H_5O_3]^-$ |
| 93.0345 | 14.15 | $[C_6H_5O]^-$ | 138.0277 | 0.73 | $[C_2H_6N_2O_5]^-$ |
| 107.0502 | 0.95 | $[C_7H_7O]^-$ | 179.0350 | 0.74 | $[C_9H_7O_4]^-$ |
| 121.0295 | 0.55 | $[C_7H_5O_2]^-$ | | | |

**Fig. 309 $MS^2$ mass spectrum of aspirin in negative mode at 30 eV collision energy (reconstructed from digitized data from the Mass Bank of North America)**



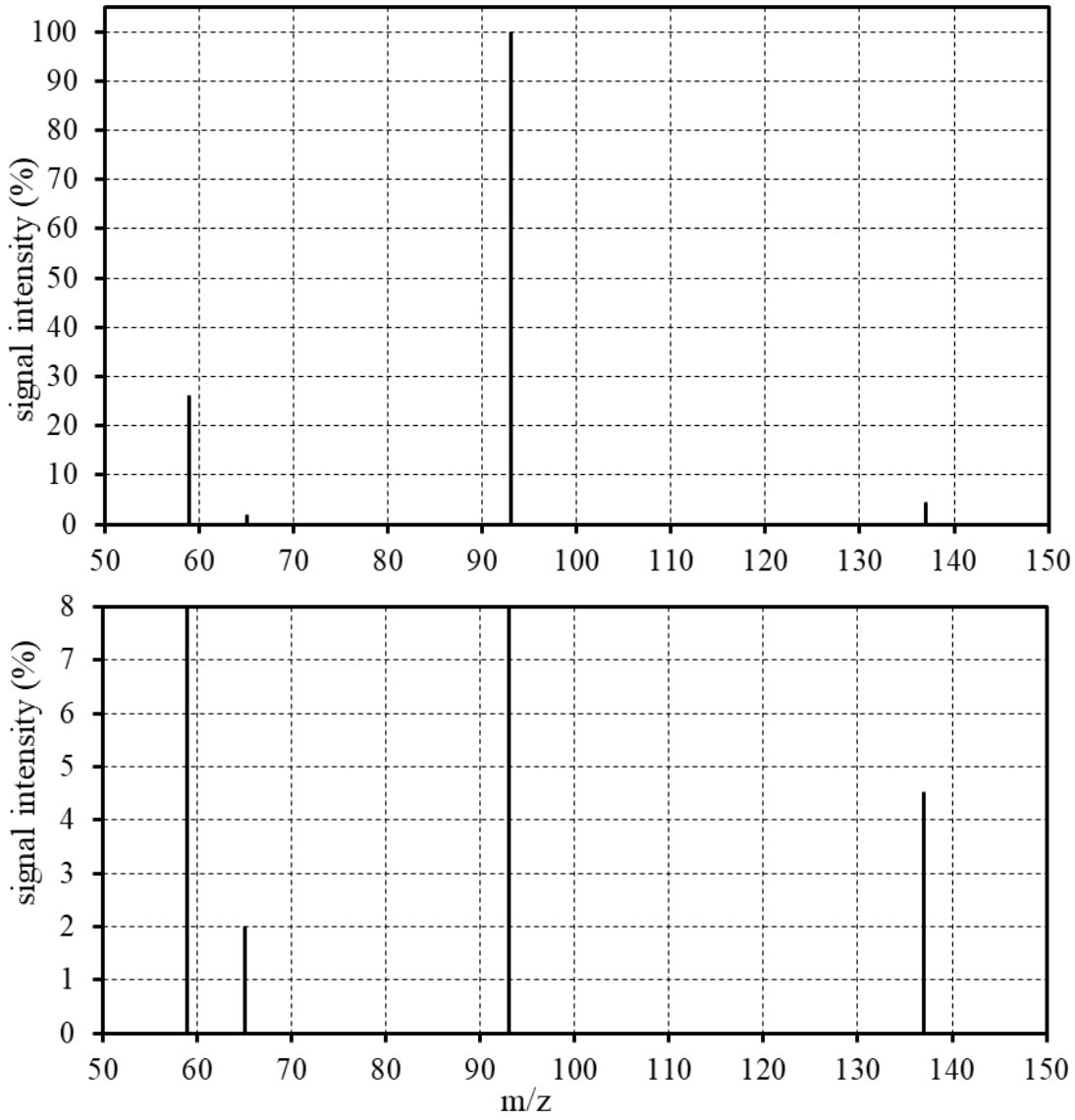

| Acetylsalicylic acid (Aspirin)<br>Negative mode – $MS^2$ – 45 eV ; precursor ion: 179.0350 $[M-H]^-$ | | | | | |
|---|---|---|---|---|---|
| **m/z** | **Relative abundance (%)** | **Assigned ionic fragment** | **m/z** | **Relative abundance (%)** | **Assigned ionic fragment** |
| 59.0138 | 33.41 | $[C_2H_3O_2]^-$ | 121.0296 | 0.79 | $[C_7H_5O_2]^-$ |
| 93.0345 | 96.20 | $[C_6H_5O]^-$ | 137.0244 | 100.00 | $[C_7H_5O_3]^-$ |
| 94.038 | 0.69 | $[CH_6N_2O_3]^-$ | 138.0278 | 0.89 | $[C_2H_6N_2O_5]^-$ |
| 107.0503 | 0.74 | $[C_7H_7O]^-$ | | | |

**Fig. 310 $MS^2$ mass spectrum of aspirin in negative mode at 45 eV collision energy (reconstructed from digitized data from the Mass Bank of North America)**



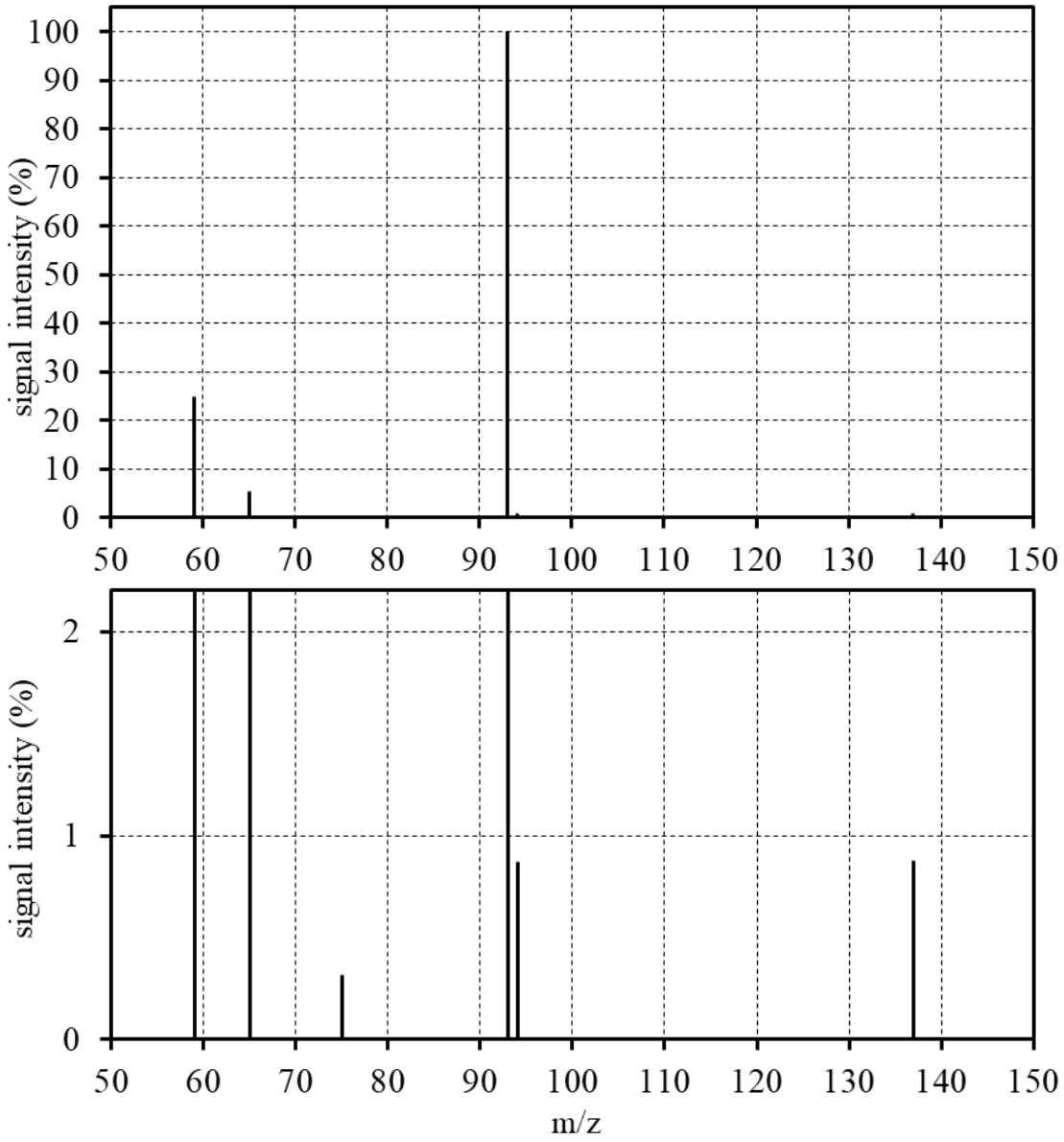

| Acetylsalicylic acid (Aspirin)<br>negative mode – $MS^2$ – 60 eV ; precursor ion: 179.0350 $[M-H]^-$ | | | | | |
|---|---|---|---|---|---|
| **m/z** | **Relative abundance (%)** | **Assigned ionic fragment** | **m/z** | **Relative abundance (%)** | **Assigned ionic fragment** |
| 59.0138 | 28.64 | $[C_2H_3O_2]^-$ | 121.0295 | 0.24 | $[C_7H_5O_2]^-$ |
| 65.0397 | 0.43 | $[C_5H_5]^-$ | 135.0452 | 0.45 | $[C_8H_7O_2]^-$ |
| 93.0345 | 100.00 | $[C_6H_5O]^-$ | 137.0244 | 22.17 | $[C_7H_5O_3]^-$ |
| 107.0502 | 0.10 | $[C_7H_7O]^-$ | 138.0277 | 0.29 | $[C_2H_6N_2O_5]^-$ |

**Fig. 311 $MS^2$ mass spectrum of aspirin in negative mode at 60 eV collision energy (reconstructed from digitized data from the Mass Bank of North America)**



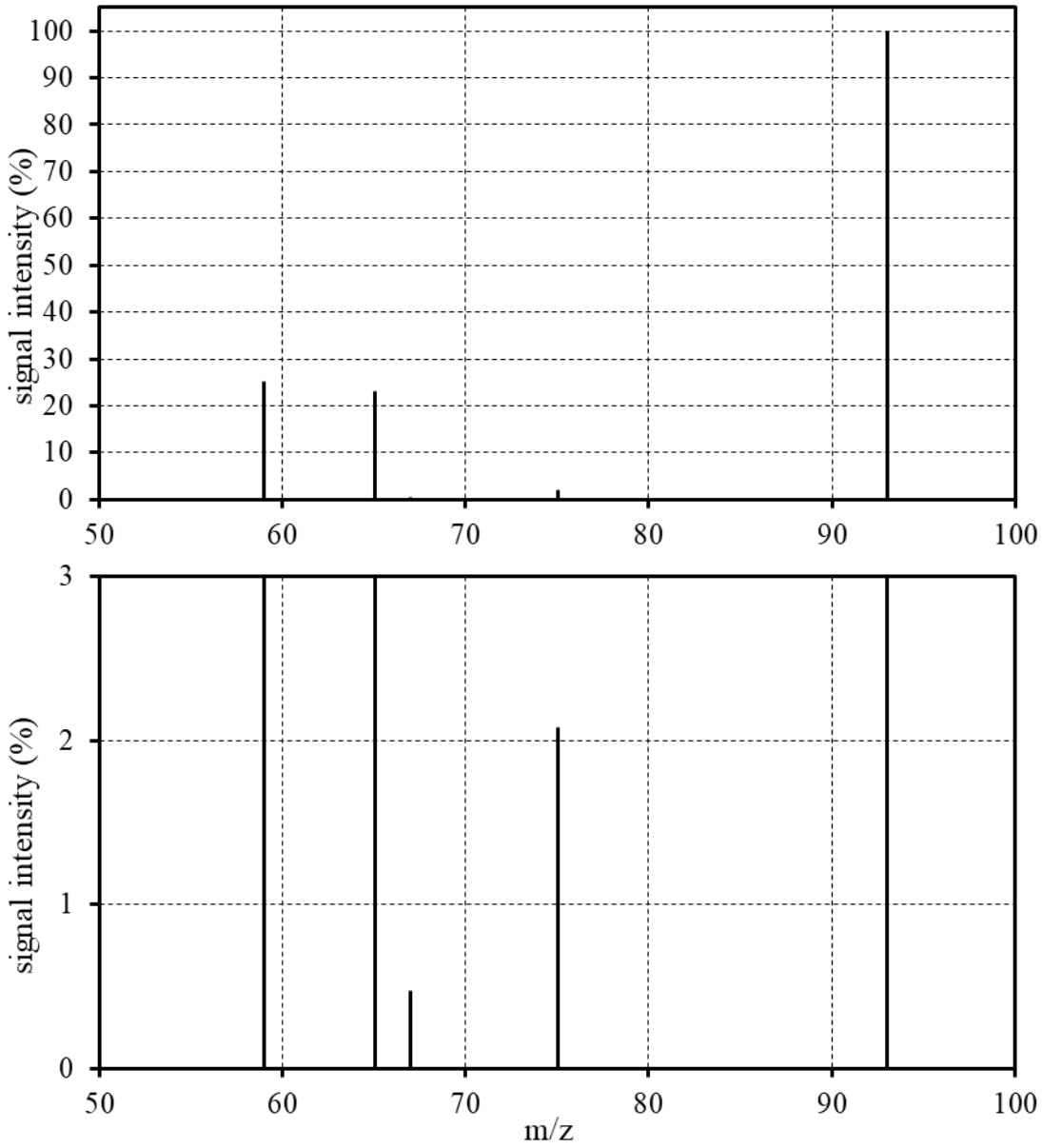

| Acetylsalicyic acid (Aspirin)<br>negative mode – $MS^2$ – 75 eV ; precursor ion: 179.0350 $[M-H]^-$ | | | | | |
|---|---|---|---|---|---|
| **m/z** | **Relative abundance (%)** | **Assigned ionic fragment** | **m/z** | **Relative abundance (%)** | **Assigned ionic fragment** |
| 59.0138 | 26.13 | $[C_2H_3O_2]^-$ | 93.0345 | 100.00 | $[C_6H_5O]^-$ |
| 65.0397 | 2.00 | $[C_5H_5]^-$ | 137.0243 | 4.52 | $[C_7H_5O_3]^-$ |

**Fig. 312 $MS^2$ mass spectrum of aspirin in negative mode at 75 eV collision energy (reconstructed from digitized data from the Mass Bank of North America)**



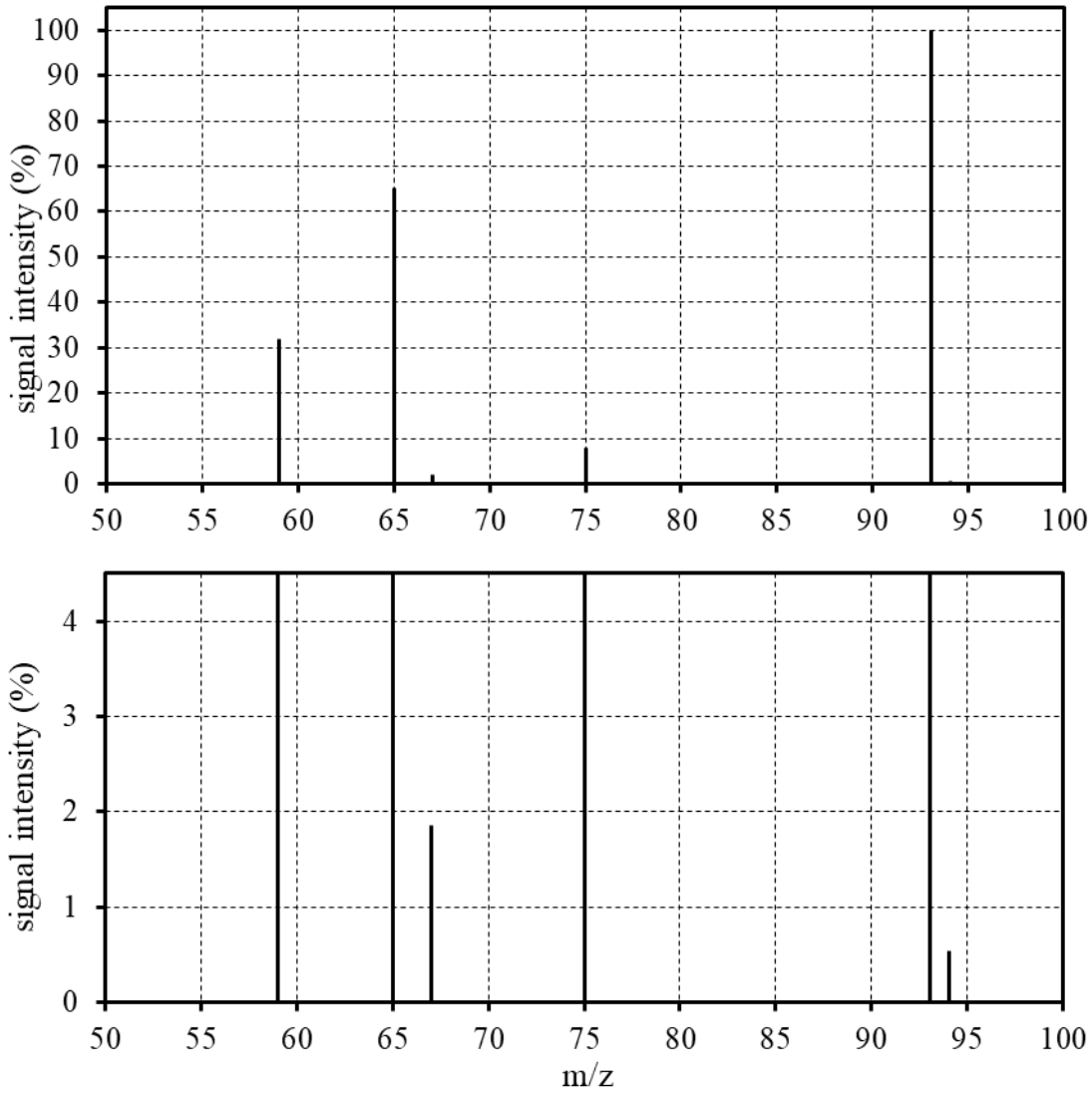

| Acetylsalicylic acid (Aspirin)<br>negative mode – $MS^2$ – 90 eV ; precursor ion: 179.0350 $[M-H]^-$ | | | | | |
|---|---|---|---|---|---|
| **m/z** | **Relative abundance (%)** | **Assigned ionic fragment** | **m/z** | **Relative abundance (%)** | **Assigned ionic fragment** |
| 59.0138 | 24.96 | $[C_2H_3O_2]^-$ | 93.0345 | 100.00 | $[C_6H_5O]^-$ |
| 65.0397 | 5.466 | $[C_5H_5]^-$ | 94.0379 | 0.87 | $[CH_6N_2O_3]^-$ |
| 75.0241 | 0.316 | $[C_6H_3]^-$ | 137.0243 | 0.88 | $[C_7H_5O_3]^-$ |

**Fig. 313 $MS^2$ mass spectrum of aspirin in negative mode at 90 eV collision energy (reconstructed from digitized data from the Mass Bank of North America)**



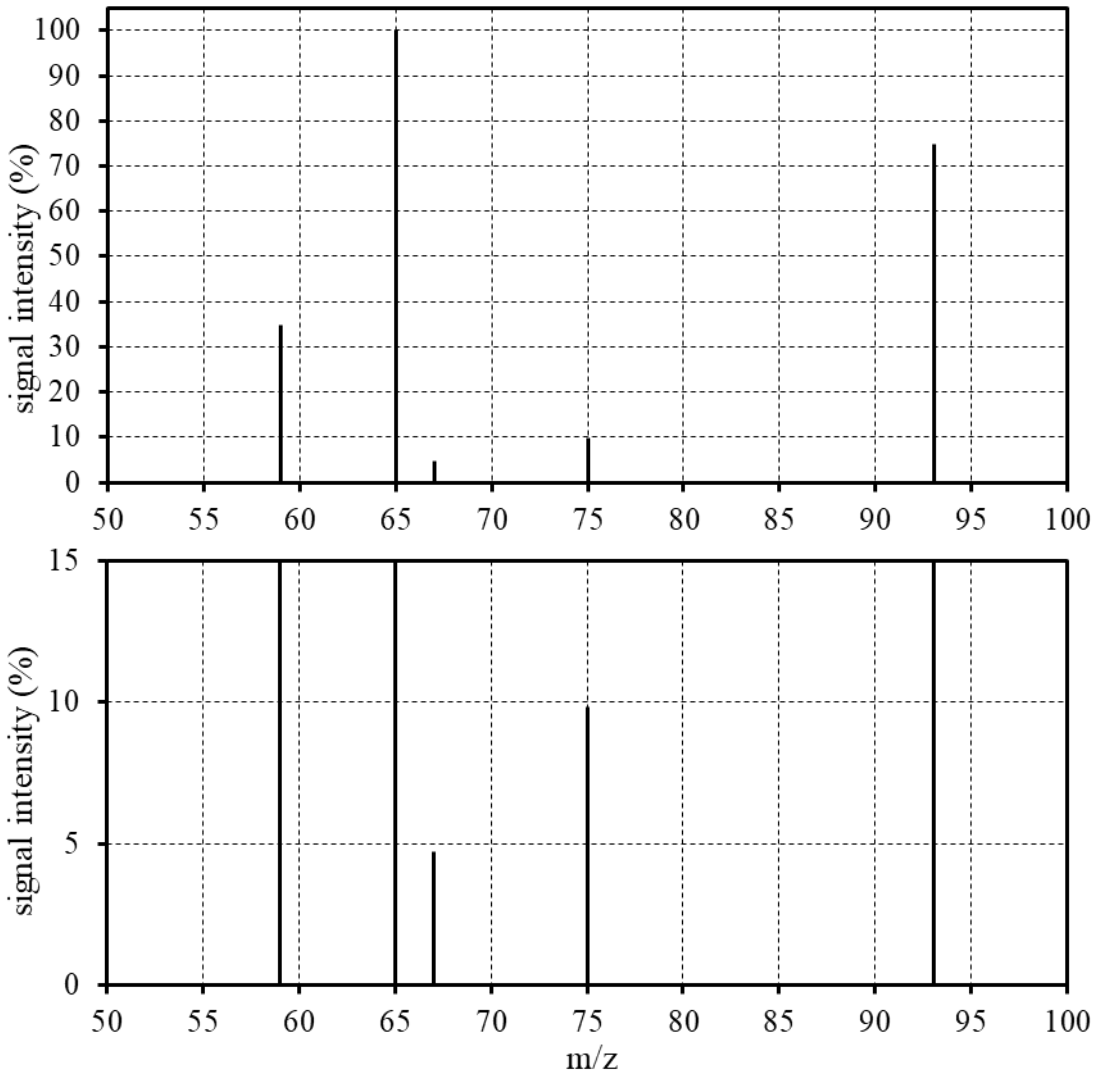

| Acetylsalicylic acid (Aspirin)<br>negative mode – $MS^2$ – 120 eV ; precursor ion: 179.0350 $[M-H]^-$ | | | | | |
|---|---|---|---|---|---|
| **m/z** | **Relative abundance (%)** | **Assigned ionic fragment** | **m/z** | **Relative abundance (%)** | **Assigned ionic fragment** |
| 59.0138 | 25.23 | $[C_2H_3O_2]^-$ | 75.0241 | 2.08 | $[C_6H_3]^-$ |
| 65.0397 | 22.98 | $[C_5H_5]^-$ | 93.0346 | 100.00 | $[C_6H_5O]^-$ |
| 67.0190 | 0.47 | $[C_4H_3O]^-$ | | | |

**Fig. 314 $MS^2$ mass spectrum of aspirin in negative mode at 120 eV collision energy (reconstructed from digitized data from the Mass Bank of North America)**




| Acetylsalicylic acid (Aspirin)<br>negative mode – $MS^2$ – 150 eV ; precursor ion: 179.0350 $[M-H]^-$ | | | | | |
|---|---|---|---|---|---|
| **m/z** | **Relative abundance (%)** | **Assigned ionic fragment** | **m/z** | **Relative abundance (%)** | **Assigned ionic fragment** |
| 59.0138 | 31.84 | $[C_2H_3O_2]^-$ | 75.024 | 7.92 | $[C_6H_3]^-$ |
| 65.0397 | 65.19 | $[C_5H_5]^-$ | 93.0346 | 100.00 | $[C_6H_5O]^-$ |
| 67.0189 | 1.85 | $[C_4H_3O]^-$ | 94.038 | 0.54 | $[CH_6N_2O_3]^-$ |

**Fig. 315 $MS^2$ mass spectrum of aspirin in negative mode at 150 eV collision energy (reconstructed from digitized data from the Mass Bank of North America)**




| Acetylsalicylic acid (Aspirin)<br>negative mode – $MS^2$ – 180 eV ; precursor ion: 179.0350 $[M-H]^-$ | | | | | |
|---|---|---|---|---|---|
| **m/z** | **Relative abundance (%)** | **Assigned ionic fragment** | **m/z** | **Relative abundance (%)** | **Assigned ionic fragment** |
| 59.0138 | 34.88 | $[C_2H_3O_2]^-$ | 75.0241 | 9.85 | $[C_6H_3]^-$ |
| 65.0397 | 100.00 | $[C_5H_5]^-$ | 93.0345 | 74.69 | $[C_6H_5O]^-$ |
| 67.0189 | 4.71 | $[C_4H_3O]^-$ | | | |

**Fig. 316 $MS^2$ mass spectrum of aspirin in negative mode at 180 eV collision energy (reconstructed from digitized data from the Mass Bank of North America)**

For comparison, Figures 308 - 316 show the $MS^2$ mass spectra of aspirin in negative mode. The precursor ion **[M-H]$^-$** with **m/z** 179.0350, obtained by electrospray ionization (**ESI**), was fragmented by collisional fragmentation with energies ranging from 15 eV to 180 eV. As can be seen, the fragmentation of the precursor ion is lower in the negative mode than in the positive mode.

## 5.10 Identification and quantification of N,N-dimethyl barbiturates by gas chromatography coupled to mass spectrometry

Some 5-substituted representatives of barbituric acid are used as sedative hypnotics. The pharmacological action is to activate the inhibition of neuronal transmission mediated by γ-aminobutyric acid (GABA). The most common are amobarbital, butalbital, pentobarbital, phenobarbital and secobarbital. Barbital (5,5-diethylbarbituric acid) was used as a sleeping pill under the name "Veronal" until 1950.

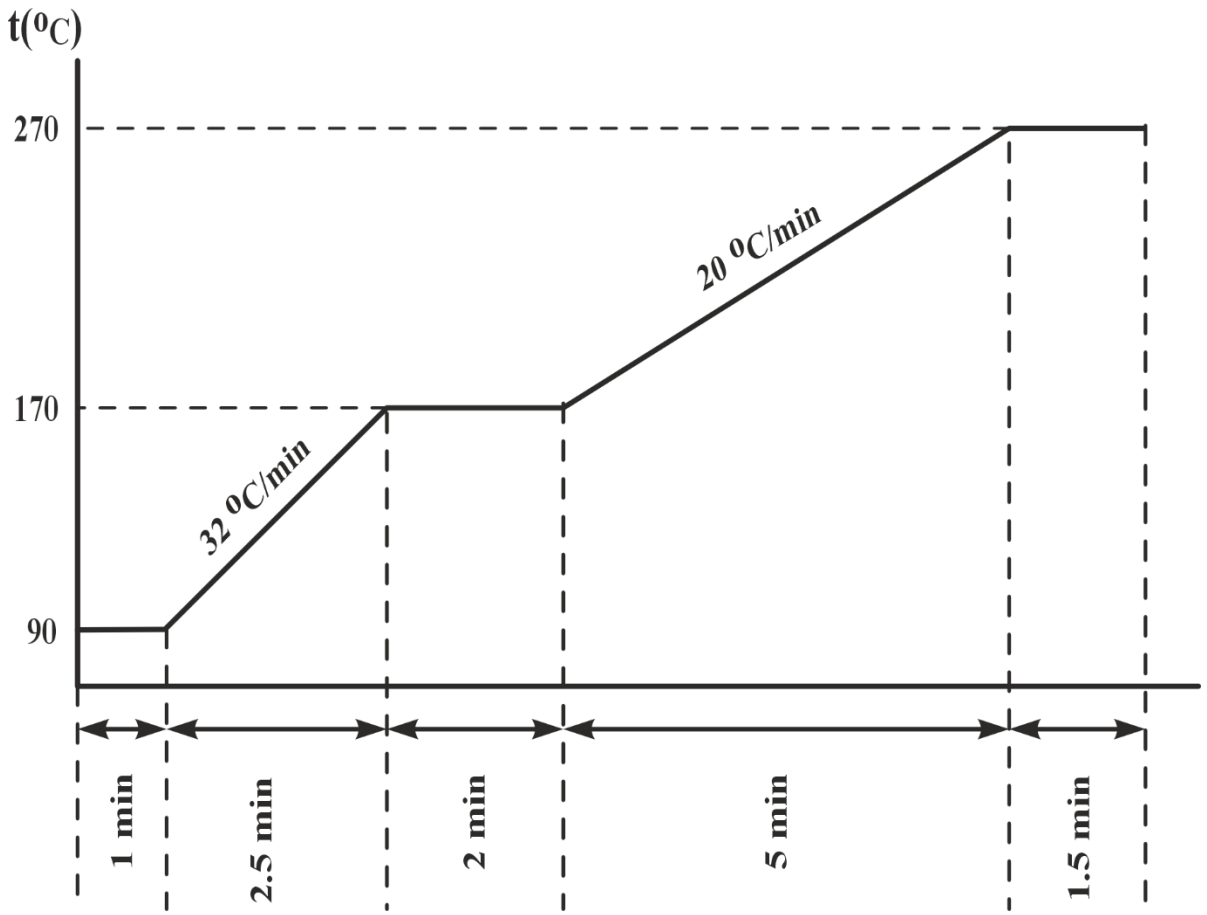



**Fig. 317 Temperature program used in SIM-chromatographic separation of N,N-dimethylbarbiturates (adapted from [4])**

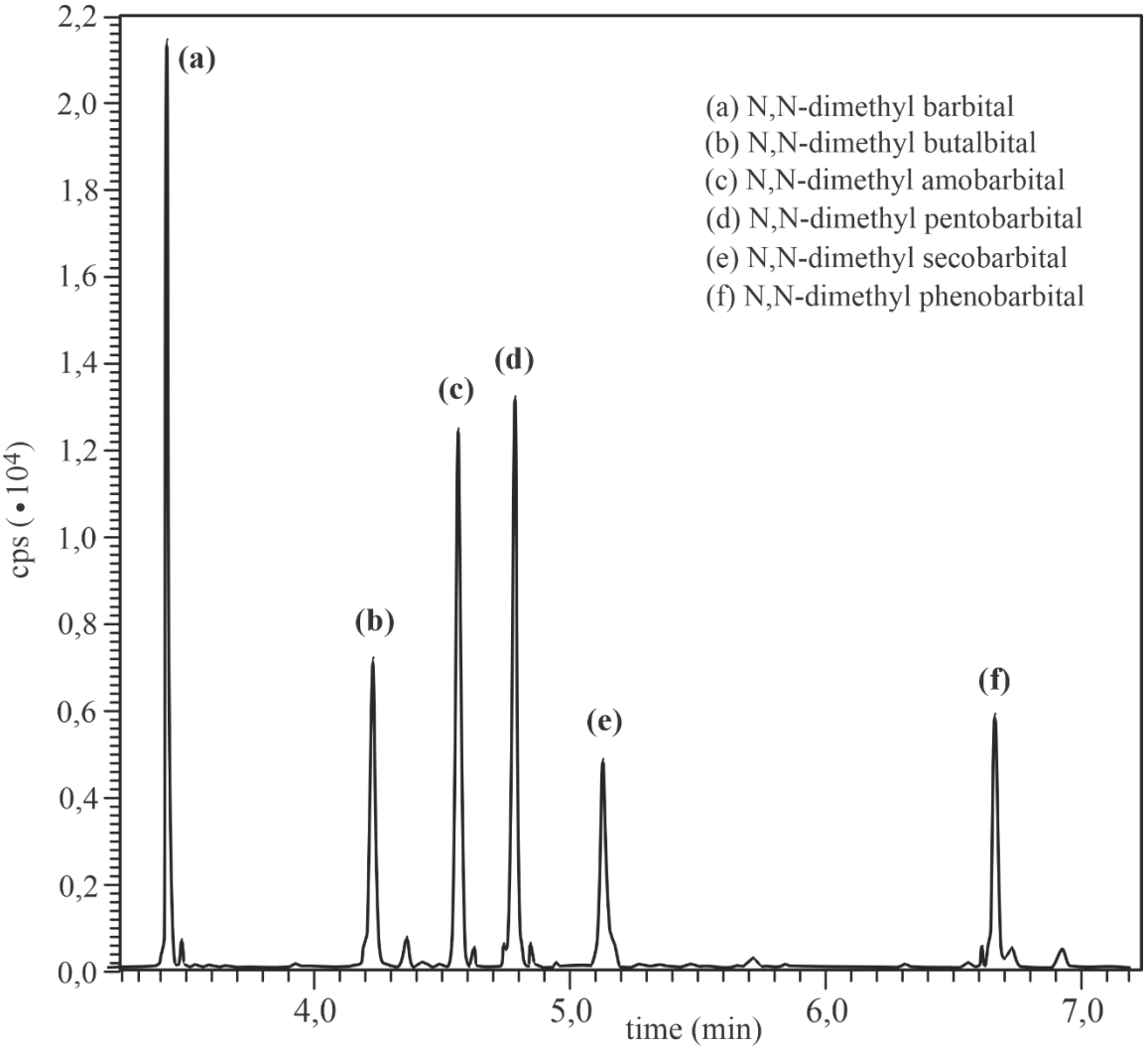



**Fig. 318 Gas chromatographic separation (TIC detection) of N-derivatized barbiturates with programmed temperature (according to [4])**

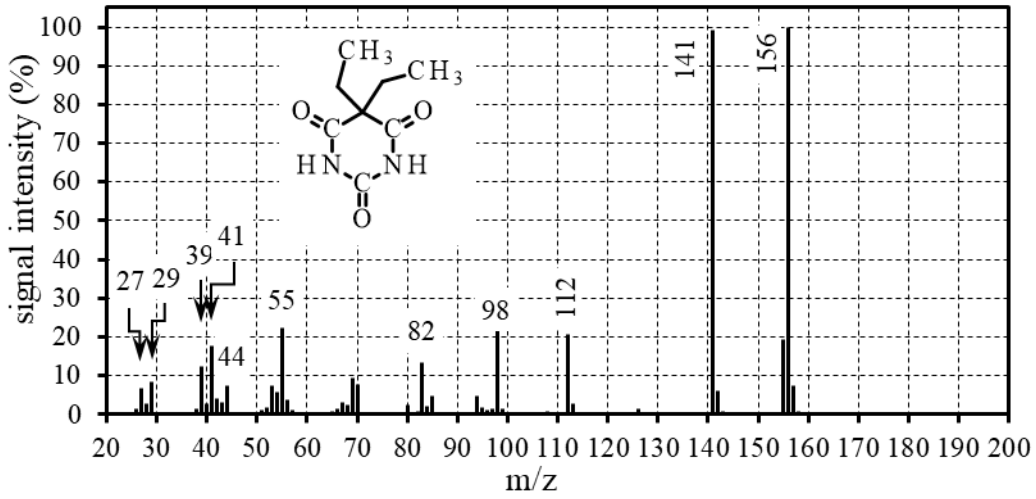



**Fig. 319 Mass spectrum of barbital (5,5-diethylbarbituric acid), EI ionization (based on NIST data, spectrum no. 352179)**

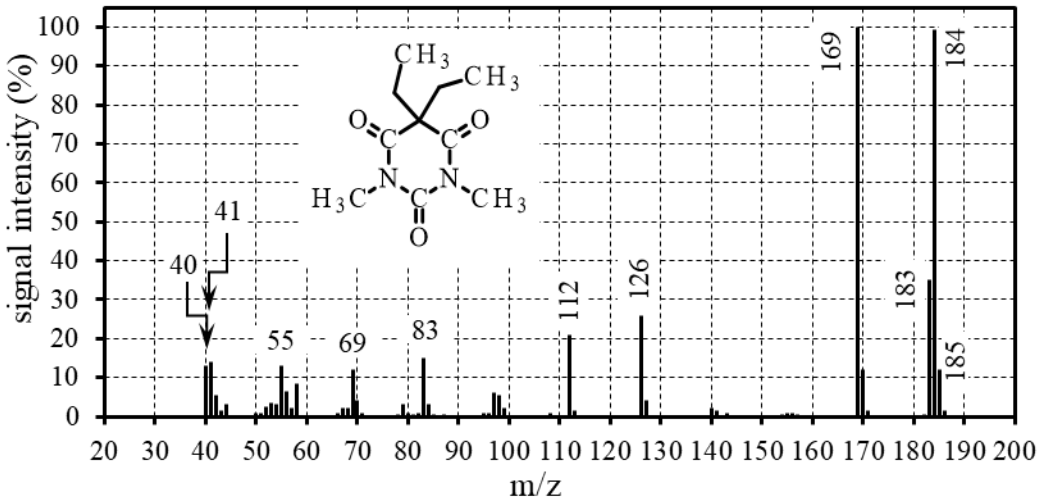



**Fig. 320 Mass spectrum of N,N-dimethyl barbital, EI ionization (recreated from NIST data, spectrum no. 9843)**

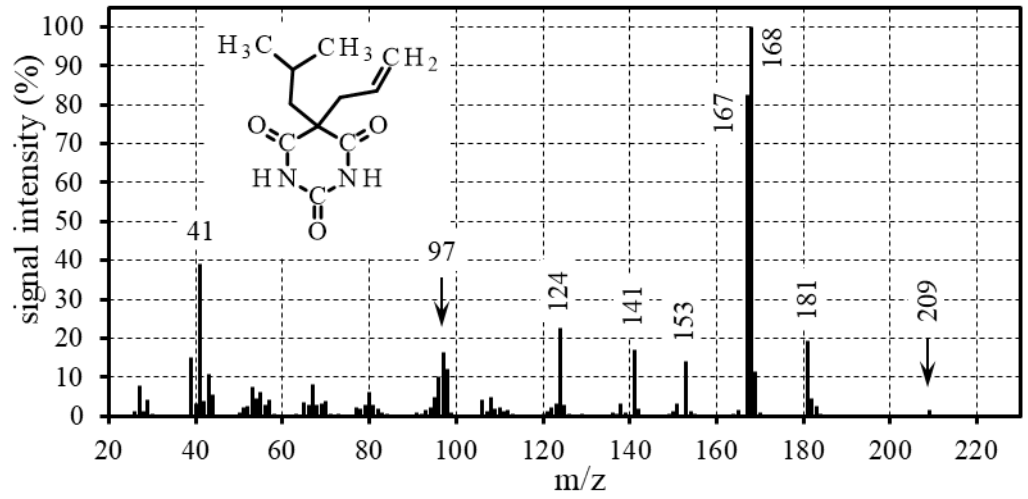



**Fig. 321 Mass spectrum of butalbital, EI ionization (recreated from NIST data, spectrum no. 250568)**

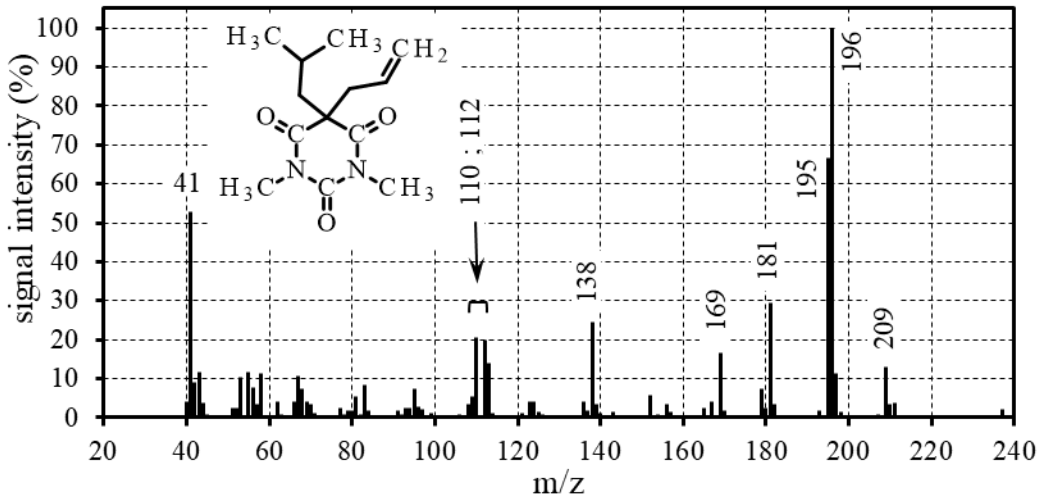



**Fig. 322 Mass spectrum of N,N-dimethylbutalbital, EI ionization (redrawn according to [4])**

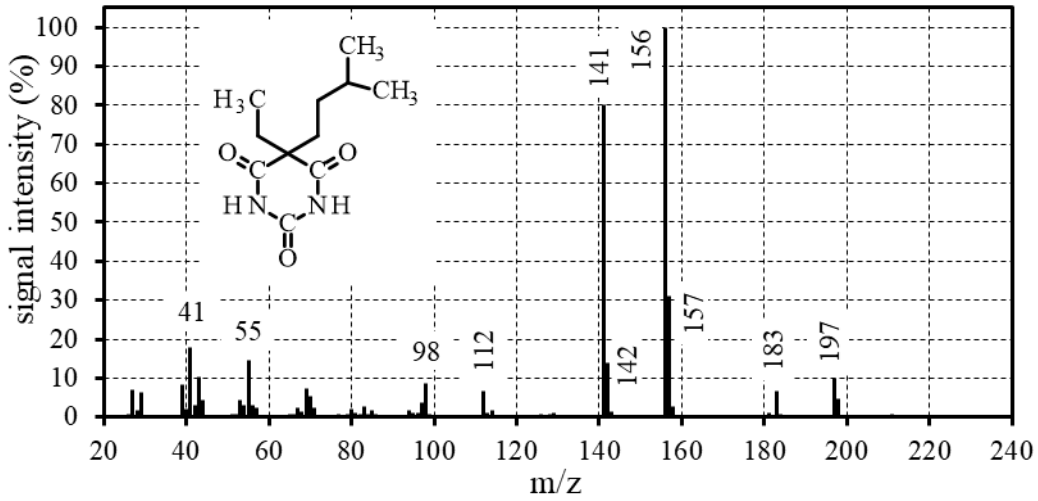



**Fig. 323 Mass spectrum of amobarbital, EI Ionization (reworked according to NIST data, spectral number 250567)**

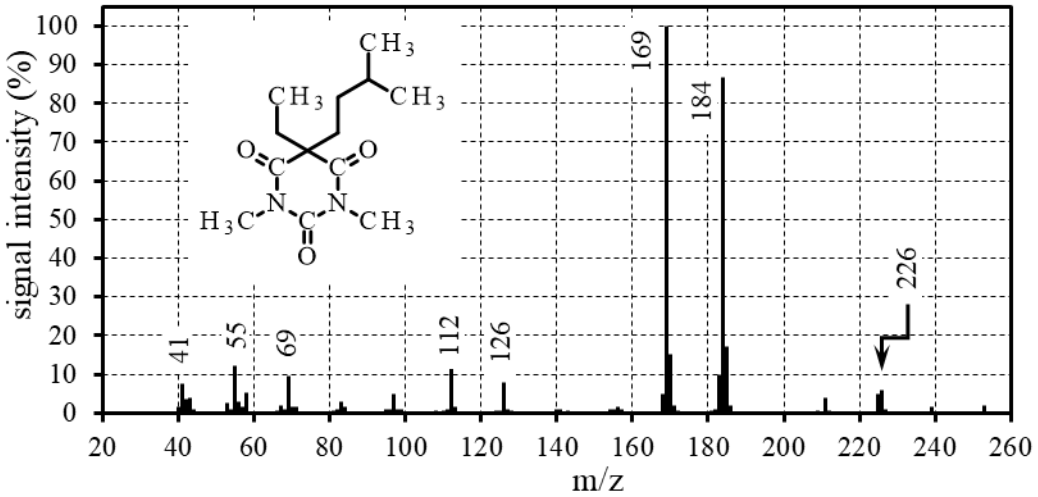



**Fig. 324 Mass spectrum of N,N-dimethyl amobarbital, EI ionization (recreated from NIST data, spectrum no. 12376)**

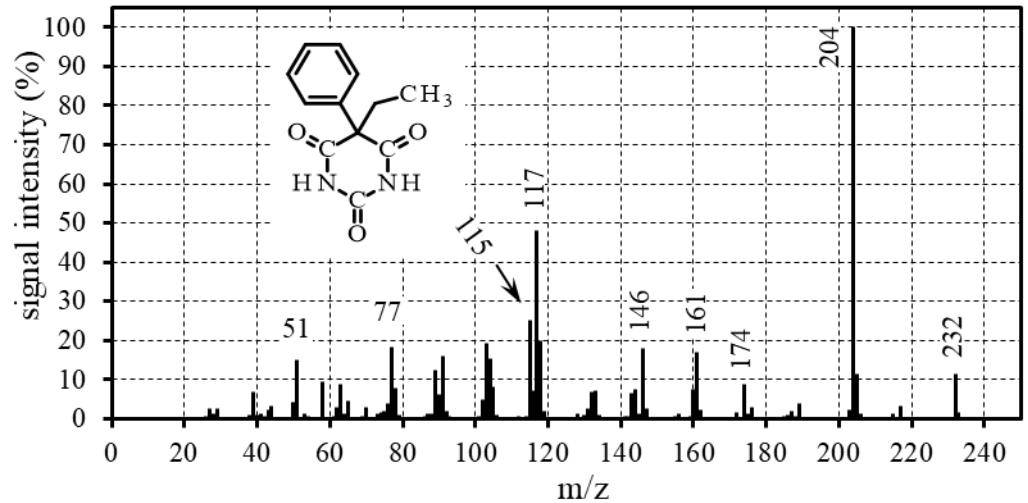



**Fig. 325 Mass spectrum of phenobarbital, EI ionization (recreated from NIST data, spectrum no. 408715)**

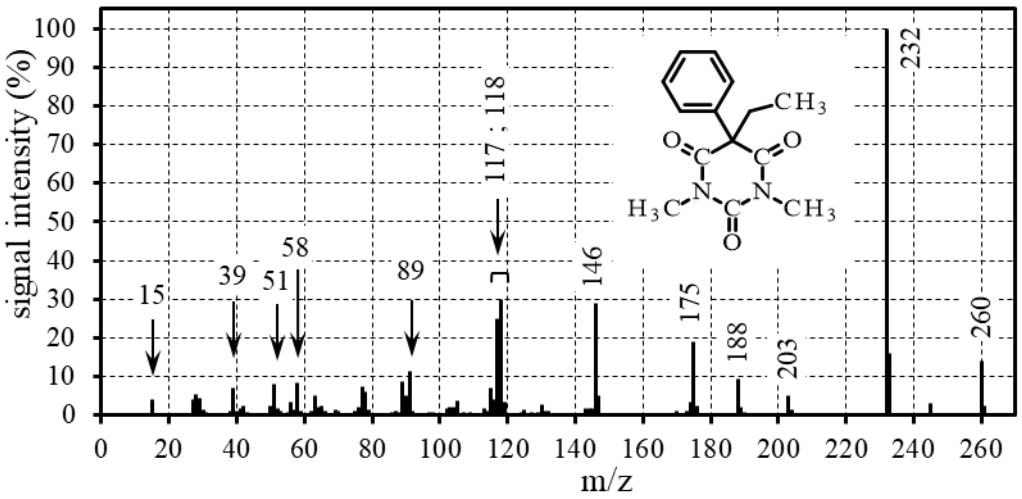



**Fig. 326 Mass spectrum of N,N-dimethyl phenobarbital, EI ionization (recreated from NIST data, spectrum no. 23007)**

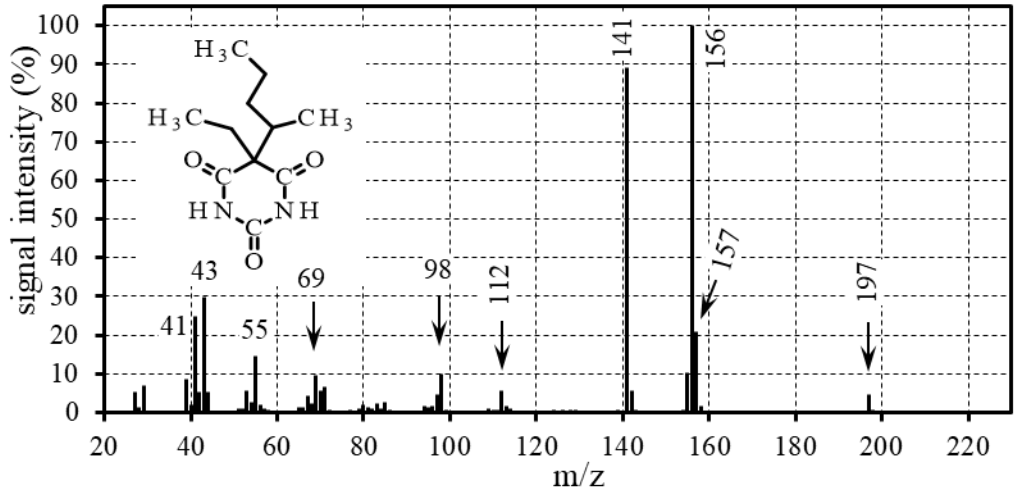



**Fig. 327 Mass spectrum of pentobarbital, EI ionization (recreated from NIST data, spectrum no. 352145)**

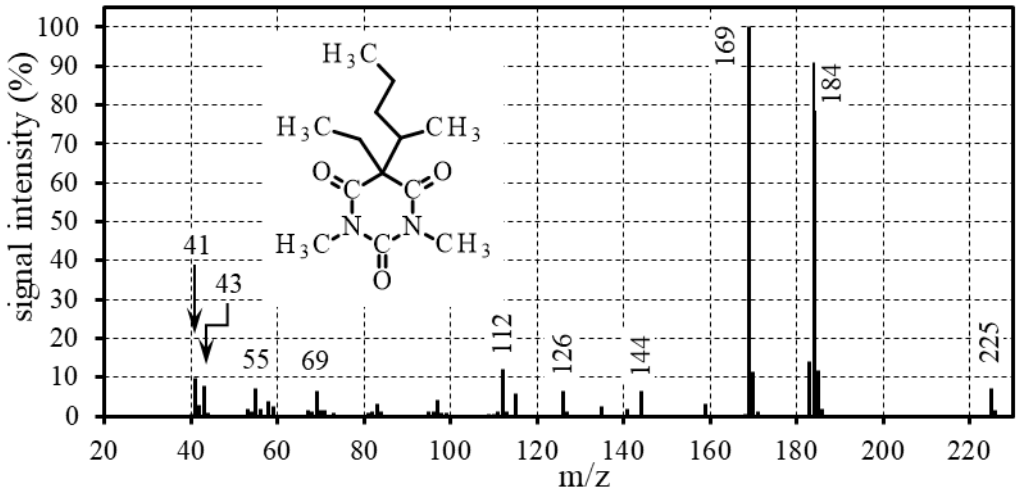



**Fig. 328 Mass spectrum of N.N-dimethyl pentobarbital, EI ionization (recreated from NIST data, spectrum no. 22977)**

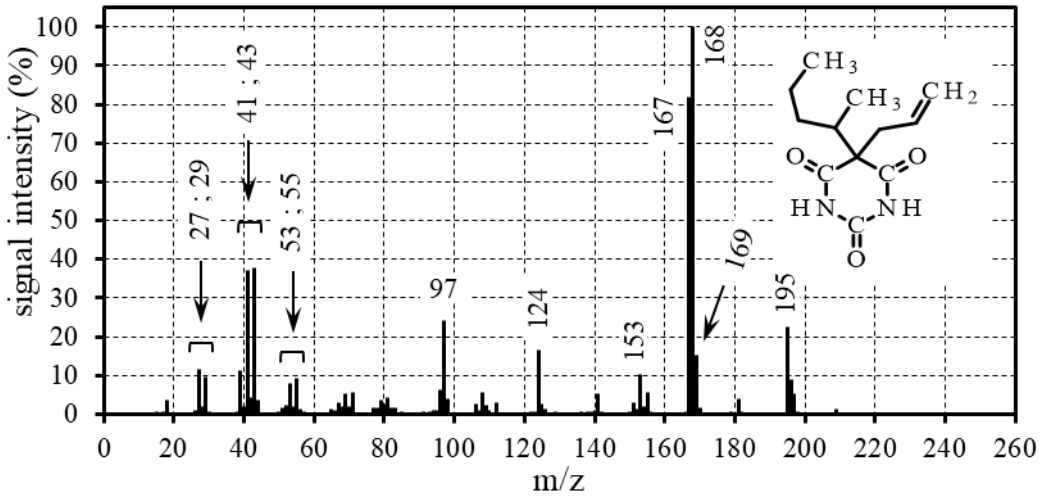



**Fig. 329 Mass spectrum of secobarbital, EI ionization (recreated from NIST data, spectrum no. 232637)**

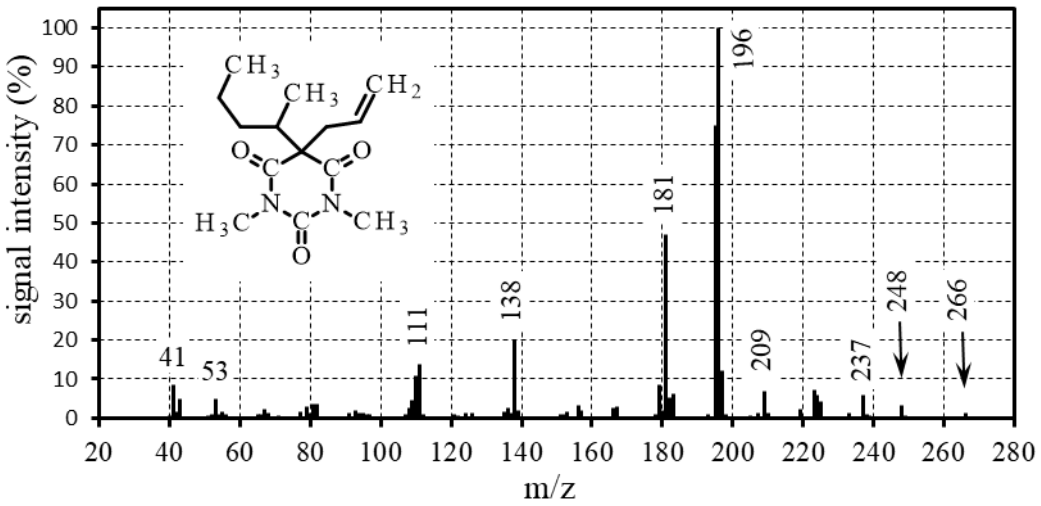



**Fig. 330 Mass spectrum of N,N-dimethyl secobarbital, EI ionization (recreated from NIST data, spectrum no. 12914)**

In parallel with the clinical use of barbiturates, there are cases of abuse of barbiturates that require their analysis not only in the usual pharmaceutical forms but also in biological fluids (blood, urine) [1]. Most of the analytical methods of choice are based on gas chromatography coupled with mass spectrometry (GC/MS) in different configurations. To improve the specificity of detection and the reliability of quantitative determination, the application of GC/MS has been preceded by microextraction procedures [2].

To improve the gas chromatographic separation and for a safer identification of some barbiturate representatives, prior derivatization of sample components by methylation at the 3- and 5-positions (on nitrogen atoms) has been proposed and tested [3,4]. N,N-dimethylated derivatives being less polar, provide superior gas chromatographic separation under non-polar stationary phase chromatography. As methylating reagent, trimethylanilinium hydroxide was used (Fig. 331). By performing gas chromatographic separation in the selected ion monitoring (SIM) regime with an appropriate temperature program, the separation of barbiturates is complete (Figure 318). The

internal diameter of the gas chromatography capillary column (Zebron ZB-1) was 0.25 mm and the length was 15 m. The ionization temperature (70 eV electron flux electron impact) was maintained at 280 $^{o}$C [4].

Figures 319 shows the mass spectrum of barbital and Figures 320 to 330 show the mass spectra of N,N-dimethylated derivatives with the dominant signals indicated, recommended for identification and quantitative determination. The spectra have been reconstructed from digitized data from the NIST Spectral Collection.

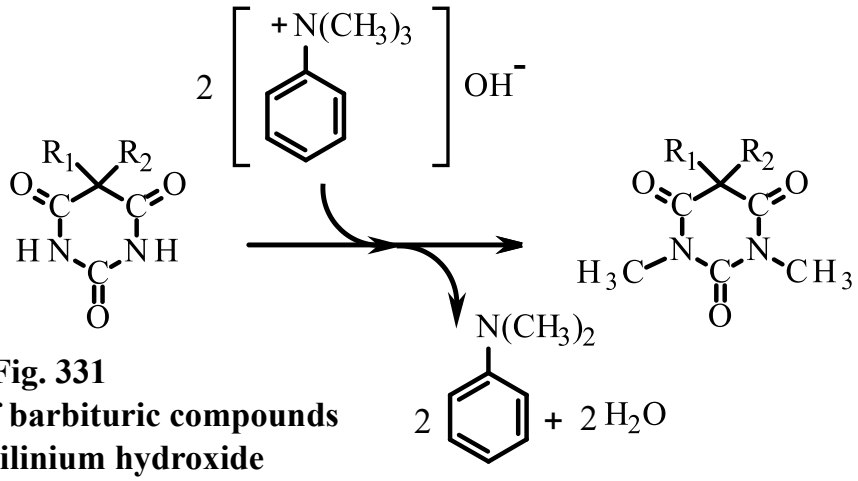



**Fig. 331**
**Derivatization of barbituric compounds with trimethylanilinium hydroxide**

**Tabel 21 Significant Δ(m/z) differences between the dominant signals of barbiturates and the corresponding N,N-dimethylated derivatives**

| | | | |
|---|---|---|---|
| **N,N-dimethyl barbital** | 126 | 141 | 156 |
| **barbital** | 112 | 169 | 184 |
| **Δ(m/z)** | 14 | 28 | 28 |

| | | | |
|---|---|---|---|
| **N,N-dimethyl butalbital** | 195 | 196 | |
| **butalbital** | 167 | 168 | |
| **Δ(m/z)** | 28 | 28 | |

| | | | |
|---|---|---|---|
| **N,N-dimethyl amobarbital** | 169 | 184 | 185 |
| **amobarbital** | 141 | 153 | 157 |
| **Δ(m/z)** | 28 | 28 | 28 |

| | | | |
|---|---|---|---|
| **N,N-dimethyl phenobarbital** | 175 | 232 | |
| **phenobarbital** | 117 | 204 | |
| **Δ(m/z)** | 28 | 28 | |

| | | | |
|---|---|---|---|
| **N,N-dimethyl secobarbital** | 181 | 196 | 209 |
| **secobarbital** | 167 | 168 | 195 |
| **Δ(m/z)** | 14 | 28 | 14 |

| | | | |
|---|---|---|---|
| **N,N-dimethyl pentobarbital** | 169 | 184 | |
| **pentobarbital** | 141 | 156 | |
| **Δ(m/z)** | 28 | 28 | |

When MS signals of the barbiturates are compared with the corresponding derivatized forms, constant shifts, **Δ(m/z)** = 28 Da and **Δ(m/z)** = 14 Da, are observed, indicating cleavage of one or two methylene (>$CH_2$) fragments (Table 21).

Derivatization of barbiturates allows for a higher quality gas chromatographic separation, and the intense MS signals are suitable for both reliable identification and quantitative determination (Table 22).

**Table 22 Recommended m/z signals for the identification and quantification of N,N-dimethylated derivatives of barbiturates (adapted from [4]).**

| Analyte (derivatized compound) | Recommended signals for identification (m/z) | Recommended signal for quantitative determination (m/z) |
|---|---|---|
| N,N-dimethyl barbital | 126 ; 169 | 184 |
| N,N-dimethyl butalbital | 169 ; 181 | 196 |
| N,N-dimethyl amobarbital | 226 ; 169 | 184 |
| N,N-dimethyl phenobarbital | 175 ; 146 | 232 |
| N,N-dimethyl pentobarbital | 225 ; 169 | 184 |
| N,N-dimethyl secobarbital | 209 ; 181 | 196 |

**Sources cited in application example 5.10**

[1] *R. Meatherall*: GC/MS Confirmation of Barbiturates in Blood and Urine.
**J. Forensic. Sci., 1997:42**(6), 1160-1170

[2] *B.J. Hall, J.S. Brodbelt*: Determination of Barbiturates by Solid-Phase Microextraction (SPME) and Ion Trap Gas Chromatography-Mass Spectrometry.
**J. Chromatogr. A., 1997:777**(2), 275-282

[3] *R.H. Liu, A.M. McKeehan, C. Edwards, G. Foster, W.D. Bentley, J.G. Landner, A.S. Walia*: Improved Gas Chromatography/Mass Spectrometry Analysis of Barbiturates in Urine Using Centrifuge-based solid-phase Extraction, Methylation with d5-Pentobarbital as Internal Standard.
**J. Forensic. Sci., 1994:39**(6), 1504-1514

[4] *L.L. Johnson, U. Garg*: "**Quantitation of Amobarbital, Butalbital, Pentobarbital, Phenobarbital and Secobarbital in Urine, Serum and Plasma Using Gas Chromatography – Mass Spectrometry (GC-MS)**" în **Clinical Applications of Mass Spectrometry – Methods and Protocols**, *U. Garg şi C.A. Hammett-Stabler* editors, chap. 7, p. 65-74
**Humana Press, 2010** [ISBN: 978-1-60761-458-6]

## 5.11 Particularities of some phosphodiesterase ($PDE_5$) inhibitors in mass spectrometric analysis

Drugs used to treat erectile dysfunction (sildenafil, tadalafil, and vardenafil), phosphodiesterase-type enzyme ($PDE_5$) inhibitors have been the subject of studies using various mass spectrometric approaches for fragmentation patterns [1,2], highlighting of photo-transformation products [3,4], detection in dietary supplements [5], and identification in counterfeit products [6].

Liquid chromatography (**HPLC**) coupled to electrospray ionization (**ESI**) MS/MS mass spectrometry has been used for several phosphodiesterase inhibitor analogs [1,2]. The mass spectrometer, as a general detector tuned to all ions formed (total ion chromatography - **TIC**), as a selective detector tuned to selected ions (selected ion chromatography - **SIC**) or as a multiple reaction monitoring (**MRM**) [6] is used.

**R**: $-CH_3$ tadalafil

**R**: $-CH_2CH_3$ homotadalafil

**R**: $-(CH_2)_3CH_3$ N-butyltadalafil

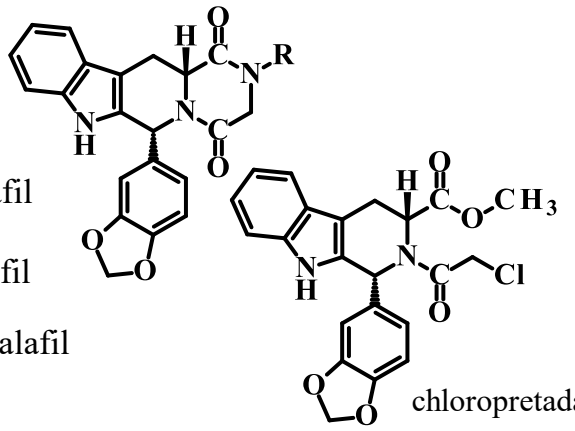
**R**: $-(CH_2)_7CH_3$ N-octyltadalafil

**R**: -ciclopentil cyclopentyltadalafil

**R**: -H demethyltadalafil

**R**: $-NH_2$ aminotadalafil

**R**: $-NH-C(O)-CH_3$ acetaminotadalafil




chloropretadalafil

**Fig. 332 Structures of tadalafil analogues detected in food supplements using ESI-MS/MS (according to [1])**

Figure 332 shows the structures of tadalafil and its analogues: homotadalafil, N-butyltadalafil, N-octyltadalafil, cyclopentyltadalafil, demethyltadalafil, aminotadalafil, acetaminotadalafil, and chloropretadalafil, which are found in some dietary supplements.

*C.L. Lee* and co-workers [8] developed a method based on $MS^2$ mass spectrometry for the identification of 39 phosphodiesterase inhibitors. The selected precursor ion was the protonated molecular ion, $\mathbf{[M+H]^+}$, and its collisional fragmentation was performed at energies of 10, 20 and 30 eV.

Figure 333 shows the high resolution $MS^2$ mass spectrum of tadalafil obtained by electrospray ionization in the positive ionization mode. The drying gas was nitrogen at 350 $^oC$. The voltage applied to the capillary tube was 4000 V.

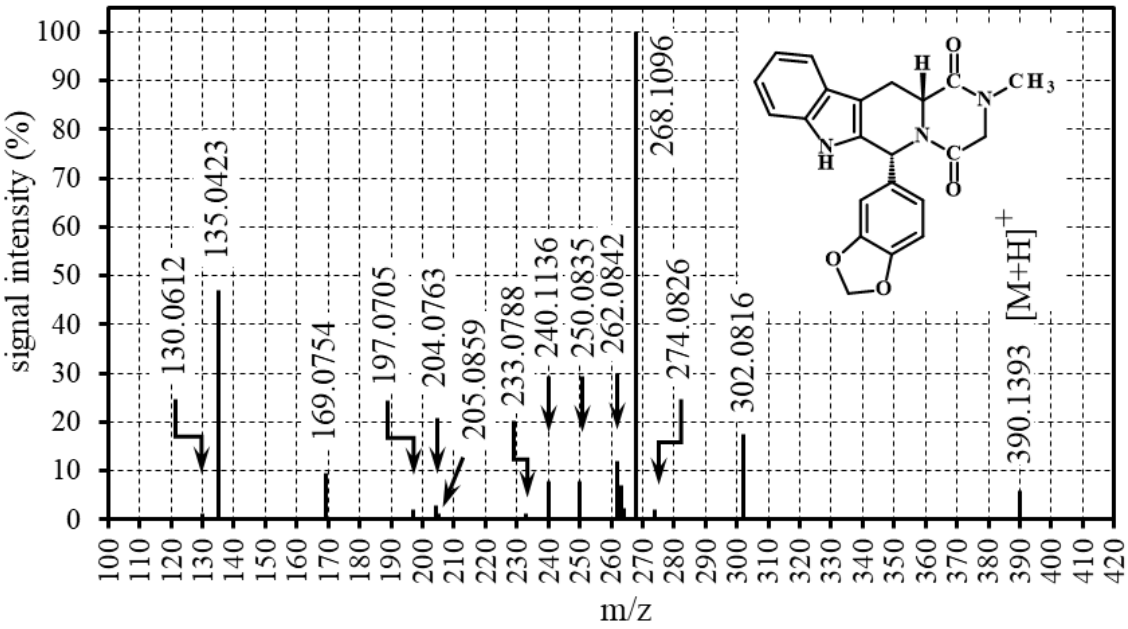



**Fig. 333 High resolution $MS^2$ mass spectrum of the compound tadalafil, recorded by ESI ionization in positive mode and Q-TOF analysis; precursor ion: $[M+H]^+$, m/z 390.1393 (reconstructed from HMBD 0014958).**

Recording the $MS^2$ spectrum allows more reliable identification of the analyte compared to the primary MS spectrum, and recording the $MS^3$ spectrum with more precursor ions provides greater confidence. *Pang* and coworkers [2] specifically looked at differentiating between tadalafil and a certain analog (aminotadalafil).

A plausible mechanism of the tadalafil ESI-$MS^2$ fragmentation pathways and the structures of the major ion fragments are shown in Figure 334 with delineation of the common ions of tadalafil analogs **(A)** and the ions resulting from individual tadalafil analogs **(B)**.

Figures 335 and 336 show the $MS^2$ spectra of Tadalafil (precursor ion **m/z** 390.1) and Tadalafil analogue (aminotadalafil, precursor ion with **m/z** 391.2) respectively.

Up to two routes were proposed for the discriminatory $MS^3$ analysis of tadalafil and aminotadalafil.

According to the first $MS^3$ fragmentation sequence, the primary precursor ion $\mathbf{[M+H]^+}$, resulting directly from the ESI ionization, is subjected to fragmentation by

collision with neutral atoms (argon). From the resulting spectrum the $[M+H]^+$ ion of **m/z** 390 is selected, and from the resulting fragments, the ion of **m/z** 268 is selected, which is the precursor ion for the second fragmentation of tadalafil (Fig. 337). For aminotadalafil, a similar sequence has been elected ($[M+H]^+$ →391→ 269→ ..,, Fig 338).

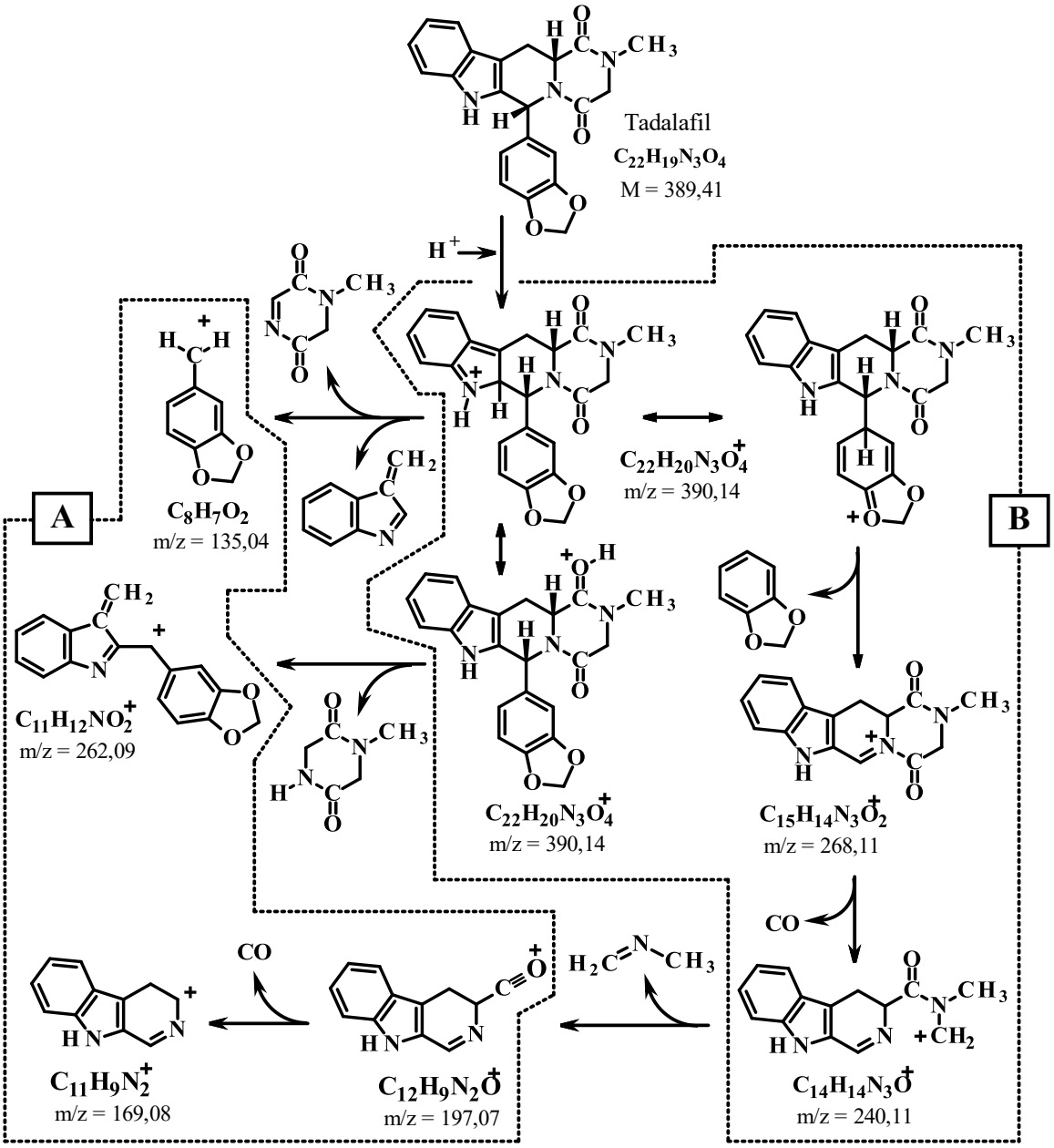



**Fig. 334 Plausible mechanism of ESI-MS/MS fragmentation of tadalafil (reconstructed from [1])**
**(A) Ions common to tadalafil analogs**
**(B) Ions specific to individual analogs**

In the second $MS^3$ fragmentation sequence the primary precursor ion $[M+H]^+$, resulting directly from the ESI ionization is subjected to fragmentation by collision

with neutral atoms (argon). From the resulting spectrum the **[M+H]**$^+$ ion of **m/z** 390 is selected, and from the resulting fragments the ion of **m/z** 273 is chosen, which is the precursor ion for the second fragmentation of tadalafil (Fig. 339). For aminotadalafil, a similar sequence has been elected (**[M+H]**+ ⟶ 391 ⟶274 ⟶ …, Fig 340).

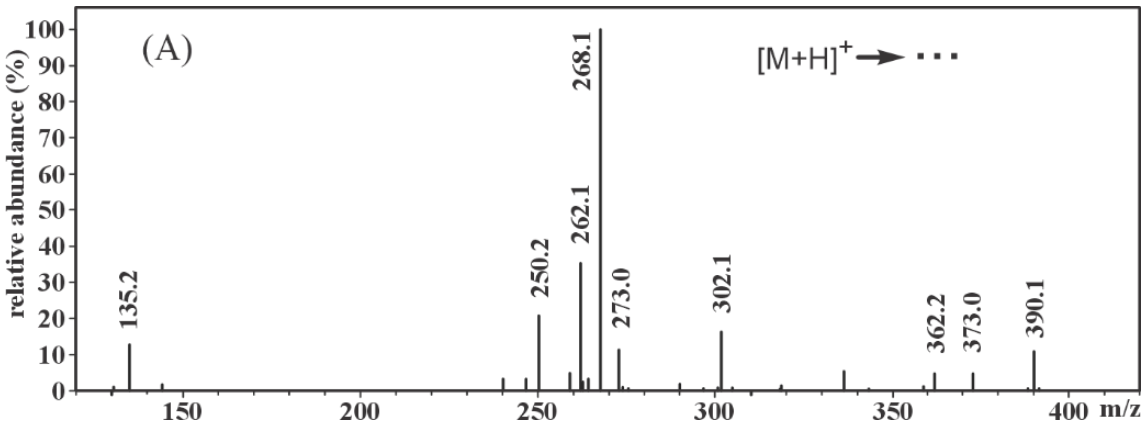



**Fig. 335 MS$^2$ spectrum of tadalafil [2]**

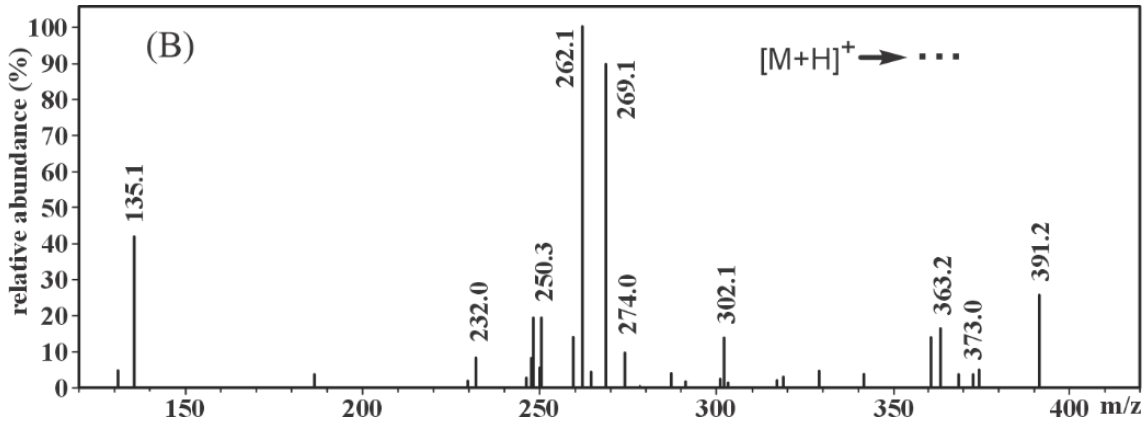



**Fig. 336 MS$^2$ spectrum of aminotadalafil [2]**

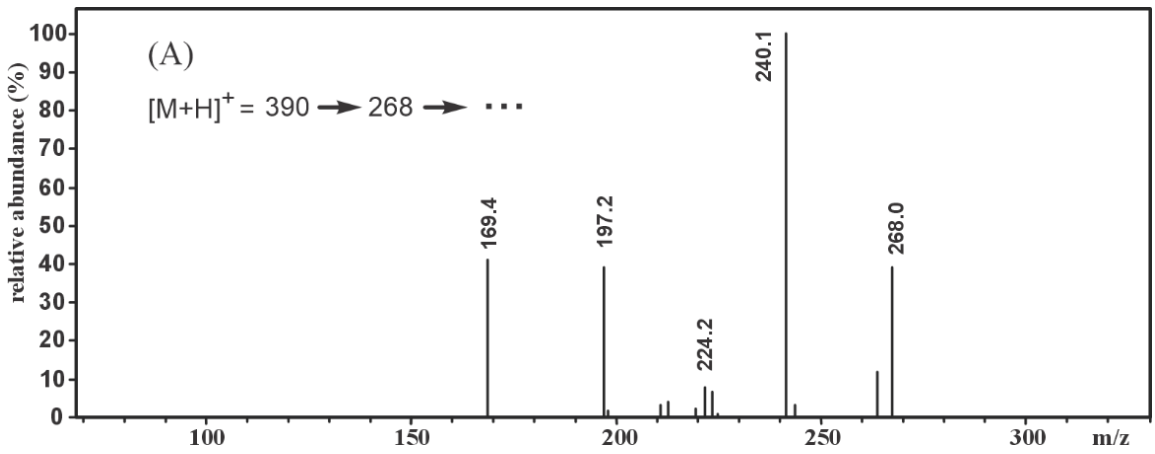



**Fig. 337 MS$^3$ spectrum of tadalafil [2]**

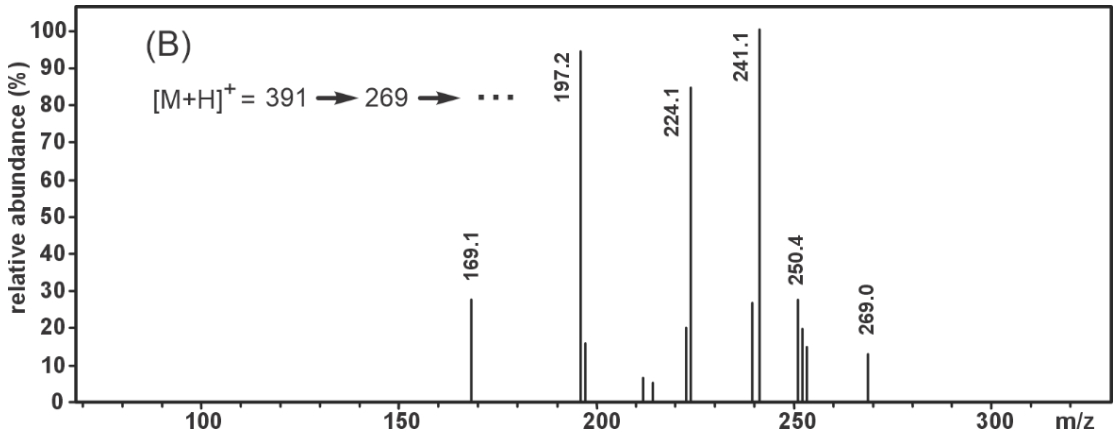



**Fig. 338 $MS^3$ spectrum of aminotadalafil [2]**

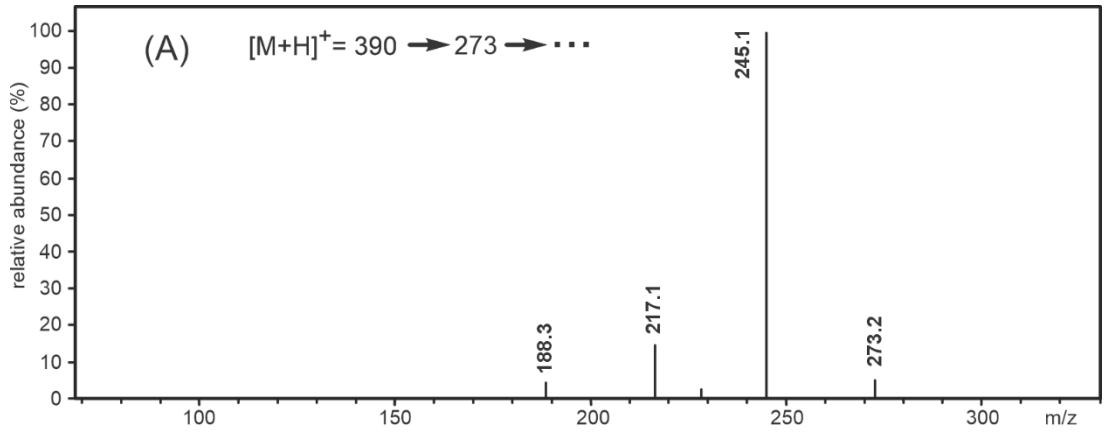



**Fig. 339 $MS^3$ spectrum of tadalafil [2]**

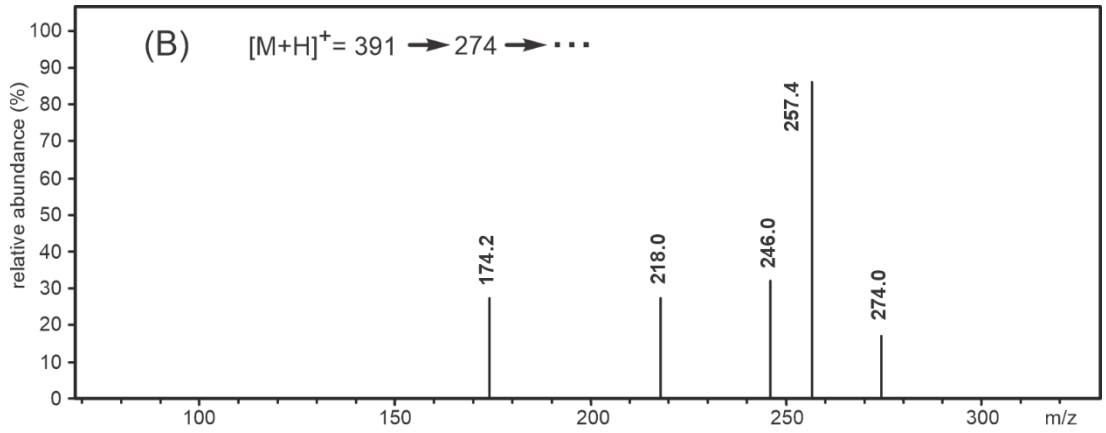



**Fig. 340 $MS^3$ spectrum of aminotadalafil [2]**

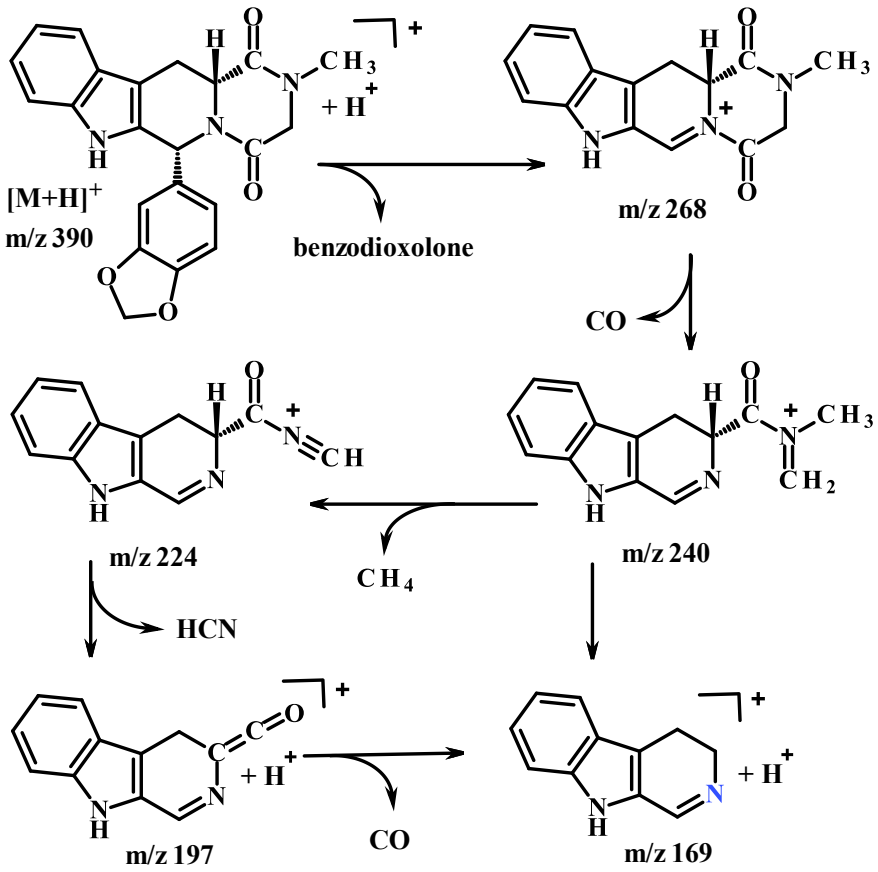



**Fig. 341 Fragmentation of tadalafil ([M+H]+ → 390 → 268 → . . . ) (according to *Peng Zou1*, *Peiling Hou1*, *Sharon Sze-Yin Oh*, *Min-Yong Low* and *Hwee-Ling Koh* [2])**

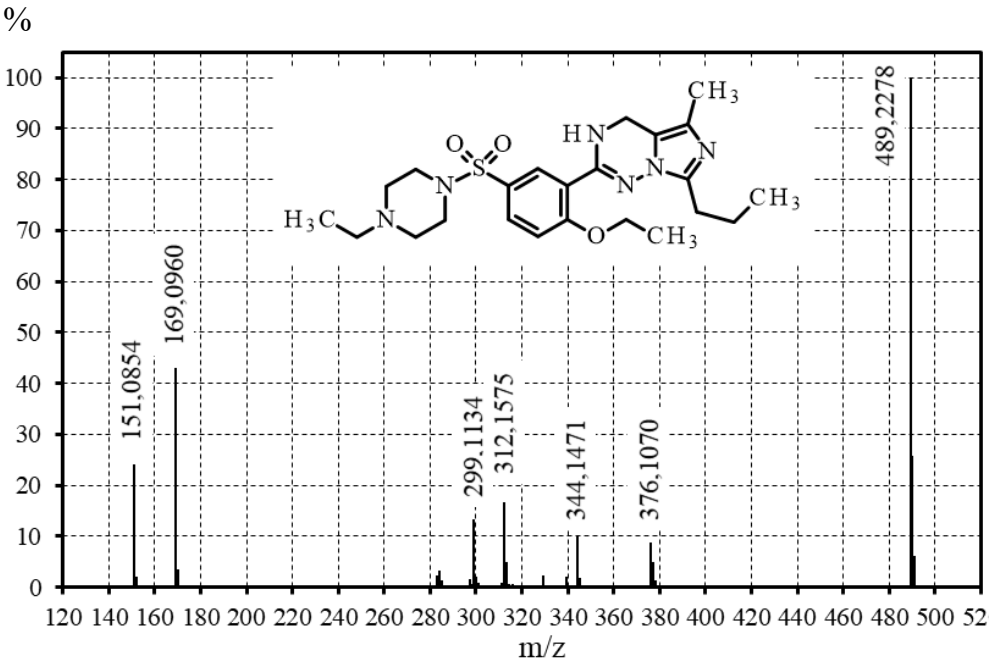



**Fig. 342 High resolution $MS^2$ mass spectrum of vardenafil (precursor m/z 489, collision energy 20 eV) (reconstructed from MoNa collection data, spectrum AU235904 and [8])**

Similar procedures for the identification of other phosphodiesterase inhibitors have been developed and recommended for quantitative analysis in other publications [6,7,8]. Table 23 lists the ion **m/z** values obtained by ESI primary ionization and **$[M+H]^+$** precursor ion fragmentation at three collision energies (10, 20, and 40 eV) for the major members of the compound class and some of their analogs. The $MS^2$ mass spectrum of vardenafil is shown in Figure 342.

The paper published by *C.L. Kee* and co-workers [9] is a comprehensive summary of methods for the analytical detection of phosphodiesterase inhibitors as dietary supplement additives using electospray ionization $MS^2$ mass spectrometry.

**Tabel 23 $MS^2$ characteristic ions of phosphodiesterase inhibitors (from [8])**

| Compound | Precursor ion $[M+H]^+$ (m/z) | Collision (eV) | Fragmentation ions (m/z) in parenthesis: relative intensity (%) | | |
|---|---|---|---|---|---|
| | | | (1) | (2) | (3) |
| Acetaminotadalafil $C_{23}H_{20}N_4O_5$ | 433,1514 | 10 | 433,1516 (100) | 311,1153 (32) | 135,0444 (20) |
| | | 20 | 135,0446 (100) | 262,0874 (62) | 311,1152 (53) |
| | | 40 | 262,0877 (110) | 135,0445 (65) | 205,0890 (42) |
| Acetylvardenafil $C_{25}H_{34}N_6O_3$ | 467,2742 | 10 | 467,2779 (100) | - | - |
| | | 20 | 467,2753 (100) | - | - |
| | | 40 | 151,0884 (100) | 112,0962 (38) | 341,1613 (36) |
| Aminotadalafil $C_{21}H_{18}N_4O_4$ | 391,1405 | 10 | 169,1042 (100) | 391,1407 (38) | 135,1613 (14) |
| | | 20 | 269,1038 (100) | 135,0444 (51) | 262,0879 (23) |
| | | 40 | 169,0759 (100) | 262,0866 (83) | 135,0442 (54) |
| Benzylsildenafil $C_{28}H_{34}N_6O_4S$ | 551,2439 | 10 | 551,2441 (100) | - | - |
| | | 20 | 551,2439 (100) | 377,1279 (7) | - |
| | | 40 | 377,1283 (100) | 134,0961 (85) | 312,1577 (23) |
| Carbodenafil $C_{24}H_{32}N_6O_3$ | 453,2607 | 10 | 453,2623 (100) | 339,1457 (18) | - |
| | | 20 | 339,1459 (100) | 453,2608 (60) | 311,1145 (29) |
| | | 40 | 311,1149 (100) | 166,0975 (17) | 147,0076 (15) |
| Chlorodenafil $C_{19}H_{21}ClN_4O_3$ | 389,1380 | 10 | 389,1399 (100) | - | - |
| | | 20 | 389,1399 (100) | 361,1086 (25) | 285,1372 (10) |
| | | 40 | 285,1375 (100) | 311,1168 (45) | 361,1086 (42) |
| Chloropretadalafil $C_{22}H_{19}ClN_2O_5$ | 427,1061 | 10 | 427,1087 (100) | 135,0460 (72) | 334,1098 (40) |
| | | 20 | 135,0459 (100) | 334,1097 (50) | 274,0889 (28) |
| | | 40 | 274,0889 (100) | 135,0460 (69) | 262,0883 (21) |
| Cinnamildenafil $C_{32}H_{38}N_6O_3$ | 555,3077 | 10 | 555,3090 (100) | 117,0704 (10) | 437,2303 (3) |
| | | 20 | 117,0704 (100) | 555,3086 (83) | 437,2309 (30) |
| | | 40 | 117,0705 (100) | 115,0550 (7) | 355,1776 (5) |
| Cyclopentynafil $C_{26}H_{36}N_6O_4S$ | 529,2596 | 10 | 529,2603 (100) | 461,1978 (4) | - |
| | | 20 | 529,2600 (100) | 461,1978 (25) | - |
| | | 40 | 461,1965 (100) | 311,1508 (45) | 283,1197 (42) |
| Demethylhongdenafil $C_{24}H_{32}N_6O_3$ | 453,2614 | 10 | 453,2618 (100) | - | - |
| | | 20 | 453,2619 (100) | - | - |
| | | 40 | 113,1078 (100) | 297,1355 (60) | 325,1339 (30) |
| Demethyltadalafil $C_{21}H_{17}N_3O_4$ | 376,1295 | 10 | 254,0927 (100) | 376,1294(57) | 135,0434 (19) |
| | | 20 | 254,0926 (100) | 135,0436 (54) | 376,1290 (7) |
| | | 40 | 262,0864 (100) | 169,0753 (69) | 205,0876 (60) |

**Tabel 23 (continued)**

| Compound | Precursor ion $[M+H]^+$ (m/z) | Collision (eV) | Fragmentation ions (m/z) in parenthesis: relative intensity (%) | | |
|---|---|---|---|---|---|
| | | | (1) | (2) | (3) |
| Desulfovardenafil $C_{17}H_{21}N_4O_2$ | 313,1667 | 10 | 313,1662 (100) | 151,0862 (8) | - |
| | | 20 | 313,1658 (100) | 151,0858 (84) | - |
| | | 40 | 151,0856 (100) | 256,0987 (5) | - |
| Dichlorodenafil $C_{19}H_{20}Cl_2N_4O_2$ | 407,1035 | 10 | 407,1014 (100) | - | - |
| | | 20 | 407,1013 (100) | - | - |
| | | 40 | 350,0310 (100) | 379,0693 (95) | 380,0952 (33) |
| Dimethylsildenafil $C_{23}H_{32}N_6O_4S$ | 489,2278 | 10 | 489,2293 (100) | - | - |
| | | 20 | 489,2291 (100) | - | - |
| | | 40 | 113,1081 (100) | 283,1207 (76) | 311,1214 (38) |
| Dimethylthiosildenafil $C_{23}H_{32}N_6O_3S_2$ | 505,2042 | 10 | 505,2035 (100) | - | - |
| | | 20 | 505,2032 (100) | 327,1244 (5) | - |
| | | 40 | 299,0945 (100) | 113,1069 (95) | 327,1274 (45) |
| Homosildenafil $C_{23}H_{32}N_6O_4S$ | 489,2281 | 10 | 489,2285 (100) | - | - |
| | | 20 | 489,2288 (100) | - | - |
| | | 40 | 113,1080 (100) | 127,1246 (75) | 297,1365 (49) |
| Hongdenafil $C_{25}H_{34}N_6O_3$ | 467,2768 | 10 | 467,2787 (100) | - | - |
| | | 20 | 467,2785 (100) | - | - |
| | | 40 | 111,0931 (100) | 127,1246 (75) | 297,1365 (49) |
| Hydroxychlorodenafil $C_{19}H_{23}ClN_4O_3$ | 391,1531 | 10 | 391,1530 (100) | - | - |
| | | 20 | 391,1528 (100) | - | - |
| | | 40 | 313,1299 (100) | 285,1344 (72) | 363,1214 (15) |
| Hydroxyhomosildenafil $C_{23}H_{32}N_6O_5S$ | 505,2233 | 10 | 505.2237 (100) | - | - |
| | | 20 | 505,2239 (100) | - | - |
| | | 40 | 283,1194 (100) | 100,0970 (92) | 129,1022 (90) |
| Hydroxyhongdenafil $C_{25}H_{34}N_6O_4$ | 483,2717 | 10 | 483,2690 (100) | - | - |
| | | 20 | 483,2719 (100) | - | - |
| | | 40 | 143,1169 (100) | 100,0730 (63) | 297,1430 (62) |
| Hydroxythiohomosildenafil $C_{23}H_{32}N_6O_4S_2$ | 521,2005 | 10 | 521,2005 (100) | - | - |
| | | 20 | 521,2004 (100) | - | - |
| | | 40 | 299,0971 (100) | 129,1021 (82) | 100,0966 (54) |
| Hydroxyvardenafil $C_{23}H_{32}N_6O_5S$ | 505,2231 | 10 | 505,2234 (100) | - | - |
| | | 20 | 505,2234 (100) | - | - |
| | | 40 | 151,0870 (100) | 312,1593 (45) | 505,2235 (43) |
| Icariin $C_{33}H_{40}O_{15}$ | 677,2433 | 10 | 531,1869 (100) | 677,2440 (59) | 369,1330 (23) |
| | | 20 | 531,1862 (100) | 369,1346 (84) | 129,0561 (7) |
| | | 40 | 369,1351 (100) | 313,0718 (25) | - |
| Mirodenafil $C_{26}H_{37}N_5O_5S$ | 532,2593 | 10 | 532,2605 (100) | - | - |
| | | 20 | 532,2610 (100) | - | - |
| | | 40 | 296,1422 (100) | 312,1369 (64) | 532,2603 (30) |
| Nitrodenafil $C_{17}H_{19}N_5O_4$ | 358,1516 | 10 | 358,1503 (100) | - | - |
| | | 20 | 358,1501 (100) | 330,1196 (46) | 284,1260 (15) |
| | | 40 | 284,1259 (100) | 256,0968 (19) | 136,0496 (16) |
| N-Octylnortadalafil $C_{29}H_{33}N_3O_4$ | 488,2544 | 10 | 366,2136 (100) | 488,2509 (78) | 135,0391 (19) |
| | | 20 | 366,2136 (100) | 135,0392 (57) | 488,2497 (15) |
| | | 40 | 135,0391 (100) | 169,0707 (71) | 262,0912 (31) |
| Norneosildenafil $C_{22}H_{29}N_5O_4S$ | 460,2010 | 10 | 460,2028 (100) | - | - |
| | | 20 | 460,2038 (100) | - | - |
| | | 40 | 283,1215 (100) | 299,1162 (71) | 312,1596 (39) |

**Tabel 23 (continued)**

| Compound | Precursor ion $[M+H]^+$ (m/z) | Collision (eV) | Fragmentation ions (m/z) in parenthesis: relative intensity (%) | | |
|---|---|---|---|---|---|
| | | | (1) | (2) | (3) |
| Norneovardenafil $C_{18}H_{20}N_4O_4$ | 357,1568 | 10 | 357,1578 (100) | - | - |
| | | 20 | 357,1572 (100) | 151,0872 (28) | 329,1250 (9) |
| | | 40 | 151,0870 (100) | 300,0882 (8) | 123,0920 (5) |
| Oxohongdenafil $C_{25}H_{32}N_6O_4$ | 481,2558 | 10 | 481,2567 (100) | - | - |
| | | 20 | 481,2556 (100) | 453,2606 (18) | 410,2168 (10) |
| | | 40 | 297,1353 (100) | 410,2197 (64) | 396,2019 (56) |
| Piperidinoacetildenafil $C_{24}H_{31}N_5O_3$ | 438,2504 | 10 | 438,2503 (100) | - | - |
| | | 20 | 438,2502 (100) | - | - |
| | | 40 | 297,1344 (100) | 341,1601 (44) | 325,1303 (42) |
| Pseudovardenafil $C_{22}H_{29}N_5O_4S$ | 460,2013 | 10 | 460,2043 (100) | - | - |
| | | 20 | 460,2042 (100) | 151,0889 (8) | - |
| | | 40 | 151,0883 (100) | 312,1605 (28) | 460,2038 (19) |
| Sildenafil $C_{22}H_{30}N_6O_4S$ | 475,2113 | 10 | 475,2113 (100) | - | - |
| | | 20 | 475,2117 (100) | - | - |
| | | 40 | 100,0994 (100) | 283,1187 (87) | 311,1489 (35) |
| Tadalafil $C_{22}H_{19}N_3O_4$ | 390,1440 | 10 | 268,1084 (100) | 390,1448 (49) | 135,0435 (22) |
| | | 20 | 268,1083 (100) | 135,0439 (69) | 262,0861 (26) |
| | | 40 | 135,0438 (100) | 169,0756 (84) | 262,0860 (81) |
| Thiohomosildenafil $C_{23}H_{32}N_6O_3S_2$ | 505,2046 | 10 | 505,2037 (100) | - | - |
| | | 20 | 505,2048 (100) | - | - |
| | | 40 | 113,1067 (100) | 299,0964 (80) | 327,1265 (50) |
| Thioquinapiperifil $C_{24}H_{28}N_6OS$ | 449,2123 | 10 | 449,2125 (100) | 204,1387 (38) | - |
| | | 20 | 204,1384 (100) | 449,2124 (21) | - |
| | | 40 | 204,1381 (100) | 186,1275 (34) | 118,0646 (18) |
| Thiosildenafil $C_{22}H_{30}N_6O_3S_2$ | 491,1906 | 10 | 491,1908 (100) | - | - |
| | | 20 | 491,1905 (100) | - | - |
| | | 40 | 299,0955 (100) | 100,0998 (90) | 313,1138 (39) |
| Udenafil $C_{25}H_{36}N_6O_4S$ | 517,2597 | 10 | 517,2607 (100) | - | - |
| | | 20 | 517,2603 (100) | - | - |
| | | 40 | 517,2604 (100) | 283,1200 (91) | 112,1121 (90) |
| Vardenafil $C_{23}H_{32}N_6O_4S$ | 489,2273 | 10 | 489,2305 (100) | - | - |
| | | 20 | 489,2304 (100) | 151,0881 (5) | - |
| | | 40 | 151,0885 (100) | 312,1602 (36) | 489,2294 (32) |

**Sources cited in application example 5.11**

[1] *J.-m. Lee, H. Hong, H.B. Oh, B. Moon*: Fragmentation Pathways of Tadalafil and Its Analogues in Electrospray Ionization Tandem Mass Spectrometry.
**Bulletin of the Korean Chemical Society 2017:39**(2), 1-7

[2] *Peng Zou1, Peiling Hou1, Sharon Sze-Yin Oh, Min-Yong Low and Hwee-Ling Koh*: Electrospray tandem mass spectrometric investigations of tadalafil and its analogue
**Rapid Communications in Mass Spectrometry 2006:20**(22), 3488-3490

[3] *J. Aceña, S. Pérez, P.Gardinali, J.L. Abad, P. Eichhorn, N. Heuett, D. Barceló*: Structure Elucidation of Phototransformation Products of Unapproved Analogs of the Erectile Dysfunction Drug Sildenafil in Artificial Freshwater with UPLC-Q Extractive-MS.
**Journal of Mass Spectrometry 2014:49**(12), 1279-1289

[4] *P. Eichhorn, S. Pérez, J. Aceña, P. Gardinali, J.L. Abad, D. Barceló*: Identification of Phototransformation Products of Sildenafil (Viagra) and Its N-demethylated Human Metabolite Under Simulated Sunlight.
**Journal of Mass Spectrometry 2012:47**(6), 701-711

[5] *S. Ahn, J.Y. Hong, M.K. Hong, Y.P. Jang, M.S. Oh, J.H. Jung, J. Hong*: Structural Determination of Sildenafil and Its Analogues in Dietary Supplements by Fast-atom Bombardment Collosion Induced Dissociation Tandem Mass Spectrometry.
**Rapid Communications in Mass Spectrometry 2009:23**(19), 3158-3166

[6] *M.E. Abdel-Hamid*: Determination of Sildenafil, Tadalafil and Vardenafil in Tablets and Adulterated Herbal Products by ESI-MS-MS.
**Journal of Liquid Chromatography & Related Technologies 2006:29**(4), 591-603

[7] *W-S. Ku, H-J. Cho, I-S. Yoon, J.H. Kim, B-J. Cha, J.S. Kim, K-M. Kim, S-K. kang, S-J. Chung, C-K. Shim, D-D. Kim*: Rapid and Sensitive Determination of Udenafil in Plasma by LC-MS/MS for Intranasal Pharmacokinetic Study in Rats.
**Chem. Pharm. Bull., 2011:59**(9), 1083-1088

[8] *S. Lee, D. Ji, M. Park, K.H. Chung*: Development of a Comprehensive Spectral Library of Sildenafil and Related Active Analogues Using LC-Q TOF-MS and Its Application for Screening Counterfeit Pharmaceuticals.
**Forensic Science International 2015:257**(December), 182-188
(**http://dx.doi.org/10.1016/j.forsciint.2015.08.016**)

[9] C-L. Kee, X. Ge, V. Gilard, M. Malet-Martino, M-Y. Low: A Review of Synthetic Phosphodiesterase Type 5 Inhibitors (PDE-5i) as Adulterants in Dietary Supplements.
**Journal of Pharmaceutical and Biomedical Analysis 2018:147**(5 January), 250-277 (**shttp://dx.doi.org/10.1016/j.jpba.2017.07.031**)

## 5.12 Determination of β-Methasone 17-valerate by HPLC and mass spectrometry

Betamethasone esterified at the 17- or 21-position with valerianic acid has been detected as an illegal additive in some cosmetic products. A combined chromatographic (HPLC, Figure 344)-mass spectrometric method has been developed for the determination of these and other related compounds [1]. Figure 343 and Table 24 show the $MS^2$ mass spectrum (graphical and digitized) of β-methasone 17-valerate obtained by positively polarized electrospray ionization (ESI, spray voltage 4.5 kV, nitrogen spray gas at 200 $^oC$) after dissociation of the precursor ion **$[M+H]^+$** with **m/z** 477.2646.

The isomers of interest are separable by liquid chromatography on a $C_{18}$ column (150 mm x 2.0 mm i.d.) using the gradient elution method with two solutions: (A) formic acid solution (0.1 %) in acetonitrile; (B) formic acid solution (0.1 %) in water. The initial mixture consists of solutions (A) and (B) in a volume ratio of 25:75. The composition of the eluent changes linearly over 30 minutes to a final volume ratio of 95:5. Detection of betamethasone valerate isomer is performed in Selected Ion Monitoring (SIM) mode based on the **$[M+H]^+$** ion (Figure 344). The analytical method provides a linear response over the concentration range 0.3 - 100 μg mg/ml of isomers.

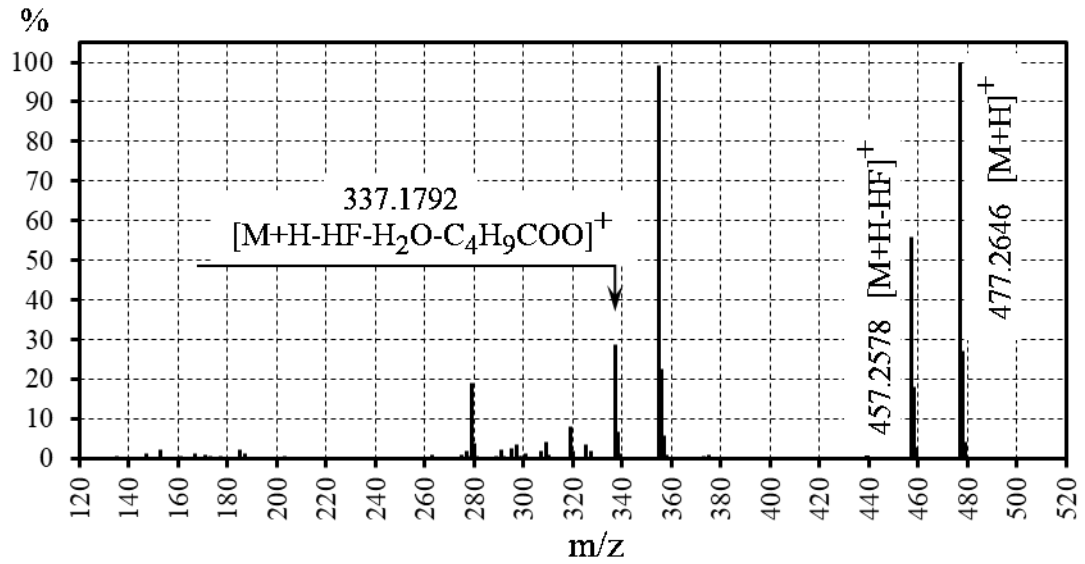



**Fig. 343 Mass spectrum of β-methasone 17-valerate ($MS^2$, positive mode, ESI ionization, collision energy 10 eV, precursor ion [M+H]+, MoNa AU283301).**

The mass spectra of the isomers are qualitatively similar, but with some differences in the relative abundance of the signals: the **$[M+H-HF-H_2O-CH_3(CH_2)_3COO]^+$** ion at **m/z** 337.1909 present in the $MS^2$ spectrum of 17-valerate betamethasone is absent in the spectrum of the 21-valerate betamethasone isomer. On the other hand, the signal of the **$[M+H-HF]^+$** ion with **m/z** 457,2586 is weaker for the 17-valerate than for the 21-valerate of betamethasone.

**Table 24. Mass spectrum of β-methasone 17-valerate ($MS^2$, positive mode, ESI ionization, collision energy 10 eV, (assignment of ion fragments) [1]**

| m/z | (%) | Assignment | m/z | (%) | Assignment |
|---|---|---|---|---|---|
| 135.0800 | 0.58 | $[C_9H_{11}O]^+$ | 301.1580 | 1.32 | $[C_{22}H_{21}O]^+$ |
| 147.0794 | 1.348 | $[C_{10}H_{11}O]^+$ | 307.1689 | 2.05 | $[C_{21}H_{23}O_2]^+$ |
| 153.0895 | 2.378 | $[C_9H_{13}O_2]^+$ | 309.1833 | 4.37 | $[C_{21}H_{25}O_2]^+$ |
| 161.0943 | 0.62 | $[C_{11}H_{13}O]^+$ | 310.1873 | 1.06 | $[C_{20}{}^{13}CH_{25}O_2]^+$ |
| 167.1051 | 1.252 | $[C_{10}H_{15}O_2]^+$ | 319.1682 | 8.29 | $[C_{22}H_{23}O_2]^+$ |
| 171.0799 | 1.012 | $[C_{12}H_{11}O]^+$ | 320.1717 | 2.03 | $[C_{21}{}^{13}CH_{23}O_2]^+$ |
| 173.0948 | 0.69 | $[C_{12}H_{13}O]^+$ | 325.1777 | 3.47 | $[C_{21}H_{25}O_3]^+$ |
| 177.0906 | 0.76 | $[C_{11}H_{13}O_2]^+$ | 326.1837 | 0.10 | $[C_{20}{}^{13}CH_{25}O_3]^+$ |
| 185.0943 | 2.30 | $[C_{13}H_{13}O]^+$ | 327.1945 | 1.89 | $[C_{21}H_{27}O_3]^+$ |
| 187.0744 | 1.45 | $[C_{12}H_{11}O_2]^+$ | 337.1792 | 28.71 | $[C_{22}H_{25}O_3]^+$ |
| 203.1058 | 0.64 | $[C_{13}H_{15}O_2]^+$ | 338.1824 | 6.86 | $[C_{21}{}^{13}CH_{25}O_3]^+$ |
| 263.1420 | 1.04 | $[C_{19}H_{19}O]^+$ | 339.1830 | 1.25 | $[C_{20}{}^{13}C_2H_{25}O_3]^+$ |
| 275.1423 | 0.92 | $[C_{20}H_{19}O]^+$ | 355.1904 | 99.28 | $[C_{26}H_{24}F]^+$ |
| 277.1572 | 2.01 | $[C_{20}H_{21}O]^+$ | 356.1933 | 22.56 | $[C_{25}{}^{13}CH_{24}F]^+$ |
| 278.1645 | 0.72 | $[C_{19}{}^{13}CH_{21}O]^+$ | 357.1909 | 5.97 | $[C_{24}{}^{13}C_2H_{24}F]^+$ |
| 279.1735 | 19.23 | $[C_{20}H_{23}O]^+$ | 358.1897 | 1.09 | $[C_{25}H_{26}O_2]^+$ |
| 280.1768 | 3.93 | $[C_{19}{}^{13}CH_{23}O]^+$ | 373.1990 | 0.78 | $[C_{22}H_{29}O_5]^+$ |
| 281.1838 | 0.72 | $[C_{18}{}^{13}C_2H_{23}O]^+$ | 375.1971 | 0.88 | $[C_{22}H_{28}FO_4]^+$ |
| 289.1586 | 0.70 | $[C_{21}H_{21}O]^+$ | 439.2479 | 0.91 | $[C_{27}H_{35}O_5]^+$ |
| 291.1731 | 2.23 | $[C_{21}H_{23}O]^+$ | 457.2578 | 56.02 | $[C_{27}H_{37}O_6]^+$ |
| 292.1777 | 0.82 | $[C_{20}{}^{13}CH_{23}O]^+$ | 458.2616 | 18.18 | $[C_{26}{}^{13}CH_{37}O_6]^+$ |
| 295.1689 | 2.65 | $[C_{20}H_{23}O_2]^+$ | 459.2623 | 2.88 | $[C_{25}{}^{13}C_2H_{37}O_6]^+$ |
| 297.1845 | 3.47 | $[C_{20}H_{25}O_2]^+$ | 477.2646 | 100.00 | $[C_{27}H_{38}FO_6]^+$ |
| 298.1876 | 0.77 | $[C_{19}{}^{13}CH_{25}O_2]^+$ | 478.2673 | 27.27 | $[C_{26}{}^{13}CH_{38}FO_6]^+$ |
| 299.1803 | 0.63 | $[C_{20}H_{24}FO]^+$ | 479.2707 | 4.30 | $[C_{25}{}^{13}C_2H_{38}FO_6]^+$ |

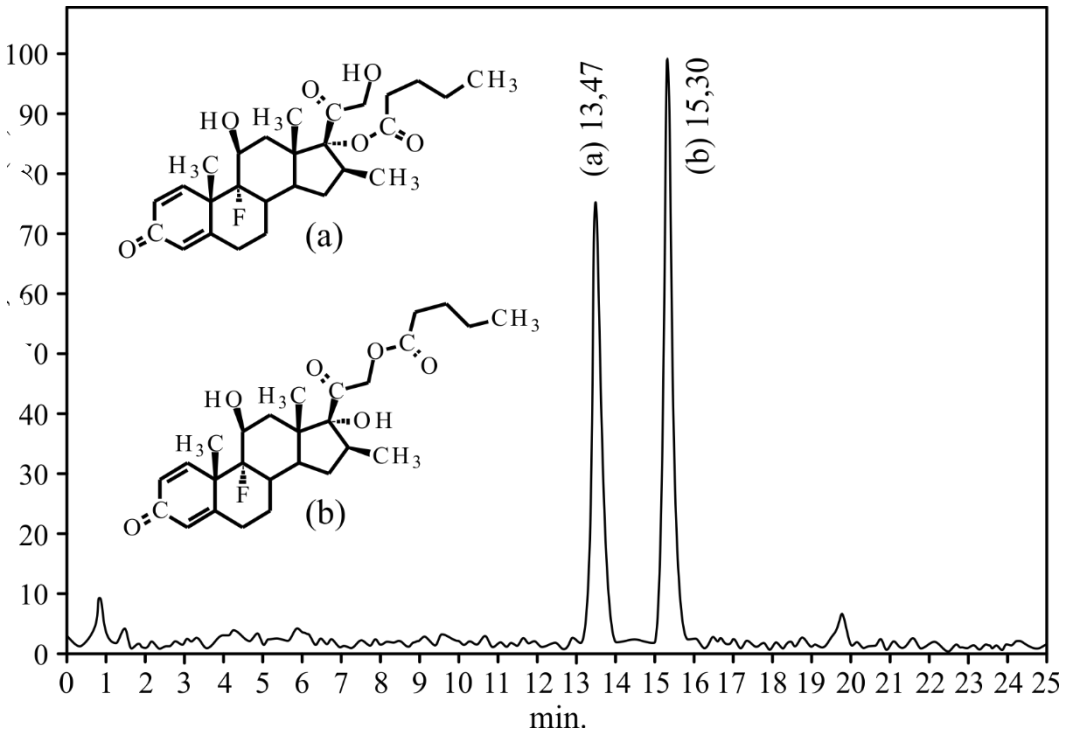



**Fig. 344 Chromatographic separation (SIM) of betamethasone 17-valerate (a) and betamethasone 21-valerate (b) (adapted from [1])**

**Source cited in sample application 5.12**

[1] *J. Fiori, V. Andrisano*: LC-MS Method for the Simultaneous Deterination of Six Glucocorticoids in Pharmaceutical Formulations and Counterfeit Cosmetic Products. **Journal of Pharmaceutical and Biomedical Analysis**, http://dx.doi.org/10.1016/j.jpba.2013.12.026

### 5.13 Study of buspirone metabolites

Buspirone is used in the treatment of anxiety disorders but has been shown to be ineffective in psychosis. It is full agonist of presynaptic 5-$HT_{1A}$ receptors and partial agonist of postsynaptic 5-$HT_{1A}$ receptors. When taken orally, the major metabolite is 1-(2-pyrimidinyl)piperazine [1,2]. Liquid chromatography coupled to mass spectrometry has been used to identify additional metabolites [3,4].

Figures 345, 346 and 347 show the $MS^1$ mass spectra and Figures 348, 349, 350, 351 and 352 show the $MS^2$ mass spectra of buspirone obtained in various sampling cone potentials and with different collision energies. The fragmentation scheme (Figure 353) corresponds to the masses of principal ions in the $MS^1$ spectrum.

Twenty-five buspirone metabolites resulting from hydroxylation, N-dealkylation, O-methylation, and glucuronidation reactions were separated by liquid chromatography and their structures were identified by comparison their $MS^2$ spectra with the corresponding buspirone spectrum. The method allowed the identification of two new metabolites: despyrimidyl-buspirone and despyrimidyl-piperazine-buspirone [3].

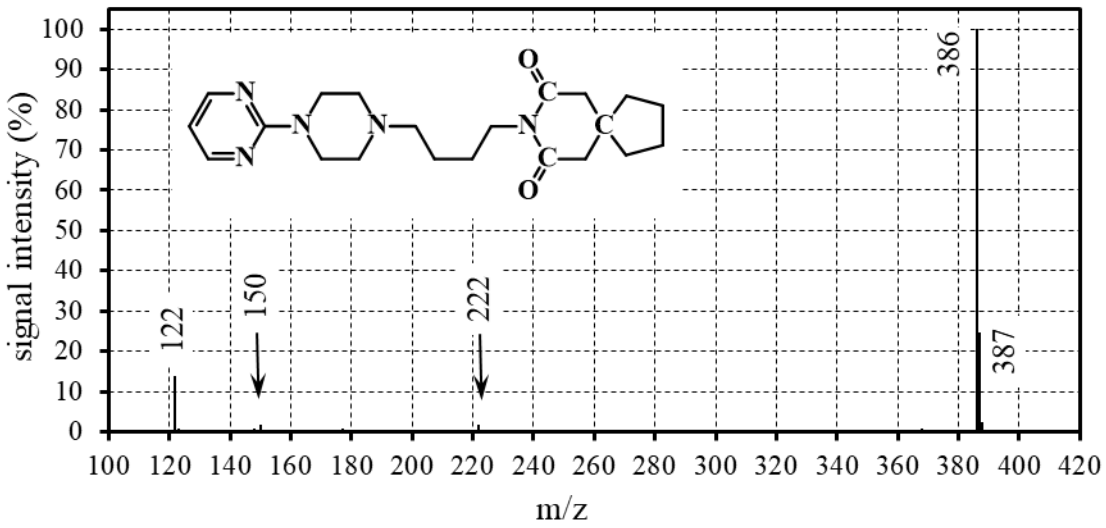



**Fig. 345 Buspirone MS[1] ESI, positive mode – Sampling cone at 45 V**

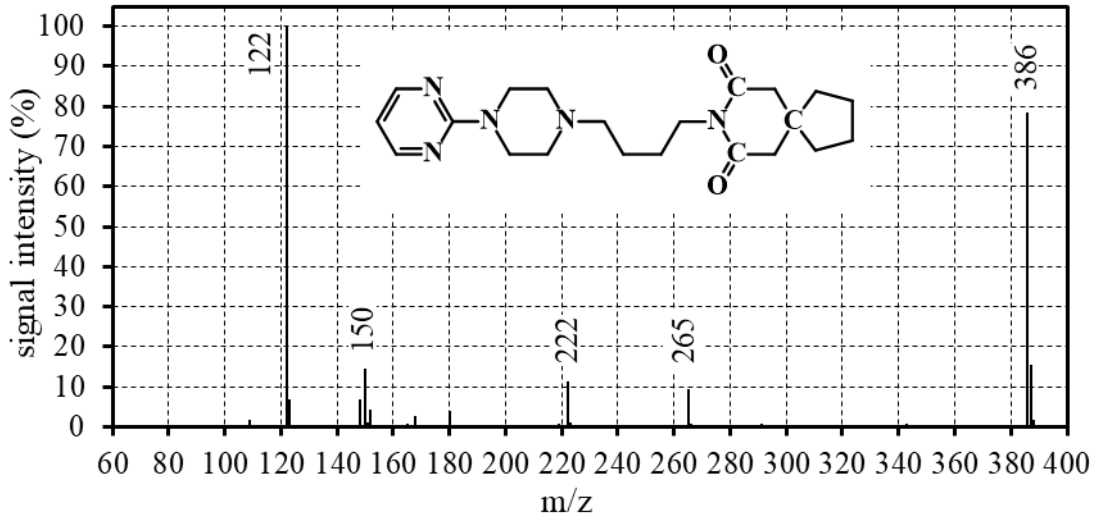



**Fig. 246 MS[1] mass spectrum of buspirone (positive ionization ESI, sampling cone voltage: 60 V (taken and adapted from MoNa database, spectrum No WA002986)**

**Table 25 MS[1] mass spectrum of buspirone (positive ionization ESI, sampling cone voltage: 60 V (digitalized form)**

| Buspirone MS[1] positive mode – Sampling cone at: 60 V Exact mass: 385,2478 | | | | | | | |
|---|---|---|---|---|---|---|---|
| **m/z** | **Relative abundance (%)** | **m/z** | **Relative abundance (%)** | **m/z** | **Relative abundance (%)** | **m/z** | **Relative abundance (%)** |
| 109 | 1,60 | 151 | 1,201 | 219 | 0,801 | 291 | 0,801 |
| 122 | 100,00 | 152 | 4,301 | 222 | 11,411 | 343 | 0,801 |
| 123 | 6,71 | 165 | 0,801 | 223 | 1,201 | 386 | 78,48 |
| 148 | 6,71 | 168 | 2,501 | 265 | 9,41 | 387 | 15,31 |
| 150 | 14,511 | 180 | 3,901 | 266 | 0,8011 | 388 | 1,60 |

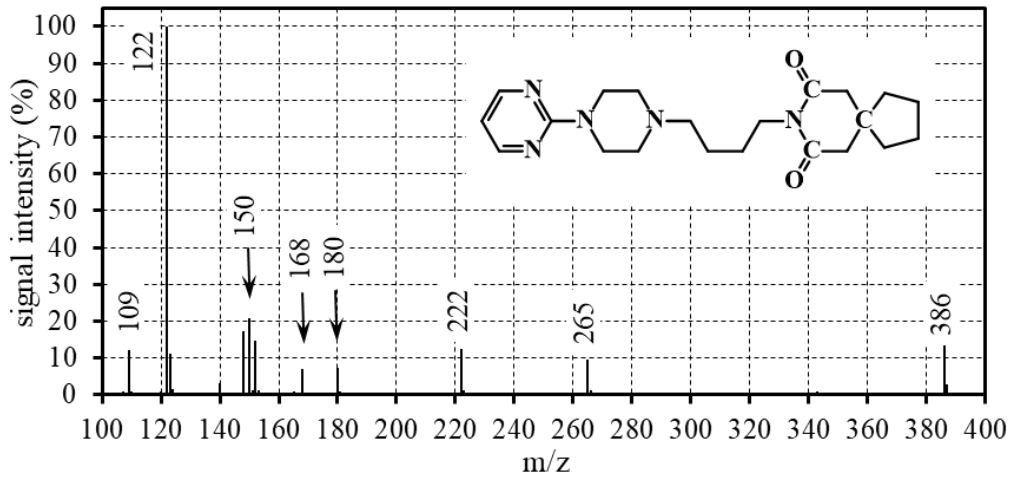



**Fig. 347 MS[1] mass spectrum of buspirone (positive ionization ESI, sampling cone voltage: 75 V (according to MoNa database, No WA002986)**

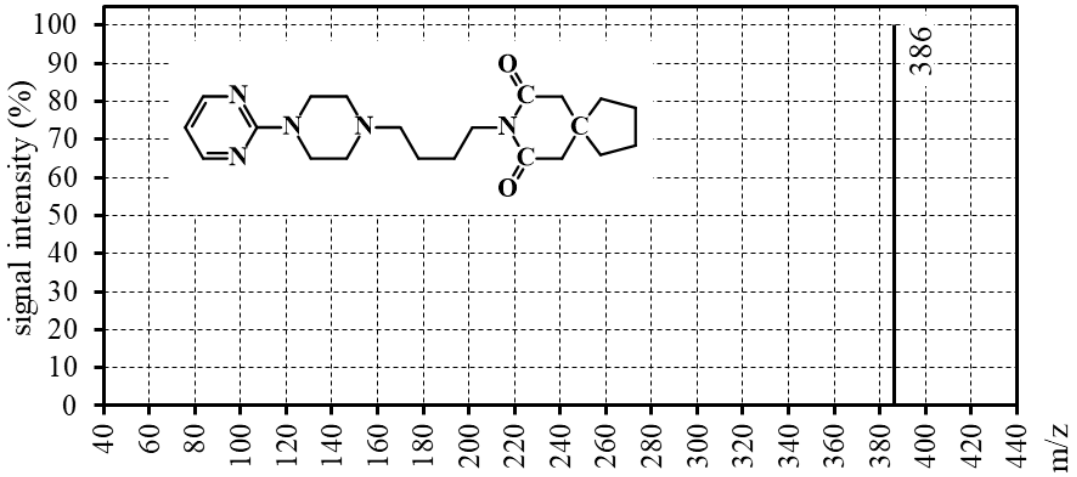



**Fig. 348 MS[2] mass spectrum of buspirone, precursor ion m/z 386 (CID fragmentation, argon collision gas at 10 eV) [3]**

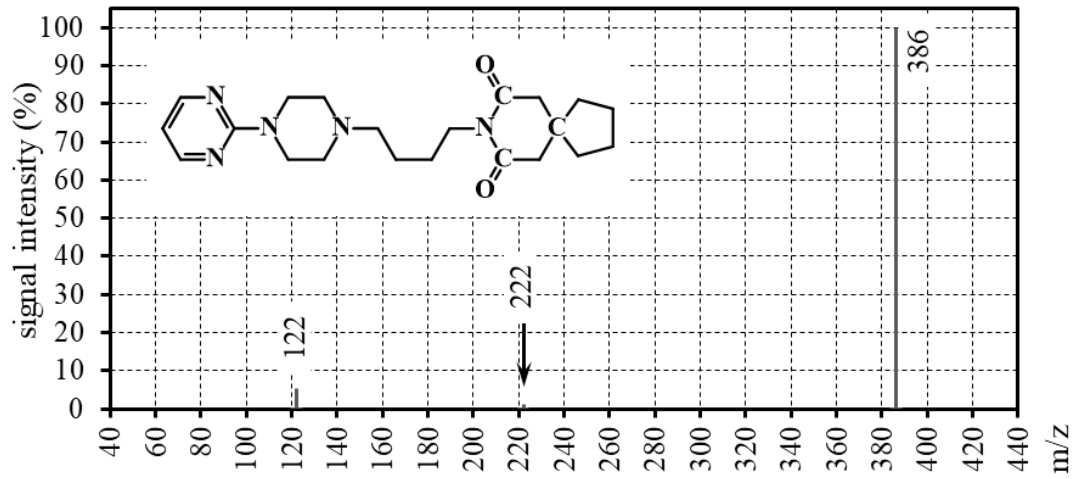



**Fig. 349 MS[2] mass spectrum of buspirone, precursor ion m/z 386 (CID fragmentation, argon collision gas at 20 eV) (reconstructed from [3] and MoNa no. WA002986)**

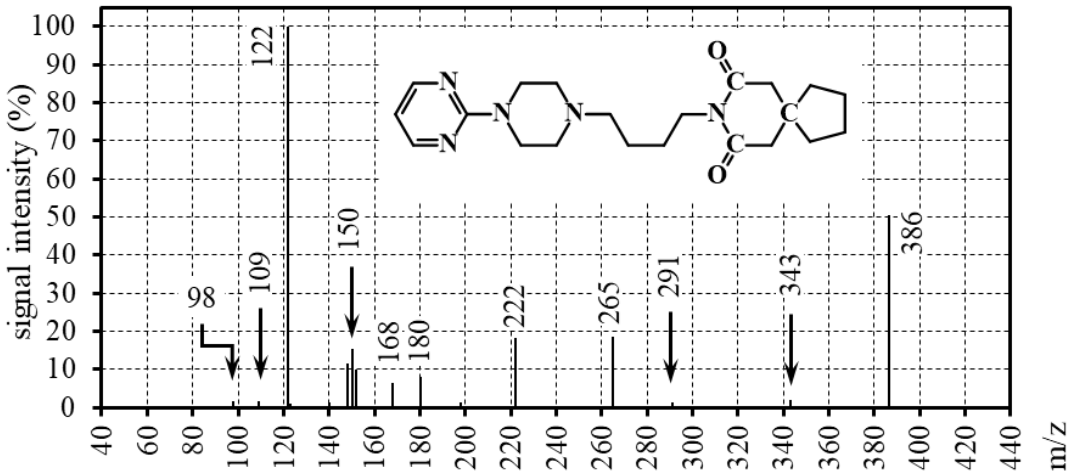



**Fig. 350 $MS^2$ mass spectrum of buspirone, precursor ion m/z 386 (CID fragmentation, argon collision gas at 30 eV) (reconstructed from [3] and MoNa no. WA002986)**

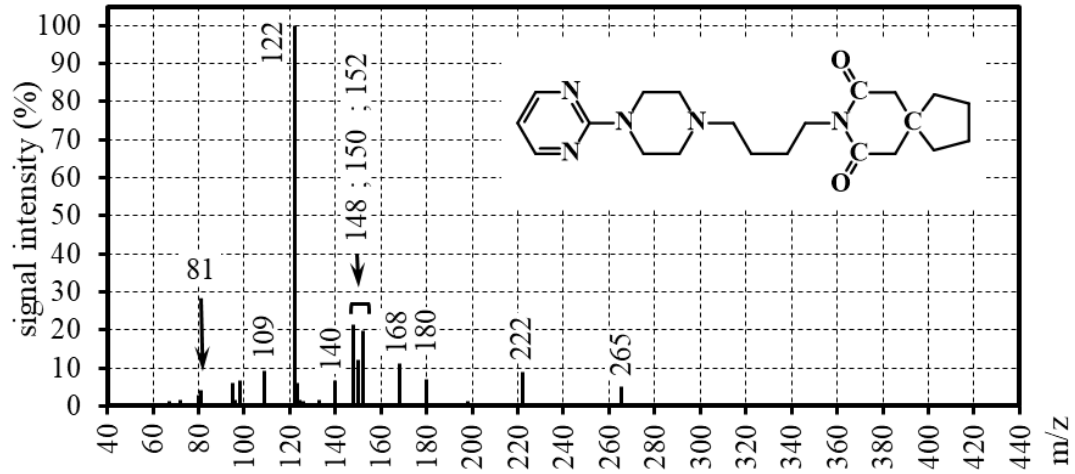



**Fig. 351 $MS^2$ mass spectrum of buspirone, precursor ion m/z 386 (CID fragmentation, argon collision gas at 40 eV) [3]**

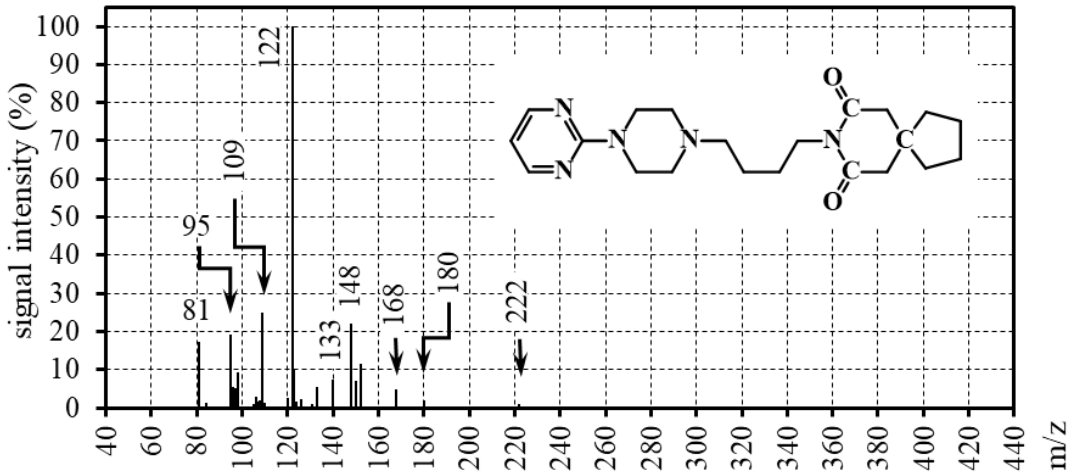



**Fig. 352 $MS^2$ mass spectrum of buspirone, precursor ion m/z 386 (CID fragmentation, argon collision gas at 50 eV) [3]**

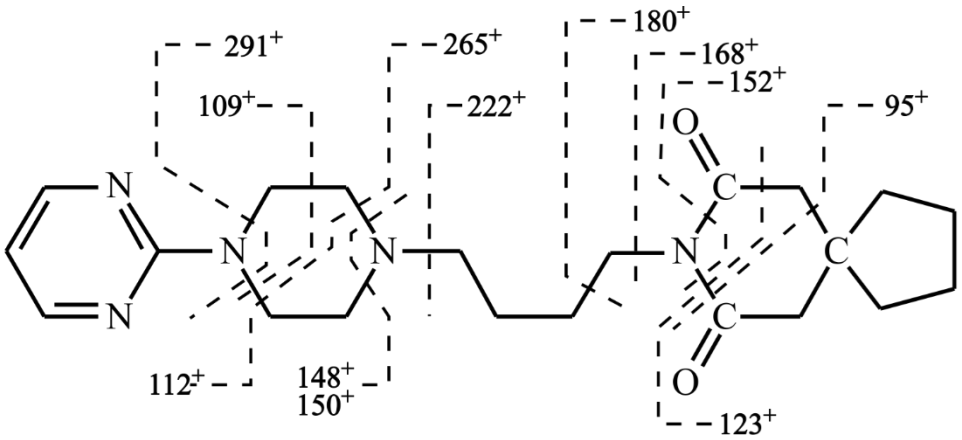



**Fig. 353 Possible fragmentation diagram of buspirone (reconstructed from [3] and [4])**

**Sources cited in the example application 5.13**

[1] *G. Tunnicliff*: Molecular Basis of Buspirone's Anxiolitic Action. **Pharmacology & Toxicology 1991:69**(3), 149-156

[2] *K.P. Zuideveld, J. Rusic-Pavietic, H.J. Maas, L.A. Peletier, P.H. Van der Graaf, M. Danhof*: Pharmacokinetic-Pharmacodynamic Modeling of Buspirone and Its Metabolite 1-(2-Pyrimidinyl)-piperazine in Rats. **The Journal of Pharmacology and Experimental Therapeutics 2002:303**(3), 1130-1137

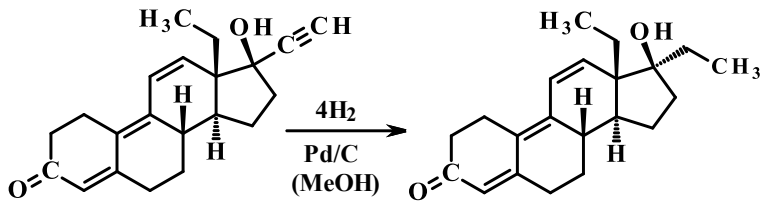
[3] *E.H. Kerns, R.A. Rourick, K.J. Volk, M.S. Lee*: Buspirone Metabolite Structure Profile Using a Standard Liquid Chromatographic – Mass Spectrometric Protocol. **Journal of Chromatography B: Biomedical Sciences and Applications 1997:698**(1-2), 133-145 (**https://doi.org/10.1016/S0378-4347(97)00254-5**)

[4] *M.S. Lee*: LC/MS Applications in Drug Development (Cap. 6, Pag. 127) **John Wiley & Sons, Inc. 2002**

## 5.14 Detection and determination of tetrahydrogestrinone in doping control

Illegal doping substances in the category of natural or semi-synthetic steroids are frequently used to boost sporting performance. There is a real competition between the trend towards the development of increasingly difficult-to-detect substances and the analytical methods developed for the identification and quantitative determination of these compounds in various pharmaceutical forms and in biological fluids [1]. Most analytical methods are based on chromatographic separation (liquid or gas phase) coupled with selective detection and quantitative determination by various spectrometric configurations [2].

One substance used in this context is tetrahydrogestrinone, a potent agonist of androgen and progesterone receptors [2], which was secretly synthesized by chemist *Patrick Arnold* with the goal of producing a difficult-to-detect and difficult-to-identify compound used to enhance athletic performance. The synthesis involved the catalytic reduction of gestrinone in a methanolic medium [3] (Figure 354).




gestrinone tetrahydrogestrinone

**Fig. 354 Synthesis of tetrahydrogestrinone**

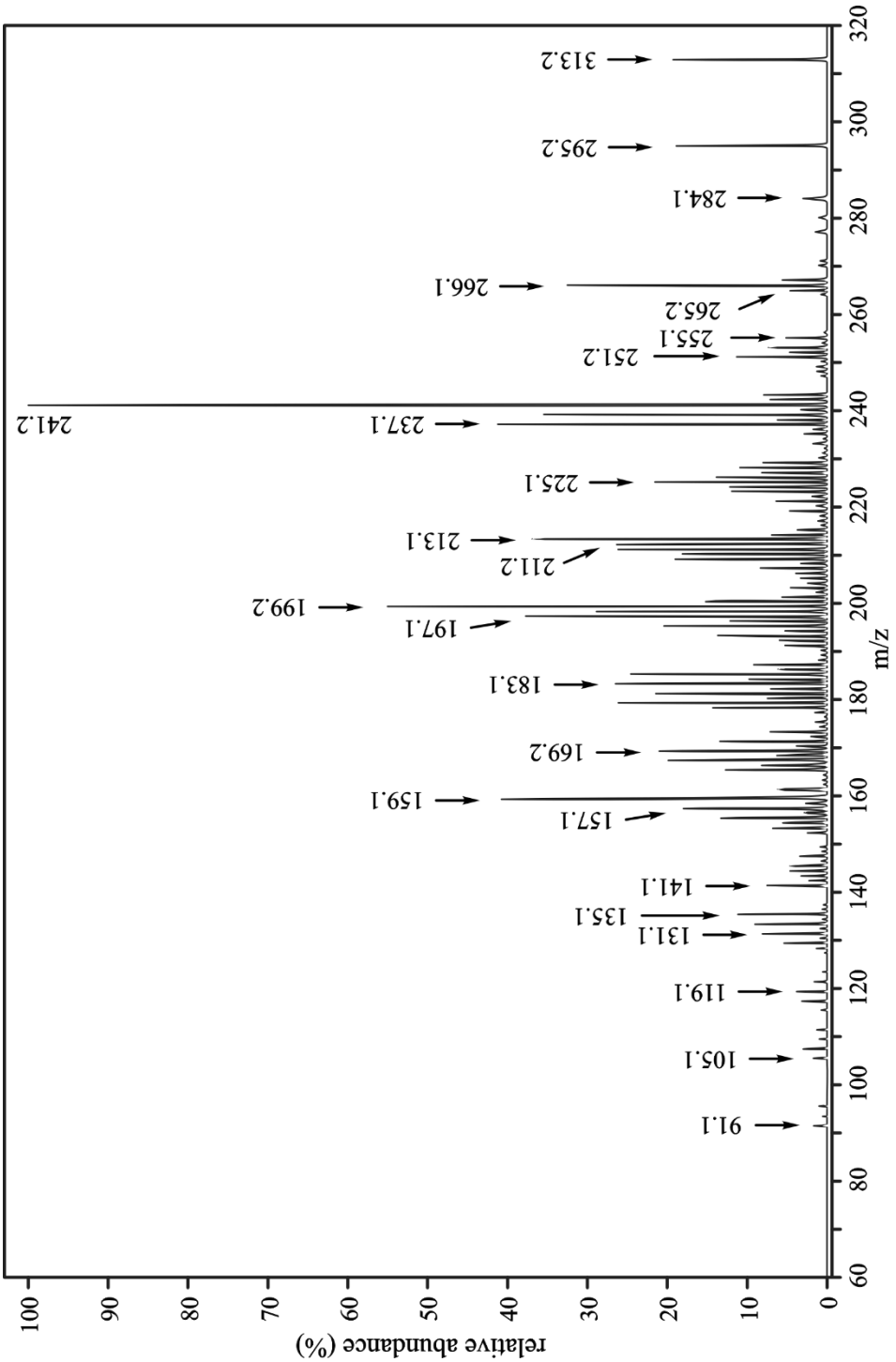



**Fig. 355 $MS^2$ mass spectrum of tetrahydrogestrinone (primary ionization ESI, collision gas: nitrogen, collision energy: 40 eV) precursor ion: m/z 313.2 $[M+H]^+$ (reconstructed from [4])**

Chromatographic methods with $MS^2$ mass spectrometric detection have been developed for the reliable and selective detection of tetrahydrogestrinone [4,5]. Figure 355 shows the $MS^2$ mass spectrum obtained by primary electrospray ionization (ESI), nitrogen impact fragmentation (impact energy 40 eV), with the main signals indicated. Some signals are also associated with other gestrinone analogs, but the signals at **m/z** ratios 199, 241, and 313 are considered to have sufficient specificity for the detection and identification of tetrahydrogestrinone [4]. Figure 356 shows the fragmentation leading to these ions. A later publication [5] completes the list of characteristic signals in the $MS^2$ mass spectrum of tetrahydrogestrinone recommended for reliable identification by primary electrospray ionization and chemical collision fragmentation (CID) at a collision energy of 15 eV (Table 26).

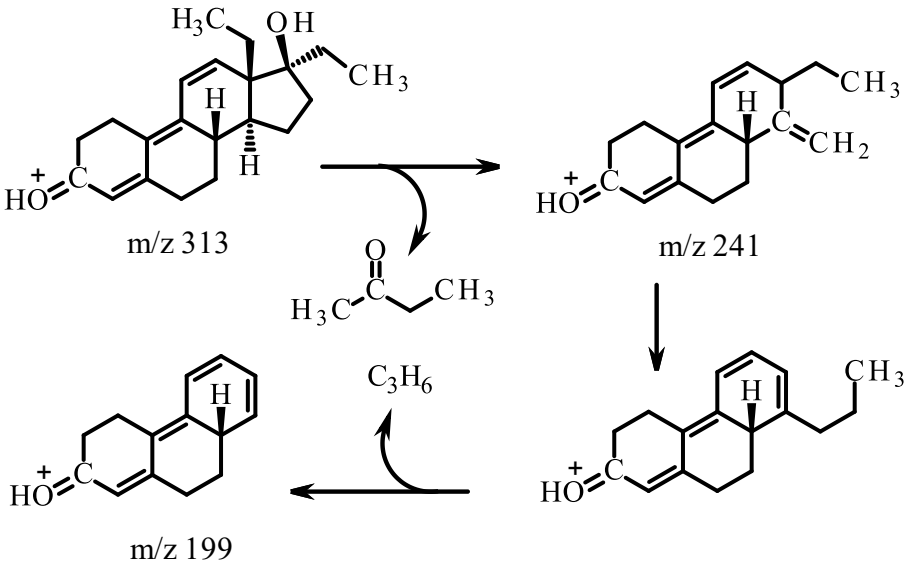



**Fig. 356 $[M+H]^+$ ion fragmentation pathway with formation of tetrahydrogestrinone characteristic signals (adapted from [4])**

**Tabel 26 Characteristic m/z signals in the $MS^2$ spectra of tetrahydrogestrinone, recommended for identification and quantification, by ESI primary ionization and collisional fragmentation (precursor ion $[M+H]^+$ with m/z 313.2162 and collision energy 15 eV, according to [5]).**

| m/z (fragment) | Elemental composition | EU** | m/z (fragment) | Compoziţie elementară | EU** |
|---|---|---|---|---|---|
| 313,2162 * | $[C_{21}H_{29}O_2]^+$ | 7,5 | 213,1274 | $[C_{15}H_{17}O]^+$ | 7,5 |
| 266,1666 | $[C_{19}H_{22}O]^+$ | 9,0 | 211,1118 | $[C_{15}H_{15}O]^+$ | 8,5 |
| 241,1587 | $[C_{17}H_{21}O]^+$ | 7,5 | 197,0961 | $[C_{14}H_{13}O]^+$ | 8,5 |
| 239,1431 | $[C_{17}H_{19}O]^+$ | 8,5 | 159,0805 | $[C_{11}H_{11}O]^+$ | 6,5 |
| 225,1274 | $[C_{16}H_{17}O]^+$ | 8,5 | | | |

*precursor ion **$[M+H]^+$** ** **EU** equivalent unsaturation (relation 73)

The enhanced resolution of the data in Table 26 (**m/z** ratios displayed to four decimal places) allows determining the molecular formula of the ion fragments and calculating the equivalent unsaturation (**EU**) according to equation (73).

$$EU = 1 + \frac{1}{2} \cdot \sum_{i=1}^{4} \left( v_{i-2} \right) \cdot n_i \qquad (73)$$

where: $\mathbf{v_i}$ is the valence of the chemical element number "**i**";

$\mathbf{n_i}$ is the number of atoms of the chemical element of number "**i**" in the molecule or ion under consideration.

Equivalent unsaturation is the measure that expresses the number of additional covalent bonds (compared to the "**σ**" single bond) or the number of cycles in the molecular or ionic formation. In the case of neutral molecules (but not radicals), the equivalent unsaturation is a positive integer. In the case of ionic or radical formations, the **EU** value may be a fractional number. Knowing the equivalent unsaturation (calculable from the molecular formula) helps to associate an **m/z** value in the mass spectrum with a molecular/ionic structure.

As an example, for the formula $C_{21}H_{28}O_2$, corresponding to the neutral tetrahydrogestrinone molecule, the equivalent unsaturation is:

$$EU(C_{21}H_{28}O_2) = 1 + \frac{1}{2} \cdot \left[ (4-2) \cdot 21 + (1-2) \cdot 28 + (2-2) \cdot 2 \right] = 8$$

Indeed, in the neutral molecule of tetrahydrogestrinone, the sum of double bonds and cycles is 8 (Figure 354).

For the formula $C_{21}H_{29}O_2$, corresponding to the molecular ion $\mathbf{[C_{21}H_{29}O_2]^+}$, the equivalent unsaturation is non-integer:

$$EU\left[C_{21}H_{29}O_2\right]^+ = 1 + \frac{1}{2} \cdot \left[ (4-2) \cdot 21 + (1-2) \cdot 29 + (2-2) \cdot 2 \right] = 7{,}5$$

**Sources cited in application example 5.14**

[1] *R. Kazlauskas*: "**Designer Steroids**" în **Doping in Sports**, editors: *D. Thiema* and *P. Hemmersbach*, cap. 7, pag. 154-185
**Springer 2010** [ISBN: 978-3-540-7908-7]

[2] *A.K. Death, K.C.Y. McGrath, R. Kazlauskas, D.J. Handelsman*: Tetrahydrogestrinone Is a Potent Androgen and Progestin.
**The Journal of Clinical Endocronology & Metabolism 2004:89**(5), 2498-2500

[3] *D.H. Catlin, M.H. Sekera, B.D. Ahrens, B. Startevic, Y-C. Chang, C.K. Hatton*: Tetrahydrogestrinone: Discovery, Synthesis and Detection in Urine.
**Rapid Communications in Mass Spectrometry 2004:18**(12), 1245-1249

[4] *M. Thevis, U. Bommerich, G. Opfermann, W. Schänzer*: Characterization of Chemically Modified Steroids for Doping Control Purposes by Electrospray Ionization Tandem Mass Spectrometry.
**Journal of Mass Spectrometry 2005:40**(4), 494-502

[5] *F. Guan, L.R. Soma, Y. Luo*: Collision-Induced Dissociation Pathways of Anabolic Steroids by Electrospray Ionization Tandem Mass Spectrometry. **J. Am. Soc. Mass Spectrom., 2006:17**(4), 477-489

### 5.15 Detection and analytical determination of diuretics abused in sports

In addition to their usual therapeutic use, diuretics are abused in some sports (like various combat sports and weightlifting) to reduce body weight or to mask the presence of doping substances in urine samples [1]. Because of this, the International Olympic Committee's Medical Commission has been monitoring the use of diuretics in sports competitions since 1988.

Most diuretics are excreted in the urine in unchanged chemical form. Detection is based on solid extraction techniques, chromatographic separation (liquid or gas) and the confirmation of chemical identity is realized by mass spectrometric techniques [2].

In 1990, *Song-Ja Park* and coworkers proposed an original method for the separation, determination, and chemical confirmation of commonly used diuretics [3]. The novel feature is the transformation of diuretics into permethylated derivatives, chemical species with reduced polarity and more advantageous chromatographic properties. The gas chromatographic separation is based on a capillary column (16 m, 0.2 mm inner diameter) with hydrophobic stationary phase (SE-30, 0.33 μm). The column temperature program is shown in Figure 357. The temperature of the gas chromatograph injection unit is maintained at 290 $^{o}$C.

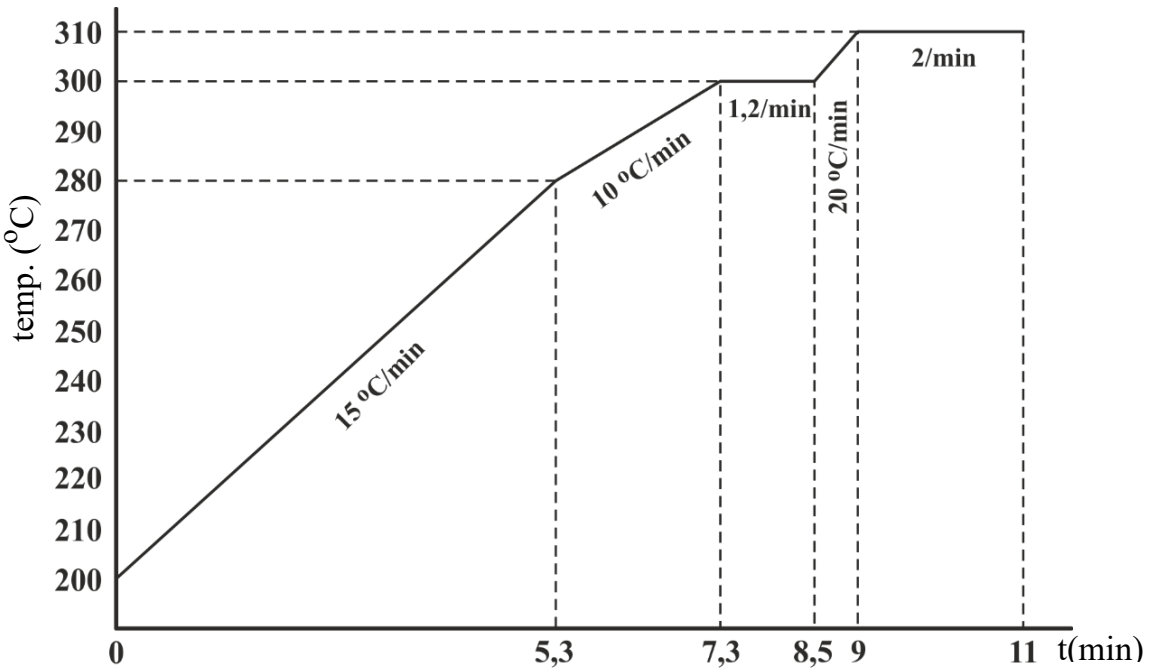



**Fig. 357 Temperature program of a capillary column used in the gas chromatographic separation of abused diuretics [3]**

The chromatogram and separation efficiency of some permethylated derivatives are shown in Figure 358. The structures of the targeted components are shown in Figure 359 (methylated positions are indicated in bold). In the usual way, mass spectrometric detection is performed in the TIC (total ion chromatogram) mode. A set of 12 per-methylated diuretics can be separated with good efficiency under the mentioned gas chromatographic conditions.

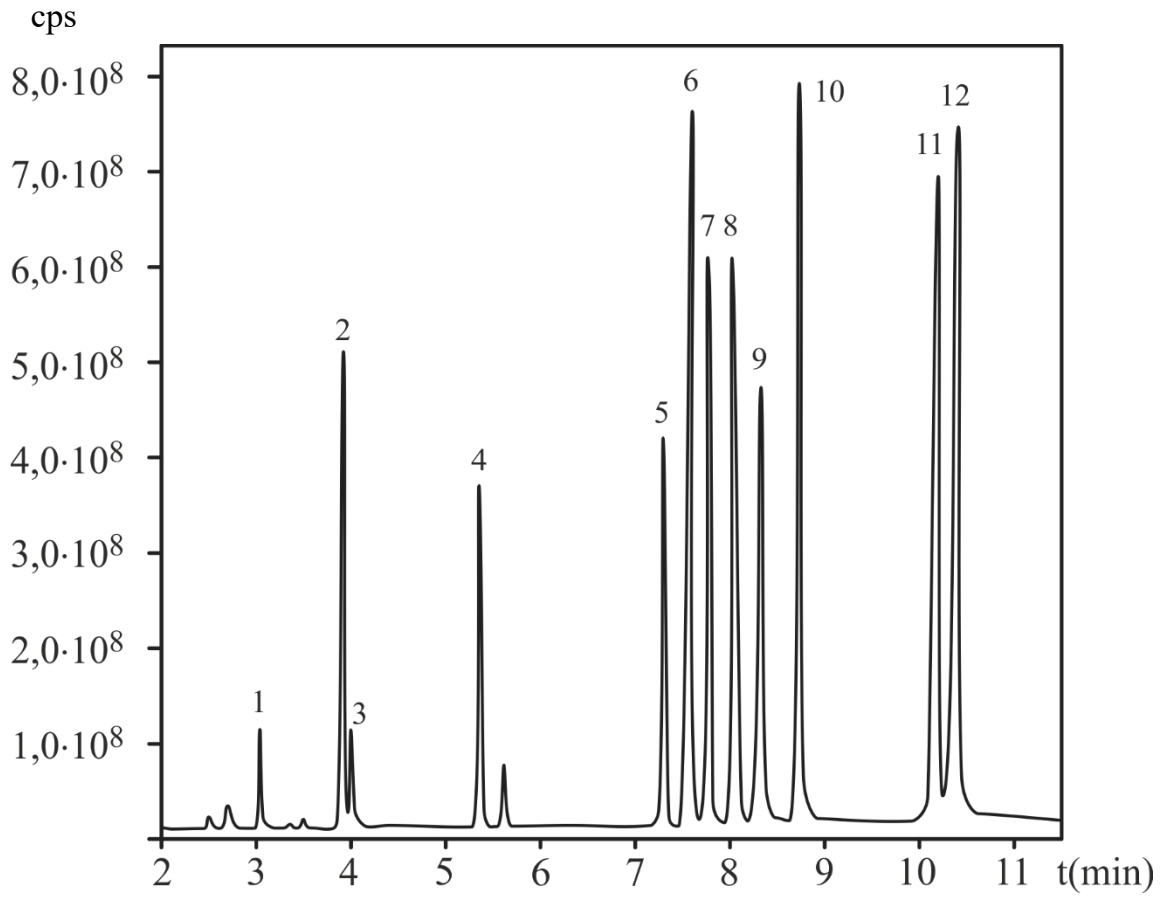
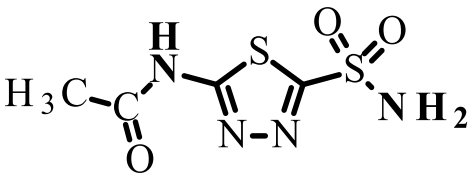



**Fig. 358 Gas chromatographic separation of permethylated derivatives of 12 diuretics: (1) acetazolamide, (2) etacrynic acid, (3) amiloride, (4) dichlofenamide, (5) furosemide, (6) mefruside, (7) chlortalidone, (8) bumetanide, (9) hydrochlorotiazide, (10) triamterene, (11) spironolactone, (12) bendrofluomethiazide (reconstructed according to [3])**

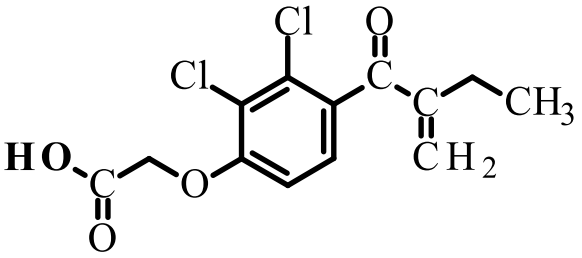
*M. Thevis* and co-workers have extended the gas chromatographic method coupled with mass spectrometry (70 eV electron impact ionization, SIM detection mode) to other permethylated representatives of the diuretic class [4]. Table 27 shows the list of recommended MS signals for the identification and determination of permethylated derivatives of diuretic substances abused in sport.

Figures 360, 361, and 362 represent the fragmentation patterns of tetra-methyl-hydrochlorothiazide, trimethyl-bumetanide and hexamethyl-triamterene in mass spec-

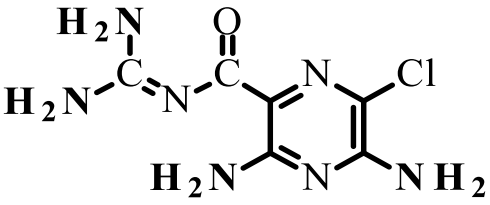
trometric ($MS^1$) analysis using primary impact ionization with an electron flux of 70 eV energy.



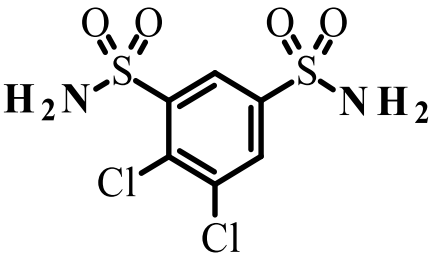
**acetazolamide**



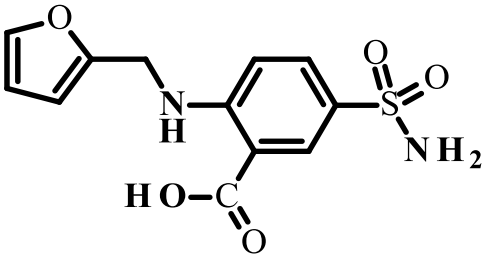
**etacrynic acid**



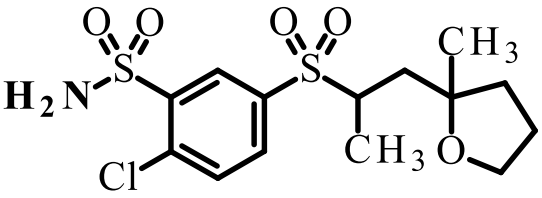
**amiloride**



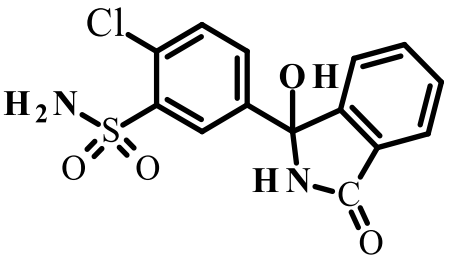
**dichlofenamide**



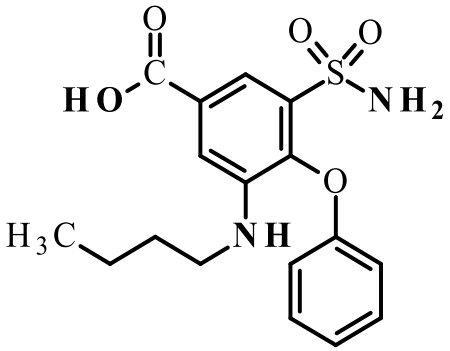
**furosemide**



**mefruside**

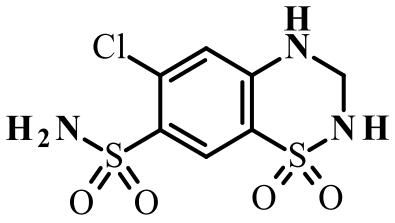


**chlortalidone**

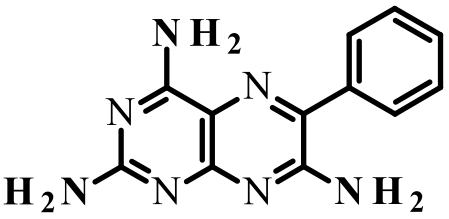


**bumetanide**

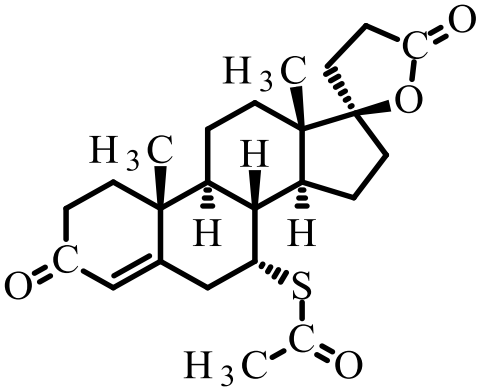
**Fig. 359 The structures of diuretics associated with some chromatographic peaks in Figure 358 and/or listed in Table 27**



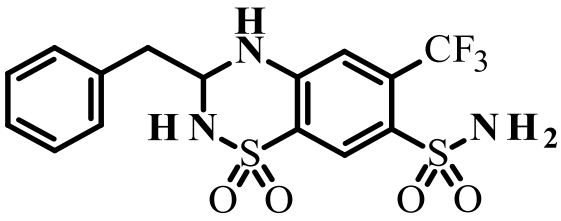
hydrochlorotiazide



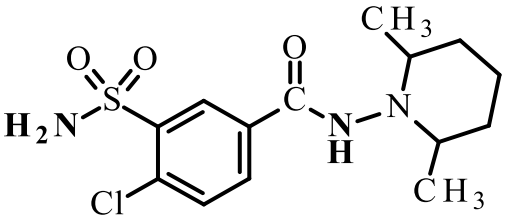
triamterene



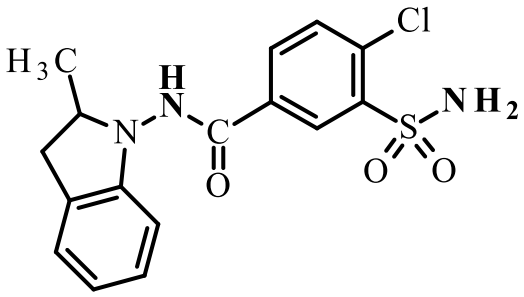
spironolactone



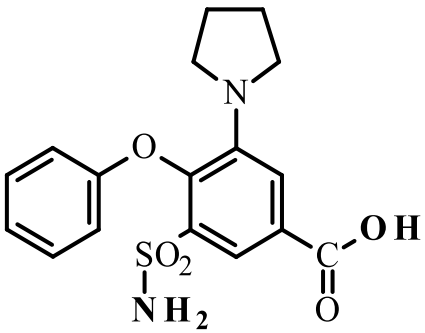
bendrofluometiazide



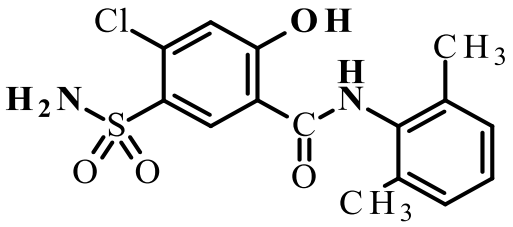
clopamide



indapamide

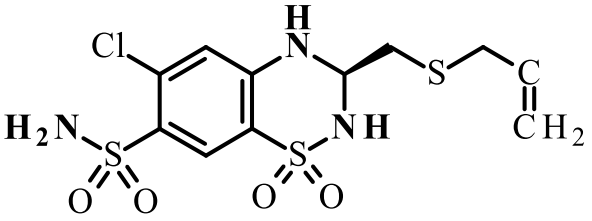


piretamide

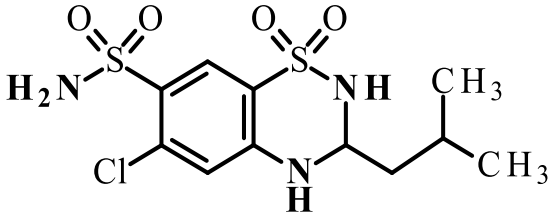


xipamide

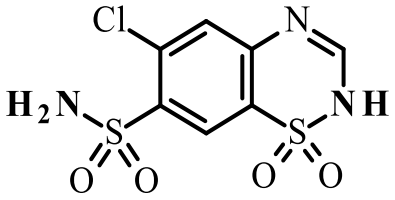
**Fig. 359 The structures of diuretics associated with some chromatographic peaks in Figure 358 and/or listed in Table 27 (continued)**



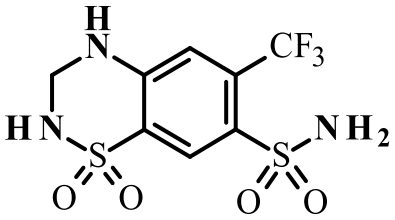
**altiazide**



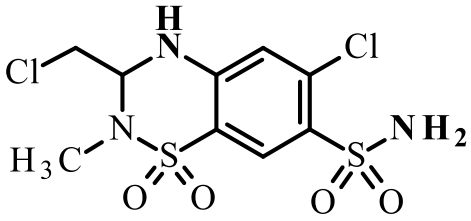
**buthiazide (butizide)**



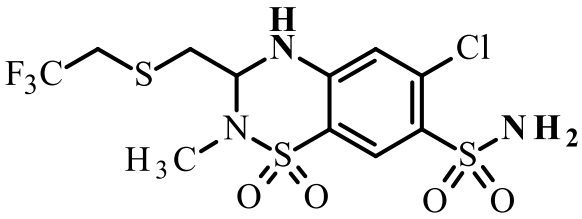
**chlorothiazide**



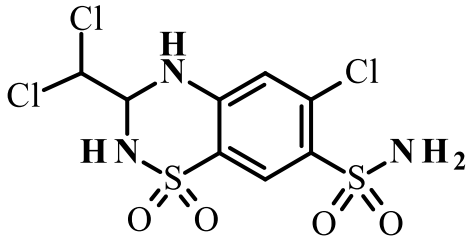
**hydrofluomethiazide**



**methiclothiazide**



**polythiazide**



**trichloromethiazide**

**Fig. 359 The structures of diuretics associated with some chromatographic peaks in Figure 358 and/or listed in Table 27 (continued)**

**Table 27 Characteristic signals of permethylated derivatives of some diuretics (ionization EI 70 eV) - the base signal is shown in bold (from [4]).**

| Nr. | Permethylated active compound | m/z permethylated compound | CAS number of unmethylated compound | Ionic fragments (m/z) |
|---|---|---|---|---|
| **1** | trimethyl-acetazolamide | 264 | 216665-38-2 | **249** ; 108 ; 83 ; 43 |
| **2** | tetramethyl-chlortalidone | 394 | 77-36-1 | **363** ; 287 ; 255 ; 176 |
| **3** | methyl etacrynate | 316 | 58-54-8 | 316 ; 281 ; **261** ; 243 |
| **4** | hexamethyl-triamterene | 337 | 396-01-0 | **336** ; 322 ; 307 ; 294 |
| **5** | dimethyl-clopamide | 373 | 636-54-4 | 139 ; 127 ; **111** ; 55 |
| **6** | trimethyl-indapamide | 407 | 26807-65-8 | 246 ; **161** ; 132 - 91 |
| **7** | trimethyl-bumetanide | 406 | 28395-03-1 | **406** ; 363 ; 318 ; 254 |
| **8** | trimethyl-furosemide | 372 | 54-31-9 | 372 ; 96 ; **81** ; 53 |
| **9** | trimethyl-piretamide | 404 | 55837-27-9 | 404 ; **295** ; 266 ; 219 |
| **10** | tetramethyl-xipamide | 410 | 14293-44-8 | **410** ; 379 ; 290 ; 121 |
| **11** | tetramethyl-altiazide | 440 | 5588-16-9 | **352** ; 244 ; 145 ; 42 |
| **12** | tetramethyl-bendroflumethiazide | 477 | 77-48-3 | **386** ; 278 ; 91 ;42 |
| **13** | tetramethyl-buthiazide | 409 | 2043-38-1 | **352** ; 244 ; 42 |
| **14** | trimethyl-chlorothiazide | 337 | 58-94-6 | 337 ; 245 ; 339 ; 230 |
| **15** | tetramethyl-hydrochlorothiazide | 353 | 58-93-5 | 353 ; **310** ; 288 ; 218 |
| **16** | tetramethyl-hydroflumethiazide | 387 | 135-09-1 | **387** ; 344 ; 252 ; 172 |
| **17** | trimethyl-methiclothiazide | 402 | 135-09-9 | **352** ; 244 |
| **18** | trimethyl-polithiazide | 481 | 346-18-9 | **352** ; 244 ; 42 |
| **19** | tetramethyl-trichloromethiazide | 435 | 133-67-5 | **352** ; 244 ; 42 |

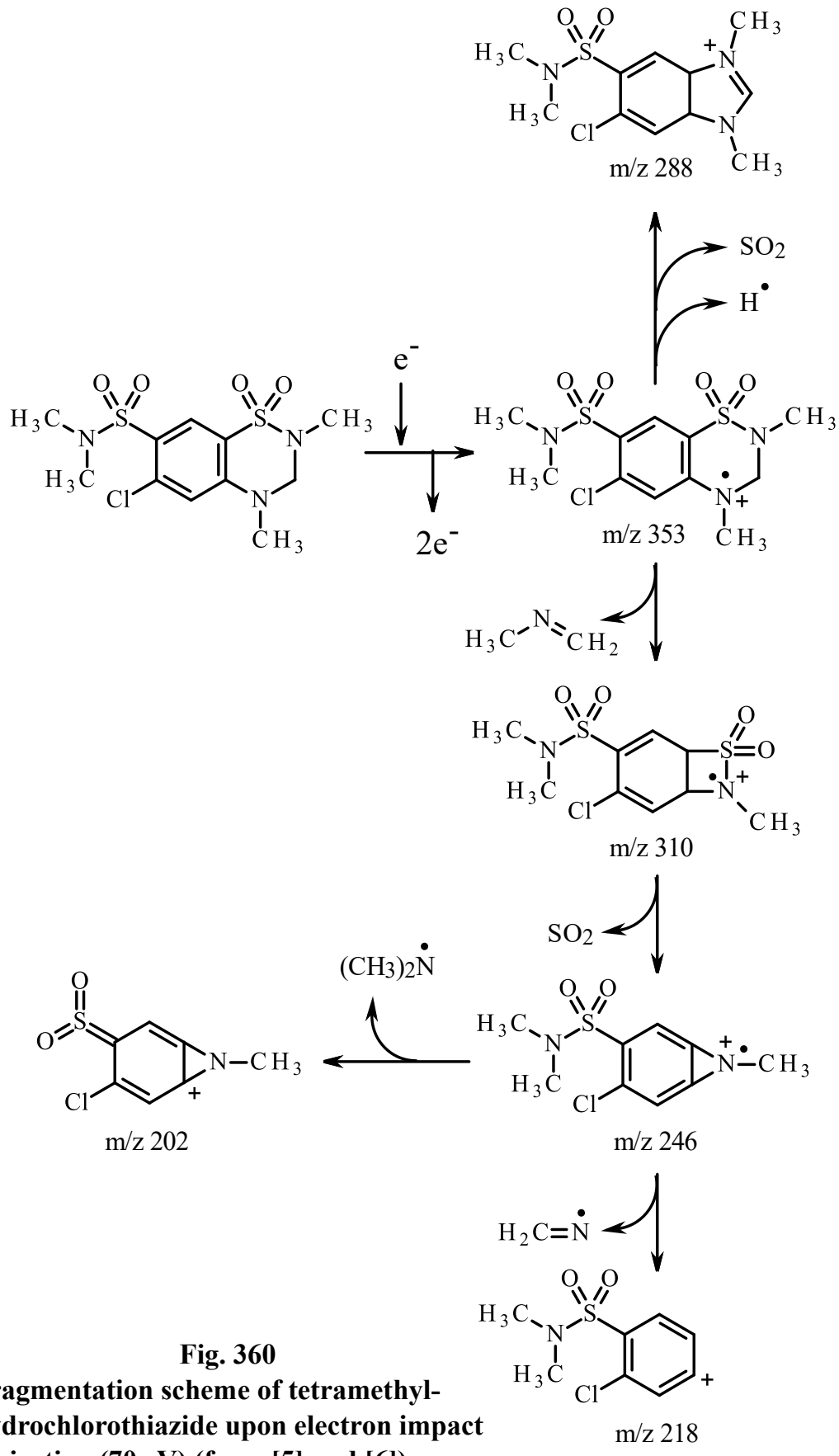



**Fig. 360**
**Fragmentation scheme of tetramethyl-hydrochlorothiazide upon electron impact ionization (70 eV) (from [5] and [6])**

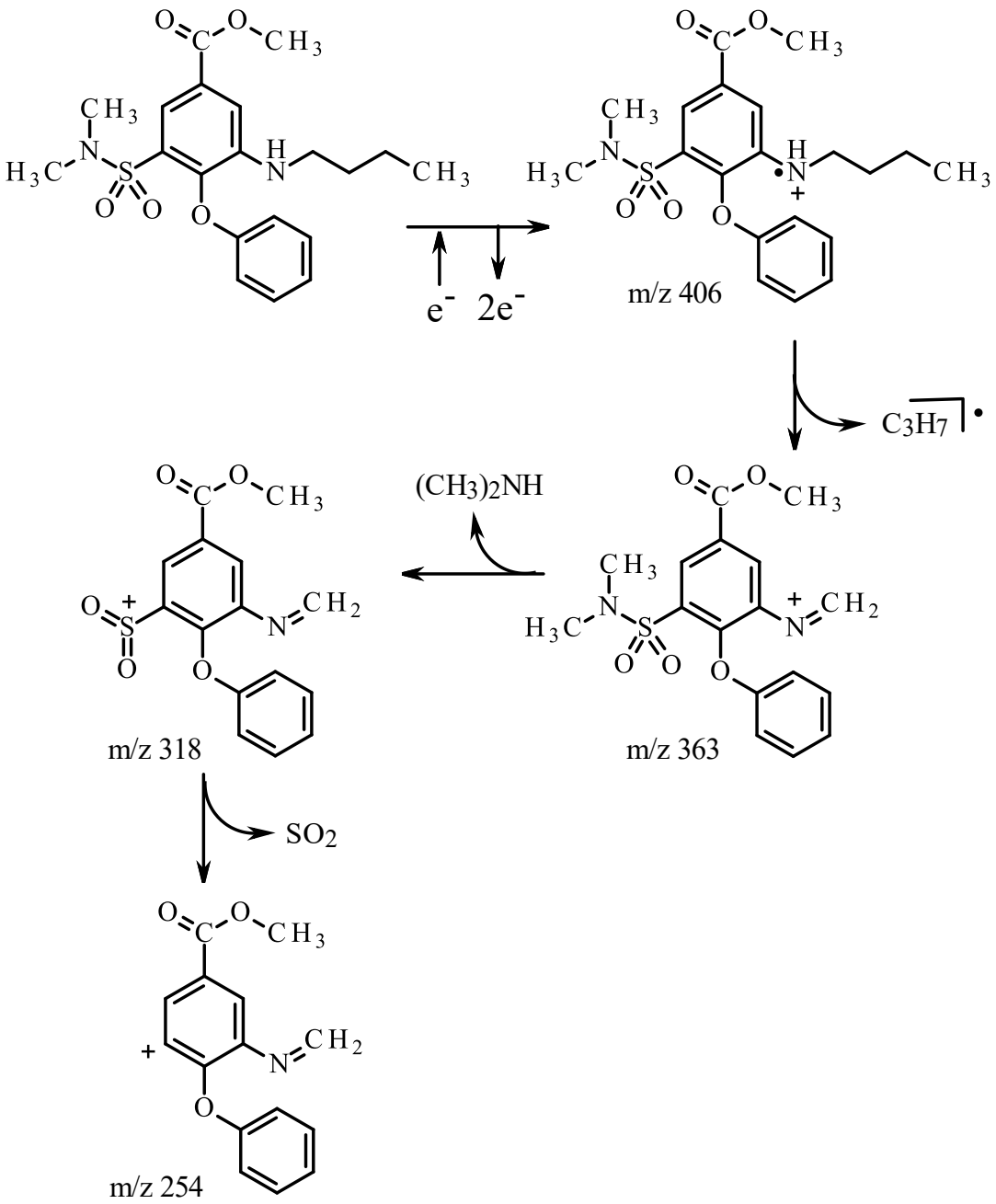



**Fig. 361 Fragmentation scheme of trimethyl-bumetazide upon electron impact ionization (70 eV) (from [5] and [6])**

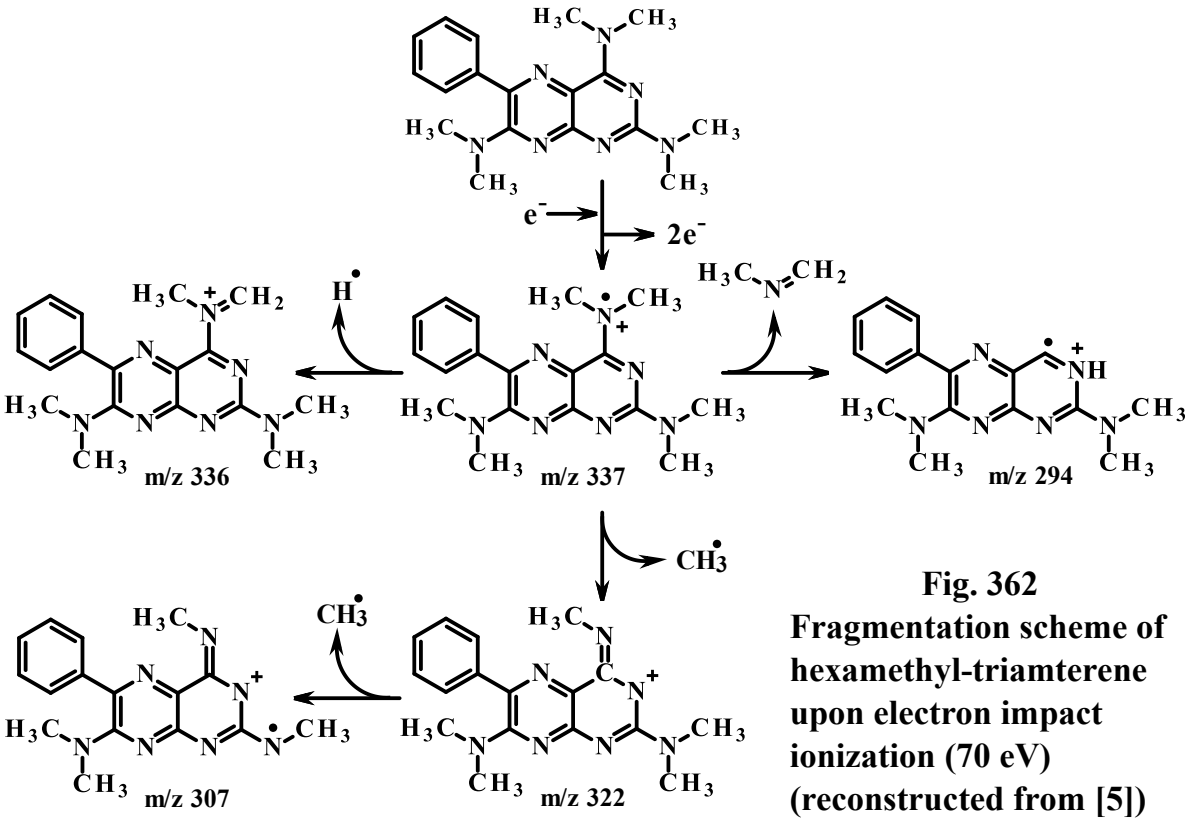



**Fig. 362**
**Fragmentation scheme of hexamethyl-triamterene upon electron impact ionization (70 eV) (reconstructed from [5])**

**Sources cited in application example 5.15**

[1] *A.B. Cadwallader, X. de la Torre, A. Tieri, F. Botrè*: The Abuse of Diuretics as Performance-Enhancing Drugs and Masking Agents in Sport Doping: Pharmacology, Toxicology and Analysis.
**British Journal of Pharmacology 2010:161**(1), 1-18

[2] *M. Kolmonen, A. Leinonen, A. Pelander, I. Ojanperä*: A General Screening Method for Doping Agents in Human Urine by Solid Phase Extraction and Liquid Chromatography/Time of Flight Mass Spectrometry
**Analytica Chimica Acta 2007:585**(1), 94-102

[3] *Song-Ja Park, Hee-Soo Puo, Yun-Je Kim, Mi-Sook Kim, Jongsei Park*: Systematic Analysis of Diuretic Doping Agents by HPLC Screening and GC/MS Confirmation.
**Journal of Analytical Toxicology 1990:14**(2), 84-90

[4] *M. Thevis*: Mass Spectrometry in Sports Drug Testing – Characterization of Prohibited Substances and Doping Control – Analytical Assays, Capitol 3.5. John Wiley & Sons, 2010 [ISBN: 978-0-41327-2]

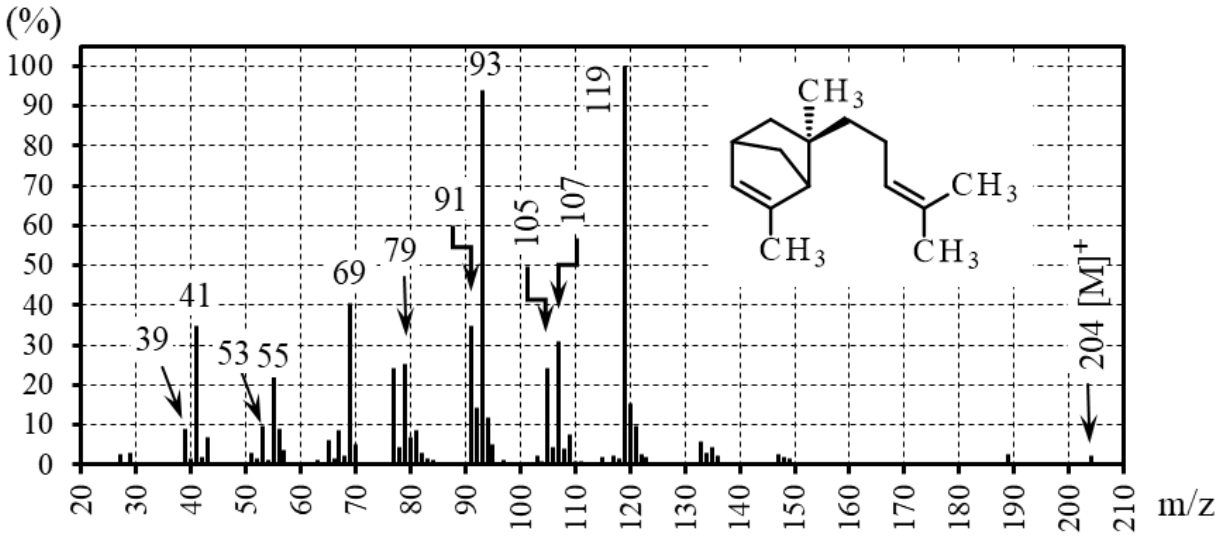
[5] *A.F. Casy*: Electron Impact Mass Spectrometry of Diuretic Agents.
**Journal of Pharmaceutical and Biomedical Analysis 1987:5**(3), 247-257

[6] *C.N. Yoon, T.H. Lee, J. Park*: Mass Spectrometry of Methyl and Methyl-d3 Derivatives of Diuretic Agents.
**Journal of Analytical Toxicology 1990:14**(2), 96-101

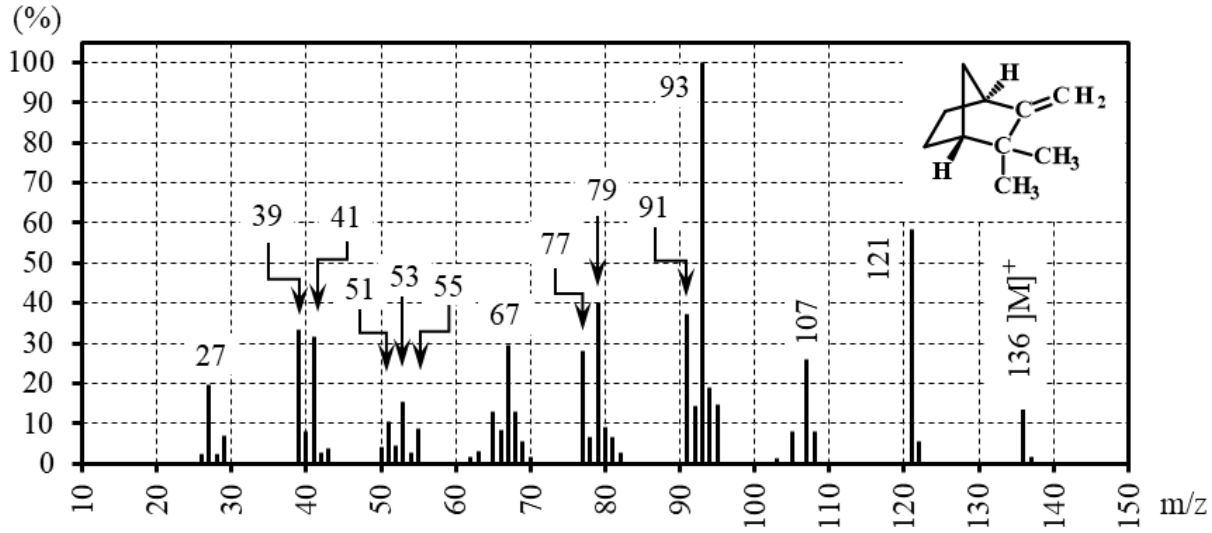
# Appendix

# $MS^1$-EI spectra of some pharmaceutically and toxicologically relevant substances

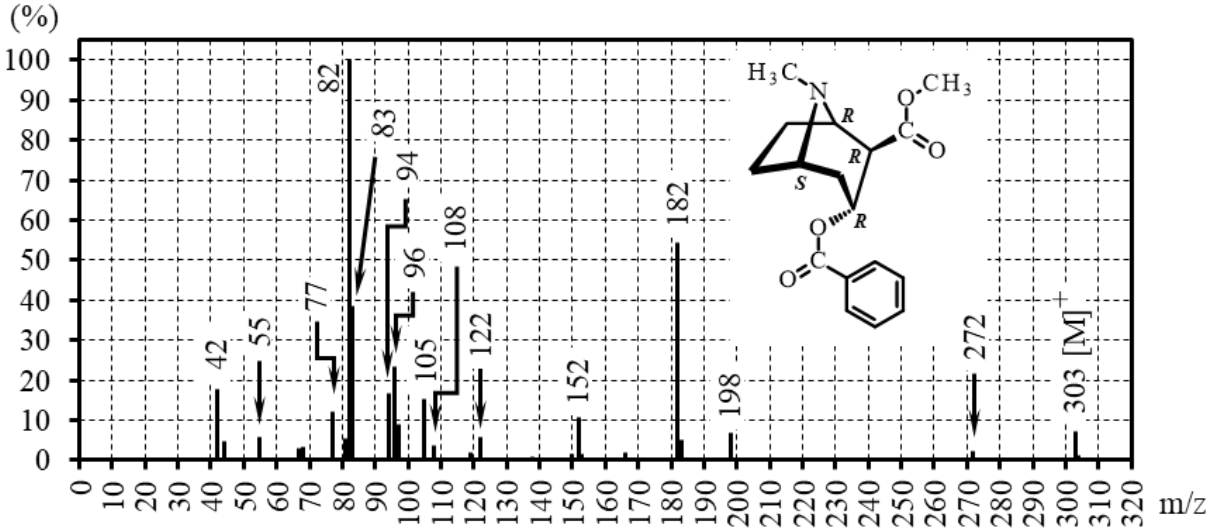
## (verified against established databases: NIST, SDBS, MoNa, MassBankRecord)



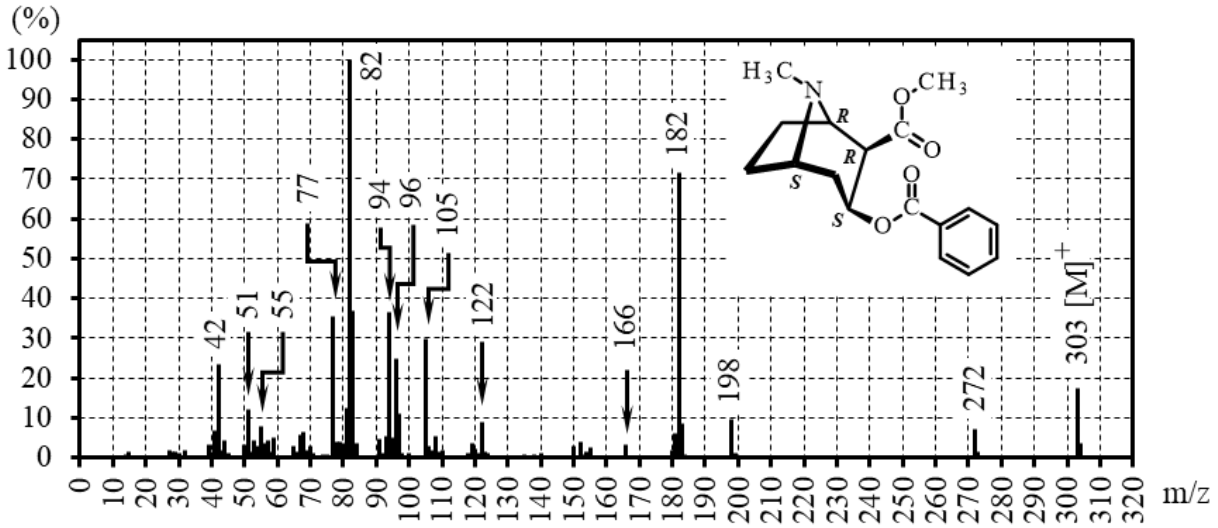

*(E)*-α-Bergamotene – CAS 17699-05-7 – EI – NIST 412425



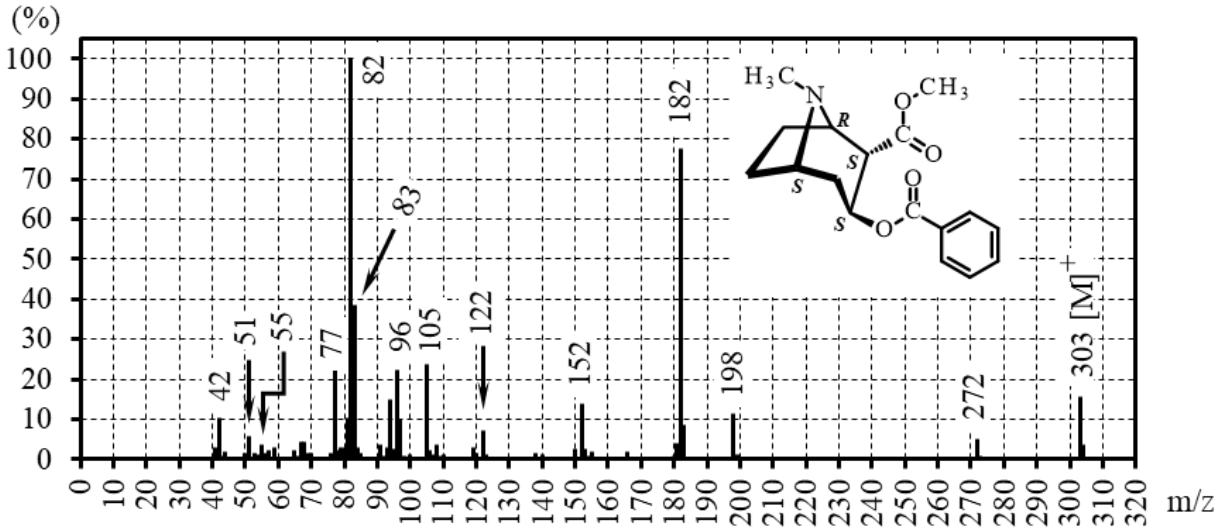

*(E)*-Camphene – CAS 79-92-5 – EI – NIST 114297



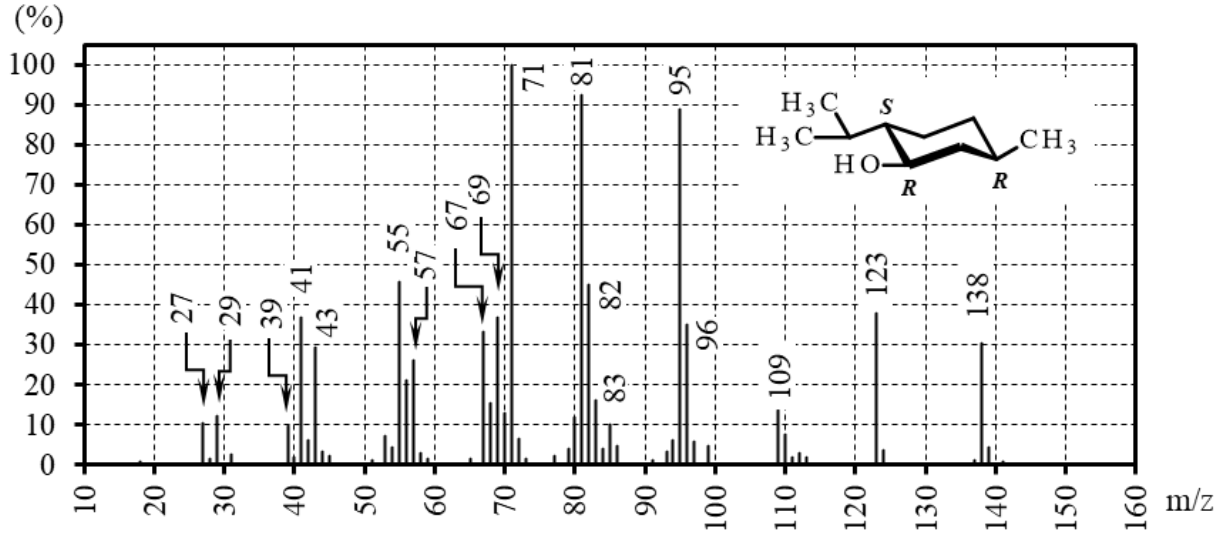

*1R*,*2R*,*3R*,*5S*-Allococaine – CAS 668-19-9 – EI – NIST 122751



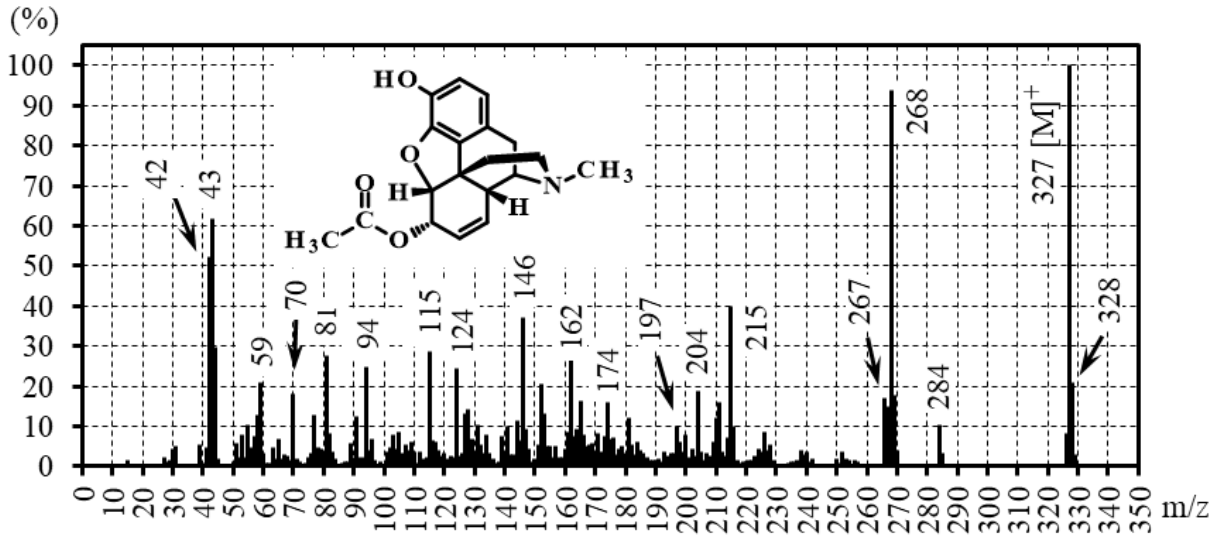

*1R*,*2R*,*3S*,*5S*-Cocaine – CAS 50-36-5 – EI – NIST 113834



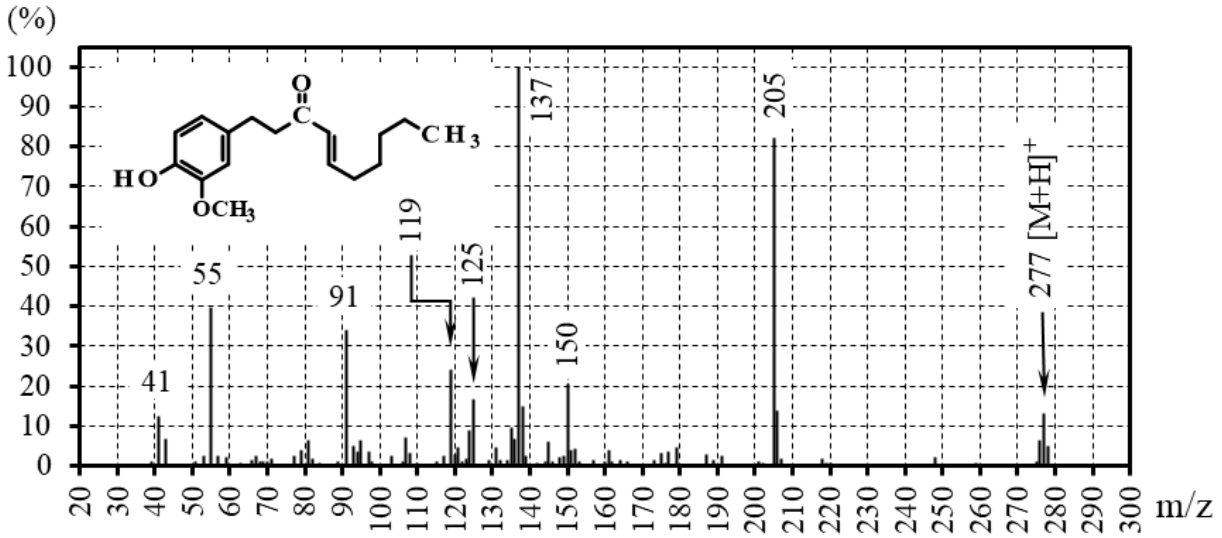

*1R*,*2S*,*3S*,*5S*-Pseudococaine – CAS 478-73-9 – EI – NIST 248638



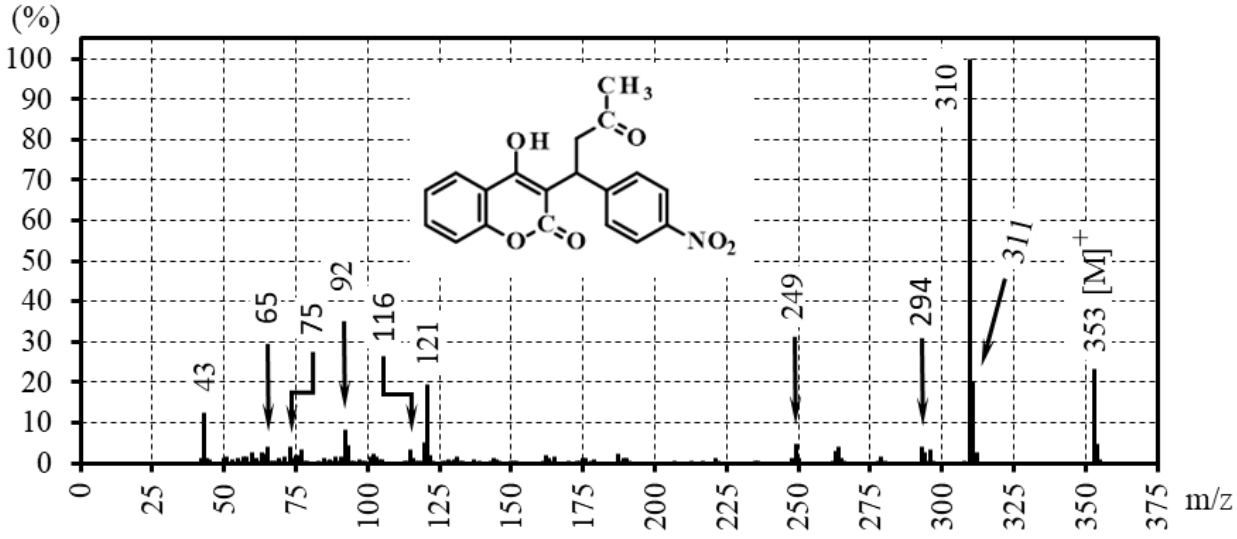

*1R*,*2S*,*5R*-(-)-Menthol – CAS 89-78-1 – EI – NIST 232390



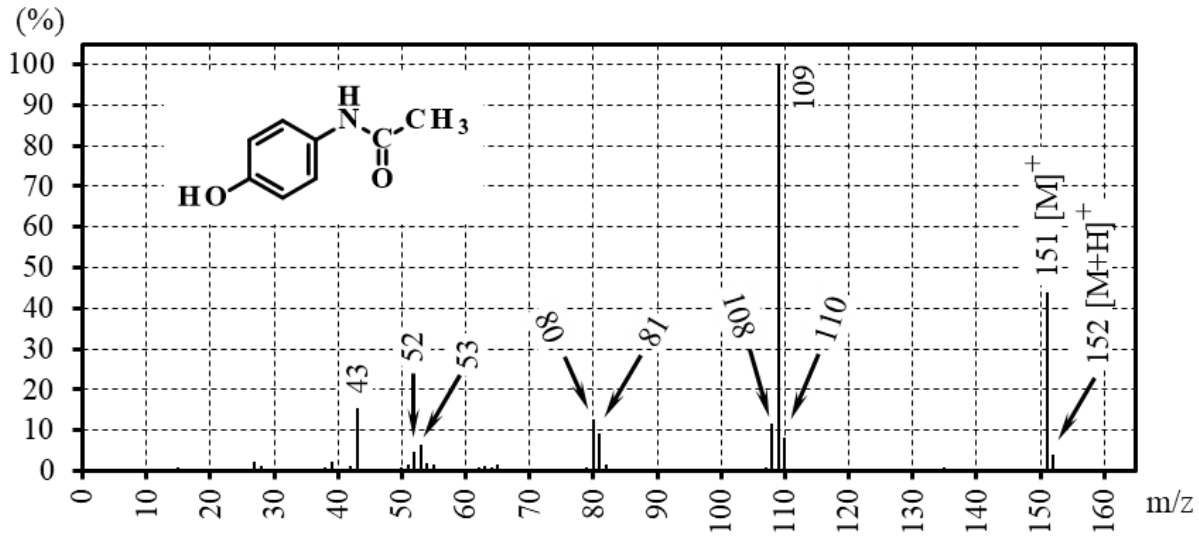

*6*-Monoacetylmorphine – CAS 2784-73-8 – EI – NIST 352203



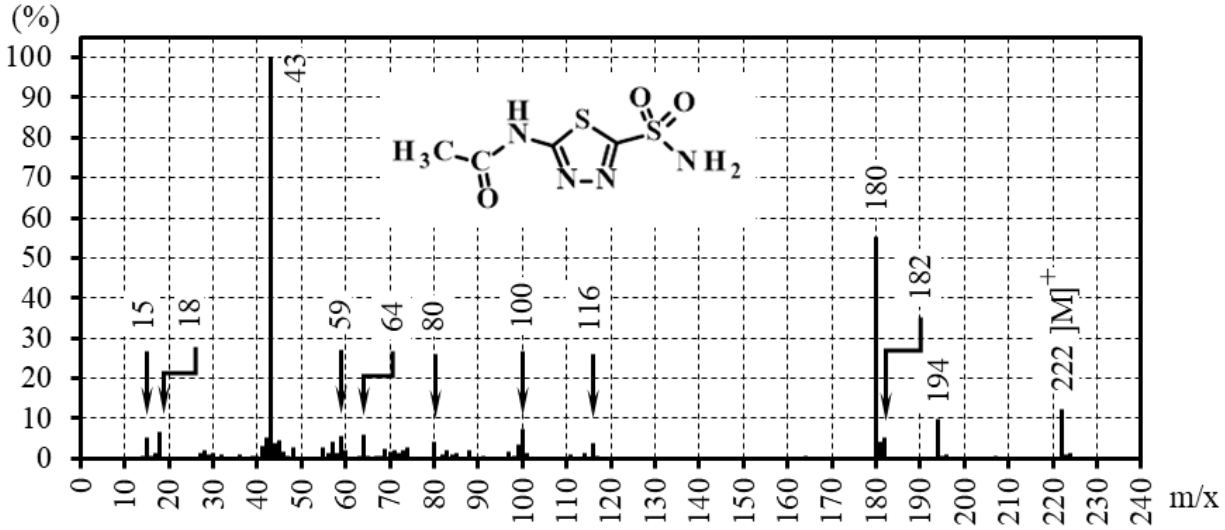

*6*-Shogaol – CAS 555-66-8 – EI 25 eV – MoNa JP007241



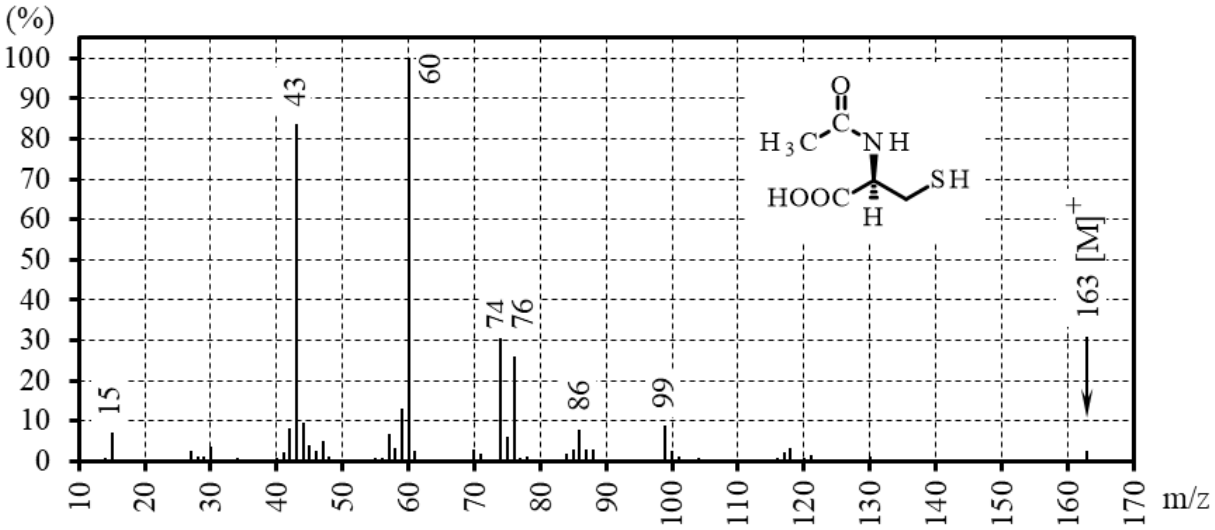

Acenocoumarol – CAS 152-72-7 – EI – NIST 247018



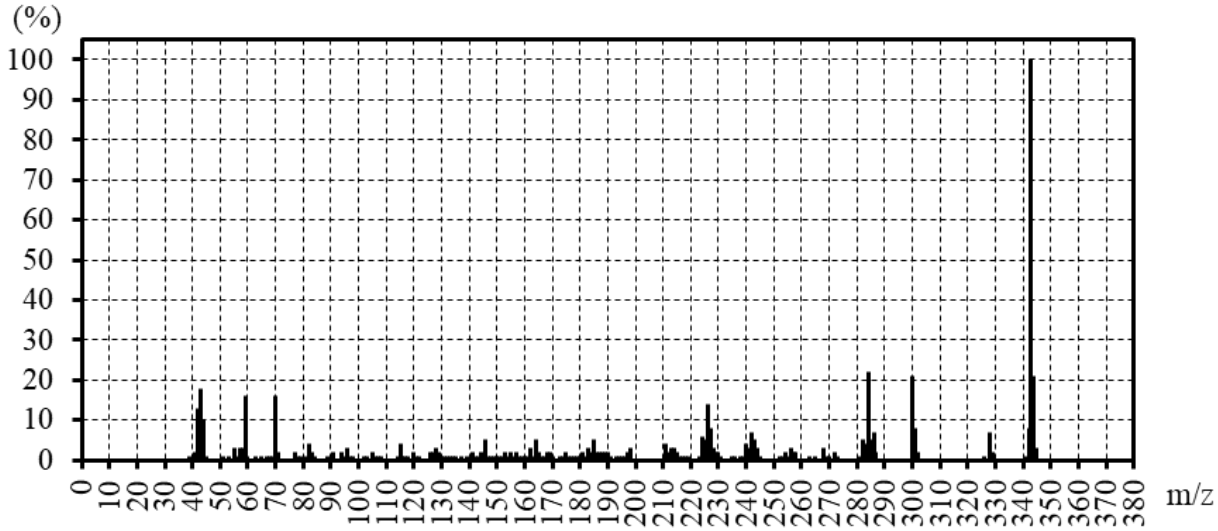

Acetaminophen (Paracetamol) – CAS 103-90-2 – NIST 229798



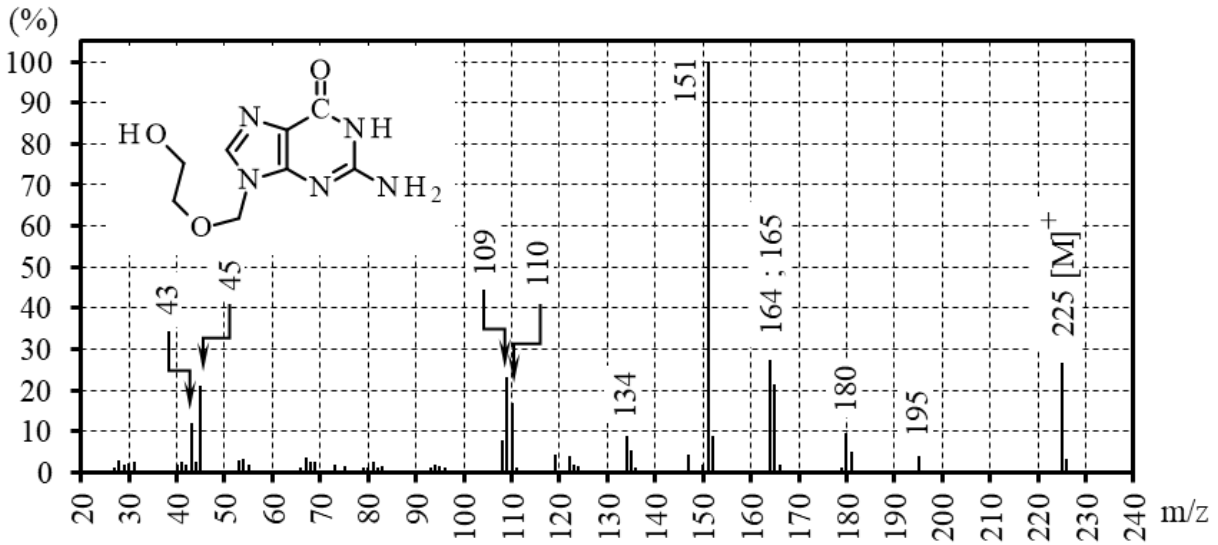

Acetazolamide - CAS 59-66-5 - EI - NIST 239163



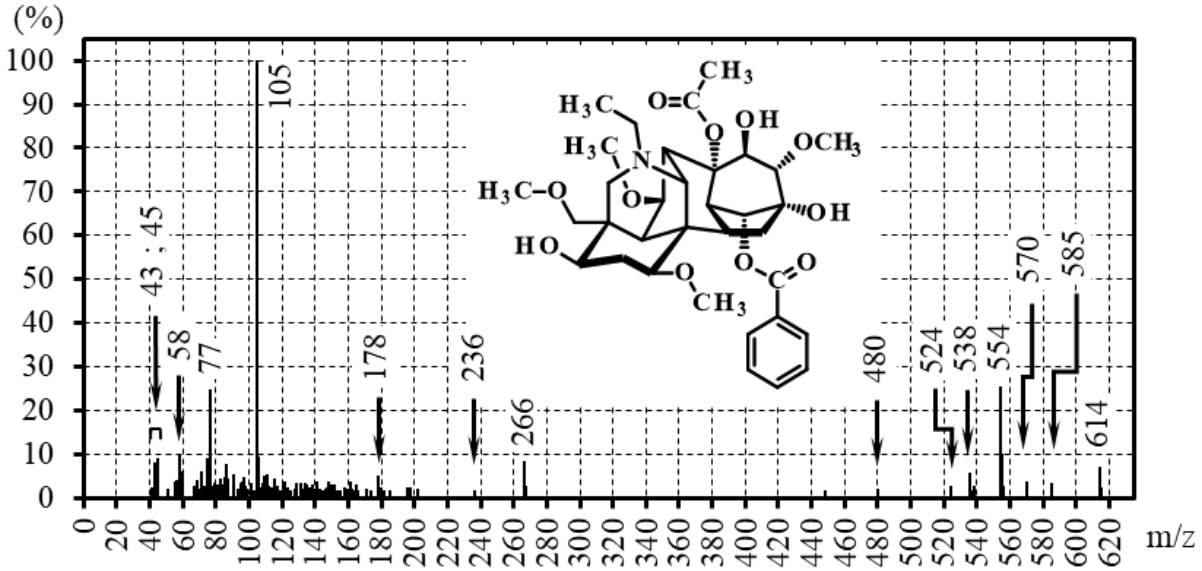

Acetylcysteine - CAS 616-91-1 - NIST 230766



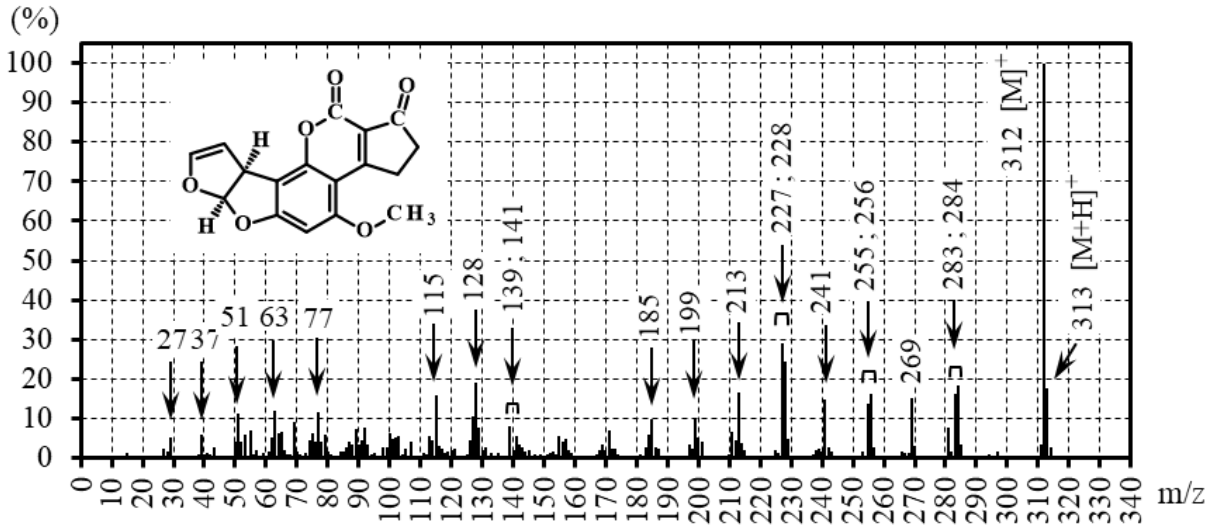

Acetyldihydrocodeine - CAS 3861-72-1 - EI - NIST 58782



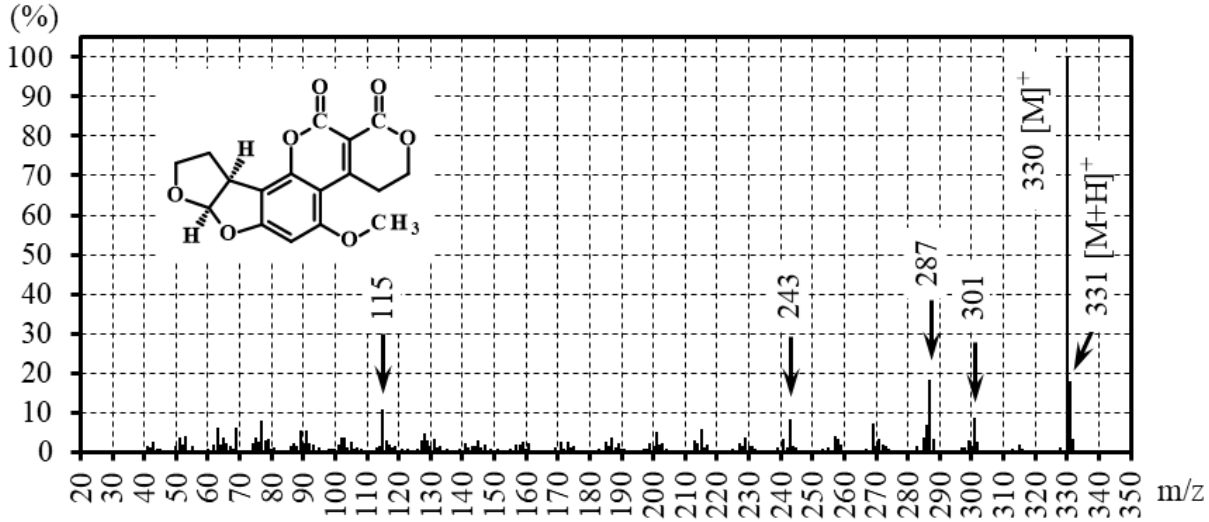

Aciclovir - 70 eV - 254 Oc - 160 Oc - SDBS 52101



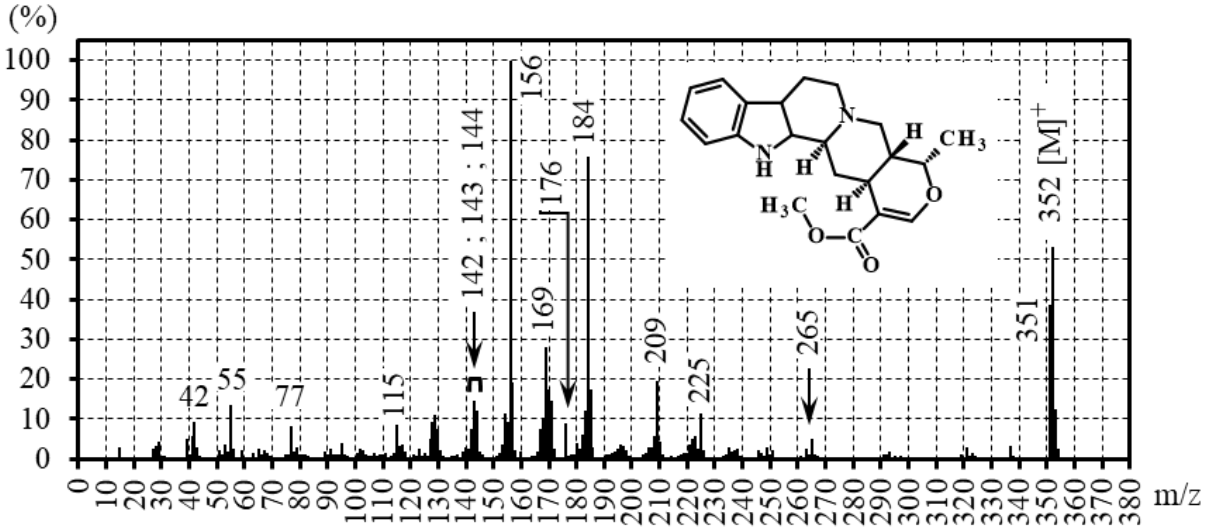

Aconitine - CAS 302-27-2 - NIST 247168



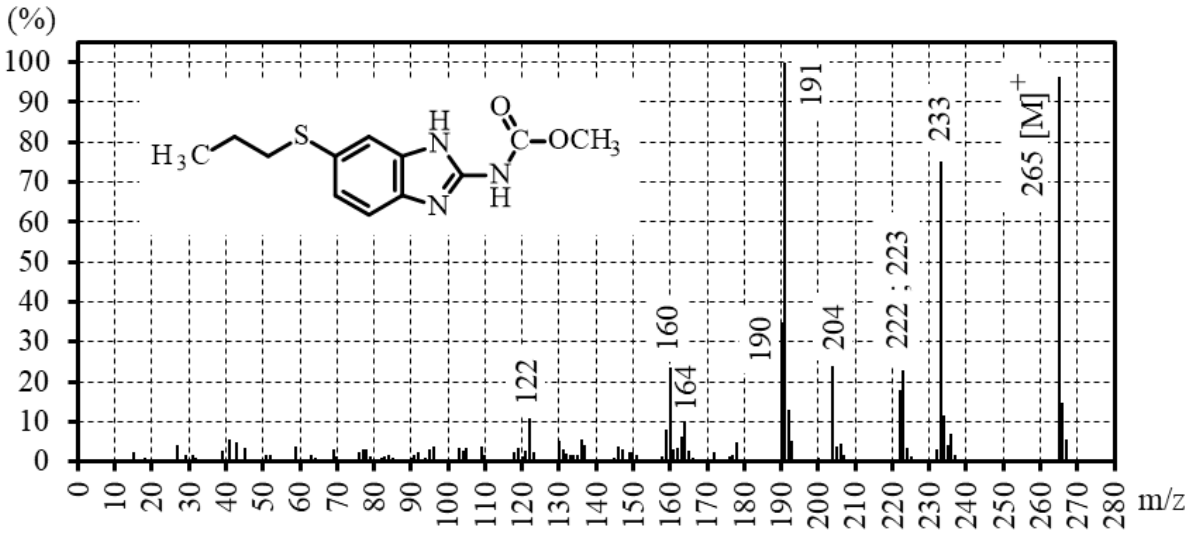

Aflatoxin B1 - CAS 1162-65-8 - NIST 341311



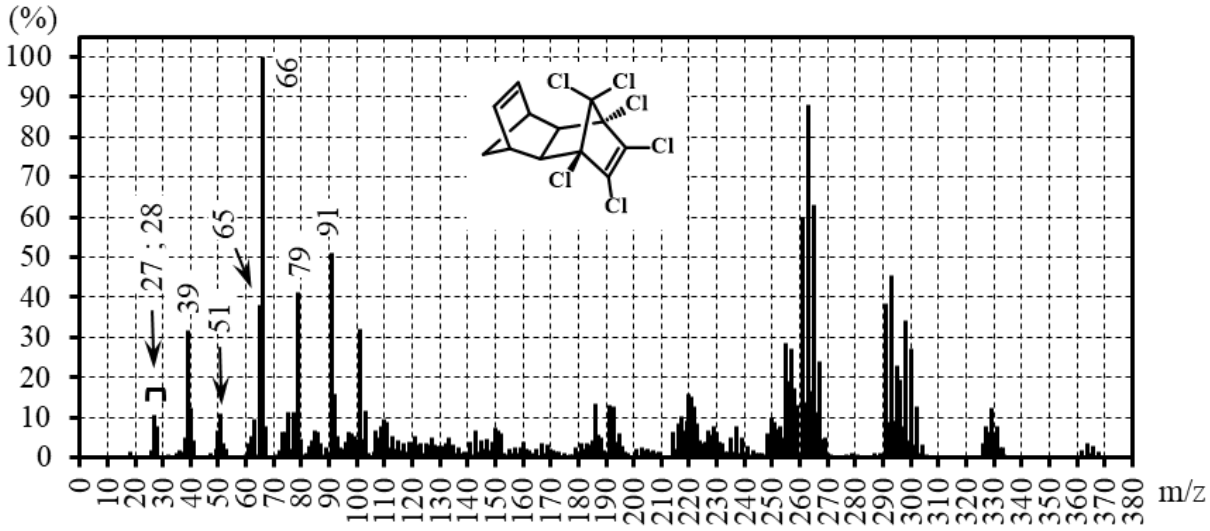

Aflatoxin G2 - CAS 7241-98-7 - EI - NIST 246958



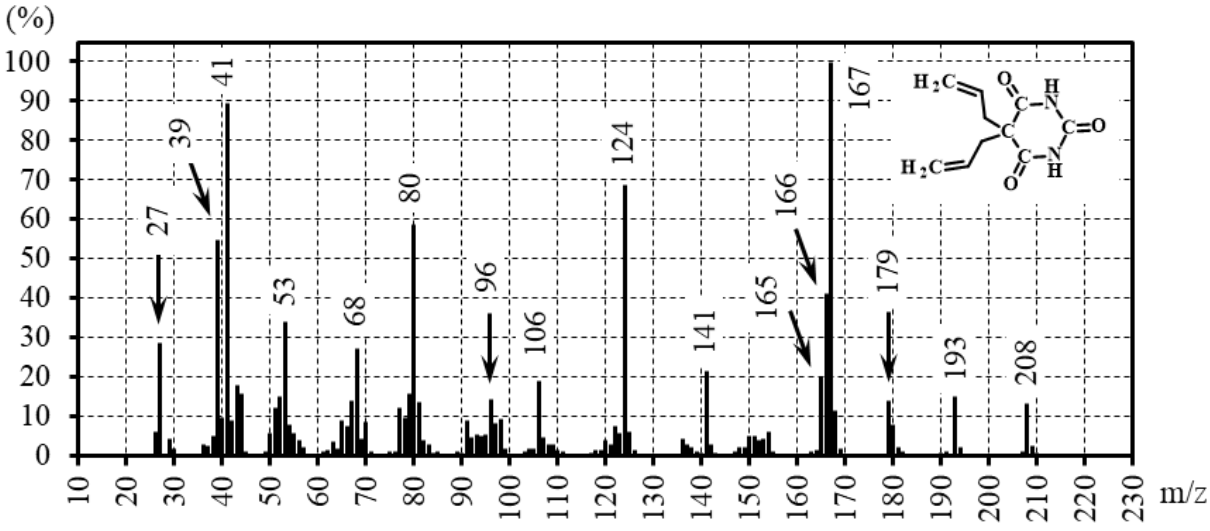

Ajmalicine (δ yohimbine) - CAS 483-04-5 - EI - NIST 241831



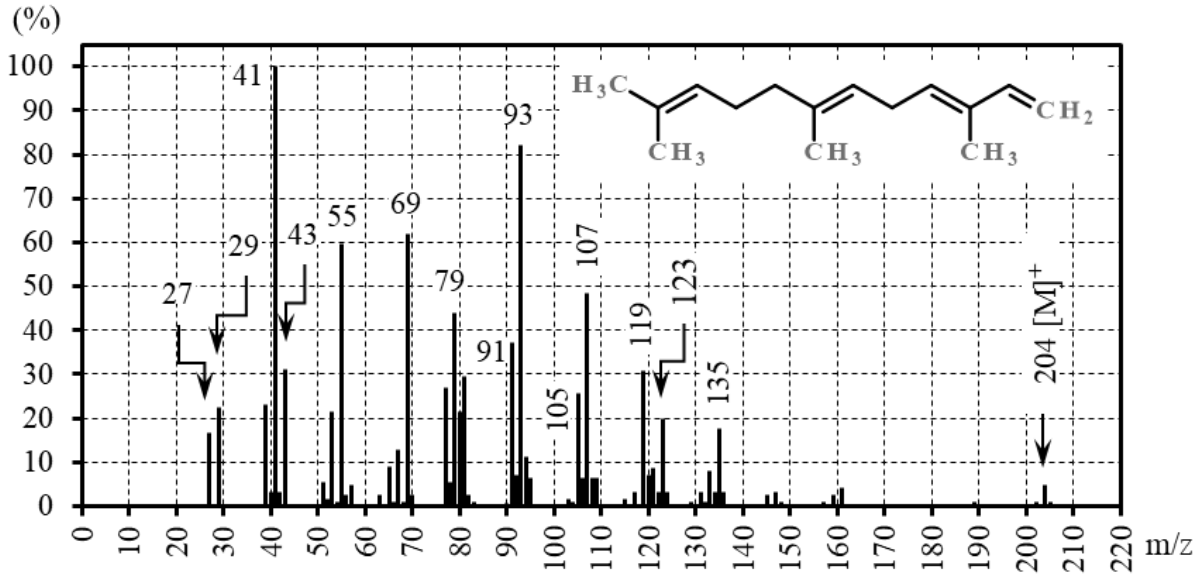

Albendazole – CAS 54965-21-8 - EI - SDBS nr. 51606



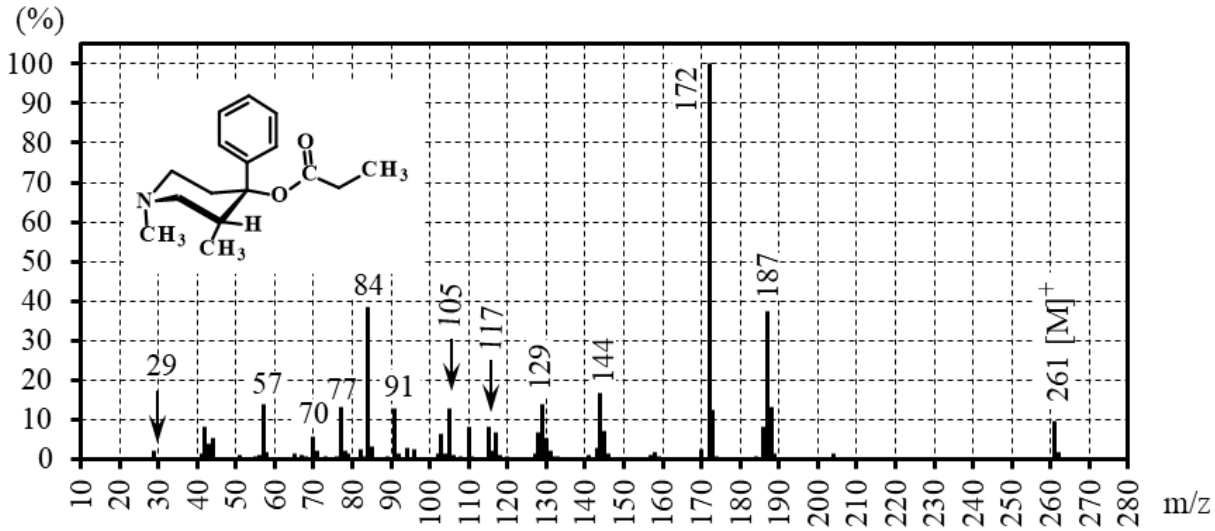

Aldrin - CAS 309-00-2 - EI – NIST 118956



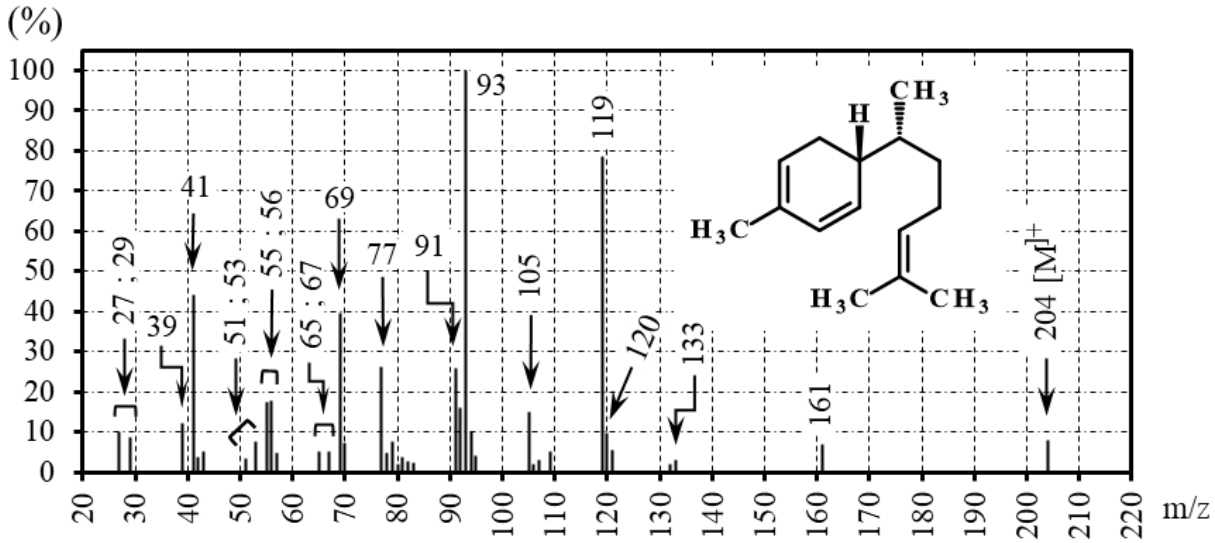

Allobarbital - CAS 52-43-7 - EI - NIST 9575



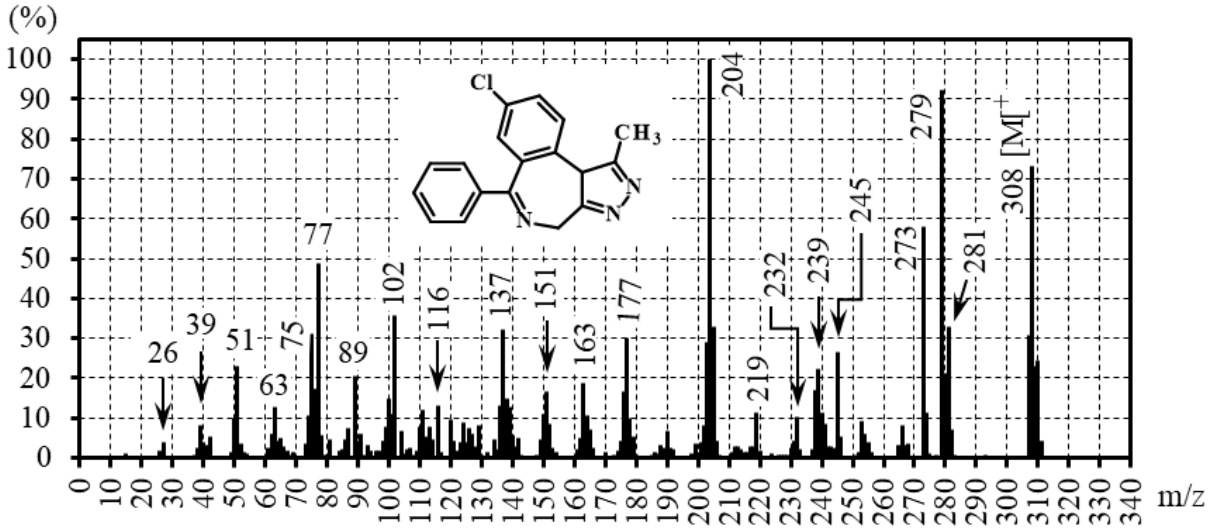

α -(*E*,*E*) Pharnesene - CAS 502-61-4 - EI - NIST 9209



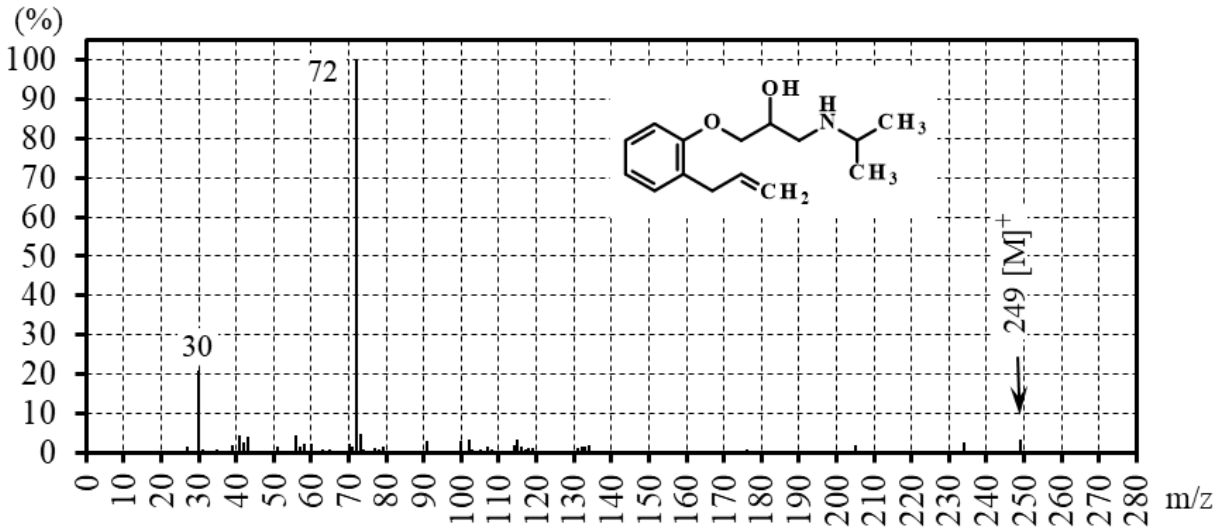

Alphaprodine - CAS 77-20-3 - EI - NIST 246499



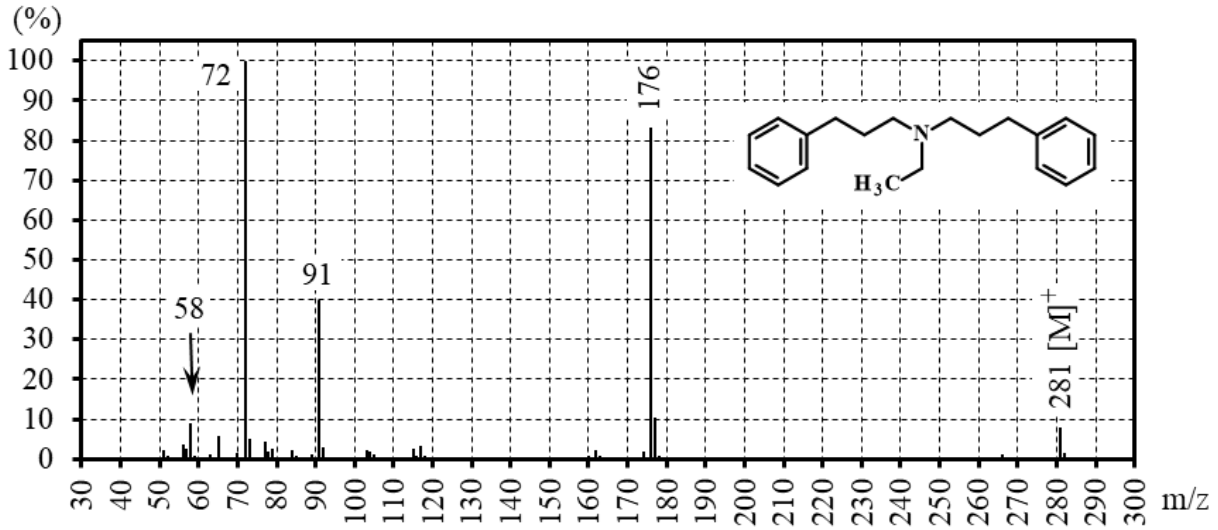

α-zingiberene CAS 495-60-3- NIST 70231



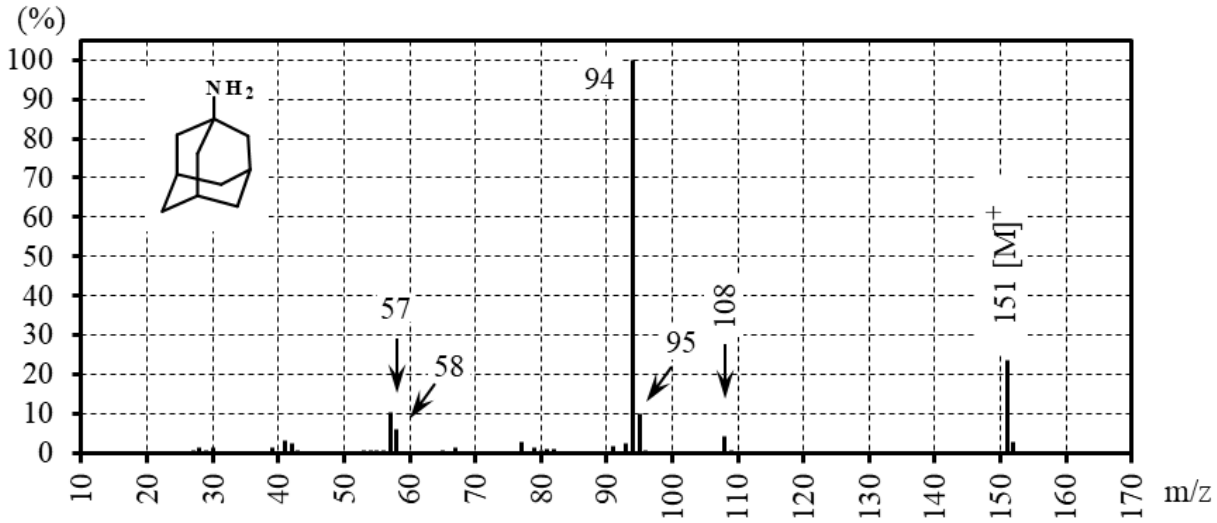

Alprazolam (Xanax) - CAS 28981-97-7 - EI - NIST 250574



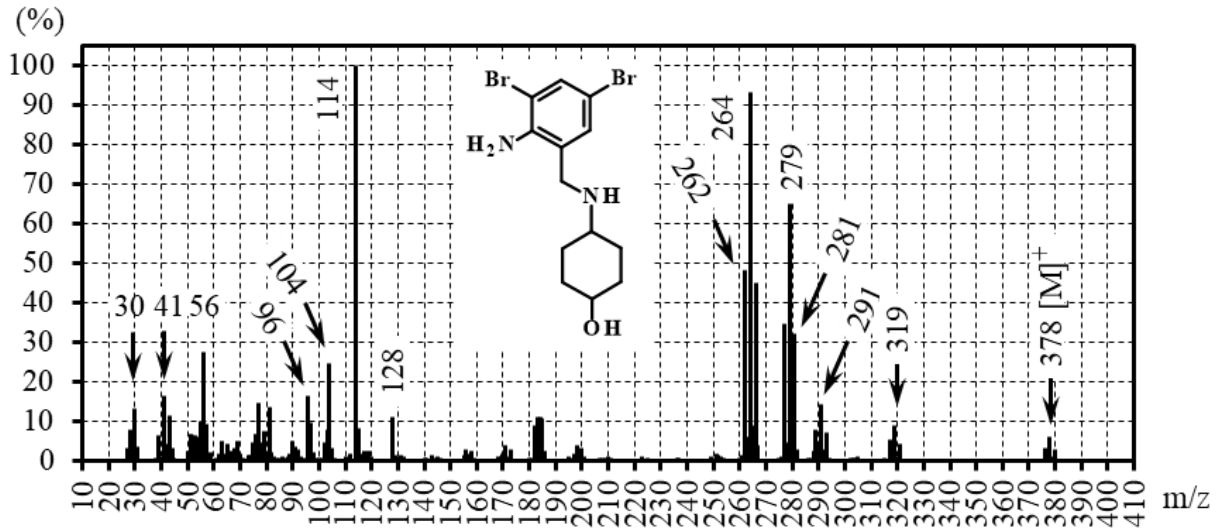

Alprenolol - CAS 13655-52-2 - NIST 42318



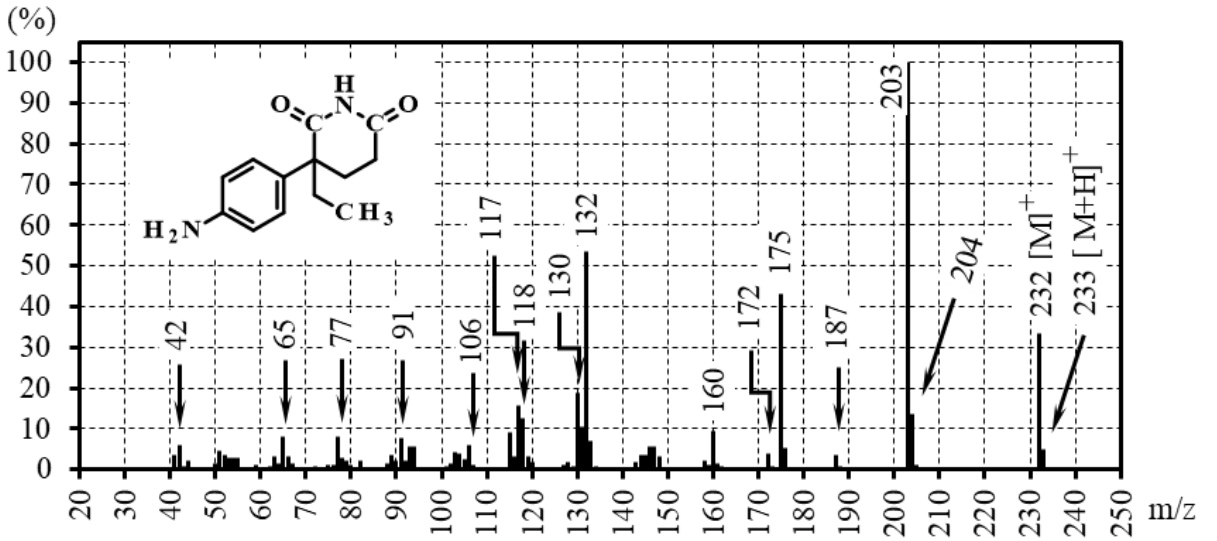

Alverine - CAS 150-59-4 - EI - NIST 137005



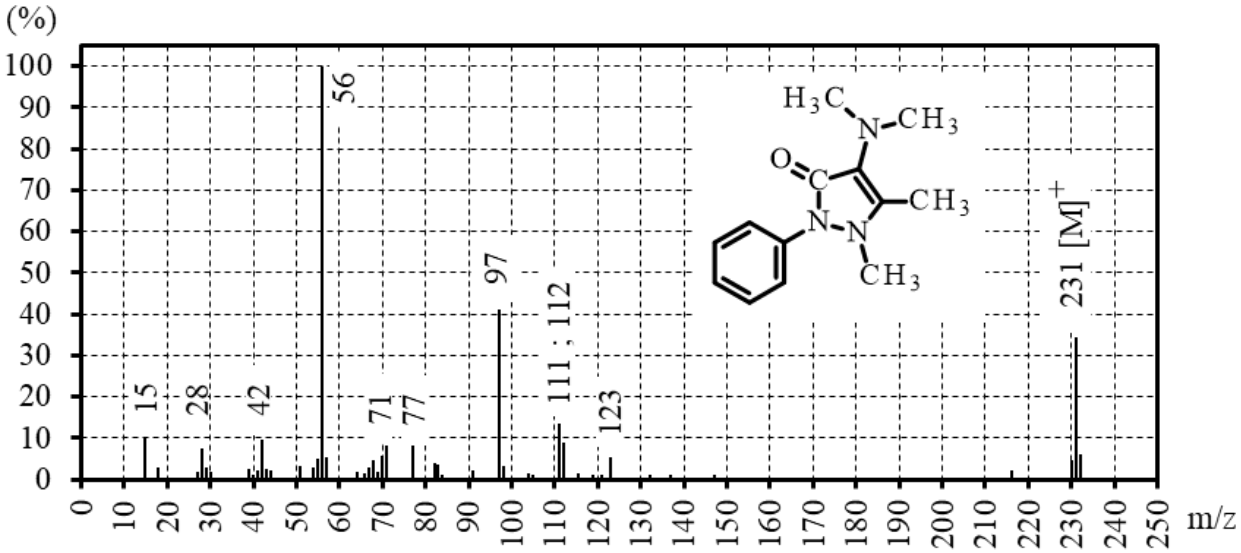

Amantadine - CAS 768-94-5 - EI - NIST 232354



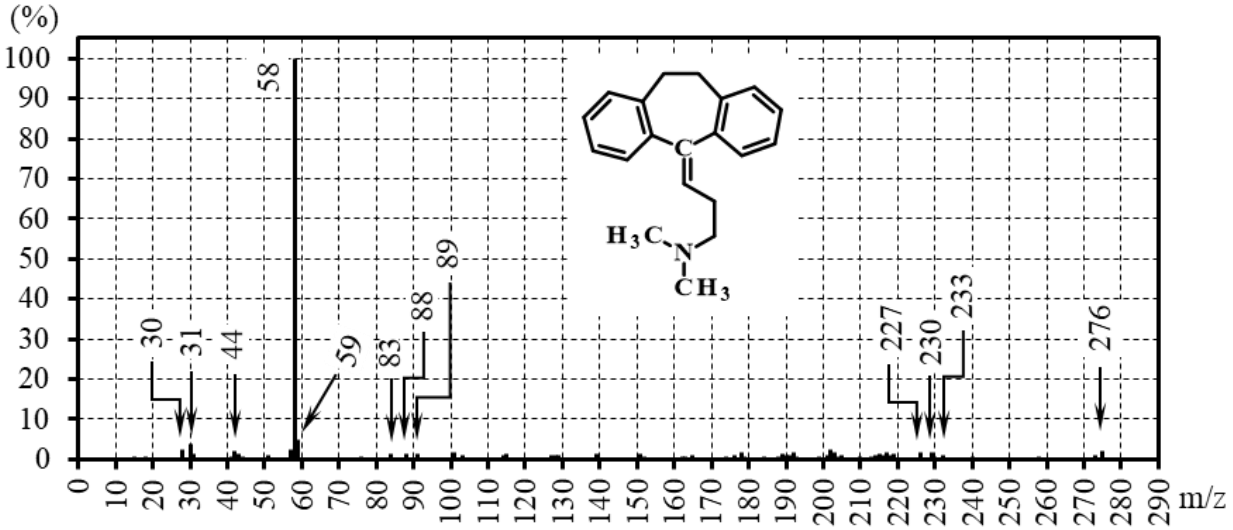

Ambroxol - CAS 18683-91-5 - EI - NIST 292178



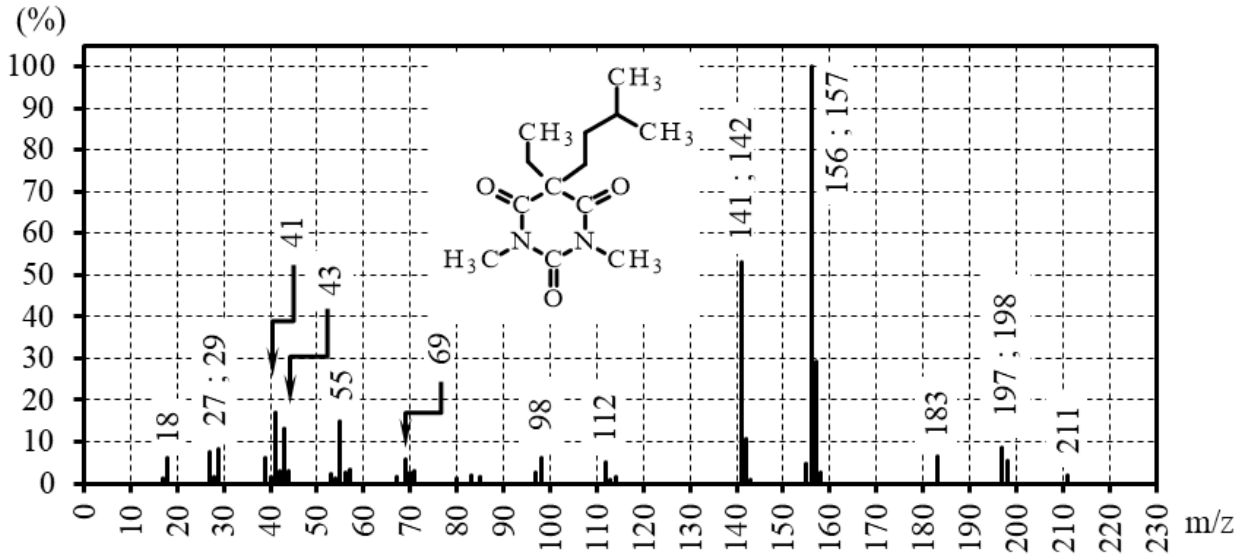

Aminoglutethimide - CAS 125-84-8 - EI - NIST 247719



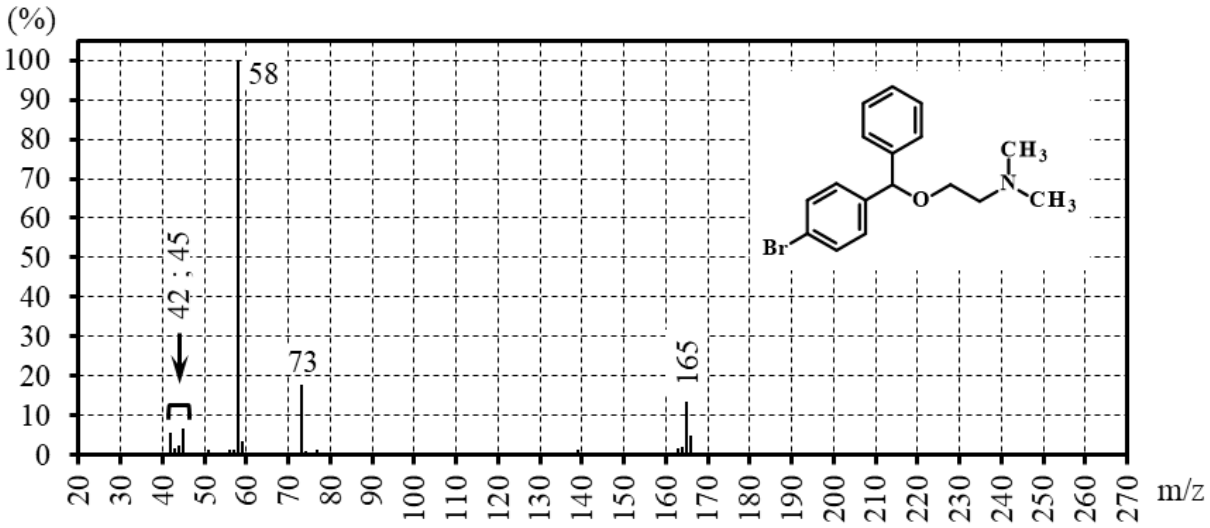

Aminophenazone (Aminopyrine) - CAS 58-15-1 - EI - SDBS 13092



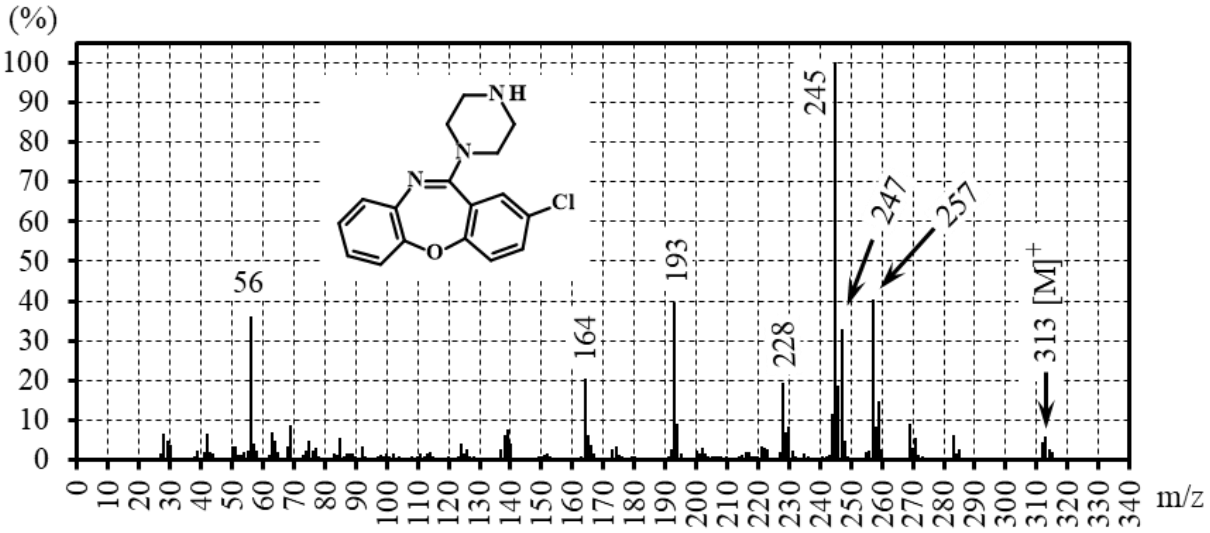

Amitriptyline - CAS 50-48-6 - EI - NIST 42327



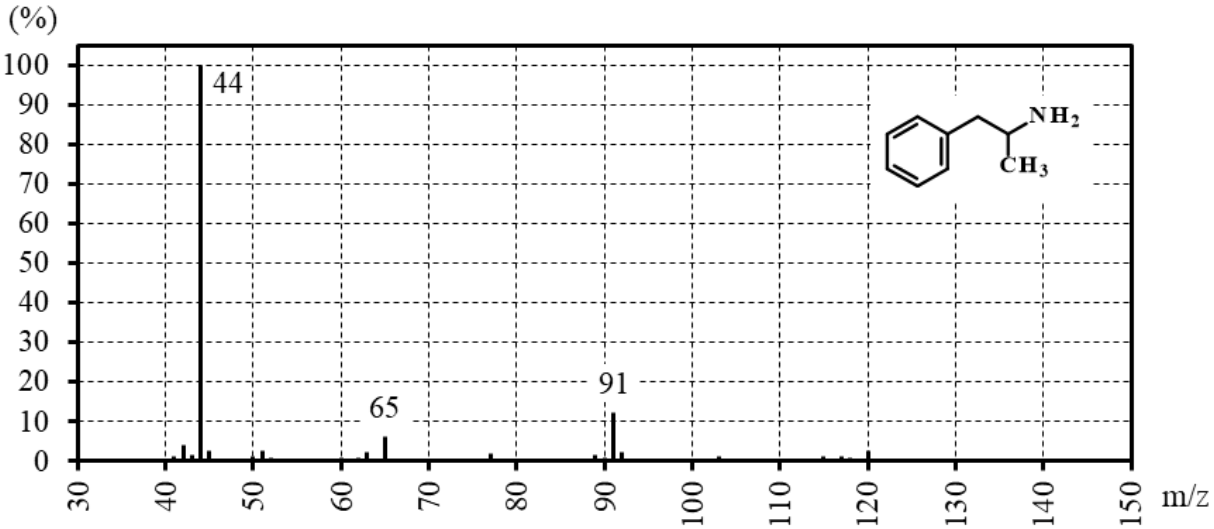

Amobarbital - CAS 57-43-2 - EI - SDBS 6965



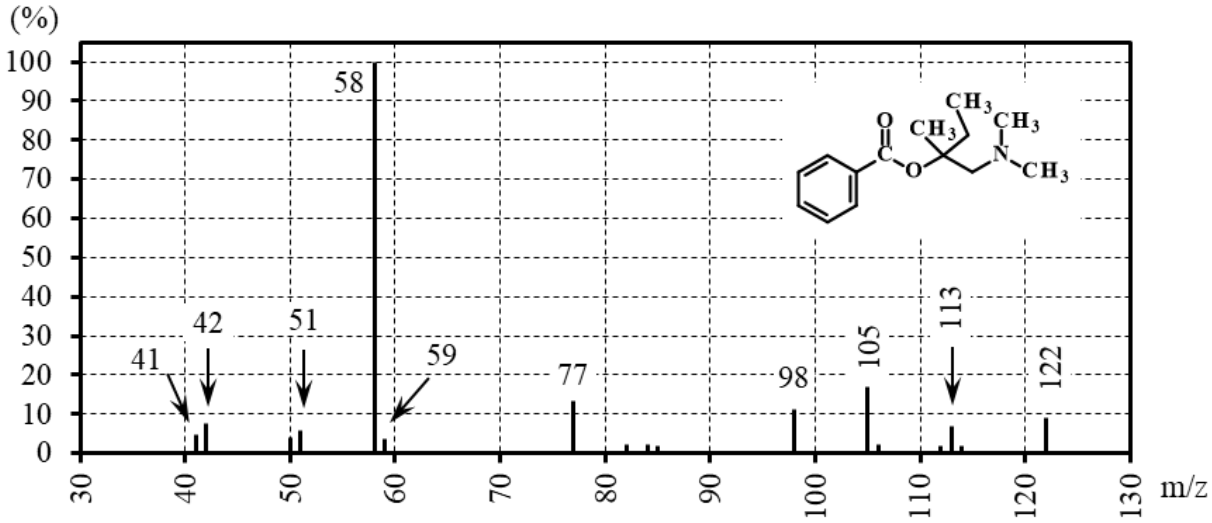

Amodryl (Bromazine) - CAS 118-23-0 - EI - NIST 247732



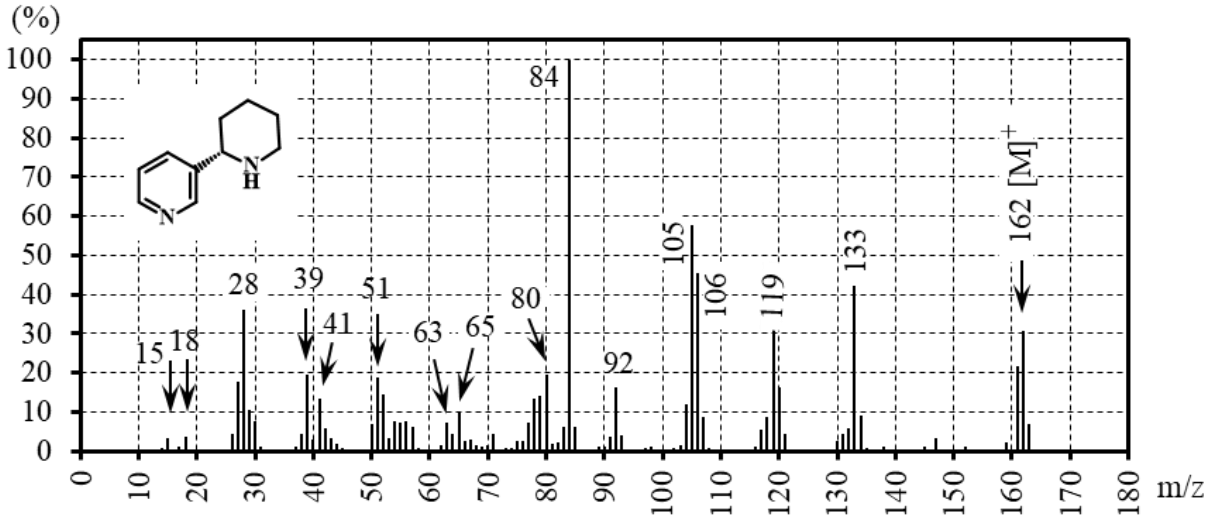

Amoxapine (Amoxan , Ascendin) - CAS 14028-44-5 - EI - NIST 352177



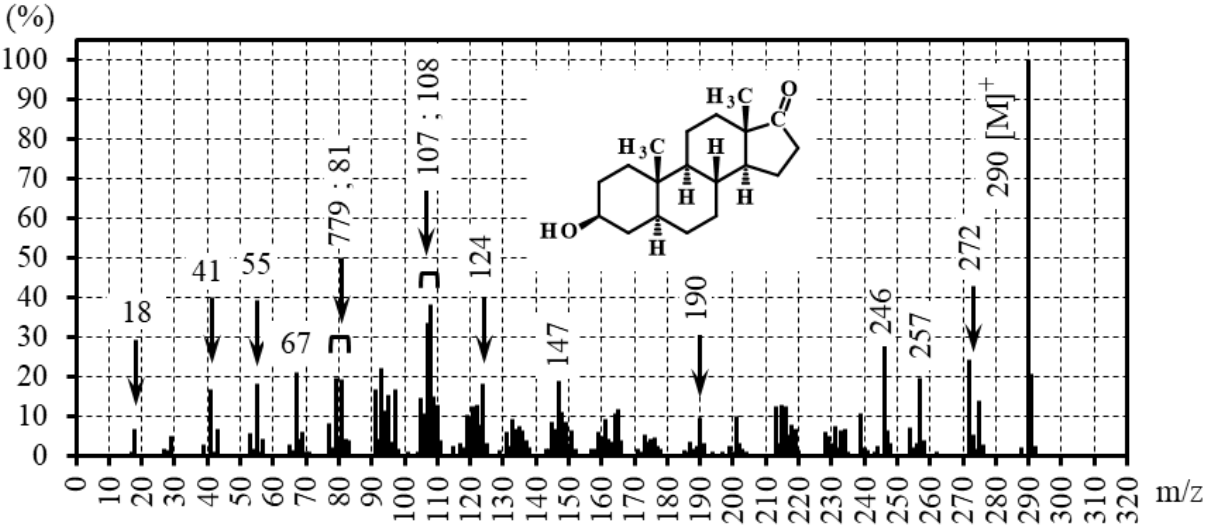

Amphetamine - CAS 300-62-9 - EI - NIST 335467



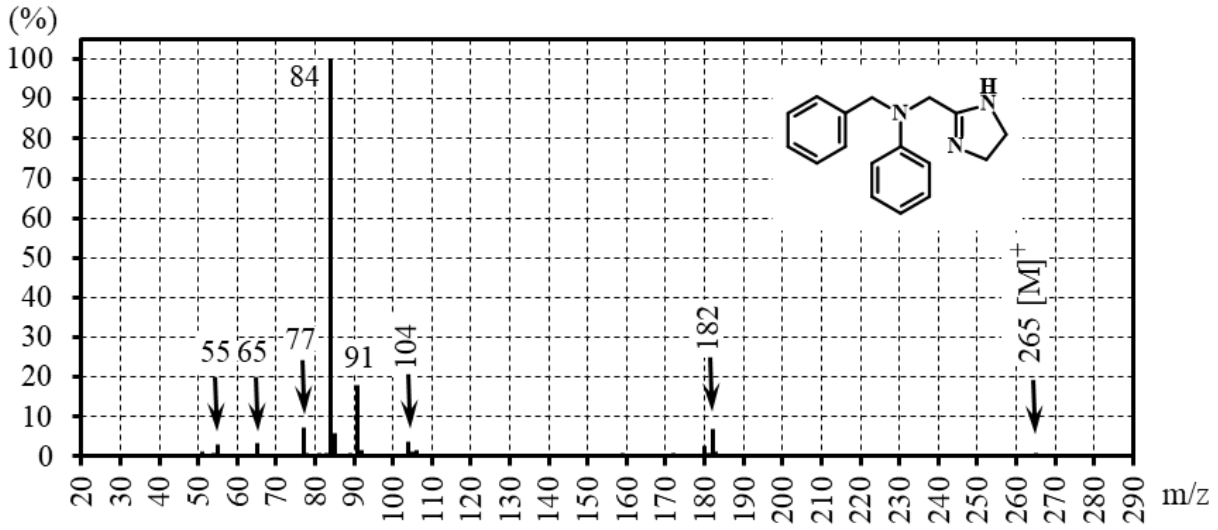

Amylocaine (Stovaine etc) - CAS 644-26-8 - EI - NIST 120490



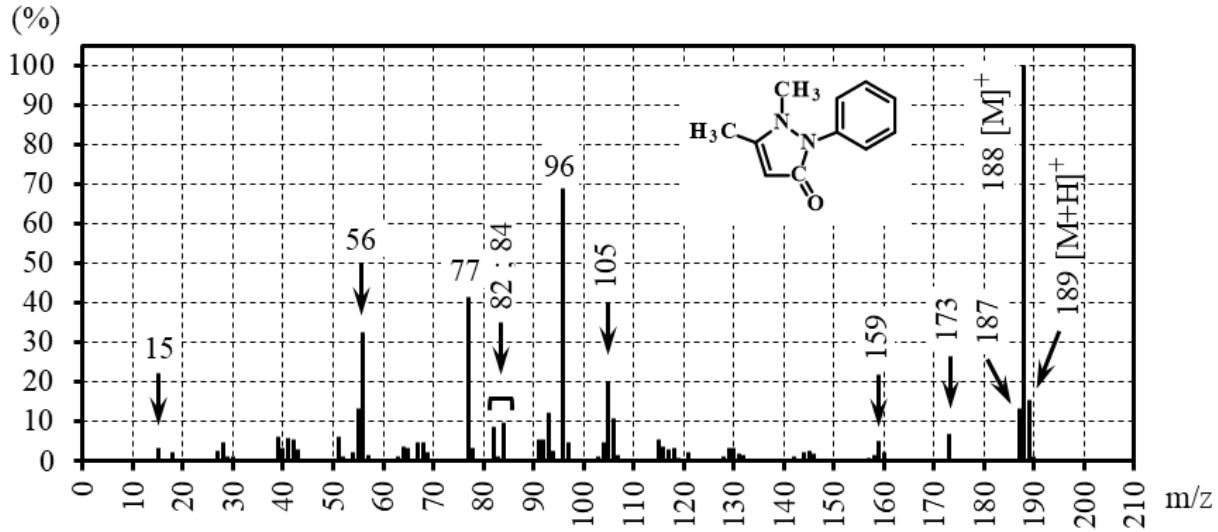

Anabasine - CAS 494-52-0 - EI - NIST 5877



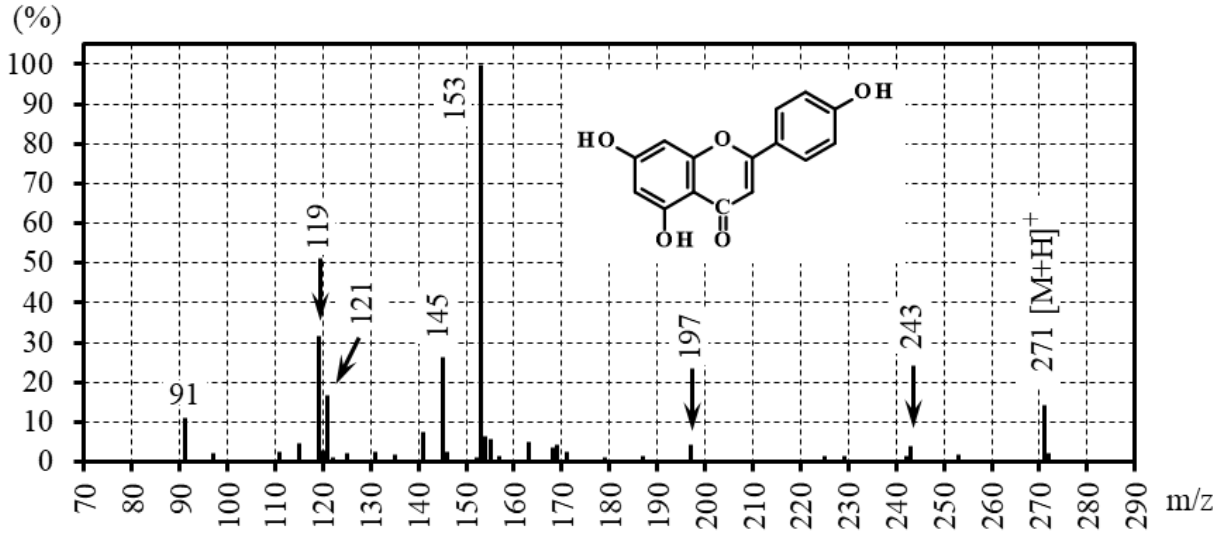

Androsterone - CAS 53-41-8 - EI source 190 oC , sample 120 oC - SDBS 10024



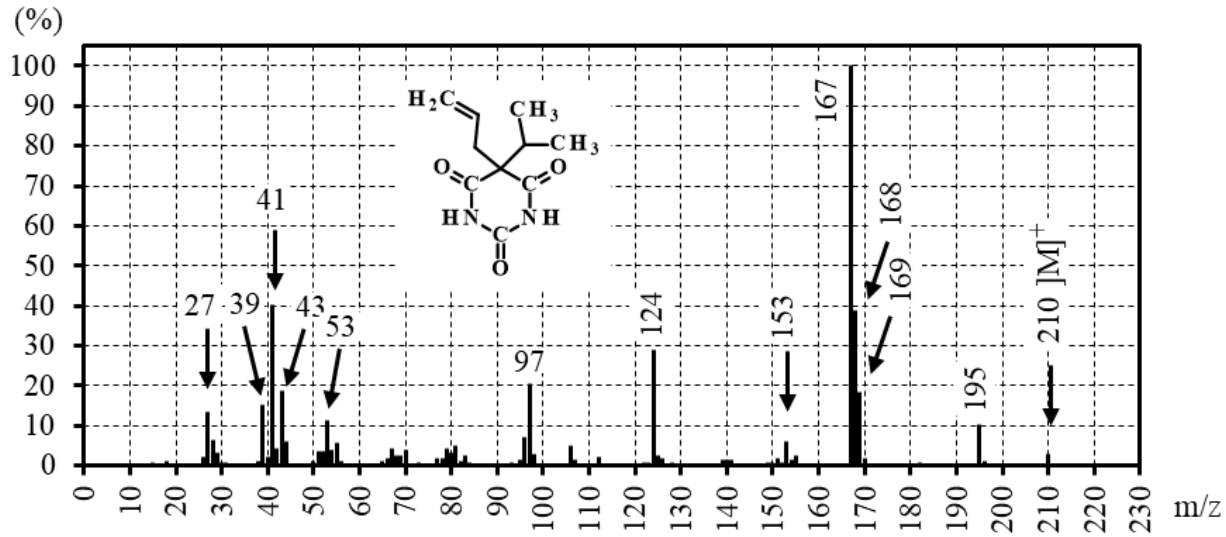

Antazoline - CAS 91-75-8 - EI - NIST 246530



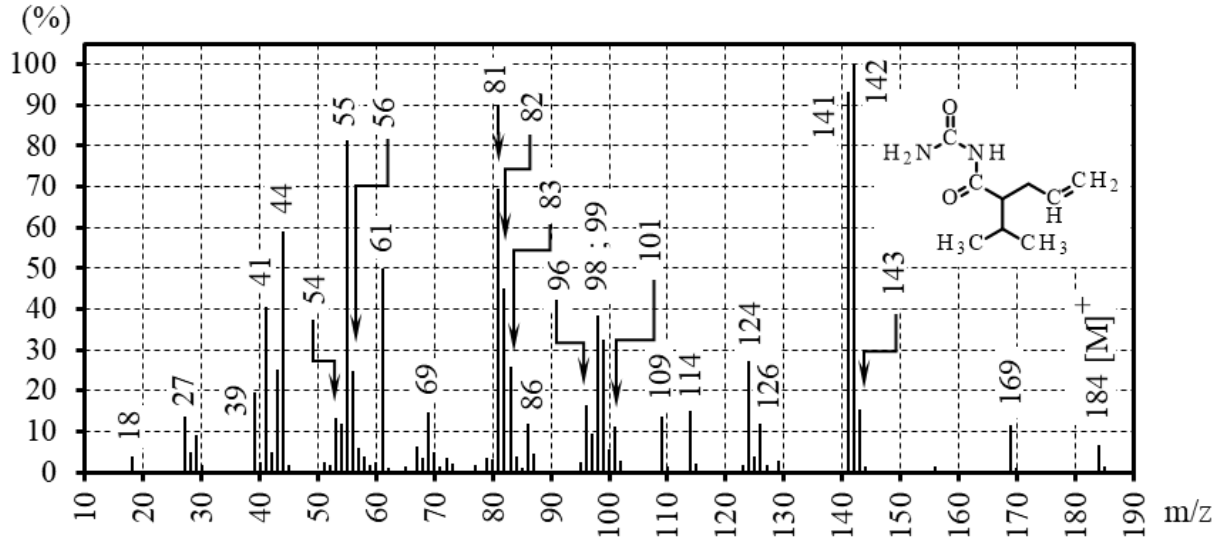

Antipyrine - CAS 60-80-0 - EI 75 eV - Source 150 °C ; sample 120 °C - SDBS 22106



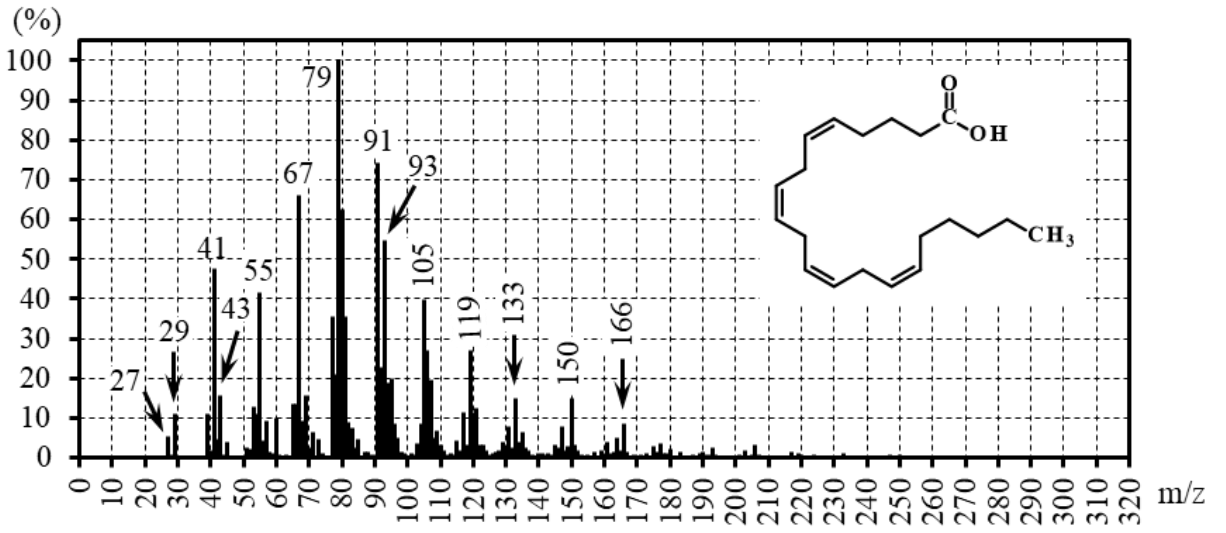

Apigenin - CAS 520-36-5 - MS2 - ESI Coll 50 3V - Prec (M+H)+ MassBankRecord



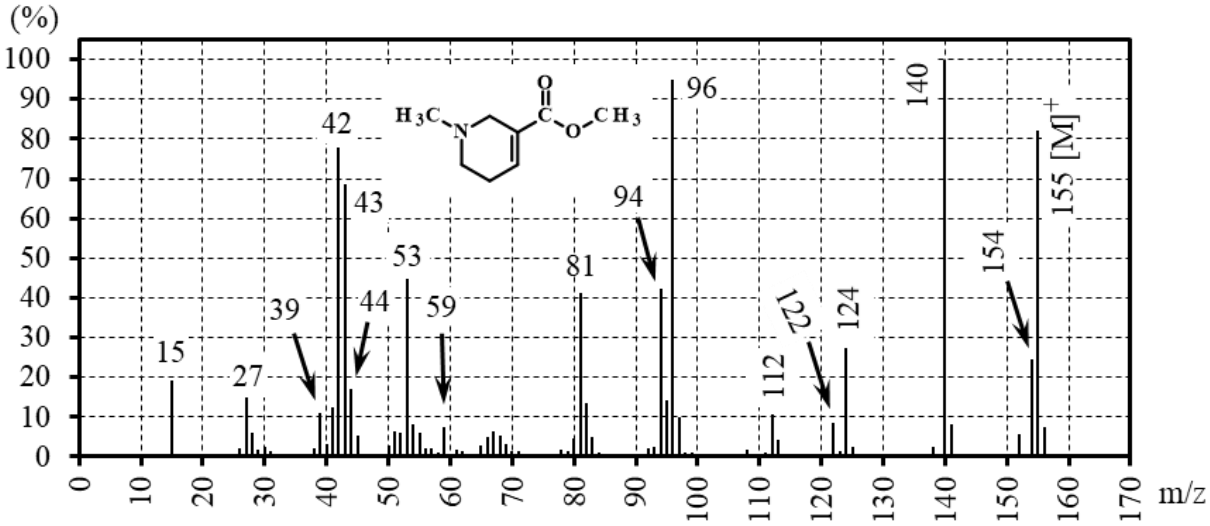

Aprobarbital - CAS 77-02-1 - EI - NIST 42293



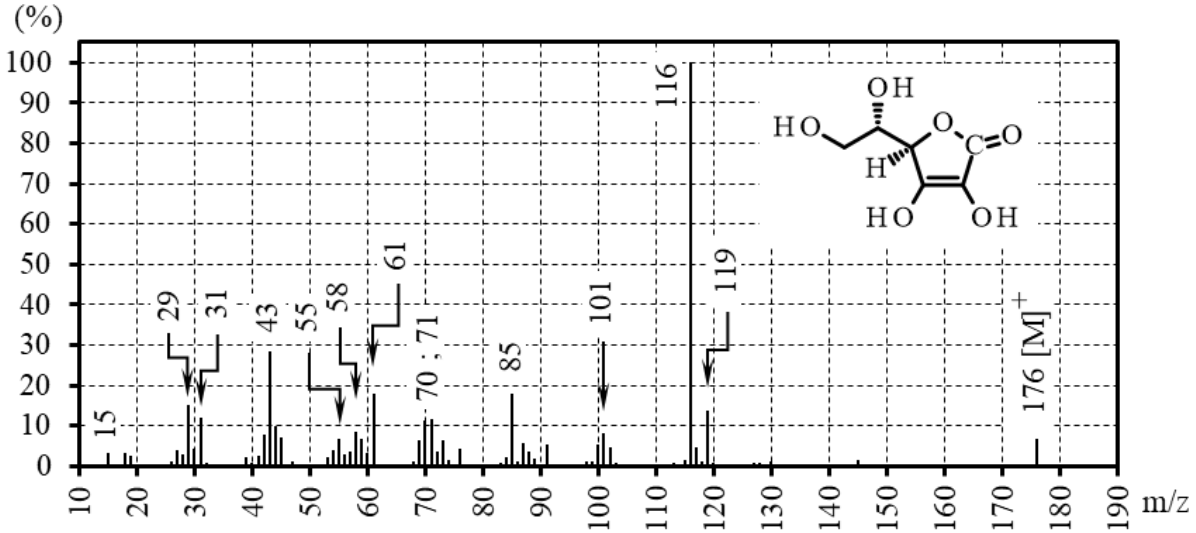

Apronal - CAS 528-92-7 - EI 75 eV - 190 oC-110 oC - SDBS 34431



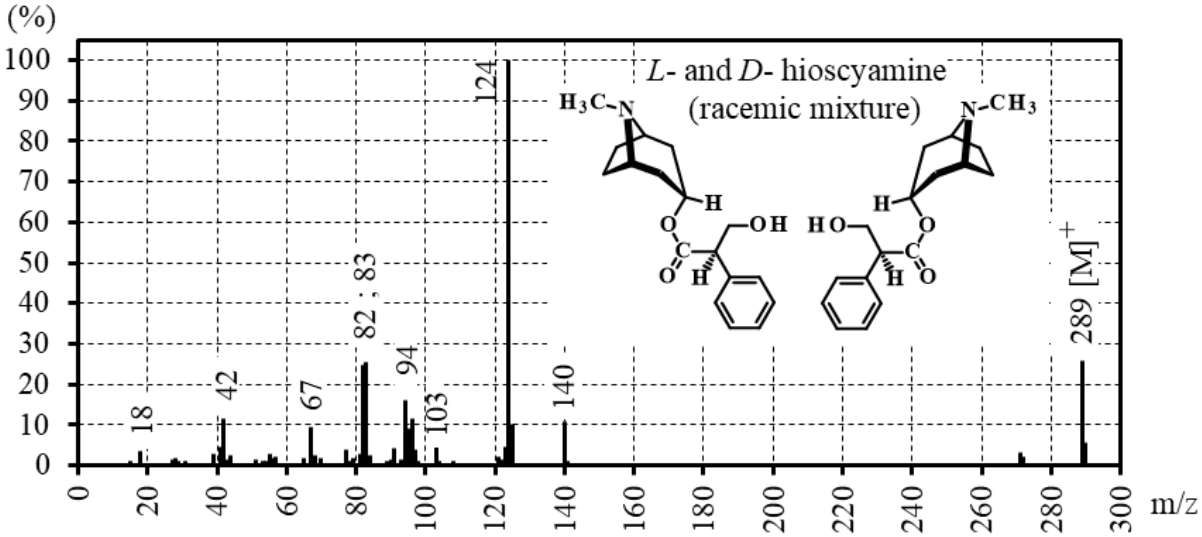

Arachidonic acid - CAS 506-32-1 - M1 - ESI - NIST 333229



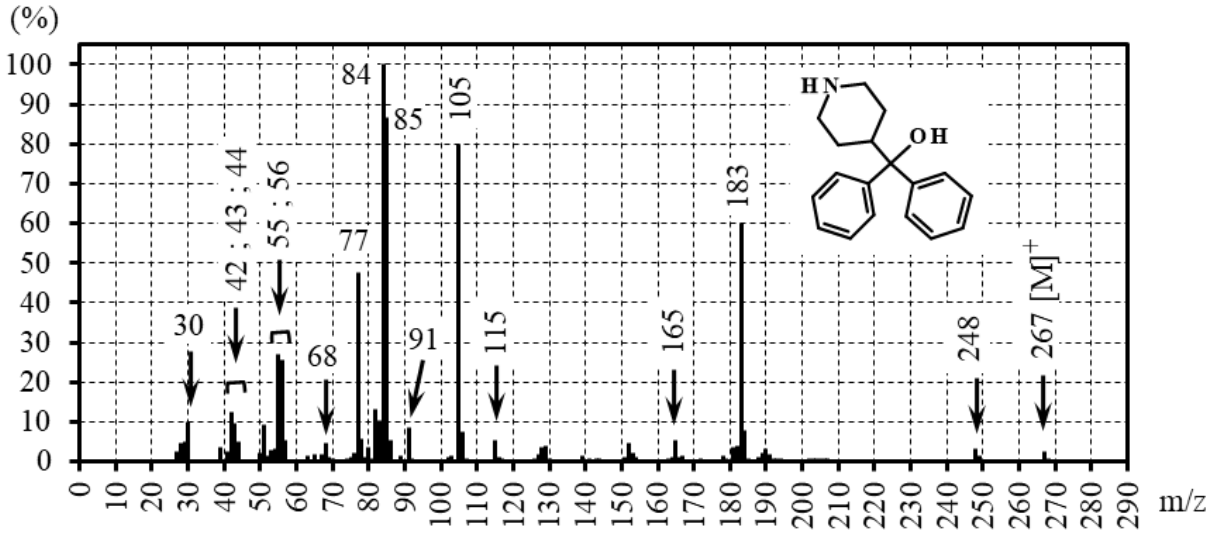

Arecoline - CAS 63-75-2 - EI - NIST 233747



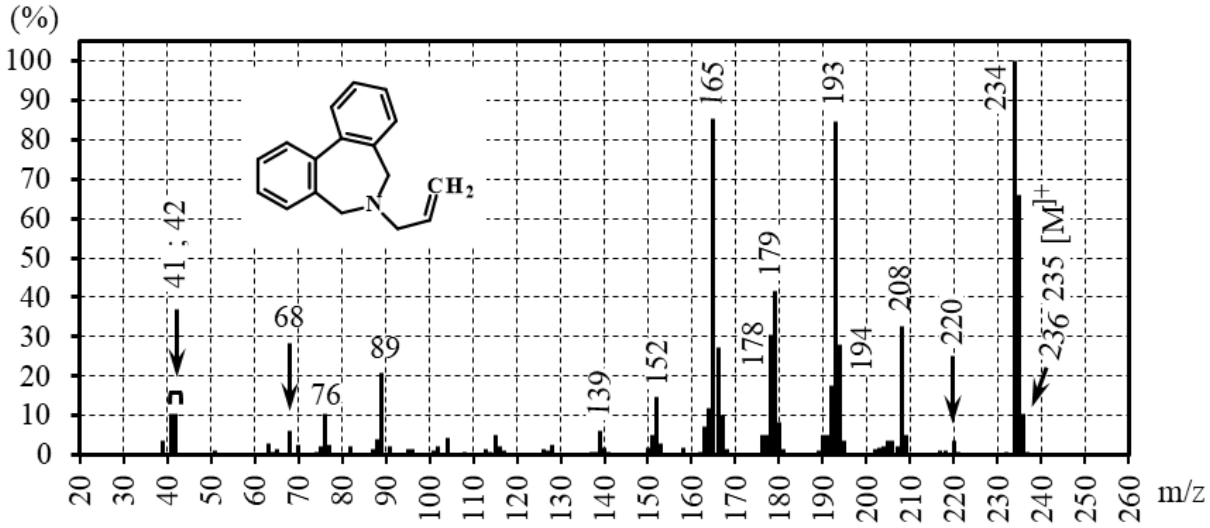

Ascorbic acid - CAS 50-81-7 - EI - NIST 228563



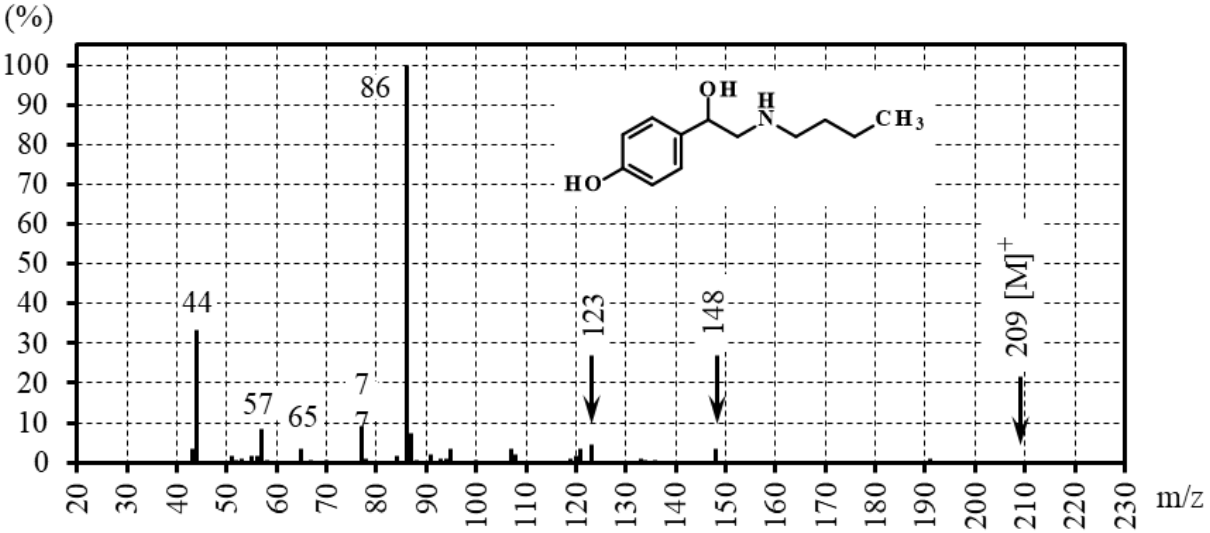

Atropine - CAS 51-55-8 - EI - SDBS nr. 8717



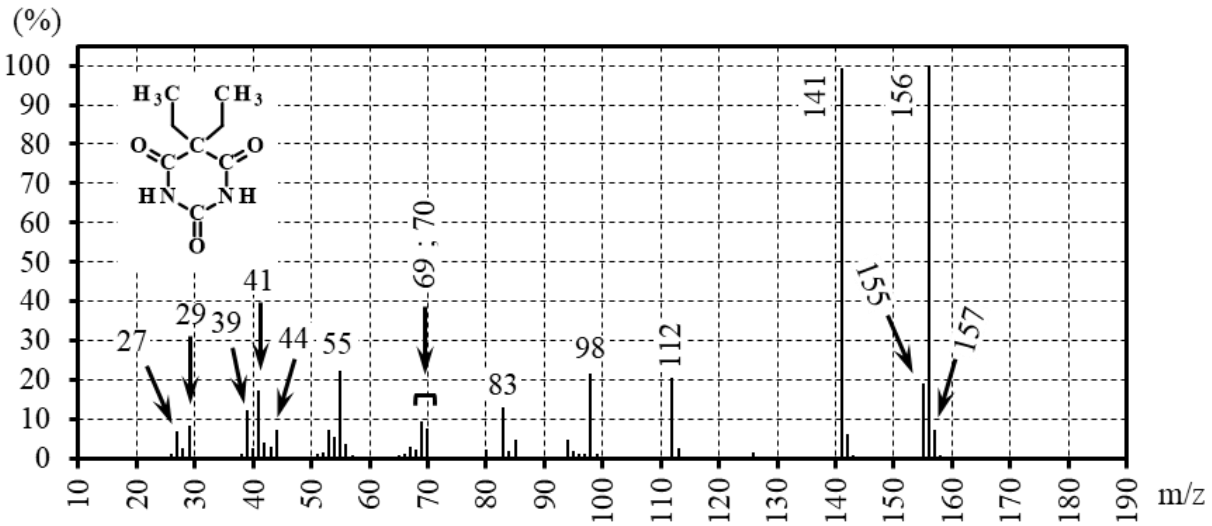

Azacyclonol - CAS 115-46-8 - EI - NIST 408710



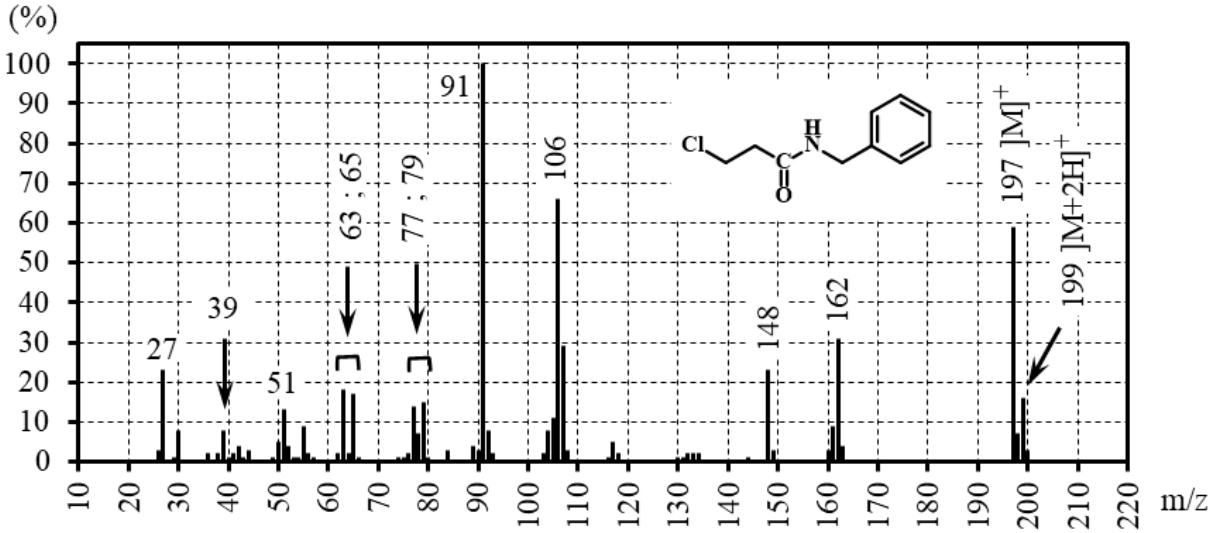

Azapetine - CAS 146-36-1 - EI - NIST 246330



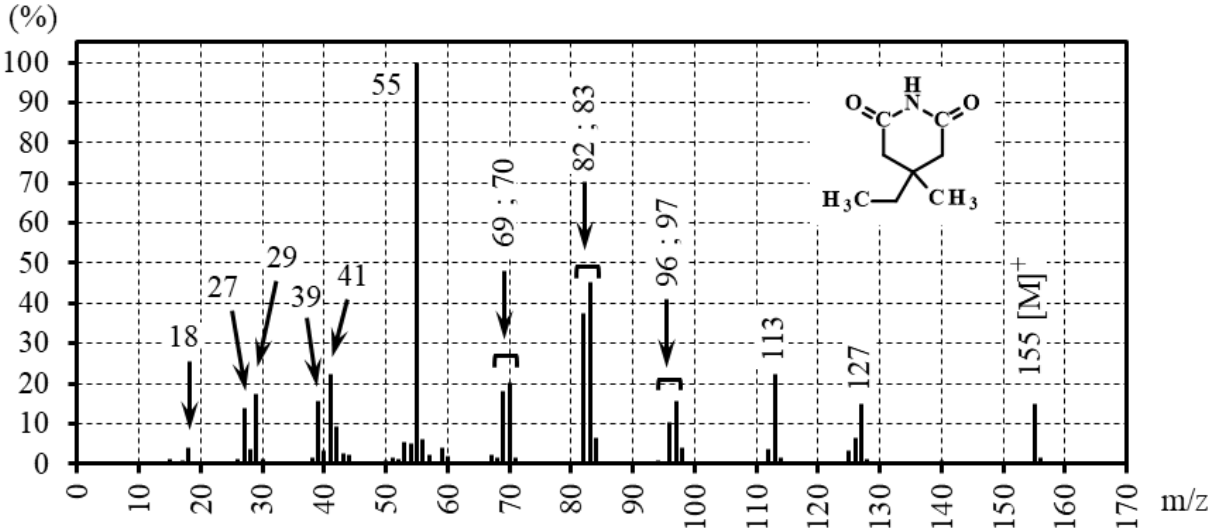

Bamethan - CAS 3703-79-5 - EI - NIST 248797



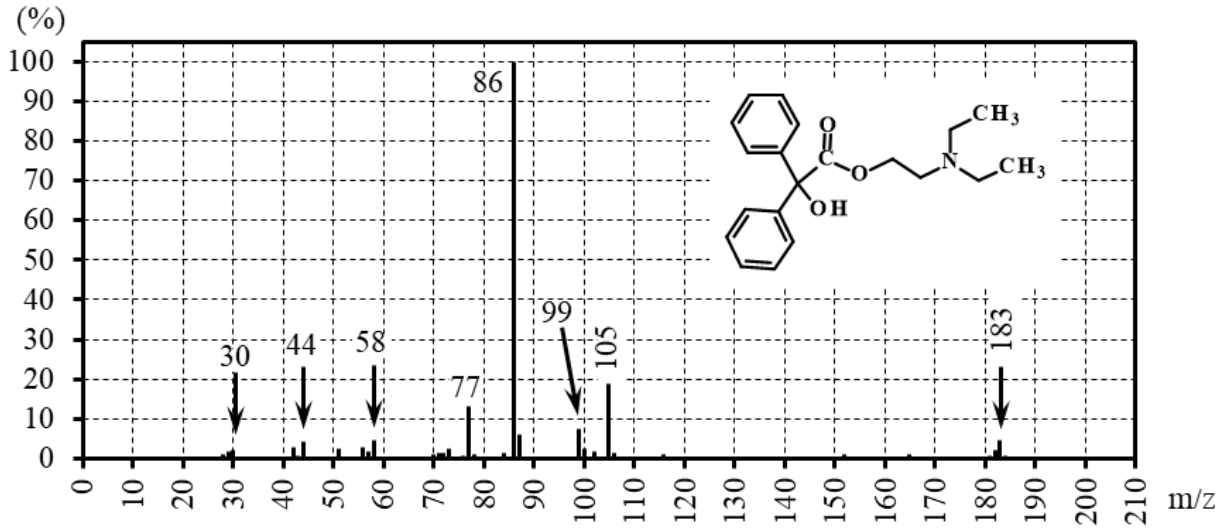

Barbital - CAS 57-44-3 - EI - NIST 352179



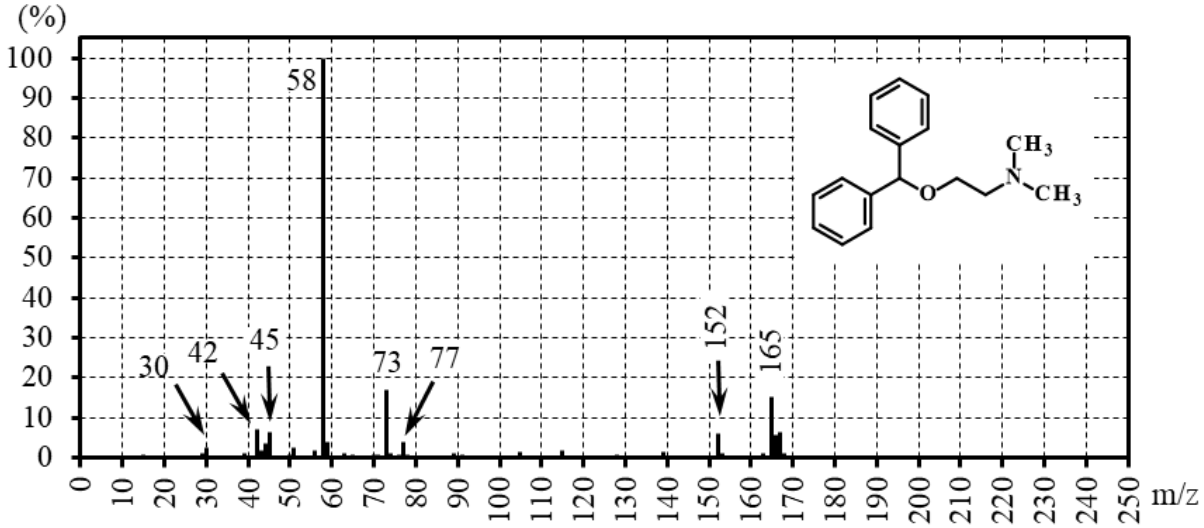

Beclamide - CAS 501-68-8 - EI - NIST 298605



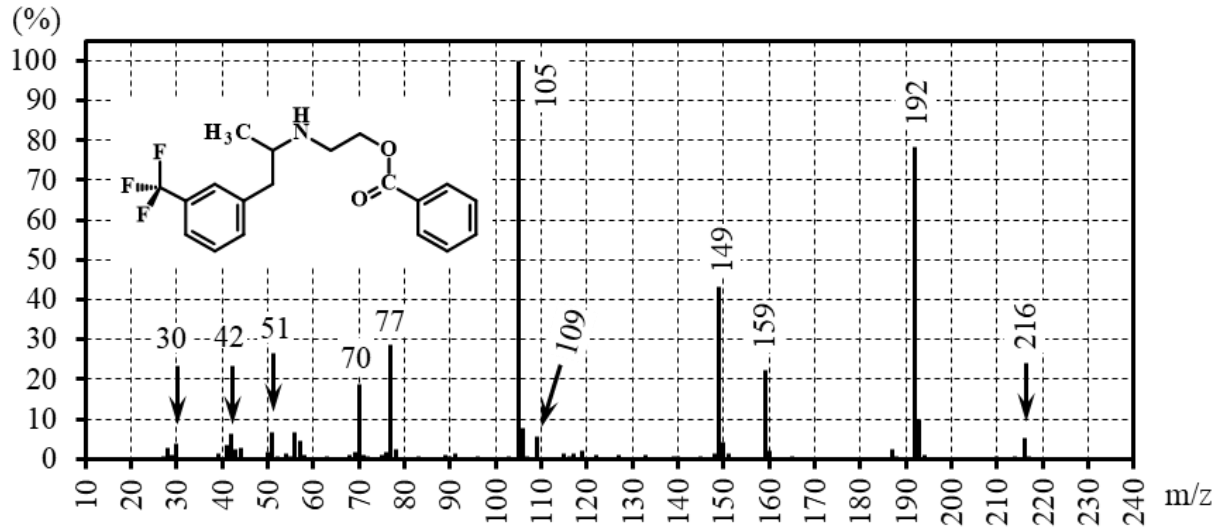

Bemegride - CAS 64-65-3 - EI - NIST 231873



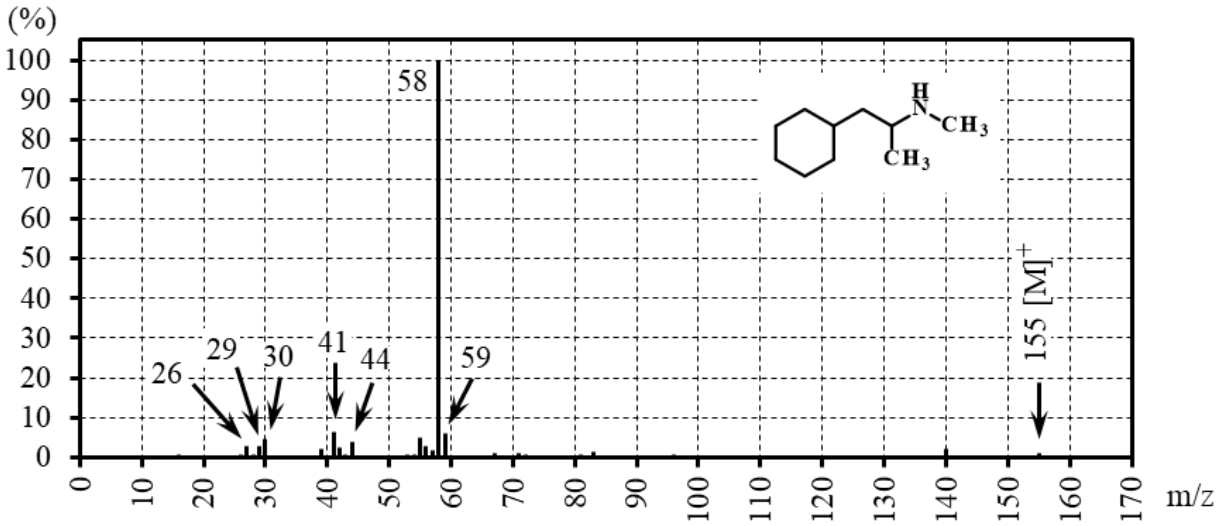

Benactyzine - CAS 302-40-9 - EI - NIST 408698



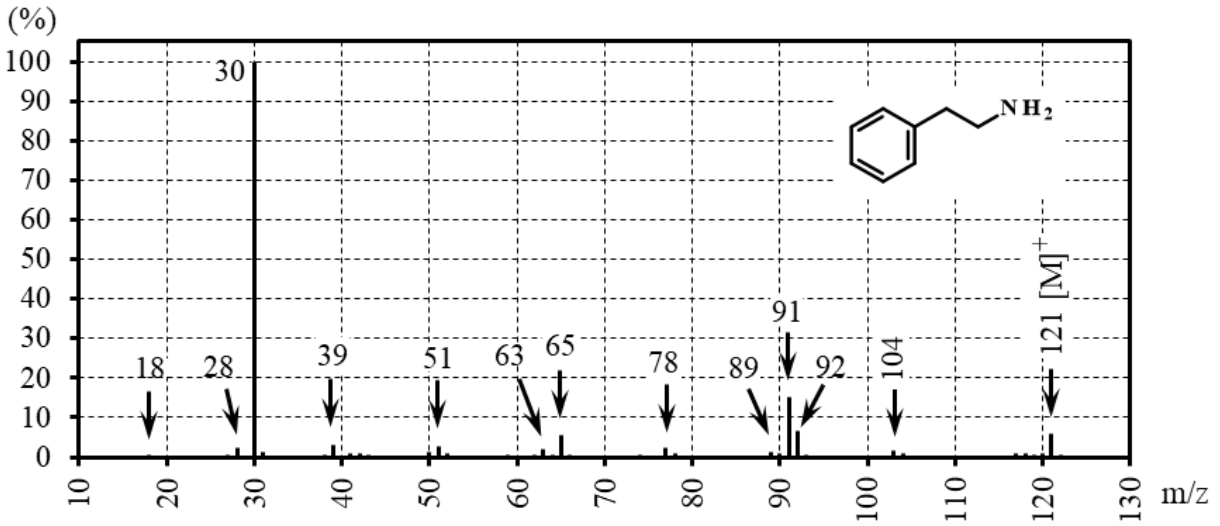

Benadryl (Diphenhydramine) - CAS 58-73-1 - EI - NIST 250549



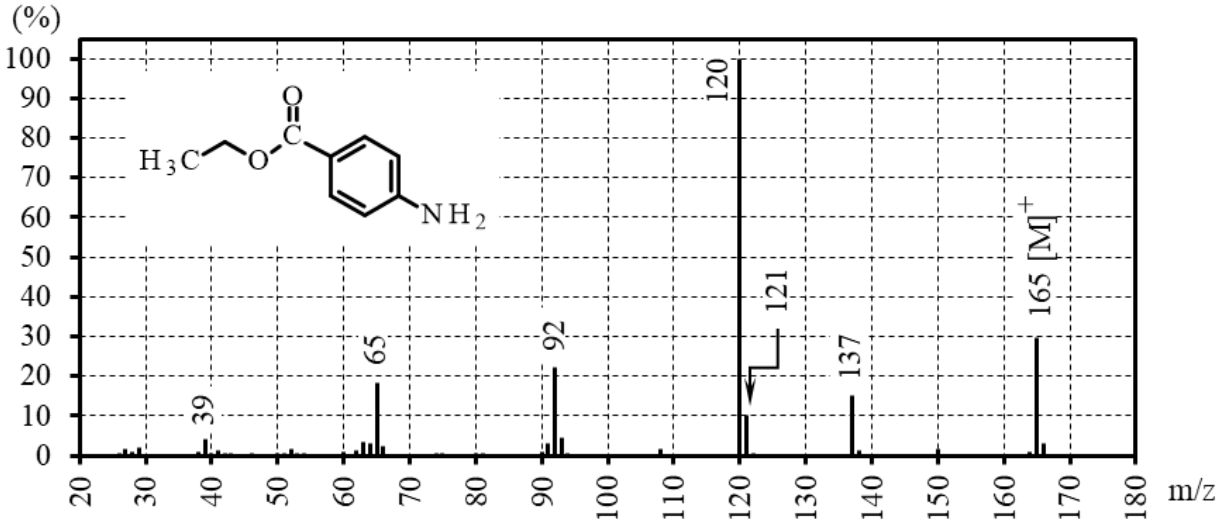

Benfluorex - CAS 23602-78-0 - EI - NIST 292037



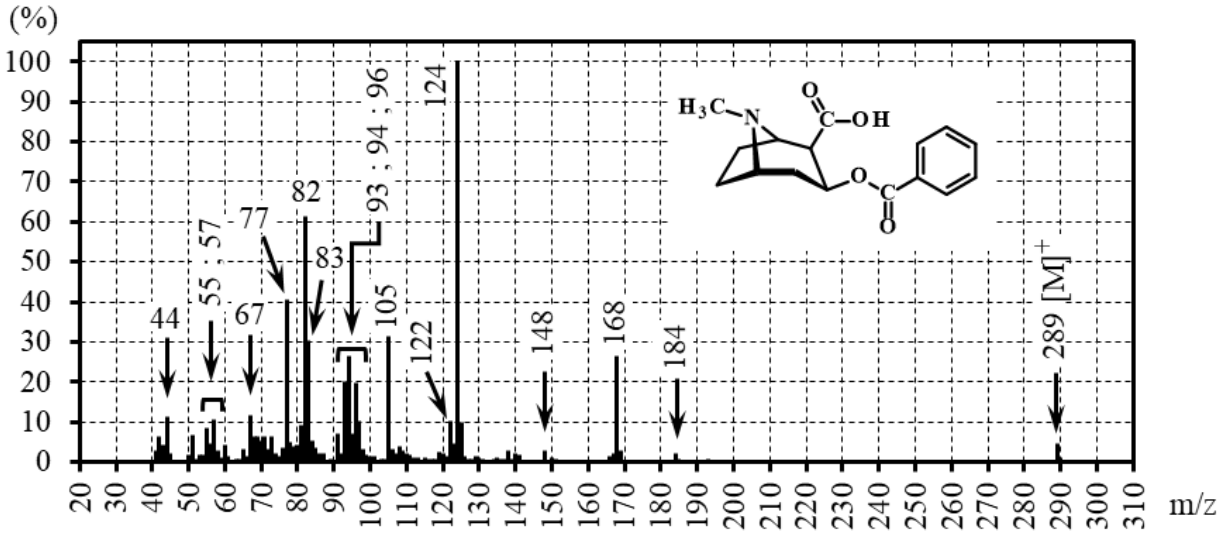

Benzedrex (Propylhexedrine) - CAS 101-40-6 - EI - NIST 42436



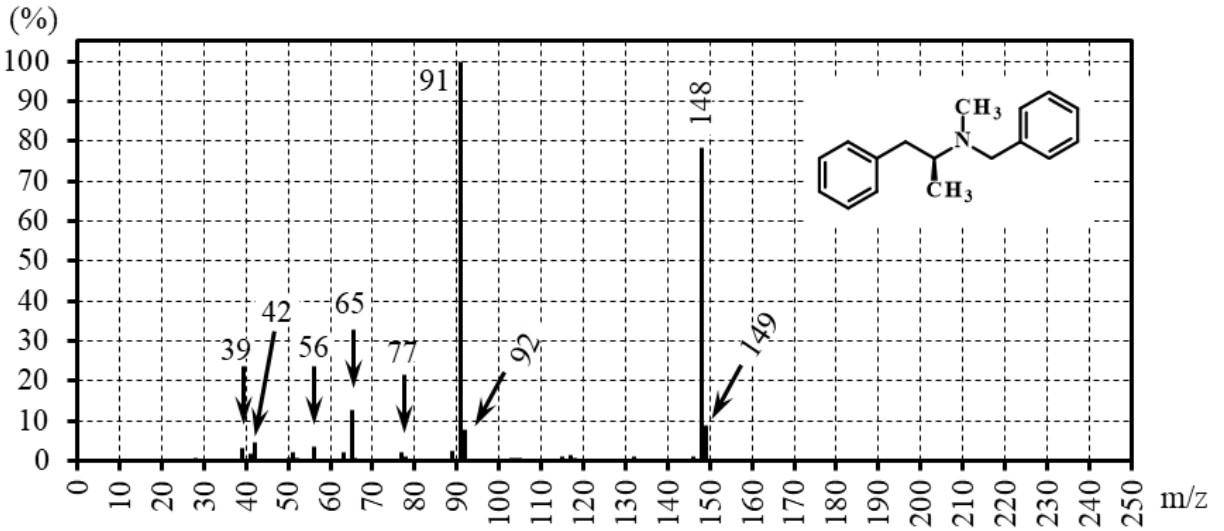

Benzeneethanamine (Phenethylamine) - CAS 64-04-0 - EI - NIST 229486



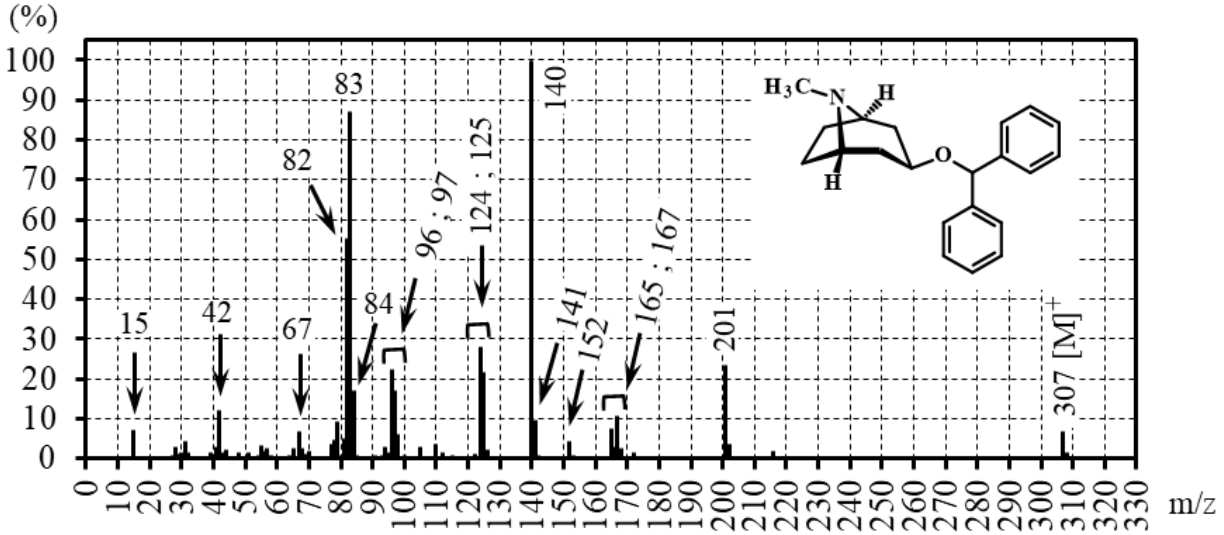

Benzocaine - CAS 94-09-7 - EI - NIST 408497



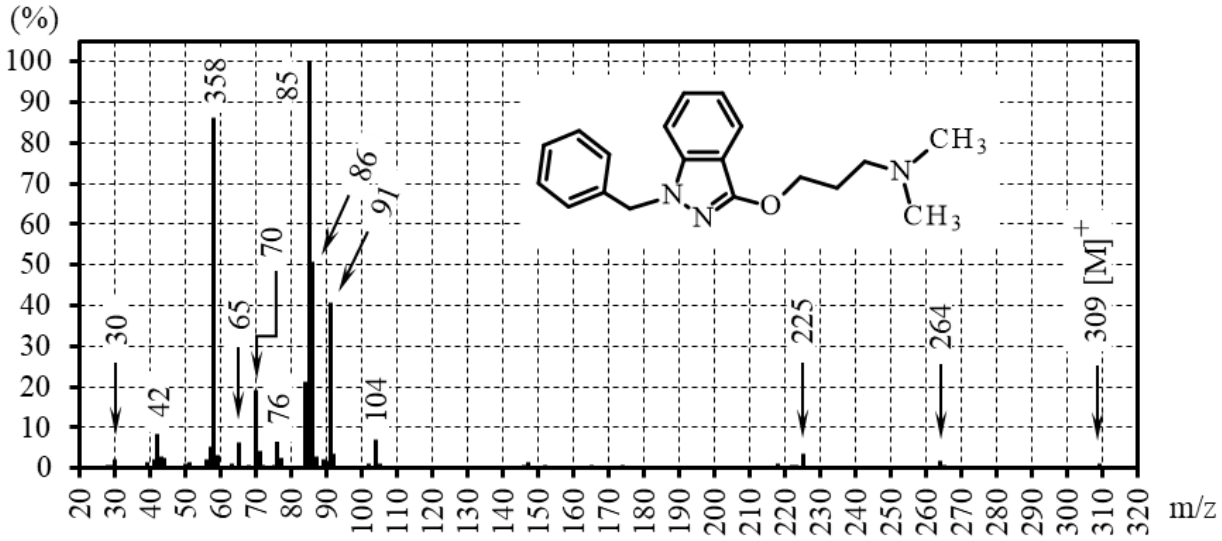

Benzoylecgonine - CAS 519-09-5 - EI - NIST 246709



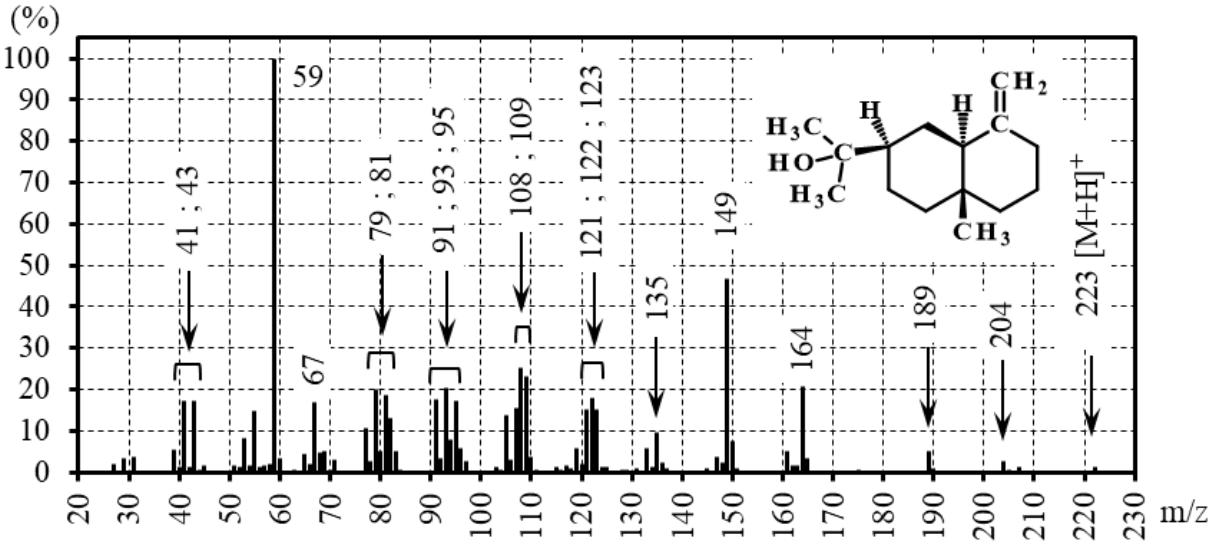

Benzphetamine - CAS 156-08-1 - EI - NIST 250592



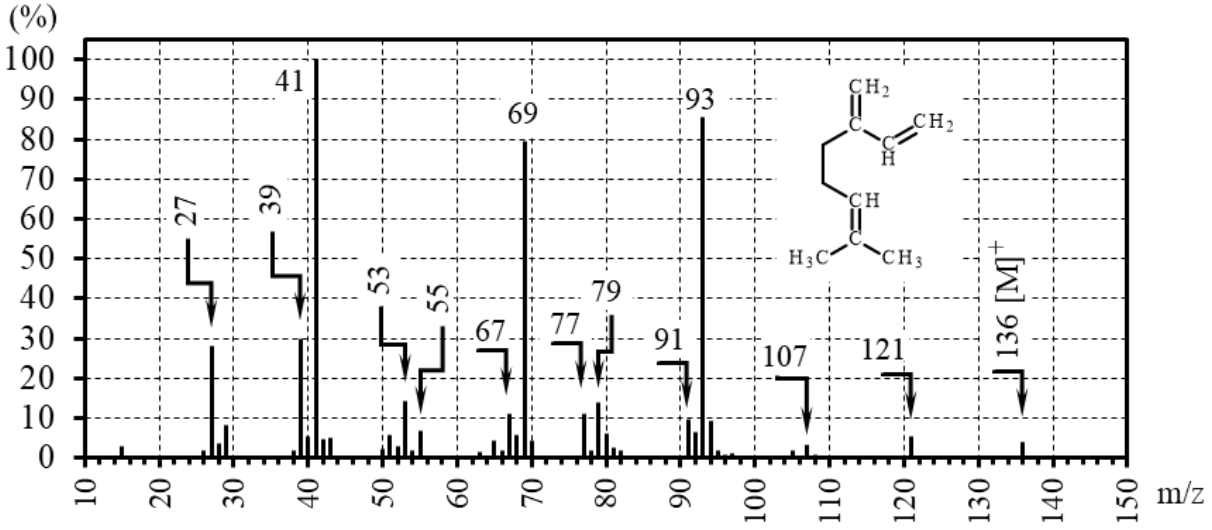

Benztropine - CAS 86-13-5 - EI - NIST 238579



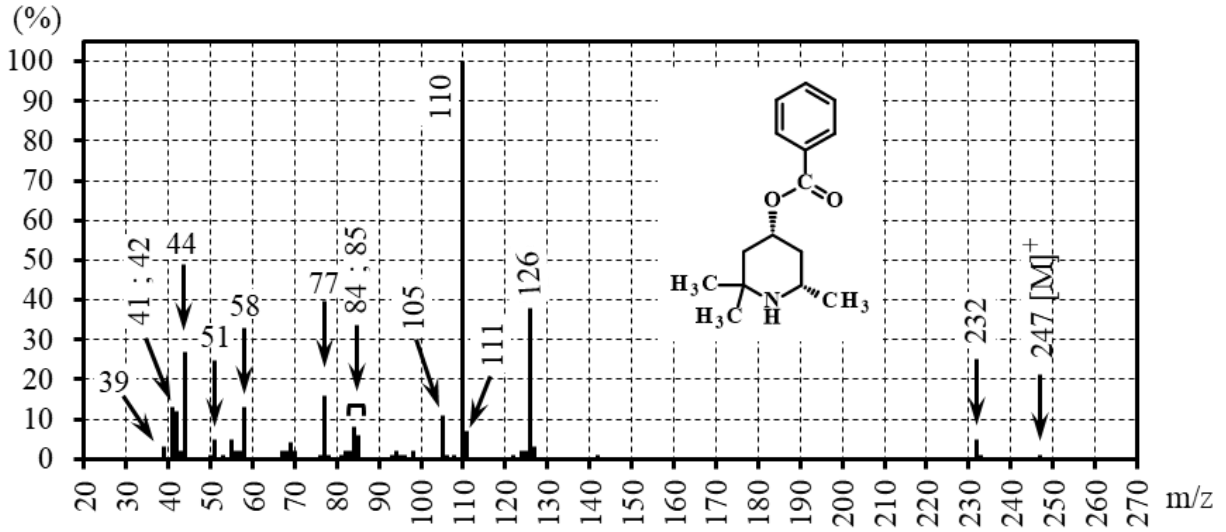

Benzydamine (in Tantum Verde) - CAS 642-72-8 - EI - NIST nr. 408054



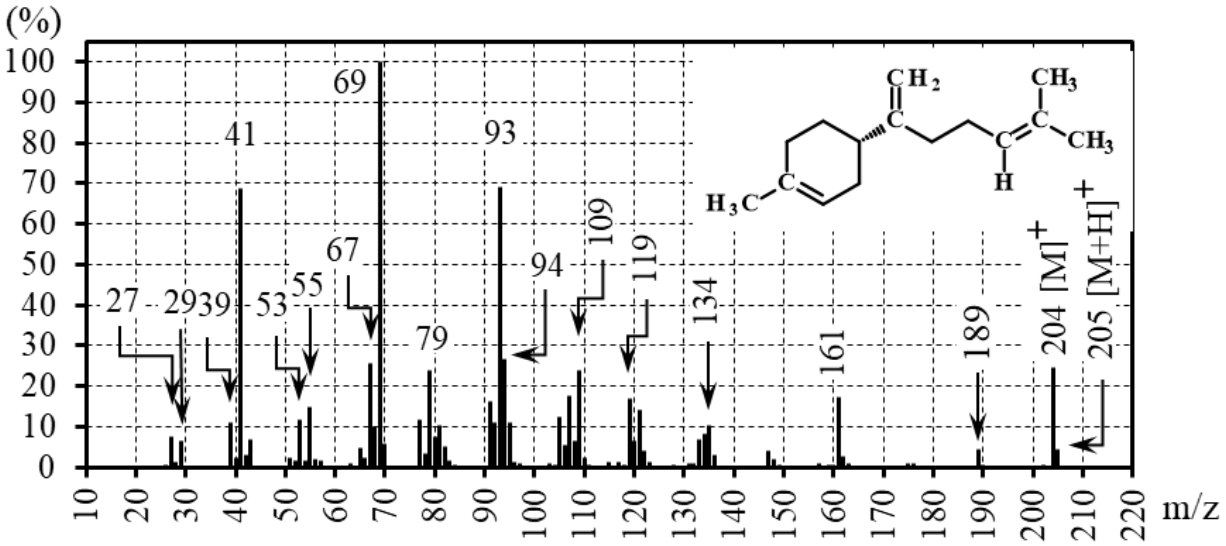

β Eudesmol CAS 473-15-4 - EI - NIST 334000



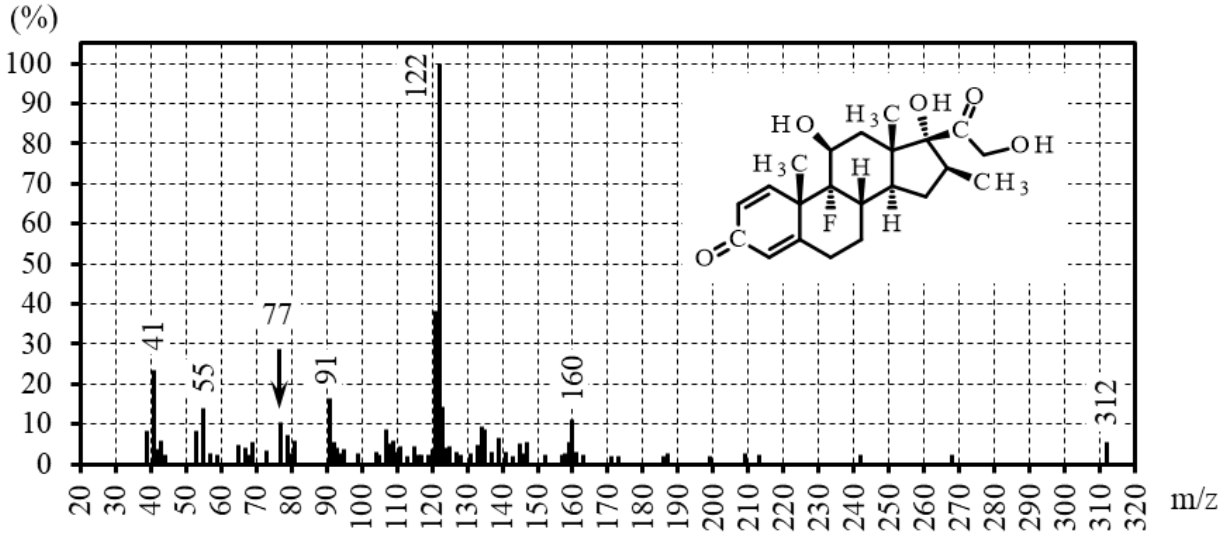

β Myrcene - CAS 123-35-3 EI - MS1 - positive mode - NIST 3301



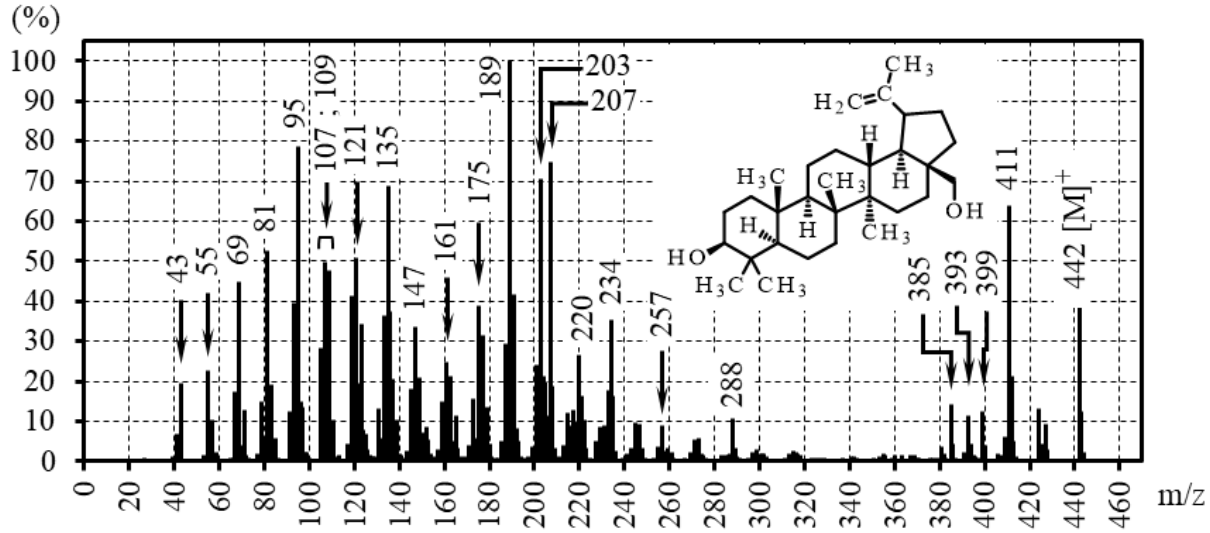

β.-Eucaine - CAS 500-34-5 - EI - NIST 298603



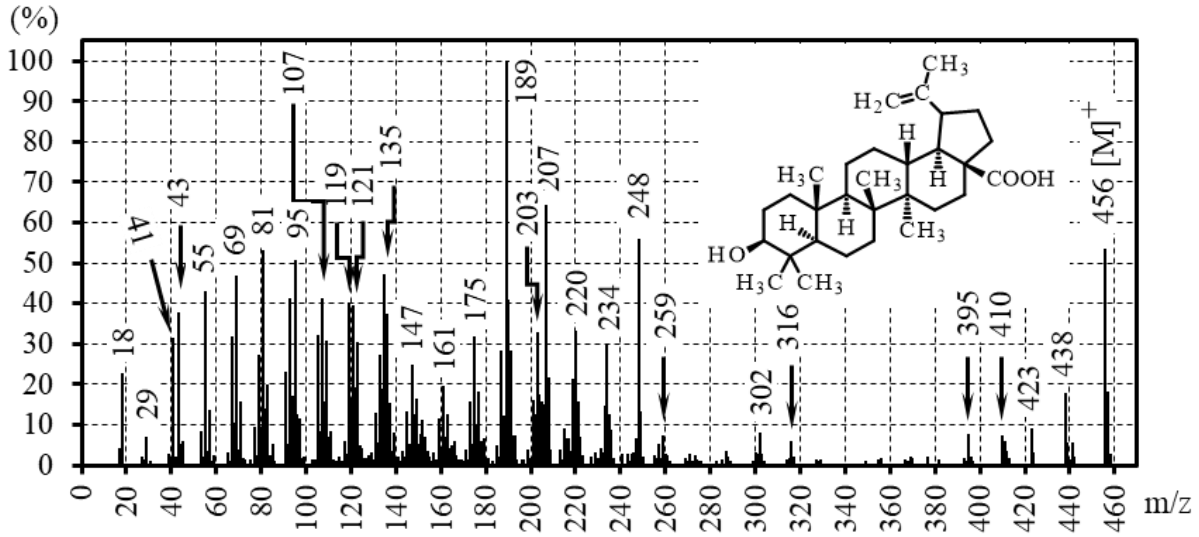

β-Bisabolene - CAS 495-61-4 - NIST 9219



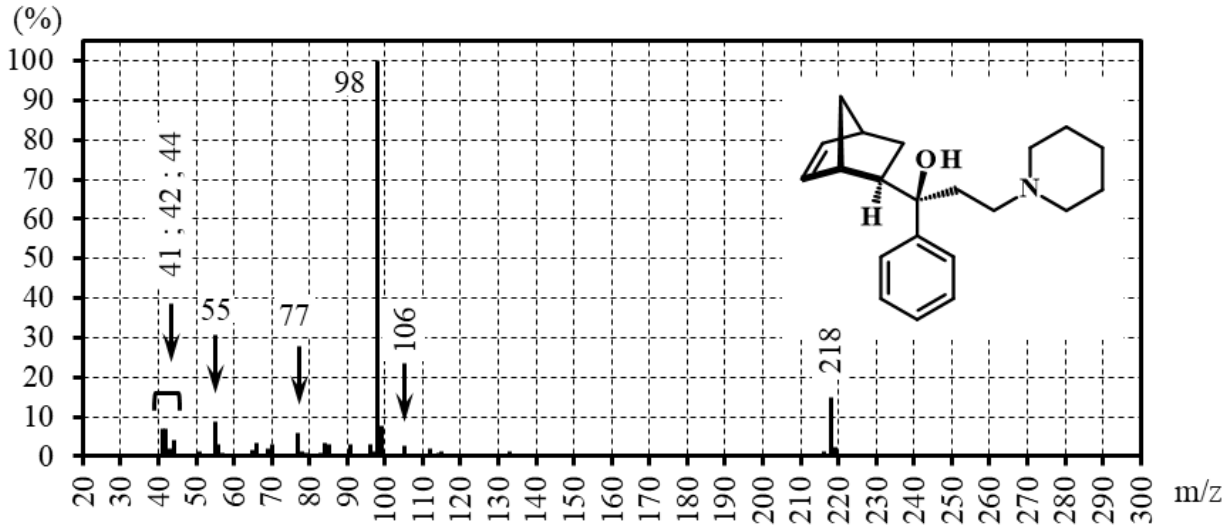

beta-Methasone - CAS 378-44-9 - EI - NIST 74535



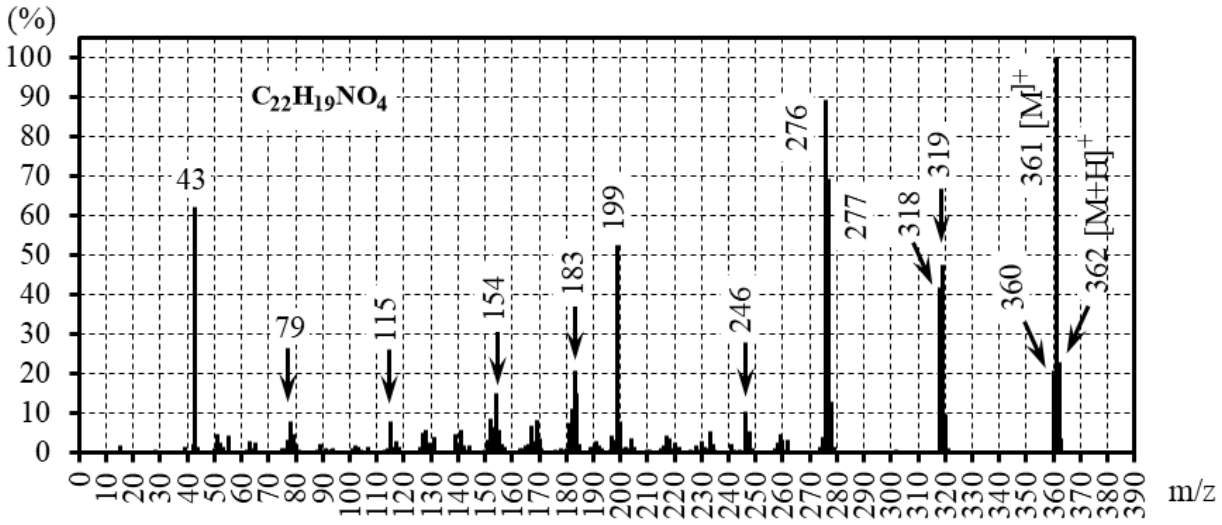

Betulin - CAS 473-98-3 - EI - NIST 63047



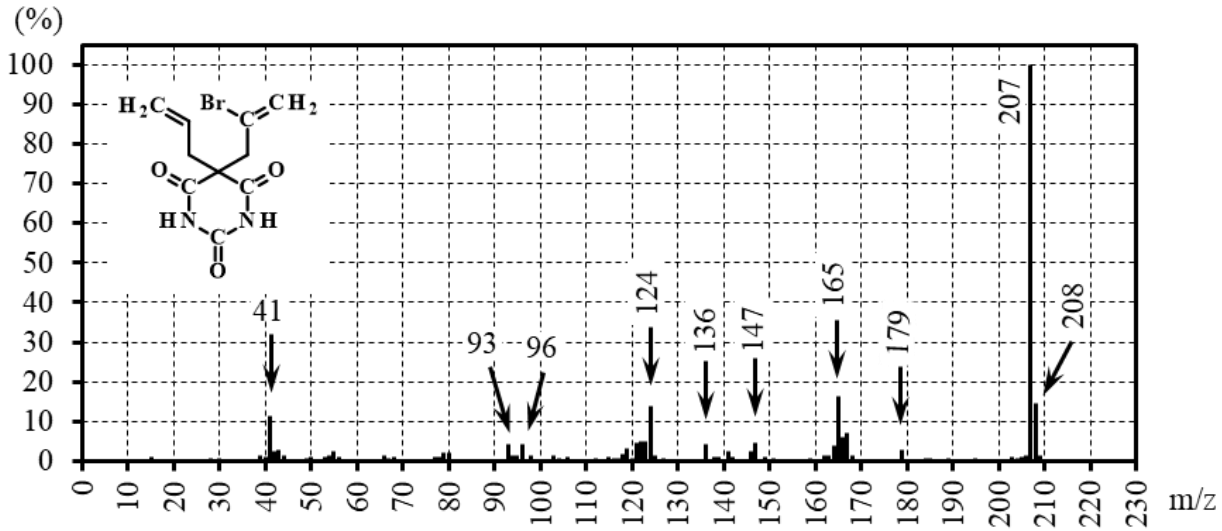

Betulinic acid - CAS 472-15-1 - EI 70 eV - SDBS nr 34273



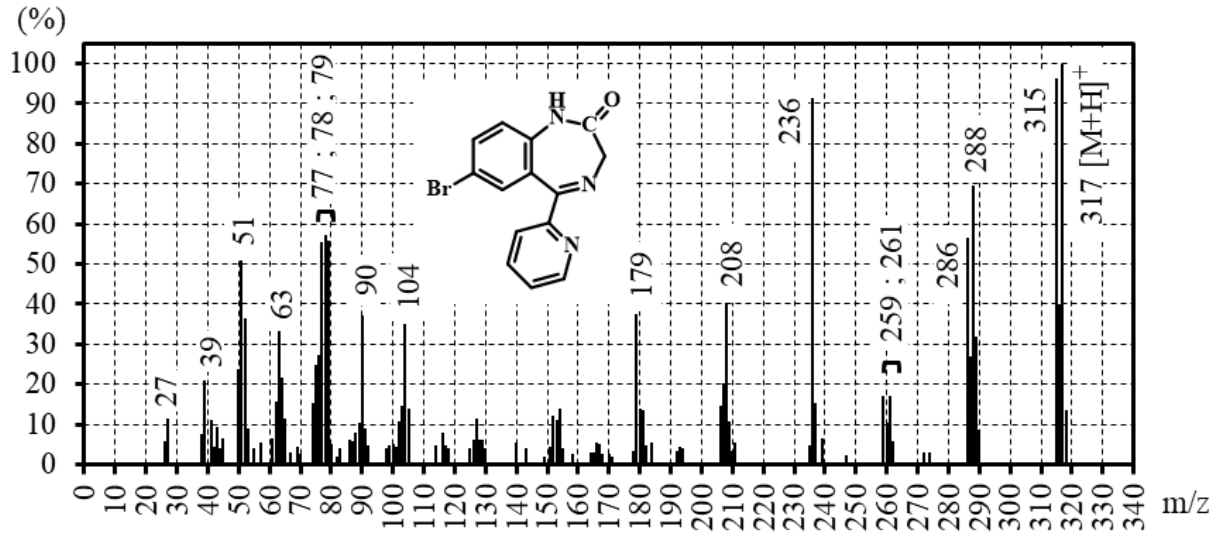

Biperiden - CAS 514-65-8 - EI - NIST 247729



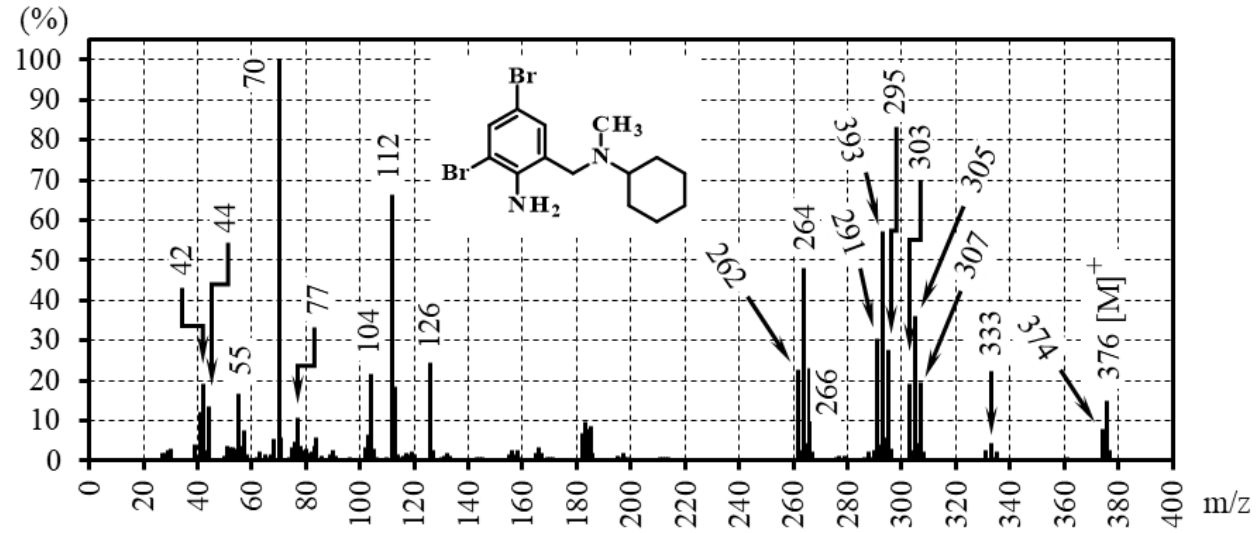

Bisacodyl - CAS 603-50-9 - EI - NIST 408689



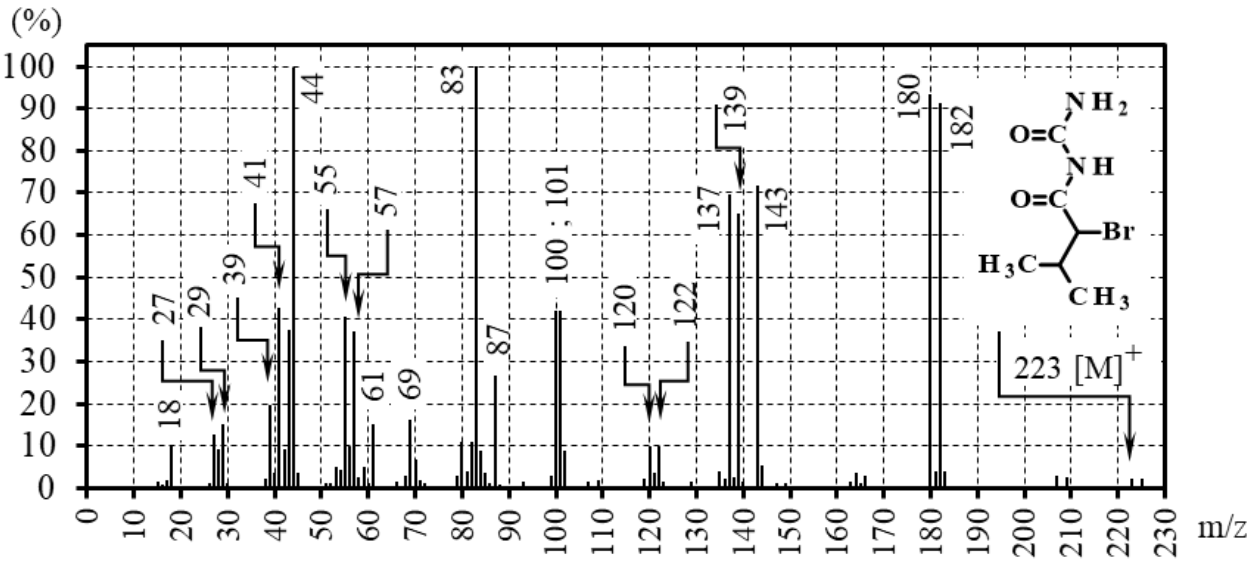

Brallobarbital - CAS 561-86-4 - EI - NIST 42338



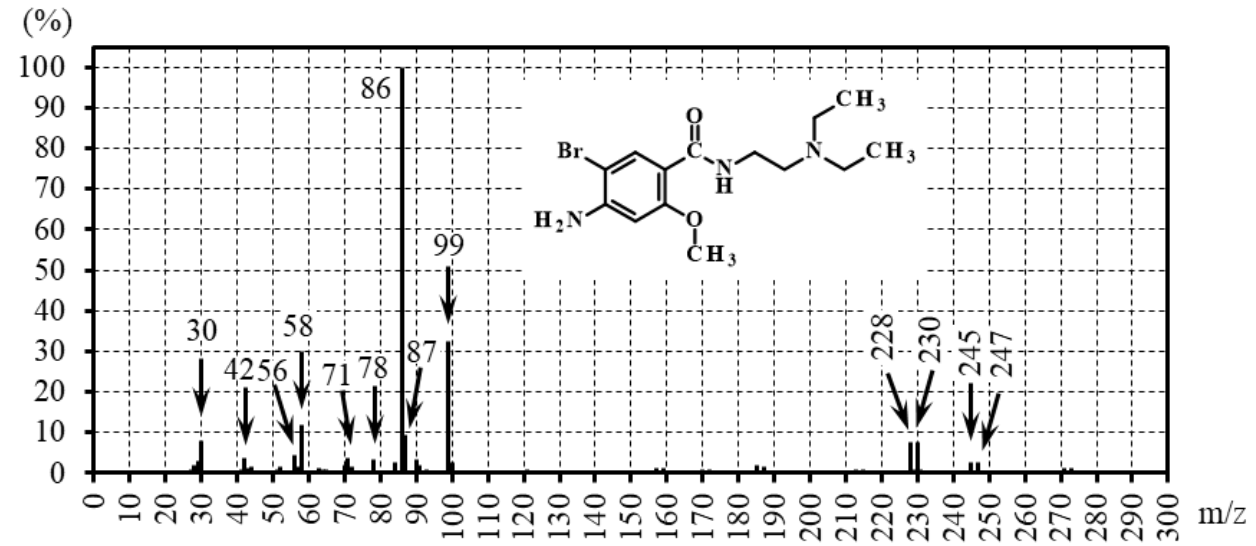

Bromazepam - CAS 1812-30-2 - EI - NIST 107109



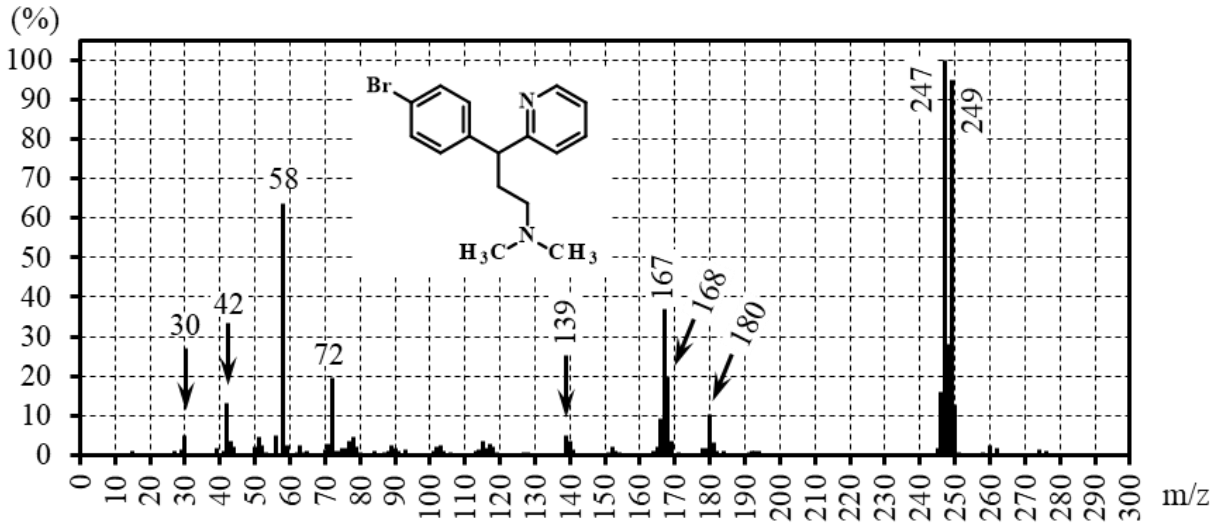

Bromhexine - CAS 3572-43-8 - NIST 408573



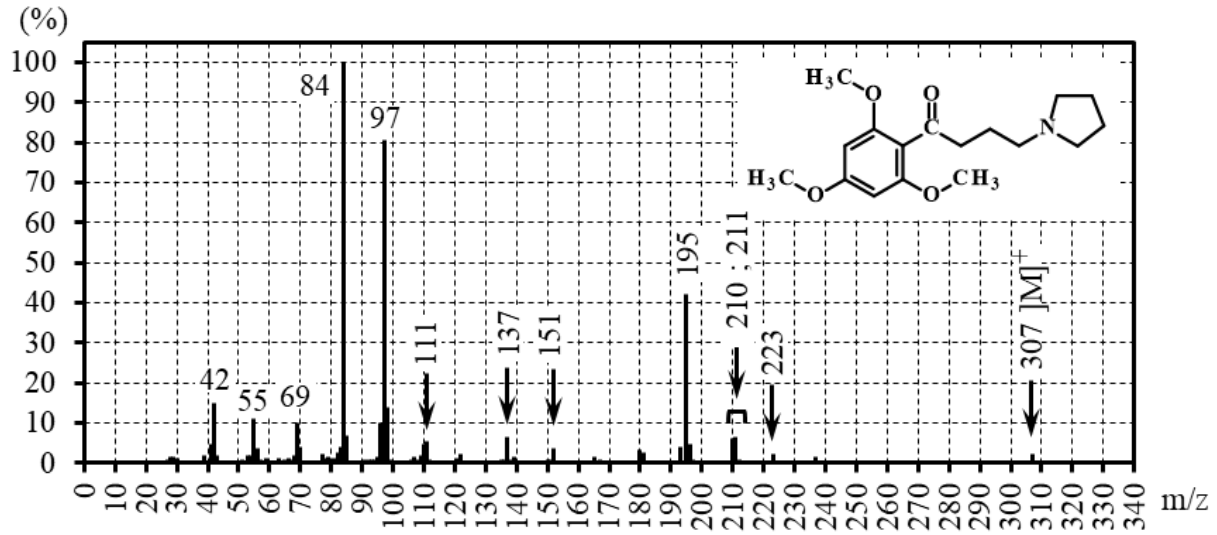

Bromisoval - CAS 496-67-3 - EI 75 eV - 190 oC, 130 oC, SDBS 34922



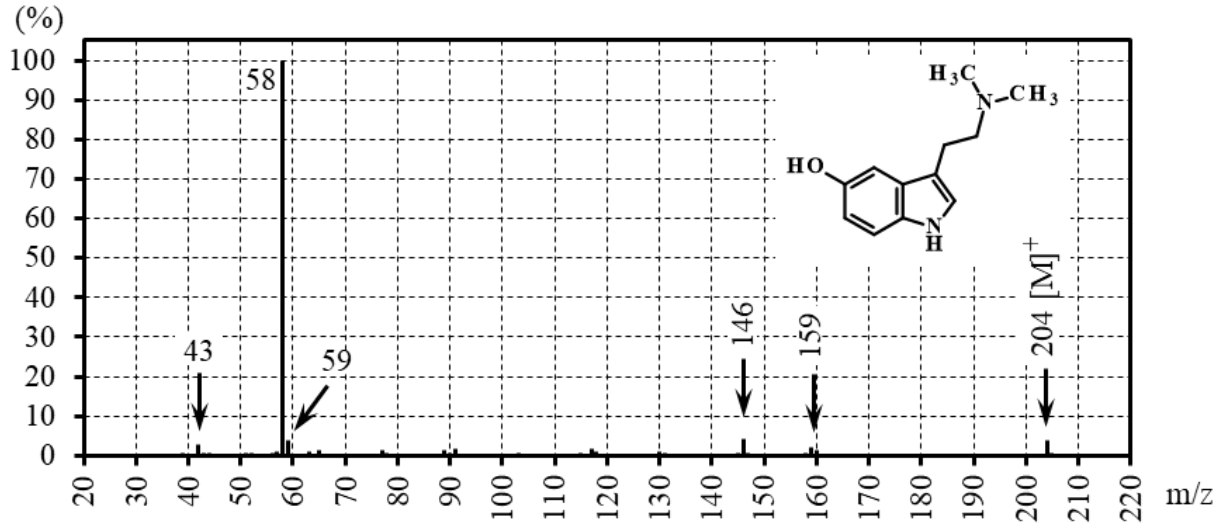

Bromopride - CAS 4093-35-0 - EI - NIST 292169



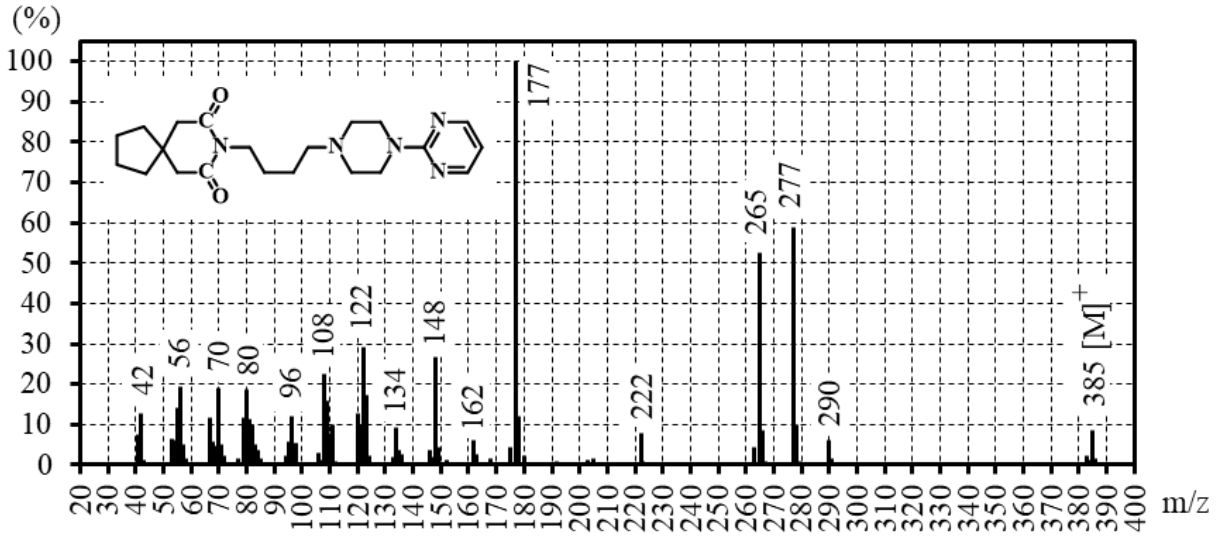

Brompheniramine - CAS 86-22-6 - EI - NIST 250546



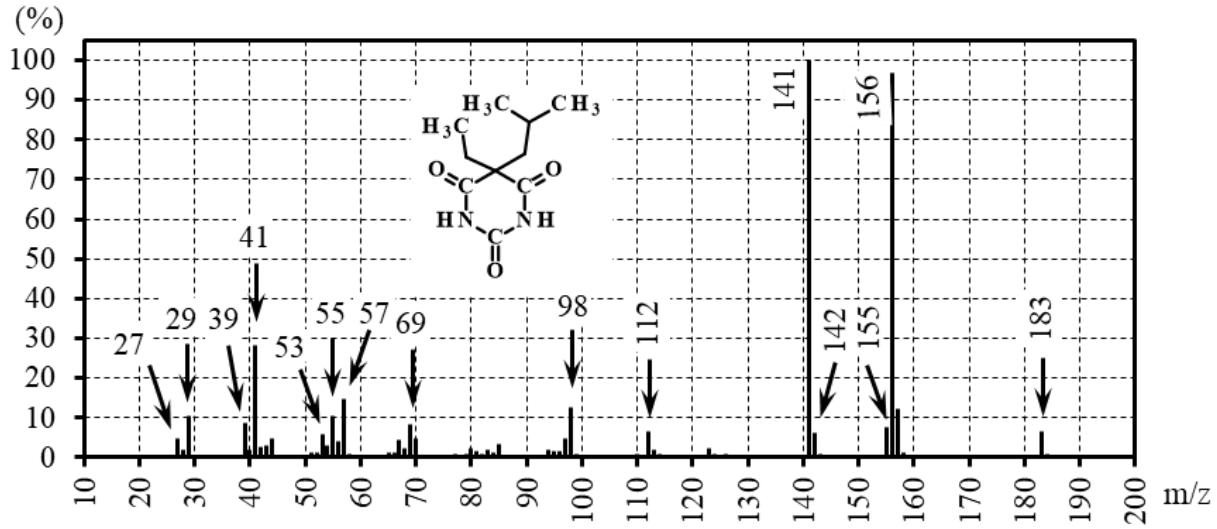

Buflomedil - CAS 55837-25-7 - EI - NIST 292107



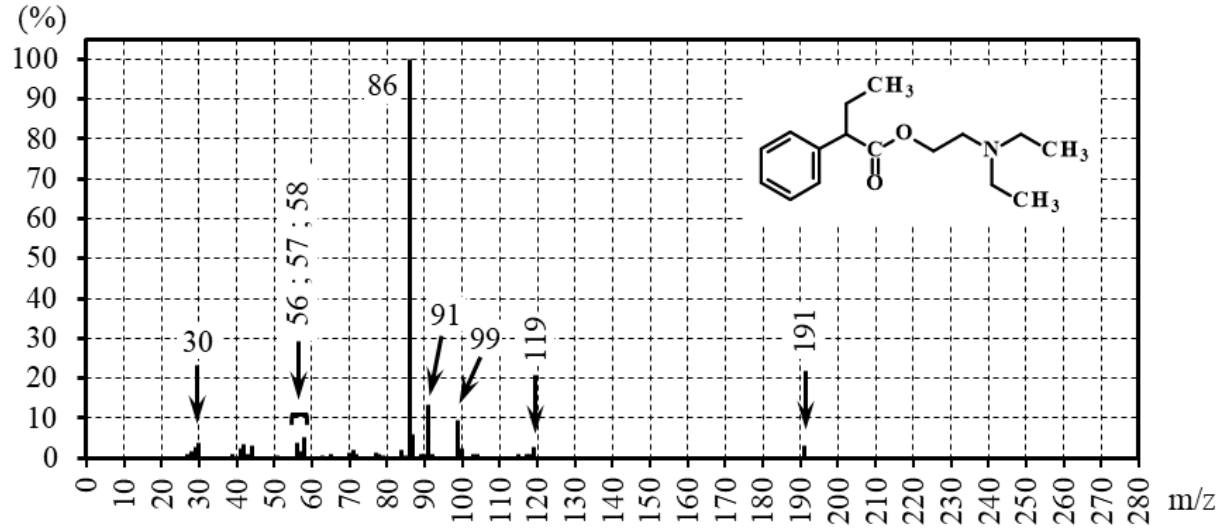

Bufotenin - CAS 487-93-4 - EI - NIST 312457



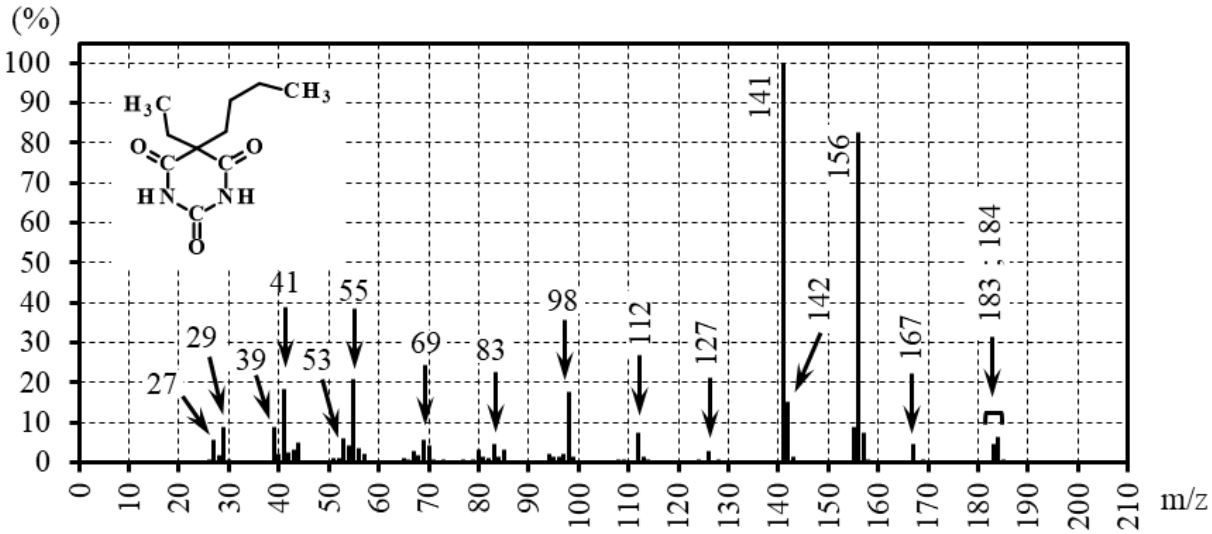

Buspirone - CAS 36505-84-7 - EI - NIST 248867



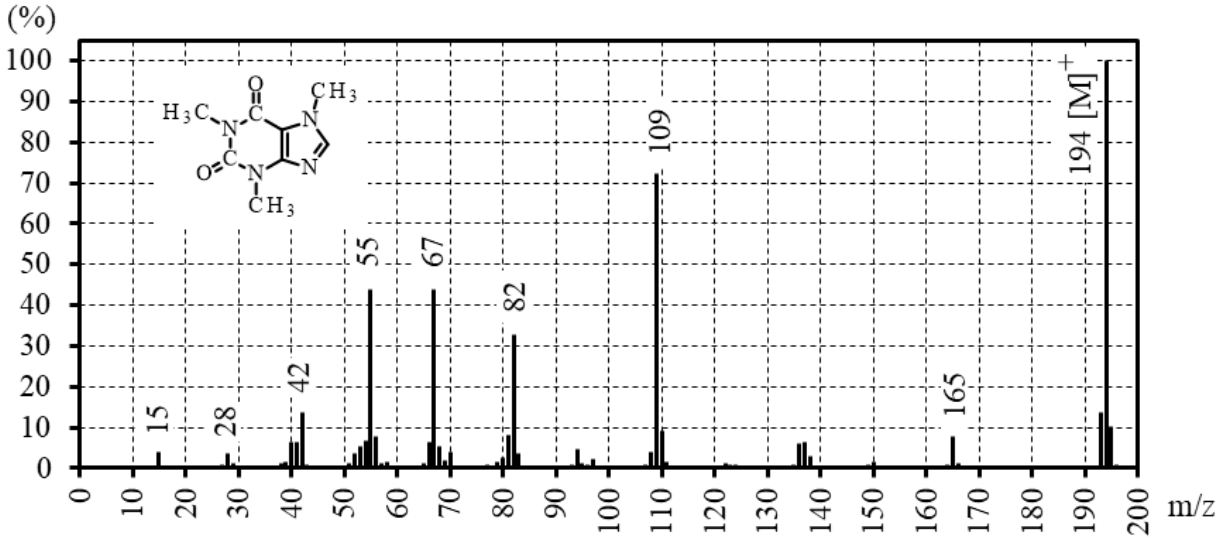

Butabarbital - CAS 125-40-6 - EI - NIST 352195



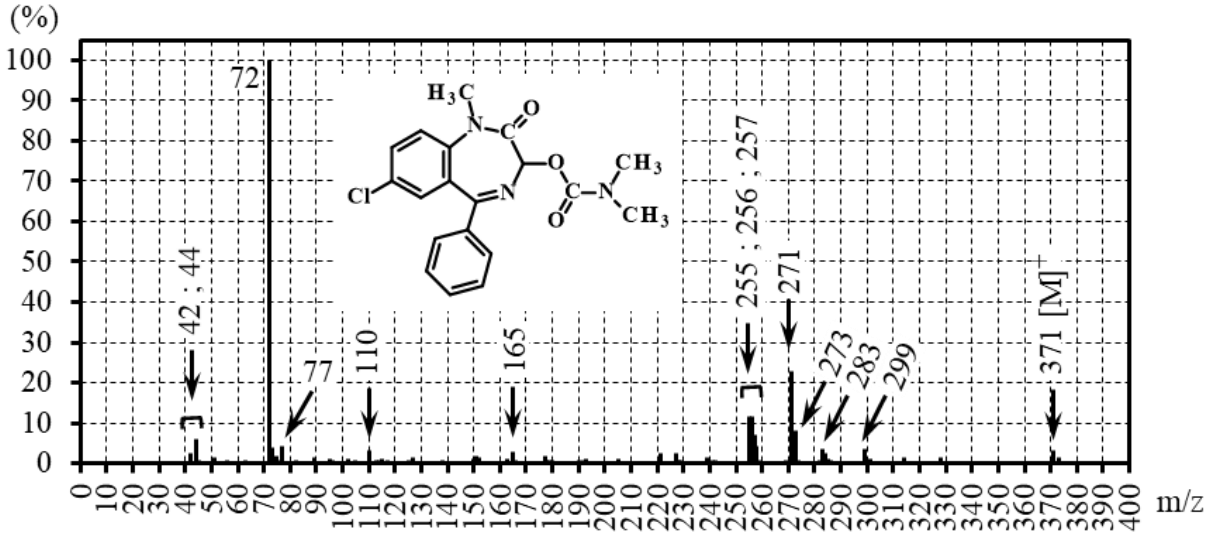

Butetamate - CAS 14007-64-8 - EI - NIST 408309



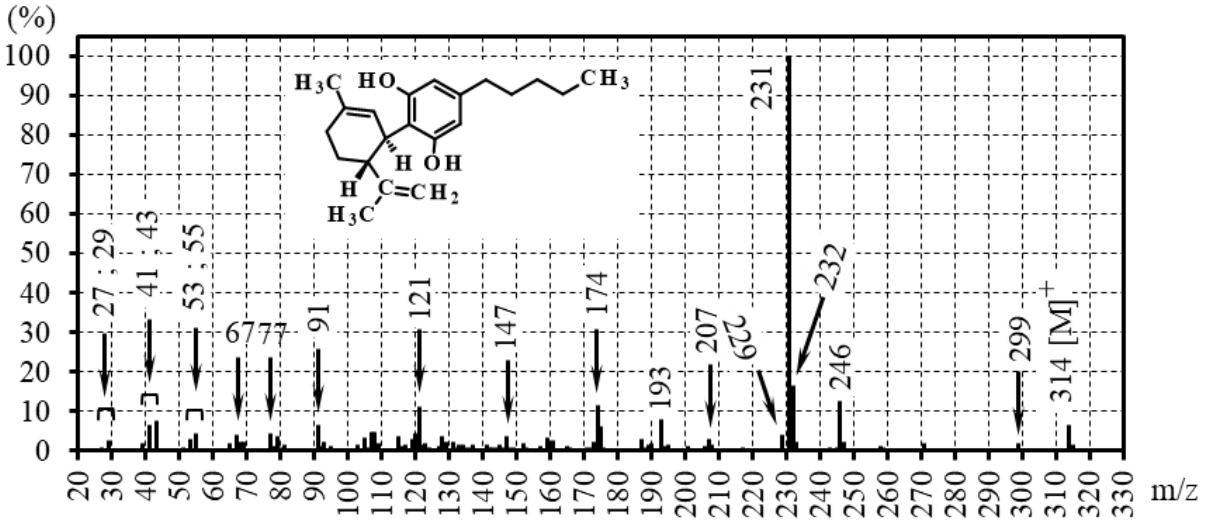

Butethal - CAS 77-28-1 - EI - NIST 352160



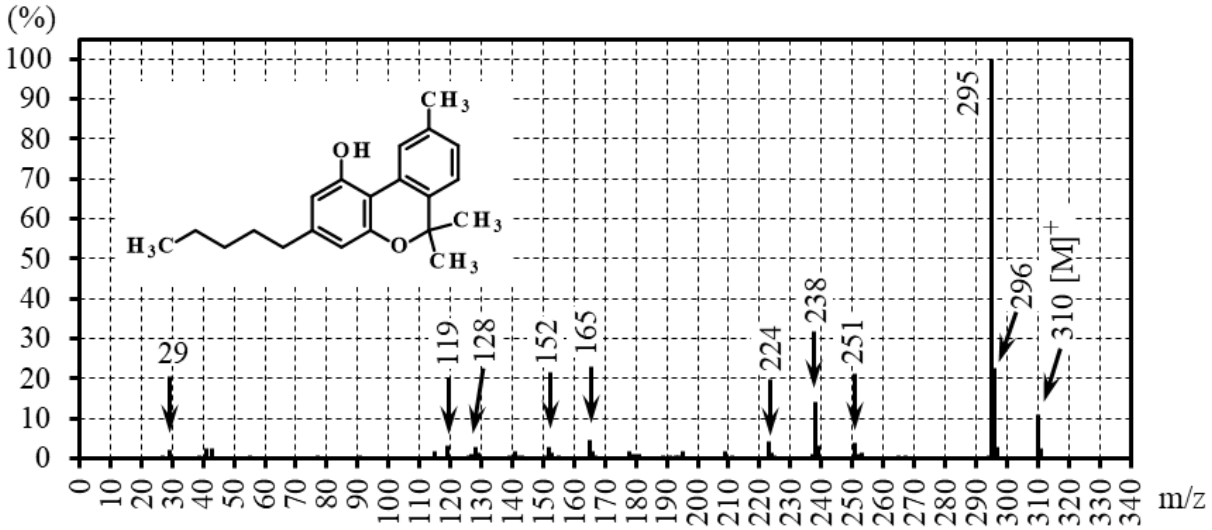

Caffeine - CAS 58-08-2 - NIST nr 290714 - EI - 70 eV



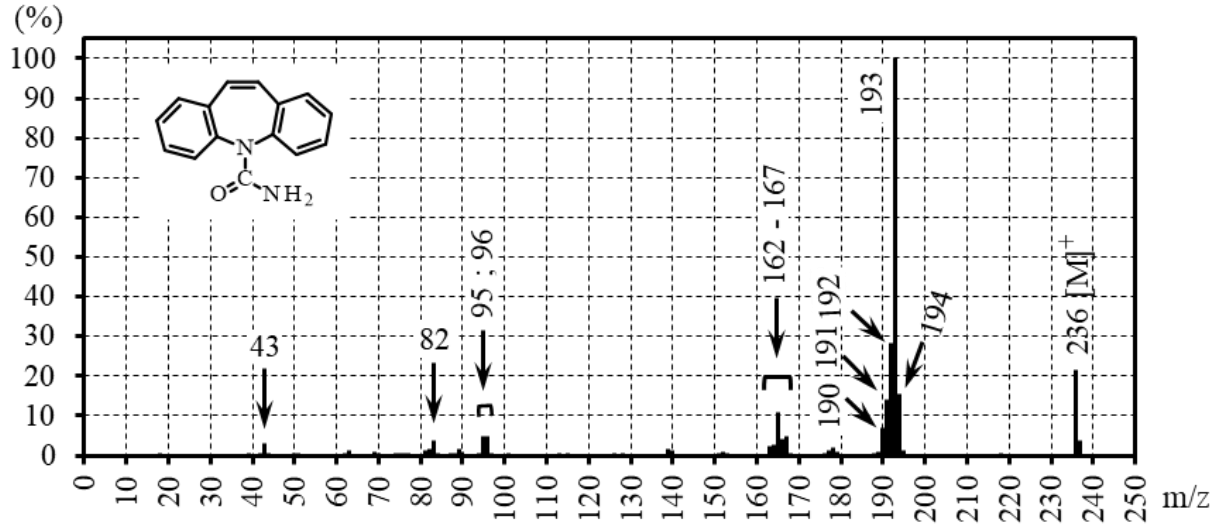

Camazepam - CAS 36104-80-0 - EI - NIST 248869



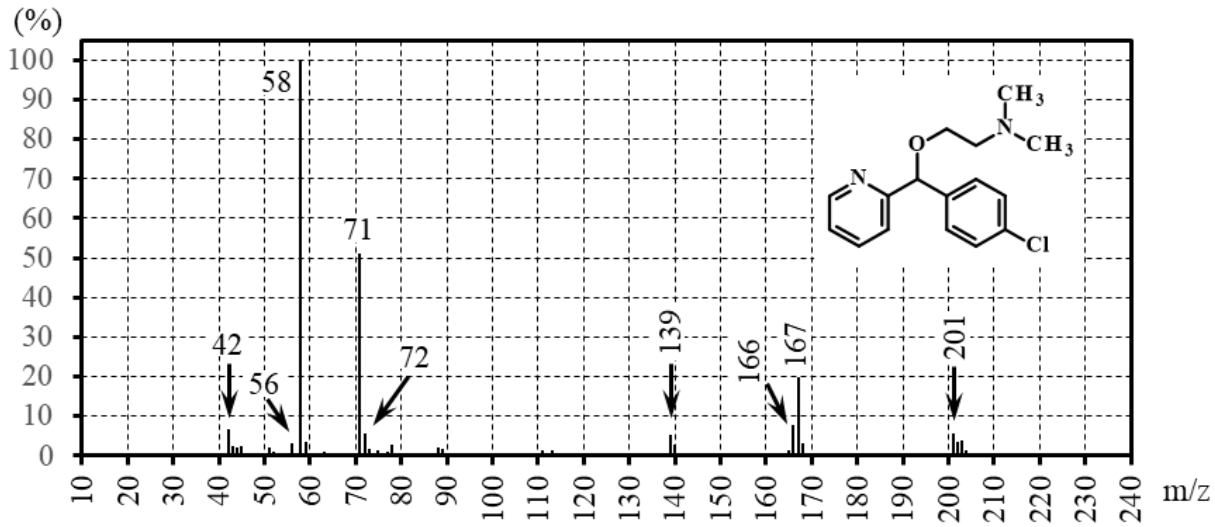

Cannabidiol - CAS 13956-29-1 - NIST 352192



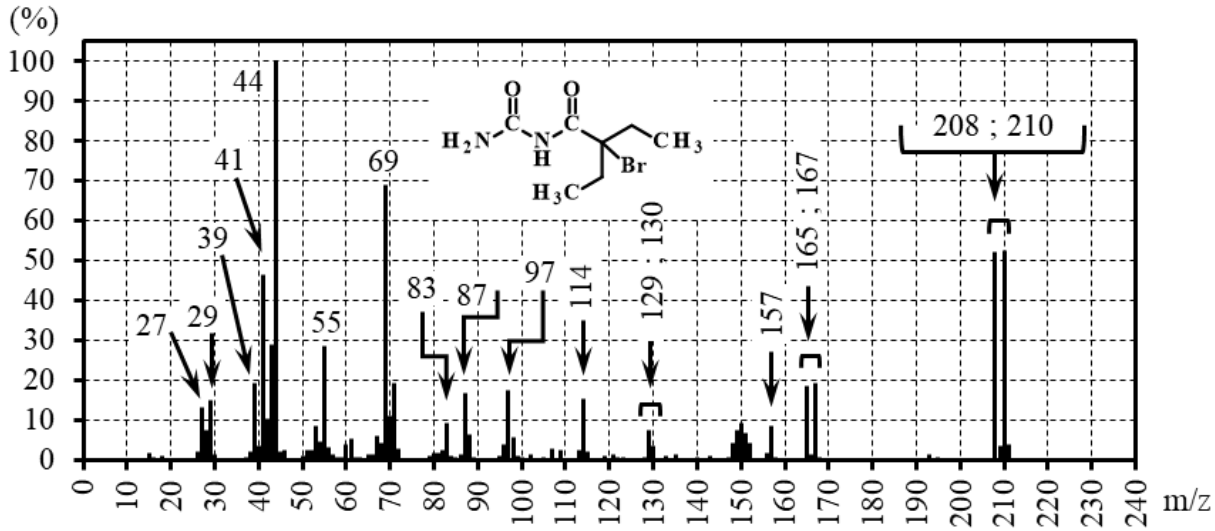

Cannabinol - CAS 521-35-7 - EI - NIST 352944



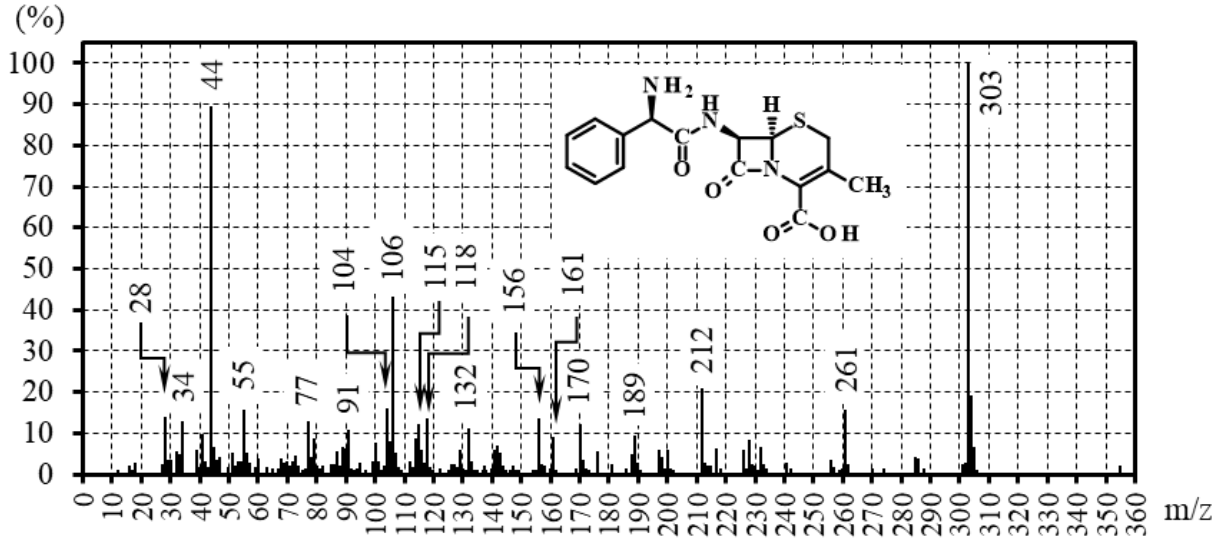

Carbamazepine - CAS 298-46-4 - EI - NIST 236284



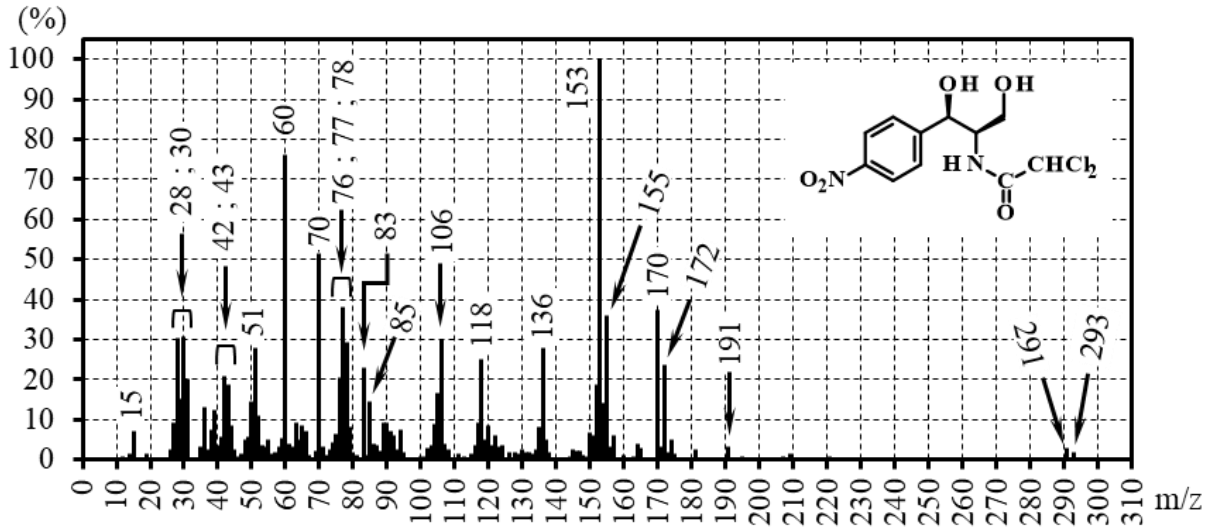

Carbinoxamine - CAS 486-16-8 - EI - NIST 334889



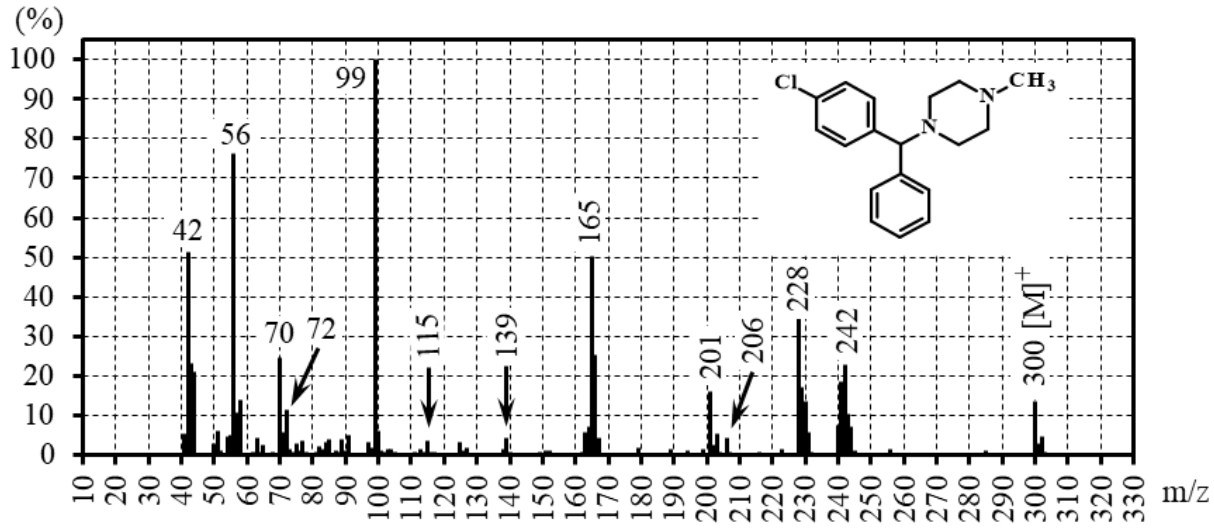

Carbromal - (Bromadal , Pinadalin) - CAS 77-65-6 - EI - NIST 250698



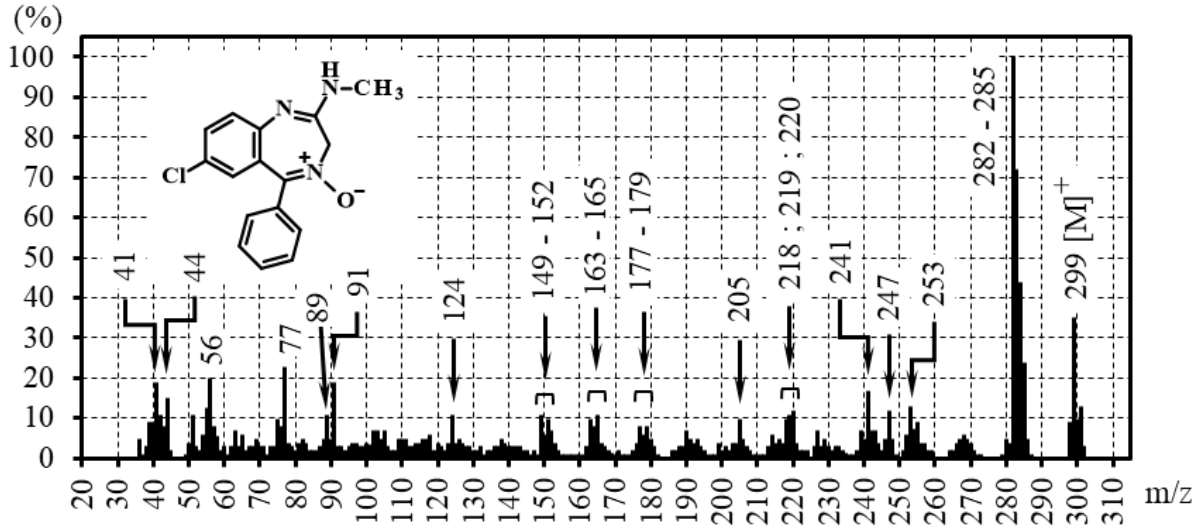

Cefalexin (Cephalexin) - CAS 15686-71-2 - EI 75 eV - SDBS nr. 14015



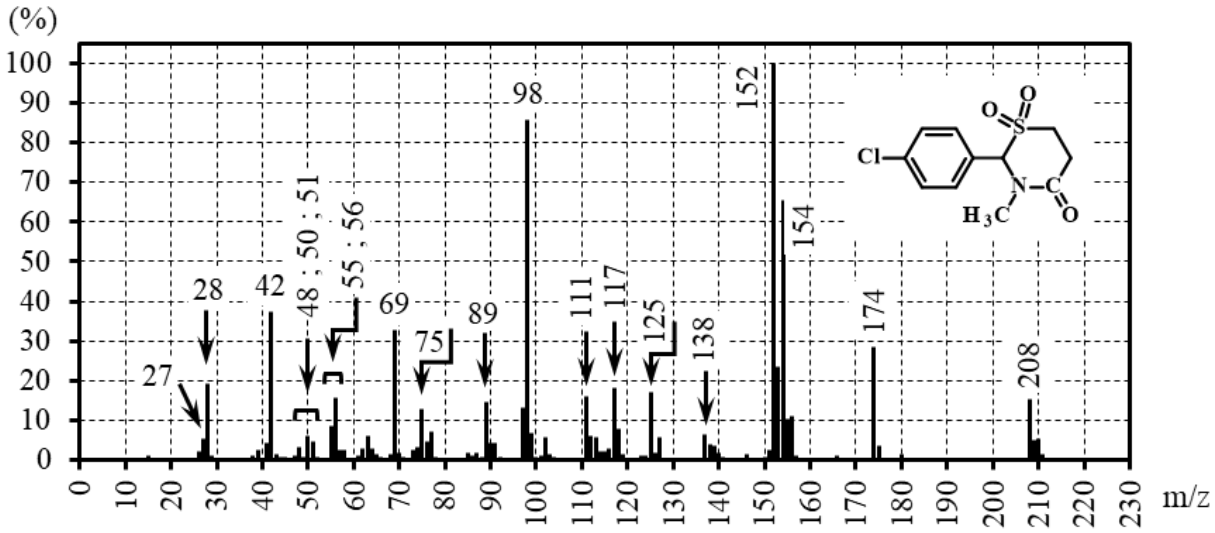

Chloramphenicol - CAS 56-75-7 - E - NIST 52747



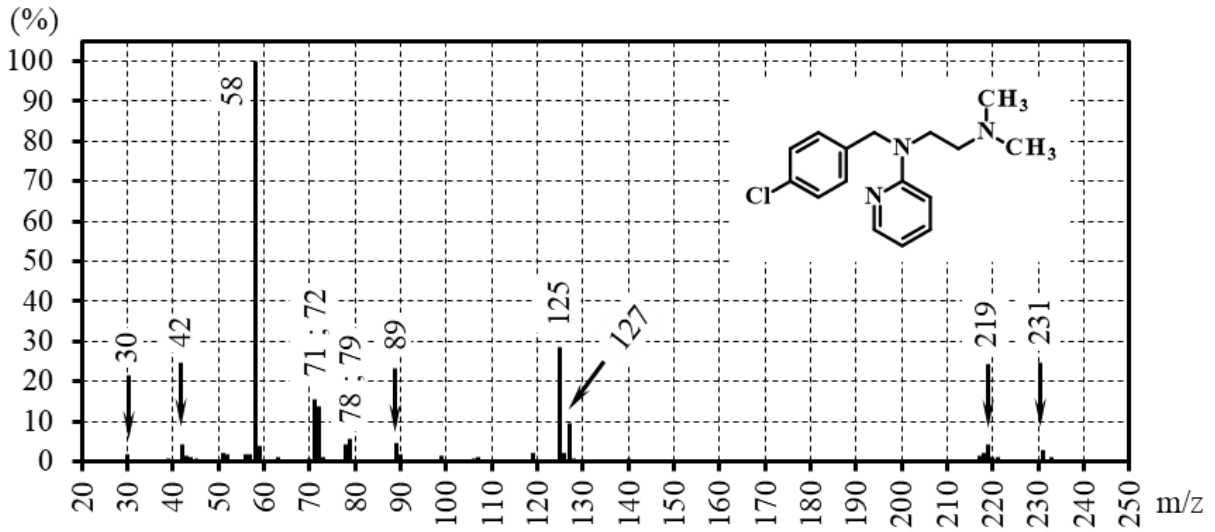

Chlorcyclizine - CAS 82-93-9 - EI - NIST 247749



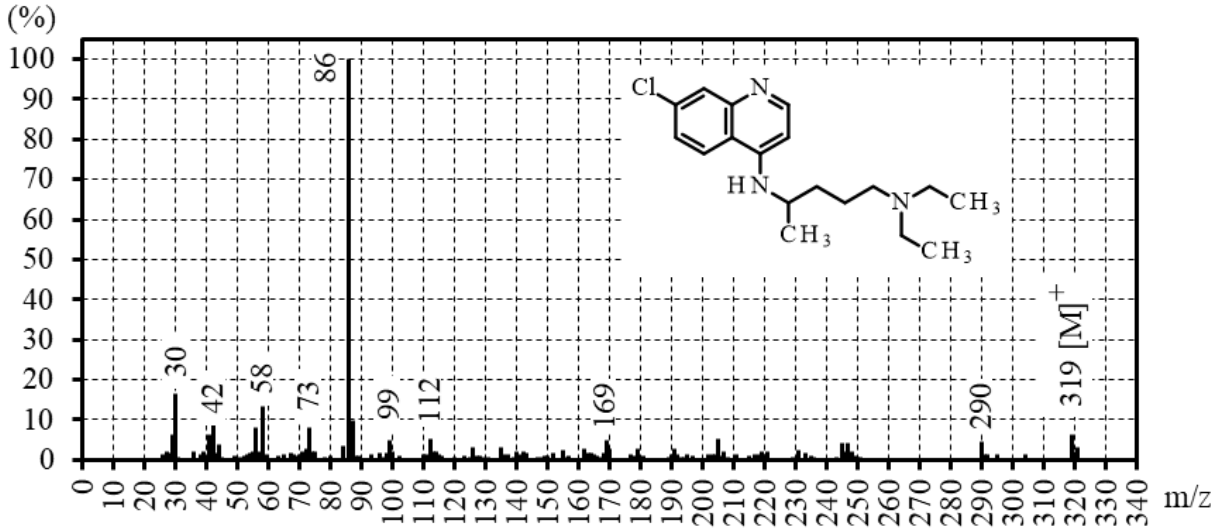

Chlordiazepoxide - CAS 58-25-3 - NIST 14316



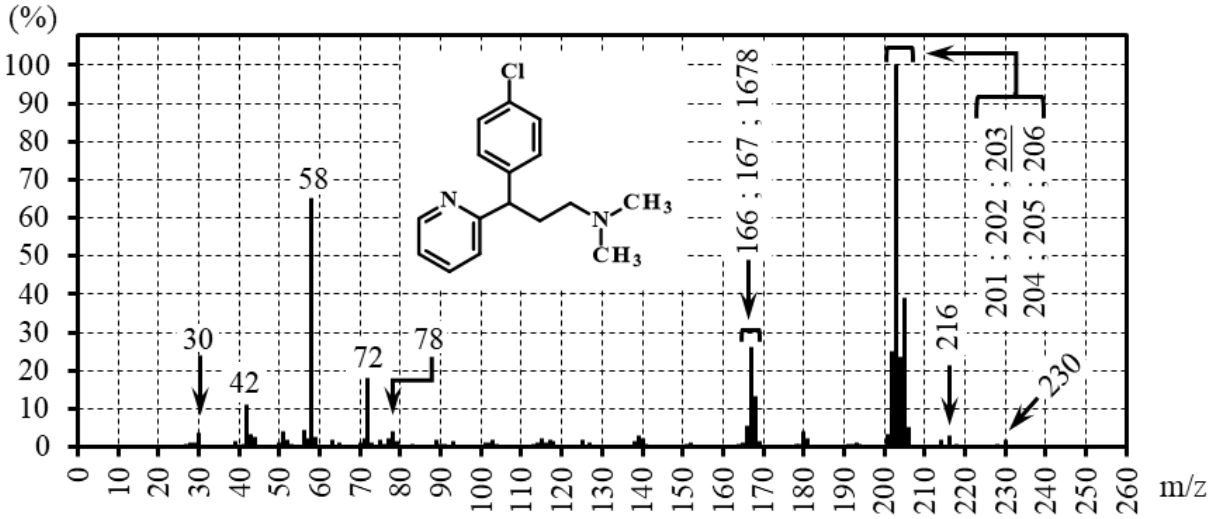

Chlormezanone - CAS 80-77-3 - EI - NIST 408569



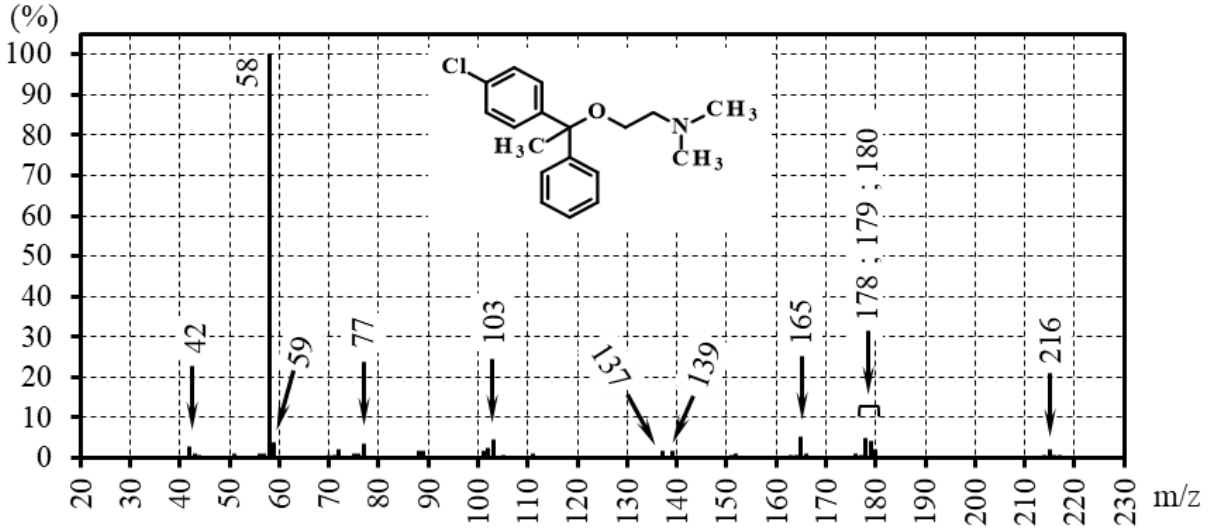

Chloropyramine - CAS 59-32-5 - NIST 417475



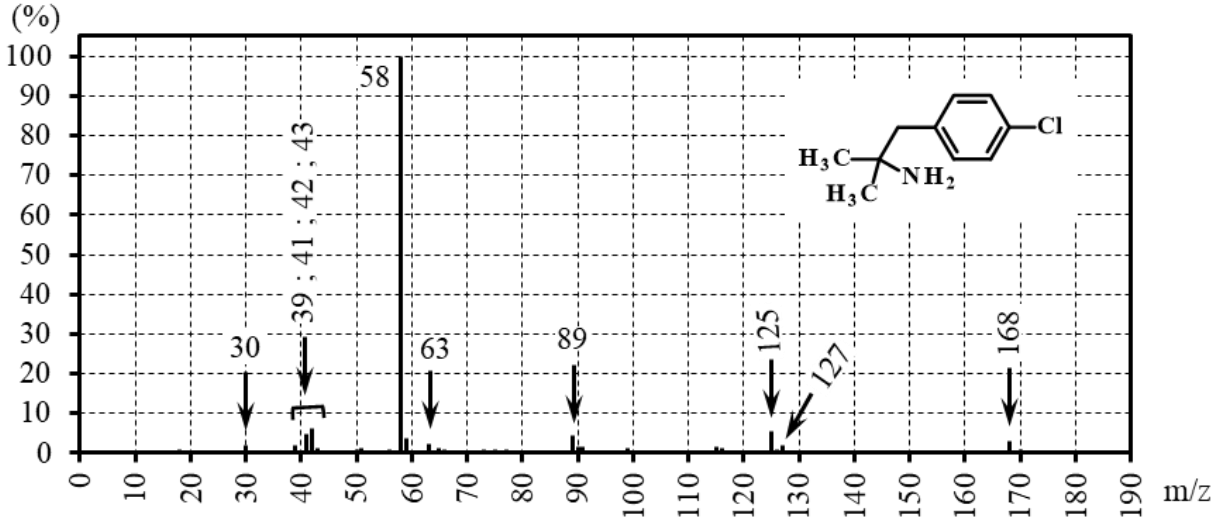

Chloroquine - CAS 54-05-7 - NIST 42361



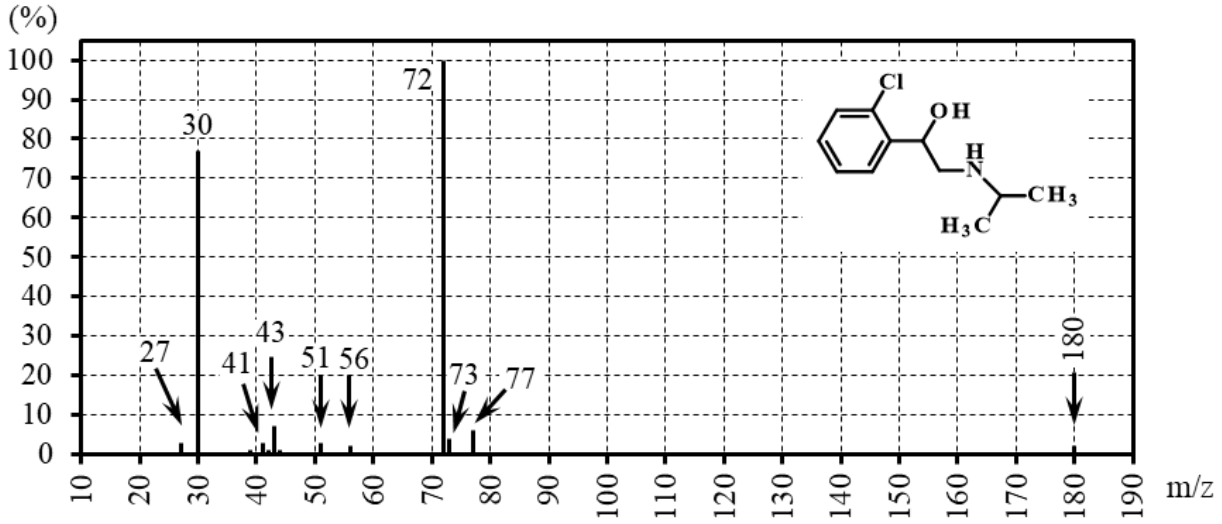

Chlorphenamine - CAS 132-22-9 - EI - NIST 342101



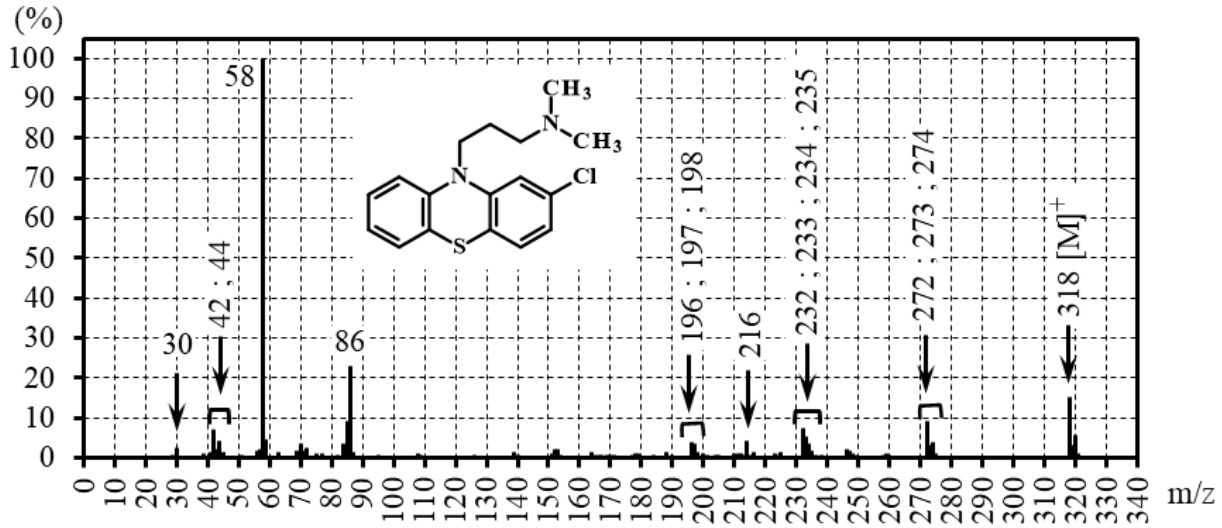

Chlorphenoxamine - CAS 77-38-3 - NIST 246811



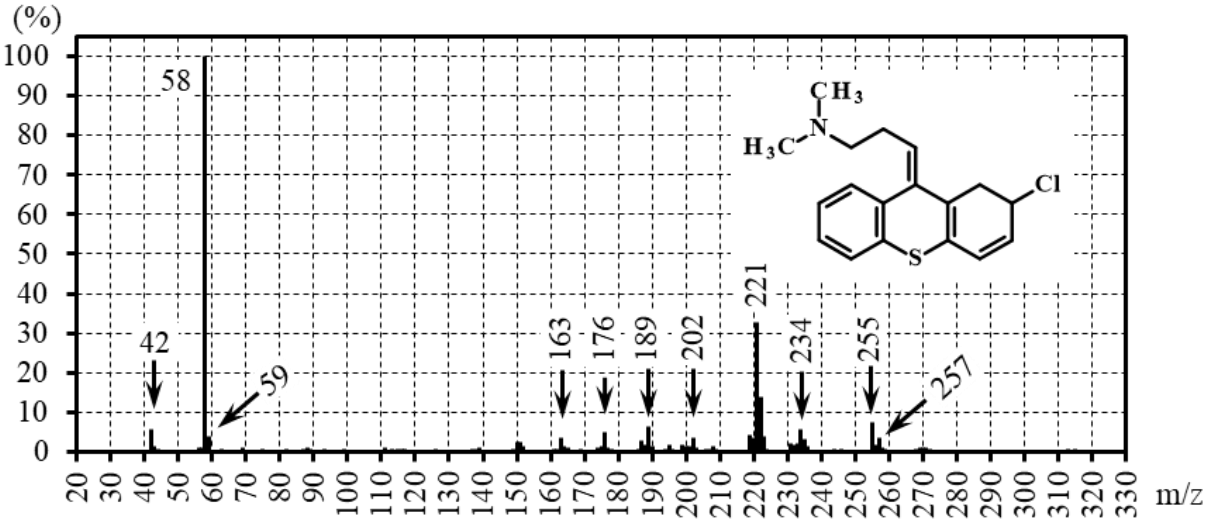

Chlorphentermine - CAS 461-78-9 - EI - NIST 408641



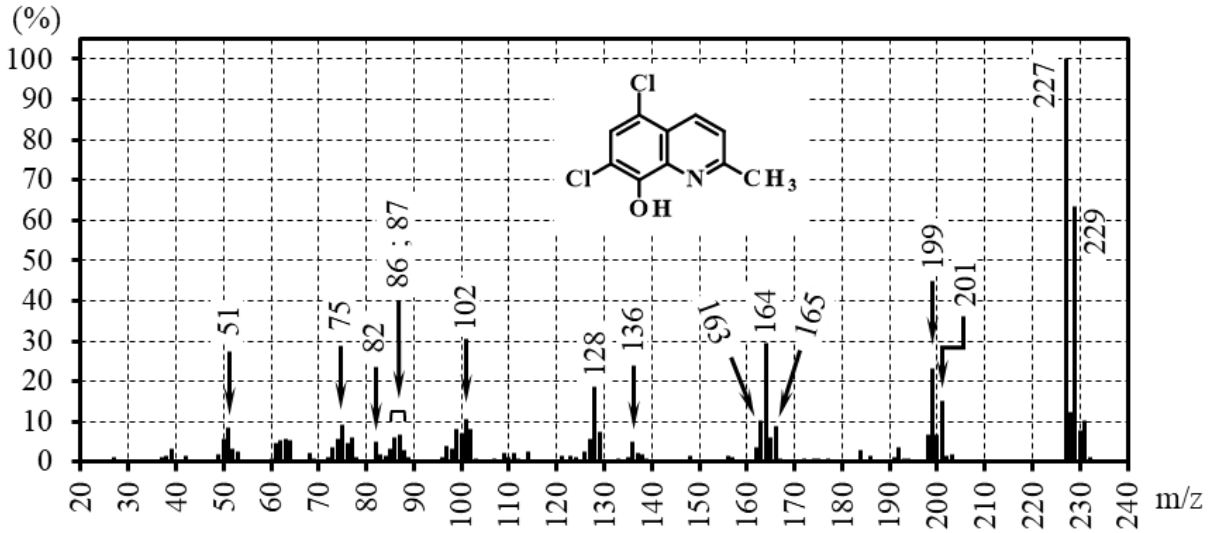

Chlorprenaline - CAS 3811-25-4 - EI - NIST 298621



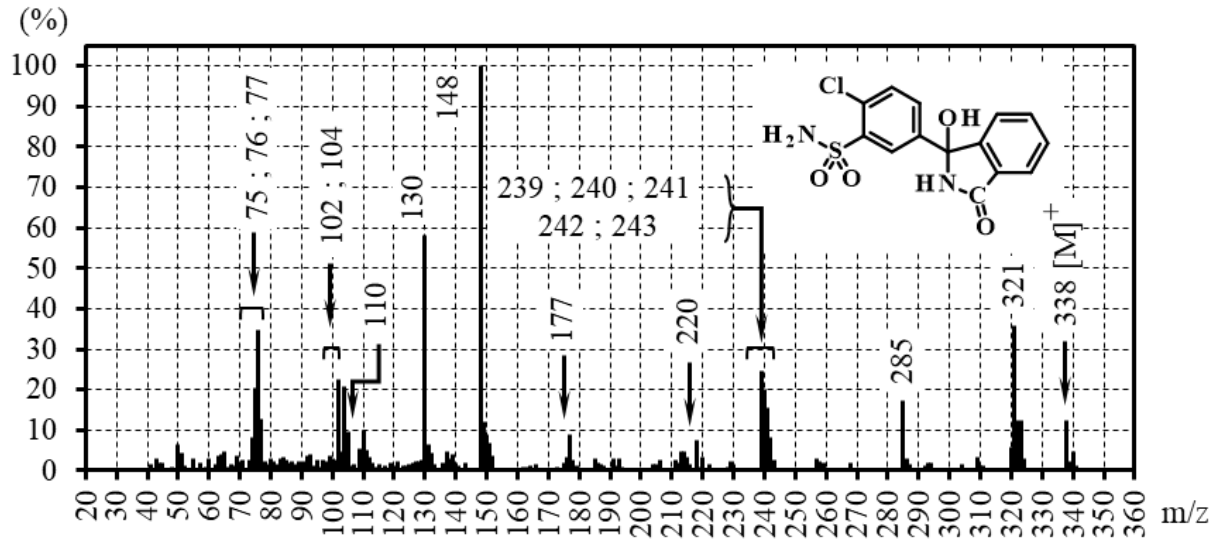

Chlorpromazine - CAS 50-53-3 = EI - NIST 291119



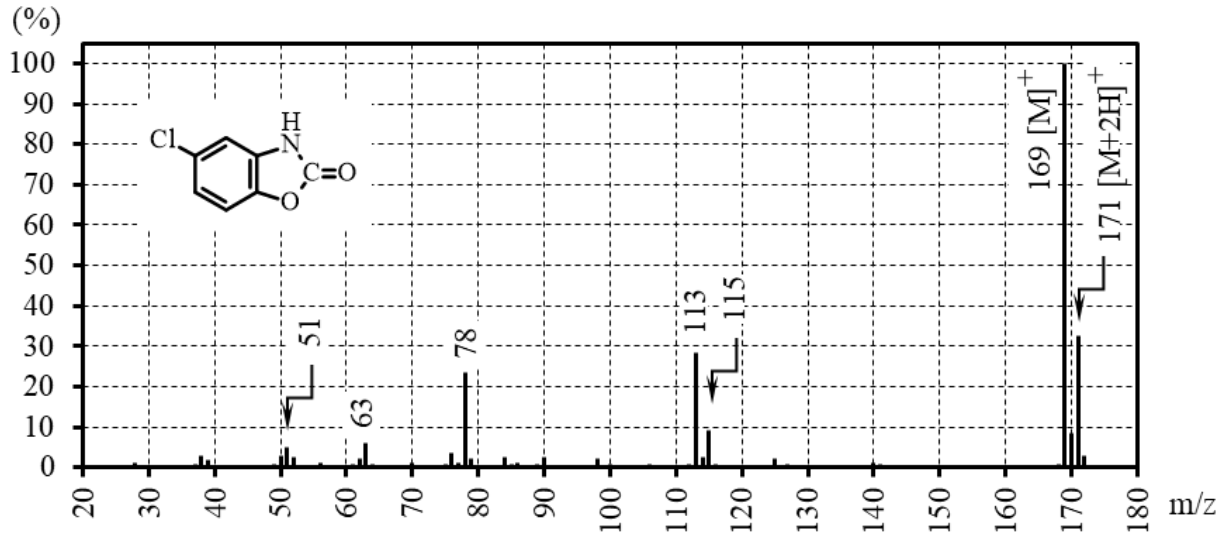

Chlorprothixene - CAS 113-59-7 - EI - NIST 247780



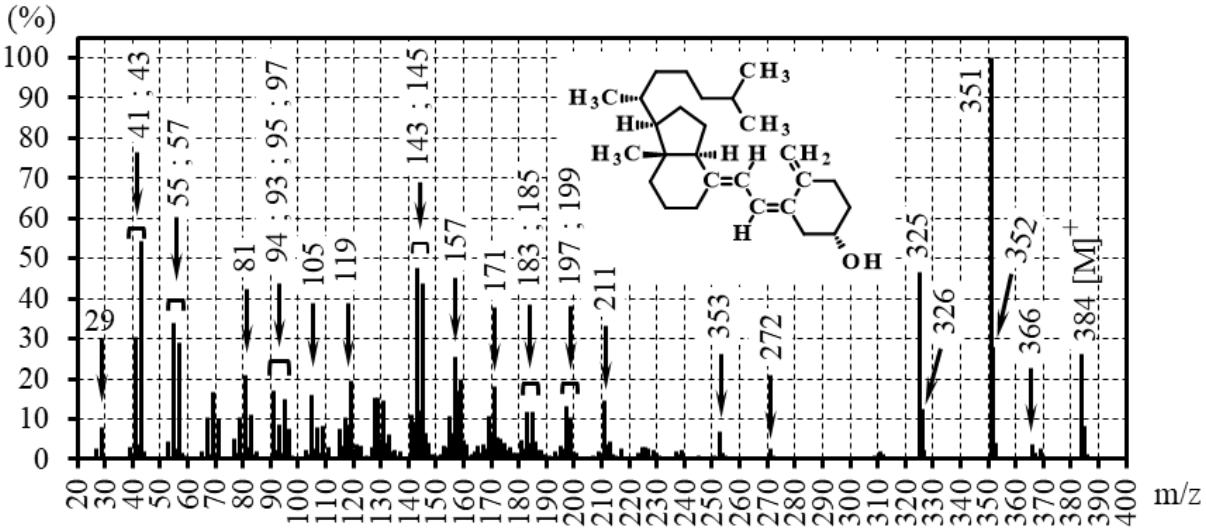

Chlorquinaldol - CAS 72-80-0 - NIST 292063



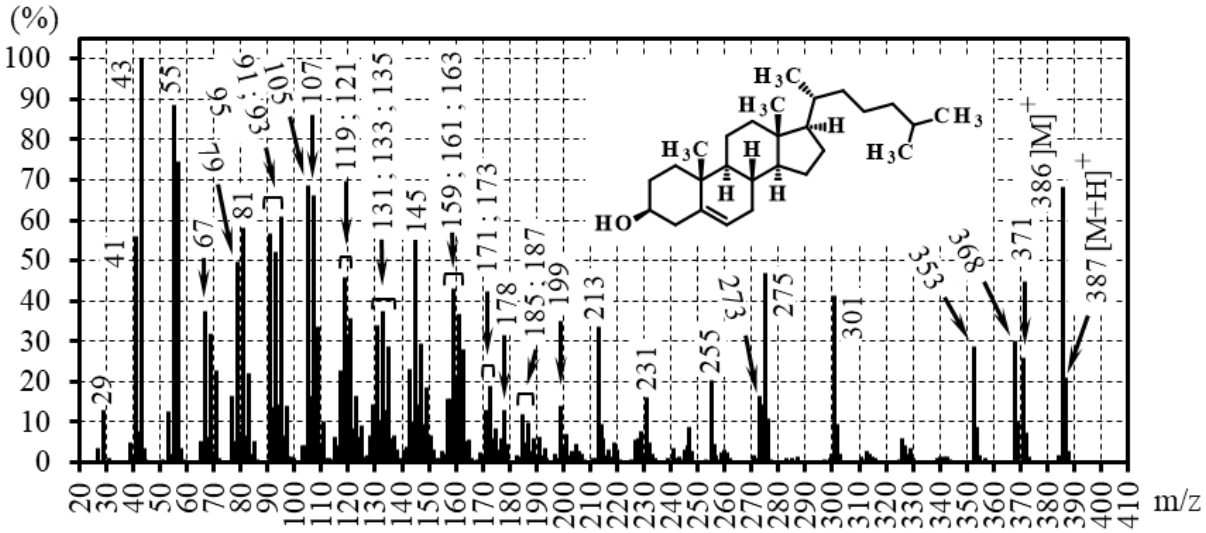

Chlortalidone - CAS 77-36-1 - NIST 246980



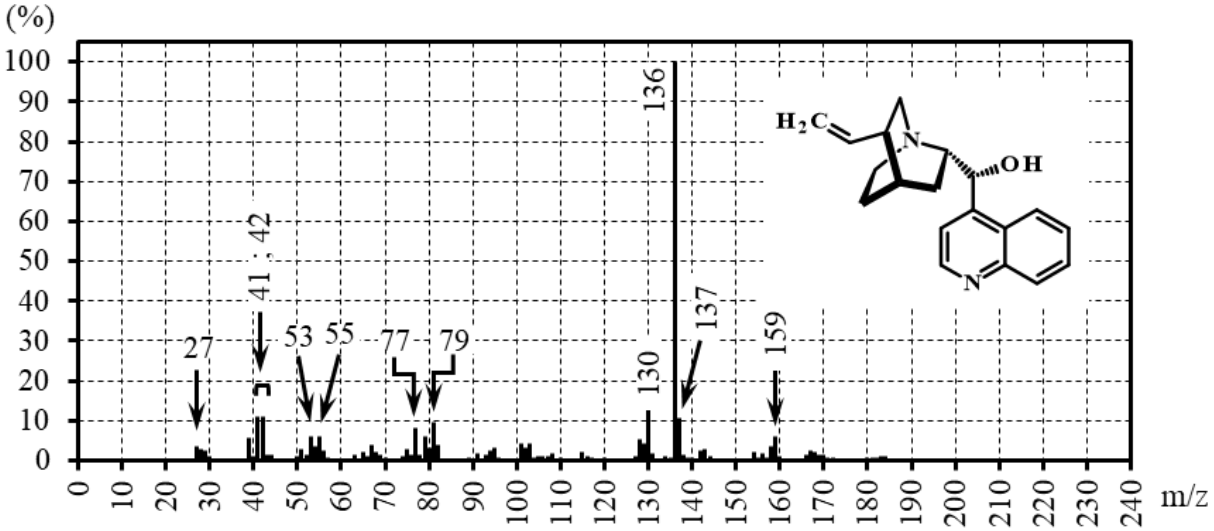

Chlorzoxazone - CAS 95-25-0 - NIST 239377



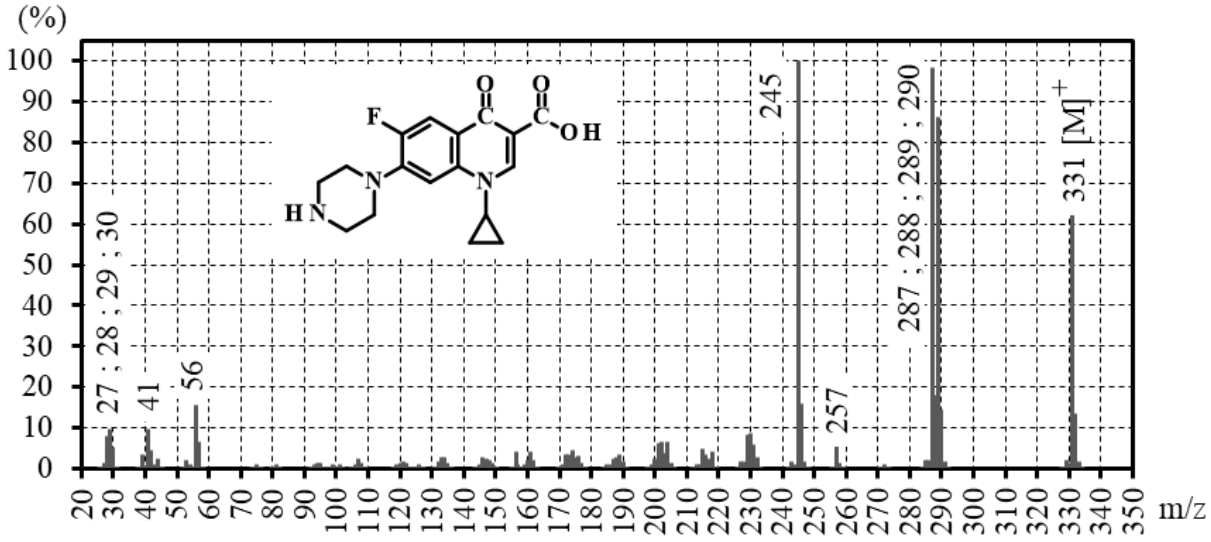

Cholecalciferol - CAS 67-97-0 - NIST 332995



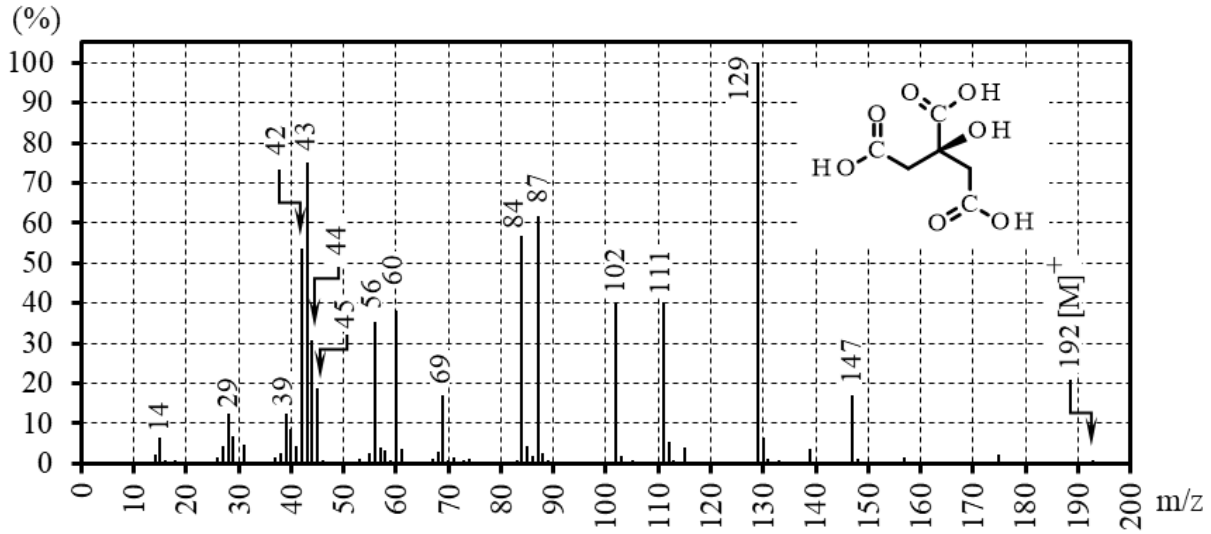

Cholesterol - CAS 57-88-5 - NIST 332884



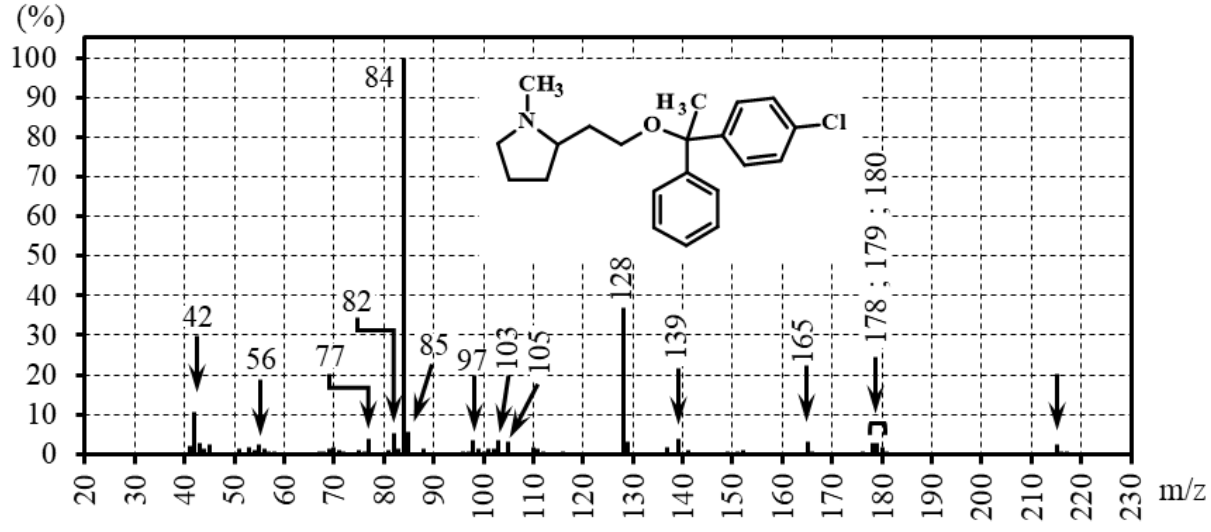

Cinchonidine - CAS 485-71-2 - EI - NIST 235882



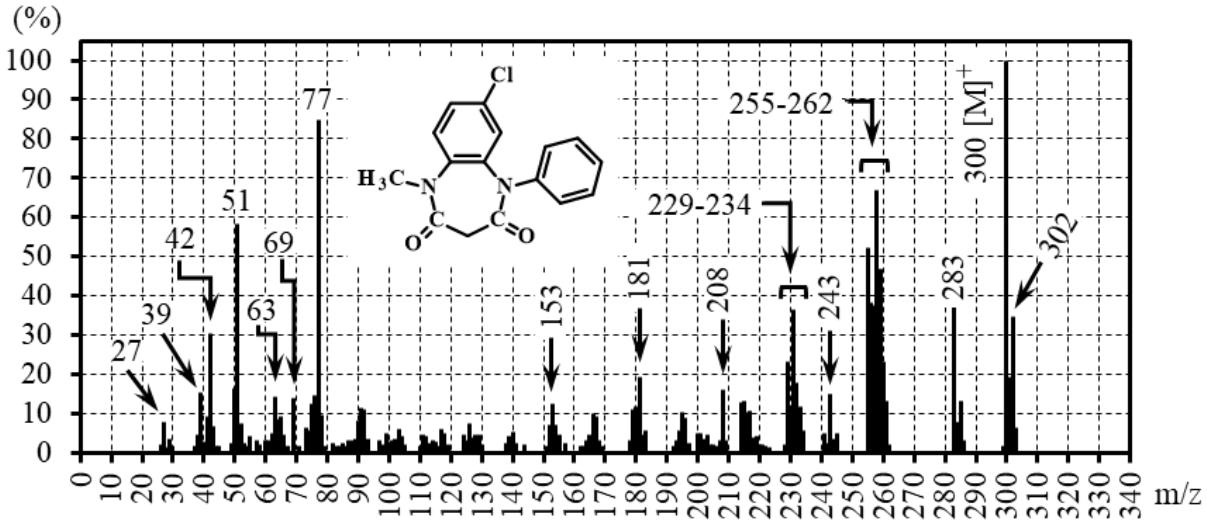

Ciprofloxacin - CAS 85721-33-1 - EI 70 eV - SDBS 53251 - 250 °C , 20 °C



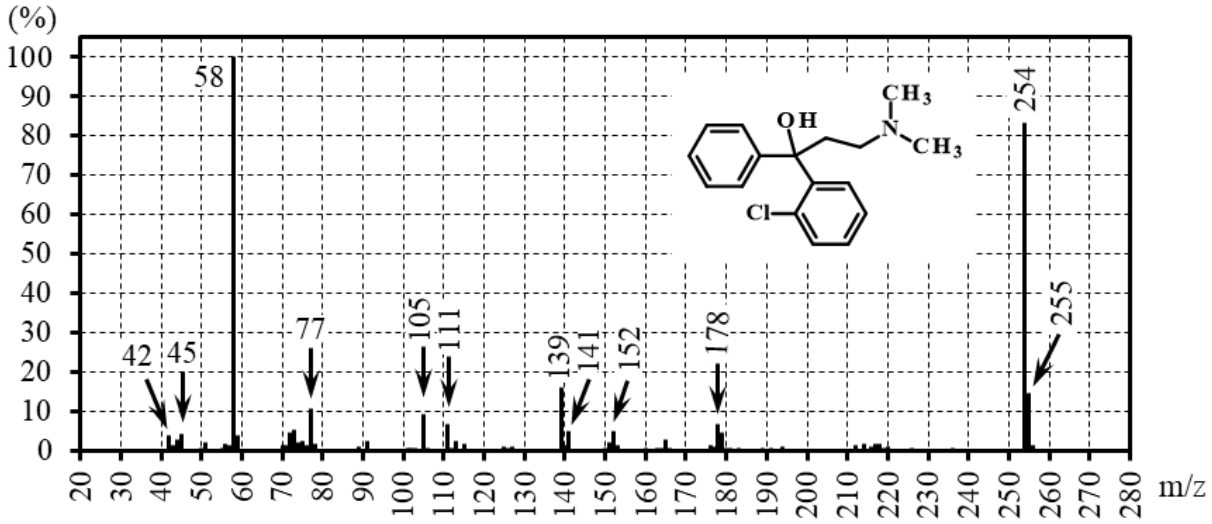

Citric acid - CAS 77-92-9 - EI - NIST 22892



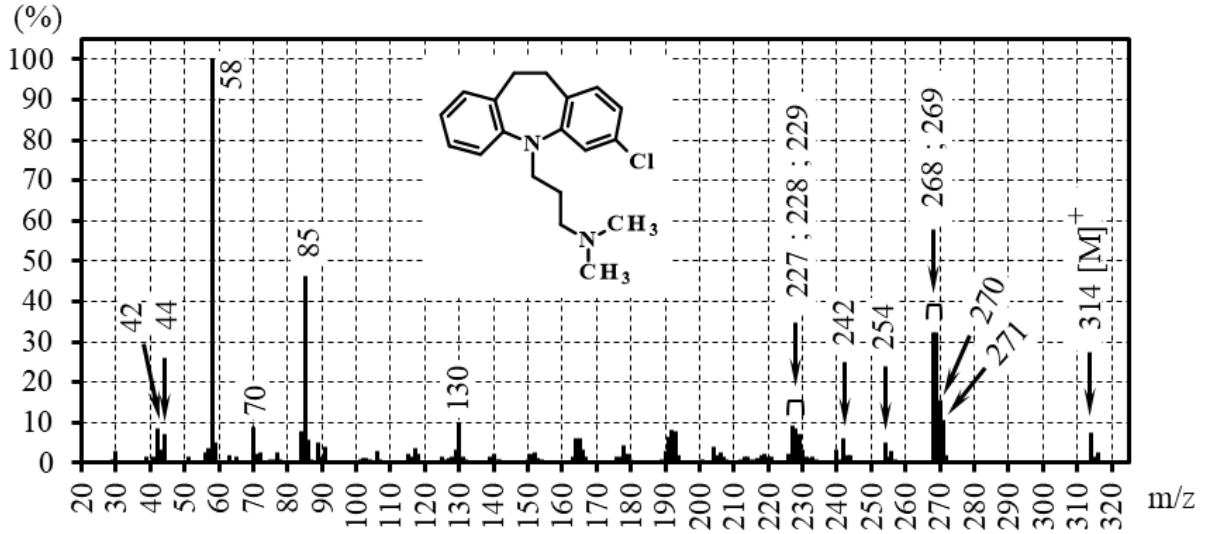

Clemastine - CAS 15686-51-8 - EI - NIST 247788



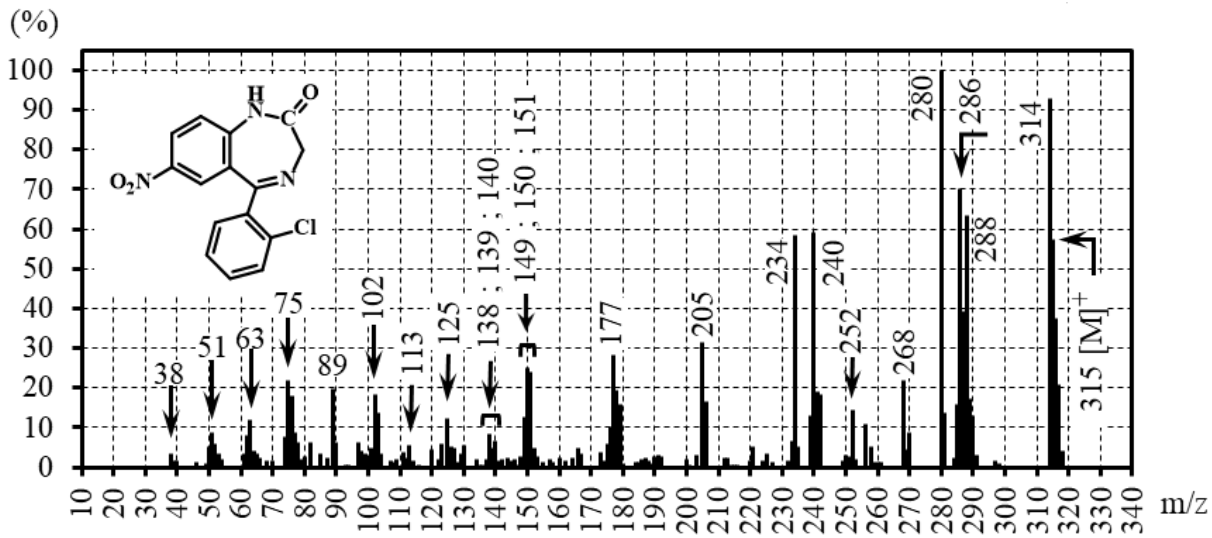

Clobazam - CAS 22316-47-8 - EI - NIST 107121



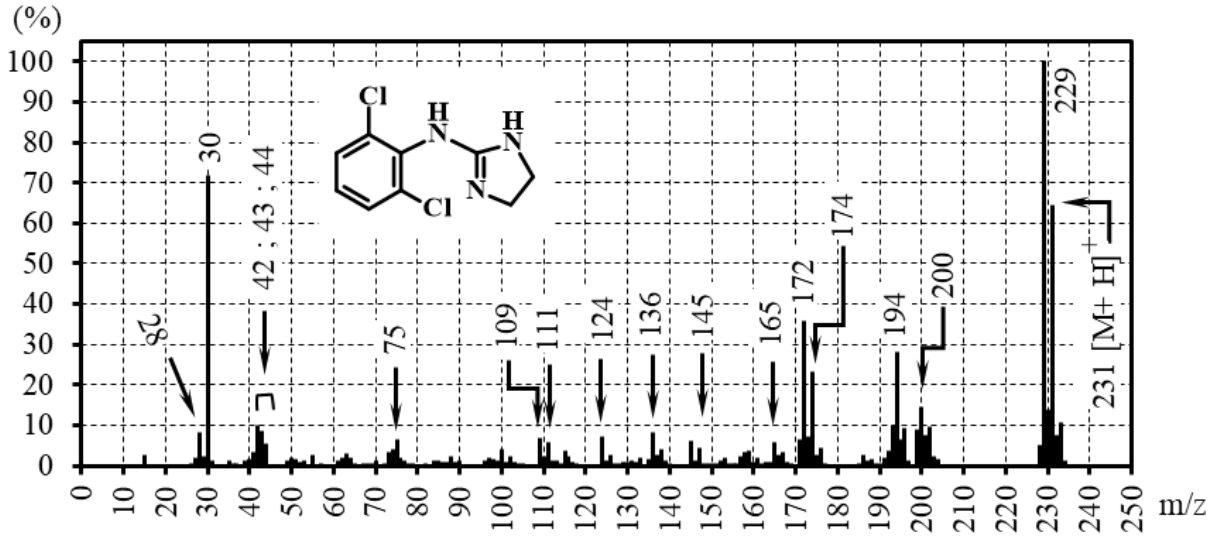

Clofedanol - CAS 791-35-5 - EI - NIST 248307



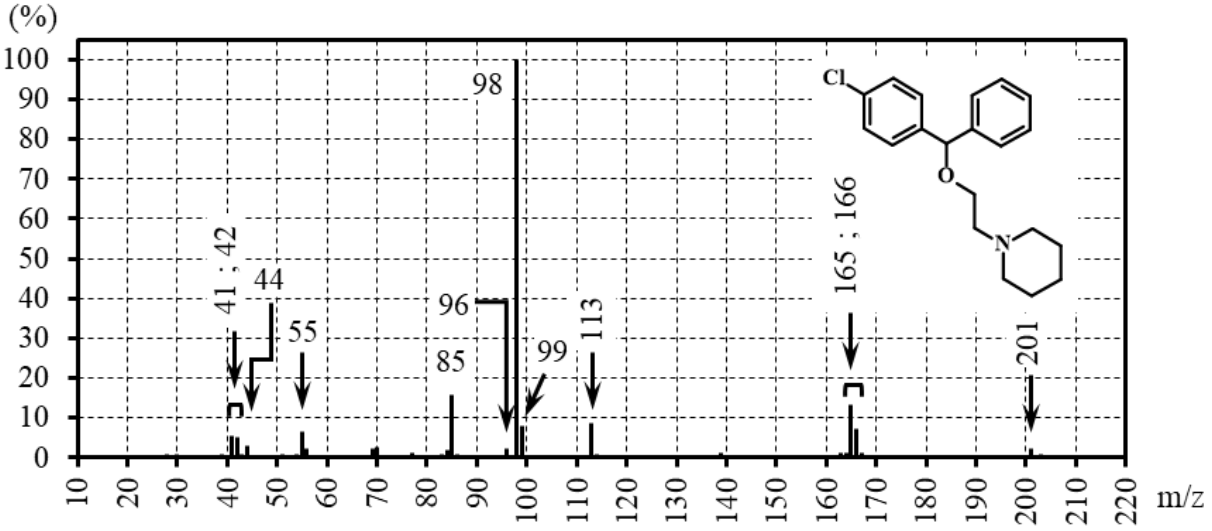

Clomopramine - CAS 303-49-1 - NIST 408658



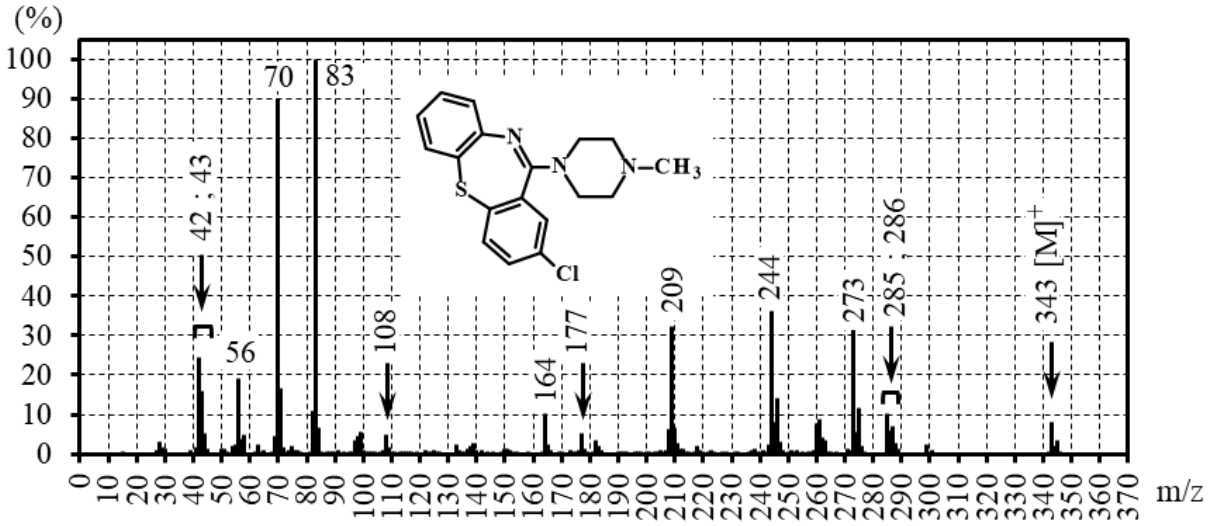

Clonazepam - CAS 1622-61-3 - EI - NIST 312384



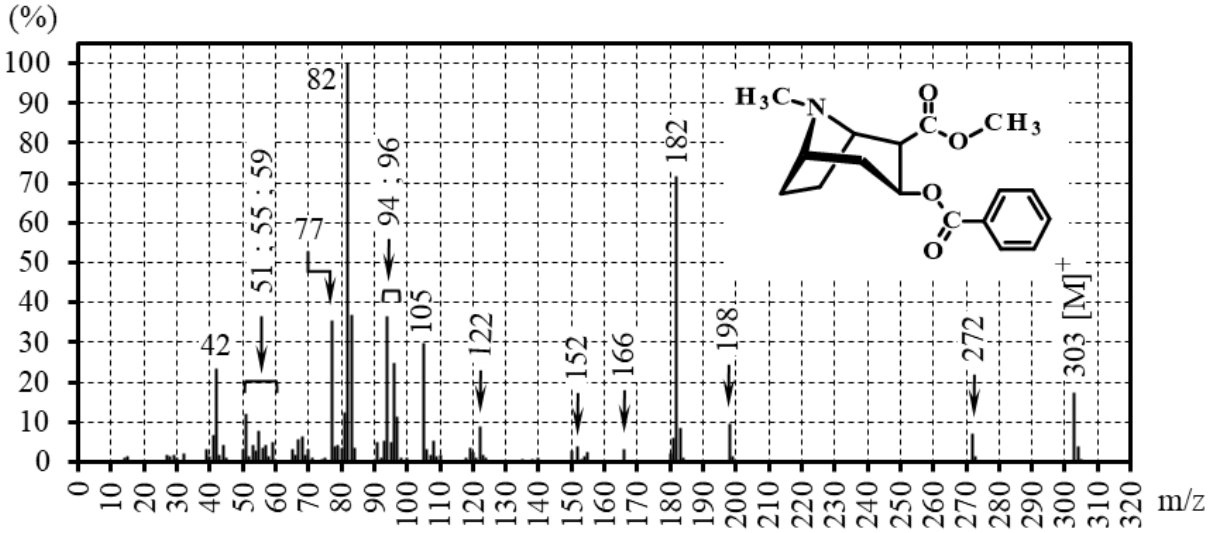

Clonidine - CAS 4205-90-7 - NIST 233859



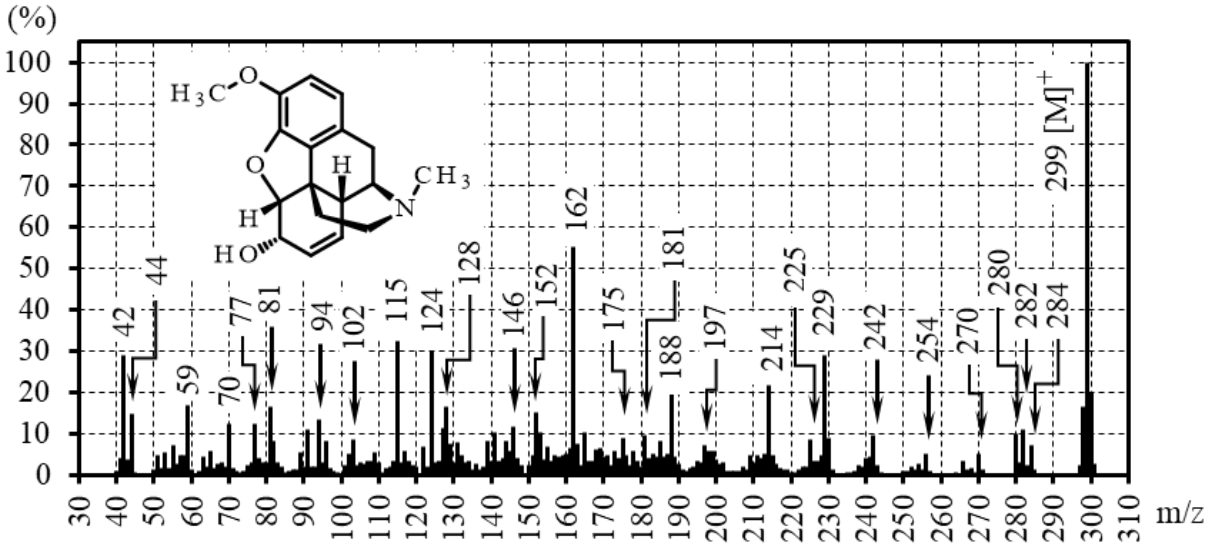

Cloperastine - CAS 3703-76-2 - EI - NIST 292020



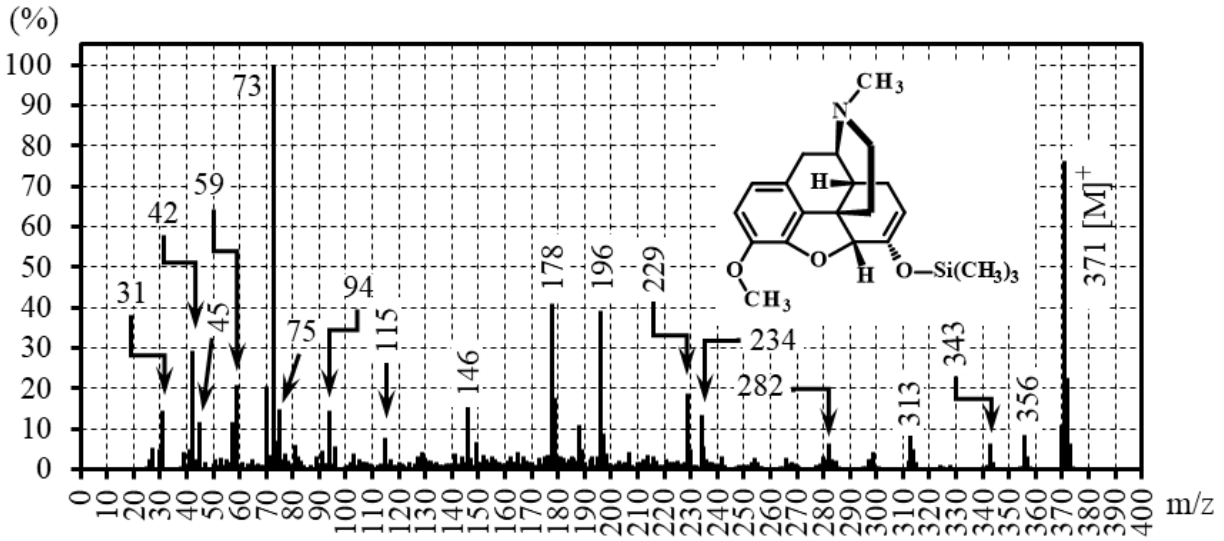

Clotiapine - CAS 2058-52-8 - EI - NIST 408767



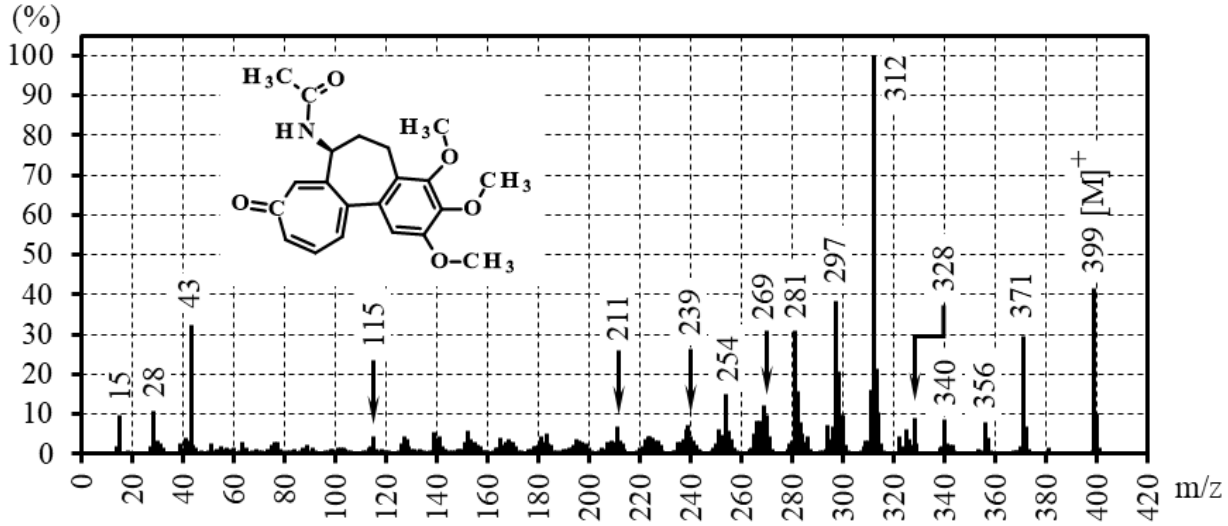

Cocaine - CAS 50-36-2 - EI - NIST 113834



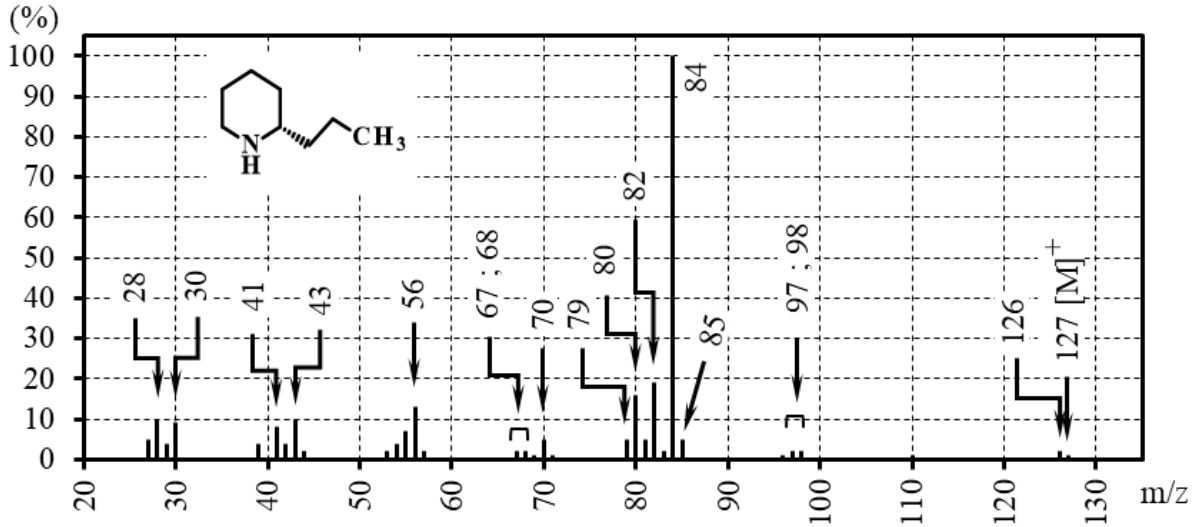

Codeine - CAS 76-57-3 - EI - NIST nr 335560



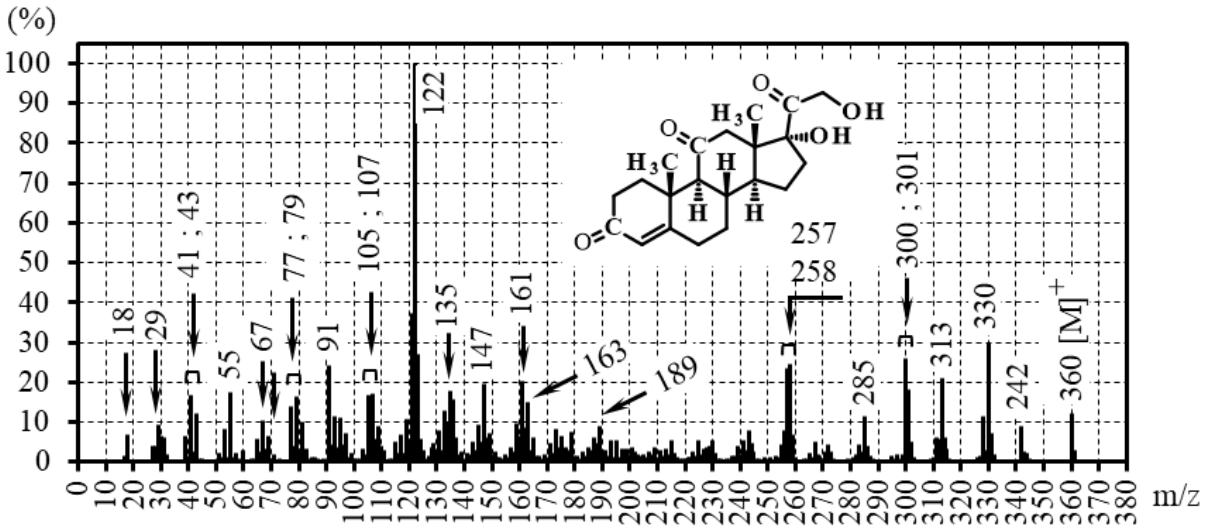

Codeine, TMS derivative - CAS 74367-14-9 - EI - NIST 107079



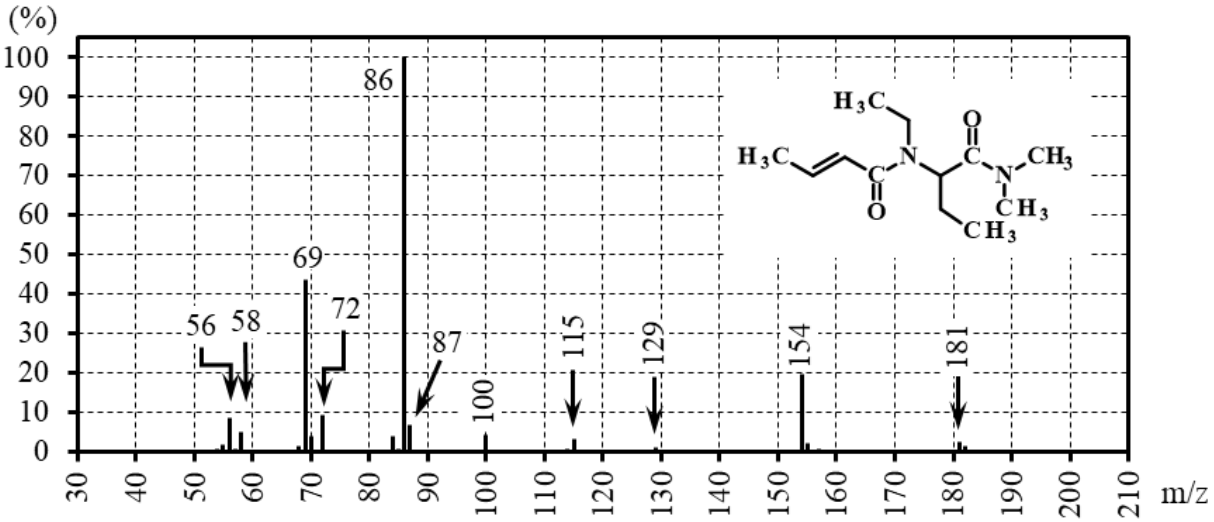

Colchicine - CAS 64-86-8 - NIST 234039



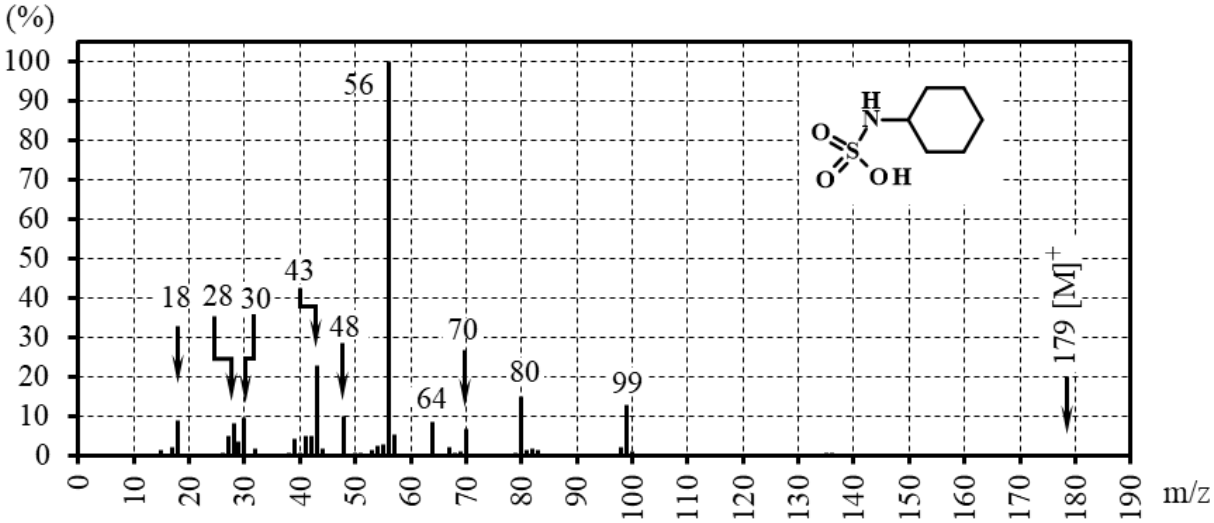

Coniine - CAS 458-88-8 - NIST 298643



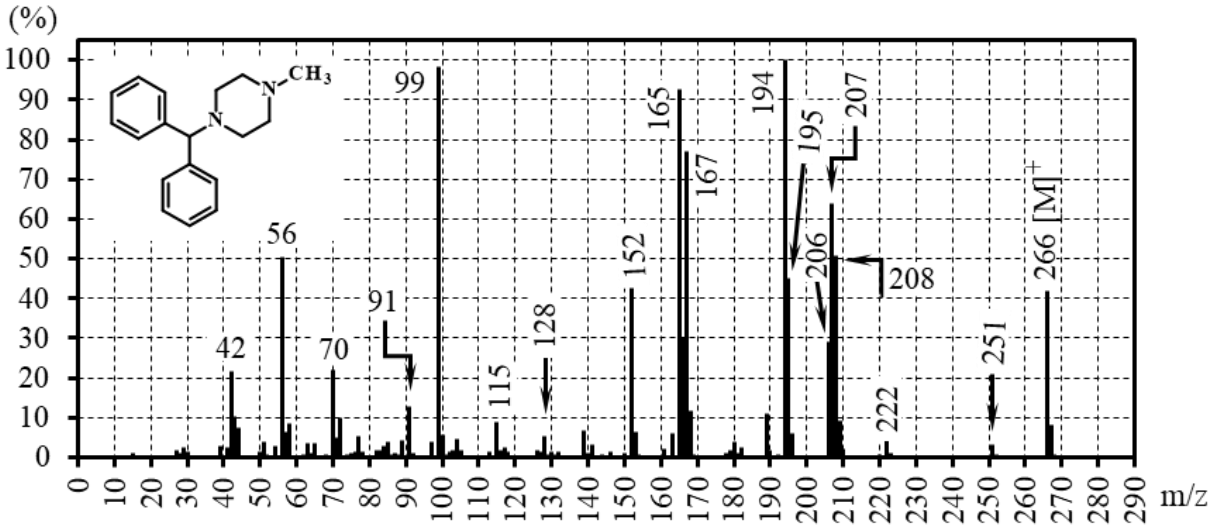

Cortisone - CAS 53-06-5 - NIST 237380



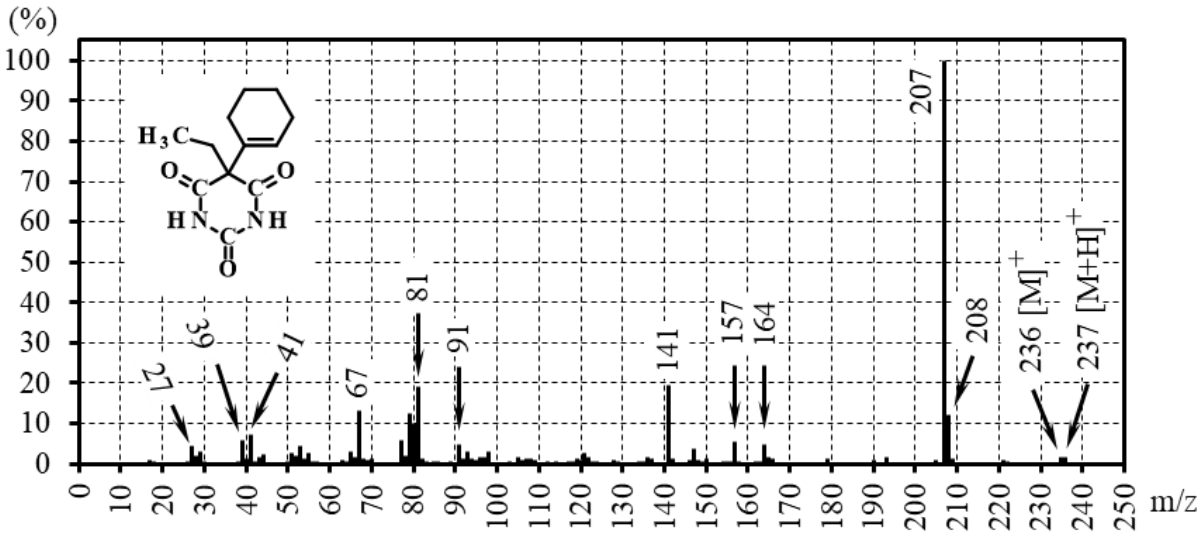

Crotetamide - CAS 6168-76-9 - EI - NIST 123836



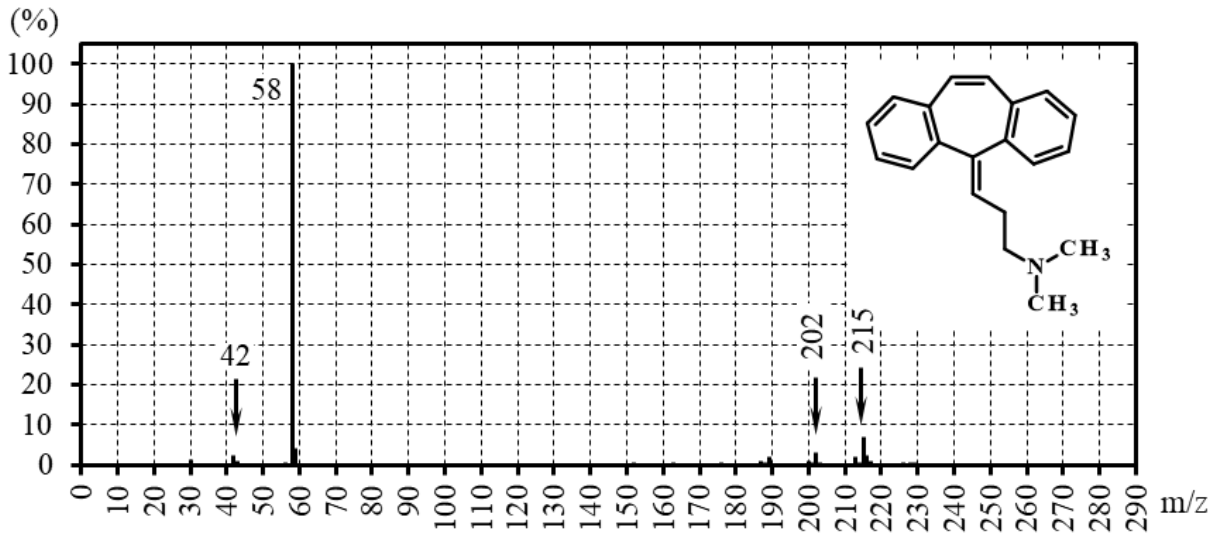

Cyclamic acid - CAS 100-88-9 - EI - NIST 230624



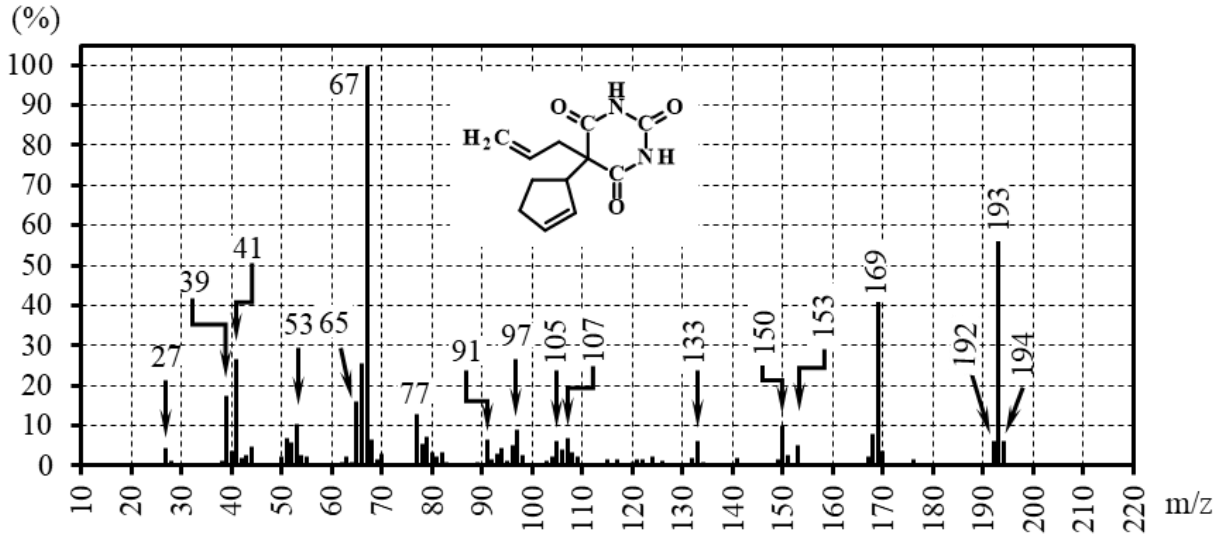

Cyclizine - CAS 82-92-8 - EI - NIST 250597



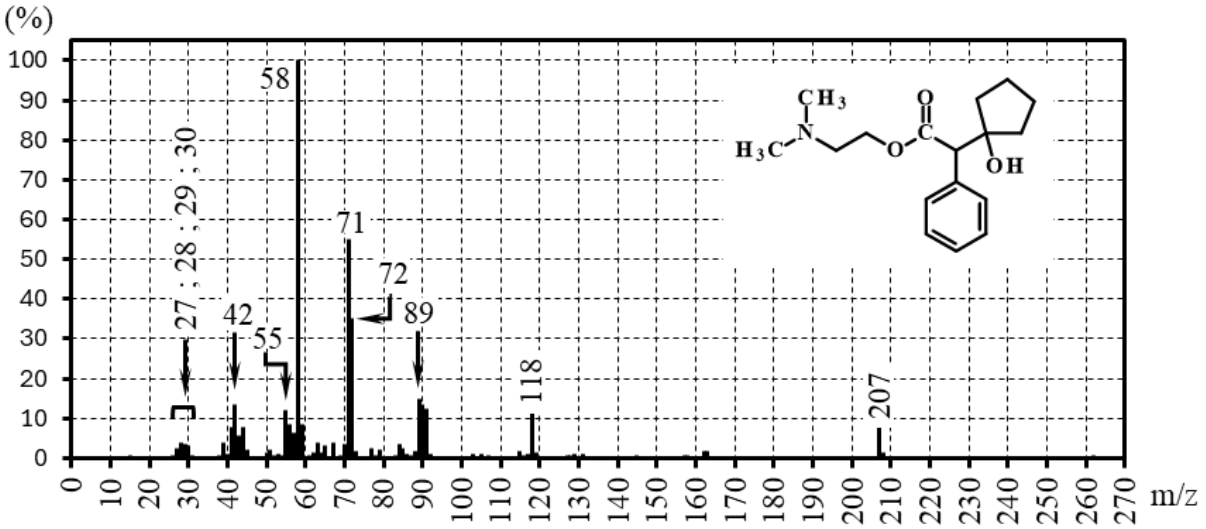

Cyclobarbital - CAS 52-31-3 - NIST 231559



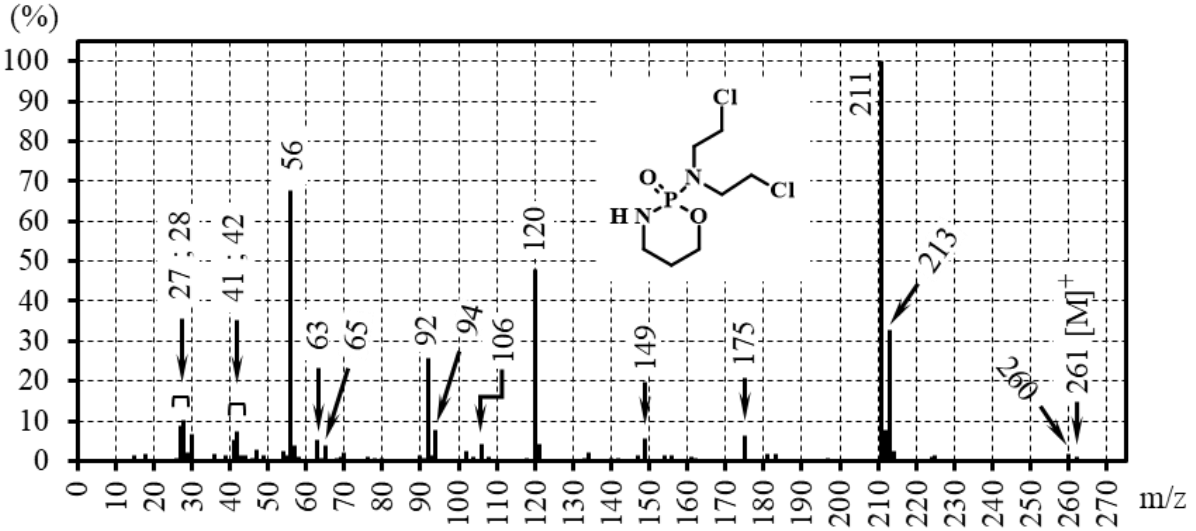

Cyclobenzaprine - CAS 303-53-7 - EI - NIST 352176



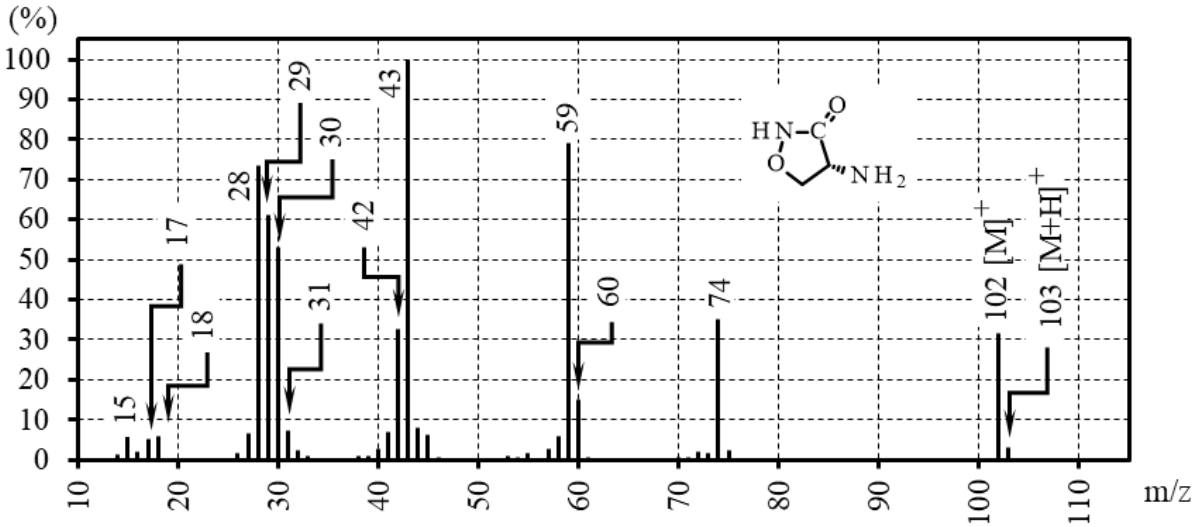

Cyclopentobarbital - CAS 76-68-6 - EI - NIST 352170



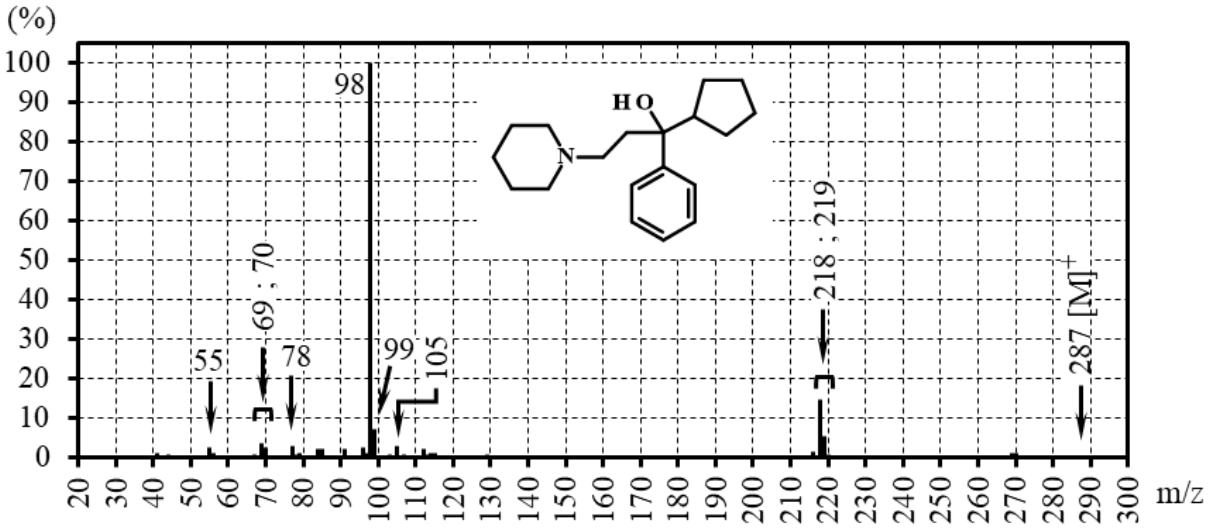

Cyclopentolate - CAS 512-15-2 - EI - NIST 292189



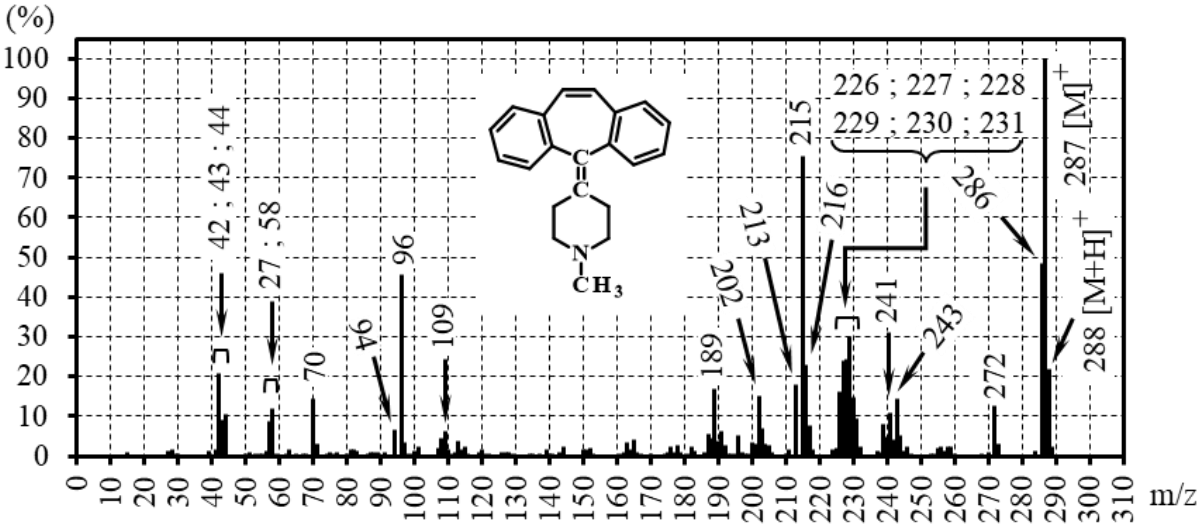

Cyclophosphamide - CAS 50-18-0 - NIST 235899



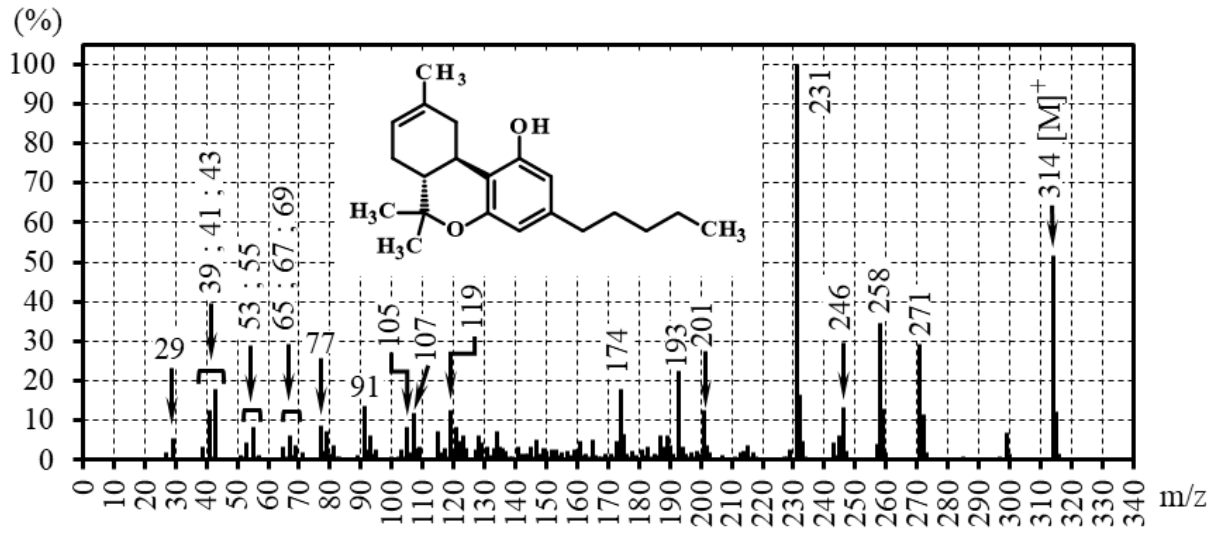

Cycloserine - CAS 68-41-7 - NIST 237050



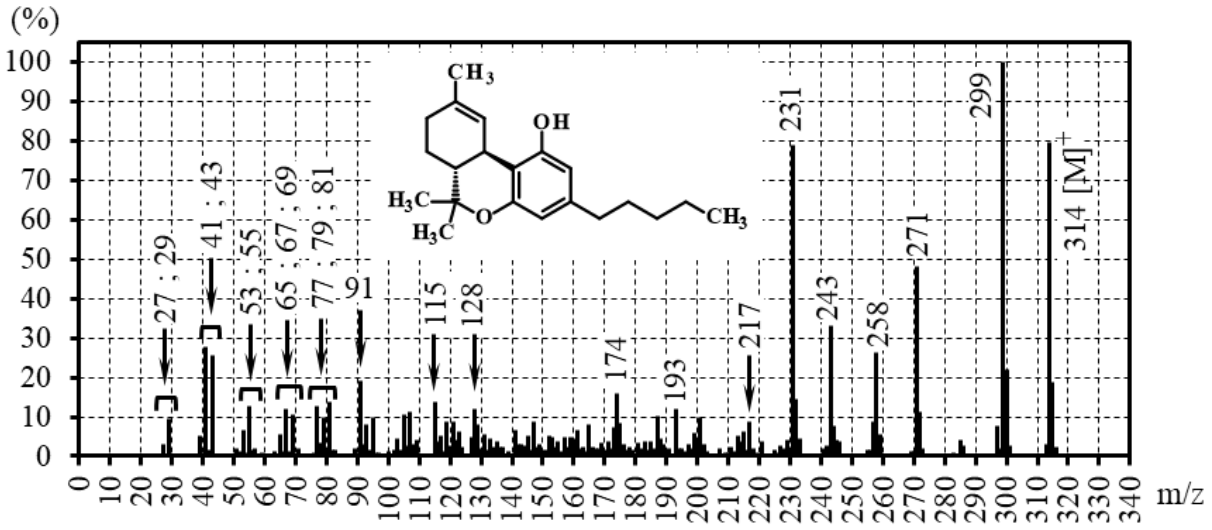

Cycrimine (Pagitane) - CAS 77-39-4 - EI - NIST 248053



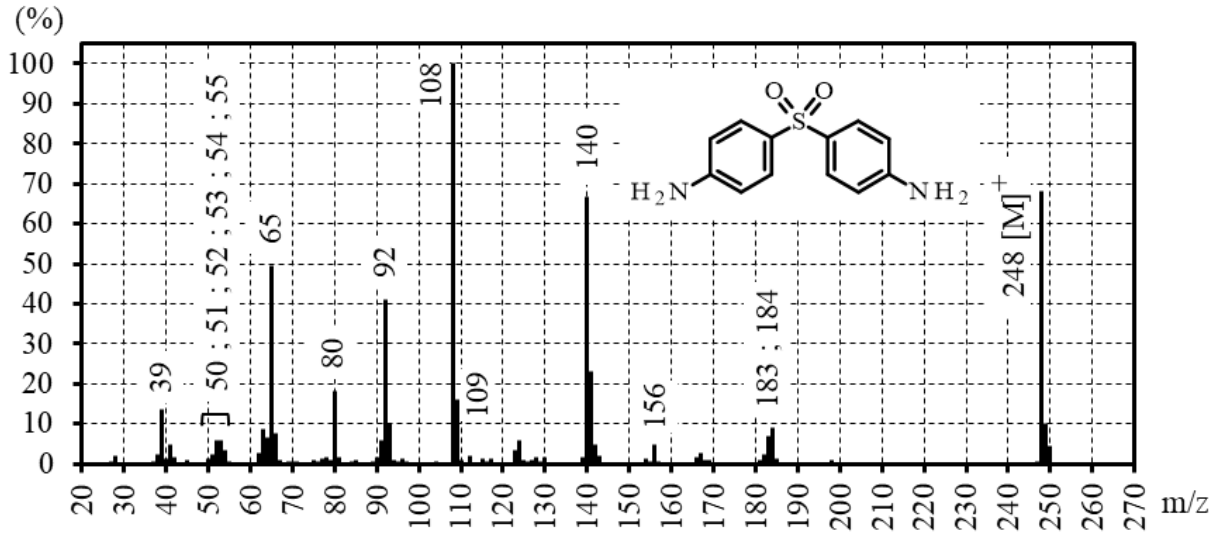

Cyproheptadine - CAS 129-03-3 - NIST 250706



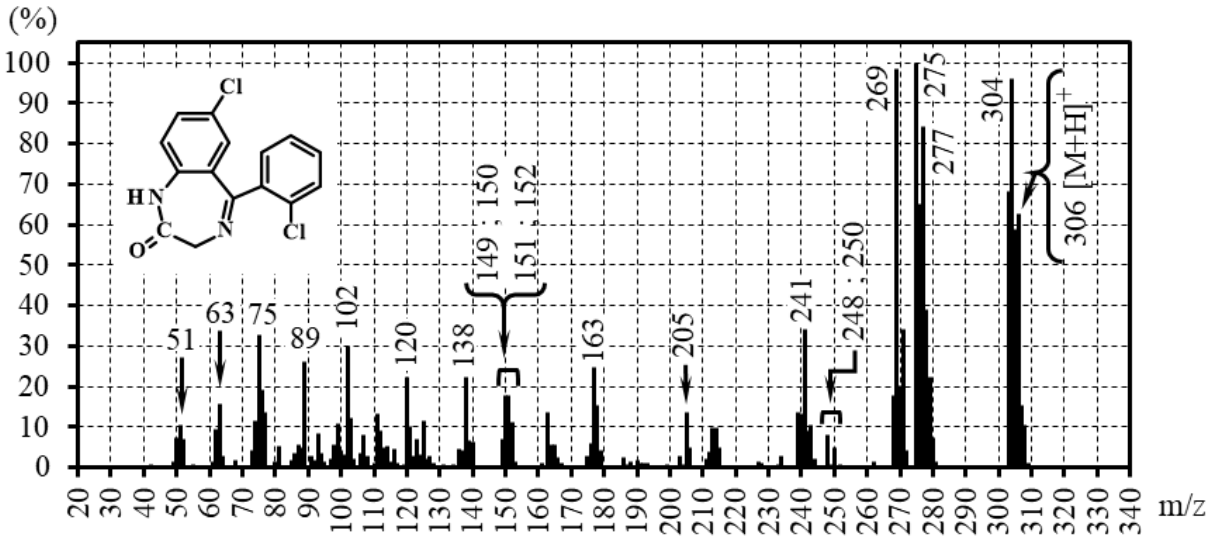

$\Delta^8$-Tetrahydrocannabinol - CAS 5957-75-5 - EI - NIST 352180



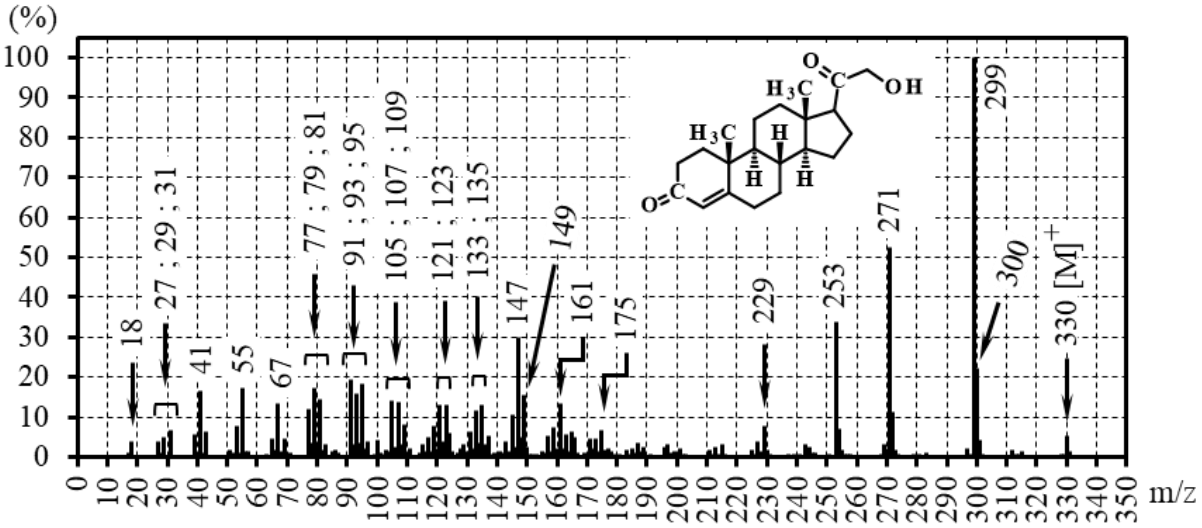

$D^9$-Tetrahydrocannabinol (Dronabinol) - CAS 1972-08-3 - EI - NIST 352175



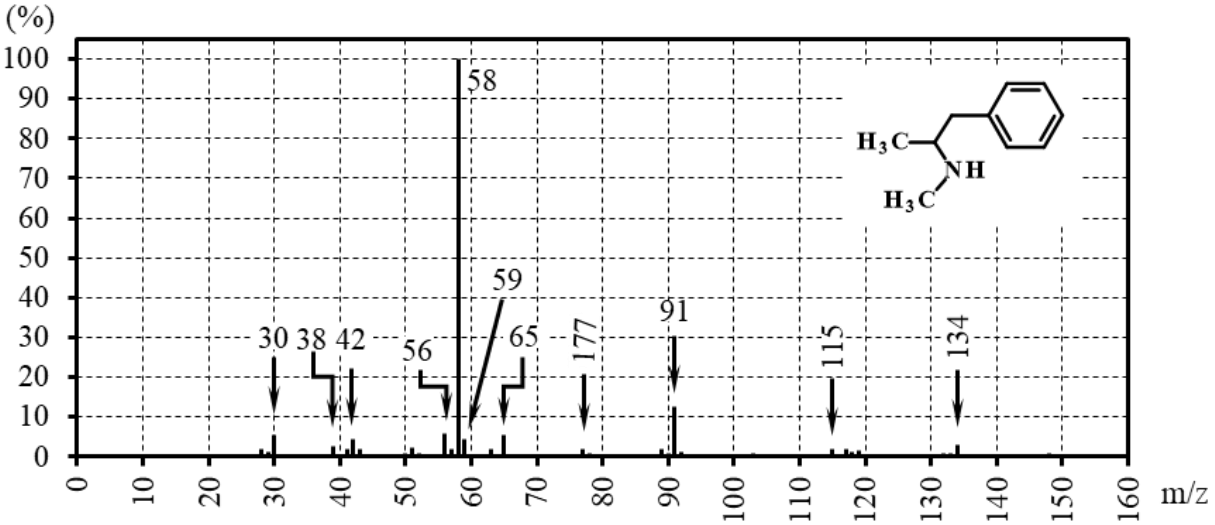

Dapsone - CAS 80-08-0 - NIST 408673



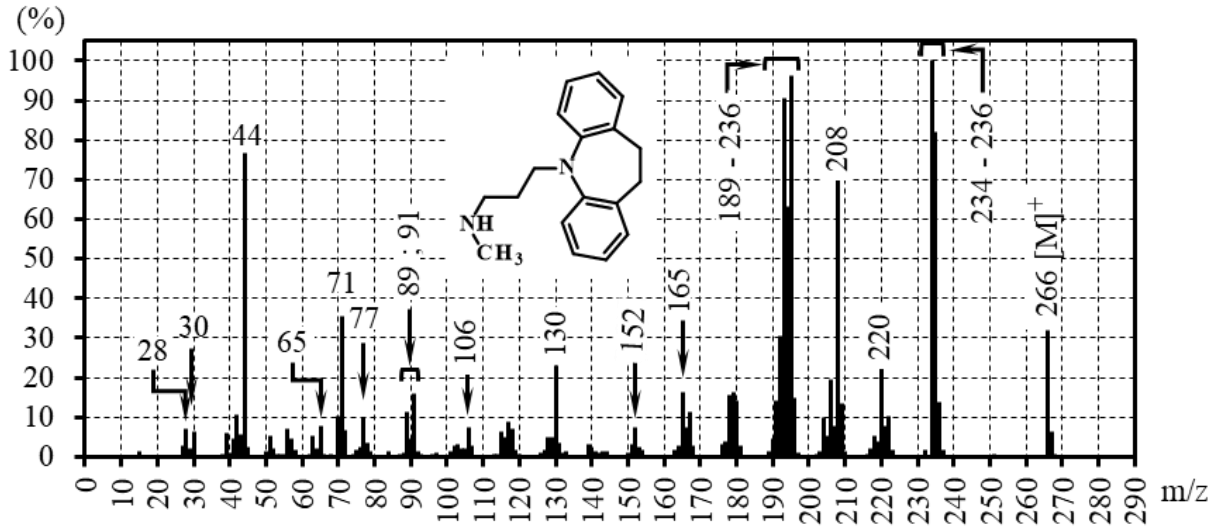

Delorazepam - CAS 2894-67-9 - EI - 248215



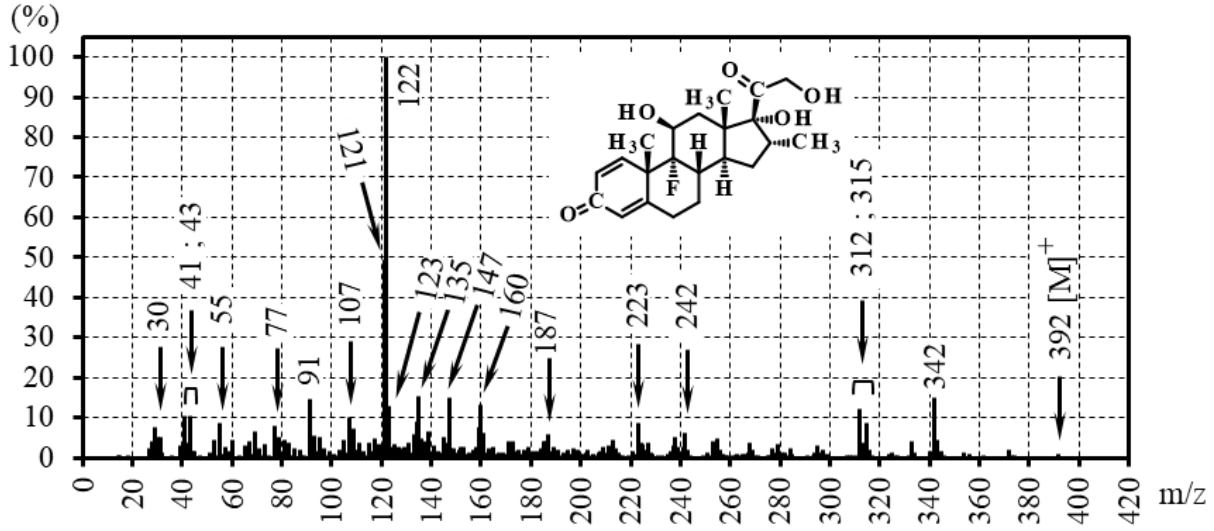

Deoxycortone - CAS 64-85-7 - NIST 235904



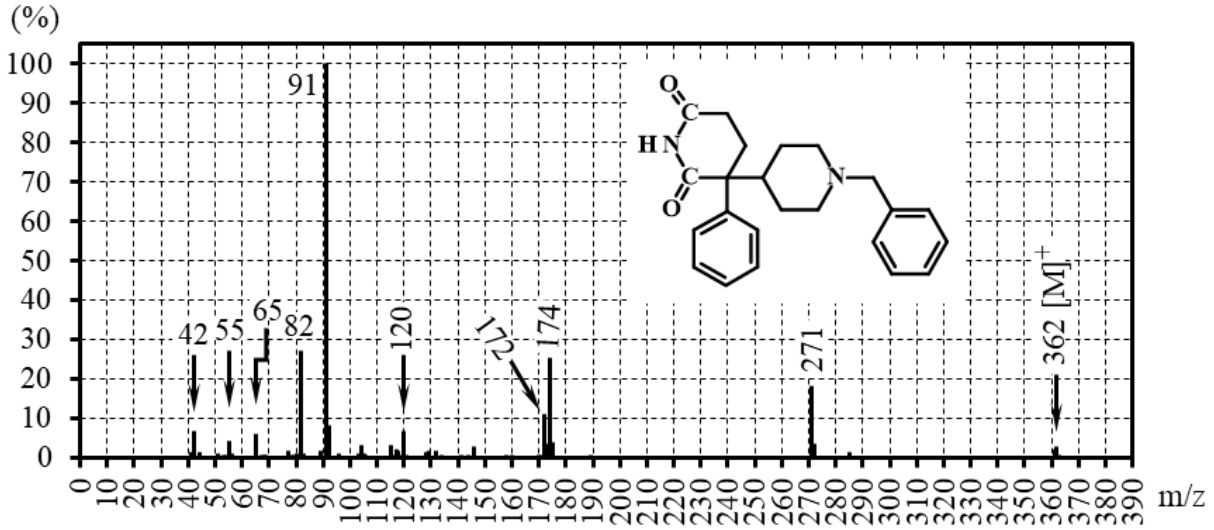

Deoxyephedrine (Pervertin, Phenethylamine) - CAS 7632-10-2 - EI - NIST 352958



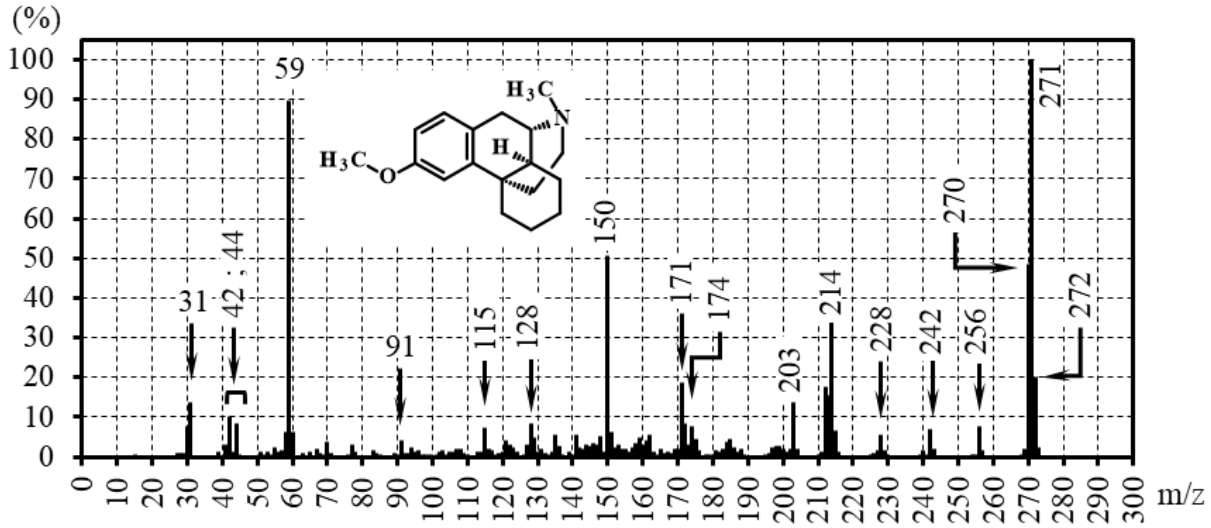

Desipramine - CAS 50-47-5 - EI - NIST 250707



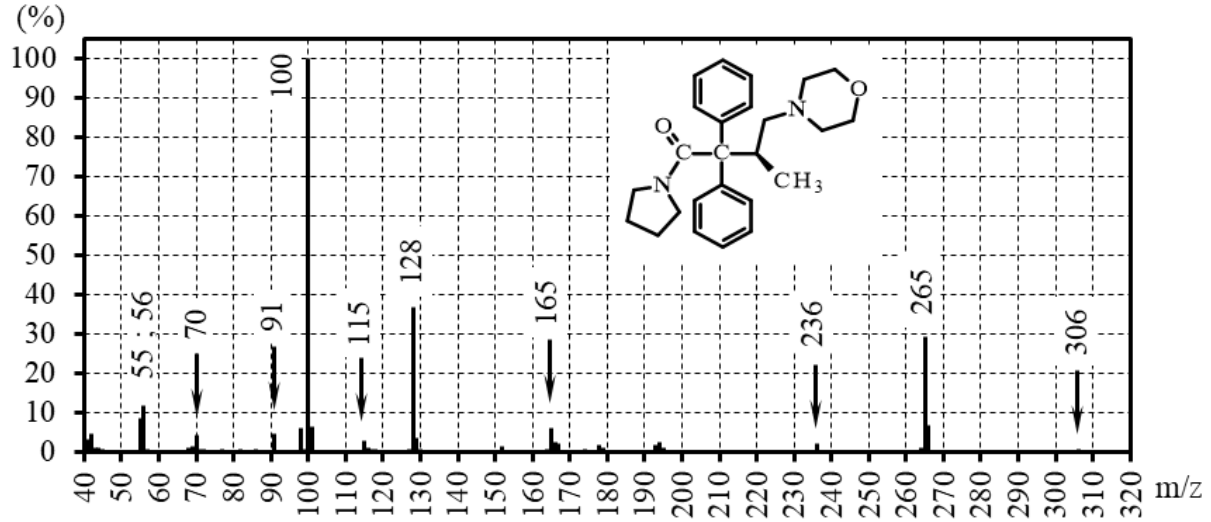

Dexamethasone - CAS 50-02-2 - NIST 235905



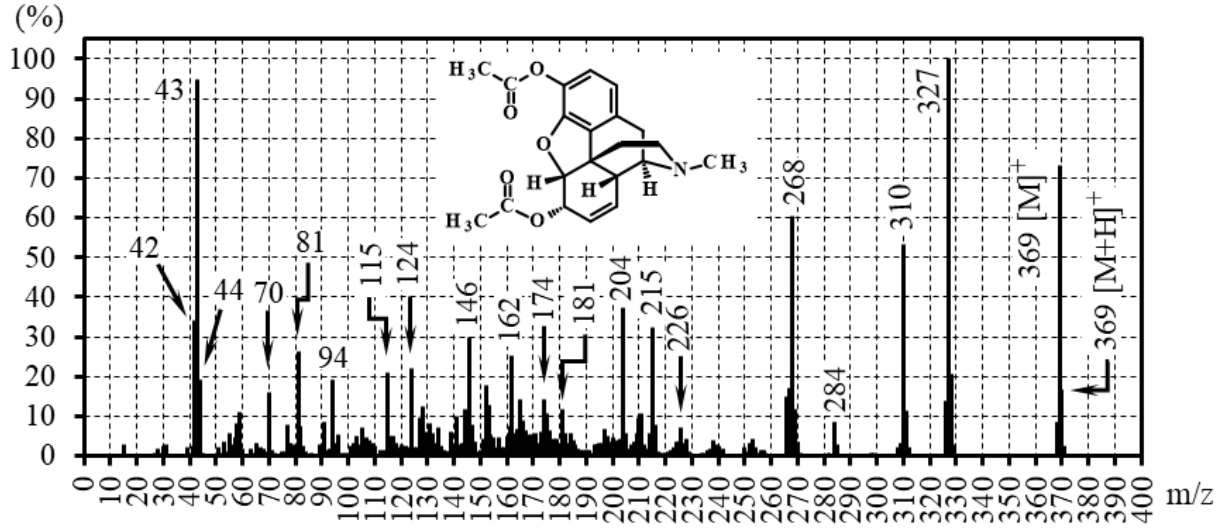

Dexetimide - CAS 21888-98-2 - EI - NIST 248890



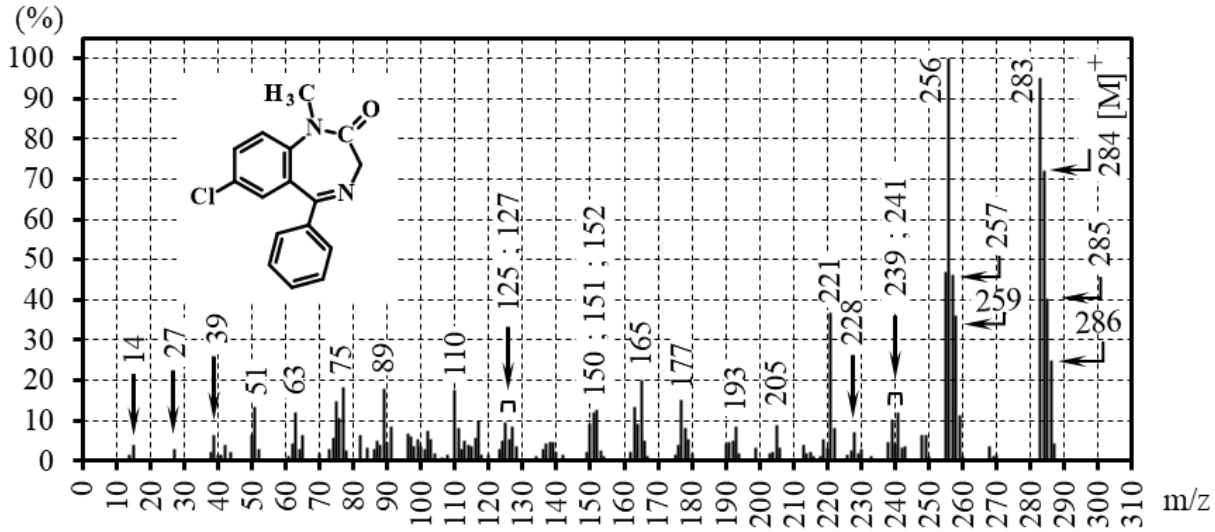

Dextromethorphan - CAS 125-71-3 - EI - NIST 235679



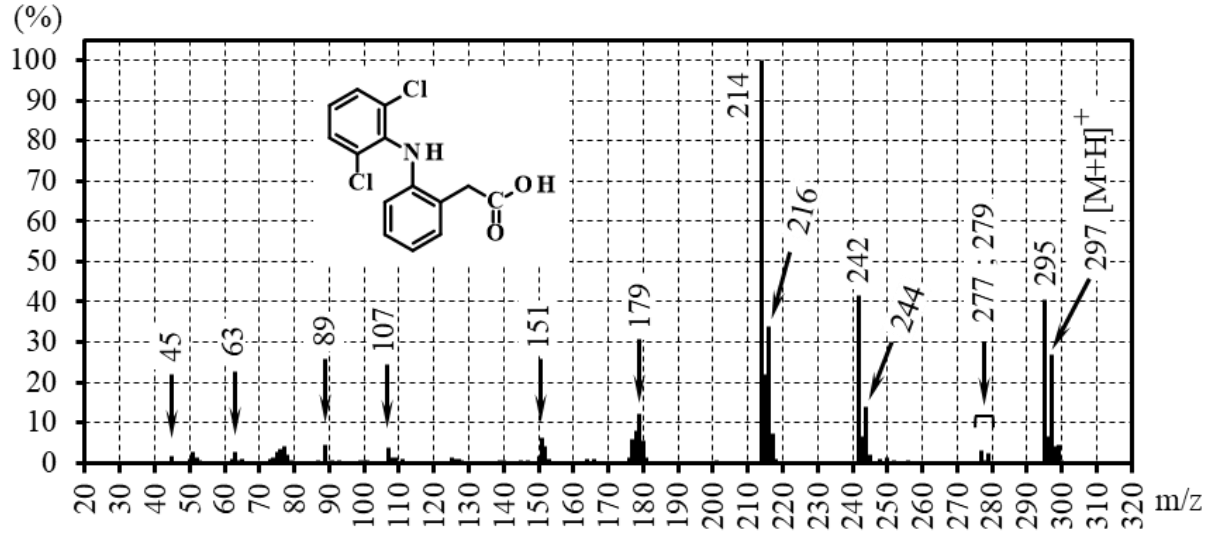

Dextromoramide - CAS 357-56-2 - EI - NIST nr. 247090



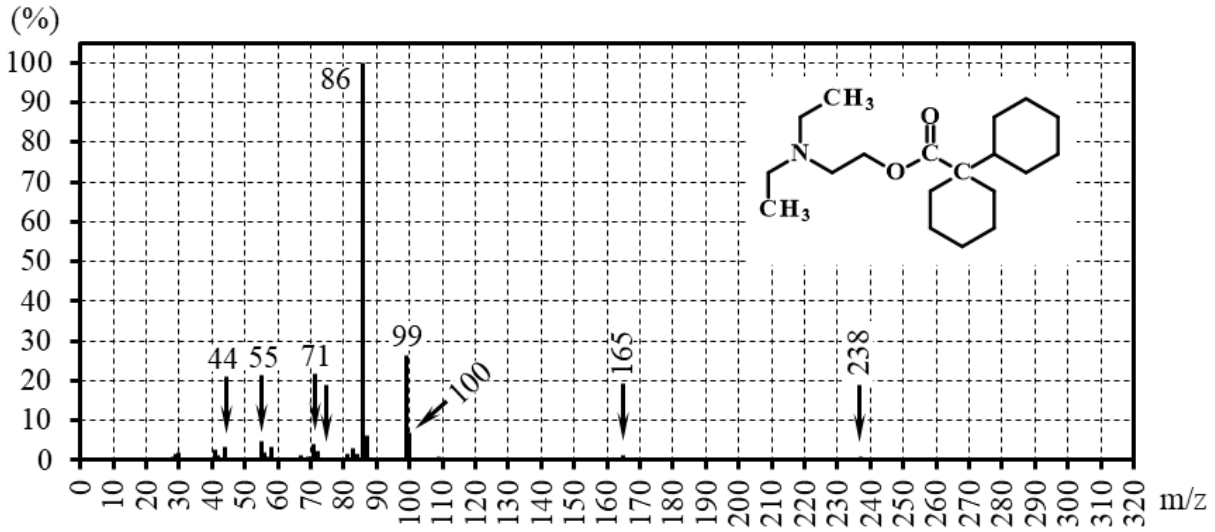

Diacetylmorphine (Heroin) - CAS 561-27-3 - EI - NIST 352937



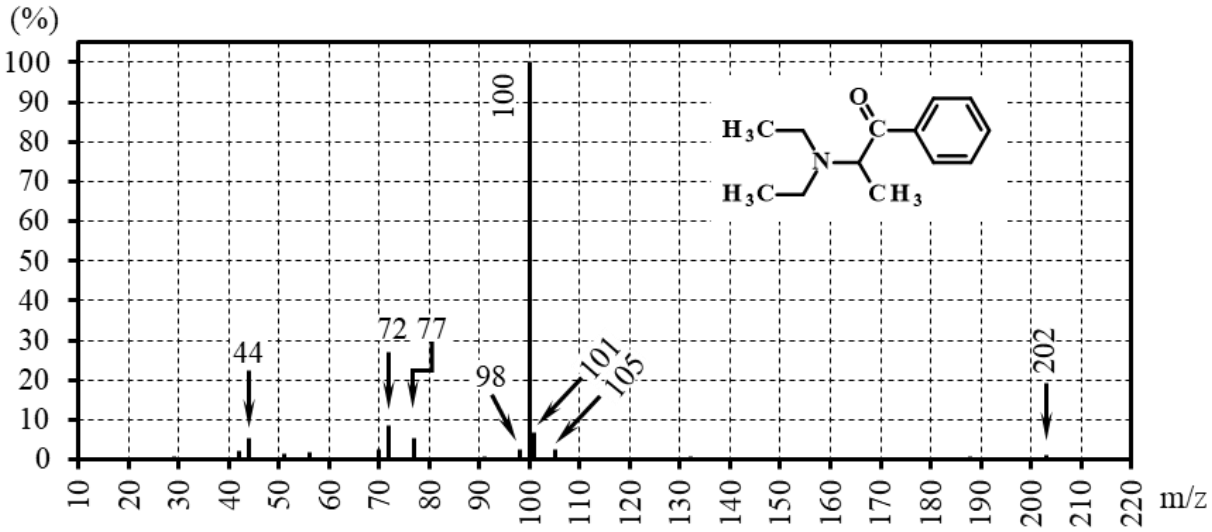

Diazepam - CAS 439-14-5 - NIST 113837



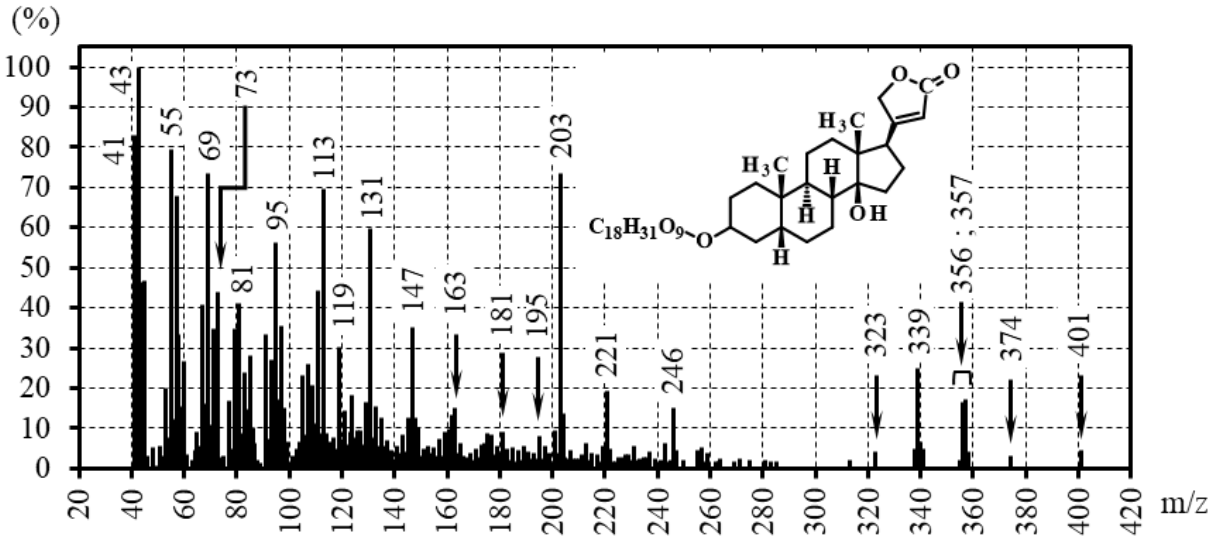

Diclofenac - CAS 15307-86-5 - NIST 397262



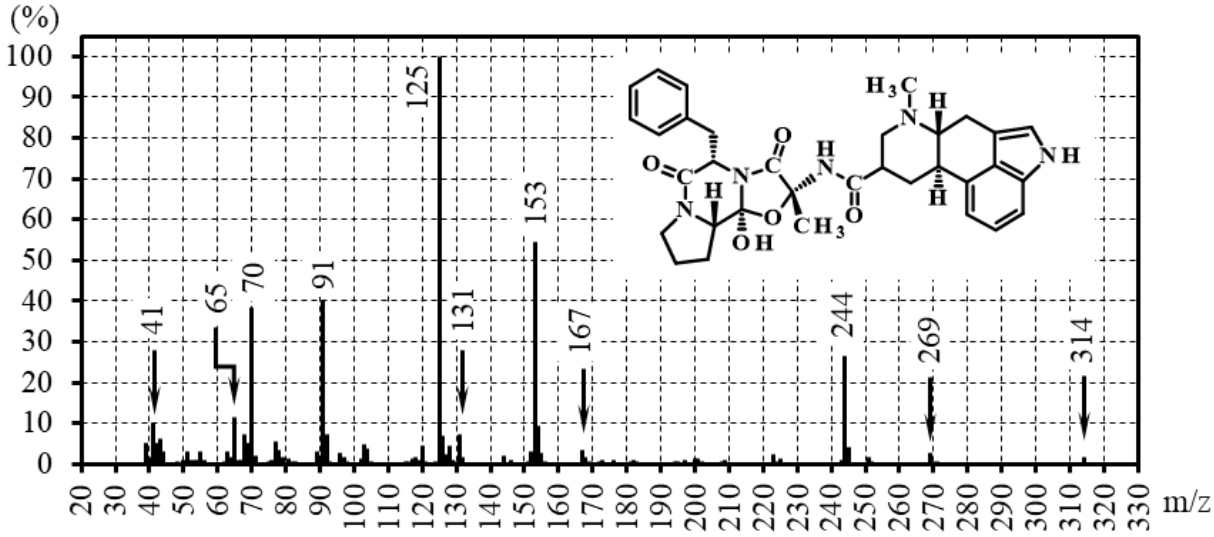

Dicyclomine - CAS 77-19-0 - EI - NIST 235662



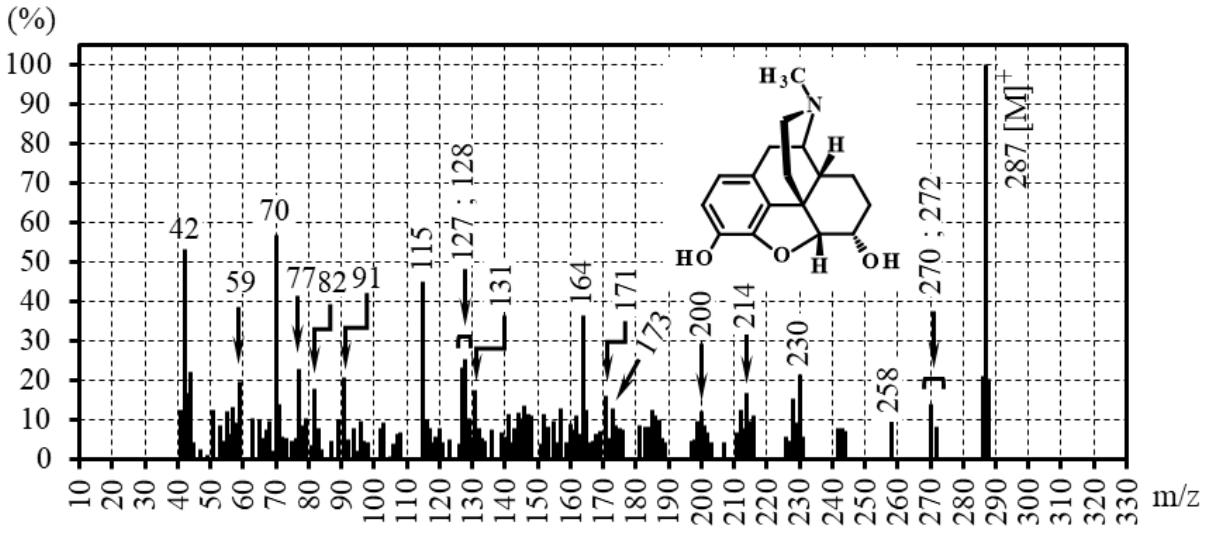

Diethylpropion (Amfepramone) - CAS 90-84-6 - EI - NIST 246177



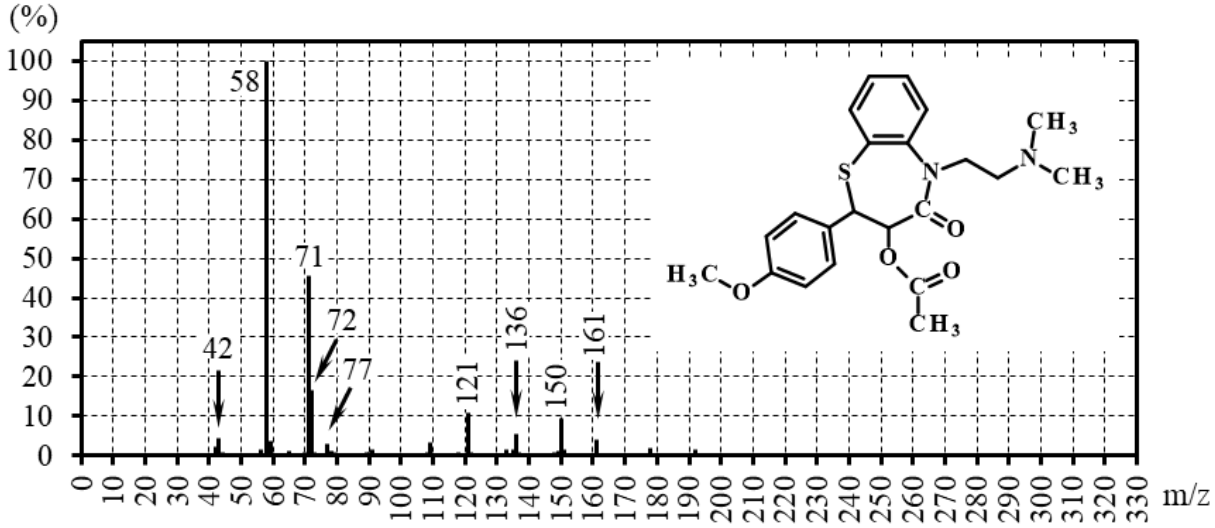

Digitoxin - CAS 71-63-6 - NIST 247912



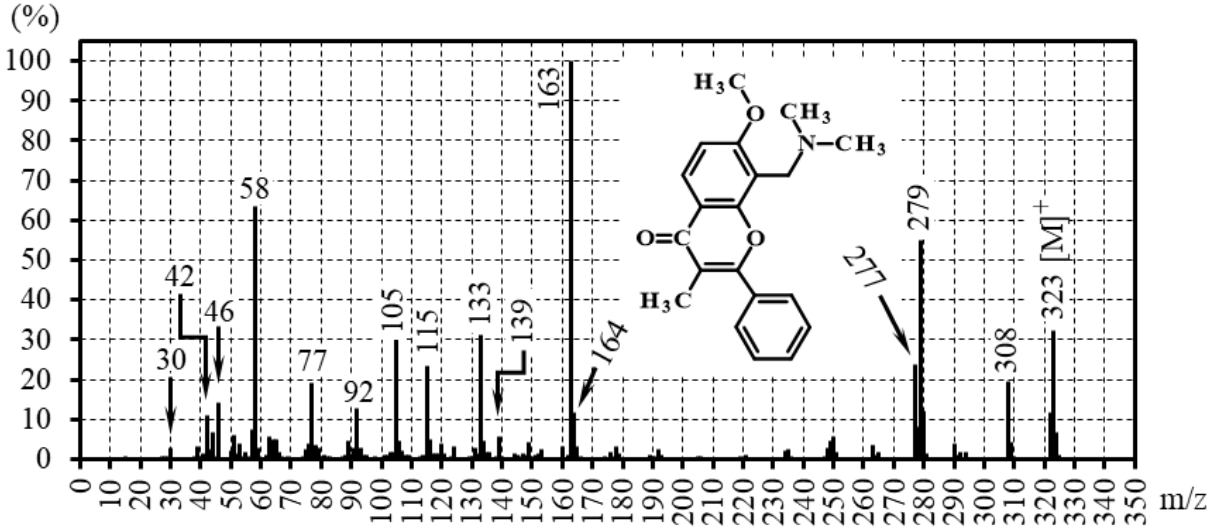

Dihydroergotamine - CAS 511-12-6 - NIST 248068



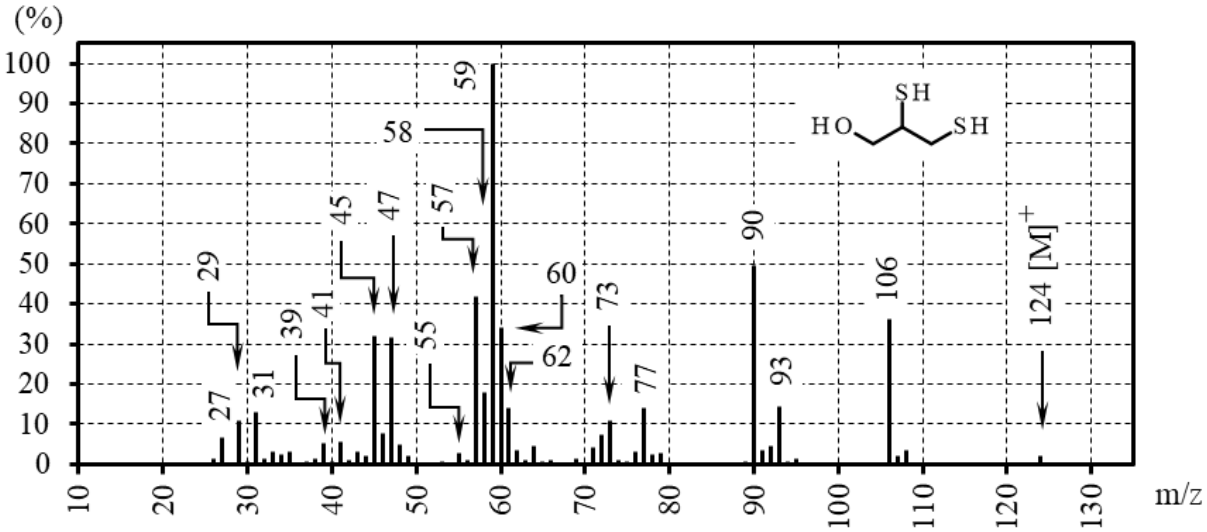

Dihydromorphine - CAS 509-60-4 - EI - NIST 247840



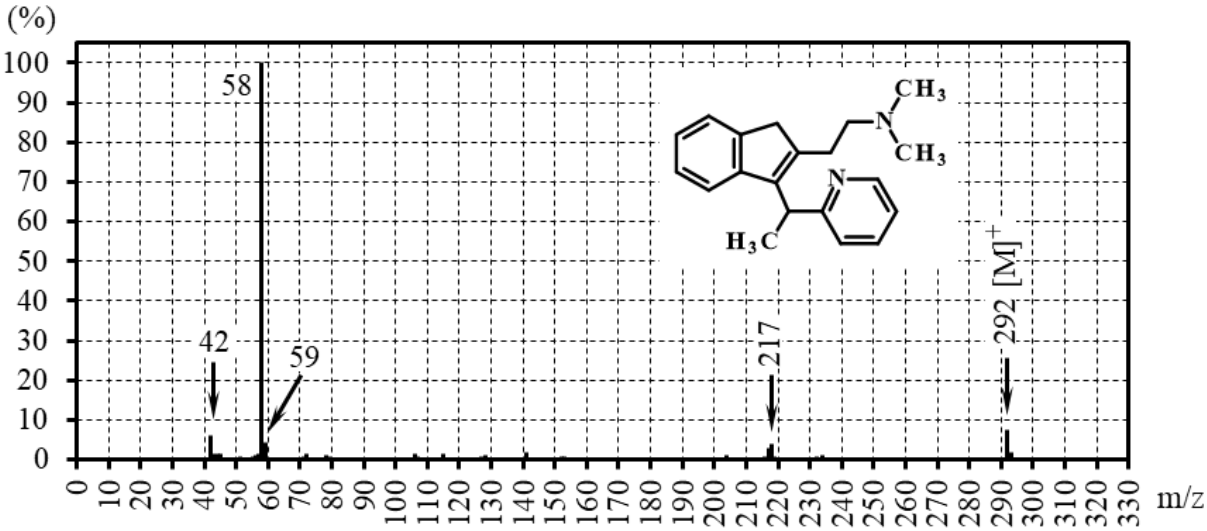

Diltiazem - CAS 42399-41-7 - EI - NIST 247122



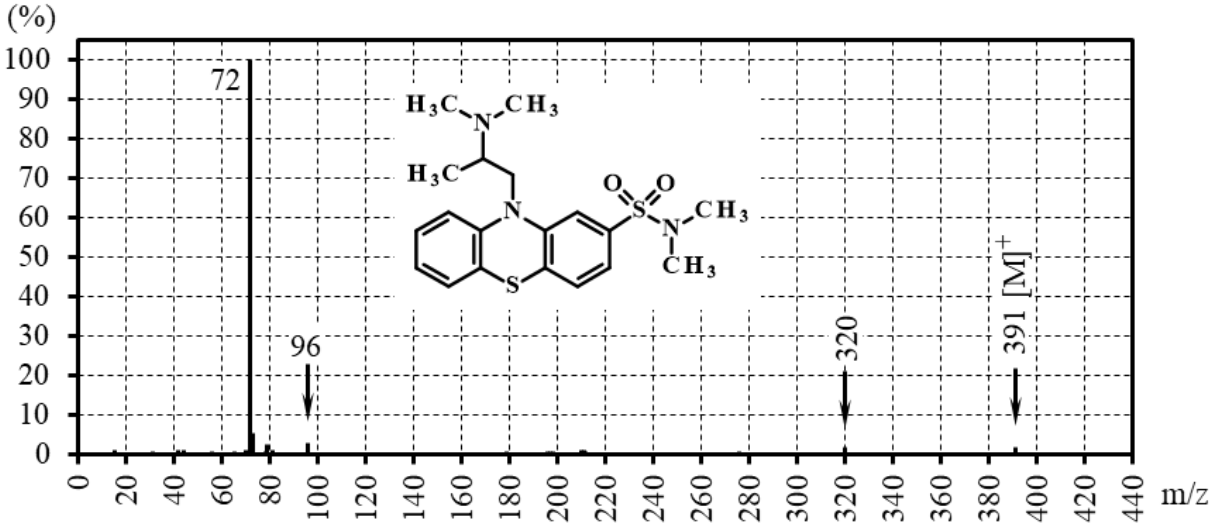

Dimefline - CAS 1165-48-6 - EI - NIST 408325



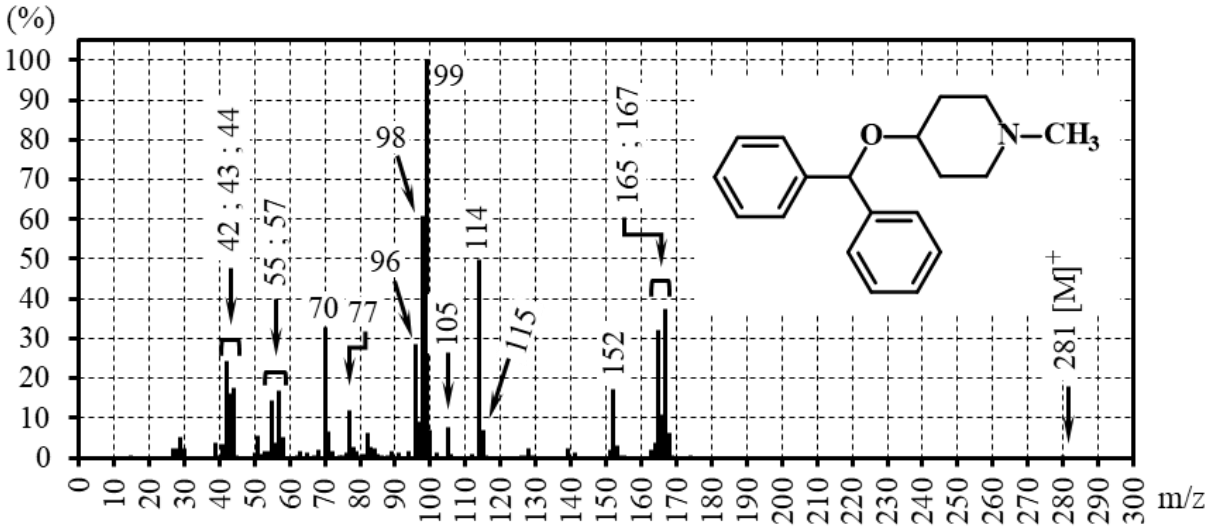

Dimercaprol - CAS 59-52-9 - NIST 291345



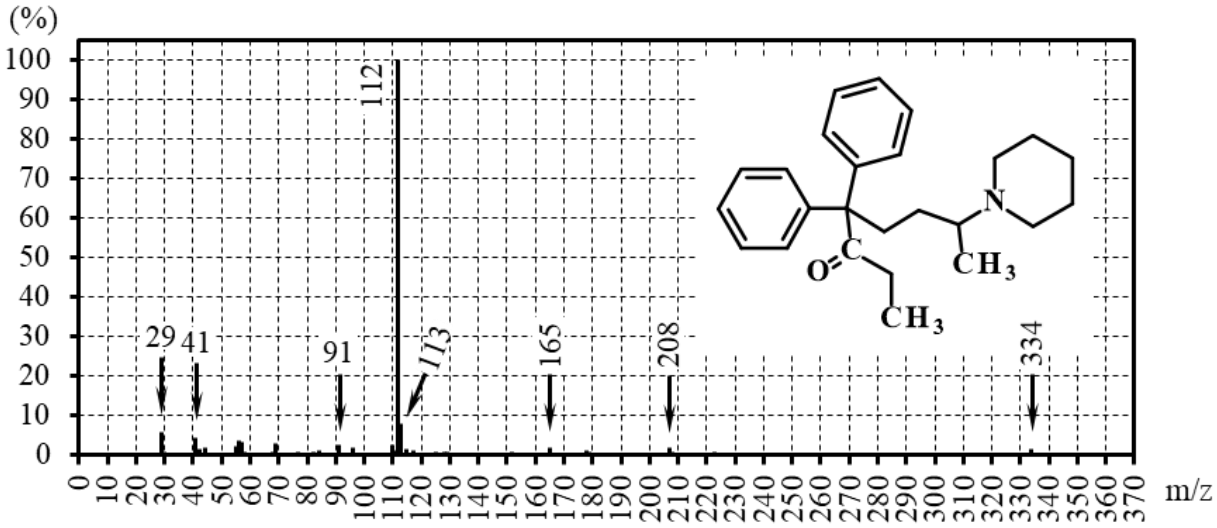

Dimetindene - CAS 5636-83-9 - EI - NIST 116715



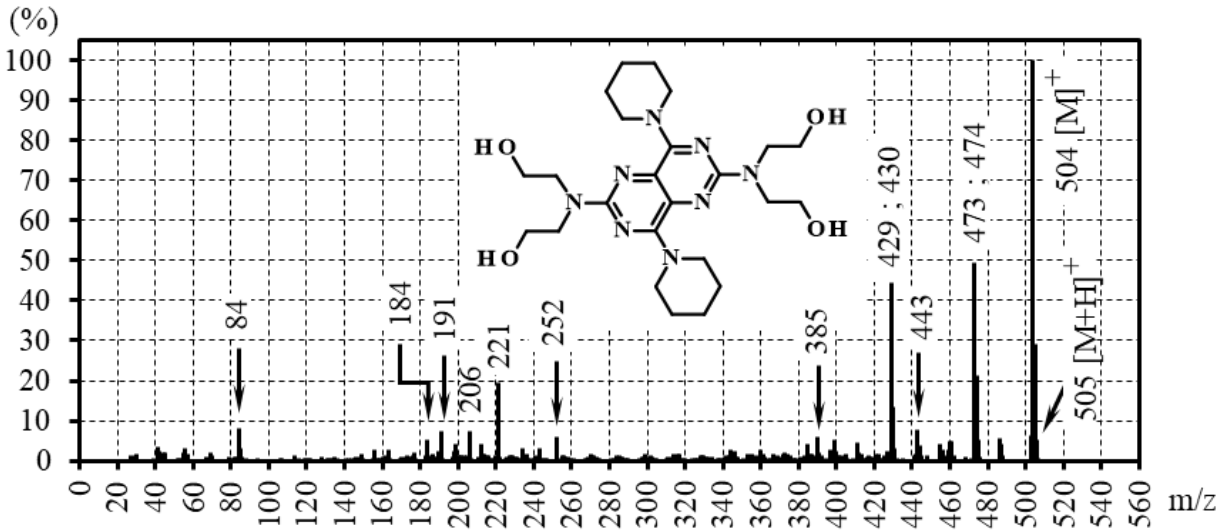

Dimetotiazine - CAS 7456-24-8 - EI - NIST 235687



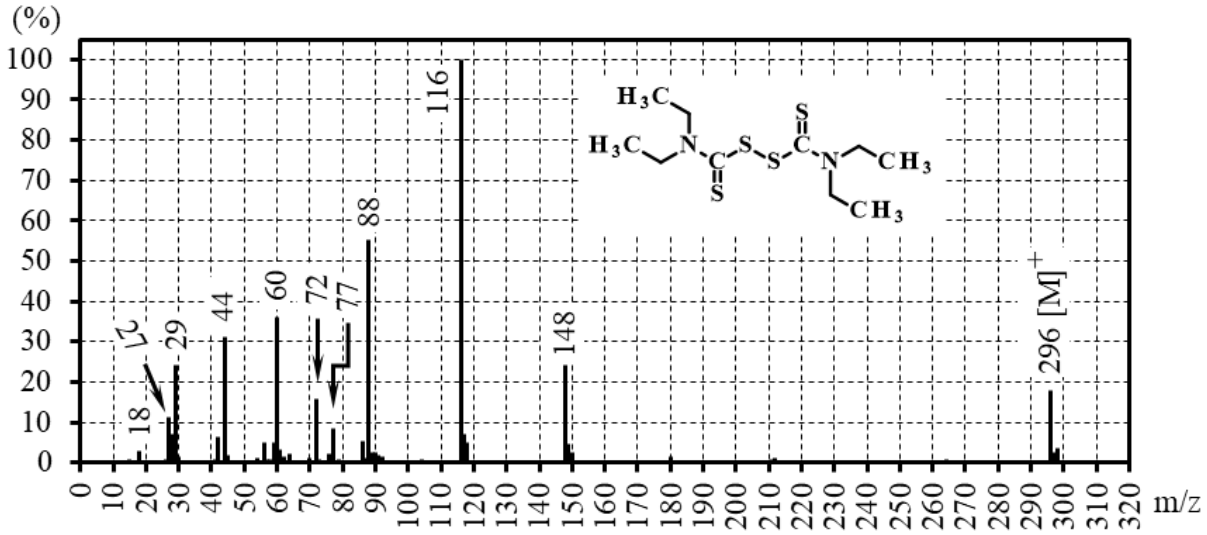

Diphenylpyraline - CAS 147-20-6 - EI - NIST 250708



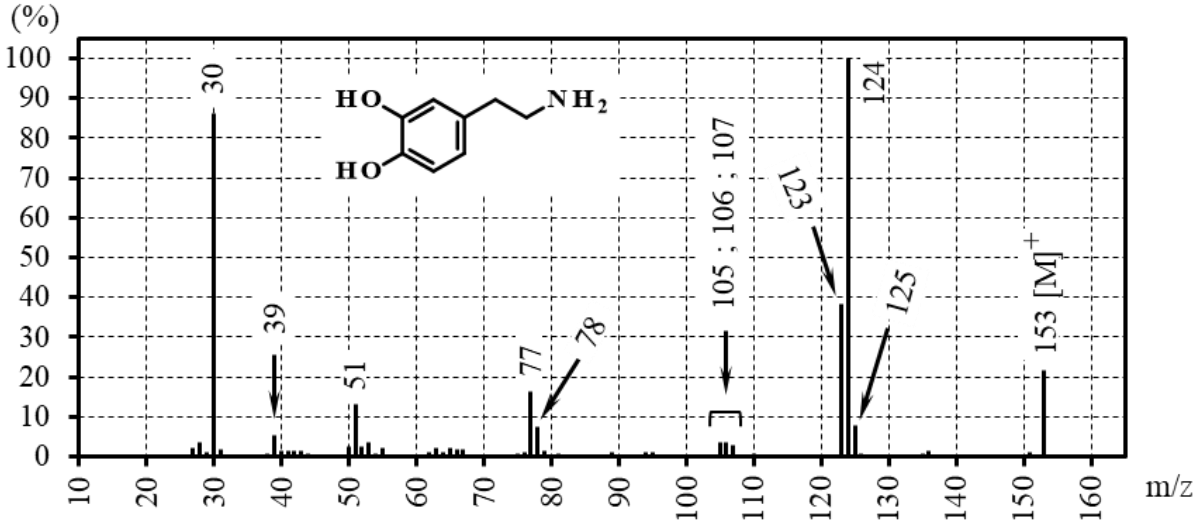

Dipipanone - CAS 467-83-4 - EI - NIST 247005



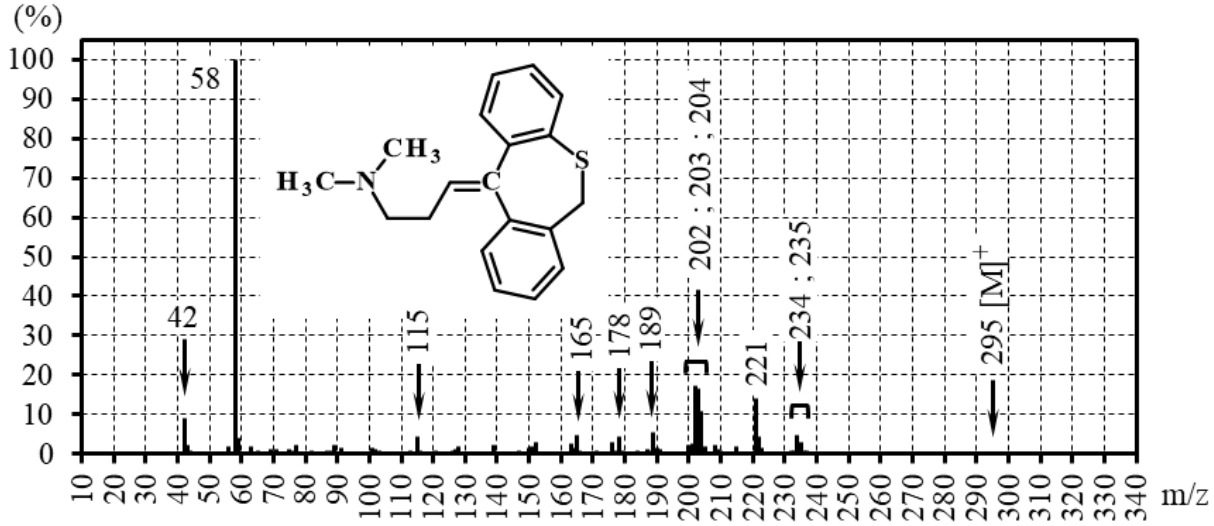

Dipyridamole - CAS 58-32-2 - NIST 237441



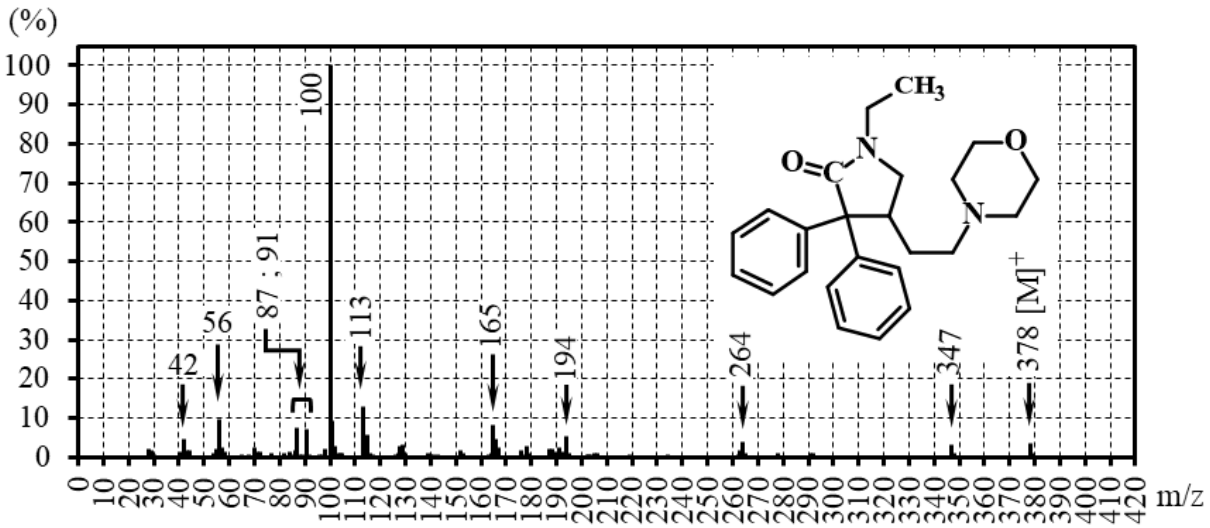

Disulfiram - CAS 97-77-8 - NIST 228650



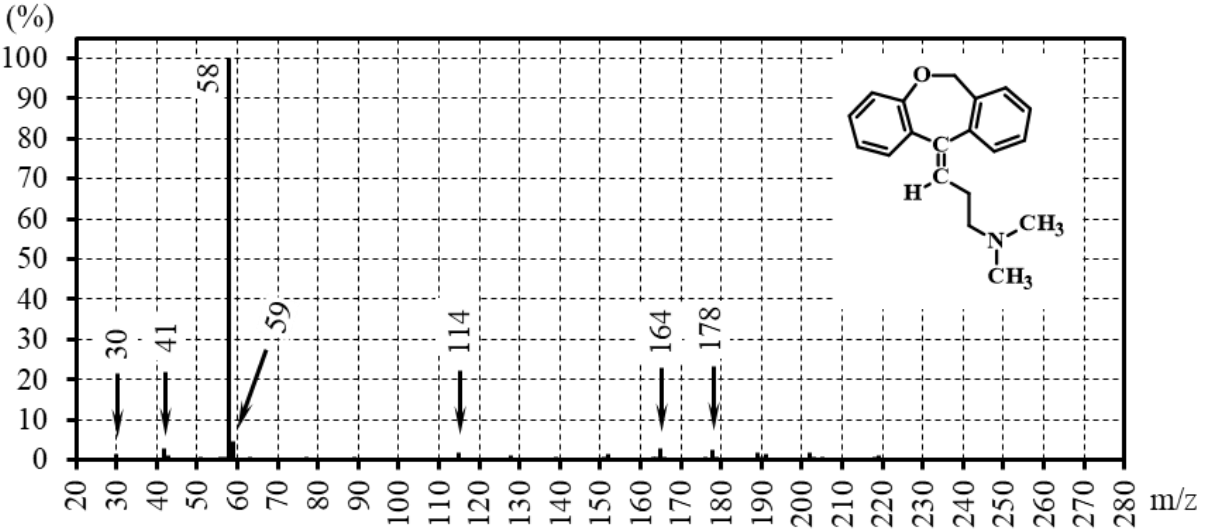

Dopamine - CAS 51-61-6 - NIST 228609



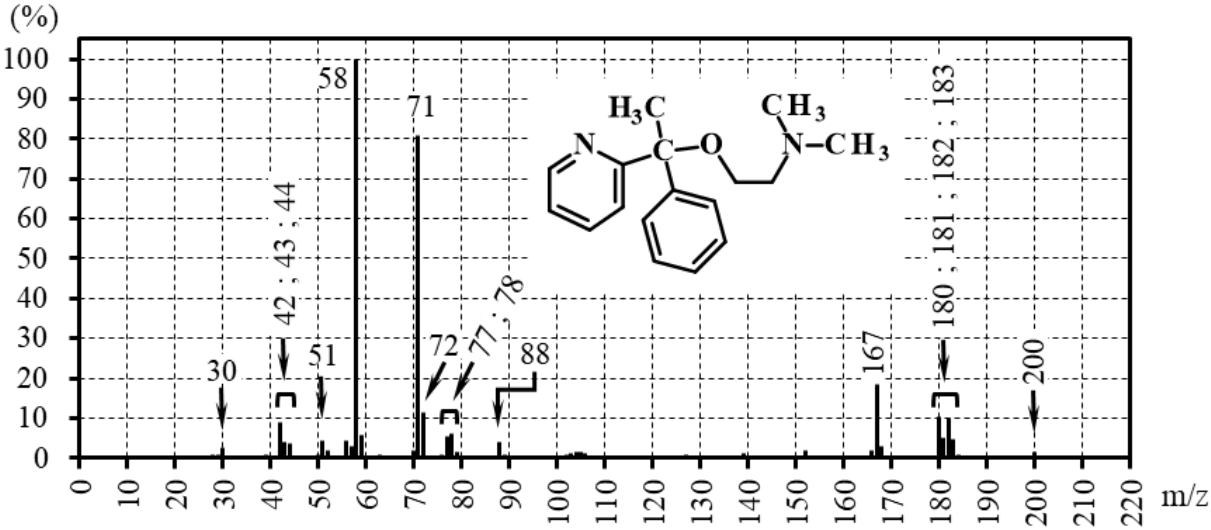

Dothiepin - CAS 113-53-1 - EI - NIST 397552



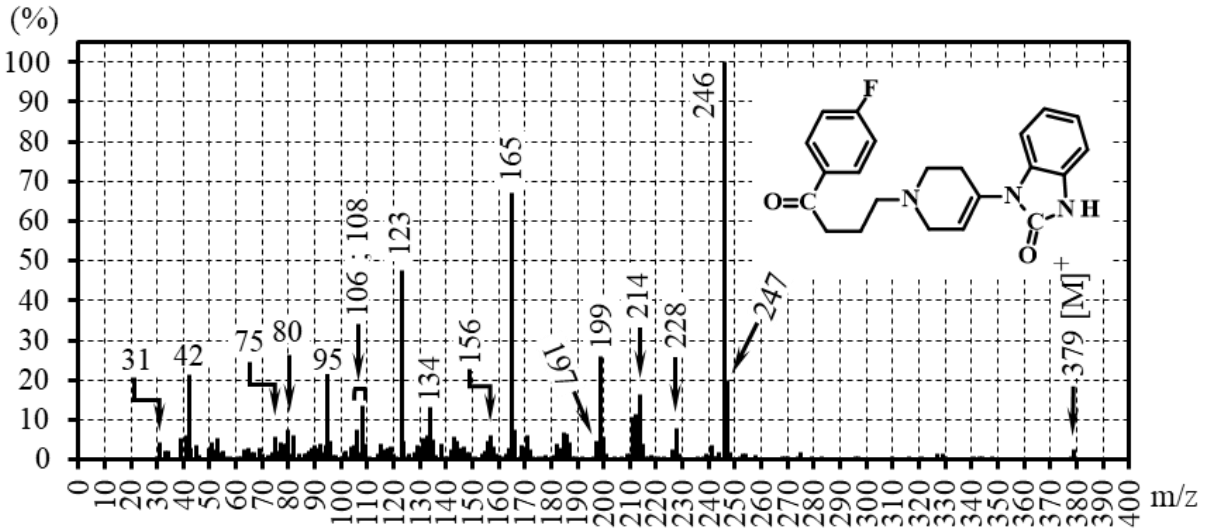

Doxapram - CAS 309-29-5 - EI - NIST 408263



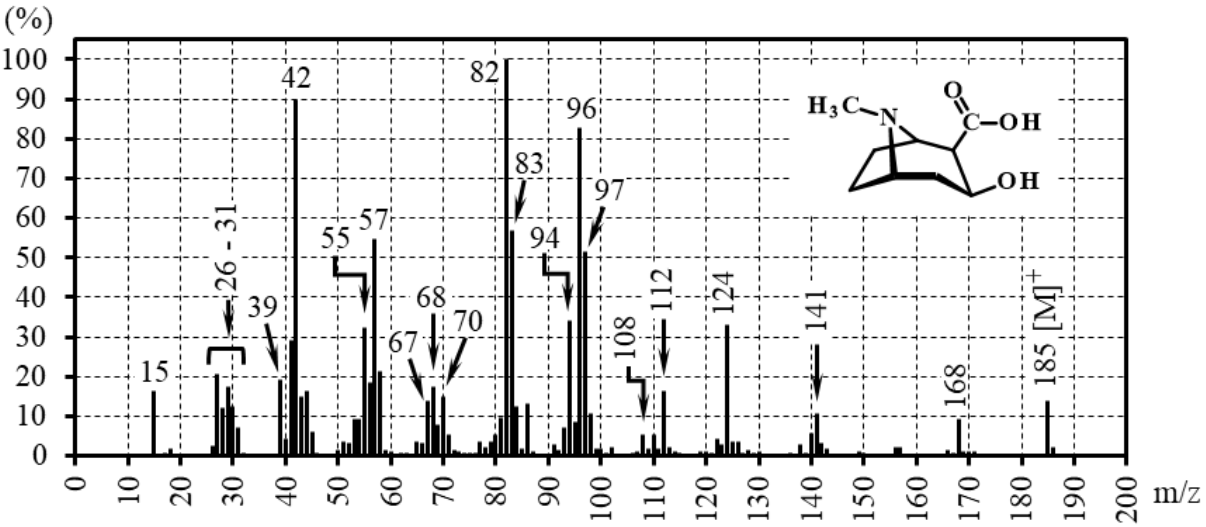

Doxepin - CAS 1668-19-5 - NIST 292030



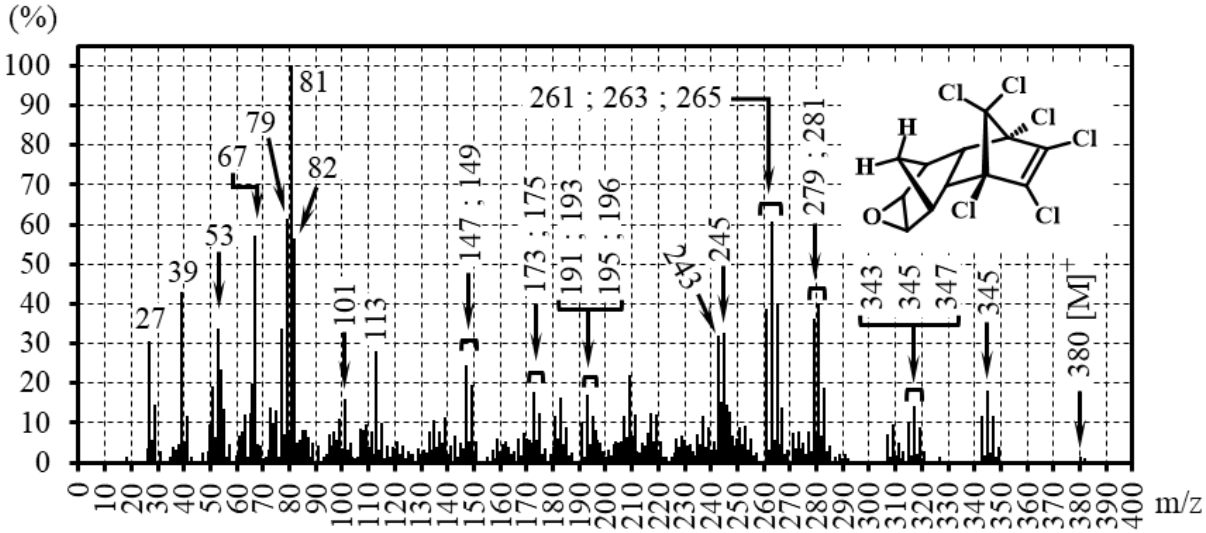

Doxylamine - CAS 469-21-6 - EI - NIST 342178



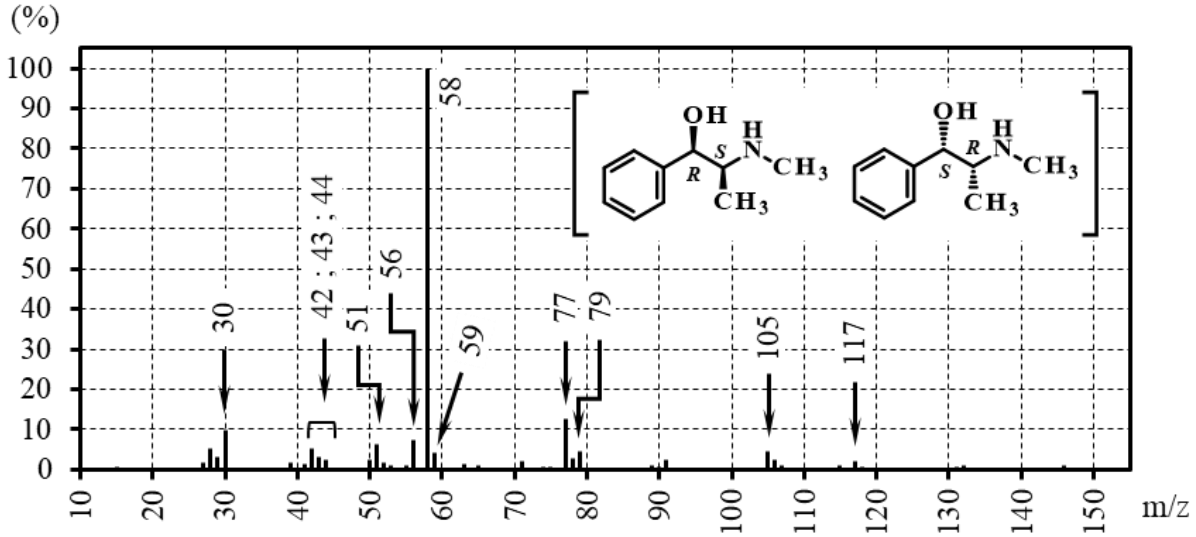

Droperidol - CAS 548-73-2 - EI - NIST 247071



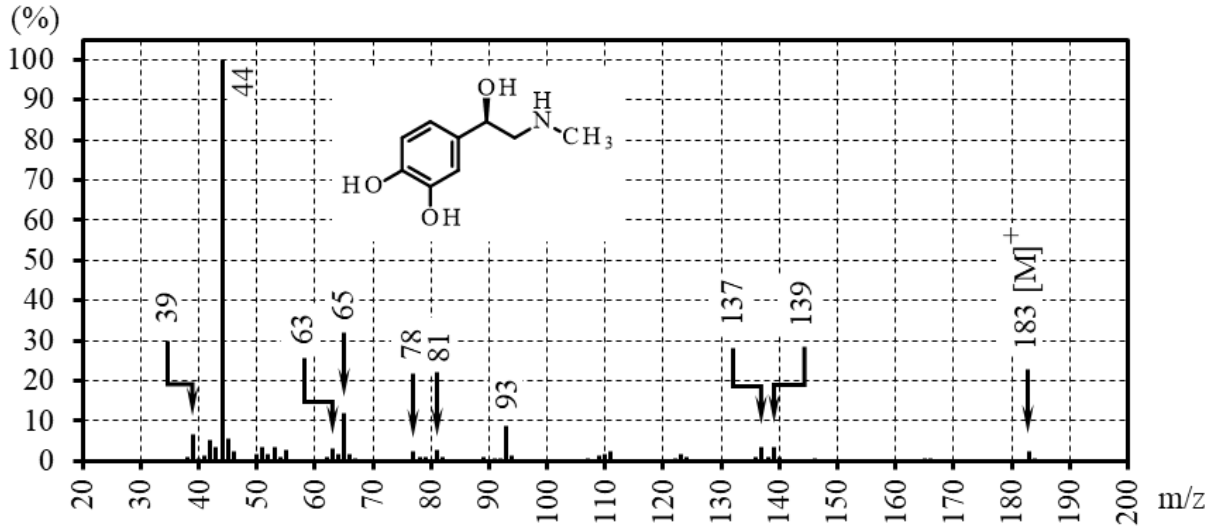

Ecgonine - CAS 481-37-8 - EI - NIST 42288



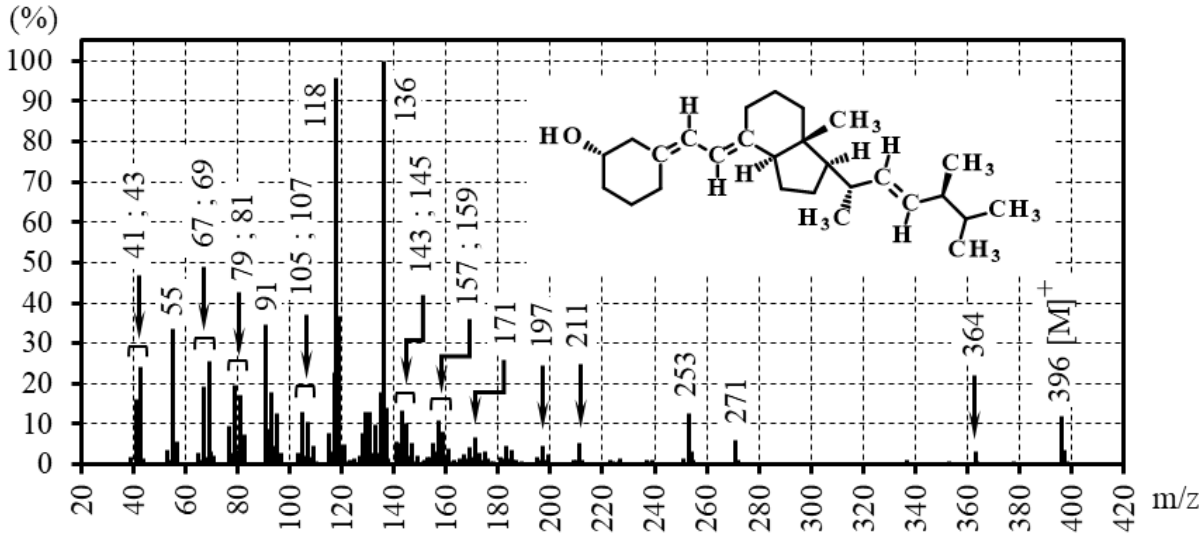

Endrin - CAS 72-20-8 - EI 75 eV source 220 $^{o}$C , sample 140 $^{o}$C - SDBS 2295



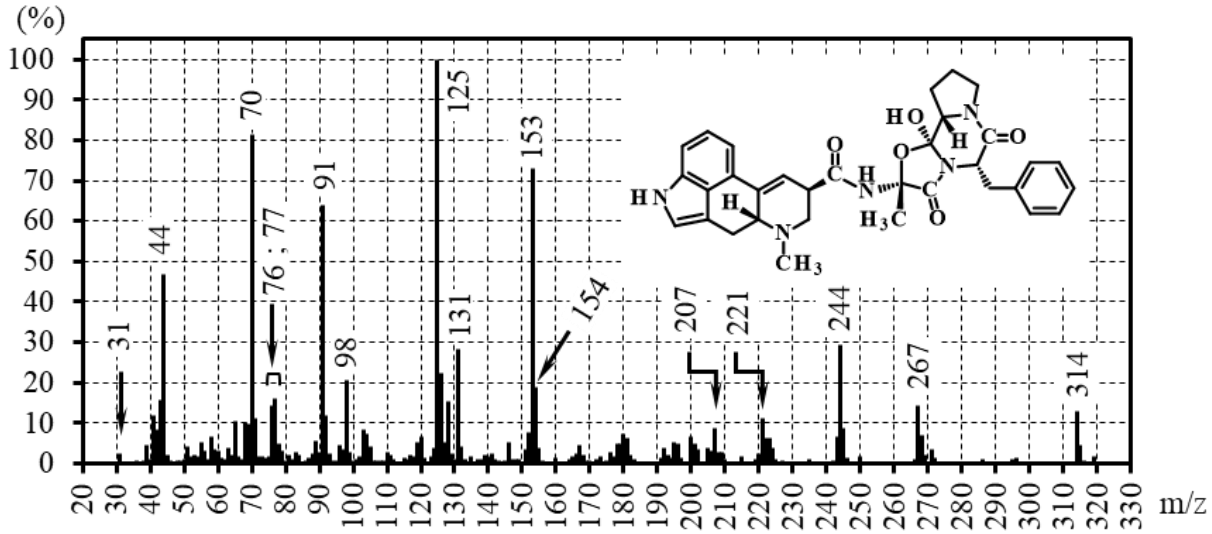

Ephedrine - CAS 299-42-3 - NIST 113823



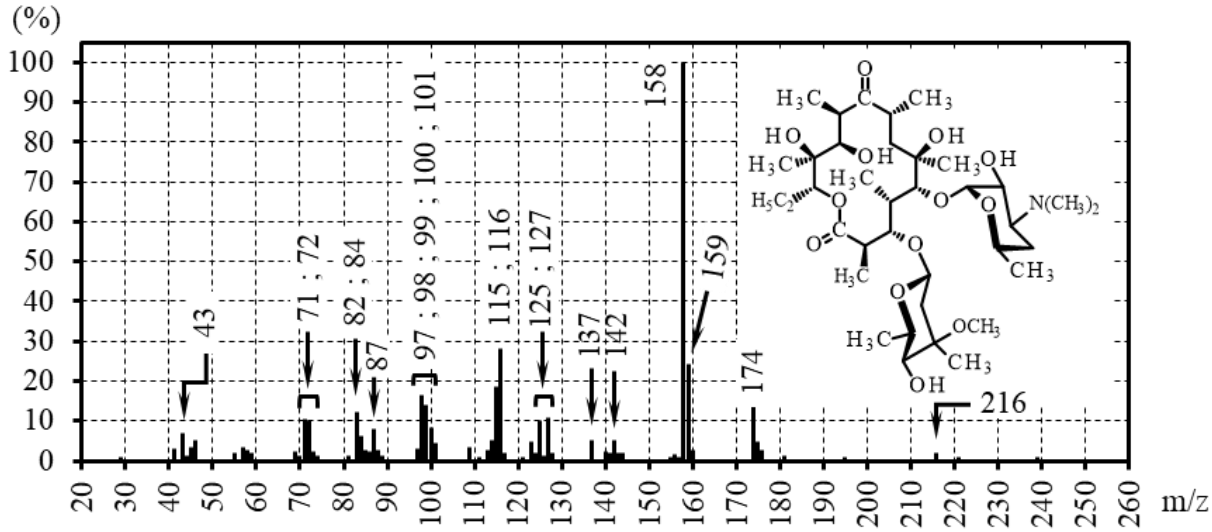

Epinephrine (Adrenaline) - CAS 51-43-4 - NIST 24257



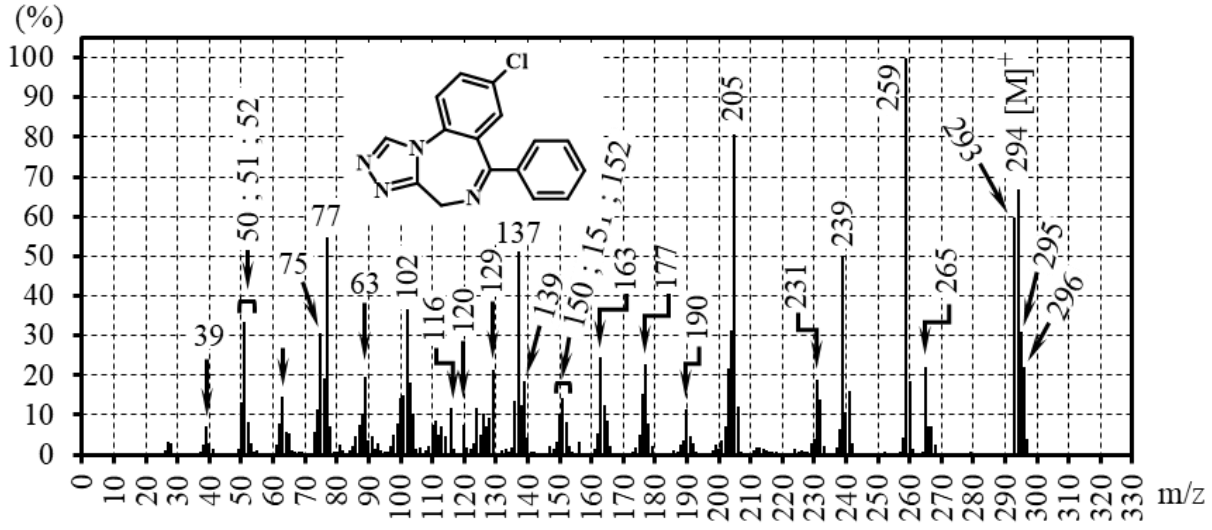

Ergocalciferol - CAS 50-14-6 - NIST 248164



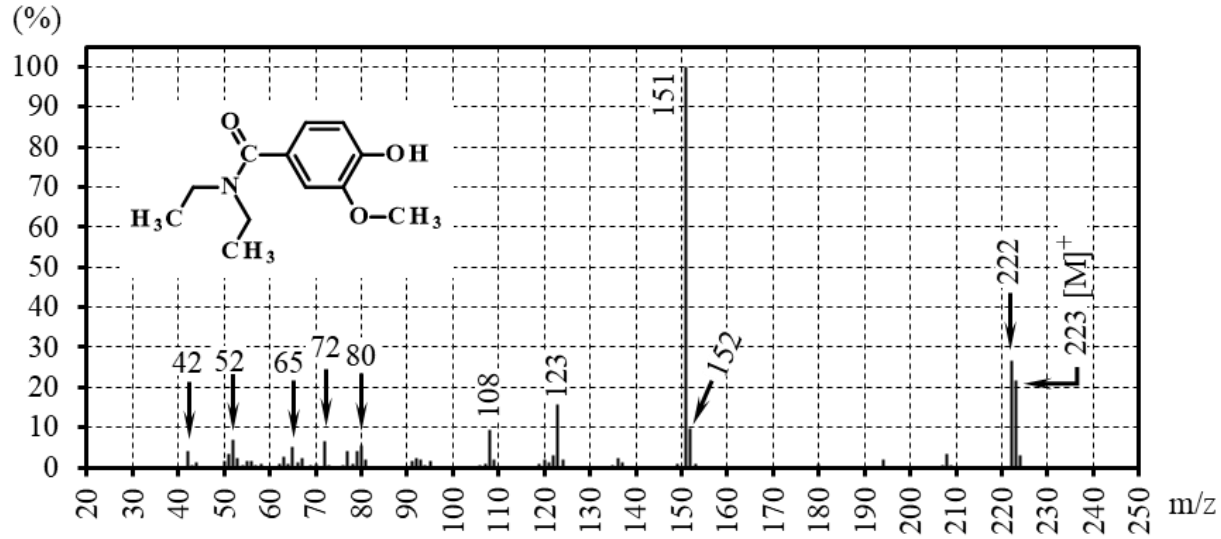

Ergotamine - CAS 113-15-5 - NIST 248677



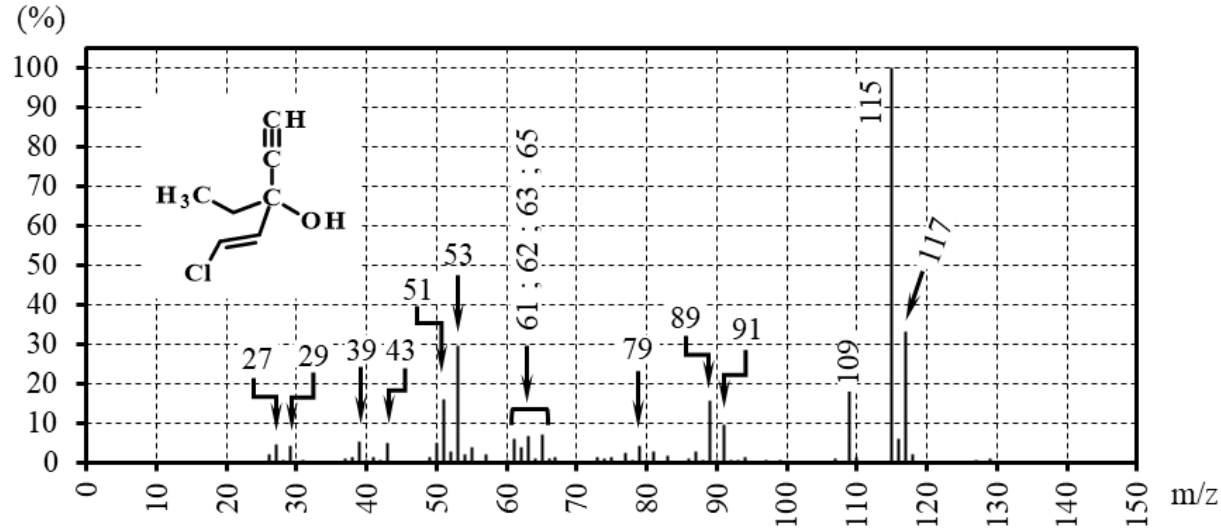

Erythromycin - CAS 114-07-8 - SDBS 22846



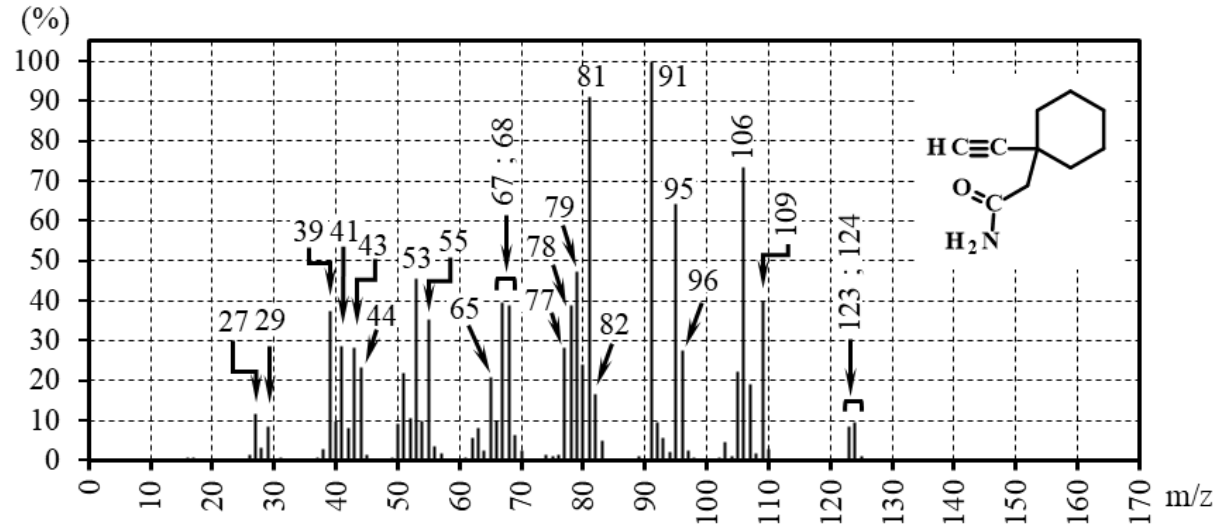

Estazolam - CAS 29975-16-4 - EI - NIST 408732



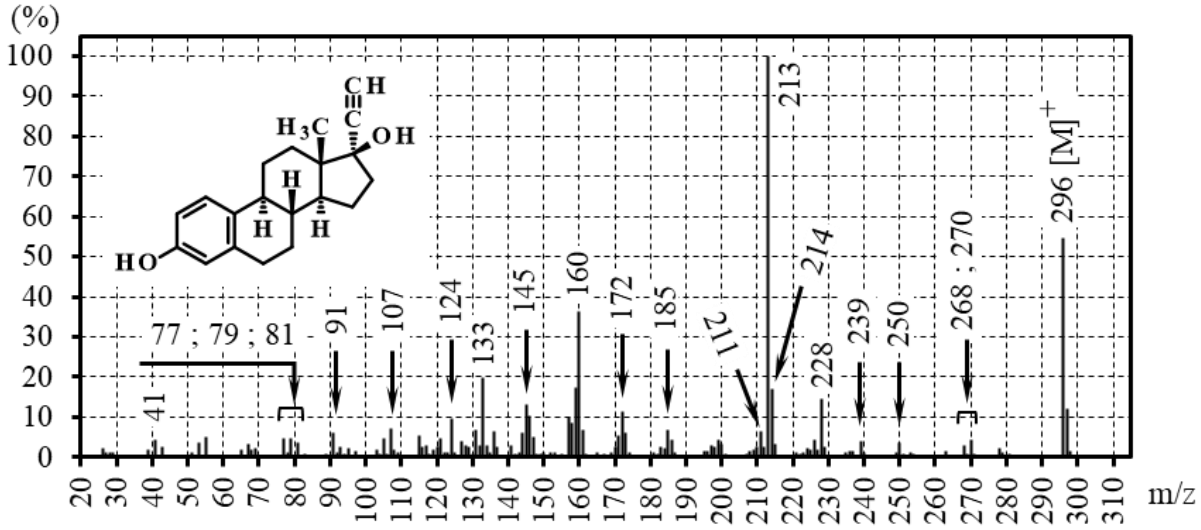

Ethamivan - CAS 304-84-7 - EI - NIST 246273



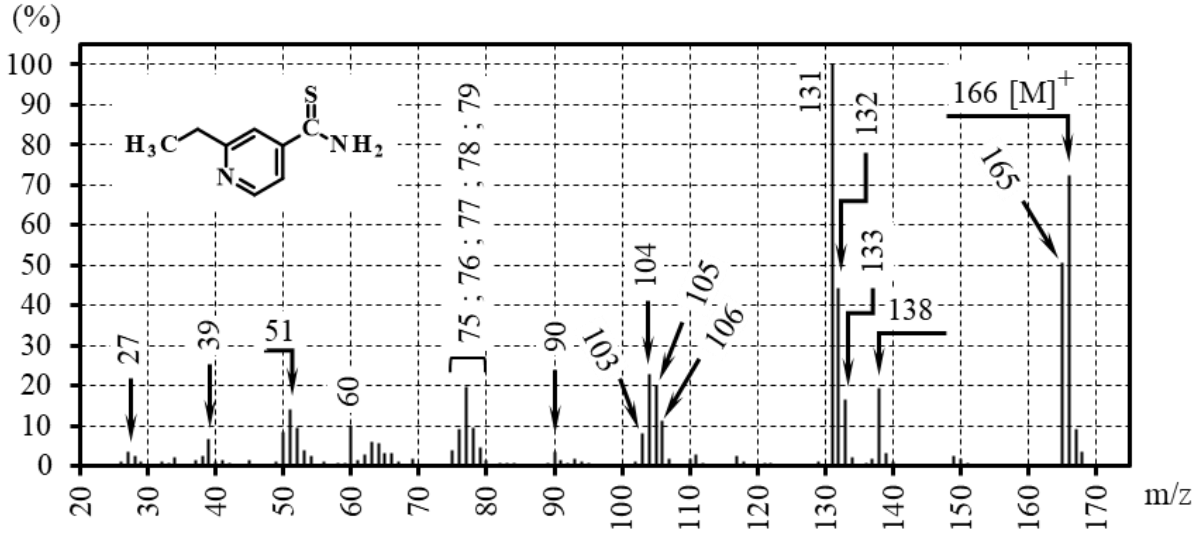

Ethchlorvynol - CAS 113-18-8 - NIST 352167



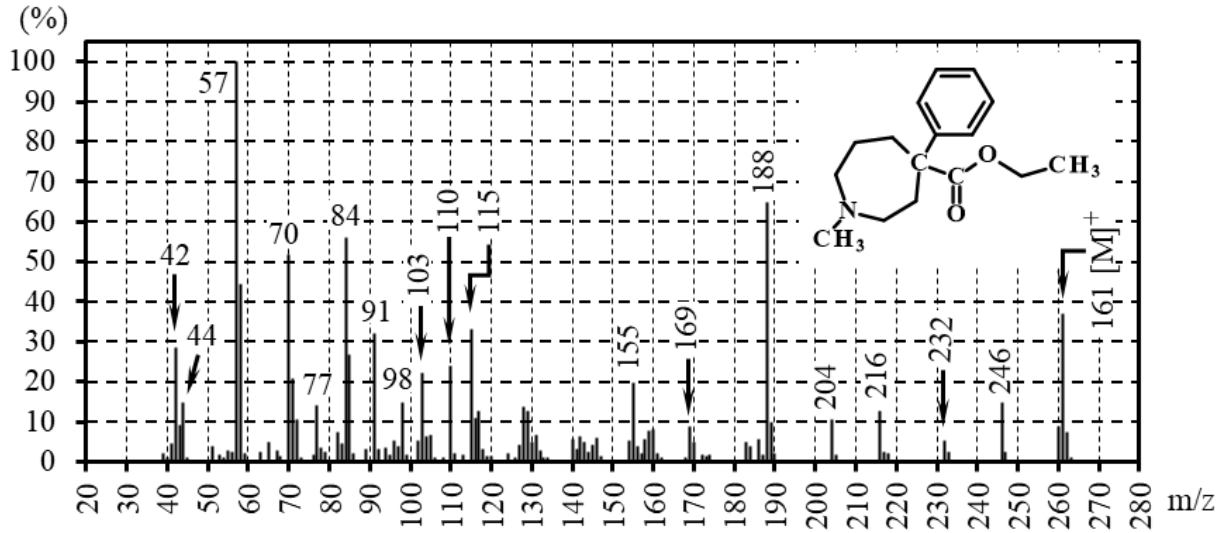

Ethinamate - CAS 126-52-3 - EI - NIST 352163



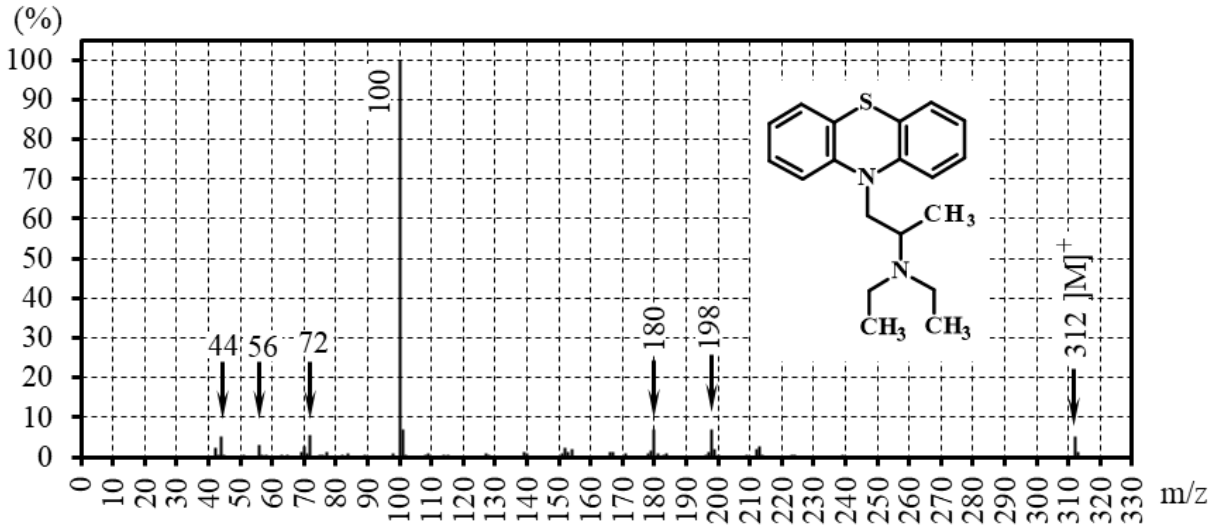

Ethinylestradiol - CAS 57-63-6 - NIST 234172



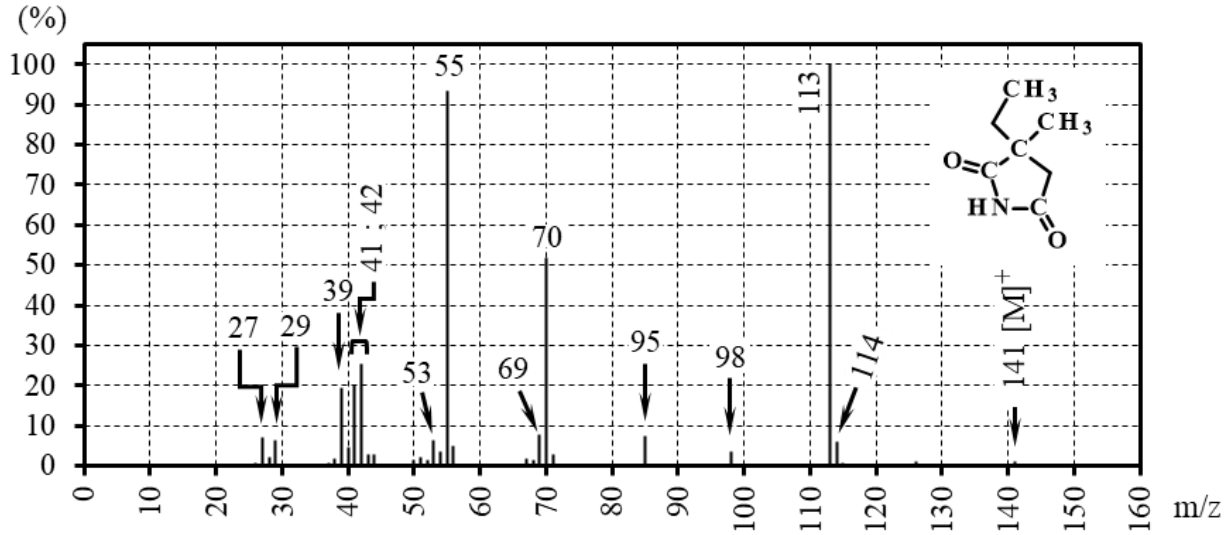

Ethionamide - CAS 536-33-4 - NIST 290504



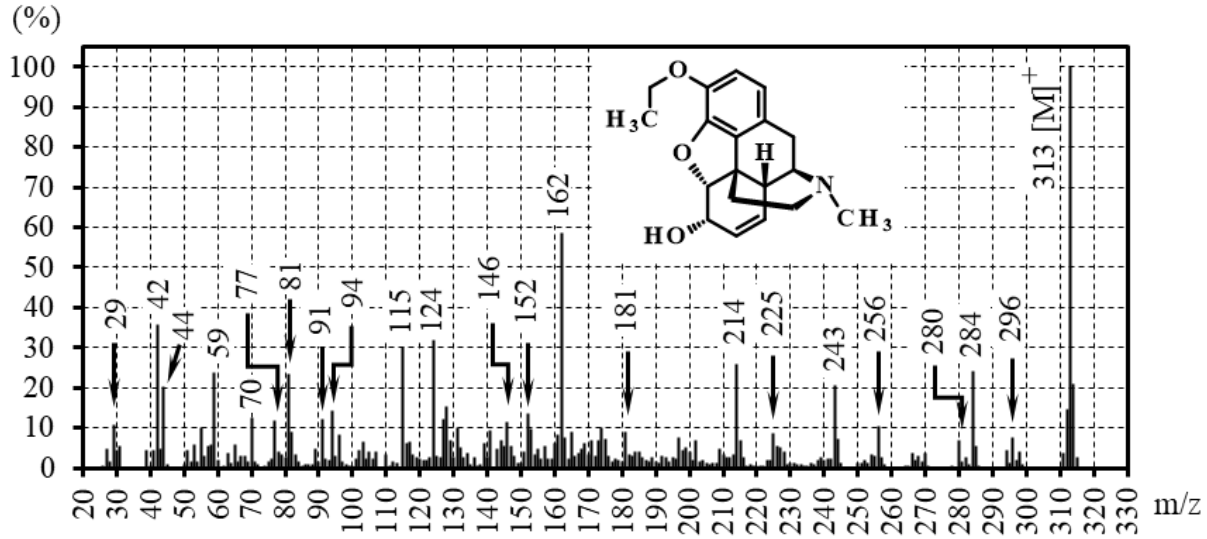

Ethoheptazine - CAS 77-15-6 - EI - NIST 246507



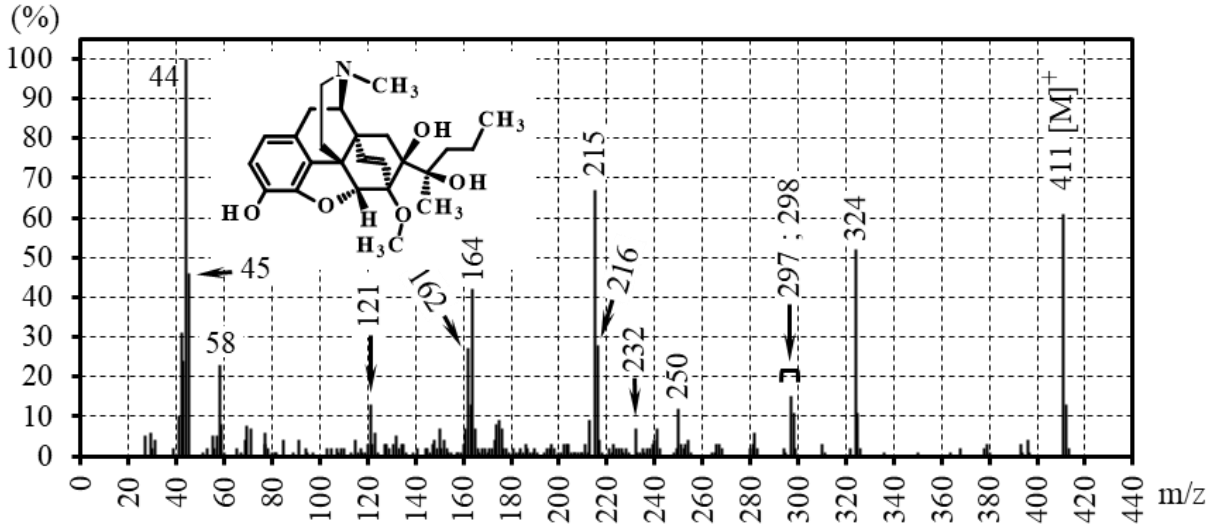

Ethopropazine - CAS 522-00-9 - EI - NIST 246857



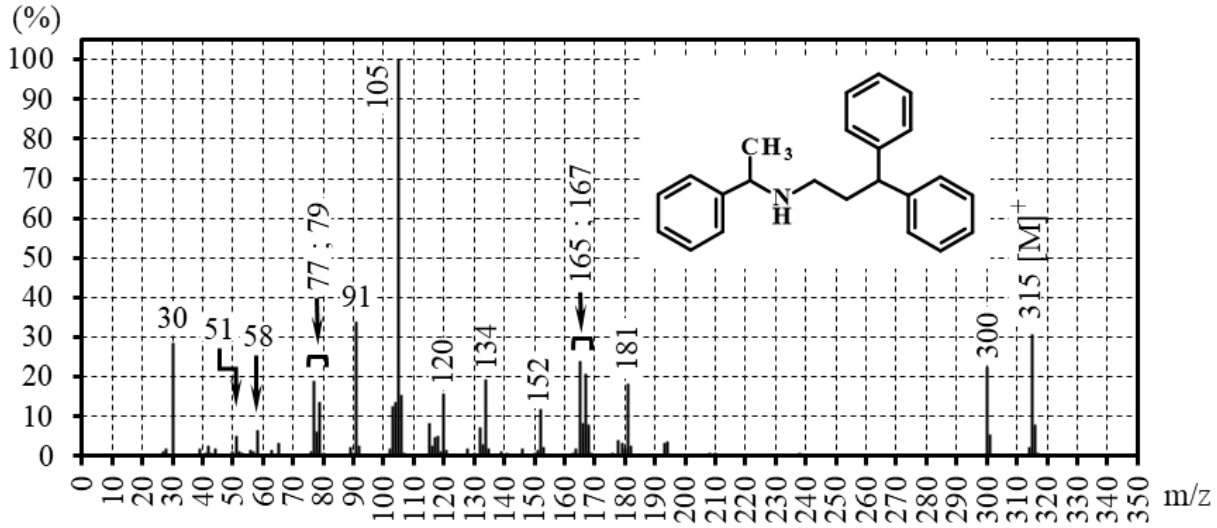

Ethosuximide - CAS 77-67-8 - EI - NIST 352149



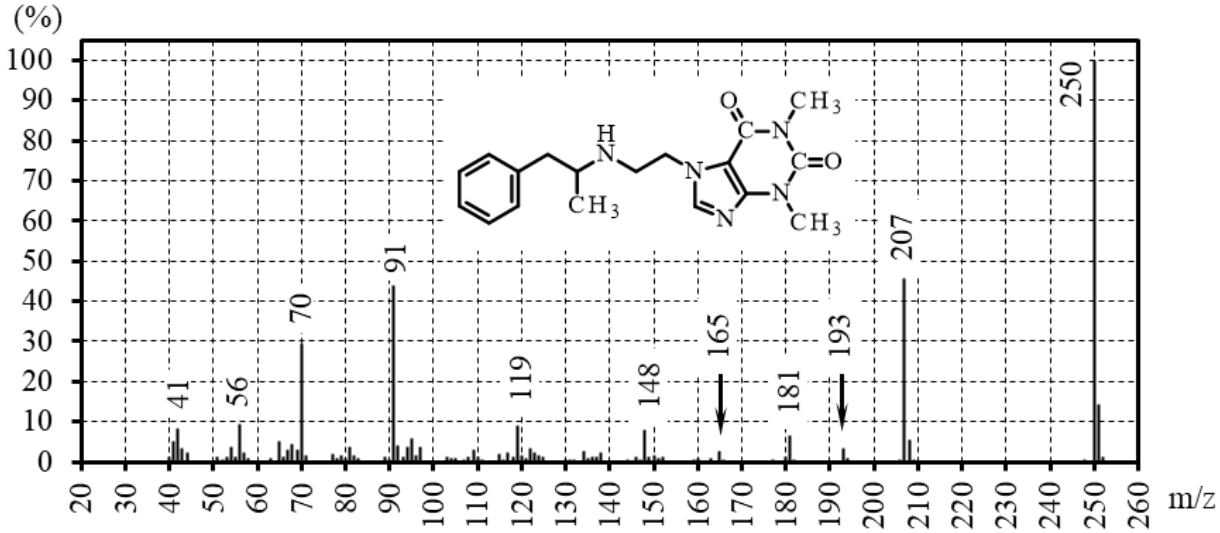

Ethylmorphine - CAS 76-58-4 - NIST 352174



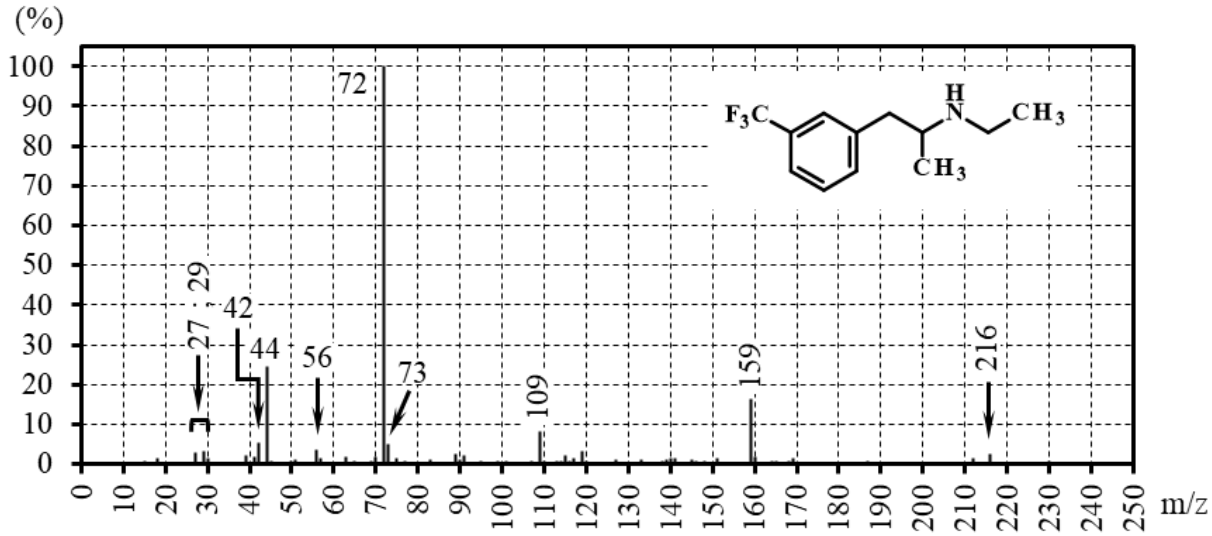

Etorphine - CAS 14521-96-1 - EI - NIST 298681



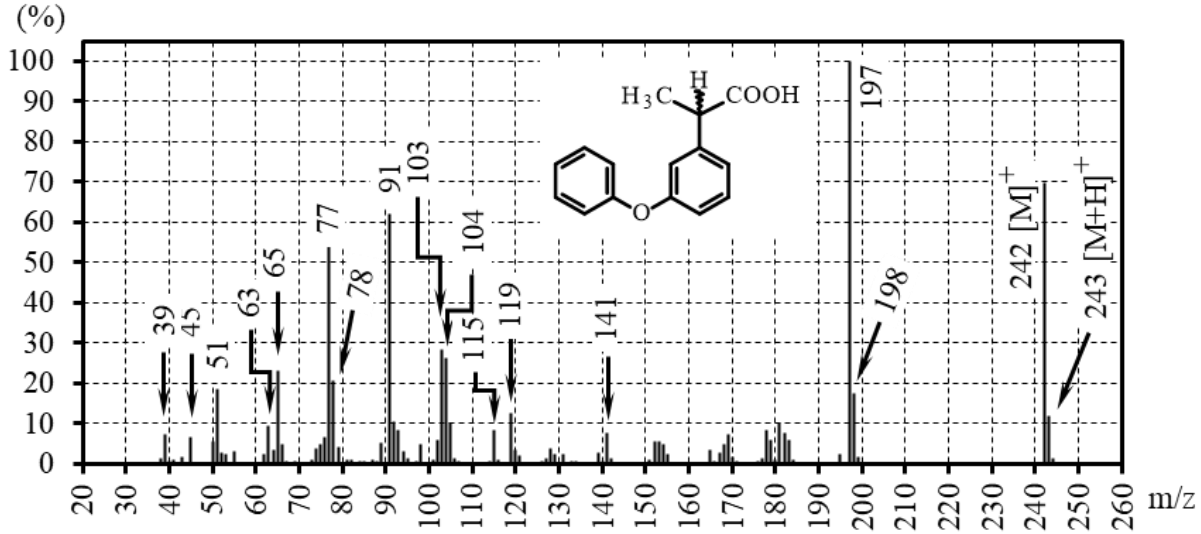

Fendiline - CAS 13042-18-7 - EI - NIST 292044



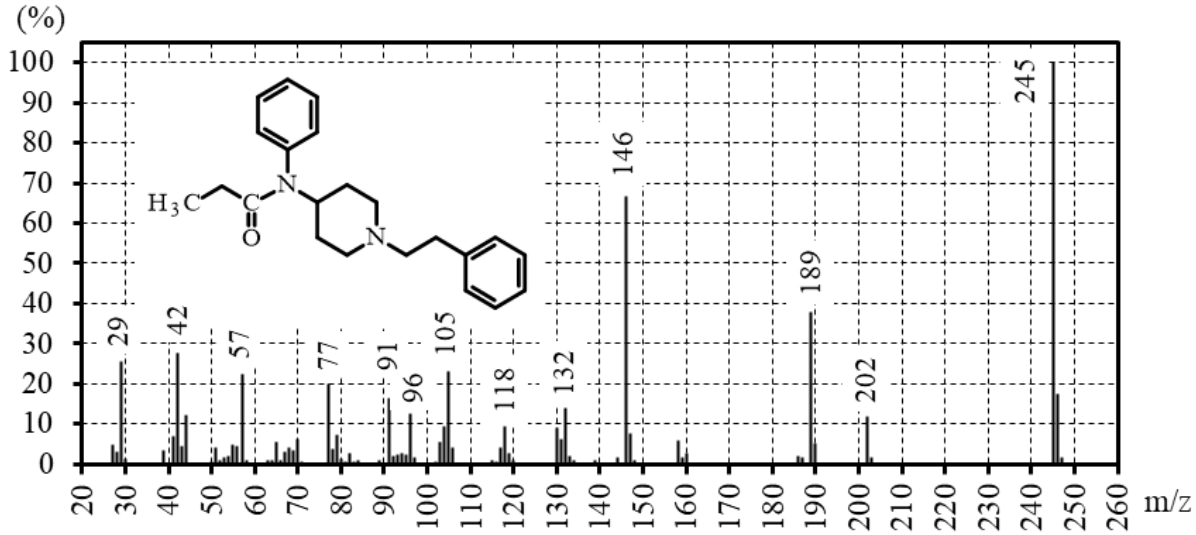

Fenethylline - CAS 3736-08-1 - NIST 335544



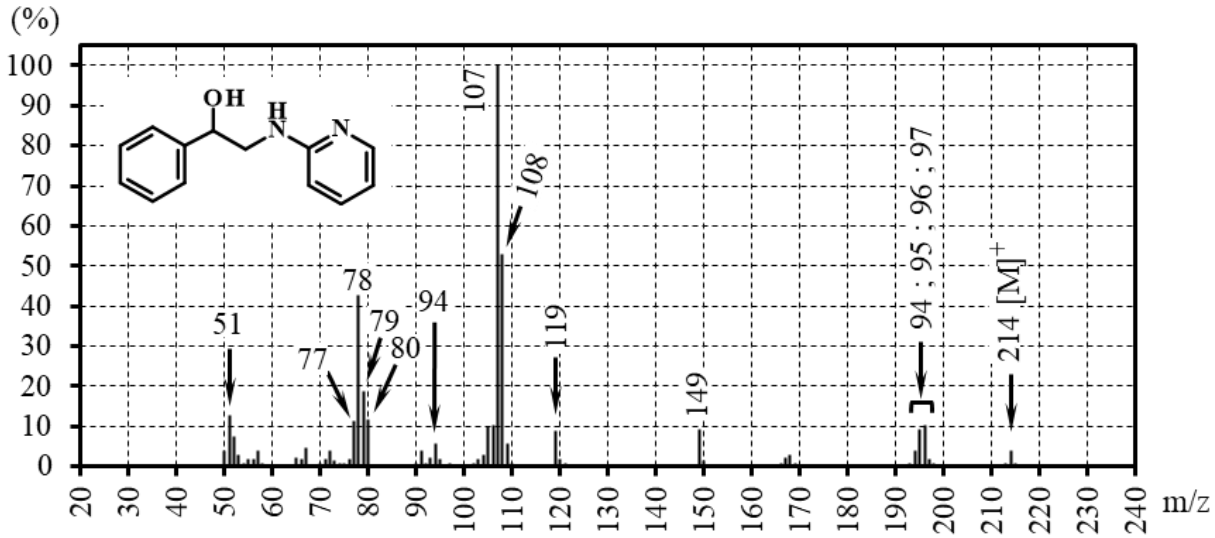

Fenfluramine - CAS 458-24-2 - EI - NIST 250583



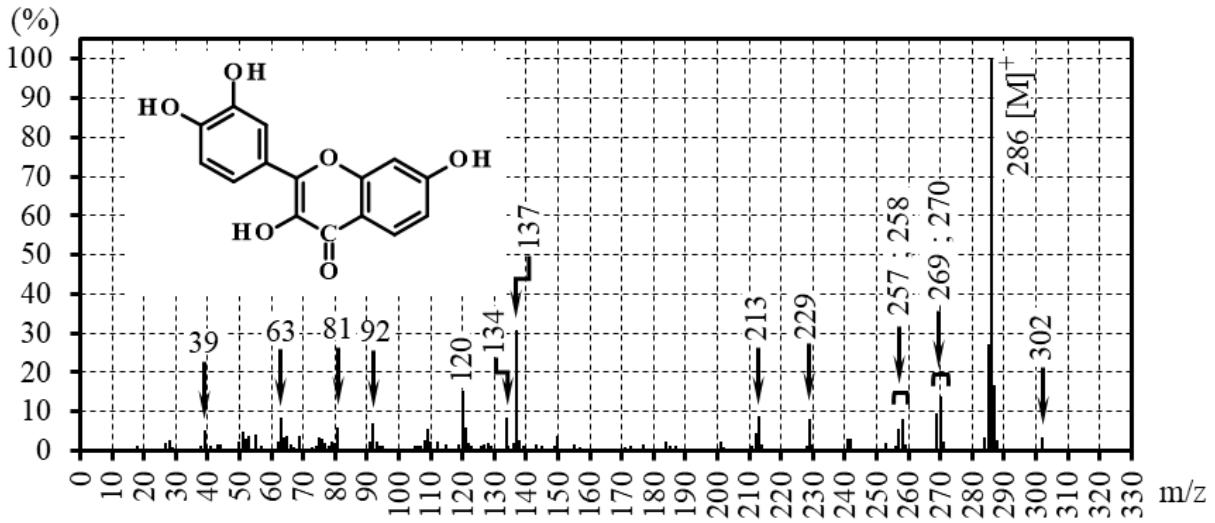

Fenoprofen - CAS 31879-05-7 - NIST 246389



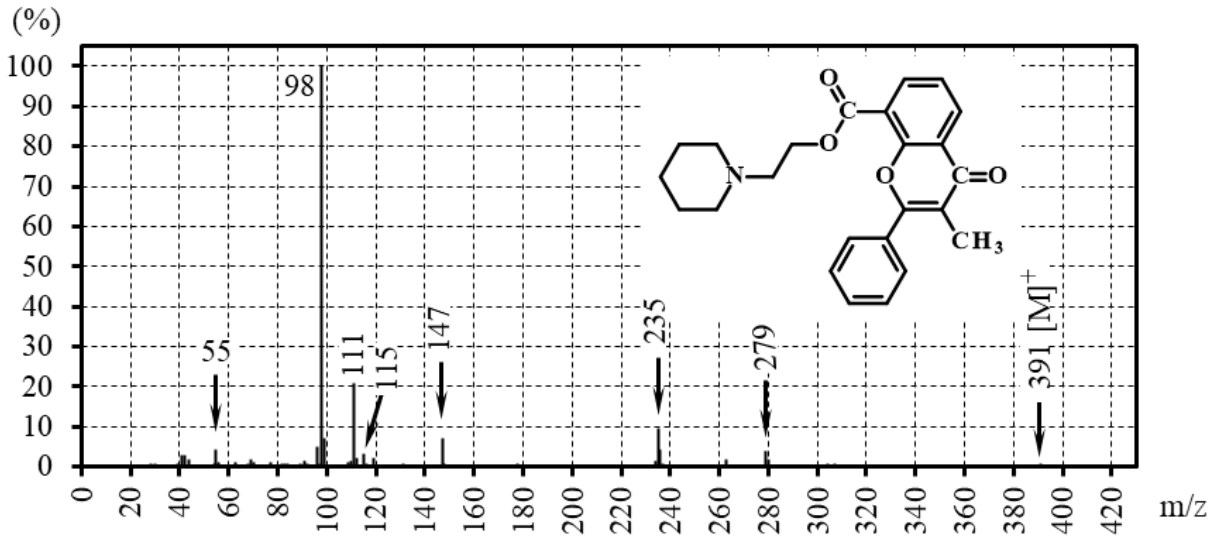

Fentanyl - CAS 437-38-7 - NIST 250541



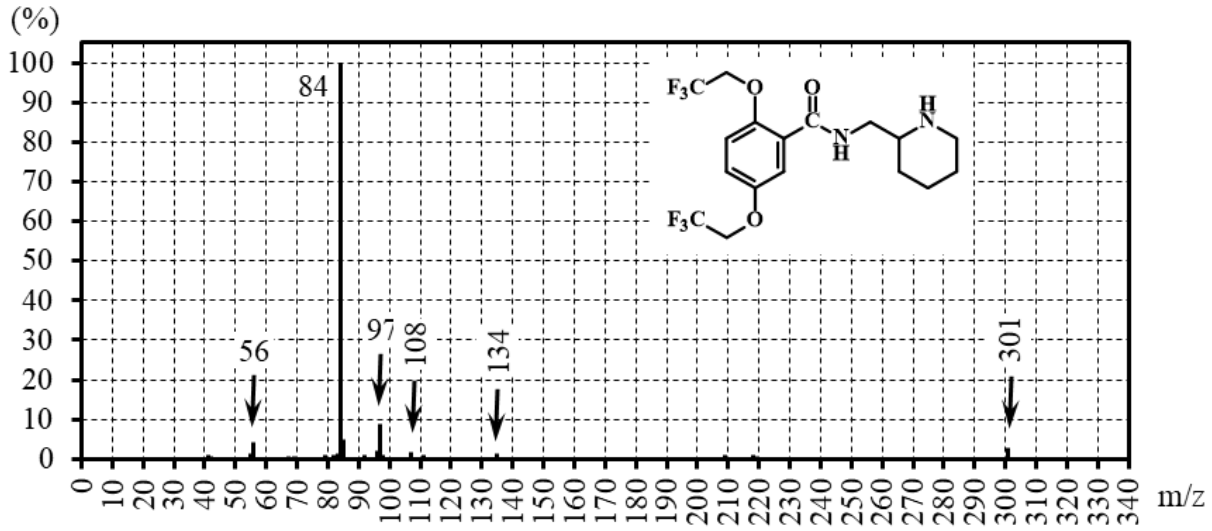

Fenyramidol - CAS 553-69-5 - EI - NIST 246223



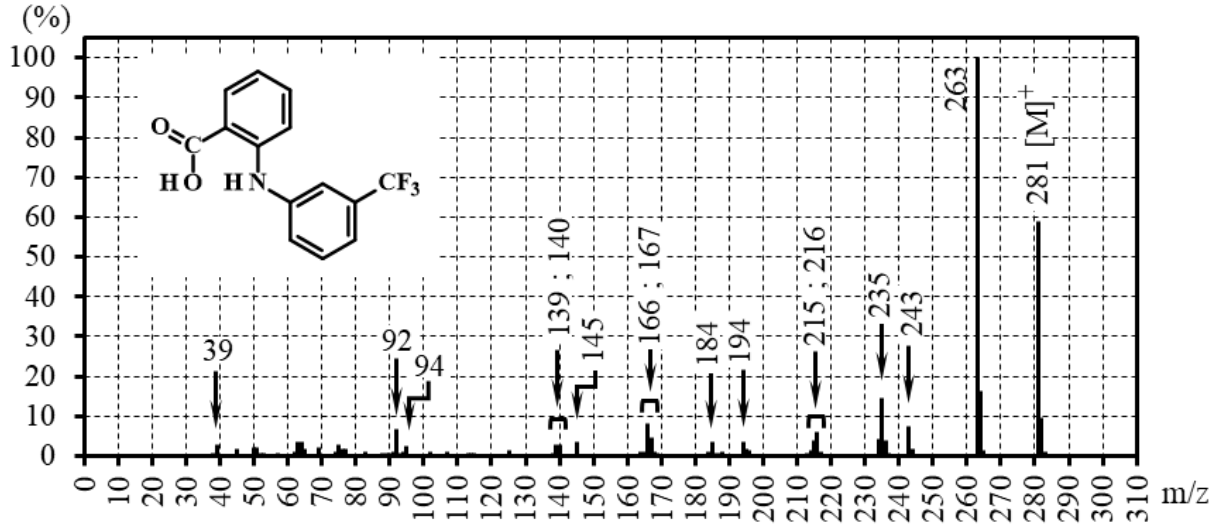

Fisetin - CAS 528-48-3 - EI 75 eV - Source 230 $^{O}$C - Sample 250 $^{O}$C - SDBS 927



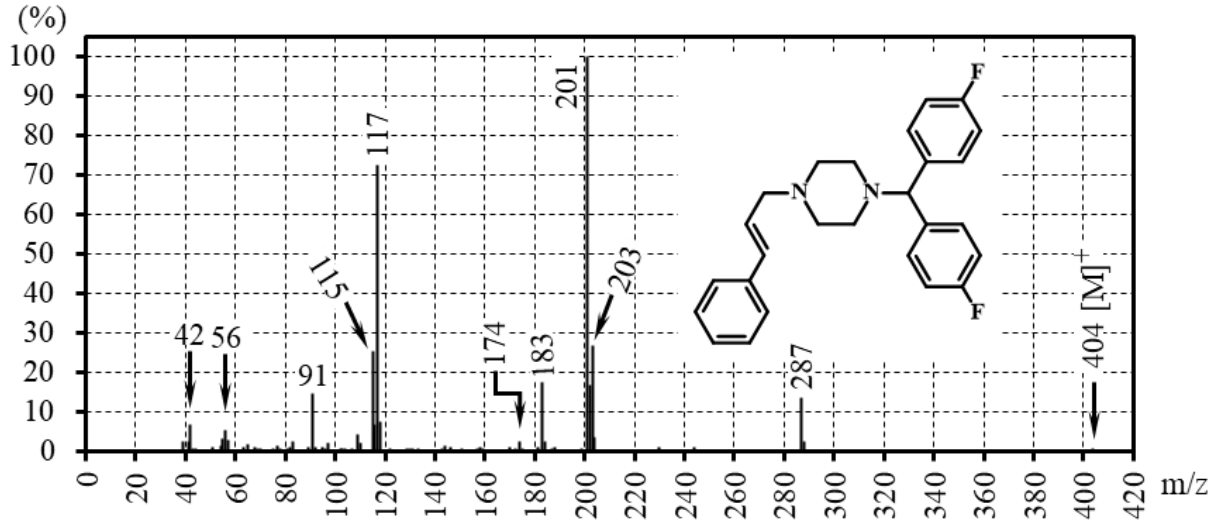

Flavoxate - CAS 15301-69-6 - EI - 235682



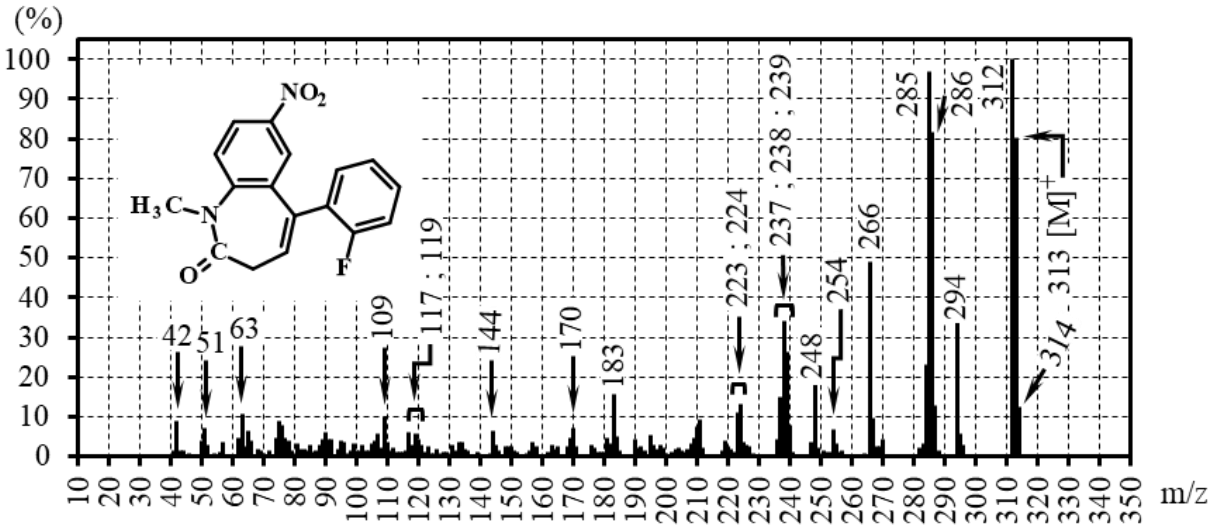

Flecainide - CAS 54143-55-4 - EI - NIST 248228



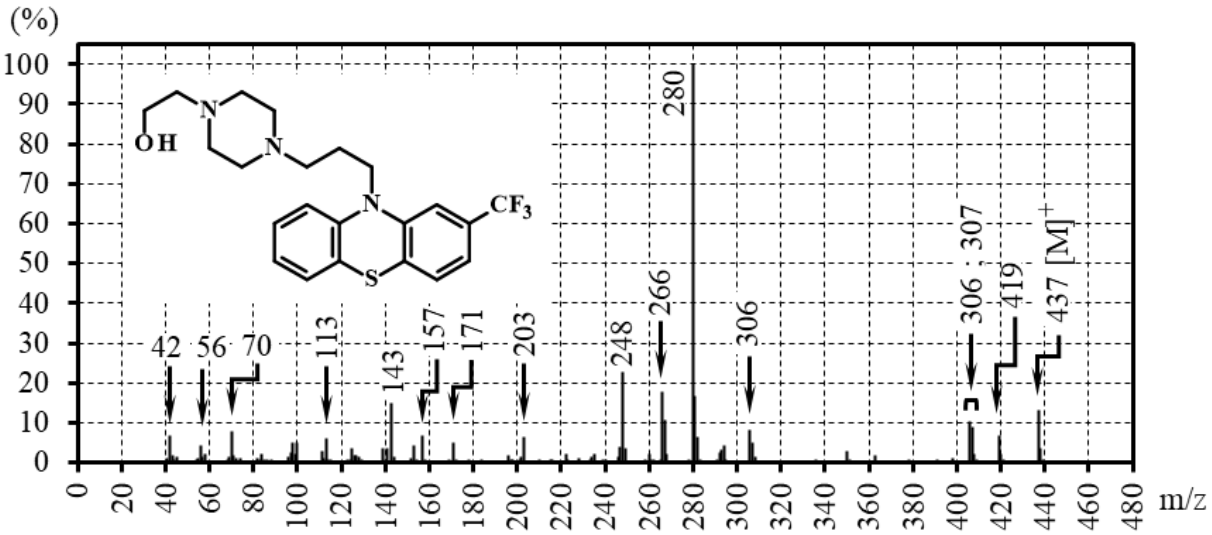

Flufenamic acid - CAS 530-78-9 - EI - NIST 133515



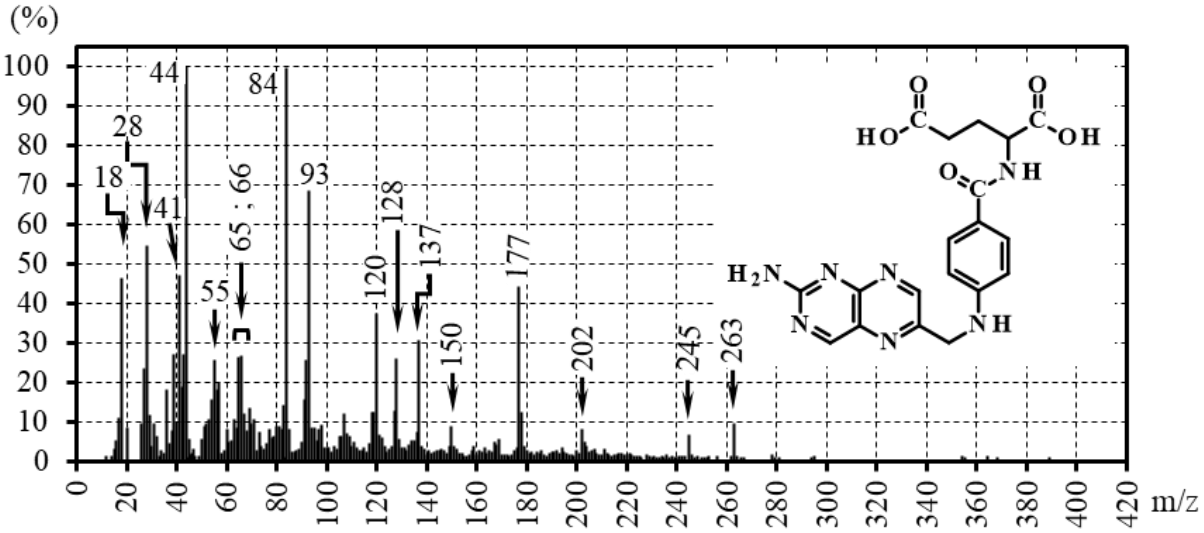

Flunarizine - CAS 52468-60-7 - EI - NIST 247479



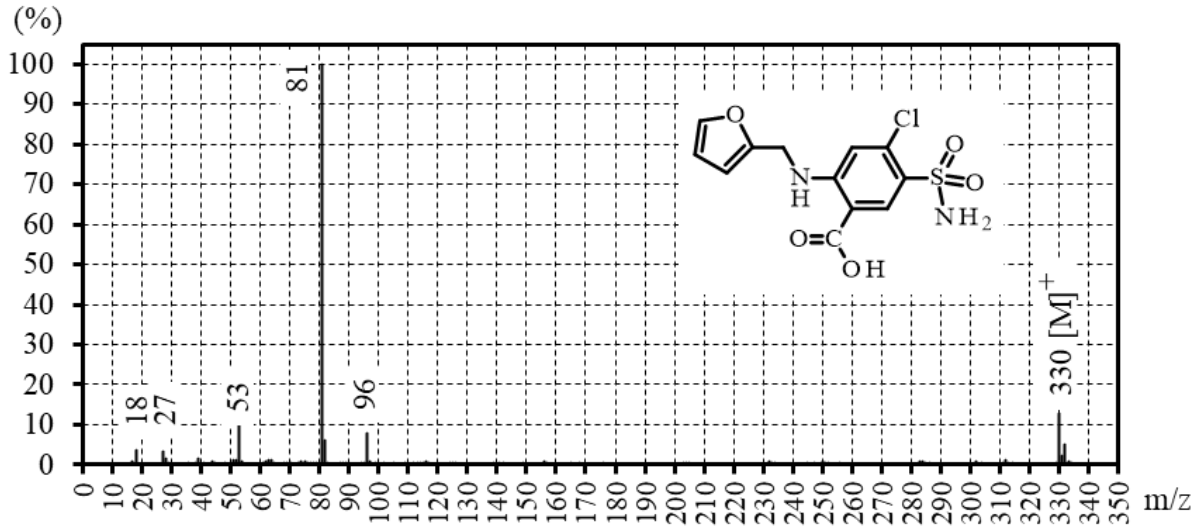

Flunitrazepam - CAS 1622-62-4 - EI - NIST 125739



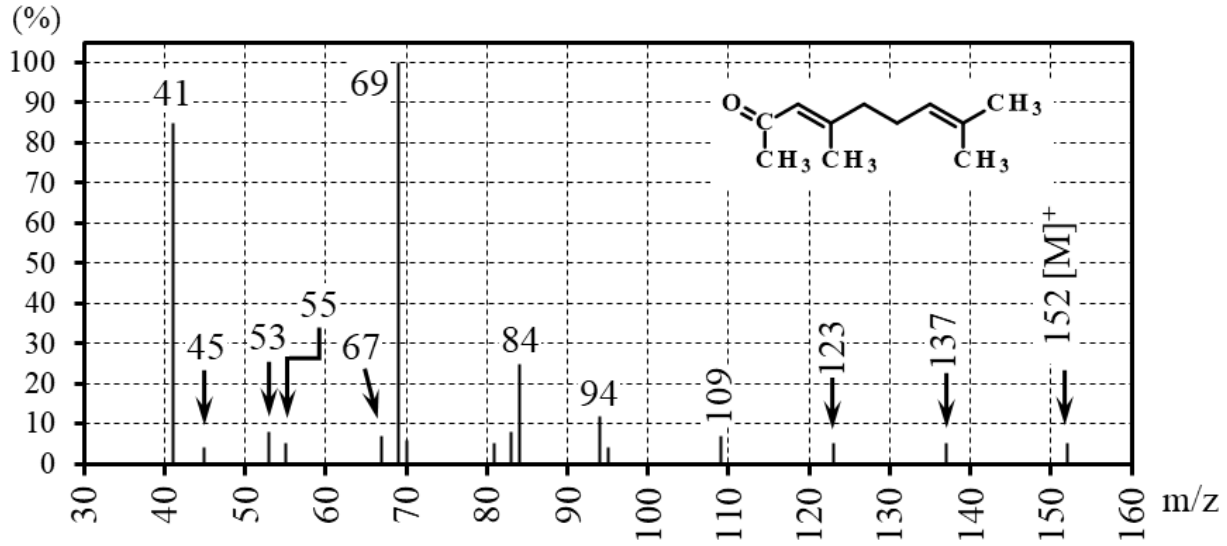

Fluphenazine - CAS 69-23-8 - EI - NIST 247652



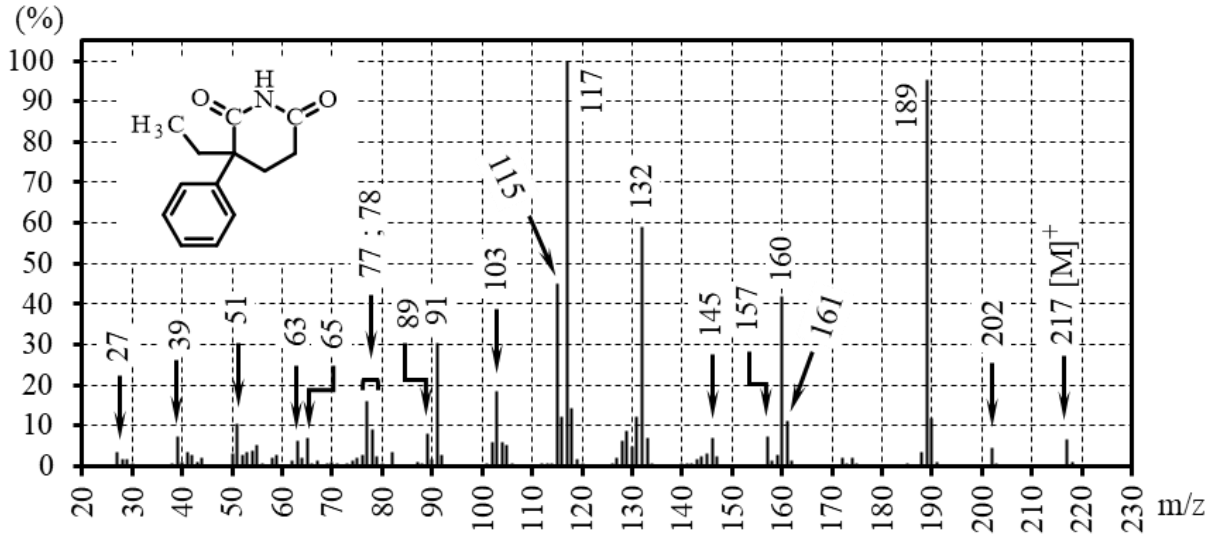

Folic acid - CAS 59-30-3 - NIST 228207



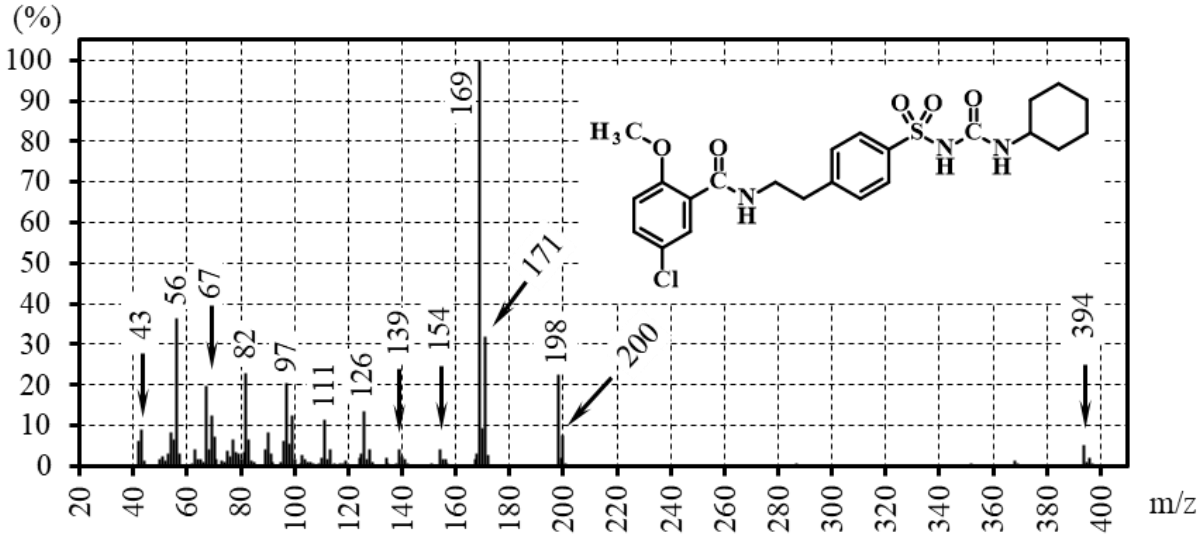

Furosemide - CAS 54-31-9 - EI 75 eV - SDBS nr. 7060



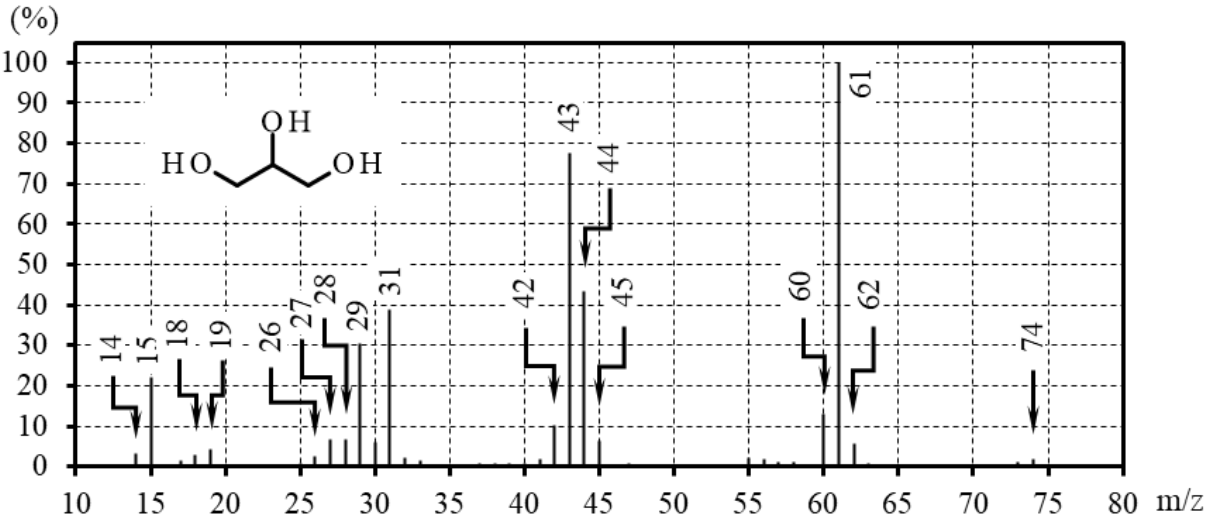

Geranial (Citral A) - EI - CAS 141-27-5 - NIST 159020



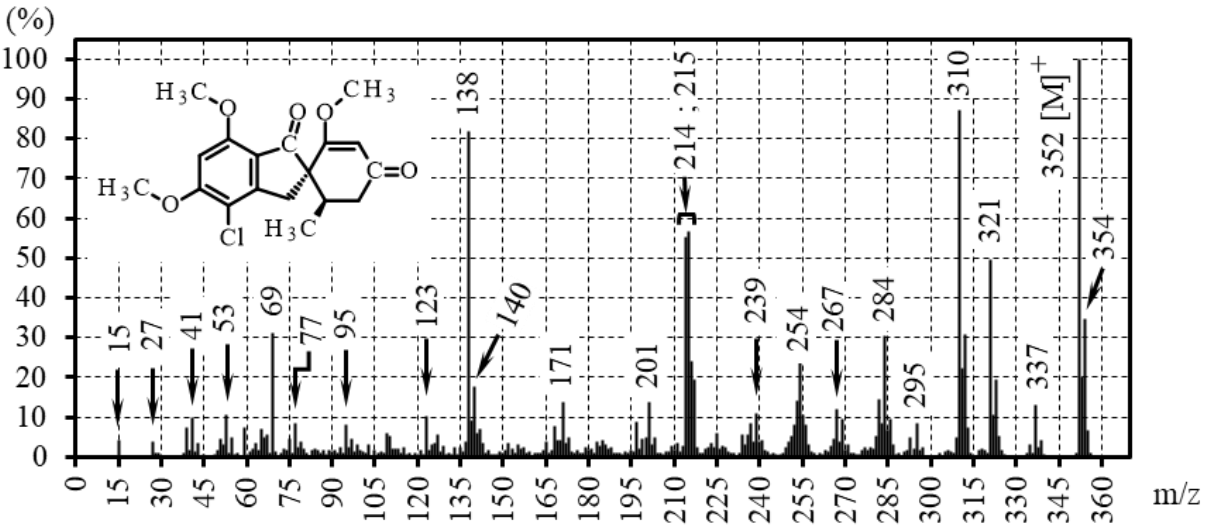

Glutethimide - CAS 77-21-4 - NIST 352165



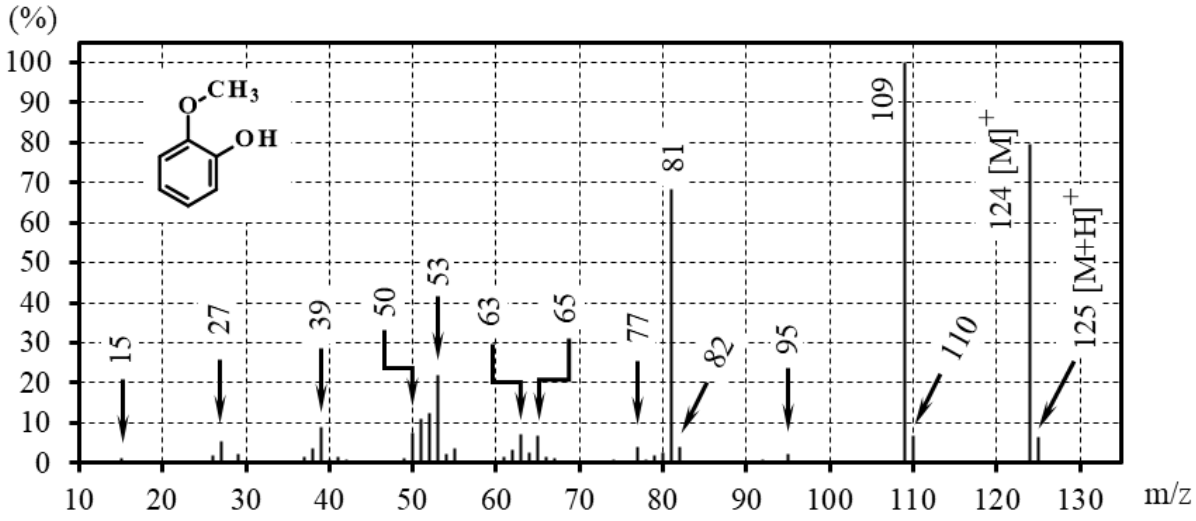

Glyburide (Glibenclamide) - CAS 10238-21-8 - NIST 247159



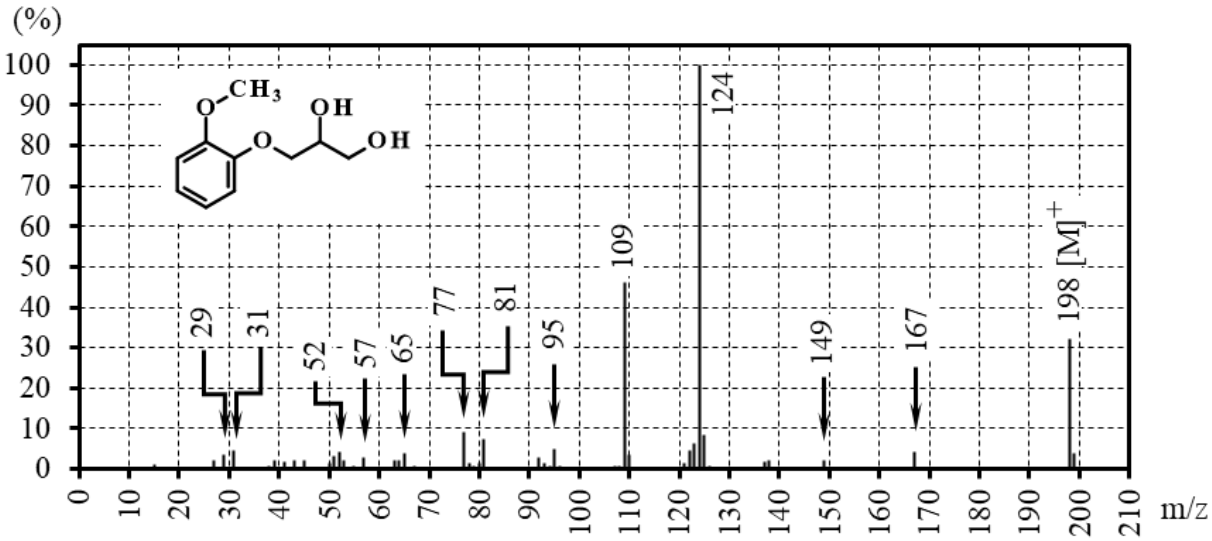

Glycerin (Glicerol) - CAS 56-81-5 - NIST 118748



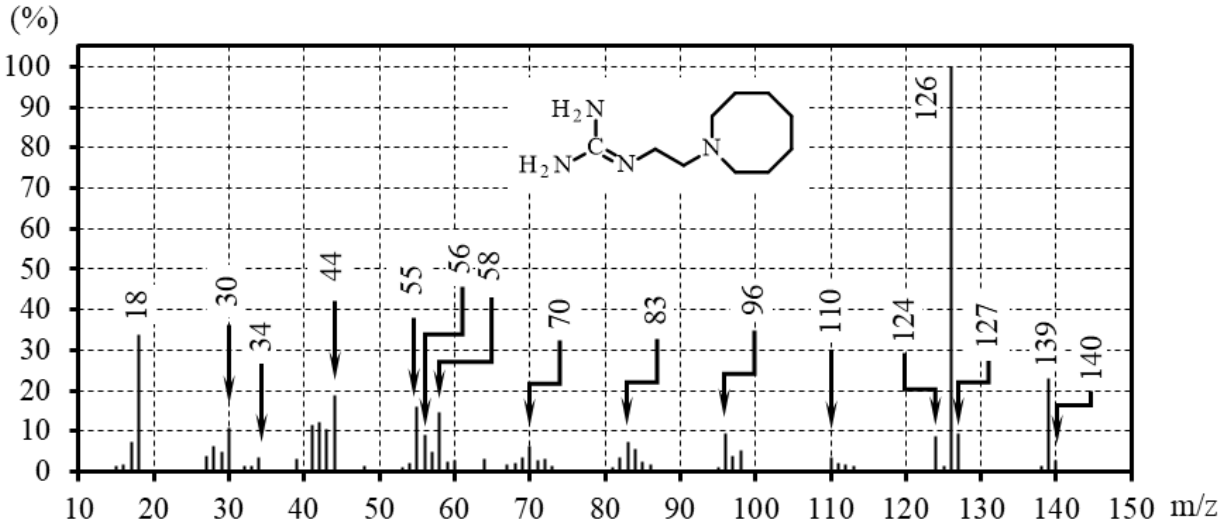

Griseofulvin - CAS 126-07-8 - NIST 238364



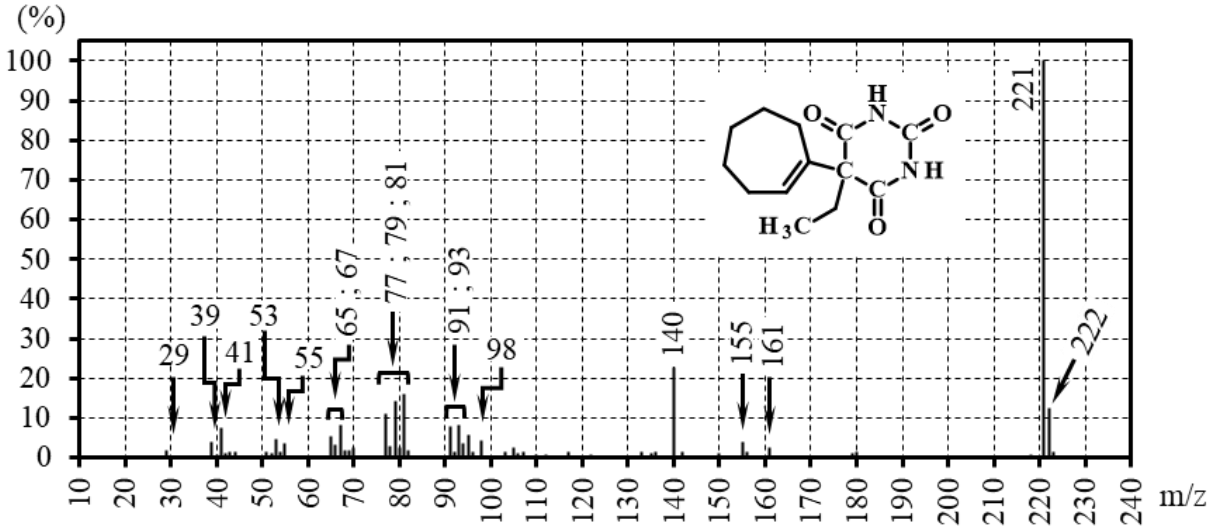

Guaiacol - CAS 90-05-1 - NIST 291437



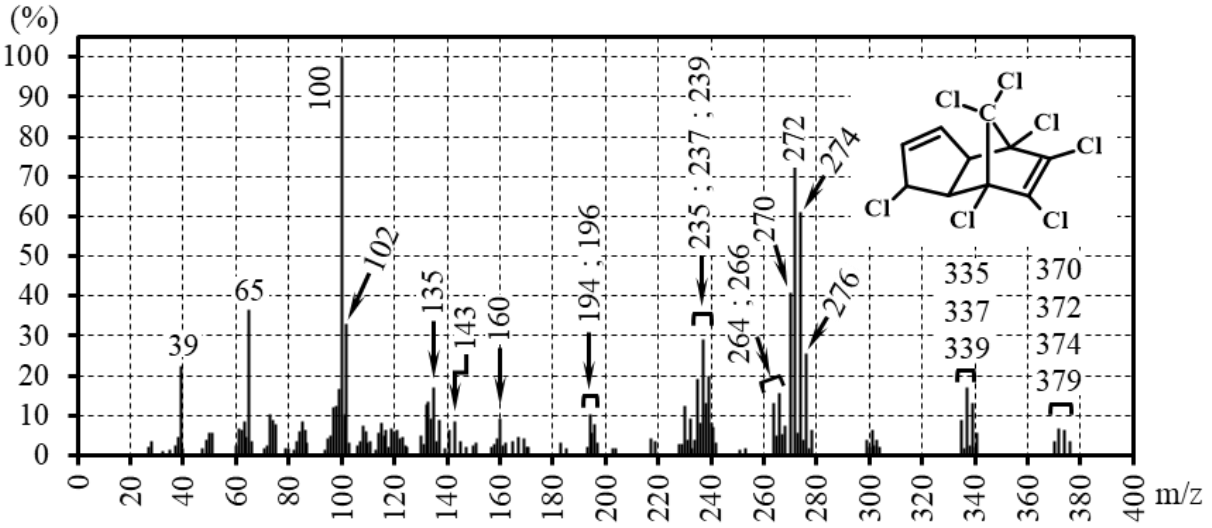

Guaifenesin - CAS 93-14-1 - NIST 232326



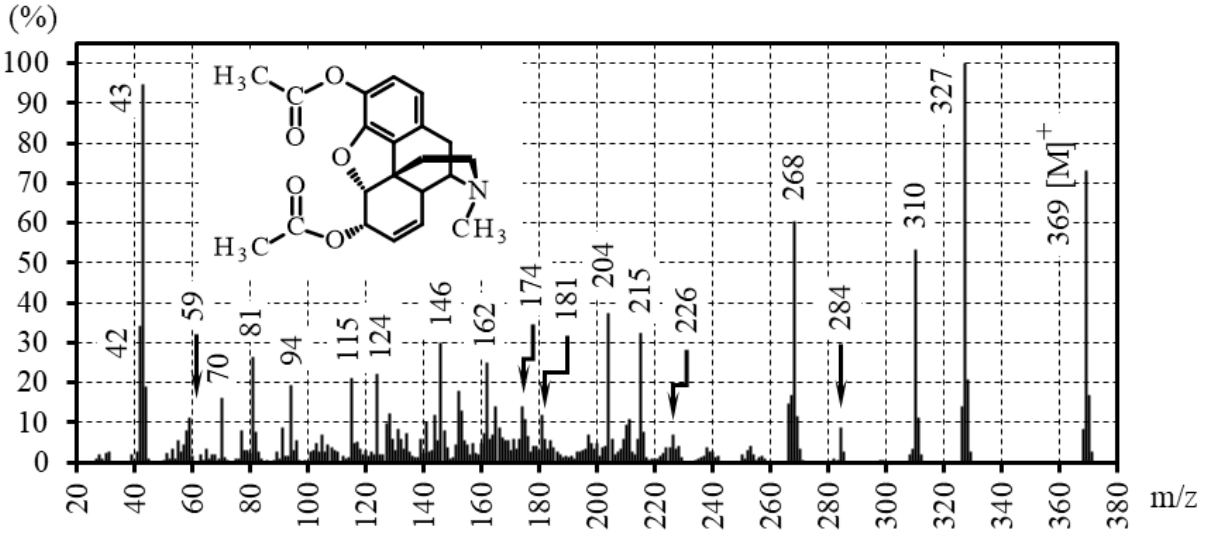

Guanethidine - CAS 645-43-2 - EI 75 eV - SDBS nr. 6851



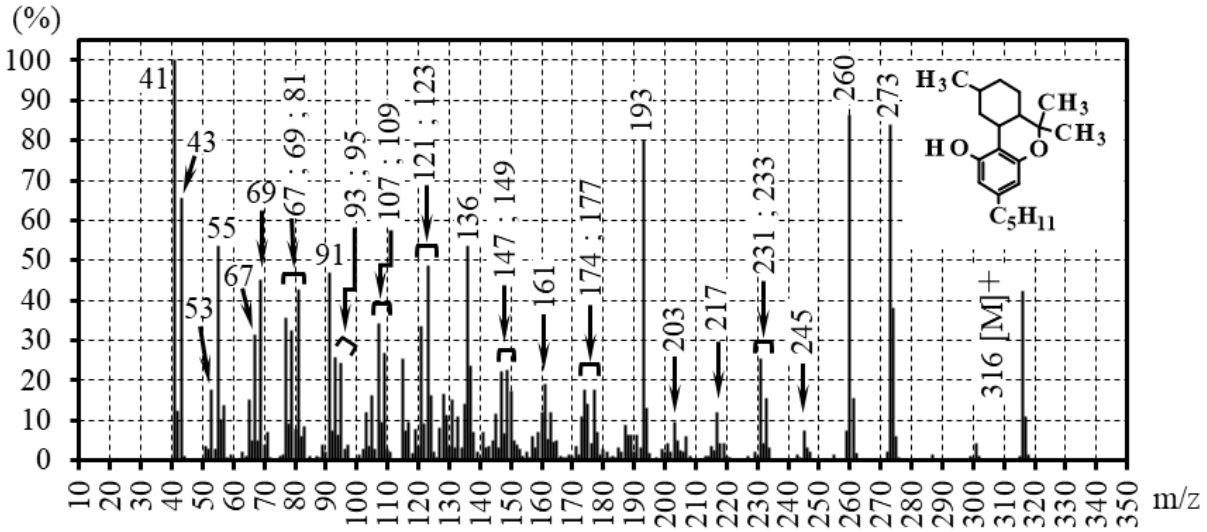

Heptabarbital - CAS 509-86-4 - EI - NIST 246436



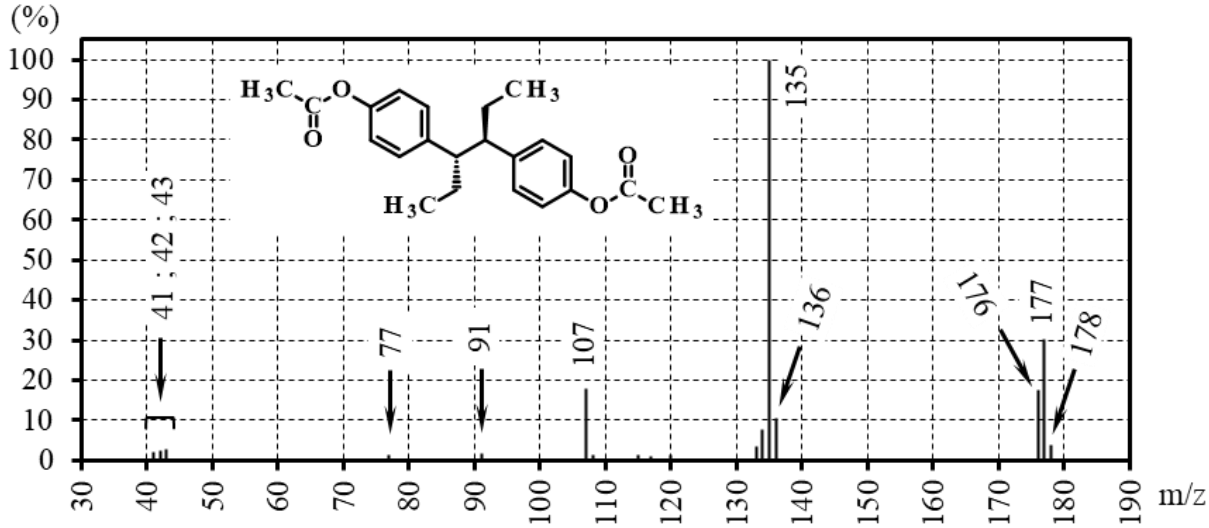

Heptachlor - CAS 76-44-8 - EI - NIST 114991



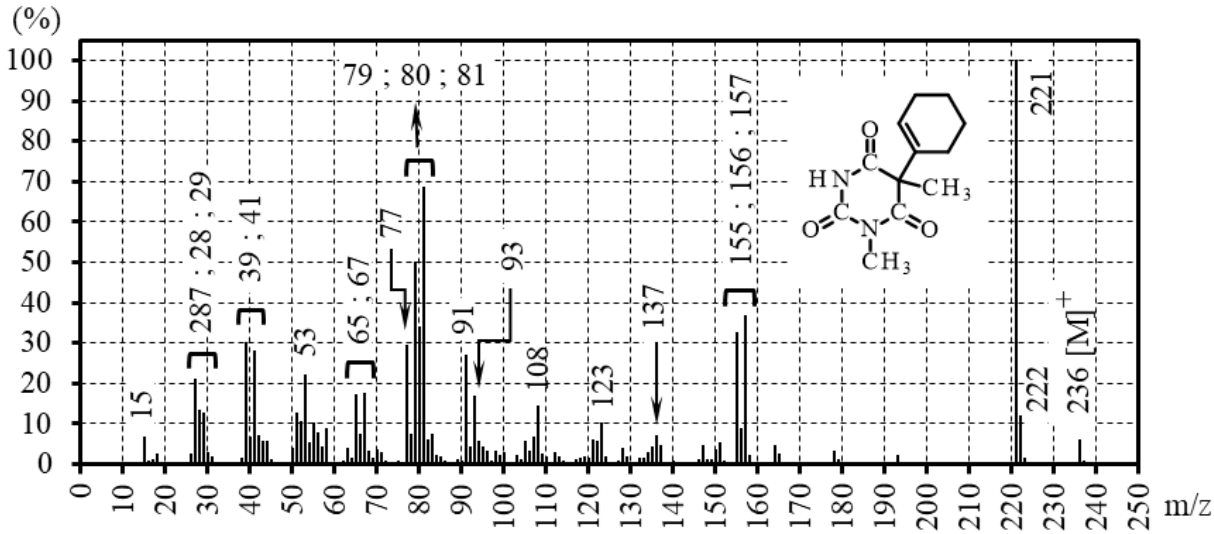

Heroin (Diacetyl morphine) - CAS 561-27-3 - EI - NIST 352937



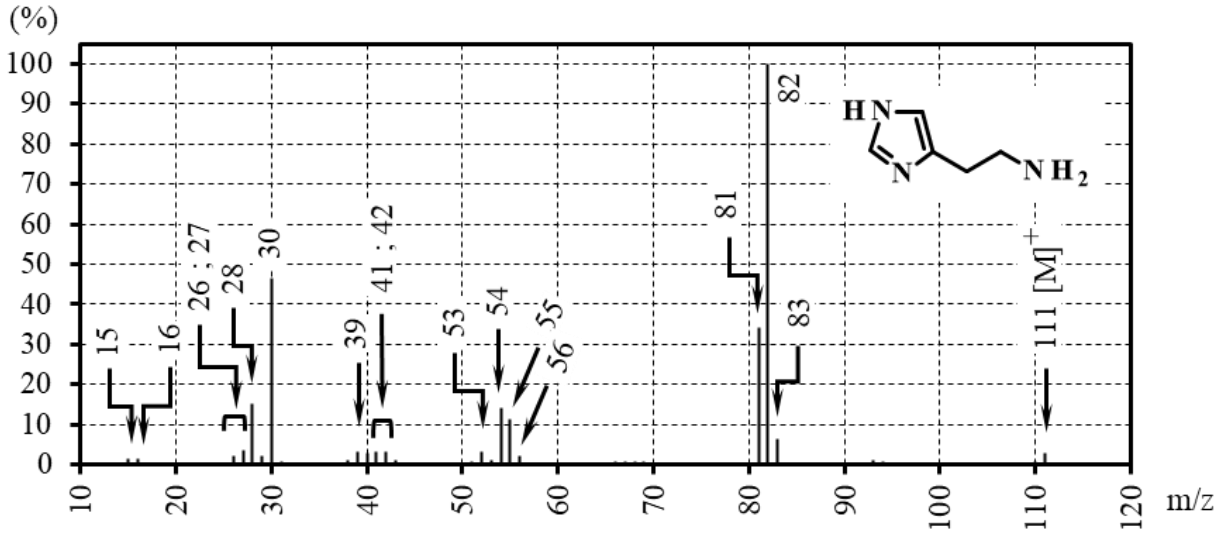

Hexahydrocannabinol - CAS 6692-85-9 - EI - NIST 247943



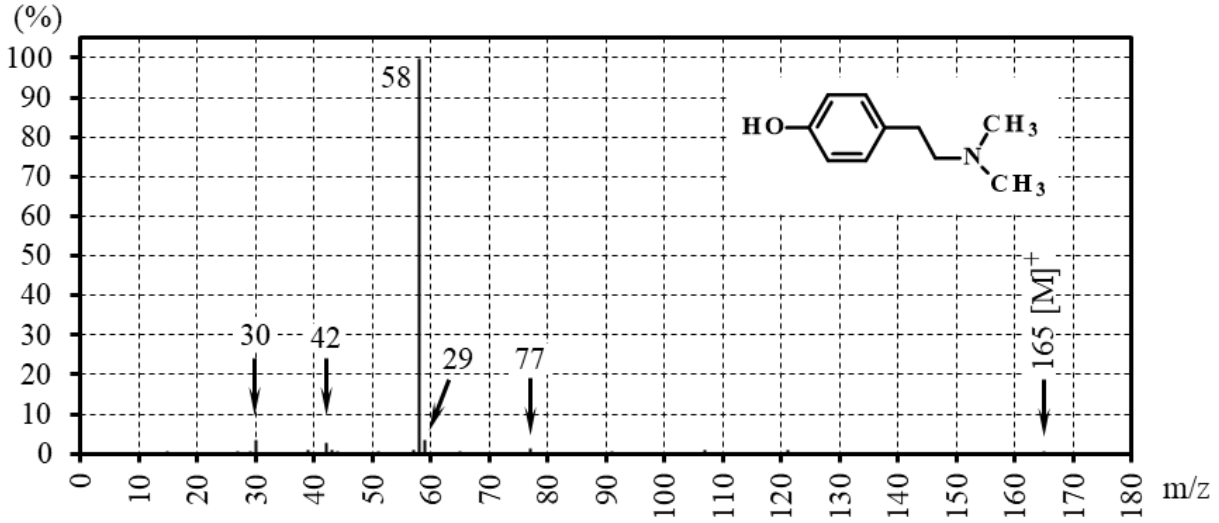

Hexestrol diacetate - CAS 4547-76-6 - SDBS 32190



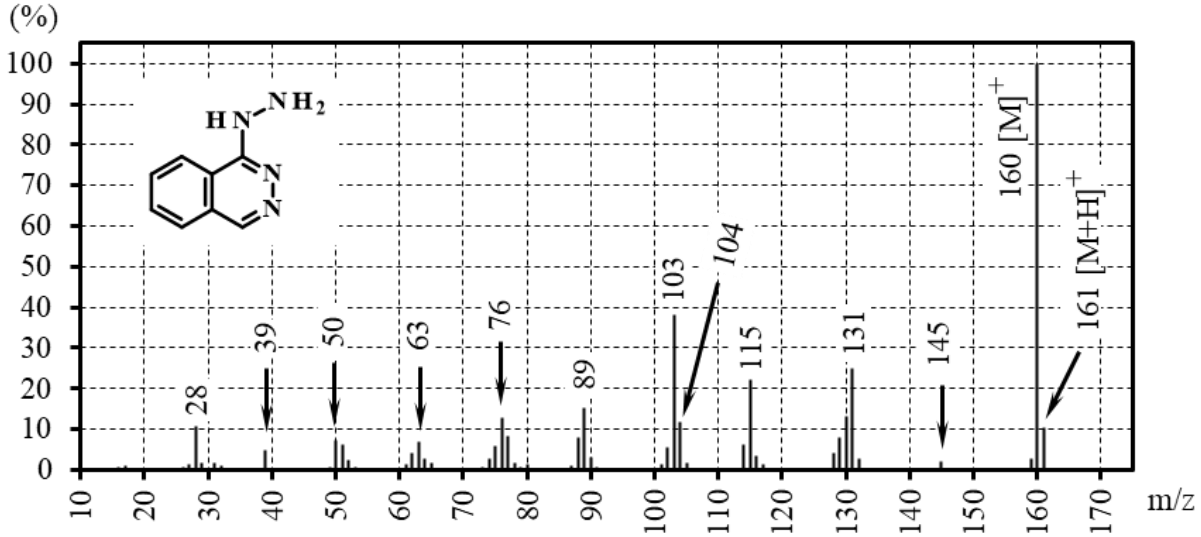

Hexobarbital - CAS 56-29-1 - EI 70 ev - NIST 286633



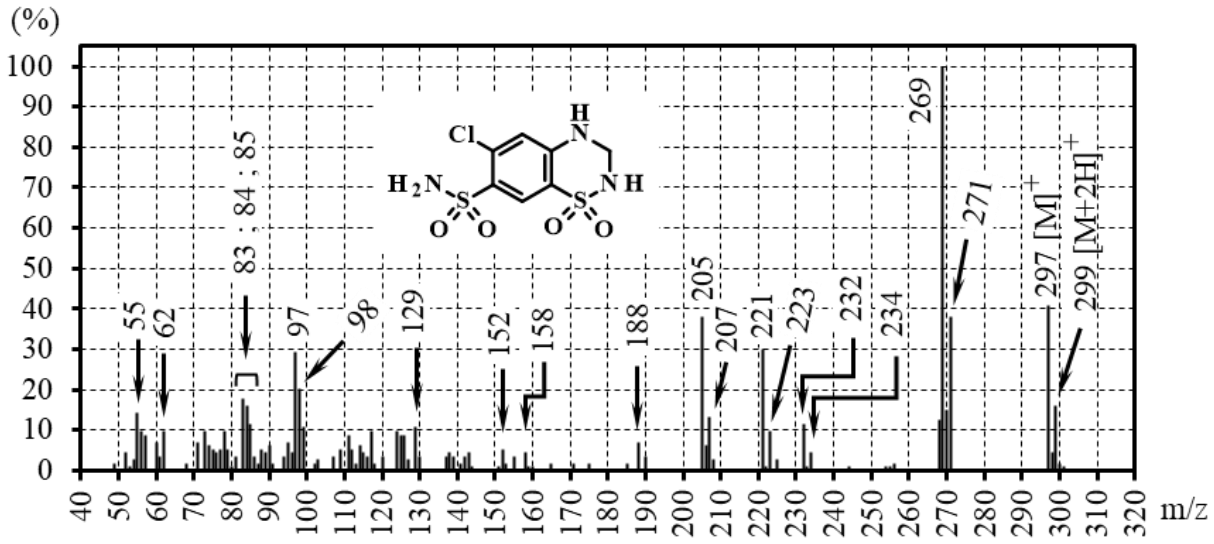

Histamine - CAS 51-45-6 - NIST 1577



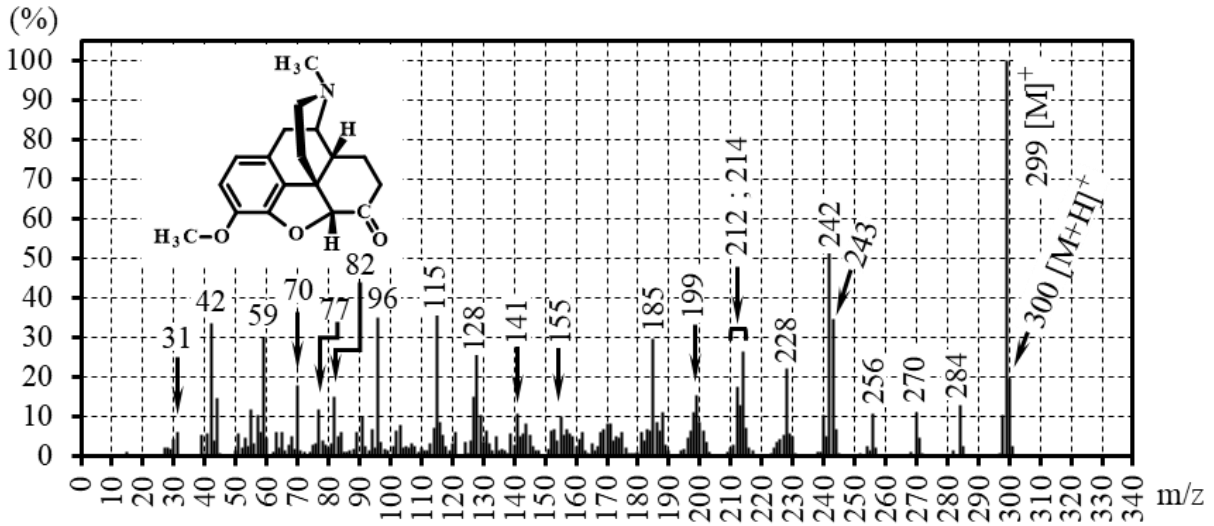

Hordenine (Eremursine, Anhaline) - CAS 539-15-1 - EI - NIST 229057



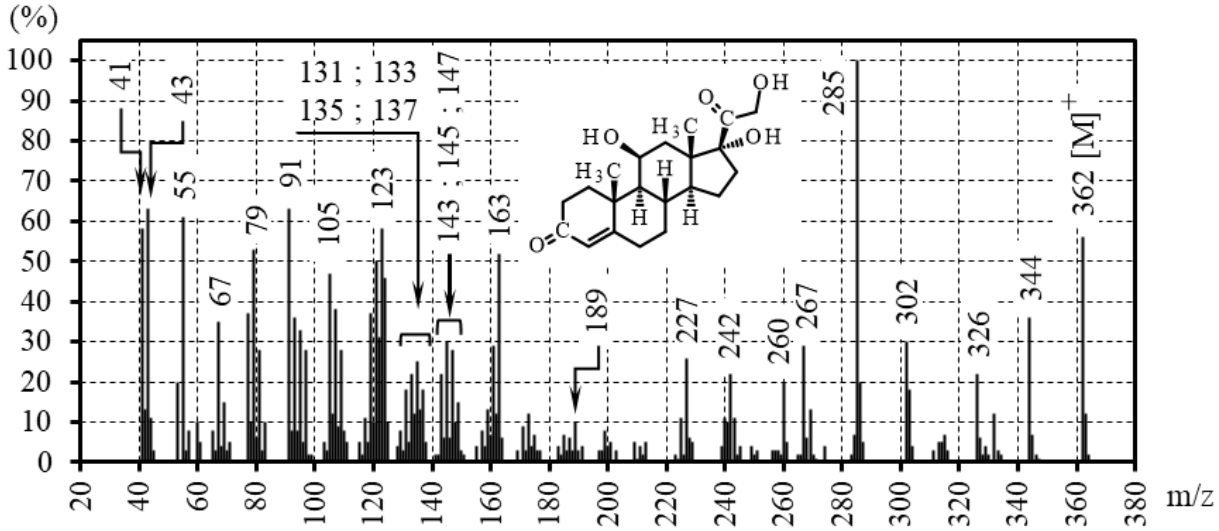

Hydralazine - CAS 86-54-4 - NIST 231803



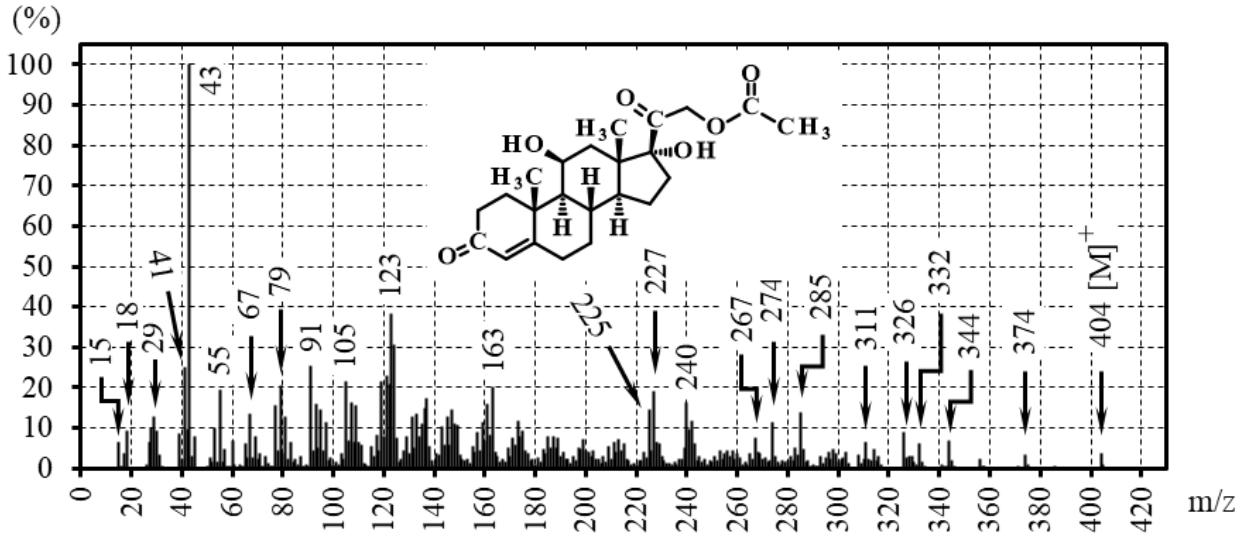

Hydrochlorothiazide - CAS 58-93-5 - NIST 74591



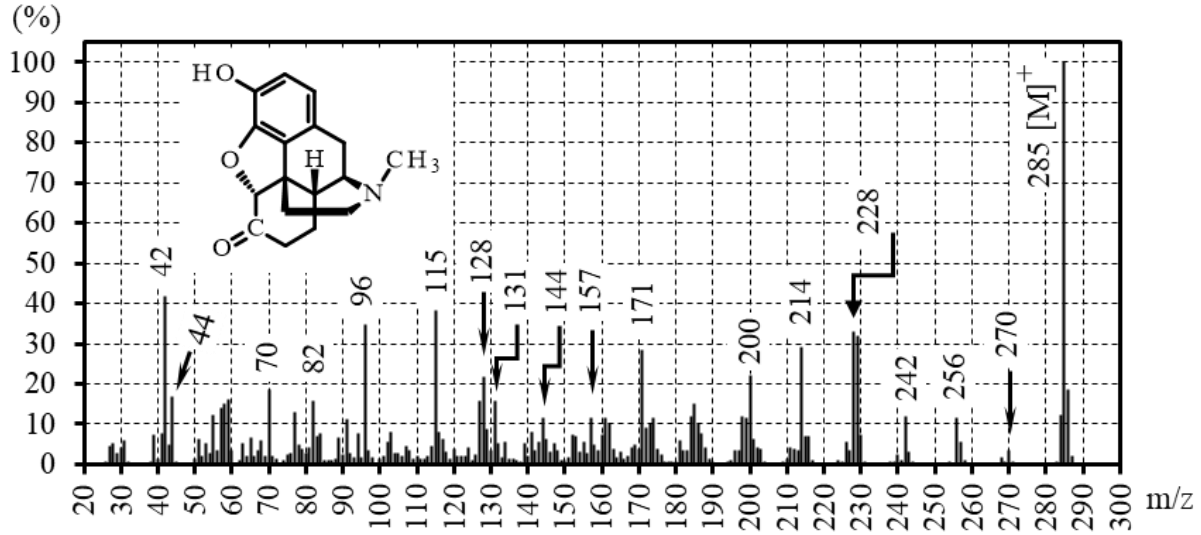

Hydrocodone - CAS 125-29-1 - EI - NIST 352146



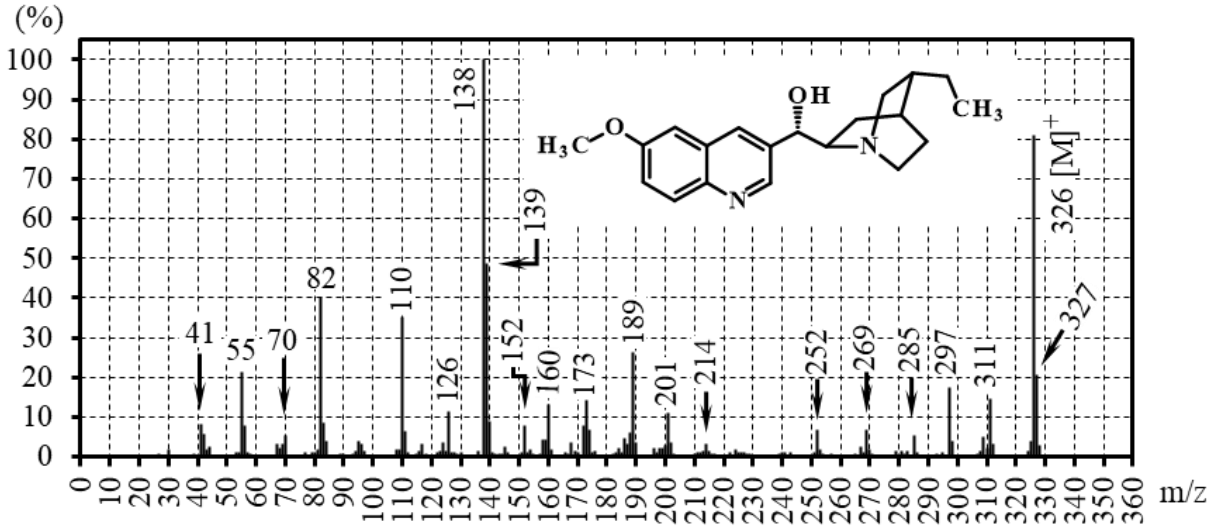

Hydrocortisone - CAS 50-23-7 - EI - NIST nr. 16228



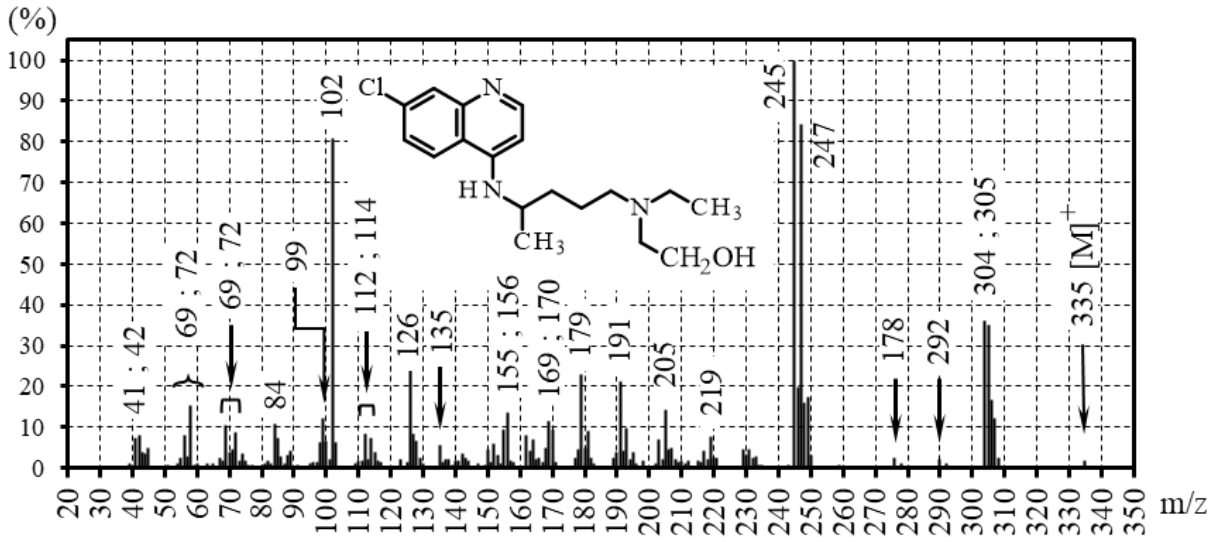

Hydrocortisone acetate - CAS 50-03-3 - NIST 234244



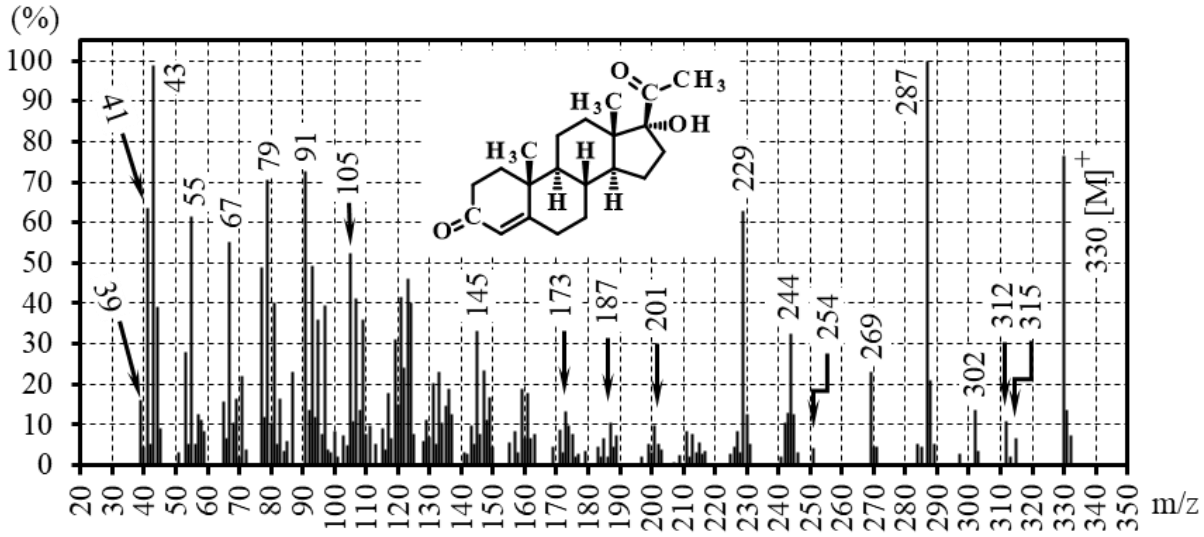

Hydromorphone - CAS 466-99-9 - EI - NIST nr. 352952



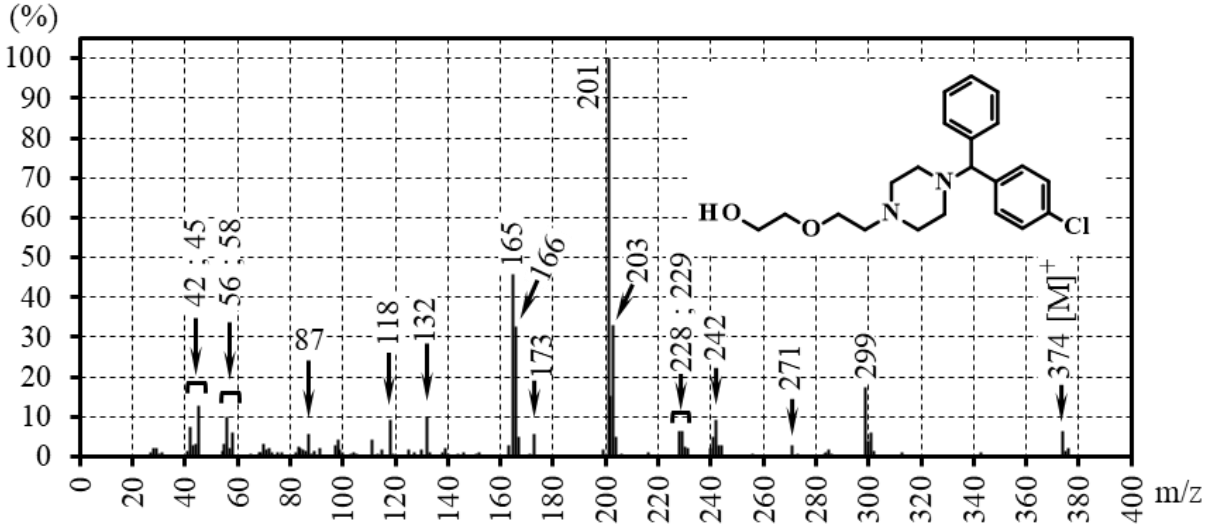

Hydroquinidine (Hydroconchinine) - CAS 1435-55 - EI - NIST 238128



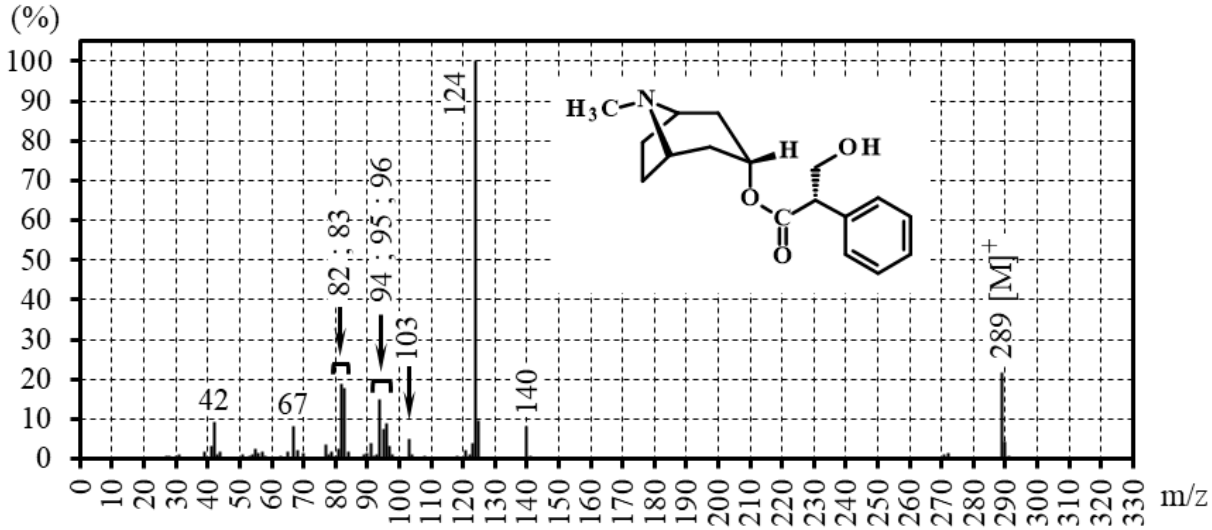

Hydroxychloroquine - CAS 118-42-3 - EI - NIST 146973



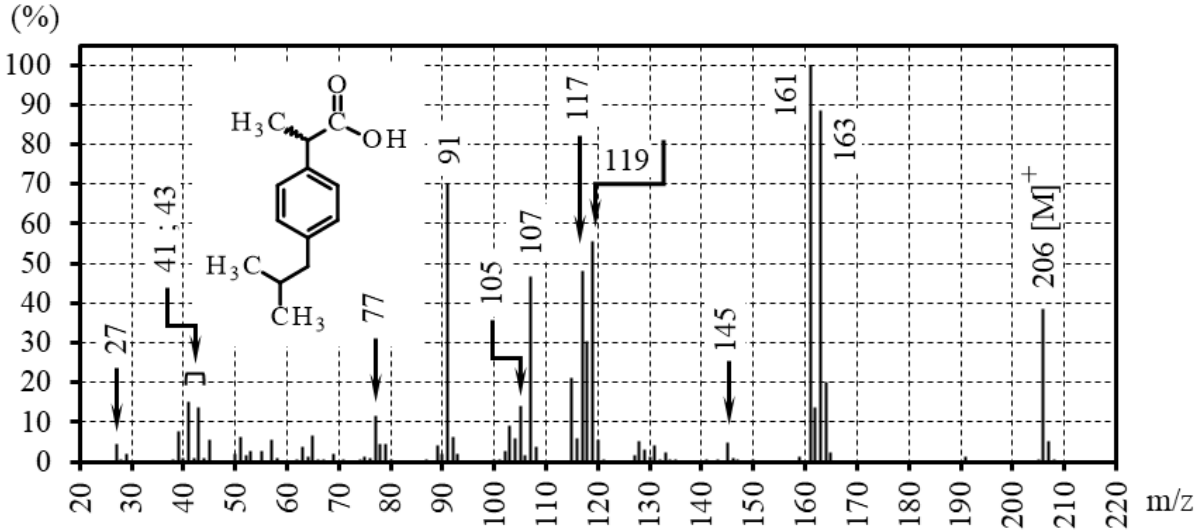

Hydroxyprogesterone - CAS 68-96-2 - NIST15392



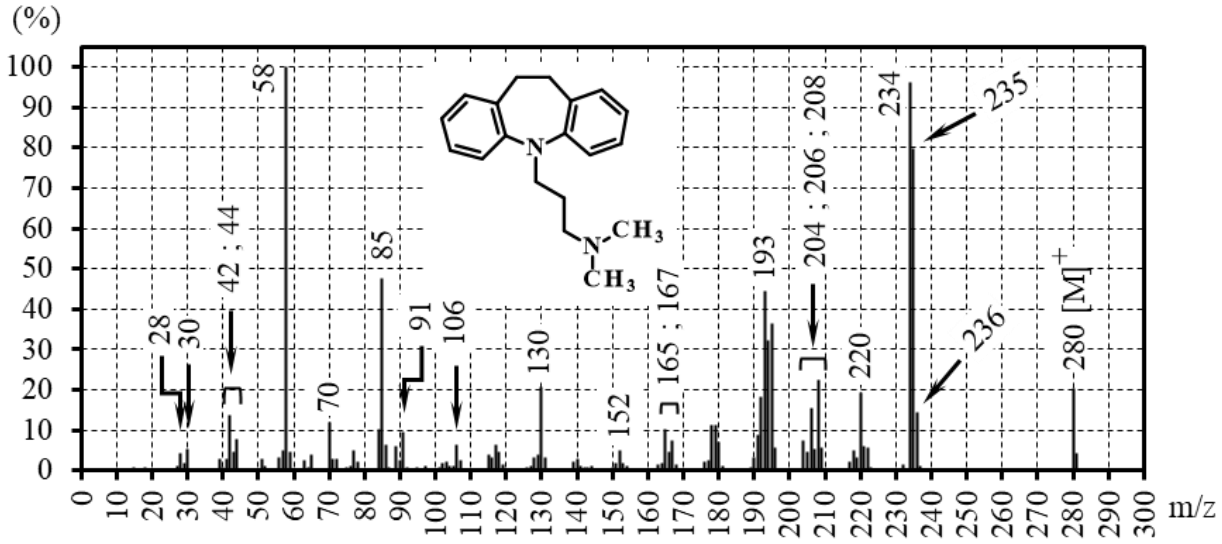

Hydroxyzine - CAS 68-88-2 - EI - NIST 250626



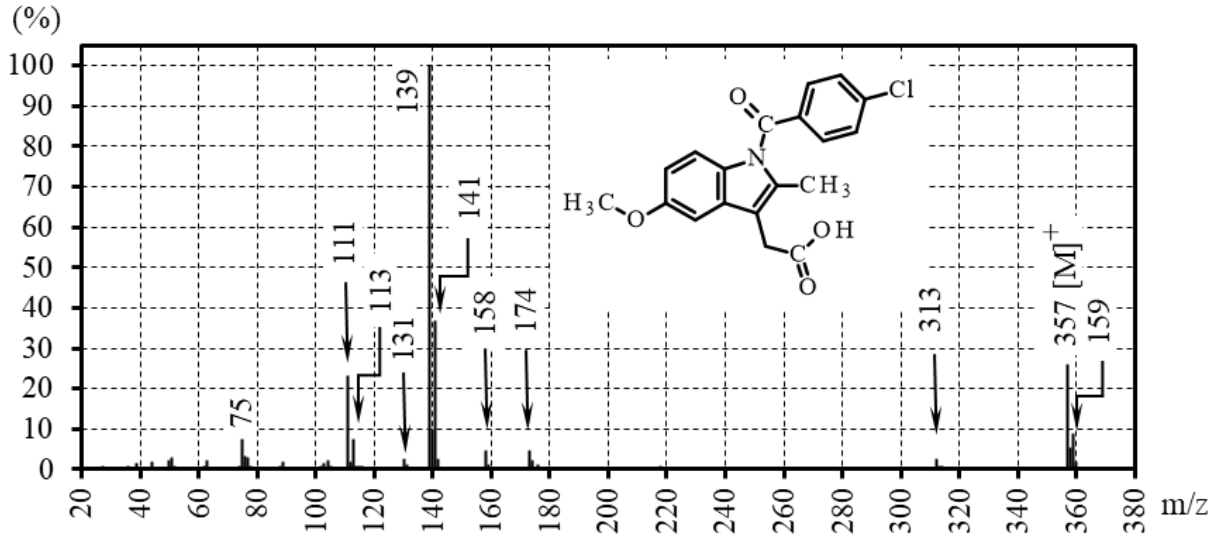

Hyoscyamine - CAS 101-31-5 - EI - NIST 233146



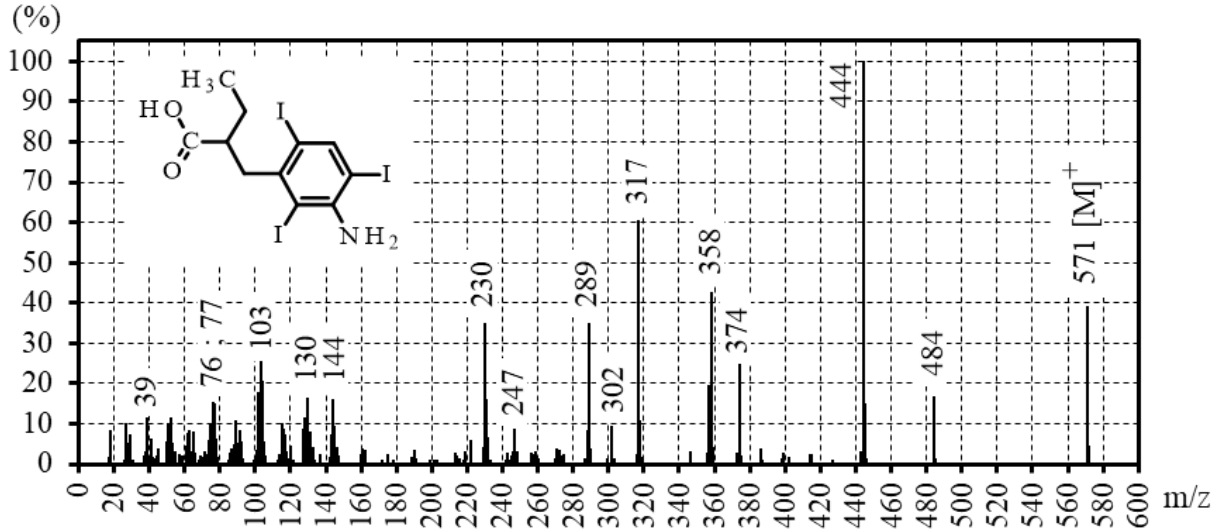

Ibuprofen - CAS 15687-27-1 - EI - NIST 352144



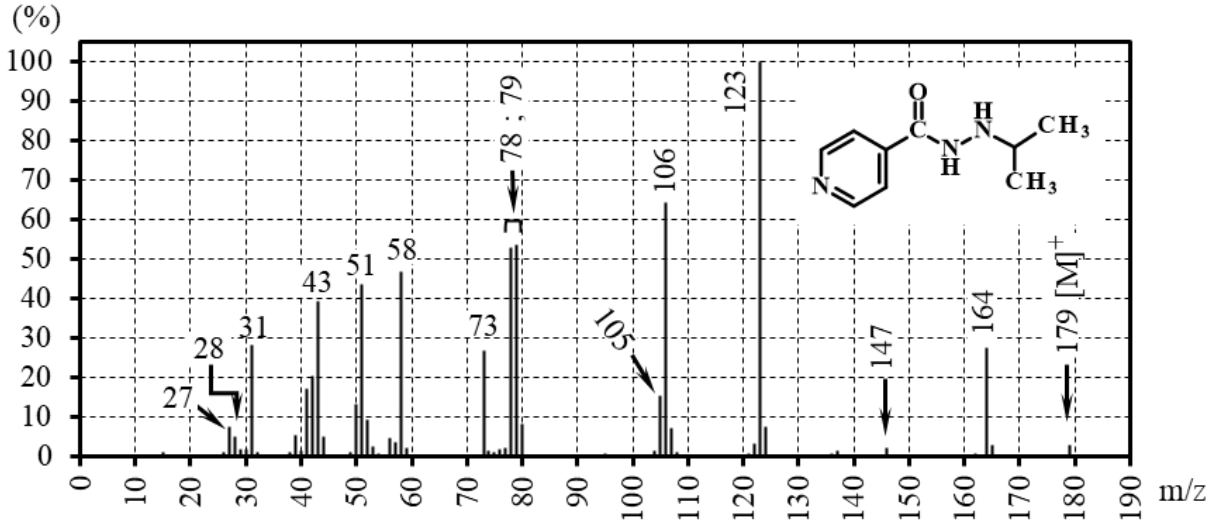

Imipramine - CAS 50-49-7 - NIST 250696



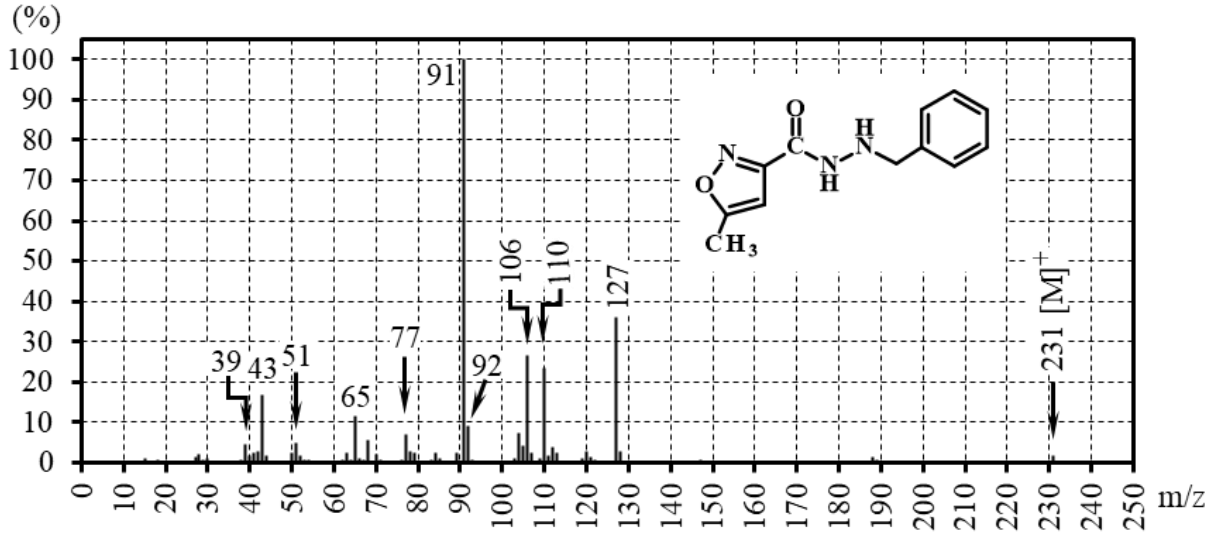

Indomethacin - CAS 53-86-1 - EI - NIST 107188



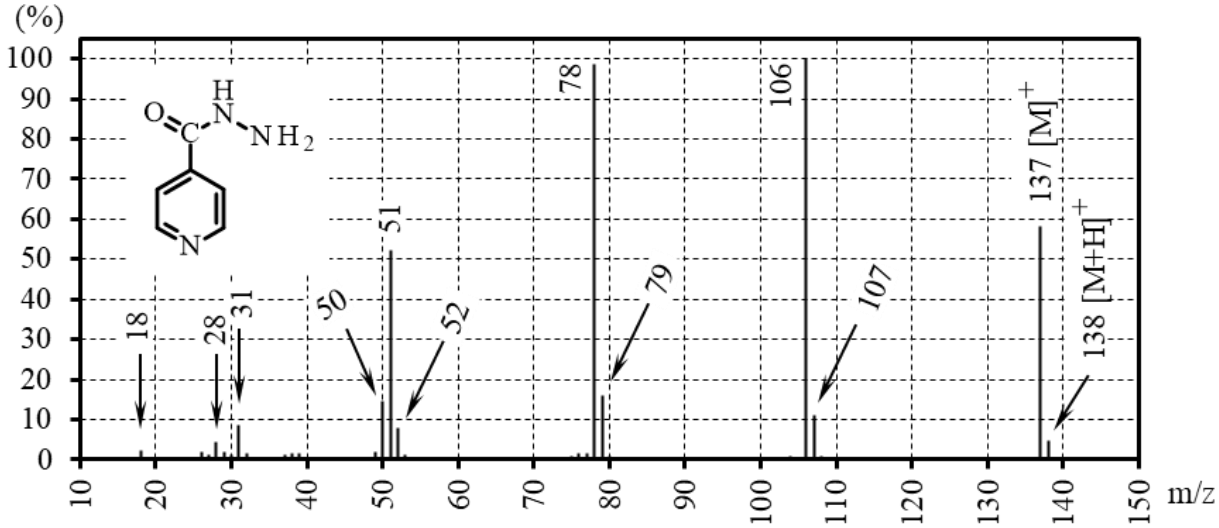

Iopanoic acid - CAS 96-83-7 - EI 75 eV - 200 °C - 150 °C - SDBS



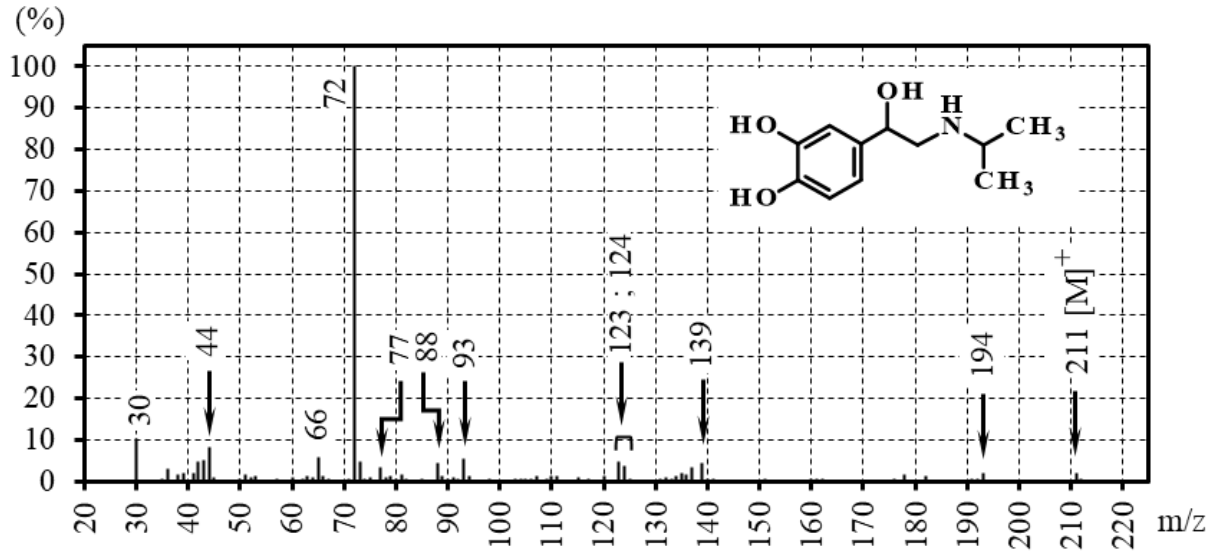

Iproniazid - CAS 54-92-2 - EI - NIST 408726



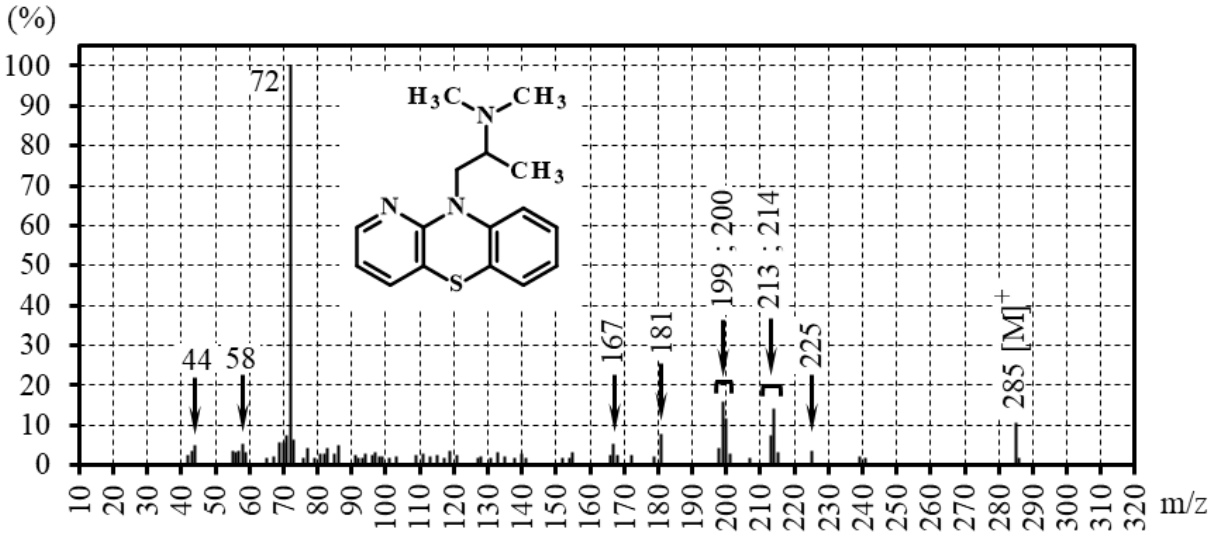

Isocarboxazid - CAS 59-63-2 - EI - NIST 250701



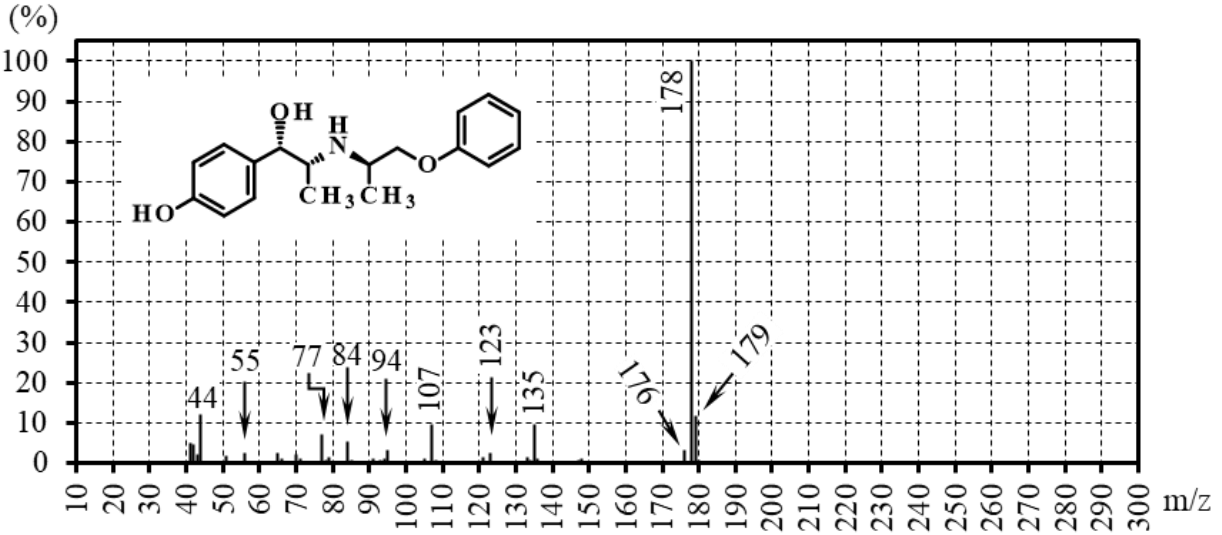

Isoniazid - CAS 54-85-3 - EI - NIST nr. 228778



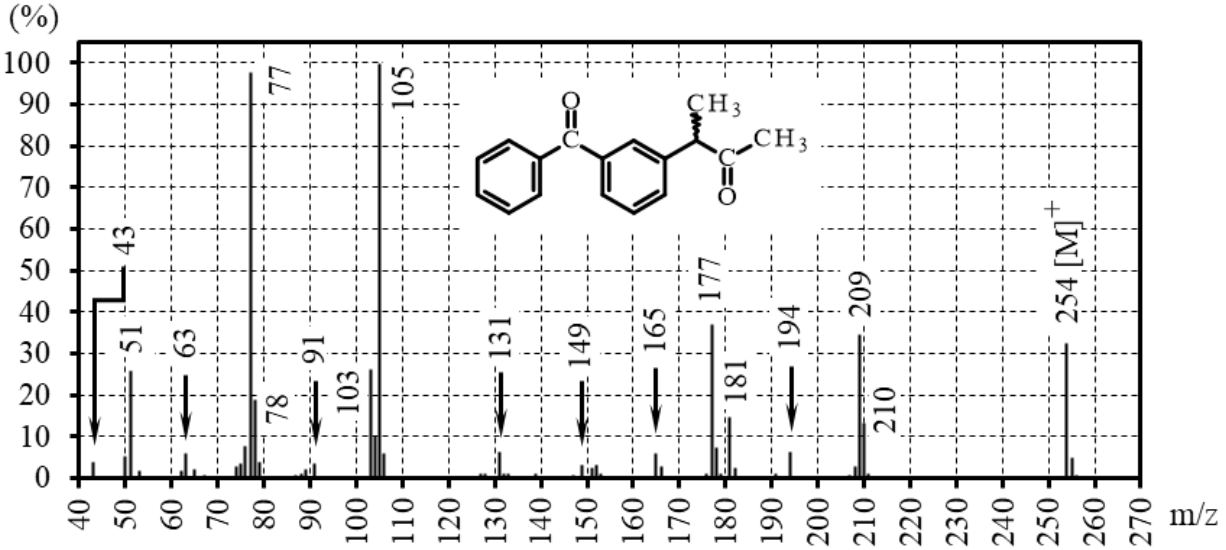

Isoprenaline (Isoproterenol) - CAS 7683-59-2 - NIST 246203



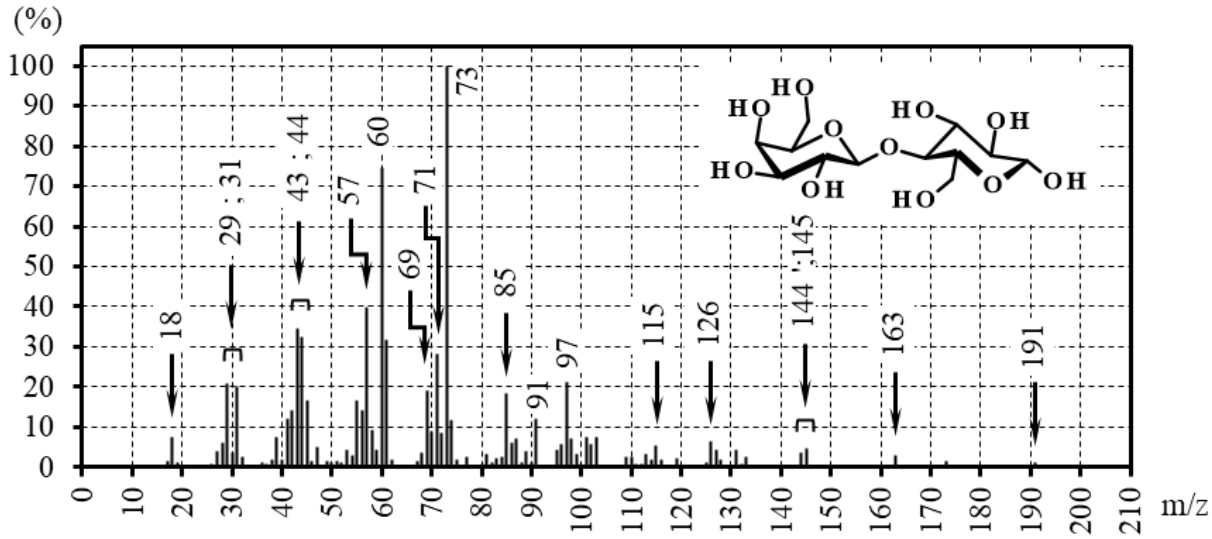

Isothipendyl - CAS 482-15-5 - EI - NIST 246682



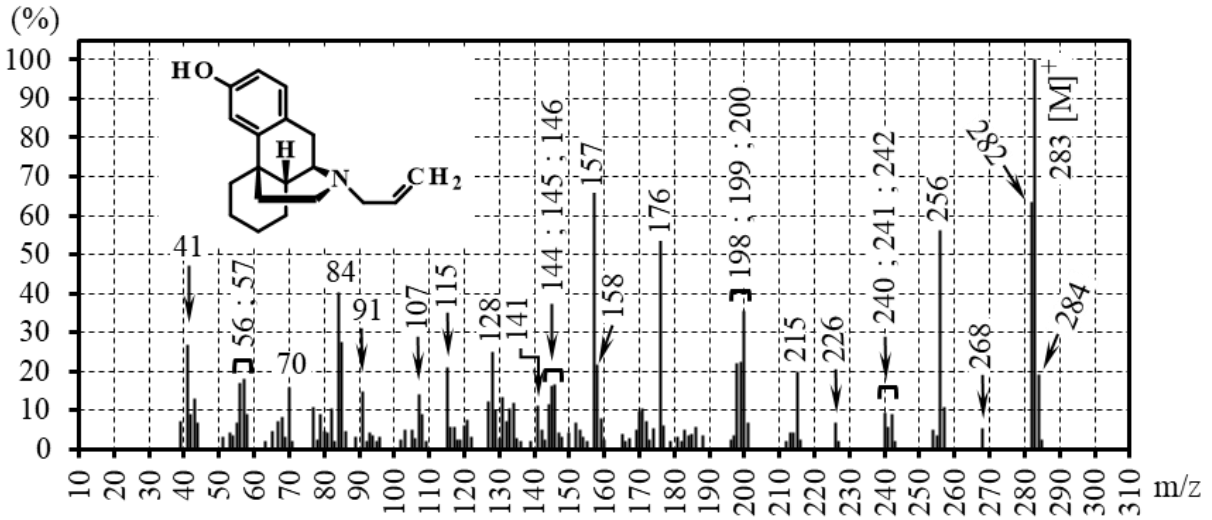

Isoxsuprine _ CAS 395-28-8 - EI - NIST 248017



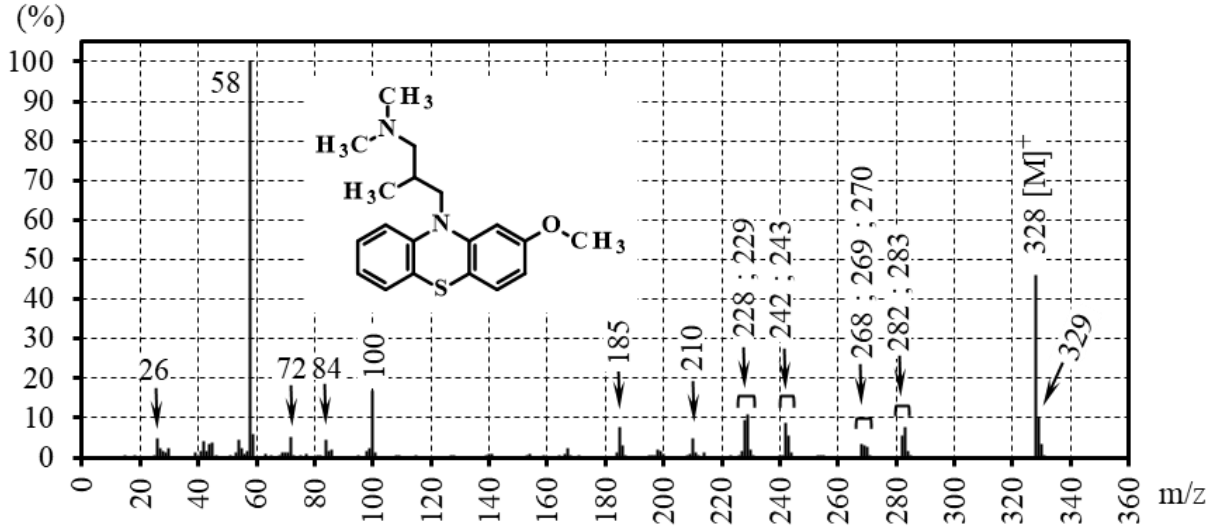

Ketoprofen- CAS 22071-15-4 - EI - NIST 248419



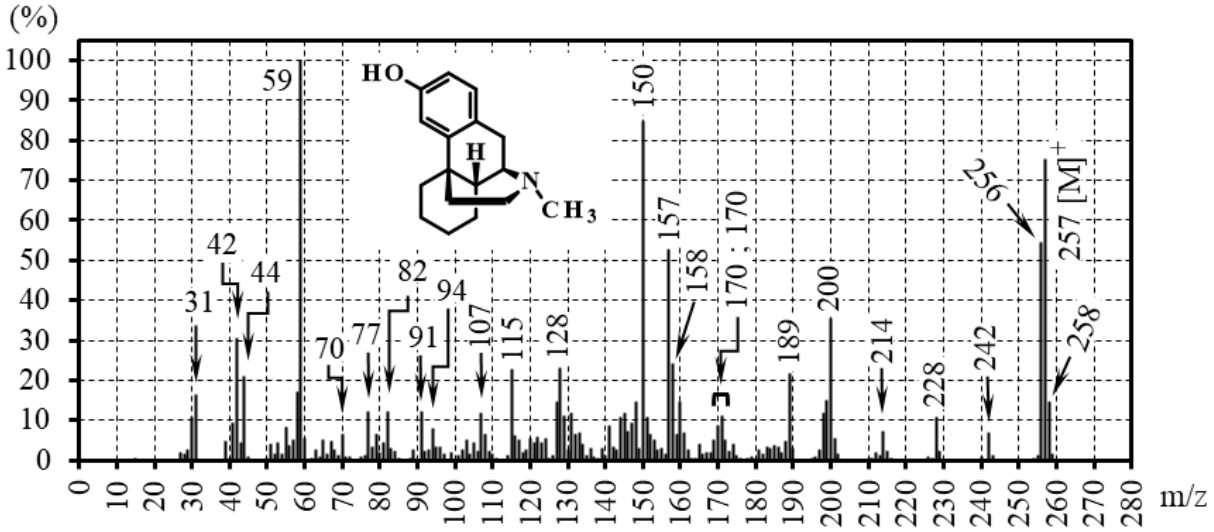

Lactose - CAS 63-42-3 - NIST 76357



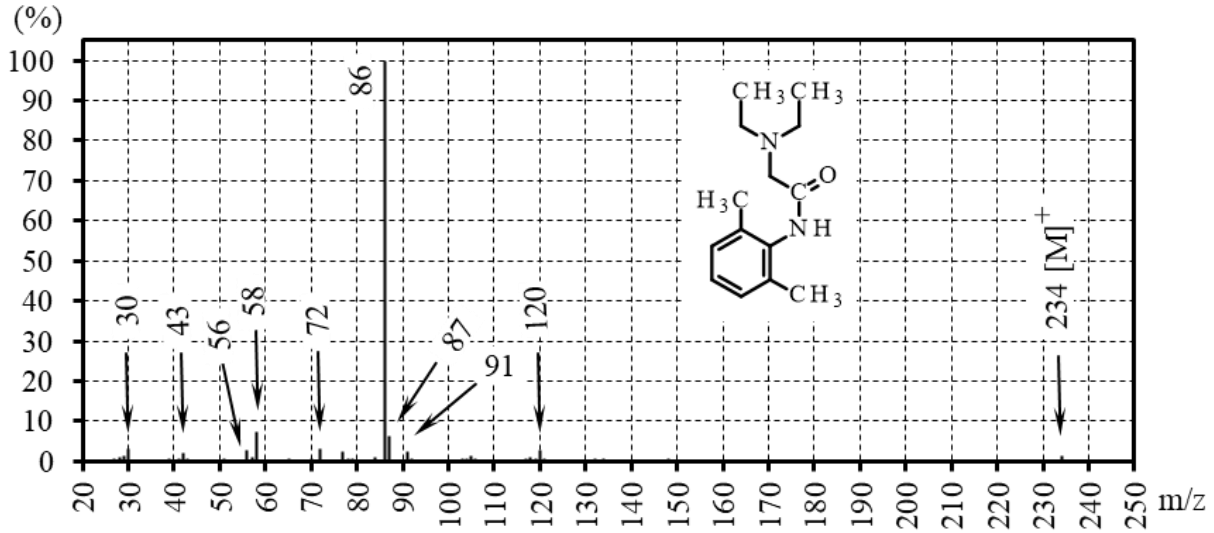

Levallorphan - CAS 152-02-3 - EI - NIST 246652



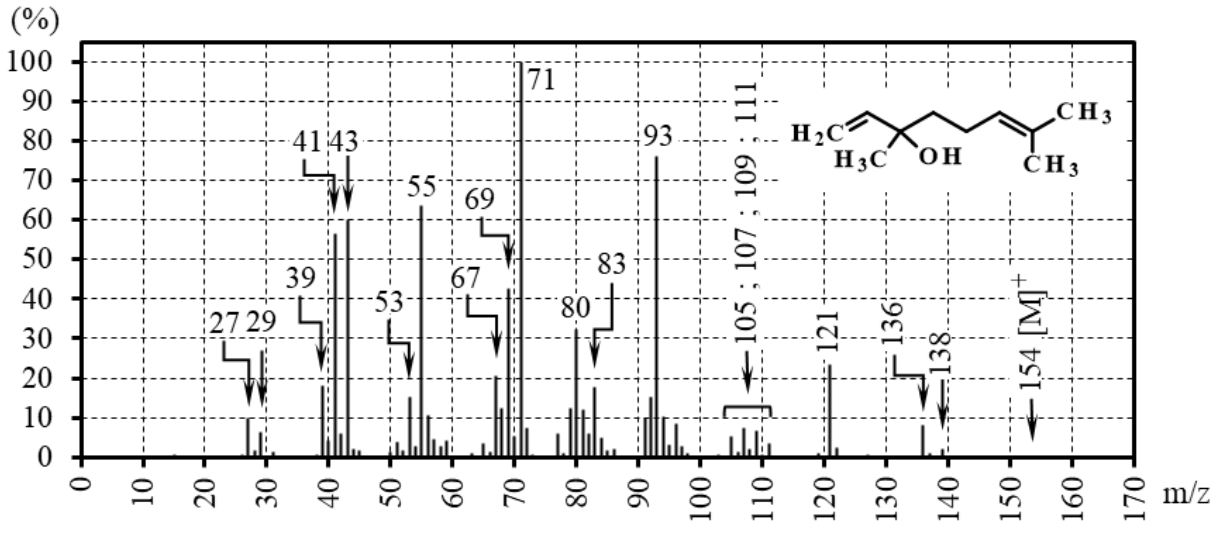

Levomepromazine - CAS 851-68-3 - EI - NIST 244417



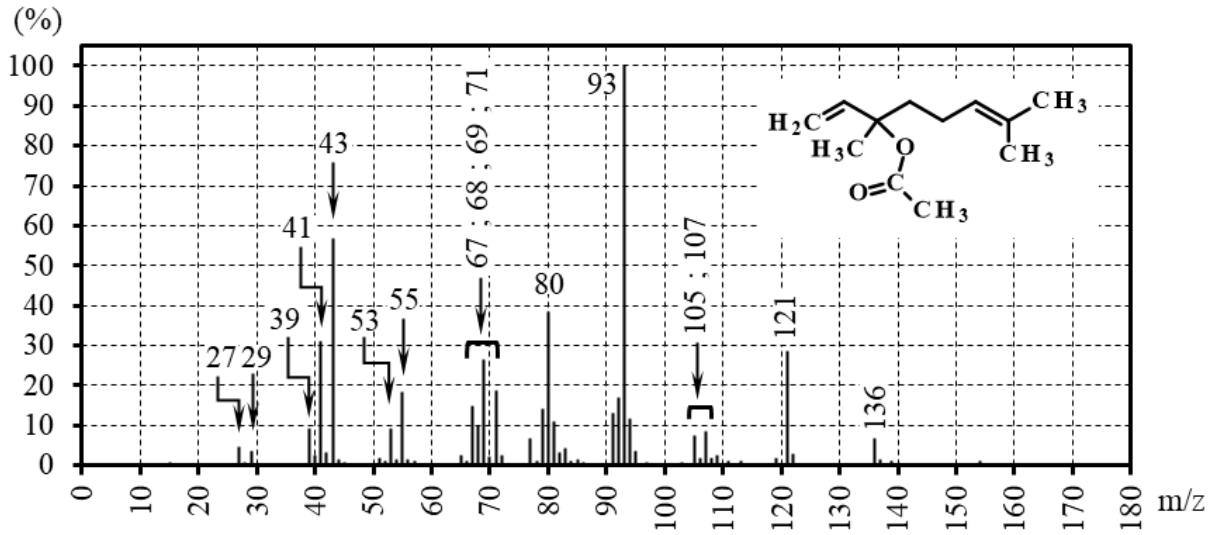

Levorphanol - CAS 77-07-6 - EI - NIST 362164



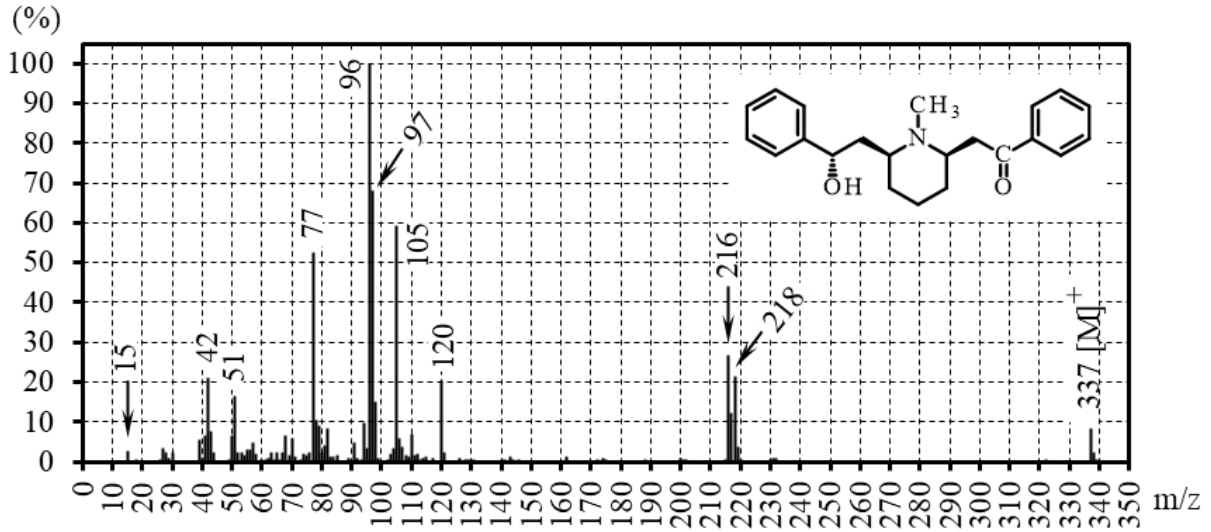

Lidocaine - CAS 137-58-6 - EI - NIST 408610



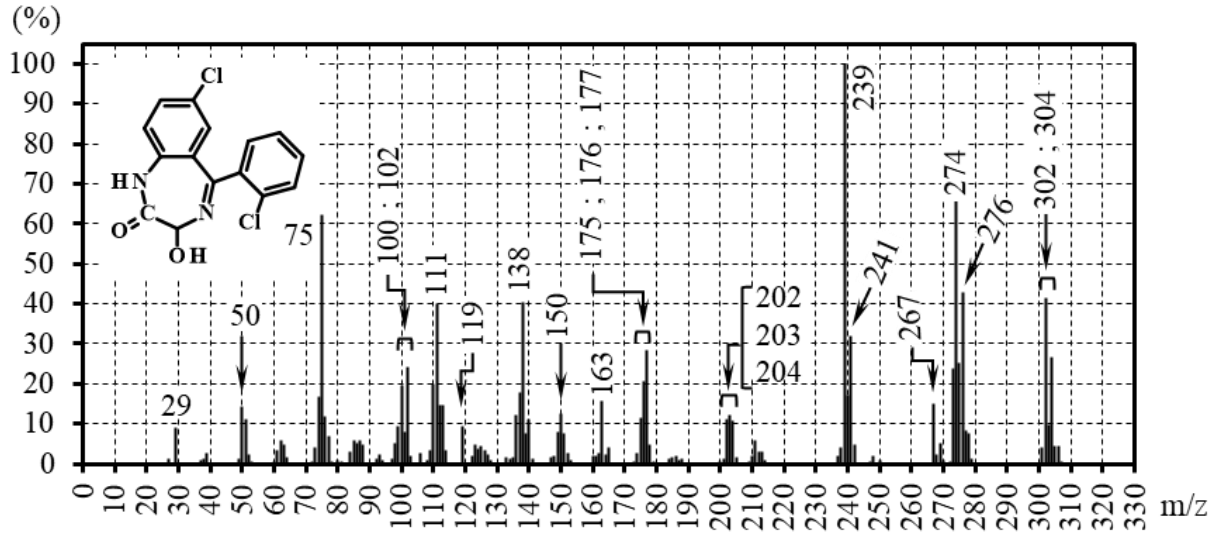

Linalool - CAS 78-70-6 - ESI - NIST 352637



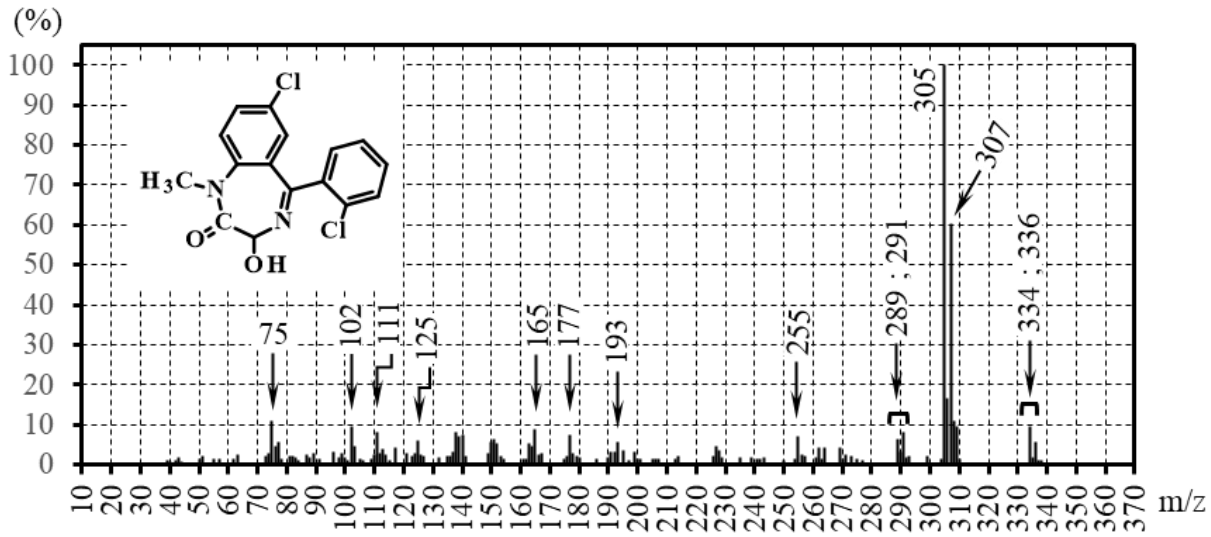

Linalyl acetate - CAS 115-95-7 - ESI - NIST 384053



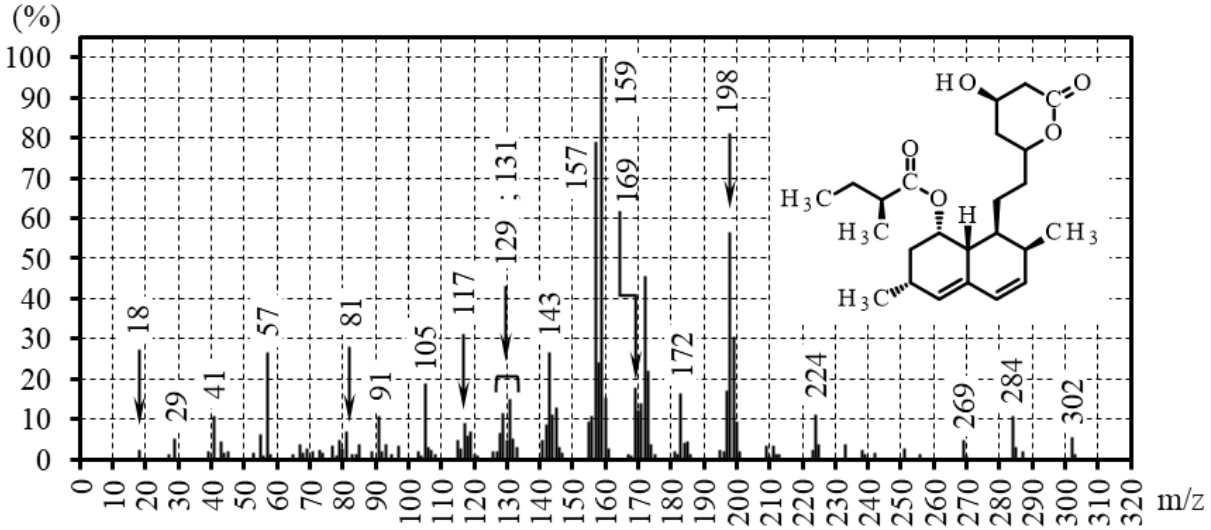

Lobeline - CAS 90-69-7 - EI - NIST 233013



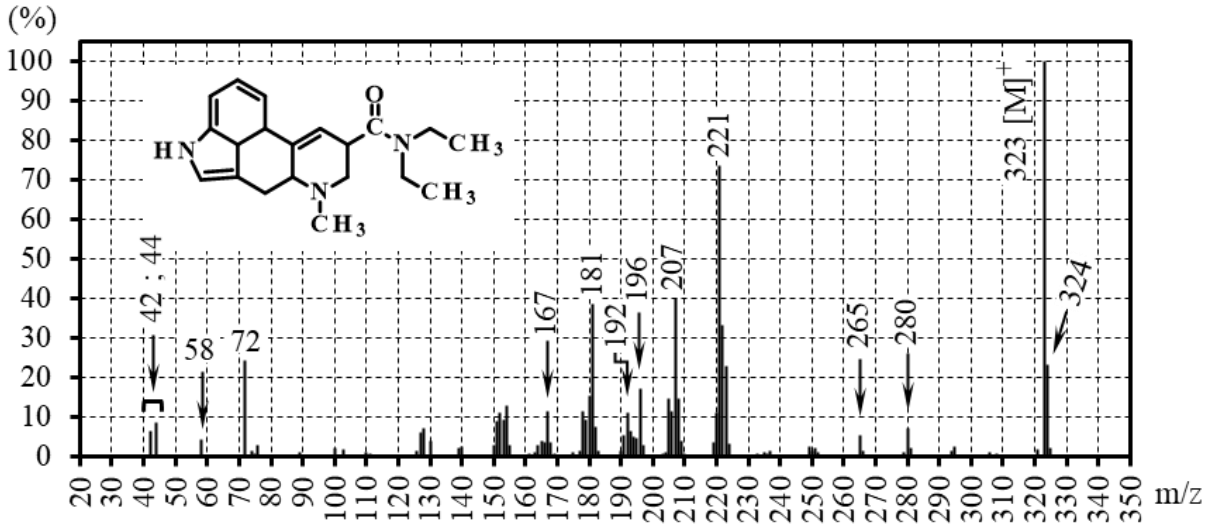

Lorazepam - CAS 846-49-1 - EI - NIST 291616



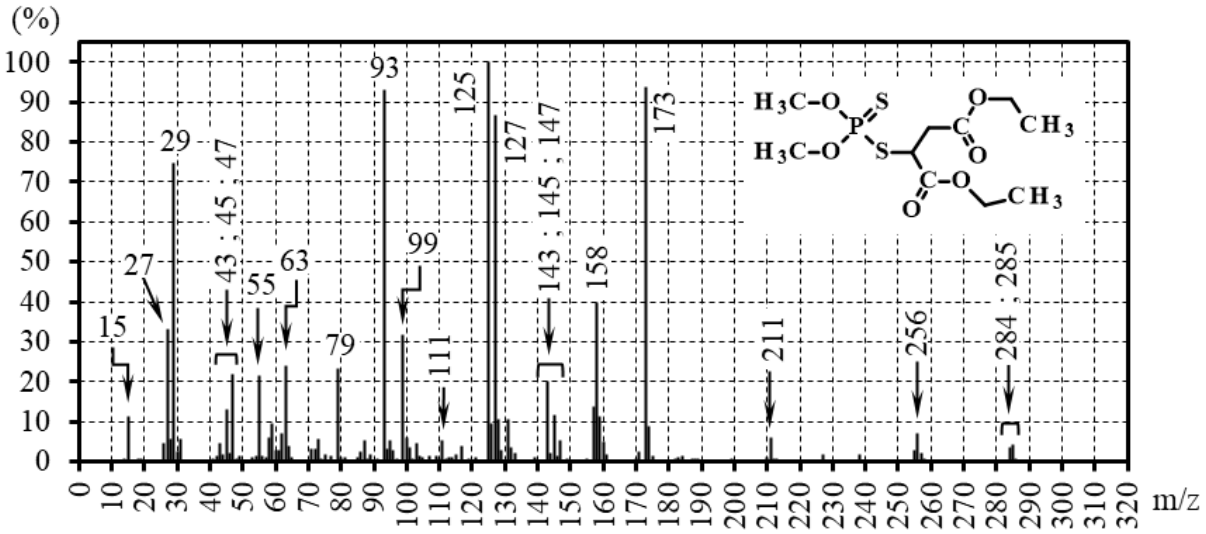

Lormetazepam - CAS 848-75-9 - EI - NIST 246967



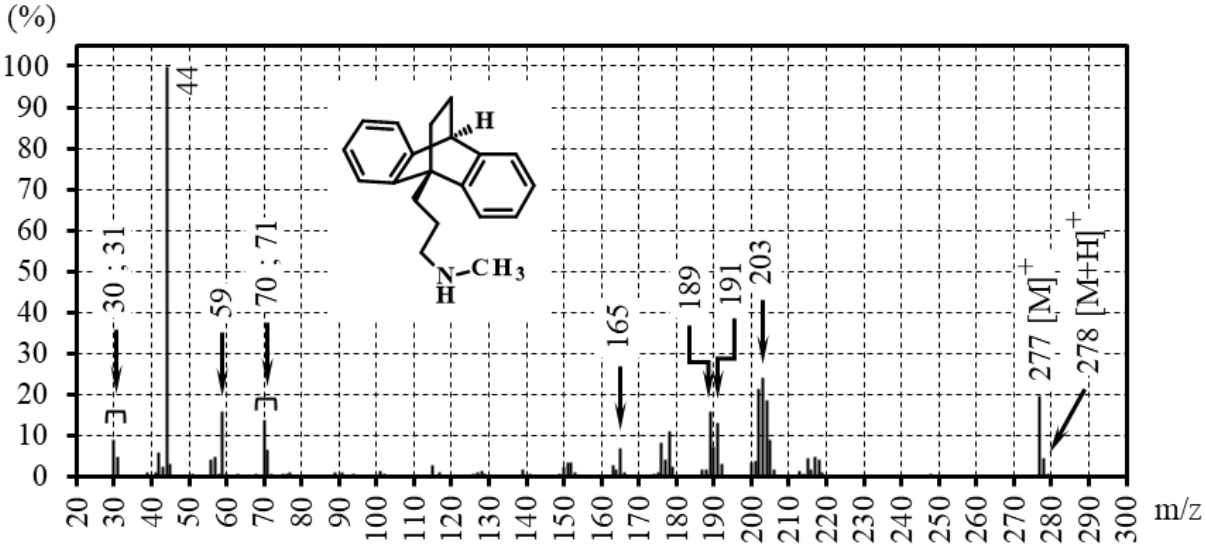

Lovastatin - CAS 75330-75-5 - EI 70 eV - SDBS 52208



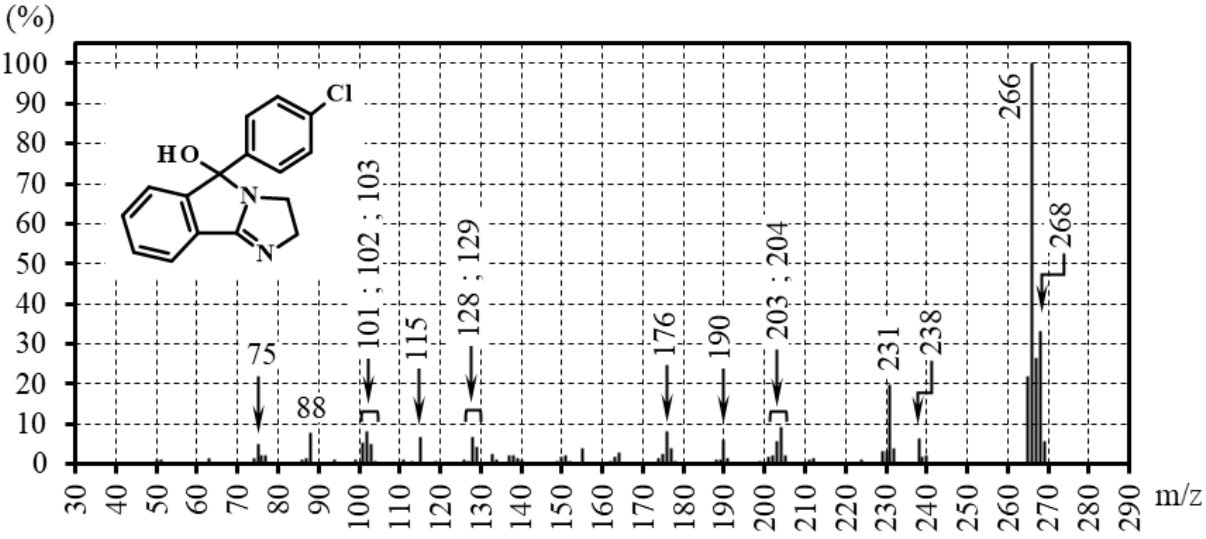

LSD (D-Lysergic acid N,N-diethylamide) - CAS 50-37-3 - EI - NIST 246915



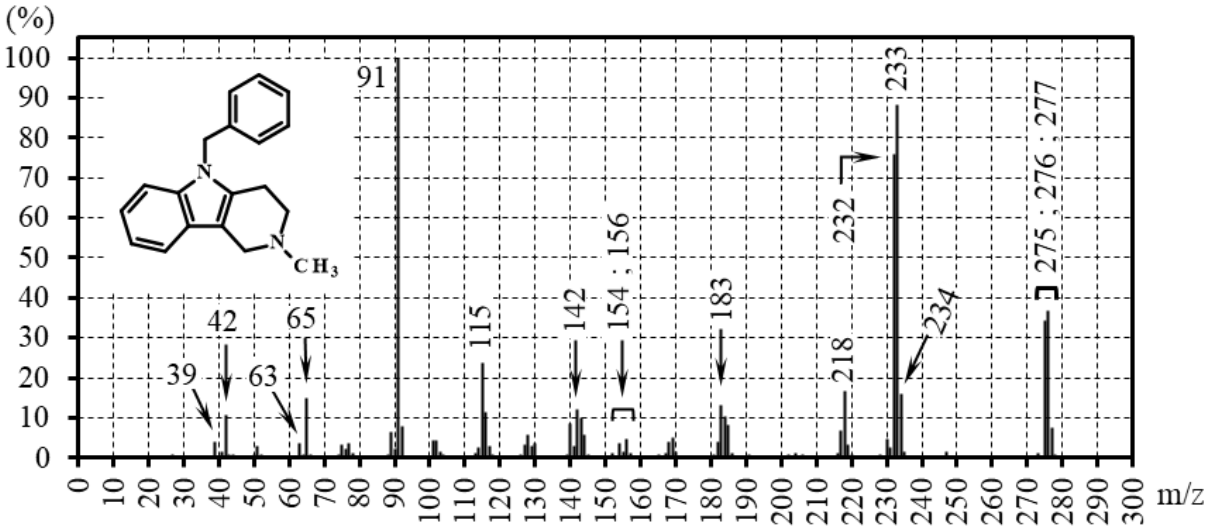

Malathion - CAS 121-75-5 - EI - NIST 118987



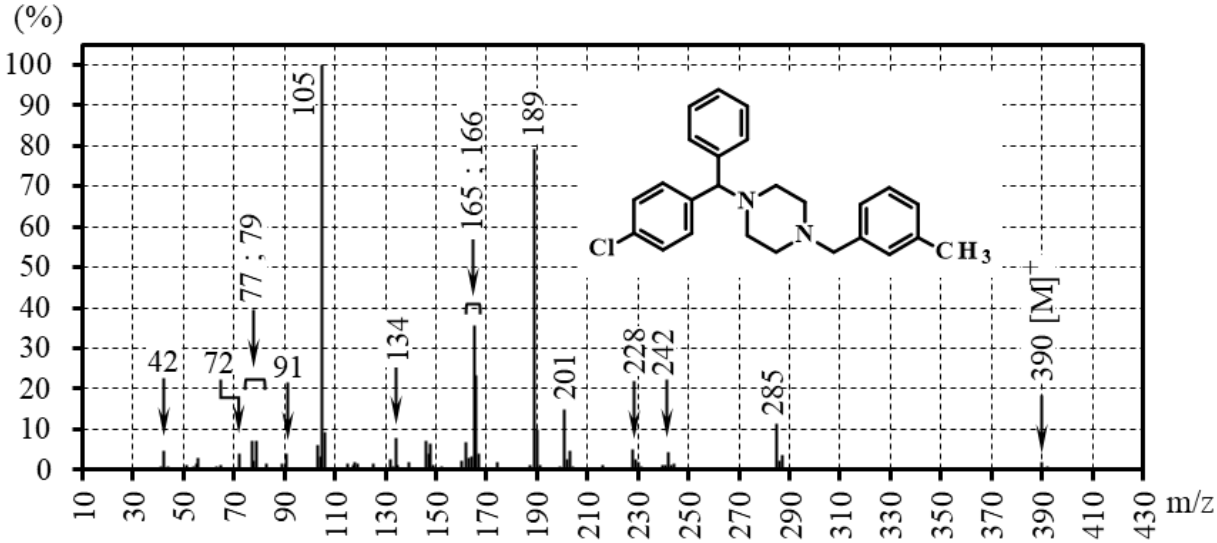

Maprotiline - CAS 10262-69-8 - NIST 246615



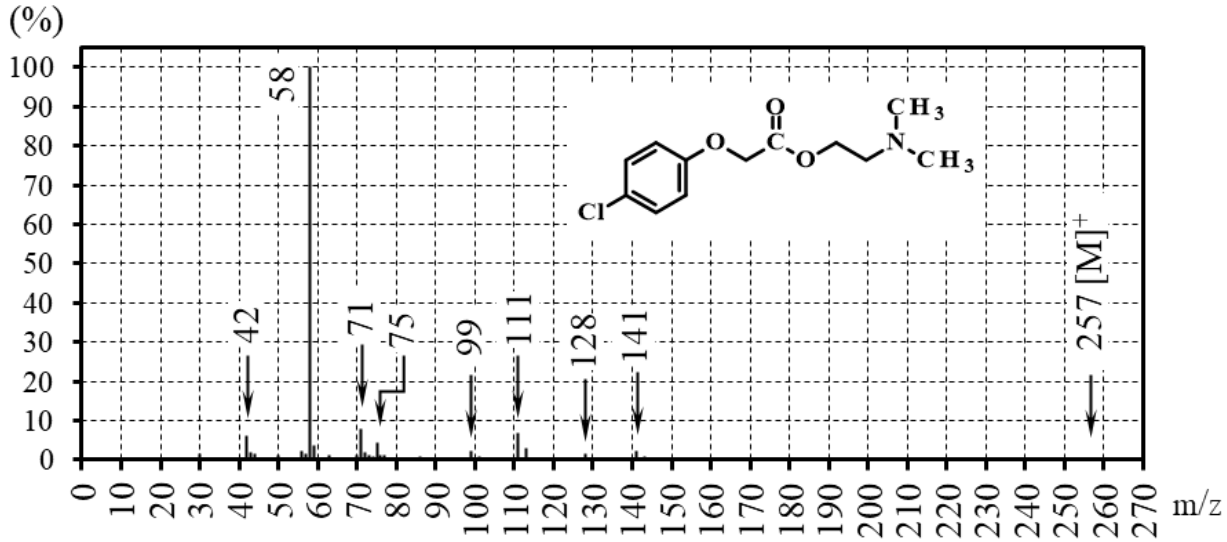

Mazindol - CAS 22232-71-9 - EI - NIST 247692



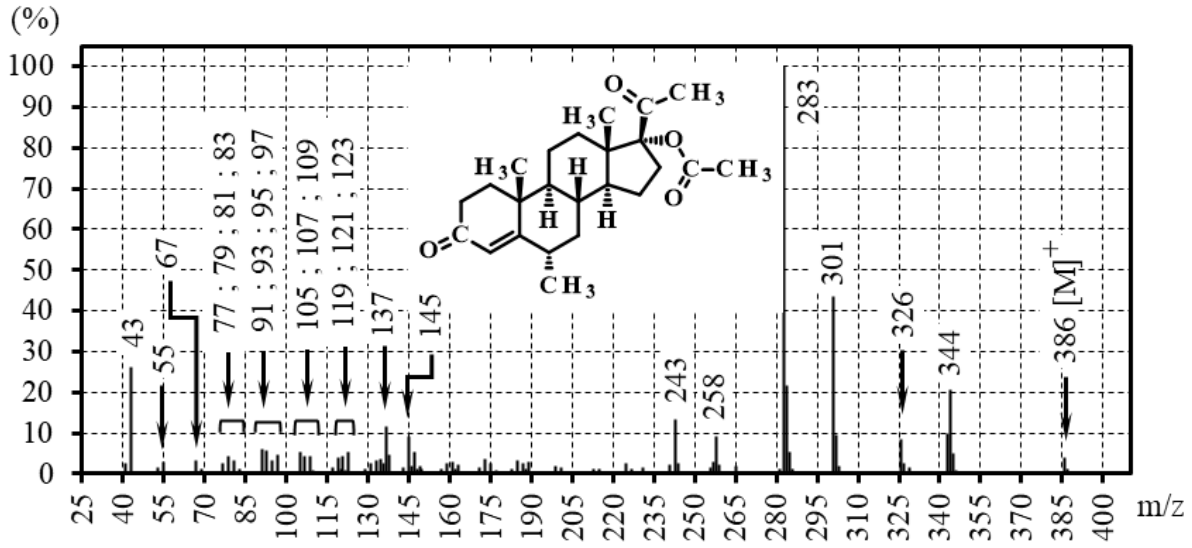

Mebhydrolin - CAS 524-81-2 - EI - NIST 408357



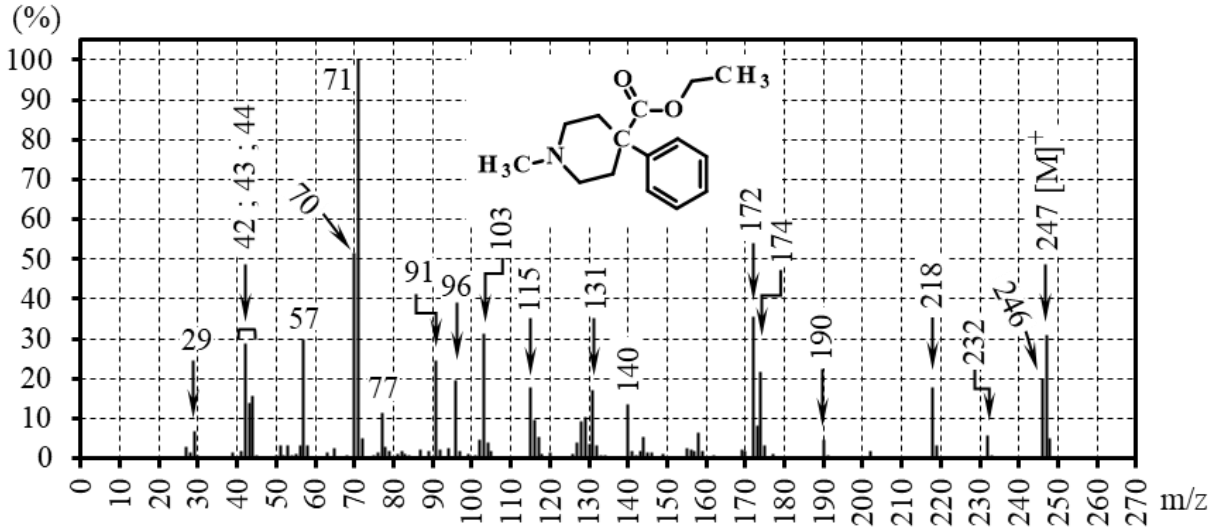

Meclizine - CAS 569-65-3 - EI - NIST 335334



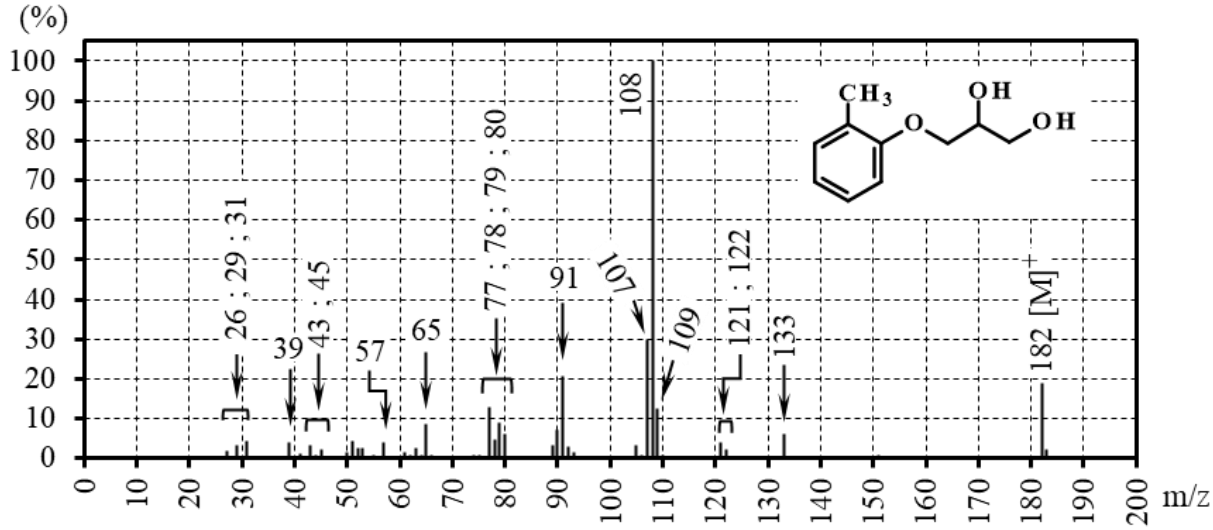

Meclofenoxate - CAS 51-68-63 - MIST 408039



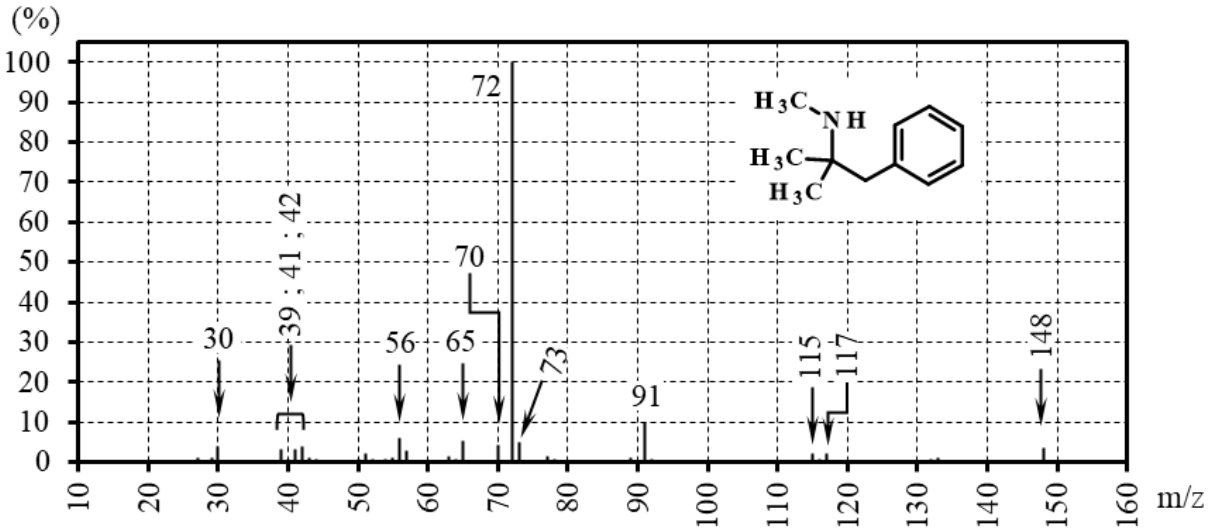

Medroxyprogesterone acetate - CAS 71-58-9 - SDBS 11518



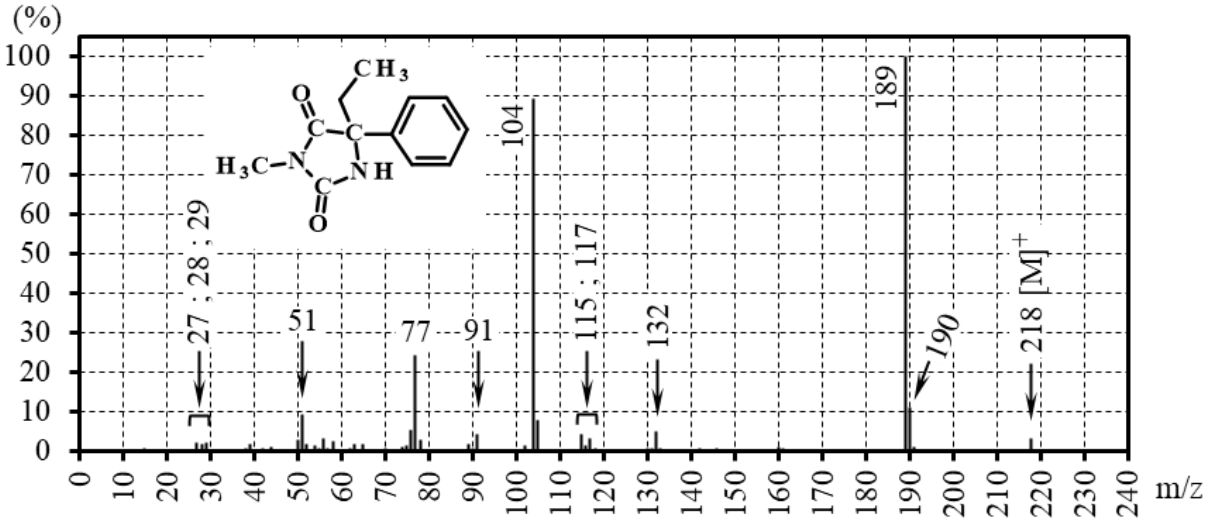

Meperidine (Pethidine , etc) - CAS 57-42-1 - EI - NIST 362938



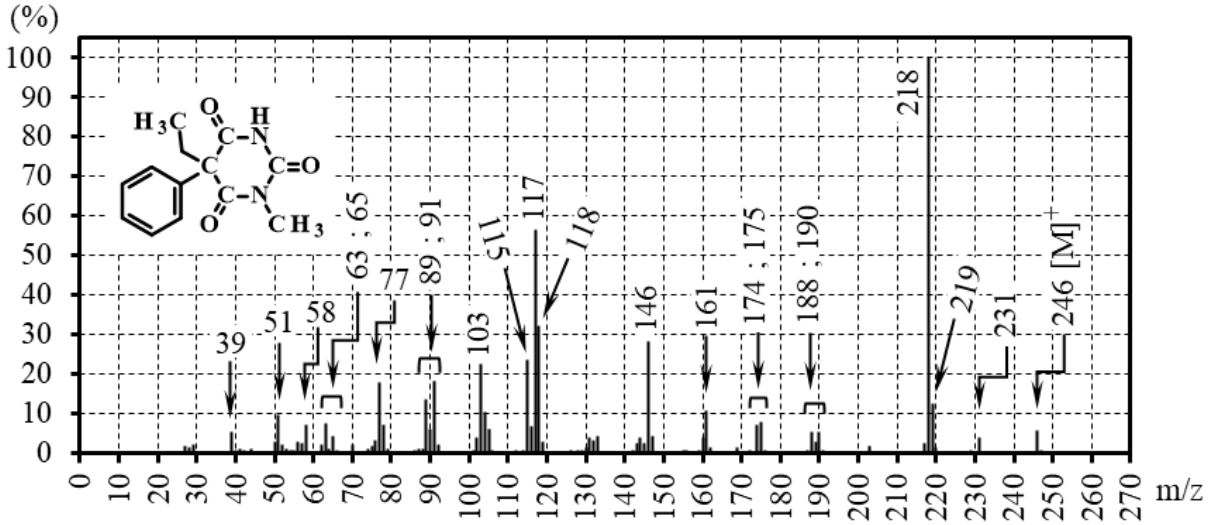

Mephenesin - CAS 59-47-2 - EI - NIST 352183



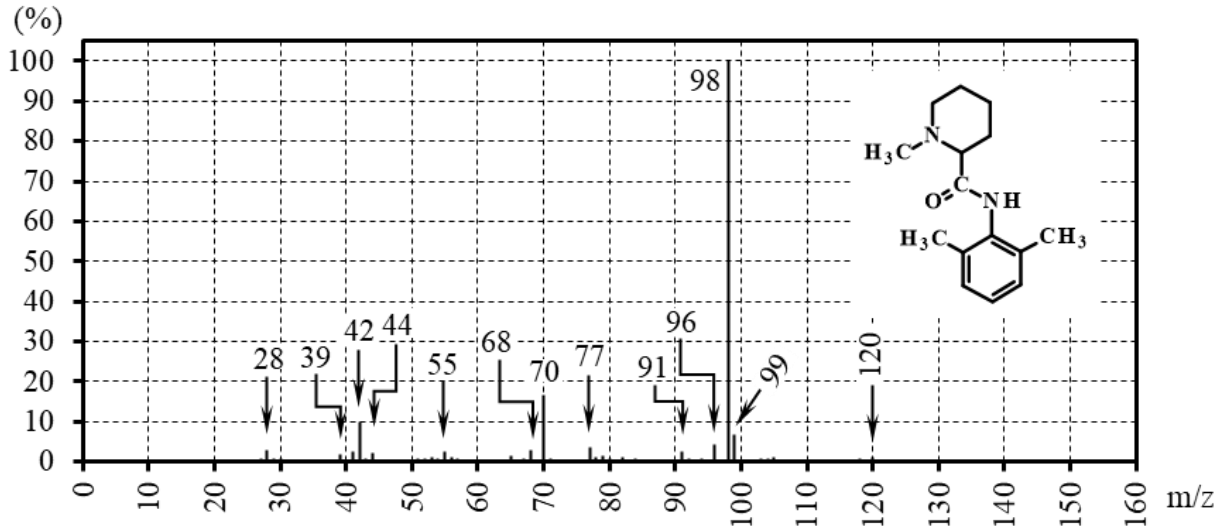

Mephentermine - CAS 100-92-5 - EI - NIST 113865



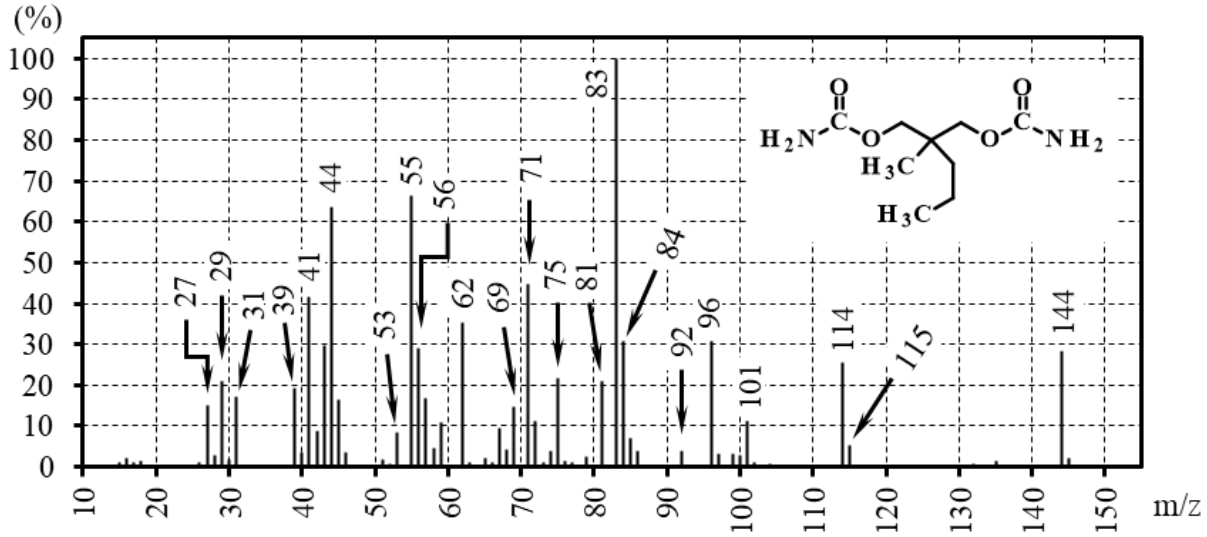

Mephenytoin - CAS 50-12-4 - EI - NIST 113831



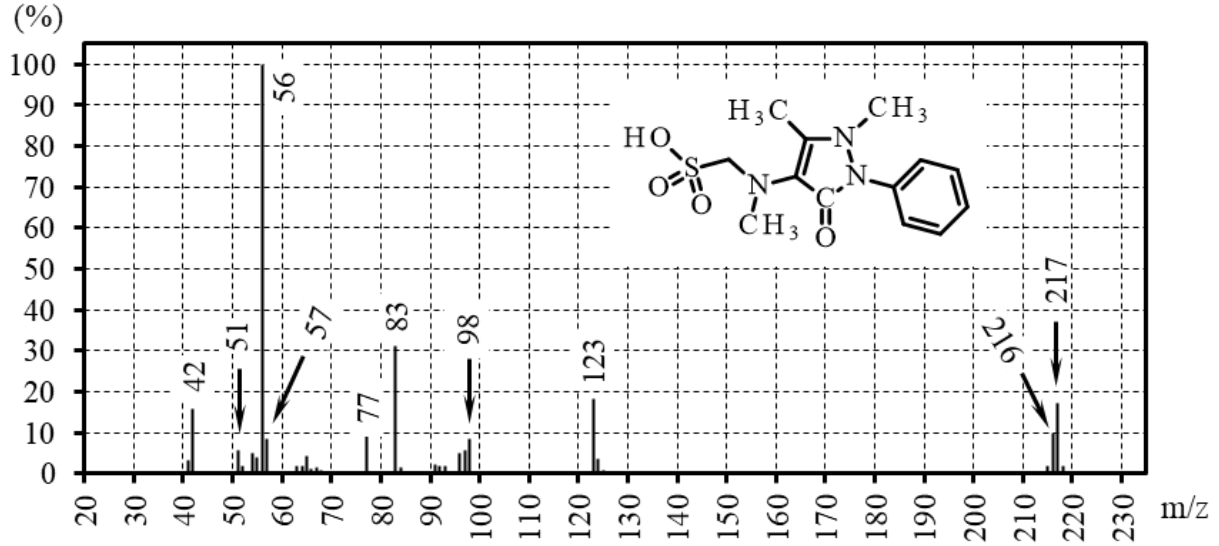

Mephobarbital - CAS 115-38-8 - EI - NIST 352171



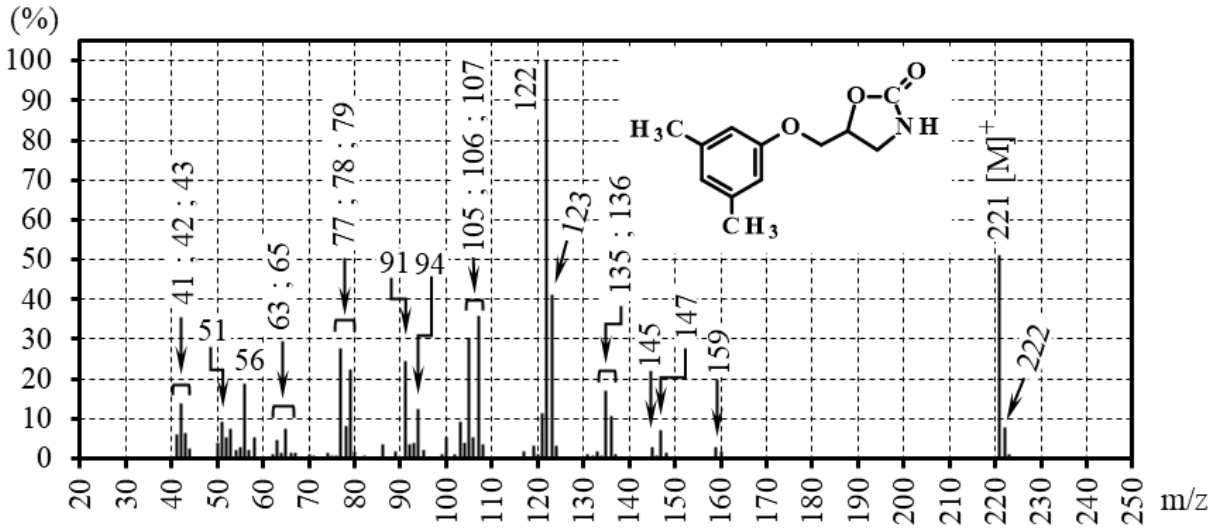

Mepivacaine - CAS 96-88-8 - EI - NIST 113842



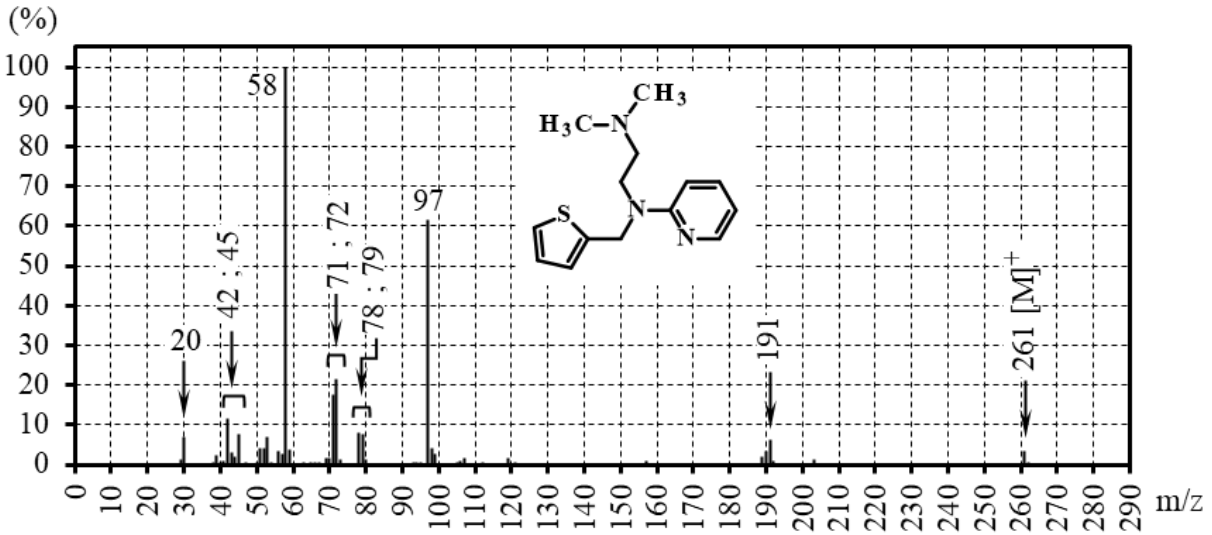

Meprobamate - CAS 57-53-4 - NIST 250606



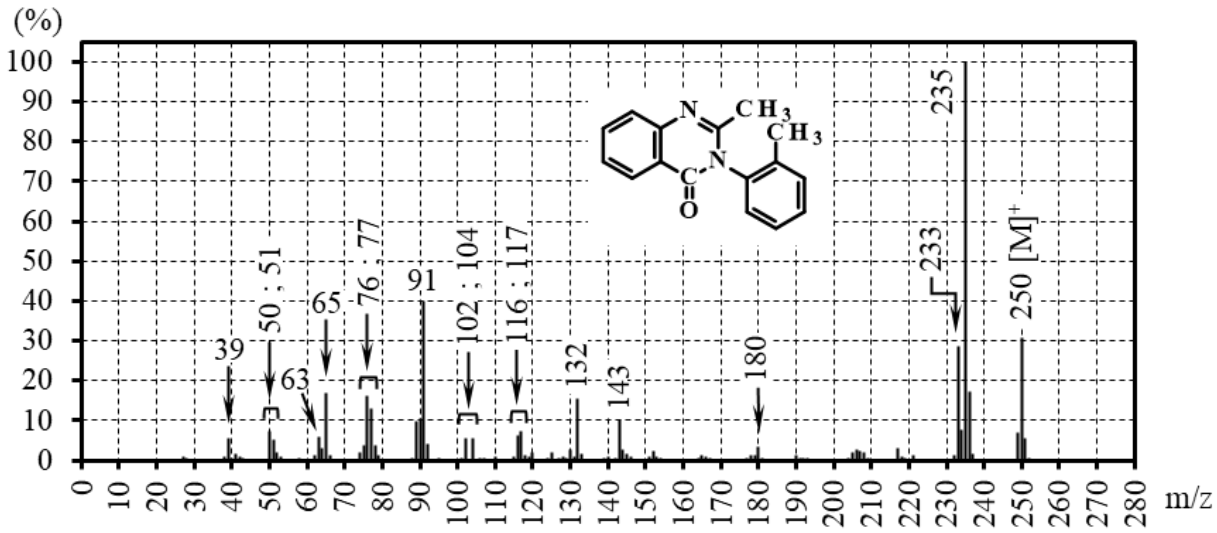

Metamizole - CAS 68-89-3 - NIST 335322



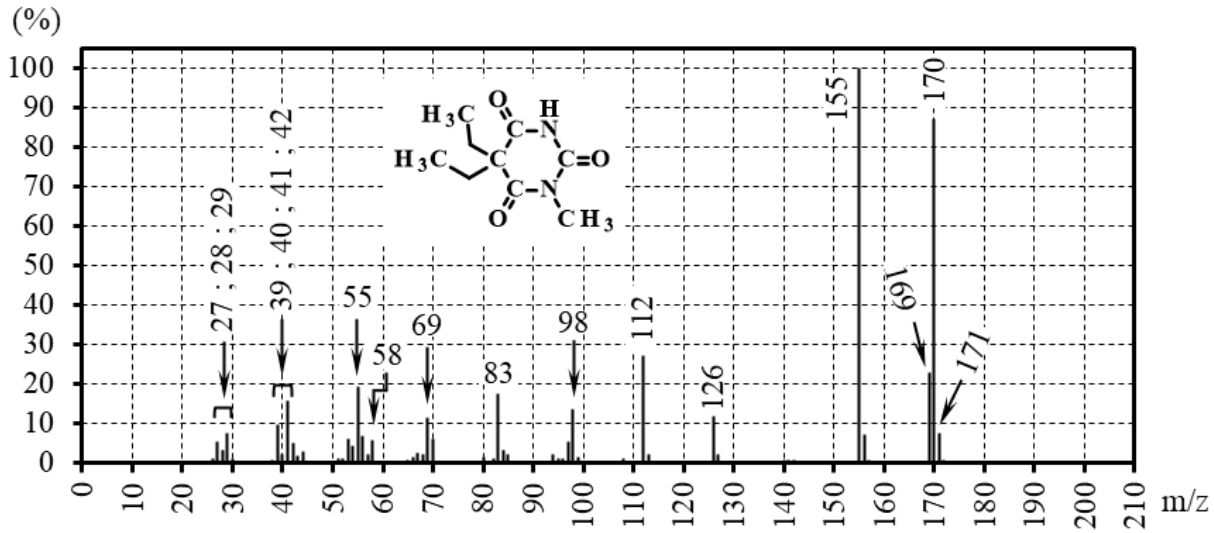

Metaxalone - CAS 1665-48-1 - EI - NIST 248039



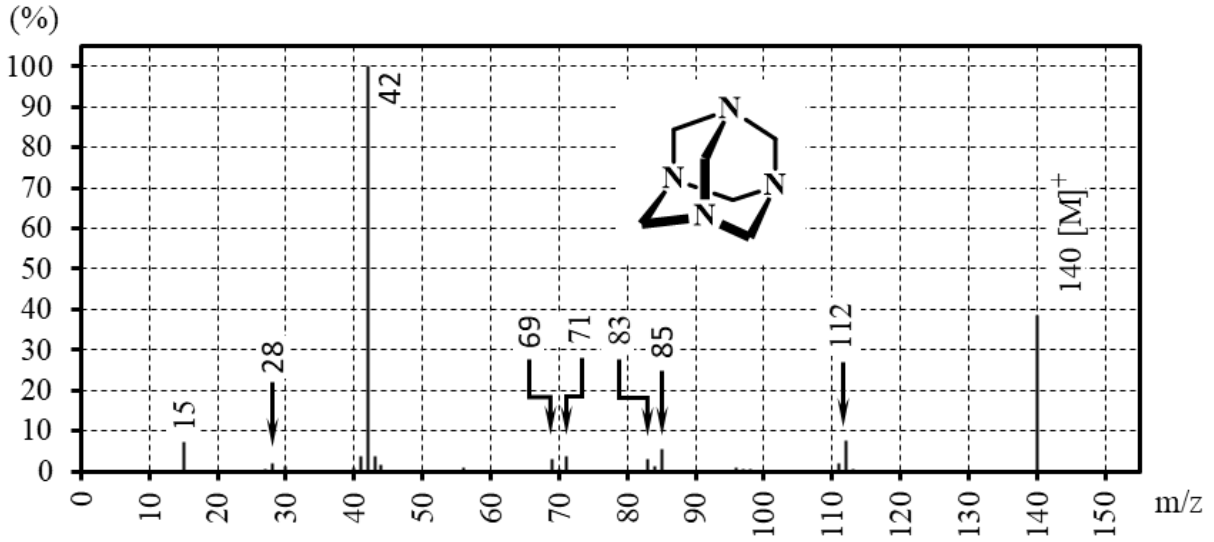

Methapyrilene - (Lulamin , Pyrathyn) - CAS 91-80-5 - EI - NIST 246498



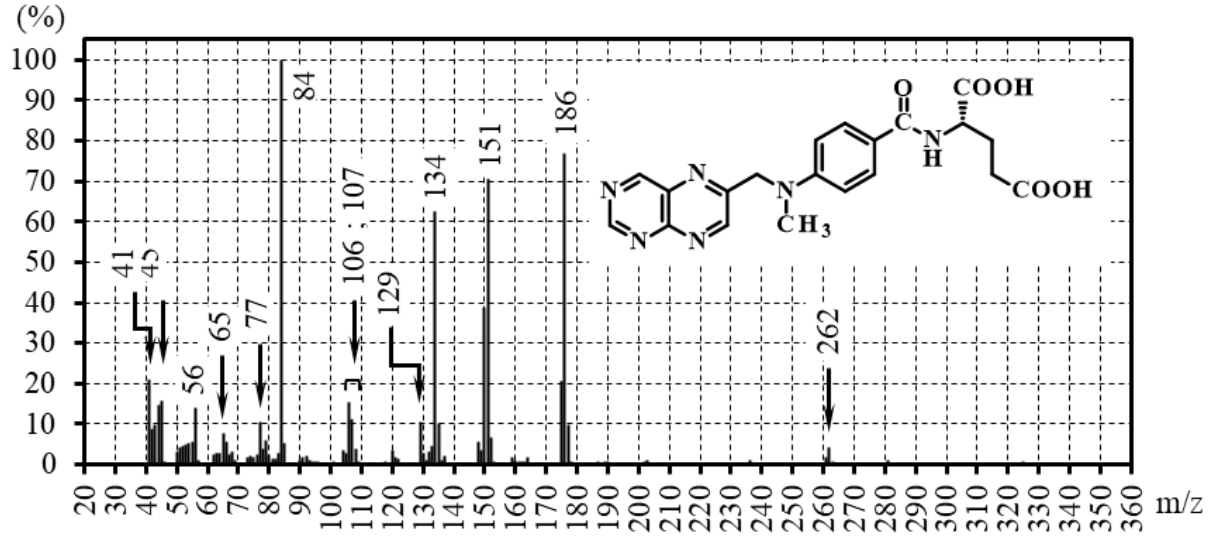

Methaqualone - CAS 72-44-6 - EI - NIST 352961



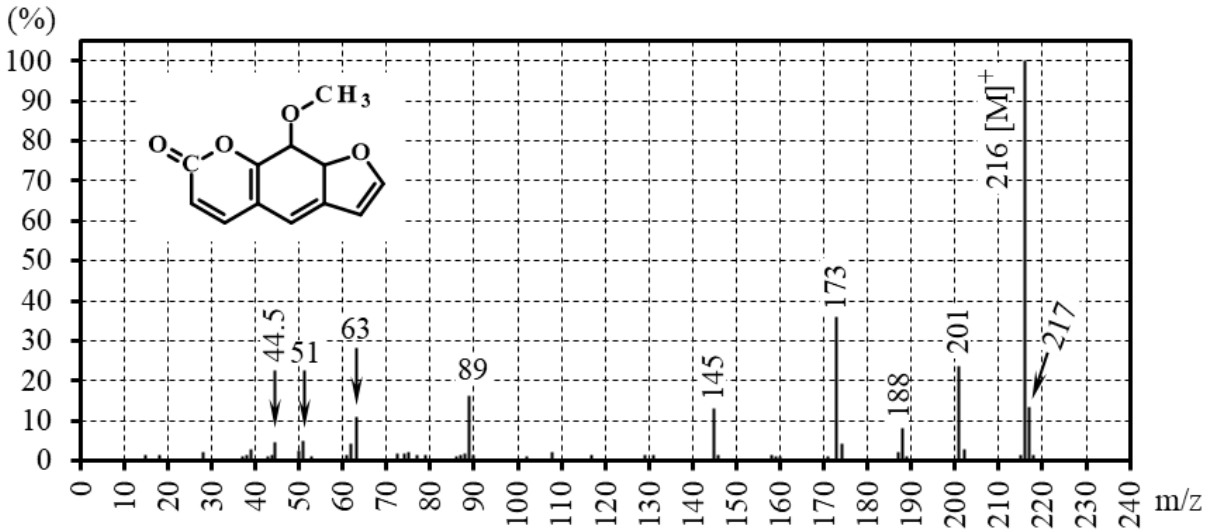

Metharbital - CAS 50-11-3 - EI - NIST 352181



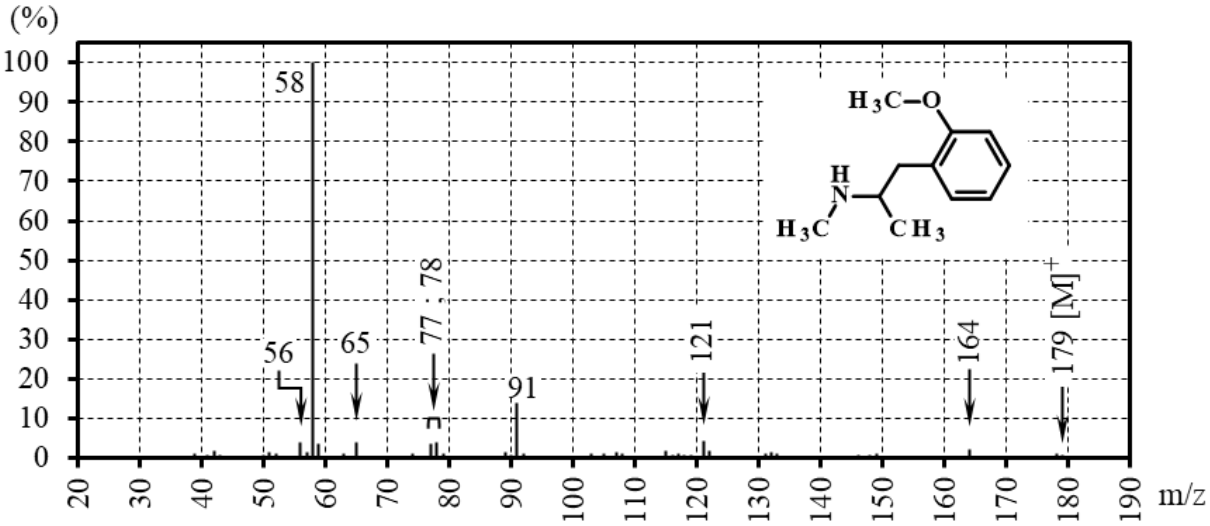

Methenamine (Urotropin) - CAS 100-97-0 - NIST 228325



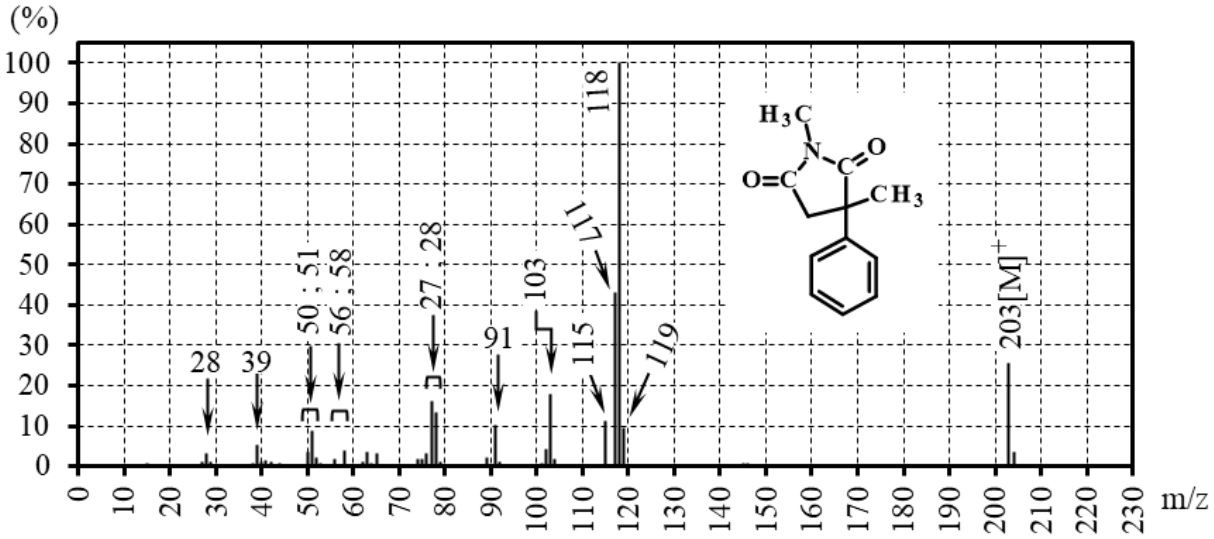

Methotrexate - CAS 59-05-2 - NIST 131571



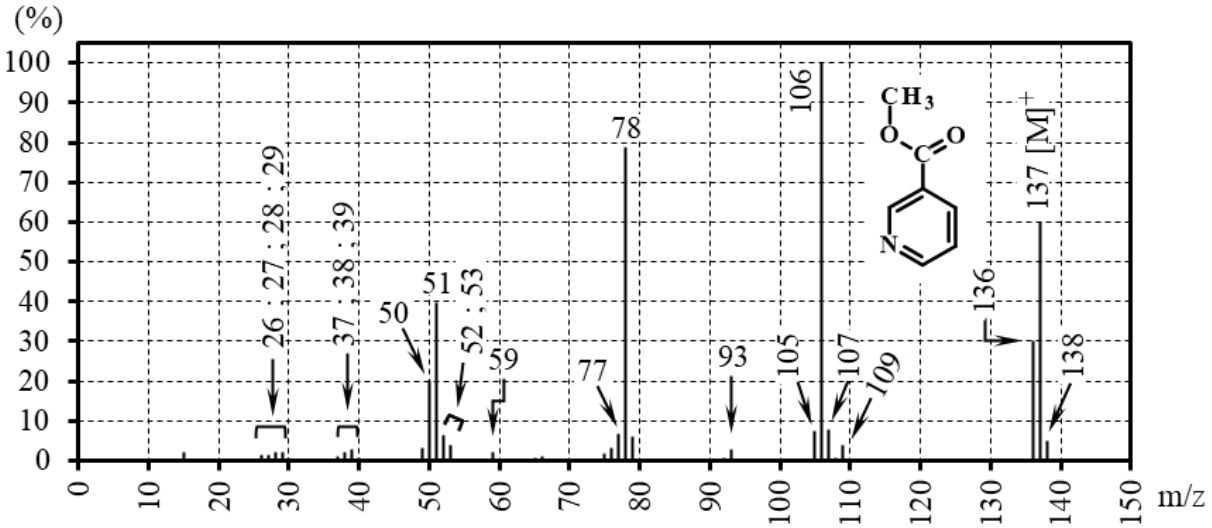

Methoxsalen (Xanthotoxin) - CAS 298-81-7 - EI 75 eV source 200 oC , sample 130 oC - SDBS 10625 - NIST 188900



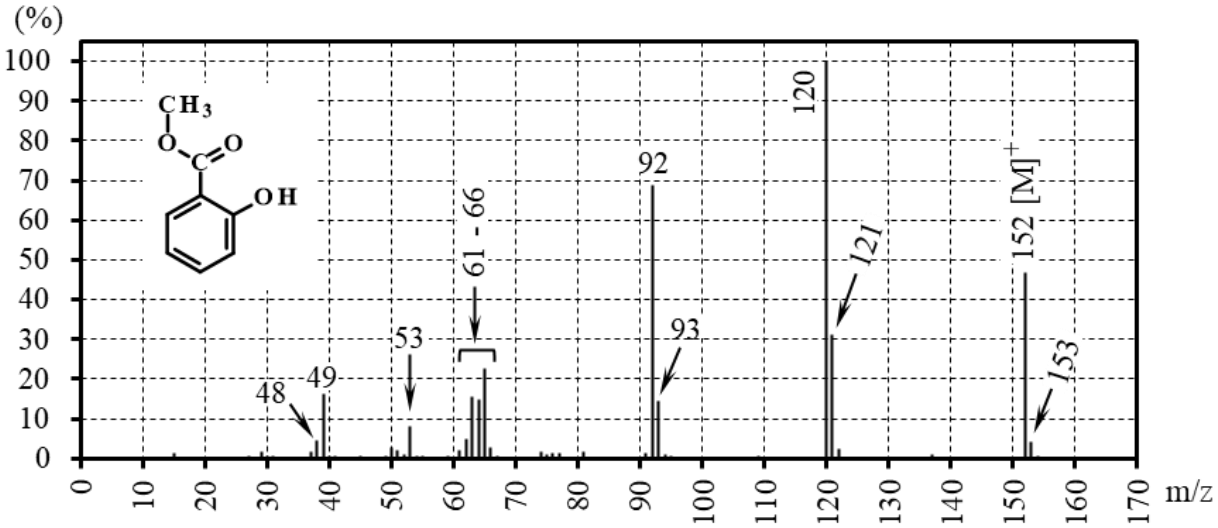

Methoxyphenamine - CAS 93-30-1 - EI - NIST 246066



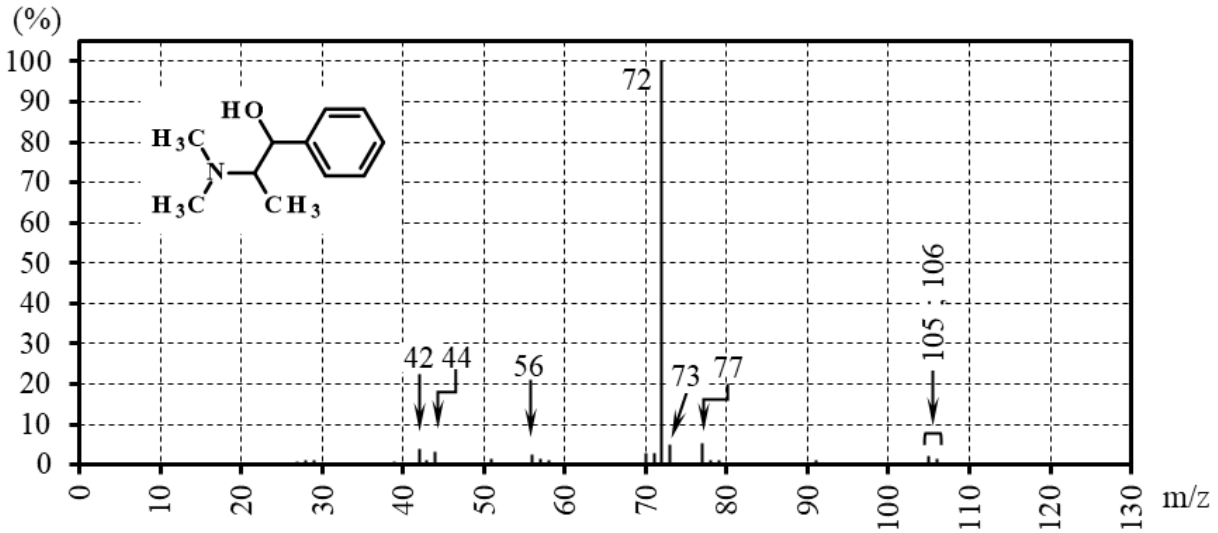

Methsuximide - CAS 77-41-8- - EI - NIST 113830



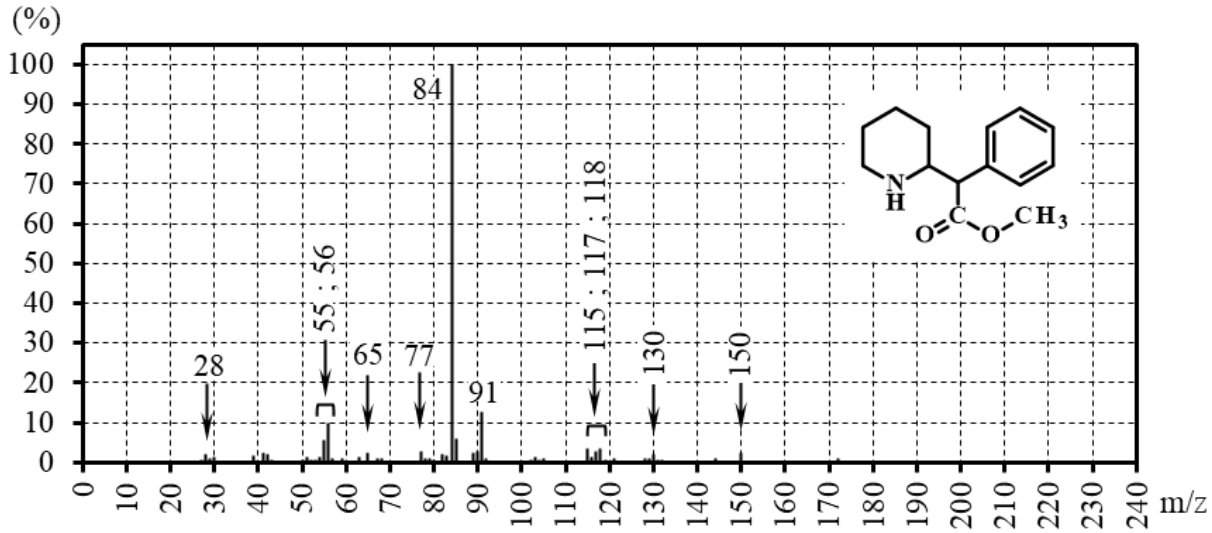

Methyl nicotinate - CAS 93-60-7 - EI - NIST 352595



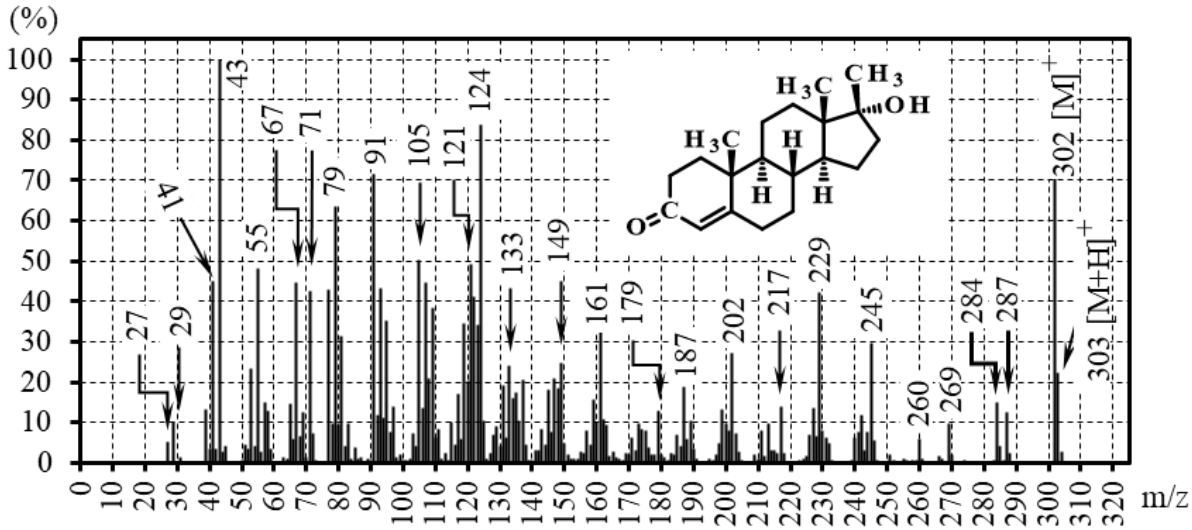

Methyl salicylate - CAS 119-36-8 - EI - NIST 291552



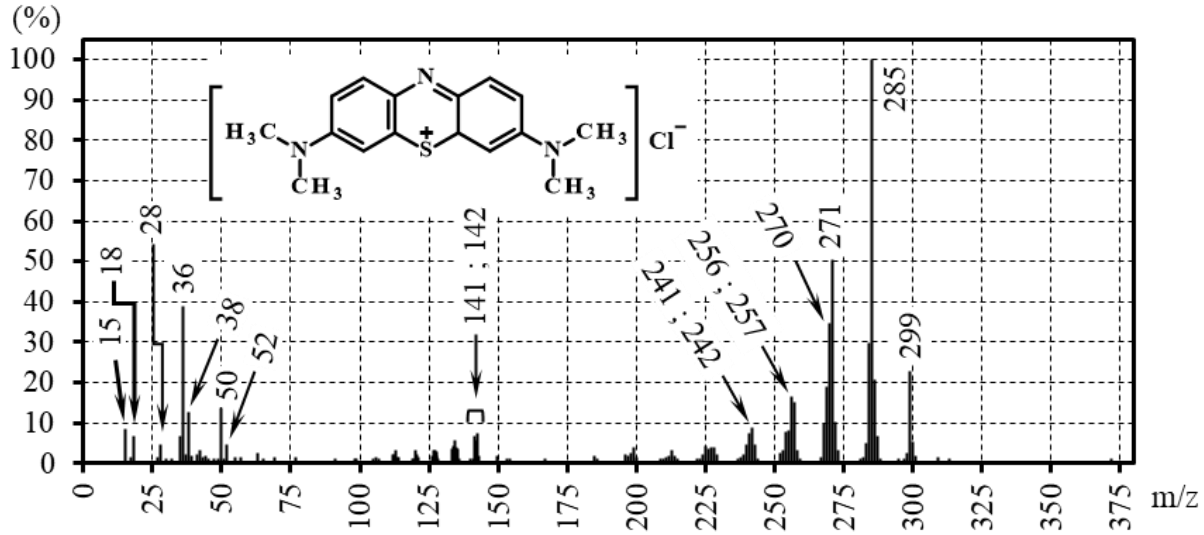

Methylephedrine - CAS 552-79-4 - EI - NIST 107881



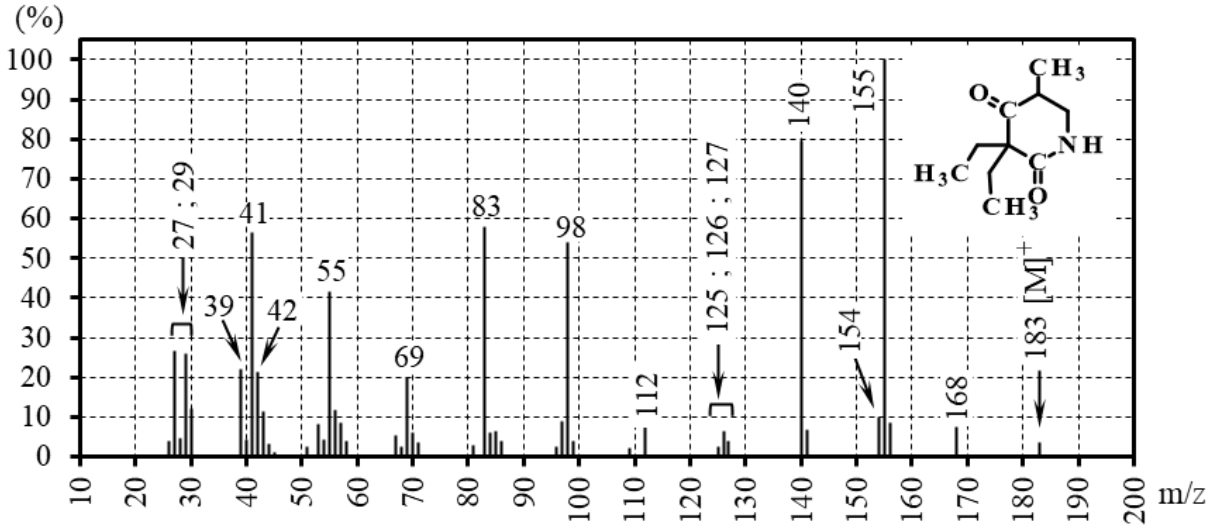

Methylphenidate - CAS 113-45-1 - EI - NIST 352161



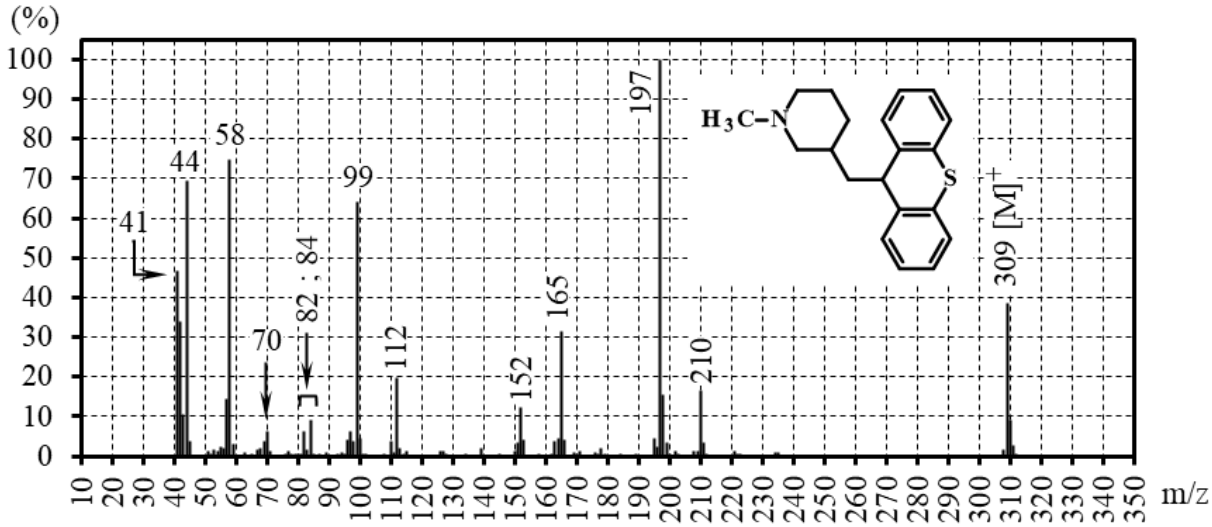

Methyltestosterone - CAS 58-18-4 - NIST 292122



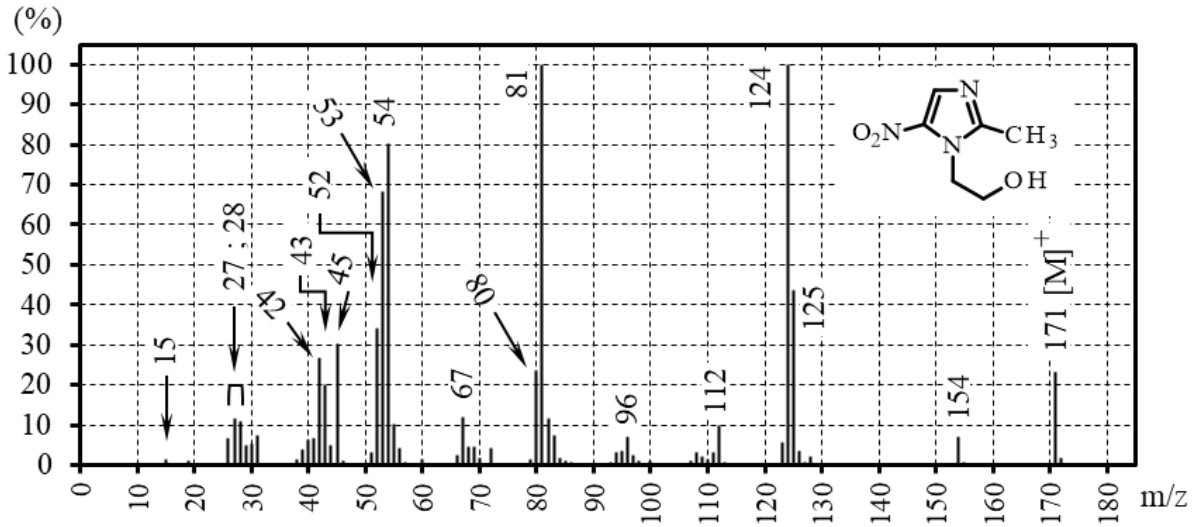

Methylthionine chloride (Methylene Blue) - CAS61-73-4 - SDBS 2609



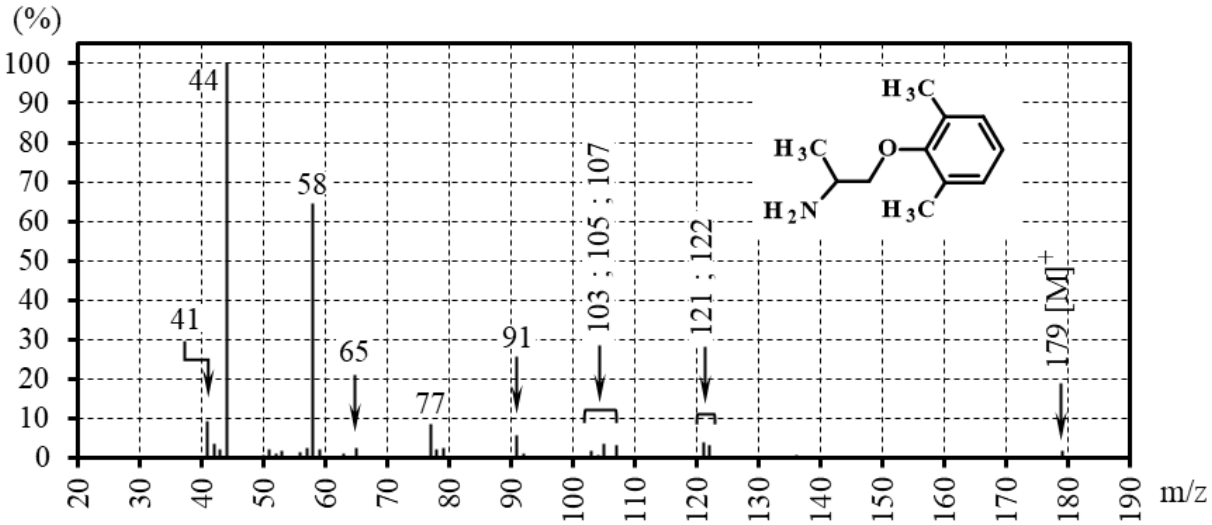

Methyprylon - CAS 125-64-4 - EI - NIST 107182



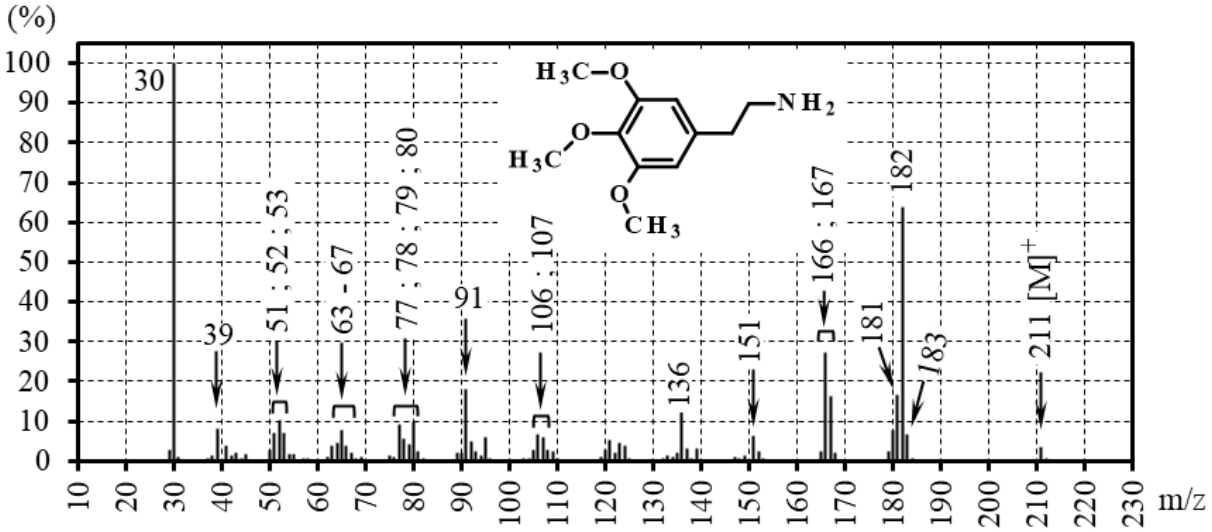

Metixene - CAS 4969-02-2 - EI - NIST 248032



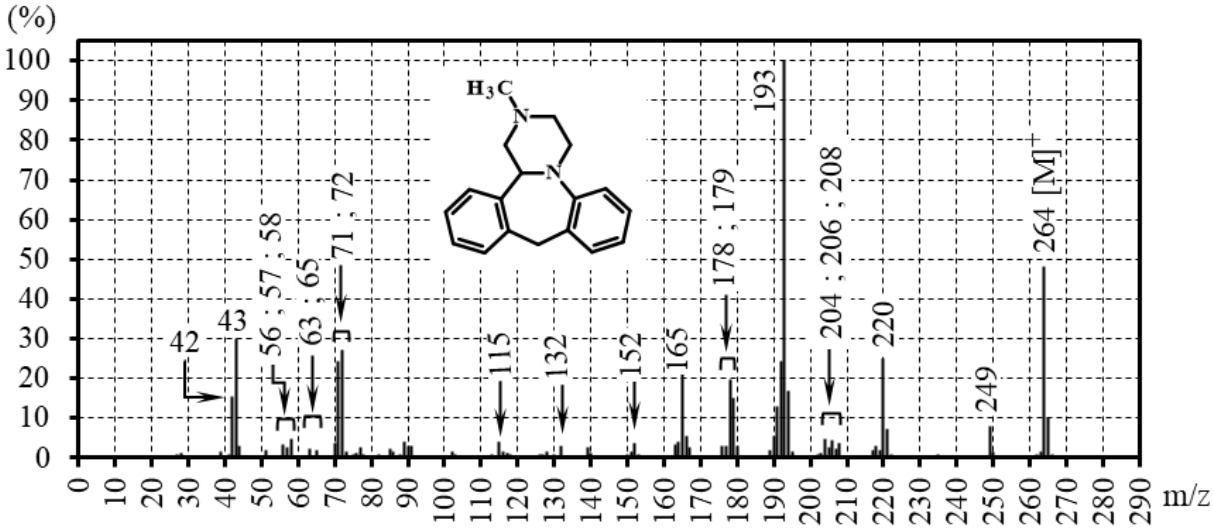

Metronidazole - CAS 443-48-1- EI - NIST nr. 352184



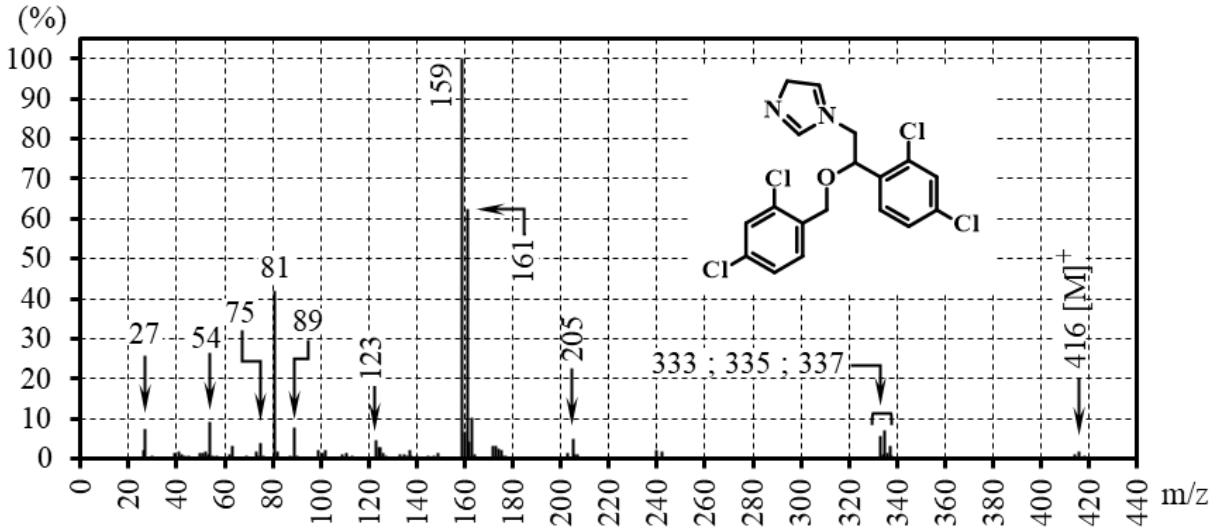

Mexiletine - CAS 31828-71-4 - EI - NIST 248218



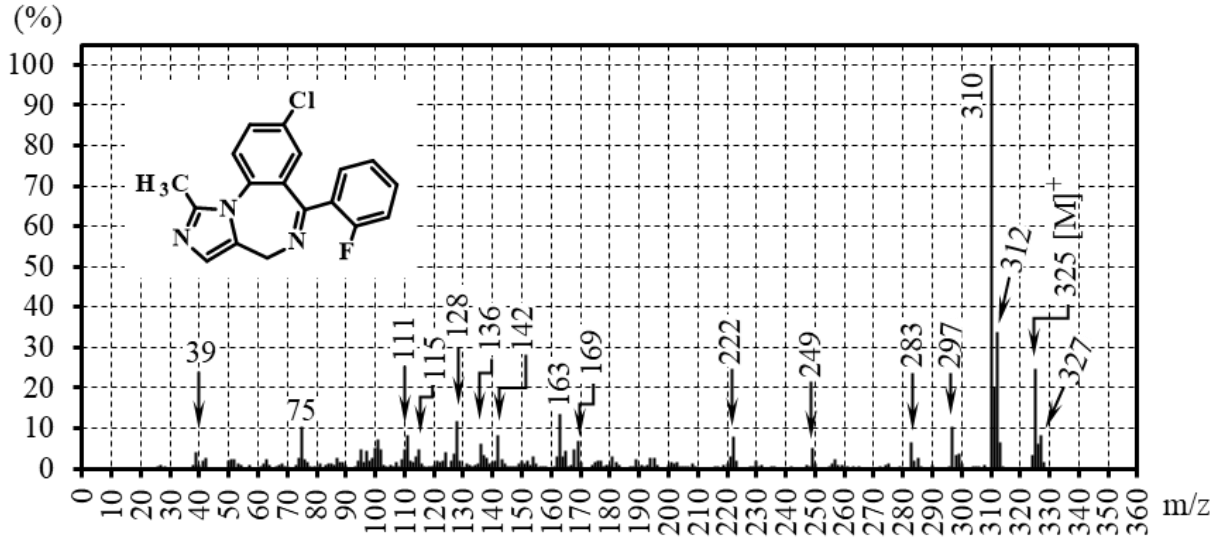

Mezcaline - CAS 54-04-6 - SI - NIST 246201



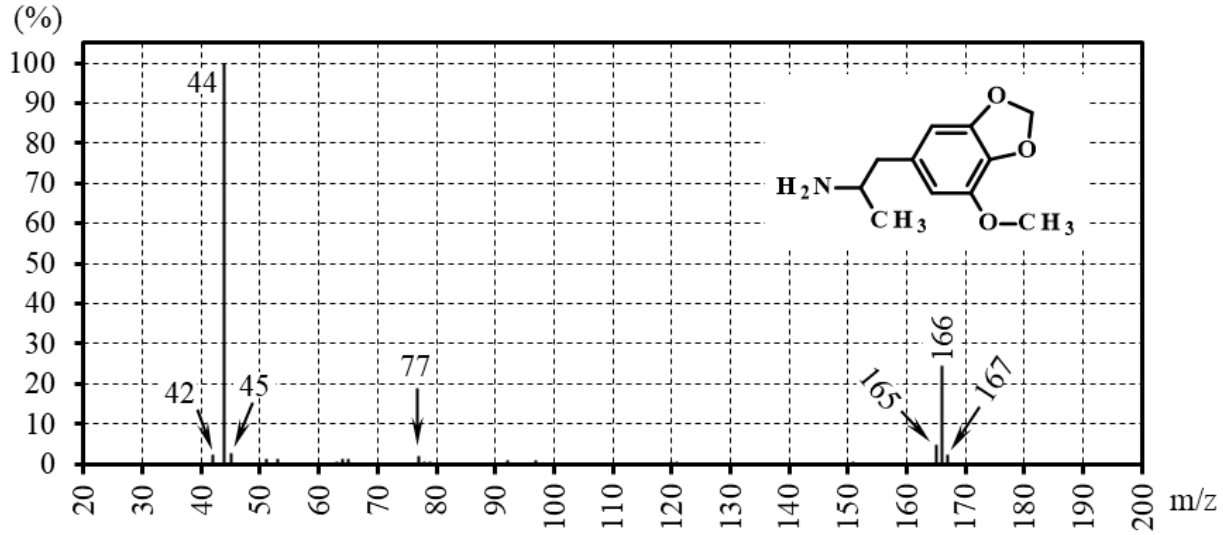

Mianserin - CAS 24219-97-4 - EI - NIST 292121



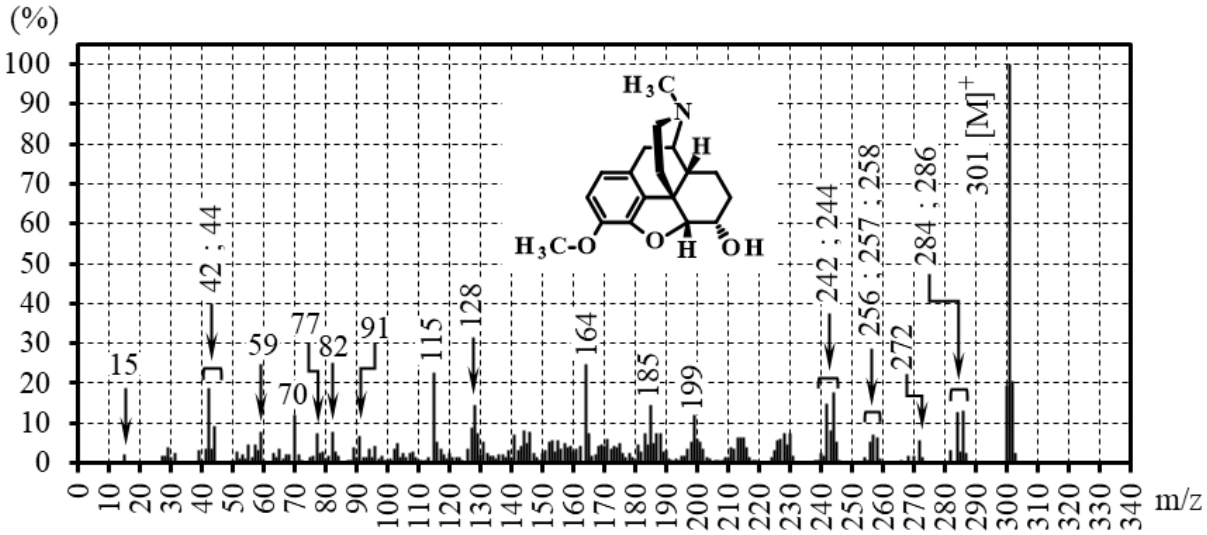

Miconazole - CAS 22916-47-8 - EI - NIST 107110



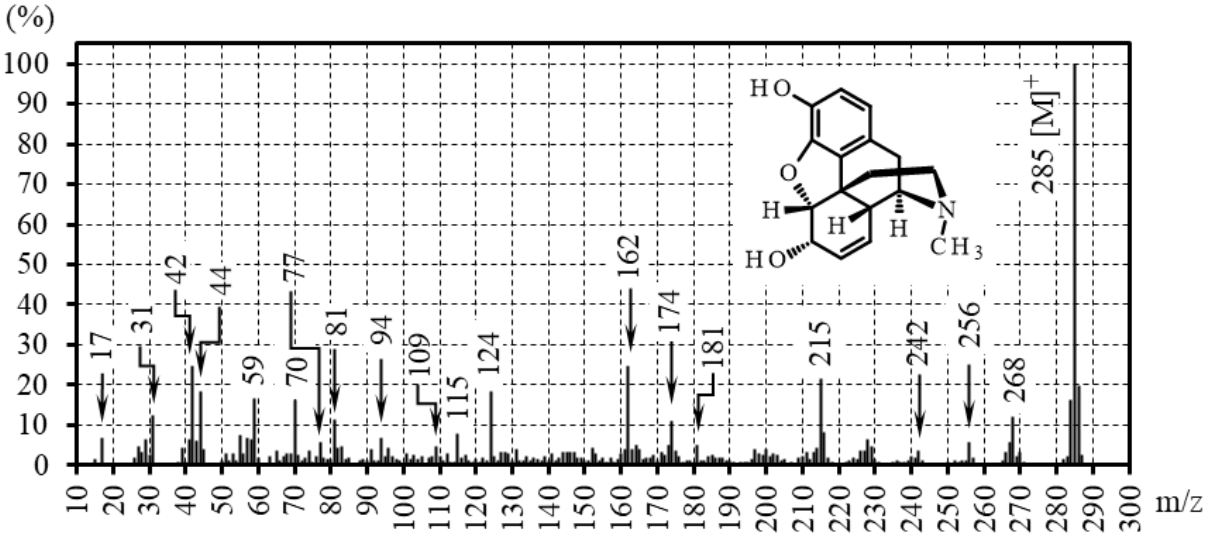

Midazolam - CAS 59467-70-8 - EI - NIST 352157



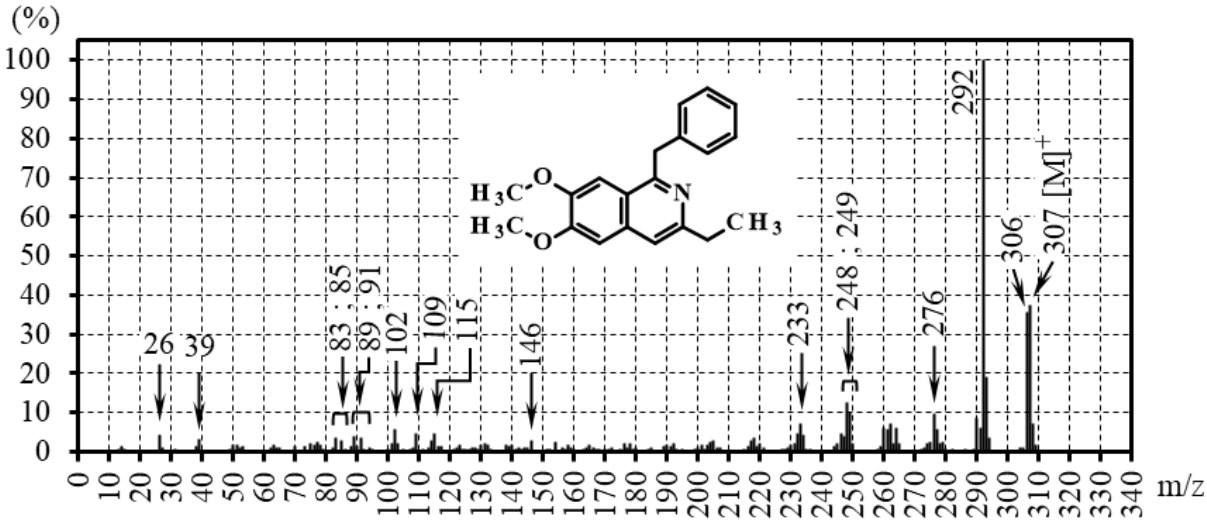

MMDA - CAS 13674-05-0 - EI - NIST 120147



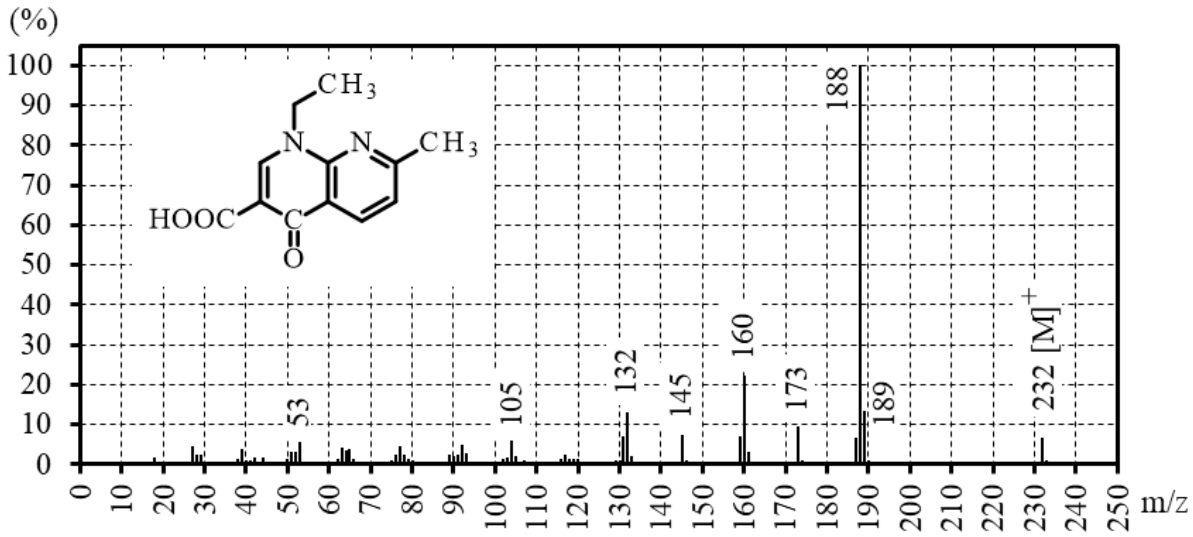

Morphinan-6-ol etc - CAS 125-28-0 - EI - NIST 250601



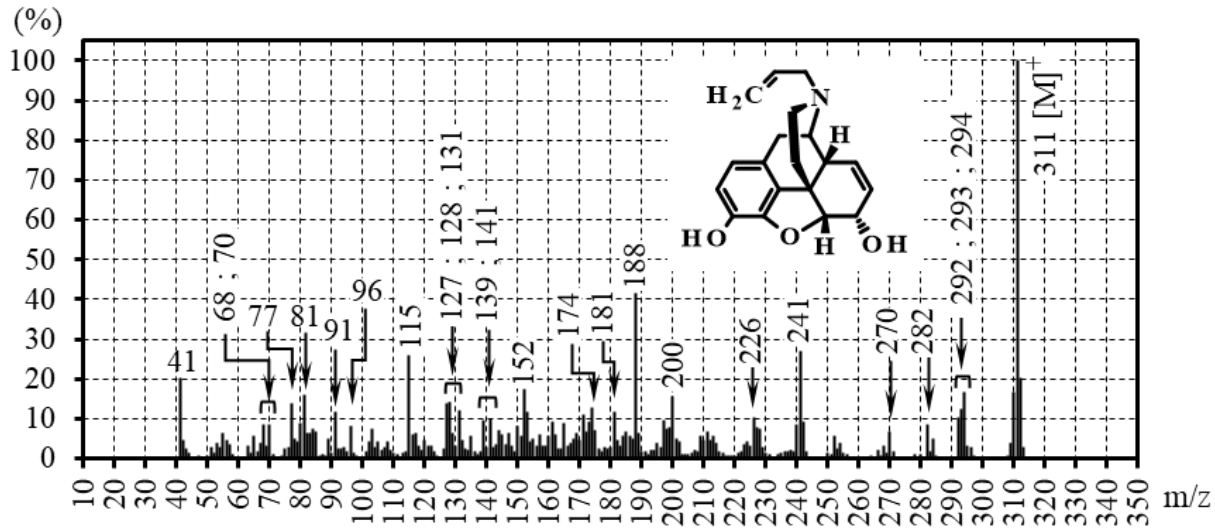

Morphine - CAS 57-27-2 - EI - NIST 42472



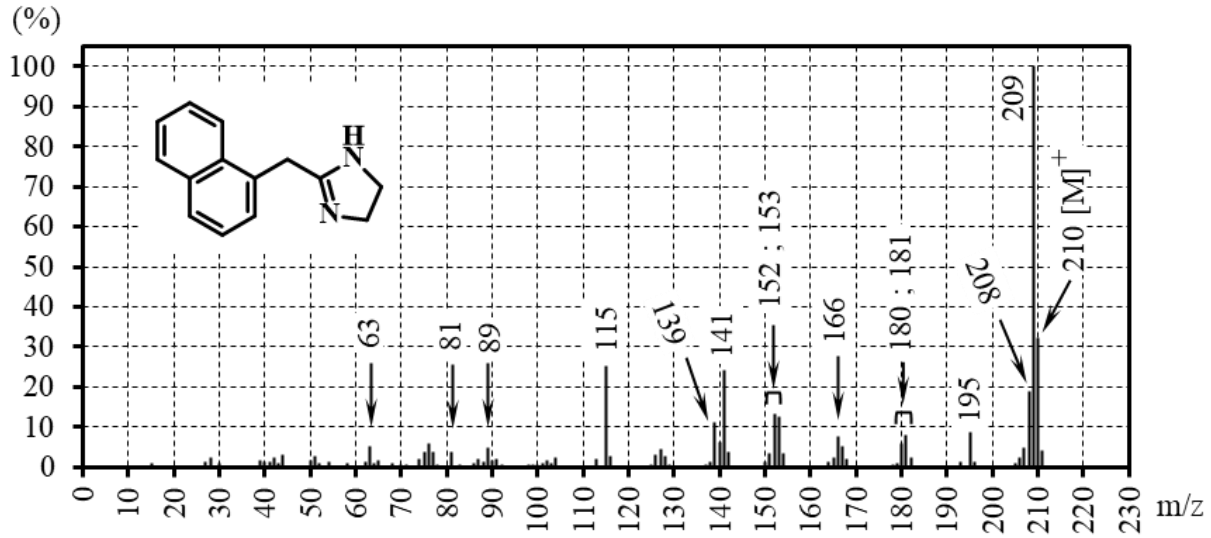

Moxaverine - CAS 10539-19-2 - EI - NIST 42352



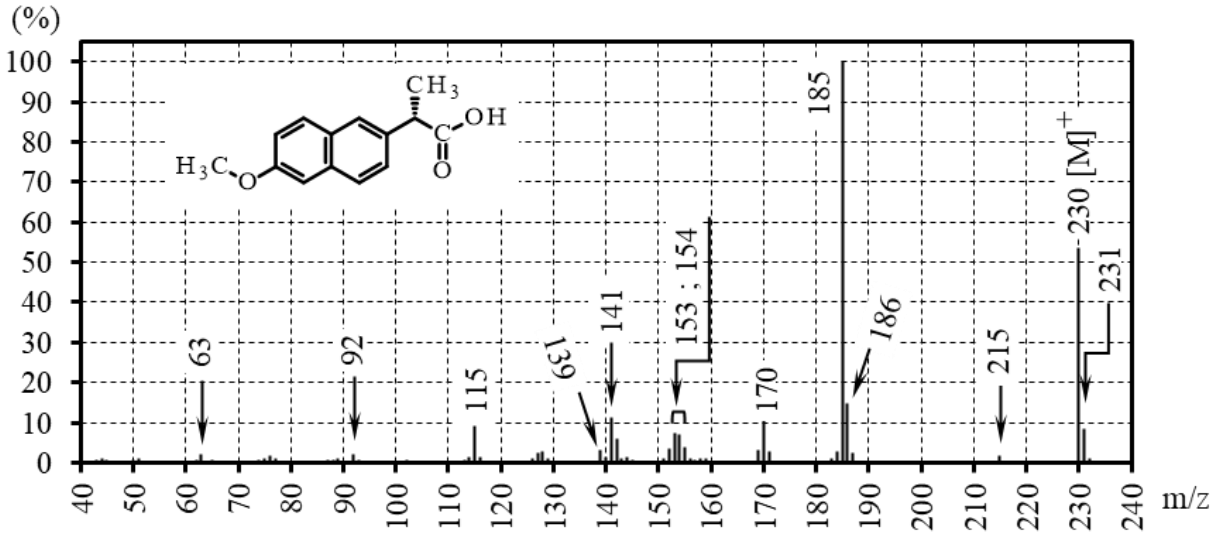

Nalidixic acid - CAS 389-08-2 - EI - SBDS 13530



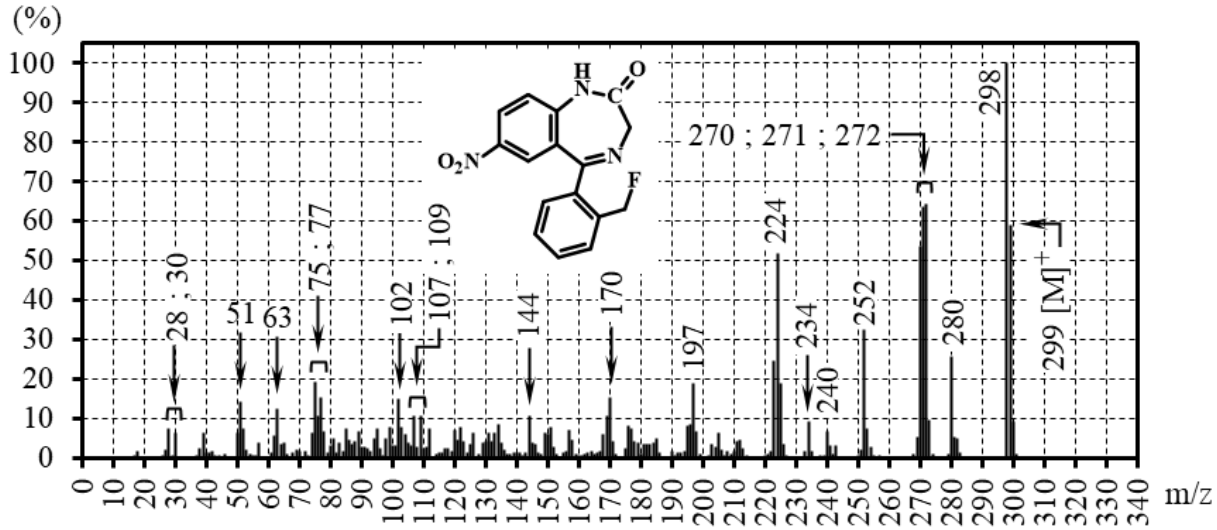

Nalorphine - CAS 62-67-9 - EI - NIST 247880



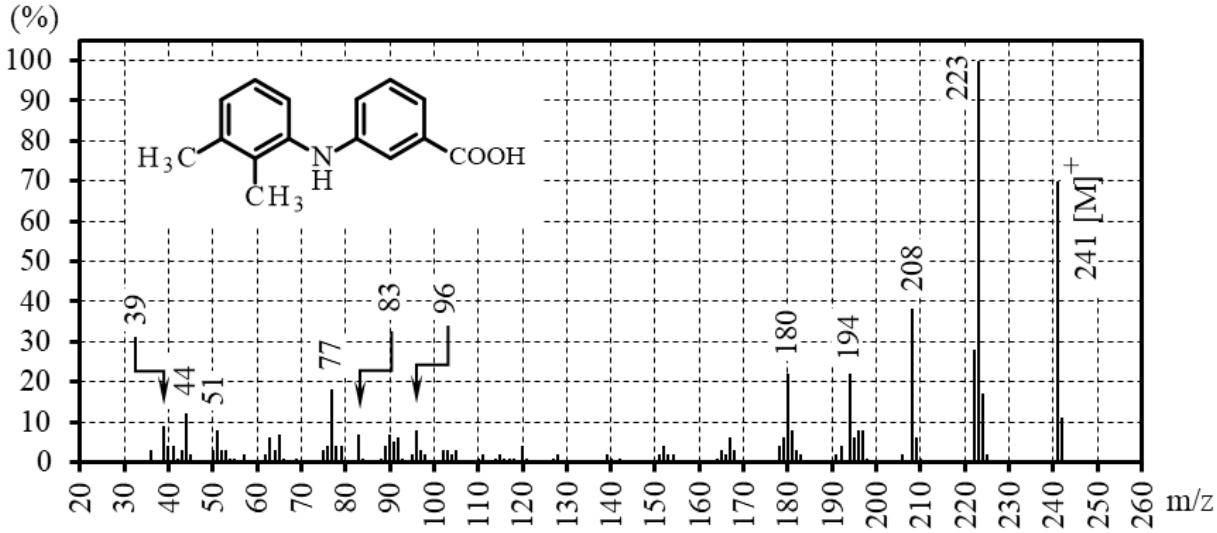

Naphazoline - CAS 835-31-4 - NIST 113854



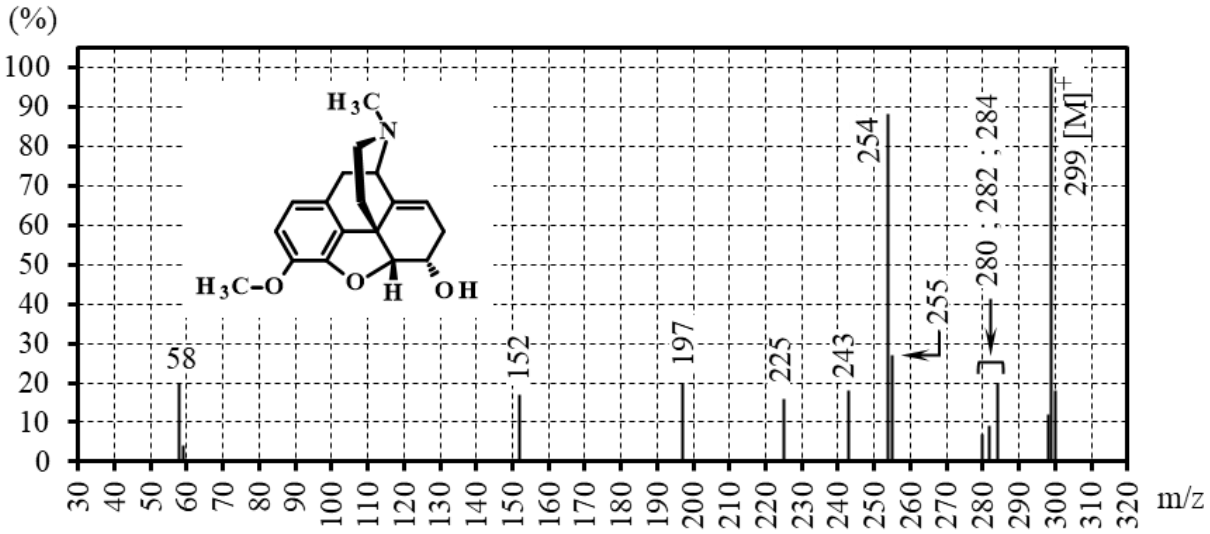

Naproxen - CAS 22204-053-1 - EI - NIST 237147



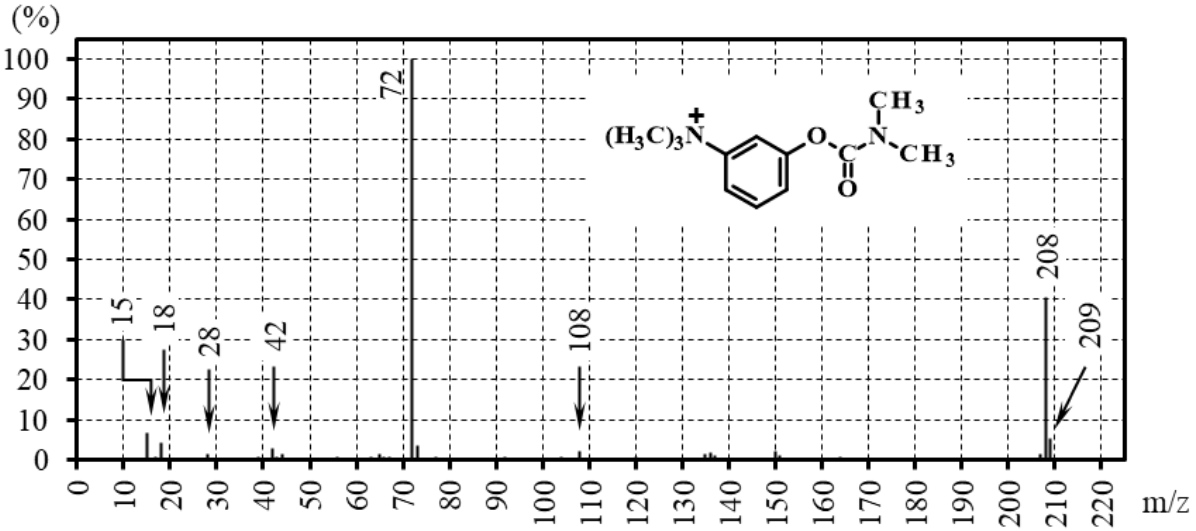

N-Desmethylflunitrazepam - CAS 2558-30-7 - EI - NIST 417081



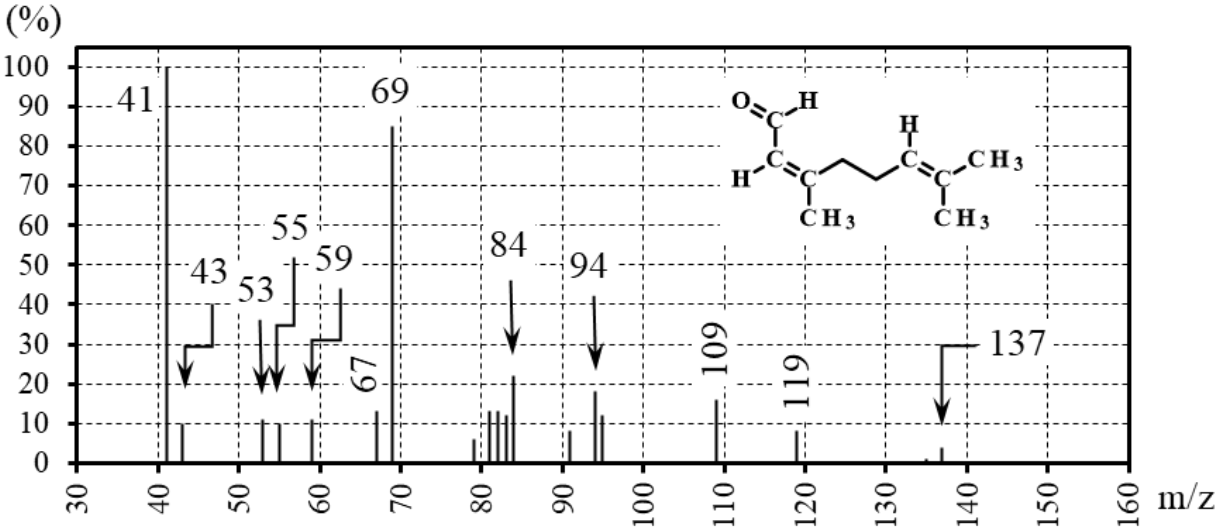

Nefenamic acid - CAS 61-68-7 - EI - NIST 298720



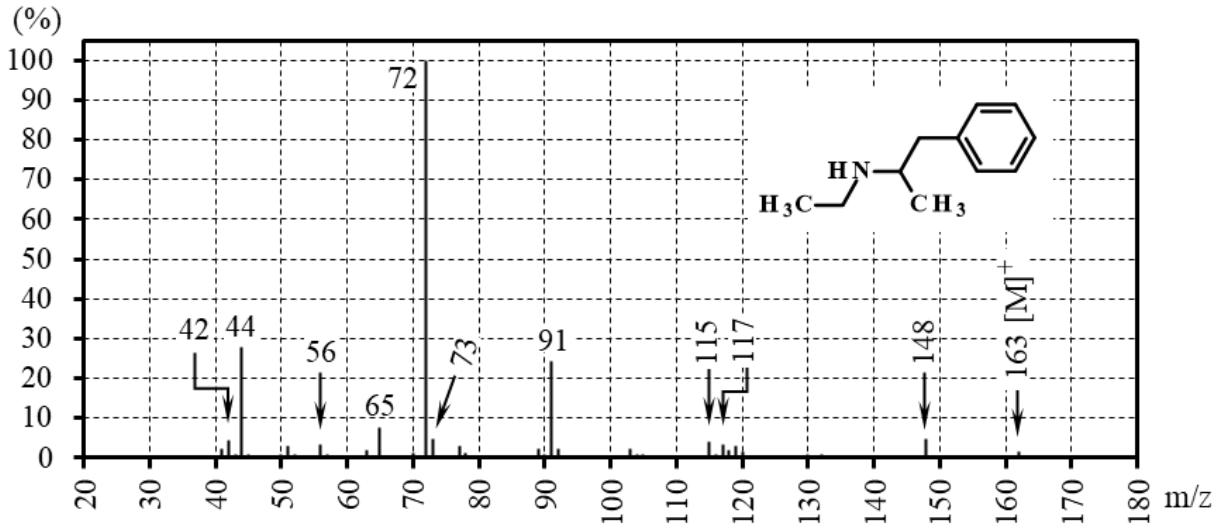

Neopine - EI - CAS 467-14-1 - NIST 64811



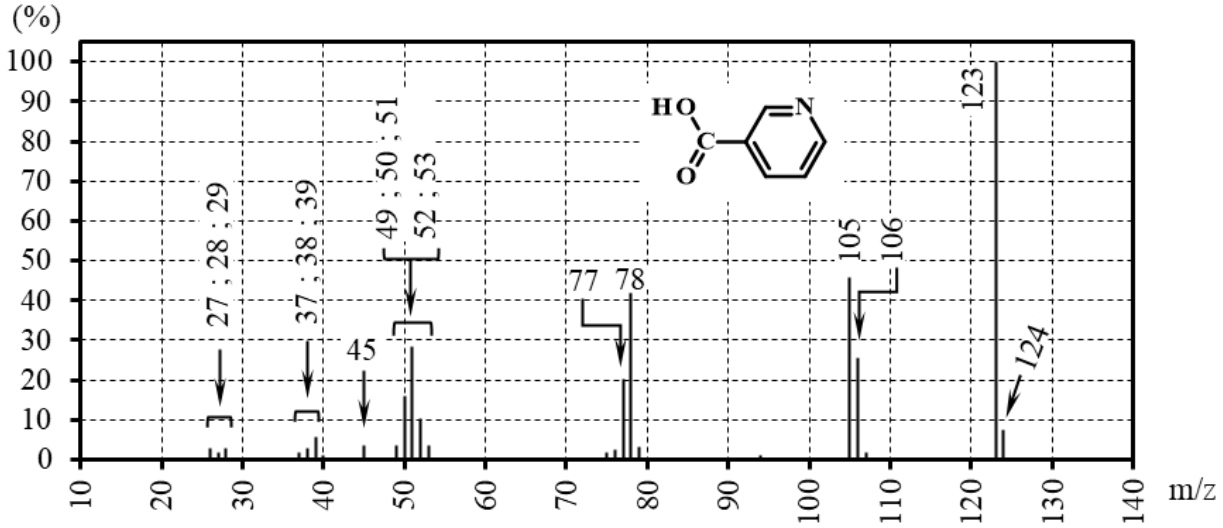

Neostigmine (cation) - CAS 59-99-4 - NIST 230961



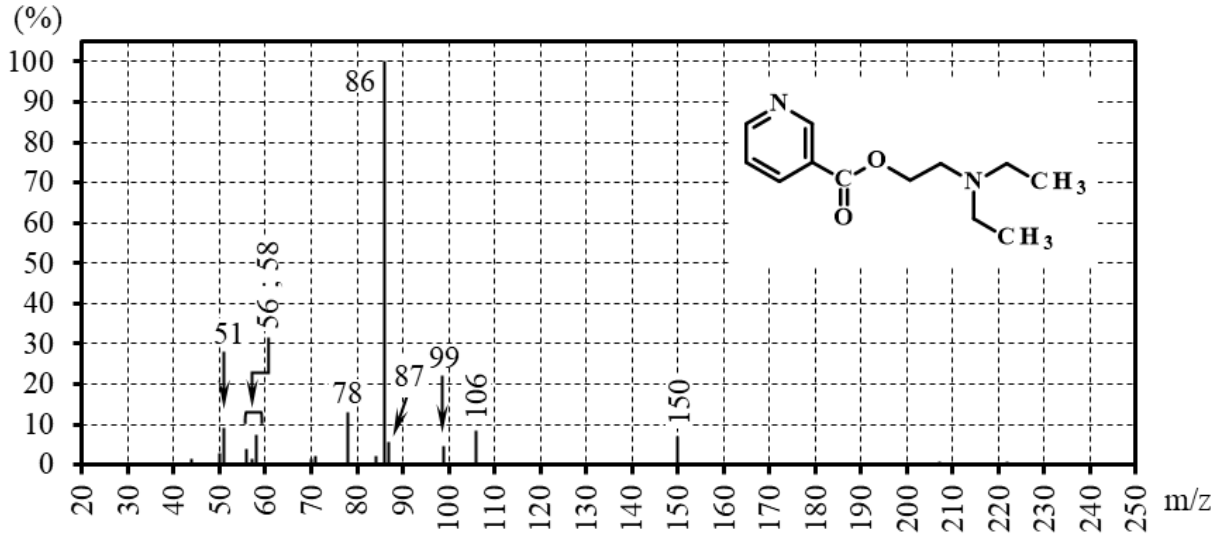

Neral (Citral B) - CAS 106-26-3 - NIST 151979



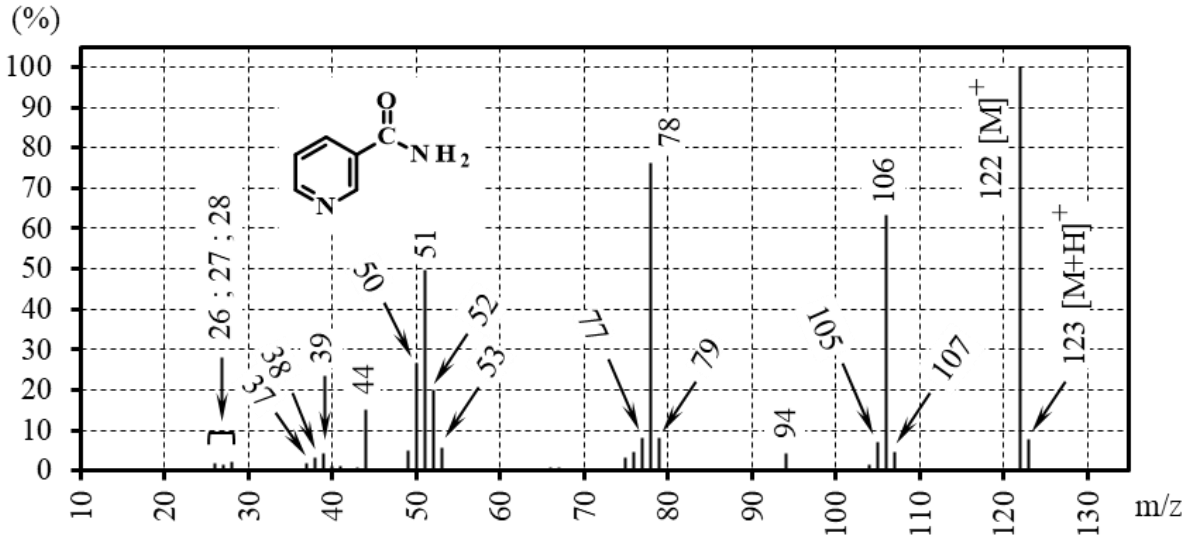

N-Ethylamphetamine - CAS 457-87-4 - EI - NIST 247926



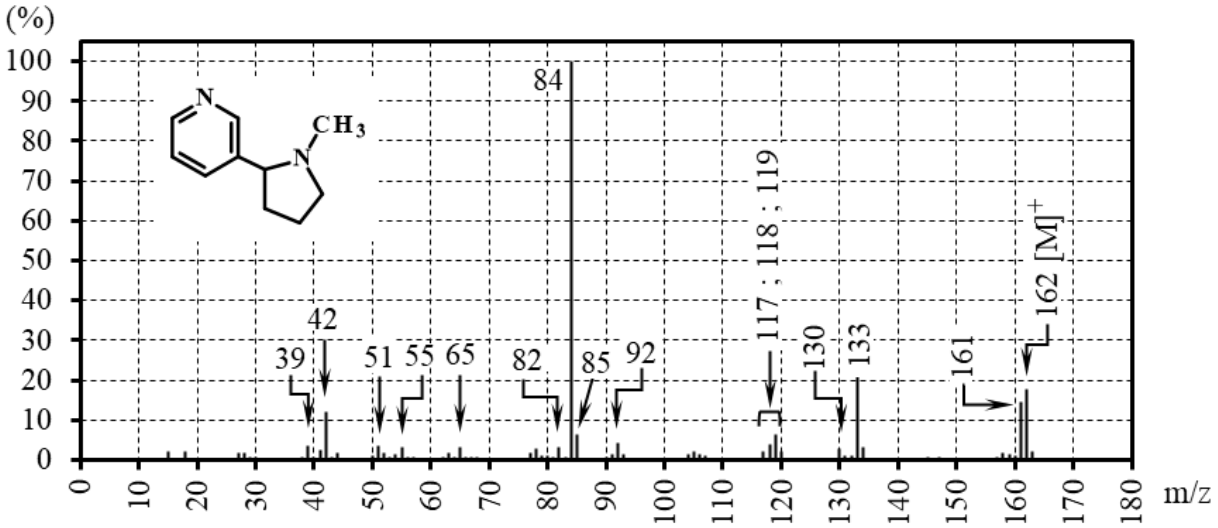

Niacin (Nicotinic acid) - CAS 59-67-6 - EI source 200 oC , sample 120 oC - SDBS 7944 - NIST 233225



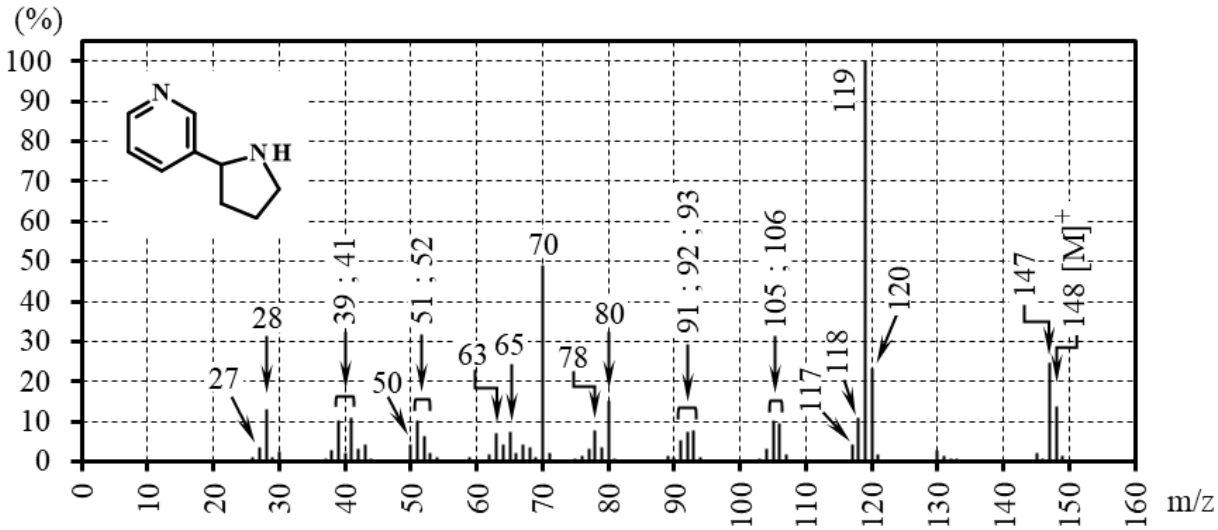

Nicametate - CAS 3099-52-3 - EI - NIST 248469



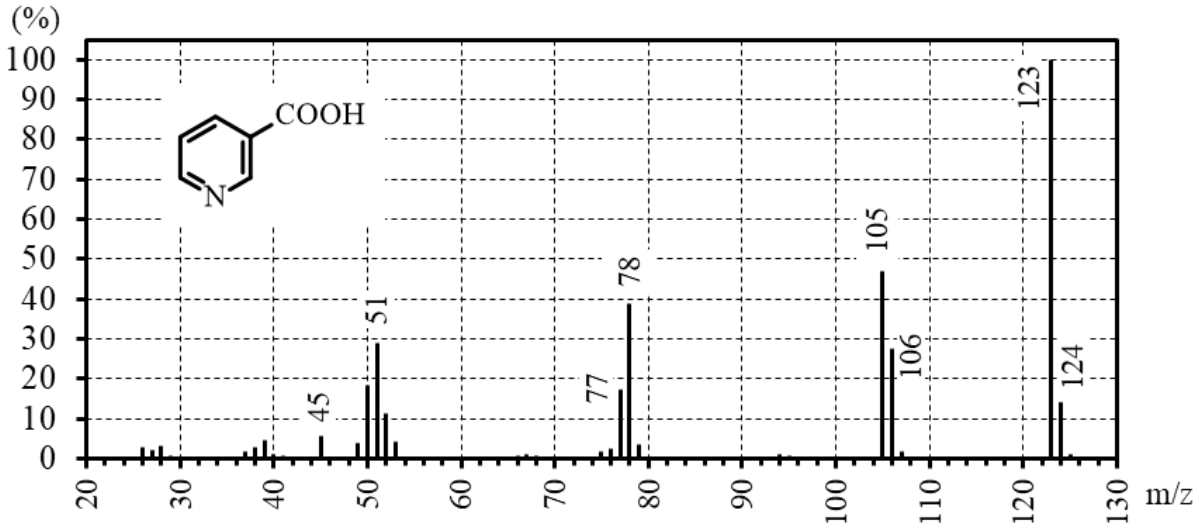

Nicotinamide (vitamin PP) - CAS 98-92-0 - NIST 290943



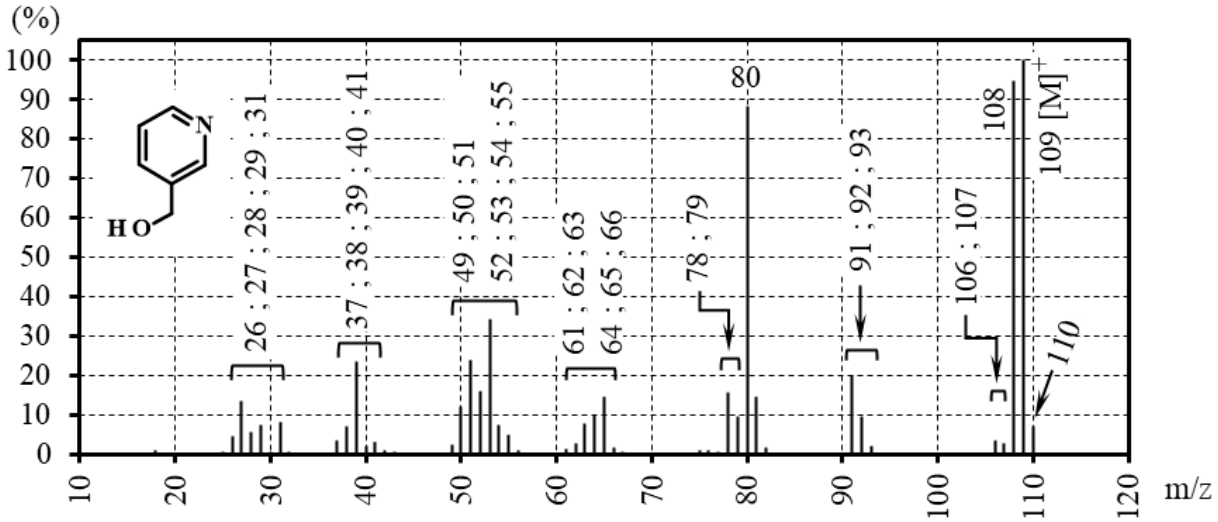

Nicotine - CAS 54-11-5 - EI - NIST 232303



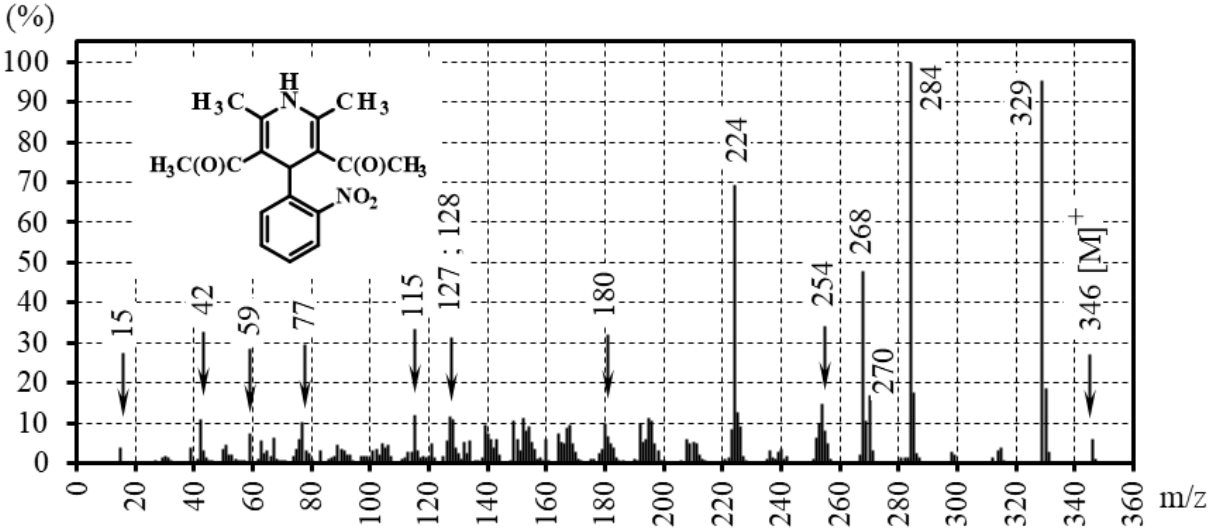

Nicotine, 1'-demethyl-, - CAS 5746-86-1 - EI - NIST 417038



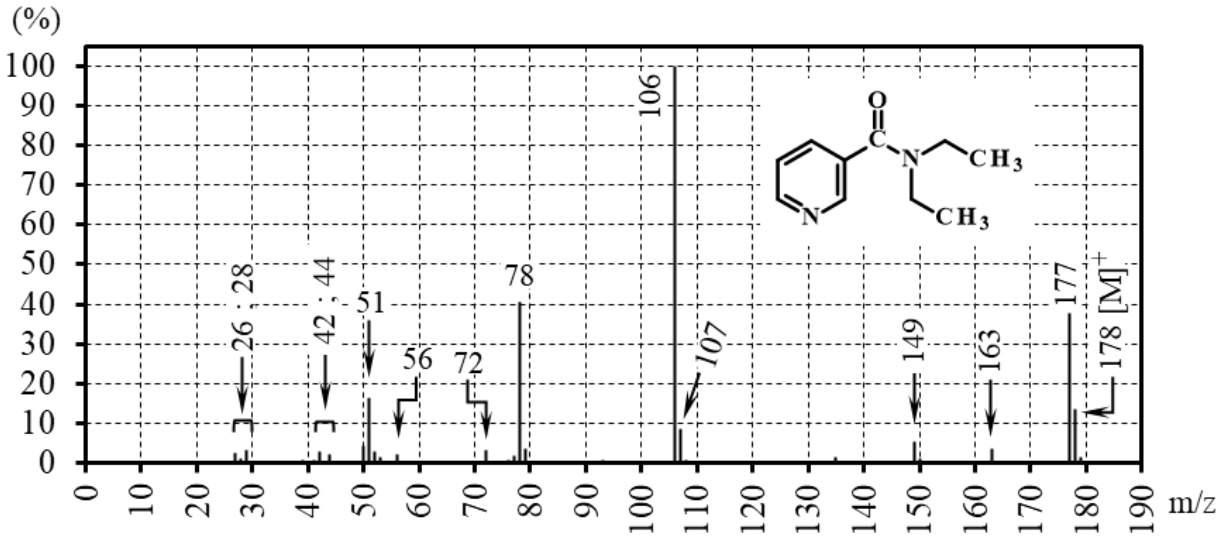

Nicotinic acid - CAS 59-67-6 - EI 70 eV - NIST nr. 233225



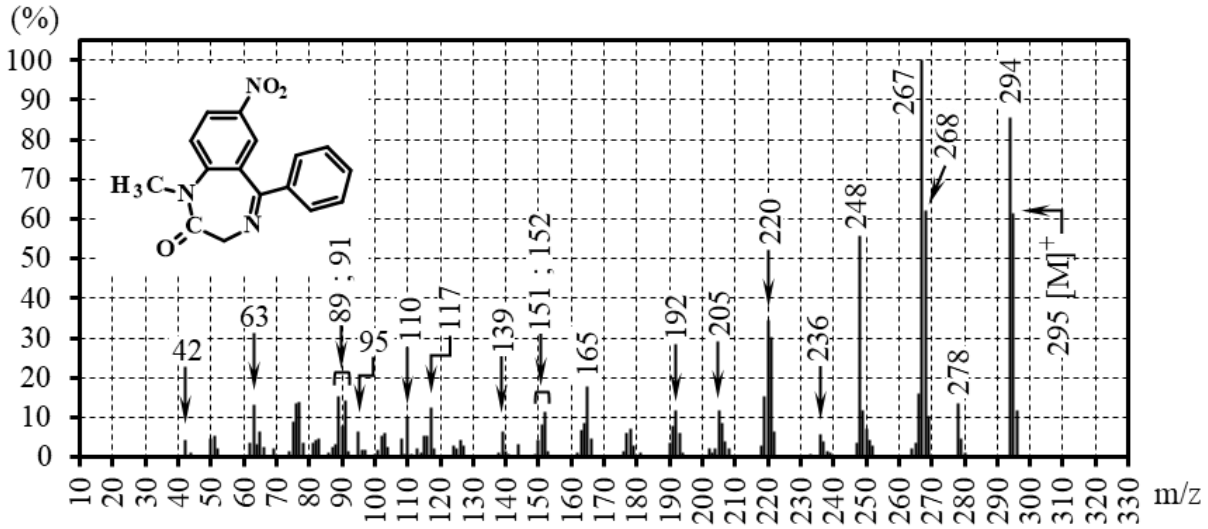

Nicotinyl alcohol - CAS 100-55-0 - EI - NIST 233597



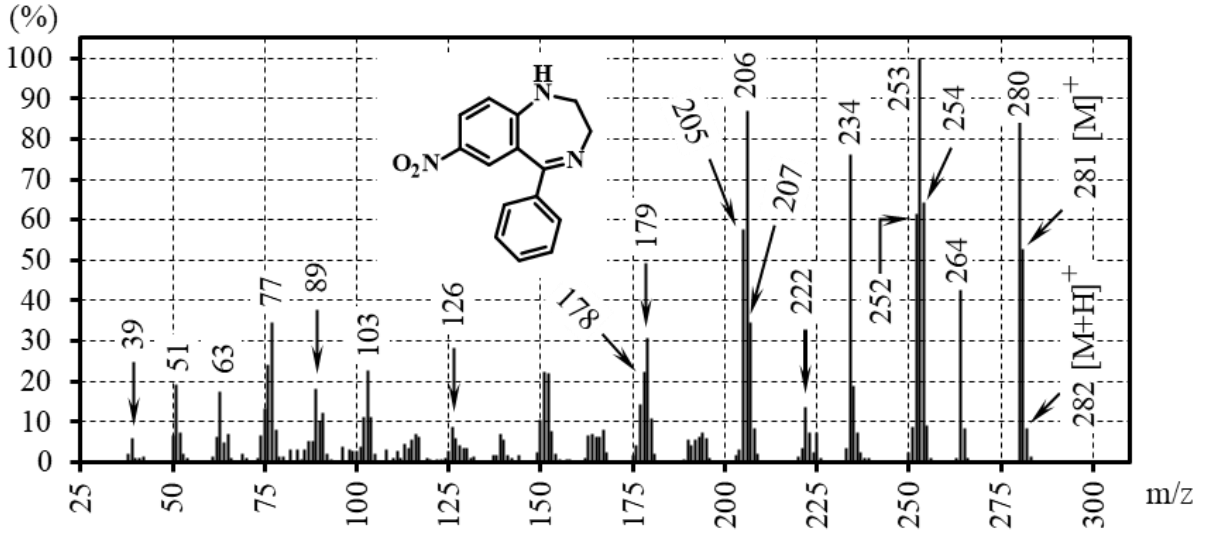

Nifedipine - CAS 21829-25-4 - NIST 341371



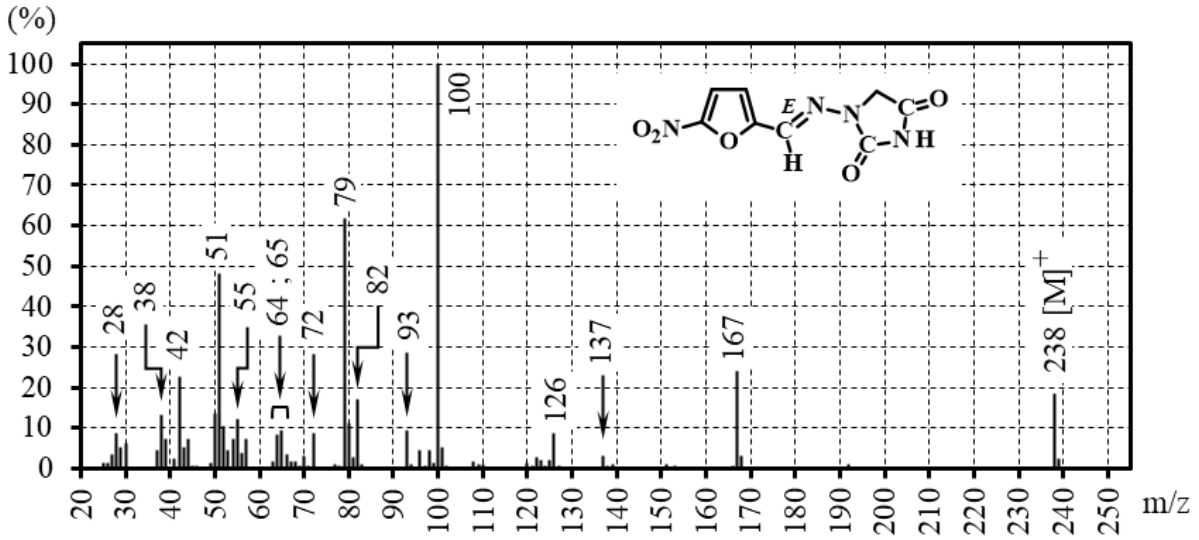

Nikethamide - CAS - 59-26-7 - EI - NIST 291418



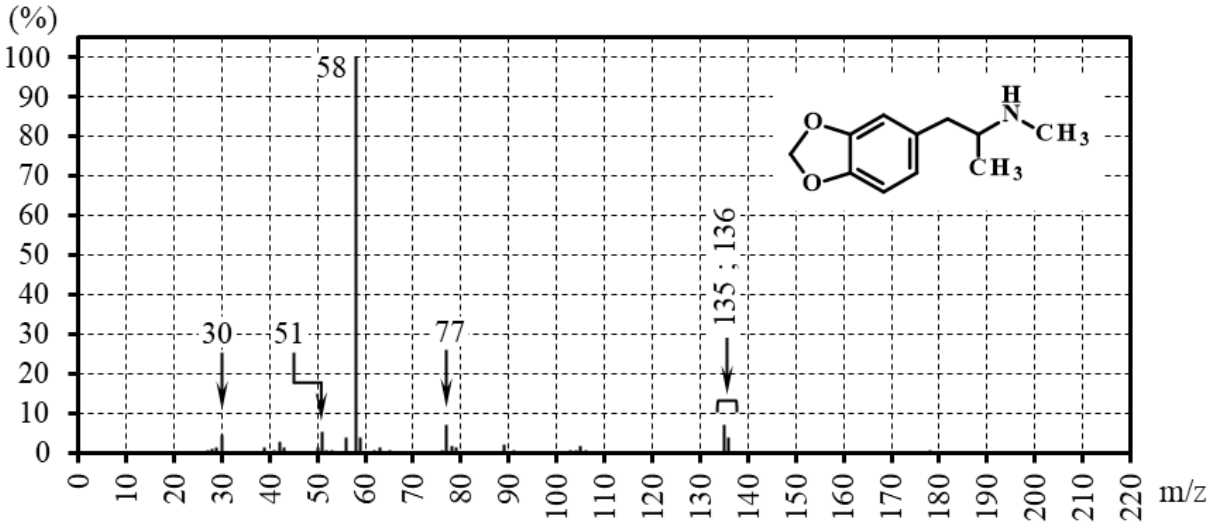

Nimetazepam - CAS 2011-67-8 - EI - NIST 248244



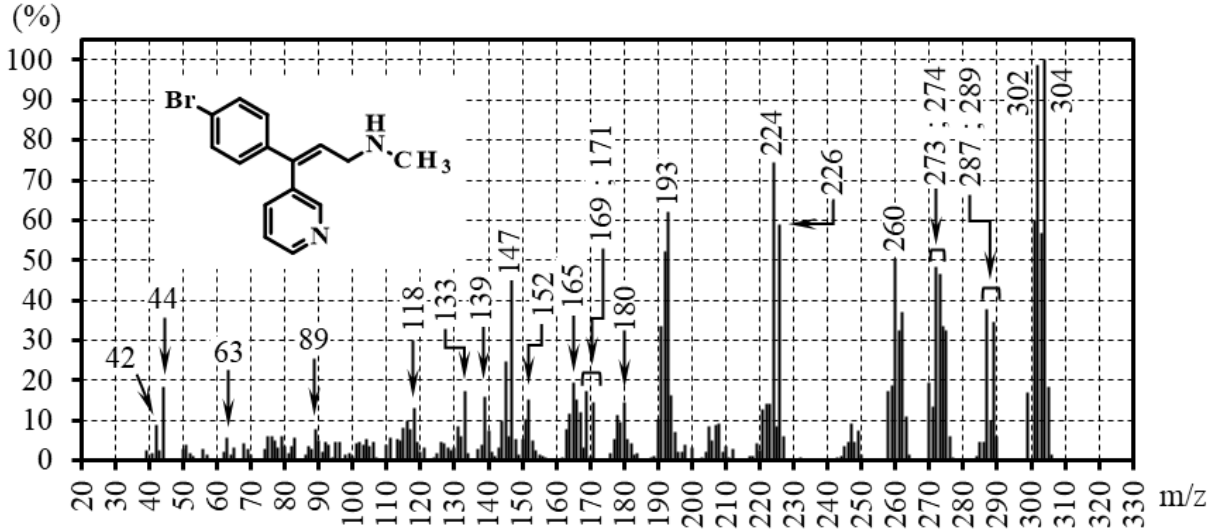

Nitrazepam - CAS 146-22-5 - NIST 312937



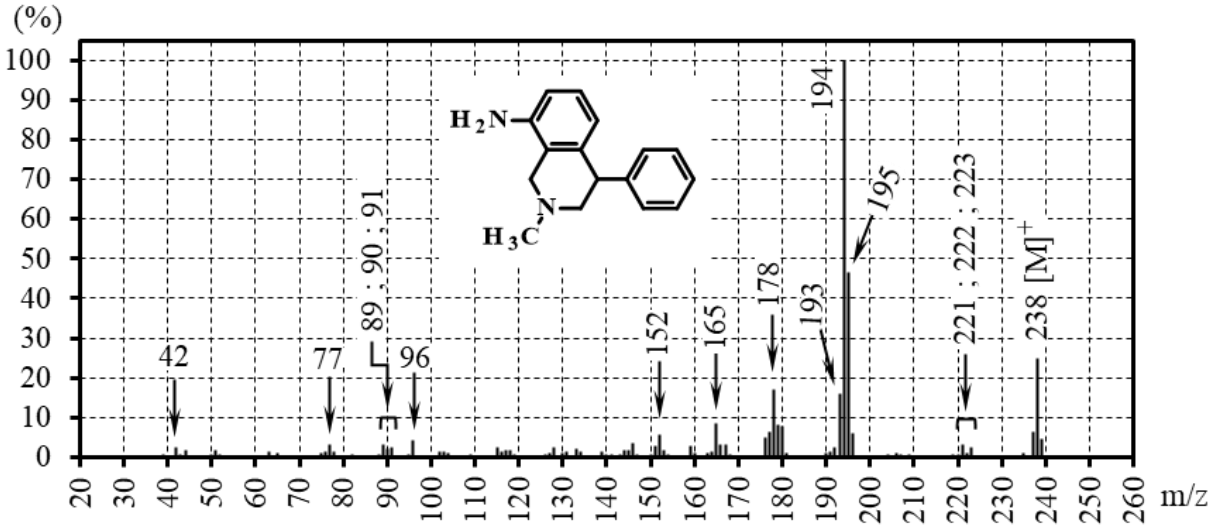

Nitrofurantoin - CAS 67-20-9 - NIST 290698



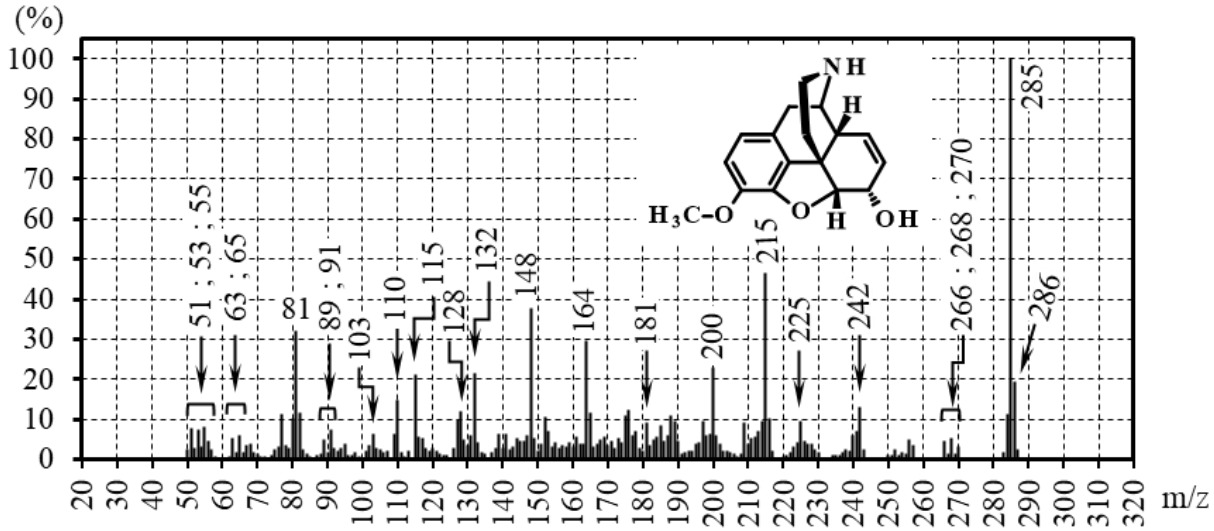

N-Methyl-3,4-methylenedioxyamphetamine (MDMA)
CAS 42542-10-9 - EI - NIST 250569



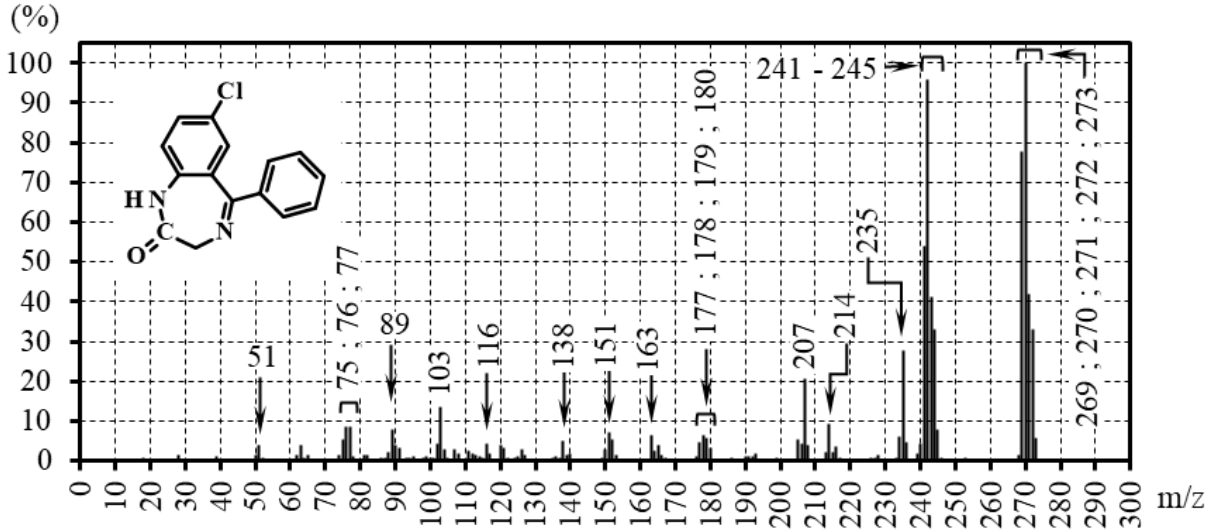

Nomelidine - CAS 60324-59-6 - EI - NIST 246795



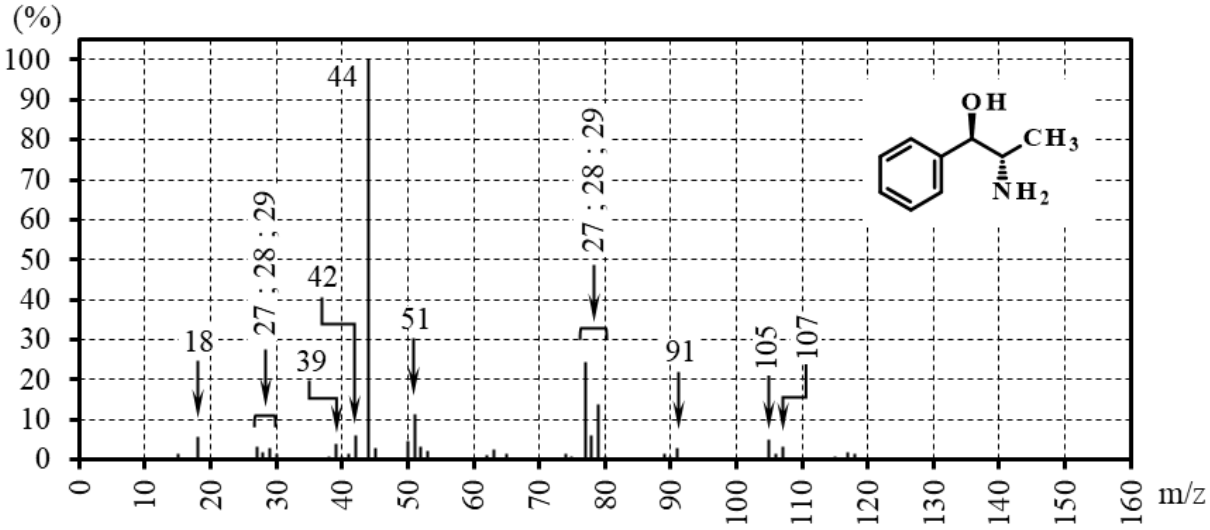

Nomifensine - CAS 24526-64-5 - EI - NIST 247189



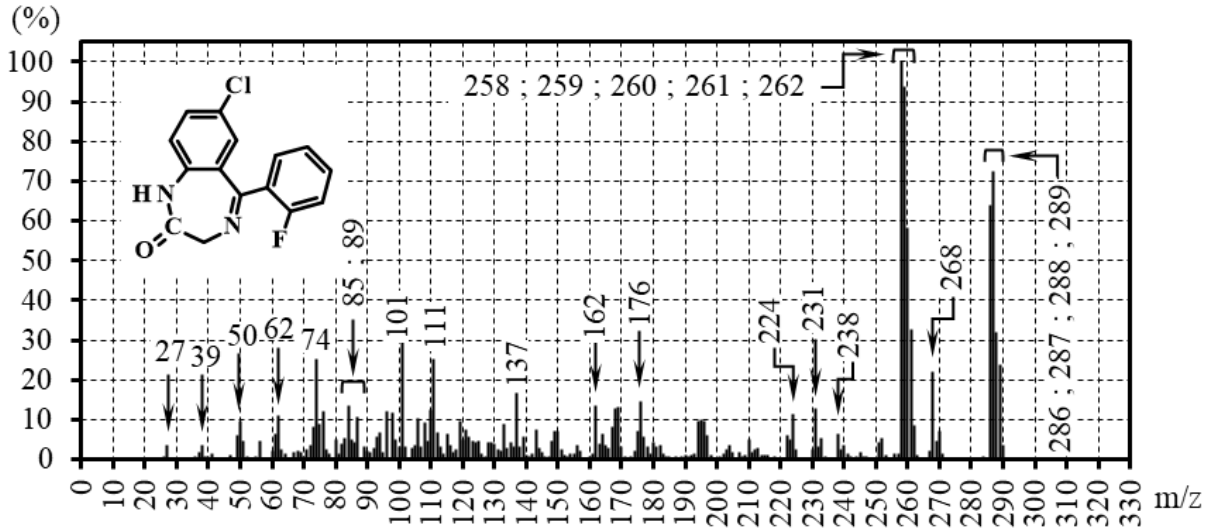

Norcodeine - CAS 467-15-2 - EI - NIST 137112



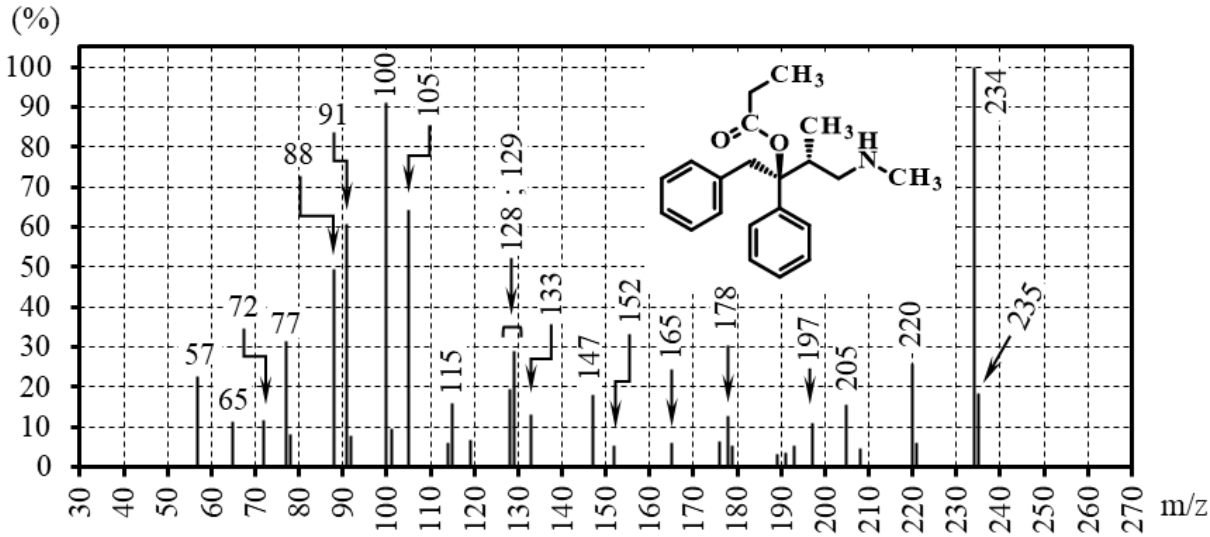

Nordazepam - CAS 1088-11-5 - EI - NIST 239791



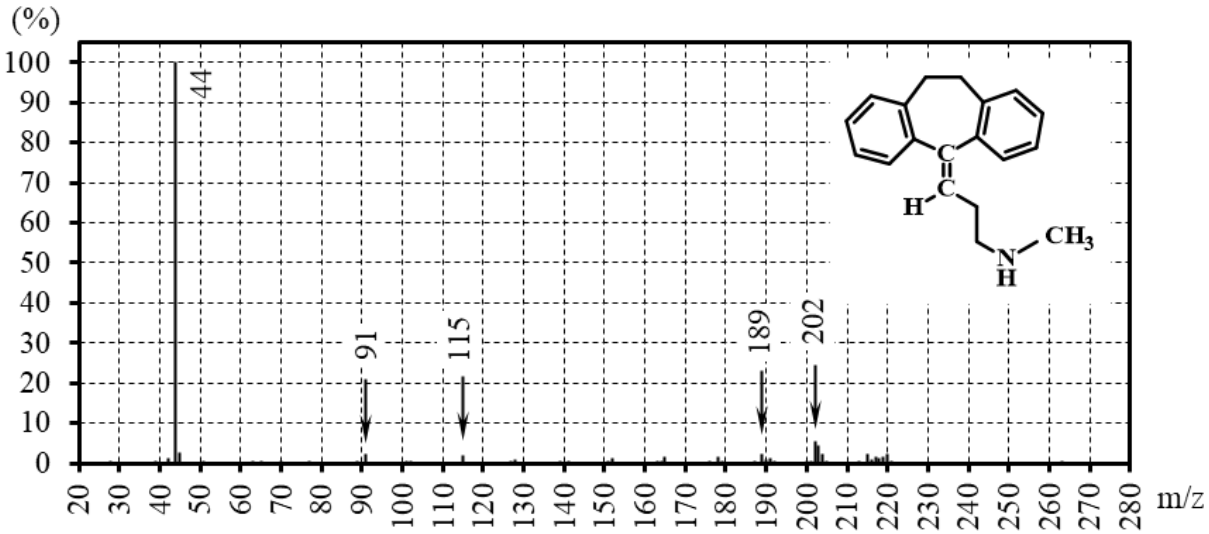

Norephedrine (-) - CAS 492-41-1 - EI - NIST 250631



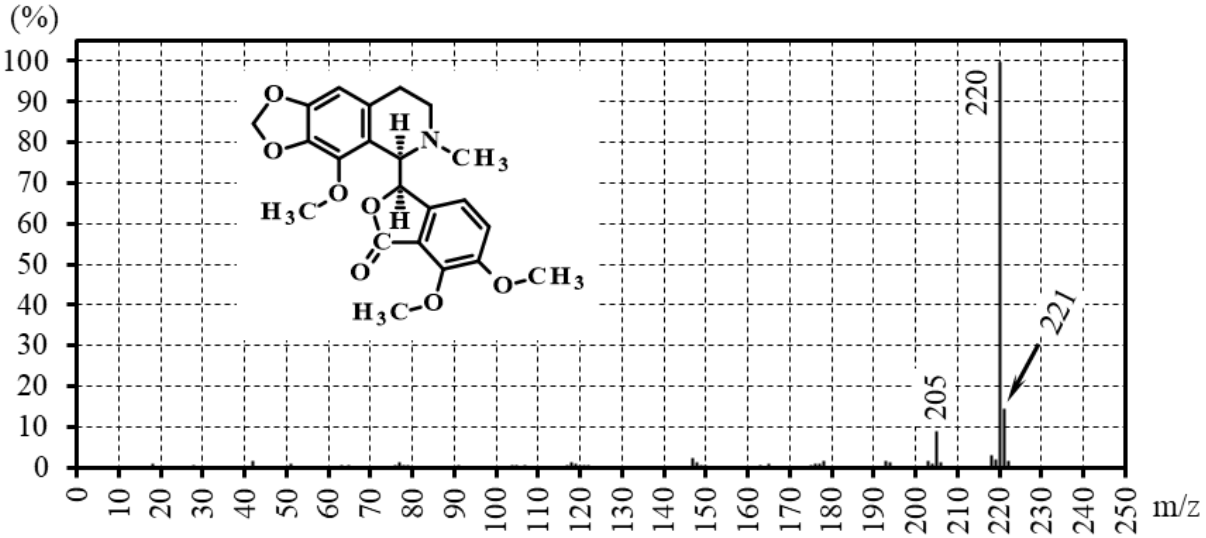

Norfludiazepam - CAS 2886-65-9 - EI - NIST 352190



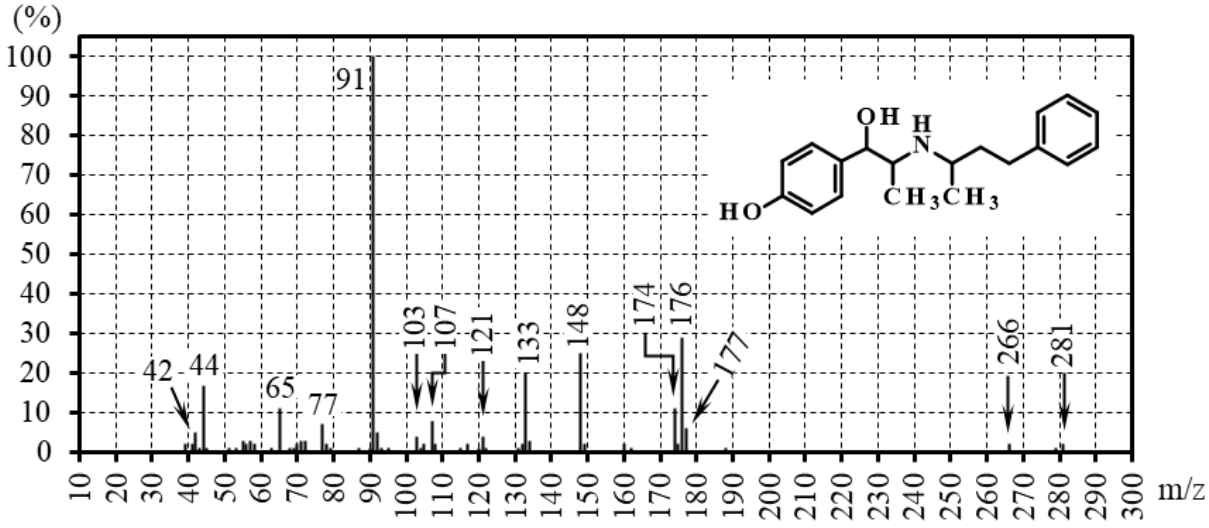

Norpropoxypheneamide – CAS 32501- EI - NIST 123368



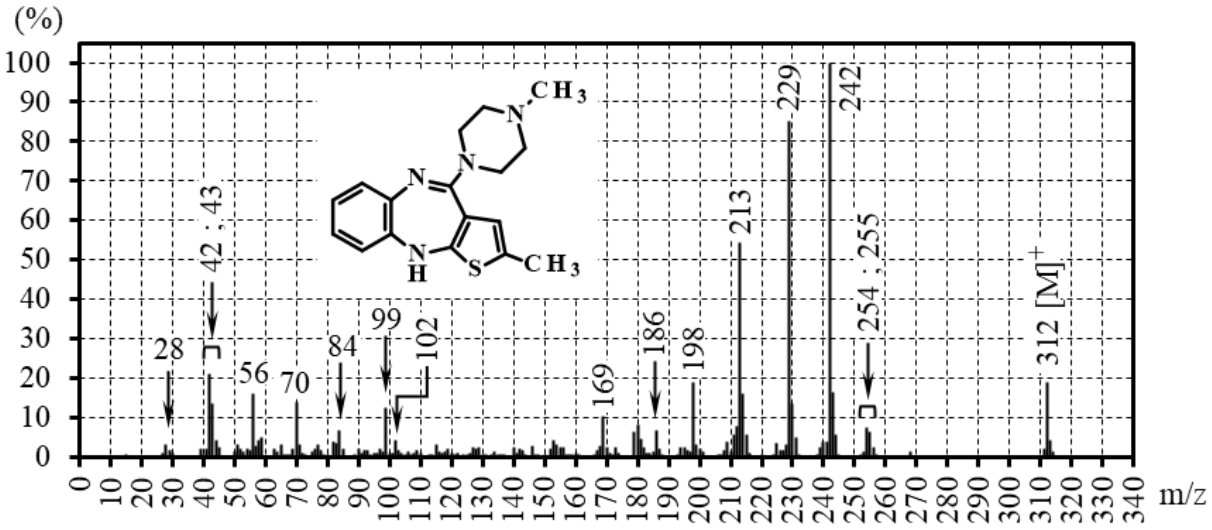

Nortriptiline - CAS 72-69-5 - NIST 408622



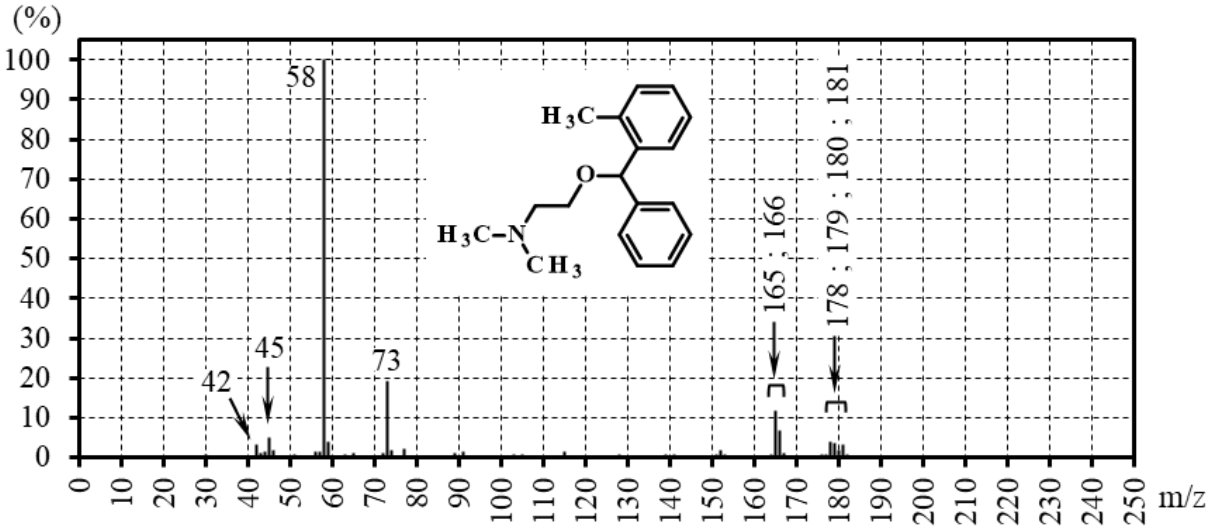

Noscapine - CAS 128-62-1 - NIST 235001



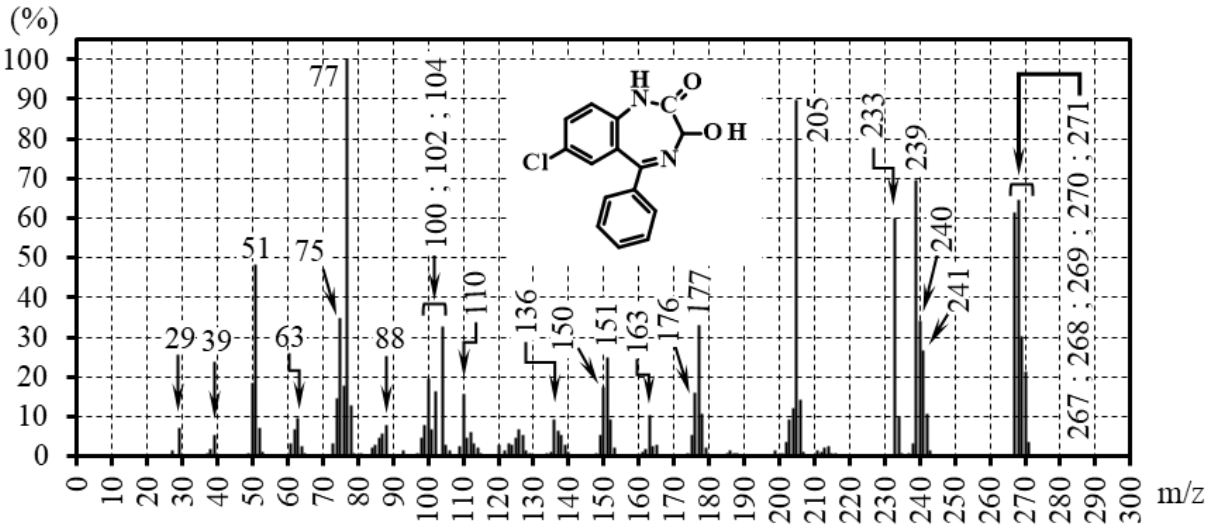

Nylidrin - CAS 447-41-6 - EI - NIST 58735



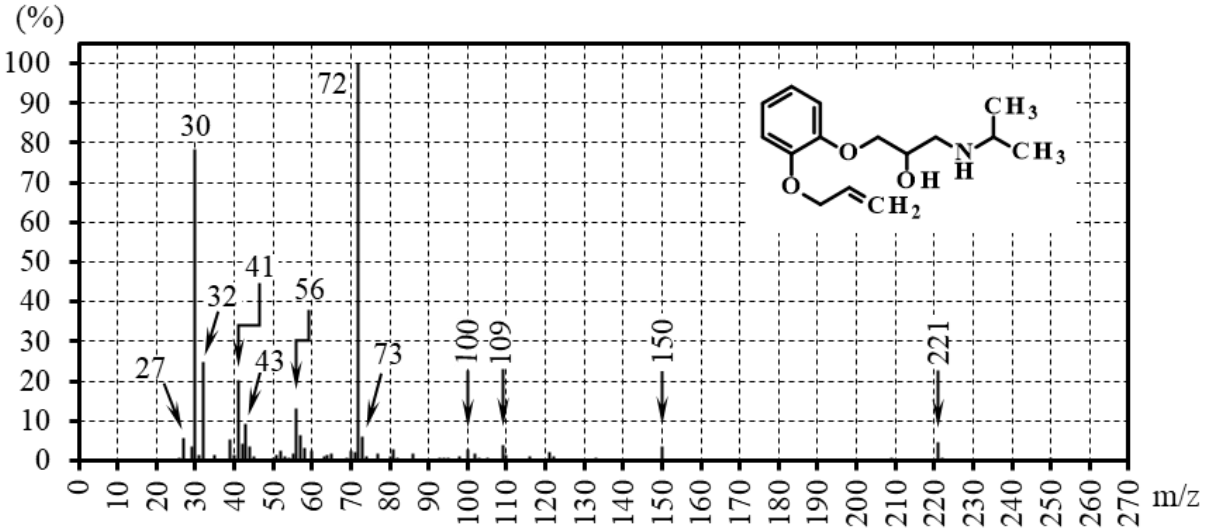

Olanzapine - CAS 132539-06-1 - EI - NIST 408782



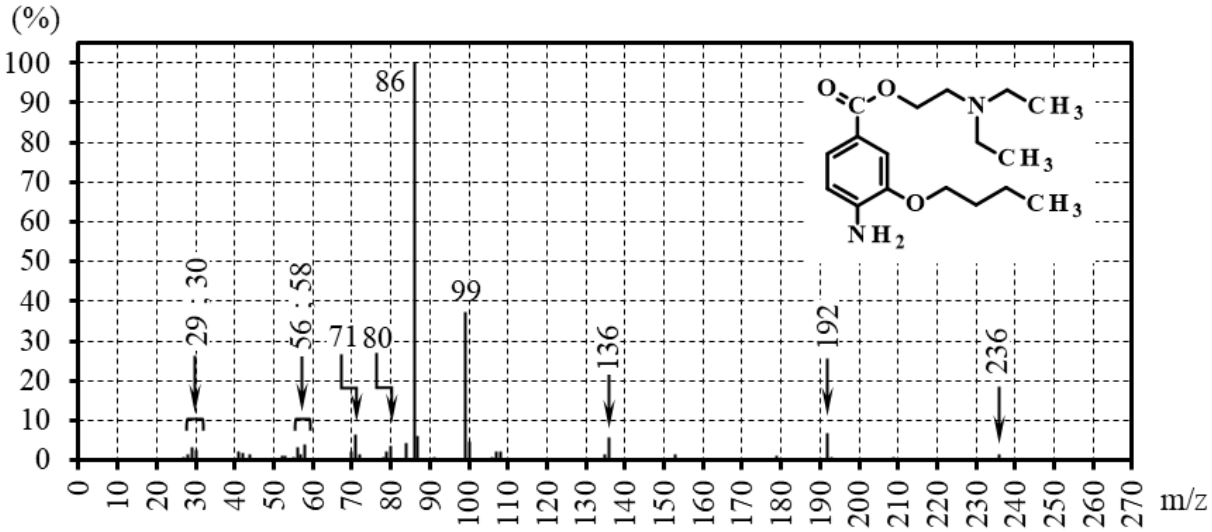

Orphenadrine - CAS 83-98-7 - EI - NIST 408590



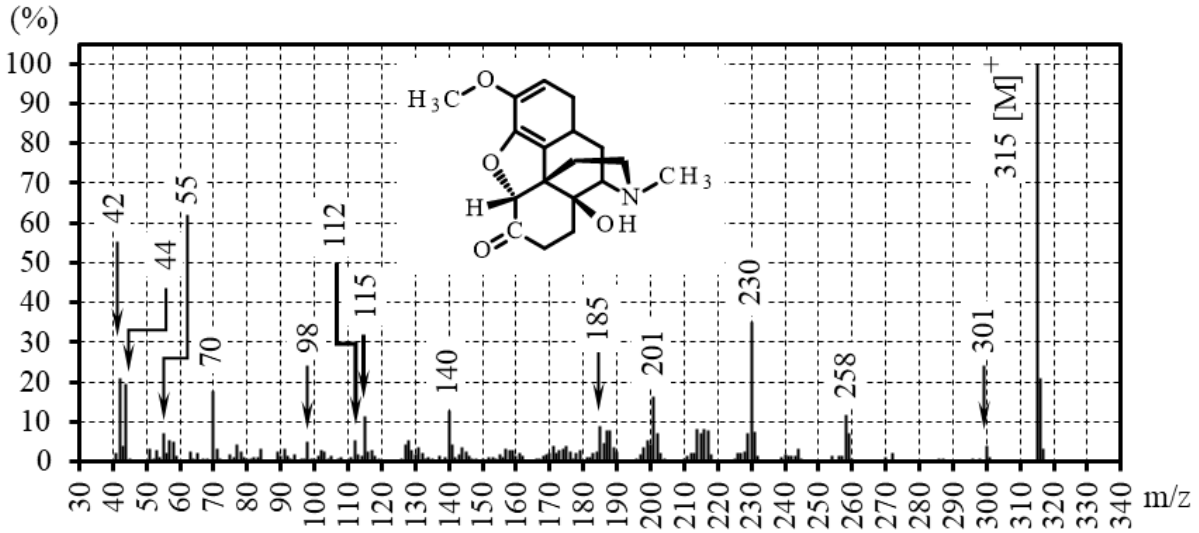

Oxazepam - CAS 604-75-1 - EI - NIST 352197



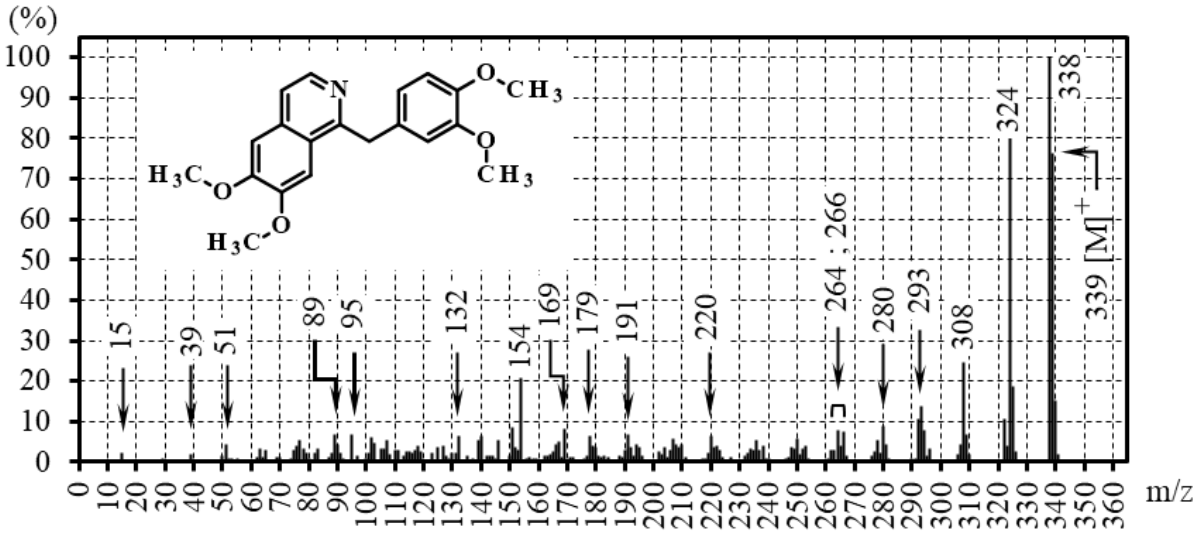

Oxprenolol - CAS 6452-71-7 - EI - NIST 107107



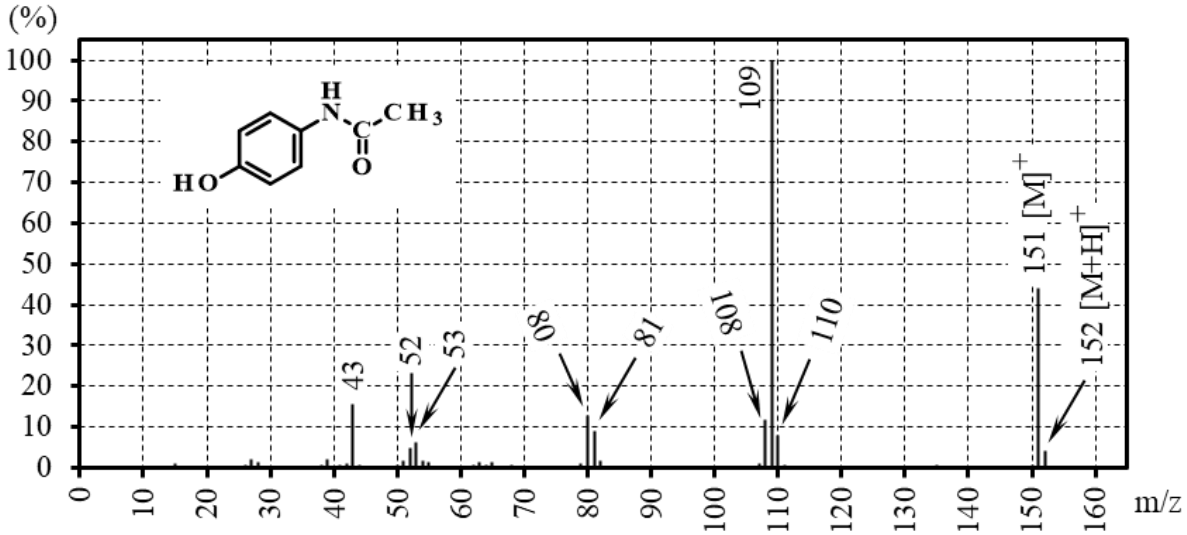

Oxybuprocaine - CAS 99-43-4 - EI - NIST 408056



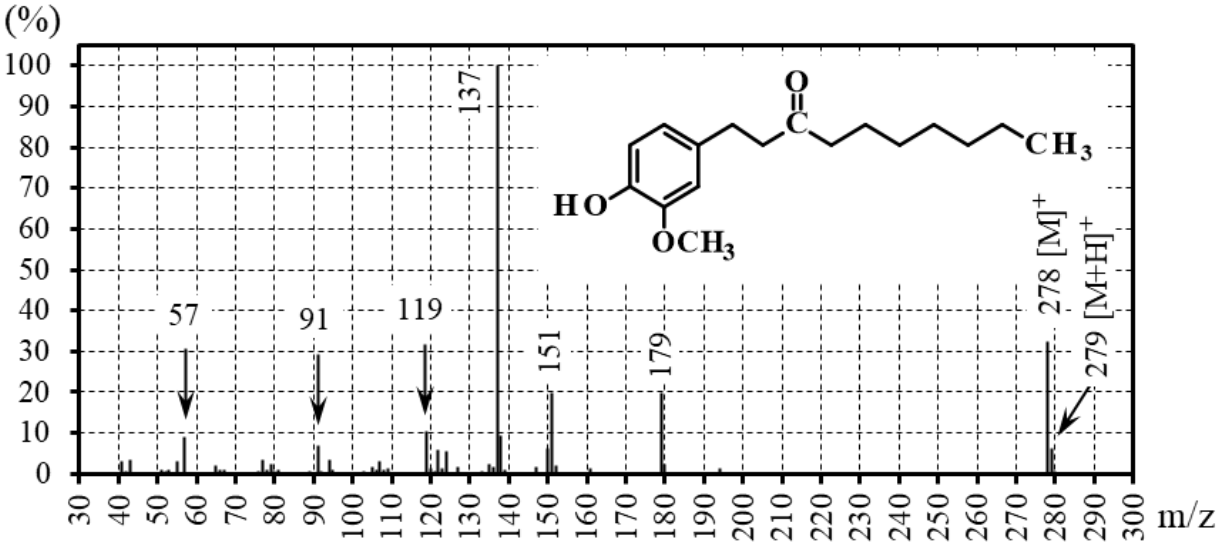

Oxycodone - CAS 76-42-6 - EI - NIST 125778



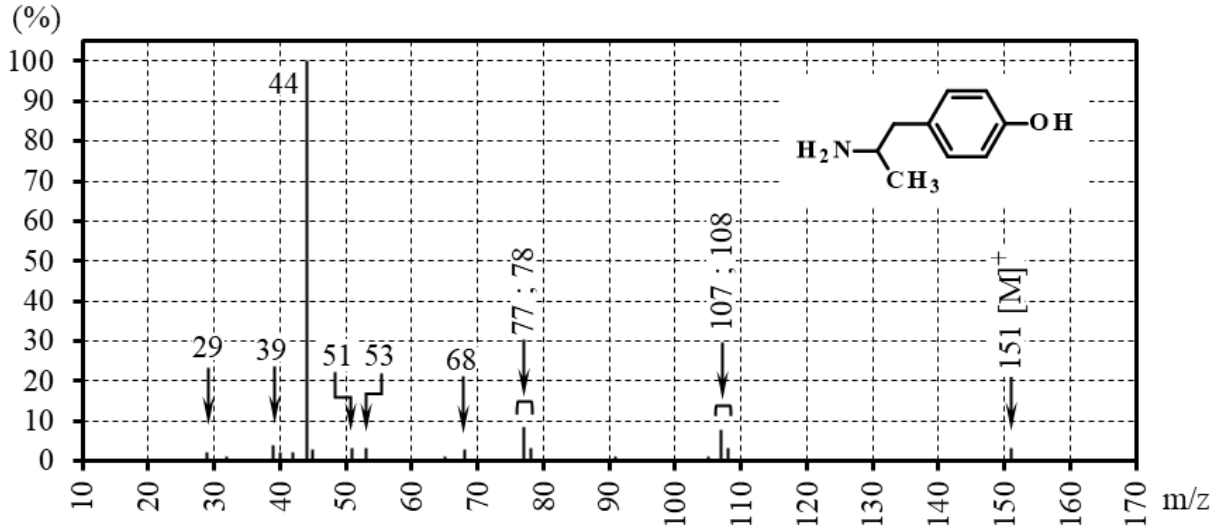

Papaverine - CAS 58-74-2 - NIST 291096



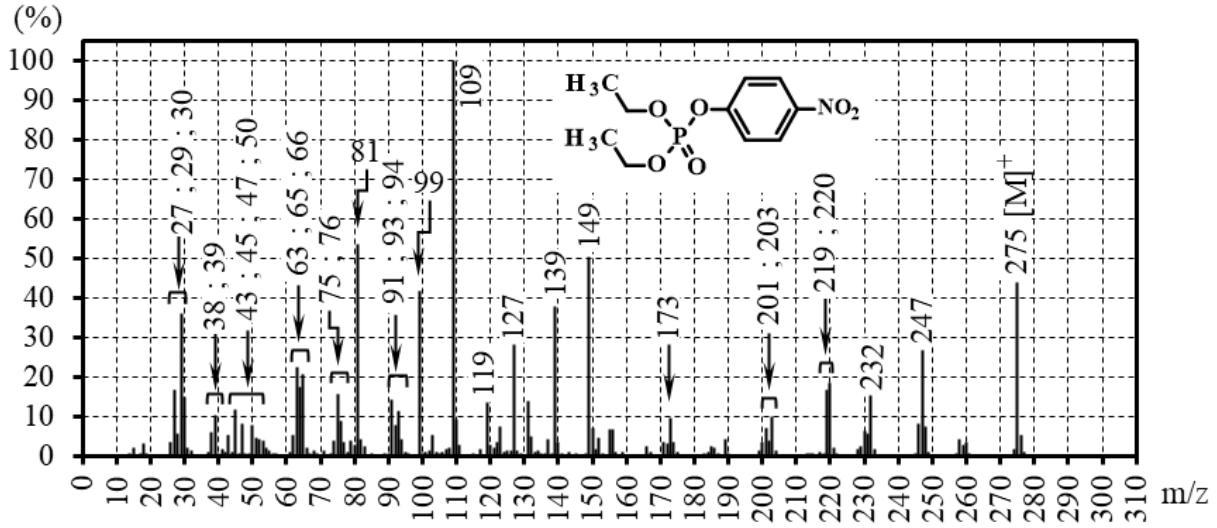

Paracetamol (Acetaminophen) - CAS 103-90-2 - NIST 229798



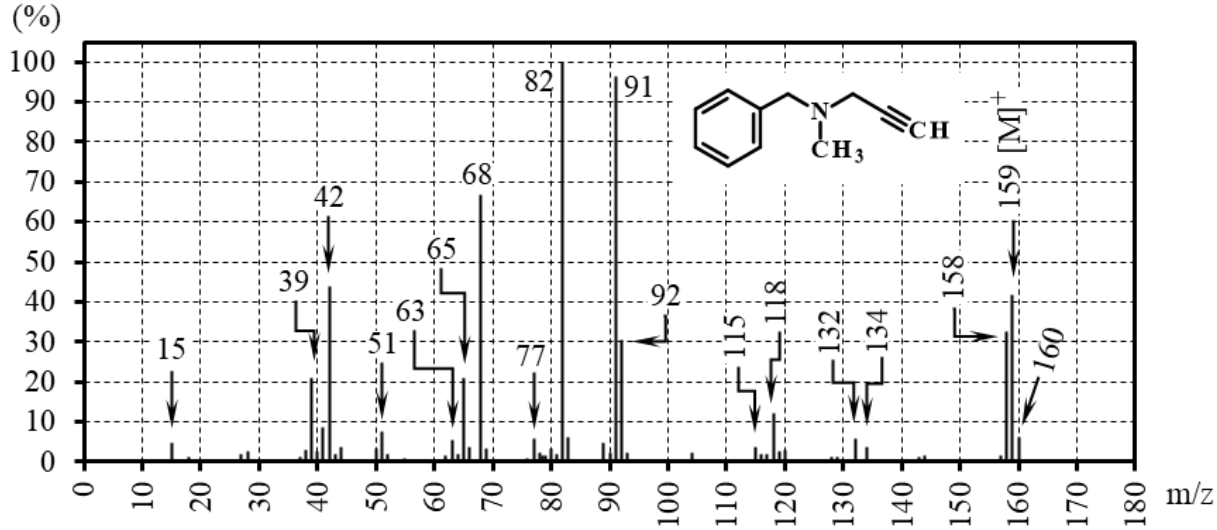

Paradol - CAS 27113-22-0 - EI - NIST 384092



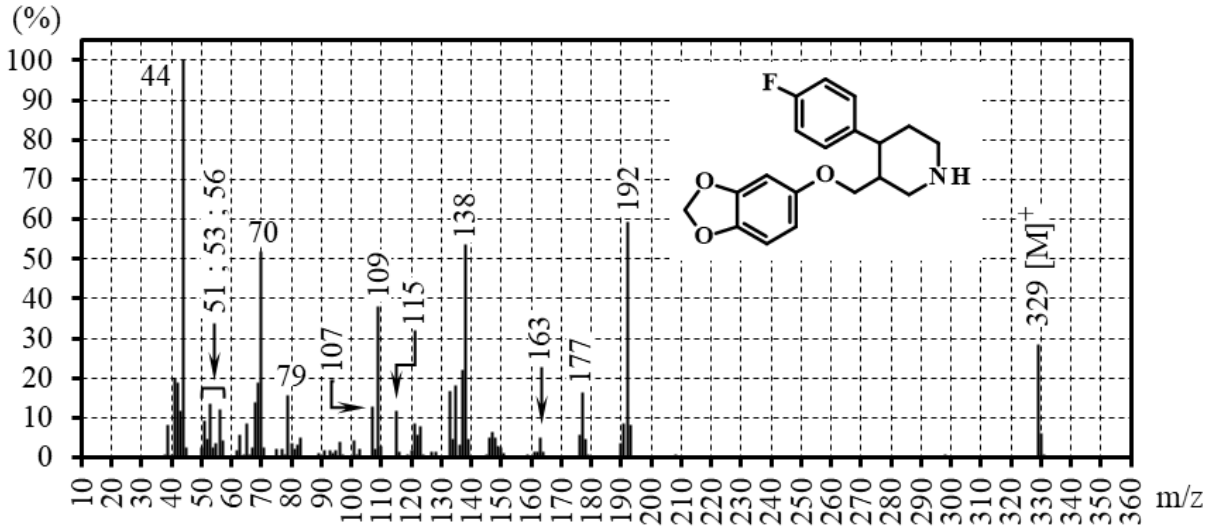

Paradrine (4-hydroxyamphetamine) - CAS 103-86-6 - EI - NIST 245970



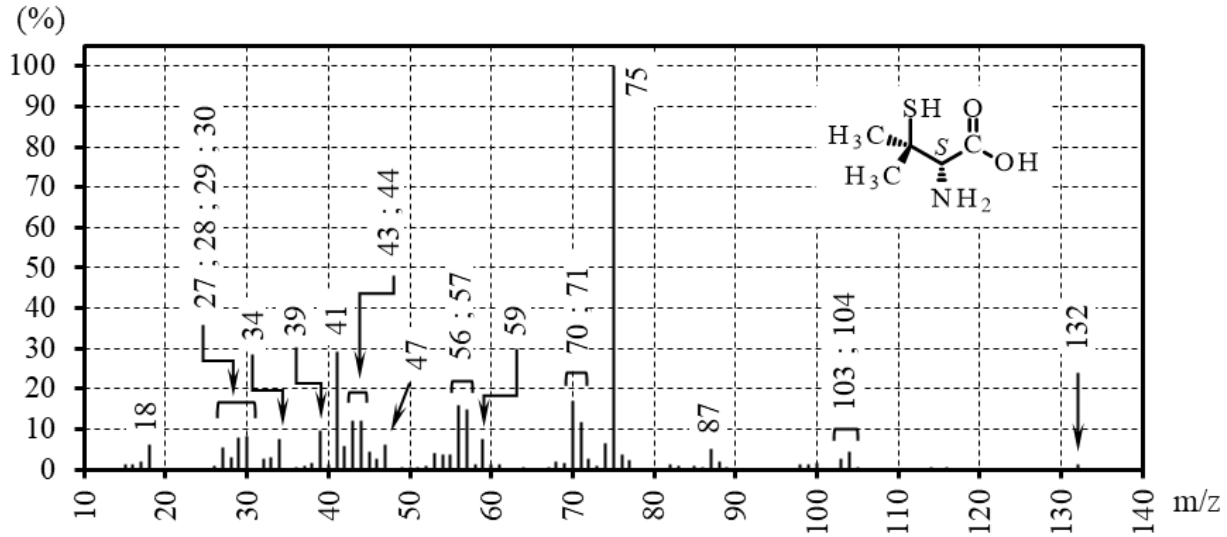

Paraoxon - CAS 311-45-5 - EI - NIST 235113



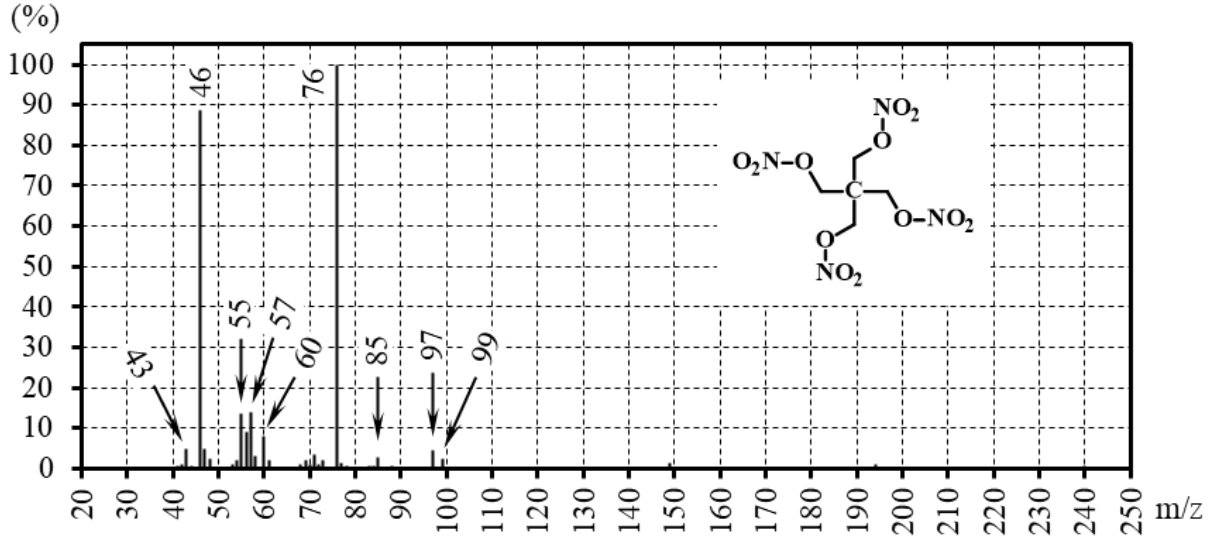

Pargyline - CAS 555-57-7 - EI 75 eV source 260 $^{o}$C , sample 190 $^{o}$C
SDBS 13504 ; NIST 235445



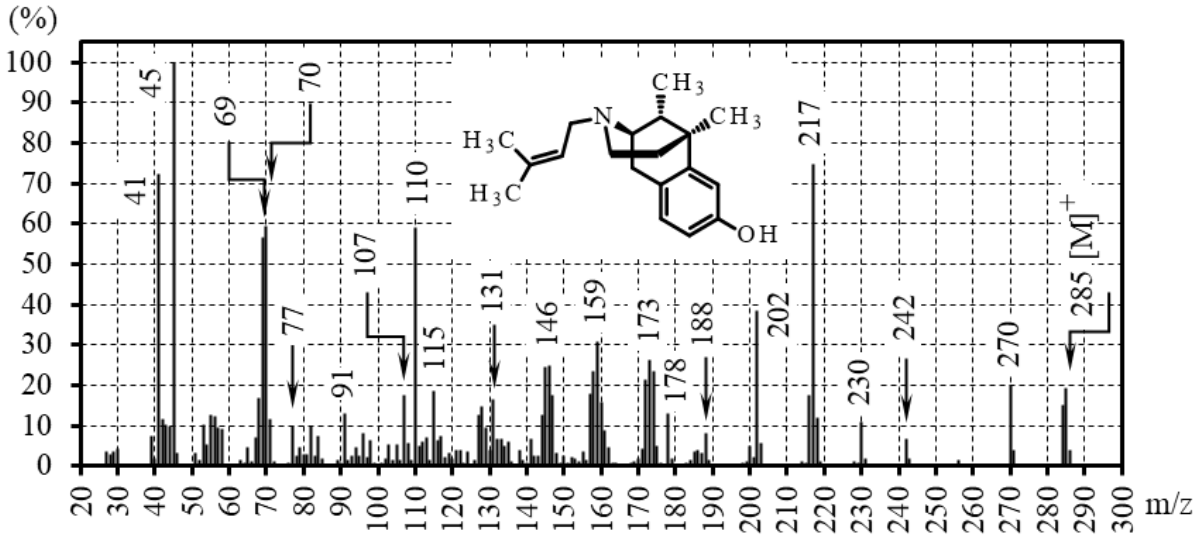

Paroxetine - CAS 61869-08-7 - EI - NIST 247287



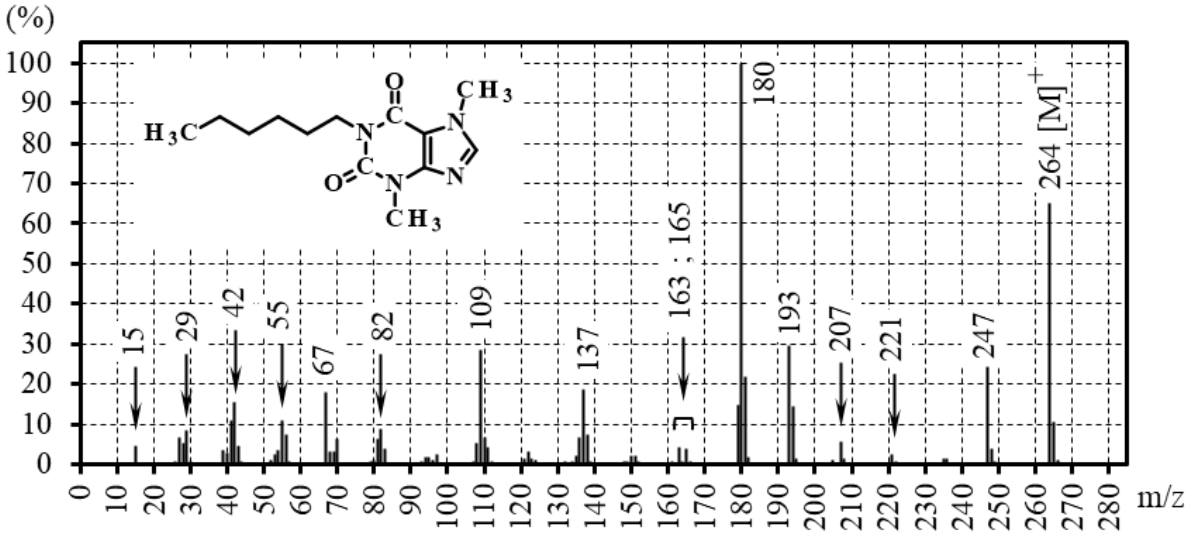

Penicillamine - CAS 52-67-5 - NIST 231231



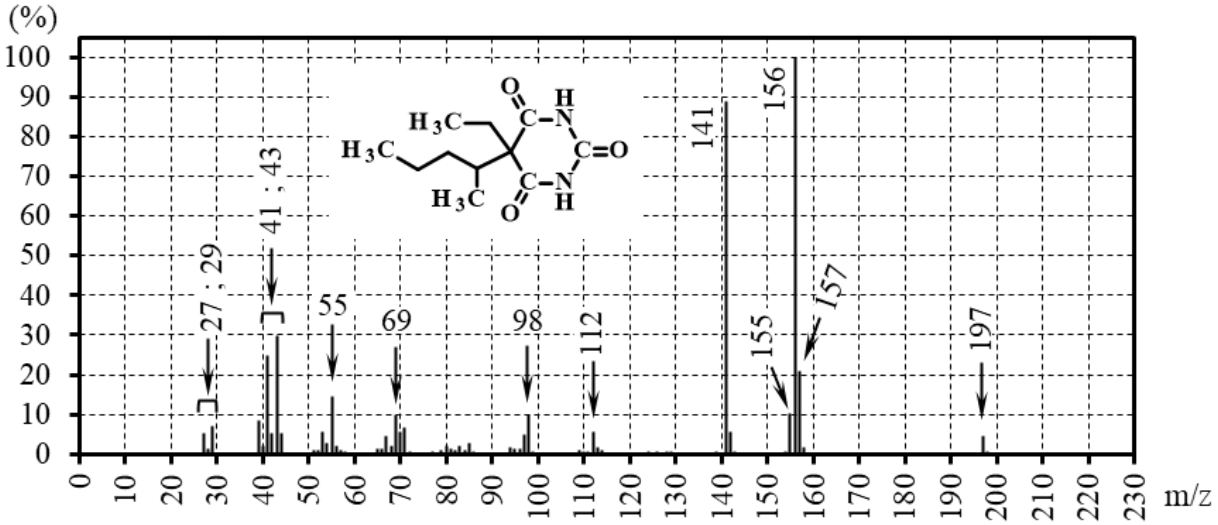

Pentaerythritol tetranitrate - CAS 78-11-5 - NIST 14982



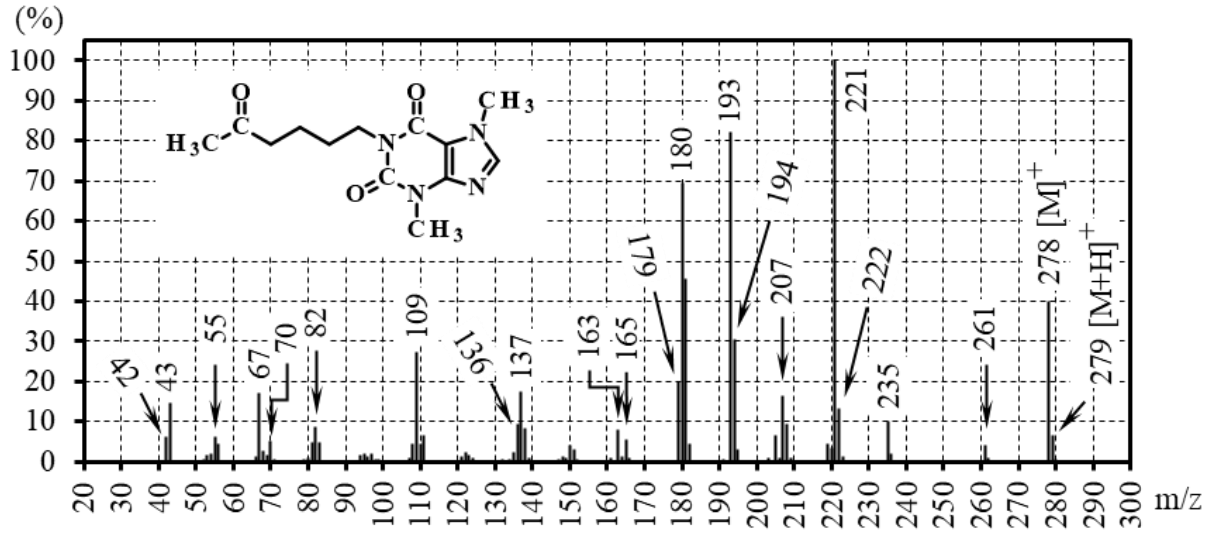

Pentazocine - CAS 359-83-1 - EI - NIST 352200



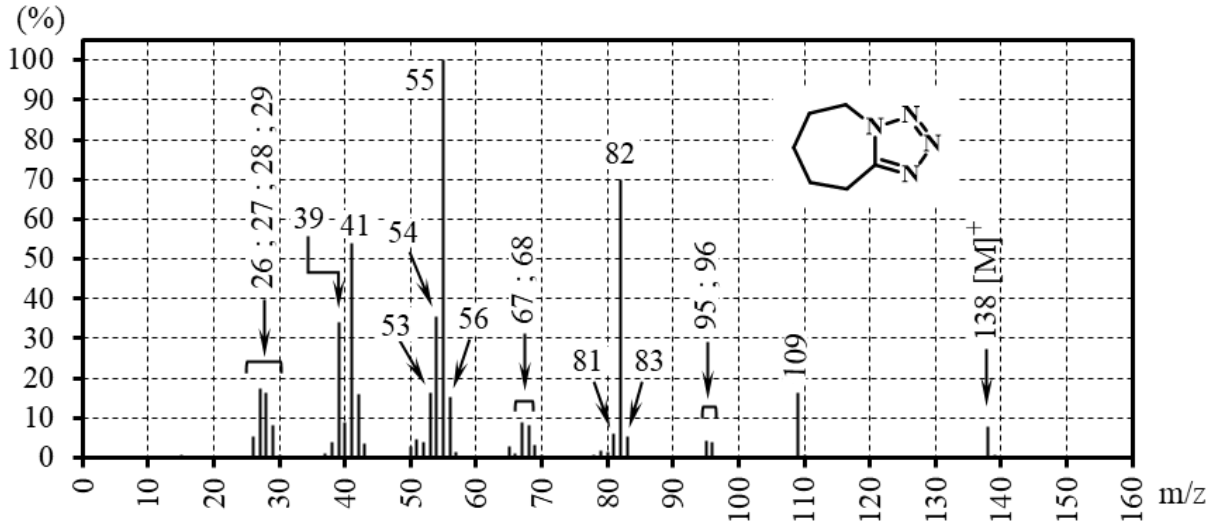

Pentifylline - CAS 1028-33-7 - NIST 135086



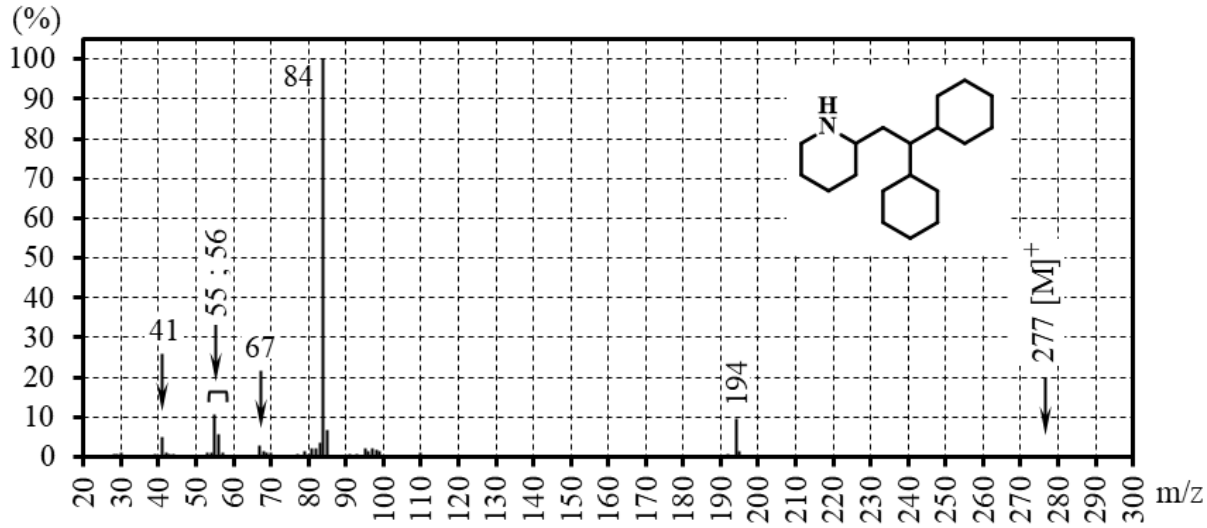

Pentobarbital - CAS 76-74-4 - EI - NIST 352145



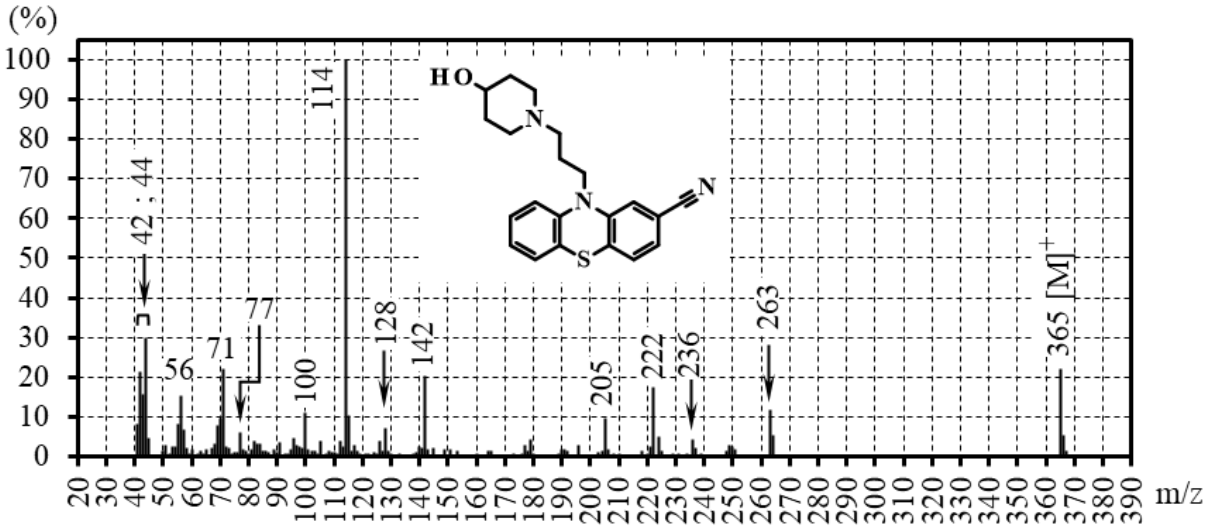

Pentoxifylline - CAS 6493-05-6 - NIST 248838



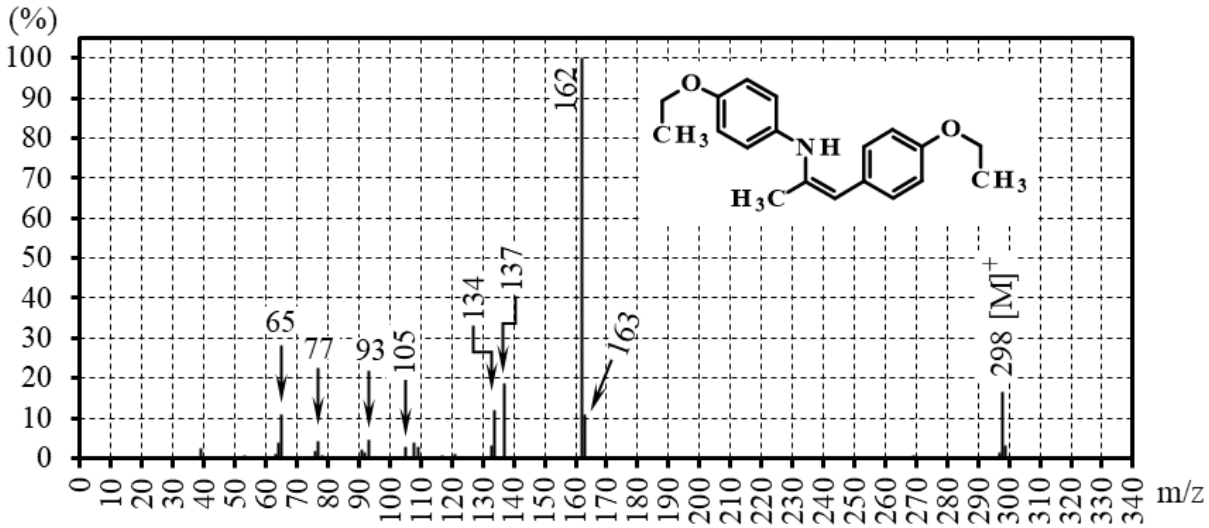

Pentylenetetrazol (Cardiazole , Angiazol) - CAS 54-95-5 - EI - NIST 290622



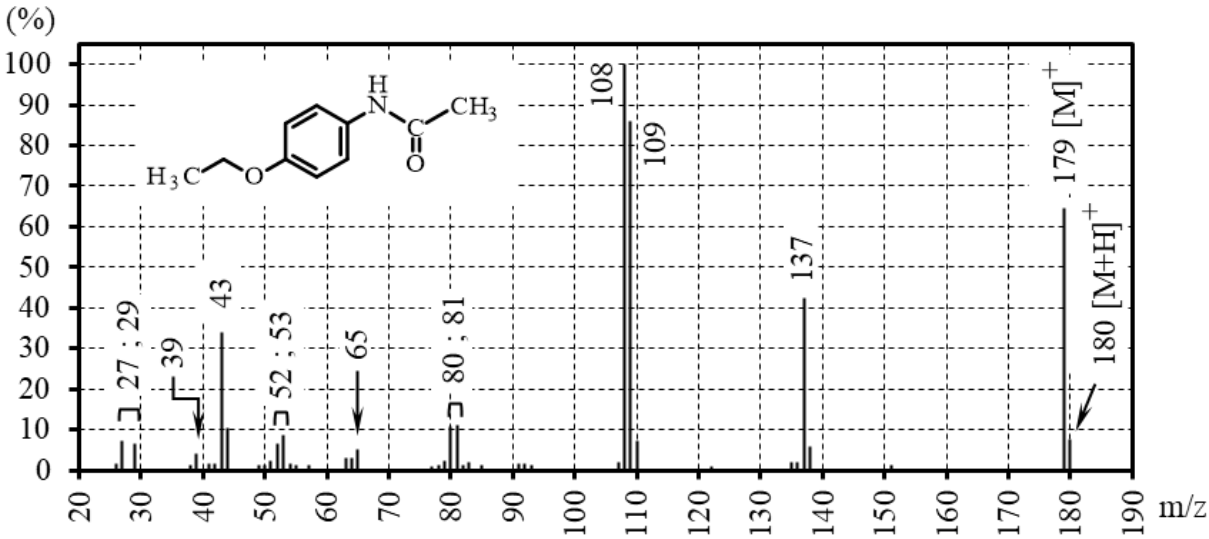

Perhexiline - CAS 6621-47-2 - EI - NIST 408719



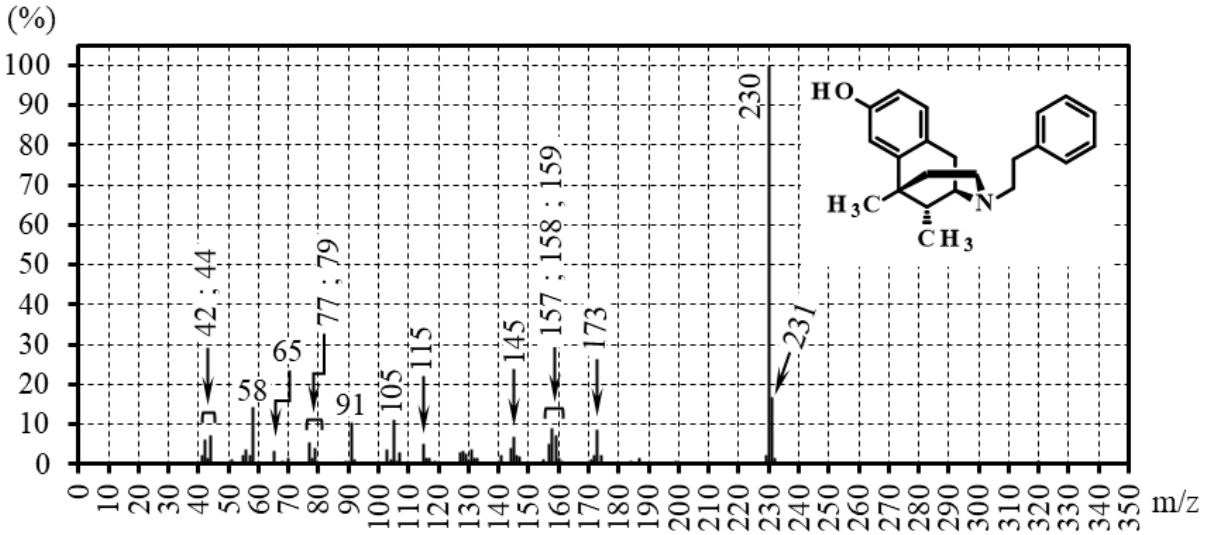

Periciazine - CAS 2622-26-6 - EI - NIST 247035



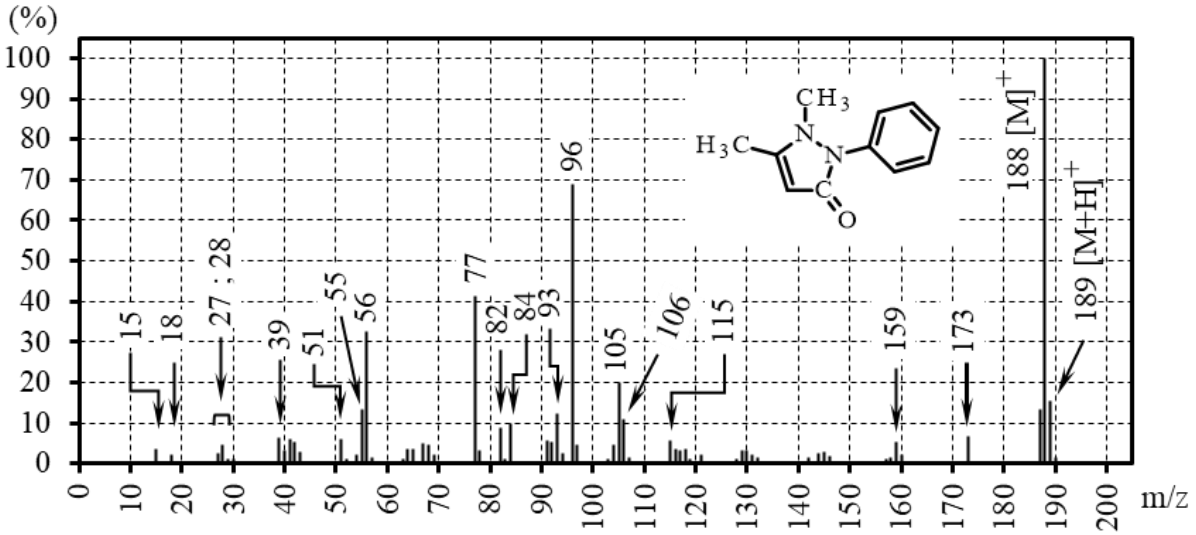

Phenacaine - CAS 101-93-9 - EI - NIST 122653



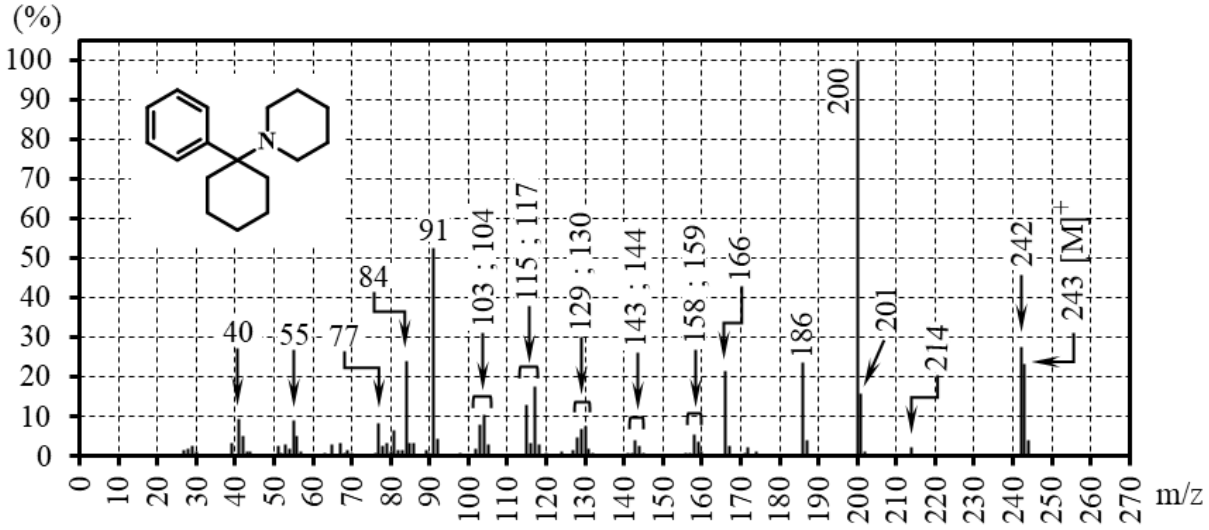

Phenacetin - CAS 62-44-2 - EI - NIST nr. 107172



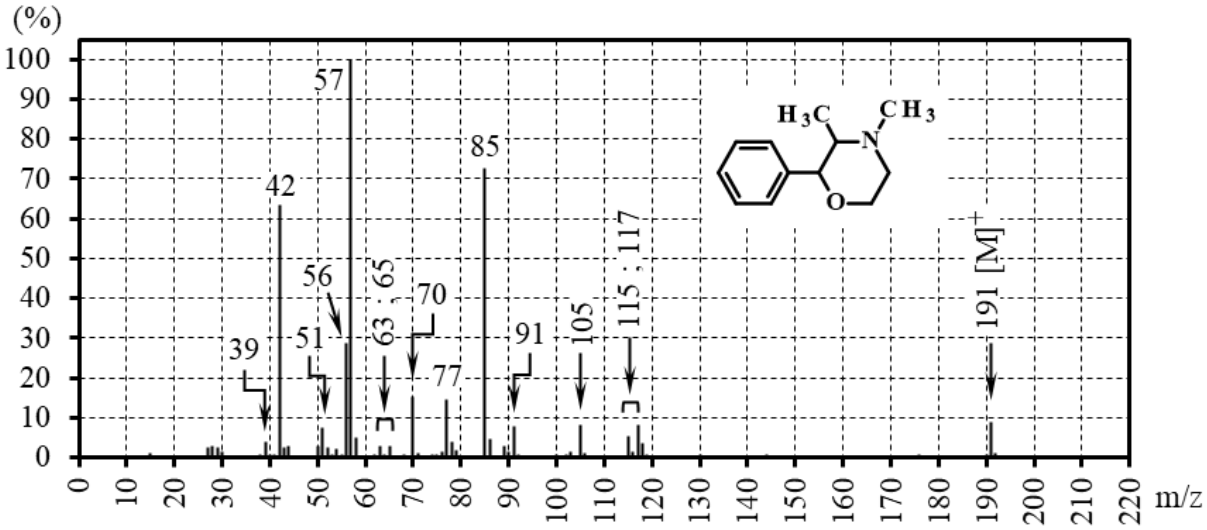

Phenazocine - CAS 127-35-5-Mass - EI - NIST 379800



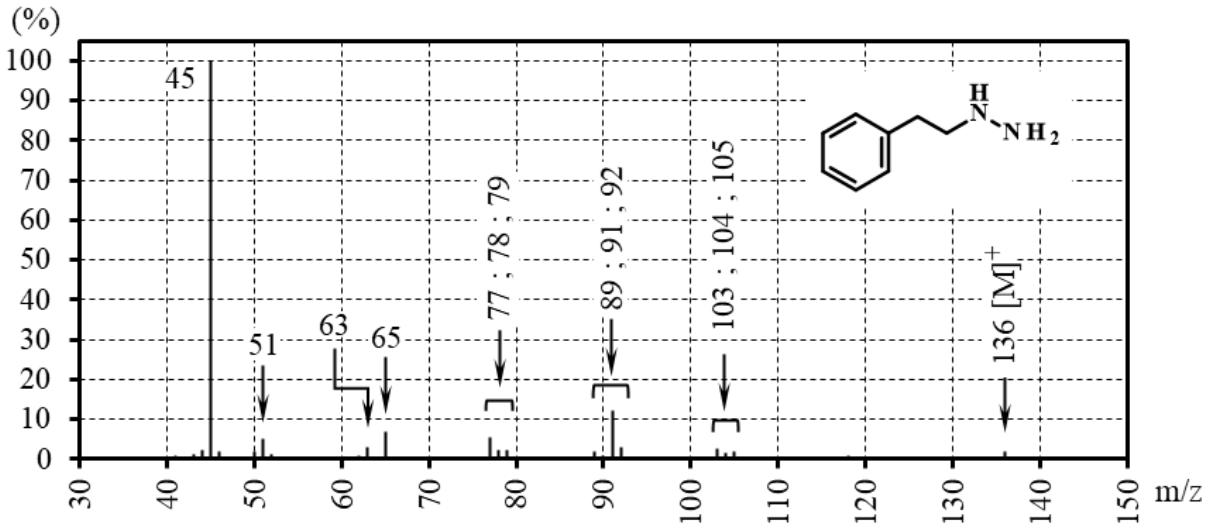

Phenazone (Antipyrine) - CAS 60-80-0 - NIST 187739 - SDBS 22106



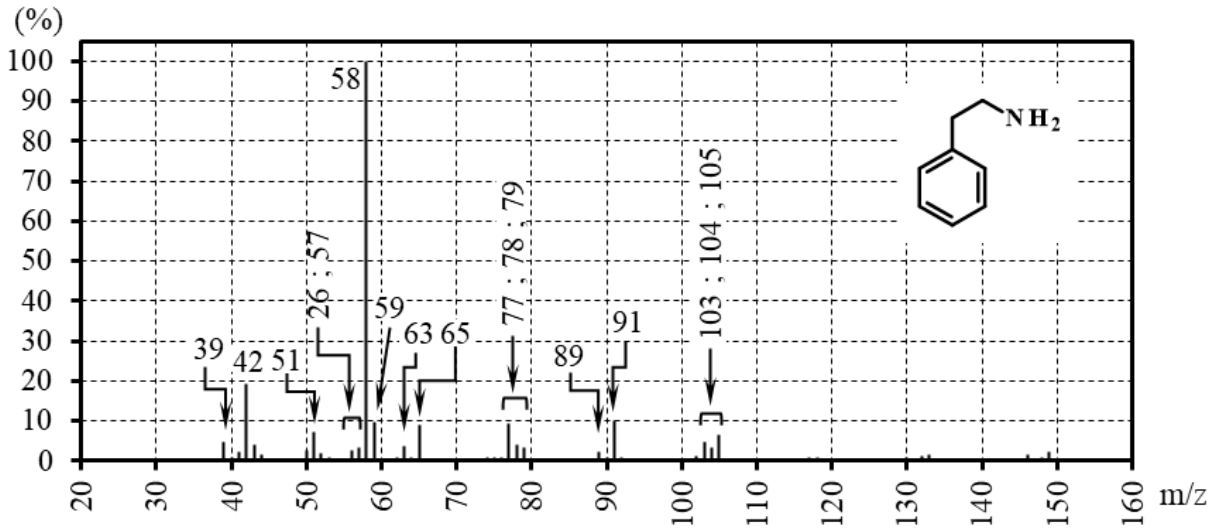

Phencyclidine - CAS 77-10-1 - EI - NIST 352151



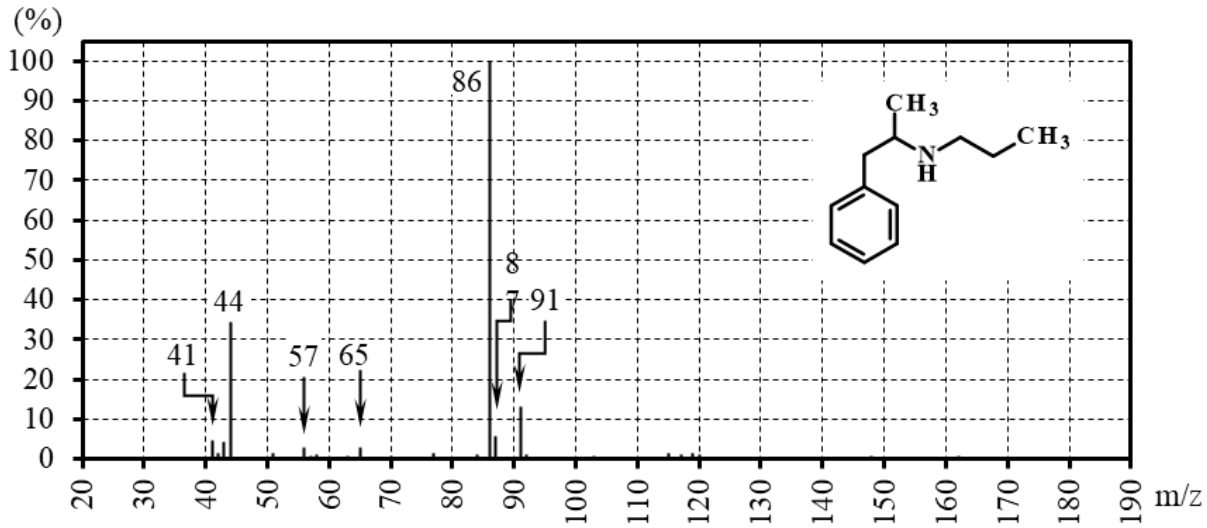

Phendimetrazine - CAS 634-03-7 - EI - NIST 113869



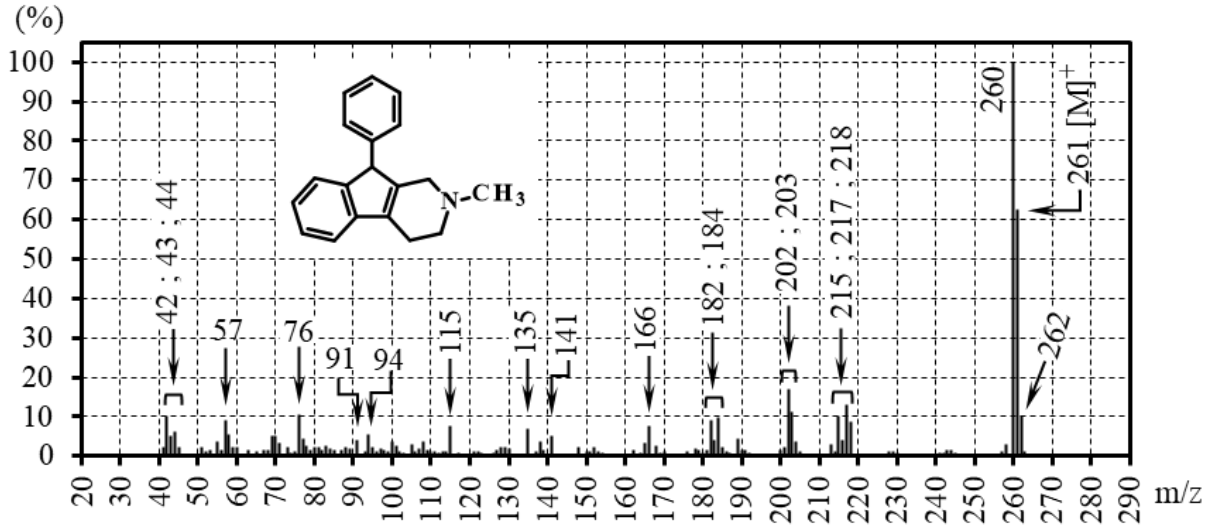

Phenelzine - CAS 51-71-8 - EI - NIST 335136



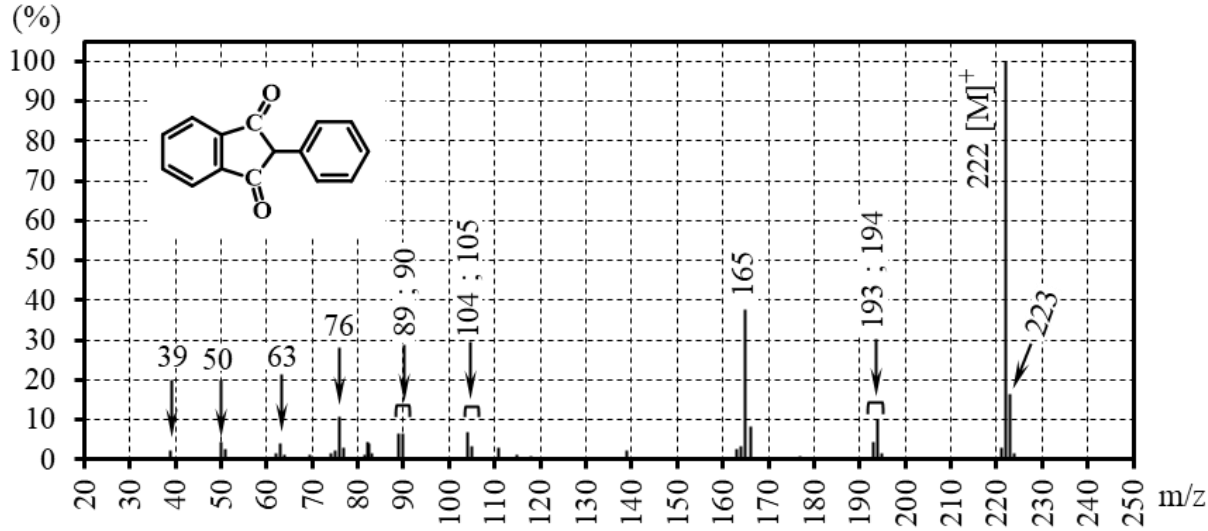

Phenethylamine - CAS 1126-71-2 - EI - NIST 397737



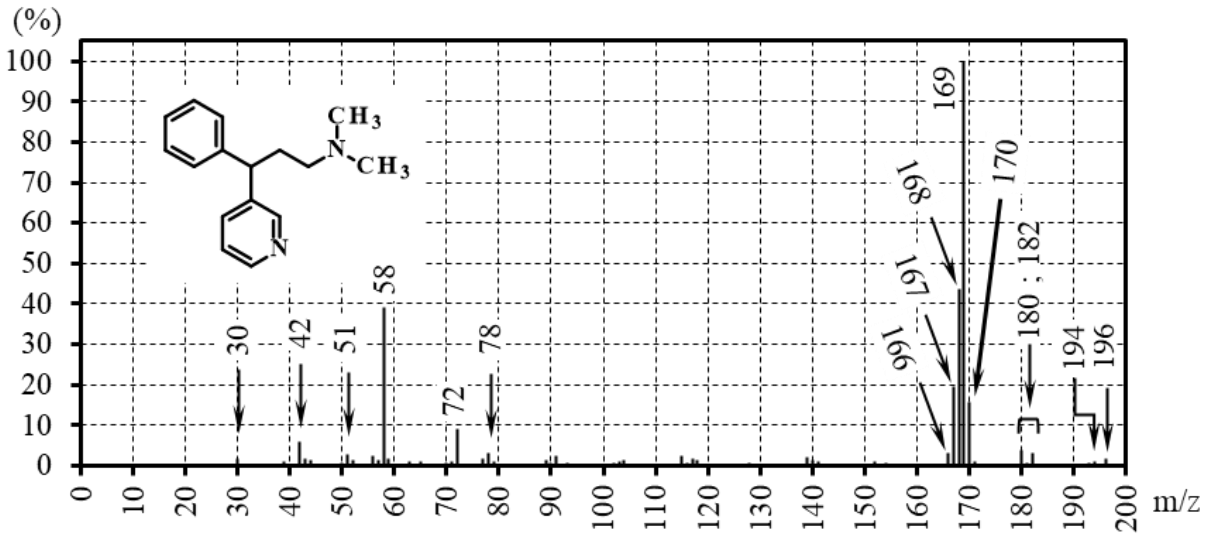

Phenethylamine, α-methyl-N-propyl- - CAS 51799-32-7 - EI - NIST 248220



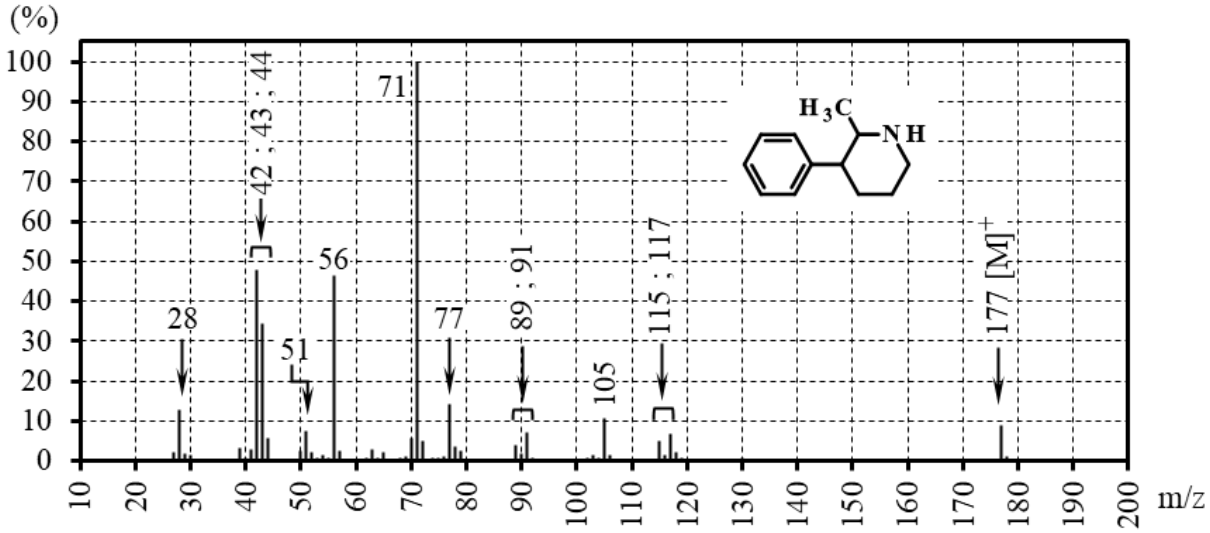

Phenindamine - CAS 82-88-2 - EI - NIST 246503



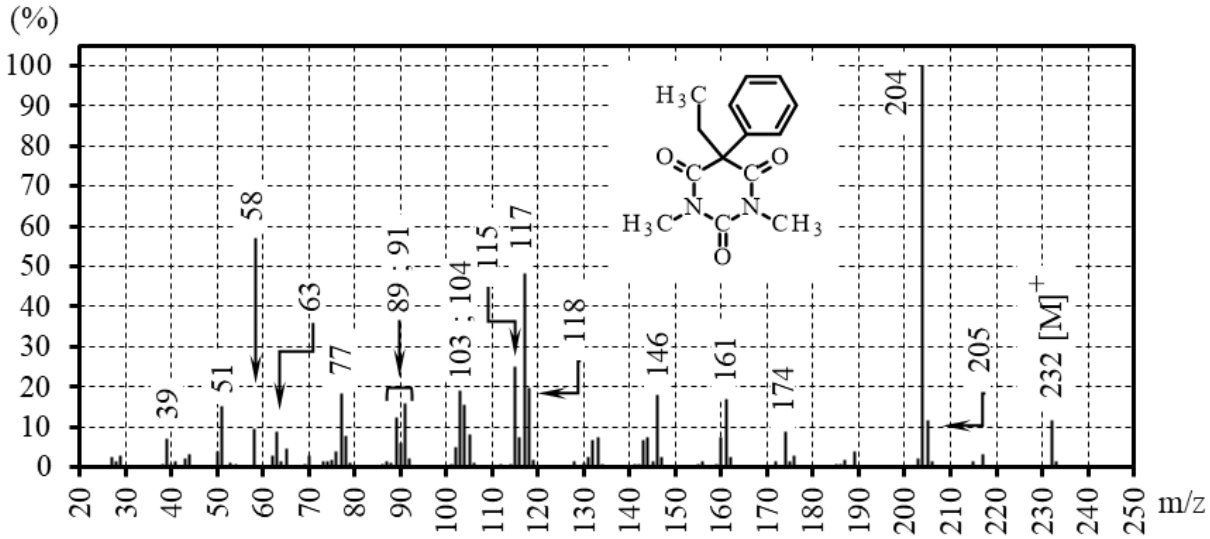

Phenindione - CAS 83-12-5 - EI 75 eV source 170 $^{o}$C , sample 120 $^{o}$C
SDBS 15621 - NIST 236131



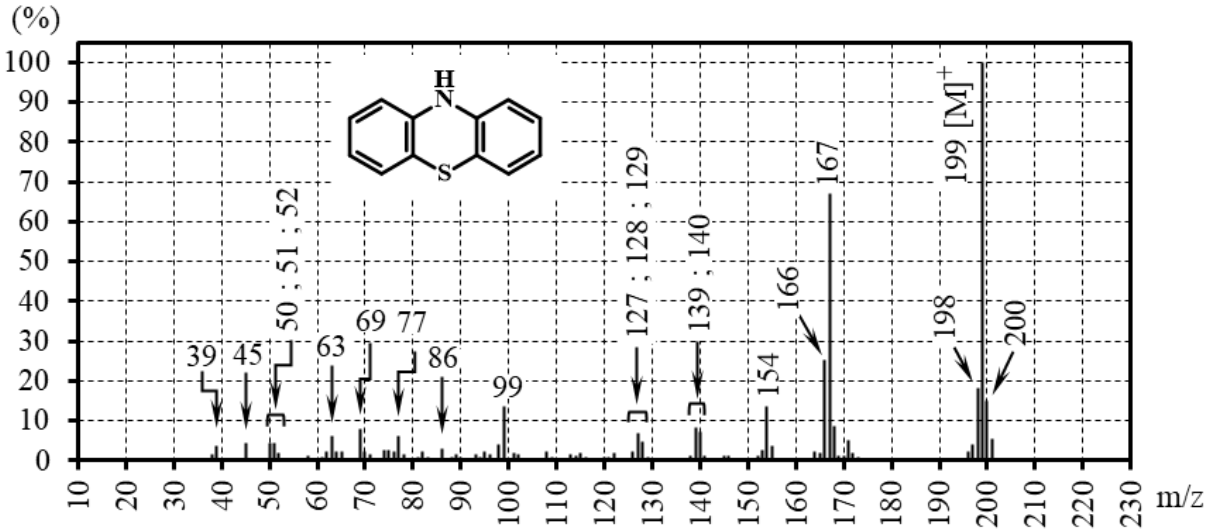

Pheniramine - CAS 86-21-5-NIST 290727



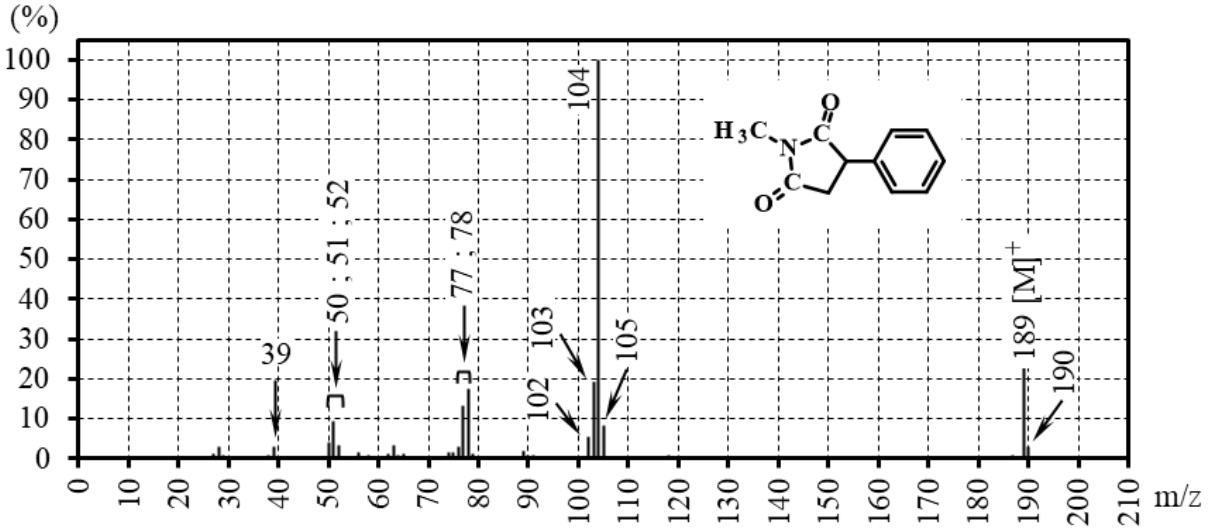

Phenmetrazine - CAS 134-49-6 - EI - NIST 408691



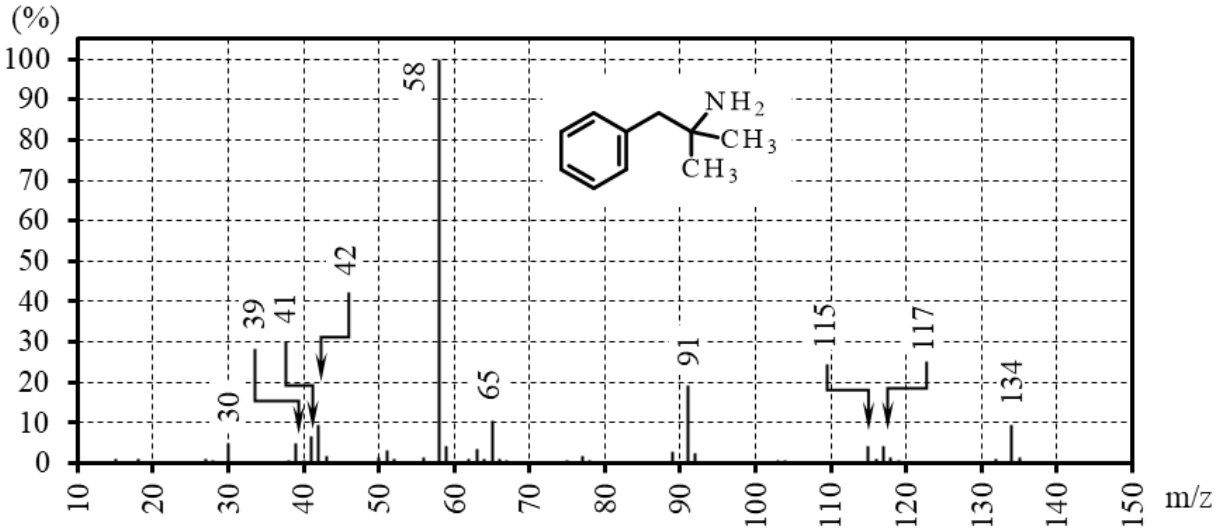

Phenobarbital - CAS 50-06-6 - EI - NIST 408715



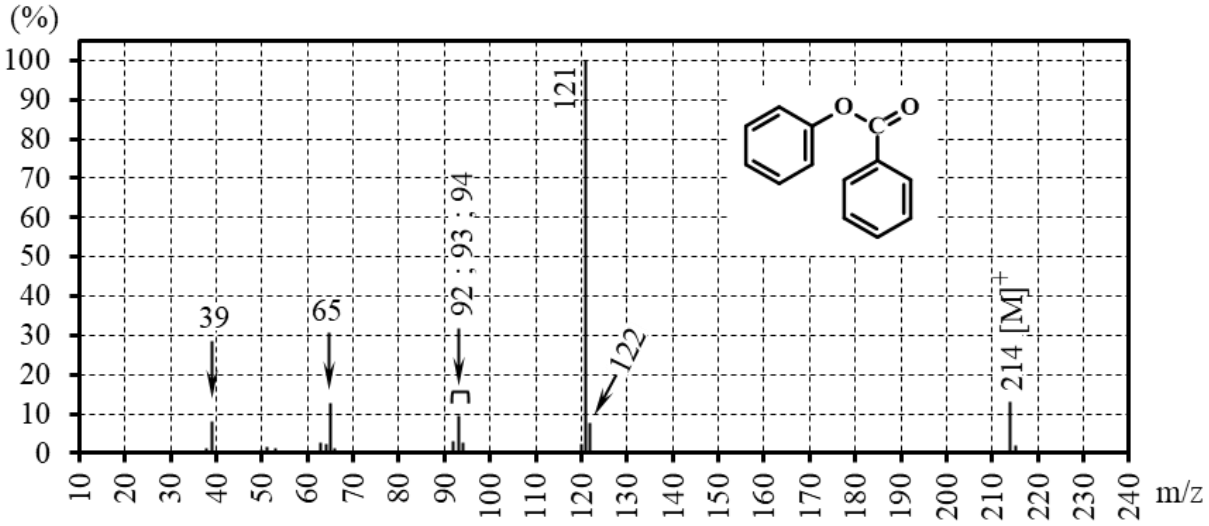

Phenothiazine - CAS 92-84-2 - EI - NIST 408667



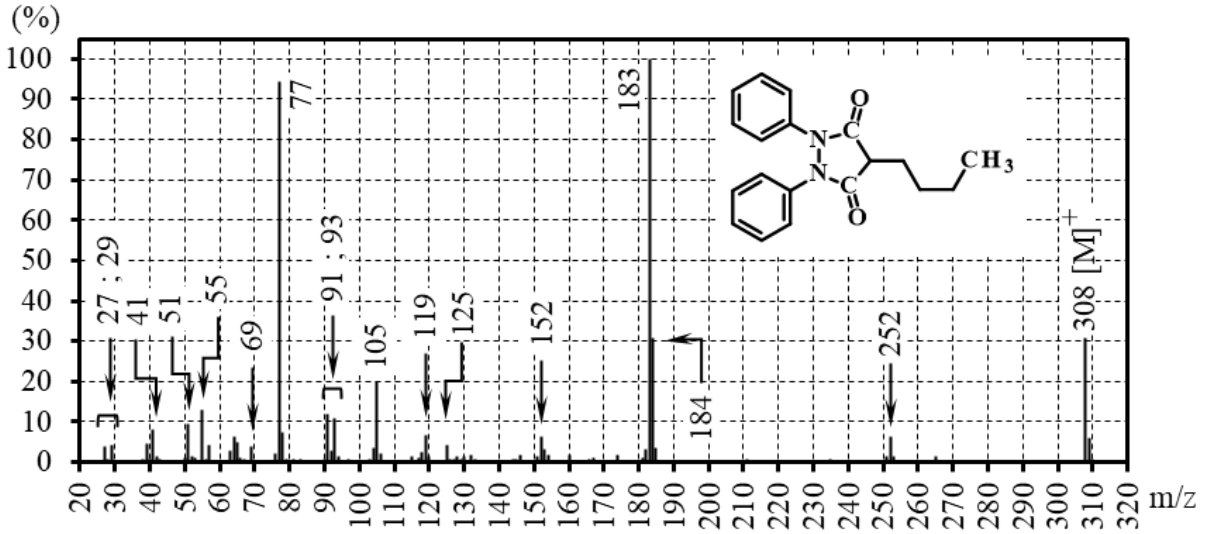

Phensuximide - CAS 86-34-0 - EI - NIST 113827



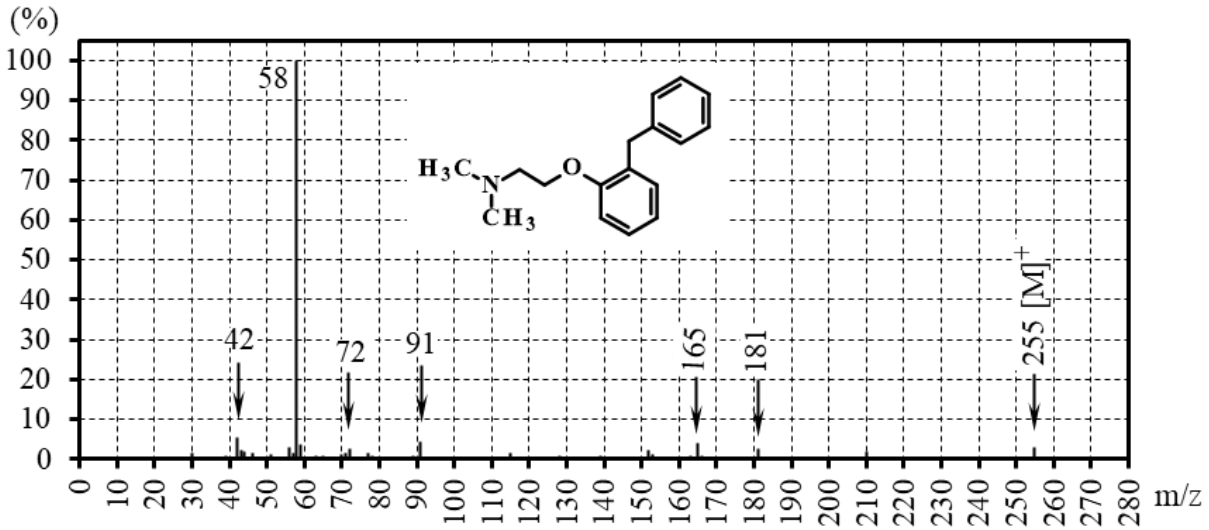

Phentermine - CAS 122-09-8 - EI - NIST 250588



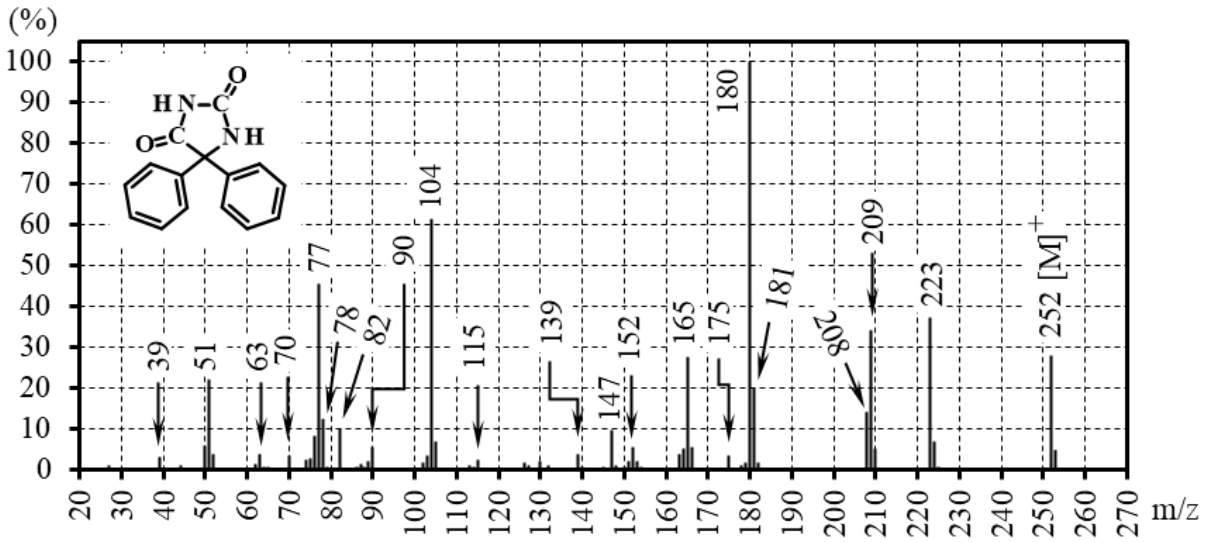

Phenyl salicylate - CAS 118-55-8 - EI - NIST 229426



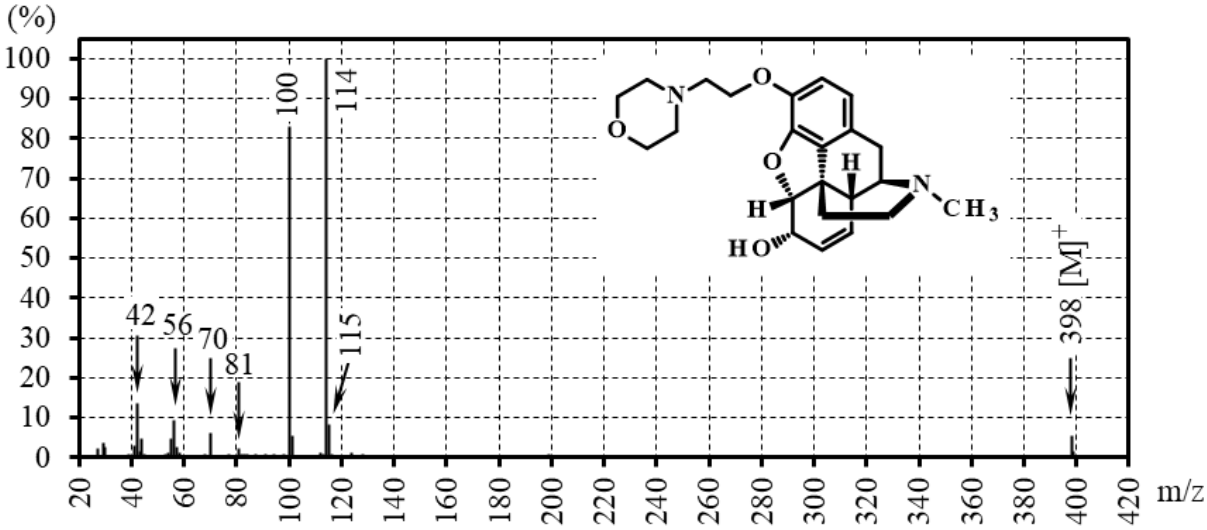

Phenylbutazone CAS 50-33-9 - EI - NIST 408762



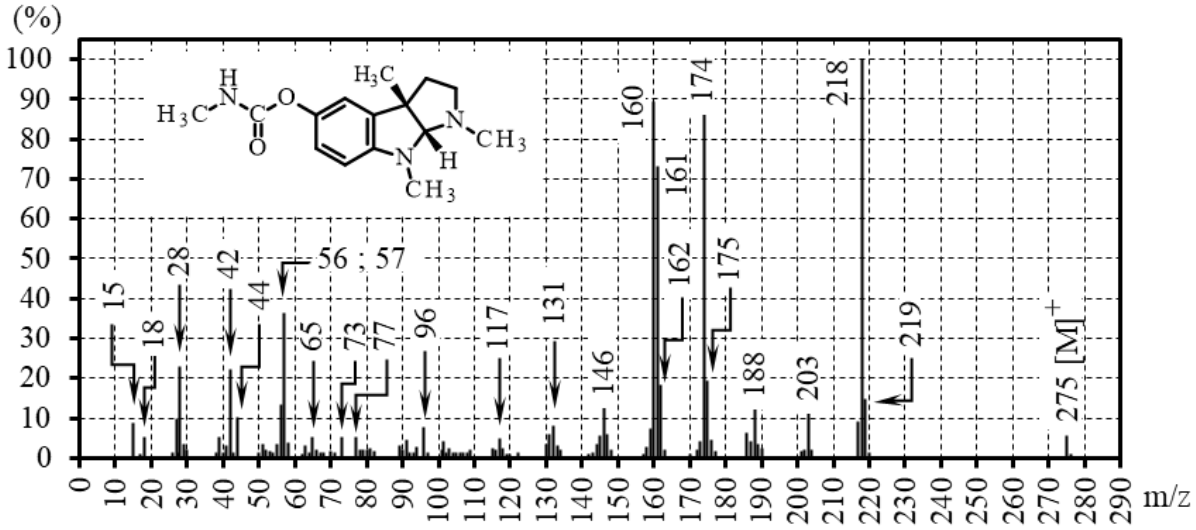

Phenyltoloxamine - CAS 92-12-6 - EI - NIST 408329



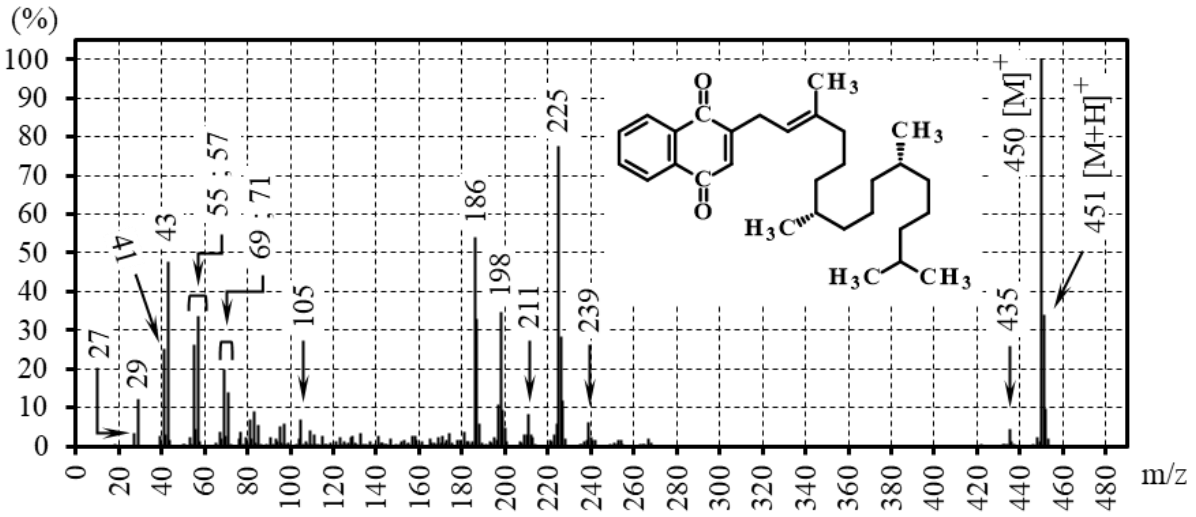

Phenytoin - CAS 57-41-0 - NIST 290661



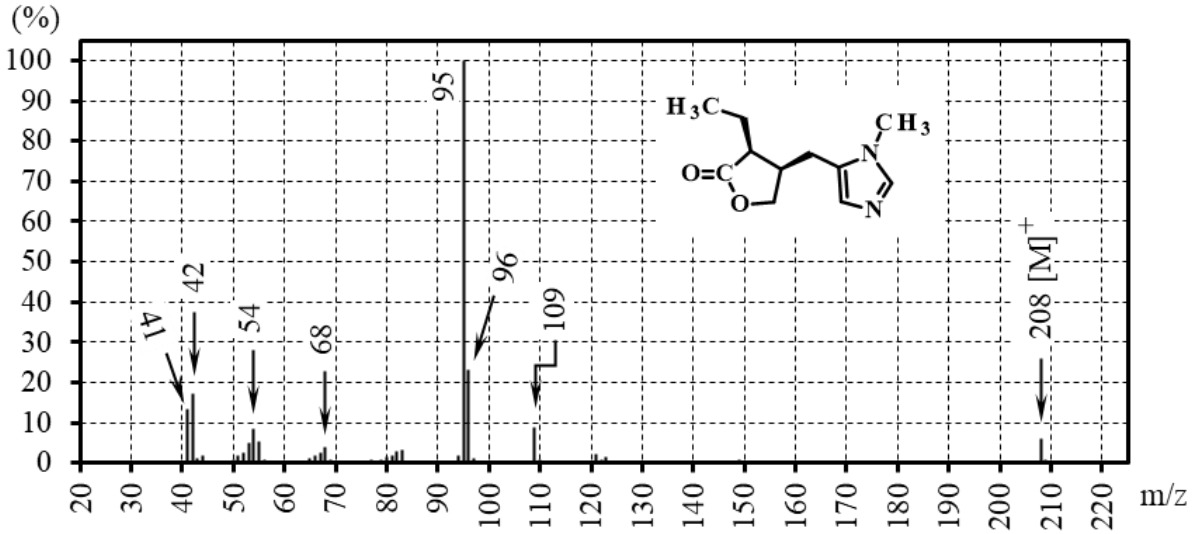

Pholcodine - CAS 509-67-1 - EI - NIST 107091



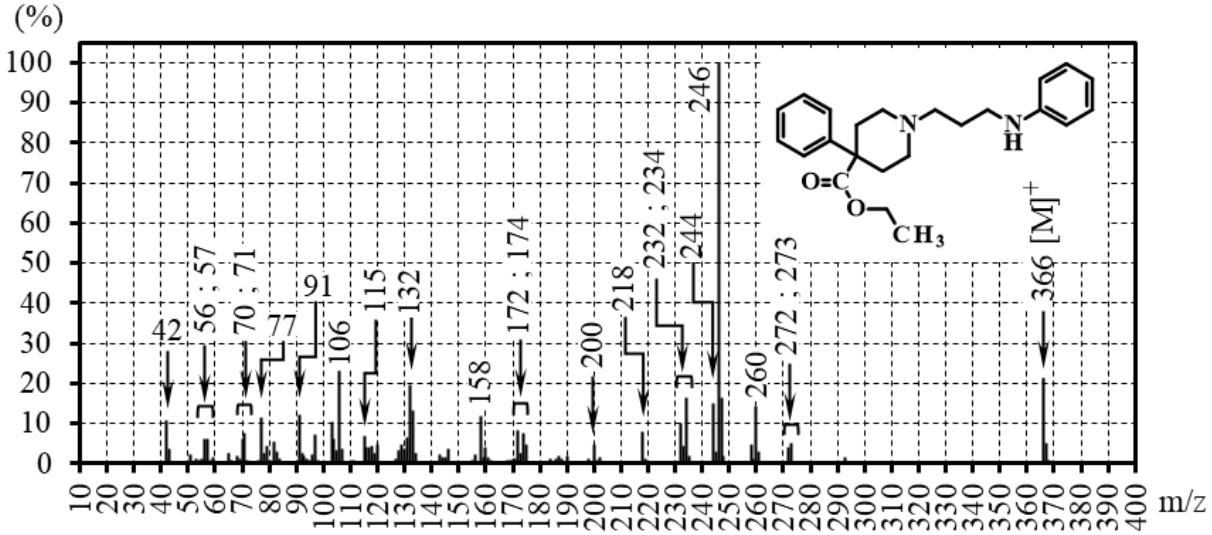

Physostigmine - CAS 57-47-6 - EI 75 eV - SDBS 11188 - NIST 221137



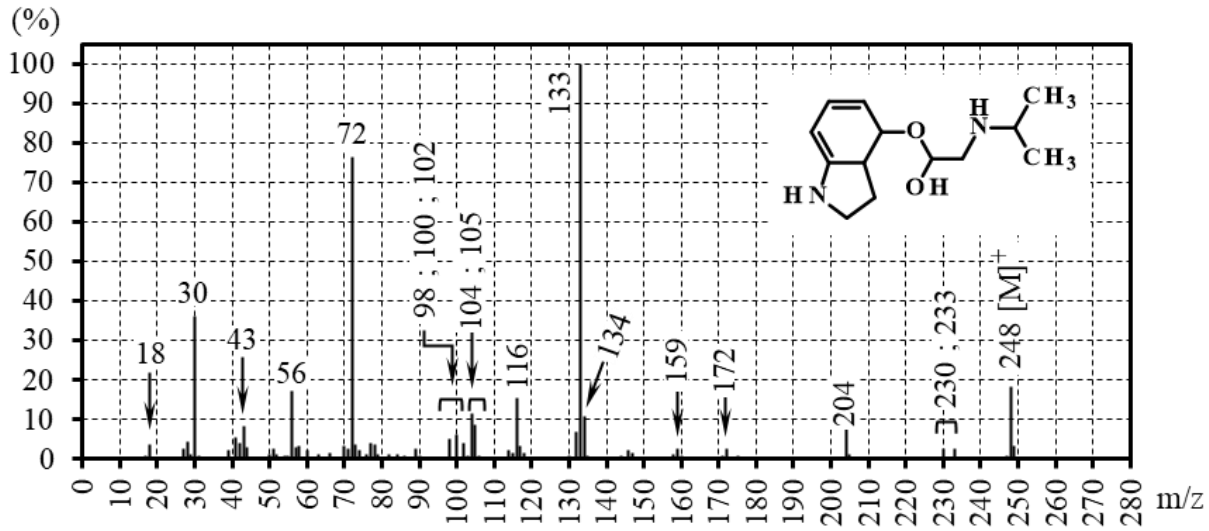

Phytomenadione (Phytonadione) - CAS 84-80-0 - NIST 233846



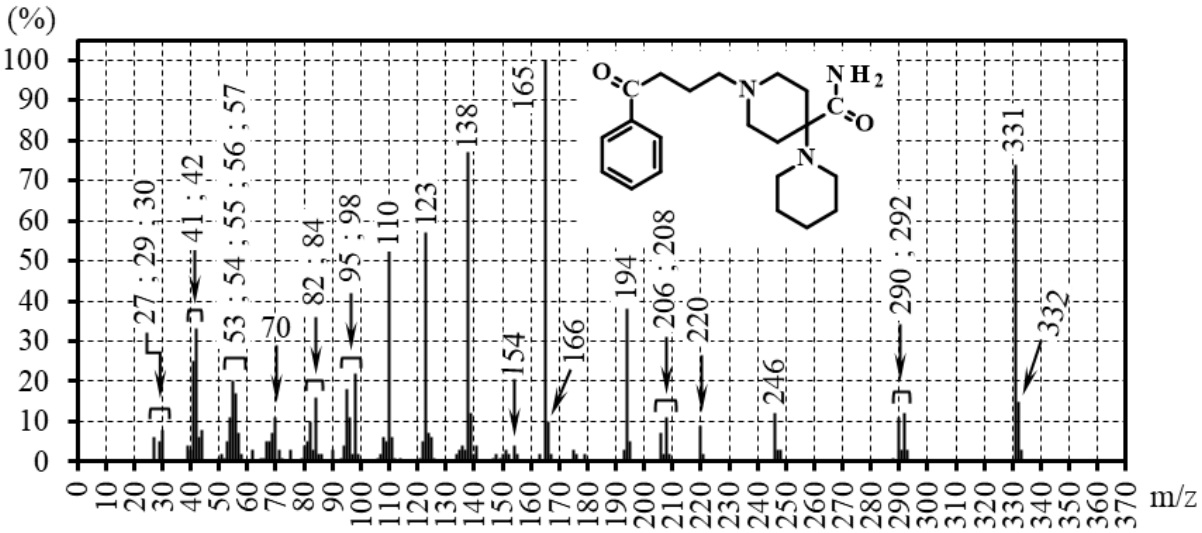

Pilocarpine - CAS 92-13-7 - EI - NIST 248003



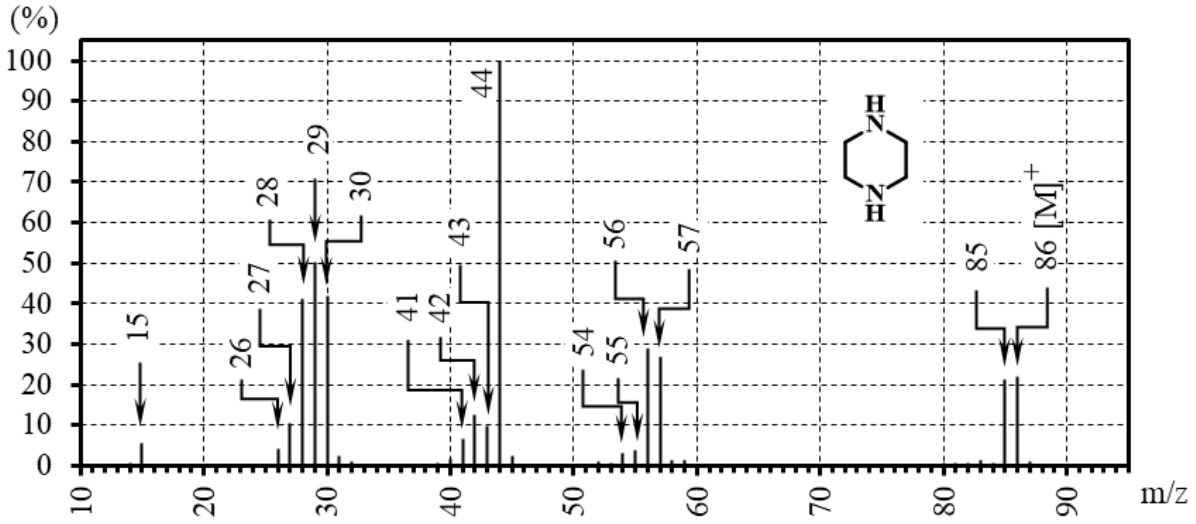

Piminodine - CAS 13495-09-5 - EI - NIST 248498



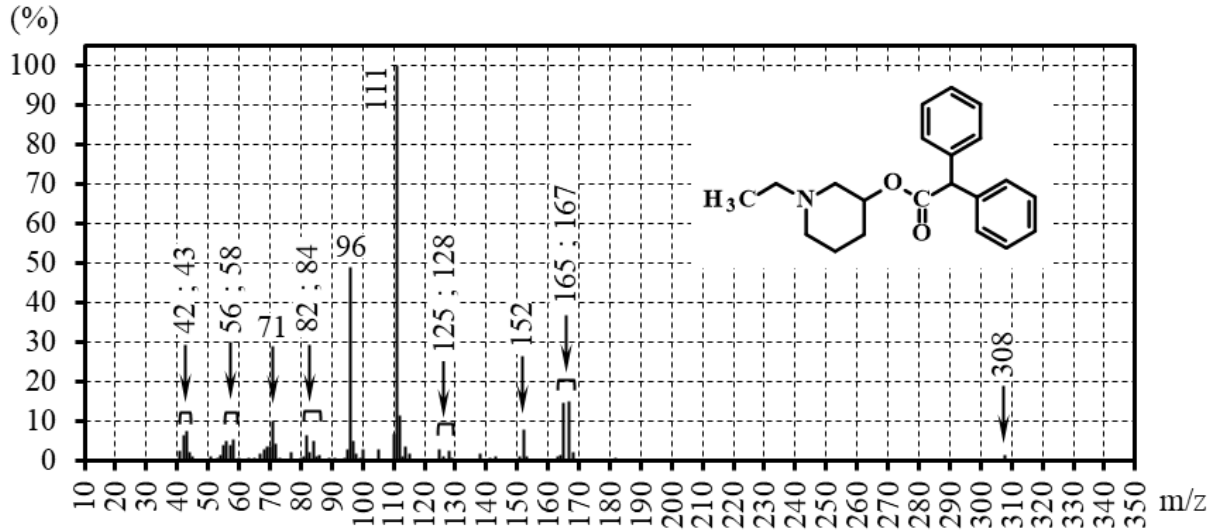

Pindolol - CAS 13523-86-9 - EI - NIST 235693



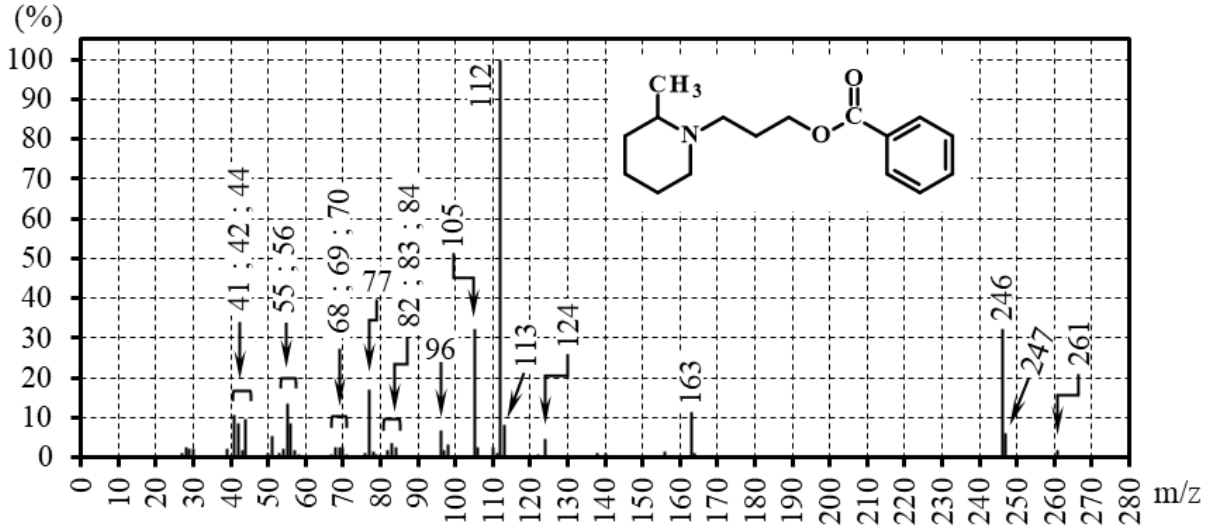

Pipamperone - CAS 1893-33-0 - EI - NIST 298766



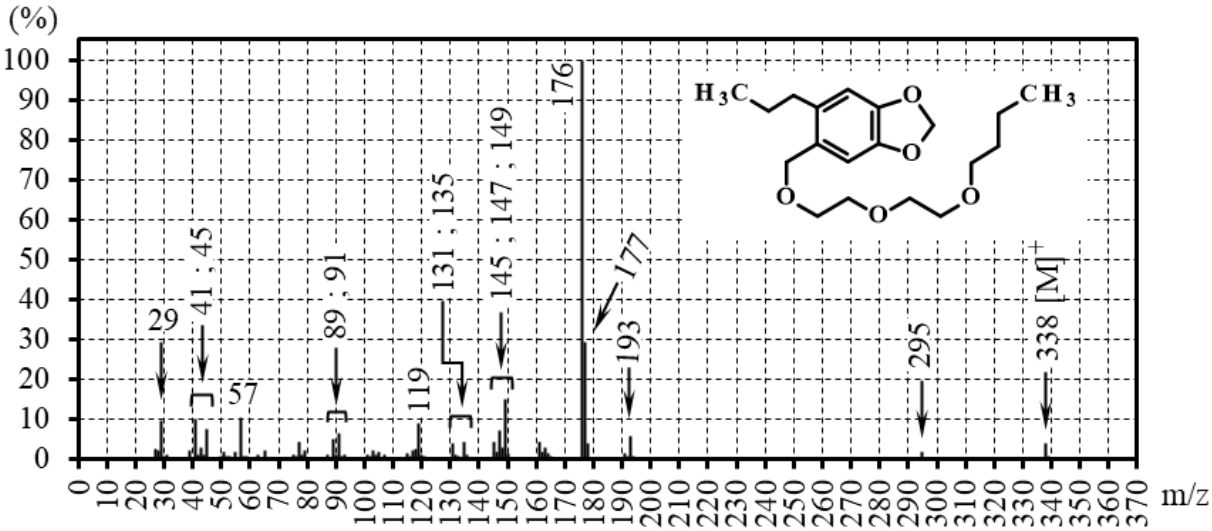

Piperazine - CAS 110-85-0 - NIST 229316



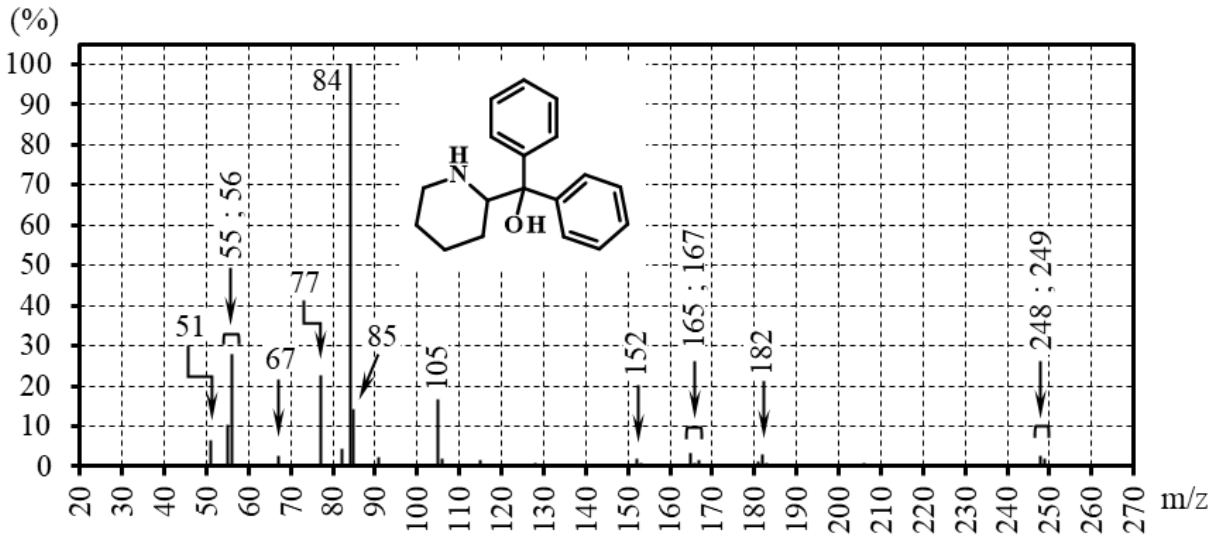

Piperidolate - CAS 82-98-4 - EI - NIST 246916



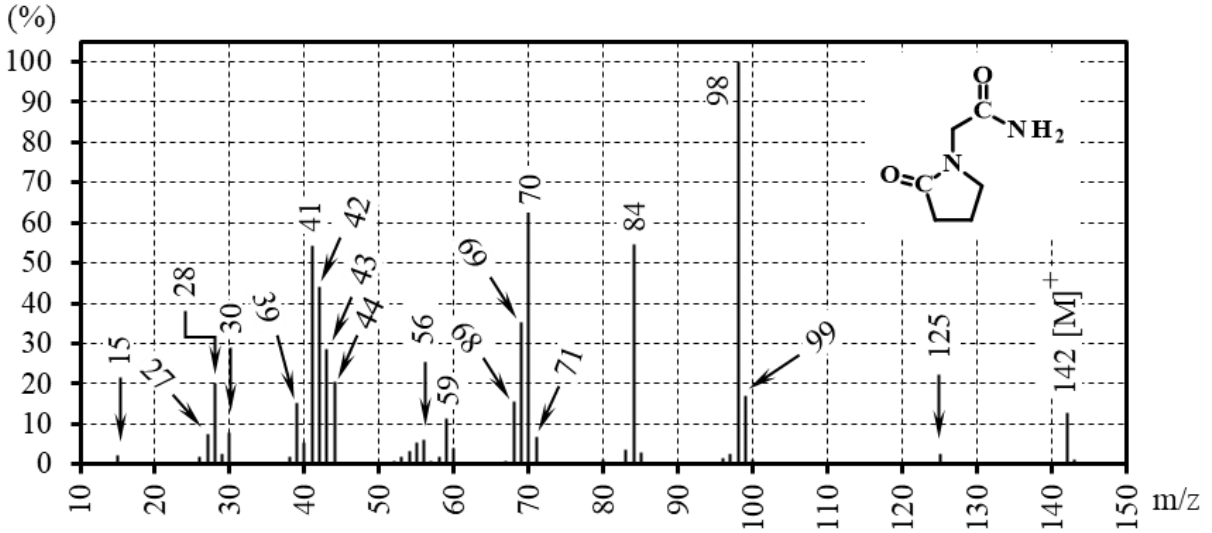

Piperocaine - CAS 136-82-3 - EI - NIST 408421



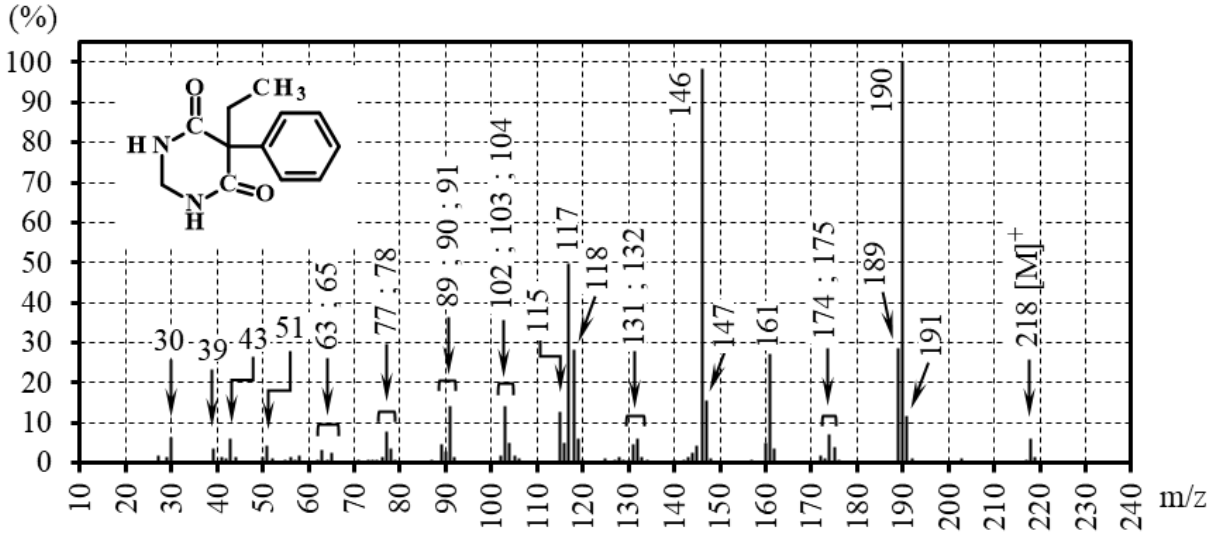

Piperonyl butoxide - CAS 51-03-6 - EI - NIST 245254



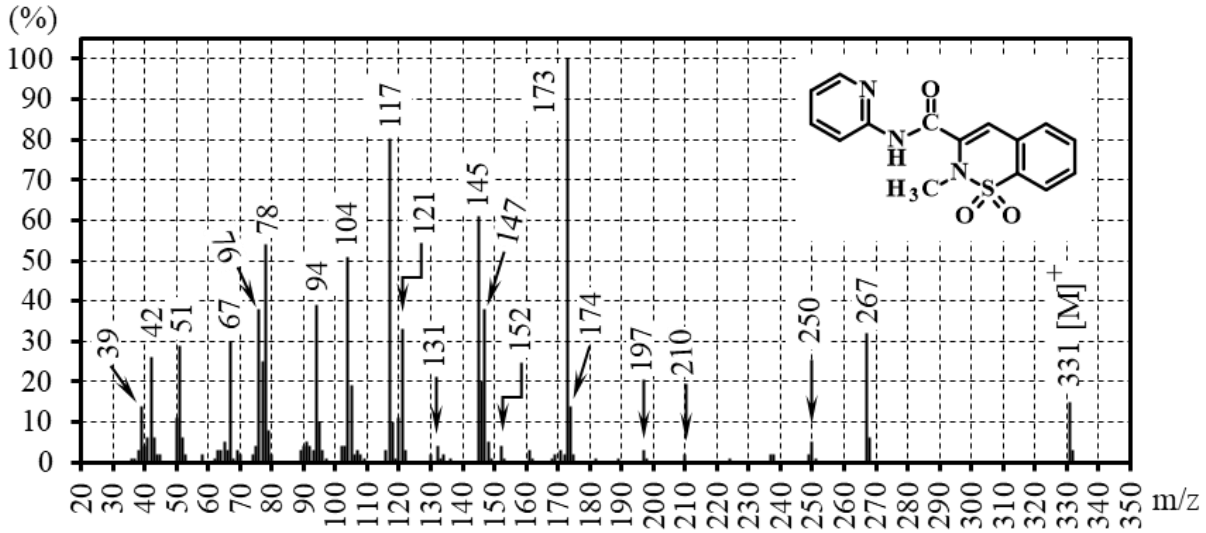

Pipradrol - CAS 467-60-7 - EI - NIST 119302



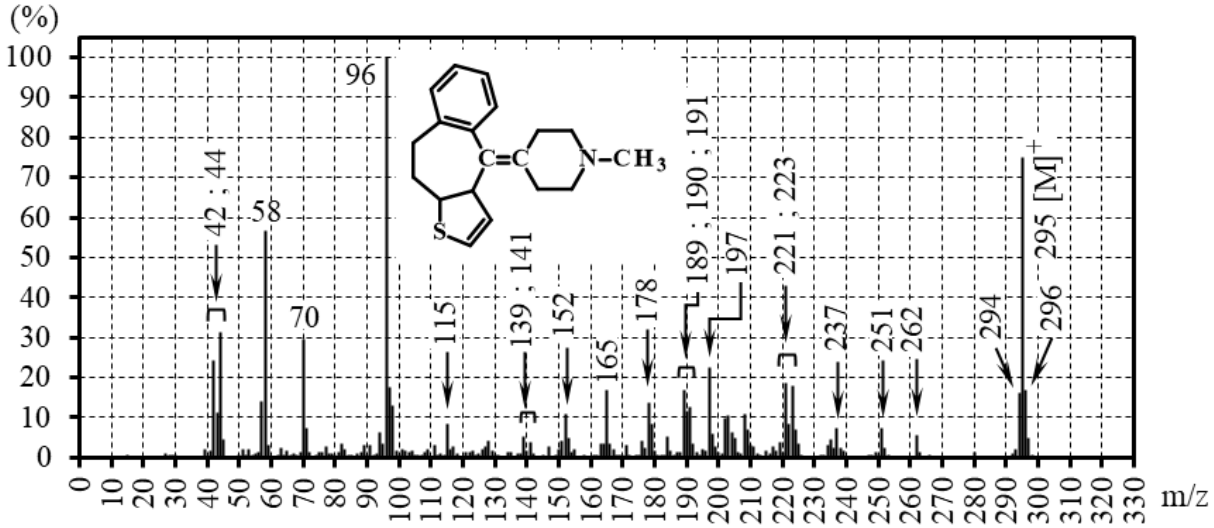

Piracetam - CAS 7491-74-9- NIST 292144



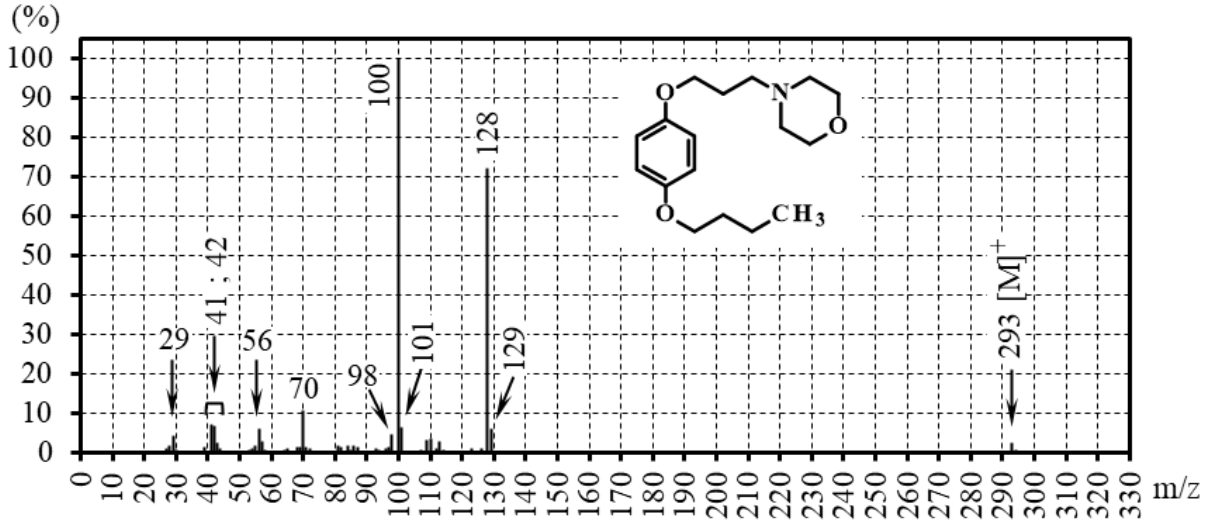

Pirimidone - CAS 125-33-7 - EI - NIST 244337



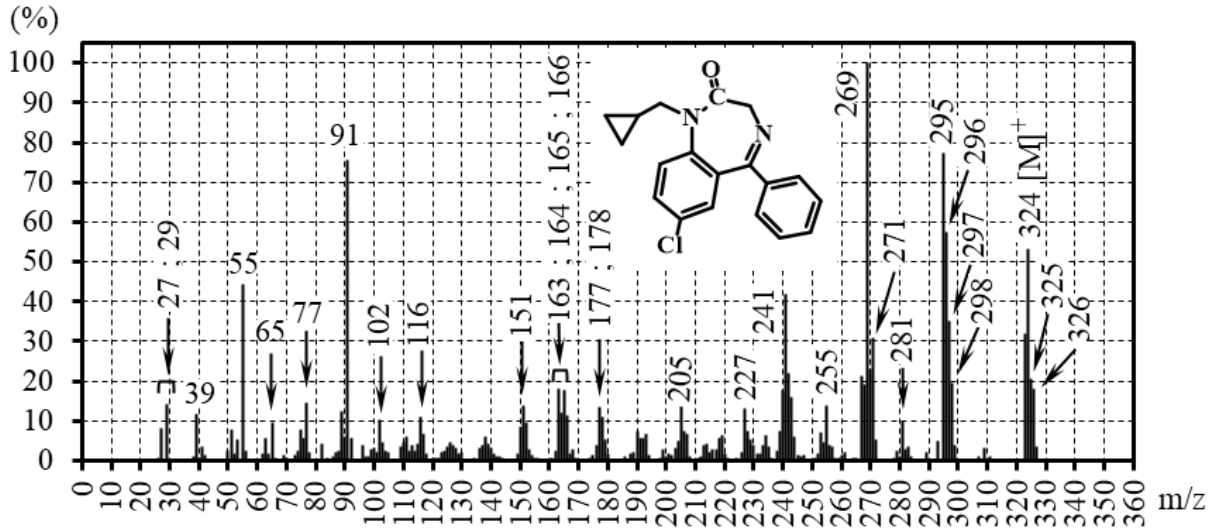

Piroxicam - CAS 36322-90-4 - NIST 298765



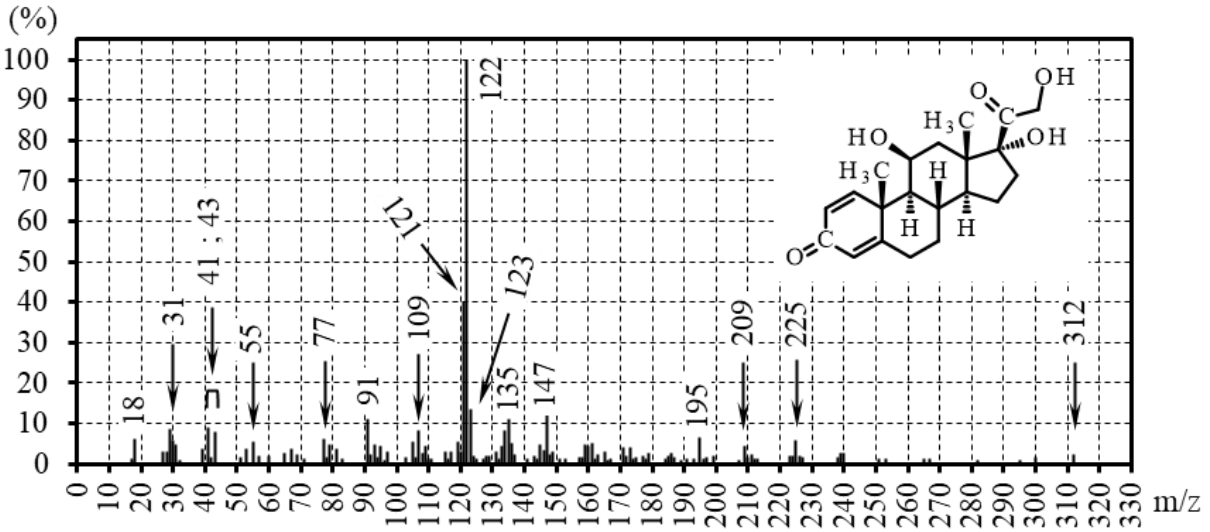

Pizotyline - CAS 15574-96-6 - EI - NIST 408672



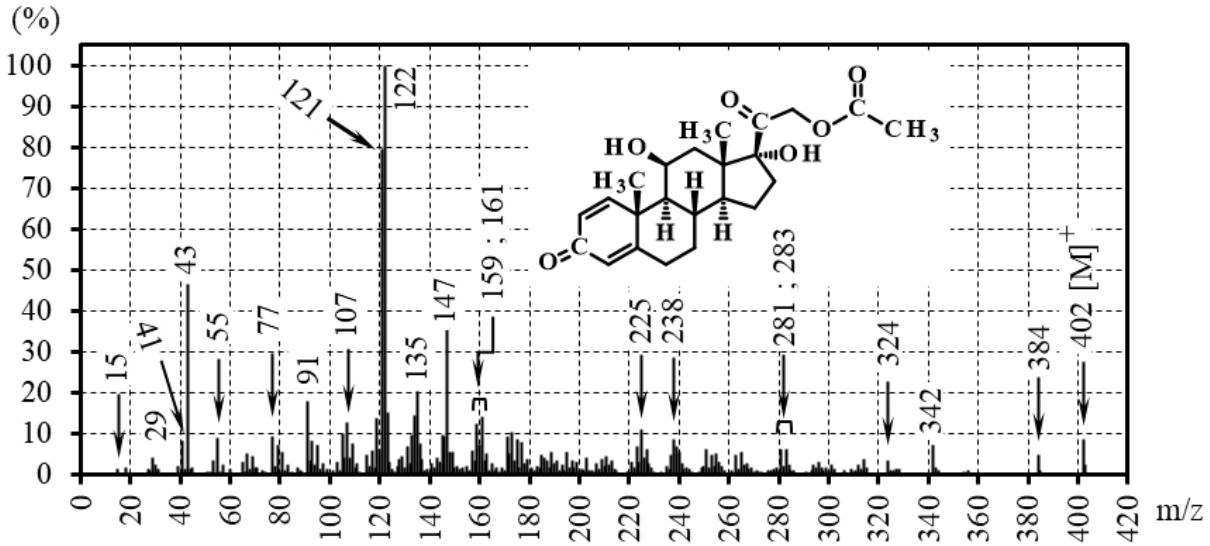

Pramocaine (Pramoxine , Tronophtane , Proxazocain) - CAS 140-65-8
EI - NIST 408053



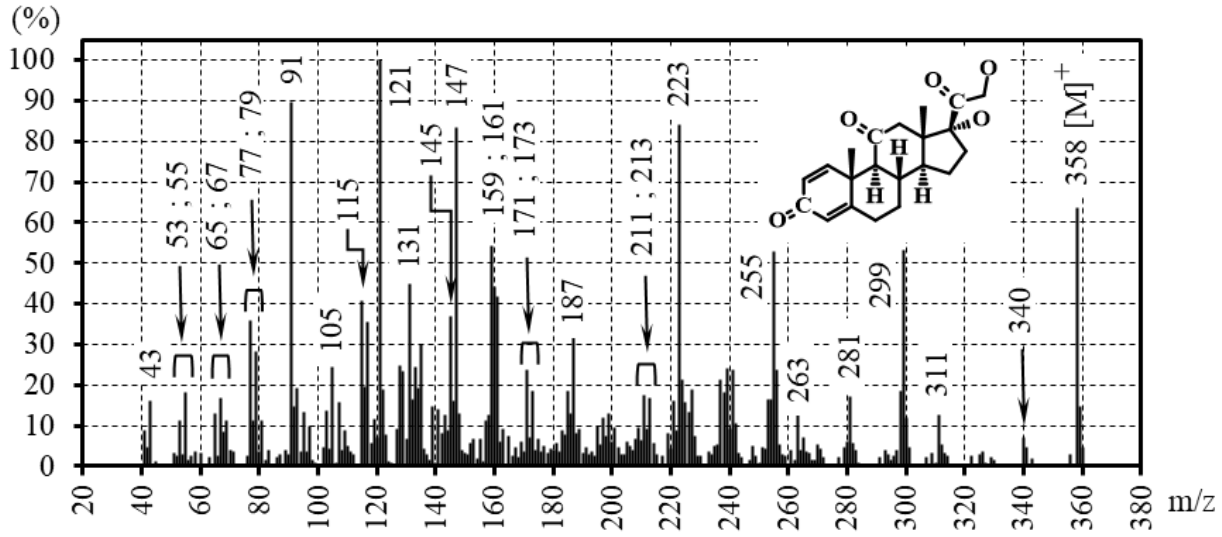

Prazepam - CAS - 2955-38-6 - EI - NIST 250562



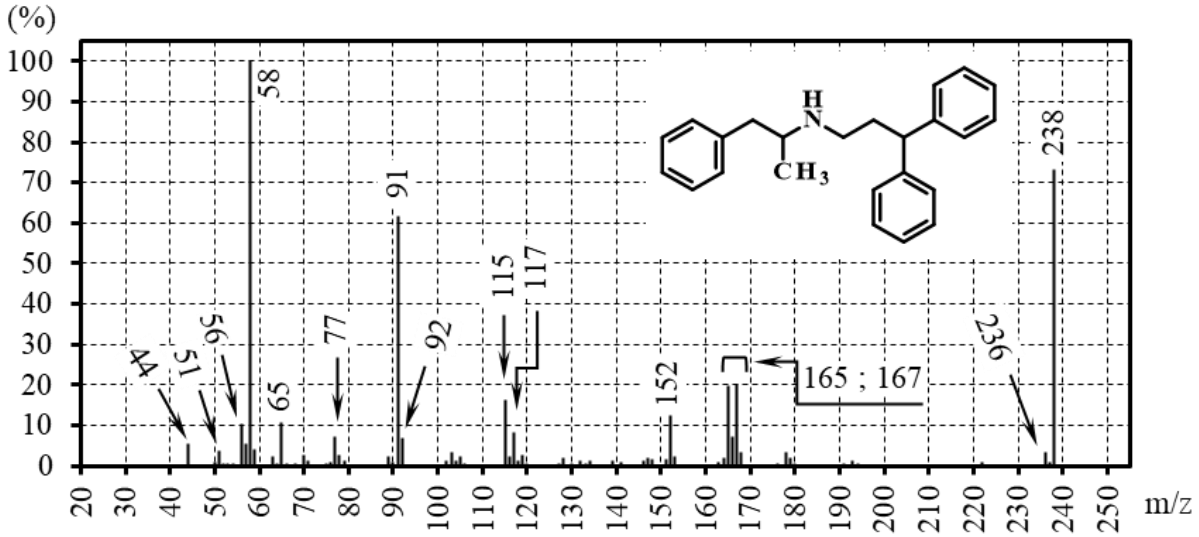

Prednisolone - CAS 50-24-8 - EI - SDBS 10998



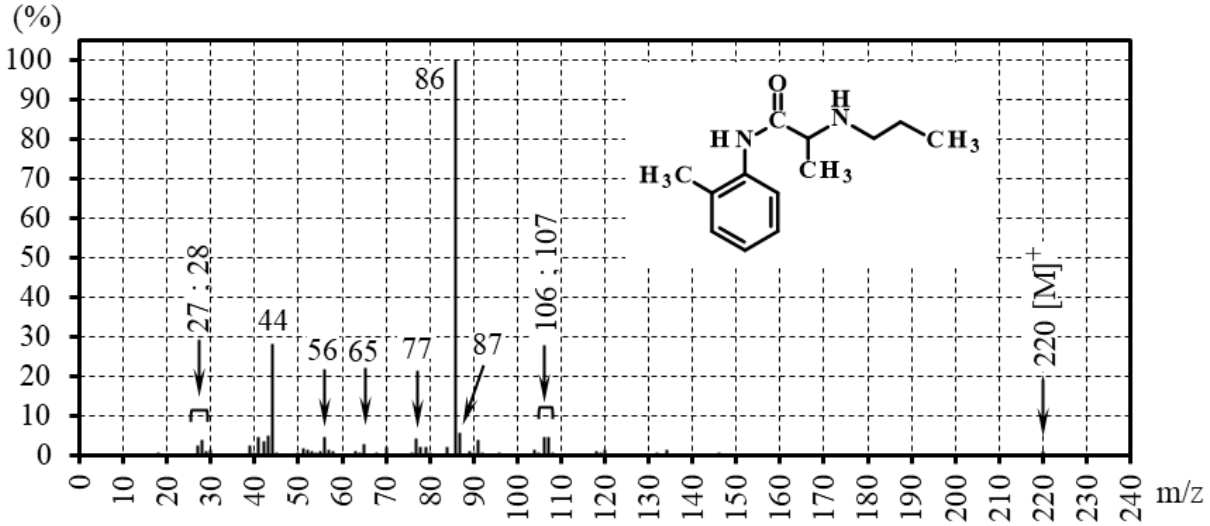

Prednisolone acetate - CAS 52-21-1 - NIST 235678



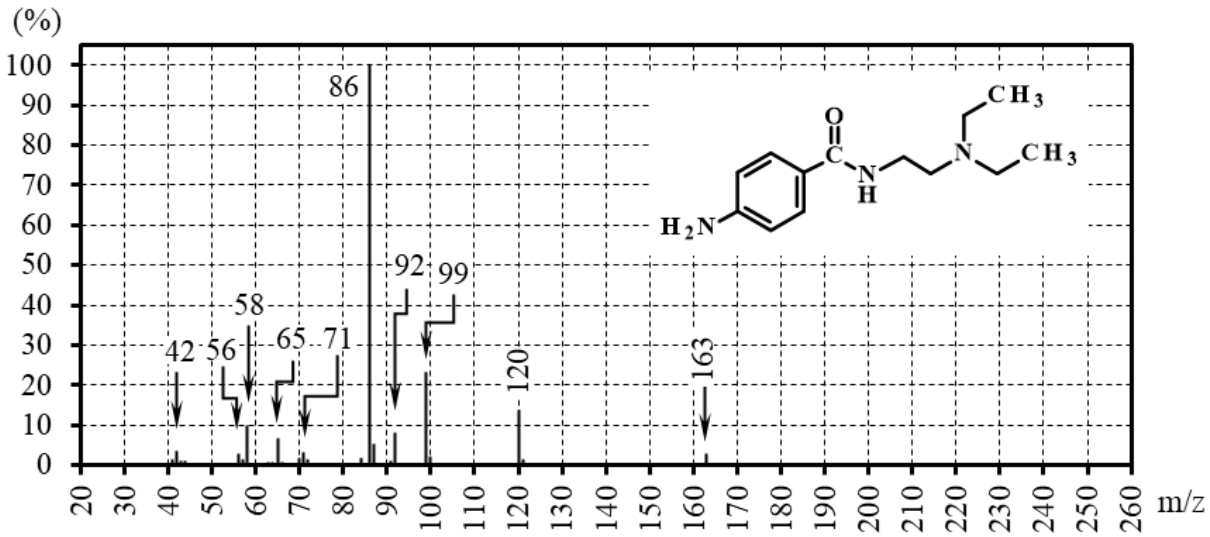

Prednisone - CAS 53-03-2 - EI - NIST 247957



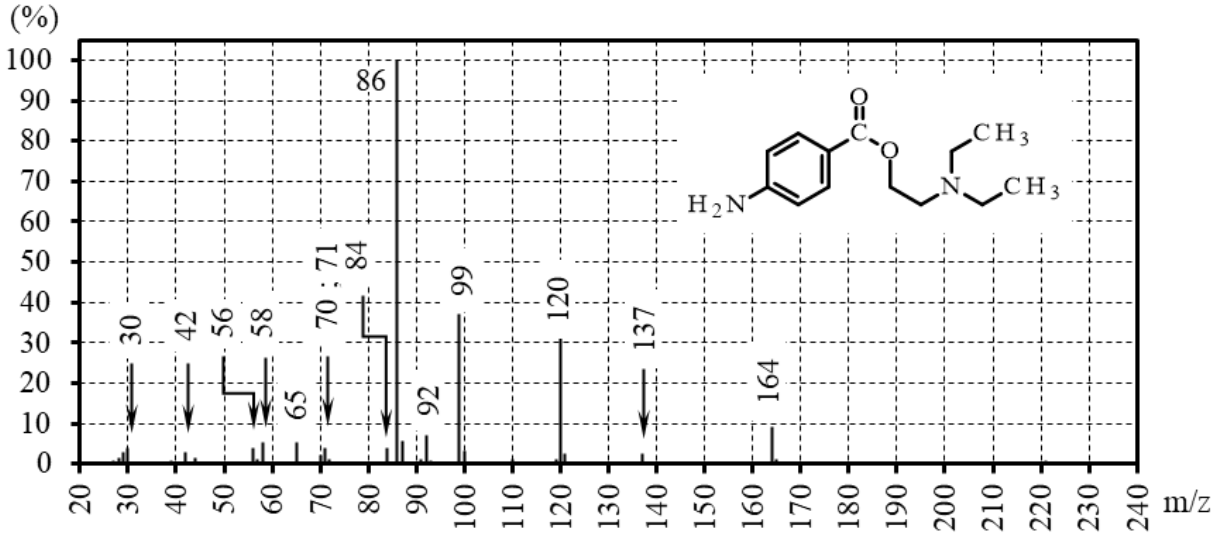

Prenylamine - CAS 300-64-7 - NIST 248510



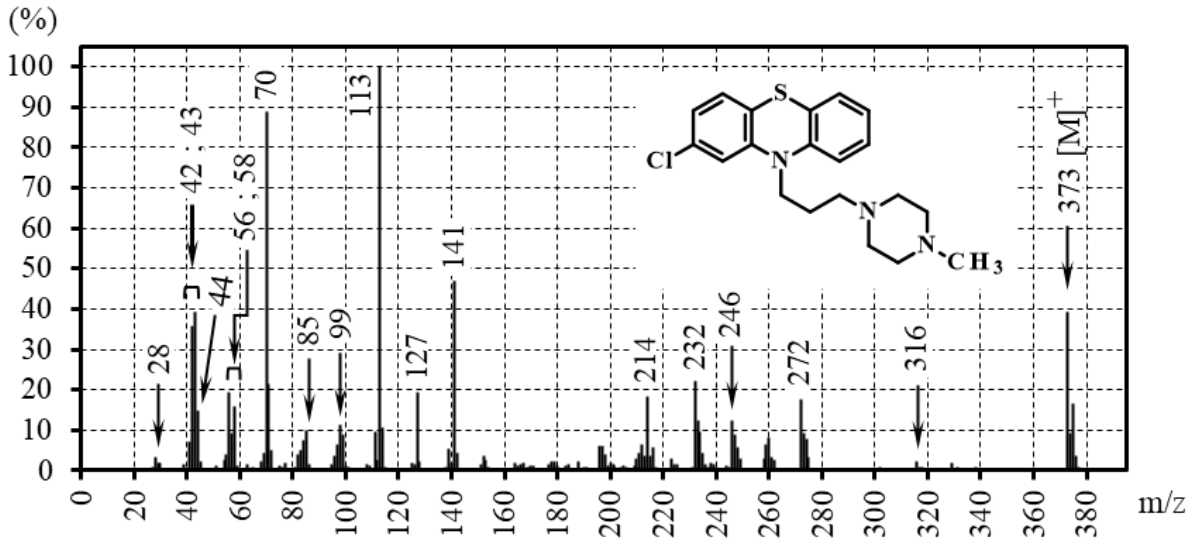

Prilocaine - CAS 721-50-6 - EI - NIST 113845



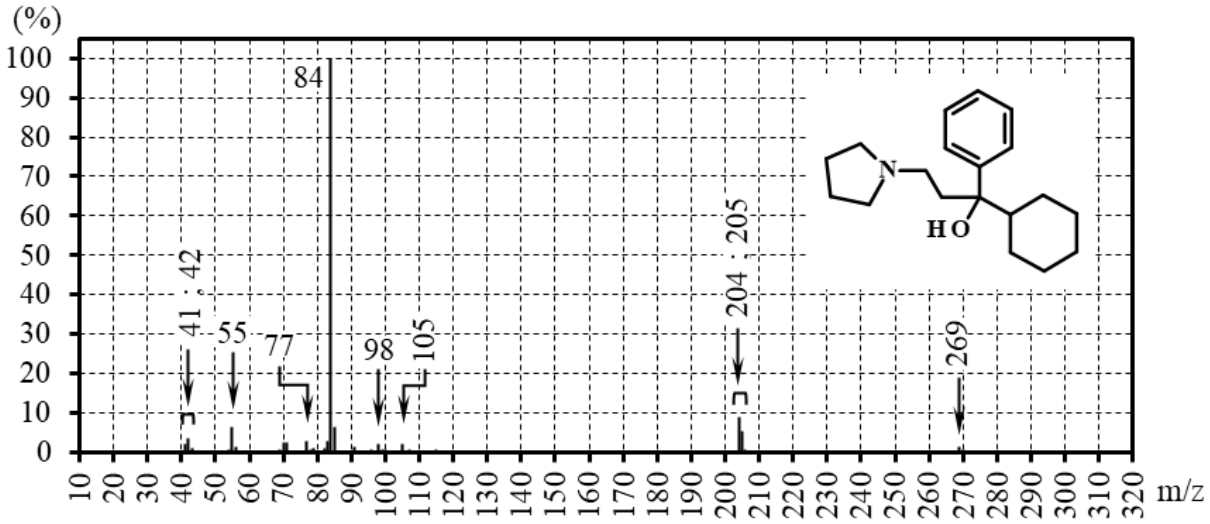

Procainamide - CAS 51-06-9 - EI - NIST 125801



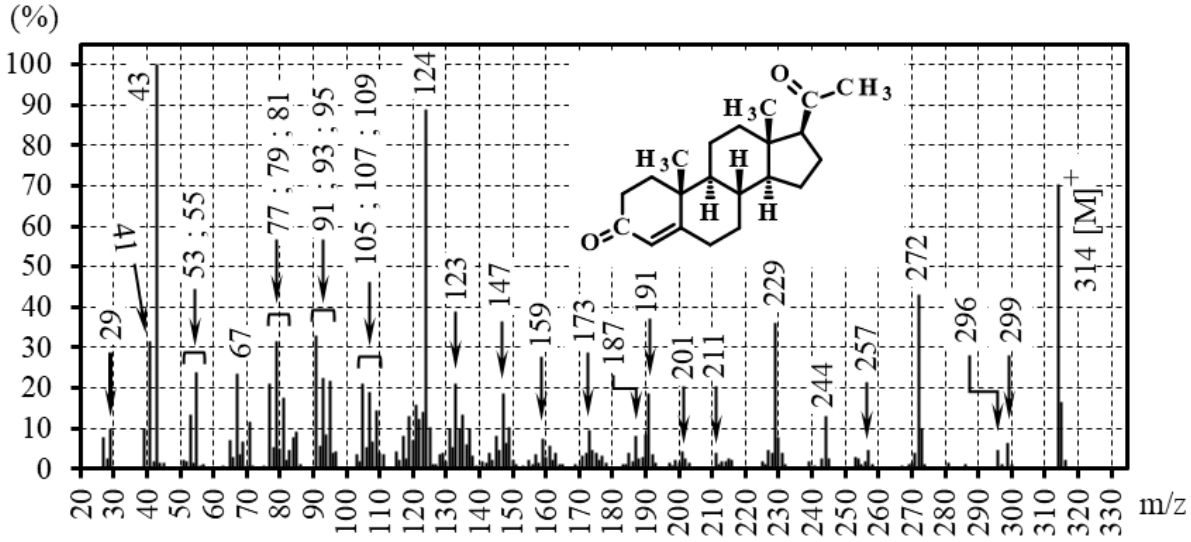

Procaine (Novocaine) - CAS 59-46-1 - EI - NIST n. 238047



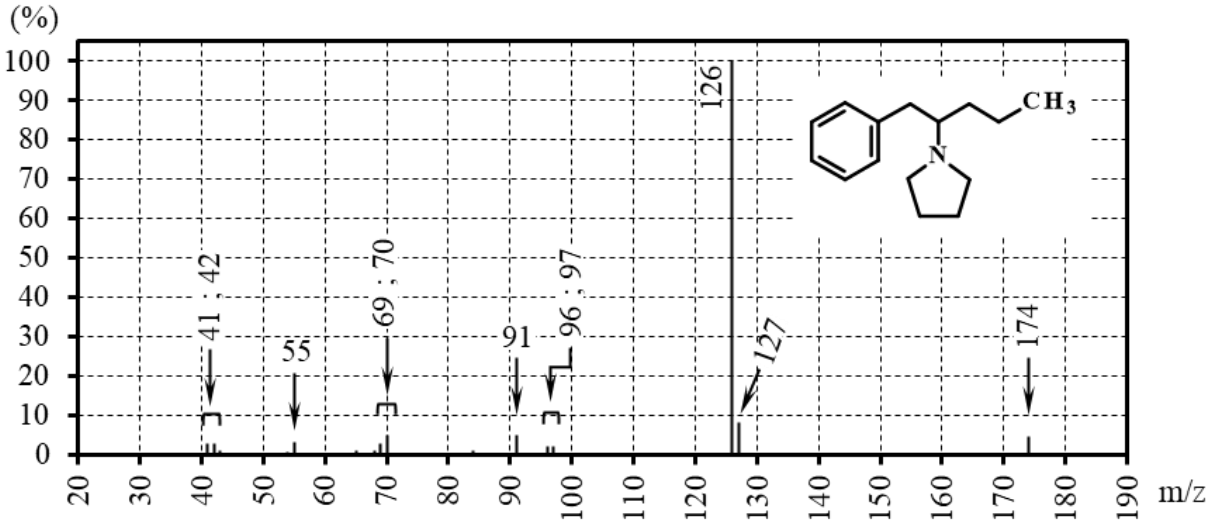

Prochloroperazine - CAS 58-38-8 - NIST 291984



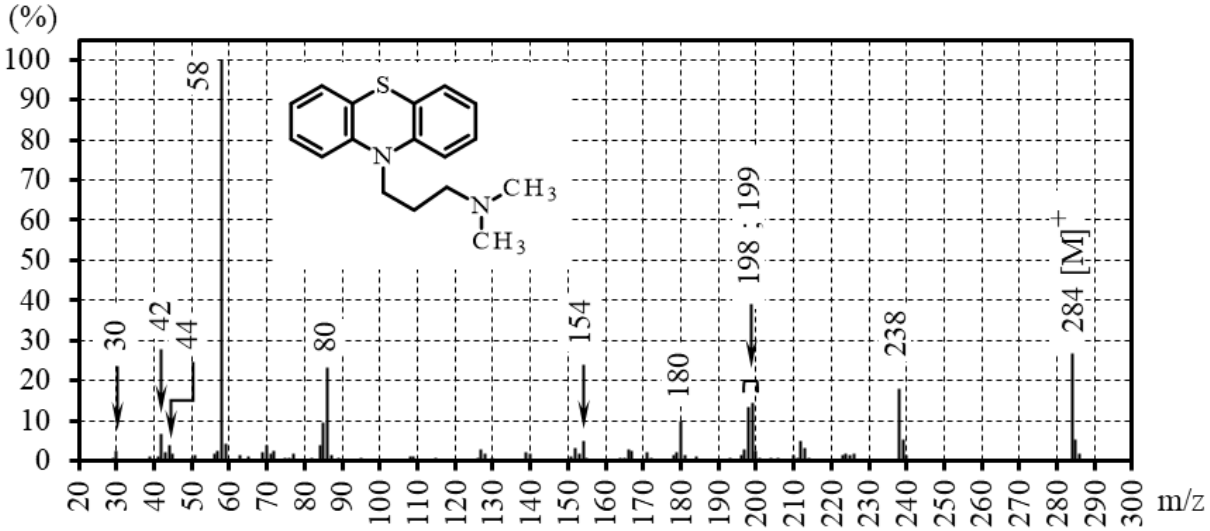

Procyclidine - CAS 77-37-2 - EI - NIST 379205



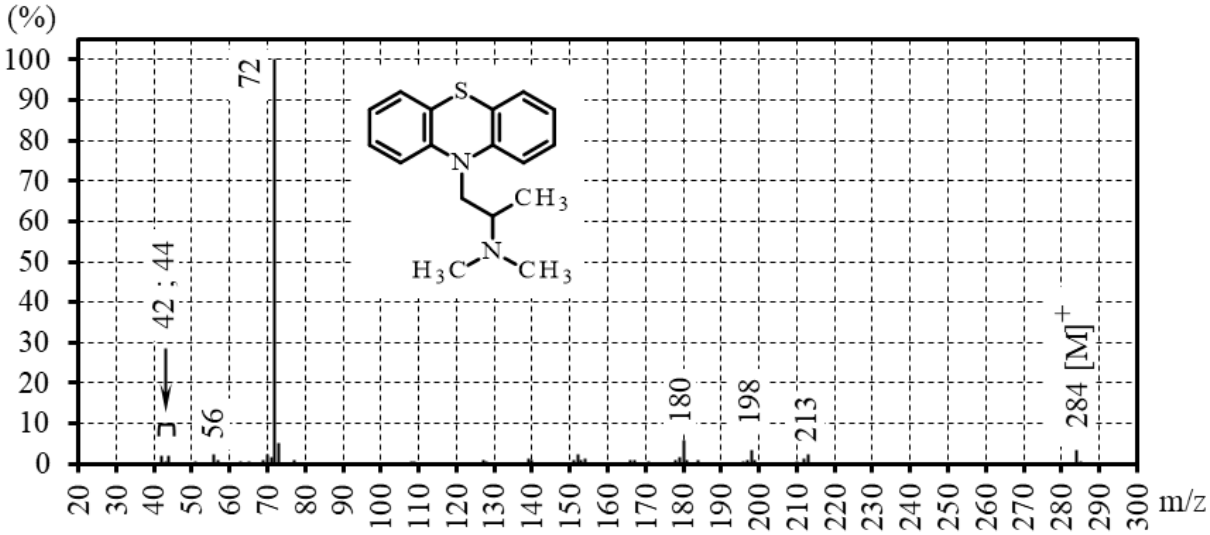

Progesterone - CAS 57-83-0 - NIST 67038



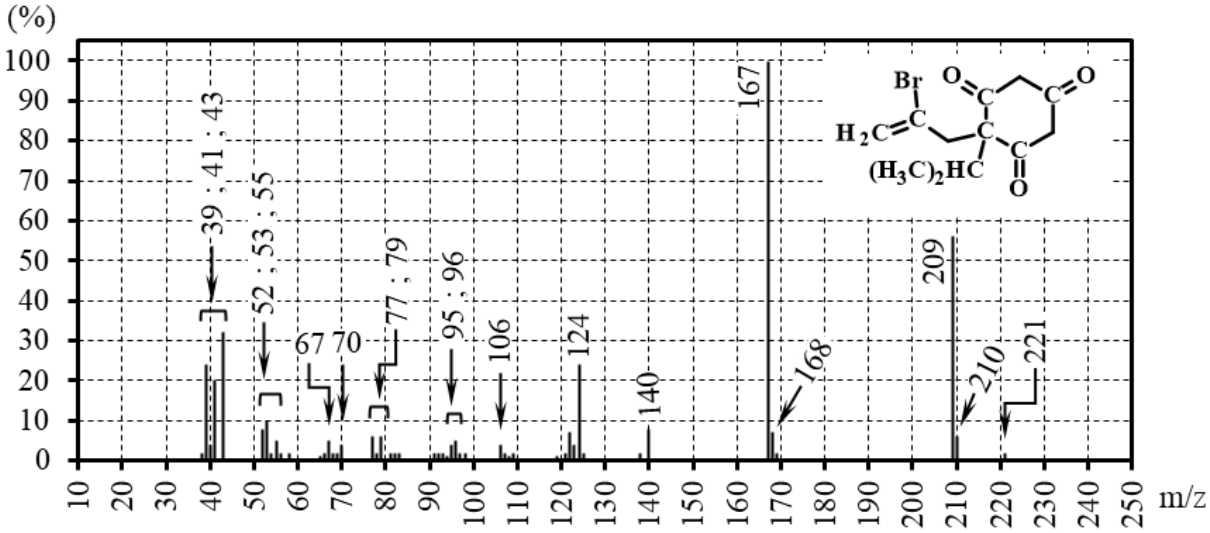

Prolintane - CAS 493-92-5 - EI - NIST 120947



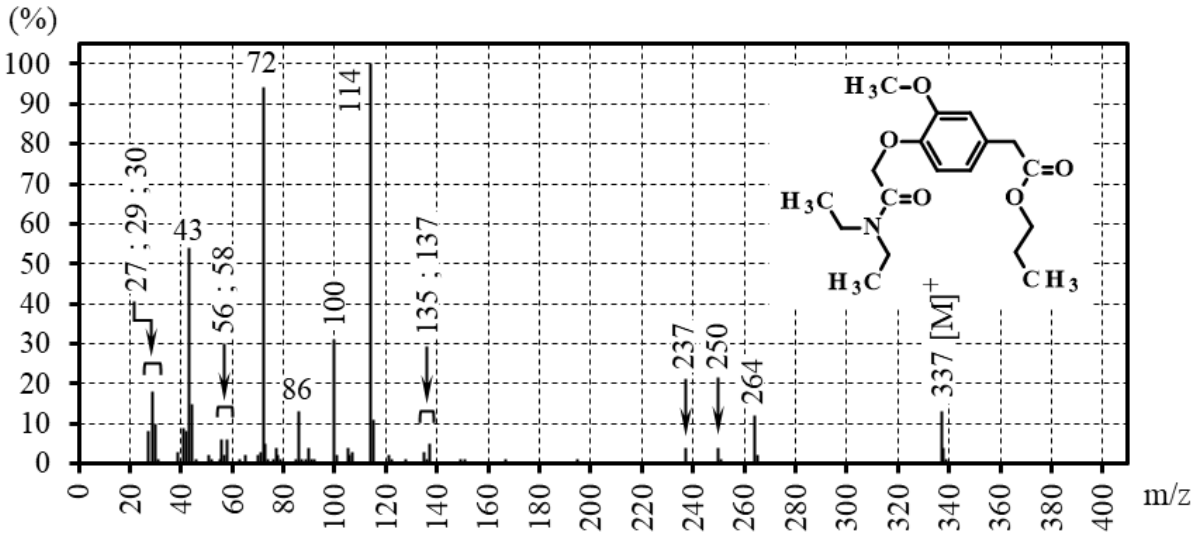

Promazine - CAS 58-40-2 - NIST 352155



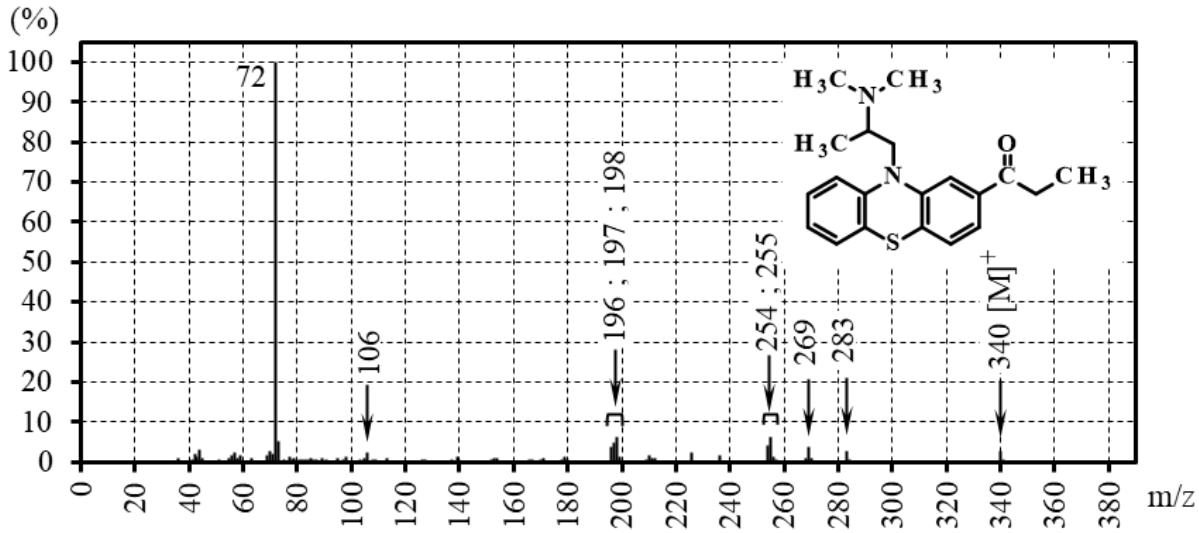

Promethazine - CAS 60-87-7 - NIST 408602



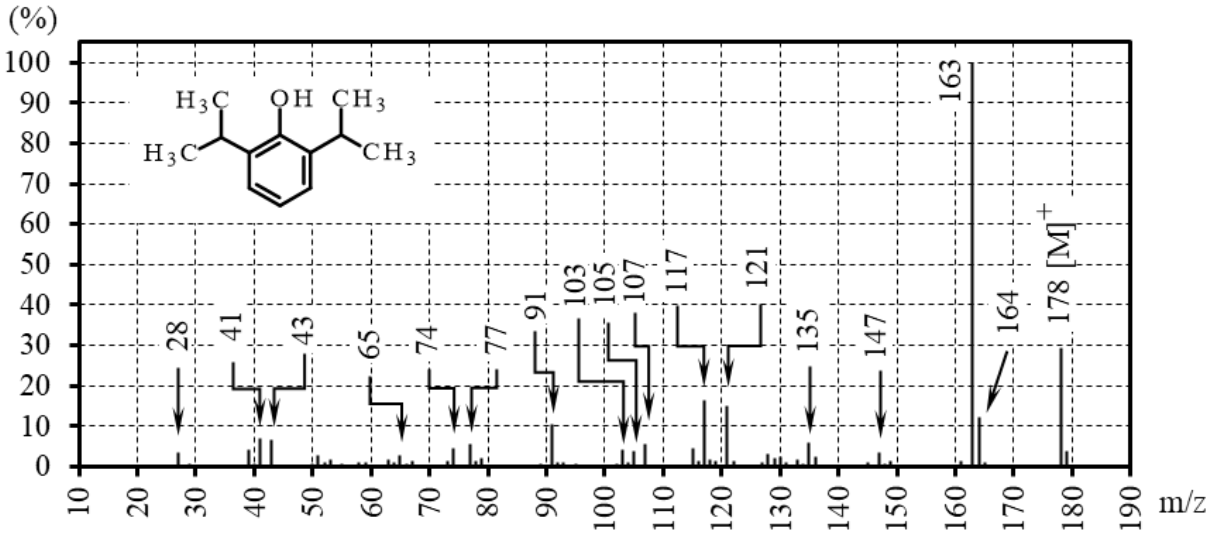

Propallylonal - CAS 545-93-7 - EI - NIST 298703



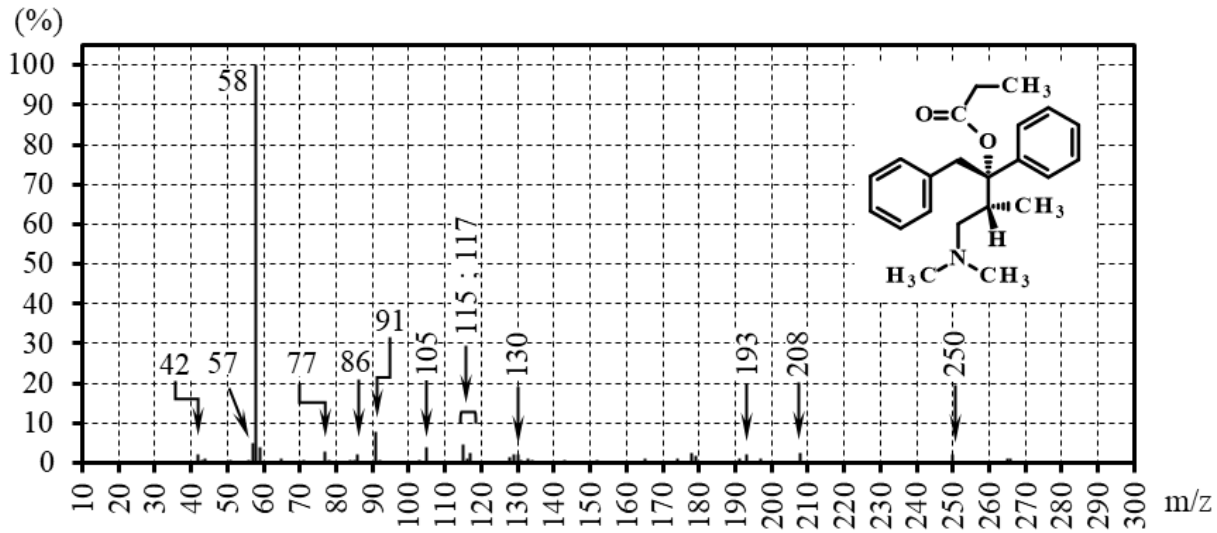

Propanidid - CAS 1421-14-3 - EI - IST 298761



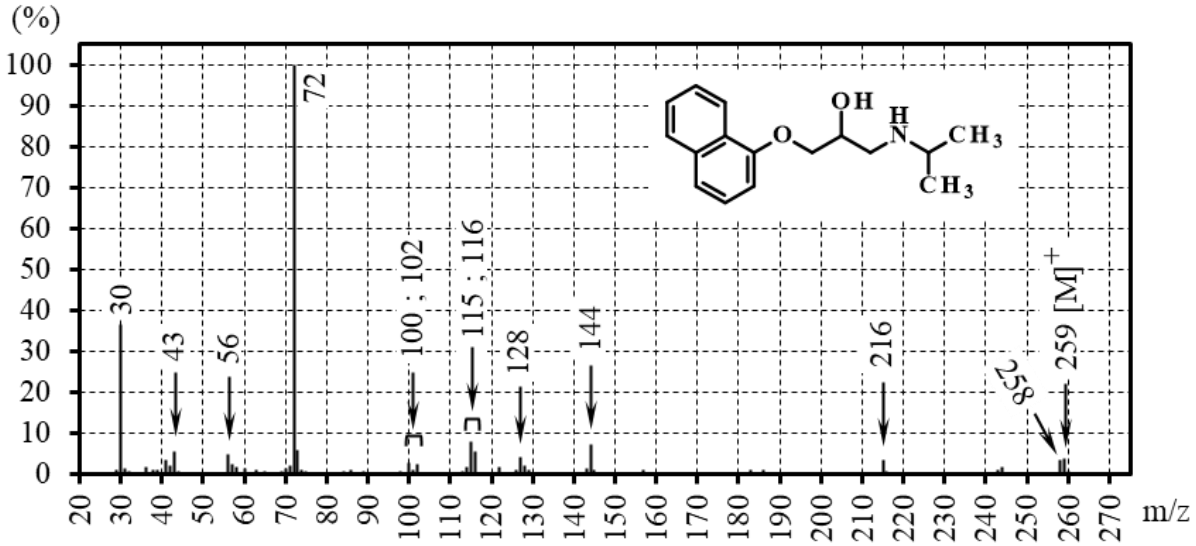

Propiomazine - CAS 362-29-8 - EI - NIST 246995



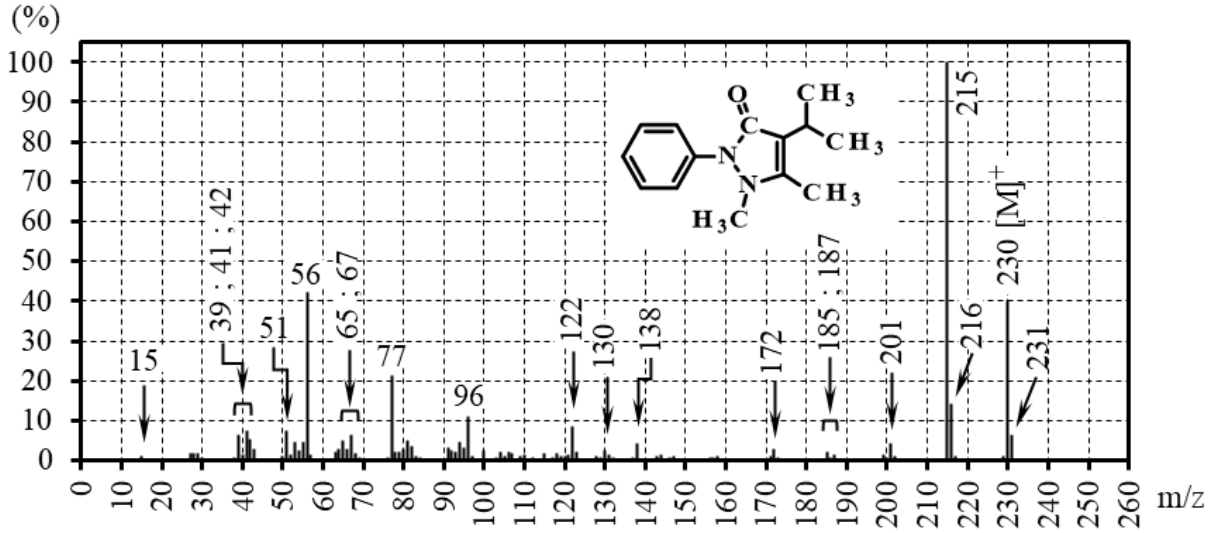

Propofol - CAS 2078-54-8 - EI - NIST 227977



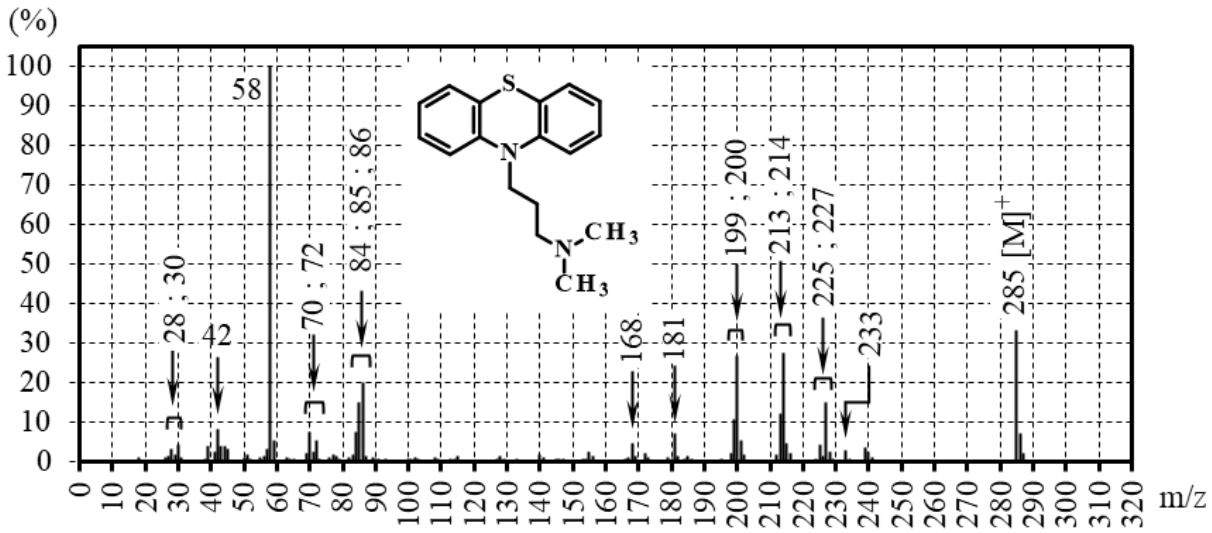

Propoxyphene - CAS 469-62-5 - EI - NIST 312352



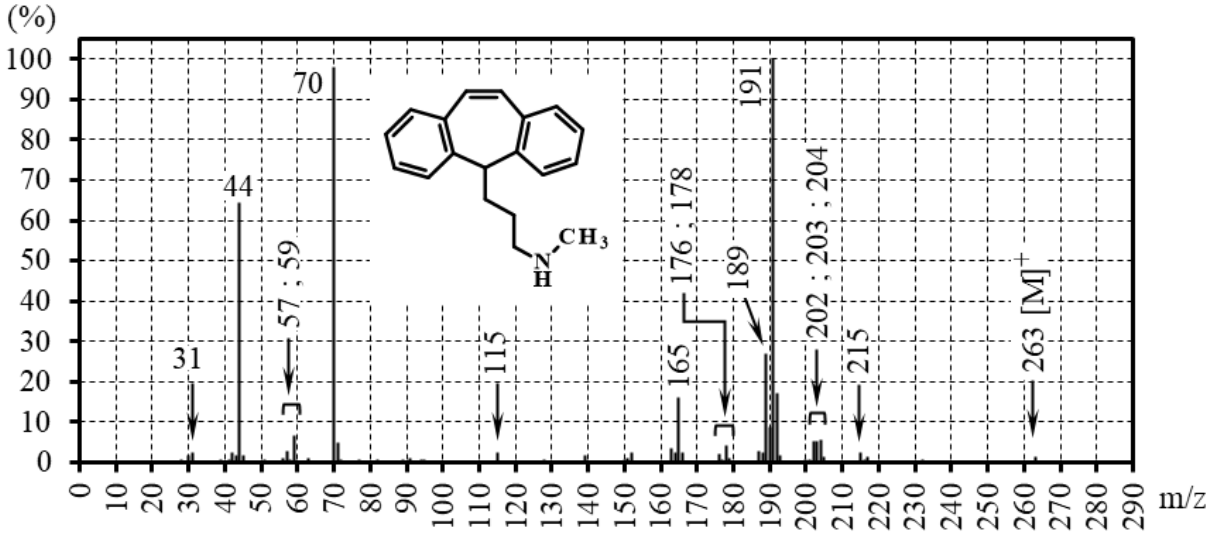

Propranolol - CAS 525-66-6 - NIST 42323



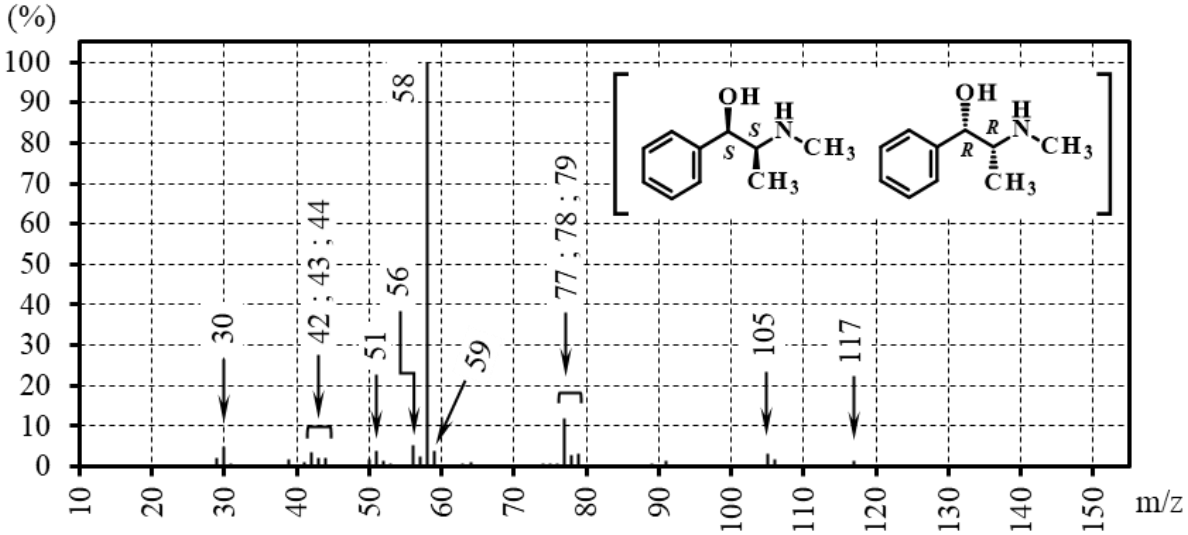

Propyphenazone - CAS 479-92-5 - EI - NIST 408684



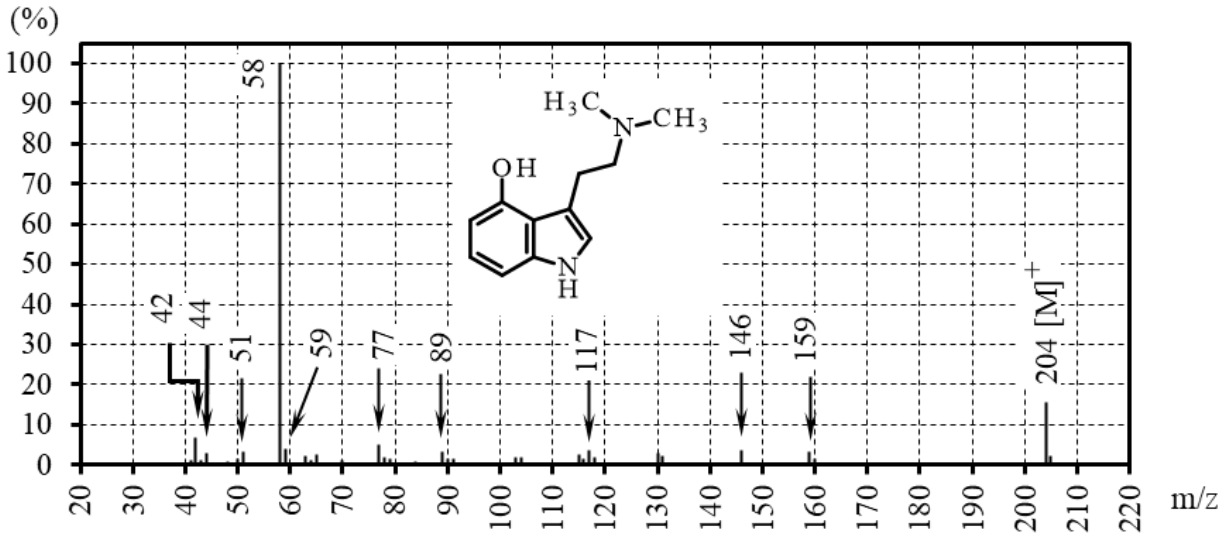

Prothipendyl - CAS 303-69-5 - EI - NIST 42336



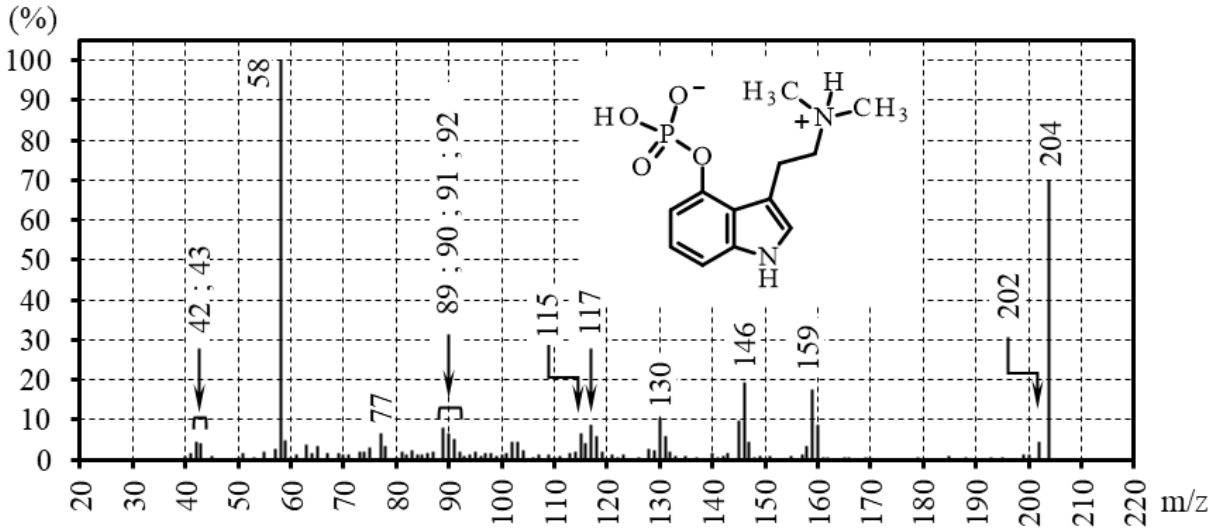

Protriptyline - CAS 438-60-8 - EI - NIST 292033



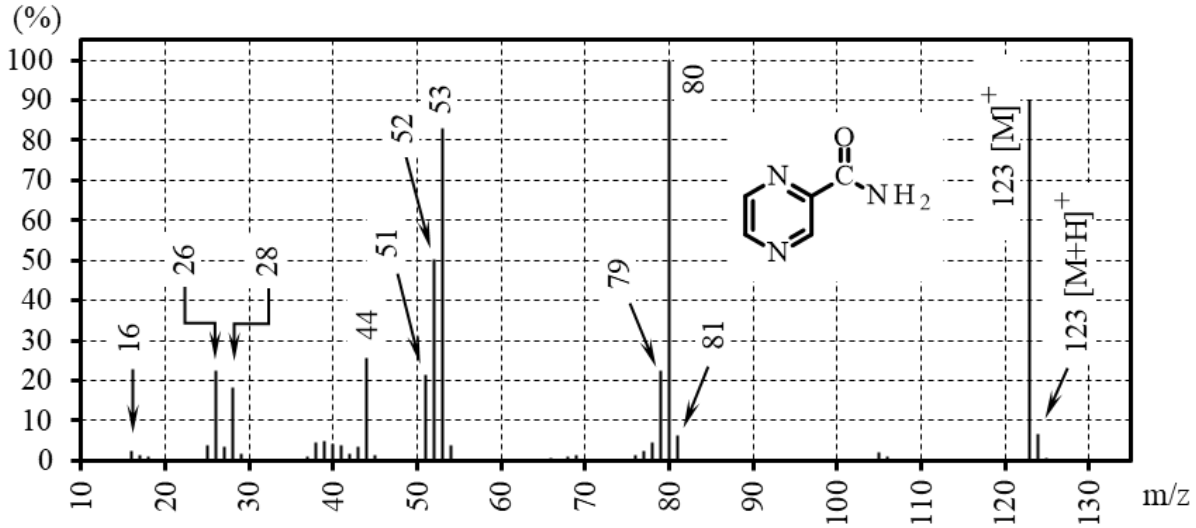

Pseudoephedrine - CAS 90-82-4 - NIST 246007



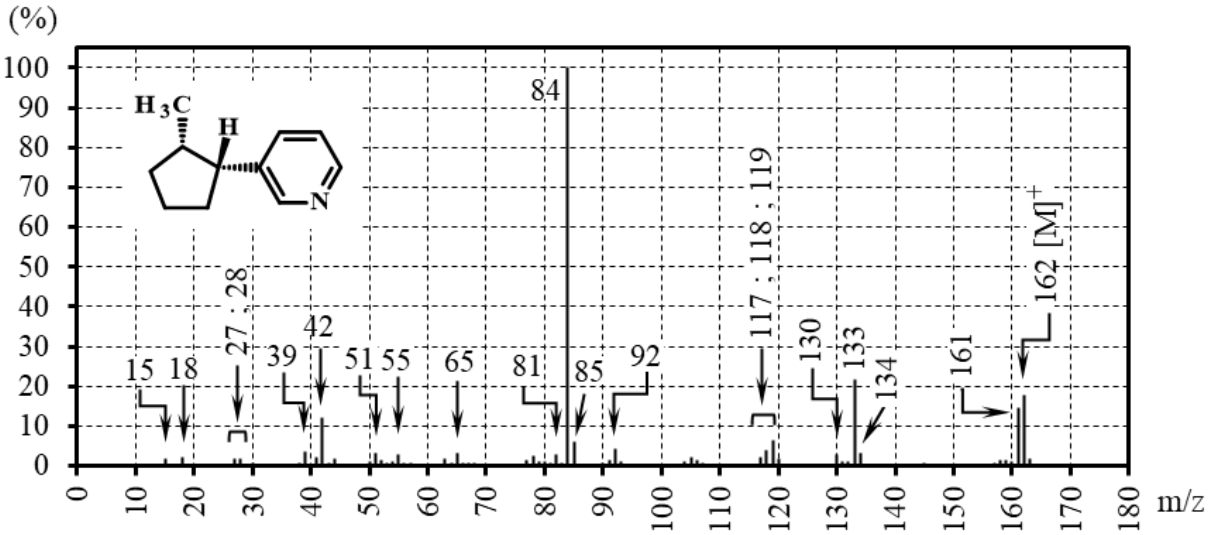

Psilocin - CAS 520-53-6 - NIST 247861



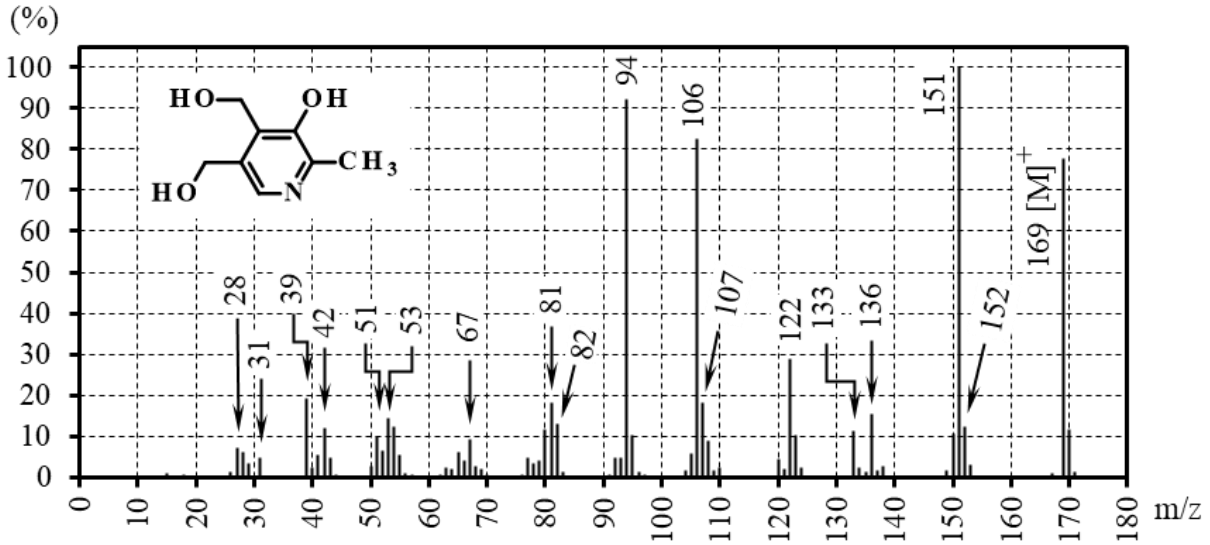

Psilocybine - CAS 520-52-5 - EI - NIST 246666



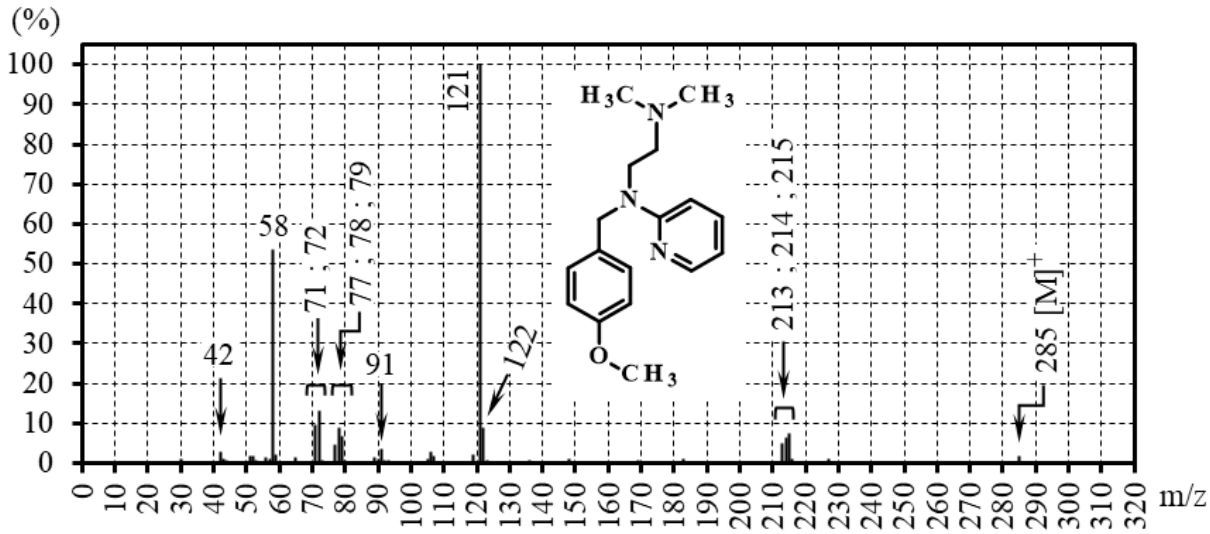

Pyrazinamide - CAS 98-96-4 - EI - NIST 118636



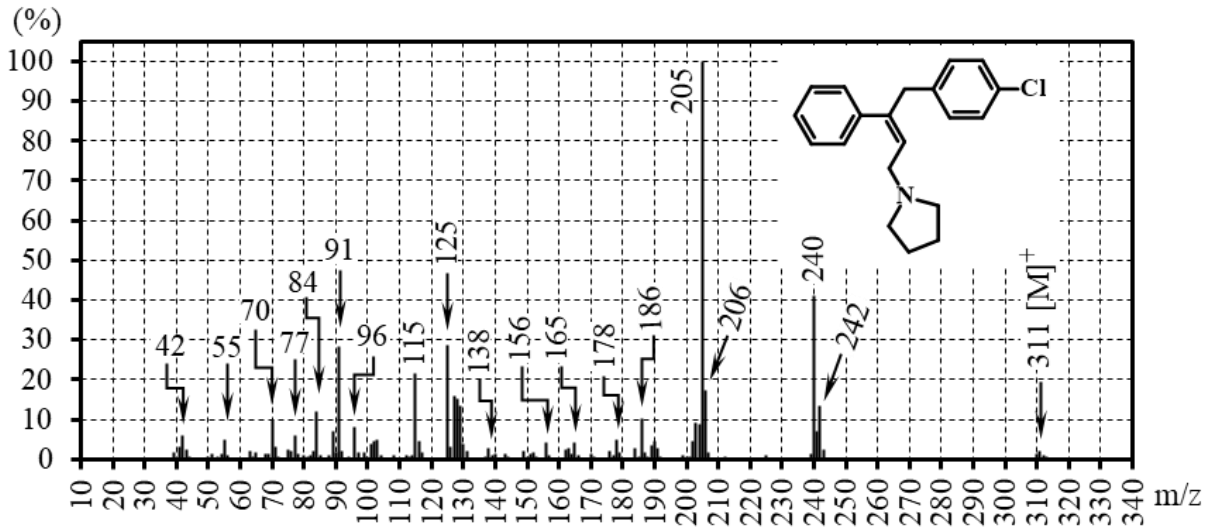

Pyridine,3-(1-methyl-2-pyrrolidinyl)-,(S) - CAS 54-11-5 - EI - NIST 232303



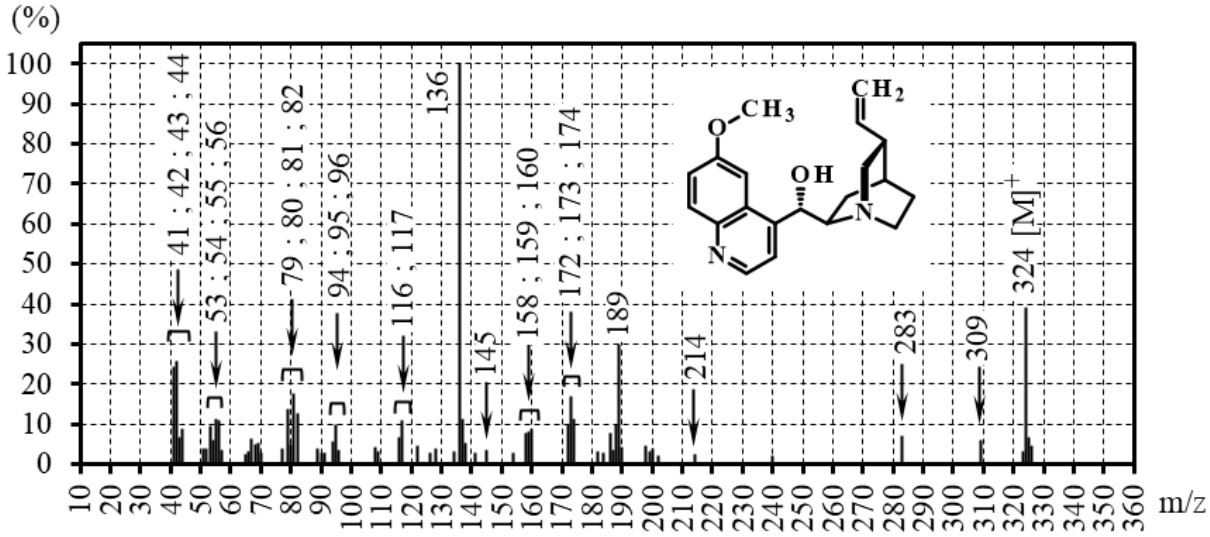

Pyridoxine - CAS 65-23-6 - NIST 228913



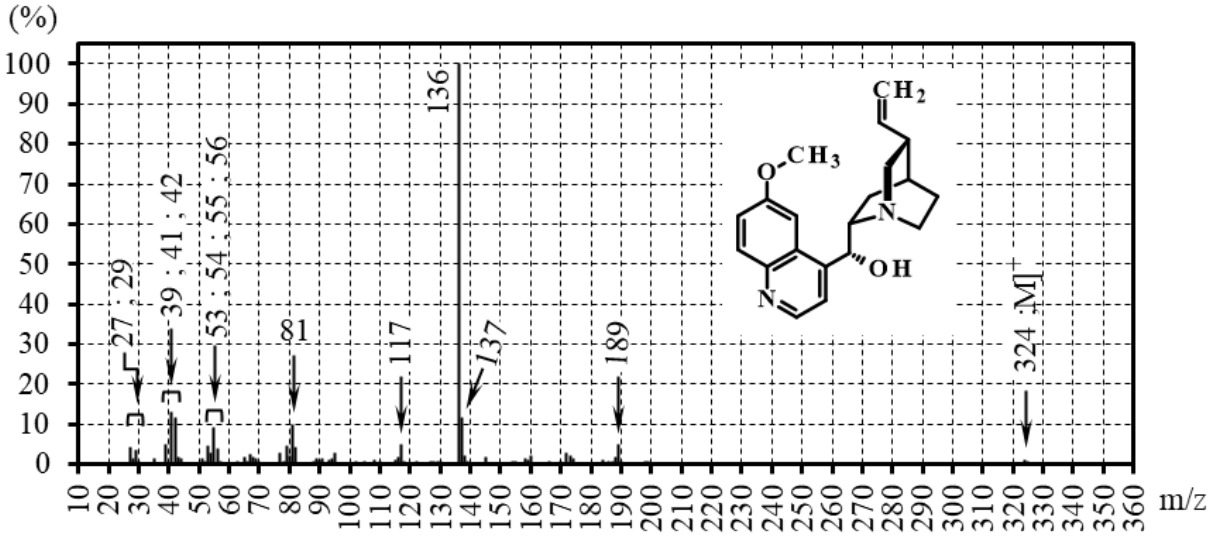

Pyrilamine - CAS 91-84-9 - EI - NIST 408611



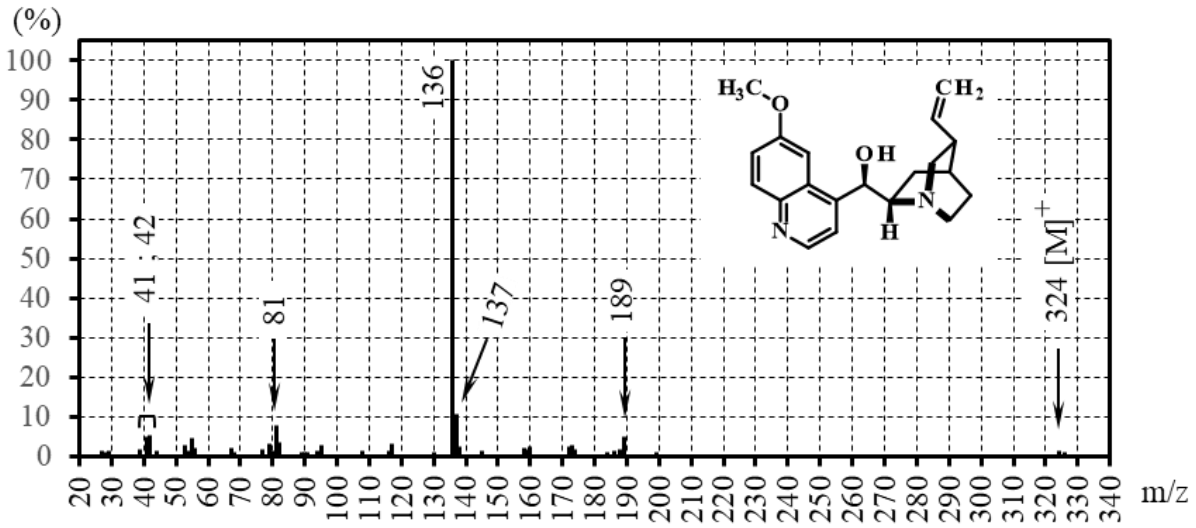

Pyrrobutamine (Pyrrobutamide , Copyronil) - CAS 91-82-7 - EI - NIST 246854



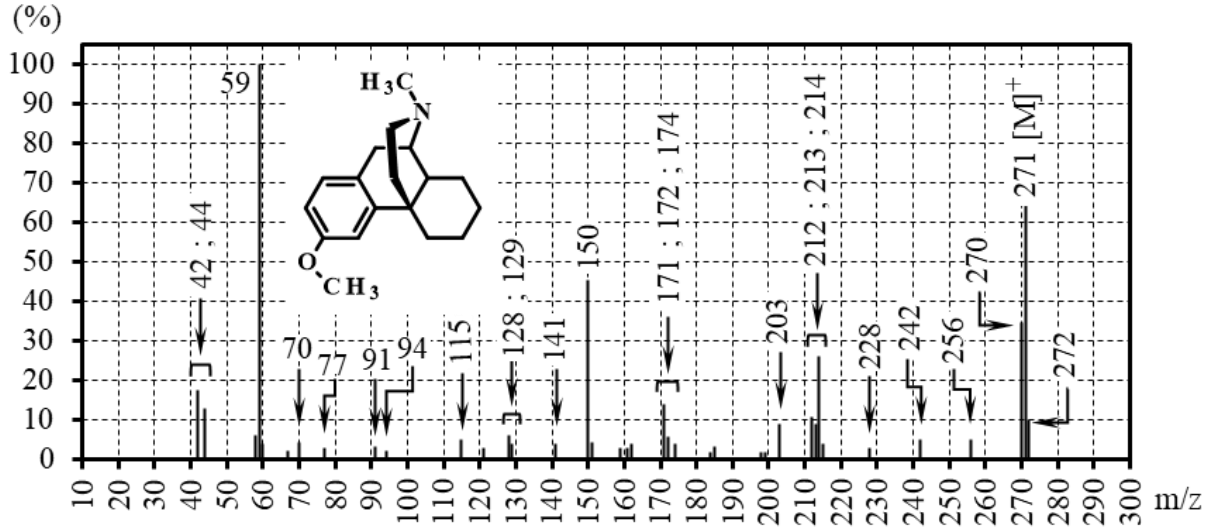

Quinidine - CAS 56-54-2 - EI - NIST 125804



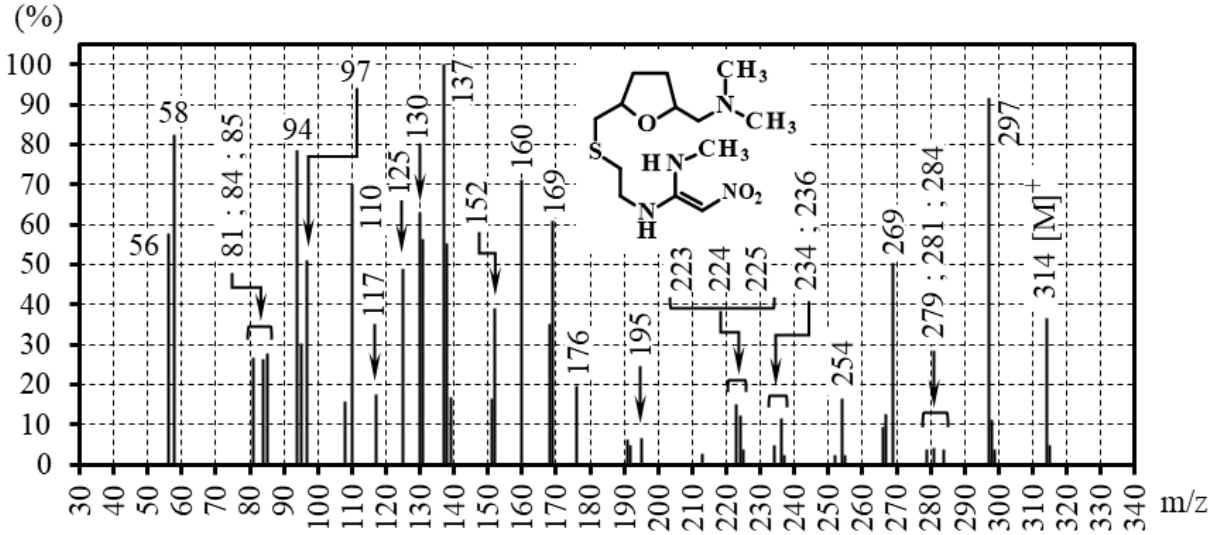

Quinine - CAS 130-95-0 - EI - NIST 107180



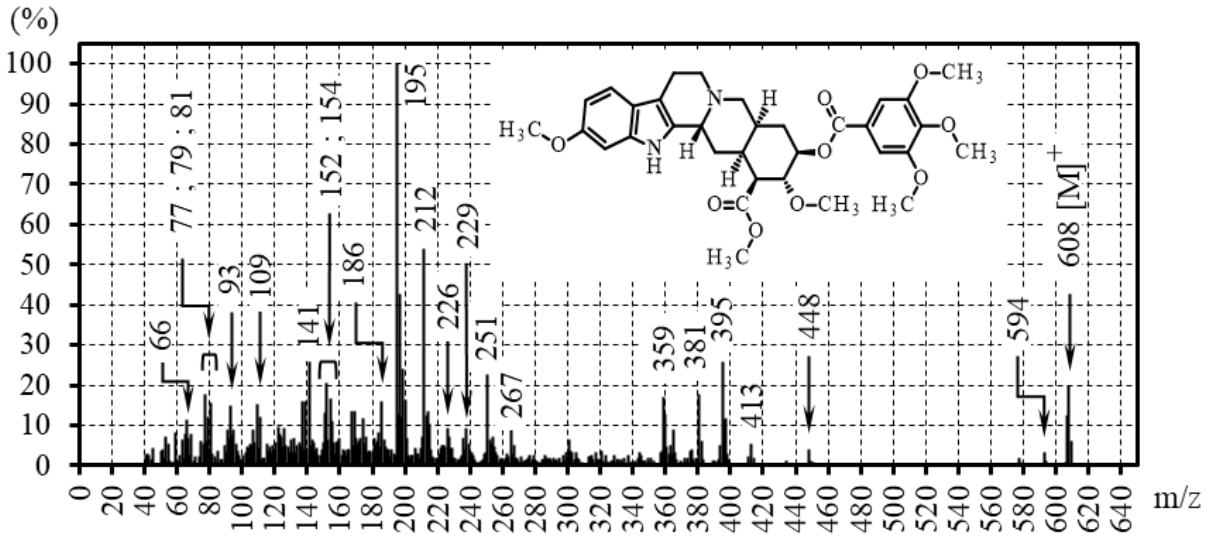

Quinine - CAS 130-95-0 - EI 75 eV - 200 $^{o}$C - 130 $^{o}$C - SDBS 2170



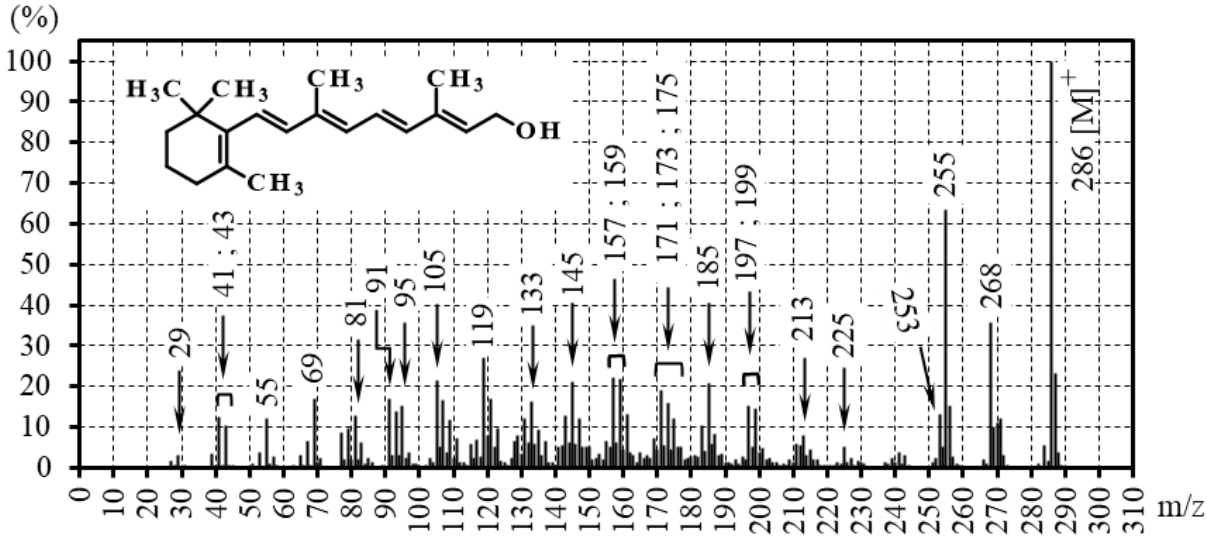

Racemethorphan - CAS 510-53-2 - EI - NIST 120960



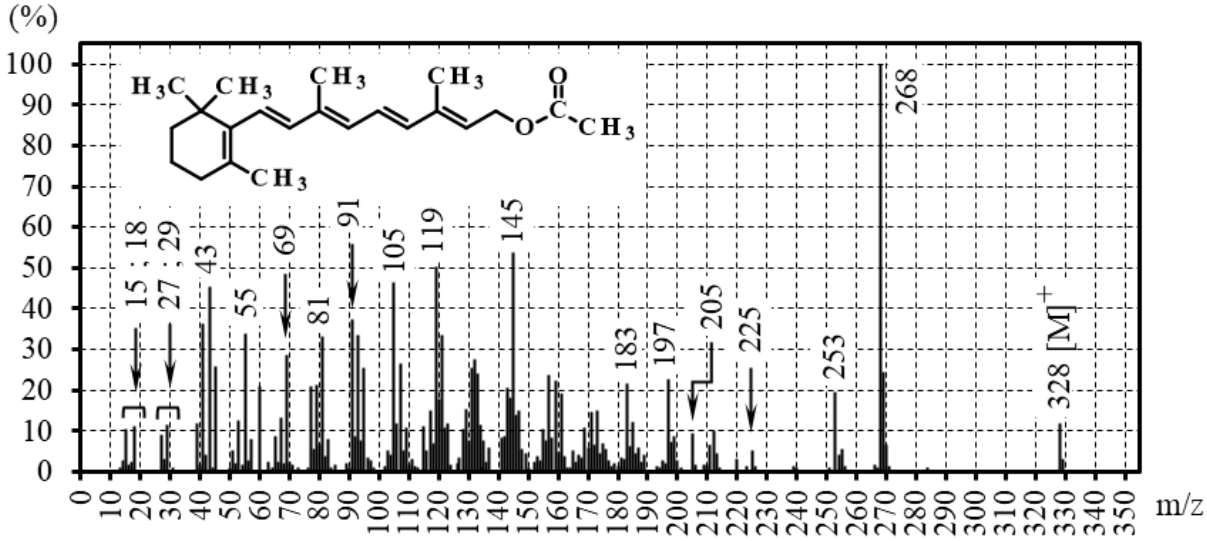

Ranitidine - CAS 66357-35-5 - EI - NIST 120443



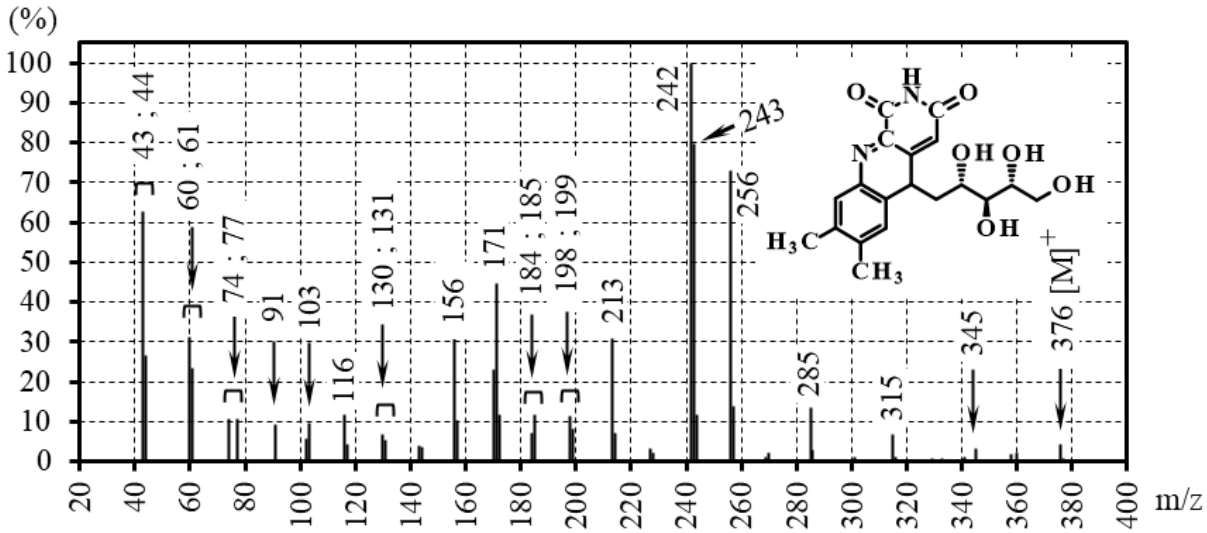

Reserpine - CAS 50-55-5 - EI 70 eV - NIST 248144



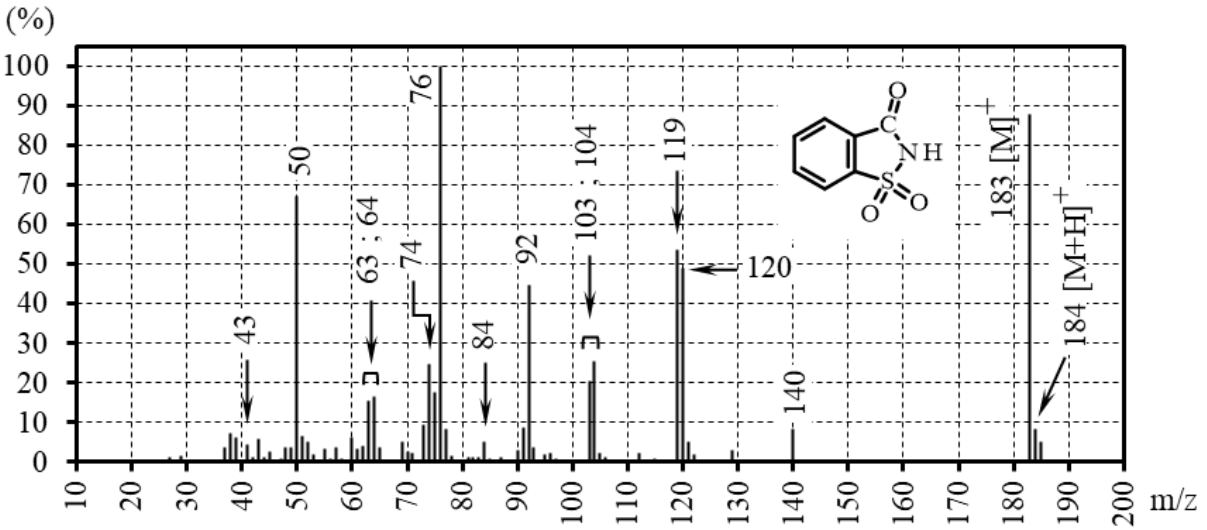

Retinol (all trans) - CAS 68-26-8 - NIST 238604



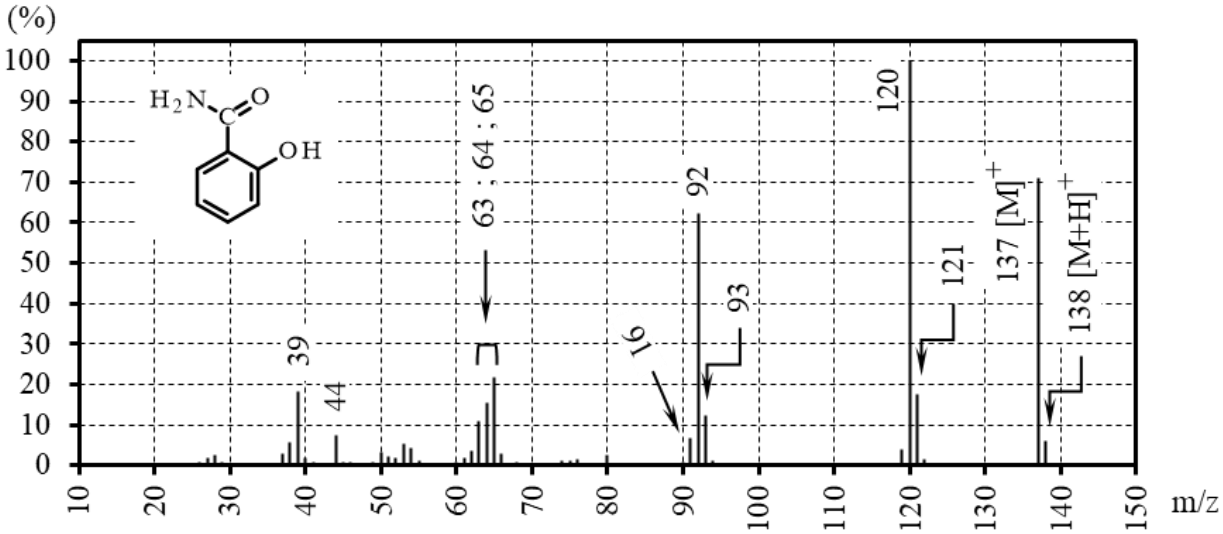

Retinol acetate - CAS 127-47-9 - SDBS 9012 - NIST 233347



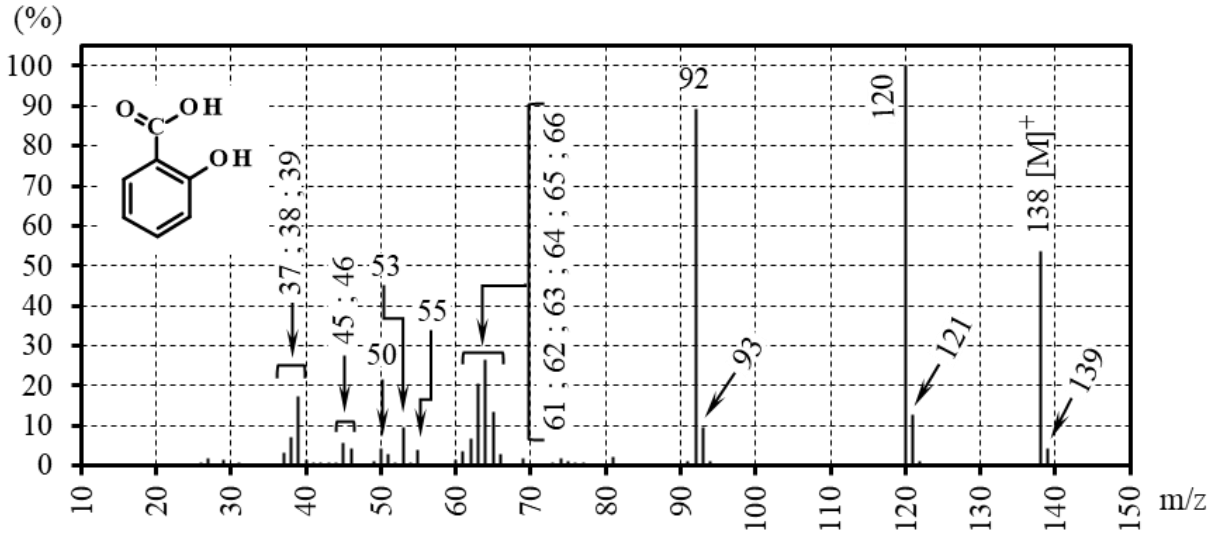

Riboflavine - CAS 83-88-5 - EI - NIST 120239



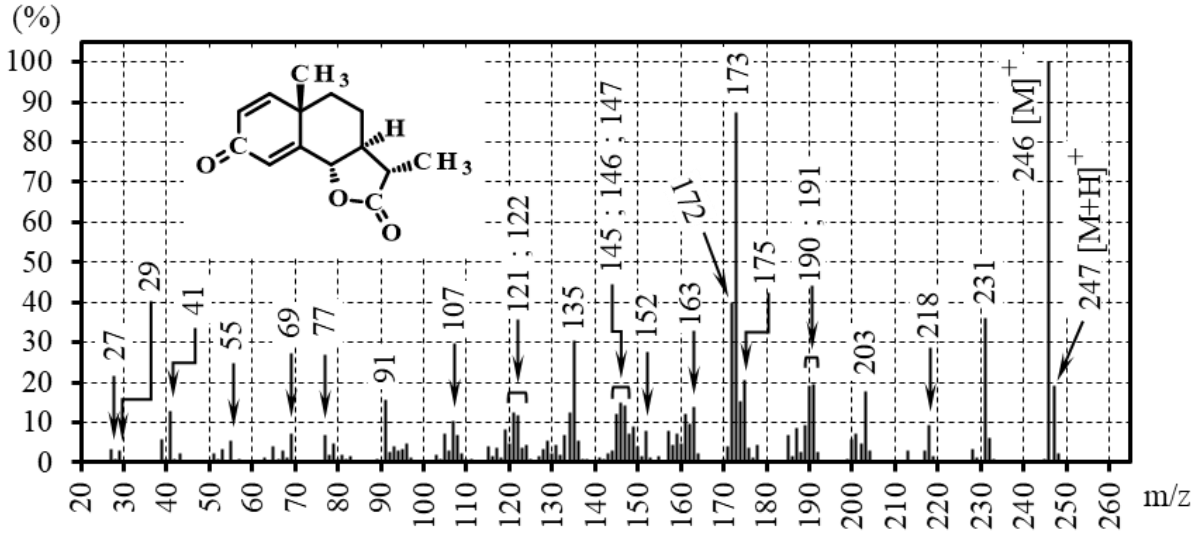

Saccharin - CAS 81-07-2 - NIST 290638



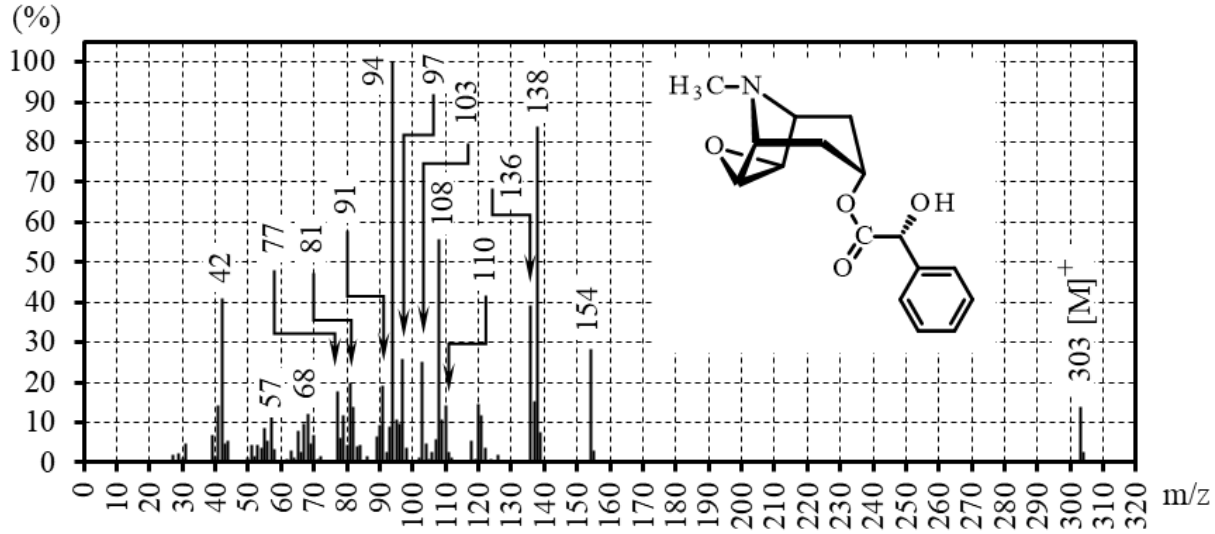

Salicylamide - CAS 65-45-2 - EI - NIST 229916



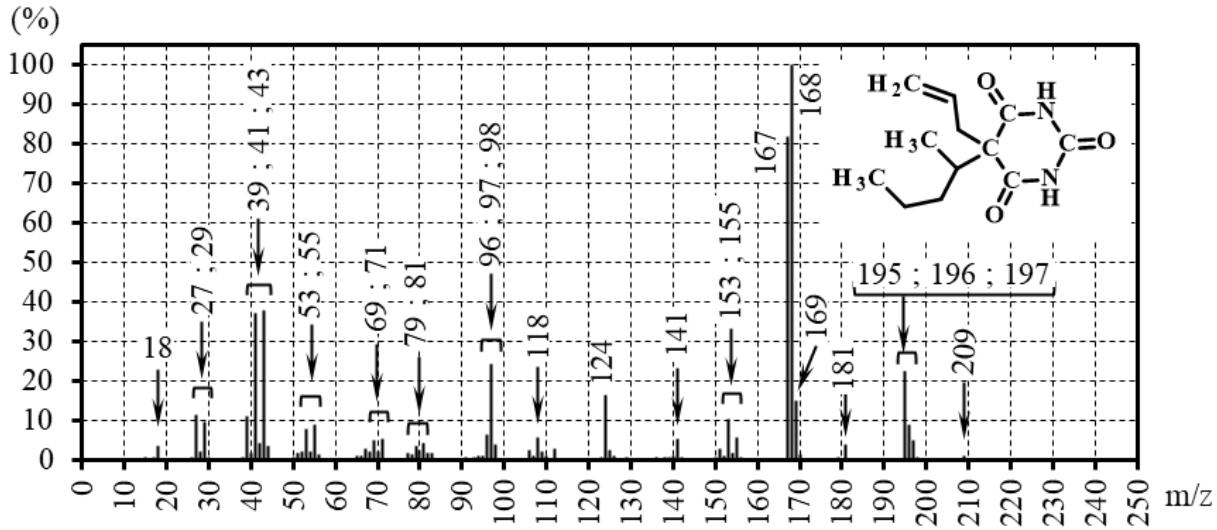

Salicylic acid - CAS 69-72-7 - EI 70 eV - NIST 375214



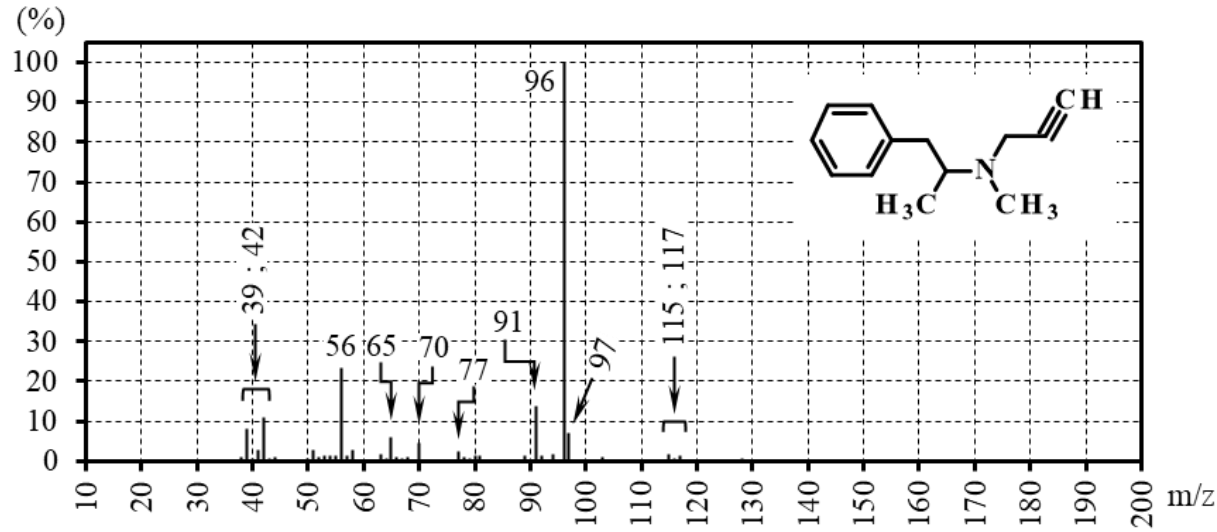

Santonin (alpha) - CAS 481-06-1 - NIST 23974



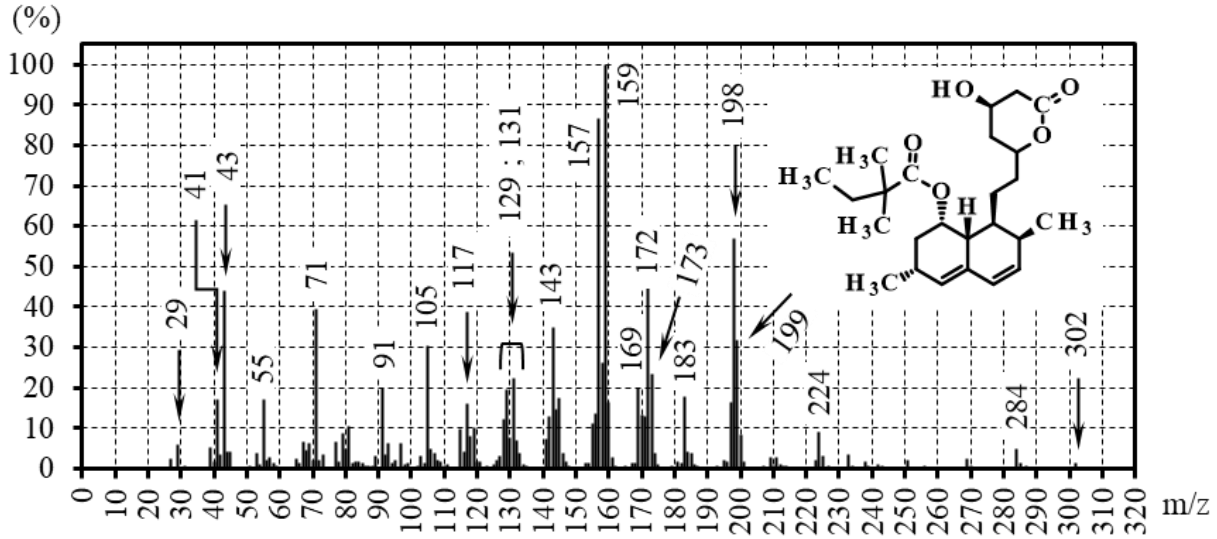

Scopolamine - CAS 51-34-3 - NIST 290684



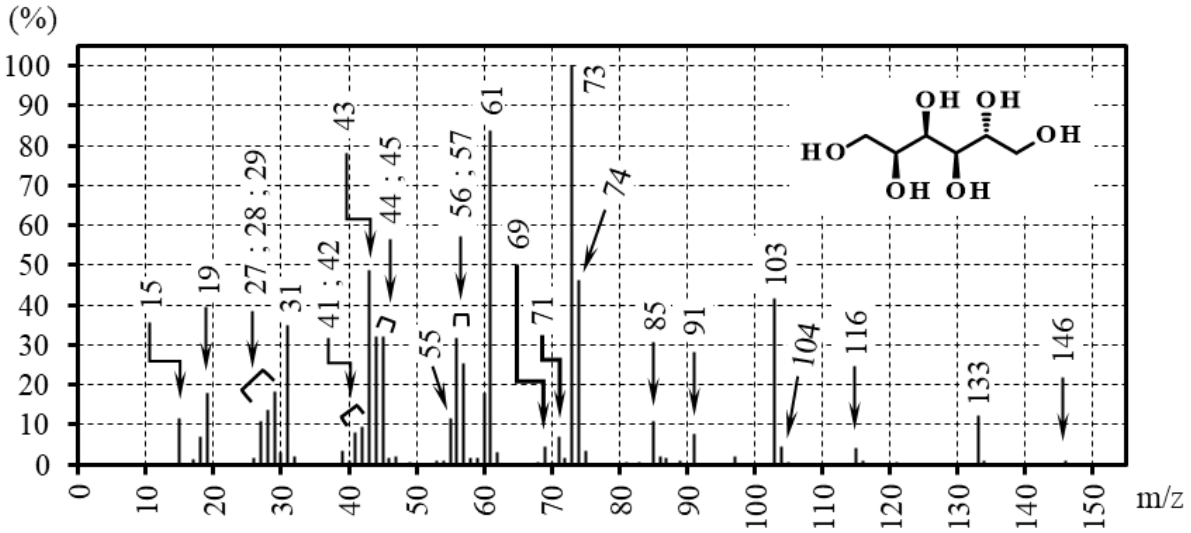

Secobarbital - CAS 76-73-3 - EI - NIST 232637



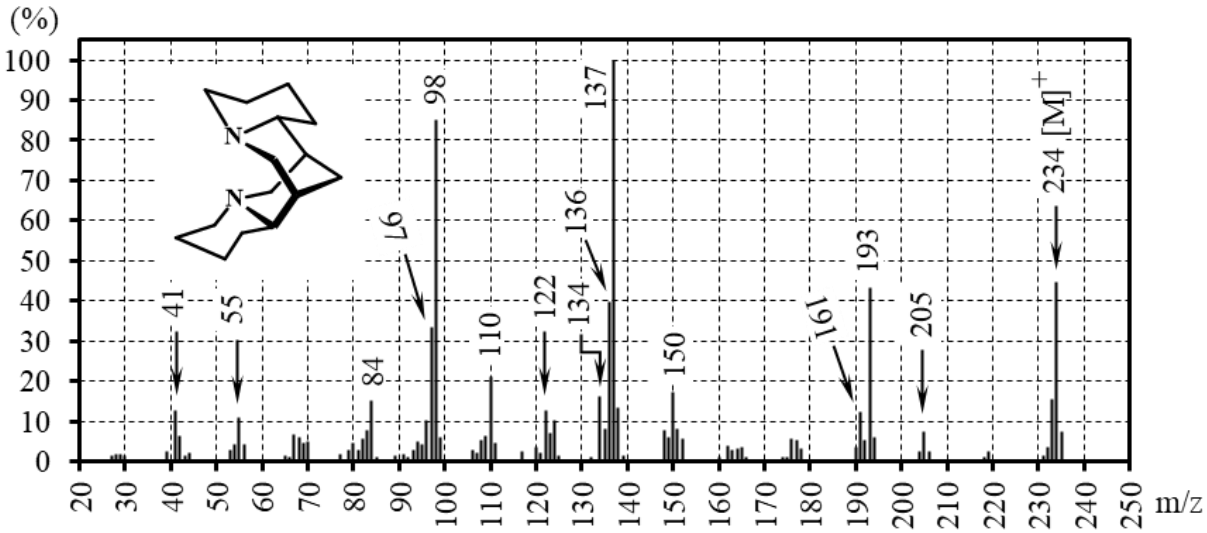

Selegiline - CAS 14611-51-9 - EI - NIST 247283



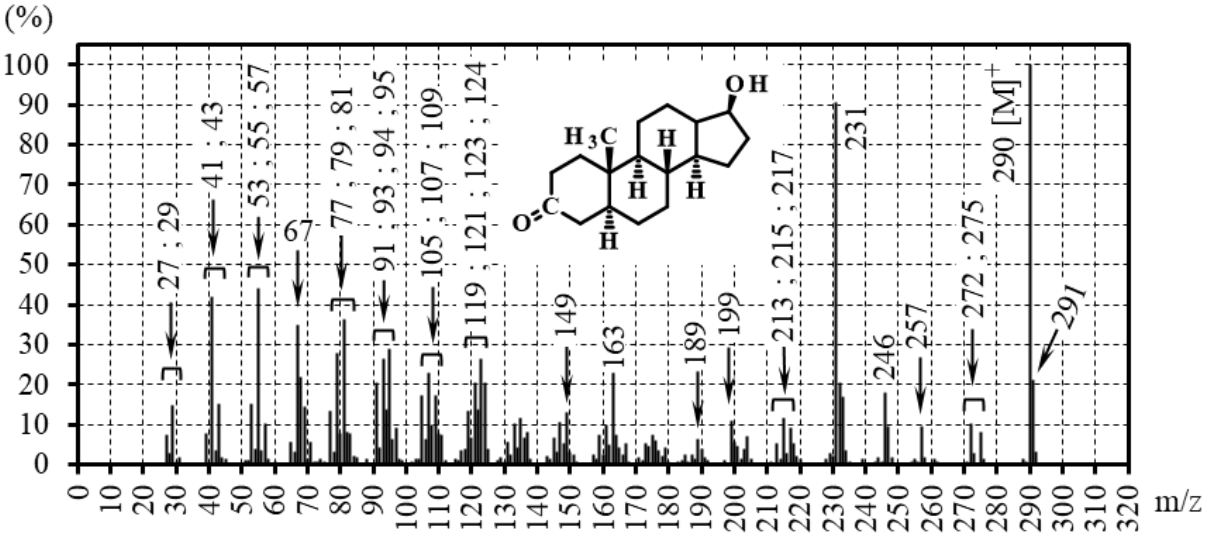

Simvastatin - CAS 79902-63-9 - EI - NIST 334005



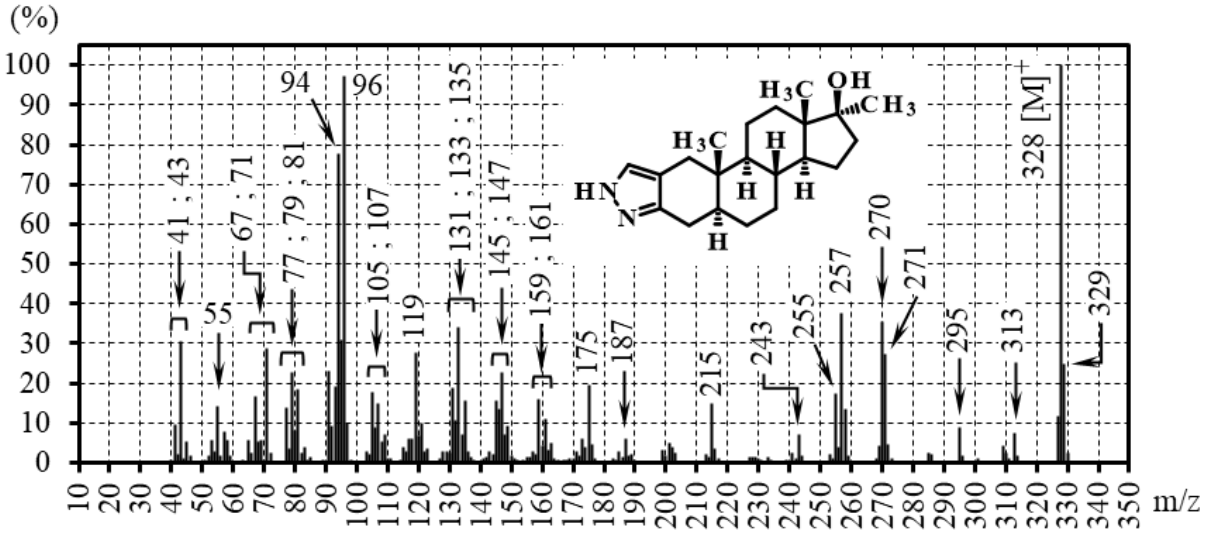

Sorbitol - CAS 50-70-4 - NIST 229600



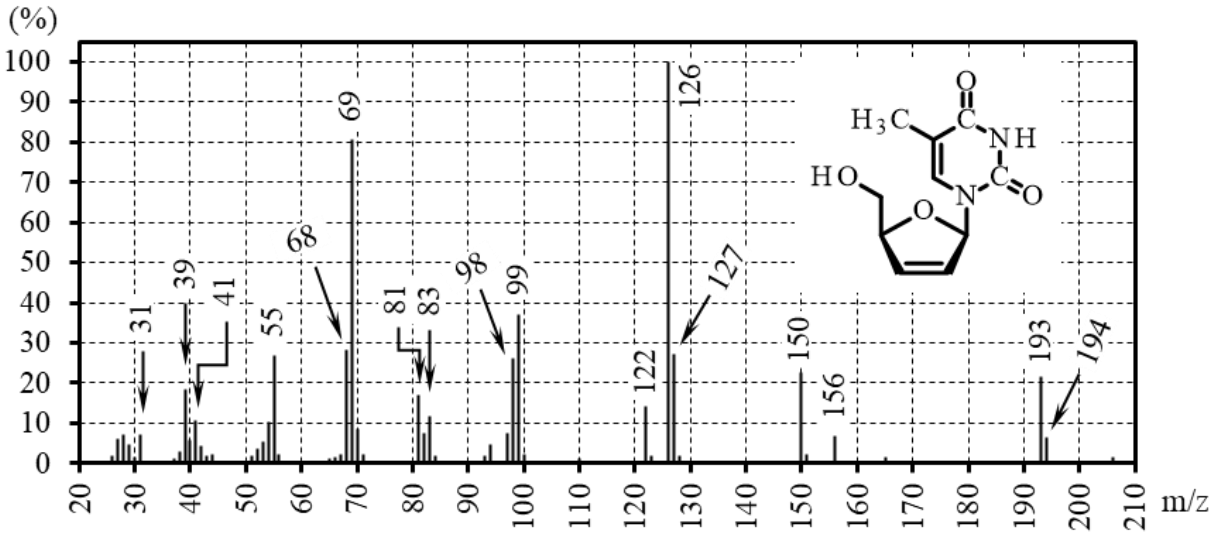

Sparteine - CAS 90-39-1 - NIST 164482 - SDBS 16462



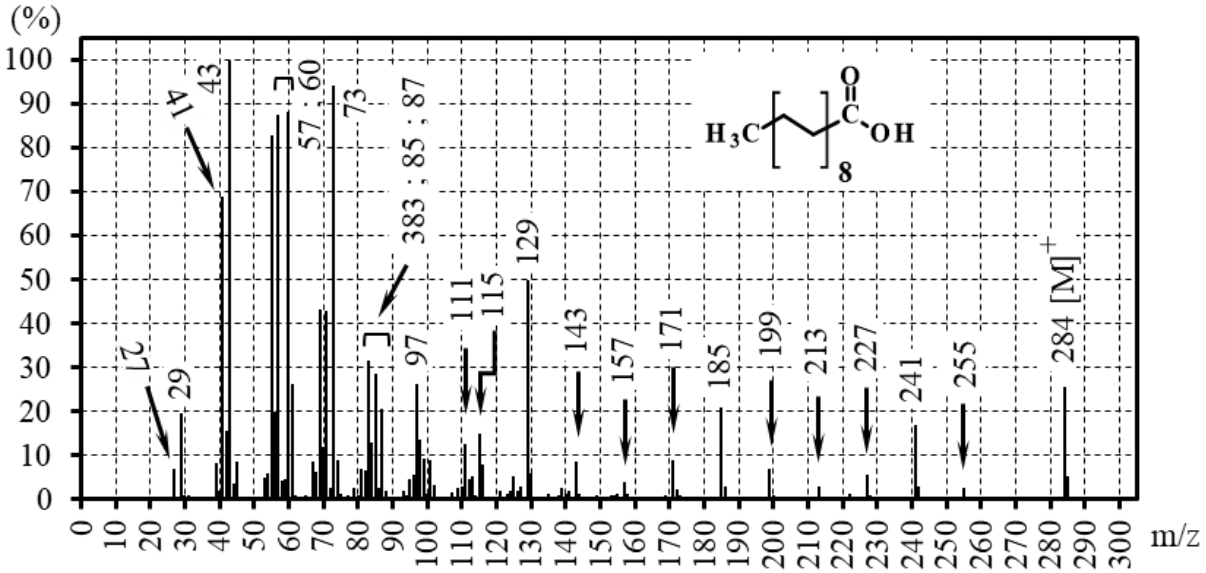

Stanolone (Dihydrotestosterone)- CAS 521-18-6 - EI - NIST 62018



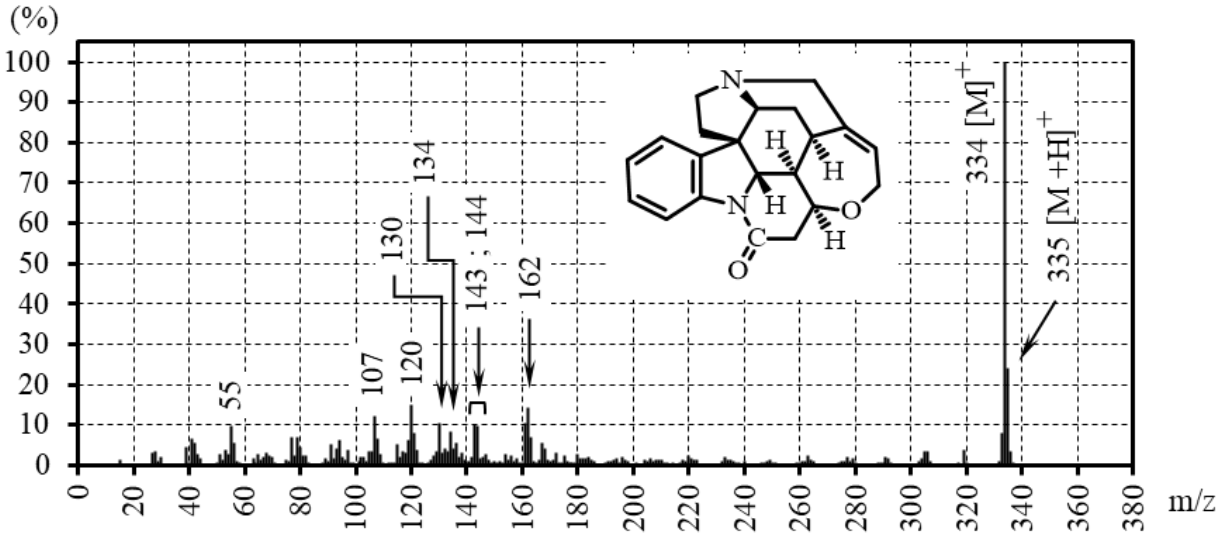

Stanozolol - CAS 10418-03-8 - EI - NIST 248148



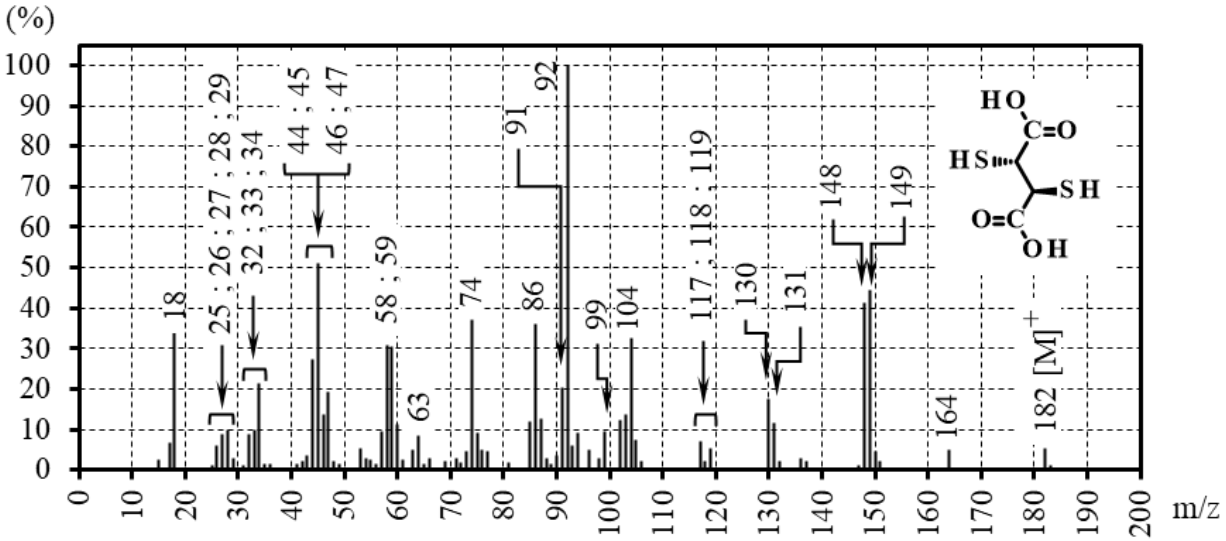

Stavudine - CAS 3056-17-5 - EI 70 eV - SDBS 52178



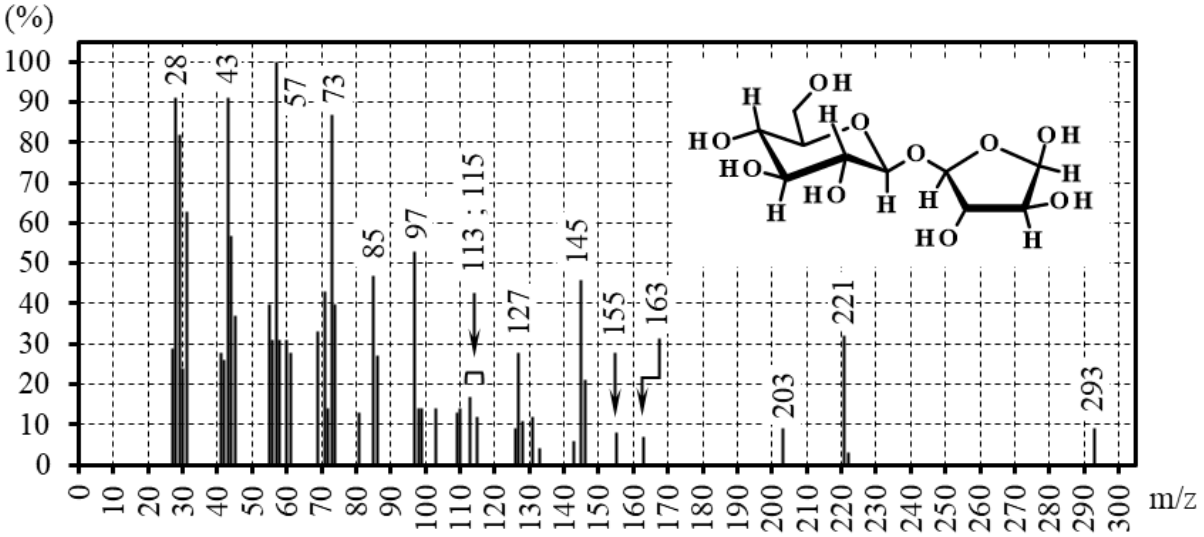

Stearic acid - CAS 57-11-4 - EI - NIST 290961



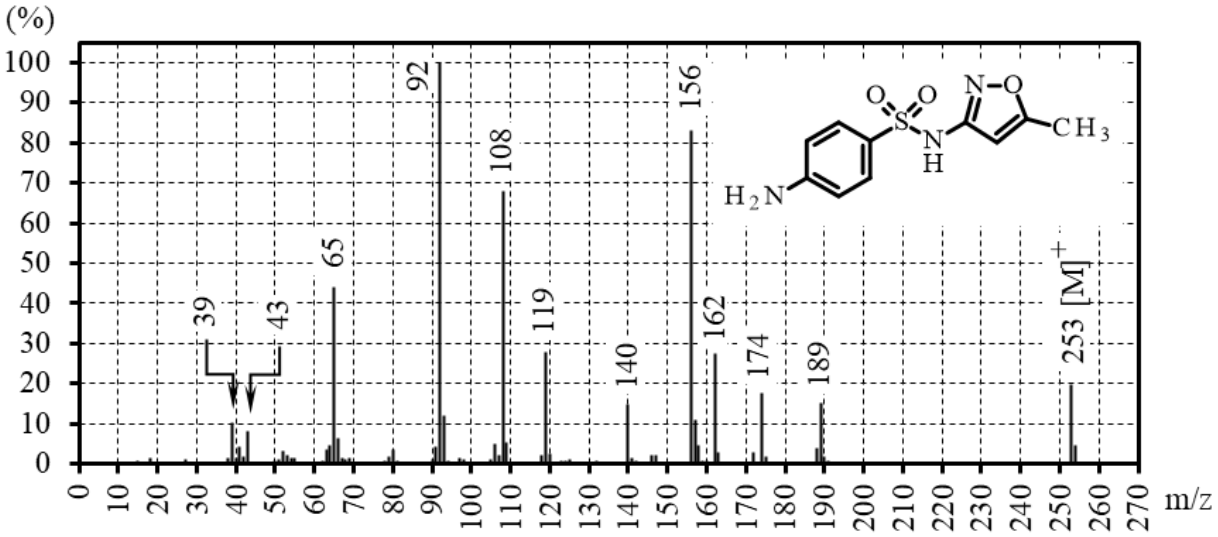

Strychnine - CAS 57-24-9 - EI - NIST 232994



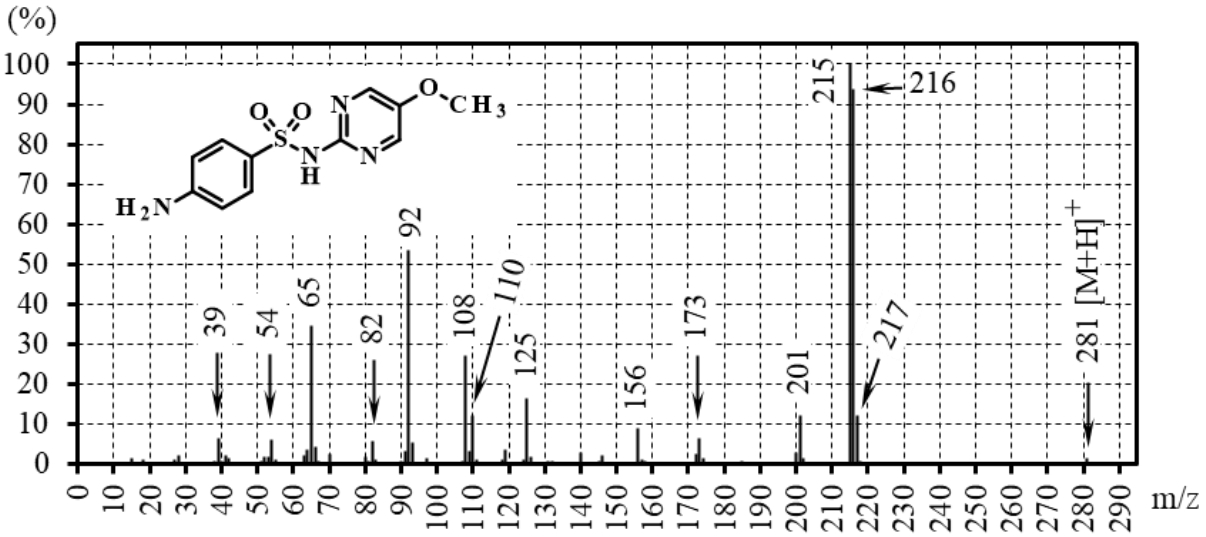

Succimer - CAS 304-55-2 - SDBS 18070



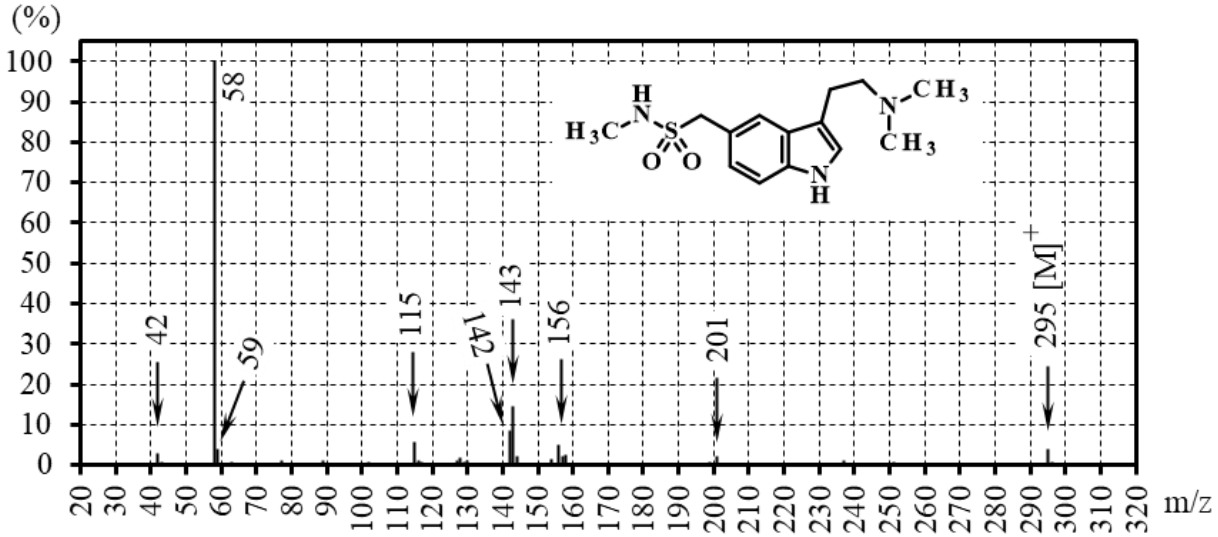

Sucrose - CAS 57-50-1 - NIST 404101



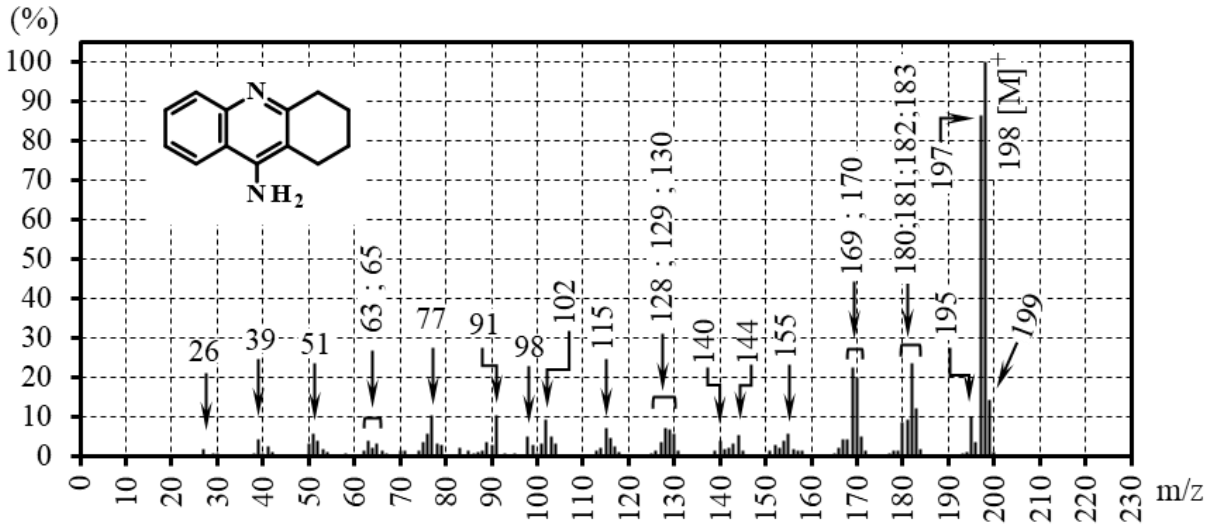

Sulfamethoxazole - CAS 723-46-6 - EI - NIST 236956



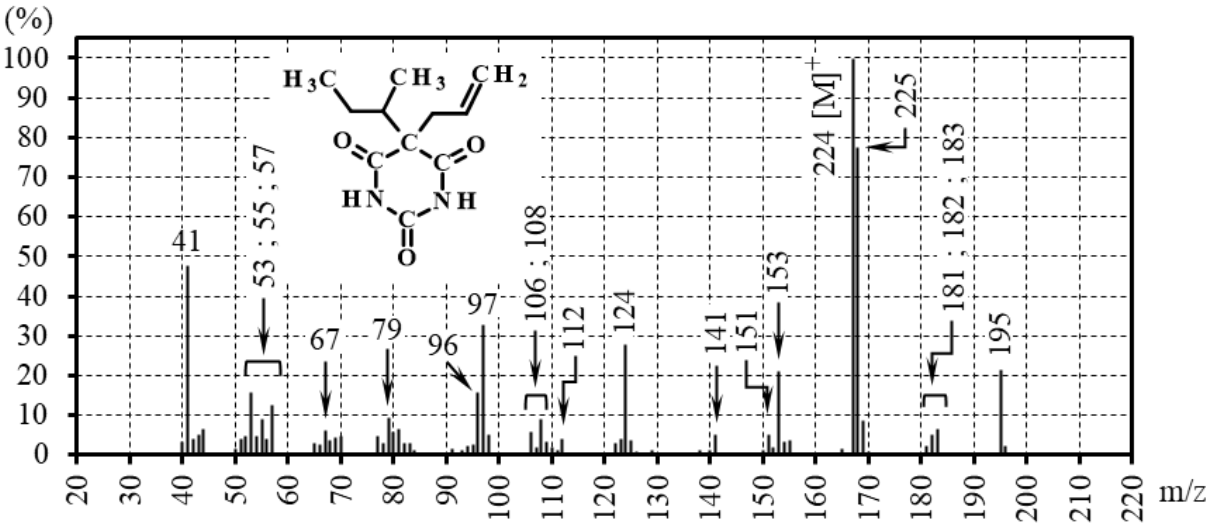

Sulfamethoxydiazine - CAS 651-06-9 - NIST 23043



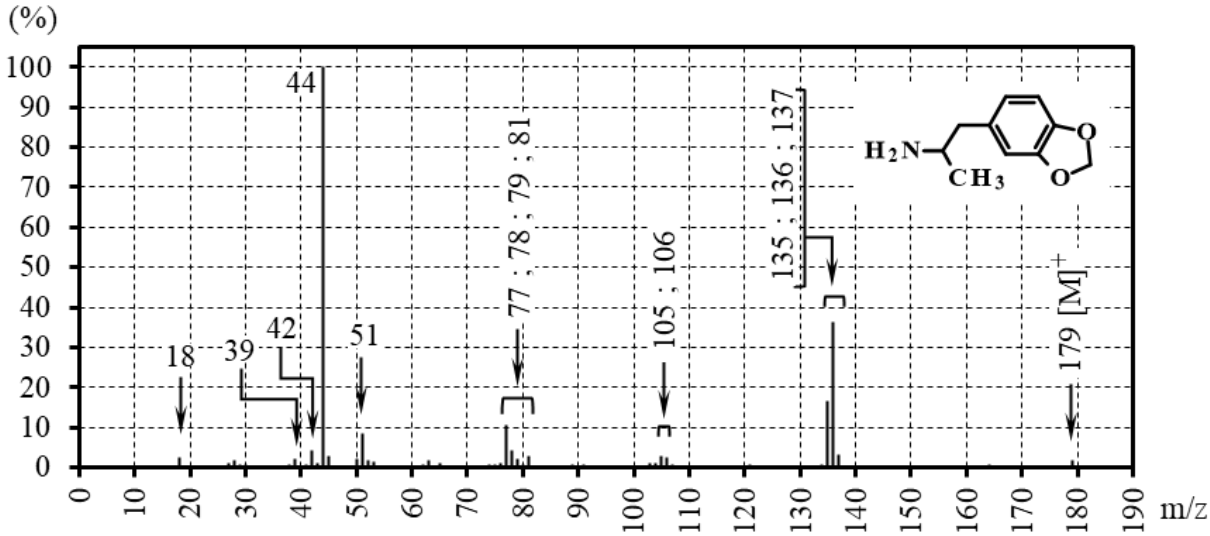

Sumatriptan - CAS 103628-46-2 - NIST 247581



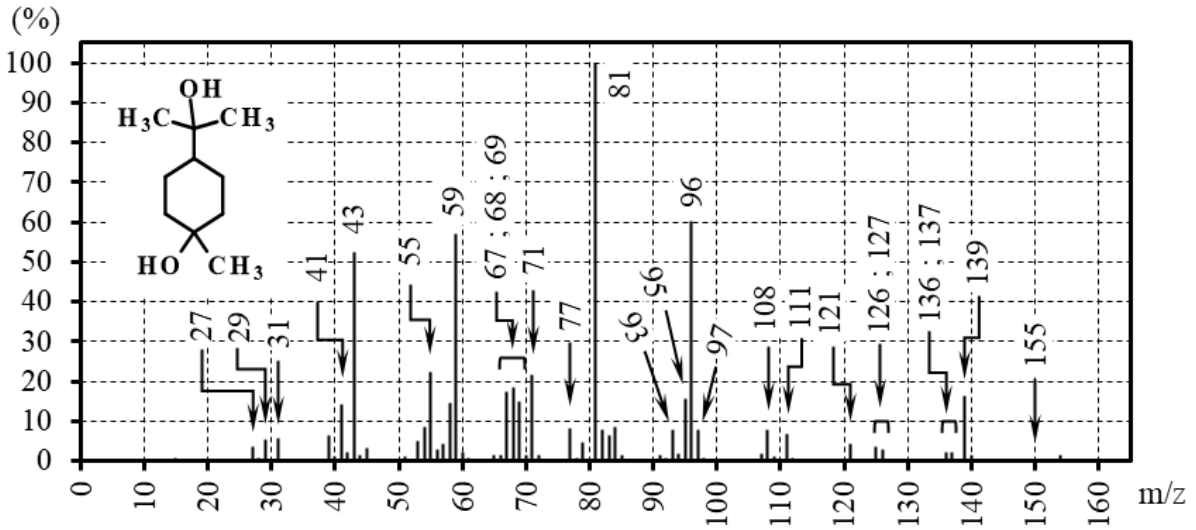

Tacrine - CAS 321-64-2 - EI - NIST 291000



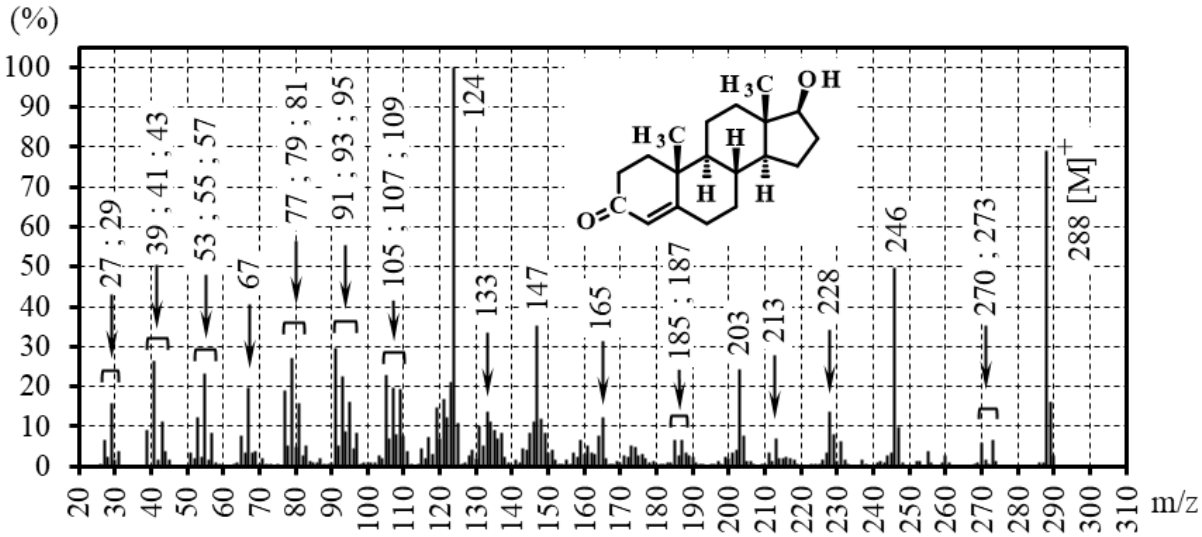

Talbutal - CAS 115-44-6 - EI - NIST 335325



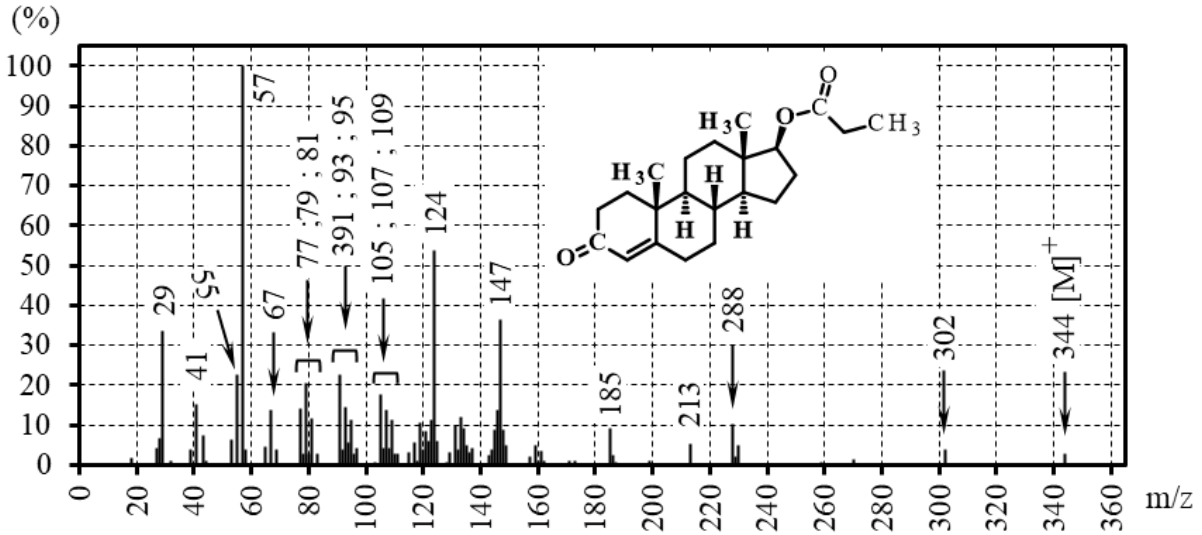

Tenamfetamine - CAS 4764-17-4 - EI - NIST 352965



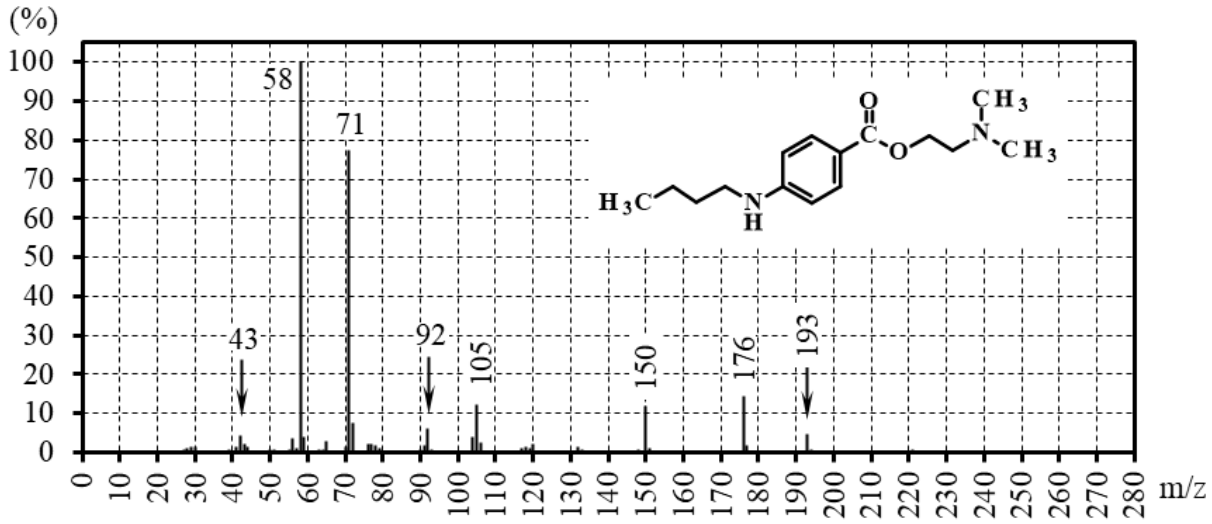

Terpin - CAS 80-53-5 - NIST 292185



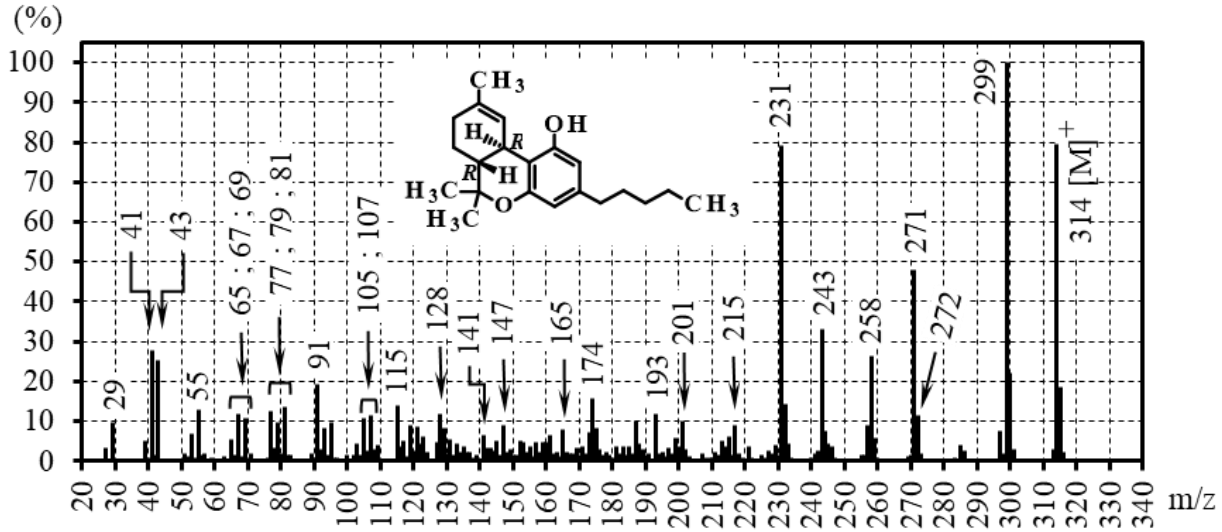

Testosterone - CAS 58-22=0 - NIST 62026



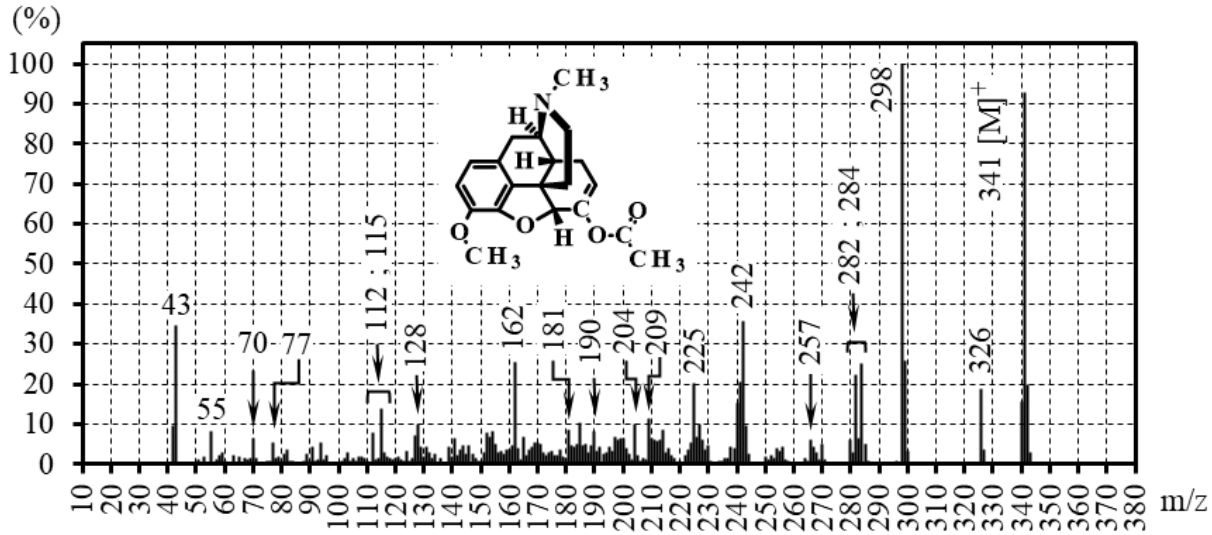

Testosterone propionate - CAS 57-85-2 - NIST 75979



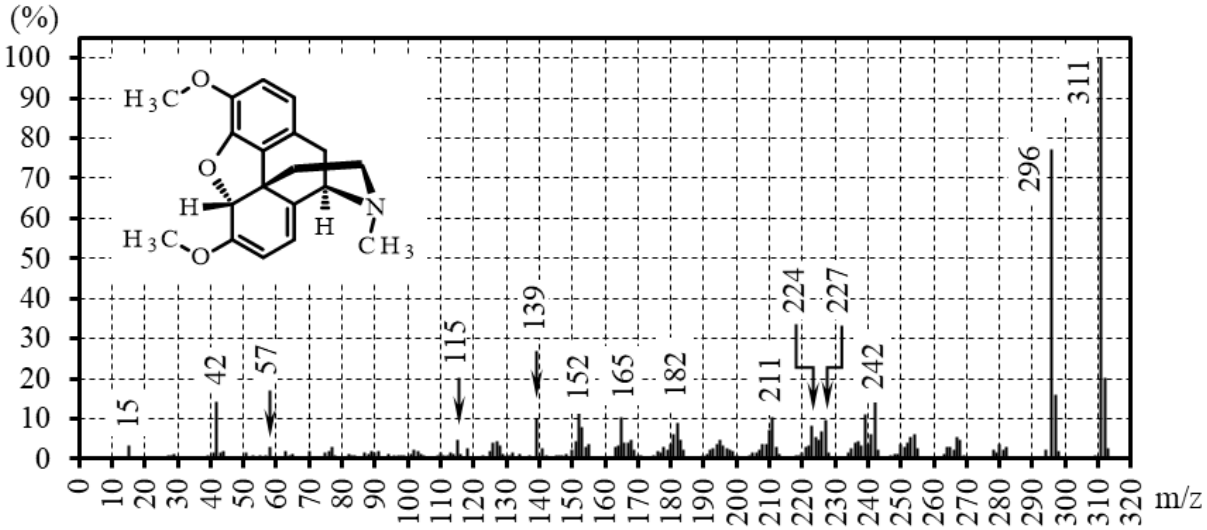

Tetracaine - CAS 94-24-6 - EI - NIST 408051



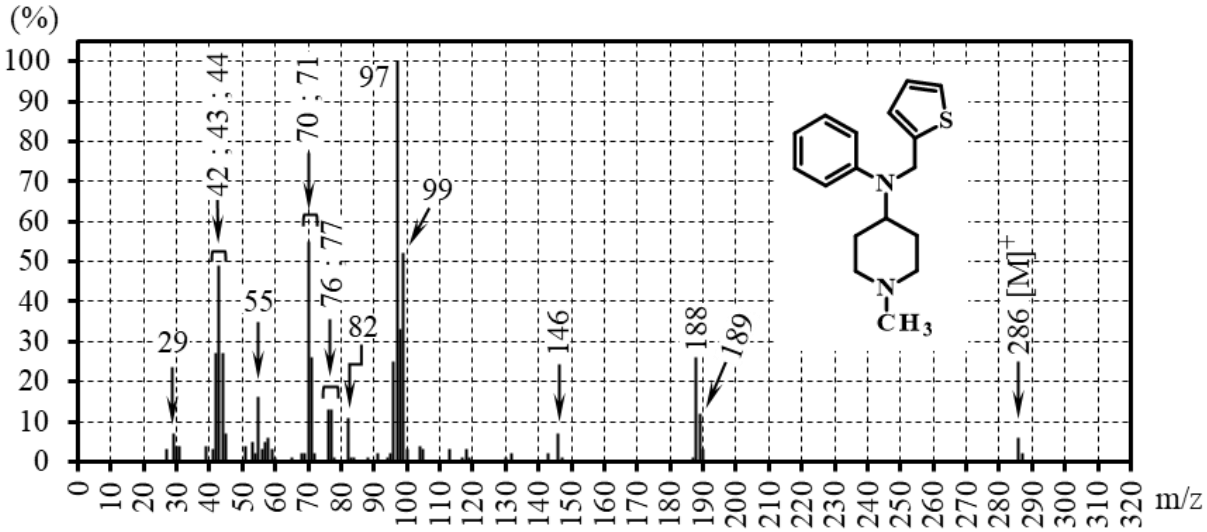

Tetrahydrocannabinol (Dronabinol) - CAS 1972-08-3 - NIST 352175



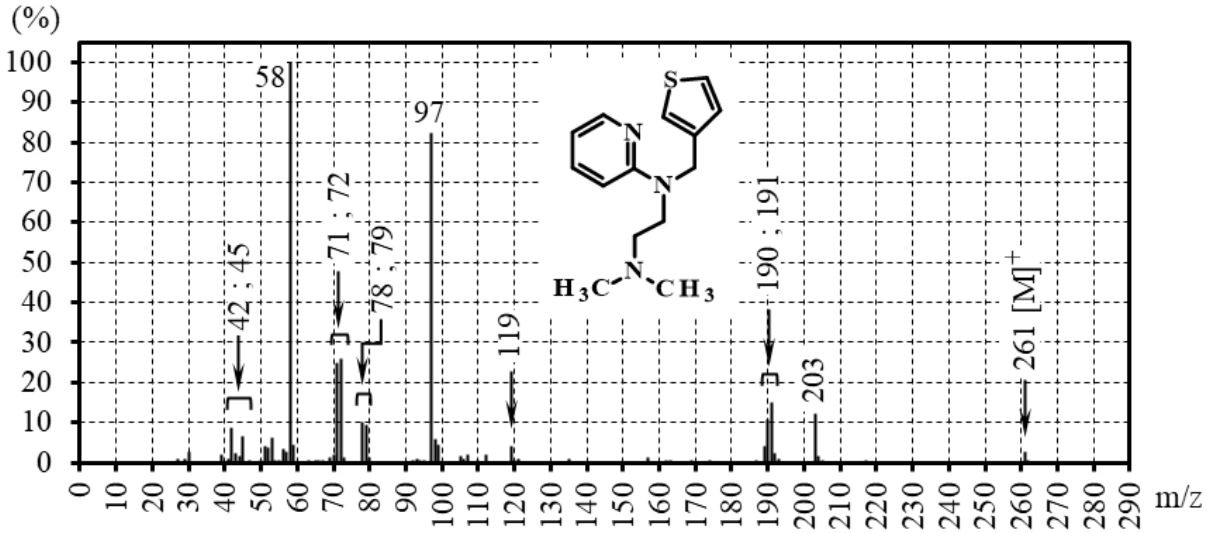

Thebacon - CAS 466-90-0 - NIST 2487531



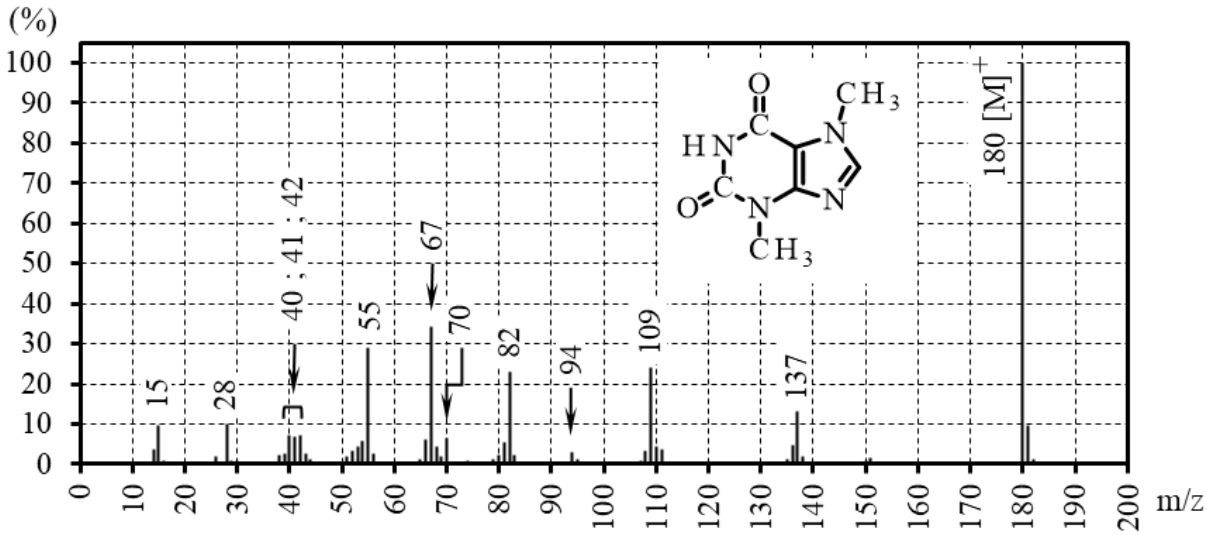

Thebaine - CAS 115-37-7 - EI - NIST 260620



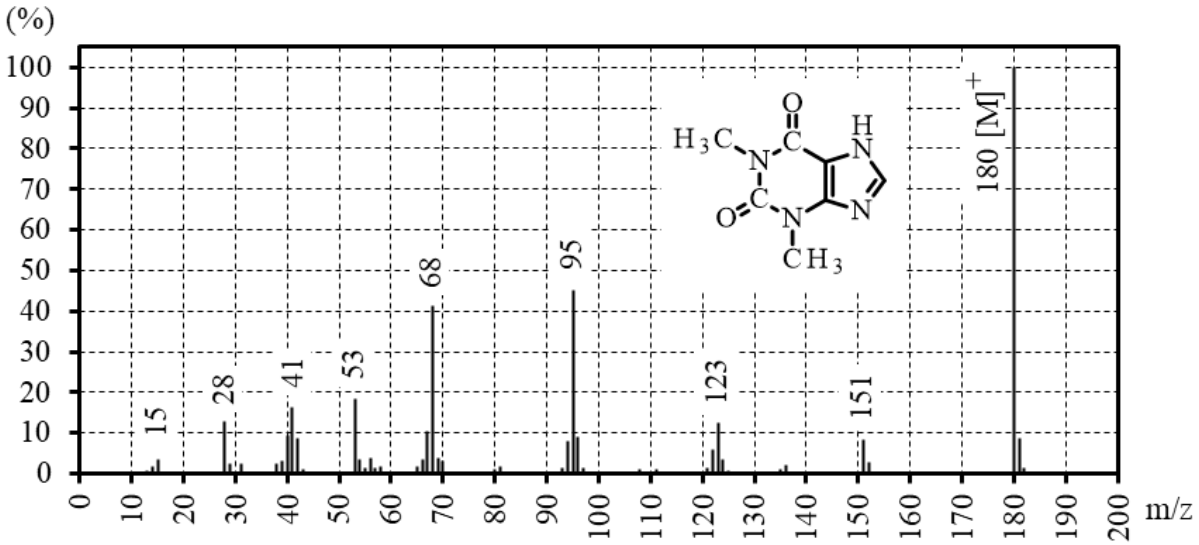

Thenalidine - CAS 86-12-4 - EI - NIST 298782



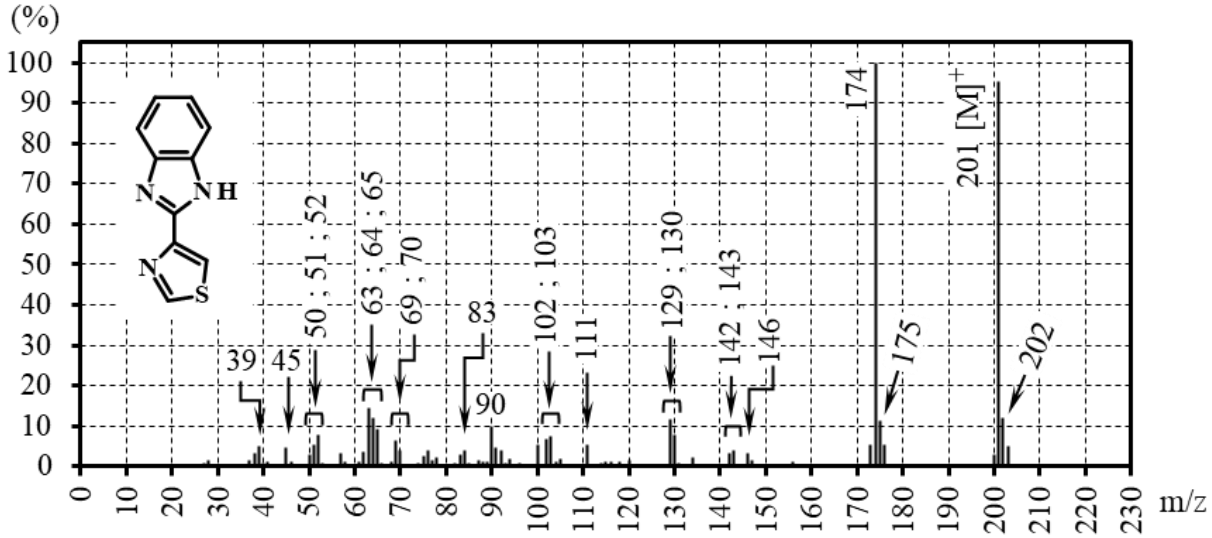

Thenyldiamine = CAS 91-79-2 - EI - NIST 270630



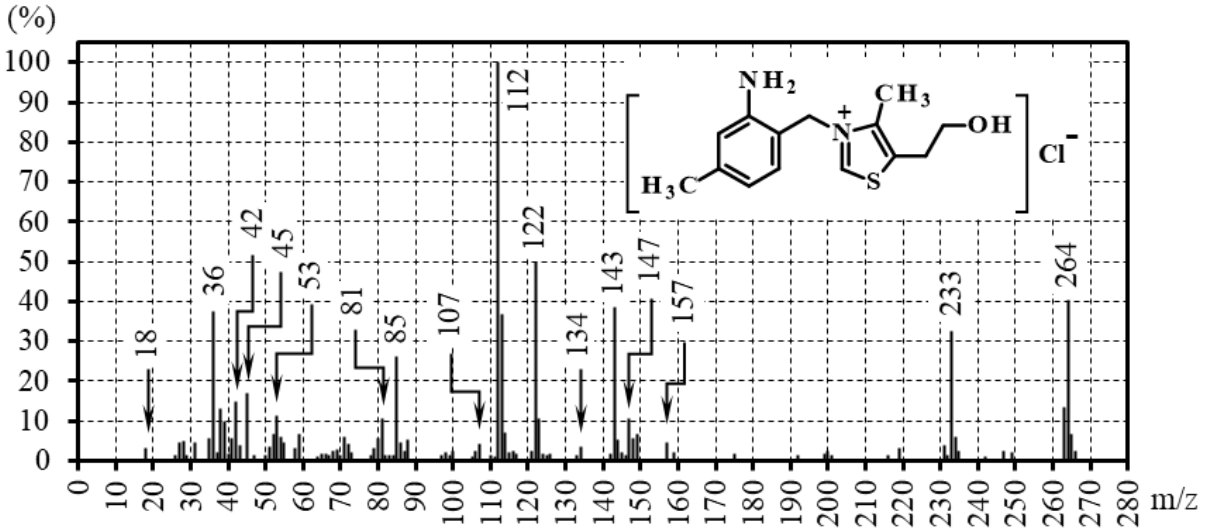

Theobromine - CAS 83-67-2 - NIST 118950



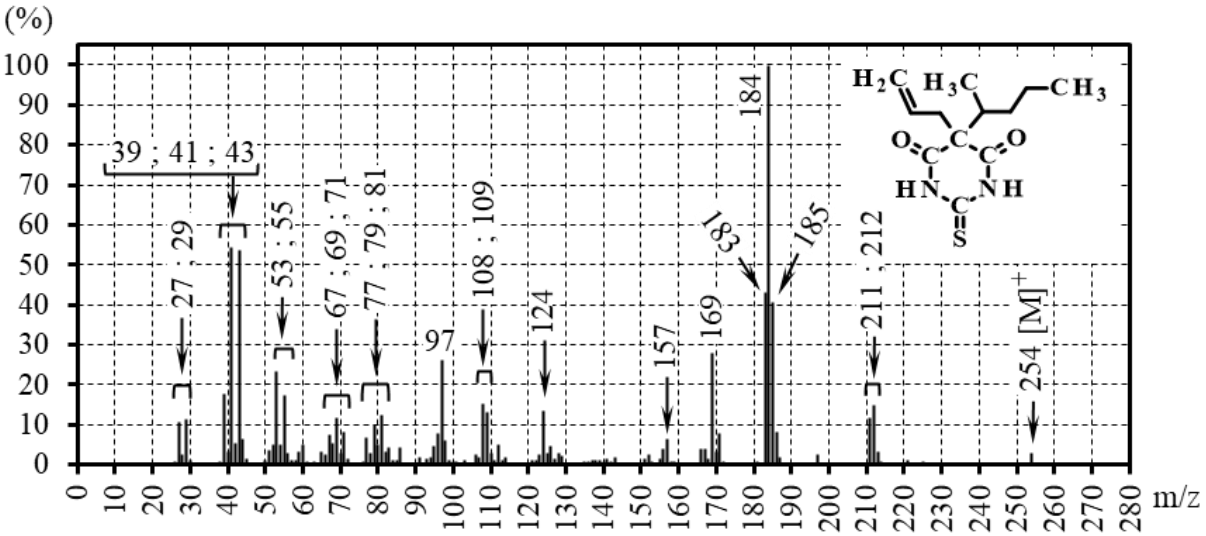

Theophylline - CAS 58-55-9 - NIST 118946 EI 70 eV



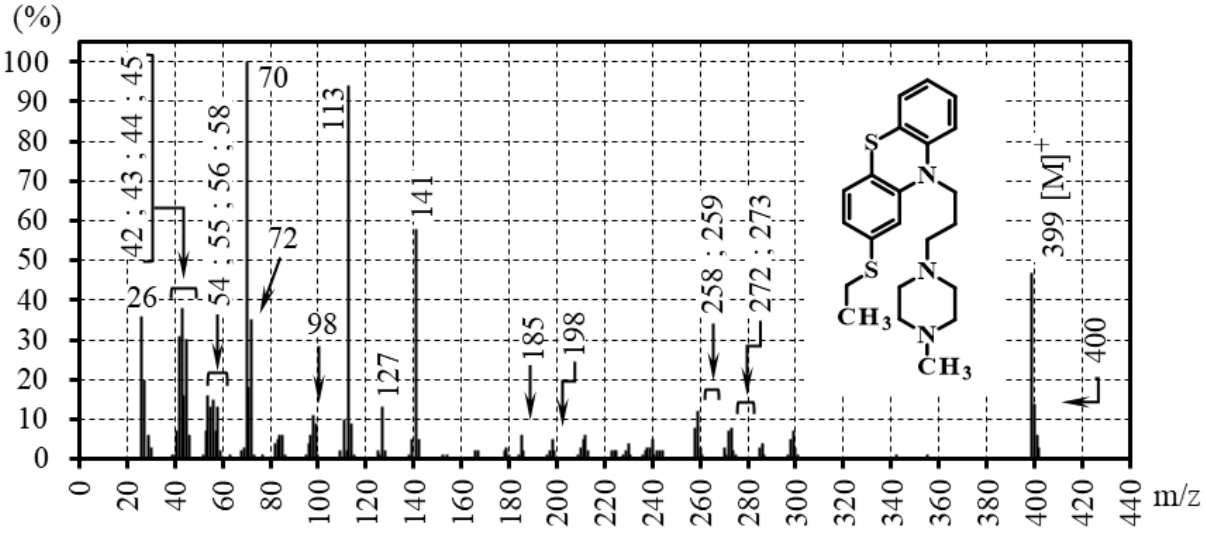

Thiabendazole - CAS 148-79-8 - EI - NIST 408784



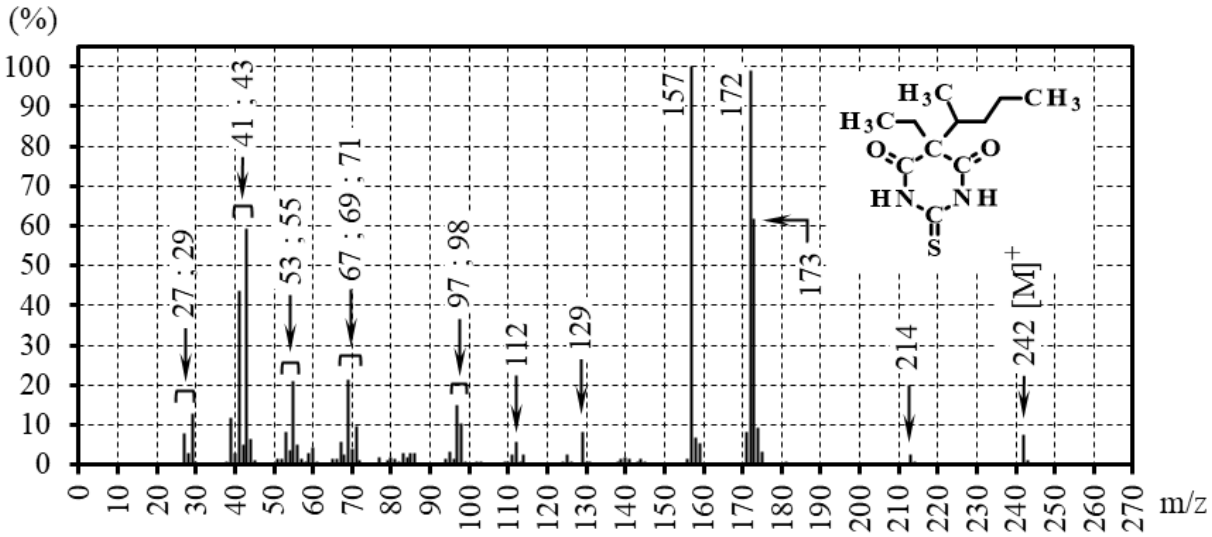

Thiamine hydrochloride - CAS 67-03-8 - EI 75 eV - SDBS 169



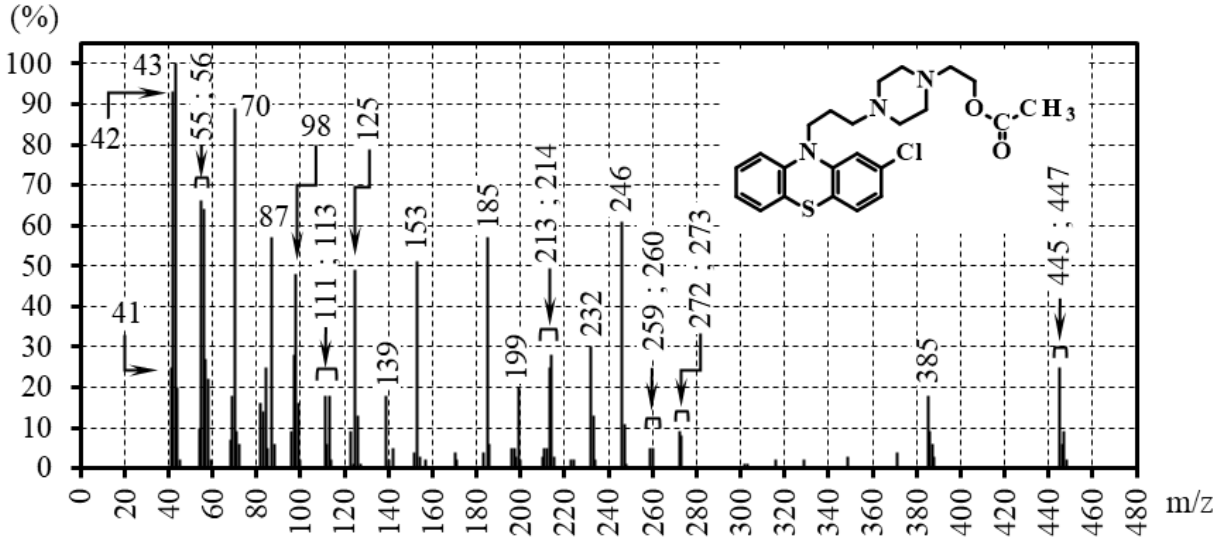

Thiamylal - CAS 77-27-0 - EI - NIST 408763



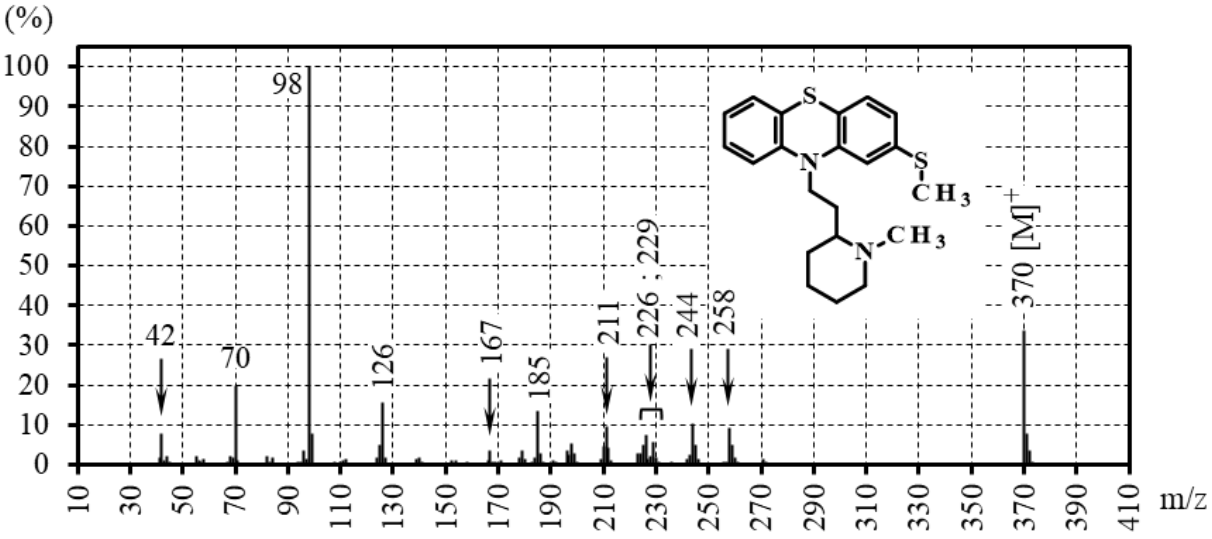

Thiethylperazine - CAS 1420-55-9 - EI - NIST 298763



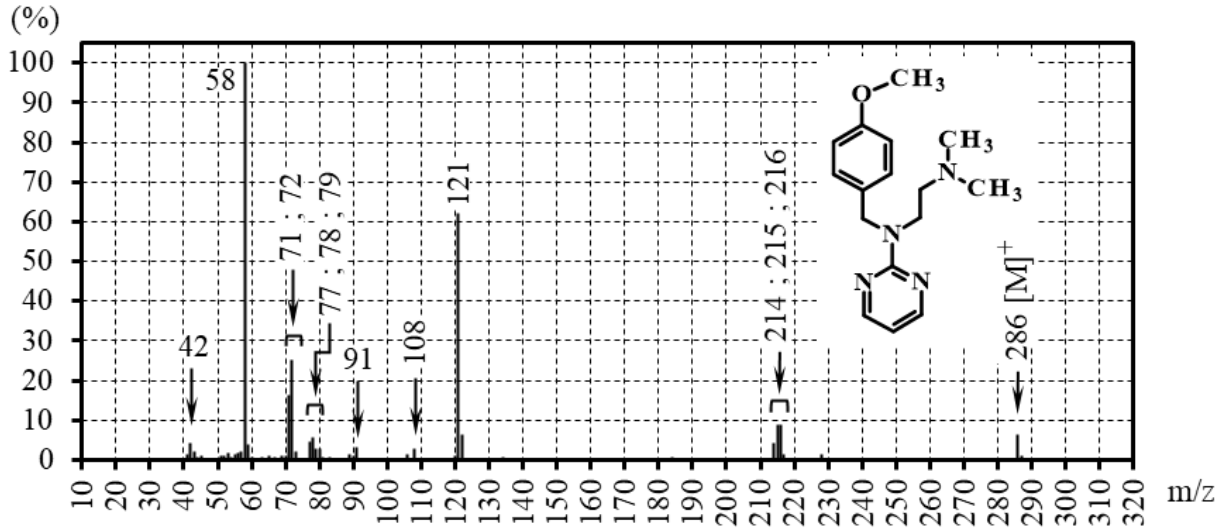

Thiopental - CAS 76-75-5 - EI - NIST 408205



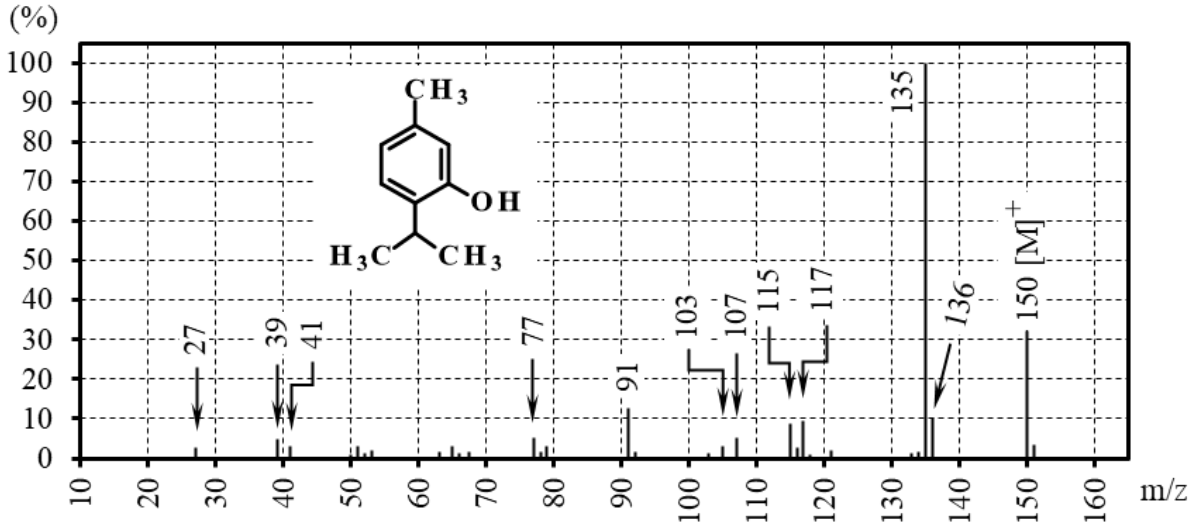

Thiopropazate - CAS 84-06-0 - EI - NIST 23700



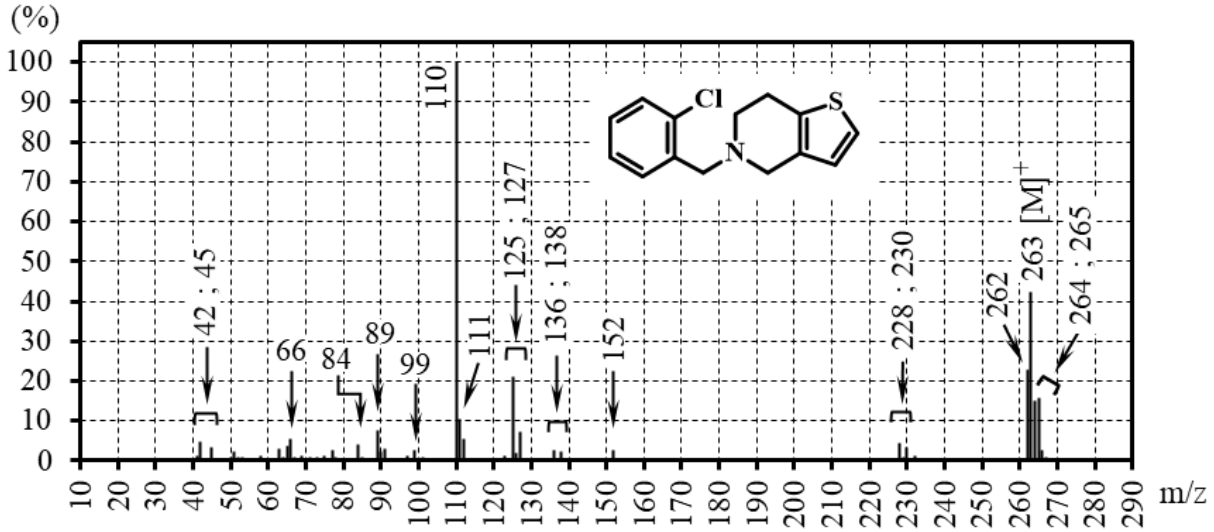

Thioridazine - CAS 50-52-2 - EI - NIST 248121



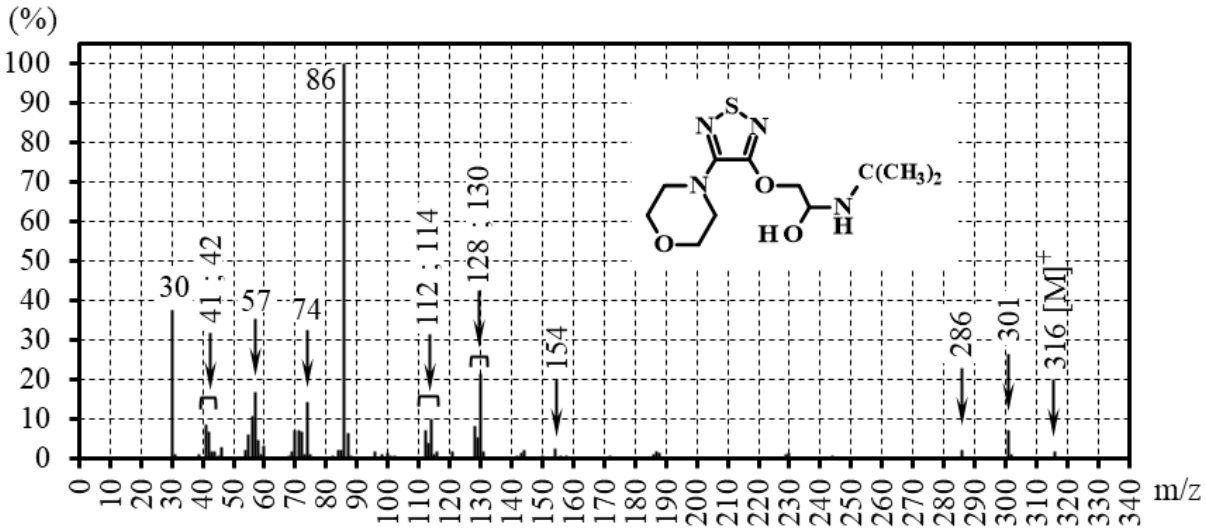

Thonzylamine - CAS 91-85-0 - EI - NIST 246690



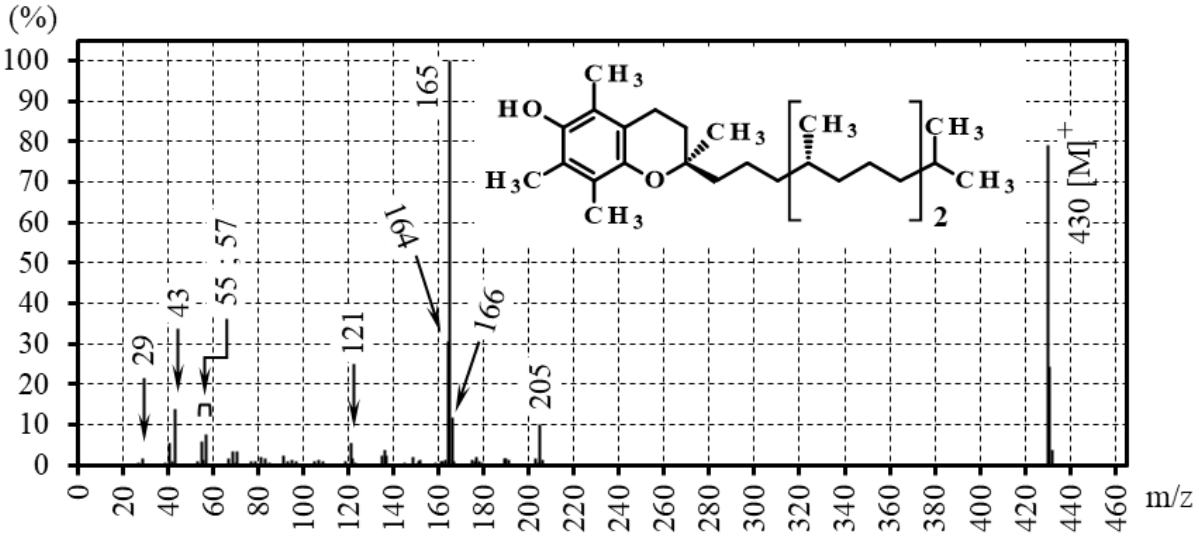

Thymol - CAS 89-83-8 - EI 75 eV - NIST 249386 - SDBS 2404



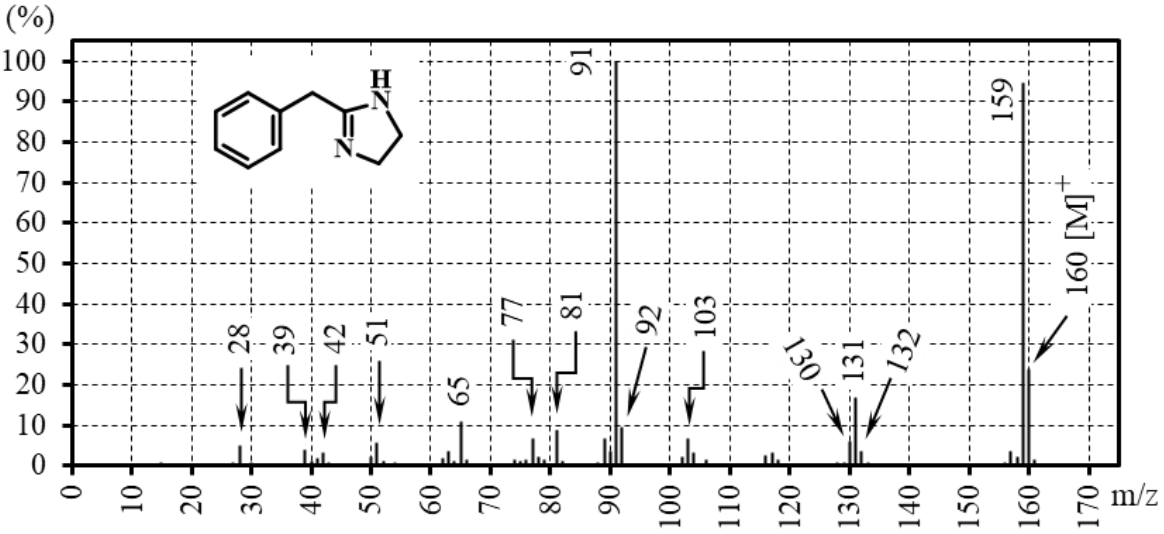

Ticlopidine - CAS 55142-85 - EI - NIST 247263



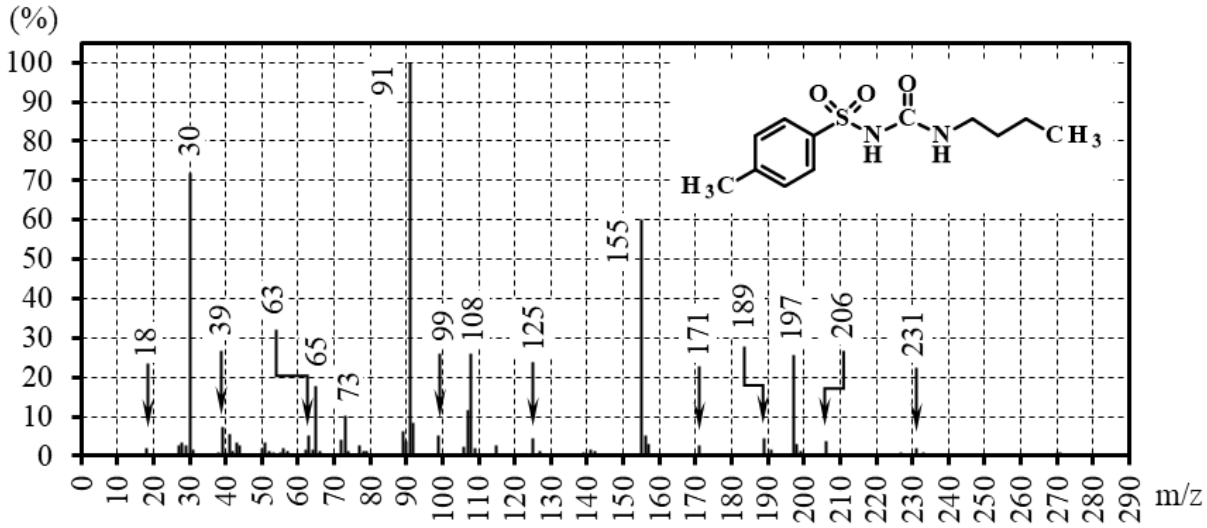

Timolol - CAS 91524-16-2 - EI - NIST 246889



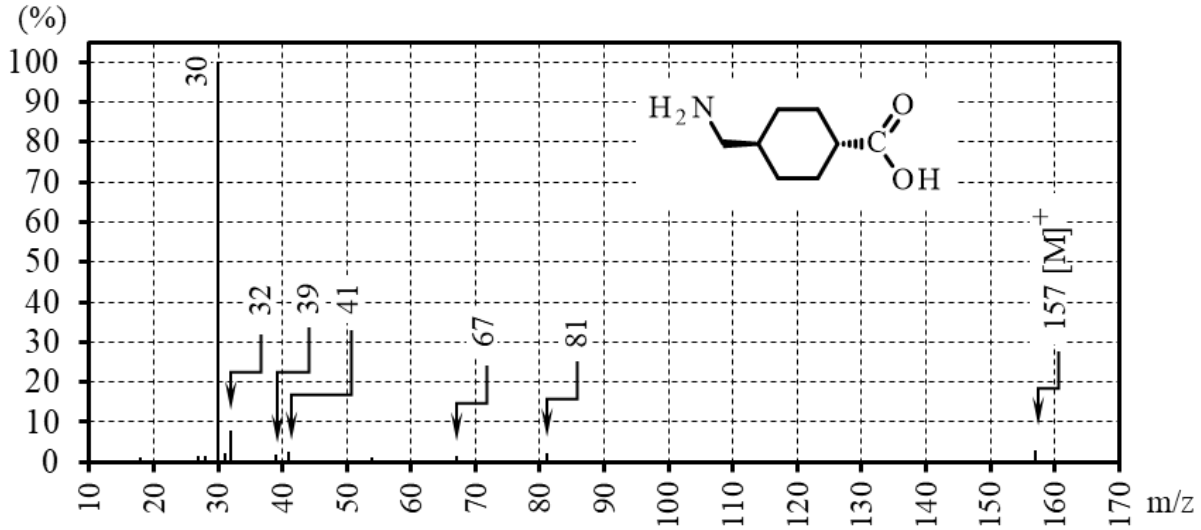

Tokopherol (alpha) - CAS 59-02-9 - NIST 374713



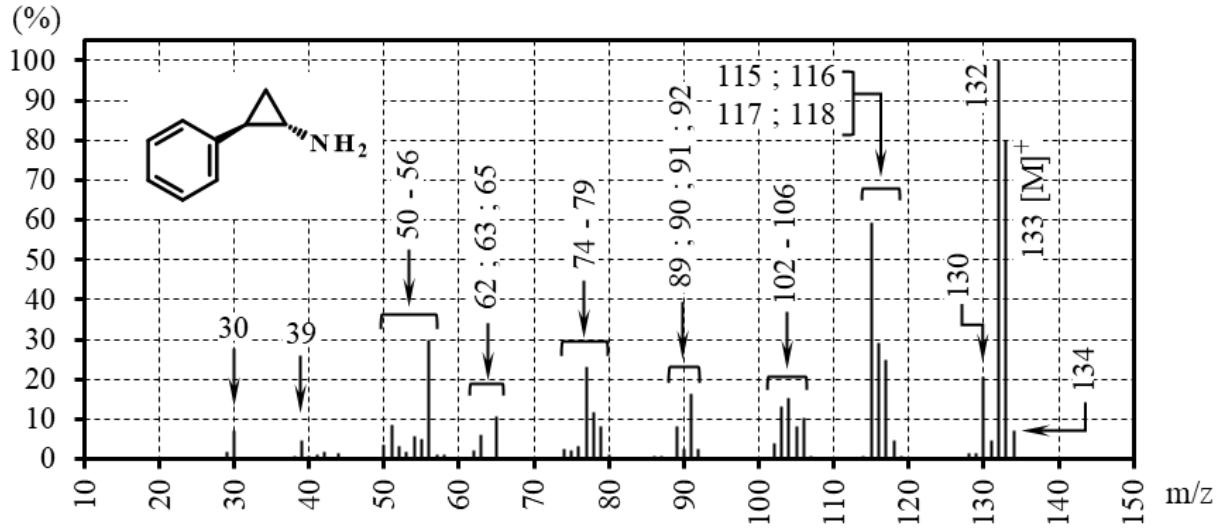

Tolazolin - CAS 59-98-3 - NIST 408031



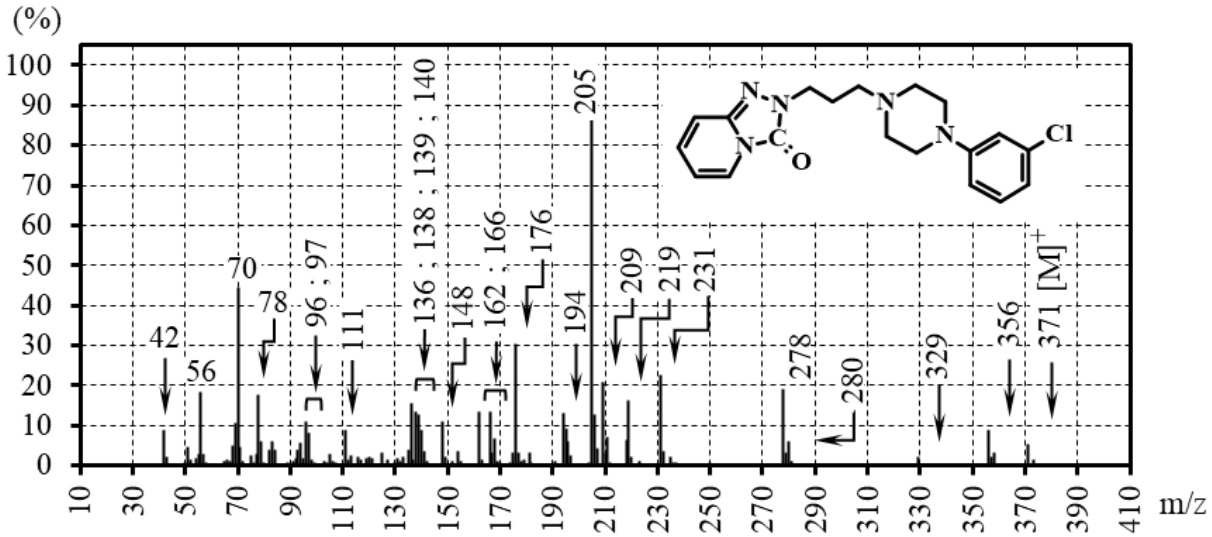

Tolbutamide - CAS 64-77-7 - NIST 242090



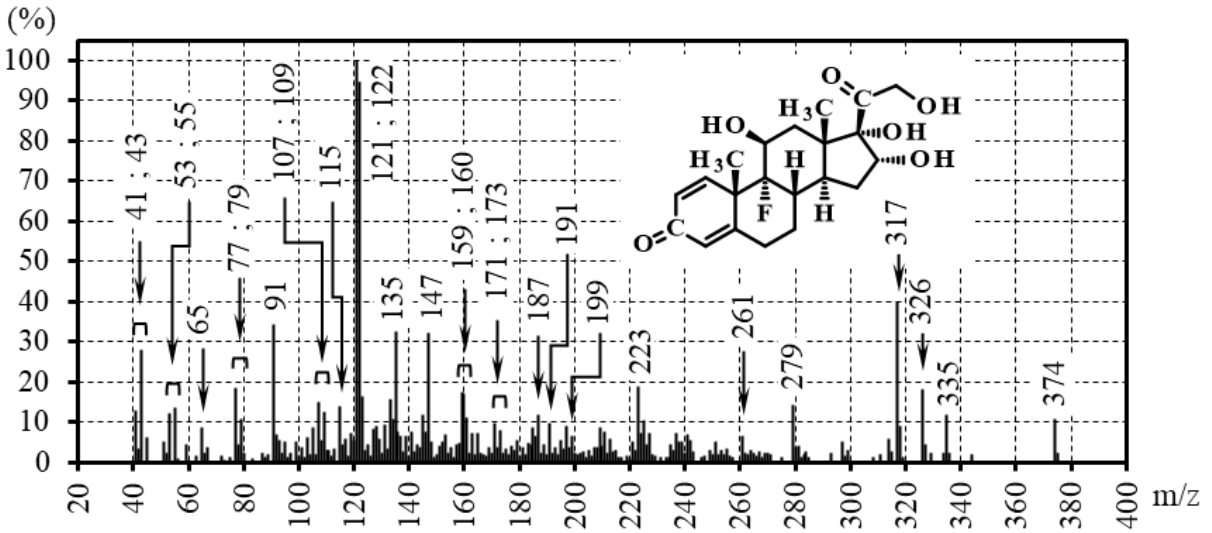

Tranexamic acid - CAS 1197-18-8 - EI 75 eV - 190 °C , 160 °C - SDBS 3530



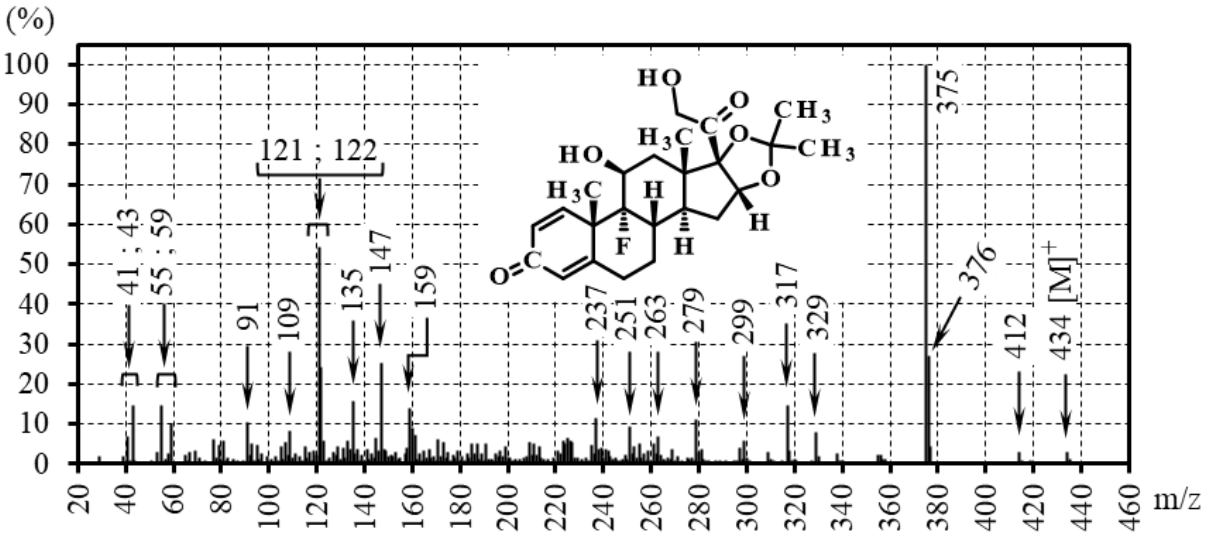

Tranylcypromine - CAS 155-09-9 - EI - NIST 245916



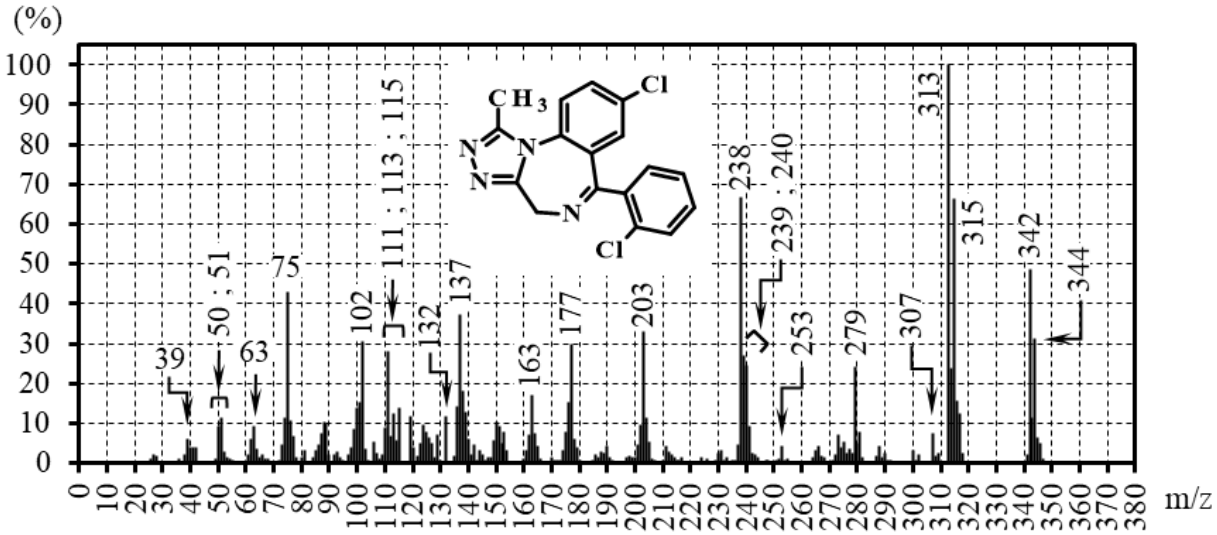

Trazodone - CAS 19794-93-5 - EI - NIST 248796



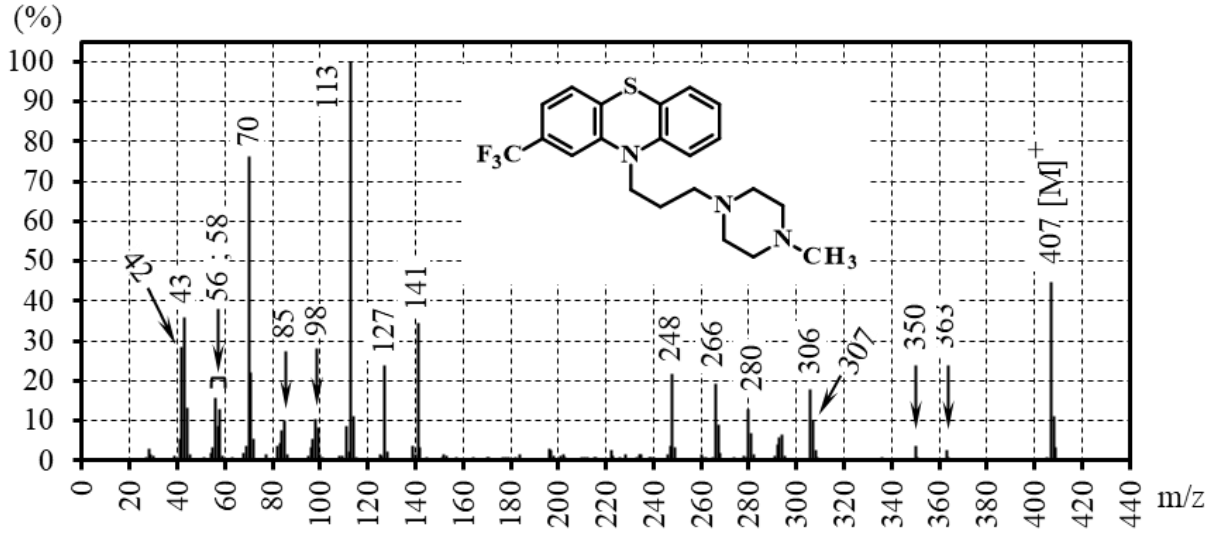

Triamcinolone - CAS 124-94-7 - NIST 248648



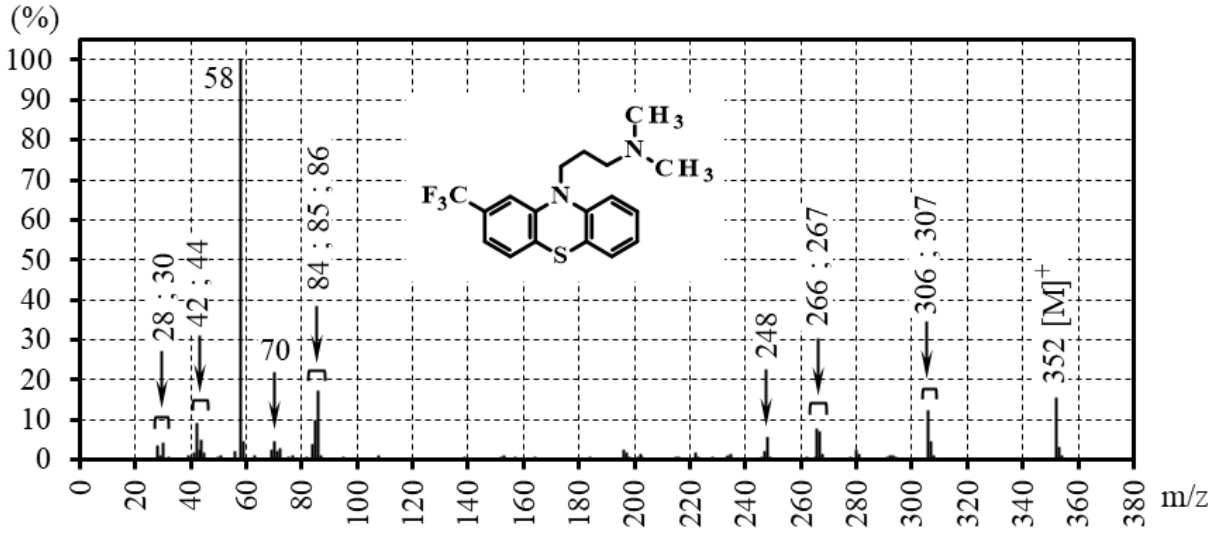

Triamcinolone acetonide - CAS 76-25-5 - NIST 236290



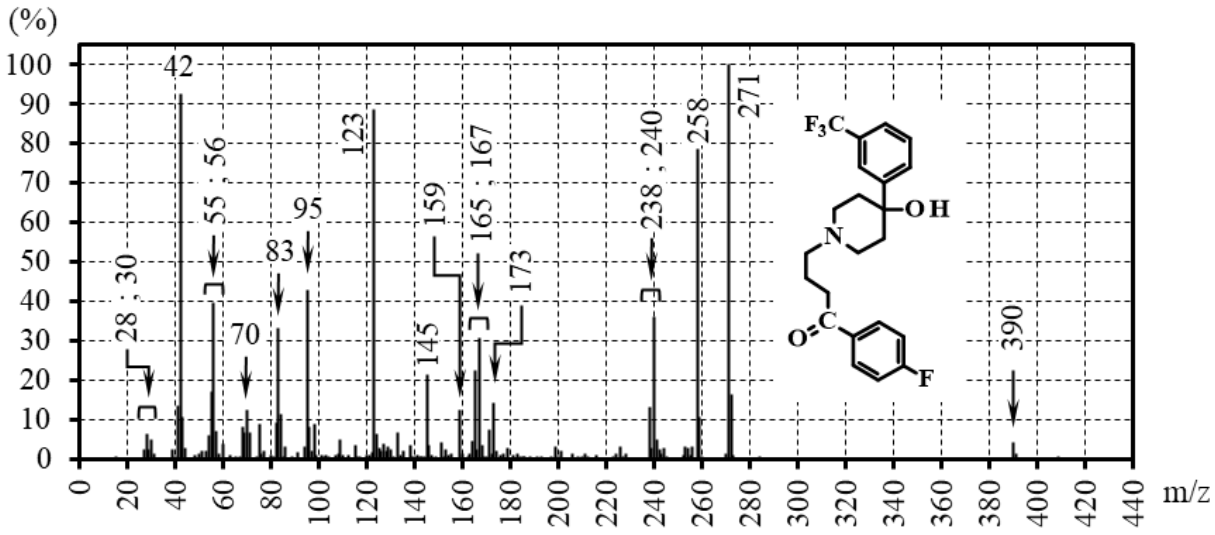

Triazolam - CAS 28911-01-5 - EI - NIST 408822



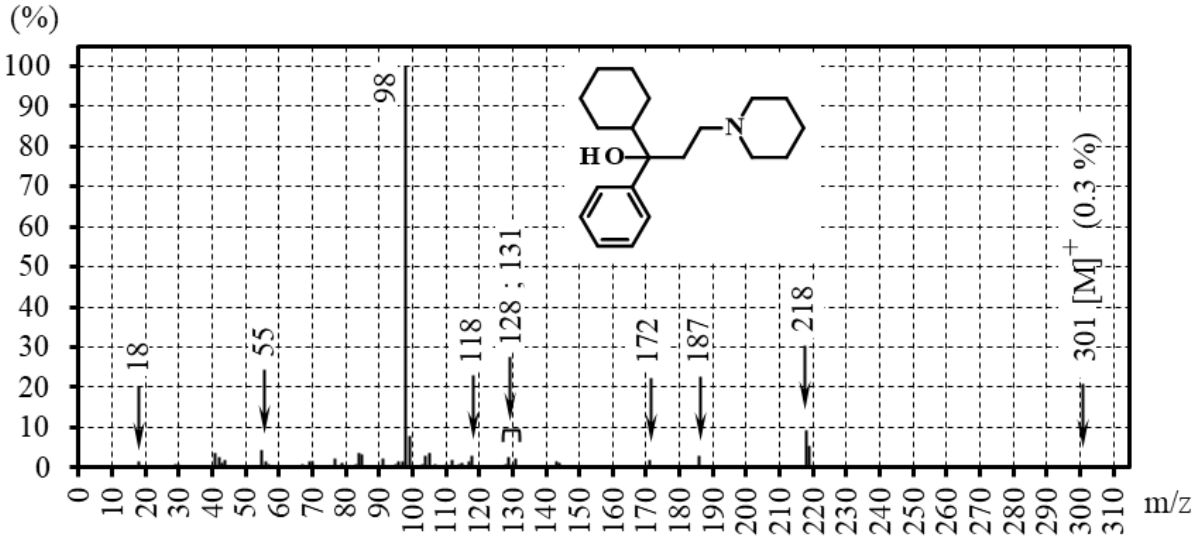

Trifluoperazine - CAS 117-89-5 - NIST 408618



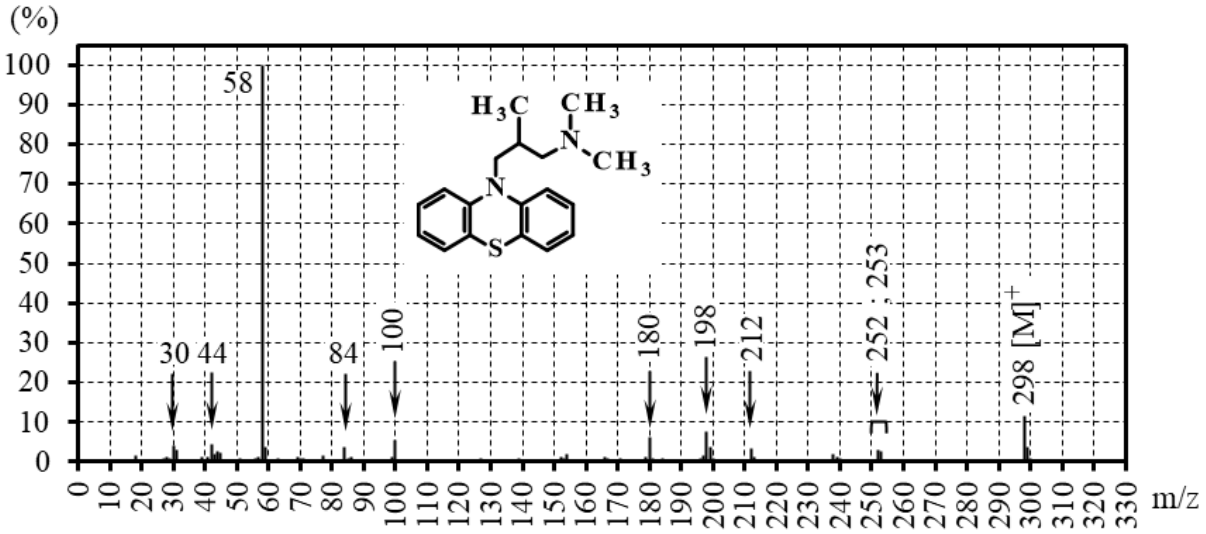

Triflupromazine - CAS 146-54-3 - EI - NIST 113868



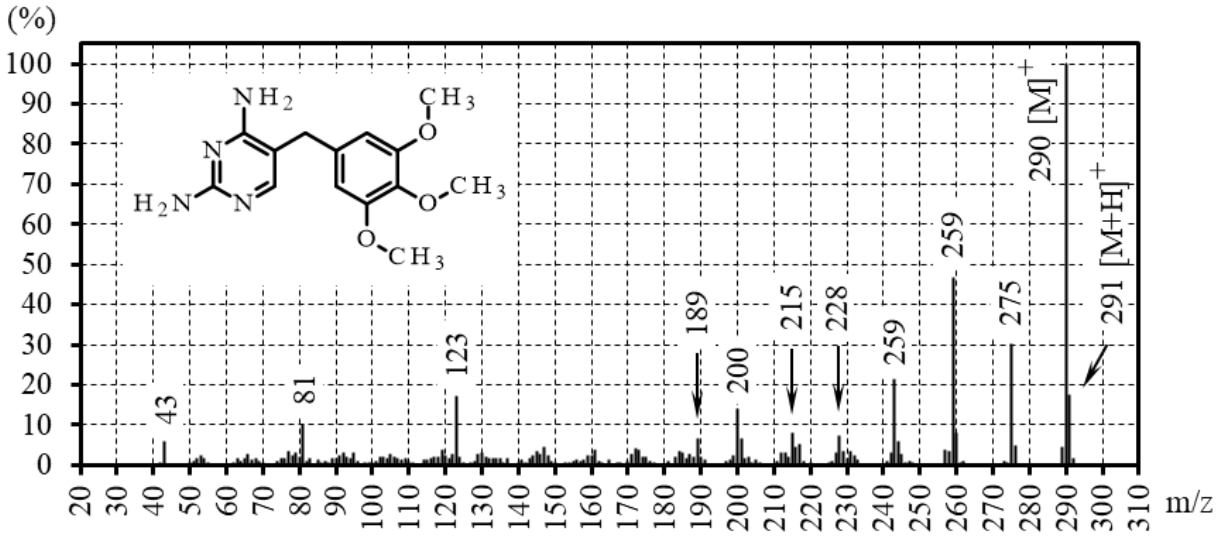

Trifuperidol - CAS 749-13-3 - EI - NIST 408744



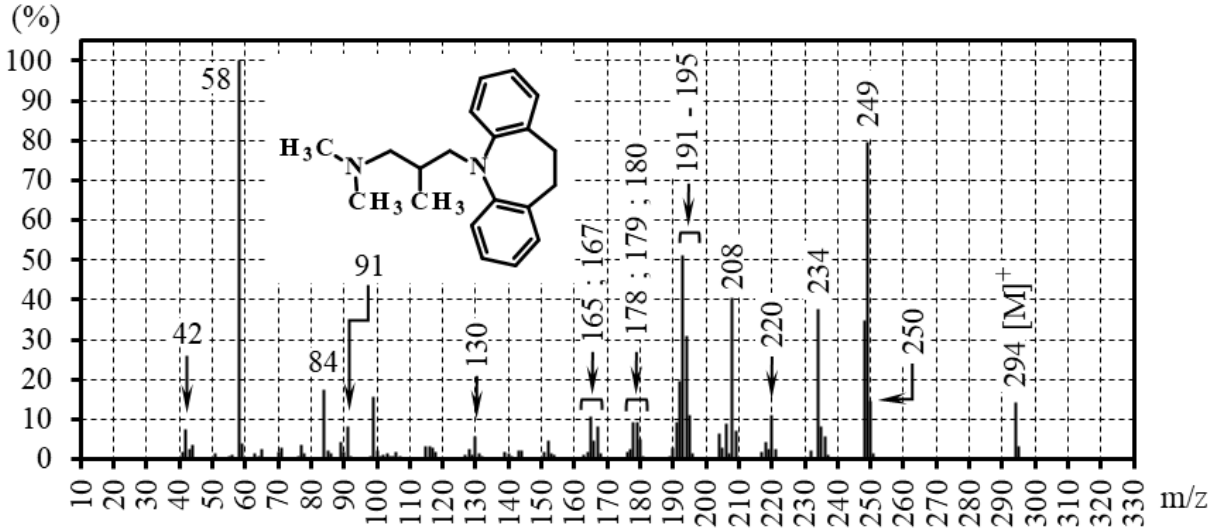

Trihexyphenidyl - CAS 114-11-6 - NIST 244993



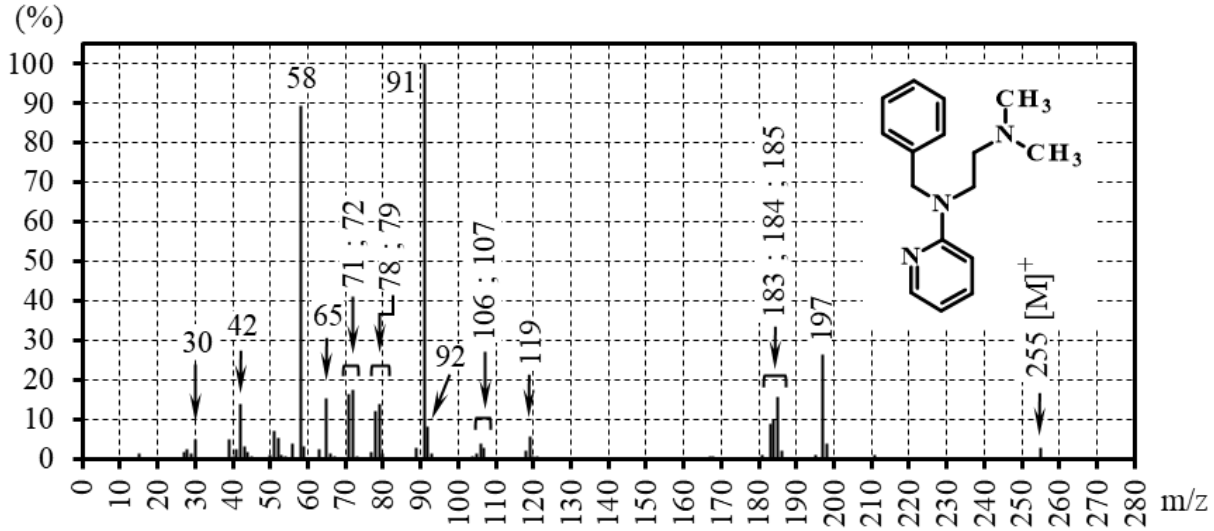

Trimeprazine - CAS 84-96-8 - EI - NIST 42348



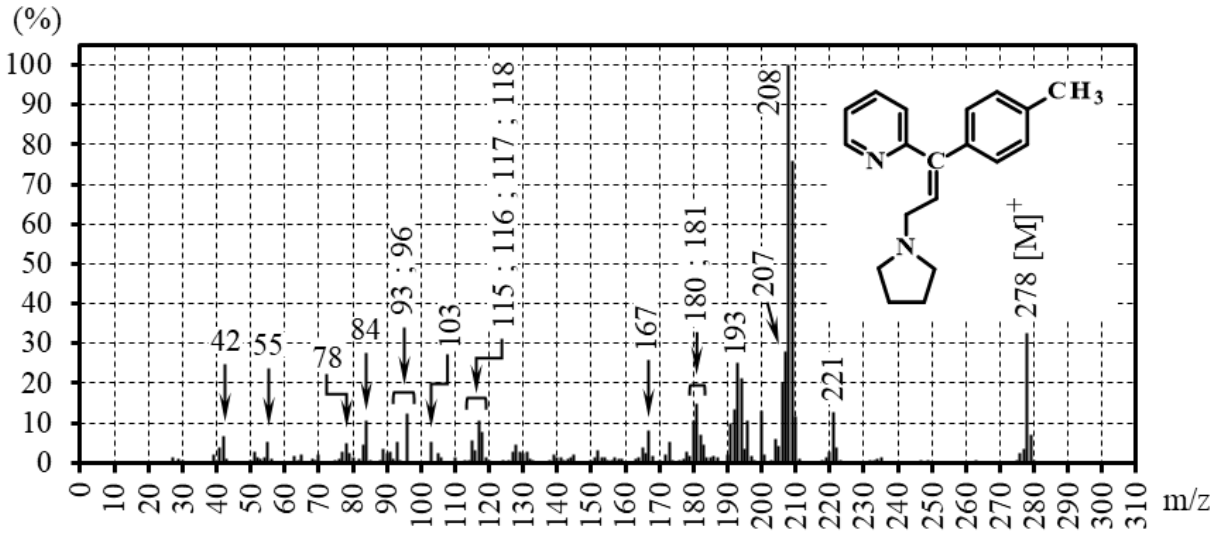

Trimethoprim - CAS 738-70-5 - EI - NIST nr. 247707



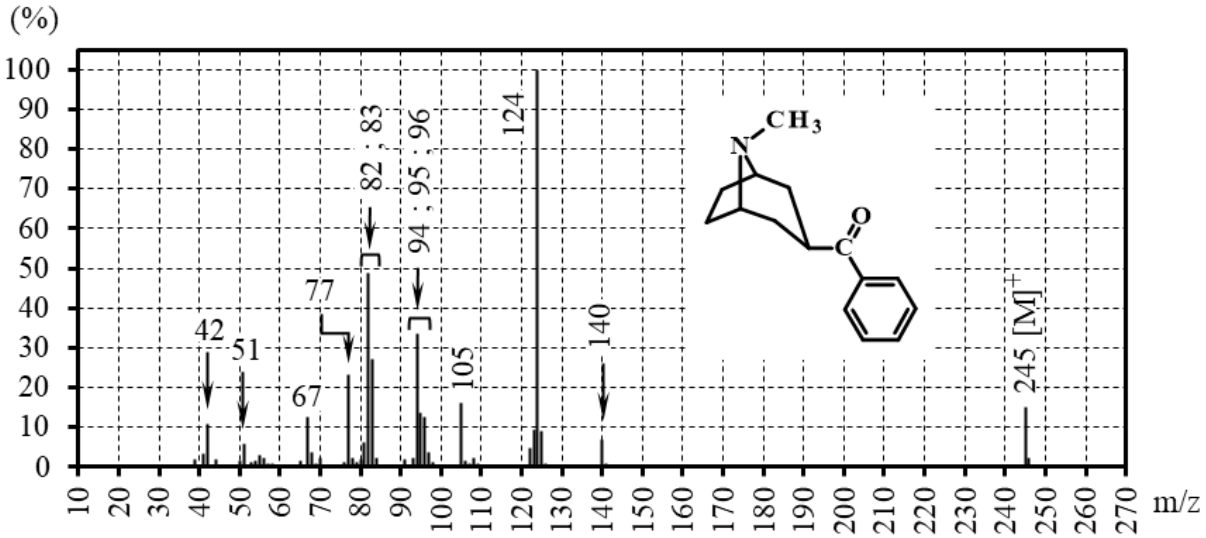

Trimipramine - CAS 739-71-9 - EI - NIST 334919



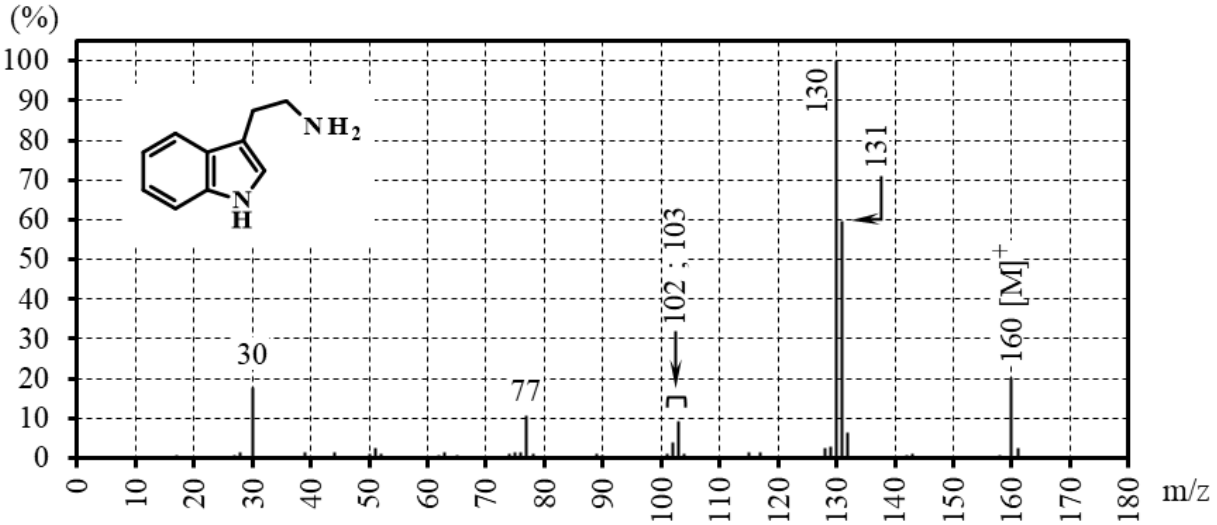

Tripelennamine - CAS 91-81-6 - EI - NIST 250622



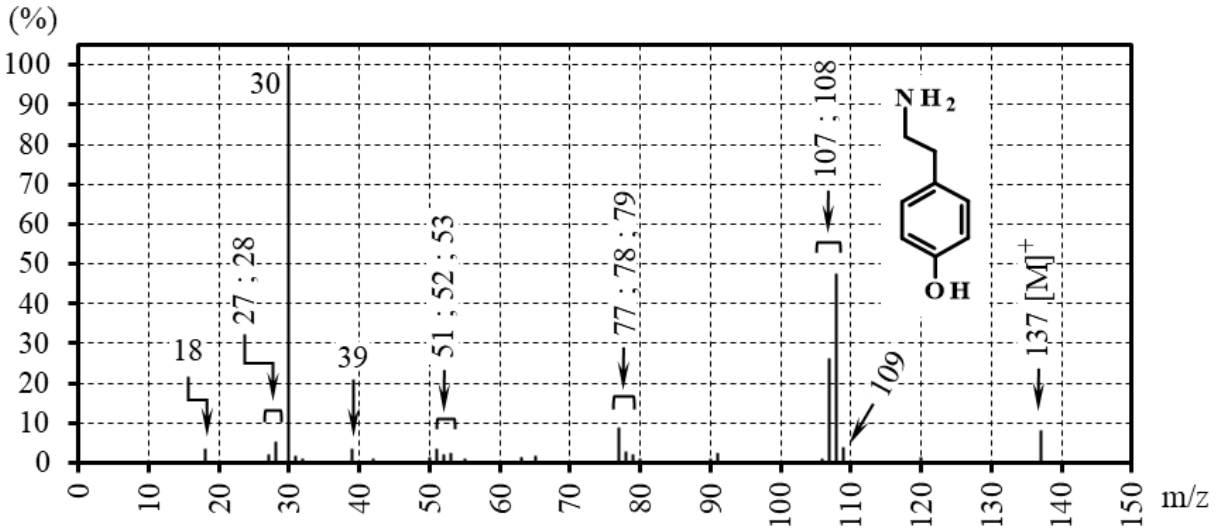

Triprolidine - CAS 486-12-4 - EI - CAS 291072



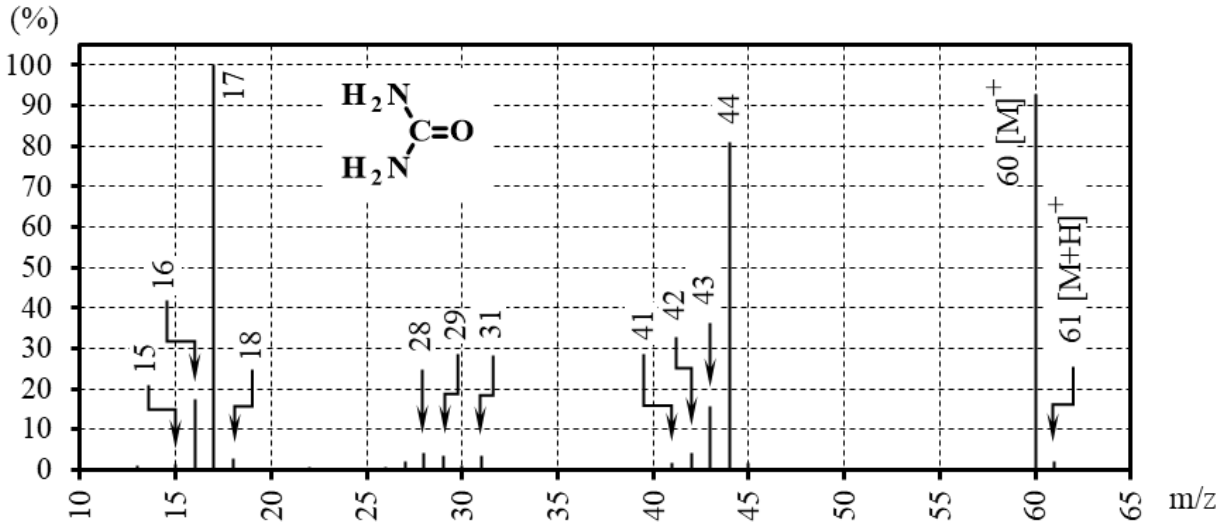

Tropacocaine - CAS 537-26-8 - NIST 246403



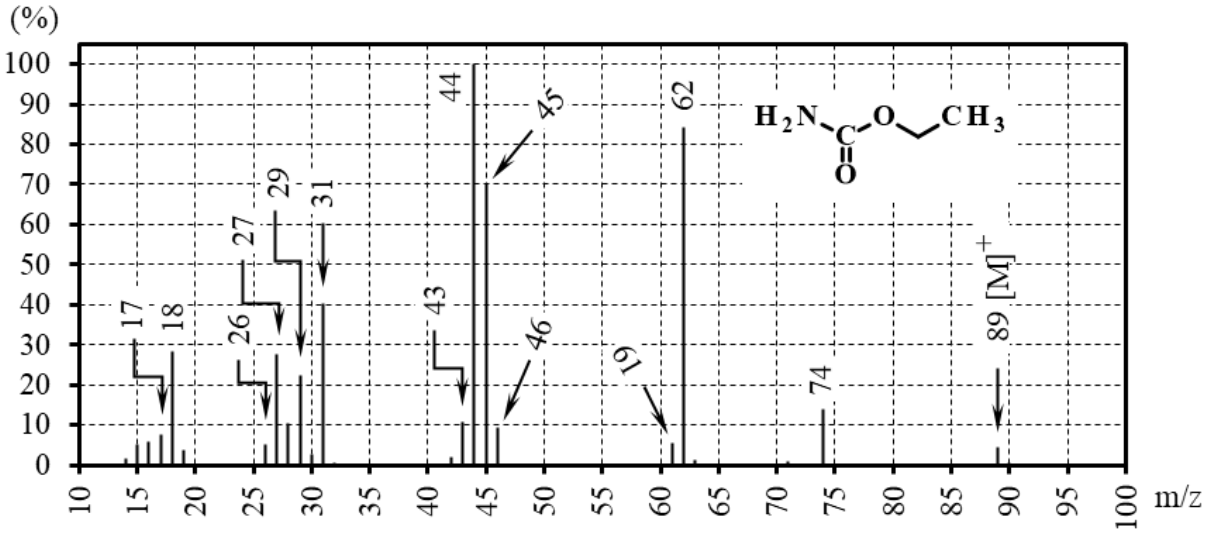

Tryptamine - CAS 61-54-1 - EI - NIST 231006



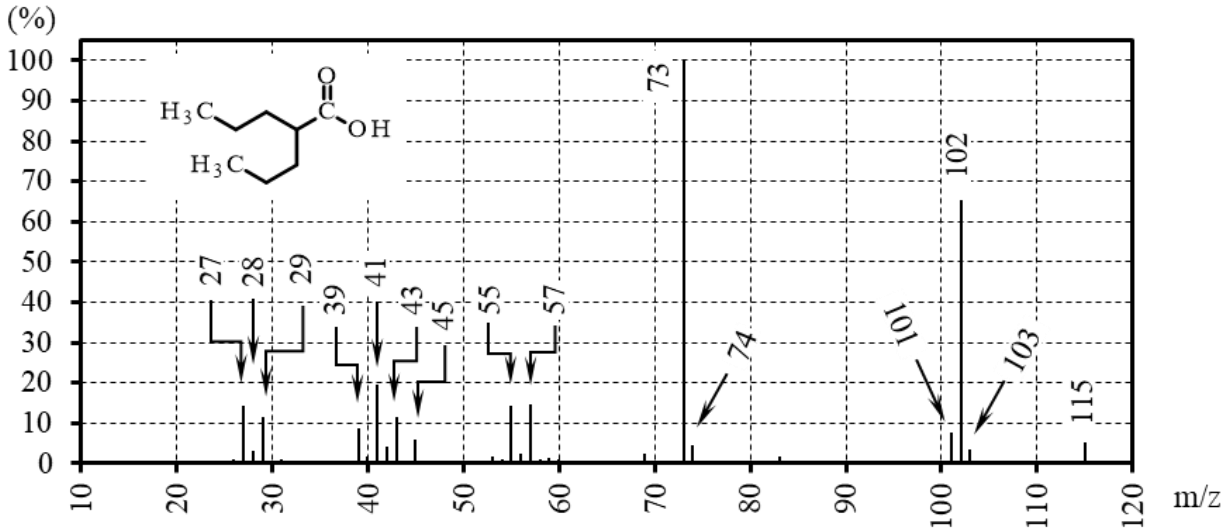

Tyrosamine (Tyramine) - CAS 51-67-2 – EI - NIST 229981



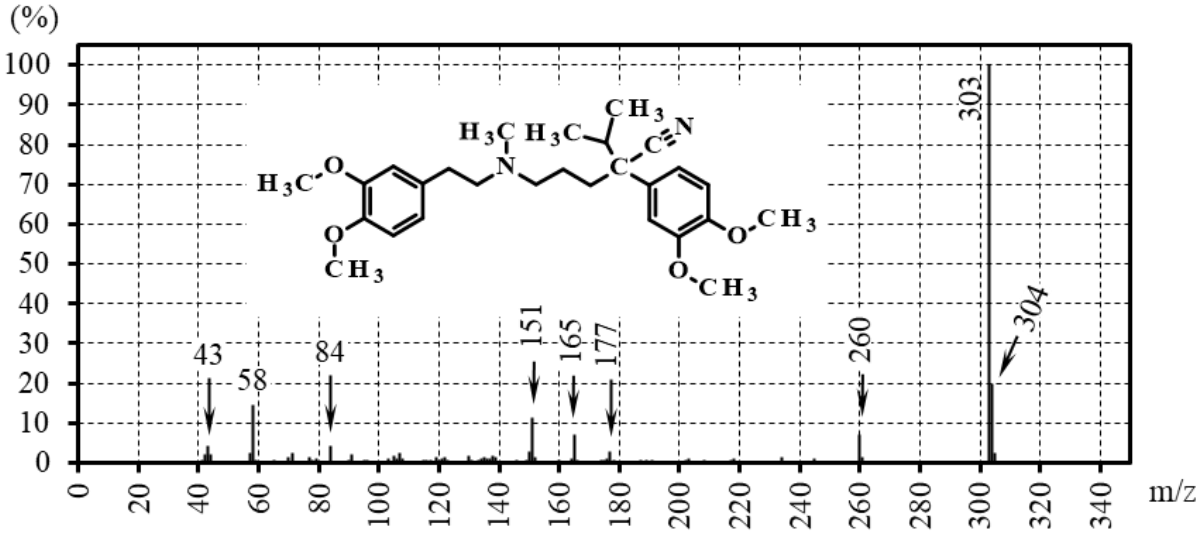

Urea - CAS 57-13-6 - NIST 229591



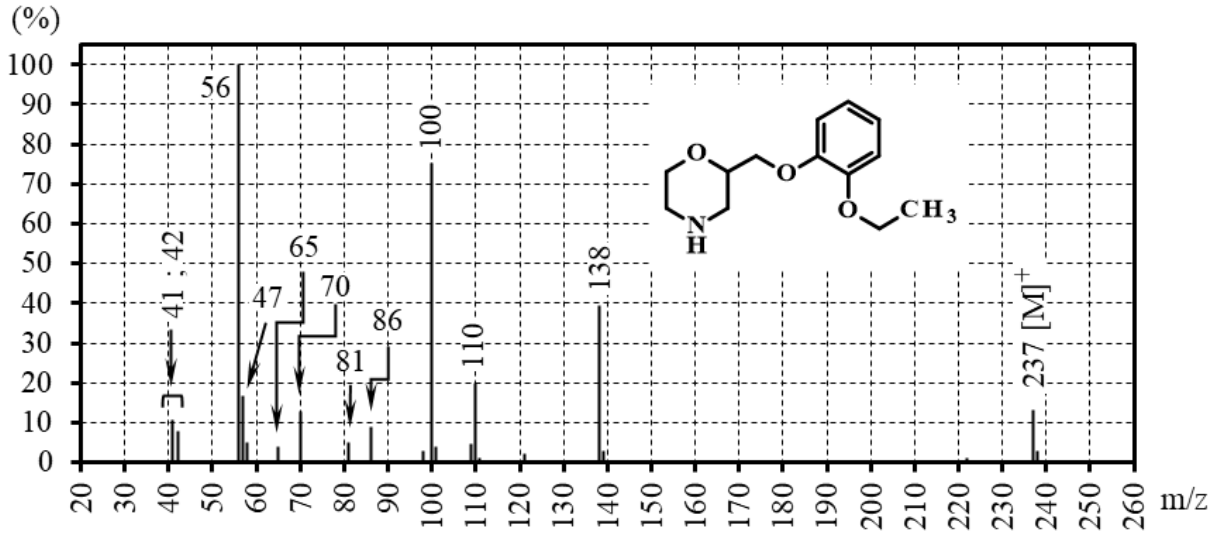

Urethane - CAS 51-79-6 - NIST 227700



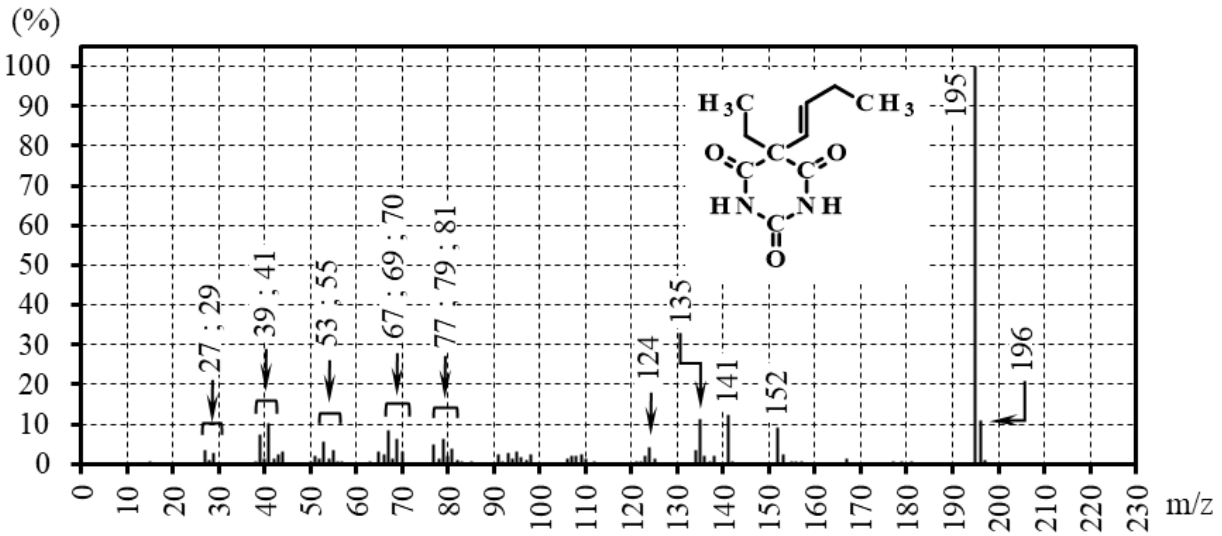

Valproic acid - CAS 99-66-1 - EI - NIST 343602



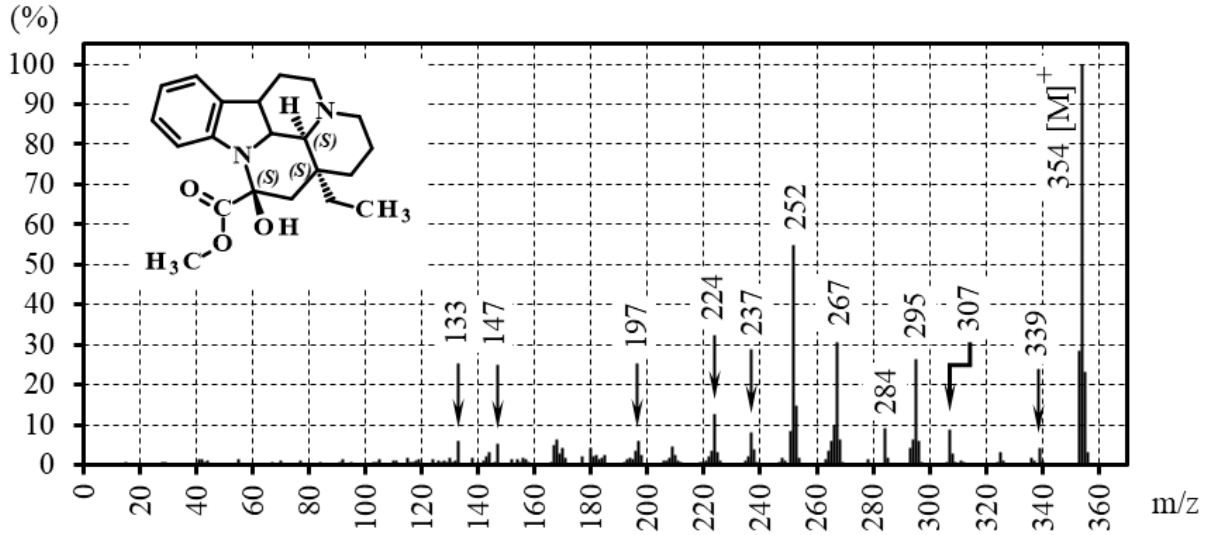

Verapamil - CAS 52-53-9 - EI - NIST 247152



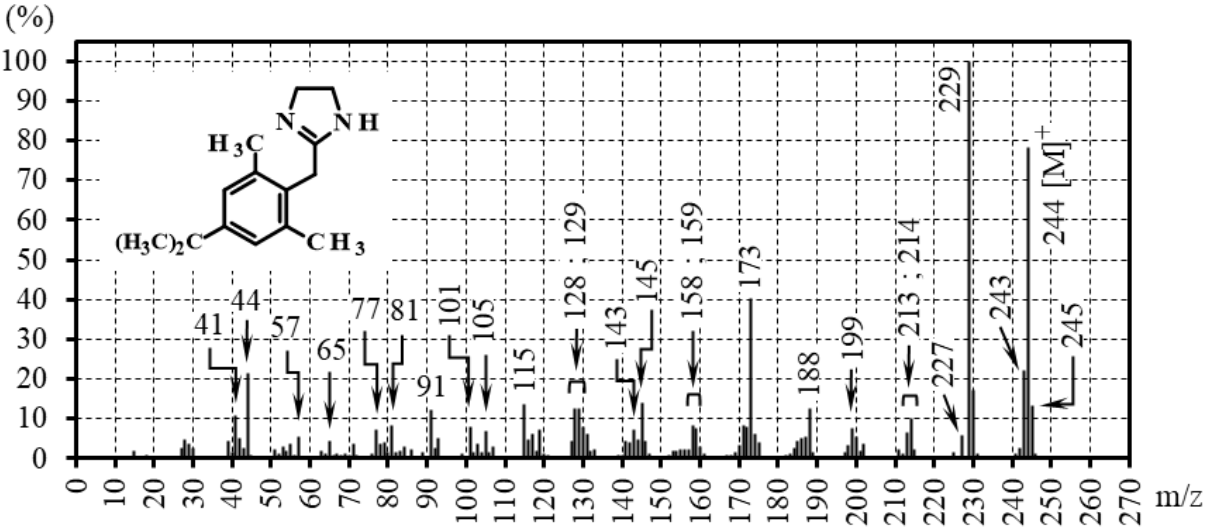

Viloxazine - CAS 46817-91-8 - EI - NIST 121041



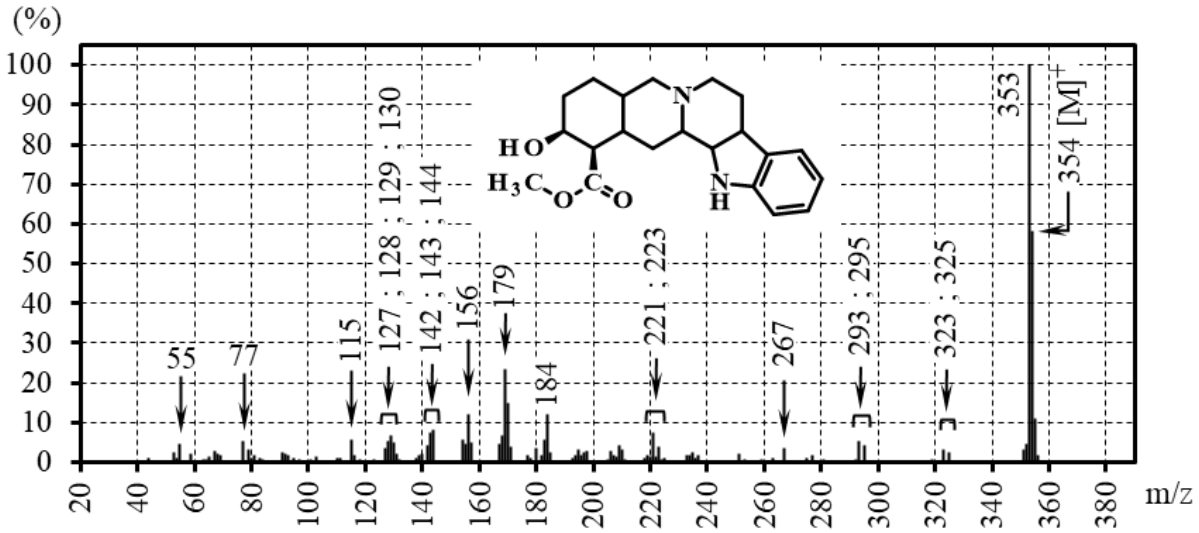

Vinbarbital - CAS 125-42-8 - EI - NIST 250623



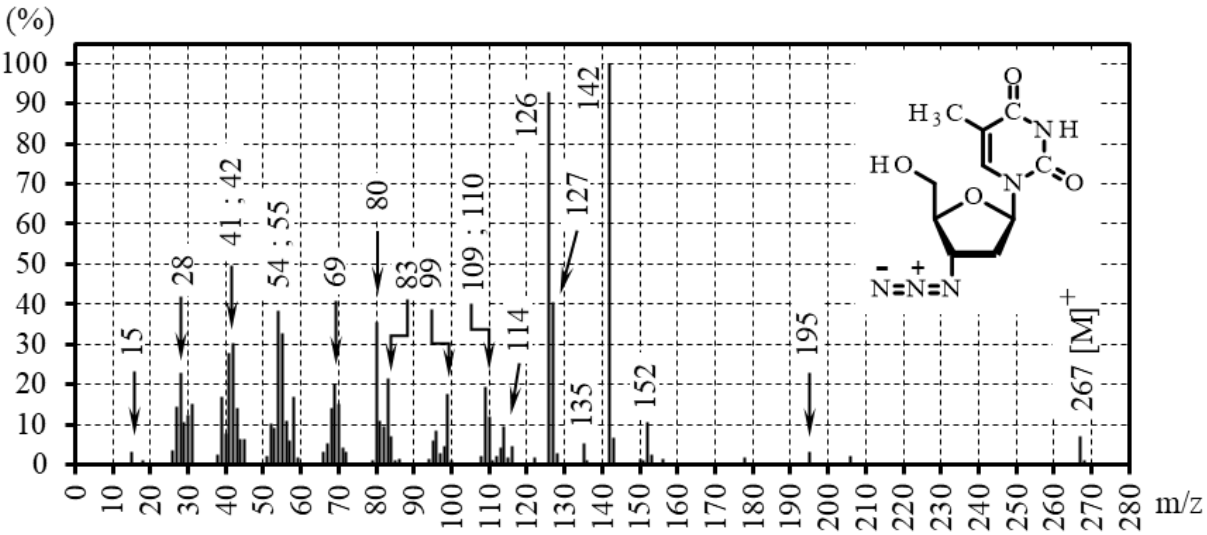

Vincamine - CAS 1617-90-9 - NIST 233872



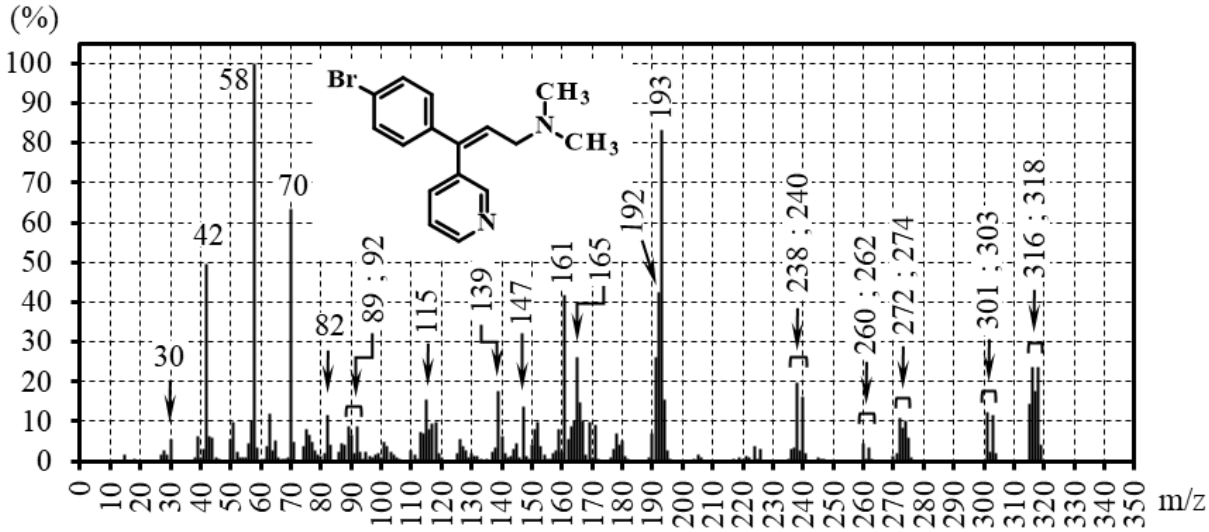

Xylometazoline (Otrivin, Otrix) - CAS 526-36-3 - EI - NIST 113858



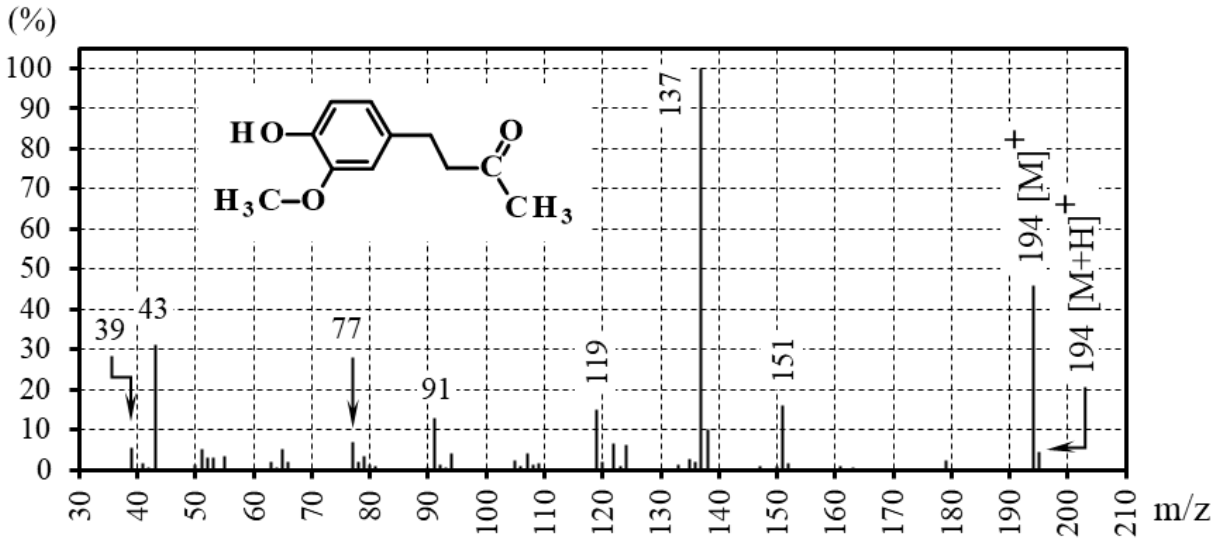

Yohimbine - CAS 146-48-5 - EI - NIST 247969



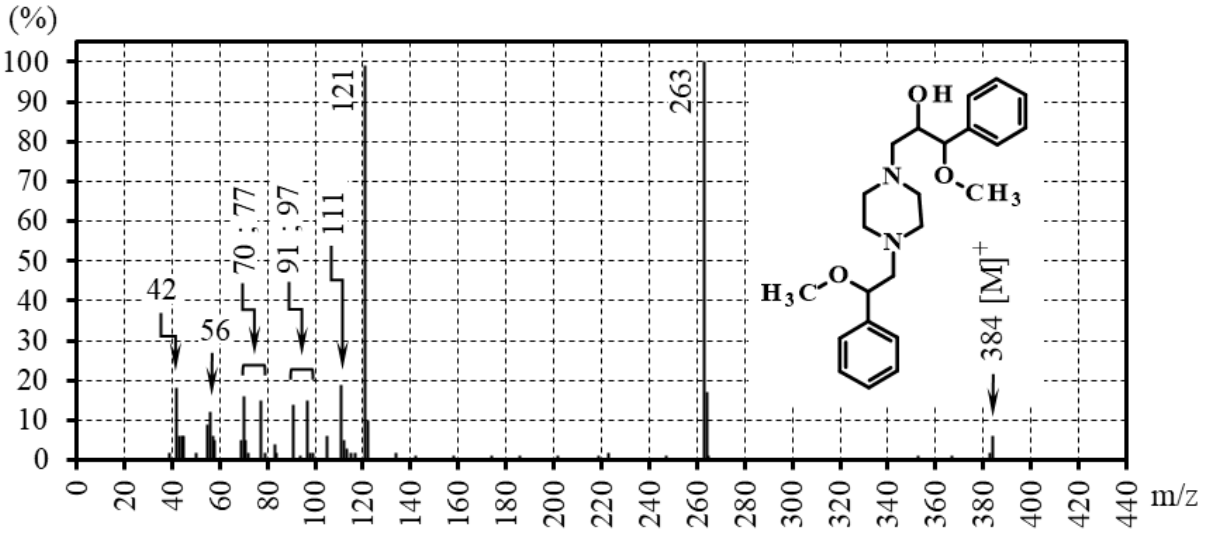

Zidovudine - CAS 30516-87-1 - EI - SDBS 51948



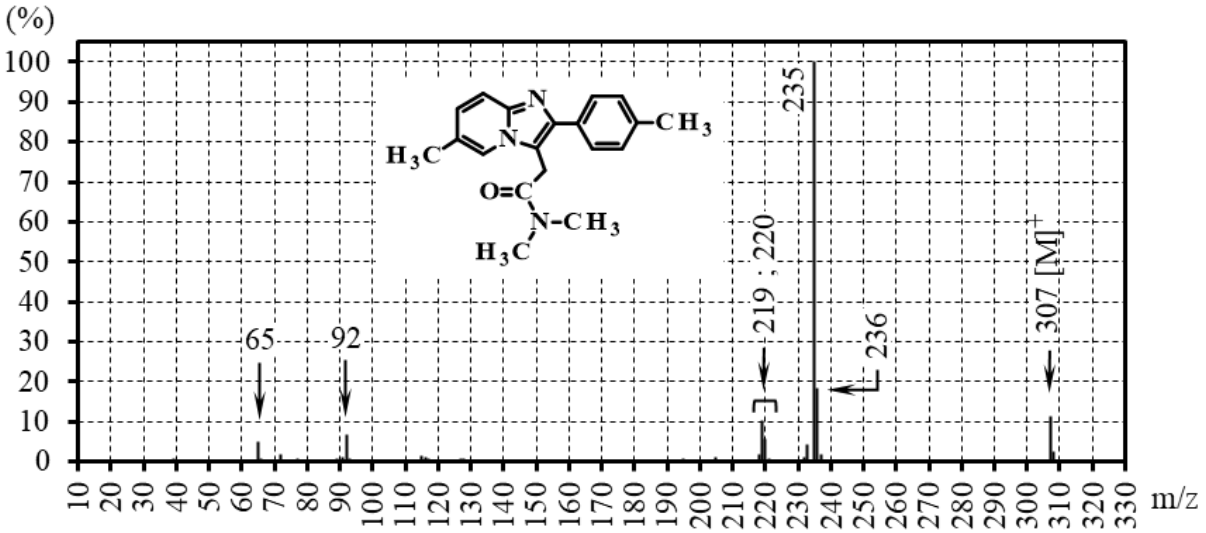

Zimeldine - CAS 56775-88-3 - EI - NIST 408751




Zingerone CAS 122-48-5 - EI MS1 - NIST 8502




Zipeprol - CAS 34758-83-3 - EI - NIST 101047




Zolpidem - CAS 82626-48-0 - EI - NIST 247600

**Furter readings on mass spectrometry**

*Aboul-Enein, H.Y.; Ali, I*: **Chiral Separations by Liquid Chromatography and Related Techniques** (volumul 90 din seria **Chromatographic Science**, *Cazes, J*. editor de serie) Marcel Dekker, Inc., 2003 [ISBN: 0-8247-4014-9]

*Adamovics, J.A*.: **Chromatographic Analysis of Pharmaceuticals** Marcel Dekker, Inc., 1997 [ISBN: 0-8247-9776-0]

*Ardrey, R.E.*: **Liquid Chromatography – Mass Spectrometry: An Introduction** John Wiley & Sons, Ltd., 2003 [ISBN: 0-471-49799-1]

*Ashcroft, A.E.*: **Ionization Methods in Organic Mass Spectrometry** The Royal Society of Chemistry, 1997 [ISBN: 0-85404-570-8]

*Bouchonnet, S.*: **Introduction to GC-MS Coupling** CRC Press, Taylor & Francis Group, 2013 [ISBN: 978-1-4665-7252-2]

*Bruno, T.J.; Svoronos, P.D.N.*: **CRC Handbook of Fundamental Correlation Chards** CRC Taylor & Francis, 2006 [ISBN: 0-8493-3250-8]

*Bruno, T.J.; Svoronos, P.N.D.*: **CRC Handbook of Fundamental Spectroscopic Correlation Charts** C.R.C. Taylor & Francis, 2005 [ISBN: 0-8493-3250-8]

*Buchanan,M.V.* (editor): ***Fourier* Transform Mass Spectrometry** American Chemical Society, Washington, 1987 [ISBN: 0-8412-1441-7]

*Castiglioni, S.; Zuccato, E.; Fanelli, R.* (editori): **Illicit Drugs in Environment – Occurence, Analysis and Fate Using Mass Spectrometry** John Wiley & Sons, Inc., 2011 [ISBN: 978-0-470-52954-8]

*Chan, Chung Chow; Lam, H.; Lee, Y.C.; Zhang, X-M.* (editori): **Analytical Method Validation and Instrument Performance Verification** John Wiley & Sons, Inc., Publication, 2004 [ISBN: 0-471-25953-5]

*Chapman, J.R.* (editor): **Methods in Molecular Biology, vol. 145 – Mass Spectrometry of Proteins and Peptides** Humana Press, Inc., 2000 [ISBN: 0-89603-609-x]

*Chapman, J,R.* (editor): **Protein and Peptide Analysis by Mass Spectrometry** Humana Press, 1996 [ISBN: 0896033457]

*Chowdhury, S.K.* (editor): **Identification and Quantification of Drugs, Metabolites and Metabolizing Enzymes by LC-MS** Elsevier, Academic Press, 2005[ISBN: 0444517103]

*Cifuentes, A.* (editor): **Advanced Mass Spectrometry in Modern Food Science and Nutrition** John Wiley & Sons, 2013 [ISBN: 978-1-118-16945-2]

*Coelho, A.V.; Catarina de Matos Ferraz Franco*: **Tandem Mass Spectrometry – Molecular Characterization** InTech, 1013 [ISBN: 978-653-51-1136-8]

*Cole, R.B.* (editor): **Electrospray and MALDI Mass Spectrometry – Fundamentals, Instrumentation, Practicalities and Biological Applications**
John Wiley & Sons, 2010 [ISBN: 978-0-471-74107-7]

*Cotter, R.J.*: **Time-of-Flight Mass Spectrometry – Instrumentation and Applications in Biological Research**
American Chemical Society, Washington, 1997 [ISBN: 0-8412-3474-4]

*Cramer, R.* (editor): **Advances in MALDI and Laser-Induced Soft Ionization Mass Spectrometry**
Springer, 2016 [ISBN: 987-3-319-04812-2]

*Currel, G.*: **Analytical Instrumentation Performance Characteristics and Quality** (Capitol 12., pag. 183-192)
John Wiley & Sons Ftd., 2000 [ISBN: 0-471-9990-8]

*Cutillas, P.R.; Timms, J.F.* (editori): **LC-MS/MS in Proteomics: Methods and Applications**
Humana Press, 2010 [ISBN: 9781607617792]

*Dass, C.*: **Fundamentals of Contemporary Mass Spectrometry**
John Wiley & Sons, 2007 [ISBN: 978-0-471-68229-5]

*Desiderio, D.M.*: **Analysis of Neuropeptides by Liquid Chromatography and Mass Spectrometry**
Elsevier, 1984 [ISBN: 0-444-42418-0]

*Downard, K.M.*: **Mass spectrometry – A Foundation Course**
The Royal Society of Chemistry, 2004 [ISBN: 0-85404-609-7]

*Downard, K.M.*(editor): **Mass Spectrometry of Protein Interaction**s
John Wiley & Sons, Inc., 2007 [ISBN: 978-0-471-79373-1]

*Dubber, M-J.*: **Application of CE, HPLC and LC-MS-MS for the Analysis and Quality Control of *Ginkgo biloba* Dosage Forms** – Thesis
Rhodes University, November 2005

*Eiceman, G.A.; Karpas, Z.*: **Ion Moblity Spectrometry**
CRC Press, Taylor & Francis Group, 2005 [ISBN: 0-203-50475-5]

*Eiceman, G.A.; Karpas, Z.; Hill jr., H.H.*: **Ion Mobility Spectrometry**
CRC Press, Taylor & Francis Group, 2014 [ISBN: 978-1-4398-5998-8]

*Eidhammer, I.; Flikka, K.; Martens, L.; Mikalsen, S-O.*: **Computational Methods for Mass Spectrometry Proteomics**
John Wiley & Sons Ltd., 2007 [ISBN: 978-0-470-51297-5]

*Ekman, R.; Silberring, J.; Estman-Brinkmalm, A.; Kraj, A.* (editori): **Mass Spectrometry – Instrumentaion, Interpretation and Applications**
John Wiley & Sons, Inc., 2009 [ISBN: 978-0-471-71395-1]

*Fay, L.B.; Kussmann, M.* (editori): **Mass Spectrometry and Nutrition Research**
The Royal Society of Chemistry, 2010 [ISBN: 978-1-84973-036-5]

*Ferrer, I.; Thurman E.M.* (editori): **Liquid Chromatography Time-of-Flight Mass Spectrometry – Principles, Tools and Applications for Accurate Mass Analysis**
John Wiley & Sons, Inc., 2009 [ISBN: 978-0-470-13797-0]

*Figerio,A.; Ghisalberti, E.L.* (editori): **Mass Spectrometry in Drug Metabolism**
Plenum Press, 1977 [ISBN: 978-1-4613-4151-2]

*Flamini, R.; Traldi, P.*: **Mass Spectrometry in Grape and Wine Chemistry**
John Wiley & Sons, Inc., 2010 [ISBN: 978-0-470-39247-8]

*Garg, U.; Hammett-Stabler, C.* (editori): **Clinical Applications of Mass Spectrometry – Methods and Protocols**
Humana Press, 2010 [ISBN: 978-1-60761-459-3]

*Ghosh,P.K.*: **Introduction to Protein Mass Spectrometry**
Academic Press – Elsevier, 2015 [ISBN: 0128021128]

*Greaves, J,; Roboz, J.*: **Mass Spectrometry for the Novice**
CRC Press, Taylor & Francis Group, 2014 [978-1-4200-8420-6]

*Gross, J.*: **Mass spectrometry – A Textbook**
Springr, 2017 [ISBN: 978-3-319-54397-0]

*deGroot, P.A.* (editor): **Handbook of Stable Isotope Analytical Techniques – vol. 1**
Elsevier, 2004 [ISBN: 0-444-51114-8]

*deGroot, P.A.* (editor): **Handbook of Stable Isotope Analytical Techniques – vol. 2**
Elsevier, 2009 [ISBN: 0-444-51115-7]

*Gross, M.L.* (editor): **High Performance Mass Spectrometry: Chemical Applications**
Americal Chemical Society, 1978 [ISBN: 0-8412-0422-5]

*Guodong, C.* (editor): **Characterization of Protein Therapeutics Using Mass spectrometry**
Springer, 2013 [ISBN: 978-1-4419-7862-2]

*Herbert, C.G.*; *Johnstone,R.A.W.*: **Mass Spectrometry Basics**
CRC Press, 2003 [ISBN: 0-8493-1354-6]

*Hillenkamp, F.; Peter-Katalinic, J.* (editori): **MALDI-MS – A Practical Guide to Instrumentation, Methods and Applications**
Wiley VCH Verlag GmbH & Co. KGaA, 2014 [ISBN: 978-3-527-67373-5]

*Hiraoka, K.* (editor): **Fundamentals of Mass Spectrometry**
Springer, 2013 [ISBN: 978-1-4514-7232-2]

*de Hoffmann, E.; Stroobant, V.*: **Mass Spectrometry – Principles and Applications**
John Wiley & Sons, Ltd., 2007 [ISBN: 978-0-470-03310-4]

*Holcapek, M.; Byrd, Wm.C.* (editori): **Handbook of Chromatography/Mass Spectrometry Techniques**
Academic Press and AOCS Press, 2017 [ISBN: 978-0-12-811732-3]

*Holmes, J.J.; Aubry, C.; Mayer. P.M.*: **Assigning Structures to Ions in Mass Spectrometry**
CRC Press, 2007 [ISBN: 978-0-8493-1950-1]

*Housby, J.N.* (editor): **Mass Spectrometry and Genomic Analysis**
Kluver Academic Publishers, 2001 [ISBN: 0-306-47595-2]

*Hübschmann, H-J.*: **Handbook of GC-MS – Fundamentals and Applications**
Wiley-VCH Verlag GmbH & Co,KGaA, 2015 [ISBN: 978-3-527-67433-6]

*Kaltashov, I.A.; Eyles, S.J.*: **Mass Spectrometry in Biophysics – Conformation and Dynamics of Biomolecules**
John Wiley & Sons, Inc., 2005 [ISBN: 0-471-45602-0]

*Kinter, M.; Sherman, N.E.*: **Protein Sequencing and Identification Using Tandem Mass Spectrometry**
John Wiley & Sons Inc., 2000 [ISBN: 0-471-32249-0]

*Kitson, F.G.; Larsen, B.S.; McEven, C.N.*: **Gas Chromatography and Mass Spactrometry**
Academic Press, 1996 [ISBN: 0-12-483385-3]

*Kohler, J.J.; Patrie, S.M.* (editori): **Mass Spectrometry of Glycoproteins – Methods and Protocols**
Humana Press, 2013 [ISBN: 978-1-62703-146-2]

*Korfmacher, W.A.* (editor): **Using Mass Spectrometry for Drug Metabolism Studies**
C.R.C. Press, 2005 [ISBN: 0-8493-1963-3]

*Korfmacher, W.A.* (editor): **Mass Spectrometry for Drug Discovery and Drug Development** (Capitol 7)
John Wiley & Sons, Inc., 2013 [ISBN: 978-0-470-94238-3]

*Kromidas, S.* (editor): **The HPLC-MS Handbook for Practitioners**
Wiley – VCH, 2017 [ISBN: 978-3-527-80920-2]

*Langman, L.J.; Snozek, C.I.H.*: **LC-MS in Drug Analysis: Methods and Protocols**
Humana Press, 2018 [ISBN: 9781493988228]

*Laskin, J.; Lifshitz, C.* (editori): **Principles of Mass Spectrometry Applied to Biomolecules**
Wiley – Interscience, 2006 [ISBN: 978-0-471-72184-0]

*Лебедев, А.Т.*: **Масс-спектрометрия в органической химии**
Москва, БИНОМ, Лаборатория знаний, 2003 [ISBN: 94774-052-4]

*Lee, M.S* (editor): **Mass Spectrometry Handbook** (Capitole 2,3,4,7)
John Wiley & Sons, Inc., 2012 [ISBN: 978-0-470-53673-5]

*Lee, M.S.*: **Integrated Strategy for Drug Discovery Using Mass Spectrometry**
John Wiley & Sons, Inc., 2005 [ISBN: 978-0-471-46127-2]

*Lee, M.S.*: **LC/MS Applications in Drug Development**
John Wiley & Sons, Inc., 2002 [ISBN: 0-471-40520-5]

*Lee, M.S.; Zhu, M.* (editori): **Mass Spectrometry in Drug Metabolism and Disposition – Basic Principles and Applications**
John Wiley & Sons, Inc., 2011 [ISBN: 978-0-470-40196-5]

*Lee, T.A.*: **A Beginner's Guide to Mass Spectral Interpretation**
John Wilew & Sons, 1998 [ISBN: 0-471-97628-8]

*Letzel, T.* (editor): **Protein and Peptide Analysis by LC-MS: Experimental Strategies**
The Royal Society of Chemistry, 2011 [ISBN: 9781849731829]

*Ma Shuguang; Chowdhury, S.K.* (editori): **Identification and Quantification of Drugs, Metabolites, Drug Metabolizing Enzymes and Transporters – Concepts, Methods and Translational Sciences**
Elsevier V.B., 2020 [ISBN: 978-0-12-820018-6]

*Mallet, A.I., Down, S.*: **Dictionary of Mass Spectrometry**
John Wiley & Sons, Ltd., 2009 [ISBN: 978-0-470-02761-5]

*March, R.E.; Todd, J.F.J.*: **Quadrupole Ion Trap Mass Spectrometry**
John Wiley & Sons, Inc., 2005 [ISBN: 978-0-471-48888-0]

*Mathiesen, R.* (editor): **Mass Spectrometry Data Analysis in Proteomics**
Springer, Humana Press, 2020 [ISBN: 978-1-4939-9744-2]

*McLafferty, F.W.; Turaček, F.*: **Interpretation of Mass Spectra**
University Science Books, Sausalito, California, 1993 [ISBN: 0-935702-25-3]

*McMaster, M.*: **LC/MS: A Practical User's Guide**
Wiley Interscience, 2005 [ISBN: 0471655317]

*McMaster, M.*: **GC/MS: A Practical User's Guide**
John Wiley & Sons Inc., 2008 [ISBN: 978-0-470-10163-6]

*Mills I, T.; Roberson, J.C.; Mathchett, C.C.; Simon, M.J.; Burns, M.D.; Ollis jr.*:
**Instrumental Data for Drug Analysis – volume 1 – 6**
C.R.C. Taylor & Francis, 2006 [ISBN: 0-8493-1974-9]

*Mistry, B.M.*: A **Handbook of Spectroscopic Data** (Capitol 5., pag. 128-236)
Oxford Book Company, Jaipur, India, 2009 [ISBN: 978-81-89473-86-0]

*Nair, H.*; Clarke, W. (editors): **Mass Spectrometry for the Clinical Laboratory**
Acad. Press., 2017 [ISBN: 978-0-12-800871-3]

*Niessen, W.M.A.*: **Current Practice of Gas Chromatography – Mass Spectrometry**
Marcel Dekker, Inc., 2001 [ISBN: 0-8247-0473-8]

*Niessen, W.M.A.*: **Liquid Chromatography – Mass Spectrometry**
CRC Press, Taylor & Francis Group, 2006 [ISBN: 978-0-8247-4082-5]

*Niessen, W.M.A.; Correa, R.A.*: **Interpretation of MS-MS Mass Spectra of Drugs and Pesticides**
John Wiley & Sons, Inc., Publication, 2017 [ISBN: 9871119294245]

*Ning, Y-C*: **Interpretation of Organic Spectra** – Capitol 4.
John Wiley & Sons, Inc. (Asia), Pte., Ltd., 2011 [ISBN: 978-0-470-82517-4]

*Oprean, I.*: **Spectrometria de masă a compuşilor organici**
Editura Dacia, Cluj, România, 1974

*Paglia, G.; Astarita, G.*: **Ion Mobility-Mass Spectrometry: Methods and Protocols**
Humana Press, 2020 [ISBN: 978-1-0716-0030-6]

*Pavia, L.D.; Lampman, G.M.; Kriz, G.S.*: **Introduction to Spectroscopy – A Guide for Students of Organic Chemistry** – Capitol 8.
Thomson Learning Inc., 2001 [ISBN: 0-03-031961-7]

*Popescu, C,; Zamfir, A.D.; Dinca, A.* (editori): **Applications of Mass Spectrometry in Life Safety**
Springer, 2008 [ISBN: 978-1-4020-8811-7]

*Pramanik, B.N.; Ganguly A.K.; Gross, M.L.* (editori): **Applied Electrospray Mass Spectrometry**
Marcel Dekker Inc., 2002 [ISBN: 0-8247-0618-8]

*Pramanik, B.N.; Lee, M.S.; Chen, G.* (editori): **Characterization of Impurities and Degradants Using Mass Spectrometry**
John Wiley & Sons Inc., 2011 [ISBN: 978-0-470-92136-4]

*Prasain, J.K.* (editor): **Tandem Mass Spectrometry – Applications and principles**
InTech, 2012 [ISBN: 978-953-51-0141-3]

*Pretsch, E.; Bühlmann, P.; Badertscher, M.*: **Structure Determination of Organic Compounds – Tables of Spectral Data**
Springer Verlag, 2009 [ISBN: 978-3-540-93809-5]

*Raftery, D.* (editor): **Mass Spectrometry in Metabolomics – Methods and Protocols**
Humana Press, 2014 [ISBN: 978-1-4939-1257-5]

*Ramanathan, R.* (editor): **Mass Spectrometry in Drug Metabolism and Pharmacokinetics**
John Wiley & Sons, Inc., 2009 [ISBN: 978-0-471-75158-8]

*Rossi, D.T.; Sinz, M.W.* (editori): **Mass Spectrometry in Drug Discovery**
Marcel Dekker, Inc., 2002 [ISBN: 0-8247-0607-2]

*Russell, D.H.* (editor): **Experimental Mass Spectrometry**
Springer Science + Business Media, 0994 [ISBN: 978-1-4899-2571-8]

*Sargent, M.; Harte, R.; Harrington, C.*: **Guidelines for Achieving High Accuracy in Isotope Dilution Mass Spectrometry (IDMS)**
LGC Limited, 2002 [ISBN: 0-85404-418-3]

*Setou, M.* (editor): **Imaging Mass Spectrometry – Protocols and Mass Microscopy**
Springer, 2010 [ISBN: 978-4-431-09425-8]

*Shalley, C.A.* (editor): **Modern Mass Spectrometry**
Springer Verlag, 2003 [ISBN: 3-540-00098-4]

*Shalley, C.*A. (editor): **Mass Spectrometry of Non-Covalent Complexes: Supramolecular Chemistry in the Gas Phase**
Wiley, 2009 [ISBN 978-0470131152]

*Shrader, S.*: **Introductory Mass Spectrometry**
CRC Press, Taylor & Francis Group, 2014 [ISBN: 978-1-4665-9585-9]

*Shvartsburg, A.A.*: **Differential Ion Mobility Spectrometry – Nonlinear Ion Transport and Fundamentals of FAIMS**
CRC Press, Taylor & Francis Group, 2009 [ISBN: 978-1-4200-5106-3]

*Smith, R.J.; Webb, M.L.* (editori): **Analysis of Drug Impurities**
Blackwell Publishing, 2007 [ISBN: 978-14051-3358-6]

*Snozek, C.L.H.; Langman, L.J.; Cotton, S.W.*: I**ntroduction to Drug Testing: The Expending Role of Mass Spectrometry**
Humana Press, New York, 2019 [ISCN: 978-1-4939-8823-5]

*Sparkman, O.D.; Penton, Z.E.; Kitson, G.F.*: **Gas Chromatography and Mass Spectrometry: A Practical Guide**
Academic Press, Inc., 2011 [ISBN: 978-0-12-373628-4]

*Spool, A.M.;* **The Practice of Tof-Sims: Time of Flight Secondary Ion Mass Spectrometry**
Momentum Press, 2016 [ISBN: 978-16065077345]

*Suelter, C.H.; Watson, J.T.* (editori): **Biomedical Applications of Mass Spectrometry**
Jonh Wiley & Sons, 1990 [ISBN: 0-471-61303-7]

*Thevis, M.*: **Mass Spectrometry in Sports Drug Testing – Characterization of Prohibited Substances and Doping Control – Analytical Assays**
John Wiley & Sons, Inc., 2010 [ISBN: 978-0-470-41327-2]

*Tsipi, D.; Botitsi, H.; Economou, A.* (editori): **Mass Spectrometry for the Analysis of Pesticide Residues and Their Metabolites**
John Wiley & Sons, Inc., 2015 [ISBN: 978-1-118-50017-0]

*Valkó, K.* (editor): **Separation Methods in Drug Synthesis and Purification**
Elsevier, 2000 [ISBN: 0-444-50007-3]

*Wang, J.;MacNeil, J.D.; Kay, J.F.* (editori): **Chemical Analysis of Antibiotic Rasidues in Food**
John Wiley & Sons, 2012 [ISBN: 978-0-470-49042-6]

*Wang, X.S.*:**Mass Spectrometric Characterization and Analysis of Anti-oxidative Properties of Medicinal Herbs** – Thesis
University of New South Wales, Sydney, 2003

*Wanner, K.; Höfner, G.* (editori): **Mass Spectrometry in Medicinal Chemistry – Applications in Drug Discovery**
Wiley-VCH Verlag GmbH & Co. KGaA, 2007 [ISBN: 978-3-527-31456-0]

*Watson, J.T.; Sparkman, O.D.*: **Introduction to Mass Spectrometry – Instrumentation, Applications and Strategies for Data Interpretation**
John Wiley & Sons, Ltd., 2007 [ISBN: 978-0-470-51634-8]

*Whittaker, D.*: **Interpreting Organic Spectra** – Capitol 2.
The Royal Society of Chemistry, 2000 [ISBN: 0-85404-601-1]

*Wilkins, C.L.; Lay jr., J.O.* (editori): **Identification of Microorganisms by Mass Spectrometry**
John Wiley & Sons, Inc., 2006 [ISBN: 978-0-471-65442-1]

*Wilkins, C.L.; Trimpin, S.* (editori): **Ion Mobility Spectrometry – Mass spectrometry – Theory and Applications**
CRC Press, Taylor & Francis Group, 2011 [ISBN: 978-1-4398-1325-6]

*Winter, D.*: **Drug Analysis by Mass Spectrometry** – Thesis
University of Canterbury, Christchurch, New Zeeland, 1986

*Yergey, A.L.; Edmonds, C.G.; Lewis, I.A.S.; Vestal, M.L.*: Liquid Chromatography/Mass Spectrometry
Springer Science + Business Media LLC, 1990 [978-1-4899-3607-3]

*Yinon, J.* (editor): **Advances in Forensic Applications of Mass Spectrometry**
CRC Press, 2004 [ISBN: 0-8493-1522-0]

*Zaitsu, K.* (editor): **Ambient Ionozation Mass Spectrometry in Life Sciences: Principles and Applications**
Elsevier, 2019 [ISBN: 9780128172209]

*Zubarev, R.*A.*; Makarov, A.*: **Orbitrap Mass Spectrometry**
Anal. Chem., 2013:85, 5228-5296